

**ELECTRONIC  
STRUCTURE AND  
PROPERTIES OF  
TRANSITION METAL  
COMPOUNDS**

# **ELECTRONIC STRUCTURE AND PROPERTIES OF TRANSITION METAL COMPOUNDS**

---

## **Introduction to the Theory**

Second Edition

**ISAAC B. BERSUKER**  
The University of Texas at Austin



A JOHN WILEY & SONS, INC., PUBLICATION

Copyright © 2010 by John Wiley & Sons, Inc. All rights reserved

Published by John Wiley & Sons, Inc., Hoboken, New Jersey  
Published simultaneously in Canada

No part of this publication may be reproduced, stored in a retrieval system, or transmitted in any form or by any means, electronic, mechanical, photocopying, recording, scanning, or otherwise, except as permitted under Section 107 or 108 of the 1976 United States Copyright Act, without either the prior written permission of the Publisher, or authorization through payment of the appropriate per-copy fee to the Copyright Clearance Center, Inc., 222 Rosewood Drive, Danvers, MA 01923, (978) 750-8400, fax (978) 750-4470, or on the web at [www.copyright.com](http://www.copyright.com). Requests to the Publisher for permission should be addressed to the Permissions Department, John Wiley & Sons, Inc., 111 River Street, Hoboken, NJ 07030, (201) 748-6011, fax (201) 748-6008, or online at <http://www.wiley.com/go/permission>.

**Limit of Liability/Disclaimer of Warranty:** While the publisher and author have used their best efforts in preparing this book, they make no representations or warranties with respect to the accuracy or completeness of the contents of this book and specifically disclaim any implied warranties of merchantability or fitness for a particular purpose. No warranty may be created or extended by sales representatives or written sales materials. The advice and strategies contained herein may not be suitable for your situation. You should consult with a professional where appropriate. Neither the publisher nor author shall be liable for any loss of profit or any other commercial damages, including but not limited to special, incidental, consequential, or other damages.

For general information on our other products and services or for technical support, please contact our Customer Care Department within the United States at (800) 762-2974, outside the United States at (317) 572-3993 or fax (317) 572-4002.

Wiley also publishes its books in a variety of electronic formats. Some content that appears in print may not be available in electronic formats. For more information about Wiley products, visit our web site at [www.wiley.com](http://www.wiley.com).

***Library of Congress Cataloging-in-Publication Data:***

Bersuker, I. B. (Isaak Borisovich)  
Electronic structure and properties of transition metal compounds :  
introduction to the theory / Isaac B. Bersuker. – 2nd ed.  
p. cm. – (Textbook for graduate and advanced undergraduate  
students)  
Includes bibliographical references and index.  
ISBN 978-0-470-18023-5 (cloth)  
1. Transition metal compounds. I. Title.  
QD172.T6B48 2010  
546'.6–dc22

2009021658

Printed in the United States of America

10 9 8 7 6 5 4 3 2 1

*To my grandsons Eugene and Kirill*

# CONTENTS

<b>Preface</b>	<b>xxi</b>
<b>Foreword to the First Edition</b>	<b>xxv</b>
<b>Mathematical Symbols</b>	<b>xxvii</b>
<b>Abbreviations</b>	<b>xxxiii</b>
<b>1 Introduction: Subject and Methods</b>	<b>1</b>
<b>1.1 Objectives, 1</b>	
Molecular Engineering and Intuitive Guesswork, 1	
Main Objectives of This Book in Comparison with Other Sources, 4	
<b>1.2 Definitions of Chemical Bonding and Transition Metal     Coordination System, 7</b>	
Chemical Bonding as an Electronic Phenomenon, 7	
Definition of Coordination System, 9	
<b>1.3 The Schrödinger Equation, 12</b>	
Formulation, 12	
Role of Approximations, 14	
<b>Summary Notes, 15</b>	
<b>References, 16</b>	

<b>2</b>	<b>Atomic States</b>	<b>18</b>
2.1	<b>One-Electron States, 18</b>	
	Angular and Radial Functions, 18	
	Orbital Overlaps: Hybridized Functions, 24	
	Spin–Orbital Interaction, 27	
	Relativistic Atomic Functions, 30	
2.2	<b>Multielectron States: Energy Terms, 35</b>	
	Electronic Configurations and Terms, 35	
	Multielectron Wavefunctions, 40	
	Slater–Condon and Racah Parameters, 42	
	The Hartree–Fock Method, 46	
	<b>Summary Notes, 51</b>	
	<b>Questions, 51</b>	
	<b>Exercises and Problems, 52</b>	
	<b>References, 52</b>	
<b>3</b>	<b>Symmetry Ideas and Group-Theoretical Description</b>	<b>54</b>
3.1	<b>Symmetry Transformations and Matrices, 54</b>	
3.2	<b>Groups of Symmetry Transformations, 60</b>	
	<i>Example 3.1.</i> The Symmetry Group of an Octahedral $O_h$ System and Its Classes, 62	
3.3	<b>Representations of Groups and Matrices of Representations, 64</b>	
3.4	<b>Classification of Molecular Terms and Vibrations, Selection Rules, and Wigner–Eckart Theorem, 69</b>	
	<i>Example 3.2.</i> Energy Terms of Electronic Configuration $e^2$ , 71	
3.5	<b>Construction of Symmetrized Molecular Orbitals and Normal Vibrations, 74</b>	
	<i>Example 3.3.</i> Construction of $E_g$ -Symmetry-Adapted $\sigma$ MOs for Octahedral $O_h$ Systems, 76	
	<i>Example 3.4.</i> Construction of $T_{2g}$ -Symmetry-Adapted $\pi$ MOs for Octahedral $O_h$ Systems, 79	
	<i>Example 3.5.</i> Normal Coordinates of a Regular Triangular Molecule $X_3$ , 80	
3.6	<b>The Notion of Double Groups, 81</b>	
	<b>Summary Notes, 82</b>	

Exercises, 82

References, 83

## **4 Crystal Field Theory 84**

### **4.1 Introduction, 84**

Brief History, 84

Main Assumptions, 85

### **4.2 Splitting of the Energy Levels of One $d$ Electron in Ligand Fields, 86**

Qualitative Aspects and Visual Interpretation, 86

Calculation of the Splitting Magnitude, 92

*Example 4.1.* Splitting of a  $d$ -Electron Term in Octahedral Crystal Fields, 94

Group-Theoretical Analysis, 97

### **4.3 Several $d$ Electrons, 99**

Case of a Weak Field, 99

Strong Crystal Fields and Low- and High-Spin Complexes, 105

*Example 4.2.* High- and Low-Spin Octahedral Complexes of Iron, 110

Energy Terms of Strong-Field Configurations, 110

Arbitrary Ligand Fields and Tanabe–Sugano Diagrams, 112

### **4.4 $f$ -Electron Term Splitting, 115**

### **4.5 Crystal Field Parameters and Extrastabilization Energy, 121**

### **4.6 Limits of Applicability of Crystal Field Theory, 126**

Summary Notes, 128

Questions, 129

Exercises and Problems, 129

References, 130

## **5 Method of Molecular Orbitals and Related Approaches 132**

### **5.1 Basic Ideas of the MO LCAO Method, 133**

Main Assumptions, 133

Secular Equation, 134

Classification by Symmetry, 135

- Symmetrized Orbitals, 138  
Simplification of the Secular Equation, 141
- 5.2 Charge Distribution and Bonding in the MO LCAO Method and the Case of Weak Covalency, 142**  
Atomic Charges and Bond Orders, 142  
*Example 5.1.* Shortcomings of Mulliken's Definition of Atomic Charges in Molecules, 145  
Bonding, Nonbonding, and Antibonding Orbitals, 147  
Case of Weak Covalency, 149  
Angular Overlap Model, 151
- 5.3 Methods of Calculation of MO Energies and LCAO Coefficients, 154**  
SCF MO LCAO Approximation, 154  
The Role of Basis Sets, 157  
Electron Correlation Effects, 161  
*Example 5.2.* Exercise: Ab Initio Calculation of  $\text{CuF}_2$  Using Hartree–Fock and MP2 Methods, 166
- 5.4 Semiquantitative Approaches, 168**  
Pseudopotentials or Effective Core Potentials (ECPs), 170  
Density-Functional Approaches, 171  
*Example 5.3.* Exercise: Calculation of  $\text{ZnCl}_2$  by the DFT Method, 178  
*Example 5.4.* Exercise: Ab Initio Calculation of the Electronic Structure of  $\text{MnO}_4^-$  Square-Planar, Tetrahedral, and Square-Based Pyramidal Configuration, 180  
Relativistic Approaches, 184
- 5.5 Semiempirical Methods, 187**  
Zero-Differential Overlap (ZDO), 188  
Extended Hückel (Hoffmann) Method, 192  
Iterative Extended Hückel Method, 193  
*Example 5.5.*  $A_{1g}$ -Type MOs of Octahedral  $\text{TiF}_6^{3-}$  Calculated Using the Extended Hückel (Wolfsberg–Helmholz) Approximation, 196  
Quasirelativistic Parameterization, 198  
*Example 5.6.* Quasirelativistic Evaluation of Energies of Ionization of Several Valence States (EIVS) of  $s$ ,  $p$ , and  $d$  Electrons of the Pt Atom, 201



- 5.6 Fragmentary Calculations, Molecular Mechanics, and Combined Quantum/Classical (QM/MM) Modeling, 201**  
Fragmentary Calculations, 202  
Molecular Mechanics, 206  
*Example 5.7.* Application of Molecular Modeling to Transition Metal Complexes with Macrocycles, 208  
Combined Quantum/Classical (QM/MM) Methods, 211  
*Example 5.8.* Oxidative Addition of H<sub>2</sub> to Pt(*t*-Bu)<sub>3</sub>)<sub>2</sub> Treated by ONIOM Version of QM/MM Methods, 215  
*Example 5.9.* Iron Picket-Fence Porphyrin Treated by the QM/MM Method with Charge Transfer (QM/MM/CT), 221
- 5.7 General Comparison of Methods, 224**  
Summary Notes, 229  
Exercises and Problems, 230  
References, 231

## **6 Electronic Structure and Chemical Bonding 238**

- 6.1 Classification of Chemical Bonds by Electronic Structure and Role of *d* and *f* Electrons in Coordination Bonding, 238**  
Criticism of the Genealogical Classification, 239  
Classification by Electronic Structure and Properties, 241  
Features of Coordination Bonds, 243  
Coordination Bonding by Pre- and Posttransition Elements, 245
- 6.2 Qualitative Aspects and Electronic Configurations, 246**  
Most Probable MO Schemes, 246  
Electronic Configurations in Low- and High-Spin Complexes, 247  
Covalence Electrons and Ionization Potentials, 251
- 6.3 Ligand Bonding, 254**  
General Considerations: Multiorbital Bonds, 254  
Monoorbital Bonds: Coordination of NH<sub>3</sub> and H<sub>2</sub>O, 259  
*Example 6.1.* Ab Initio Numerical SCF-CI Calculations of the Electronic Structure of Monoorbital Bonds: Ni(H<sub>2</sub>O)<sub>*n*</sub> and Ni(PH<sub>3</sub>)<sub>*n*</sub>, *n* = 1, 2, 261  
Diorbital Bonds: Coordination of the N<sub>2</sub> Molecule, 261  
*Example 6.2.* Electronic Structure and Bonding in FeN<sub>2</sub>, 264  
Coordination of Carbon Monoxide, 264

- Example 6.3.* Bonding and Charge Transfer in the Pt—CO Complex, 265
- Example 6.4.* Bonding in M—CO with M = Cr, Fe, Co, Ni, 267
- Example 6.5.* Bonding in Sc—CO, Ni—CO, and Ni(CO)<sub>2</sub>, 268
- $\sigma + \pi$  Bonding, 269
- Example 6.6.* Electronic Structure of Transition Metal Hexacarbonyls M(CO)<sub>6</sub>, 271
- CO Bonding on Surfaces, 273
- Bonding of NO, 275
- Example 6.7.* Coordination of NO on the Ni(111) Surface, 276
- Coordination of C<sub>2</sub>H<sub>4</sub>, 277
- Example 6.8.* Ethylene Bonding to Transition Metal Centers, 278
- Example 6.9.* Ethylene Bonding in PtCl<sub>3</sub>(C<sub>2</sub>H<sub>4</sub>)<sup>-</sup> and PdCl<sub>3</sub>(C<sub>2</sub>H<sub>4</sub>)<sup>-</sup>, 279
- Metal–Metal Bonds and Bridging Ligands, 282
- Example 6.10.* Multiple Metal–Metal Bonds in [Re<sub>2</sub>Cl<sub>8</sub>]<sup>2-</sup> and [Mo<sub>2</sub>Cl<sub>8</sub>]<sup>4-</sup>, 284
- 6.4 Energies, Geometries, and Charge Distributions, 291**
- Ionization Energies, 291
- Example 6.11.* Ab Initio Calculations of Ni(C<sub>3</sub>H<sub>5</sub>)<sub>2</sub>, 293
- Total and Bonding Energies, Geometries, and Other Properties, 295
- 6.5 Relativistic Effects, 303**
- Orbital Contraction and Valence Activity, 304
- Example 6.12.* Relativistic Effects in Catalytic Activity of Pt and Pd Complexes, 306
- Bond Lengths, Bond Energies, and Vibrational Frequencies, 307
- Example 6.13.* Relativistic Effects in Metal Hydrides, 307
- Correlation Between Spin–Orbital Splitting and Bonding, 310
- Example 6.14.* Relativistic Semiempirical Calculation of PtCl<sub>6</sub><sup>2-</sup>, 312
- Other Relativistic Effects, 315
- Summary Notes, 315**

**Exercises and Problems, 316**

**References, 318**

**7 Electronic Control of Molecular Shapes and Transformations via Vibronic Coupling 324**

**7.1 Molecular Vibrations, 325**

Adiabatic Approximation, 325

Normal Coordinates and Harmonic Vibrations, 328

Special Features of Vibrations of Coordination Systems, 336

**7.2 Vibronic Coupling, 337**

Vibronic Constants, 337

Orbital Vibronic Constants, 339

*Example 7.1.* Vibronic MO Description of Electronic Structure of  $N_2$  and CO, 342

**7.3 The Jahn–Teller Effect, 344**

The Jahn–Teller Theorem, 344

The Jahn–Teller Effect in a Twofold-Degenerate Electronic State, 351

Threefold-Degenerate Electronic States, 364

**7.4 Pseudo-Jahn–Teller Effect and the Two-Level Paradigm, 369**

Pseudo-Jahn–Teller (PJT) Instability, 369

Uniqueness of the Vibronic Mechanism of Configuration

Instability: The Two-Level Paradigm, 377

*Example 7.2.* Numerical Confirmation of PJT Origin of Instability of High-Symmetry Configurations, 379

*Example 7.3.* Numerical Calculations Confirming the PJT Origin of Configuration Instability of Coordination Systems, 380

Further Insight into the Pseudo-JTE and Hidden JTE, 381

*Example 7.4.* Comparison of Covalence versus Polarization Contributions to PJT Instability, 384

*Example 7.5.* Why Some  $ML_2$  Molecules ( $M = Ca, Sr, Ba; L = H, F, Cl, Br$ ) are Bent While Others Are Linear, 385

*Example 7.6.* Hidden JTE in  $CuF_3$ : Ab Initio Calculations, 387

**Summary Notes, 388**

**Exercises and Problems, 389**

**References, 390**

<b>8</b>	<b>Electronic Structure Investigated by Physical Methods</b>	<b>392</b>
<b>8.1</b>	<b>Band Shapes of Electronic Spectra, 393</b>	
	Qualitative Interpretation of Vibrational Broadening, 393	
	<i>Example 8.1.</i> Broad and Narrow Bands in Light Absorption and Emission by Transition Metal Complexes, 396	
	Theory of Absorption Band Shapes, 396	
	Band Shapes of Electronic Transitions between Nondegenerate States; Zero-Phonon Lines, 399	
	Types of Electronic Transitions on Intensity, 402	
	<i>Example 8.2.</i> Selection Rules for Polarized Light Absorption by the $\text{PtCl}_4^{2-}$ Complex, 403	
<b>8.2</b>	<b><i>d-d</i>, Charge Transfer, Infrared, and Raman Spectra, 405</b>	
	Origin and Special Features of <i>d-d</i> Transitions, 406	
	<i>Example 8.3.</i> <i>d-d</i> Transitions in the Absorption Spectrum of $\text{Mn}(\text{H}_2\text{O})_6^{2+}$ , 407	
	<i>Example 8.4.</i> Temperature-Dependent Absorption Spectra of $\text{K}_2\text{NaCrF}_6$ and Emerald, 410	
	Spectrochemical and Nephelauxetic Series, 411	
	Charge Transfer Spectra, 415	
	<i>Example 8.5.</i> Some Ligand $\rightarrow$ Metal or Metal $\rightarrow$ Ligand Charge Transfer Spectra, 416	
	Infrared Absorption and Raman Scattering, 417	
	<i>Example 8.6.</i> Resonance Raman Spectrum of Red $\text{K}_2[\text{Ni}(\text{dto})_2]$ in Solid State, 421	
	Transitions Involving Orbitally Degenerate States, 422	
<b>8.3</b>	<b>X-Ray and Ultraviolet Photoelectron Spectra; EXAFS, 426</b>	
	General Ideas, 426	
	<i>Example 8.7.</i> Photoelectron Spectra of Specific Coordination Systems and Their Interpretation, 429	
	Electron Relaxation; Shakeup and CI Satellites, 431	
	<i>Example 8.8.</i> Configuration Interaction Satellite to the $\text{K}^+$ 3s Emission Line in the UPS Spectrum of KF, 434	
	Chemical Shift, 436	
	<i>Example 8.9.</i> The 1s Line of Nitrogen in the XPS of Different Coordination Systems Reflecting the Variety of Its Bonding in Different Groups, 439	

- EXAFS and Related Methods, 440
- Example 8.10.* Applications of EXAFS Spectroscopy to a Variety of Problems, 442
- 8.4 Magnetic Properties, 443**
- Magnetic Moment and Quenching of Orbital Contribution, 443
- Paramagnetic Susceptibility, 447
- Electron Spin Resonance (ESR), 449
- Magnetic Exchange Coupling, 457
- Example 8.11.* Magnetic Exchange Coupling in Binuclear Copper Acetate Hydrate, 461
- Example 8.12.* The Nature of Metal–Metal Bonding in Binuclear Copper Acetate Hydrate, 462
- Spin Crossover, 465
- Magnetic Circular Dichroism (MCD), 468
- 8.5 Gamma-Resonance Spectroscopy, 472**
- The Mossbauer Effect, 472
- $\gamma$ -Resonance Spectra, 473
- Isomer Shift and Quadrupole Splitting in GRS, 474
- Hyperfine Splitting, 478
- Example 8.13.* Magnetic Hyperfine Structure in GRS of Coordination Compounds with a  $^{57}\text{Fe}$  Nucleus, 479
- Example 8.14.* Observation of Spin Crossover in the  $\gamma$ -Resonance Spectrum of  $[\text{Fe}(\text{phen})_2(\text{NCS})_2]$ , 482
- 8.6 Electron Charge and Spin Density Distribution in Diffraction Methods, 483**
- The Method of Deformation Density, 483
- Example 8.15.* Deformation Density in Sodium Nitroprusside (Direct Inspection), 485
- Example 8.16.* Metal–Metal Bonding in  $\text{Mn}_2(\text{CO})_{10}$ ; Fragment Deformation Density, 488
- Example 8.17.* Density Modeling for Fe(II)–Phthalocyanine and Co(II)–Tetraphenyl-porphyrin, 491
- Spin Densities from Neutron Scattering, 493
- Example 8.18.* Spin Distributions in Some Coordination Systems Obtained from Neutron Scattering, 494
- Summary Notes, 495**
- Exercises and Problems, 497**
- References, 500**

<b>9</b>	<b>Stereochemistry and Crystal Chemistry</b>	<b>506</b>
<b>9.1</b>	<b>Definitions. Semiclassical Approaches, 506</b>	
	The Notion of Molecular Shape, 506	
	Directed Valences, Localized Electron Pairs, and Valence Shell Electron Pair Repulsion (VSEPR), 508	
	Nonbonding Orbitals and Nodal Properties, 512	
	<i>Example 9.1.</i> Influence of Nonbonding MOs on Coordination Geometry, 513	
	Complementary Spherical Electron Density Model, 514	
	<i>Example 9.2.</i> The Inert-Gas Rule in Stereochemistry of Some Coordination Compounds, 517	
<b>9.2</b>	<b>Vibronic Effects in Stereochemistry, 519</b>	
	Nuclear Motion Effects: Relativity to the Means of Observation and Vibronic Amplification of Distortions, 519	
	Qualitative Stereochemical Effects of Jahn–Teller and Pseudo-Jahn–Teller Distortions, 522	
	<i>Example 9.3.</i> Stereochemistry of $\text{MX}_n$ Systems Controlled by Electronic Structure and Vibronic Coupling, 524	
	<i>Example 9.4.</i> Pseudo-JT Origin of Distortions in $\text{CuCl}_5^{3-}$ versus $\text{ZnCl}_5^{3-}$ , 525	
	Off-Center Position of the Central Atom, 528	
	Geometry of Ligand Coordination, 530	
	Stereochemically Active and Inert Lone Pairs, 535	
	Pseudorotations in Coordination Systems, 539	
<b>9.3</b>	<b>Mutual Influence of Ligands, 544</b>	
	The Model: <i>trans</i> and <i>cis</i> Influences in Stereochemistry, 544	
	Electronic Factors, 546	
	Vibronic Theory of Ligand Mutual Influence, 549	
<b>9.4</b>	<b>Crystal Stereochemistry, 554</b>	
	The Plasticity Effect, 554	
	Distortion Isomers, 559	
	<i>Example 9.5.</i> Origin of Distortion Isomers in $\text{Cu}(\text{NH}_3)_2\text{X}_2$ , X = Cl, Br, 559	
	Temperature-Dependent Solid-State Conformers, 562	
	Cooperative Effects: Order–Disorder and “Displacive” Phase Transitions and Helicoidal Structures, 566	
	<b>Summary Notes, 572</b>	
	<b>Exercises and Problems, 573</b>	
	<b>References, 575</b>	

<b>10 Electron Transfer, Redox Properties, and Electron-Conformational Effects</b>	<b>579</b>
<b>10.1 Electron Transfer and Charge Transfer by Coordination, 579</b>	
Intramolecular Charge Transfer and Intermolecular Electron Transfer, 579	
Redox Capacitance, 584	
<i>Example 10.1.</i> Charge Transfer by Coordination of Peroxide to Iron Porphyrin, 587	
Hard and Soft Acids and Bases, 587	
<b>10.2 Electron Transfer in Mixed-Valence Compounds, 591</b>	
Mixed-Valence Compounds as Electronic Systems; a Two-Level Dimer, 591	
<i>Example 10.2.</i> The Creutz–Taube (CT) Ion as a Mixed-Valence System, 594	
Magnetic Properties, 597	
Mixed-Valence Trimers: Coexistence of Localized and Delocalized States, 601	
<i>Example 10.3.</i> Tricenter Ferredoxin, 606	
<b>10.3 Electron-Conformational Effects in Biological Systems, 609</b>	
Distortions Produced by Excess Electronic Charge; Special Features of Metalloenzymes, 609	
Trigger Mechanism of Hemoglobin Oxygenation: Comparison with Peroxidase, 612	
<b>Summary Notes, 618</b>	
<b>Exercises and Problems, 619</b>	
<b>References, 620</b>	
<b>11 Reactivity and Catalytic Action</b>	<b>623</b>
<b>11.1 Electronic Factors in Reactivity, 623</b>	
Chemical Reactivity and Activated Complexes, 623	
Frontier Orbitals and Perturbation Theory, 627	
Orbital Symmetry Rules in Reaction Mechanisms, 630	
<i>Example 11.1.</i> Orbital Symmetry Rules and Vibronic Coupling in Formation of Cyclobutane from Ethylene with Catalyst Participation, 633	
<b>11.2 Electronic Control of Chemical Activation via Vibronic Coupling, 635</b>	

Chemical Activation by Electron Rearrangement,	635
Activation of Small Molecules by Coordination: Semiempirical Approach,	640
<i>Example 11.2.</i> Activation of Carbon Monoxide,	642
<i>Example 11.3.</i> Numerical Estimate of CO Activation by Coordination to a NiO Surface,	646
<i>Example 11.4.</i> Activation of Dinitrogen,	646
<i>Example 11.5.</i> Activation of Nitrogen Monoxide,	648
<i>Example 11.6.</i> Activation of Hydrogen,	649
<i>Example 11.7.</i> Activation of Oxygen by Hemoproteins,	650
Jahn–Teller- and Pseudo-Jahn–Teller-Induced Chemical Activation,	652
<i>Example 11.8.</i> Jahn–Teller-Induced Substitution Reactions in Octahedral Complexes with an <i>E</i> Term,	655
<b>11.3 Direct Computation of Energy Barriers of Chemical Reactions,</b>	<b>656</b>
Substitution Reactions: The <i>trans</i> Effect,	656
Ligand Coupling and Cleavage Processes,	662
CO Reductive Hydrogenation and Carbonyl Insertion Reactions,	666
Olefin Insertion Reactions,	674
<i>Example 11.9.</i> Polymerization with Ziegler–Natta Catalysts,	677
Photochemical Reactions of Organometallics,	682
<b>Summary Notes,</b>	<b>686</b>
<b>Questions and Problems,</b>	<b>687</b>
<b>References,</b>	<b>689</b>
<b>Appendixes</b>	
Appendix 1. Tables of Characters of Irreducible Representations of Most Usable Symmetry Point Groups and Direct Products of Some Representations,	692
Appendix 2. General Expressions for the Matrix Element $V_{mm'}$ of Perturbation of the States of One <i>d</i> Electron in Crystal Fields of Arbitrary Symmetry,	697
Appendix 3. Calculation of the Destabilization and Splitting of the States of One <i>d</i> Electron in Crystal Fields of Different Symmetries,	700



CONTENTS

xix

Appendix 4. Matrix Elements of Crystal Field Perturbation of a Two-Electron Term  $F(nd)^2$ ,  $V'_{ij}$ ,  $i, j = 1, 2, \dots, 7$  Expressed by One-Electron Matrix Elements  $V'_{mm}$  Given in Appendix 2, 703

Appendix 5. Matrix Elements of Crystal Field Perturbation of  $f$  Electron States, 705

**Answers and Solutions**

**707**

**Subject Index**

**745**

**Formula Index**

**753**

## PREFACE

In rewriting the first edition of this book, two goals were pursued. The first one is educational, to make the book more accessible to graduate and advanced undergraduate students and to supplement the presentation with additional “infrastructure” that allows the reader to use the book as a textbook for special courses. The second goal, although more usual, is no less important; it strives from the necessity to renew the material of the book in view of the fast development of this field during the last two decades.

For the educational goal the narrative is given in maximum possible plain language accompanied by many boxed “Examples” showing explicitly how the theory is applied to solving specific chemical problems, and each chapter is supplemented by “Summary Notes,” “Questions,” “Exercises,” and “Problems.” These supplements serve as a guide to learning and adoption of the subject by the students, and to help the instructor of the course. Some of these additions are on the level of chemical problem solving with detailed solutions given at the end of the book.

Beside these essential educational improvements the book preserves and enhances the first edition’s role as a source of information on the basics of electronic structure and properties of transition metal systems (TMSs) in its most modern understanding, and with emphasis on origins and physical meaning. All the chapters are corrected and updated, but essential changes were introduced in Chapters 5–9, especially in Chapters 5 and 8. In particular, in Chapter 5 combined quantum–classical (QM/MM) methods of modeling large organometallic systems are described and examples of QM/MM calculations for specific TMS are given. In the same chapter an extended presentation of the density-functional methods of electronic structure calculations (which have

reached widespread use also by nonexperts) is given together with examples of computations using free programs downloaded from the Internet. Similar examples are also given for semiempirical and ab initio methods of computation. In Chapter 8 some important physical methods of investigation are added, including a section on gamma-resonance spectroscopy, as well as further description of IR, Raman, and charge transfer spectra.

The special boxed “Examples” in nine chapters of the book (a total of 70) supplement the theoretical methods and results, making them more accessible and understandable. They may serve also as separate essays—solutions of chemical problems by means of theoretical methods, and therefore they are indicated on a separate line in the book Contents.

The role and place of this book among others available is outlined in the introductory Chapter 1, but I should like to note here the (unique of this kind) attempt to promote a novel, more general agenda (with a higher level of theory and understanding) of the role of electronic structure in formation and transformation of matter. With regard to TMS, the first significant level of electronic theory was reached in the 1950s–1960s by *crystal field theory*. A higher level of theory was achieved in the 1980s–1990s, based on computer developments that allowed for full molecular orbital and density-functional *electronic structure calculations*.

However, in the last two to three decades a new, higher level of understanding of the role of electronic structure in properties of matter emerged that has not yet been assimilated by the lay chemist and physicist, and still has not been introduced in teaching of this subject. The novel understanding is related to the ways in which the electrons control molecular transformation. It turns out that nuclear configuration changes are dependent on the electronic structure that essentially *involves excited electronic states*. The point is that quantum separation of ground and excited electronic states is valid only for given, fixed positions of the nuclei; any displacement of the latter mixes the initial ground and excited or degenerate states, and this mixing is crucial in understanding the origin of nuclear configuration changes. *Mixing electronic states, ground and excited, degenerate and nondegenerate, solely determines all possible nuclear configuration instabilities, distortions, and transformations*, including formation of molecular shapes and crystal lattices, conformational changes and phase transitions, chemical activation, and mechanism of chemical reactions, to mention a few.

Comprehending this nuclear-dynamical aspect of electronic structure elevates the theory to a new, higher level and facilitates a better understanding of chemical and physical phenomena. The intention of this book is to instill this advanced way of thinking in physics and chemistry. It is given in many parts of the book as a paradigm, more noticeable and explicitly in Section 7.4 with applications in subsequent chapters, especially Chapters 9–11.

In preparation of this book I benefited from the help of my students and colleagues, many of whom were mentioned in the Preface to the first edition. For

the present (second) edition I received further assistance from J. E. Boggs, P. Garcia-Fernandez, V. Z. Polinger, B. S. Tsukerblat, M. D. Kaplan, S. A. Borshch, S. S. Stavrov, G. I. Bersuker, L. F. Chibotaru, I. Ya. Ogurtsov, N. N. Gorinchoy, Wenli Zou, and Yang Liu. I am grateful also to F. A. Cotton and J. P. Fackler, Jr., for their foreword to the first edition. Special thanks are due to Professor Charles Dismukes (Princeton University), who used the first edition as a textbook to his courses and provided us with a variety of comments and questions, as well as corrections to misprints and omissions.

ISAAC B. BERSUKER  
*Austin, Texas, March 2009*

### EXTRACTS FROM THE PREFACE TO THE FIRST EDITION

Presently transition metal compounds form a number of research fields with vast applications ranging from a variety of magnetic, ferroelectric, and superconducting materials to all kinds of catalysts, to metallobiochemical systems of vital importance. The main goal of this book is to provide a comprehensive discussion of the latest developments in the study of electronic structure and related properties of transition metal coordination systems, and to present the subject in a form suitable for chemists and physicists—students, researchers, and teachers.

Most attention is paid to a better understanding of the basic principles, general features, and specifics of electronic properties affecting ligand bonding, stereochemistry and crystal chemistry, chemical reactivity, electron transfer and redox phenomena, as well as spectroscopic, magnetic, and electronic density distribution properties. The discussion of relativistic effects in bonding, presented in a book context for the first time, elucidates the origin of important properties including, for instance, the “nobleness” and the yellow color of gold.

Quite novel are the implications of vibronic effects in chemical and physical phenomena presented in this book. The concept of vibronic interactions developed during the last two decades as a perturbational approach to the coupling between the electronic motion and nuclear configuration, contributes significantly to the solution of a number of problems. These include, for instance, band shapes of electronic and photoelectron spectra, local stereochemistry and structural phase transitions in crystals, plasticity, distortion isomers, and temperature dependent conformers, molecular pseudorotations, chemical activation by coordination, and electron-conformational effects in biological systems.

One of the special features of this book is that it includes both the theory of electronic structure and its applications to various problems. Significant efforts were made to present the whole topic in a unified fashion with indications of direct and indirect links between its numerous more specific aspects, and to make the presentation understandable without oversimplification. Many examples are provided, which will assist the reader in understanding how theoretical concepts can be applied to laboratory problems.

During the preparation of this book I benefited from the help and cooperation of my students and co-workers, as well as from suggestions of many colleagues throughout the world. I am very grateful to all of them.

ISAAC B. BERSUKER  
*Austin, Texas, April 1995*

## FOREWORD TO THE FIRST EDITION

While several major treatises have been published in the English language that purport to cover the topic of this volume, none has appeared in more than a decade. Advances in computing during this time have put the tools of the theoretical chemist in the hands of the experimentalist. Use of these tools requires a working knowledge of the basis for understanding the electronic structure and properties of the transition elements and their compounds. Therefore, theoretical features of the electronic structure of transition metal compounds are an important component of the training of both the experimental and theoretical chemist contributing solutions to problems in this area. Since this chemistry permeates industrial and biological chemistry as well as catalysis, solutions to problems in this field take on considerable importance. The field of transition metal chemistry is, indeed, fortunate that Isaac Bersuker, the leading contributor to the theory of transition metal electronic structure in the late period of the former Soviet Union, has translated and edited his numerous contributions published originally in Russian and combined them with new work into this modern English language text.

Isaac Bersuker became recognized as an authority in the Soviet Union on transition metal chemistry theory with publication of his 1962 book, which in many ways covered the same material that was published in English as *An Introduction to Transition-Metal Chemistry* by L. E. Orgel (Butler and Tanner Ltd., Frome, Somerset, England, 1960). While Orgel's book was "must" reading for transition metal chemists in the West in the 1960s, Bersuker's book served the same role in the Soviet Union. To our knowledge, Bersuker's Russian language book was never fully translated into English, although one of us (JPF) had a Russian-speaking student translate much of it for him in the late 1960s. As Bersuker's interaction with Western scientists increased during the 1970s and

1980s, his contribution to the understanding of the electronic structure of metal systems became increasingly known and appreciated. While in the former Soviet Union, Bersuker directed a powerful Academy of Sciences program in Kishinev, Moldova which focused on problems involving coupling between electronic and vibrational phenomena. In 1993 he moved to the United States (Austin, Texas), where he continues to be active. He recently authored a major review on "The concept of vibronic interactions in crystal stereochemistry of transition metal compounds," *J. Coord. Chem.* **289**, 338 (1995).

Many readers of this Foreword will be familiar with Isaac Bersuker's contributions to the understanding of the Jahn–Teller effect. His book *The Jahn–Teller Effect and Vibronic Interactions in Modern Chemistry* (Plenum Press, New York, 1984) is an important contribution used by persons interested in evaluating those systems in which vibrational and electronic states have similar energy separations that interact with each other. The useful concept of *orbital vibronic constants* is first presented in text form in the Jahn–Teller volume. This topic is brought into focus for the reader of this book in Chapter 7, following along after several introductory chapters that build the basic theory of transition metal chemistry. Incidentally, relativistic effects for transition metal compounds are treated for what is perhaps the first time in a book directed toward inorganic chemistry. Molecular orbital methods are introduced and compared, various bonding types are classified, electronic band shapes are interpreted, and magnetic properties are discussed. Stereochemistry is a fundamental and important part of this book, with symmetry and group theory widely used throughout, including the classification of terms, selection rules, crystal structures, and vibronic effects (vibronic stereochemistry). The book concludes with an investigation of the electronic properties of transition metal complexes, including the use of modern techniques such as EXAFS and the development of the concepts associated with electron transfer, a topic of fundamental importance to biological catalysis. Chemical activation and the direct calculation of energy barriers in chemical reactions complete the coverage in the book. Thus the student of this text is armed with an important, even essential arsenal of theory with which to handle virtually any electronic structure problem in transition metal chemistry.

We trust that this book will be a suitable primer for every serious practitioner of modern transition metal chemistry.

F. A. COTTON  
J. P. FACKLER, JR.

## MATHEMATICAL SYMBOLS

$A$	electron affinity hyperfine constant
$A$	atomic core
$A, B$	nondegenerate terms
$A, B, C$	Racah parameters
$\mathbf{B}$	magnetic induction
$C$	redox capacitance
$C^{(i)}$	anharmonicity correction coefficients
$c$	speed of light
$c_{ij}$	LCAO coefficients
$D$	activation energy barrier height
$D_s, D_t$	low-symmetry crystal field corrections
$d$	atomic state barrier width
$E$	energy
$E, e$	double degenerate representation term
$E_{JT}$	Jahn–Teller stabilization energy
$e$	electronic charge
$e_\sigma, e_\pi$	AOM parameters
$F$	linear vibronic constant
$F_k$	radial components of crystal field matrix elements



$F^{(k)}$	Slater–Condon parameter
$F(S)$	structure factor in X-ray scattering
$F(\Omega)$	form function for spectroscopic band shapes
$f$	angular dependence function in ESR spectra
	atomic state
	linear orbital vibronic constant
	multiplicity of degeneracy
	oscillator strength
	probability of nuclear zero-phonon transition
$G$	atomic term
	quadratic vibronic constants
	symmetry operator
$G_{ij}$	group overlap integral
$g$	$g$ factor
	quadratic orbital vibronic constant
$H$	Hamiltonian
$\Delta H$	heat of reaction
$\mathcal{H}$	magnetic field intensity
$\mathcal{H}_n$	Hermite polinomial
$I$	ionization potential
	light intensity
$\mathbf{I}$	nuclear spin
$I_{ij}$	Coulomb interaction
$i, j$	atomic and molecular states
	multiply used index
$\mathbf{j}_i$	total one-electron momentum
$J$	exchange coupling constant
	quantum number
	total momentum
$K_{ij}$	exchange interaction
$K_{\Gamma}^{\Gamma}$	force (elastic) constant, APES curvature
$K_{\Gamma^*}(\Gamma)$	vibronic reduction factor
$K(\Omega)$	coefficient of light absorption
$k$	reaction rate
$k(\Omega)$	spectral density of absorption
$k^i$	force constant coefficients
$\mathbf{L}$	operator
	orbital momentum
$L$	orbital momentum quantum number
$L_i$	ligand
$L_k^i$	Laguerre polinomial
$l, m, n$	direction cosines

	quantum numbers of atomic states
	vibronic energy levels
<b>M</b>	magnetic (electric) dipole moment
	magnetization
<i>M</i>	nucleus mass
	quantum number of projection of <b>L</b>
	metal center
<i>M</i>	molecular core electronic configuration
<i>M(S)</i>	magnetic structure factor
<i>M</i> <sub>12</sub>	transition moment
<i>m</i>	electron mass
<i>n</i>	vibrational quantum number
<i>P</i>	electron transfer probability
<i>P</i> <sub><i>a</i></sub>	amplification coefficient
<i>P</i> <sub><i>μν</i></sub>	bond orders
<i>P</i> <sub><i>ik</i></sub>	operator of permutation of <i>i</i> and <i>k</i>
<i>P</i> <sub><i>l</i></sub> <sup><i>m</i></sup>	associated Legendre polinomial
<i>p</i> = <i>K</i> <sub><i>E</i></sub> ( <i>A</i> <sub>2</sub> )	vibronic reduction factor in the <i>E</i> – <i>e</i> problem
<i>Q</i>	normal (symmetrized) nuclear coordinates
<i>Q</i> <sub><i>xx</i></sub>	gradient of electric field
<i>q</i> = <i>K</i> <sub><i>E</i></sub> ( <i>E</i> )	vibronic reduction factor in the <i>E</i> – <i>e</i> problem
<i>q</i> <sub><i>i</i></sub>	MO occupation numbers (MO population)
<i>q</i> <sub><i>μ</i></sub>	atomic effective charge
$\Delta q$	orbital charge transfer
<i>R</i>	interatomic distance
	nuclear coordinate
<b>R</b> <sub><i>α</i></sub>	radius vector
<i>R</i> <sub><i>nl</i></sub>	atomic radial wavefunction
<i>r</i> <sub><i>i</i></sub>	electron coordinate
<i>r</i> , $\theta$ , $\phi$	polar coordinates
<i>S</i>	electron spin
<i>S</i> , <i>S</i> <sub><i>AB</i></sub> , <i>S</i> <sub><i>ij</i></sub>	overlap integral
<i>S</i> , <i>P</i> , <i>D</i> , <i>F</i> , ...	atomic terms
<i>s</i> , <i>p</i> , <i>d</i> , <i>f</i>	atomic one-electron states
<i>T</i>	temperature
	period of vibrations
<i>T</i> <sub>1,2</sub>	triply degenerate representations (terms)
<i>U</i>	effective potential
	electron–nuclear interaction
<i>V</i>	electron–nuclear plus nuclear–nuclear interaction
	crystal field potential
<i>v</i>	electron speed

$W$	ionic interaction potential vibronic interaction terms
$w$	intramolecular electron transfer constant
$X$	character of representation
$x, y, z$	Cartesian coordinates
$Y_{l,m}$	spherical function
$Z$	nuclear charge
$Z_{\text{eff}}$	effective charge
$\alpha$	radial wavefunction parameter
$\alpha, \beta$	multiple-use index
$\alpha, \beta$	Pauli matrices
$\beta$	anharmonicity correction Bohr magneton nephelauxetic ratio
$\Gamma$	irreducible representation (term)
$\gamma$	anharmonicity coefficient covalence parameter core screening parameter $\gamma$ quanta $\gamma$ -resonance spectroscopy line of degenerate irreducible representations
$\gamma_{AB}$	electron repulsion integral
$\Delta$	crystal field parameter electron energy gap operator (second derivatives)
$\Delta X$	change of $X$
$\delta$	chemical shift extrastabilization energy Krönecker index ( $\delta$ symbol) tunneling splitting
$\delta(x)$	delta function
$\delta X$	variation of $X$
$\varepsilon$	one-electron orbital energy
$\varepsilon, \theta$	two components of the doubly degenerate $E$ representation
$\varepsilon(\Omega)$	extinction coefficient
$\xi, \eta, \zeta$	three components of the triply degenerate $T_2$ representation
$\xi$	one-electron spin-orbital coupling constant
$\vec{\nabla}$	vector operator
$\eta$	asymmetry parameter chemical hardness relativistic contraction

$\lambda$	covalence parameter spin-orbital interaction constant
$\lambda_{\Gamma}$	dimensionless vibronic constant
$\mu$	chemical potential ligand dipole moment magnetic moment
$\nu$	vibrational frequency, vibrational quantum number
$\Omega$	electron transition frequency incident irradiation frequency
$\delta\Omega$	optical bandwidth
$\Pi$	pairing energy term of linear molecule
$\pi$	$\pi$ MO, $\pi$ bonds
$\omega$	vibrational frequency
$\Psi$	total wavefunction
$\psi$	one-electron wavefunction
$\Psi, \psi, \Phi, \varphi, \chi$	wavefunctions
$\rho, \theta, \phi$	nuclear polar coordinates
$\rho$	electron charge density
$\Delta\rho$	deformation density
$\sum_i$	summation over $i$
$\sum_{i=m}^n$	summation over $i$ from $m$ to $n$
$\sum_{ij}$	summation over $i$ and $j$ except $i = j$
$\sigma$	$\sigma$ MO, $\sigma$ bond Pauli matrix
$\tau$	lifetime, relaxation time
$\Phi$	ligand MO wavefunction multielectron wavefunction
$\varphi$	one-electron atomic or MO wavefunction
$\chi$	nuclear wavefunction relativistic spinor magnetic susceptibility

## ABBREVIATIONS

acac	acetylacetone
AES	Auger electron spectroscopy
AO	atomic orbitals
AOM	angular overlap model
AP	adiabatic potential
APE	adiabatic potential energy
APES	adiabatic potential energy surface
BA	border atom
BLYP	Becke, Lee, Yang, Parr (functional)
bipy	bipyridyl
bpym	2,2'-bipyrimidine
BSSE	basis set superposition error
bzp	bromazepan
CA	central atom
CAS	complete active space
CFT	crystal field theory
CI	configuration interaction
CNDO	complete neglect of differential overlap
CoTPP	cobalt-tetraphenylporphyrin
Cp*	pentamethylcyclopentadienide
CT	charge transfer; Creutz-Taube
DD	deformation density

DFT	density-functional theory
DSC	double self-consistency
dto	ditiooxalato
DZ	double-zeta (basis set)
ECE	electron-conformational effect
ECP	effective core potential
EELS	electron energy loss spectroscopy
EFG	electric field gradient
EH	extended Huckel (method)
EIVS	energy of ionization of the valence state
emu	electromagnetic unit
En, en	ethylenediamine
ENDOR	electron nuclear double resonance
Et	ethyl
ESR	electron spin resonance
EXAFS	extended X-ray absorption fine structure
GAMESS	generalized atomic and molecular electronic structure system
GEA	gradient expansion approximation
GGA	generalized gradient approximation (in DFT)
GRS	gamma-resonance spectroscopy
GTO	Gaussian-type orbital
Hb	hemoglobin
HDEVV	Heisenberg–Dirac–Van Vleck (Hamiltonian)
HF	Hartree–Fock
hfac	hexafluoroacetylacetonate
HFR	Hartree–Fock–Roothaan
HK	Hohenberg–Kohn (theorem)
HOMO	highest occupied MO
HS	high-spin (configuration)
HSAB	hard and soft acids and bases
IEH	iterative extended Hückel (method)
IEPA	independent electron pair approximation
ImH	imidazol
INDO	intermediate neglect of differential overlap
IrRep	irreducible representation
IT	intervalence transition
JT	Jahn–Teller
JTE	Jahn–Teller effect
KS	Kohn–Sham (equations)
LDA	local density approximation
LIESST	light-induced electron spin state trapping
LS	low-spin (configuration)

LSD	local spin density approximation
LUMO	lowest unoccupied MO
M	metal atom (center)
MCD	magnetic circular dichroism
MCZDO	multicenter zero-differential overlap
MD	molecular dynamics
MeP	metal porphyrin
MePc	metal phtalocyanine
MET	many-electron theory
MINDO	modified INDO
MM	molecular mechanics
MRCI	multireference CI
MO	molecular orbital
MO LCAO	MO-linear combinations of AO
MV	mixed valence
NDDO	neglect of diatomic differential overlap
NGR	nuclear gamma-resonance
NITet	ethylnitronylnitroxide
NMR	nuclear magnetic resonance
NR	nonrelativistic
obbz	oxamidobis(benzoato)
ONIOM	own <i>N</i> -layered integrated molecular orbital and molecular mechanics (method)
OVC	orbital vibronic constant
Ox	oxalate
pba	1,3-propylene bis(oxamato)
Ph	phenyl
PJTE	pseudo-JTE
pyz	pyrazine
QM	quantum mechanics
QM/MM	quantum mechanics/molecular mechanics
QM/MM/CT	QM/MM/charge transfer
QR	quasirelativistic
QRA	quasirelativistic approach
RE	relativistic effect
RECP	relativistic effective core potential
RHF	restricted Hartree–Fock
RTE	Renner–Teller effect
SCCC	self-consistent charge and configuration
SCF	self-consistent field
SP	square pyramidal
STO	Slater-type orbital

TBP	trigonal bipyramidal
TDDFT	time-dependent DFT
TESCT	two electronic states in chemical transformations (paradigm)
TFD	Thomas–Fermi–Dirac
TMS	transition metal system
UHF	unrestricted Hartree–Fock
UKS	unrestricted KS
UPS	ultraviolet photoelectron spectroscopy
VOIP	valence orbital ionization potential
VMO	vibronic molecular orbital
VSEPR	valence shell electron pair repulsion
XANES	X-ray absorption near-edge structure
XES	X-ray emission spectroscopy
XPS	X-ray photoelectron spectroscopy
ZDO	zero-differential overlap



---

# 1

---

## INTRODUCTION: SUBJECT AND METHODS

*The electronic theory of transition metal systems pioneers a way of thinking in chemistry.*

This chapter is intended to introduce the reader to the objectives and main purpose of the book, to define the subject and the methods of its exploration, and to determine its “ecological niche” in the rapid development of science and increasing demands for generalized information.

After a brief discussion of the main objectives and the role and place of this book among others available (Section 1.1), the definitions of chemical bonding and coordination systems are given (Section 1.2), followed by a very brief outline of the main ideas of quantum chemistry, mostly definitions employed in the subsequent presentation (Section 1.3).

### 1.1. OBJECTIVES

#### **Molecular Engineering and Intuitive Guesswork**

The beginning of the twenty-first century (even the next millennium of human civilization) inclines us to sum up the achievements in the past century and to relate our intentions to what is expected in the coming new age. In the twentieth century the theory of structure and properties of transition metal coordination compounds, as well as polyatomic systems in general, advanced tremendously

and reached impressive results. Basic understanding of the nature of chemical bonding and chemical transformations was reached and the idea of purposeful synthesis of new compounds with specific properties was promoted significantly. As a result of the rapid development of this trend in science, especially in the second half of the century, the solution of the problem of *molecular engineering*, which includes design and consequent synthesis of newly designed compounds, is approaching rapidly. *In the twenty-first century the majority of new chemical compounds will be obtained on the basis of molecular design, and we should be prepared, both practically and psychologically, to meet this challenge.*

Molecular engineering is based mainly on the knowledge of molecular structure, including electronic structure. To design a compound with specific properties, the laws that control the formation and structure of molecular systems, as well the correlation between structure and properties, must be known in detail. Therefore, *the study of electronic structure and properties of polyatomic systems is one of the most important tasks of modern chemistry* in view of its trends and developments in the near future.

However, so far the majority of chemical compounds with the required properties were obtained mainly on the basis of intuitive knowledge, without specialized molecular engineering. Thus far the preparation of new compounds has depended mainly on the skill and intuition of the researcher. On the other hand, intuition, or intuitive knowledge, does not emerge from nothing; implicitly it is based on real knowledge or, more precisely, on *understanding* (see discussion below) of the phenomena lying in the base of the processes under consideration. Intuitive guesswork is also a kind of “engineering”. The in-depth understanding of chemical phenomena based on a correctly formulated way of thinking allows one to sidestep (circumvent, jump over) the lack of detailed information about the specific process under study, and to come to a correct result that from the outside appears to be “unexpected.” The better the understanding in visual images concepts, models, and comparisons, the more fruitful the intuitive thinking.

It is clear that the smaller is the region of lack of knowledge (i.e., the less the volume of the “black box” of ignorance), the easier it is to “jump over” it. If this black box is large, the findings of intuitive guess-work are of a unique, accidental nature; they become more frequent and more purposeful with reduction of the black box. The volume of the black box decreases rapidly with the increase in our knowledge (although it may never be exactly zero). Hence the preparation of new compounds based on intuitive thinking ultimately also depends on in-depth understanding of the phenomena, understanding based on the knowledge of the laws controlling the formation of new compounds and their properties.

*Preparation of new compounds with specific properties based on either molecular engineering or intuitive conjecture requires (in both cases) knowledge of structure and properties of such compounds.*

The term “*understanding*” used above is not trivial and needs some clarification. We use this term in the following sense: *to understand the origin of a new phenomenon means to be able to reduce it to more simple (“usual”), conventional images or concepts.* To deepen or extend the understanding means to introduce

more complicated basic images to which the phenomena should be reduced. In the 1950s the basic images in the understanding of the origin of properties of transition metal compounds were created by the *crystal field theory* (Chapter 4), which arose instead of and in addition to the image of a two-electron valence bond. Subsequently, a deeper understanding was reached by introducing more complicated images (concepts) of *molecular orbitals* that continue to serve as basic images (Chapters 5 and 6). In the more recent decades new basic concepts based on *vibronic coupling* (Chapter 7) have emerged, which essentially involves excited states information, distortion, and transformation of molecular configurations. Note that the new images of understanding, being more complicated, do not fully negate the old ones, but complement them with new content. New images (concepts) are produced by the theory. With the progress of science the images become more complicated, approaching the reality.

Lack of understanding means that it is impossible to reduce the phenomenon to well-established conventional images. This requires creation of new images. Sometimes the latter differ drastically from the usual ones. In the history of science the most dramatic new images have been introduced by quantum mechanics. *The wave-particle duality*—the fact that a microscopic object (e.g., the electron) exhibits properties of both particles (i.e., it can be localized at a single point of space) and plane waves (i.e., it is delocalized over the whole space)—cannot be understood within the existing images, it must be taken as such in a conventional manner until it becomes usual.

In view of what we noted above about understanding, to make the book intelligible means to reduce the properties of transition metal compounds to basic images (concepts). Hence we should describe the newest basic images that provide understanding most appropriate to the real phenomena. The main concepts in the theory of electronic structure of coordination compounds, mentioned above (crystal fields, molecular orbitals, vibronic coupling) should be presented such as to become usual elements of thinking in chemistry (in fact, molecular orbitals are now such elements). This, in turn, requires simplicity and visualization to the greatest extent possible. *Simplicity* in this aspect means less abstracted presentation with more specific examples avoiding as much as possible bulky mathematical deductions. As pointed out by Werner Heisenberg [1.1], “even for the physicist description in plain language will be a criterion of the degree of understanding that has been reached”.

However, aspiring to simplicity involves the danger of *oversimplification*. The latter takes place when the phenomenon under consideration is presented by a “smoothed” picture in which angles are cut off and important details are omitted. For instance, in many books and papers it is stated that as a result of the Jahn–Teller effect, distorted molecular configurations should be observed. This statement is an oversimplification because, in fact, Jahn–Teller distortions can be observed only under some important additional conditions (Sections 7.3 and 9.2). Besides misunderstanding, oversimplification may create also illusions of “easy access to science,” whereas in fact much stronger efforts are needed; this may have negative influence on education and scientific thinking.

### Main Objectives of This Book in Comparison with Other Sources

Many books and review articles are devoted to the electronic structure and properties of transition metal coordination compounds or, more often, to particular aspects of this problem (see, e.g., Refs. 1.2–1.16 and references cited therein). The present book differs significantly from those sources in many respects.

First, this book attempts to give *a generalized view on the modern state of art of the whole topic* beginning from the main ideas of quantum chemistry and atomic states through theories of electronic structure and vibronic coupling to physical methods of investigation and applications to various chemical and physical problems. The advantages of this presentation, as compared with many publications devoted to a more narrow aspect of the problem, is that the latter give a generalized view of what is going on in that narrow field, whereas this book generalizes the trend as a whole, including its main particular problems.

We emphasize that *the whole trend is not equal to the sum of particular trends* (more than 2000 years ago Aristotle claimed that “the whole is more than the sum of its parts”). A general view of the topic as a whole, given as an entire subject with direct interrelations between its different, more particular aspects, provides a significantly higher level of understanding of both the particular problems and the whole trend. Presented by the same author in a unified way and on the same level, different problems should be better understood by the reader. In some aspects it is pleasing to see the unity of nature at work linking apparently unrelated observations together (see, e.g., the discussion of the statement that “nature tends to avoid degeneracies” in Section 7.4).

*Many problems treated in this book are novel*; they have not been fully considered before in books on coordination compounds. This is, first, *the concept of vibronic interactions* considered in Chapter 7, and then used to solve various problems of coordination compounds (Chapters 9–11). The treatment of *electronic structure, relativistic effects in bonding, optical band shapes, electronic and vibronic origin of stereochemistry, electron transfer in mixed-valence compounds, chemical activation by coordination*, and others is also novel. Even for those problems that were solved long before and considered repeatedly in books and review publications, renewal of their presentation updated in accordance with the novel achievements of the theory is required periodically. The previous books on electronic structure of coordination compounds with goals similar to those of particular parts of this book have long been published [1.3–1.15]; two of the most recent books were published more than 10 years ago [1.14], not long after our first edition. Special attention in many publications was paid to methods of numerical computation [1.17–1.19, 1.21, 1.22]. The majority of the present book’s sections include novel, original treatments for these “classical” problems too (see, e.g., the definition of the coordination bond given in Sections 1.2 and 6.1). In comparison with other books of this level, this book further explains the origins of phenomena based on first principles, which leads to a more in-depth understanding; it prefers physical meaning over pure description.

As mentioned in the Preface, the novelty of this book is also in its special efforts to promote a novel agenda with a higher level of theory and understanding of the role of electronic structure in formation and transformation of matter. With regard to transition metal systems (TMSs), the first significant level of electronic theory was reached in the 1950s–1960s by the *crystal field theory*. It was essentially improved in the 1980s–1990s based on computer developments that allowed for full molecular orbital *electronic structure calculations*.

However, in the last two or three decades a new, higher level of understanding of electronic structure and properties of matter emerged that is not yet fully apprehended by the lay chemist and physicist, and it still has not been introduced in teaching of this subject. Distinguished from the electronic structure of well-defined molecular shapes, the novel understanding is related to all kinds of molecular transformation. The point is that quantum separation of ground and excited electronic states (as well as the definition of degenerate states) is valid only for given, fixed positions of the nuclei; these states become mixed by nuclear displacements, and this mixing is crucial in understanding nuclear configuration changes (Section 7.4). *Mixing electronic states, ground and excited, solely determines all possible nuclear configuration instabilities, distortions, and transformations*, including formation of molecular shapes and crystal lattices, conformational changes and phase transitions, chemical activation, and chemical reactions mechanisms, to mention only a few. For a given nuclear configuration no changes are possible within just one electronic state—this is the *two electronic states in transformations* (TEST) paradigm.

Comprehending this nuclear-dynamical aspect of electronic structure elevates the theory to a new, higher level facilitates a better understanding of chemical and physical phenomena. The intention of this book is also to instill this advanced way of thinking in physics and chemistry. It is given in many parts of this book, more noticeably and explicitly in Chapter 7, Section 7.4, with applications in subsequent chapters.

This book's symbiosis of theory and applications, namely, the presentation of the general theory of electronic structure (Chapters 2–5 and 7), together with applications to chemical bonding (Chapter 6), physical methods of investigation (Chapter 8), and various chemical problems (Chapters 9–11), accompanied by 70 *Examples* of solutions of relevant specific problems, as well Summary Notes, Questions, Exercises, and Problems to each chapter, is very rare in the literature. Meanwhile, this presentation allows the reader, interested in the solutions of applied problems, to consult directly the theoretical background of these solutions and to consider their applicability to other problems. The treatment of different chemical properties from the same perspective also has the advantage of stimulating the search for new effects, rules, and laws that emerge from these direct comparisons.

To summarize, *the main objectives of this book are to give a general and most modern view on the theory of electronic structure and properties of transition metal compounds with applications to various chemical and physical problems,*

*presented in a way intelligible to students, researchers, and teachers, and usable also as a textbook for graduate and advanced undergraduate students.*

Some comments are worthwhile about the meaning of the notion “Introduction to the Theory” given in the title of the book. It means that the latter is addressed also to those who have not studied any special theory of electronic structure of transition metal coordination compounds (but who have some background in quantum theory in the volume of a regular course for chemists). It also implies that the book is not devoted to the advances of the theory itself, its sophisticated formulations and methodologies. Instead, the latest achievements of the theory are presented together with explanations of how they have been obtained (but without bulky mathematical deductions) and how they can be used to solve physical and chemical problems. Further developments of the theory itself form a part of quantum chemistry well presented in literature [1.16–1.22].

An important question concerning the *theory* is the real meaning implied by this term. The theory of electronic structure forms one of the principal parts of modern quantum chemistry (others are molecular dynamics, intermolecular interactions, molecular transformations, interaction with external fields, etc.). Its particular trend—numerical computation of the electronic structure for fixed nuclei—is at present most advanced. Modern computers and supercomputers allow us, in principle, to compute the electronic structure of any coordination system of reasonable size and to get relatively accurate figures of its energies and wavefunctions, energy barriers of chemical reactions, spectroscopic properties, and so on (see Examples in Chapters 5, 6, and 11). Note that two decades ago metal-containing systems with active *d* and *f* orbitals were a challenge to quantum chemistry [1.17, 1.21]. With the development of computers and advanced computer algorithms and programs, these calculations tend to become routine (see Examples and Problems in Chapters 5, 6, and 11).

However, the numerical data of the computed electronic structure themselves cannot be regarded as a theory. Indeed, these data characterize a single compound (for which the computation has been carried out) and, in general, they cannot be directly transferred to other compounds. From this perspective computer data seem similar to many other characteristics of the compounds obtained by different *experimental* facilities. *In fact, numerical results on electronic structure computation are outputs of a computer experiment*; the computer is thus similar to a numerical spectrometer that yields the energy spectrum and wavefunctions of the system.

To transform experimental data into a theory, the data should be properly accumulated and generalized. The latter means correlating the data with some *analytical models* obtained by simplifications and reasonable assumptions introduced in the first principles. In this way the experimental data can be rationalized and shown to express some laws, rules, trends, and characteristic orders of magnitude. The same is true for computer numerical data. The latter are thus most appreciated when they are obtained for series of compounds with similar structures and/or similar properties that can be directly generalized. In particular, this is true for different nuclear configurations of the same system—adiabatic



potential energy surfaces (APES) and chemical reaction energy barriers [1.17, 1.21, 1.22] (see Chapters 6 and 11).

Note also that *ab initio* calculated wavefunctions of coordination compounds are given in thousands of determinants that in general can be neither read nor understood without specific rationalizations by means of physically grounded simplified schemes (but they can be further processed by means of computer programs). Nevertheless, *the results of numerical calculation are of inestimable value to the theory of electronic structure; together with other experimental data, they form the informational basis of the theory and allow one to discriminate the best theoretical models among the many possible.*

Finally, as mentioned above, the book is intended to be used also as a *text-book for graduate and advanced undergraduate students*. For this purpose we introduced many Examples (offset from general text in box format) of specific applications of the theory, as well as end-of-chapter summary notes, questions, exercises, and problems with solutions deemed to make this book more accessible to chemists and physicists, including graduate and advanced undergraduate students, and usable for teaching special courses. Such courses may not necessarily include the entire book material—they can be devoted to only parts of it—but because of the interrelation between these parts and cross references, the student will be enriched with knowledge from other parts. The book is deemed to provide a solid background in and updated understanding of the laws controlling molecular properties, which is most important in pursuing further research and teaching activity on any narrower subject of this vast field.

## 1.2. DEFINITIONS OF CHEMICAL BONDING AND TRANSITION METAL COORDINATION SYSTEM

### Chemical Bonding as an Electronic Phenomenon

*Chemical bonding* is usually defined as an interaction between two or several atoms that causes the formation of a chemically stable polyatomic system (molecule, radical, molecular ion, complex, crystal, chemisorbed formation on surfaces, etc.). However, this formulation is not sufficiently rigorous, since without additional explanation it is not clear when the system should be considered as chemically stable. In fact, in this definition, admitting that chemical bonding is a kind of interaction, we introduce for the characterization of the latter a new term “chemically stable system,” which is no clearer than the initial one, the chemical bond.

One may try to discriminate chemical bonding from other (say, intermolecular) interactions by the bonding energy. However, the latter, as is well known from experimental data, is not sufficiently informative for this purpose; for chemical bonds the bonding energy varies from several to several hundred kilocalories per mole (kcal/mol), as it is thus both smaller and larger than intermolecular interaction (which reaches about 20 kcal/mol) and the hydrogen bond (1–8 kcal/mol) (compare with the energies of the bond  $\text{UBr}_5\text{—Br}$  equal to 13 kcal/mol, or the

reaction  $\text{ClO}_2 \rightarrow \text{Cl} + \text{O}_2$  equal to 4 kcal/mol [1.24]). It can also be shown that bond lengths are not always sufficiently informative with respect to the nature of the bonding.

A more rigorous discrimination of the chemical bonding can be based on the differences in electronic structure. *The main feature of chemical interaction is that it results in a significant reorganization (restructuring) of the electronic shells of the bonding atoms.* This reorganization is characterized by “collectivization” of the valence electrons and *charge transfer* (in case of different atoms). Electron collectivization is a more general characteristic of the bond since it can take place without charge transfer, whereas charge transfer cannot be realized without collectivization; the limit case of pure (100%) ionic bonds does not exist.

We define the *chemical bond* as an interaction between atoms associated with a collectivization of the valence electronic orbitals [1.25]. This definition is sufficiently rigorous and allows one to distinguish chemical bonding from, say, intermolecular interaction or physical adsorption on surfaces (according to this definition, the hydrogen bond, which is associated with electron collectivization and charge transfer, is a type of chemical bonding).

*Any rigorous definition of a physical quantity should contain, explicitly or implicitly, an indication of the means of its observation.* In the definition of the chemical bonding given above, the means of its observation are implied; the collectivization of the electrons affects all the main physical and chemical properties of the system, and therefore the set of all these properties forms an experimental criterion of chemical bonding. In this set, such an important characteristic of the bond as its energy, which is an integral feature of the bond, may be less sensitive to the electronic structure than, for instance, the electronic spectra. In the example described above, the bond  $\text{UBr}_5\text{—Br}$  with a bonding energy of  $\sim 13$  kcal/mol (which is less than the intermolecular limit of 20 kcal/mol) could be attributed to intermolecular bonding, but the electronic spectra testify to chemical bonding. Besides bonding energy and electronic spectra, chemical bonding affects essentially all other spectra in whole-range spectroscopy, magnetic and electric properties, electron and X-ray diffraction, and so on.

The electronic nature of chemical bonding leads directly to the conclusion of its quantum origin. The motions of the electrons in atomic systems can be correctly described only by means of quantum mechanics. The nature of the bonding between two neutral atoms in the hydrogen molecule was first revealed by Heitler and London in 1927 by means of a quantum-mechanical description [1.26]. It was shown that the bonding results from the so-called exchange part of the energy, which is negative and results from the *undistinguishability* of the electrons and the *Pauli principle*; the exchange energy is a quantum effect and has no classical (nonquantum) analog. The Heitler–London approximation lies at the base of the quantum electronic theory of chemical bonding and quantum chemistry.

However, it is incorrect to state that the chemical bonding is due to exchange forces that keep the neutral atoms together. The analysis of the Heitler–London approximation for the  $\text{H}_2$  molecule clearly shows that the only forces that lead to the formation of the chemical bond are the electrostatic interaction forces



between the four particles: two protons and two electrons. In fact, the bonding is caused by the quantum wave properties of the electrons. The interference of the wavefunctions of the two electrons from the two bonding hydrogen atoms, under certain conditions, results in extra electronic charge concentration in the region between the two nuclei (constructive interference), thus keeping them bonded. In many cases a significant part of the bonding energy is due to the reduction of the kinetic energy of the collectivized electrons. The separation of the exchange part of the energy results from the assumed one-electron approximation in the wavefunction when there are two or more electrons. For instance, in the case of  $\text{H}_2^+$  with a single electron, there is still chemical bonding (resulting from the same interference of the two wavefunctions occupied by one electron) in spite of the absence of exchange interaction.

*The quantum nature of the chemical bond is stipulated by the quantum-mechanical description of the motions of the electrons and nuclei.*

The quantum origin of chemical bonding contributes directly to the understanding of the main property of a chemical compound—its existence and stability. Therefore *in the study of the composition–structure–property correlation the electronic structure plays a key role*. Note that in general the term *electronic structure* implies that in addition to the ground-state energy and electron distribution (the wavefunction), the *excited states* are also known. The latter allow one to describe vibronic coupling and spectroscopic properties, as well as the behavior of the system under the influence of external perturbations, including intermolecular interactions and chemical reactions (Sections 10.1 and 11.1).

However, the electronic structure does not describe all the properties of the compound. In particular, the temperature dependence of the properties may be determined rather by *the dynamics in the nuclear subsystem*. An important feature of the system is also *the coupling of the electronic distribution to the nuclear configuration and nuclear dynamics (vibronic coupling)*.

*The electronic structure, vibronic coupling, and nuclear dynamics describe in principle all the properties of isolated molecules*. To describe chemical compounds in their different aggregate states—ensembles of interacting molecules—*quantum-statistical, thermodynamic, and kinetics studies should be employed*.

### **Definition of Coordination System**

The definition of a coordination system (coordination bond, coordination compound) is not trivial and encounters difficulties. Many previous attempts to give a compact definition based on empirical data were unsuccessful (see, e.g., the text by Cotton and Wilkinson [1.15] and Section 6.1). In view of the discussion given below in this section, these attempts failed because they tried to define the coordination compound according to the genealogy (prehistory) of its formation, whereas in fact the properties of any molecular system are determined by its structural features, primarily by its electronic structure, regardless of the method of its preparation [1.25] (properties of chemical compounds are functions of state, not functions of pass).

The usual definition of a coordination system that can be traced back to the *coordination theory* created by Alfred Werner more than a century ago [1.27] is that a complex or a coordination compound is formed by a *central atom* (CA) or ion M that can bond one or several ligands (atoms, atomic groups, ions)  $L_1, L_2, \dots$ , resulting in the system  $ML_1L_2, \dots, L_n$  (all the ligands  $L_i$  or some of them may be identical). This definition is so general that any molecular system can be considered as a coordination compound. For instance, methane can be presented as  $C^{4+}$  (M) +  $4H^-$  (4L), that is, as a coordination compound  $ML_4$  [1.15]. To avoid this misunderstanding, it was required that the ions M and ligands  $L_i$  be “real,” existing under the usual chemical conditions, and that the reaction of complex formation take place under the usual conditions.

Even with these limitations, the definition above is invalid, and there are many cases when it is misleading. For example,  $SiF_6^{2-}$  has many features of coordination compounds (Section 6.1), whereas, when presented as required by the definition as  $Si^{4+} + 6F^-$ , we encounter conflict with the fact that  $Si^{4+}$  does not exist under the usual conditions. This example can be treated as a more real composition:  $SiF_4 + 2F^-$ ; then, to include it in the definition, we must assume that M can be also a molecule, but this assumption gives rise to new controversies and misunderstandings. This and many other examples show explicitly that *it is impossible to give a general definition of coordination systems based on the genealogy of their formation*.

On the other hand, the properties of molecular compounds as functions of state are determined by their electronic structure. This statement leads directly to the idea of classification of chemical bonds and definition of coordination systems *on the basis of electronic structure* [1.25]. At present, when the electronic structure of coordination compounds is relatively well studied, the tendency to classify the chemical compounds on their methods of preparation seems somewhat old-fashioned. However, it was not old-fashioned at the time when coordination chemistry was rapidly developing, while the knowledge about electronic structure was rather poor and could not serve as a basis for classification. Note also that the way of thinking in chemistry was (and in a great measure is) more appropriate to *preparative chemistry*, but it is gradually changing to *structural chemistry*.

It is quite understandable that the definition of coordination systems based on electronic structure is more convenient to discuss after the study of electronic structure. Therefore the classification of chemical bonds and chemical compounds is given in more detail in Section 6.1. According to Section 6.1, chemical bonds can be classified after their electronic structure into three main classes (Table 6.1). The first is that of *localized valence bonds* formed by two electrons with opposite spins, by one from each of the bonding atoms, and these two electrons occupy one localized bonding orbital. These valence bonds follow the usual rules of valence of organic compounds, which can be described by one valence scheme without the assumption of resonance structures (superposition of valence schemes). Localized double, triple,  $\dots$ , bonds are also included in this class. The compounds with localized valence bonds can be called *valence compounds*.

The second class contains *linearly delocalized bonds with possible ramification* in which the valence electrons occupy one-electron molecular orbitals that are delocalized over all or a part of (but more than one) interatomic bonds (e.g., conjugated organic molecules, metallic chain structures or solids). These bonds can be called *conjugated*, or *orbital, bonds*. In fact, this class of bonds includes all organic and main-group-element compounds that cannot be described by one valence scheme.

The third class contains *the bonds that are three-dimensionally delocalized around a center: coordination bonds*. Distinct from the conjugated bonds, which are delocalized along the bonding line, the coordination bond is *three-dimensionally center-delocalized*. In other words, the coordination bond is formed by a coordination center to which the ligands are bonded via electrons that occupy one-electron orbitals, each of which involves all or several ligands. This means that, in general, there are no localized CA–ligand bonds; they are collectivized by the three-dimensionally (i.e., along several bonds CA–ligand) delocalized bonding electrons. It can be shown that the delocalization of the one-electron orbitals is realized via the *d* or *f* orbitals of the central atom, which have many lobes differently oriented in space (Section 2.1), while *s* and *p* electrons can provide only localized or linearly delocalized orbitals.

This definition allows one to discriminate the coordination bonds from valence and conjugated bonds. For instance, the two tetrahedral systems,  $\text{CH}_4$  and  $\text{CuCl}_4^{2-}$ , differ essentially in electronic structure:  $\text{CH}_4$  has four localized two-electron bonds C–H (hybridized  $sp^3$  valence bonds), whereas in  $\text{CuCl}_4^{2-}$  the bonding electrons are delocalized over all the ligands via the copper *d* electrons (coordination bond). Note that by this definition the bonds in  $\text{NH}_4^+$  and  $\text{BH}_4^-$  are valence bonds analogous to  $\text{CH}_4$  [1.28]; similarly,  $\text{BF}_3\text{—NH}_3$  is a valence compound since its electronic structure is analogous to  $\text{CF}_3\text{—CH}_3$ .

In the  $\text{SiF}_6^{2-}$  example considered above,  $\text{SiF}_4$  is a valence compound because of its localized Si–F bonds (analogies of C–F), while the bond in  $\text{SiF}_6^{2-}$  can be considered as a coordination bond because the octahedral coordination involves partially the low-lying *d* orbitals of Si, making the one-electron bonding states delocalized (Section 6.1).

With this classification of chemical bonds, the following definition of the coordination compound or, more general, coordination system can be given: *a coordination system  $ML_1L_2\cdots L_n$  consists of a coordinating atom (coordination center)  $M$  ligated to  $n$  atoms or groups of atoms (ligands)  $L_1, L_2, \dots, L_n$  by coordination bonds that are delocalized over all or several ligands*. Following this definition two main structural features characterize the coordination system: the coordination center and the three-dimensionally center-delocalized (coordination) bond. These features determine the main properties of coordination bonding discussed in this book; for a brief summary see Table 6.2.

Transition metal compounds are mostly coordination systems: even in the solid state of ionic crystals (as well as in the pure metallic state) the local features of the system are controlled by the coordination centers with properties that, in

essence, are quite similar to those of isolated coordination systems. The main reason for this similarity between molecular and local crystal properties lies in the specific role of the  $d$  electrons in both cases. Since these electrons may be active also as low-lying excited states, this book, which is devoted to transition metal systems (TMSs), mostly coordination systems, also includes partly pre- and posttransition and rare-earth systems. As emphasized in Section 6.1, in principle any atom may serve as a coordination center; active  $d$  states lacking in the free atom may occur as a result of a corresponding chemical interaction that results in  $d$ -state activation and coordination bonding.

### 1.3. THE SCHRÖDINGER EQUATION

This section presents some basic notions of quantum chemistry, the Schrödinger equation and the main approximations used in its solution for molecular systems, which we give here mainly to introduce appropriate denotations used below. There are quite a number of textbooks on this topic: the reader is referred to several texts [1.29–1.33], to mention only some of them.

#### Formulation

Following the formal scheme of quantum mechanics [1.29], each physical quantity  $L$  (energy, momentum, coordinate, etc.) is correlated with an *operator*  $\mathbf{L}$  (a symbol that denotes a certain mathematical operation), such that the experimentally observed values of this quantity  $L = L_n$ ,  $n = 1, 2, \dots$ , are the eigenvalues of the following *operator equation*

$$\mathbf{L}\Psi_n = L_n\Psi_n, \quad n = 1, 2, \dots \quad (1.1)$$

The eigenfunction  $\Psi_n$  (the wavefunction) contains information about all properties of the system in the state with  $L = L_n$ .

For the main physical quantities the form of the operator  $\mathbf{L}$  is well known. In quantum chemistry, the most important quantity is the energy of the system  $E$ . The operator of energy is the Hamilton operator  $\mathbf{H}$ , called the *Hamiltonian*. Therefore the operator equation for the energy is

$$\mathbf{H}\Psi_n = E_n\Psi_n \quad (1.2)$$

This is the *Schrödinger equation for stationary states* (for which the energy has a definite value). For nonstationary states that are time-dependent, the Schrödinger equation is ( $\hbar$  is the Planck constant and  $i$  is the imaginary unit,  $i^2 = -1$ ):

$$i\hbar\frac{\partial\Psi}{\partial t} = \mathbf{H}\Psi \quad (1.3)$$

Equation (1.2) is a particular case of Eq. (1.3).

The Hamiltonian  $H$  (hereafter we denote operators in italic type) includes the operators of the kinetic energies of the electrons and nuclei  $T$  and the potential energy of all the interactions between them  $U$ ,  $H = T + U$ . In the *nonrelativistic approximation* these interactions are purely electrostatic. Taking account of relativistic effects, the dependence of the masses on velocity, as well as magnetic spin-orbital and spin-spin interactions, should be included. This can be done on the basis of the *Dirac equation* discussed in Sections 2.1 and 5.4 (see also Sections 5.5 and 6.5).

The total kinetic energy is the sum of the kinetic energy operators of each particle  $T = p^2/2\mu$ , where  $\vec{p} = -i\hbar\vec{\nabla}$  is the operator of the momentum ( $\vec{\nabla}$  is a gradient vector with components  $\partial/\partial x$ ,  $\partial/\partial y$ , and  $\partial/\partial z$ ; do not confuse the imaginary unit  $i$ ,  $i^2 = -1$ , with the summation index, which is often also expressed as  $i$ ) and  $\mu$  is its mass:

$$T = \sum_i \frac{-\hbar^2 \Delta_i}{2\mu_i} \quad (1.4)$$

This equation accounts for the fact that  $p^2 = (-i\hbar\nabla)^2 = -\hbar^2\Delta$ , where  $\Delta$  is a usual differential operator ( $\nabla^2 = \Delta$ ),  $\Delta_i\Psi = \partial^2\Psi/\partial x_i^2 + \partial^2\Psi/\partial y_i^2 + \partial^2\Psi/\partial z_i^2$ .

The operator  $U$  contains the sum of the Coulomb attractions and repulsions. The attraction of the  $i$ th electron to the  $\alpha$  nucleus is  $U_{i\alpha} = -Z_\alpha e^2/r_{i\alpha}$ , where  $e$  is the numerical value of the charge of the electron,  $Z_\alpha$  is the order number of the element in the periodic table equal to the positive charge of the nucleus,  $r_{i\alpha} = |\mathbf{r}_i - \mathbf{R}_\alpha|$  is the electron-nucleus distance, and  $\mathbf{r}_i$  and  $\mathbf{R}_\alpha$  are the radius vectors of the electron and nucleus, respectively. The Coulomb repulsion between the electrons is  $U_{ij} = e^2/r_{ij}$ , and between the nuclei it is  $U_{\alpha\beta} = Z_\alpha Z_\beta e^2/R_{\alpha\beta}$ , where  $r_{ij} = |\mathbf{r}_i - \mathbf{r}_j|$  and  $R_{\alpha\beta} = |\mathbf{R}_\alpha - \mathbf{R}_\beta|$  are the interelectron and internuclei distances, respectively.

Thus the Schrödinger equation for a molecular system of  $n$  electrons with mass  $m$  and  $N$  nuclei with masses  $M_\alpha$  can be expressed as

$$[T + U]\Psi_k = E_k\Psi_k$$

or in a more explicit form as

$$\left[ \sum_i^n \frac{-\hbar^2 \Delta_i}{2m} + \sum_\alpha^N \frac{-\hbar^2 \Delta_\alpha}{2M_\alpha} - \sum_i^n \sum_\alpha^N \frac{Z_\alpha e^2}{r_{i\alpha}} + \sum_{i<j} \frac{e^2}{r_{ij}} + \sum_{\alpha<\beta} \frac{Z_\alpha Z_\beta e^2}{R_{\alpha\beta}} - E_k \right] \Psi_k(\mathbf{r}_1, \mathbf{r}_2, \dots, \mathbf{r}_n; \mathbf{R}_1, \mathbf{R}_2, \dots, \mathbf{R}_N) = 0 \quad (1.5)$$

This equation is in fact a linear differential equation of the second order (of elliptical type) with respect to  $3(n + N)$  variables  $\mathbf{r}_i$  and  $\mathbf{R}_\alpha$ . It yields a nontrivial

solution for only discrete values  $E_k$ , which are thus the only possible stationary energy values of the system, as well as their corresponding wavefunctions  $\Psi_k$ . The latter, as mentioned above, contains the information of all the (nonrelativistic) properties of the system in the state with the energy  $E_k$ . In particular,  $\Psi_k$  also contains complete information about the electronic and nuclear charge distribution:  $|\Psi(\mathbf{r}_1, \mathbf{r}_2, \dots, \mathbf{R}_1, \mathbf{R}_2, \dots)|^2$  equals the probability of finding the first electron at  $\mathbf{r}_1$ , the second at  $\mathbf{r}_2$ , and so on (Section 5.2).

*The exact solution of the Schrödinger equation allows one, in principle, to determine a priori all the properties of any polyatomic system and its behavior in different conditions.* Note that in all cases when exact solutions of Eq. (1.5) have been obtained, they were in good agreement with the experimental data, and in many cases the results of calculation have an accuracy rivaling experiment.

### Role of Approximations

In the early stages of development of quantum mechanics, the Schrödinger equation raised some hopes that it could describe the entire chemistry, rendering many experimental approaches unnecessary. In a 1929 publication [1.34] one of the founders of quantum mechanics, P. A. M. Dirac, stated that “the underlying physical laws necessary for the mathematical theory of a large part of physics and the whole chemistry are thus completely known, and the difficulty is only that the exact application of these laws leads to equations much too complicated to be soluble.” After 80 years this statement remains valid; there are still principal difficulties in obtaining exact solutions of Eq. (1.5) for molecular systems with many particles, although the achievements in this field are impressive. With the growth of computers, exact solutions of Eq. (1.5) or even more complicated equations that include relativistic effects become possible for a limited number of electrons and nuclei. This number is increasing, but for relatively large numbers of particles the results of numerical computations become difficult to perceive and almost impossible to interpret directly.

For instance, as mentioned above, the wavefunction of a system with tens of particles emerges from the numerical calculations spread on thousands of determinants. With the increase in the number of particles the numerical information yielded by the computer becomes so vast that it is useless. To rationalize these data and to be able to solve Eq. (1.5) for larger molecular systems, *simplifications* by introducing *approximations and/or analytical models* are absolutely necessary (see also the discussion at the end of Section 5.6).

Thus *the exact numerical solution of the Schrödinger (Dirac) equation for large molecular systems is at present, in general, an irrational task.* The problem of electronic structure can be solved by introducing approximate methods of solution of Eq. (1.5) that allow one to obtain energies  $E_k$  and wavefunctions  $\Psi_k$  in a convenient form and to evaluate the physical and chemical quantities with the required accuracy. The choice of the approximation that is optimal for the solution of a specific problem for a given molecular system and analysis of the results in view of the approximations made is one of the most important (and sometimes most difficult) problems of quantum chemistry.

Most approximations used in modern quantum chemistry are aimed at the separation of variables in Eq. (1.5). These approximations can be divided into three main groups:

1. Separation of the nuclear dynamics from the electronic motions—the adiabatic approximation (Section 7.1).
2. Substitution of the local interactions between the electrons given by the Coulomb terms  $e^2/r_{ij}$  by some averaged interaction that is an additive function of  $r_i$  and  $r_j$  (neglect of correlation effects)—the one-electron approximation, followed by an account for correlation effects by different methods (Section 5.3).
3. Presentation of the one-electron function of many centers—molecular orbitals (MOs), by a sum of one-center functions; atomic orbitals (AOs), the approximation of molecular orbitals as linear combinations of atomic orbitals (MO LCAO) (Section 5.1); and related approximations in the density-functional approaches (Section 5.4).

These approximations are discussed in Chapters 2, 4, 5, and 7.

## SUMMARY NOTES

1. *Molecular engineering* of new compounds—the forefront of modern chemistry—is based on knowledge and understanding of the laws that control the structure and properties of molecular systems. Intuitive guesswork is an art of the researcher based on the same premises.
2. *Understanding* a new phenomenon means being able to reduce it to already known (conventional) images and conceptions. New images and conceptions are produced by the theory that is a generalization of experimental data.
3. *The chemical bond* is defined as an interaction between atoms that collectivizes the motion of some or all of their valence electrons. The bonding is produced by electrostatic forces between the electrons and nuclei as their motion is described by means of quantum mechanics.
4. Different kinds of *chemical bonds should be classified by their electronic structure*, not by the way they are obtained—properties of chemical compounds are functions of state, not functions of pass.
5. Coordination compounds are defined as having a central atom—a coordination center forming *three-dimensionally delocalized bonds* with two or more ligands. Such bonds are produced by significant participation of *d* or *f* electrons, which are present in transition metal atoms, but can be activated in some other atoms under the ligand influence or by excitation.
6. The basis of electronic structure studies is quantum chemistry, the main equation of which is the *Schrödinger equation*. To solve this equation



for practically important molecular systems, three *main simplifications* are employed: (a) separation of electronic and nuclear motions (adiabatic approximation), (b) separation of the variables of the electrons (one-electron approximation), and (c) presentation of the molecular orbitals as a linear combination of atomic orbitals (MO LCAO approximation).

7. One of the main goals of this book is to promote a general view (understanding) of the whole subject by presenting the theory of electronic structure interlinked with physical methods of investigation and applications to a variety of chemical problems. The whole subject is more than a sum of its particular topics considered elsewhere.
8. Another goal is to make the book accessible to lay chemists and physicists, including graduate and advanced undergraduate students, and usable also as a textbook for corresponding courses. For this purpose the discussion of the topics are presented together with many examples and illustrations of applications of the theory to specific transition metal systems, as well as summary notes, questions, exercises, and problems.

## REFERENCES

- 1.1. W. Heisenberg, *Physics and Philosophy*, Harper, New York, 1958, p. 168.
- 1.2. L. Pauling, *The Nature of Chemical Bond*, Cornell Univ. Press, Ithaca, NY, 1960.
- 1.3. L. E. Orgel, *Introduction to Transition-Metal Chemistry*, Methuen, London, 1960 (2nd ed., 1966).
- 1.4. J. S. Griffith, *The Theory of Transition-Metal Ions*, Cambridge Univ. Press, 1961.
- 1.5. C. J. Ballhausen, *Introduction to Ligand Field Theory*, McGraw-Hill, New York, 1962.
- 1.6. I. B. Bersuker and A. V. Ablov, *The Chemical Bond in Complex Compounds* (Russ), Știința, Kishinev, 1962; I. B. Bersuker, *Structure and Properties of Coordination Compounds* (Russ.), Khimia, Leningrad, 1971 (2nd ed., 1976; 3rd ed., 1986).
- 1.7. C. J. Ballhausen and H. B. Gray, *Molecular Orbital Theory*, Benjamin, New York, 1964.
- 1.8. H. L. Schlafer and G. Gliemann, *Basic Principles of Ligand Field Theory*, Wiley, New York, 1969.
- 1.9. C. K. Jorgensen, *Modern Aspects of Ligand Field Theory*, North-Holland, Amsterdam, 1971.
- 1.10. C. J. Ballhausen, *Molecular Electronic Structure of Transition Metal Complexes*, McGraw-Hill, New York, 1979.
- 1.11. J. K. Burdett, *Molecular Shapes. Theoretical Models of Inorganic Stereochemistry*, Wiley, New York, 1980.
- 1.12. T. A. Albright, J. K. Burdett, and M.-H. Whangbo, *Orbital Interaction in Chemistry*, Wiley, New York, 1985.
- 1.13. R. Hoffmann, *Solids and Surfaces: A Chemist's View of Bonding in Extended Structures*, VCH, New York, 1988.



- 1.14. E. I. Solomon and A. B. P. Lever, eds., *Inorganic Electronic Structure and Spectroscopy*, Vols. I, II, Wiley, New York, 1999.
- 1.15. F. A. Cotton and G. Wilkinson, *Advanced Inorganic Chemistry: A Comprehensive Text*, Wiley, New York, 1992 (6th ed., 1999).
- 1.16. I. B. Bersuker, *The Jahn-Teller Effect*, Cambridge Univ. Press, Cambridge, UK, 2006.
- 1.17. A. Veillard, ed., *Quantum Chemistry: The Challenge of Transition Metal and Coordination Chemistry*, NATO ASI Series C, Vol. 176, Reidel, Dordrecht, 1986.
- 1.18. M. Dupuis, ed., *Supercomputer Simulation in Chemistry*, Lecture Notes in Chemistry, Vol. 44, Ed. Springer-Verlag, Heidelberg, 1986.
- 1.19. P. Coppens and M. B. Hall, eds., *Electron Distribution and the Chemical bond*, Plenum, New York, 1982.
- 1.20. I. B. Bersuker and V. Z. Polinger, *Vibronic Interactions in Molecules and Crystals*, Springer-Verlag, New York, 1989.
- 1.21. D. R. Salahub and M. C. Zerner, eds., *The Challenge of d and f electrons, Theory and Computation*, ACS Symposium Series N 394, Washington, DC, 1989.
- 1.22. K. Lipkowitz and D. Boyd, eds., *Reviews in Computational Chemistry*, VCH, New York, Vols. 1–26, 1990–2008.
- 1.23. D. Braga, P. J. Dyson, F. Grepioni, and B. F. G. Johnson, *Chem. Rev.* **94**, 1585 (1994).
- 1.24. L. V. Gurvitz, G. V. Karachevtsev, and V. N. Kontdrat'ev, *Energies of Chemical Bond Cleavage. Ionization Potentials and Electron Affinities. Reference Book* (Russ.), Nauka, Moscow, 1974.
- 1.25. I. B. Bersuker, in *Brief Chemical Encyclopedia* (Russ.), Vol. 5, Soviet Encyclopedia, Moscow, 1967, pp. 627–636.
- 1.26. W. Heitler and F. London, *Phys. Z.* **44**, 455 (1927).
- 1.27. G. B. Kauffman, ed., *Coordination Chemistry. A Century of Progress (1893–1993)*, ACS Symposium Series 565, ACS, Washington, DC, 1994.
- 1.28. R. F. W. Bader and M. E. Stephen, *J. Am. Chem. Soc.* **97**, 7391 (1975).
- 1.29. W. Kauzmann, *Quantum Chemistry. An Introduction*, Academic Press, New York, 1957.
- 1.30. R. McWeeny, *Methods of Molecular Quantum Mechanics*, 2nd ed., Academic Press, New York, 1989.
- 1.31. I. N. Levine, *Quantum Chemistry*, 3rd ed., Allyn & Bacon, Boston, 1983.
- 1.32. R. J. Silbey, R. A. Alberty, and M. G. Bawendi, *Physical Chemistry*, 4th ed., Wiley, Hoboken, NJ, 2005.
- 1.33. P. von R. Schleyer et al., eds., *Encyclopedia of Computational Chemistry*, Vols. 1–5, Wiley, 1998.
- 1.34. P. A. M. Dirac, *Proc. Roy. Soc.* **A123**, 714 (1929).

---

# 2

---

## ATOMIC STATES

*Atomic states are the primary characteristics of the interacting atoms forming the transition metal system (TMS). They determine practically all the properties of TMS described in this book.*

This chapter presents a brief general introduction to the subject and the main formulas used in the following chapters (for more details on atomic states, see Refs. 2.1–2.5).

### 2.1. ONE-ELECTRON STATES

#### Angular and Radial Functions

The one-electron approximation for a multielectron system is based on the assumption that each electron moves independently in an averaged field created by all the other electrons and nuclei. This assumption allows one to perform a complete separation of the variables, that is, to describe the motion of the electron by its own coordinates, independent of the coordinates of other electrons. The one-electron approximation, although widely used, is, strictly speaking, not valid in many-electron systems because it neglects *electron correlation effects* (Section 5.3), but it is the most convenient starting approximation.

For an atom it is also assumed that the averaged field in which the electron moves has spherical symmetry. Under this assumption the one-electron

---

*Electronic Structure and Properties of Transition Metal Compounds: Introduction to the Theory,*  
Second Edition By Isaac B. Bersuker  
Copyright © 2010 John Wiley & Sons, Inc.

wavefunction, solutions of the Schrödinger equation [Eq. (1.5)], can be presented as a product of the radial  $R(r)$  and angular  $Y(\theta, \phi)$  parts, where  $r, \theta, \phi$  are the polar coordinates with the origin at the nucleus. In the approximation of hydrogenlike functions the one-electron states—*atomic orbitals* (AOs)—are described by the same quantum numbers  $n, l, m$ , as in the hydrogen atom:  $n = 1, 2, \dots$ ;  $l = 0, 1, 2, \dots, (n - 1)$ ;  $m = 0, \pm 1, \pm 2, \dots, \pm l$ . Then

$$\psi_{lmn} = R_{nl}(r)Y_{lm}(\theta, \phi) \quad (2.1)$$

where  $Y_{lm}(\theta, \phi)$  is a spherical function,

$$Y_{l,m}(\theta, \phi) = \left[ \frac{(2l+1)(l-m)!}{4\pi(l+m)!} \right]^{1/2} P_l^m(\cos \theta) e^{im\phi} \quad (2.2)$$

and  $P_l^m(x)$  is an associated Legendre polynomial:

$$P_l^m(x) = (1-x^2)^{m/2} (d^{l+m}/dx^{l+m}) \frac{(x^2-1)^l}{2^l l!} \quad (2.3)$$

For  $l = 0, m = 0$  ( $s$  states), the function (2.2) does not depend on the angles  $\theta$  and  $\phi$ , and the function (2.1) depends only on the distance between the electron and the nucleus  $r$ ; its diagram in space has the form of a continuous sphere (Fig. 2.1).

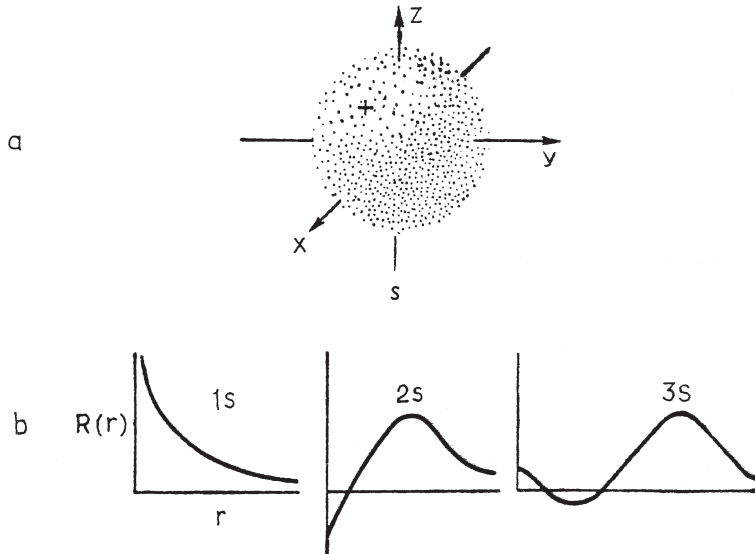


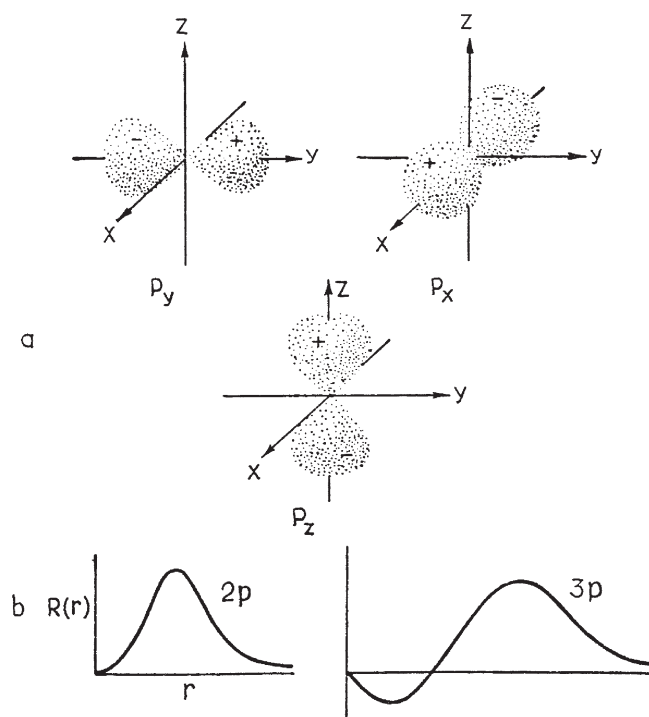
**FIGURE 2.1.** Schematic representation of angular (a) and radial (b) distributions of atomic  $s$  functions.

For  $l = 1$  ( $p$  states),  $m = 0, \pm 1$ , that is, there are three functions (2.2), two of which (with  $m = 1$  and  $m = -1$ ) are complex-conjugated. Since for a free atom the one-electron energies  $\varepsilon_{nl}$  are independent of  $m$  and all the three states have the same energy (threefold degeneracy), any linear combination of these three functions is also a wavefunction with the same energy (in any combination only three such functions are independent). Therefore it is often convenient to express them in the real form (Table 2.1 and Fig. 2.2).

Similarly, real combinations of functions (2.1) can be chosen for the five  $d$  states ( $l = 2, m = 0, \pm 1, \pm 2$ ) shown in Table 2.1 (Fig. 2.3). Note that diagramming  $p, d, \dots$  functions becomes possible after the choice of convenient linear combinations of functions (2.2), which are real and allow for visual presentation. Hence the picture of these  $p, d, f, \dots$ , one-electron states in absence of external perturbations is rather conventional; any of the combinations of degenerate  $p(d, f)$  states is also a  $p(d, f)$  state. *Only under external perturbations do the lobes acquire a specific orientation and a real physical meaning that determines the charge distribution.*

Other real combinations of  $d$  functions may be preferred dependent on the symmetry of the external perturbation acting upon the atom (Chapter 4).

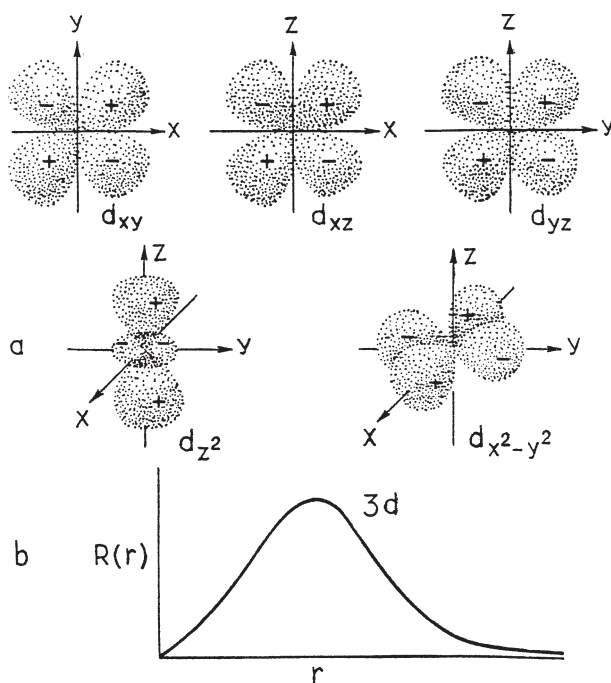
Similarly, for seven  $f$  functions ( $l = 3, m = 0, \pm 1, \pm 2, \pm 3$ ) two sets of real angular parts are commonly used (Table 2.2 and Fig. 2.4). The first set,



**FIGURE 2.2.** Angular (a) and radial (b) distributions of atomic  $p$  functions.

**TABLE 2.1. Orthonormalized Real Angular Parts of One-Electron  $s$ ,  $p$ , and  $d$  Functions  $Y_{lm}(\theta, \phi)$** 

Denotation	$Y_{lm}$ in Polar Coordinates	$Y_{lm}$ in Cartesian Coordinates
$s$	$(4\pi)^{-1/2}$	$(4\pi)^{-1/2}$
$p_x$	$(3/4\pi)^{1/2} \sin \theta \cos \phi$	$(3/4\pi)^{1/2} r^{-1} x$
$p_y$	$(3/4\pi)^{1/2} \sin \theta \sin \phi$	$(3/4\pi)^{1/2} r^{-1} y$
$p_z$	$(3/4\pi)^{1/2} \cos \theta$	$(3/4\pi)^{1/2} r^{-1} z$
$d_{z^2}$	$(5/16\pi)^{1/2} (3 \cos^2 \theta - 1)$	$(5/16\pi)^{1/2} r^{-2} (3z^2 - r^2)$
$d_{x^2-y^2}$	$(15/16\pi)^{1/2} \sin^2 \theta \cos 2\phi$	$(15/16\pi)^{1/2} r^{-2} (x^2 - y^2)$
$d_{xy}$	$(15/16\pi)^{1/2} \sin^2 \theta \sin 2\phi$	$(15/4\pi)^{1/2} r^{-2} xy$
$d_{xz}$	$(15/4\pi)^{1/2} \sin \theta \cos \theta \cos \phi$	$(15/4\pi)^{1/2} r^{-2} xz$
$d_{yz}$	$(15/4\pi)^{1/2} \sin \theta \cos \theta \sin \phi$	$(15/4\pi)^{1/2} r^{-2} yz$

**FIGURE 2.3.** Illustration of angular (a) and radial (b) distributions of atomic  $d$  states.

called *cubic*, is convenient when atomic states in cubic fields are considered (Section 4.4). The second set is preferable for lower symmetries. The functions of one set can be easily obtained as a linear combination of the functions of

**TABLE 2.2. Orthonormalized Real Angular Parts of One-Electron Atomic  $f$  Functions  $Y_{3m}(\theta, \phi)$**

Detonation	$Y_{3m}$	
	Polar Coordinates	Cartesian Coordinates
<i>Cubic Set</i>		
$f_{x^3}$	$(7/16\pi)^{1/2} \sin \theta \cos \phi (5 \sin^2 \theta \cos^2 \phi - 3)$	$(7/16\pi)^{1/2} r^{-3} x (5x^2 - 3r^2)$
$f_{y^3}$	$(7/16\pi)^{1/2} \sin \theta \sin \phi (5 \sin^2 \theta \sin^2 \phi - 3)$	$(7/16\pi)^{1/2} r^{-3} y (5y^2 - 3r^2)$
$f_{z^3}$	$(7/16\pi)^{1/2} (5 \cos^3 \theta - 3 \cos \theta)$	$(7/16\pi)^{1/2} r^{-3} z (5z^2 - 3r^2)$
$f_{xyz}$	$(105/16\pi)^{1/2} \sin^2 \theta \cos \theta \sin 2\phi$	$(105/4\pi)^{1/2} r^{-3} xyz$
$f_{x(z^2-y^2)}$	$(105/16\pi)^{1/2} \sin \theta \cos \phi (\cos^2 \theta - \sin^2 \theta \sin^2 \phi)$	$(105/16\pi)^{1/2} r^{-3} x (z^2 - y^2)$
$f_{y(x^2-z^2)}$	$(105/16\pi)^{1/2} \sin \theta \sin \phi (\cos^2 \theta - \sin^2 \theta \cos^2 \phi)$	$(105/16\pi)^{1/2} r^{-3} y (z^2 - x^2)$
$f_{z(x^2-y^2)}$	$(105/16\pi)^{1/2} \sin^2 \theta \cos \theta \cos 2\phi$	$(105/16\pi)^{1/2} r^{-3} z (x^2 - y^2)$
<i>Low-Symmetry Set</i>		
$f_{z^3}$	$(17/16\pi)^{1/2} (5 \cos^3 \theta - 3 \cos \theta)$	$(17/16\pi)^{1/2} r^{-3} z (5z^2 - 3r^2)$
$f_{xz^2}$	$(21/32\pi)^{1/2} \sin \theta \cos \phi (5 \cos^2 \theta - 1)$	$(21/32\pi)^{1/2} r^{-3} x (5z^2 - r^2)$
$f_{yz^2}$	$(21/32\pi)^{1/2} \sin \theta \sin \phi (5 \cos^2 \theta - 1)$	$(21/32\pi)^{1/2} r^{-3} y (5z^2 - r^2)$
$f_{xyz}$	$(105/16\pi)^{1/2} \sin^2 \theta \cos \theta \sin 2\phi$	$(105/4\pi)^{1/2} r^{-3} xyz$
$f_{z(x^2-y^2)}$	$(105/16\pi)^{1/2} \sin^2 \theta \cos \theta \cos 2\phi$	$(105/16\pi)^{1/2} r^{-3} z (x^2 - y^2)$
$f_{x(x^2-3y^2)}$	$(35/32\pi)^{1/2} \sin^3 \theta \cos 3\phi$	$(35/32\pi)^{1/2} r^{-3} x (x^2 - 3y^2)$
$f_{y(3x^2-y^2)}$	$(35/32\pi)^{1/2} \sin^3 \theta \sin 3\phi$	$(35/32\pi)^{1/2} r^{-3} y (3x^2 - y^2)$

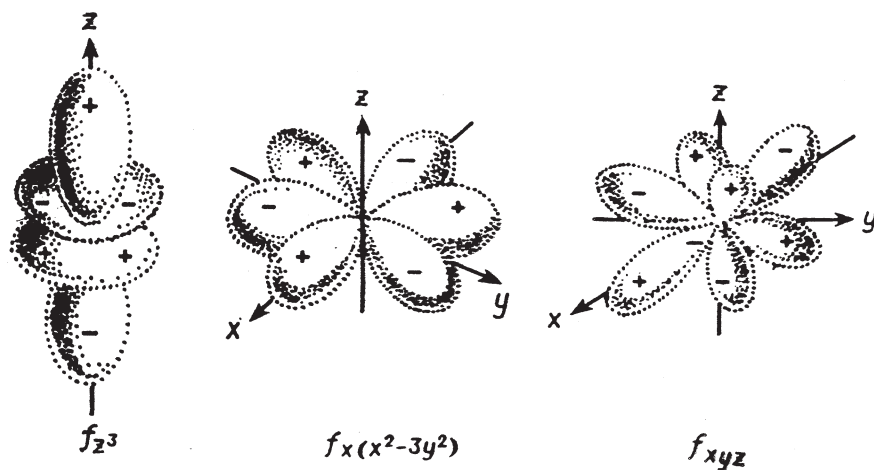


**FIGURE 2.4.** Angular distributions for some atomic one-electron wavefunctions  $f$ .

the other set (e.g.,  $f_{y^3} = -[10^{1/2}f_{y(3x^2-y^2)} + 6^{1/2}f_{yz^2}]/4$ ). Again, all these and other linear combinations of atomic functions acquire physical sense only under external perturbations that lower the spherical symmetry.

The radial functions  $R_{nl}(r)$  in (2.1) for one-electron hydrogenlike atoms can also be presented in an analytic form as follows ( $\alpha = Z/na_0$ , where  $Z$  is the nuclear charge and  $a_0$  is the Bohr radius):

$$R_{nl}(r) = \left[ \frac{(n-l-1)!}{((n+l)!)^3 2n} \right]^{1/2} (2\alpha)^{l+3/2} \exp(-\alpha r) r^l L_{n+l}^{2l+1}(2\alpha r) \quad (2.4)$$

where  $L_k^i(x)$  is the so-called Laguerre polynomial:

$$L_k^i(x) = \frac{d^i}{dx^i} \left[ e^x \frac{d^k}{dx^k} (x^k e^{-x}) \right] \quad (2.5)$$

Expressions for several of the most usable radial functions are given in Table 2.3.

Hydrogenlike functions (2.4) can be used for approximate estimations of some properties of nonhydrogen (many-electron) atoms, provided the real charge is substituted by the effective charge  $Z_{\text{eff}}$ . Different approximations are used to choose  $Z_{\text{eff}}$  in the wavefunction. One of them is purely empirical, based on fitting the one-electron energies calculated by this wavefunction with the experimental ionization potentials.

Instead of the hydrogenlike function (2.4), *Slater-type nodeless atomic functions* are often used in molecular calculations. These functions have the general

**TABLE 2.3. Expressions for Some Radial Parts of One-Electron Hydrogenlike Atomic Functions  $R_{nl}$  ( $\alpha = Z/na_0$ )**

Function	Expression
$R_{10}$	$2\alpha^{3/2}e^{-\alpha r}$
$R_{10}$	$2\alpha^{3/2}e^{-\alpha r}(1 - \alpha r)$
$R_{21}$	$(2/\sqrt{3})\alpha^{5/2}r e^{-\alpha r}$
$R_{30}$	$\frac{2}{3}\alpha^{3/2}e^{-\alpha r}(3 - 6\alpha r + 2\alpha^2 r^2)$
$R_{31}$	$(2\sqrt{2}/3)\alpha^{5/2}r e^{-\alpha r}(2 - \alpha r)$
$R_{32}$	$(4/3\sqrt{10})\alpha^{7/2}r^2 e^{-\alpha r}$
$R_{40}$	$\frac{2}{3}\alpha^{3/2}e^{-\alpha r}(3 - 9\alpha r + 6\alpha^2 r^2 - \alpha^3 r^3)$
$R_{41}$	$(2/\sqrt{15})\alpha^{5/2}r e^{-\alpha r}(5 - 5\alpha r + \alpha^2 r^2)$
$R_{42}$	$(2/3\sqrt{5})\alpha^{7/2}r^2 e^{-\alpha r}(3 - \alpha r)$
$R_{43}$	$(2/3\sqrt{35})\alpha^{9/2}r^3 e^{-\alpha r}$

form

$$R_n(r) = Nr^{n^*-1} \exp \left[ \frac{-(Z - \gamma)r}{n^*a_0} \right] \quad (2.6)$$

where  $N$  is the normalization constant,  $n^*$  is the effective principal quantum number,  $\gamma$  is the screening constant, and  $Z - \gamma$  is the effective nuclear charge, and there are simple rules for evaluating their magnitudes for each electronic configuration [2.2]. Sometimes the parameters of the Slater function (2.6) are considered as variational variables to be determined from the condition of the minimum of energy of the system.

In more accurate calculations numerical Hartree–Fock (HF) wavefunctions, discussed in Section 2.2, are used as one-electronic states. Computed HF one-electron wavefunctions are available for all the atoms and their ionized states [2.6, 2.7]. For practical use analytical presentations of the numerical functions are more convenient [2.8, 2.9].

Atomic orbitals (AOs) are most important in the calculation of molecular orbitals (MOs) by the LCAO methods (Chapter 5). There are many aspects to the choice of atomic orbitals in the calculation of MOs and the chemical bonding (see *basis sets* in MO calculations, Section 5.3).

### Orbital Overlaps: Hybridized Functions

As mentioned above, the well-known and widely used presentation of hydrogenlike one-electron orbitals in atoms in the form of  $s, p, d, f, \dots$  is based on the assumption of spherical symmetry of the field in which each electron moves, because only spherical symmetry allows for solutions in the form of spherical functions (2.2). If the field, under external influence, becomes nonspherical, these atomic states are no longer independent. They mix, and the degree of this mixing, or *hybridization*, is determined by the symmetry and strength of the external field and the energy gaps between the admixed orbitals. This is one of the obvious consequences of chemical interactions (bonding) in which the atom under consideration takes part.

One of the basic features of two atoms that determine their ability to interact with each other chemically is the “diffusiveness” (extension in space) and mutual orientation of their atomic states in space expressed by the *orbital overlap* (Section 5.2). If atom  $A$  is presented by its AO  $\varphi_A$ , and atom  $B$  by  $\varphi_B$ , then the expression

$$S_{AB} = \int \varphi_A \varphi_B d\tau \quad (2.7)$$

is called the *overlap integral*.

It should be noted that it is the integral (total) overlap  $S_{AB}$  that characterizes the formation of a chemical bond between neutral atoms. The presence of local regions of overlap (*differential overlap*) is necessary but not sufficient for the



bond formation, because the local overlaps may have different signs in different regions and thus compensate each other in the integral overlap. On the other hand, the overlap integral (2.7) itself, although indicating the possibility of bonding, is not sufficiently informative for characterizing all the bonding features. Another important parameter determining the bonding is the energy gap between the overlapping orbitals (Section 5.2).

Symmetry considerations provide a way to estimate whether the integral (2.7) is zero without its actual calculation. Group-theoretical rules (Section 3.4) allow us to do this easily. Sometimes, the evaluation of the integral (2.7) can also be done using rather simple visual considerations. Indeed, it is well known that any transformation of the variables under the sign of the integral does not change its value. This means that if one can find a transformation of the coordinates for which one of the two functions  $\varphi_A$  or  $\varphi_B$  changes its sign, whereas the other does not, then  $S_{AB} = -S_{AB} = 0$ .

For example, take  $\varphi_A = s^A$  and  $\varphi_B = p_x^B$  (the bonding line is assumed to be along  $z$ ). Then  $S_{AB} = \int s^A p_x^B d\tau = 0$  because the coordinate transformation  $x' = -x$  (reflection in the plane  $yz$ ) changes the sign of  $p_x^B$  ( $p_x' = -p_x$ ) and does not change the sign of  $s^A$  (see Fig. 2.1 and Table 2.1). On the other hand,  $\int s^A p_z d\tau \neq 0$  since in this case the two functions  $s^A$  and  $p_z$  are not changed under the symmetry operations of the system.

The symmetry of the region of orbital overlap between two atoms is of great importance for characterization of their bonding. Depending on this symmetry, one can distinguish the so-called  $\sigma$ ,  $\pi$ ,  $\delta$ , ... bonds. A more rigorous foundation of this classification of chemical bonds in diatomics is based on the quantized values of the projection of the electron angular momentum on the internuclear axis of the molecule characterized by its quantum numbers  $\lambda = 0, 1, 2, \dots$ , which correspond to  $\sigma, \pi, \delta, \dots$  bonds, respectively.

For a  $\sigma$  bond the orbital overlap region is symmetric with respect to the line of bonding between the atoms, which means that the electron density of the bond (Section 5.2) has axial symmetry (Fig. 2.5). The wavefunction of the system with this bond is independent of the angle of rotation around the molecular axis; the projection of the angular momentum on this axis (and its quantum number  $\lambda$ ) is zero. For a  $\pi$  bond the overlap is symmetrical with respect to the plane comprising the molecular axis (Fig. 2.6), and  $\lambda = 1$ . In the  $\delta$  bond there are two mutually perpendicular planes of symmetry that cross at the molecular axis,  $\lambda = 2$  (Fig. 2.7) (Hereafter positive orbital lobes are shadowed).

Obviously, not all atomic functions can be employed in the formation of diatomic bonds of given symmetry. For instance,  $s$  functions never form  $\pi$  bonds because they do not have the required symmetry of reflection in the plane crossing the molecular axis. Similarly,  $p$  functions cannot form  $\delta$  bonds since they lack two mutually perpendicular planes of symmetry. On the other hand, under certain conditions  $d$  functions can form both  $\delta$  and  $\pi$  bonds, as well as  $\sigma$  bonds,  $p$  functions can form  $\pi$  and  $\sigma$  bonds, while  $s$  function can form  $\sigma$  bonds only. However, strong relativistic effects violate these rules (see below in this section and in Section 6.5).

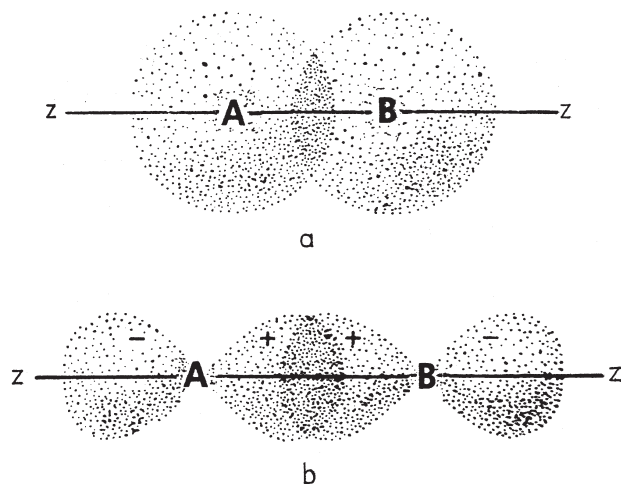


FIGURE 2.5. Interatomic  $\sigma$  overlaps: (a)  $s-s$ , (b)  $(p_\sigma - p_\sigma)$ .

The notions of  $\sigma, \pi, \delta, \dots$  bonds, which have a rigorous physical sense in the case of diatomics, may become less definitive and rather conventional in some polyatomic systems, especially in coordination compounds with three-dimensionally delocalized bonds. Indeed, for the latter the same AOs of the CA can take part in the formation of  $\sigma$  bonds with one ligand and  $\pi$  bonds with another (for examples of  $\sigma + \pi$  bonds, see Section 6.3). As mentioned above, in the case of transition metal coordination compounds, pure localized (separated) bonds CA—ligand, strictly speaking, make little sense, but they can be well defined as ligand—complex bonds.

The greater the orbital overlap, *ceteris paribus*, the stronger the bonding (Section 5.2). Therefore, the binding favors spatially oriented orbitals, and this explains the formation of *hybridized orbitals* induced by chemical bonding. As mentioned above, the separation of atomic one-electron orbitals into  $s, p, d, f, \dots$  is a rigorous consequence of the spherical symmetry of the field. Hence *in the free atom there are neither hybridized orbitals nor "directed valencies"; they are formed under the influence of the external (bonding) fields.*

Figure 2.8a shows the two independent  $s$  and  $p_z$  orbitals, while in Fig. 2.8b the mixed (hybridized)  $s + p_z$  and  $s - p_z$  functions are illustrated. The hybridized AOs are much more oriented in space along the  $z$  and  $-z$  axes, respectively, than are the pure  $s$  and  $p_z$  orbitals, thus favoring stronger chemical bonds with two other atoms in these directions. It is just this enhanced bonding that induces the  $sp$  hybridization.

Provided the geometry of the molecular system formed by the interacting atoms is known, the hybridized orbitals can be obtained from the condition of orthogonality and normalization [2.10]. The following types of hybridized orbitals are widely used:  $sp$ , linear coordination;  $sp^2$ , trigonal-planar;  $sp^3$  and  $sd^3$ ,

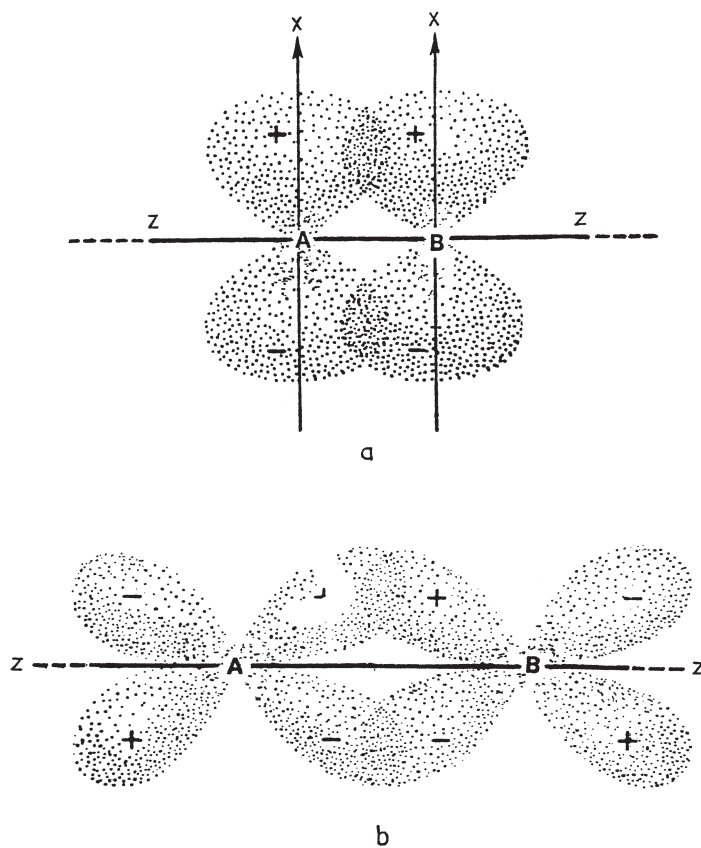


FIGURE 2.6. Interatomic  $\pi$  overlaps: (a)  $p_\pi - p_\pi$ ; (b)  $d_\pi - d_\pi$ .

tetrahedral;  $d^2sp^3$ , octahedral; and so on. Table 2.4 gives some of the hybridized functions. As stated in Sections 1.2 and 6.1,  $d$  orbitals form three-dimensional delocalized bonds rather than localized hybrid bonds.

### Spin-Orbital Interaction

The relativistic features of atomic orbitals are considered in the next subsection, and relativistic effects are discussed in Section 6.5 (and in other parts of this book), but one of these effects, the spin-orbital interaction, is most important in quantum chemistry and cannot be avoided even in nonrelativistic approaches. Spin-orbital interaction in polyatomic systems with nonzero spin affects almost all their properties (as illustrated multiply in the next chapters).

It is known that the electron possesses a spin momentum  $\mathbf{s}$ , and that its projection has two values,  $s_z = \pm \frac{1}{2}\hbar$ , corresponding to its two possible positions with respect to the axis of quantization: spinup and spindown. Taking into account

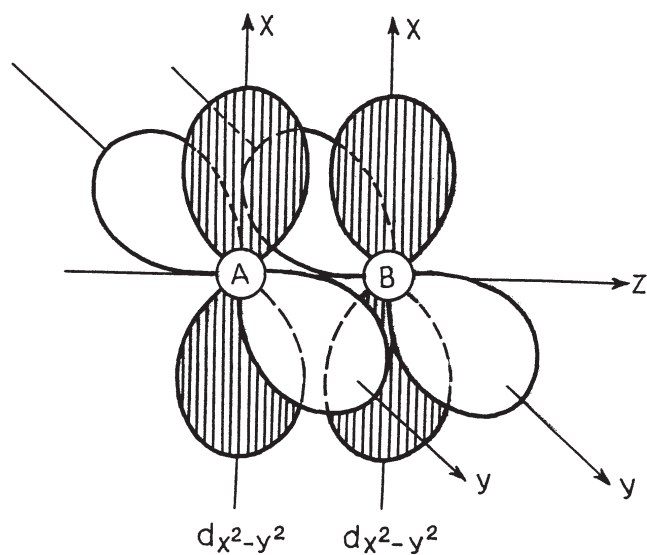


**FIGURE 2.7.** Interatomic  $\delta d_{x^2-y^2}^A - d_{x^2-y^2}^B$  overlap that has two perpendicular planes of symmetry that cross the axis of bonding.

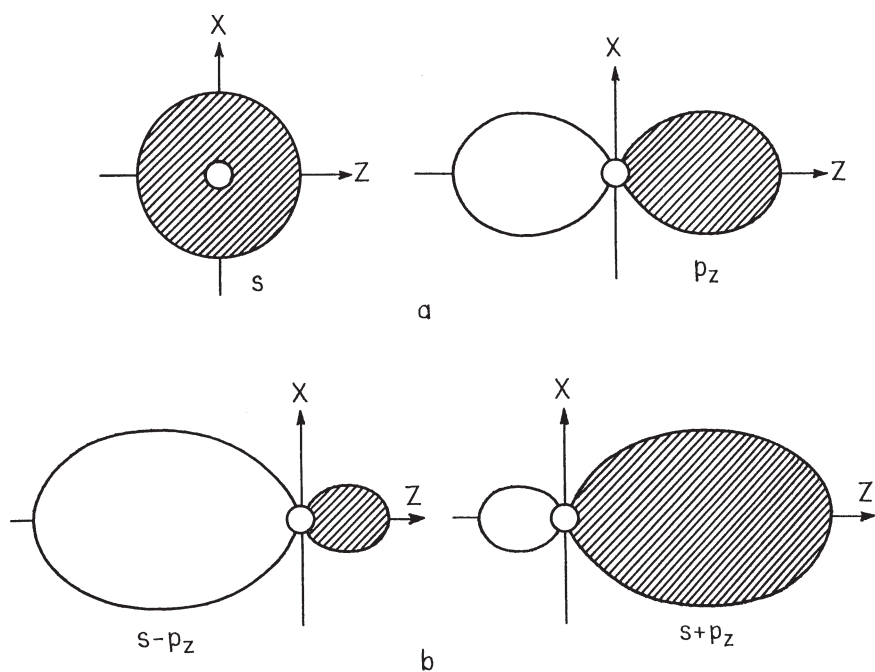


**FIGURE 2.8.**  $sp$  hybridization: (a) free  $s$  and  $p_z$  orbitals; (b) hybridized  $s+p_z$  and  $s-p_z$  orbitals.

**TABLE 2.4. Some Hybridized Atomic Orbitals**

Type of Hybridization	Hybridized Orbitals
$sp$ (along $x$ )	$2^{-1/2}(s + p_x), 2^{-1/2}(s - p_x)$
$sp^2$ (in $xy$ plane)	$3^{-1/2}(s + \sqrt{2}p_x)$ $3^{-1/2}(s - p_x/\sqrt{2} + \sqrt{3}p_y/\sqrt{2})$ $3^{-1/2}(s - p_x/\sqrt{2} - \sqrt{3}p_y/\sqrt{2})$
$sp^3$ (tetrahedral)	$\frac{1}{2}(s + p_x + p_y + p_z)$ $\frac{1}{2}(s + p_x - p_y - p_z)$ $\frac{1}{2}(s - p_x + p_y - p_z)$ $\frac{1}{2}(s - p_x - p_y + p_z)$
$d^2sp^3$	$6^{-1/2}(s + \sqrt{3}p_z + \sqrt{2}d_{z^2})$ $6^{-1/2}(s - \sqrt{3}p_z + \sqrt{2}d_{z^2})$ $12^{-1/2}(\sqrt{2}s + \sqrt{6}p_y - d_{z^2} + \sqrt{3}d_{x^2-y^2})$ $12^{-1/2}(\sqrt{2}s - \sqrt{6}p_y - d_{z^2} + \sqrt{3}d_{x^2-y^2})$ $12^{-1/2}(\sqrt{2}s + \sqrt{6}p_x - d_{z^2} - \sqrt{3}d_{x^2-y^2})$ $12^{-1/2}(\sqrt{2}s - \sqrt{6}p_x - d_{z^2} - \sqrt{3}d_{x^2-y^2})$

this spin and assuming that it is independent of the orbital motion of the electrons, we should multiply the one-electron orbital function (2.1) by the spin function determining the spin state, and to add the spin quantum numbers  $m_s = \pm\frac{1}{2}$  to the three orbital quantum number  $n, l, m$ .

Complications begin when we take into account that the spin momentum is associated with a magnetic moment of the electron (the *Bohr magneton*). Indeed, the orbital motion of the electron creates a magnetic field and the magnetic moment of the electron interacts with the magnetic field of orbital motion. This is the *spin-orbital interaction*. It is obvious that the spin-orbital interaction is different for the two spin positions, spinup along the orbital magnetic field and spindown in the opposite direction, resulting in the *spin-orbital splitting* of the energy levels.

The energy of interaction of the electron spin  $\mathbf{s}$  with the magnetic field of its orbital motion that has the momentum  $\mathbf{l}$  is a relativistic effect [not included in the Schrödinger equation (1.5)] that emerges from Dirac's equation [2.5]. For the operator of this interaction  $H_{SO}$ , we have

$$H_{SO} = \xi(r)(\mathbf{l}, \mathbf{s}) \quad \xi(r) = -\frac{e}{2m^2c^2r} \frac{dV(r)}{dr} \quad (2.8)$$

where  $V(r)$  is the potential energy of the electron in the atom. For light atoms  $H_{SO}$  can be considered as a perturbation of the nonrelativistic states. Then the

energy correction due to the spin–orbital interaction can be obtained by perturbation theory. In the first order these corrections are equal to the diagonal matrix elements of the perturbation (2.8). Usually they are characterized by the *one-electron spin–orbital constant*  $\xi_{nl}$

$$\xi_{nl} = \hbar^2 \int \xi(r) R_{nl}^2(r) r^2 dr \quad (2.9)$$

where  $R_{nl}(r)$  is the radial part of the atomic wavefunction of the perturbed state ( $nl$ ). For a Coulomb field  $V = Ze/r$

$$\begin{aligned} \xi_{nl} &= \frac{Ze^2\hbar^2}{2m^2c^2a_0^3} \int r^{-3} R_{nl}(r) r^2 dr \\ &= \frac{e^2\hbar^2}{2m^2c^2a_0^3 n^3 l(l+1)(l+1/2)} Z^4 \end{aligned} \quad (2.10)$$

Here  $l \neq 0$ ; for  $l = 0$ ,  $H_{SO} = 0$ :  $s$  states are not subject to spin–orbital splitting.

From expression (2.10) it is seen that the constant of spin–orbital interaction  $\xi$  for an electron in a hydrogenlike atom is strongly dependent on the atomic number  $Z$  (proportional to  $Z^4$ ). For instance, for a  $3d$  electron  $\xi_{3d} = 1.4 \times 10^{-2} Z^4 \text{ cm}^{-1}$ , and for a  $4d$  electron  $\xi_{4d} = 6.1 \times 10^{-3} Z^4 \text{ cm}^{-1}$ . It follows that the influence of spin–orbital interactions becomes very strong in heavy atoms and for large  $Z$  values it can no longer be taken as a small perturbation; it should be considered along with other electrostatic interactions in the atom. In this case the wavefunction of the electron cannot be taken as a product of its orbital and spin parts.

### Relativistic Atomic Functions

Relativistic atomic states become of great importance in the study of electronic structure and properties of transition metal compounds (Sections 5.4 and 6.5). For large electron speeds  $v$  that are realized in heavy atoms, the dependence of the mass of the electron on its speed and the magnetic moment of the electron [not included in the Schrödinger equation (1.5)] should be taken into account. This is done in the Dirac equation, which, in the absence of external magnetic fields, can be written as follows [2.5]:

$$(\alpha c\mathbf{p} + eU + mc^2)\Psi = E\Psi \quad (2.11)$$

Formally, this equation is somewhat similar to the Schrödinger equation (1.5), but in fact, Eq. (2.11) is much more complicated than (1.5). First, (2.11) is a matrix equation of the fourth rank, which means that there is a system of four coupled equations to be solved. This is due to the matrices  $\alpha$  and  $\beta$ . They are (the  $\beta$  matrix is employed later):

$$\alpha = \begin{pmatrix} 0 & \sigma \\ \sigma & 0 \end{pmatrix} \quad \beta = \begin{pmatrix} I & 0 \\ 0 & -I \end{pmatrix} \quad (2.12)$$

where the components of the vector–matrix  $\sigma$  are the well-known Pauli matrices:

$$\sigma_x = \begin{pmatrix} 0 & 1 \\ 1 & 0 \end{pmatrix} \quad \sigma_y = \begin{pmatrix} 0 & -i \\ i & 0 \end{pmatrix} \quad \sigma_z = \begin{pmatrix} 1 & 0 \\ 0 & -1 \end{pmatrix} \quad (2.13)$$

and  $I$  is a unit matrix:

$$I = \begin{pmatrix} 1 & 0 \\ 0 & 1 \end{pmatrix} \quad (2.14)$$

Other notations in (2.11) are usual:  $c$  is the speed of light and  $p = -i\hbar\nabla$  [hence  $\alpha c\mathbf{p}$  means  $-i\hbar c(\alpha_x \partial/\partial x + \alpha_y \partial/\partial y + \alpha_z \partial/\partial z)$ ].

According to the fourth-rank equation (2.11), its solution  $\Psi$ , the wavefunction, is also fourth component. Indeed, it resembles a column four-vector, which is called a *bispinor* [2.5]:

$$\Psi = \begin{pmatrix} \Psi^{(1)} \\ \Psi^{(2)} \\ \Psi^{(3)} \\ \Psi^{(4)} \end{pmatrix} = \begin{pmatrix} \varphi \\ \chi \end{pmatrix} \quad (2.15)$$

where  $\varphi$  and  $\chi$  are spinors composed of the 1,2 and 3,4 components, respectively. The presentation of the solution (2.15) as two spinors has a specific physical meaning, since when the ratio  $v/c$  is not very large, the first spinor  $\varphi$  is much larger than the second one  $\chi$ , and the latter can be neglected.

The physical meaning of the wavefunction  $\Psi$  of (2.15) that emerges from quantum mechanics is, in general, the same as in the nonrelativistic case:  $|\Psi^{(1)}|^2 d\tau$  means the probability of finding the electron in the volume  $d\tau$  near point 1. Then  $|\Psi|^2 = \Psi^* \Psi$ , and the product of the column vector  $\Psi$  with its complex-conjugated  $\Psi^*$  [which is a row vector  $(\Psi^{(1)*}, \Psi^{(2)*}, \Psi^{(3)*}, \Psi^{(4)*})$ ] yields

$$|\Psi|^2 = |\Psi^{(1)}|^2 + |\Psi^{(2)}|^2 + |\Psi^{(3)}|^2 + |\Psi^{(4)}|^2 \quad (2.16)$$

or

$$|\Psi|^2 = |\varphi|^2 + |\chi|^2 \quad (2.17)$$

Thus the density of position probability equals the sum of the contributions of all the components of the relativistic wavefunction. In particular, when the electron speed is not very large (e.g., in the region far from the nucleus), the major contribution comes from the large component  $\varphi$ , and  $|\Psi|^2 \approx |\varphi|^2$

To estimate relativistic effects as compared to the nonrelativistic properties, the constant  $\alpha = \frac{1}{137}$ , called *the fine-structure constant*, is introduced (do not confuse this  $\alpha$  constant with the  $\alpha$  parameter in the nonrelativistic radial functions in

Table 2.3 and the  $\alpha$  matrices above). In atomic units the speed of light  $c \cong 137$ . On the other hand, the electron speed  $v$  at the nucleus in the same units is equal to  $Z$ , the nuclear charge. Hence the magnitude  $\alpha Z$  equals the ratio of the electron speed to the speed of light at the nucleus, where this ratio is maximal.

In the spherically symmetric field of the nucleus, the relativistic solution is characterized by four quantum numbers (which are somewhat similar to the non-relativistic ones):

1. The principal quantum number  $n = 1, 2, 3, \dots$ , which has the same meaning as in the nonrelativistic atom.
2. The azimuthal quantum number  $l = 0, 1, 2, \dots, (n-1)$ , which denotes the states corresponding to  $s, p, d, \dots$ , respectively; distinct from the Schrödinger atom, in the relativistic case,  $l$  is no longer the quantum number of the orbital angular momentum.
3.  $j = |l \pm \frac{1}{2}|$ , the angular momentum quantum number that is always positive (as  $l$  is) and half-integer; it takes at most two values.
4.  $m$ , the magnetic quantum number that can take all half-odd-integer values from  $-j$  to  $+j$  [ $m = j, j-1, \dots, -(j-1), -j$ ].

With these quantum numbers  $n_l j m$ , for  $s$  electrons, we have  $j = \frac{1}{2}, m = \pm \frac{1}{2}$  (two states); for  $p$  electrons:  $j = \frac{1}{2}$  with  $m = \pm \frac{1}{2}$  (two states) and  $j = 3/2$  with  $m = \pm \frac{1}{2}, \pm \frac{3}{2}$  (four states); for  $d$  electrons:  $j = \frac{3}{2}$  with  $m = \pm \frac{1}{2}, \pm \frac{3}{2}$  (four states) and  $j = \frac{5}{2}$  with  $m = \pm \frac{1}{2}, \pm \frac{3}{2}, \pm \frac{5}{2}$  (six states). Usually the magnetic quantum number (similar to the nonrelativistic spin quantum number  $m_s$ ) is not indicated, and hence we have two  $ns_{1/2}$  states, two  $np_{1/2}$  and four  $np_{3/2}$  states, four  $nd_{3/2}$  and six  $nd_{5/2}$  states, six  $nf_{5/2}$  and eight  $nf_{7/2}$  states, and so on.

For these states the four-component wavefunctions are [2.5, 2.11]:

$$\Psi_{n_l j m} = (N_{n_l j m})^{1/2} \begin{pmatrix} g a_1 Y_{l, m-1/2} \\ g a_2 Y_{1, m+1/2} \\ -i f a_3 Y_{2j-1, m-1/2} \\ -i f a_4 Y_{2j-1, m+1/2} \end{pmatrix} \quad (2.18)$$

where  $Y_{lm}$  are the spherical harmonics (2.2),  $N_{n_l j m}$  is the normalization factor determined from the condition  $\int |\Psi_{n_l j m}|^2 d\tau = 1$  [taking into account Eq. (2.16)], and  $a_i$  are constants as follows:

$$a_1 = \left( \frac{l + \frac{1}{2} \pm m}{2l + 1} \right)^{1/2}$$

$$a_2 = \left( \frac{l + \frac{1}{2} \mp m}{2l + 1} \right)^{1/2}$$



$$a_3 = \left( \frac{2j - l + \frac{1}{2} \mp m}{4j - 2l + 1} \right)^{1/2} \quad (2.19)$$

$$a_4 = \left( \frac{2j - l + \frac{1}{2} \pm m}{4j - 2l + 1} \right)^{1/2}$$

where in the symbol  $\pm$  the sign of  $j - l$  should be taken, whereas in  $\mp$  its opposite is implied, and  $g$  and  $f$  are the radial parts of the wavefunction:  $g$  is the same for the two components  $\Psi^{(1)}$  and  $\Psi^{(2)}$  of the large spinor, while  $f$  is the same for  $\Psi^{(3)}$  and  $\Psi^{(4)}$  of the small spinor [Eq. (2.18)]. Their general expressions are somewhat awkward [2.5] [they can be presented as a product of an exponent with a polynomial similar to (2.4)], but it is important that *the  $f$  component is  $\alpha Z$  times smaller than the  $g$  one*. Table 2.5 presents some explicit expressions for relativistic  $s$  and  $p$  functions in a hydrogenlike atom given with accuracy up to terms  $\alpha Z$  included [2.11].

Some interesting features emerge from the relativistic functions as compared with the nonrelativistic ones. First, the relativistic  $s$  functions are spherically symmetric, quite similar to the nonrelativistic case. But surprisingly, in contrast to the nonrelativistic  $p$  orbitals, the  $p_{1/2}$  states are also spherically symmetric. This can be easily confirmed by substituting the four components of any of the two  $p_{1/2}$  functions from Table 2.5 into Eq. (2.16). It appears to be a general trend: relativistic atomic functions with the same  $j$  and  $m$  quantum numbers have the same angular dependence of the corresponding position density. This means not only that  $s_{1/2}(\frac{1}{2})$  and  $p_{1/2}(\frac{1}{2})$  have identical (in this case spherically symmetric) angular dependence of the position density but also that  $p_{3/2}(\frac{3}{2})$  and  $d_{3/2}(\frac{3}{2})$ ,  $d_{5/2}(\frac{5}{2})$ , and  $f_{5/2}(\frac{5}{2})$  have similar angular electron cloud distribution.

The  $p_{3/2}(\frac{1}{2})$  distribution is also different from that of the nonrelativistic  $p$  states. Indeed, using Eq. (2.16) with the data in Table 2.5, one can easily find that the angular dependence of the electron distribution in this state is  $\cos^2 \theta + \frac{1}{3}$  (instead of  $\cos^2 \theta$  in the  $p_z$  function); that is, it has also a  $\frac{1}{3}$  weighted  $s$ -type spherically symmetric distribution. The  $p_{3/2}(\frac{3}{2})$  functions yield an angular distribution identical to the nonrelativistic case.

The  $s$ -type distribution in the relativistic  $p$  states [ $p_{1/2}$  and  $p_{3/2}(\frac{1}{2})$ ] is very important for the bonding properties of corresponding atoms, especially in their ability to form pure  $\sigma$  and  $\pi$  bonds (see below). Another feature of these functions is that they have no angular nodes; it can be shown that all the relativistic atomic functions have no radial nodes, either. Indeed, the radial nodes in the large component  $g$  never coincide with those of the smaller component  $f$ , and hence at the points where  $g^2$  is zero  $f^2$  gives a non-zero contribution of the order of  $(\alpha Z)^2 = (Z/137)^2$ . Thus in the relativistic presentation, strictly speaking, there are no points of zero radial distribution of electron position density.

All the foregoing effects in the relativistic atomic states are significant if and only if the spin-orbital interaction is sufficiently strong. For zero (or negligible) spin-orbital splitting all the  $p$  states are degenerate (the energies of  $p_{1/2}$  and  $p_{3/2}$

**TABLE 2.5. Relativistic Atomic Wavefunctions for a Hydrogenlike Atom to the First Order in  $\alpha Z^a$** 

Atomic State	$\sqrt{N}$	Spinors	Radial Part	Angular Part	
				$m = \frac{1}{2}$	$m = -\frac{1}{2}$
$1s_{1/2}$	1	$\varphi$	$e^{-r}$	1 0	0 -1
		$\chi$	$\alpha Z e^{-r}$	$\frac{1}{2}i \cos \theta$ $\frac{1}{2}i \sin \theta e^{i\phi}$	$-\frac{1}{2}i \sin \theta e^{-i\phi}$ $\frac{1}{2}i \cos \theta$
$2s_{1/2}$	$(\frac{1}{8})^{1/2}$	$\varphi$	$e^{-r/2}[1 - (r/2)]$	1 0	0 -1
		$\chi$	$\alpha Z e^{-r/2}[1 - (r/4)]$	$\frac{1}{2}i \cos \theta$ $\frac{1}{2}i \sin \theta e^{i\phi}$	$-\frac{1}{2}i \sin \theta e^{-i\phi}$ $\frac{1}{2}i \cos \theta$
$2p_{1/2}$	$(\frac{1}{32})^{1/2}$	$\varphi$	$r e^{-r/2}$	$-(1/\sqrt{3}) \cos \theta$ $-(1/\sqrt{3}) \sin \theta e^{i\phi}$	$(1/\sqrt{3}) \sin \theta e^{-i\phi}$ $-(1/\sqrt{3}) \cos \theta$
		$\chi$	$\alpha Z e^{-r/2}[1 - (r/6)]$	$(\frac{3}{4})^{1/2} i$ 0	0 $(\frac{3}{4})^{1/2} i$
$2p_{3/2}$	$(\frac{1}{32})^{1/2}$	$\varphi$	$r e^{-r/2}$	$(\frac{2}{3})^{1/2} \cos \theta$ $-(\frac{1}{6})^{1/2} \sin \theta e^{i\phi}$	$-(\frac{1}{6})^{1/2} \sin \theta e^{-i\phi}$ $-(\frac{2}{3})^{1/2} \cos \theta$
		$\chi$	$\alpha Z r e^{-r/2}$	$(\frac{3}{32})^{1/2} i (\cos^2 \theta - \frac{1}{3})$ $(\frac{3}{32})^{1/2} i \sin \theta \cos \theta e^{i\phi}$	$-(\frac{3}{32})^{1/2} i \sin \theta \cos \theta e^{-i\phi}$ $(\frac{3}{32})^{1/2} i (\cos^2 \theta - \frac{1}{3})$
$2p_{3/2}$	$(\frac{1}{32})^{1/2}$	$\varphi$	$r e^{-r/2}$	$(1/\sqrt{2}) \sin \theta e^{i\phi}$ 0	0 $(1/\sqrt{2}) \sin \theta e^{-i\phi}$
		$\chi$	$\alpha Z r e^{-r/2}$	$(\frac{1}{32})^{1/2} i \sin \theta \cos \theta e^{i\phi}$ $(\frac{1}{32})^{1/2} i \sin^2 \theta e^{2i\phi}$	$(\frac{1}{32})^{1/2} i \sin^2 \theta e^{-2i\phi}$ $-(\frac{1}{32})^{1/2} i \sin \theta \cos \theta e^{-i\phi}$

Source: Powel [2.11].

<sup>a</sup>The radial coordinate  $r$  is given in  $a_0/Z$  units, while the function as a whole is in  $(Z^3/\pi a_0^3)^{1/2}$  units.

states coincide), and then any of their linear combination is also an eigenfunction with the same energy. In particular, the combinations

$$\begin{aligned} \left(\frac{2}{3}\right)^{1/2} p_{3/2,1/2} - \left(\frac{1}{3}\right)^{1/2} p_{1/2,1/2} &\sim p_z \\ \left(\frac{1}{2}\right)^{1/2} p_{3/2,3/2} + \left(\frac{1}{3}\right)^{1/2} p_{1/2,-1/2} - \left(\frac{1}{6}\right)^{1/2} p_{3/2,-1/2} &\sim p_x \\ \left(\frac{1}{2}\right)^{1/2} p_{3/2,3/2} - \left(\frac{1}{3}\right)^{1/2} p_{1/2,-1/2} + \left(\frac{1}{6}\right)^{1/2} p_{3/2,-1/2} &\sim p_y \end{aligned} \quad (2.20)$$

have the angular behavior of the corresponding  $p_z$ ,  $p_x$ , and  $p_y$  nonrelativistic atomic  $p$  functions. A sufficiently large separation between the  $p_{1/2}$  and  $p_{3/2}$  states caused by the spin-orbital interaction (as compared with the bonding effects) makes this orbital mixing impossible, thus realizing the relativistic behavior of the corresponding atomic states.

More complicated are the orbital overlaps of relativistic functions. When two atoms  $A$  and  $B$  are characterized by four-component wavefunctions of the type (2.15), their overlap, similar to that in (2.16), is given by the following expression:

$$\begin{aligned} S_{AB} = \int \Psi_A^* \Psi_B d\tau = \int \left[ \Psi_A^{(1)*} \Psi_B^{(1)} \right. \\ \left. + \Psi_A^{(2)*} \Psi_B^{(2)} + \Psi_A^{(3)*} \Psi_B^{(3)} + \Psi_A^{(4)*} \Psi_B^{(4)} \right] d\tau \end{aligned} \quad (2.21)$$

With the relativistic functions in Table 2.5, the idea of  $\sigma$ ,  $\pi$ , and  $\delta$  bonds changes significantly. Indeed, only the overlap of  $s_{1/2}^A - s_{1/2}^B$  functions is of pure  $\sigma$  type, quite similar to the overlap of the corresponding nonrelativistic orbitals. The  $p_{1/2}^A - p_{1/2}^B$  overlap is essentially different from both  $p_z^A - p_z^B$   $\sigma$  overlap and  $p_x^A - p_x^B$  ( $p_y^A - p_y^B$ )  $\pi$  overlap. The direct substitution of the four-component functions from Table 2.5 into Eq. (2.21) (in fact, only the large  $\varphi$  component should be tried since the  $\chi$  spinor is much smaller, and, in any case, it yields the same angular dependence as does the  $\varphi$  spinor) shows that  $p_{1/2}^A(\frac{1}{2}) - p_{1/2}^B(\frac{1}{2})$  overlap has  $\frac{1}{3}\sigma$  bonding character and  $\frac{2}{3}\pi$  antibonding, or vice versa,  $\frac{1}{3}\sigma$  antibonding and  $\frac{2}{3}\pi$  bonding (see Section 6.5 and Fig. 6.32). Similarly, the  $p_{3/2}^A(\frac{1}{2}) - p_{3/2}^B(\frac{1}{2})$  overlap comprises  $\frac{2}{3}$  of  $\sigma$  bonding and  $\frac{1}{3}$  of  $\pi$  antibonding, or vice versa,  $\frac{2}{3}$  of  $\sigma$  antibonding and  $\frac{1}{3}$  of  $\pi$  bonding. The  $p_{3/2}^A(\frac{3}{2}) - p_{3/2}^B(\frac{3}{2})$  overlap is the same as for nonrelativistic  $p$  functions. These conclusions are important to the analysis of the electronic structure and bonding in heavy-atom coordination compounds (Section 6.5).

## 2.2. MULTIELECTRON STATES: ENERGY TERMS

### Electronic Configurations and Terms

For more than one electron in the atom, the picture of electronic structure becomes significantly more complicated. In the one-electron approximation the

multielectron wavefunction is composed of one-electron functions following specific rules that depend on the magnitudes of the spin-orbital and interelectron interactions. When ignoring these interactions, the electron can be distributed among the one-electron orbitals of the type (2.1) with the quantum numbers  $n, l, m, m_s$  following the *Pauli principle*. This distribution—the numbers of electrons in  $s, p, d, f$  states—forms the *electron configuration* of the atom. With the spin-orbital and interelectron interactions taken into account there may be many states of the same electron configuration that differ with respect to energy and spin values.

Methods of determining the states of a given electron configuration are vary according different for different relationships between the spin-orbital and interelectron interactions. For light atoms (to approximately the middle of the periodic table) the spin-orbital interaction is no larger than  $\sim 10^3 \text{ cm}^{-1}$  (see Table 2.7, below), and hence it is much weaker than the interelectron interaction, which is of the order of  $10^4 \text{ cm}^{-1}$ . In this case *Russell-Saunders LS coupling* takes place, for which the orbital and spin momenta of the electrons  $\mathbf{l}_i$  and  $\mathbf{s}_i$  are summed up separately into the total orbital momentum  $\mathbf{L} = \sum_i \mathbf{l}_i$  and total spin momentum  $\mathbf{S} = \sum_i \mathbf{s}_i$ ; the spin-orbital interaction is considered afterward and results in the total electronic angular momentum  $\mathbf{J} = \mathbf{L} + \mathbf{S}$ . In the *LS coupling* scheme the wavefunction of the atom is a solution of Eq. (1.1) for the operators  $L^2, L_z, S^2, S_z$ , and is characterized by the following quantum numbers:

- $L$ , the total momentum:  $L = 0, 1, 2, \dots$
- $M = \sum_i m_i$ , the projection  $L_z$  of the total momentum  $\mathbf{L}$ :  $M = L, L - 1, \dots, 0, -1, \dots, -L$  ( $2L + 1$  values)
- $S$ , the total spin
- $M_S = \sum_s m_s$ , the projection  $S_z$  of the total spin  $\mathbf{S}$ :  $M_S = S, S - 1, \dots, -S$  ( $2S + 1$  values)

The set of states with the same values of  $L$  and  $S$ , but different  $M$  and  $M_S$ , in all  $(2L + 1)(2S + 1)$  states, forms the *atomic term*. The terms with  $L = 0, 1, 2, 3, 4, 5, \dots$  are denoted by the capital letters  $S, P, D, F, G, H$ , respectively, with denotation of the *spin multiplicity* (the number of spin states) equal to  $2S + 1$  as a superscript in the left-hand side. For instance, the term with  $L = 1$  and  $S = 1$  (spin triplet) is denoted by  ${}^3P$ .

Because of different charge distributions and spin orientations in different one-electron states (Fig. 2.1) and hence different interelectron interactions, the energies of different terms (even with the same electronic configuration) are significantly different. These differences can be calculated and expressed by the *Slater-Condon, or Racah, parameters*. Table 2.6 lists the relative energies of the terms of  $d^n$  configurations expressed by Racah parameters  $A, B, C$ . They are obtained as explained later in this section.

The analysis shows that in all the cases the state with the lowest energy, the ground state, corresponds to the term of maximum possible (in the configuration

**TABLE 2.6. Energy Terms of Electronic  $d^n$  Configurations Expressed by Racah Parameters  $A, B, C$** 

Electronic Configuration	Term <sup>a</sup>	Relative Electron Interaction Energy <sup>b</sup>
$d^1, d^9$	${}^2D$	
$d^2, d^8$	${}^3F$	$A - 8B$
	${}^3P$	$A + 7B$
	${}^1G$	$A + 4B + 2C$
	${}^1D$	$A - 3B + 2C$
	${}^1S$	$A + 14B + 7C$
$d^3, d^7$	${}^4F$	$3A - 15B$
	${}^4P$	$3A$
	${}^2H, {}^2P$	$3A - 6B + 3C$
	${}^2G$	$3A - 11B + 3C$
	${}^2F$	$3A + 9B + 3C$
	${}^2D', {}^2D''$	$3A + 5B + 5C \pm (193B^2 + 8BC + 4C^2)^{1/2}$
$d^4, d^6$	${}^5D$	$6A - 21B$
	${}^3H$	$6A - 17B + 4C$
	${}^3G$	$6A - 12B + 4C$
	${}^3F', {}^3F''$	$6A - 5B + \frac{11}{2}C \pm \frac{3}{2}(68B^2 + 4BC + C^2)^{1/2}$
	${}^3D$	$6A - 5B + 4C$
	${}^3P', {}^3P''$	$6A - 5B + \frac{11}{2}C \pm \frac{1}{2}(912B^2 - 24BC + 9C^2)^{1/2}$
	${}^1I$	$6A - 15B + 6C$
	${}^1G', {}^1G''$	$6A - 5B + \frac{15}{2}C \pm \frac{1}{2}(708B^2 - 12BC + 9C^2)^{1/2}$
	${}^1F$	$6A + 6C$
	${}^1D', {}^1D''$	$6A + 9B + \frac{15}{2}C \pm \frac{3}{2}(144B^2 + 8BC + C^2)^{1/2}$
	${}^1S', {}^1S''$	$6A + 10B + 10C \pm 2(193B^2 + 8BC + 4C^2)^{1/2}$
$d^5$	${}^6S$	$10A - 35B$
	${}^4G$	$10A - 25B + 5C$
	${}^4F$	$10A - 13B + 7C$
	${}^4D$	$10A - 18B + 5C$
	${}^4P$	$10A - 28B + 7C$
	${}^2I$	$10A - 24B + 8C$
	${}^2H$	$10A - 22B + 10C$
	${}^2G'$	$10A - 13B + 8C$
	${}^2G''$	$10A + 3B + 10C$
	${}^2F'$	$10A - 9B + 8C$
	${}^2F''$	$10A - 25B + 10C$
	${}^2D', {}^2D''$	$10A - 3B + 11C \pm 3(57B^2 + 2BC + C^2)^{1/2}$
	${}^2D'''$	$10A - 4B + 10C$
	${}^2P$	$10A + 20B + 10C$
	${}^2S$	$10A - 3B + 8C$

<sup>a</sup>Terms with the same  $L$  and  $S$  are distinguished by primes.<sup>b</sup>Energies of  $d^{10-n}$  configurations differ from those of  $d^n$  by a constant shift.

**TABLE 2.7. Constants of Spin–Orbital Coupling  $\lambda$  for Some Transition Metal  $3d$  Ions in Their Ground States**

Ion	Electronic Configuration	Ground State	$\lambda$ (cm <sup>-1</sup> )
Ti <sup>3+</sup>	$d^1$	${}^2D$	154
V <sup>3+</sup>	$d^2$	${}^3F$	104
V <sup>2+</sup>	$d^3$	${}^4F$	55
Cr <sup>3+</sup>	$d^3$	${}^4F$	87
Cr <sup>2+</sup>	$d^4$	${}^5D$	57
Mn <sup>3+</sup>	$d^4$	${}^5D$	85
Mn <sup>2+</sup> , Fe <sup>3+</sup>	$d^5$	${}^6S$	0
Fe <sup>2+</sup>	$d^6$	${}^5D$	-100
Co <sup>2+</sup>	$d^7$	${}^4F$	-180
Ni <sup>2+</sup>	$d^8$	${}^3F$	-335
Cu <sup>2+</sup>	$d^9$	${}^3D$	-852

under consideration) spin multiplicity and maximum orbital momentum for this multiplicity. This is the well-known *Hund rule*. For example, for the electronic configuration  $[A](nd)^2$  (where  $[A]$  denotes the inner closed shell), for instance,  $V^{3+}$ , the possible terms, as shown below and in Table 2.6, are  ${}^3F$ ,  ${}^1D$ ,  ${}^3P$ ,  ${}^1G$ , and  ${}^1S$ . Following Hund's rule, the ground term is  ${}^3F$ , because it has the maximal spin  $S = 1$  (spin multiplicity  $2S + 1 = 3$ ), and with the maximal spin it also has the maximal orbital momentum  $L = 3$  (the  ${}^3P$  term also has the maximal spin  $S = 1$ , but its orbital momentum  $L = 1$  is lower).

The origin of Hund's rule can be understood when one considers the fact that the maximum spin means that the electrons occupy as many separate one-electron orbitals with parallel spin orientations as possible (in the same orbital, two electrons have mutually compensating opposite spins). For such electrons the negative exchange interaction that lowers the energy is maximal (the exchange between electrons with opposite spins is zero). In addition, together with the requirement of maximum orbital momentum, it favors the electron charge distribution over the largest possible volume of the atom, thus lowering the interelectron electrostatic repulsion.

In the approximation of the  $LS$  coupling under consideration the total momentum of the atom is  $\mathbf{J} = \mathbf{L} + \mathbf{S}$ , its quantum number  $J$  acquires all the values by one from  $L + S$  to  $|L - S|$ :  $J = L + S, L + S - 1, \dots, |L - S|$ . When the spin–orbital interaction is included, the energy levels with different  $J$  values may be different. The magnitude of this spin–orbital splitting can be obtained by means of perturbation theory. Following Eq. (2.8), the operator of the spin–orbital interaction in a multielectron atom can be written in the following form:

$$H_{SO} = \sum_i \xi(\mathbf{r}_i)(\mathbf{l}_i, \mathbf{s}_i) \quad (2.22)$$

which in the case of  $LS$  coupling can be transformed to

$$H_{SO} = \lambda(\mathbf{L}, \mathbf{S}) \quad (2.23)$$

where  $\lambda$  is a combination of radial integrals of the type (2.9), called *the spin-orbital constant* of the atom (or ion).

The spin-orbital constant  $\lambda$  plays a significant role in quantum chemistry and the theory of physical methods of investigation of molecular systems.  $\lambda$  can be either positive or negative, unlike the analogous spin-orbital constant for one-electron  $\xi_{nl}$ , which is always positive [see Eqs. (2.9) and (2.10)]. Besides theoretical calculations,  $\lambda$  can be obtained from experimental data using *the rule of Landé intervals*. Indeed,  $\mathbf{J} = \mathbf{L} + \mathbf{S}$ ,  $J^2 = L^2 + S^2 + 2(\mathbf{L}, \mathbf{S})$  and hence

$$(\mathbf{L}, \mathbf{S}) = \frac{J^2 - L^2 - S^2}{2} \quad (2.24)$$

On the other hand, it is known from quantum mechanics that the mean value of the squares of the momenta are  $\langle J^2 \rangle = J(J+1)$ ,  $\langle L^2 \rangle = L(L+1)$ ,  $\langle S^2 \rangle = S(S+1)$ , and hence the mean value of the perturbation (2.23), the first correction  $\Delta E_j$  to the energy level with the corresponding  $J$  value of the  $LS$  term under consideration, is

$$\Delta E_j = \lambda \langle (\mathbf{L}, \mathbf{S}) \rangle = \frac{\lambda[J(J+1) - L(L+1) - S(S+1)]}{2} \quad (2.25)$$

Hence, for the energy difference between two levels of the same  $LS$  term with consecutive  $J$  values, we have

$$E_{J+1} - E_J = \Delta E_{J+1} - \Delta E_J = \lambda(J+1) \quad (2.26)$$

This is the rule of Landé intervals, which enables us to obtain easily the  $\lambda$  values using experimental (spectroscopic) data on the energy differences between the components of the multiplet spectrum. Table 2.7 shows some of the values of  $\lambda$  obtained in this way. As one can see,  $\lambda > 0$  for electronic configurations  $d^n$  with  $n < 5$ , and  $\lambda < 0$  for  $n > 5$  (for  $d^5L = 0$  and  $\lambda = 0$ ). In the case of heavy atoms  $\lambda$  increases rapidly with  $Z$  reaching values of several thousand wavenumbers ( $\text{cm}^{-1}$ ). For rare-earth elements there is an approximate empirical formula [2.12]:

$$\lambda = 200 (Z - 55) \text{ cm}^{-1} \quad (2.27)$$

For heavy atoms the  $LS$  coupling approximation becomes invalid because the spin-orbital interaction is not as small as the interelectron repulsion. In these cases the presentation (2.23) with separate summation of the orbital momenta of the electrons into the total orbital momentum  $\mathbf{L}$ , and the spin momenta into the total spin  $\mathbf{S}$  is ungrounded. For sufficiently strong spin-orbital interactions

the opposite limit case is used in which the orbital  $\mathbf{l}_i$  and spin  $\mathbf{s}_i$  momenta of each electron are first summed up, resulting in its total momentum  $\mathbf{j}_i = \mathbf{l}_i + \mathbf{s}_i$ , and then these one-electron total momenta  $\mathbf{j}_i$  are summarized, yielding the total momentum of the atom  $\mathbf{J} = \sum_i \mathbf{j}_i$ . This is the so-called *j-j coupling scheme*. Examples of *j-j* coupling are considered in Section 5.5 and Examples 5.6 and 6.14.

In many cases the intermediate picture between the *LS* and *jj* coupling schemes is more appropriate. With care, these cases can also be handled by the *LS* approximation [2.3].

### Multielectron Wavefunctions

In the one-electron approximation to the study of multielectron systems, each electron is described by a wavefunction that does not contain the coordinates of the other electrons, and the total wavefunction is constructed by the one-electron functions following certain rules. The main requirement for the total wavefunction is that it be antisymmetric with respect to the permutation of the (orbital and spin) coordinates of any two electrons. This condition follows from the quantum-mechanical *principle of indistinguishability* of identical particles with half-integer spins, and results directly in *the Pauli principle*.

To obey the condition of antisymmetry with respect to electron permutations, the presentation of the full wavefunction  $\Phi$  in the form of a determinant composed of one-electron functions (the so-called Slater determinant) is most convenient. For  $n$ -electron systems with closed shells, we obtain

$$\Phi(1, 2, \dots, n) = (n!)^{-1/2} \begin{vmatrix} \psi_1(1) & \psi_1(2) & \cdots & \psi_1(n) \\ \psi_2(1) & \psi_2(2) & \cdots & \psi_2(n) \\ \vdots & \vdots & \ddots & \vdots \\ \psi_n(1) & \psi_n(2) & \cdots & \psi_n(n) \end{vmatrix} \quad (2.28)$$

where each number  $1, 2, \dots, n$  in parentheses is the shorthand notation for the three orbital and one spin coordinates of the corresponding electron, and the factor  $(n!)^{-1/2}$  occurs as a result of normalization (the one-electron functions  $\psi_i$  are assumed to be orthonormalized).

From (2.28) one can easily verify that the function  $\Phi$  has the required symmetry properties. Indeed, the interchange of the coordinates of any two electrons, say 1 with 2, is equivalent to the interchange of two columns of the determinant (1 and 2), and this changes the sign of the latter.

If the one-electron functions are characterized by the four quantum numbers  $n, l, m, m_s$ , then the full wavefunction is determined by the set of quantum numbers of all the occupied one-electron states, which can be denoted as follows:

$$\Phi(n_1 l_1 m_1 m_{s1}; n_2 l_2 m_2 m_{s2}; \cdots; n_n l_n m_n m_{sn}) \quad (2.29)$$



For electrons of the same shell ( $nl$ ), the quantum numbers  $n$  and  $l$  may be omitted, and the two values of the spin quantum number can be denoted by “+” and “-.” For instance, for two equivalent (i.e., with the same  $n$ )  $d$  electrons with quantum numbers  $m_1 = 2, m_{s1} = \frac{1}{2}$  and  $m_2 = 1, m_{s2} = -\frac{1}{2}$  the wavefunction can be written as  $\Phi(2^+, 1^-)$ . As mentioned above, the one-electron functions in the  $LS$  coupling scheme under consideration are presented as a product of the orbital and spin parts,  $\psi(nlmm_s) = \varphi_{nlm}(\mathbf{r}_i, \theta, \phi)\eta_i(m_s)$ , where  $\varphi_{nlm}$  is determined by Eq. (2.1) and  $\eta_i(m_s)$  is the spin state function.

Using these denotations, we demonstrate below how the possible electronic terms of a given configuration can be revealed. Consider an example of two  $d$  electrons above the closed shell of an atom, namely, the configuration  $[A](nd)^2$ . There are five orbital  $d$  states, each having two spin states, hence 10 states are to be occupied by the two electrons under the condition that each state accept only one electron. The number of possible pairs of states equals the number of combination of 10 by 2:  $C_{10}^2 = 10 \times 9/2 = 45$ . For each of these 45 possible states of the  $d^2$  configuration, there is a wavefunction  $\Phi(m_1m_{s1}; m_2m_{s2})$  determined after Eq. (2.28).

If we neglect the interelectron interaction, all these 45 states have the same energy, and there is a 45-fold degeneracy. In Table 2.8 the wavefunctions for these 45 states are grouped according to the values of the quantum numbers of the projection of the summary orbital momentum of the two electrons  $M = m_1 + m_2$  and summary spin  $M_s = m_{s1} + m_{s2}$ . Such tables can be easily composed for any electron configuration of the atom. Then, to obtain the possible terms, one has to separate the groups of states that have the same  $L$  and  $S$ , but different  $M$  and  $M_s$  ( $2L + 1)(2S + 1)$  states in each group (each term).

**TABLE 2.8. All Possible 45 States of Two-Electron  $(nd)^2$  Configuration (in One-Electron Approximation) Classified by Quantum Numbers  $M$  and  $M_s$**

$M$	$M_s$		
	1	0	-1
4		$\Phi(2^+; 2^-)$	
3	$\Phi(2^+; 1^+)$	$\Phi(2^+; 1^-), \Phi(2^-; 1^+)$	$\Phi(2^-; 1^-)$
2	$\Phi(2^+; 0^+)$	$\Phi(2^+; 0^-), \Phi(2^-; 0^+), \Phi(1^+; 1^-)$	$\Phi(2^-; 0^-)$
1	$\Phi(2^+; -1^+)$	$\Phi(2^+; -1^-), \Phi(2^-; -1^+)$	$\Phi(2^-; -1^-)$
	$\Phi(1^+; 0^+)$	$\Phi(1^+; 0^-), \Phi(1^-; 0^+)$	$\Phi(1^-; 0^-)$
0	$\Phi(2^+; -2^+)$	$\Phi(2^+; -2^-), \Phi(2^-; 2^+)$	$\Phi(2^-; -2^-)$
	$\Phi(1^+; -1^+)$	$\Phi(1^+; -1^-), \Phi(1^-; -1^+), \Phi(0^+; 0^-)$	$\Phi(1^-; -1^-)$
-1	$\Phi(1^+; -2^+)$	$\Phi(1^+; -2^-), \Phi(1^-; -2^+)$	$\Phi(1^-; -2^-)$
	$\Phi(0^+; -1^+)$	$\Phi(0^+; -1^-), \Phi(0^-; -1^+)$	$\Phi(0^-; -1^-)$
-2	$\Phi(0^+; -2^+)$	$\Phi(0^+; -2^-), \Phi(0^-; -2^+), \Phi(-1^+; -1^-)$	$\Phi(0^-; -2^-)$
-3	$\Phi(-1^+; -2^+)$	$\Phi(-1^+; -2^-), \Phi(-1^-; -2^+)$	$\Phi(-1^-; -2^-)$
-4		$\Phi(-2^+; -2^-)$	

It is seen from Table 2.8 that the largest value,  $M = 4$ , is possible only in combination with  $M_s = 0$ . Since  $M = L, L - 1, \dots$ , and  $M_s = S, S - 1, \dots$ , the largest  $L$  is also 4 with  $S = 0$ . Thus the term with the largest  $L$  is the spin singlet  ${}^1G$ . This term has  $(2L + 1)(2S + 1) = 9$  states with  $M_s = 0$  and  $M = 4, 3, 2, 1, 0, -1, -2, -3, -4$ . They can be easily found in Table 2.8 and eliminated.

From the remaining states the senior one is that with  $M = 3$  and  $M_s = 1$ . It belongs to the term with  $L = 3$  and  $S = 1$ , specifically, to the  ${}^3F$  term that has  $(2L + 1)(2S + 1) = 21$  states with  $M = 3, 2, 1, 0, -1, -2, -3$ , and  $M_s = 1, 0, -1$  for each  $M$  value. Eliminating them from Table 2.8, we again find the senior state with  $M = 2$  and  $M_s = 0$  that belongs to the  ${}^1D$  term (five states). In a similar way we also find the  ${}^3P$  term (9 states) and the  ${}^1S$  term (one state), thus counting all the 45 states. Hence for the configuration  $[A](nd)^2$  the terms  ${}^1G, {}^3F, {}^1D, {}^3P$ , and  ${}^1S$  are possible. Similarly, the possible terms of all the other configurations  $d^n$  listed in Table 2.6 were found.

The wavefunctions of the atomic terms with certain  $L, M, S$ , and  $M_s$  values  $\Psi(LMSM_s)$  can be found as a linear combination of the functions  $\Phi(m_1m_{s1}; m_2m_{s2})$  [see (2.28)] that satisfy the condition of being an eigenfunction of the operators  $L^2, S^2, L_z, S_z$ . The method of their determination based on the symmetry properties of these operators is given in special manuals [2.1–2.4, 2.13,]. In particular, if the functions are known for some of the  $M$  and  $M_s$  values, they can also be found for other quantum numbers using the following relationships:

$$\begin{aligned} &= (L_x \pm iL_y)\Psi(LMSM_s) \\ &= \hbar[(L \pm M + 1)(L \mp M)]^{1/2}\Psi(L, M \pm 1, S, M_s) \end{aligned} \quad (2.30)$$

$$\begin{aligned} &= (S_x \pm iS_y)\Psi(LMSM_s) \\ &= \hbar[(S \pm M_s + 1)(S \mp M_s)]^{1/2}\Psi(L, M, S, M_s \pm 1) \end{aligned} \quad (2.31)$$

Table 2.9 gives some of the widely used wavefunctions for the terms  ${}^3F$  and  ${}^3P$  of the configurations  $d^2$  and  $d^8$ , as well as  ${}^4F$  and  ${}^4P$  for the configurations  $d^3$  and  $d^7$ . The functions are given for one value of the spin quantum number  $M_s$ ; for the other values of  $M_s$  they can be found from the relation (2.31). The configurations  $d^1, d^4, d^6$ , and  $d^9$ , using the principle of *complementary electronic configurations* (see below), can be presented as one-electron configurations above a closed shell; their functions  $\Psi(L, M, S, M_s)$  coincide with  $\psi(nlmm_s)$ .

### Slater–Condon and Racah Parameters

As mentioned above, without the electron interaction presented by the term  $H' = \sum e^2/r_{ij}$  in the Hamiltonian, all terms of a given electron configuration have the same energy. When the electron interaction is included, the energies of different terms diverge due to the differences in the electron repulsion and exchange interaction. To determine this energy-level splitting, one can consider the electron interaction  $H'$  as a perturbation and solve the perturbation theory

**TABLE 2.9.** Wavefunctions  $\Psi(LMSM_s)$  of Some Terms of  $d^2$  and  $d^3$  Configurations Expressed as Linear Combinations of Determinant Functions  $\Phi(m_1m_{s1}; m_2m_{s2}; \dots)$

Term	$\Psi(LMSM_s)$	$\sum_i C_i \Phi$
${}^3F(d^2)$	$\Psi(3\ 3\ 1\ 1)$	$\Phi(2^+; 1^+)$
	$\Psi(3\ 2\ 1\ 1)$	$\Phi(2^+; 0^+)$
	$\Psi(3\ 1\ 1\ 1)$	$\sqrt{\frac{3}{5}}\Phi(2^+; -1^+) + \sqrt{\frac{2}{5}}\Phi(1^+; 0^+)$
	$\Psi(3\ 0\ 1\ 1)$	$\sqrt{\frac{1}{5}}\Phi(2^+; -2^+) + \sqrt{\frac{4}{5}}\Phi(1^+; -1^+)$
	$\Psi(3\ -1\ 1\ 1)$	$\sqrt{\frac{3}{5}}\Phi(1^+; -2^+) + \sqrt{\frac{2}{5}}\Phi(0^+; -1^+)$
	$\Psi(3\ -2\ 1\ 1)$	$\Phi(0^+; -2^+)$
	$\Psi(3\ -3\ 1\ 1)$	$\Phi(-1^+; -2^+)$
${}^3P(d^2)$	$\Psi(1\ 1\ 1\ 1)$	$\sqrt{\frac{2}{5}}\Phi(2^+; -1^+) - \sqrt{\frac{3}{5}}\Phi(1^+; 0^+)$
	$\Psi(1\ 0\ 1\ 1)$	$\sqrt{\frac{4}{5}}\Phi(2^+; -2^+) - \sqrt{\frac{1}{5}}\Phi(1^+; -1^+)$
	$\Psi(1\ -1\ 1\ 1)$	$\sqrt{\frac{2}{5}}\Phi(1^+; -2^+) - \sqrt{\frac{3}{5}}\Phi(0^+; -1^+)$
${}^4F(d^3)$	$\Psi(3\ 3\ \frac{3}{2}\ \frac{3}{2})$	$\Phi(2^+; 1^+; 0^+)$
	$\Psi(3\ 2\ \frac{3}{2}\ \frac{3}{2})$	$\Phi(2^+; 1^+; -1^+)$
	$\Psi(3\ 1\ \frac{3}{2}\ \frac{3}{2})$	$\sqrt{\frac{2}{5}}\Phi(2^+; 1^+; -2^+) + \sqrt{\frac{3}{5}}\Phi(2^+; 0^+; -1^+)$
	$\Psi(3\ 0\ \frac{3}{2}\ \frac{3}{2})$	$\sqrt{\frac{4}{5}}\Phi(2^+; 0^+; -2^+) + \sqrt{\frac{1}{5}}\Phi(1^+; 0^+; -1^+)$
	$\Psi(3\ -1\ \frac{3}{2}\ \frac{3}{2})$	$\sqrt{\frac{2}{5}}\Phi(2^+; -1^+; -2^+) + \sqrt{\frac{3}{5}}\Phi(1^+; 0^+; -2^+)$
	$\Psi(3\ -2\ \frac{3}{2}\ \frac{3}{2})$	$\Phi(1^+; -1^+; -2^+)$
	$\Psi(3\ -3\ \frac{3}{2}\ \frac{3}{2})$	$\Phi(0^+; -1^+; -2^+)$
${}^4P(d^3)$	$\Psi(1\ 1\ \frac{3}{2}\ \frac{3}{2})$	$\sqrt{\frac{3}{5}}\Phi(2^+; 1^+; -2^+) - \sqrt{\frac{2}{5}}\Phi(2^+; 0^+; -1^+)$
	$\Psi(1\ 0\ \frac{3}{2}\ \frac{3}{2})$	$\sqrt{\frac{1}{5}}\Phi(2^+; 0^+; -2^+) - \sqrt{\frac{4}{5}}\Phi(1^+; 0^+; -1^+)$
	$\Psi(1\ -1\ \frac{3}{2}\ \frac{3}{2})$	$\sqrt{\frac{3}{5}}\Phi(2^+; -1^+; -2^+) - \sqrt{\frac{2}{5}}\Phi(1^+; 0^+; -2^+)$

problem, taking the functions  $\Psi(LMSM_s)$  as zeroth-order functions. The corresponding secular equation of perturbation theory is then essentially simplified because the operators  $L^2$ ,  $S^2$ ,  $L_z$ , and  $S_z$  commute with  $H'$ . This means that with the functions  $\Psi$  that are eigenfunctions of the operators above, only matrix elements of the perturbation  $H'$  that are diagonal in  $L$  and  $S$  are nonzero, and they are the same for different  $M$  and  $M_s$ . In other words, the energy corrections  $\Delta E$  caused by electron interaction are the same for all states with the same  $LS$  value, and can be found directly as diagonal matrix elements:

$$\Delta E(L, S) = \int \frac{\sum e^2}{r_{ij}} |\Psi(LMSM_s)|^2 d\tau \quad (2.32)$$

Off-diagonal matrix elements of  $H'$  may also be nonzero if the wavefunctions of the two states pertain to different configurations, and they were calculated in the Hartree–Fock or other approximation *without including correlation effects* (the exact wavefunctions are mutually orthogonal and yield zero off-diagonal matrix elements of  $H'$ ). To judge which such states can interact, a simple symmetry argument can be invoked:  $H'$  is invariant to all symmetry operations of the atom (spherical group) and thus belongs to the totally symmetric representation of this group (Chapter 3), and hence integrals such as (2.32) are nonzero only if the two states from different configurations have the same symmetry. This is the origin of the term *configuration interaction* used to evaluate the electron correlation effects (see Section 5.3 for more details).

The way of calculation of integrals of the type (2.32) is well known. Since  $\Psi$  is a linear combination of  $\Phi$  in Table 2.9, Eq. (2.32) can be reduced to integrals of the following type:

$$\int \Phi^*(m_1, m_{s1}, \dots) \frac{e^2}{r_{ij}} \Phi(m'_1 m'_{s1}, \dots) d\tau \quad (2.33)$$

This integral equals zero when the two functions  $\Phi$  differ by more than two one-electron states. Indeed, different one-electron functions are orthogonal to each other, and since  $r_{12} = |\mathbf{r}_1 - \mathbf{r}_2|$  depends on the coordinates of only two electrons, the integration over the other coordinates with orthogonal functions yields zero. For instance

$$\int \Phi^*(2^+; 1^-; 0^+) \sum_{i,j} \frac{1}{r_{ij}} \Phi(1^+; 2^-; 0^-) d\tau = 0$$

whereas

$$\int \Phi^*(2^+; 1^-; 0^+) \sum_{i,j} \frac{1}{r_{ij}} \Phi(2^+; 2^-; 1^+) d\tau \neq 0$$

Thus only four one-electron functions (two from each side) can differ in the nonzero integrals (2.33); denote them by  $a, b, c$ , and  $d$ . Then the expression for  $\Delta E$  is reduced to a sum of two-electron integrals of the following type:

$$[ab|cd] = \int a^*(1)b(1) \frac{e^2}{r_{12}} c^*(2)d(2) d\tau_1 d\tau_2 \quad (2.34)$$

In the notation on the left-hand side of Eq. (2.34), widely employed in quantum chemistry,  $a$  and  $b$  are one-electron functions of the first electron, while  $c$  and  $d$  contain the coordinates of the second electron. Some of these one-electron functions can coincide. In particular, the following integrals

$$[aa|bb] = I(a, b) = \int a^*(1)a(1) \frac{e^2}{r_{12}} b^*(2)b(2) d\tau_1 d\tau_2 \quad (2.35)$$

$$[ab|ba] = K(a, b) = \int a^*(1)b(1)\frac{e^2}{r_{12}}b^*(2)a(2) d\tau_1 d\tau_2 \quad (2.36)$$

are most usable. The first one, called *the Coulomb integral*, equals the energy of the electrostatic repulsion of two electron clouds described by the one-electron probability distributions  $a^2(1)$  and  $b^2(2)$ , respectively.  $K(a, b)$  is termed *the exchange integral* representing the energy decrease caused by the exchange interaction between the two electrons in the states  $a$  and  $b$ .

To calculate the integral (2.34), the following expression is useful:

$$\frac{1}{r_{12}} = \sum_{k=0}^{\infty} K_k(r_1, r_2) P_k(\cos \gamma_{12}) \quad (2.37)$$

where

$$K_k(r_1, r_2) = \begin{cases} r_1^k/r_2^{k+1} & \text{if } r_1 < r_2 \\ r_2^k/r_1^{k+1} & \text{if } r_2 < r_1 \end{cases} \quad (2.38)$$

and  $P_k(\cos \gamma_{12})$  is the Legendre polynomial [Eq. (2.3) with  $m = 0$ ] of the argument  $\cos \gamma_{12} = \cos \theta_1 \cos \theta_2 + \sin \theta_1 \sin \theta_2 \cos(\phi_1 - \phi_2)$ . Substituting the one-electron functions  $a, b, c$ , and  $d$  by their expressions of the type (2.1) together with (2.37) and (2.38) into (2.34) and using some orthogonality conditions for the spherical functions, one can integrate over the angular coordinates, thus reducing the expression for  $[ab|cd]$  to a limited number of two-electron radial integrals of the following type:

$$\begin{aligned} R^{(k)}(abcd) &= e^2 \int \int R_{n(a)l(a)}^*(r_1) R_{n(b)l(b)}(r_1) K_k(r_1, r_2) \\ &\quad \times R_{n(c)l(c)}^*(r_2) R_{n(d)l(d)}(r_2) r_1^2 r_2^2 dr_1 dr_2 \end{aligned} \quad (2.39)$$

For the Coulomb and exchange contributions, the following notations are used:

$$R^{(k)}(aabb) = F^{(k)} \quad (2.40)$$

$$R^{(k)}(abba) = G^{(k)} \quad (2.41)$$

The constants  $F^{(k)}$  and  $G^{(k)}$  are referred to as *Slater–Condon parameters*. For electrons that have the same  $n$  and  $l$  values (such electrons are called *equivalent* because of their equivalent orbitals), all the radial integrals  $R^{(k)}$  are of the  $F^{(k)}$  type. In atomic calculations the parameters  $F_k$  are more convenient; they differ from  $F^{(k)}$  by a numerical coefficient. For instance, for equivalent  $d$  electrons the nonzero  $F_k$  parameters are

$$F_0 = F^{(0)} \quad F_2 = \frac{1}{49} F^{(2)} \quad F_4 = \frac{1}{144} F^{(4)} \quad (2.42)$$

Finally, in many cases combinations of Slater–Condon parameters, known as *Racah parameters*, are used:

$$A = F_0 - 49F_4 \quad B = F_2 - 5F_4 \quad C = 35F_4 \quad (2.43)$$

The correction to the energy due to electron interactions and hence the relative energies of atomic terms of  $d^n$  configuration expressed in terms of Racah parameters  $A, B, C$  are given in Table 2.6.

To calculate the Racah parameters, as seen from expression (2.39), the radial wavefunctions of the atomic one-electron states are needed. More often it is preferred to consider the values  $A, B, C$  as empirical parameters and to determine them from the comparison of the calculated energies with those determined experimentally from spectroscopic data. For the electronic configuration  $[A](nd)^2$  discussed above, the energy difference between the terms  ${}^3F$  and  ${}^3P$  is  $E({}^3P) - E({}^3F) = 15B$  (Table 2.6). On the other hand, the experimental value of this splitting, for instance, for  $V^{3+}(3d^2)$ , is  $\approx 13000 \text{ cm}^{-1}$ ; hence  $B \approx 870 \text{ cm}^{-1}$ . Some values of the Racah parameters for transition metal ions and their complexes are given in Tables 4.7 (Section 4.5) and 8.3 (Section 8.2). Sometimes the following estimations for Slater–Condon parameters for  $f$  electrons are useful [2.14]:  $F_4 \leq 0.202F_2$ , and  $F_6 \leq 0.0306F_2$ .

In many cases there is no need for detailed calculation of the energy terms for all possible electron configurations of the atom because for some of them the electronic terms can be revealed directly from other configurations using *the principle of complementary configurations*. According to this principle, the configuration with  $n$  equivalent electrons has the same types of terms as the configuration  $N - n$ , where  $N$  is the number of electrons in the closed shell under consideration. The reason is that formally the problem of  $n$  electrons is equivalent to that of  $N - n$  “holes,” and hence the problem of  $n$  particles can be reduced to that of  $N - n$  (other) particles. The reduction of computation work by using this principle is significant; for the configuration  $d^9$  the terms are equivalent to those of  $d^1$ , for  $d^8$  - to  $d^2$ , for  $d^7$  - to  $d^3$ , and so on. The rule is also valid for half-filled shells for which all the orbital states are occupied (orbitally closed shell). This means that for  $d^4$  one can use the configurations of  $d^{5-4} = d^1$  ( $d^5$  is a half-filled shell), for  $d^6$  - that of  $d^{10-6} \rightarrow d^4 \rightarrow d^1$ , and so on. Thus all the terms of  $d^n$  configurations can be reduced to those of  $d^1$  and  $d^2$ . Tables 2.6 and 2.9 are based on this principle.

### The Hartree–Fock Method

The Hartree–Fock method of calculation is of general importance serving as a starting point to many other methods of investigation of multiparticle systems. For multielectron systems (atoms, molecules, crystals) the Hartree–Fock method [2.1–2.4] yields the best solutions (one-electron functions and energies) compatible with the approximation of full separation of the electron variables, that is, ignoring correlation effects (Section 5.3). The importance of this method and its

self-consistent procedure can hardly be overestimated because *it lies in the base of the entire gamut of modern computational chemistry and physics.*

To disclose the essence of this method, let us begin with the *Hartree* approximation. Assume that each electron can be considered as moving independently in an averaged field created by the nucleus and the other electrons. This means that its wavefunction  $\varphi_i(\mathbf{r}_i)$  is independent of the variables of other electrons, and the expression  $|\varphi_i(\mathbf{r}_i)|^2$  is the probability density of finding the  $i$ th electron at point  $r_i$ . Since the probability of simultaneously occurring independent events equals the product of probabilities of each event, the electronic wavefunction of the system as a whole can be presented in the form of a simple product of the one-electron functions  $\varphi_i(\mathbf{r}_i)$ :

$$\Phi(\mathbf{r}_1, \mathbf{r}_2, \dots, \mathbf{r}_n) = \varphi_1(\mathbf{r}_1)\varphi_2(\mathbf{r}_2) \cdots \varphi_n(\mathbf{r}_n) \quad (2.44)$$

This means that  $|\Phi|^2$  is the density of the probability of finding electron 1 at  $\mathbf{r}_1$ , electron 2 at  $\mathbf{r}_2$ , and so on. The functions  $\varphi_i(\mathbf{r})$  are assumed to be orthonormalized:

$$\int \varphi_i^*(\mathbf{r})\varphi_j(\mathbf{r}) d\tau = \delta_{ij} \quad i, j = 1, 2, \dots, n \quad (2.45)$$

Hereafter in this book,  $\delta_{ij}$  means *the Kroneker index* (or  $\delta$  symbol):

$$\delta_{ij} = \begin{cases} 0 & \text{if } i \neq j \\ 1 & \text{if } i = j \end{cases} \quad (2.46)$$

To determine the functions  $\varphi(\mathbf{r})$ , *the variational principle* can be employed. This principle states that the functions (2.44) sought for must obey the condition of the minimal total energy  $E$  of the system,  $\delta E = 0$  (here  $\delta$  means variation, not to be confused with the Kroneker index  $\delta_{ij}$ ) calculated with the Hamiltonian  $H$  of the Schrödinger equation:

$$E = \int \Phi^* H \Phi d\tau \quad (2.47)$$

$$\delta E = \delta \int \Phi^* H \Phi d\tau = 0 \quad (2.48)$$

By substituting (2.44) into (2.48) with the Hamiltonian from Section 1.3 and varying the unknown functions  $\varphi_i(\mathbf{r}_i)$ , one finds the following system of equations for these functions:

$$[H^0 + V_k(\mathbf{r}) - \varepsilon_k] \varphi_k(\mathbf{r}) = 0 \quad k = 1, 2, \dots, n \quad (2.49)$$

where  $H^0$  is the part of the Hamiltonian that contains the kinetic energy  $T$  and the energies of interaction with the nuclei  $U_\alpha$ :

$$H^0 = T - \sum_{\alpha} U_{\alpha} = -\frac{\hbar^2}{2m} \Delta - \sum_{\alpha} \frac{e^2 Z_{\alpha}}{|\mathbf{r} - \mathbf{R}_{\alpha}|} \quad (2.50)$$

and  $V_k(\mathbf{r})$  is the sum of the energies of the electrostatic repulsive interaction of the  $k$ th electron with the charges of the  $i$ th electrons distributed in space with the densities  $e|\varphi_i(\mathbf{r}_i)|^2$ :

$$V_k(\mathbf{r}) = \sum_{i \neq k} e^2 \int \frac{|\varphi_i(\mathbf{r}')|^2}{|\mathbf{r} - \mathbf{r}'|} d\tau \quad (2.51)$$

The system of equations (2.49) describes the full separation of the variables of the electrons; each of its  $n$  equations contains the coordinates of only one electron. They are complicated, integrodifferential equations (the unknown function is under both differentiation and integration) that can be solved by means of a special iteration procedure termed *the self-consistent field (SCF) method*. The fundamentals of this method are as follows.

Assume that we have a set of functions  $\varphi_k(\mathbf{r})$ —the initial set—obtained, for instance, by ignoring the electron interaction [i.e., assuming  $V_k(\mathbf{r}) = 0$  in Eq. (2.49)]. With these functions, all the terms  $V_k(r)$  after (2.51) and their sum (the average potential of interaction of one electron with all the others) can be evaluated. By substituting these terms into the system (2.49), one obtains  $n$  independent simple differential equations that can be solved numerically. These solutions yield a new system of functions  $\varphi'$  (and eigenvalues  $\varepsilon'$ ) that are more accurate than the initial set  $\varphi$  because the electron interaction has been accounted for. With the more accurate functions one can calculate more accurate potentials of the interelectronic interaction  $V'_k(\mathbf{r})$  and again solve Eqs. (2.49) with these better potentials, and so on, until the new eigenfunctions  $\varphi_k$  and new eigenvalues  $\varepsilon_k$  coincide with the previous values (within the accuracy required). The solutions obtained in this way are called *self-consistent solutions*. The self-consistent method described above was suggested first by Hartree [2.15].

However, as shown by Fock [2.16], the presentation (2.44) of the wavefunction  $\Phi$  as a simple product of one-electron functions  $\varphi$  does not satisfy the condition of undistinguishability of the electrons that requires the total wavefunction to be antisymmetric with respect to the permutation of the coordinates of any two electrons. To obey this condition in the case of a closed-shell system, the wavefunction  $\Phi$  should be presented in the form of the determinant (2.28) constructed by the functions  $\varphi_i(\mathbf{r})$ . The substitution of this determinant function into Eq. (2.48) and the consequent variation of the functions  $\varphi_k(\mathbf{r})$  yields the following system of equations instead of (2.49):

$$\begin{aligned} & \left[ H^0 + 2 \sum_{i=1}^{n/2} \frac{e^2 \int \varphi_i^*(\mathbf{r}') \varphi_i(\mathbf{r}')}{|\mathbf{r} - \mathbf{r}'|} d\tau' - 2\varepsilon_{kk} \right] \varphi_k(\mathbf{r}) \\ & - \sum_{i=1}^{n/2} \left[ \frac{e^2 \int \varphi_i^*(\mathbf{r}') \varphi_k(\mathbf{r}')}{|\mathbf{r} - \mathbf{r}'|} d\tau' - \varepsilon_{ik} \right] \varphi_i(\mathbf{r}') = 0 \end{aligned} \quad (2.52)$$



Here it is taken into account that in accordance with the assumption of a closed shell, the number of electrons  $n$  is even, and in each of the orbital states  $\varphi_k(\mathbf{r})$  there are two electrons with opposite spins. The second sum in (2.52) is the so-called exchange correction that arises additionally [as compared with (2.49)] from the undistinguishability principle, the *exchange interactions*. Exchange interactions are nonzero for electrons with the same spin states only, and therefore the number of terms in the second sum in (2.52) is half that in the first sum, the electrostatic interactions.

The term with  $i = k$  from the exchange sum that corresponds to the interaction of the electron with itself vanishes automatically since it is present in both sums of (2.52) with opposite signs [the remaining term with  $i = k$  in the first sum (which has the factor 2) denotes the electrostatic interaction of the  $i$ th electron with the other one in the same orbital state  $\varphi_i(\mathbf{r})$  but with an opposite spin].

The constants  $\varepsilon_{ik}$  occur as Lagrange factors at the condition of normalization and orthogonality of the functions  $\varphi_k$  and  $\varphi_i$  (2.45). The most part of these constants can be eliminated by substituting  $\varphi_i$  with their linear combinations  $\varphi'_i$ . In other words, we can perform a unitary transformation [see Eq. (3.11)] of the set of functions  $\varphi_i$  to another set  $\varphi'_i$  for which the off-diagonal values  $\varepsilon'_{ik}$  become zero. Unitary transformations do not change the initial determinant function (2.28) and hence the energy of the system [2.17].

Denoting the remaining diagonal value  $\varepsilon_{kk} = E_k$  and introducing the operator  $P_{ik}$  that interchanges the indices  $i$  and  $k$  of the function on which it acts, we have (the prime at  $\varphi'$  is omitted):

$$\left[ H^0 + \sum_i \frac{e^2 \int \varphi_i^*(\mathbf{r}') (2 - P_{ik}) \varphi_i(\mathbf{r}')}{|\mathbf{r} - \mathbf{r}'|} d\tau' - E_k \right] \varphi_k(\mathbf{r}) = 0 \quad k = 1, 2, \dots, \frac{n}{2} \quad (2.53)$$

This is *the system of Hartree–Fock (HF) self-consistent field (SCF) equations* for a multielectron system with a closed electronic shell. It can be solved in the same manner as discussed above for the Hartree equations yielding self-consistent one-electron states—wavefunctions  $\varphi_k(\mathbf{r})$  and eigenvalue  $E_k$ . The latter has the physical meaning of the one-electron orbital energy in the self-consistent state  $\varphi_k(\mathbf{r})$ .

Equations (2.53) can be written in the form of a usual Schrödinger equation:

$$F^k \varphi_k(\mathbf{r}) = E_k \varphi_k(\mathbf{r}) \quad (2.54)$$

where

$$F^k = H^0 + \sum_i \frac{e^2 \int \varphi_i^*(\mathbf{r}') (2 - P_{ik}) \varphi_i(\mathbf{r}')}{|\mathbf{r} - \mathbf{r}'|} d\tau' \quad (2.55)$$

is the Fock effective one-electron Hamiltonian, sometimes called *Fockian*. Multiplying Eq. (2.53) or (2.54) by  $\varphi_k(r)$  from the left-hand side and integrating over  $r$ , one finds

$$\begin{aligned} E_k &= H_{kk}^0 + \sum_i (2[ii|kk] - [ik|ki]) \\ &= H_{kk}^0 + \sum_i [2I(i, k) - K(i, k)] \end{aligned} \quad (2.56)$$

where the notation (2.35) for the Coulomb integral  $I(i, k) = [ii|kk]$  and (2.36) for the exchange one  $K(i, k) = [ik|ki]$  are used. Accounting for the expression (2.50) for  $H^0$ , we conclude that the self-consistent energy of the  $k$ th electron in the one-electron state equals the sum of its kinetic energy, the energy of interaction with the nuclei, and the energy of the Coulomb and exchange interelectron interactions.

In fact,  $E_k$  equals the energy that must be applied to withdraw the  $k$ th electron from the atom, *the ionization energy*, provided all the other one-electron states are not changed by the transition to the ionized state. This statement is known as *the Koopmans theorem* [2.18]. For many coordination systems the Koopmans theorem is invalid because of the significant changes in the one-electron states (interelectron interaction) caused by the elimination of one electron; on ionization the remaining electrons relax to new self-consistent states (see Sections 6.2, 6.4, 8.3, etc.).

For the sum of the one-electron energies of the  $n$  electrons, we have

$$2 \sum_{k=1}^{n/2} E_k = 2 \sum_{k=1}^{n/2} H_{kk}^0 + 2 \sum_{k=1}^{n/2} [2I(i, k) - K(i, k)] \quad (2.57)$$

It is important that in this sum the interelectron interaction is included twice: once in the sum of the interaction of a given  $i$ th electron with all the others (including the  $k$ th electron) and the second time in the sum of the interaction of the  $k$ th electron with all the others also including the  $i$ th one. Therefore, to obtain the total energy of the system  $E$ , the interelectron interaction should be subtracted once from the expression (2.57). Hence

$$E = 2 \sum_{k=1}^{n/2} H_{kk}^0 + \sum_{k=1}^{n/2} [2I(i, k) - K(i, k)] \quad (2.58)$$

For a system with an open shell of electrons the Hartree–Fock equations (2.53) become much more complicated. This problem is discussed further in Section 5.3.

**SUMMARY NOTES**

1. *Atomic states* are basic elements (elementary bricks) of electronic structure of transition metal systems (TMSs).
2. The usually presented space distributions of the degenerate  $p, d, \dots$  states of free atoms are virtual; they become real (in the sense of charge distribution) only under external perturbations, such as by bonding to other atoms, in which case they may also become mixed, hybridized. *Hybridization* is thus a bonding effect.
3. The interaction between the magnetic moment of the electron spin and the magnetic field of its orbital motion (*spin-orbital interaction*) is one of the most essential relativistic effects, unavoidable even in nonrelativistic treatment of molecular systems. Spin-orbital interaction is much more significant for TMS than for organic compounds.
4. *Relativistic atomic functions* have some peculiar properties making them much different from nonrelativistic (NR) ones. In particular, their radial part has no nodes, the  $p_{1/2}$  function is spherical symmetric (similar to the NR  $s$  function), and their overlap does not produce pure  $\sigma$  or pure  $\pi$  bonding (they are mixed, etc.; see also Section 6.5).
5. Each *electronic configuration* of multielectron atoms produces several electronic terms with different electron spins and distributions over the one-electron states. *Electronic terms* have different energies and wavefunctions because of the differences in electron repulsion and exchange interaction.
6. In the iterative *self-consistent field* (SCF) approximation the averaged field for each electron is calculated first with some guesswork functions and are used to solve equations to obtain better wavefunctions, which are used to recalculate the (better) averaged field, and so on, until the resulting energy and wavefunction coincide with the previous one. This *Hartree-Fock SCF procedure* is a starting point in almost all the modern methods of calculation of electronic structure.

**QUESTIONS**

Answer the following questions (explain your answer): *True or false?*

- 2.1. The charge distribution of a  $d$  electron in a free transition metal atom has the characteristic angular features of a  $d$  function in Fig. 2.3.
- 2.2. As a result of orbital  $sp^3$  hybridization, a free carbon atom has four tetrahedrally directed valences.
- 2.3. Spin-orbital interaction is zero for  $s$  electrons.
- 2.4. For both light and heavy atoms the total electronic wavefunction of an atom equals the product of the orbital and spin wavefunctions.

- 2.5. The overlap integral between the orbitals of two atoms cannot be larger than unity.
- 2.6. For transition metal compounds the spin-orbital coupling is negligible.
- 2.7. Slater-Condon parameters describe the interelectron interaction in atoms.

### EXERCISES AND PROBLEMS

*Note:* Asterisks indicate advanced exercises and problems.

- P2.1.** Use Eqs. (2.1)–(2.5) to calculate the explicit radial and angular atomic functions for  $5d$  and  $5f$  electrons. How many nodes (zeros) have the radial functions? Are there nodes in the corresponding relativistic radial atomic functions?
- P2.2.** Albright and Burdett [2.19, p. 28] stated that hybridized  $sp^3$  atomic functions are nonorthogonal to each other. On the other hand, in Section 2.1 of this book, it is stated that the coefficients of the hybridized functions are determined from the condition of their orthogonality. Resolve this controversy by showing that the hybridized functions of any type ( $sp^2$ ,  $sp^3$ , and  $d^2sp^3$  orbitals in Table 2.4) are mutually orthogonal.
- P2.3.** Explain the difference between Russell-Saunders  $LS$  and heavy-atom  $j-j$  coupling of moments and spins of electrons in atoms. Give examples of these two types of coupling in interelectron interactions.
- P2.4.** From the list of the terms of electronic  $d^n$  configurations and their energies as a function of Racah parameters in Table 2.6, we can see that the complementary configurations  $d^n$  and  $d^{10-n}$  have the same terms and energy functions (the latter may differ by a constant meaning by just the energy read off.). Explain why this occurs.
- \*P2.5.** Using Tables 2.6, 4.7, and 8.3, construct the energy-level diagrams (positions of term energies) for the first row transition metal ions with electronic configurations  $[A](3d)^2$  and  $[A](3d)^3$ , respectively. Take the energy read off at the Racah parameter  $A = 0$ .
- P2.6.** On the basis of the system of equations (2.53), formulate in writing how, step by step, the iterative SCF procedure is used to solve the problem of electronic structure. What is the physical meaning of the orbital energies  $E_k$  and wavefunctions  $\phi_k(\mathbf{r})$  obtained from these solutions?

### REFERENCES

- 2.1. H. Eyring, J. Walter, and G. E. Kimball, *Quantum Chemistry*, Wiley, New York, 1947.
- 2.2. J. C. Slater, *Quantum Theory of Atomic Structure*, Mc-Graw-Hill, New York, 1960.
- 2.3. E. U. Condon, *The Theory of Atomic Spectra*, Cambridge Univ. Press, Cambridge, UK, 1959.

- 2.4. P. Gombas, *Theorie und Lösungsmethoden des Mehrteilchenproblems der Wellenmechanik*, Basel, 1950.
- 2.5. H. A. Bethe and E. E. Salpeter, *Quantum Mechanics of One and Two-Electron Atoms*, Springer, Berlin, 1957.
- 2.6. F. Herman and S. Skillman, *Atomic Structure Calculations*, Prentice-Hall, Englewood Cliffs, NJ, 1963.
- 2.7. S. Fraga and J. Karwowski, *Tables of Hartree-Fock Atomic Data*, Univ. Alberta, Canada, 1974,
- 2.8. E. Clementi, *IBM J. Res. Devel.* **9**, 2 (1965), Supplement, *Tables of Atomic Functions*, IBM, 1965, Tables 1–45.
- 2.9. J. W. Richardson, W. C. Nieuwpoort, and R. R. Powell, *J. Chem. Phys.* **36**, 1057 (1962); J. W. Richardson, P. R. Powell, and W. C. Nieuwpoort, *ibid.*, **38**, 796 (1963).
- 2.10. J. N. Murrell, S. F. A. Kettle, and J. M. Tedder, *Valence Theory*, Wiley, New York, 1965.
- 2.11. R. E. Powel, *Chem. Educ.* **45**, 558 (1968).
- 2.12. M. A. El'yashevich, *Rare Earth Spectra* (Russ.), Moscow, Gostechteorizdat, 1953.
- 2.13. H. L. Schlafer and G. Glieman, *Basic Principles of Ligand Field Theory*, Wiley, New York, 1969.
- 2.14. C. K. Jorgensen, *Kgl. danske Vid.* **29**, 1 (1955).
- 2.15. D. Hartree, *The Calculations of Atomic Structures*, Wiley, New York, 1957.
- 2.16. V. A. Fock, *Z. (Zeitschrift) Phys.* **61**, 126 (1930); **62**, 795 (1930).
- 2.17. J. C. Slater, *Electronic Structure of Molecules*, McGraw-Hill, New York, 1963.
- 2.18. T. Koopmans, *Physica* **1**, 104 (1933).
- 2.19. T. A. Albright and J. K. Burdett, *Problems in Molecular Orbital Theory*, Oxford Univ. Press, New York, 1992.

---

# 3

---

## SYMMETRY IDEAS AND GROUP-THEORETICAL DESCRIPTION

*In the theory of electronic structure and properties of transition metal coordination compounds the ideas of symmetry are of great, sometimes fundamental importance.*

The most complete description of symmetry properties is achieved in the mathematical group theory. In this chapter we give minimum information about some rules worked out by group-theoretical methods that are required for a better understanding of the presentation in this book (for more details on group theory see, e.g., Refs. 3.1–3.8).

### 3.1. SYMMETRY TRANSFORMATIONS AND MATRICES

*Molecular symmetry* is the property of a molecule to remain invariant under certain rotations and reflections in space and permutations of identical particles. These rotations, reflections, and permutations are called *symmetry operations*, or *symmetry transformations*. For instance, in the equilateral planar-triangular configuration of the molecule  $V_3$ , the symmetry transformations are (Fig. 3.1) rotations around the  $Oz$  axis (which is perpendicular to the plane of the molecule) by angles  $2\pi/3$ ,  $4\pi/3$ ,  $2\pi$ , and around the axes  $A_1B_1$ ,  $A_2B_2$ , and  $A_3B_3$  by angles  $\pi$  and  $2\pi$ , as well as reflection in the planes that comprise these axes and are perpendicular to the plane of the molecule, and reflection in the plane of the triangle.

---

*Electronic Structure and Properties of Transition Metal Compounds: Introduction to the Theory,*  
Second Edition By Isaac B. Bersuker  
Copyright © 2010 John Wiley & Sons, Inc.

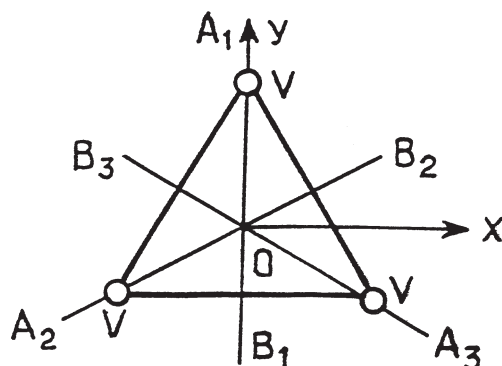


FIGURE 3.1. Symmetry elements of an equilateral triangle.

For the simplest symmetry operations in space, namely, rotation and reflections (for crystals there are also translations), there are conventional notations. The *rotation* around some axis by the angle  $2\pi/n$  is denoted by  $C_n$ . It is obvious that if, after some rotation, the molecule is matched with itself, it will behave in the same way when this rotation is repeated an integer number of times.

The result of *consequent performance of two symmetry operations is defined as their product*. If  $C_n$  is a symmetry operation of the molecule, then  $C_n \cdot C_n = C_n^2$  is also a symmetry operation. In general,  $C^p$  with any integer  $p$  is also a symmetry operation. In particular,  $C_n^n$  is a rotation by an angle  $2\pi$  that does not change the position of the molecule in space; this is the *identical operation E*; hence  $C_n^n = E$ . The axis of rotation in the  $C_n$  operation is called the *symmetry axis of the order n*, or *n-fold axis*.

The symmetry operation  $\sigma$  denotes the *reflection in a plane*; obviously,  $\sigma^2 = E$ . If there is also an axis of symmetry, the reflection in the plane containing this axis is denoted by  $\sigma_v$  or  $\sigma_d$ , while the reflection in the plane perpendicular to the axis of symmetry is  $\sigma_h$ . The consequent performance of the operations  $C_n$  and  $\sigma_h$ , their product  $C_n \cdot \sigma_h = S_n$ , is called the *reflection-rotation operation*. In particular, the rotation by an angle  $\pi$  ( $C_2$ ) followed by the reflection in the plane perpendicular to the rotation axis  $\sigma_h$ , is the *inversion operation I* with respect to the point where the axis crosses the plane:  $I = S_2 = C_2 \cdot \sigma_h$ . From these simple operations all the symmetry transformations of molecules can be deduced.

The term *transformations* for these rotations and reflections comes from their mathematical expression by simple linear transformations of the coordinate system. For instance, the rotation of the molecule by an angle  $\phi$  around the axis  $Oz$  is equivalent to the transformation of the coordinate system in which the point  $M(x, y, z)$  is transferred to  $M'(x', y', z')$  and

$$\begin{aligned} x' &= x \cos \phi + y \sin \phi \\ y' &= -x \sin \phi + y \cos \phi \\ z' &= z \end{aligned} \tag{3.1}$$

Such transformations are used very often; therefore, it is convenient to simplify their notation. First, let us write Eq. (3.1) in a more symmetric form:

$$\begin{aligned}x' &= \cos \phi \cdot x + \sin \phi \cdot y + 0 \cdot z \\y' &= -\sin \phi \cdot x + \cos \phi \cdot y + 0 \cdot z \\z' &= 0 \cdot x + 0 \cdot y + 1 \cdot z\end{aligned}\tag{3.1'}$$

We see that the transformation (3.1) is determined by a set of coefficients that can be arranged in a quadratic table:

$$A = \begin{pmatrix} \cos \phi & \sin \phi & 0 \\ -\sin \phi & \cos \phi & 0 \\ 0 & 0 & 1 \end{pmatrix}\tag{3.2}$$

This table is called *the matrix of the transformation* (3.1). By means of the matrix  $A$ , the transformation of  $M$  into  $M'$  can be written in a much simpler (compact) form:

$$M' = AM\tag{3.3}$$

where  $A$  means that a special operation given by the system of equation (3.1) (and denoted by the matrix  $A$ ) should be performed on the coordinates of  $M$ .

The transformation of an arbitrary function of coordinates  $f(x, y, z)$  via the transformation of the coordinates (3.1) can be written in a similar way:

$$f(x', y', z') = Af(x, y, z)\tag{3.3'}$$

Here  $A$  means that the operation (3.1) should apply to all the coordinates, and in this way the whole function  $f$  changes. The symbol  $A$ , indicating a certain operation to be performed over the function that follows  $A$ , is called an *operator*. Hence each symmetry transformation can be presented by a certain matrix-operator.

If one performs a backrotation (i.e., a rotation by the angle  $-\phi$ ) on the same system, then the point  $M'$  is transferred back to  $M$ , and it can be shown using Eqs. (3.1) that the transformation of  $M'(x', y', z')$  into  $M(x, y, z)$  has the following form:

$$\begin{aligned}x &= x' \cos \phi - y' \sin \phi \\y &= x' \sin \phi + y' \cos \phi \\z &= z'\end{aligned}\tag{3.4}$$



with the matrix

$$A' = \begin{pmatrix} \cos \phi & -\sin \phi & 0 \\ \sin \phi & \cos \phi & 0 \\ 0 & 0 & 1 \end{pmatrix} \quad (3.5)$$

This transformation can be written more compactly as

$$M = A'M' \quad (3.6)$$

Obviously the consequent application of the operations  $A$  and  $A'$  to point  $M$  transfers this point into itself; hence

$$AA'M = M \quad (3.7)$$

or  $AA' = E$ , the identical transformation. It can be shown that  $E$  is always a diagonal unity matrix with zero off-diagonal elements and units in the diagonal positions. In particular, in the three-dimensional case discussed above, we obtain

$$E = \begin{pmatrix} 1 & 0 & 0 \\ 0 & 1 & 0 \\ 0 & 0 & 1 \end{pmatrix} \quad (3.8)$$

which corresponds to the transformation:

$$\begin{aligned} x &= x' \\ y &= y' \\ z &= z' \end{aligned} \quad (3.9)$$

The condition  $AA' = E$  means that  $A$  and  $A'$  are *mutually inverse matrices*. If some transformation is described by the matrix  $A$ , then the inverse transformation  $A'$  is described by the inverse matrix  $A^{-1}$ . The latter can be obtained from the former by means of a simple transposition of the columns by rows [compare  $A'$  after (3.5) with  $A$  after (3.2)]. This operation is called *transposition* of the matrix. For any real and unitary (see below) transformation the inverse matrix is just the transposed matrix.

The reflection operation can be presented in a manner quite similar to that for rotations. For instance, the reflection in the plane  $xy$  corresponds to the transformation  $x' = x$ ,  $y' = y$ , and  $z' = -z$  with the matrix

$$A = \begin{pmatrix} 1 & 0 & 0 \\ 0 & 1 & 0 \\ 0 & 0 & -1 \end{pmatrix} \quad (3.9')$$

while the inversion is

$$\begin{aligned} x' &= -x \\ y' &= -y \\ z' &= -z \end{aligned} \quad A = \begin{pmatrix} -1 & 0 & 0 \\ 0 & -1 & 0 \\ 0 & 0 & -1 \end{pmatrix} \quad (3.10)$$

In the general case of  $n$  coordinates  $x_1, x_2, \dots, x_n$  ( $n$ -dimensional space) their linear transformation, similar to (3.1) or (3.10) for the three-dimensional space, can be conveniently written as follows:

$$x'_i = \sum_j a_{ij} x_j, \quad i = 1, 2, \dots, n \quad (3.11)$$

where  $a_{ij}$  are the coefficients of the transformation. The matrix  $A$  corresponding to this transformation is

$$A = \begin{pmatrix} a_{11} & a_{12} & \dots & a_{1n} \\ a_{21} & a_{22} & \dots & a_{2n} \\ \vdots & \vdots & & \vdots \\ a_{n1} & a_{n2} & \dots & a_{nn} \end{pmatrix} \quad (3.12)$$

The matrices (3.2), (3.5), (3.8)–(3.10) are particular cases of the matrix (3.12) for three-dimensional transformations.

It can be shown that for rotations and reflections the matrix elements  $a_{ij}$  obey certain relationships of orthogonality and normalization:

$$\sum_j a_{jk} a_{jl} = \delta_{kl} \quad (3.13)$$

where  $\delta_{kl}$  is the Kronecker index (2.46):  $\delta_{kl} = 1$  if  $k = l$  and  $\delta_{kl} = 0$  if  $k \neq l$ .

The linear transformations that obey the condition (3.13) are called *unitary transformations*. It can be easily checked that the three-dimensional transformations (rotations and reflections) are unitary transformations. Thus all the molecular space symmetry operations are unitary transformations.

Let us perform two consequent unitary transformations:

$$\begin{aligned} x'_j &= \sum_{k=1}^n a_{jk} x_k & j &= 1, 2, \dots, n \\ x''_i &= \sum_j b_{ij} x'_j & i &= 1, 2, \dots, n \end{aligned} \quad (3.14)$$

or in a more compact form

$$\begin{aligned} M' &= AM \\ M'' &= BM' \end{aligned} \quad (3.14')$$

The result of the two transformations can also be obtained directly by one transformation of  $x$  into  $x''$ :

$$x_i'' = \sum_{k=1}^n c_{ik} x_k \quad i = 1, 2, \dots, n \quad (3.15)$$

or

$$M'' = CM \quad (3.15')$$

where  $C$  is the matrix of this transformation. On the other hand, by substitution of the first of Eqs. (3.14') into the second one, we have

$$M'' = BM' = BAM$$

Thus [cf. (3.15')]

$$C = B \cdot A \quad (3.16)$$

Determined in this way, *the matrix  $C$  equals the product of the matrices  $B$  and  $A$* . Its elements can be found by substituting the first Eq. (3.14) into the second one:

$$x'' = \sum_j b_{ij} x_j' = \sum_j b_{ij} \sum_k a_{jk} x_k = \sum_{j,k} b_{ij} a_{jk} x_k \quad (3.15'')$$

Hence

$$c_{ik} = \sum_j b_{ij} a_{jk} \quad (3.17)$$

In other words, the matrix elements of the product of two matrices equals the sum of the products of the elements of each row of the multiplier with the elements of the corresponding column of the multiplicand. In this context it is worthwhile to emphasize that the product of two matrices (two symmetry operations) is, in general, not commutative (the multiplier and multiplicand are not interchangeable):

$$B \cdot A \neq A \cdot B \quad (3.18)$$

Thus the consecutive application of two transformations (two symmetry operations) can be described by one matrix equal to the product of the matrices of the two transformations. Obviously, the identical transformation  $E$  multiplied by any matrix  $A$  does not change it:  $E \cdot A = A$ .

To conclude this section: (1) each symmetry transformation of the molecule corresponds to some matrix-operator, (2) inverse transformation corresponds to

the inverse matrix, (3) the identity operation corresponds to the unity matrix, and (4) the consecutive application of two symmetry operations corresponds to the product of their matrices.

Thus the geometric properties of symmetry are translated into the language of matrices–operators; this is important for direct use of group-theoretical considerations in evaluation of structure and properties of matter.

### 3.2. GROUPS OF SYMMETRY TRANSFORMATIONS

One of the most important properties of a molecule is that its *symmetry transformations form a group in the mathematical sense of this word*. A *group* is a set of elements (of any nature) that satisfies the following conditions:

1. The operation of multiplication of two elements is defined, the product of any two elements being also an element of the set under consideration.
2. The multiplication obeys the law of associativity:  $(AB) \cdot C = A \cdot (BC)$ , where  $A$ ,  $B$ , and  $C$  are elements of the set.
3. Among the elements there is an identity one  $E$ , that is, an element which in the product with another one does not change the latter.
4. For each element there is an inverse element that satisfies the condition  $A \cdot A^{-1} = E$ .

It can be shown that the set of symmetry operations of a molecule satisfies all four of these conditions for a group. Indeed, the product of two symmetry operations, defined as their consecutive application, is also a symmetry operation; each of them matches the molecule with itself (by definition), and hence their product also matches the molecule with itself. Then the identity element is the identical transformation (say, the rotation by an angle  $2\pi$ ), and the inverse element, as shown above, is given by the inverse transformation. The associative law can also be easily checked.

Thus the set of symmetry transformations forms a group in the mathematical sense of the word, and this means that all the results of the mathematical theory of groups can be used directly to reveal the properties of symmetry operations and their role in physical and chemical properties of the molecule. Next, we formulate briefly some useful group-theoretical rules.

The number of elements in the group is called *the order of the group*. For a molecule the order of the group can be either a finite, or an infinite number. The latter is realized, for instance, in linear molecules for which the number of rotations is infinite, since rotations by any angle around the axis of the molecule is a symmetry operation (in this case the group is continuous). If the order of the group is not a simple number, then some subgroups can be separated from the group, which means that within the set of elements of the group there are smaller sets that form smaller groups.

Two elements,  $A$  and  $B$ , are called *conjugated* if there is such a third element  $P$  for which

$$A = P \cdot B \cdot P^{-1} \quad (3.19)$$

It can be shown that if  $A$  is conjugated with  $B$ , and  $B$  is conjugated with  $C$ , then  $A$  is conjugated with  $C$ . This property allows one to separate the elements of the group into smaller sets in which all the elements are mutually conjugated. These sets are called *classes*.

There is a simple geometric rule that enables one to easily separate the symmetry operations into classes. Denote by  $A$  the rotation around the  $Oa$  axis by an angle  $\phi$ , and by  $B$  the rotation by the same angle around another axis  $Ob$ . If there is an element  $P$  of the group that transforms the axis  $Ob$  into  $Oa$ , then  $A = PBP^{-1}$ , and  $A$  and  $B$  belong to the same class. The proof of this rule emerges directly from geometric concepts and can be easily checked. Separation of the group elements into classes is very important for applications.

Note that all the molecular symmetry groups are *point groups* for which any set of consecutive symmetry operations leaves at least one point of the system unchanged. Otherwise, these operations are not symmetry operations because they displace the molecule and it does not match with itself. For crystals there is also translation symmetry, but the local properties can still be described by point groups.

The simplest point groups are as follows (Fig. 3.2). The groups  $C_n$ ,  $n = 1, 2, \dots$  contain one axis of symmetry of the  $n$ th order and  $n$  elements:  $C_n, C_n^2, C_n^3, \dots, C_n^n = E$ . The groups  $C_{nh}$  and  $C_{nv}$  can be obtained by adding reflection planes  $\sigma_h$  and  $\sigma_v$ , respectively, to the  $n$ th-order axis (in  $C_{\infty h}$  and  $C_{\infty v}$  the order of the symmetry axis is infinite). The group  $D_{nh}$  is obtained by adding a perpendicular second-order axis to the main  $n$ th axis (this also creates reflection planes; see below). Most important for coordination compounds are

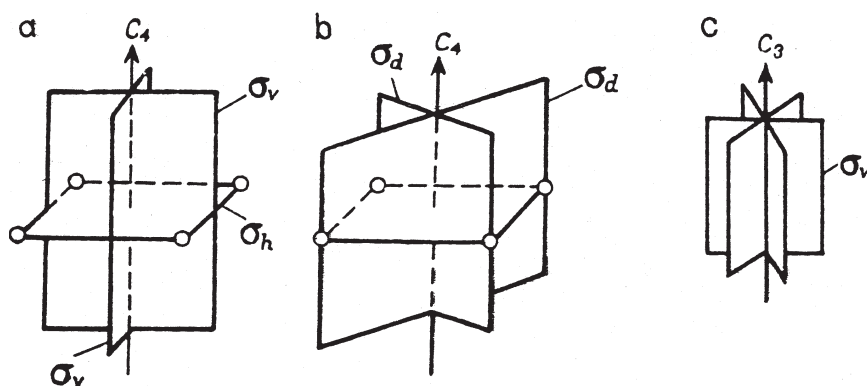


**FIGURE 3.2.** Symmetry elements of some point groups: (a) fourth-order axis  $C_4$  and symmetry planes  $\sigma_v$  and  $\sigma_h$  of the  $C_{4h}$  group; (b)  $\sigma_d$  planes of the same group  $C_{4h}$ ; (c) the threefold axis  $C_3$  and symmetry planes  $\sigma_v$  of the  $C_{3v}$  group.

the cubic groups, tetrahedral  $T$ ,  $T_d$ , and  $T_h$ , and octahedral  $O$  and  $O_h$ , as well as icosahedral groups  $I$  and  $I_h$ . The description of these groups in detail is given in special manuals mentioned above. Example 3.1 illustrates the details in the description of the cubic  $O_h$  group.

### EXAMPLE 3.1

#### The Symmetry Group of an Octahedral $O_h$ System and Its Classes

Consider as an example the octahedral  $O_h$  group, which corresponds to the symmetry operations of an octahedral complex with identical ligands. It includes all the symmetry elements of a cube (Fig. 3.3): three axes of the fourth order  $C_4$  lining the centers of opposite faces of the cube (in octahedral complexes they line two ligands in the *trans* position) and three axes of the second order that coincide with the  $C_4$  axes:  $C_2 = C_4^2$ ; four axes of the third order  $C_3$  that coincide with the diagonals of the cube; six axes of the second order  $C_2'$  connecting the midpoints of the opposite edges; a center of symmetry (inversion operation  $I$ ); three reflection planes parallel to the faces of the cube  $\sigma_h$ ; and six reflection planes  $\sigma_d$ , each containing two opposite edges.

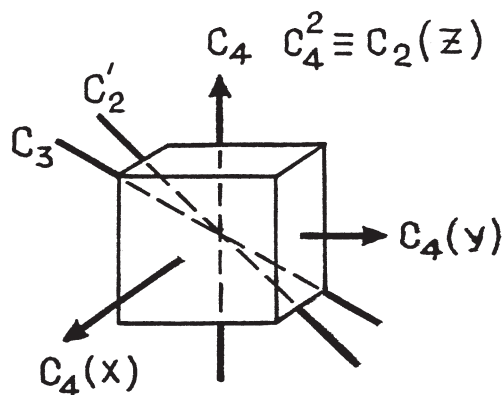


FIGURE 3.3. Symmetry axes of a cube.

To determine the number of elements (the order of the group) and their distribution over the classes, it is convenient to begin with the subgroup  $O$  of the  $O_h$  group, which is also known as a separate group of all the rotations of the octahedron (without reflections). According to the geometric rule of distribution of the symmetry operations into classes formulated above, rotations by the same angle around different axes enter the same class if among the elements of the group  $O$  under consideration there are such rotations that transfer one axis into another. Using this rule one can establish that in the  $O$  group there are 24 elements that form five classes:

1. *Class E*, which contains one element (the identical element always forms a separate class)
2. *Class C<sub>4</sub>*, containing six elements, three rotations  $C_4$ , and three rotations  $C_4^3$  around the fourth-order axes;  $C_4^3$  means  $3 \times$  rotation by the angle  $2\pi/4$ , which is equivalent to  $C_4^{-1}$ , the element inverse to  $C_4$  describing the rotation around  $C_4$  by an angle of  $-2\pi/4$
3. *Class C<sub>4</sub><sup>2</sup> = C<sub>2</sub>*, containing three rotations by an angle  $\pi$  around the fourth-order axis  $C_4$
4. *Class C<sub>3</sub>*, containing eight rotations by angles  $2\pi/3$  and  $-2\pi/3$  around the third-order axis (the elements  $C_3$  and  $C_3^2$ )
5. *Class C<sub>2</sub>'*, containing six rotations by angle  $\pi$  around the second-order axis

The elements of the octahedral group  $O_h$  can be obtained from the elements of the  $O$  group by multiplying each of them by the element  $S_2 = I$ , the inversion in the center of the cube. We then have:  $E \cdot I = I$ ,  $C_3 \cdot I = S_6$ ,  $C_4 \cdot I = S_4$ ,  $C_2' \cdot I = \sigma_d$ , and  $C_2 \cdot I = \sigma_h$ . This results in a doubling of the number of elements and classes. Hence the  $O_h$  group has 48 elements distributed in 10 classes (the number of elements is indicated in parentheses):  $E(1)$ ,  $C_4(6)$ ,  $C_2(3)$ ,  $C_3(8)$ ,  $C_2'(6)$ ,  $I(1)$ ,  $S_4(6)$ ,  $\sigma_h(3)$ ,  $S_6(8)$ , and  $\sigma_d(6)$ . Each of these symmetry transformations corresponds to a matrix, and all these matrices form the same group, as the transformations; the relationships obtained above for symmetry transformations are equally valid for the appropriate matrices—operators. Table 3.1 (see also Table A1.11) shows all these classes together with the corresponding irreducible representations and their characters discussed in the next section.

**TABLE 3.1. Irreducible Representations and Characters of the Octahedral Point Group  $O_h^a$**

$O_h$	$E$	$6C_4$	$3C_4^2=C_2$	$8C_3$	$6C_2'$	$S_2=I$	$6S_4$	$3\sigma_h$	$8S_6$	$6\sigma_d$
$A_{1g}$	+1	+1	+1	+1	+1	+1	+1	+1	+1	+1
$A_{1u}$	+1	+1	+1	+1	+1	-1	-1	-1	-1	-1
$A_{2g}$	+1	-1	+1	+1	-1	+1	-1	+1	+1	-1
$A_{2u}$	+1	-1	+1	+1	-1	-1	+1	-1	-1	+1
$E_g$	+2	0	+2	-1	0	+2	0	+2	-1	0
$E_u$	+2	0	+2	-1	0	-2	0	-2	+1	0
$T_{1g}$	+3	+1	-1	0	-1	+3	+1	-1	0	-1
$T_{1u}$	+3	+1	-1	0	-1	-3	-1	+1	0	+1
$T_{2g}$	+3	-1	-1	0	+1	+3	-1	-1	0	+1
$T_{2u}$	+3	-1	-1	0	+1	-3	+1	+1	0	-1

<sup>a</sup>See also Table A1.11.

### 3.3. REPRESENTATIONS OF GROUPS AND MATRICES OF REPRESENTATIONS

As is known from quantum mechanics, the state of the system with given energy  $\varepsilon$  (the eigenstate) is determined by the wavefunction  $\psi$  or, more general, by a set of wavefunctions  $\psi_1, \psi_2, \dots, \psi_f$  that satisfy the Schrödinger equation (1.5):

$$H\psi_n = \varepsilon\psi_n \quad n = 1, 2, \dots, f \quad (3.20)$$

If  $f > 1$ , there are more than one state with the same energy  $\varepsilon$  and the term is  $f$ -fold degenerate (the functions  $\psi_n$  are assumed to be linearly independent). It is easy to check that if all these functions satisfy Eq. (3.20), then any of the linear combinations  $a_1\psi_1 + a_2\psi_2 + \dots + a_f\psi_f$  with arbitrary coefficients  $a_1, a_2, \dots, a_f$ , satisfies the same equation.

Let us apply a symmetry operation  $G$  to both parts of Eq. (3.20):

$$G(H\psi_n) = G(\varepsilon_n\psi_n) \quad (3.21)$$

By definition,  $G$  does not change the molecule and hence its Hamiltonian  $H$ . This means that  $G(H\psi) = H(G\psi)$ . On the other hand,  $\varepsilon_n$  is a constant; hence  $G(\varepsilon_n\psi_n) = \varepsilon_n(G\psi_n)$ . Thus Eq. (3.21) yields

$$H(G\psi_n) = \varepsilon_n(G\psi_n) \quad (3.21')$$

It is seen that the function  $\psi'_n = G\psi_n$  [i.e., the  $\psi_n$  transformed by the symmetry operation  $G$  as required by the rule (3.3')] also satisfies the Schrödinger equation with the same energy  $\varepsilon_n$ . But there are only  $f$  such independent functions. Therefore,  $\psi'_n$  must coincide with one of them or (more general) with their linear combination:

$$\psi'_n = \sum_k^f G_{nk}\psi_k \quad n = 1, 2, \dots, f \quad (3.22)$$

where  $G_{nk}$  are some constants.

We thus obtained  $f$  equations that show how the  $f$  linearly independent functions  $\psi_1, \psi_2, \dots, \psi_f$  transform to a new system of functions  $\psi'_1, \psi'_2, \dots, \psi'_f$  by the symmetry operation  $G$ . The transformation is determined by the constants  $G_{nk}$ , which can be written in the form of a matrix, quite similar to the coordinate transformations (3.12) (Section 3.1):

$$G = \begin{pmatrix} G_{11} & G_{12} & \cdots & G_{1f} \\ G_{21} & G_{22} & \cdots & G_{2f} \\ \vdots & \vdots & & \vdots \\ G_{f1} & G_{f2} & \cdots & G_{ff} \end{pmatrix} \quad (3.23)$$



For another symmetry transformation, we can similarly obtain another matrix. Counting all the symmetry transformations, that is, all the elements of the symmetry group of the molecule under consideration, we obtain a set of matrices of the dimension  $f$ ; their number is equal to the number of elements in the group. These matrices form *the representation of the group*, with  $f$  as its dimensionality, while the set of functions  $\psi_1, \psi_2, \dots, \psi_f$ , by means of which the matrices were obtained, is called *the basis of the representation*.

It can be shown that to obtain the group representation there is no need to use the set of basis functions that are wavefunctions of the system with given energy. To obtain the transformations (3.22), the only requirement imposed on the basis functions is that they be independent and transform to each other by symmetry transformations. The three-dimensional matrices of symmetry rotations and reflections introduced above can serve as an example of such a representation of the group (for this representation the coordinates  $x, y, z$  serve as basis functions). But it is important that *the wavefunctions of the system can serve as a basis of the group representation*.

By using different basis sets one, can obtain different representations for the same group; the number of possible representations is thus infinite. However, not all of these representations are independent and not all of the independent representations are important to the applications.

Let us first introduce the notion of equivalent representations. Assume that by means of a set of basis functions  $\psi_1, \psi_2, \dots, \psi_p$  we obtained a representation  $G$  of the group. Apply to these functions some linear transformation of the type (3.22) with the transformation constants given by some matrix  $S$ . As a result of this transformation, we obtain another set of functions  $\psi'_1, \psi'_2, \dots, \psi'_p$ , which can also serve as a basis of another representation  $G'$ . It can be shown that there is a certain relationship between the matrices  $G$  of the former and  $G'$  of the latter representations:

$$G' = S^{-1}GS \quad (3.24)$$

The representations  $G$  and  $G'$  related by (3.34) are called *equivalent representations*.

By comparison with (3.19), one can see that the relationship between the matrices of equivalent representations coincides with the condition of conjugation of the (belonging to the same class) symmetry operations corresponding to these matrices, provided that  $S$  belongs to the same group.

An important feature of equivalent representations is that their matrices, related by (3.24), have the same characters  $X$ . *The character of a matrix  $X(G)$  equals the sum of its diagonal elements:*

$$X(G) = G_{11} + G_{22} + \dots + G_{ff} = \sum_i^f G_{ii} \quad (3.25)$$

In particular, the character of the identical transformation  $E$  corresponding to the unity matrix with all the diagonal elements  $G_{ii} = 1, i = 1, 2, \dots, f$  equals

the dimensionality of the representation  $f$ :

$$X(E) = f \quad (3.26)$$

Let us show that the characters of the matrices of equivalent representations coincide:

$$X(G) = X(G') \quad (3.27)$$

Indeed, using the rule of multiplication of matrices (3.17), we can obtain from (3.24) the following relations:

$$X(G') = \sum_i G'_{ii} = \sum_i \sum_j \sum_k S_{ik}^{-1} G_{kl} S_{li} = \sum_k \sum_l G_{kl} \delta_{kl} = \sum_k G_{kk} = X(G)$$

where the elements of the inverse matrix  $S^{-1}$  are denoted by  $S_{ik}^{-1}$  and the relation

$$\sum_i S_{ik}^{-1} S_{li} = \delta_{kl}$$

is employed [cf. Eq. (3.13)].

Since all the elements of the same class are related by (3.24), the characters of their matrices obey the condition (3.27), that is, *the matrices of the elements of the same class have the same characters*.

Another important feature of the group representation is the possibility of reducing them to *irreducible representations* (often denoted as IrReps and sometimes called *symmetry types*). When passing from a given basis of functions to another (equivalent) by means of some linear transformation, it may be possible to divide the whole set of functions into smaller sets of  $f_1, f_2, \dots, f_r$  ( $f_1 + f_2 + \dots + f_r = f$ ) functions, so that in each smaller set they transform to one another (by symmetry transformations) not involving the functions of other sets. In other words, each of these sets can serve as a basis of a representation of smaller dimensionality. The larger representation is thus *reducible*. If such a separation of the basis sets cannot be carried out by linear transformations, then the representation is called *irreducible*.

By means of a linear transformation of the basis set the matrices of a reducible representation can be reduced to the form, in which the nonzero matrix elements lie within some smaller square tables (submatrices) that occupy diagonal positions, out of which all the matrix elements are zero as follows:

$$\left( \begin{array}{ccc}
 \begin{array}{c} G_{ij} \\ i, j = 1, 2, \dots, f_1 \end{array} & & 0 \\
 \begin{array}{c} \dots \\ G_{kl} \\ k, l = f_1 + 1, \dots, f_1 + f_2 \end{array} & & \dots \\
 0 & & \begin{array}{c} \dots \\ G_{md} \\ m, d = f - f_r, \dots, f \end{array} \end{array} \right) \quad (3.28)$$

If the dimensionality of these submatrices cannot be lowered by linear transformations of the basis functions, then each of them is a matrix of an IrRep and the set of such (equal in dimensionality and similar in position) submatrices forms an IrRep. Hence the reducible representation of the dimensionality  $f$  can be characterized by  $r$  sets of matrices of lower dimensionality,  $f_1, f_2, \dots, f_r$  ( $f_1 + f_2 + \dots + f_r = f$ ), each realizing an IrRep of the group. This procedure is called *decomposition of the reducible representation into irreducible parts*.

It follows from the presentation of the matrix of the reducible representation in the form (3.28) that its character equals the sum of the characters of the irreducible representations to which the reducible one is reduced. Denoting the characters of the reducible and irreducible representations by  $X(G)$  and  $X^{(\alpha)}(G)$ , respectively, we have

$$X(G) = \sum_{\alpha} a^{(\alpha)} X^{(\alpha)}(G) \quad (3.29)$$

where  $a^{(\alpha)}$  is the number of times that the  $\alpha$  IrRep enters the reducible one.

The characters obey some orthogonality relationships. The latter are based on the orthogonality relation for the matrix elements of the matrices of the representations [cf. (3.13)]:

$$\sum_G G_{ik}^{(\alpha)} G_{lm}^{(\beta)} = \frac{g}{f_{\alpha}} \delta_{\alpha\beta} \delta_{il} \delta_{km} \quad (3.30)$$

which means that if the two IrRep are different,  $\alpha \neq \beta$ , the above sum is zero. In particular, assuming that  $\beta$  is a unity representation, we have

$$\sum_G G_{ik}^{(\alpha)} = 0 \quad (3.31)$$

for any nonunity representation  $\alpha$ . Several interesting consequences follow from Eq. (3.30) [For direct use of Eq. (3.31), see Section 3.4]. In particular, the sum (over all the symmetry operations  $G$ ) of the products of characters  $X^{(\alpha)}(G)$  and  $X^{(\beta)}(G)$  of two irreducible representations  $\alpha$  and  $\beta$  is equal to zero if the two representations are different, and to the order of the group  $g$  if they coincide:

$$\sum_G X^{(\alpha)}(G)X^{(\beta)}(G) = g\delta_{\alpha\beta} \quad (3.32)$$

Multiplying the left and the right sides of (3.29) by  $X^{(\beta)}(G)$ , summing over  $G$ , and taking into account the relation (3.32), we get

$$a^{(\beta)} = \frac{1}{g} \sum_G X(G)X^{(\beta)}(G) \quad (3.33)$$

This relation, known as *the formula of decomposition of reducible representations into irreducible parts*, solves directly the problem of finding whether a certain IrRep is included in the reducible one, provided that the characters of both the latter and former are known. Many symmetry problems can be solved by this formula.

Let us also list (without derivation) some important rules concerning IrReps and their characters:

1. The number of nonequivalent IrReps of a group equals the number of its classes  $r$ .
2. The sum of the squares of the dimensionalities of the IrReps equals the order of the group  $g$ :  $f_1^2 + f_2^2 + \dots + f_r^2 = g$ .
3. The dimensionalities of the IrReps of the group are divisors of its order.
4. Among the IrReps there is the so-called unity representation realized by one basis function that is totally symmetric with respect to all the symmetry operations of the group; all the characters of the matrices of the unity representation are equal to one.
5. The characters of the matrices of the IrRep  $\Gamma$ , which is a direct product of the representations  $\alpha$  and  $\beta$ , equals the products of the characters of the corresponding matrices of these representations.

The term *direct product of representations* needs some clarification. Denote the sets of basis functions of the representations  $\alpha$  and  $\beta$  by  $\psi_\alpha$  and  $\psi_\beta$ , respectively. Then the direct product of the representations  $\alpha$  and  $\beta$  is the representation  $\gamma$  realized by the set of functions from the products  $\psi^{(\alpha)}\psi^{(\beta)}$ . If  $\psi^{(\alpha)}$  and  $\psi^{(\beta)}$  coincide, the new representation with the characters  $[X(G)]^2$  decomposes into two representations [3.1, 3.7]:

1. The representation of symmetric product with the characters

$$[X]^2(G) = \frac{1}{2}\{[X(G)]^2 + X(G^2)\} \quad (3.34)$$

## 2. Representations of the antisymmetric product with the characters

$$\{X\}^2(G) = \frac{1}{2}\{[X(G)]^2 - X(G^2)\} \quad (3.35)$$

The two products, symmetric and antisymmetric, play an important role in the description of physical properties of molecules (see below in Example 3.2).

The general properties of IrReps and their characters, especially the orthonormalization conditions of the type (3.30), allow one to calculate the values of all the characters. They are calculated and tabulated for all the symmetry groups. *Appendix A1* gives the tables of characters of the most usable molecular point groups, including information about symmetry properties of Cartesian coordinates and rotations, while Table 3.1 in Example 3.1 shows the symmetry elements, their classes, and the IrReps of octahedral systems with  $O_h$  symmetry. Each column of Table 3.1 presents 1 of the 10 classes of this group. The number of its elements is indicated by a coefficient to the denotation of the class, while the rows correspond to the 10 IrReps. The notations are those due to Mulliken 3.9: one-dimensional representations are denoted by  $A$  and  $B$ , and two-, three-, four- and five-dimensional by  $E$ ,  $T$ ,  $G$ , and  $H$ , respectively. In practice the notations of Bethe are also used, in which only one letter,  $\Gamma$ , with indices, is employed (Section 3.6). If the group includes the inversion operation  $I$ , all the representations have an additional index, either  $g$  or  $u$ , indicating the parity of the basis functions with respect to the operation of inversion:  $g$  means evenness (gerade), while  $u$  means oddness (ungerade).

The knowledge of the characters of the IrReps of the symmetry group enables us to describe all the properties of the molecule related to its symmetry.

### 3.4. CLASSIFICATION OF MOLECULAR TERMS AND VIBRATIONS, SELECTION RULES, AND WIGNER-ECKART THEOREM

In this and subsequent sections some important applications of the group-theoretical rules, discussed above, are considered briefly.

*Classification of molecular terms on symmetry* is at present unavoidable in any rational description of electronic structure and properties of molecules. As shown above, the set of wavefunctions of an eigenstate forms a basis of the representation of the group of symmetry transformations of the molecule. It can be shown that this representation is irreducible. Hence we have a direct correspondence between (1) the energy terms of the molecular system and their wavefunctions and (2) the IrReps of its group of symmetry transformations. This forms the basis for the classification of molecular states on symmetry.

Each energy term is correlated with an IrRep of the symmetry group of the molecular system. *The dimensionality of the representation indicates the degeneracy of the term*, that is, the number of functions that transform to each other by the symmetry operations and hence the number of states with the same energy, while the characters of the matrices of the IrReps describe the symmetry properties of

these wavefunctions. For instance, for a molecular system with the symmetry described by the group  $O_h$  (Table 3.1), the following types of energy terms are possible: nondegenerate  $A_{1g}, A_{1u}, A_{2g}, A_{2u}$ ; double degenerate,  $E_g$  and  $E_u$ ; and threefold degenerate,  $T_{1g}, T_{1u}, T_{2g}, T_{2u}$  (see Section 3.5, Examples 3.3 and 3.4, and Solutions to Problems P3.5 and P3.6).

Quite similar to energy terms, *normal vibrations* (Section 7.1) can be classified on symmetry types of the symmetry group of the system. It can be shown that by symmetry transformations, normal nuclear displacements in vibrations with a given frequency transform into each other, realizing an IrRep of the symmetry group, similar to the symmetry transformations of the wavefunctions of a given term in Eqs. (3.21)–(3.23). Therefore, each normal vibration belongs to an IrRep of the symmetry group that determines the symmetry and degeneracy of the vibration (Section 3.5).

The classification of molecular terms and vibrations on symmetry is most important in different applications. Besides describing of the symmetry properties, it allows us to solve many problems, including construction of molecular orbitals with given symmetry (Section 3.5), possible normal vibration (Section 3.5), energy-level splitting in external fields (Section 4.2), selection rules for matrix elements describing observable properties (e.g., in light absorption; see Section 8.1), evaluation of the possible terms of given electron configurations, and so on.

Consider *selection rules for matrix elements*. The most general form of a matrix element representing molecular properties is

$$\int \Psi_1^* \mathbf{f} \Psi_2 d\tau \quad (3.36)$$

where  $\mathbf{f}$  is a scalar, vector, or tensor operator describing the physical property under study (Section 1.3), while  $\Psi_1$  and  $\Psi_2$  are the wavefunctions of two states of the system. In particular,  $\Psi_1 = \Psi_2$  for the diagonal matrix element.

Direct calculation of (3.36) is often difficult mainly because the wavefunctions are unknown. However, *the selection rules*—the general rules indicating whether the matrix element (3.36) is zero or nonzero—can be solved using symmetry ideas and the group-theoretical results without calculation of the integral. For this purpose knowledge of the symmetry properties of the operator  $\mathbf{f}$  and of the wavefunctions  $\Psi_1$  and  $\Psi_2$  is needed. Using this classification on symmetry,  $\Psi_1$  and  $\Psi_2$  can be directly attributed to the corresponding IrReps, and the same can be done for  $\mathbf{f}$  by considering its behavior under the operations of the symmetry group.

Equation (3.36) is a definite integral, a number, and as such it is independent of coordinate transformations  $G$  performed under the sign of the integral. This means that

$$\int F_i d\tau = \int G F_i d\tau \quad (3.37)$$

where we denoted  $F_i = \Psi_1 \mathbf{f} \Psi_2$ . On the other hand, considering  $F_i$  as one of the functions of a basis realizing some representation  $\gamma$  of the group, we obtain [after Eq. (3.22)]

$$G F_i = \sum_k G_{ik}^{(\gamma)} F_k$$

and hence

$$\int F_i d\tau = \int \sum_k G_{ik}^{(\gamma)} F_k d\tau$$

Now, by summing up the left- and right hand sides of this equation over all the symmetry operations  $G$  of the group, the integral at the left (which is independent of  $G$ ) is just multiplied by the number of elements  $g$ . Hence

$$g \int \Psi_1^* \mathbf{f} \Psi_2 d\tau = \sum_k \int F_k \sum_G G_{ik}^{(\gamma)} d\tau \quad (3.38)$$

But the sum  $\sum_G G_{ik}^{(\gamma)}$ , following (3.31), is nonzero only when  $\gamma$  is a unity representation, and is zero for all the other representations. On the other hand, the representation  $\gamma$  of the product  $F = \Psi_1^* \mathbf{f} \Psi_2$  equals the product of representations of  $\Psi_1$ ,  $\mathbf{f}$ , and  $\Psi_2$ . Thus we arrived at the fundamental rule: *the matrix element (3.36) is nonzero if and only if the product of representations to which  $\Psi_1$ ,  $\mathbf{f}$ , and  $\Psi_2$  belong contains the unity representation.*

To obtain selection rules for operators of physical magnitudes using this rule some simple procedures should be carried out. Provided that the representations of the wavefunctions  $\Psi_1$  and  $\Psi_2$  and the operator  $\mathbf{f}$  are known, they should be multiplied, and then, using Eq. (3.33), one should determine whether the product of these three representations contains the unity representation. For the latter all the characters are equal to a unity, while the characters of the product of the representations equal the product of their characters. Note that if the two functions  $\Psi_1$  and  $\Psi_2$  are equal [and hence (3.36) is a diagonal matrix element], the product of their representations must be taken as a symmetric product with the characters after (3.34):  $[X^2](G) = \frac{1}{2}\{[X(G)]^2 + X(G^2)\}$ .

Another important application of group theory is the *determination of energy terms of electron configurations*. In Section 2.2, atomic energy terms are listed in Table 2.6. Similarly, different molecular terms are formed from any given electron configuration by distributing the electrons over the possible combinations of one-electron orbital and spin states of this configuration. Example 3.2 explains in detail how the application of group-theoretical rules essentially simplifies this procedure using the two-electron configuration  $e^2$  as an example.

### EXAMPLE 3.2

#### *Energy Terms of Electronic Configuration $e^2$*

Different terms of the same electron configuration are produced by all possible combinations of its one-electron orbital and spin functions (Section 2.2). There are four two-electron combinations of the one-electron functions of the two twofold degenerate  $E$  states in the  $e^2$

configuration. According to Section 3.3 [Eqs. (3.34) and (3.35)], the irreducible representations (IrReps) of these four states can be found by decomposition of the reducible representation of their direct product into IrReps using Eq. (3.33). The characters of the reducible representation of the direct product of two representation are equal to the product of their characters. For the octahedral group  $O_h$ , using Table A1.11 [or Eq. (3.1)], we can easily see that for the direct product  $E \times E$  the reducible characters are

$G$	$E$	$C'_2$	$C_4$	$C_2$	$C_3$	$I$	$S_4$	$S_6$	$\sigma_h$	$\sigma_d$
$X(G)$	4	0	4	1	0	4	0	1	4	0

Even without using Eq. (3.33) we can see by direct inspection that these characters equal the sum of those in  $A_1$ ,  $A_2$ , and  $E$ . Hence  $E \times E = A_1 + A_2 + E$ .

The same three terms emerge from the  $e^2$  configuration in any cubic group ( $T_d$ ,  $O$ ) and any other group that has a threefold axis of symmetry. However, for  $C_{4v}$ ,  $C_{4h}$ ,  $D_{4h}$ , and  $D_{4v}$ , as well as for any group of the type  $C_{4nv,h}$  or  $D_{4nv,h}$ , where  $n$  is an integer (the axis of symmetry is a multiple of 4) the decomposition for  $e^2$  is different:  $E \times E = A_1 + A_2 + B_1 + B_2$ . This is an important distinction between the two kinds of possible symmetries of TMS.

So far we considered only the orbital parts of the one-electron states. To account for the possible spin states, the direct product of two IrRep's can be decomposed into a symmetric part and an antisymmetric part given by Eqs. (3.34) and (3.35), respectively. Using these formulas we easily can separate the symmetric [#] and antisymmetric {#} parts:

$$[E \times E] = A_1 + E$$

$$\{E \times E\} = A_2$$

Now we can engage the Pauli principle or, more generally, the condition that the total wavefunction be antisymmetric with regard to the permutation (exchange of coordinates) of the two electrons. This means that for the symmetric orbital part the spin function should be antisymmetric, and hence the two spins should be antiparallel ( $\uparrow\downarrow$ ) with the total spin equal to zero; the two terms  $A_1$  and  $E$  are singlets,  $^1A_1$  and  $^1E$ . On the contrary, the orbitally antisymmetric term  $A_2$  must be accompanied by a symmetric spin function ( $\uparrow\uparrow$ ) with a total spin  $S = 1$  meaning a spin triplet ( $2S+1 = 3$ ),  $^3A_2$ . Thus the final solution is that the electronic configuration  $e^2$  has three terms:  $^1A_1$ ,  $^1E$ , and  $^3A_2$ .

If we denote the two orbitals of the degenerate  $e$  state by  $|\theta\rangle$  and  $|\varepsilon\rangle$  and the spin states by arrows as above, we can present the four



wavefunctions of these terms as follows [3.10]:

$$\begin{aligned}
 {}^3A_2 &= |\theta \uparrow; \varepsilon \uparrow\rangle \\
 {}^1A_1 &= \frac{1}{\sqrt{2}}(|\varepsilon \uparrow; \varepsilon \downarrow\rangle + |\theta \uparrow; \theta \downarrow\rangle) \\
 {}^1E_\theta &= \frac{1}{\sqrt{2}}(|\varepsilon \uparrow; \varepsilon \downarrow\rangle - |\theta \uparrow; \theta \downarrow\rangle) \\
 {}^1E_\varepsilon &= \frac{1}{\sqrt{2}}(|\theta \uparrow; \varepsilon \downarrow\rangle + |\theta \downarrow; \varepsilon \uparrow\rangle)
 \end{aligned}$$

From many other group-theoretical rules very useful in applications, we formulate here (without proof) the *Wigner–Eckart theorem*. The degenerate state of the system belongs to the IrReps with a dimensionality greater than unity ( $E$ ,  $T$ , etc.), and its matrices have several rows and columns. In this case it is convenient to attribute the wavefunctions of the term to the corresponding rows of the representation. For instance, for the threefold degenerate  $T_{1u}$  term of the  $O_h$  group the three wavefunctions transform under symmetry operations as the three coordinates  $x$ ,  $y$ ,  $z$ , respectively (Table A1.11). Hence each of them represents a row of the representation  $T_{1u}$ . The three functions of the  $T_{2g}$  term (also threefold degenerate) transform as the three products of coordinates  $xy$ ,  $xz$ , and  $yz$ , respectively. In general,  $\Gamma$  denotes the representation of the term and  $\gamma$  are its rows.

Consider the matrix element

$$\int \Psi^*(\Gamma_1\gamma_1) f_{\Gamma\gamma} \Psi(\Gamma_2\gamma_2) d\tau \equiv \langle \Gamma_1\gamma_1 | f_{\Gamma\gamma} | \Gamma_2\gamma_2 \rangle \quad (3.39)$$

where  $f_{\Gamma\gamma}$  is an operator of a physical magnitude that transform as the  $\gamma$  row of the  $\Gamma$  representation and  $\Gamma_1\gamma_1$ ,  $\Gamma_2\gamma_2$  are the representations and their rows for the two wavefunctions. The notation of the integral (3.39) given in the right-hand side is widely used in practice. The Wigner–Eckart theorem states that the matrix element (3.39) can be reduced to the following form [3.5]:

$$\langle \Gamma_1\gamma_1 | f_{\Gamma\gamma} | \Gamma_2\gamma_2 \rangle = \langle \Gamma_1 || f_\Gamma || \Gamma_2 \rangle \cdot \langle \Gamma_1\gamma_1, \Gamma\gamma | \Gamma_2\gamma_2 \rangle \quad (3.40)$$

where  $\langle \Gamma_1 || f_\Gamma || \Gamma_2 \rangle$  is the *reduced matrix element* dependent on the representations  $\Gamma_1$ ,  $\Gamma$ ,  $\Gamma_2$ , but not on their rows, and  $\langle \Gamma_1\gamma_1, \Gamma\gamma | \Gamma_2\gamma_2 \rangle$  are the *Clebsh–Gordan coefficients* for which there are ready-made tables.

The essence of the Wigner–Eckart theorem (3.40) is that for degenerate states there is no need to calculate all matrix elements for all rows of the representation; if one knows at least one matrix element, the reduced matrix element can be obtained from (3.40), and then all the others can be calculated using the tabulated Clebsh–Gordan coefficients. The theorem also limits the number of possible independent parameters of the problem with given symmetry.

### 3.5. CONSTRUCTION OF SYMMETRIZED MOLECULAR ORBITALS AND NORMAL VIBRATIONS

In the methods of molecular orbitals—linear combinations of atomic orbitals (MO LCAO, Chapter 5), as well as in many other related problems, it is necessary to construct an LCAO that transforms after the IrReps of the symmetry group of the system. Consider as an example an octahedral complex with  $O_h$  symmetry. The six ligand  $\sigma$  orbitals (with respect to the ligand–metal bond, Section 2.2),  $\sigma_1, \sigma_2, \dots, \sigma_6$ , are shown in Fig. 3.4. By the symmetry operations of the octahedral group  $O_h$  these functions transform to each other; the transformed functions can be written as follows:

$$\sigma'_i = C_{i1}\sigma_1 + C_{i2}\sigma_2 + \dots + C_{i6}\sigma_6 \quad i = 1, 2, \dots, 6 \quad (3.41)$$

The coefficients  $C_{ij}$  of these six transformations form the matrix of the representation for the symmetry operation used, and the number of such matrices equals the number of symmetry operations in the group. The set of these matrices forms the reducible representation of the transformation (3.41). If all coefficients

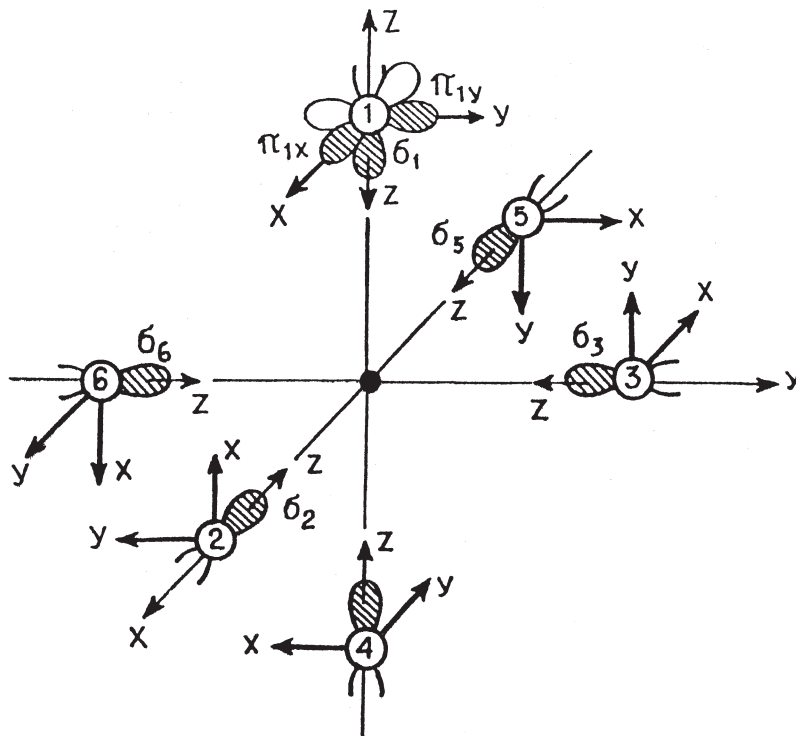


FIGURE 3.4. Space orientation of the  $\pi_{1x}$ ,  $\pi_{1y}$ , and  $\sigma_n$  ( $n = 1, 2, \dots, 6$ ) ligand orbitals in an octahedral complex (cf. Fig. 5.1).

of the matrices are known, it is easy to calculate their characters with Eq. (3.25), and then to decompose the reducible representation into irreducible parts using Eq. (3.33). The types of IrReps obtained in this way are just that sought for, to which the MOs—linear combinations of the six  $\sigma$  orbitals of the ligand—pertain.

However, to obtain the characters of the symmetry transformation (3.41), there is no need to perform these transformations and to find all the coefficients  $C_{ij}$ . Instead, one can use the following rule: *the character of the representation for a given symmetry transformation equals the number of atoms that remain unmoved by this transformation.*

Let us illustrate this rule by applying the transformation  $C_4$  of the  $O_h$  group, the rotation by an angle  $\pi/2$  around the axis  $Oz$ . As seen from Fig. 3.4, by this rotation two ligands, 1 and 4, remain unmoved from their positions and hence, following the abovementioned rule,  $X(C_4) = 2$  (for the transformation of the six ligand  $\sigma$  functions). This result can be checked directly. Indeed, by the  $C_4$  rotation the new function  $\sigma'$  can be easily expressed by the old ones:  $\sigma'_1 = \sigma_1, \sigma'_2 = \sigma_6, \sigma'_3 = \sigma_2$ , and so on. This can be conveniently written in the form of a general transformation (3.41):

$$\begin{aligned}\sigma'_1 &= 1 \cdot \sigma_1 + 0 \cdot \sigma_2 + 0 \cdot \sigma_3 + 0 \cdot \sigma_4 + 0 \cdot \sigma_5 + 0 \cdot \sigma_6 \\ \sigma'_2 &= 0 \cdot \sigma_1 + 0 \cdot \sigma_2 + 0 \cdot \sigma_3 + 0 \cdot \sigma_4 + 0 \cdot \sigma_5 + 1 \cdot \sigma_6 \\ \sigma'_3 &= 0 \cdot \sigma_1 + 1 \cdot \sigma_2 + 0 \cdot \sigma_3 + 0 \cdot \sigma_4 + 0 \cdot \sigma_5 + 0 \cdot \sigma_6 \\ \sigma'_4 &= 0 \cdot \sigma_1 + 0 \cdot \sigma_2 + 0 \cdot \sigma_3 + 1 \cdot \sigma_4 + 0 \cdot \sigma_5 + 0 \cdot \sigma_6 \\ \sigma'_5 &= 0 \cdot \sigma_1 + 0 \cdot \sigma_2 + 1 \cdot \sigma_3 + 0 \cdot \sigma_4 + 0 \cdot \sigma_5 + 0 \cdot \sigma_6 \\ \sigma'_6 &= 0 \cdot \sigma_1 + 0 \cdot \sigma_2 + 0 \cdot \sigma_3 + 0 \cdot \sigma_4 + 1 \cdot \sigma_5 + 0 \cdot \sigma_6\end{aligned}\quad (3.42)$$

The matrix of this transformation is

$$\begin{pmatrix} 1 & 0 & 0 & 0 & 0 & 0 \\ 0 & 0 & 0 & 0 & 0 & 1 \\ 0 & 1 & 0 & 0 & 0 & 0 \\ 0 & 0 & 0 & 1 & 0 & 0 \\ 0 & 0 & 1 & 0 & 0 & 0 \\ 0 & 0 & 0 & 0 & 1 & 0 \end{pmatrix}\quad (3.43)$$

and it is seen that the sum of the diagonal elements is indeed  $X(C_4) = 2$ .

Using this rule, we can obtain directly all the characters of the reducible representation  $\Gamma$  for all the symmetry transformations of the  $O_h$  group:

$G$	$E$	$C'_2$	$C_4$	$C_2$	$C_3$	$I$	$S_4$	$S_6$	$\sigma_h$	$\sigma_d$
$X(G)$	6	0	2	2	0	0	0	0	4	2

(3.44)

This representation can be decomposed into irreducible parts by means of Eq. (3.33):

$$\Gamma - \rightarrow A_{1g} + E_g + T_{1u} \quad (3.45)$$

Thus the symmetrized (group) orbitals of the type  $\sigma$  formed as linear combinations of the  $\sigma$  AOs of the six ligands of an octahedral complex should belong to one of the following IrReps of the  $O_h$  group:  $A_{1g}$ ,  $E_g$ ,  $T_{1u}$ . To construct the appropriate linear combinations of the atomic  $\sigma$  functions that transform after these representations, look first for the simple one,  $A_{1g}$ . Since its matrices are one-dimensional and the characters are units, the  $A_{1g}$ -type linear combination of  $\sigma$ -type AOs of the ligands for any symmetry operation of the  $O_h$  group transforms into itself. The only combination of this type is their sum:

$$\Psi(A_{1g}) = \sigma_1 + \sigma_2 + \sigma_3 + \sigma_4 + \sigma_5 + \sigma_6 \quad (3.46)$$

Indeed, any symmetry operation transforms  $\sigma_i$  into  $\sigma_j$ , and this does not change the sum (3.46).

For degenerate representations  $E_g$  ( $f = 2$ ) and  $T_{1u}$  ( $f = 3$ ), the procedure is more complicated. To construct the symmetrized orbital  $\psi^{(\alpha)}$  that belongs to the  $\alpha$  irreducible representation the *projection formula* can be employed [3.7]:

$$\psi^{(\alpha)} = \frac{f_\alpha}{g} \sum_G X^{(\alpha)}(G) G \psi \quad (3.47)$$

where  $\psi$  is an arbitrary function of the basis set (when there are recurring representations of the same symmetry, this relation should be slightly modified [3.3]). To use (3.47), one must choose a function  $\psi$  from the basis, apply to this function the symmetry operations  $G$ , multiply by its character in the representation  $\alpha$ , and sum up the results over all the operations  $G$  of the group. The result will be either a linear combination of different functions of the basis sought for or zero. The latter case means that the initial function  $\psi$  has not been chosen properly (it does not enter the  $\alpha$  representation) and another one should to be tried. Example 3.3 shows how  $E_g$ -type orbitals can be constructed following the same rules.

### EXAMPLE 3.3

#### Construction of $E_g$ -Symmetry-Adapted $\sigma$ MOs for Octahedral $O_h$ Systems

Let us apply Eq. (3.47) to find the MOs that transform after the  $E_g$  representation of the octahedral  $O_h$  group. Take  $\sigma_1$  as the initial  $\psi$ . From Table 3.1, one can see that for the  $E_g$  representation  $X(C'_2) = X(C_4) = X(S_4) = X(\sigma_d) = 0$ , and hence the corresponding symmetry transformations do not contribute to the sum (3.47). Then

- For the identical transformation  $E$ :  $X(E) = 2$ ,  $E\sigma_1 = \sigma_1$ .
- For eight rotations  $C_3$ :  $X(C_3) = -1$ , and each of the following transformations takes place twice (for rotations by an angle  $2\pi/3$  and  $-2\pi/3$ , respectively):  $C_3\sigma_1 = \sigma_2$ ,  $C_3\sigma_2 = \sigma_1$ ,  $C_3\sigma_3 = \sigma_5$ ,  $C_3\sigma_5 = \sigma_3$ ,  $C_3\sigma_4 = \sigma_6$ ,  $C_3\sigma_6 = \sigma_4$  (for four axes  $C_3$ , respectively).
- For three rotations:  $C_2^2 = C_2$ :  $X(C_2) = 2$ , and  $\sigma_1$  transforms once in  $\sigma_1$  and twice in  $\sigma_4$ .
- For the inversion operation  $I$ :  $X(I) = 2$ ,  $I \cdot \sigma_1 = \sigma_4$ .
- For eight rotation–reflections  $S_6$ :  $X(S_6) = -1$ , and  $\sigma_1$  transforms consecutively into  $\sigma_2$ ,  $\sigma_3$ ,  $\sigma_5$ , and  $\sigma_6$ , respectively, twice in each of them, similar to the transformation  $C_3$ .
- For three reflections  $\sigma_h$ :  $X(\sigma_h) = 2$ , and  $\sigma_1$  transforms once in  $\sigma_4$  and twice in itself ( $\sigma_1$ ).

Factoring in all these transformations and character values, and substituting them into Eq. (3.47), we have

$$\begin{aligned}\psi_1(E_g) &= \frac{2}{48}[2\sigma_1 - 1 \cdot (2\sigma_2 + 2\sigma_3 + 2\sigma_5 + 2\sigma_6) + 2 \cdot (\sigma_1 + 2\sigma_4) \\ &\quad + 2\sigma_4 - 1 \cdot (2\sigma_2 + 2\sigma_3 + 2\sigma_5 + 2\sigma_6) + 2(\sigma_4 + 2\sigma_1) \\ &= \frac{1}{6}(2\sigma_1 + 2\sigma_4 - \sigma_2 - \sigma_3 - \sigma_5 - \sigma_6)\end{aligned}\quad (3.48)$$

This is just one of the  $E_g$  functions sought for, with an accuracy up to the normalization factor  $N$ ; neglecting ligand–ligand overlap,  $N = (\frac{1}{12})^{1/2}$ . To obtain the other  $E_g$  function ( $E_g$  is twofold degenerate), we should repeat the procedure above, taking consecutively  $\sigma_2$  and  $\sigma_3$  as the probe functions  $\psi$ . Owing to the equivalence of all the ligands in the  $O_h$  symmetry, we can conclude directly that for  $\psi \sim \sigma_2$  and  $\psi \sim \sigma_3$  we obtain, respectively,  $\psi'(E_g) = N[2\sigma_2 + 2\sigma_5 - \sigma_1 - \sigma_3 - \sigma_4 - \sigma_6]$ , and  $\psi''(E_g) = N[2\sigma_3 + 2\sigma_6 - \sigma_1 - \sigma_2 - \sigma_3 - \sigma_4]$  (with  $\sigma_4$ ,  $\sigma_5$ , and  $\sigma_6$  taken as  $\psi$ , we obtain the same three functions  $\psi_1$ ,  $\psi'_2$ , and  $\psi''_2$ ).

However, one can easily check that these three  $E_g$  functions are not mutually orthogonal and hence are not linearly independent. Therefore, from the two functions  $\psi'_2$  and  $\psi''_2$ , only one combination should be constructed that transforms after the  $E_g$  representation and is orthogonal to  $\psi_1$ . Because each of the functions  $\psi'_1$  and  $\psi''_2$  transforms after  $E_g$ , any of their linear combinations belongs to  $E_g$ . It can be easily shown that the combination that is orthogonal to (3.48) is

$$\psi_2(E_g) = \frac{1}{2}(\sigma_2 + \sigma_5 - \sigma_3 - \sigma_6)\quad (3.49)$$

The two functions (3.48) and (3.49) represent the  $E_g$  state sought for (see Table 5.1 in Section 5.1).

For atomic  $\pi$  functions the procedure used to obtain adapted MOs is more complicated because the geometric rule of finding the characters of the reducible representation of the type (3.44) should be modified. Indeed, as seen from Fig. 3.4, the  $\pi$  orbitals of each ligand have two orientations in space (say,  $p_{1x}$  and  $p_{1y}$  for ligand 1), and therefore they do not necessarily transform into themselves under symmetry operations that leave the ligand in its initial position. For instance, under the  $C_4$  rotation of the octahedron ligand 1 remains unchanged, but its  $\pi$  functions change:  $p'_{1x} \rightarrow -p_{1y}$ ,  $p'_{1y} \rightarrow -p_{1x}$  (Fig. 3.4). Therefore the above-mentioned geometric rule for finding character values in the case of  $\pi$  functions modifies as follows. The character of the representation of a given symmetry transformation equals the number of  $\pi$  functions that remain unchanged by this transformation minus the number of functions that change their sign. Example 3.4 shows how the  $T_{2g}$ -type  $\pi$  orbital is constructed.

In a similar way, the normal vibrations of the system can be determined. As mentioned in Section 3.4, nuclear displacements in normal vibration with a given frequency have the same transformation properties as wavefunctions of a given energy term, that is they belong to one of the IrReps of the symmetry group following group-theoretical rules. Applying the symmetry transformations of the group to the normal displacements, we obtain a set of matrices of these transformations that forms the *full vibrational representation*. This representation is reducible and can be decomposed in IrReps using Eq. (3.33). The IrReps obtained in this way are just the types of normal vibrations of the system.

To obtain the characters of the vibrational representation, we must also obtain the set of matrices of the symmetry transformations of the normal displacements of the nuclei and sum up their diagonal elements. To do so, several simplifications are possible. First, since unitary transformations of coordinates do not change the characters of their matrices, we can perform transformations on Cartesian coordinates instead of normal ones. The matrices of transformations of Cartesian coordinates are simple, they are given by Eqs. (3.2), (3.5), (3.8), and (3.10) for several symmetry operations.

Second, since we don't need the whole matrix but only their diagonal elements, only the coordinates of the atoms that remain unmoved by the symmetry transformation should be factored in, as those of the atoms' interchanging positions will not be on the diagonal of the matrix. For a symmetry rotation  $C(\phi)$  on an angle  $\phi$ , the transformation matrix is given by (3.2) with the character

$$\chi_C(\phi) = 1 + 2 \cos \phi \quad (3.50)$$

If there are  $N_C$  unmoved atoms in this rotation, each of them gives the same contribution, and hence (3.53) should be multiplied by  $N_C$ . However, as we look only to vibrational displacements, we should exclude the translational and rotational displacement of the molecule as a whole. From the corresponding matrices we find that each of these two transformations gives the same contribution

**EXAMPLE 3.4*****Construction of  $T_{2g}$ -Symmetry-Adapted  $\pi$  MOs for Octahedral  $O_h$  Systems***

For the  $12\pi$  functions of six ligands in octahedral systems of  $O_h$  symmetry (Fig 3.4), the identical transformation  $E$  leaves unchanged all  $\pi$  functions, and hence  $X(E) = 12$ . For  $C_3$  rotations no  $\pi$  functions remain unchanged or changing sign:  $X(C_3) = 0$ . The same is true for  $C_2'$ :  $X(C_2') = 0$ . For  $C_4$  rotations two ligands (e.g., 1 and 4) remain at their initial positions, but their  $p_\pi$  functions transform to each other, and hence  $X(C_4) = 0$ , whereas under the rotation  $C_2 = C_4^2$  these functions only change sign:  $p'_{1x} = -p_{1x}$ ,  $p'_{1y} = -p_{1y}$ ,  $p'_{4x} = -p_{4x}$ ,  $p'_{4y} = -p_{4y}$ . Hence  $X(C_2) = -4$ . Similarly, we find all the other characters of the reducible representation:

$G$	$E$	$C_2'$	$8C_3$	$6C_4$	$C_2$	$I$	$6S_4$	$8S_6$	$3\sigma_h$	$6\sigma_d$
$X(G)$	12	0	0	0	-4	0	0	0	0	0

(3.51)

Using Eq. (3.33), one can easily decompose this representation  $\Gamma$  into irreducible parts:

$$\Gamma \rightarrow T_{1g} + T_{2u} + T_{2g} + T_{1u} \quad (3.52)$$

Thus the ligand  $\pi$  functions in the  $O_h$  group can realize symmetrized orbitals of the threefold degenerate type  $T_{1g}$ ,  $T_{1u}$ ,  $T_{2g}$ , and  $T_{2u}$  only, and hence these  $\pi$  functions take part only in such MO types.

To find these MOs, it is most convenient to use the projection formula (3.47). Taking as the starting function  $\psi$ , one of the  $\pi$  functions of a ligand (e.g.,  $\pi_{2y}$ ), one can easily obtain the following for the  $T_{2g}$  representation:

$$\psi(T_{2g}) = \frac{1}{2}(\pi_{2y} + \pi_{3x} + \pi_{5x} + \pi_{6y}) \quad (3.53)$$

Taking the other  $\pi$  orbitals as reference functions in the formula (3.47), we obtain the other two  $T_{2g}$  functions, as well as the  $T_{1g}$ ,  $T_{1u}$ , and  $T_{2u}$  combinations, all in all 12 symmetrized MOs formed by 12 ligand  $\pi$  functions (Table 5.1).

In the same way any other functions sets can be transformed (projected) to symmetrized combinations that belong to certain IrReps of the symmetry group.

$1 + 2 \cos \phi$ . Hence the total character of a rotational transformation is

$$\chi_C(\phi) = (N_C - 2)(1 + 2 \cos \phi) \quad (3.54)$$

In particular, for the identical transformation  $E$ ,  $\phi = 0$ , and  $\chi(E) = 3(N - 2)$ . In a similar way we find that for reflection in a plane  $\sigma$

$$\chi(\sigma) = N_\sigma \quad (3.55)$$

while for inversion (see the matrix (3.8))

$$\chi(I) = -3N_I \quad (3.56)$$

and for rotation-reflection axes  $S(\phi)$ ,  $\chi(S) = N_S(-1 + 2 \cos \phi)$ , where  $N_\sigma$ ,  $N_I$ , and  $N_S$  are the corresponding numbers of atoms that remain unmoved by the transformation, see Example 3.5.

### EXAMPLE 3.5

#### Normal Coordinates of a Regular Triangular Molecule $X_3$

A regular triangular molecule  $X_3$  has  $D_{3h}$  symmetry (Fig. 3.1) with six classes of symmetry transformations (six IrReps), shown in Table A1.5. To obtain the characters of the full vibrational representation, we apply Eqs. (3.54)–(3.56) to each class of symmetry transformation, respectively. For the identical operation  $E$ , all atoms remain unmoved and in Eq. (3.54) with  $N_C = 3$  and  $\phi = 0$ , we obtain  $\chi(E) = 3$ . For the  $\sigma_h$  reflection  $N_\sigma = 3$ ; hence  $\chi(\sigma_h) = 3$ . For the  $C_3$  rotation  $\phi = 2\pi/3$ ,  $N_C = 0$ , and  $\chi(C_3) = 0$ . Similarly,  $\chi(S_3) = \chi(C_3) \cdot \chi(\sigma_h) = 0$ ,  $\chi(C_2) = 1$ , and  $\chi(\sigma_v) = 1$ . Thus the characters of the full vibrational representation are

$G$	$E$	$\sigma_h$	$C_3$	$S_3$	$C_2$	$\sigma_v$
$\chi(G)$	3	3	0	0	1	1

Now, using Eq. (3.33), or by direct inspection, we can see that this reducible representation equals the sum  $A_1 + E'$ . The  $X_3$  molecule thus has one totally symmetric  $A_1$  and one double degenerate  $E'$  normal vibrations. They are shown in Fig. 7.3. To get the coordinate displacements in these vibrations one can use the projection formula (3.47) applying it to the atomic displacements, one at a time.



### 3.6. THE NOTION OF DOUBLE GROUPS

As mentioned in Section 2.2, with the spin–orbital interaction included, the stationary states of the system are classified by the quantum number  $J$  of the total momentum  $\mathbf{J} = \mathbf{L} + \mathbf{S}$ ;  $J = L + S, L + S - 1, \dots, |L - S|$ . This classification is of special importance in systems with sufficiently strong spin–orbital interaction (strong relativistic effects, see Sections 2.1, 5.4, 5.5, and 6.5).

If  $S$  is a half-integer (for an odd number of electrons),  $J$  is also a half-integer. The states with half-integer  $J$  values are described not by simple functions, but by two-component spinors (cf. the relativistic description of atomic states with four-component bispinors in Section 2.1, which, in quasirelativistic approaches, are reduced to two-component spinors; see Sections 5.4 and 5.5). Under symmetry operations, the two-component spinors, unlike simple functions, transform in a special way by realizing the so-called *two-valued representations* [3.7].

The two-valued representations are not real representations in the sense described above and do not obey the orthogonality relationships of the types (3.30)–(3.33). Therefore, their inclusion in the point groups significantly complicates the applications. To avoid these difficulties the notion of *double groups* is introduced.

Let us consider a usual point group and formally add to its symmetry operations an additional element  $Q$  describing a rotation by the angle  $2\pi$  around some axis. Assume that  $Q$  is not identical with the  $E$  operation  $Q \neq E$ , but that  $Q^2 = E$ . Then the number of elements of the group is doubled because each operation  $G$  is complemented by a new operation  $QG$ . In particular,  $C_n^n = Q$ ,  $C_n^{2n} = E$ ,  $\sigma^2 = Q$ ,  $\sigma^4 = E$ , and so on. It can be shown that in such a group with formally doubled elements (double group) the double-valued representations describing the symmetry properties of states with half-integer  $J$  values (bispinors) decompose into two single-valued representations that have usual group-theoretical properties. Therefore, if the elements of the double group—its IrReps and their characters—are known, the states with half-integer spin values can be considered in the same manner as described above, provided that they are attributed to double groups.

The double-groups properties can be obtained in a manner similar to those for the simple groups using general theorems of group theory. The doubling of the number of elements does not necessarily double the number of classes (and hence representations) of the group. For instance, in the group of rotations of a cube  $O$  there are 24 elements and five classes considered above (Section 3.2), while in the corresponding double group  $O'$  (the double groups are denoted by the same letters as the simple groups, with a prime) there are 48 elements and eight classes, and the new representations are  $E'_1$ ,  $E'_2$ , and  $G'$  (Appendix 1, Table A1.13).

Some remarks regarding the notations are in order. The representations of the double groups corresponding to the two-valued representations of the simple groups are marked by primes (after Mulliken):  $E'$  and  $G'$  for twofold and fourfold representations, respectively. In the literature, especially for double groups,

the Bethe notations are also widely used. Therefore the following *table of correspondence* for these two types of notations may be useful:

$$\begin{array}{c|c|c|c|c|c|c|c|c}
 \text{Mulliken:} & A & B & E & T_1 & T_2 & E'_1 & E'_2 & G' \\
 \hline
 \text{Bethe:} & \Gamma_1 & \Gamma_2 & \Gamma_3 & \Gamma_4 & \Gamma_5 & \Gamma_6 & \Gamma_7 & \Gamma_8
 \end{array} \quad (3.57)$$

Direct products of IrReps of double groups (as well as simple groups and simple and double groups) are given in Appendix 1, Table A1.14.

### SUMMARY NOTES

1. *Symmetry description* of molecular systems by means of group-theoretical parameters provides for very useful qualitative understanding and quantitative evaluation of their properties.
2. *Symmetry operations* (transformations) of a molecular system can be conveniently described by matrices that form a *mathematical group*. This allows one to apply group theory to the analysis and description of molecular properties.
3. The *irreducible representations (IrReps)* or *symmetry types* of the group and the *characters* of their transformation matrices (the sum of their diagonal elements) are the most important group parameters. The symmetry operations are divided into classes in which their transformation matrices have the same characters. There are tables of classes, IrReps, and their characters for all symmetry groups (see Appendix).
4. Application of group theory to the description of molecular properties is based on the fact that the *energy levels and wavefunctions*—solutions of the Schrödinger equation—*belong necessarily to one of the symmetry types* (IrReps) of the symmetry group of the system, and hence all the stationary states of the system can be classified on symmetry.
5. *Group-theoretical description* allows one to evaluate a variety of important properties of the system, including the possible types of energy states and wavefunctions, symmetry-adapted molecular orbitals, selection rules for transitions between the energy states, possible spontaneous distortions of high-symmetry configurations, and so on. The results of this chapter are used thoroughly in all the other parts of this book.

### EXERCISES

- 3.1. Reveal all the symmetry operations of a hexagonal prism.
- 3.2. Determine the symmetry group of NH<sub>3</sub> (pyramidal), CuF<sub>3</sub> (planar), CH<sub>2</sub>—CH<sub>2</sub>, [ReH<sub>9</sub>]<sup>2-</sup> (tricapped trigonal prism), H<sub>4</sub>[W(CN)<sub>8</sub>] (square antiprism), K<sub>4</sub>[W(CN)<sub>8</sub>] (dodecahedron), and [Ni(CN)<sub>5</sub>]<sup>3-</sup> (square pyramid).

- 3.3. Using the tables of IrReps in the Appendix 1, evaluate the selection rules for electric-dipole and magnetic-dipole optical transitions between the  $A$ ,  $E$ , and  $T$  states in systems with  $O_h$ ,  $T_d$ ,  $D_{3d}$ ,  $D_{2h}$ ,  $D_{4h}$ , and  $I_h$  symmetries. [*Hint*: The components of electric-dipole and magnetic-dipole operators (Section 8.1) transform as corresponding Cartesian coordinates  $x$ ,  $y$ ,  $z$ , and rotations  $R_x$ ,  $R_y$ ,  $R_z$ , respectively.]
- 3.4. Using the tables of characters of IrReps in Appendix 1, show that for cubic groups the symmetric products  $[E \times E] = A_1 + A_2 + E$ ,  $[T \times T] = A + E + T_1 + T_2$ , while for the  $C_{4v}$  group  $[E \times E] = A_1 + A_2 + B_1 + B_2$ .
- 3.5. Following the procedure of building symmetrized (symmetry-adapted)  $A_{1g}$  and  $E_g$ -type  $\sigma$  MOs and  $T_{2g}$   $\pi$  MOs given in Section 3.5 and in Examples 3.2 and 3.3, construct  $\sigma$ - and  $\pi$ -type MOs for the other  $T_{1g}$  and  $T_{2u}$  symmetry types of octahedral complexes of  $O_h$  symmetry in Table 5.1.
- 3.6. Similar to Exercise 3.5 above, construct  $\sigma$ - and  $\pi$ -type MO's for tetrahedral molecular systems with  $T_d$  symmetry (Table 5.2).
- 3.7. Using the tables of IrReps in Appendix 1, find the selection rules for the tensor of polarizabilities  $\alpha_{ij}$  (Section 8.2) for molecular systems with  $O_h$  symmetry. (*Hint*: The components of any tensor  $\alpha_{xx}$ ,  $\alpha_{xy}$ , etc. transform as the corresponding products of Cartesian coordinates  $xx$ ,  $xy$ , etc.)
- 3.8. Example 3.2 shows in detail how to determine the energy terms of the electron configuration  $e^2$ . Obtain in the same way the energy terms of the electron configuration  $t^2$  in systems with cubic symmetries  $T_d$ ,  $O$ , and  $O_h$ .

## REFERENCES

- 3.1. R. Hochstrasser, *Molecular Aspects of Symmetry*, Benjamin, New York, 1966.
- 3.2. F. A. Cotton, *Chemical Applications of Group Theory*, 2nd ed., Interscience, New York, 1971.
- 3.3. J. P. Fackler, Jr., *Symmetry in Coordination Chemistry*, Academic Press, New York, 1979.
- 3.4. I. G. Kaplan, *Symmetry of Many-Electron Systems*, Physical Chemistry Series, E. M. Loebl, ed., Vol. 34, Academic Press, New York, 1975.
- 3.5. H. Bethe, *Ann. Phys.* 3, 133 (1929).
- 3.6. S. Sugano, Y. Tanabe, and H. Kamimura, *Multiplets of Transition-Metal Ions in Crystals*, Academic Press, New York, 1970.
- 3.7. L. Landau, and E. Lifshitz, *Quantum Mechanics*, 3rd ed., Nauka, Moscow, 1974, Chapter 12.
- 3.8. B. S. Tsukerblat, *Group Theory in Chemistry and Spectroscopy. A Simple Guide to Advanced Usage*, Academic Press, New York, 1994.
- 3.9. R. S. Mulliken, *Phys. Rev.* 43, 279 (1933).
- 3.10. P. Garcia-Fernandez, I. B. Bersuker, and J. E. Boggs, *J. Chem. Phys.* 125, 104102 (2006).

---

# 4

---

## CRYSTAL FIELD THEORY

*Simple model theories can often be used as a basis for correct understanding of rather complicated phenomena.\**

The crystal field theory in its application to transition metal compounds discussed in this chapter may serve as an illustration to this statement.

### 4.1. INTRODUCTION

#### **Brief History**

The basis for crystal field theory (CFT) was created by Bethe in 1929 in his classical work “Term splitting in crystals” [4.2]. This publication contains, in essence, all the main elements of modern theory. The first period of development of the CFT in the 1930s is related to the papers by Van Vleck and his coworkers (see Refs. 4.1, 4.3, and references cited therein) in which the origin of the magnetic properties of transition metal ions in crystals was revealed.

The theoretical results obtained by Van Vleck were aimed at “crystalline” effects; their general relevance to coordination compounds was not realized at that time. Nevertheless, some important results illustrating the efficiency of the CFT

\*There is an expression of Enrico Fermi: “A really good theoretical physicist can obtain right answers even with wrong formulas.” Paraphrasing this apothegm, Van Vleck wrote [4.1]: “A really good theoretical chemists can obtain right answers with wrong models.”

were obtained, including explanation of magnetic behavior in the cases of weak and strong ligand fields, reduction of the orbital magnetic moment by the crystal field, temperature dependence of magnetic susceptibility, and the Jahn–Teller effect.

The second period of CFT development, the period of its vigorous growth, began in the 1950s. In works by Ilse, Hartmann, Orgel, Moffitt, Ballhausen, Jorgensen, and others (see Refs. 4.4–4.9 and references cited therein), CFT successfully was shown to explain the origin of absorption spectra in the visible and related regions (the origin of colors), as well as a series of other optical, electric, magnetic, thermodynamic, and electron spin resonance (ESR) properties of transition metal systems (TMSs).

Historically, CFT in its application to inorganic complexes can be considered as a direct extension of prequantum electrostatic considerations. Electrostatic theory, first developed by Kossel [4.10] and Magnus [4.11], is based on the assumption that the central ion and the ligands are kept together by ion–ion or ion–dipole electrostatic interactions. Despite very limited possibilities, the pure electrostatic approach was rather stimulating at the time. It was further developed after the creation of quantum mechanics, which allows for a more adequate description of these ideas.

### Main Assumptions

In its applications to transition metal coordination compounds, CFT is based on the following main assumptions (basic statements):

1. *The transition metal coordination compound (as it is described in Section 1.2) is stable because of the electrostatic interaction between the central atom (CA) or ion and ligands—ions or dipoles.*
2. *The CA is considered with its detailed electronic structure, while the ligands are assumed to be “structureless” sources of electrostatic fields (sometimes allowing for their polarization in the field of the CA and the other ligands).*
3. *The structure and properties of the system based on this model are described by means of quantum mechanics.*

Only statement 1 was employed in the old prequantum theory. Basic assumptions 2 and 3 allow one to consider phenomena that have a quantum nature and take place mainly within the electronic shell of the CA, but do not involve explicitly the electronic structure of the ligands. Despite this significant limitation (for more details, see Section 4.6), CFT, within the limits of its applicability, is a rather efficient means of investigating many aspects of the electronic structure and properties of transition metal compounds.

In accordance with the basic statements of the CFT, the electronic structure of a coordination system is determined by the Schrödinger equation (1.5) with the Hamiltonian  $H$

$$H = H_0 + V + W \quad (4.1)$$

where  $H_0$  includes all the intraatomic interactions in the CA—the kinetic energy of its  $n$  electrons and the interaction between them and with the nucleus,  $V$  is the interaction between the CA electrons and the ligands taken as point charges  $q_i$  or dipoles  $\mu_i$ , and  $W$  is the electrostatic interaction of the positive charge  $Ze$  of the CA nucleus with the ligand charges or dipoles (as above,  $Z$  is the order number of the element in the periodic table and  $e$  is the absolute value of the electronic charge).

Taking the origin of the polar coordinate system at the nucleus, we can denote the  $N$  ligand coordinates by  $\mathbf{R}_i(R_i, \vartheta_i, \phi_i)$ ,  $i = 1, 2, \dots, N$ . Then

$$V = - \sum_i^N \sum_j^n \frac{eq_j}{|\mathbf{r}_j - \mathbf{R}_i|} \quad (4.2)$$

and

$$W = \sum_i^N \frac{Ze q_i}{R_i} \quad (4.3)$$

If  $q_i < 0$ , then the term (4.3) provides the required CA–ligand negative interaction energy due to which the complex is stable. In this case the term  $V$  after (4.2) is positive, and hence the electron–ligand interaction destabilizes the complex. This situation is quite usual in real systems; the CA is electropositive and the ligands are electronegative. Formally, there is a possibility that  $q_i$  is positive, and then  $V$  is negative, providing the necessary stabilization energy, as  $W$  is destabilizing; this model seems to be unreal except when the electrons are formally substituted by positive holes (Section 4.2).

The term  $W$  after (4.3) is seldom considered in CFT explicitly because calculation of the absolute values of stabilization (bonding) energies is beyond the possibilities of this theory. On the other hand,  $W$  is independent of the electron coordinates, and therefore it is constant with respect to the electronic properties, considered in CFT. As usual in quantum chemistry, the valence electrons of the CA are most important in chemical phenomena. Therefore the number of electrons  $n$  in Eq. (4.2) is often the number of the valence electrons, while  $Ze$  is the effective charge of the remaining core.

## 4.2. SPLITTING OF THE ENERGY LEVELS OF ONE $d$ ELECTRON IN LIGAND FIELDS

### Qualitative Aspects and Visual Interpretation

In accordance with the assumptions of the CFT, the main effect of complex formation is produced by the ligands' field, which changes the electronic structure

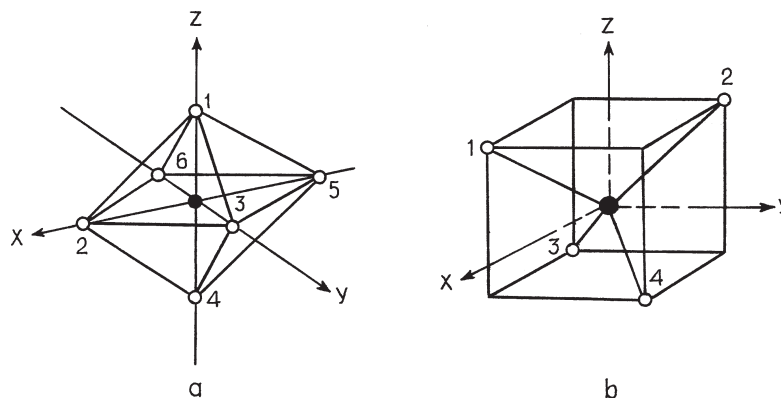


FIGURE 4.1. Ligand numeration in octahedral (a) and tetrahedral (b) complexes.

of the CA. The problem of calculating atomic states in external fields of different symmetries (different ligand positions) was solved by Bethe [4.2]. *The main effect of ligand influence on the states of the CA is the splitting of its energy levels.* The origin of this splitting is known in quantum mechanics as the *Stark effect*.

Consider the simplest (from the CFT perspective) case when the central ion of an octahedral complex (Fig. 4.1a) contains only one  $d$  electron over the closed shell, as, for instance, in  $[\text{Ti}(\text{H}_2\text{O})_6]^{3+}$ . The ground state of the  $\text{Ti}^{3+}$  ion is  ${}^2D$  (Section 2.2, Table 2.6). This term has an orbital momentum  $L = 2$ , an orbital degeneracy  $2L + 1 = 5$ , and a spin  $S = \frac{1}{2}$  (doublet state). The five orbital states are just the five possible angular states of the only  $d$  electron given in Table 2.1, with identical radial parts. As seen from Fig. 2.3, the three orbitals  $d_{xy}$ ,  $d_{xz}$ ,  $d_{yz}$  ( $t_{2g}$  orbitals) are oriented in space in such a way that their distribution maxima (their lobes) fall into the region in between the coordinate axes. The lobes of the remaining two orbitals,  $d_{z^2}$  and  $d_{x^2-y^2}$  ( $e_g$  orbitals), are oriented exactly along the axes.

Compare the electron distributions in the two types of  $d$  states,  $e_g$  and  $t_{2g}$ , say,  $d_{x^2-y^2}$  ( $e_g$ ) and  $d_{xy}$  ( $t_{2g}$ ), illustrated in Fig. 4.2. Because the ligands have negative charges (ligand-dipoles are oriented with the negative pole to the CA), we easily conclude that in octahedral complexes the  $d_{x^2-y^2}$  electron is subject to a stronger electrostatic repulsion from the ligands than is the  $d_{xy}$  one. Hence the electron energies of these two states (which are equal in the free ion), under the electrostatic influence of the ligands become different; the  $d_{x^2-y^2}$  energy level is higher than the  $d_{xy}$  one. All three  $t_{2g}$  states ( $d_{xy}$ ,  $d_{xz}$ ,  $d_{yz}$ ) are fully equivalent with respect to the six ligands, and therefore they have the same (lower) energy, forming a threefold-degenerate term. It can be shown that the two  $e_g$  states also have equal energies, forming a twofold-degenerate term.

Thus the five  $d$  states that have the same energy in the free atom (or ion) are divided into two groups of states with different energies under the octahedral field of the ligands. In other words, *the fivefold-degenerate  $D$  term of the free*

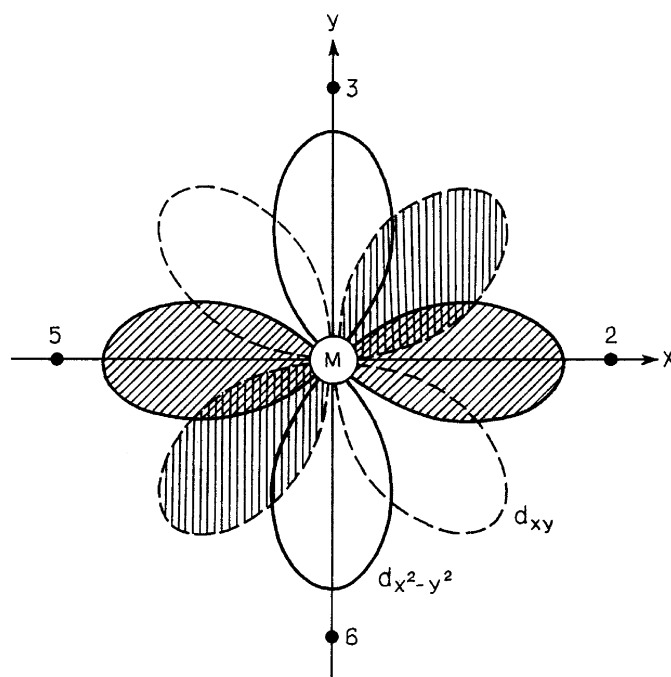


**FIGURE 4.2.** Comparison of electron distributions in the two  $d$  states,  $d_{x^2-y^2}$  (solid lines) and  $d_{xy}$  (dashed lines) with respect to the four ligands in the  $xy$  plane (the positive lobes of both functions are shadowed).

ion is split in the field of the ligands of an octahedral complex into two terms: threefold-degenerate  ${}^2T_{2g}$  and twofold-degenerate  ${}^2E_g$ :

$${}^2D \rightarrow {}^2T_{2g} + {}^2E_g \quad (4.4)$$

The denotation here is that due to Mulliken (Sections 3.3 and 3.6). Note that one-electron states of the same symmetry are denoted by corresponding lowercase letters ( $t_{2g}$ ,  $e_g$ , etc.) as distinct from many-electron terms denoted by capital letters.

It follows from these considerations that the splitting (4.4) occurs as a result of the smaller repulsion (from the ligands) of the  $t_{2g}$  states than  $e_g$  states, but all five states are destabilized in the field of the ligands. For applications, it is convenient to present this effect quantitatively as a sum of two effects: *destabilization and splitting*. This is illustrated in Fig. 4.3; the corresponding calculations of the destabilization  $E_0$  and splitting  $\Delta$  values are given below.

Visually, the destabilization equals the energy of repulsion of the CA electrons from the ligand charges when they are assumed to have spherically symmetric distribution around the central atom; this repulsion  $E_0$  is the same for all five  $d$  electrons. Obviously the destabilization must be compensated for by the attraction



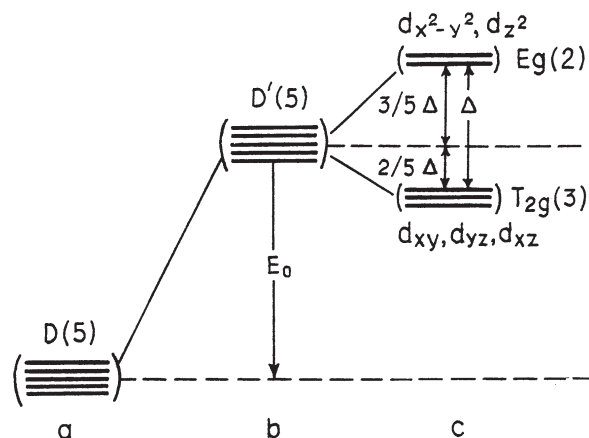


**FIGURE 4.3.** Destabilization  $E_0$  and splitting  $\Delta$  of the atomic  $D$  term in the field of six ligands in an octahedral complex (the degeneracies are indicated in parantheses): (a) free atom; (b) spherical averaged ligand field; (c) octahedral field.

term  $W$  between the CA core and ligands in Eq. (4.3); otherwise the complex is not stable.

For a tetrahedral complex the qualitative picture of the term splitting is inverse to that of the octahedral case. Indeed, in the tetrahedral environment of four ligands the  $t_{2g}$  orbitals are oriented with their lobes much closer to the ligands than are the  $e_g$  orbitals, and hence the former are subject to stronger repulsion than the latter. Therefore the energy levels of the  $t_{2g}$  orbitals are higher than those of  $e_g$ . Symmetry considerations and the calculations given below show that in the tetrahedral system, again, the three  $t_{2g}$  states, as well as the two  $e_g$  states, remain degenerate, forming the  $T_2$  and  $E$  terms, respectively (in the case of a tetrahedron there is no inversion symmetry and no classification of the terms by  $g$  and  $u$ ; see Section 3.4 and Appendix 1). Hence, in a tetrahedral complex, the  $D$ -term splitting is (Fig. 4.4b)

$$D \rightarrow T_2 + E \quad (4.5)$$

which is very similar to that of an octahedral complex (4.4). However, in contrast to the octahedral case, the  $T_2$  term is higher in energy than the  $E$  term, and the splitting magnitude, as well as the destabilization energy, is smaller.

Both octahedral and tetrahedral symmetries appertain to the cubic groups of symmetry (Appendix 1). Figure 4.4 also shows splitting of the atomic  $D$  term in the field of eight ligands at the corners of a cube. If the symmetry of the ligand field is lowered, the terms  $T_2$  and  $E$  may be subject to further splitting. Consider the case of a tetragonally distorted octahedron formed by the elongation of the regular octahedron along one of its diagonals, say,  $z$ . In this case the energies of the two  $e_g$  orbitals,  $d_{x^2-y^2}$  and  $d_{z^2}$ , are no longer equal, since the repulsion

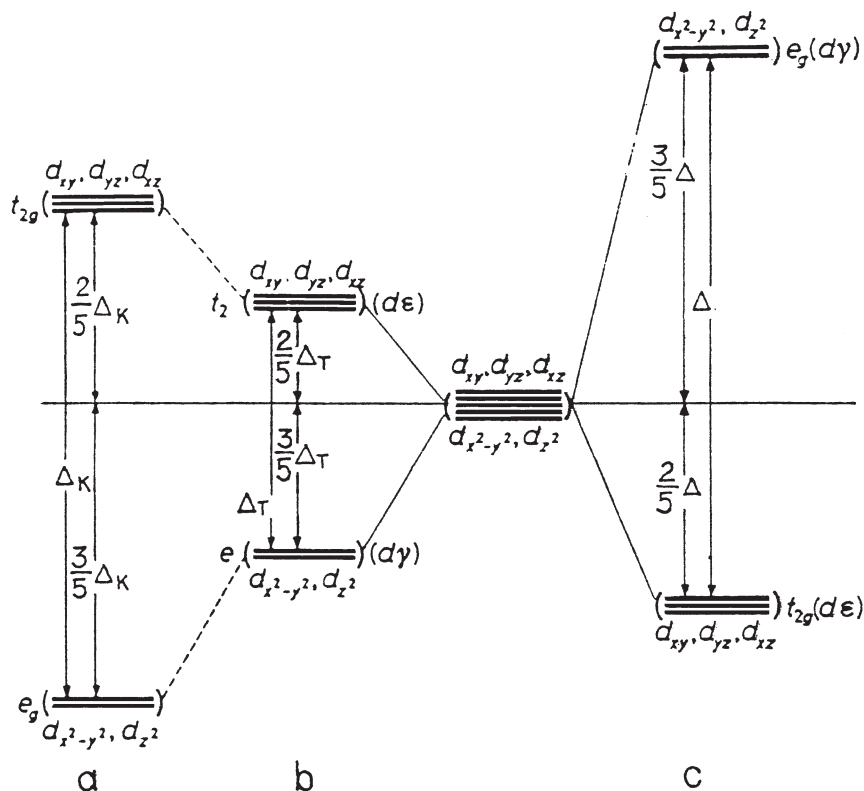


**FIGURE 4.4.** Splitting of the  $D$  term in cubic (a), tetrahedral (b), and octahedral (c) fields of the ligands.

is lower in the latter. The three  $t_{2g}$  states do not remain equivalent, either; two of them,  $d_{xz}$  and  $d_{yz}$ , experience (equally) less repulsion from the ligands than does  $d_{xy}$ . Therefore, in the tetragonally distorted octahedron the atomic  $D$  term splits into four terms, from which only  $E_g(d_{xz}, d_{yz})$  remains twofold-degenerate (Fig. 4.5). If the symmetry of the ligand field is further lowered (e.g., if the two axes,  $x$  and  $y$ , are nonequivalent), the twofold-degenerate term splits as well.

For a CA with more than one  $d$  electron, the visual interpretation of the splitting becomes more complicated but the main idea remains the same; in the CFT model the energies of the states that are degenerate in the free atom (ion) may differ because of the variation in repulsion from the ligands.

If the number of  $d$  electrons above the closed shell equals nine, the visual interpretation of the splitting becomes possible again; it is quite similar to that of  $d^1$ , considered above. Indeed, the  $d^9$  configuration can be formally presented as one positive electronic charge above the closed-shell  $d^{10}$  configuration, that is, a  $d$  hole in the  $d^{10}$  shell (see the principle of complementary configurations [4.15] in Section 2.2). The behavior of the states of the  $d$  hole in the field of the ligands

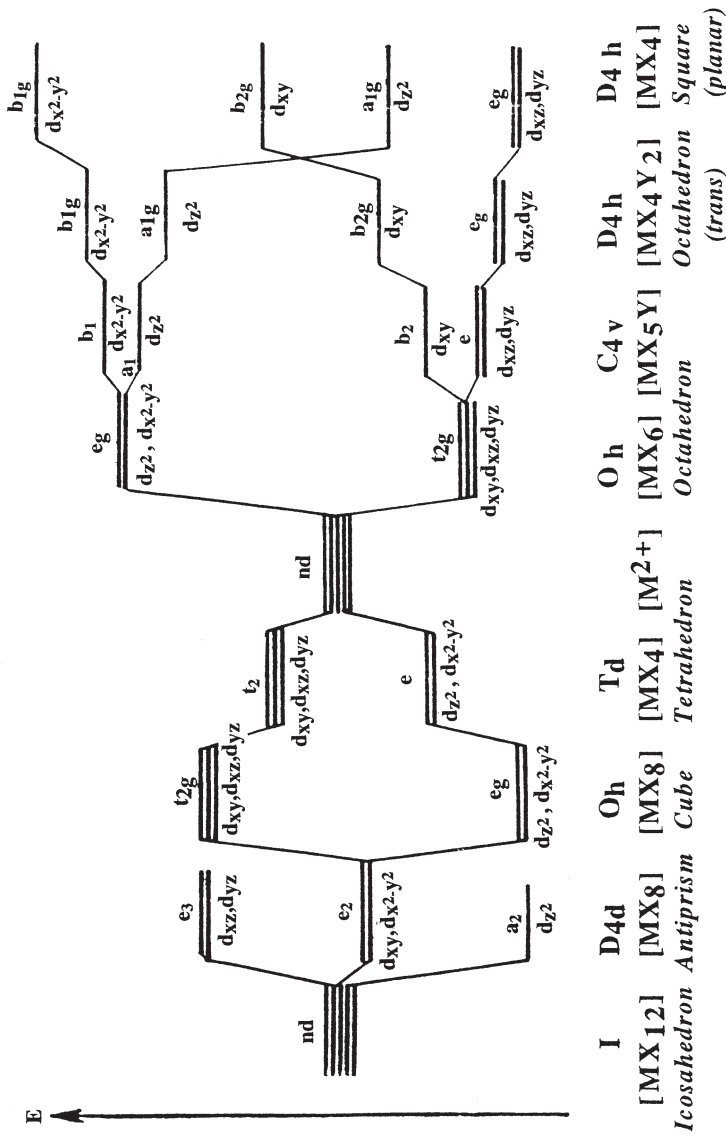


**FIGURE 4.5.** Splitting of  $d$  orbital energy levels in ligand fields of different symmetries. In  $\text{MX}_5\text{Y}$  and  $\text{MX}_4\text{Y}_2$  complexes the splitting of the  $T_{2g}$  and  $E_g$  terms can be inverted depending on the ratio of field strengths  $X/Y$ . (After Schmidtke [4.12].)

is the same as for one  $d$  electron, with the distinction that the charge of the  $d$  hole is opposite that of the  $d$  electron, and hence the sign of the interaction with the ligands changes from repulsion to attraction. For these reasons the ground state of the  $d^9$  configuration (the  $d$  hole) is also  ${}^2D$ , as for the  $d^1$  configuration, and its splitting in crystal fields of different symmetries has the same components as does  $d^1$ , but with their mutual arrangement inverse to that of  $d^1$ . *This rule of inverse term splitting for complimentary electron configurations is valid for any pair of electronic configuration,  $d^n$  and  $d^{10-n}$  ( $n = 1, 2, 3, 4$ ), in which the number of, respectively,  $d$  electrons and  $d$  holes over the closed shell  $d^{10}$  is the same.*

### Calculation of the Splitting Magnitude

The quantitative evaluation of energy-level splitting of the CA in the field of ligands is relatively simple. The calculations should be based on the Schrödinger equation (1.5) with the Hamiltonian (4.1). As mentioned above, the term  $W$  after (4.3) is not important for the splitting since it is independent of electron coordinates. To simplify the calculations, further assumptions are introduced in the CFT. In this section we assume that the term  $V$ , the electron–ligand interaction, is much smaller than the intraatomic interactions described by  $H_0$ , and hence  $V$  can be considered as a perturbation to the solutions of  $H_0$ . This assumption is valid if the resulting term splitting obtained in this way is smaller than the energy gap between the terms of the free atom or ion (solutions of  $H_0$ ). In Sections 4.3 and 4.4 this statement is subject to modification.

Consider the case of one  $d$  electron above the closed shell, that is, the electron configuration of the CA  $[A]d^1$ , where  $[A]$  denotes the atomic closed-shell configuration. The solution for the free ion with the Hamiltonian  $H_0$  yields the fivefold orbitally degenerate  ${}^2D$  term. To reveal the modifications of this term under the perturbation  $V$  after (4.2), one has to solve the perturbation theory problem, which in the case of fivefold degeneracy reduces to the secular equation of the fifth order with respect to the energy level corrections  $\varepsilon$ :

$$\|V_{mm'} - \varepsilon\delta_{mm'}\| = 0 \quad m, m' = 2, 1, 0, -1, -2 \quad (4.6)$$

or in more detail

$$\begin{vmatrix} V_{22} - \varepsilon & V_{21} & V_{20} & V_{2-1} & V_{2-2} \\ V_{12} & V_{11} - \varepsilon & V_{10} & V_{1-1} & V_{1-2} \\ V_{02} & V_{01} & V_{00} - \varepsilon & V_{0-1} & V_{0-2} \\ V_{-12} & V_{-11} & V_{-10} & V_{-11} - \varepsilon & V_{-1-2} \\ V_{-22} & V_{-21} & V_{-20} & V_{-2-1} & V_{-22} - \varepsilon \end{vmatrix} = 0 \quad (4.7)$$

where, in accordance with (4.2)

$$V_{mm'} = \sum_i e q_i \int \frac{\psi_m^* \psi_{m'}}{|\mathbf{r} - \mathbf{R}_i|} d\tau \quad (4.8)$$

**TABLE 4.1. Coefficients  $A_{mm'}$  and  $B_{mm'}$  in Matrix Elements of the Crystal Field for a  $d$  Electron (4.9)<sup>a</sup>**

$m$	$(63/\sqrt{4\pi})A_{mm'}$					$(35/\sqrt{4\pi})B_{mm'}$				
	$m'$					$m'$				
	2	1	0	-1	-2	2	1	0	-1	-2
2	1	$-\sqrt{5}$	$\sqrt{15}$	$-\sqrt{35}$	$\sqrt{70}$	$-\sqrt{20}$	$\sqrt{30}$	$-\sqrt{20}$	0	0
1	$\sqrt{5}$	-4	$\sqrt{30}$	$-\sqrt{40}$	$\sqrt{35}$	$-\sqrt{30}$	$\sqrt{5}$	$\sqrt{5}$	$-\sqrt{30}$	0
0	$\sqrt{15}$	$-\sqrt{30}$	6	$-\sqrt{30}$	$\sqrt{15}$	$-\sqrt{20}$	$-\sqrt{5}$	$\sqrt{20}$	$-\sqrt{5}$	$-\sqrt{20}$
-1	$\sqrt{35}$	$-\sqrt{40}$	$\sqrt{30}$	-4	$\sqrt{5}$	0	$-\sqrt{30}$	$\sqrt{5}$	$\sqrt{5}$	$-\sqrt{30}$
-2	$\sqrt{70}$	$-\sqrt{35}$	$\sqrt{15}$	$-\sqrt{5}$	1	0	0	$-\sqrt{20}$	$\sqrt{30}$	$-\sqrt{20}$

<sup>a</sup>  $D_{mm'} = (4\pi)^{1/2}\delta_{mm'}$ .

and the functions of the  $d$  states are taken in their general form (2.2) (not as real combinations in Table 2.1) with the indices  $m$  and  $m'$  listed in (4.6).

The general expression for  $V_{mm'}$  (which is most important in the CFT) is obtained in Appendix 2, Eq. (A2.8):

$$\begin{aligned}
 V_{mm'} = \sum_i e q_i [ & A_{mm'} F_4(R_i) Y_4^{m-m'}(\vartheta_i, \phi_i) + B_{mm'} F_2(R_i) Y_2^{m-m'}(\vartheta_i, \phi_i) \\
 & + D_{mm'} F_0(R_i) Y_0^{m-m'}(\vartheta_i, \phi_i) ] \quad (4.9)
 \end{aligned}$$

where  $A_{mm'}$ ,  $B_{mm'}$ , and  $D_{mm'}$  are some constants (determined by corresponding Clebsch–Gordan coefficients) given in Table 4.1, while the functions  $F_k(R)$  [not to be confused with the Slater–Condon constants  $F_k$  after (2.32)] is given by the expression

$$F_k(R) = R^{-(k+1)} \int_0^R r^k R_{nl}^2(r) r^2 dr + R^k \int_R^\infty r^{-(k+1)} R_{nl}^2(r) r^2 dr \quad (4.10)$$

with radial functions  $R_{n2}(r)$  after Table 2.3 (not to be confused with the ligand coordinates  $R$ ); they can be calculated and expressed in analytical form (A2.10). In Example 4.1 and Appendix 3 calculations of the splitting magnitude  $\Delta$  in systems of different symmetry are shown in more detail.

Analyzing the crystal field splitting obtained in Example 4.1 and in Appendix 3, one can see that it has some interesting general features. In particular, there is always *the preservation of the center of gravity*—the sum of the energy level displacements (from the  $E_0$  value) multiplied by their degeneracies equals zero. For instance, for the splitting  $D \rightarrow T_{2g} + E_g$ , we have  $2 \cdot \frac{3}{5}\Delta - 3 \cdot \frac{2}{5}\Delta = 0$ . This rule enables us to predict some relations between the energy-level positions with respect to  $E_0$ . As compared with the octahedron, the corresponding splitting in the tetrahedron, as mentioned above, is inverted and smaller (Fig. 4.4).

**EXAMPLE 4.1*****Splitting of a  $d$ -Electron Term in Octahedral Crystal Fields***

By way of example, let us calculate the splitting of a  $d$  electron term in an octahedral field of six identical ligands at the corners of a regular octahedron. The ligand charges and coordinates are (Fig. 4.1a)

$$\begin{aligned} q_i &= q & R_i &= R & i &= 1, 2, \dots, 6 \\ \vartheta_1 &= 0 & \vartheta_2 &= \vartheta_3 = \vartheta_5 = \vartheta_6 &= \frac{\pi}{2} & \vartheta_4 &= \pi \\ \phi_2 &= 0 & \phi_3 &= \frac{\pi}{2} & \phi_5 &= \pi & \phi_6 &= \frac{3\pi}{2} \end{aligned} \quad (4.11)$$

Substituting these values into Eq. (4.9) and taking into account the data of Table 4.1, we find that  $V_{21} = V_{20} = V_{2-1} = V_{10} = V_{1-1} = V_{1-2} = V_{0-1} = V_{0-2} = V_{-1-2} = 0$ , and only four matrix elements,  $V_{00}$ ,  $V_{11}$ ,  $V_{22}$ , and  $V_{2-2}$ , are nonzero:

$$\begin{aligned} V_{22} &= V_{-2-2} = eq[6F_0(R) + \frac{1}{6}F_4(R)] \\ V_{11} &= V_{-1-1} = eq[6F_0(R) - \frac{2}{3}F_4(R)] \\ V_{00} &= eq[6F_0(R) + F_4(R)] \\ V_{-22} &= V_{2-2} = \frac{5}{6}eqF_4(R) \end{aligned} \quad (4.12)$$

With these matrix elements the roots of Eq. (4.7) can be obtained directly:

$$\begin{aligned} \varepsilon_1 &= V_{00} \\ \varepsilon_2 &= V_{22} + V_{2-2} \\ \varepsilon_3 &= V_{22} - V_{2-2} \\ \varepsilon_4 &= \varepsilon_5 = V_{11} \end{aligned} \quad (4.13)$$

Then we note that  $V_{22} + V_{2-2} = V_{00}$  and  $V_{22} - V_{2-2} = V_{11}$ . Finally the roots  $\varepsilon$ —perturbation corrections to the atomic energy levels—are

$$\begin{aligned} \varepsilon_1 &= \varepsilon_2 = V_{00} = eq[6F_0(R) + F_4(R)] \\ \varepsilon_3 &= \varepsilon_4 = \varepsilon_5 = V_{11} = eq[6F_0(R) - \frac{2}{3}F_4(R)] \end{aligned} \quad (4.14)$$

Thus, in accordance with the above-described qualitative results, the  $d$  electron energy levels ( ${}^2D$  term) are split by the octahedral ligand field into twofold ( $E_g$ )- and threefold ( $T_{2g}$ )-degenerate terms. Furthermore, Eqs. (4.14) allow one to obtain the expressions for absolute values and signs of the splitting  $\Delta$  and destabilization energy  $E_0$ . Indeed,

from (4.10) it is seen that all the functions  $F_k(R)$  are positive,  $F_k > 0$ . Therefore  $V_{00} > V_{11}$ , and the twofold-degenerate  $E_g$  term is higher in energy than the  $T_{2g}$  one. *The splitting  $\Delta$  is the main CFT parameter.* We have

$$\Delta = \varepsilon(E_g) - \varepsilon(T_{2g}) = \frac{5}{3}eqF_4(R) \quad (4.15)$$

Then the expressions for the energies (4.14) can be rewritten as follows:

$$\begin{aligned} \varepsilon(E_g) &= E_0 + \frac{3}{5}\Delta \\ \varepsilon(T_{2g}) &= E_0 - \frac{2}{5}\Delta \end{aligned} \quad (4.16)$$

where

$$E_0 = 6eqF_0(R) \quad (4.17)$$

is just the average energy of repulsion of the  $d$  electron from six negative charges  $q$  when they are uniformly distributed over a sphere of radius  $R$  with the center at the CA, the destabilization energy. Similarly, the splitting and destabilization can be calculated for other types of coordination given in Appendix 3.

Using (A3.14), we have

$$\varepsilon(T_2) = E_0^T + \frac{2}{5}\Delta_T \quad (4.18)$$

$$\varepsilon(E) = E_0^T - \frac{3}{5}\Delta_T \quad (4.19)$$

where

$$\Delta_T = \frac{20}{27}eqF_4(R) \quad (4.20)$$

$$E_0^T = 4eqF_0(R) \quad (4.21)$$

Note that with the same  $R$  and  $q$ ,  $\Delta_T = -\frac{4}{9}\Delta$ , that is, the splitting magnitude in tetrahedral symmetry, *ceteris paribus*, is  $\frac{4}{9}$  times the octahedral splitting.

In the cubic coordination (eight ligands at the corners of a cube) the splitting and destabilization energy are qualitatively similar to those of the tetrahedral case, but 2 times larger in magnitude [Eqs. (A3.17) and (A3.18)]:

$$\Delta_C = \frac{40}{27}eqF_4(R) = 2\Delta_T \quad (4.22)$$

$$E_0^C = 8eqF_0(R) = 2E_0^T \quad (4.23)$$

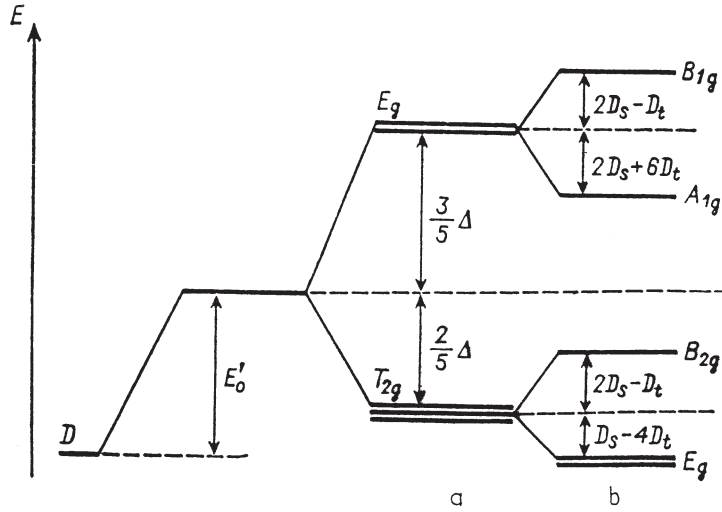


**FIGURE 4.6.** Splitting of the energy levels of  $d$  states ( $D$  term) in regular octahedral field (a) and tetragonally distorted (elongated octahedral) field (b);  $E'_0$  is the spherical-symmetric destabilization.

For tetragonally distorted octahedra the description of the splitting requires, in addition to the main CFT parameter  $\Delta$ , two parameters  $D_s$  and  $D_t$  (A3.7):

$$D_s = \frac{2}{7}eq[F_2(R_2) - F_2(R_1)] \quad (4.24)$$

$$D_t = \frac{2}{21}eq[F_4(R_2) - F_4(R_1)] \quad (4.25)$$

where  $R_1$  and  $R_2$  are the distances between the CA and the axial and equatorial ligands, respectively. With these parameters, the energy levels of the  $d$  states in the tetragonally distorted octahedron are (Fig. 4.6):

$$\begin{aligned} \varepsilon(A_{1g}; d_{z^2}) &= E'_0 + \frac{3}{5}\Delta - 2D_s - 6D_t \\ \varepsilon(B_{1g}; d_{x^2-y^2}) &= E'_0 + \frac{3}{5}\Delta + 2D_s - D_t \\ \varepsilon(B_{2g}; d_{xy}) &= E'_0 - \frac{2}{5}\Delta + 2D_s - D_t \\ \varepsilon(E_g; d_{xz}, d_{yz}) &= E'_0 - \frac{2}{5}\Delta - D_s + 4D_t \end{aligned} \quad (4.26)$$

where [cf. (4.17)]

$$E'_0 = eq[2F_0(R_1) + 4F_0(R_2)] \quad (4.27)$$

and  $\Delta$  is the same as in Eq. (4.15).

A planar-quadratic complex can be considered as the limit case of a tetragonally distorted octahedron with  $R_1 \rightarrow \infty$ . Then  $F_k(R_1) \rightarrow 0$ ,  $D_t = \frac{2}{35}\Delta$



(Appendix 3), and only two independent parameters,  $D_s$  and  $\Delta$ , are needed to describe the splitting (Fig. 4.6). Following (A3.10), we obtain

$$\begin{aligned}\varepsilon(A_{1g}; d_{z^2}) &= E_0'' + \frac{9}{35}\Delta - 2D_s \\ \varepsilon(B_{1g}; d_{x^2-y^2}) &= E_0'' + \frac{19}{35}\Delta + 2D_s \\ \varepsilon(B_{2g}; d_{xy}) &= E_0'' - \frac{16}{35}\Delta + 2D_s \\ \varepsilon(E_g; d_{xz}, d_{yz}) &= E_0'' - \frac{6}{35}\Delta - D_s\end{aligned}\quad (4.28)$$

with  $\Delta$  after (4.15) and

$$E_0'' = 4eqF_4(R) \quad (4.29)$$

If the ligand is a point dipole, the term splitting is qualitatively the same, as in the case of point charges. Assuming that the dimensions of the dipole with the dipole moment  $\mu$  are much smaller than the distance to the CA, one can obtain the following expression for the splitting magnitude in the octahedral case (A3.3):

$$\Delta = -\frac{5}{3}e\mu F_4'(R) \quad (4.30)$$

where the prime at  $F$  means its derivative [cf. (4.15)]; note that  $F_4' < 0$ .

For more complicated coordination the calculations can be carried out in a similar way, first evaluating the matrix elements  $V_{mm'}$  after (4.9), and then solving the secular equation (4.7). For lower symmetries (including those resulting from different ligands), numerical solutions of (4.7) may be necessary. The results for planar trigonal coordination, trigonal bipyramid and antiprism, and some other cases can be found in Ref. 4.13; another example, a semicoordinated octahedron prism of  $C_{2v}$  symmetry with 1 : 4 : 2 stereochemistry (of the type  $\text{NbF}_7^{2-}$ ) has been considered [4.14].

### Group-Theoretical Analysis

Let us discuss now the problem of term splitting from the point of view of symmetry considerations, given in Chapter 3, without employing the secular equation (4.7). For a free atom the group of symmetry transformations is the group of rotations of a sphere  $R(3)$  that has an infinite number of elements and many irreducible representations (IrReps). The spherical functions  $Y_L^M(\vartheta, \phi) = P_L^M(\cos \vartheta)e^{iM\phi}$ , where  $P_L^M$  is an associated Legendre polynomial [see (2.2)], can be taken as a basis of this group. For each  $L$  value there are  $2L + 1$  spherical functions with different  $M$  ( $M = 0, \pm 1, \dots, \pm L$ ), which transform to each other by the symmetry transformations of the group and produce the IrRep of dimensionality  $2L + 1$ . Hence the atomic terms have a  $(2L + 1)$ -fold degeneracy.

For the spherical group the characters of the matrices of the representations for a rotation by an angle  $\phi$  can be calculated by the following formula [4.2]:

$$X(\phi) = \frac{\sin(L + \frac{1}{2})\phi}{\sin \frac{1}{2}\phi} \quad (4.31)$$

When the atom is introduced in an external field of, for instance,  $O_h$  symmetry, the symmetry of the system as a whole (the atom plus the field) becomes  $O_h$ , and only those symmetry transformations (rotations) that comply with the  $O_h$  restrictions remain. The number of symmetry transformations is thus reduced, which means that the IrRep of the spherical group, to which the atomic term of  $(2L + 1)$ -fold degeneracy belongs, may become reducible in the  $O_h$  group (Section 3.3). The reducible representation can be decomposed into several IrReps of smaller dimensionality, to which several energy terms of lower degeneracy belong—the term splits.

To determine the term splitting, the representation of the spherical group with the dimensionality  $2L + 1$  should be decomposed into IrReps of the  $O_h$  group. This problem is solved completely by means of the relation (3.33). Consider, for example, the atomic term  $D$  in the octahedral complex of  $O_h$  symmetry, discussed above. For this term  $L = 2$ ,  $2L + 1 = 5$ . To employ (3.33), one has to calculate first the characters  $X(G)$  of the representation of the spherical group with  $L = 2$  for all operations  $G$  of the  $O_h$  group. For the first classes that include rotations only (Table 3.1) the characters can be calculated after (4.31). For the remaining five classes the symmetry elements are those of the first five classes multiplied by the operation of inversion  $I$  (Section 3.2), and hence their characters can be determined as a product of the characters of the two factors. Since the functions of the basis (the spherical functions with  $L = 2$ ) are invariant with respect to the inversion transformation [ $X(I) = 1$ ], the characters for the elements of the five classes with inversion are the same as that without inversion.

For instance, for the element  $C'_2$  (rotation by an angle  $\pi$ ), using (4.31) with  $L = 2$ , we obtain

$$X(\pi) = \frac{\sin \frac{5}{2}\pi}{\sin(\pi/2)} = 1$$

and for the element  $\sigma_d = C'_2 I$ :

$$X(\sigma_d) = X(C'_2) \cdot X(I) = 1 \cdot 1 = 1$$

In a similar way one can obtain the characters for all the other symmetry operations of the  $O_h$  group listed in Table 3.1, as follows:

$G$	$E$	$6C_4$	$3C_4^2 = 3C_2$	$8C_3$	$6C'_2$	$I$	$6S_4$	$3\sigma_h$	$8S_6$	$6\sigma_d$
$X(G)$	5	-1	1	-1	1	5	-1	1	-1	1

(4.32)

Now, using Eq. (3.33), one can find out the irreducible representations of the  $O_h$  group comprised in the reducible representation (4.32). We have

**TABLE 4.2. Types of Symmetry (Irreducible Representations of the Tables in Appendix 1) to Which the Atomic States with Given Quantum Numbers  $L(l)$  or  $J(j)$  Belong in the Point Groups of Different Symmetries<sup>a</sup>**

$L$ or $J$	$O_h$	$T_d$	$D_3$	$D_{4h}$	$C_{4v}$	$C_{2v}$
0	$A_{1g}$	$A_1$	$A_1$	$A_{1g}$	$A_1$	$A_1$
1	$T_{1u}$	$T_2$	$A_2 + E$	$A_{2u} + E_u$	$A_1 + E$	$A_1 + B_1 + B_2$
2	$E_g$	$E$	$E$	$A_{1g} + B_{1g}$	$A_1 + B_1$	$2A_1$
	$T_{2g}$	$T_2$	$A_1 + E$	$B_{2g} + E_g$	$B_2 + E$	$A_2 + B_1 + B_2$
3	$A_{2u}$	$A_1$	$A_2$	$B_{1u}$	$B_2$	$A_2$
	$T_{1u}$	$T_2$	$A_2 + E$	$A_{2u} + E_u$	$A_1 + E$	$A_1 + B_1 + B_2$
	$T_{2u}$	$T_1$	$A_1 + E$	$B_{2u} + E_u$	$B_1 + E$	$A_1 + B_1 + B_2$
4	$A_{1g}$	$A_1$	$A_1$	$A_{1g}$	$A_1$	$A_1$
	$E_g$	$E$	$E$	$A_{1g} + B_{1g}$	$A_1 + B_1$	$2A_1$
	$T_{1g}$	$T_1$	$A_2 + E$	$A_{2g} + E_g$	$A_2 + E$	$A_2 + B_1 + B_2$
	$T_{2g}$	$T_2$	$A_1 + E$	$B_{2g} + E_g$	$B_2 + E$	$A_2 + B_1 + B_2$
5	$E_u$	$E$	$E$	$A_{1u} + B_{1u}$	$A_2 + B_2$	$2A_2$
	$T_{1u}$	$T_2$	$A_2 + E$	$A_{2u} + E_u$	$A_1 + E$	$A_1 + B_1 + B_2$
	$T_{2u}$	$T_1$	$A_1 + E$	$B_{2u} + E_u$	$B_1 + E$	$A_1 + B_1 + B_2$

<sup>a</sup>Belonging to several types of symmetry in the cases of  $L \neq 0$  or  $J \neq 0$  can be interpreted as a corresponding splitting.

$$a^{(A_{1g})} = \frac{1}{48}(5-6+3-8+6+5-6+3-8+6) = 0$$

$$a^{(E_g)} = \frac{1}{48}(10+0+6+8+0+10+0+6+8+0) = 1$$

and so on. In this way one finds that  $a^{(E_g)} = 1$ ,  $a^{(T_{2g})} = 1$ , and all the other  $a^{(\beta)} = 0$ . It follows that the fivefold-degenerate  $D$  term in the field of  $O_h$  symmetry splits into two terms: twofold-degenerate  $E_g$  and threefold-degenerate  $T_{2g}$ :  $D \rightarrow E_g + T_{2g}$ . Quite similarly, one can find the splitting in all other cases of this kind.

Table 4.2 gives the IrReps (symmetry types) to which the orbital states of a free atom (spherical functions) belong in fields of different symmetries; comparison of symmetry types in different groups gives the expected splitting of the corresponding terms. For instance, the  $D$  term ( $L = 2$ ) splits into  $E_g + T_{2g}$  in the  $O_h$  group,  $E + A_1 + E$  in the  $D_3$  group,  $A_{1g} + B_{1g} + B_{2g} + E_g$  in the  $D_{4h}$  group, and so on. Similar correlations between the symmetry representations that show the possible term splitting when passing from higher symmetries to lower ones in other cases are given in Table 4.3.

### 4.3. SEVERAL $d$ ELECTRONS

#### Case of a Weak Field

If the electron configuration of the CA contains more than one  $d$  electron above the closed shell, the picture of possible energy terms and their splitting in the ligand fields is significantly complicated by the interaction between the

**TABLE 4.3. Correlations of the Irreducible Representations of the  $O_h$  and  $D_{4h}$  Symmetry Groups with Their Subgroups Indicating the Corresponding Symmetry Transformations and Splitting**

Group	Subgroup			Group	Subgroup	
	$T_d$	$D_{4h}$	$D_3$		$D_{4h}$	$C_{4v}$
$A_{1g}$	$A_1$	$A_{1g}$	$A_1$	$A_{1g}$	$A_1$	$A_1$
$A_{1u}$	$A_2$	$A_{1u}$	$A_1$	$A_{1u}$	$A_2$	$A_2$
$A_{2g}$	$A_2$	$B_{1g}$	$A_2$	$A_{2g}$	$A_2$	$B_1$
$A_{2u}$	$A_1$	$B_{1u}$	$A_2$	$A_{2u}$	$A_1$	$B_2$
$E_g$	$E$	$A_{1g} + B_{1g}$	$E$	$B_{1g}$	$B_1$	$A_1$
$E_u$	$E$	$A_{1u} + B_{1u}$	$E$	$B_{1u}$	$B_2$	$A_2$
$T_{1g}$	$T_1$	$A_{2g} + E_g$	$A_2 + E$	$B_{2g}$	$B_2$	$B_1$
$T_{1u}$	$T_2$	$A_{2u} + E_u$	$A_2 + E$	$B_{2u}$	$B_1$	$B_2$
$T_{2g}$	$T_2$	$B_{2g} + E_g$	$A_1 + E$	$E_g$	$E$	$A_2 + B_2$
$T_{2u}$	$T_1$	$B_{2u} + E_u$	$A_1 + E$	$E_u$	$E$	$A_1 + B_1$

$d$  electrons. If the ligand field is not very strong, the atomic terms can still be classified by the quantum number of the atomic total momentum  $L$ , and the influence of the ligands can be taken as a perturbation of the atomic terms; this is *the case of weak ligand field*.

The term *weak field* is discussed below in more detail (in particular, see the beginning of Section 4.4 for some different terminology). Here we emphasize that under the influence of the weak field of the ligands the  $LS$  coupling between the  $d$  electrons (Section 2.2) is not destroyed, and the term with the highest spin is the ground term. Therefore the complexes with weak ligand fields are also called *high-spin complexes*.

For several  $d$  electrons the main effect of ligand fields, as for one  $d$  electron, is energy term splitting. However, unlike the  $d^1$  case, the visual interpretation of the splitting of the terms of  $d^n$  configuration ( $n > 1$ ) is difficult. But the cause of the splitting is the same; in the ligand field, the atomic (multielectron) states that have the same energy in the free atom (ion), are subject to different repulsion from the ligands owing to their different orientation with respect to these ligands.

Quantitatively, for the electronic configuration of the CA  $A(nd)^2$  in the ligand field, which is weaker than the interaction between the  $d$  electrons, one can consider first the possible states of the free atom (ion) and find its terms, as is done in Section 2.2, and then determine the influence of the ligand field as a perturbation for each of these terms separately. For two  $d$  electrons the possible terms are (Table 2.6)  ${}^3F$ ,  ${}^3P$ ,  ${}^1G$ ,  ${}^1D$ , and  ${}^1S$ , with the  ${}^3F$  term being the ground state. Their wavefunctions  $\Psi(LMSM_s)$  are given in Section 2.2, Table 2.8. The perturbation operator, following Eq. (4.2), is

$$\begin{aligned}
V' &= \sum_{\alpha} eq_{\alpha} \left( \frac{1}{|\mathbf{r}_1 - \mathbf{R}_{\alpha}|} + \frac{1}{|\mathbf{r}_2 - \mathbf{R}_{\alpha}|} \right) \\
&= V(\mathbf{r}_1) + V(\mathbf{r}_2)
\end{aligned} \tag{4.33}$$

Calculation of the matrix elements of this perturbation is relatively not difficult because the operators  $V(\mathbf{r}_i)$  depend on the orbital coordinates of only one electron (and not on spin coordinates). Presenting the two-electron wavefunction  $\Psi$  by the determinant functions  $\Phi(m_1 m_{s1}; m_2 m_{s2})$  (Table 2.8), one can see that the matrix element of  $V'$  is nonzero if and only if the two spin quantum numbers  $m_{s1}$  and  $m_{s2}$  and one of the  $m$  values ( $m_1$  or  $m_2$ ) in the two functions are identical. This can be expressed as follows:

$$\begin{aligned}
&\langle \Psi(m_1 m_{s1}; m_2 m_{s2}) | V' | \Psi(m'_1 m'_{s1}; m'_2 m'_{s2}) \rangle \\
&= \delta_{m_1 m'_{s1}} \delta_{m_2 m'_{s2}} (V_{m_1 m_1'} \delta_{m_2 m_2'} + V_{m_2 m_2'} \delta_{m_1 m_1'} - V_{m_1 m_2} \delta_{m_1' m_2'} \\
&\quad - V_{m_1' m_2'} \delta_{m_1 m_2})
\end{aligned} \tag{4.34}$$

Here  $V_{mm'}$  are the one-electron matrix elements (4.9), calculated above. Using (4.34), one can obtain the expressions for all the two-electron matrix elements  $\langle 1 | V' | 2 \rangle$  by the known one-electron matrix elements  $V_{mm'}$ ; they are given in Appendix 4.

By way of example, let us consider the ground-state term  ${}^3F$  of the  $d^2$  configuration in the octahedral field of  $O_h$  symmetry. The wavefunctions are given in Table 2.8. The term  ${}^3F$  is orbitally sevenfold-degenerate ( $L = 3, 2L + 1 = 7$ ), and the secular equation of the perturbation theory is of the seventh order [cf. Eq. (4.7)]:

$$\|V'_{ij} - \varepsilon \delta_{ij}\| = 0 \quad i, j = 1, 2, \dots, 7 \tag{4.35}$$

Assuming, as above, that the ligands are point charges and using expressions from Appendix 4 for  $V'_{ij}$  and (4.9) for  $V_{mm'}$  with the ligand coordinates (4.11), we have  $V'_{12} = V'_{14} = V'_{16} = V'_{17} = V'_{23} = V'_{24} = V'_{25} = V'_{27} = V'_{34} = V'_{35} = V'_{36} = V'_{45} = V'_{46} = V'_{47} = V'_{56} = V'_{57} = V'_{67} = 0$ . Besides

$$V'_{11} = V'_{77} \quad V'_{22} = V'_{66} \quad V'_{33} = V'_{55} \tag{4.36}$$

With these matrix elements the secular equation (4.35) yields the following roots:

$$\begin{aligned}
\varepsilon_1 &= V'_{44} \\
\varepsilon_{2,3} &= V'_{22} + (\frac{5}{3})^{1/2} V'_{15} \\
\varepsilon_{4,5,6,7} &= \frac{1}{2} \{ (V'_{11} + V'_{33}) \pm [(V'_{11} - V'_{33})^2 + 4(V'_{15})^2]^{1/2} \}
\end{aligned} \tag{4.37}$$

Substituting again  $V'_{ij}$  after (A4.1) and  $V_{mm'}$  after (4.12), we find the perturbation corrections to the energy levels in the ligand field (the symmetry types in the  $O_h$  group are shown in parentheses):

$$\begin{aligned}\varepsilon_1(^3A_g) &= 2V_{00} = eq[12F_0 + 2F_4] \\ \varepsilon_{2,3,4}(^3T_{2g}) &= V_{00} + V_{11} = eq[12F_0 + \frac{1}{3}F_4] \\ \varepsilon_{5,6,7}(^3T_{1g}) &= \frac{1}{5}V_{00} + \frac{2}{5}V_{11} = eq[12F_0 - F_4]\end{aligned}\quad (4.38)$$

Or, introducing the main parameter  $\Delta$  of the CFT after (4.15) and the destabilization energy  $E_0$  after (4.17), we have

$$\begin{aligned}\varepsilon(^3A_{2g}) &= 2E_0 + \frac{6}{5}\Delta \\ \varepsilon(^3T_{2g}) &= 2E_0 + \frac{1}{5}\Delta \\ \varepsilon(^3T_{1g}) &= 2E_0 - \frac{3}{5}\Delta\end{aligned}\quad (4.39)$$

It follows that the atomic orbitally sevenfold-degenerate  $^3F$  term in the octahedral field of six ligands splits into three terms: one orbitally nondegenerate  $^3A_{2g}$  and two threefold degenerate  $^3T_{2g}$  and  $^3T_{1g}$ :

$$^3F \rightarrow ^3A_{2g} + ^3T_{2g} + ^3T_{1g}\quad (4.40)$$

Since  $\Delta$  and  $E_0$  are positive,  $^3T_{1g}$  is the ground term, and  $^3T_{2g}$  and  $^3A_{2g}$  follow consecutively (Fig. 4.7).

The wavefunctions of the terms (4.39) can be obtained as solutions of the secular equation (4.35) in the form of linear combinations of the atomic functions  $\Psi(LMSM_s)$ . They are given in Table 4.4 [for the spin triplet the functions for only one spin value are given; the others can be obtained by the transformation (2.31)].

The splitting of other terms of the  $[A](nd)^2$  configuration is obtained similarly:

$^1D$  term:

$$\begin{aligned}\varepsilon(^1E_g) &= eq[12F_0 + \frac{4}{7}F_4] = 2E_0 + \frac{12}{35}\Delta \\ \varepsilon(^1T_{2g}) &= eq[12F_0 - \frac{8}{21}F_4] = 2E_0 - \frac{8}{35}\Delta\end{aligned}\quad (4.41)$$

$^3P$  term:

$$\varepsilon(^3T_{2g}) = 12eqF_0 = 2E_0\quad (4.42)$$

$^1G$  term:

$$\begin{aligned}\varepsilon(^1A_{1g}) &= eq[12F_0 + \frac{2}{3}F_4] = 2E_0 + \frac{2}{5}\Delta \\ \varepsilon(^1E_g) &= eq[12F_0 + \frac{2}{21}F_4] = 2E_0 + \frac{2}{35}\Delta \\ \varepsilon(^1T_{2g}) &= eq[12F_0 - \frac{13}{21}F_4] = 2E_0 - \frac{13}{35}\Delta \\ \varepsilon(^1T_{1g}) &= eq[12F_0 + \frac{1}{3}F_2E_0 + \frac{1}{5}\Delta]\end{aligned}\quad (4.43)$$

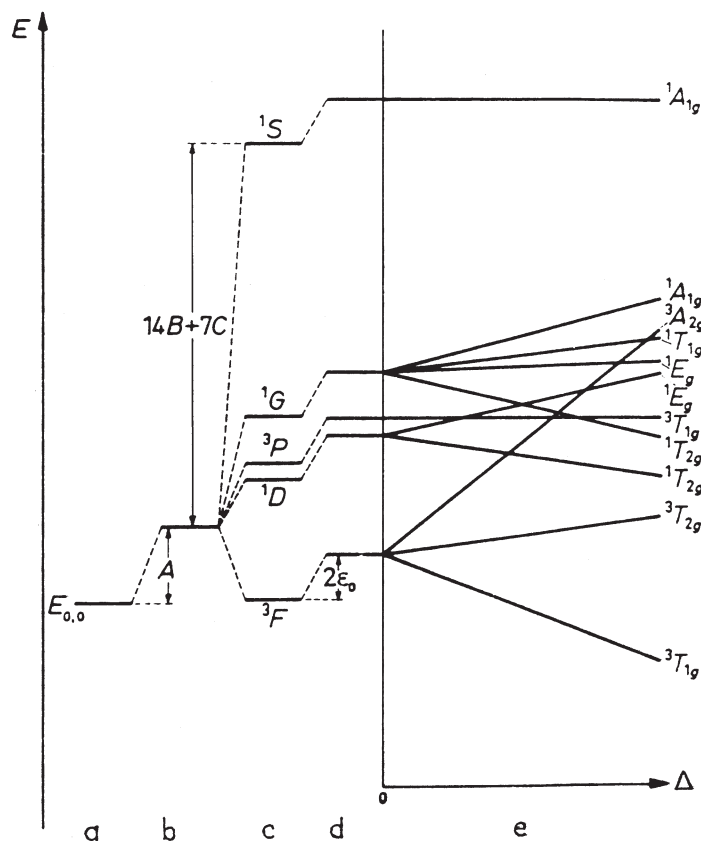


**FIGURE 4.7.** Splitting of the terms of the electronic  $d^2$  configuration in octahedral ligand fields in the weak-field limit: (a)  $d$ -electron energy level; (b) interelectron interaction (spherical averaged part); (c) interelectron interaction—formation of atomic terms (Section 2.2); (d) ligand field destabilization; (e) ligand field splitting as a function of  $\Delta$ .

$^1S$  term:

$$\varepsilon(^1A_{1g}) = 12eqF_0 = 2E_0 \quad (4.44)$$

These splittings are illustrated in Fig. 4.7; the destabilization energy—the averaged electron interaction equal to the Racah parameter  $A$  (Section 2.2, Table 2.6)—is also shown.

The calculations above are carried out in the weak-field approximation, in which the perturbation theory is applied to each atomic term separately. Therefore *the criterion of validity of the weak-field approximations is that the term splitting is much smaller than the energy gap between the terms*. As seen from Fig. 4.7, for  $d^2$  configurations this criterion is fulfilled if  $\Delta$  is sufficiently small. For large

**TABLE 4.4. Wavefunctions of Component States of the  ${}^3F(d^2)$  Term (Split in the Octahedral Field of  $O_h$  Symmetry) Expressed by Linear Combinations of the Atomic Functions  $\Psi$  ( $LMSM_s$ ) of Table 2.8<sup>a</sup>**

Type of Symmetry (Component Terms)	$\sum_i C_i \Psi_i$
$A_{2g}$	$(\frac{1}{2})^{1/2} [\Psi(3\ 2\ 1\ 1) - \Psi(3\ -2\ 1\ 1)]$
$T_{1g}$	$(\frac{5}{8})^{1/2} \Psi(3\ -3\ 1\ 1) + (\frac{3}{8})^{1/2} \Psi(3\ 1\ 1\ 1)$ $\Psi(3\ 0\ 1\ 1)$
$T_{2g}$	$(\frac{5}{8})^{1/2} \Psi(3\ 3\ 1\ 1) + (\frac{3}{8})^{1/2} \Psi(3\ -1\ 1\ 1)$ $(\frac{3}{8})^{1/2} \Psi(3\ 3\ 1\ 1) - (\frac{5}{8})^{1/2} \Psi(3\ -1\ 1\ 1)$ $(\frac{1}{2})^{1/2} [\Psi(3\ 2\ 1\ 1) + \Psi(3\ -2\ 1\ 1)]$ $(\frac{3}{8})^{1/2} \Psi(3\ -3\ 1\ 1) - (\frac{5}{8})^{1/2} \Psi(3\ 1\ 1\ 1)$

<sup>a</sup>The component with  $M_s = 1$  only is shown; the states with  $M_s = -1$  and  $M_s = 0$  can be found by transformations using Eq. (2.31).

$\Delta$  values the components of the split terms even cross each other, rendering the approximation of weak field invalid.

For complexes with symmetries lower than  $O_h$  the degenerate terms are subject to further splitting as shown in Table 4.2. For quantitative estimates one can use the results of Appendix 3. For a tetragonally distorted (elongated) octahedron with the coordinates (A3.4), the nonzero matrix elements  $V'_{ij}$  are the same as in the regular octahedron. Hence the roots of the secular equation (4.35) for the splitting of the  ${}^3F$  term are given by the same general expressions (4.37) in which the matrix elements  $V_{mm'}$  are those of Eq. (A3.5), not (4.12). Therefore, as distinct from the regular octahedron, the tetragonally elongated one yields five different roots, two of which are twofold-degenerate:

$$\begin{aligned}
 \varepsilon_1({}^3A_{2g}) &= V_{00} + V_{22} + V_{2-2} \\
 \varepsilon_2({}^3B_{2g}) &= V_{00} + V_{22} - V_{2-2} \\
 \varepsilon_3({}^3A'_{2g}) &= \frac{8}{5}V_{11} + \frac{2}{5}V_{22} \\
 \varepsilon_{4,5}({}^3E'_g) &= V_{11} + \frac{4}{5}V_{22} + \frac{1}{5}V_{00} \\
 &\quad - [\frac{1}{25}(V_{22} - V_{00})^2 + \frac{3}{5}(V_{2-2})^2]^{1/2} \\
 \varepsilon({}^3E''_g) &= V_{11} + \frac{4}{5}V_{22} + \frac{1}{5}V_{00} \\
 &\quad + [\frac{1}{25}(V_{22} - V_{00})^2 + \frac{3}{5}(V_{2-2})^2]^{1/2}
 \end{aligned} \tag{4.45}$$

It is seen that, in accordance with the group-theoretical results (Table 4.3), in tetragonal fields  $T_{2g}$  and  $T_{1g}$  terms of the octahedron undergo further splitting:  $T_{2g} \rightarrow B_{2g} + E'_g$ ,  $T_{1g} \rightarrow A'_{2g} + E''_g$ . The wavefunctions of these states can be obtained in the usual fashion from the functions in Tables 2.8 and 4.4.

For a square-planar complex with the CA in the center of the square the energy levels are given by Eq. (4.37) with the matrix element  $V_{mm'}$  after (A3.9).



In the case of tetrahedral symmetry with four point charges at the corners of a tetrahedron and the CA in the center [with the coordinates (A3.11)], splitting of the  ${}^3F$  term of the  $d^2$  configuration results in three terms,  ${}^3T_1$ ,  ${}^3T_2$ , and  ${}^3A_2$ :

$$\begin{aligned}\varepsilon({}^3T_1) &= \frac{1}{5}V_{00} + \frac{9}{5}V_{11} = eq[8F_0 + \frac{4}{9}F_4] = 2E_0^T + \frac{3}{5}\Delta_T \\ \varepsilon({}^3T_2) &= V_{00} + V_{11} = eq[8F_0 - \frac{4}{27}F_4] = 2E_0 - \frac{1}{5}\Delta_T \\ \varepsilon({}^3A_2) &= 2V_{00} = eq[8F_0 - \frac{8}{9}F_4] = 2E_0^T - \frac{6}{5}\Delta_T\end{aligned}\quad (4.46)$$

As with one  $d$  electron, the tetrahedral splitting is similar to the octahedral one, but with the inverse order of the energy levels:  $\varepsilon({}^3A_2) < \varepsilon({}^3T_2) < \varepsilon({}^3T_1)$  [cf. (4.39)]. Again,  $E_0^T = \frac{2}{3}E_0$  and  $\Delta_T = -\frac{4}{9}\Delta$ , provided that the ligand charges  $q$  and their distances  $R$  to the CA are the same as in the octahedron.

For systems with lower symmetries the calculations are more difficult, but they can be reduced by using the method of equivalent operators [4.15] or irreducible tensor operators [4.16, 4.17]. The tables of spectroscopic coefficients for  $p$ ,  $d$ , and  $f$  configurations [4.18] are rather useful for such calculations.

The qualitative picture of term splitting for electronic configurations  $[A](nd)^n$  with  $n > 2$  in fields of lower symmetry can be found directly by using the complementary rule (Section 2.2): configurations  $d^n$  and  $d^{10-n}$  have mutually inverted schemes of term splitting. In the weak-field case this rule is also valid for the pairs of configurations  $d^n$  and  $d^{5-n}$ . Therefore the splitting of the terms of the electronic configuration  $d^3$  can be obtained from that of  $d^2$ . In particular, the ground state  ${}^4F$  has the same three terms  ${}^4T_{1g}$ ,  ${}^4T_{2g}$ , and  ${}^4A_{2g}$  as the  ${}^3F$  state of the  $d^2$  configuration, but they are arranged in an inverse sequence:  $\varepsilon(T_{1g}) > \varepsilon(T_{2g}) > \varepsilon(A_{2g})$ , with energy spacing  $\frac{3}{5}\Delta$ ,  $-\frac{1}{5}\Delta$ , and  $-\frac{6}{5}\Delta$ , respectively, from the nonsplit level (Fig. 4.8). The average destabilization energy in the case of  $d^3$  is  $3E_0$  instead of  $2E_0$  for the  $d^2$  configuration (in the approximation under consideration it is proportional to the number of  $d$  electrons) and, again, the preservation rule for the center of gravity of the multiplet is obeyed (Section 4.2):

$$3\varepsilon(T_{1g}) + 3\varepsilon(T_{2g}) + \varepsilon(A_{2g}) = 0$$

For other configurations the scheme of term splitting can be evaluated similarly; for high-spin configurations the scheme for  $d^4$  corresponds to the inverted one of  $d^1$  (i.e., it is the same as for  $d^9$ ); for  $d^5$  (term  ${}^6S$ ) there is no splitting; the configuration  $d^6$  corresponds to the inverted  $d^4$ , which is analogous to  $d^1$ ;  $d^7$  corresponds to  $d^2$ , and  $d^8$  to  $d^3$  (i.e., to inverted  $d^2$ );  $d^9$  is similar to inverted  $d^1$ .

### Strong Crystal Fields and Low- and High-Spin Complexes

In the other limit case, opposite to the weak-field one, the effect of the ligand field on the states of the CA is strong; it surpasses the electrostatic interaction between the electrons. In this case the orbital coupling between the electrons is broken

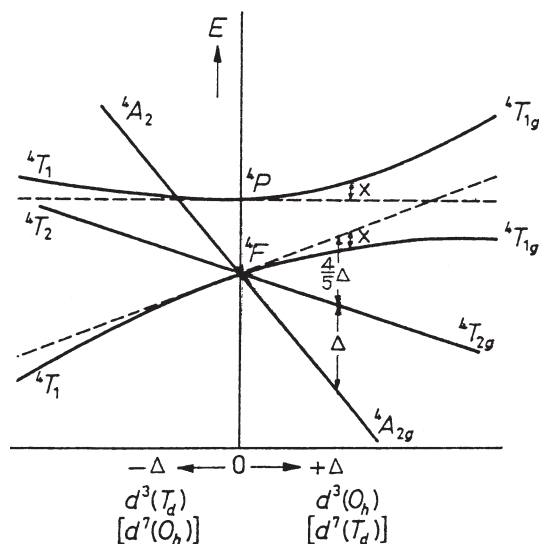


**FIGURE 4.8.** Splitting of the ground-state term  ${}^4F$  of the  $d^3(d^7)$ -electron configuration in octahedral  $O_h$  and tetrahedral  $T_d$  ligand fields as a function of the CFT parameter  $\Delta$  with the  $T_{1g}(F)-T_{1g}(P)$  interaction included.

and the states with definitive total momentum quantum numbers  $L$  ( $S$ ,  $P$ ,  $D$ , etc., states), strictly speaking, cease to exist. In other words, each  $d$  electron chooses its orientation in space under the influence of the ligand field rather than the other  $d$  electrons. This is the *strong-ligand-field limit*. [A formally similar situation takes place when the orbital coupling between the electrons is broken by the spin-orbital interaction (cf. the  $j-j$  coupling scheme in Sections 2.2 and 4.4).

It follows that when the ligand field is strong, it makes no sense to speak about atomic term splitting, since the terms themselves are destroyed. To determine the states in this case, one should first find the orientations of each  $d$  state in the ligand field neglecting the electron interaction, and then evaluate the possible terms of the system taking into account the interaction of the electrons in these crystal-field-oriented electronic states.

As shown in Section 4.2, for one  $d$  electron in the octahedral field of the ligands there are two nonequivalent kinds of orbital states: the more stable  $t_{2g}$  states ( $d_{xy}$ ,  $d_{xz}$ ,  $d_{yz}$ ) in which the electrostatic repulsion from the six ligands is smaller, and the less stable (higher in energy by  $\Delta$ ) states  $e_g$  ( $d_{x^2-y^2}$ ,  $d_{z^2}$ ) in which the repulsion from the ligands is larger. Hence in the strong ligand field, neglecting the electron interaction, the  $d$  electrons occupy first the  $t_{2g}$  orbitals (maximum six electrons) and then the  $e_g$  orbitals (four electrons); the electron configuration is  $(t_{2g})^n$  for  $n \leq 6$ , and  $(t_{2g})^6(e_g)^{n-6}$  for  $n > 6$ . The energy terms can be obtained from these configurations by including the electron interaction.

Consider the atomic electron configuration  $[A](nd)^2$ . In strong ligand fields, as stated above, the two  $d$  electrons in the ground state of an octahedral complex occupy two  $t_{2g}$  orbitals (the state with two electrons in one orbital is higher in energy) forming the  $(t_{2g})^2$  configuration. In the excited states one of the two  $d$  electrons can occupy the  $e_g$  orbital and form the  $(t_{2g})^1(e_g)^1$  configuration, which is higher than  $(t_{2g})^2$  by  $\Delta$ , and the two electrons can occupy the  $e_g$  orbitals, resulting in the excited  $(e_g)^2$  configuration, also higher by  $\Delta$  than  $(t_{2g})^1(e_g)^1$  [and by  $2\Delta$  than  $(t_{2g})^2$ ].

Thus the  $d^2$  configuration in the strong octahedral field forms three configurations,  $(t_{2g})^2$ ,  $(t_{2g})^1(e_g)^1$ , and  $(e_g)^2$ , situated consecutively with an energy spacing  $\Delta$  (Fig. 4.9c). In each of these configurations the electron interaction yields several terms similar to the term formation in the free atom (Section 2.2). The method for evaluating the energy terms is discussed below; the resulting terms for the  $(t_{2g})^2$  configuration expressed by Racah parameters (2.43) are as follows:

$$\begin{aligned}\varepsilon^3(T_{1g}) &= A - 5B \\ \varepsilon(^1T_{2g}) &= A + B + 2C \\ \varepsilon(^1E_g) &= A + B + 2C \\ \varepsilon(^1A_{1g}) &= A + 10B + 5C\end{aligned}\tag{4.47}$$

Splitting of the configurations that emerge from  $d^2$  is shown in Fig. 4.9e. In particular, the ground state of the  $(t_{2g})^2$  configuration  $^3T_{1g}$  is the same as in the weak-field limit. However, the sequence and spacing of the excited states is essentially different. Table 4.5 gives the electronic configurations and the ground-state terms for all the atomic configurations  $d^n$  in strong octahedral and tetrahedral ligand fields. By comparison with the corresponding cases of weak fields, one can see that differences occur for  $n = 4, 5, 6, 7$  in octahedral symmetry, and for  $n = 3, 4, 5, 6$  in tetrahedral systems. It is important that in these cases the spin multiplicity of the ground state is always lower in the strong-field limit than in the weak field. Therefore the complexes with strong ligand fields are called *low-spin complexes*, as distinct from complexes with weak ligand fields, which are *high-spin complexes*.

One consequence of this result is the statement that, depending on the ligand properties (ligand field strength), there may be complexes of the same metal in the same oxidation state with two different kinds of spin multiplicity of the ground state (and hence different magnetic properties). This phenomenon is confirmed experimentally on a wide range of TMS and it is widely used in their investigation. In particular, there may be a coexistence of the two magnetic states in a narrow range of external magnetic fields or temperature (see spin crossover in Section 8.4). Together with the elucidation of the origin of the colors (Section 8.2), this explanation of magnetic behavior of transition metal complexes is one of the most important achievements of the CFT. The two cases of ligand fields, weak and strong, remain equally important in the MO theory and are discussed again in Section 6.2 (cf. Table 4.5 with Tables 6.3 and 6.4).

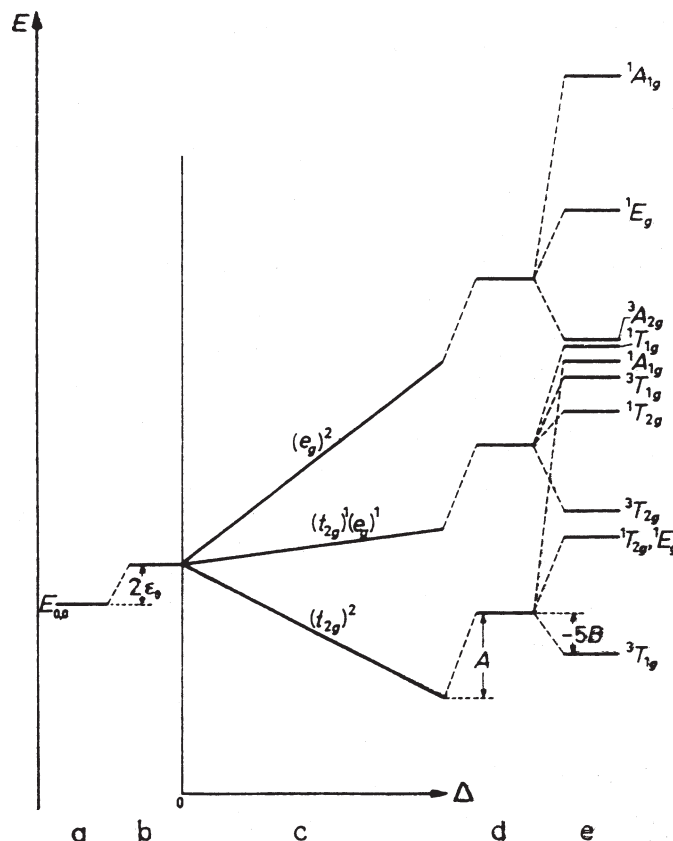


**FIGURE 4.9.** Splitting of the terms of the  $d^2$  configuration in strong fields of octahedral symmetry: (a)  $d$ -electron energy level; (b) ligand field destabilization; (c) ligand field splitting as a function of  $\Delta$ ; (d) electron interaction destabilization; (e) electron interaction splitting.

The criterion of validity of the strong-field limit, similar to the weak-field case, follows from its assumptions. Since the splitting caused by the electron interactions are determined for each of the three configurations  $(t_{2g})^2$ ,  $(t_{2g})^1(e_g)^1$ , and  $(e_g)^2$  separately, the results are valid when the splitting is smaller than the energy gap  $\Delta$  between them. For splitting of the  $(t_{2g})^2$  configuration, the maximum distance between its components after (4.47) is  $15B + 5C$ ; hence the condition of validity of the strong-field approach is  $15B + 5C \ll \Delta$ . Otherwise the terms of the same symmetry from different configurations become strongly mixed [e.g.,  ${}^1T_{2g}$  from  $(t_{2g})^2$  with  ${}^1T_{2g}$  from  $(t_{2g})^1(e_g)^1$ ], and it is said that there is a *configuration interaction*.

For more than two  $d$  electrons, the criterion of validity of the strong-field approximation can be established similarly. Of special interest are the cases of

**TABLE 4.5. Electronic Configuration and Ground-State Terms of Octahedral and Tetrahedral Complexes in the Case of Strong Ligand Fields<sup>a</sup>**

Number of $d$ Electrons	Octahedral Complex		Tetrahedral Complex	
	Electronic Configuration	Ground-State Term	Electronic Configuration	Ground-State Term
$d^1$	$t_{2g}$	${}^2T_{2g}$	$e$	${}^2E$
$d^2$	$(t_{2g})^2$	${}^3T_{1g}$	$(e)^2$	${}^3A_2$
$d^3$	$(t_{2g})^3$	${}^4A_{2g}$	$(e)^3$	${}^2E$
$d^4$	$(t_{2g})^4$	${}^3T_{1g}$	$(e)^4$	${}^1A_1$
$d^5$	$(t_{2g})^5$	${}^2T_{2g}$	$(e)^4t_2$	${}^2T_2$
$d^6$	$(t_{2g})^6$	${}^1A_{1g}$	$(e)^4(t_2)^2$	${}^3T_1$
$d^7$	$(t_{2g})^6e_g$	${}^2E_g$	$(e)^4(t_2)^3$	${}^4A_2$
$d^8$	$(t_{2g})^6(e_g)^2$	${}^3A_{2g}$	$(e)^4(t_2)^4$	${}^2T_1$
$d^9$	$(t_{2g})^6(e_g)^3$	${}^2E_g$	$(e)^4(t_2)^5$	${}^2T_2$
$d^{10}$	$(t_{2g})^6(e_g)^4$	${}^1A_{1g}$	$(e)^4(t_2)^6$	${}^1A_1$

<sup>a</sup>Compare with Tables 6.3 and 6.4.

$d^4$ ,  $d^5$ ,  $d^6$ , and  $d^7$  in octahedral complexes and  $d^3$ ,  $d^4$ ,  $d^5$ , and  $d^6$  in tetrahedral systems, for which the two limit cases differ by the spin of the ground state. Let us introduce the notion of *pairing energy*  $\Pi$  defined as the difference between the energies of multielectron interactions in low- and high-spin complexes, respectively, divided by the number of pairings destroyed by the low-spin  $\rightarrow$  high-spin transition. It is obvious that the low-spin state is preferable if

$$\Pi < \Delta \quad (4.48)$$

On the contrary, if

$$\Pi > \Delta \quad (4.49)$$

the high-spin state is the ground state.

Comparison of the data in Table 2.6 for the relative energies of the terms of  $d^n$  configurations with the expressions (4.47) allows one to obtain the following relations [4.15]:

$$\begin{aligned} \Pi(d^4) &= 6B + 5C \\ \Pi(d^5) &= \frac{15}{2}B + 5C \\ \Pi(d^6) &= \frac{5}{2}B + 4C \\ \Pi(d^7) &= 4B + 4C \end{aligned} \quad (4.50)$$

and if the Racah parameters  $B$  and  $C$  can be assumed the same in different configurations, then

$$\Pi(d^6) < \Pi(d^7) < \Pi(d^4) < \Pi(d^5) \quad (4.51)$$

Some interesting consequences follow from Eqs. (4.48)–(4.51): (1) the pairing energy is the lowest for the  $d^6$  configuration, and hence the low-spin state is preferable in octahedral complexes with this configuration as compared with others *ceteris paribus*; and (2) as  $\Delta$  is significantly smaller for tetrahedral complexes than for octahedral systems, the low-spin configuration for the former is much less probable than for the latter. Finally, by comparisons [4.15], it was shown that for  $d^6$  and  $d^5$  configurations the state with intermediate spins ( $S = 1$  for  $d^6$  and  $S = \frac{3}{2}$  for  $d^5$ ) is less probable. Several high-spin and low-spin iron complexes are shown in Example 4.2.

### EXAMPLE 4.2

#### *High- and Low-Spin Octahedral Complexes of Iron*

The conclusions presented above have many confirmations in the experimental data (Chapters 8–11). With specific  $\Delta$  values for different CAs and ligands retrieved from spectroscopic data [some of which are listed in Table 8.2 and in the spectrochemical series (8.23) and (8.24)], one can see that, for instance, the complex  $[\text{Fe}(\text{NO}_2)_6]^{3-}$  should be in the low-spin configuration  $(t_{2g})^5$  with all the five  $d$  electrons in the three  $t_{2g}$  orbitals resulting in one unpaired electron and total spin  $S = \frac{1}{2}$ , because  $\text{NO}_2^-$  ligands produce large  $\Delta$  splittings [one of the largest according to the spectrochemical series (8.24)], whereas  $[\text{FeBr}_6]^{3-}$  is a high-spin complex [ $\text{Br}^-$  is a weak-field ligand, the weakest in the series (8.23) and (8.24)] with all five electrons unpaired [electron configuration  $(t_{2g})^3(e_g)^2$ ] and total spin  $S = \frac{5}{2}$ . The ground terms of these two complexes are  ${}^2T_{2g}$  and  ${}^6S$ , respectively.

### Energy Terms of Strong-Field Configurations

Energy terms of strong-field configurations can be formed by means of a procedure similar to that used in the formation of atomic terms (Section 2.2). Let us illustrate this by the example of the ground-state configuration  $(t_{2g})^2$ .

There are three  $t_{2g}$  functions of the  $d$  electron,  $d_{xy}$ ,  $d_{xz}$ , and  $d_{yz}$ , that we denote here by  $\varphi_1$ ,  $\varphi_2$  and  $\varphi_3$ , respectively, and each of them is associated with two spin states denoted, as above, by “+” and “−.” Hence we should distribute the two electrons in six one-electron states,  $\varphi_1^+$ ,  $\varphi_1^-$ ,  $\varphi_2^+$ ,  $\varphi_2^-$ ,  $\varphi_3^+$ ,  $\varphi_3^-$ , making 15 possibilities [ $C_6^2 = 6!/2!(6-2)! = 6 \cdot 5/2 = 15$ ]. Thus there are 15 determinant functions  $\Phi(\varphi_i^\pm, \varphi_j^\pm)$  of the type (2.28) that have different total spin projection values:  $M_s = 1, 0, -1$ . Let us group the 15 functions with respect to  $M_s$  (cf. Table 2.8):

$M_s = 1$ :

$$\Phi(\varphi_1^+, \varphi_2^+) \quad \Phi(\varphi_1^+, \varphi_3^+) \quad \Phi(\varphi_2^+, \varphi_3^+) \quad (4.52)$$

$M_s = -1$ :

$$\Phi(\varphi_1^-, \varphi_2^-) \quad \Phi(\varphi_1^-, \varphi_3^-) \quad \Phi(\varphi_2^-, \varphi_3^-) \quad (4.53)$$

$M_s = 0$ :

$$\begin{aligned} &\Phi(\varphi_1^+, \varphi_1^-) \quad \Phi(\varphi_2^+, \varphi_2^-) \quad \Phi(\varphi_3^+, \varphi_3^-) \\ &\Phi(\varphi_1^-, \varphi_1^+) \quad \Phi(\varphi_2^-, \varphi_2^+) \quad \Phi(\varphi_3^-, \varphi_3^+) \\ &\Phi(\varphi_1^-, \varphi_2^+) \quad \Phi(\varphi_1^-, \varphi_3^+) \quad \Phi(\varphi_2^-, \varphi_3^+) \end{aligned} \quad (4.54)$$

Since for spin triplets  $S = 1$  and  $M_s = 1, 0, -1$ , while for singlets  $S = 0$ ,  $M_s = 0$ , we conclude that among the 15 functions, 9 of which belong to triplets, while the remaining 6 form singlets. To find them, one can use symmetry considerations. The two one-electron  $t_{2g}$  states transform after the  $T_{2g}$  representation of the  $O_h$  group of symmetry. To determine the possible terms of the  $(t_{2g})^2$  configuration, one must find the irreducible representations in the product  $T_{2g} \times T_{2g}$  using the relation (3.33) and the characters of the  $O_h$  group given in Table 3.1:  $T_{2g} \times T_{2g} = T_{1g} + T_{2g} + E_g + A_{1g}$ . On the other hand, the symmetry properties of the  $d$  functions show that the three functions (4.52) with  $M_s = 1$  transform as  $T_{1g}$ , the three functions (4.54) with  $M_s = -1$  have the same symmetry  $T_{1g}$ , and from the functions (4.53) with  $M_s = 0$  one can also form three linear combinations that transform after the same representation  $T_{1g}$  (the method to select functions and construct linear combinations that transform after certain types of symmetry is given in Section 3.5). These nine functions form the term  ${}^3T_{1g}$ . To satisfy the remaining representations  $T_{2g}$ ,  $E_g$ , and  $A_{1g}$  with the remaining six singlet functions from (4.54), we have the only possibility:  ${}^1T_{2g}$ ,  ${}^1E_g$ , and  ${}^1A_{1g}$ . Thus the  $(t_{2g})^2$  configuration yields the following terms:  ${}^3T_{1g}$ ,  ${}^1T_{2g}$ ,  ${}^1E_g$ ,  ${}^1A_{1g}$  (see also Problem P3.9). Using the functions (4.52) through (4.54) and the group-theoretical formula (3.47), one can construct the functions for all these terms. They are given in Table 4.6.

The energy difference between the four terms of the  $d^2$  configuration is caused by the corresponding differences in the interelectron interaction described by the matrix elements of the operator  $\sum_{i,j} e^2/r_{ij}$ . The latter, in accordance with the strong-field approximation, can be considered as a perturbation of the states of the  $(t_{2g})^2$  configuration. Taking the 15 states (4.52)–(4.54) as a basis, we solve the secular equation of the perturbation theory to find 15 values of energy corrections  $\varepsilon$ .

On the other hand, we already know the symmetrized linear combinations of these functions given in Table 4.6, which transform after the IrReps of the symmetry group of the system, and hence these functions are correct zeroth-order functions of the perturbation theory. With these functions the corrections are equal to the diagonal matrix elements of the electron interaction  $\sum_{i,j} e^2/r_{ij}$ .

**TABLE 4.6. Wavefunctions of States of the Configuration  $(t_{2g})^2$  in Strong Ligand Fields as Linear Combinations of the Two-Electron Functions  $\Phi_k$  ( $\varphi_i^\pm, \varphi_j^\pm$ )**

Term	$M_s$	$\sum_k C_k \Phi_k$
${}^3T_{1g}$	1	$\Phi(\varphi_1^+; \varphi_2^+)$ $\Phi(\varphi_1^+; \varphi_3^+)$ $\Phi(\varphi_2^+; \varphi_3^+)$
	0	$(1/\sqrt{2})[\Phi(\varphi_1^+; \varphi_2^-) + \Phi(\varphi_1^-; \varphi_2^+)]$ $(1/\sqrt{2})[\Phi(\varphi_1^+; \varphi_3^-) + \Phi(\varphi_1^-; \varphi_3^+)]$ $(1/\sqrt{2})[\Phi(\varphi_2^+; \varphi_3^-) + \Phi(\varphi_2^-; \varphi_3^+)]$
	-1	$\Phi(\varphi_1^-; \varphi_2^-)$ $\Phi(\varphi_1^-, \varphi_3^-)$ $\Phi(\varphi_2^-, \varphi_3^-)$
		$(1/\sqrt{2})[\Phi(\varphi_1^+; \varphi_2^-) - \Phi(\varphi_1^-; \varphi_2^+)]$ $(1/\sqrt{2})[\Phi(\varphi_1^+; \varphi_3^-) - \Phi(\varphi_1^-; \varphi_3^+)]$ $(1/\sqrt{2})[\Phi(\varphi_2^+; \varphi_3^-) - \Phi(\varphi_2^-; \varphi_3^+)]$
${}^1E_g$	0	$(1/\sqrt{2})[\Phi(\varphi_2^+; \varphi_2^-) - \Phi(\varphi_3^+; \varphi_3^-)]$
${}^1A_{1g}$	0	$(1/\sqrt{6})[2\Phi(\varphi_1^+; \varphi_1^-) - \Phi(\varphi_2^+; \varphi_2^-) - \Phi(\varphi_3^+; \varphi_3^-)]$ $(1/\sqrt{3})[\Phi(\varphi_1^+; \varphi_1^-) + \Phi(\varphi_2^+; \varphi_2^-) + \Phi(\varphi_3^+; \varphi_3^-)]$

Methods of calculation of such matrix elements are discussed in Section 2.2. The results can be expressed by Slater–Condon or Racah parameters. In the case under consideration they yield the energies given by Eq. (4.47). For the other configurations  $(t_{2g})^1(e_g)^1$  and  $(e_g)^2$  of  $d^2$ , the possible energy terms can be found quite similarly, resulting in the scheme of energy terms for the  $[A](nd)^2$  states in a strong octahedral field given in Fig. 4.9.

The quantitative criterion of validity of the strong-field limit coincides with the criterion of applicability of the perturbation theory: the term splitting must be much smaller than the energy gap  $\Delta$  between the electronic configurations in the ligand field.

### Arbitrary Ligand Fields and Tanabe–Sugano Diagrams

If the ligand field is of intermediate strength for which neither the weak-field nor strong-field criterion is realized, the problem should be solved with the ligand field and electron interactions considered simultaneously. For a specific system the calculations can be carried out by numerical computation. However, a general understanding (and sometimes practical results) can be obtained when starting from one of the limit cases, for which the problem can be solved analytically, with subsequent corrections on the abovementioned term interactions, or configuration interaction.

For instance, for the electronic configuration  $[A](nd)^2$ , as a result of the splitting in octahedral ligand fields in the weak-field limit, some of the terms of the same symmetry (originating from different atomic terms) are quite close in



energy (Fig. 4.7):  ${}^1T_{2g}({}^1D)$  and  ${}^1T_{2g}({}^1G)$ ,  ${}^1E_g({}^1D)$  and  ${}^1E_g({}^1G)$ . Other terms [e.g.,  ${}^3T_{1g}({}^3F)$  and  ${}^3T_{1g}({}^3P)$ ,  ${}^1A_{1g}({}^1G)$  and  ${}^1A_{1g}({}^1S)$ ] are apparently not so close, but may also interact significantly. In the strong field limit examples of close-in-energy terms are  ${}^1A_{1g}(t_{2g})^2$  and  ${}^1A_{1g}(e_g)^2$ ,  ${}^1T_{2g}(t_{2g})^2$  and  ${}^1T_{2g}(t_{2g})(e_g)$ , and so on.

These relatively close-in-energy terms of the same symmetry influence each other, they “interact,” and it can be shown that the interacting energy levels diverge. Therefore, we can say that *there is a repulsion of terms with the same symmetry*. Another formulation of this rule is that *the terms of the same symmetry do not intersect (nonintersection rule)*. Figure 4.8 illustrates this effect for the  ${}^4T_{1g}(F) - {}^4T_{1g}(P)$  repulsion in octahedral [ ${}^4T_1(F) - {}^4T_1(P)$  in tetrahedral] complexes.

The magnitude of repulsion (divergence) of two terms of the same symmetry  $\Gamma$  as a result of their interaction  $\Delta E(\Gamma)$  can be evaluated by perturbation theory considering the electron interaction  $\sum e^2/r_{ij}$  and the ligand field potential  $V$  after Eq. (4.33) as perturbations. Denote the wavefunctions of the two interacting terms by  $\Psi_1$  and  $\Psi_2$  and the energy gap between them by  $2\delta$ . Taking the energy reference in the middle of this gap, we have for the secular equation of the perturbation theory:

$$\begin{bmatrix} -\delta - \varepsilon & H_{12} \\ H_{21} & \delta - \varepsilon \end{bmatrix} = 0 \quad (4.55)$$

where

$$H_{12} = \int \Psi_1^* \left[ \frac{\sum e^2}{r_{ij}} + V \right] \Psi_2 d\tau \quad (4.56)$$

is the term interaction energy.

The solutions of (4.55)—corrections to the energies of the interacting terms  $\varepsilon$ —are

$$\varepsilon_{1,2} = \pm(\delta^2 + H_{12}^2)^{1/2} \quad (4.57)$$

and hence

$$\Delta E = \varepsilon_2 - \varepsilon_1 - 2\delta = 2[(\delta^2 + H_{12}^2)^{1/2} - \delta] \quad (4.58)$$

We emphasize that the matrix element  $H_{12}$  after (4.56) equals zero if the two wavefunctions  $\Psi_1$  and  $\Psi_2$  belong to different symmetry types (see selection rules for matrix elements, Section 3.4). For  $H_{12} = 0$ ,  $\Delta E = 0$ , and therefore *the terms of different symmetry do not interact* (they intersect). Certainly, if there are more than two interacting terms, the order of the secular equation (4.55) increases respectively.

**TABLE 4.7. Some Numerical Values for the Racah Parameters  $B$  and  $C$  (in  $\text{cm}^{-1}$ ) and  $\gamma = C/B$  for Transition Metal Ions  $M^{2+}$  and  $M^{3+}$**

$M^{2+}$	$B$	$C$	$\gamma$	$M^{3+}$	$B$	$C$	$\gamma$
Ti <sup>2+</sup>	695	2910	4.19	—	—	—	—
V <sup>2+</sup>	755	3255	4.31	V <sup>3+</sup>	862	3815	4.43
Cr <sup>2+</sup>	810	3565	4.40	Cr <sup>3+</sup>	918	4133	4.50
Mn <sup>2+</sup>	860	3850	4.78	Mn <sup>3+</sup>	965	4450	4.61
Fe <sup>2+</sup>	917	4040	4.41	Fe <sup>3+</sup>	1015	4800	4.73
Co <sup>2+</sup>	971	449	4.63	Co <sup>3+</sup>	1065	5120	4.81
Ni <sup>2+</sup>	1030	4850	4.71	Ni <sup>3+</sup>	1115	5450	4.89

With the corrections (4.58) included, the energies of the terms are no longer bound to a certain assumption of the strength of the ligand field and are independent of the reference limit case taken as a starting point. Figure 4.10 shows the correlation of the terms of the  $[A](nd)^2$  configuration in octahedral fields of strong, weak, and intermediate strength.

It follows that for arbitrary strength of ligand fields the energy term splitting depends not only on the CFT parameter  $\Delta$  but also on the initial energy spacing of the atomic terms. The latter can be defined, as in Table 2.6 for the  $d^2$  configuration, by three Racah parameters:  $A$ ,  $B$ , and  $C$ . Parameter  $A$  determines the energy of destabilization by the average electron interaction, which is the same for all the terms (see Table 2.6 and Fig. 4.7) and can be excluded by an appropriate choice of the energy reference.

Parameters  $B$  and  $C$  can be obtained from the empirical spectroscopic data of free atoms and ions (Section 2.2). Table 4.7 lists these parameters for some transition metal ions (most usable in coordination chemistry) together with their ratio  $\gamma = C/B$  (see also Table 8.3). The  $\gamma$  value does not differ much for different ions (for rough approximate estimations it may be assumed that  $C \approx 4.5B$ ). Assuming that  $\gamma$  is known, one can reduce the number of parameters determining the relative energy-level positions to two:  $\Delta$  and  $B$ . Then, by choosing the scale in  $B$  units, one obtains the energies as a function of only one parameter  $\Delta$ .

Energy-level diagrams as functions of the CFT parameter  $\Delta$  for all the  $d^n$  configurations ( $n = 2, 3, 4, 5, 6, 7, 8$ ) given in Fig. 4.11 were constructed by Tanabe and Sugano [4.19]. In these diagrams the energy readoff is taken at the ground state. Therefore, for the electronic configuration  $d^n$  with  $n = 4, 5, 6, 7$  in octahedral fields ( $n = 3, 4, 5, 6$  in tetrahedral fields) at a certain value of  $\Delta$  (more precisely,  $\Delta/B$ ), there is a term crossing, the ground-state changes, and all the energy levels on the diagram are subject to a break. Usually at this break the ground-state multiplicity also changes, and there is a transition from the weak ligand field to the strong field. The Tanabe–Sugano diagrams give the most complete information about the electronic structure of the system in the CFT model. For improvements in these diagrams with respect to the spin–orbital interaction see, for instance, Ref. 4.20.

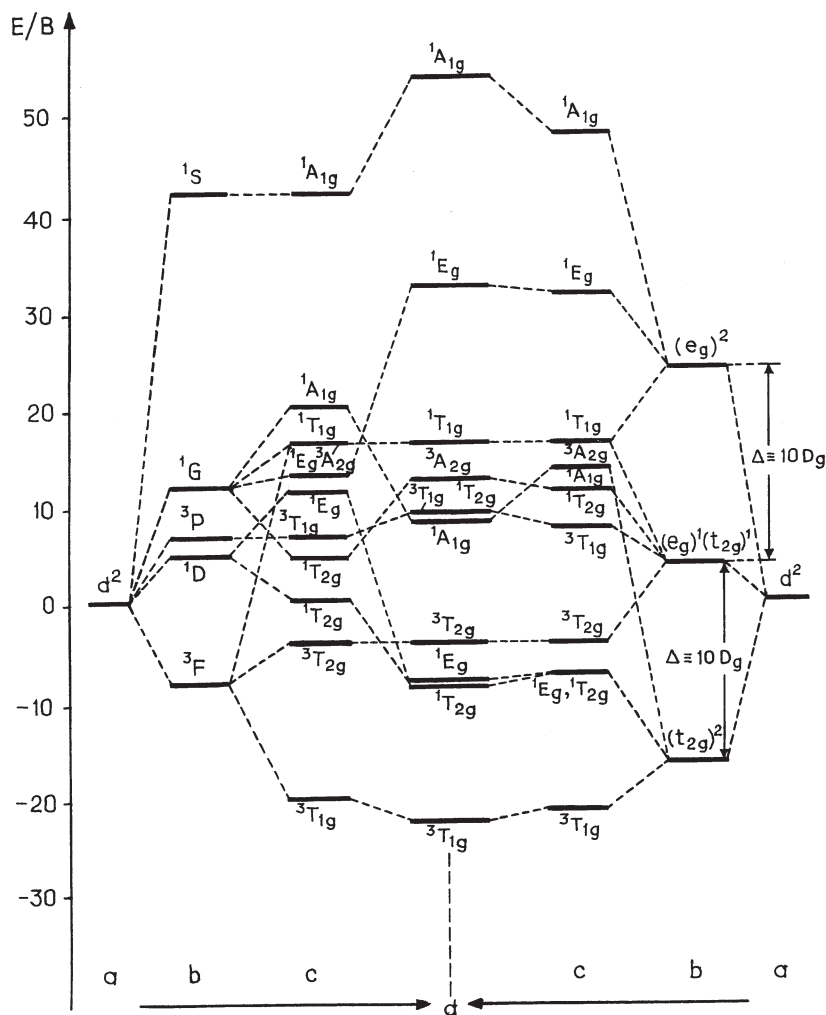


**FIGURE 4.10.** Correlation of the energy terms of the electronic  $d^2$  configuration in weak, strong, and intermediate ligand fields of octahedral symmetry. From left to right (weak field): (a)  $d$  levels; (b) with interelectron interaction; (c) with interelectron interaction in the ligand field. From right to left (strong field): (a)  $d$  levels; (b)  $d$ -level terms in the ligand field; (c) in the ligand field with interelectron interaction; (d) arbitrary field:  $d$ -level terms in ligand fields with interelectron and term interactions included. (From Schlafer and Gliemann [4.7].)

**4.4. f-ELECTRON TERM SPLITTING**

One important feature of  $f$  electrons is that they are usually screened from the ligand field by the outer  $s, p, d$  electrons and hence they are less affected by

the ligands than the  $d$  electrons. On the other hand,  $f$  electrons are subject to stronger spin-orbital coupling [Eq. (2.27)]. Hence, distinct from compounds with  $d$  electrons, where the spin-orbital coupling is assumed to be smaller than both the ligand field and interelectron interactions, in  $f$ -electron systems the ligand field is smaller than both the interelectron and spin-orbital interactions.

In fact, following Bethe [4.2], we should compare three important magnitudes: electron interaction, ligand field potential, and spin-orbital interaction. With these three magnitudes, three cases are significant in the CFT:

1. *Weak field*—the ligand potential is weaker than both interelectron and spin-orbital interactions.
2. *Intermediate field*—the ligand field is smaller than the interelectron interaction, but larger than the spin-orbital coupling.

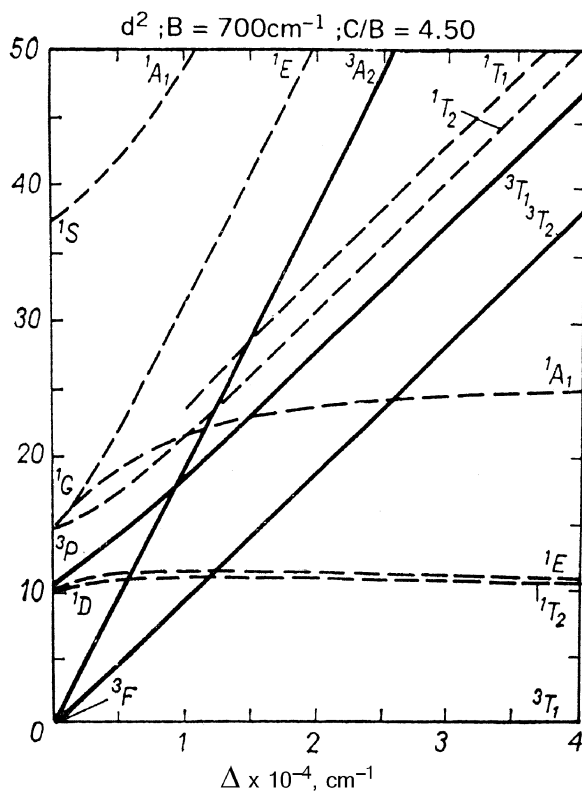


**FIGURE 4.11a.** Tanabe-Sugano diagrams: energy levels as a function of octahedral crystal fields  $\Delta$  in  $10^3 \text{ cm}^{-1}$ . For convenience, the energy levels with multiplicities different from the ground-state ones are given by dashed lines. The indices  $g$  and  $u$  are omitted. Some levels of minor significance are not shown.

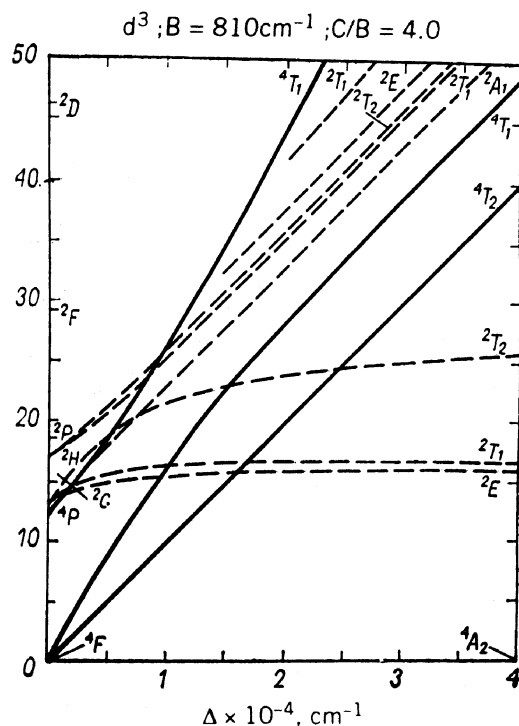


FIGURE 4.11b. (Continued)

3. *Strong field*—the ligand field potential is stronger than both the interelectron and spin-orbital interactions.

For  $d$  electrons case 1 is not important, and therefore it is usually ignored (cases 2 and 3 are called *weak-* and *strong-field cases*, respectively).

For  $f$  electrons in weak fields (1) the atomic terms should be characterized (in addition to  $L$  and  $S$ ) by the quantum number  $J = L + S - 1, \dots, |L - S|$ , which factors in the spin-orbital interaction (Section 2.2). Since the total spin  $S$  can be a semiinteger,  $J$  may also be a semiinteger. For instance, for one  $f$  electron with  $L = 3, S = \frac{1}{2}$ , and with the spin-orbital interaction included,  $J = \frac{7}{2}$  and  $\frac{5}{2}$ , so its states are  ${}^2F_{7/2}, {}^2F_{5/2}$  (the  $J$  value is indicated as a subscript). The weak-field approximation here means that the splitting of each of these terms by the ligand field can be considered separately.

Visual interpretation of the charge distribution in the states with the total momentum quantum number  $J$  and the splitting of these states in ligand fields of different symmetries is not so straightforward, as in the case of  $d$  electrons, where the spin-orbital interaction can be approximately neglected. Qualitatively, the splitting of  $f$  states can be easily obtained by means of the group-theoretical

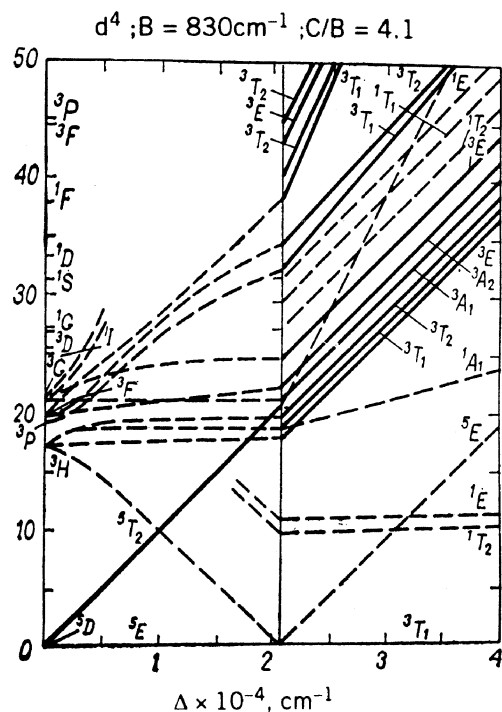


FIGURE 4.11c. (Continued)

rules (Sections 3.4 and 4.2), while quantitative calculations can be performed by perturbation theory.

However, some grade of understanding of the situation can be reached by using the model of pure orbital states, that is, neglecting the spin-orbital coupling. In particular, considering the angular distributions of atomic  $f$ -electron functions from the cubic set, given in Table 2.2 and Fig. 2.4, and the corresponding electrostatic repulsion of the electron in these states from six point charges (or dipoles) of an octahedral complex, one can conclude that in the three states  $f_{x^3}$ ,  $f_{y^3}$ , and  $f_{z^3}$ , the repulsion is the greatest (and equal for all of them). In the other three states  $f_{x(y^2-z^2)}$ ,  $f_{y(z^2-x^2)}$ , and  $f_{z(x^2-y^2)}$ , it is also equal but smaller than in the previous three states, and in the  $f_{xyz}$  state it is the smallest (in tetrahedral systems, analogously to the  $d$  electron states, the picture is inverted).

Thus the sevenfold orbitally degenerate  $F$  term of the free atom (ion) with one  $f$  electron is split by the octahedral ligand field into three terms from which one is nondegenerate and two are threefold-degenerate. It can be shown that the symmetries of these states are  $A_{2u}$ ,  $T_{2u}$ , and  $T_{1u}$ , respectively (Fig. 4.12).

Hence the splitting  $F \rightarrow A_{2u} + T_{2u} + T_{1u}$  is similar to that obtained above for the  $F$  term of the  $d^2$  configuration in octahedral fields (Figs. 4.7 and 4.8), with

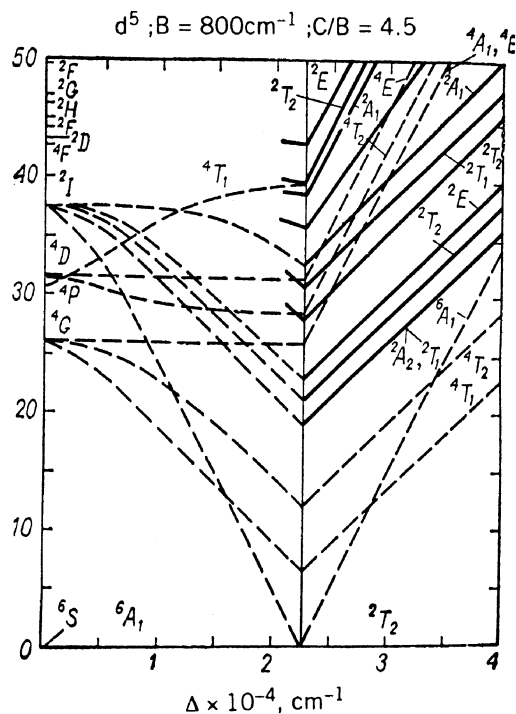


FIGURE 4.11d. (Continued)

an inverted ordering and opposite parity of the terms,  $u$  instead of  $g$ ;  $f$  states, unlike the  $d$  ones, are odd with respect to reflections.

By way of example, we also show the scheme of splitting of the energy levels of an  $f$  electron in the field of a hexagonal biprism with the sixfold axis along  $z$  (Fig. 4.13), which is realized, for instance, in uranyl complexes [4.21]. Here the low-symmetry set of one-electron atomic angular  $f$  functions of Table 2.2 is used. Splitting of the orbital states in other cases in ligand fields of different symmetries can be revealed using Table 4.2.

Quantitative calculations of the energy term splitting of  $f$  electrons can be carried out similarly to that for  $d$  electrons, considered above. To do this, the secular equation (4.6) of the seventh order (for one  $f$  electron) must be solved. For the matrix elements  $V_{mm'}$  one can obtain expressions of the type (4.9) for arbitrary positions of the ligands [4.22]. They are given in Appendix 5.

However, as stated above, in the case of  $f$  electrons the spin-orbital interaction can be stronger than the ligand field, and hence the latter should be considered as a perturbation to the atomic states classified by the quantum number  $J$  of the total momentum  $\mathbf{J} = \mathbf{L} + \mathbf{S}$ . Qualitatively, the splitting of the  $J$  term can be obtained by applying group-theoretical rules given in Section 3.4. If  $J$  is an integer, the splitting coincides completely with that expected for the corresponding

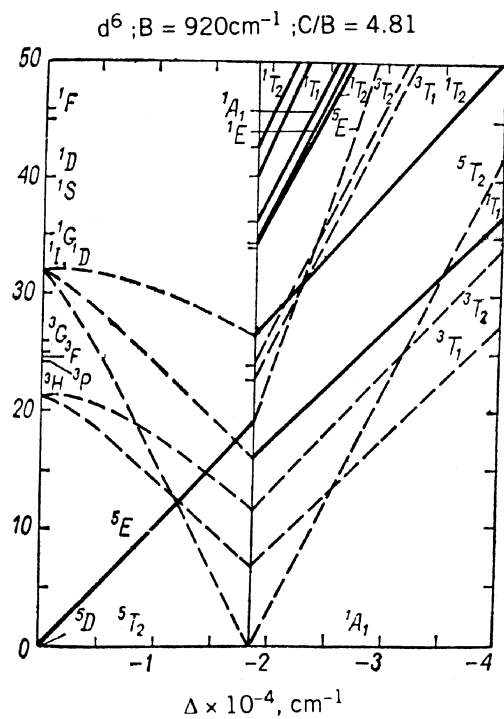


FIGURE 4.11e. (Continued)

$L$  value. For semiinteger  $J$  values, the double groups of symmetry discussed in Section 3.6 should be employed, and the terms should be classified according to their irreducible representations  $E'_1$ ,  $E'_2$  (twofold-degenerate),  $G'$  (fourfold) or, respectively,  $\Gamma_6$ ,  $\Gamma_7$ ,  $\Gamma_8$  in Bethe's notations. The splitting is evaluated, as usual, by means of Eq. (3.33) with the characters given in the corresponding tables of Appendix 1. Some results for most usable cases are given in Table 4.8.

**TABLE 4.8. Splitting of Atomic Terms with Semiinteger  $J$  Values in Ligand Fields of Different Symmetries**

$J$	Cubic Symmetry $O'$	Tetragonal Symmetry $D'_4$	Hexagonal Symmetry $D'_6$
$\frac{1}{2}$	$E'_1$	$E'_1$	$E'_2$
$\frac{3}{2}$	$G'$	$E'_1 + E'_2$	$E'_2 + E'_3$
$\frac{5}{2}$	$E'_2 + G'$	$E'_1 + 2E'_2$	$E'_1 + E'_2 + E'_3$
$\frac{7}{2}$	$E'_1 + E'_2 + G'$	$2E'_1 + 2E'_2$	$E'_1 + 2E'_2 + E'_3$
$\frac{9}{2}$	$E'_1 + 2G'$	$3E'_1 + 2E'_2$	$E'_1 + 2E'_2 + 2E'_3$
$\frac{11}{2}$	$E'_1 + E'_2 + 2G'$	$3E'_1 + 3E'_2$	$2E'_1 + 2E'_2 + 2E'_3$



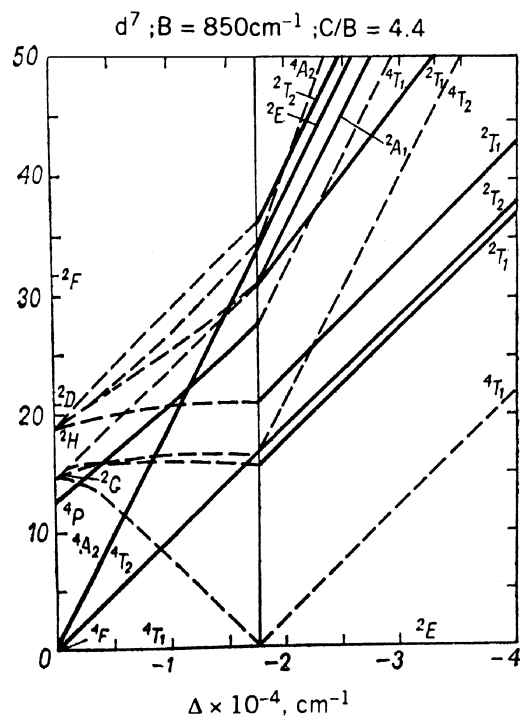


FIGURE 4.11f. (Continued)

For quantitative calculations the ligand field, spin-orbital interaction, and electron interaction should be included in the perturbation simultaneously. Such calculations are carried out numerically (see, e.g., Ref. 4.17). Similar to  $d$  electrons, the method of equivalent operators and irreducible tensor operators may be useful for such calculations [4.15–4.18].

#### 4.5. CRYSTAL FIELD PARAMETERS AND EXTRASTABILIZATION ENERGY

The most valuable results of the CFT are based on its semiempirical versions that yield general qualitative and semiquantitative conclusions. In these versions the electronic structure of the system is described by means of one (or several) parameters that can be obtained from independent experimental data or from comparison of the theory with the experiments (see also Section 4.6). Therefore the meaning of the CFT parameters is of great importance.

The main parameters of the  $d^n$ -term splitting in cubic fields (cube, octahedron, tetrahedron) is the energy gap  $\Delta$  between the  $e_g$  and  $t_{2g}$  one-electron states, which is often denoted as  $10D_q$ . According to Eqs. (4.15) and (4.30), for six

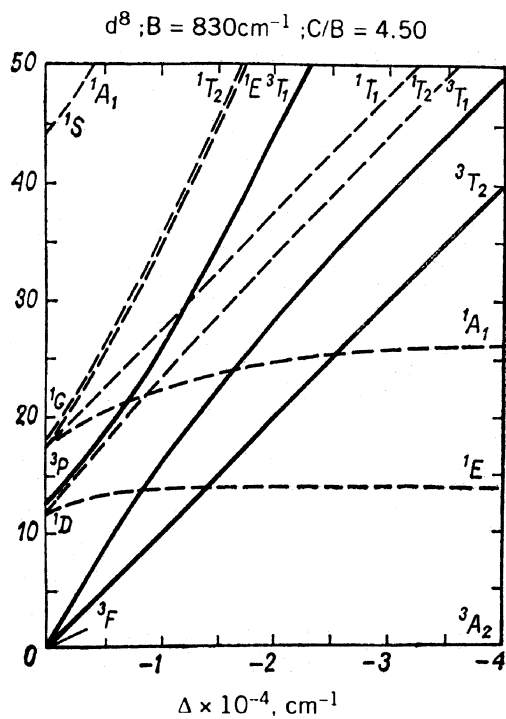


FIGURE 4.11g. (Continued)

ligand–point charges  $q$  at the corners of a regular octahedron, we obtain

$$\Delta = \frac{5}{3}eqF_4(R) \quad (4.59)$$

where the function  $F_4(R)$  is defined by Eq. (4.10) and  $R$  is the interatomic CA–ligand distance, while for the similar case of ligand–dipole moments  $\mu$ , we have

$$\Delta = -\frac{5}{3}e\mu F_4'(R) \quad (4.60)$$

For a tetrahedron  $\Delta_T = -\frac{4}{9}\Delta$ , while for a cube  $\Delta_C = 2\Delta_T = -\frac{8}{9}\Delta$  [Eqs. (4.20) and (4.22)].

Direct calculation of  $\Delta$  after Eqs. (4.59) and (4.60) does not have sufficient credibility because of the rough assumptions on which CFT is based on. However some rules in the relative changes of  $\Delta$  in series of similar compounds can be carried out from these relations quite satisfactorily. According to Eqs. (4.59) and (4.60),  $\Delta$  depends on three parameters. Two of them,  $q$  (or  $\mu$ ) and  $R$ , characterize the ligand, its charge and position, respectively, while the third one ( $\alpha$ ) is the effective parameter of the CA radial  $nd$  function in the  $F_k(R)$  functions

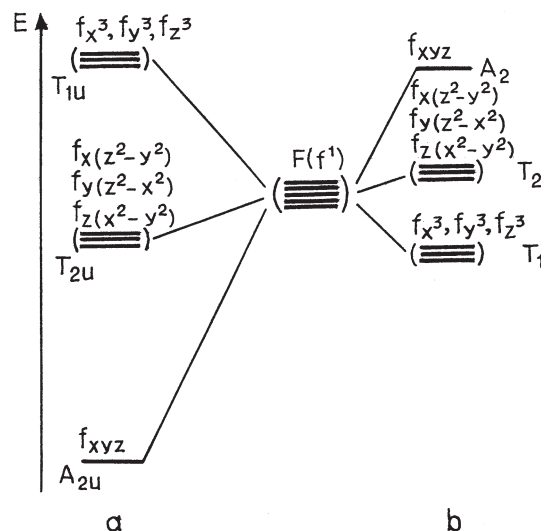


**FIGURE 4.12.** Splitting of the atomic energy levels of one  $f$  electron in octahedral (a) and tetrahedral (b) ligand fields (the spin-orbital interaction is neglected).

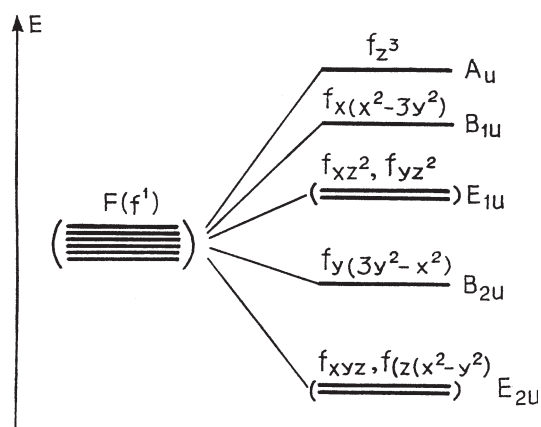


**FIGURE 4.13.** Splitting of one  $f$ -electron energy levels in the field of a hexagonal bipyramid.

measuring the strength of the coupling of the  $d$  electron to the CA nuclei. In the same group of transition metals (e.g., in the iron group) the  $\alpha$  values for different metals in the same oxidation state are close (the ionization potentials determining approximately the  $\alpha$  value differ in this series by no more than 10–15%). Hence for such a series  $\Delta$  depends mostly on the ligand field. Therefore  $\Delta$  is called the *ligand field parameter*.

When passing from the elements of the first transition group to the second and third ones, the  $\alpha$  value decreases significantly, and hence the parameter  $\Delta$  increases. Indeed, following (A2.14),  $F_4(R)$  decreases with increasing  $\alpha$  [for actual values of interatomic distances  $R$  the derivative  $F_4'(x) < 0$ ,  $x = \alpha R$ ]. The data on absorption spectra confirm these conclusions (Section 8.2). For instance, for hydrated transition metal ions of the first transition group,  $\Delta$  varies in the limits 7500–12,500  $\text{cm}^{-1}$  and 13,500–21,000  $\text{cm}^{-1}$  for the oxidation states +2 and +3, respectively, while for the second and third transition groups  $\Delta$  is larger by 30–70%. Different ligands can be arranged in a *spectrochemical series* with respect to the splitting  $\Delta$  that they produce in a complex of the same metal discussed in Section 8.2.

Another parameter of the splitting that may be useful in practice is the *energy of extrastabilization*  $\delta$ , which equals the energy difference between the initial nonsplit term (but destabilized by the average ligand repulsion energy  $E_0$ ) and the new ground term after the splitting. The term *stabilization* for this magnitude may be misleading because the electron–ligand interaction is repulsion (destabilization). In fact, the new ground state is just less destabilized than the electronic states on average, and it is implied that this “less destabilization” can be considered as an additional stabilization [i.e., in addition to that produced by the main attractive term (4.3) minus the average destabilization energy  $E_0$  in Eq. (4.17)].

The  $\delta$  value can be easily obtained from the expression for  $\Delta$  and the rule of preservation of the center of gravity (Section 4.2). For the electronic configuration  $[A](nd)^1$  in an octahedral field  $\delta = \frac{2}{5}\Delta$  (Fig. 4.3), while in the tetrahedral fields  $\delta_T = \frac{3}{5}\Delta_T = \frac{4}{15}\Delta$ , and in the eight-coordinate cube  $\delta_C = 2\delta_T = \frac{8}{15}\Delta$  [see Fig. 4.4 and Eqs. (4.20) and (4.22)]. On the basis of these relations and accounting for the electron occupation of different orbitals in the weak- and strong-field limits, the extrastabilization energies for different electron configurations  $d^n$  are given in Table 4.9.

One feature of the extrastabilization energy that emerges from this table is its nonmonotonous change with the number of  $d$  electrons. In particular, for high-spin complexes  $\delta$  is zero for  $d^0$ ,  $d^5$ , and  $d^{10}$ , and has two maxima at  $d^3$  and  $d^8$ . This “two-humped” behavior is confirmed qualitatively by many experimental data. By way of an illustrative example the *heat of formation* of bivalent and trivalent transition metal aqua complexes as a function of  $d^n$  is shown in Fig. 4.14. It is seen that, indeed,  $\Delta H$  has two maxima and three minima as predicted by CFT (note that the extrastabilization energy is to be added to the main bonding energy, which is shown in Fig. 4.14 by a solid line).

However, in Table 4.9 the changes in electron interactions by passing from one configuration to another are ignored. Meanwhile, they may be significantly different. For instance, for the  $d^2$  configuration in the weak-field limit, according to the data in Table 2.6, the energy of interaction between the two electrons in the ground state  ${}^3T_{1g}({}^3F)$  (in the  ${}^3T_{1g}$  term originating from the atomic  ${}^3F$  term) equals  $A - 8B$ , whereas in the strong-field case in the ground state  ${}^3T_{1g}(t_{2g})^2$  [i.e., for the same term  ${}^3T_{1g}$  originating from the strong field configuration  $(t_{2g})^2$ ] it equals  $A - 5B$  [see Eqs. (4.47) and Fig. 4.9]. The destabilization energies  $E_0$

**TABLE 4.9. Energy of Extrastabilization  $\delta$  in Ligand Fields of Different Symmetries in Units of the Crystal Field Parameter  $\Delta^a$** 

Electronic Configuration	Examples of Ions	High Spin			Low Spin		
		Octahedron	Tetrahedron	Cube	Octahedron	Tetrahedron	Cube
$d^0$	Sc <sup>2+</sup>	0	0	0	0	0	0
$d^1$	Ti <sup>3+</sup>	$\frac{2}{5}$	$\frac{4}{15}$	$\frac{8}{15}$	$\frac{2}{5}$	$\frac{4}{15}$	$\frac{8}{15}$
$d^2$	V <sup>3+</sup>	$\frac{4}{5}$	$\frac{8}{15}$	$\frac{16}{15}$	$\frac{4}{5}$	$\frac{8}{15}$	$\frac{16}{15}$
$d^3$	Cr <sup>3+</sup>	$\frac{6}{5}$	$\frac{16}{45}$	$\frac{32}{45}$	$\frac{6}{5}$	$\frac{4}{5}$	$\frac{8}{5}$
$d^4$	Mn <sup>3+</sup>	$\frac{3}{5}$	$\frac{8}{45}$	$\frac{16}{45}$	$\frac{8}{5}$	$\frac{16}{15}$	$\frac{32}{15}$
$d^5$	Mn <sup>2+</sup> , Fe <sup>3+</sup>	0	0	0	2	$\frac{8}{9}$	$\frac{16}{9}$
$d^6$	Fe <sup>2+</sup> , Co <sup>3+</sup>	$\frac{2}{5}$	$\frac{4}{15}$	$\frac{8}{15}$	$\frac{12}{5}$	$\frac{32}{45}$	$\frac{64}{45}$
$d^7$	Co <sup>2+</sup>	$\frac{4}{5}$	$\frac{8}{15}$	$\frac{16}{15}$	$\frac{9}{5}$	$\frac{8}{15}$	$\frac{16}{15}$
$d^8$	Ni <sup>2+</sup>	$\frac{6}{5}$	$\frac{16}{45}$	$\frac{32}{45}$	$\frac{6}{5}$	$\frac{16}{45}$	$\frac{32}{45}$
$d^9$	Cu <sup>2+</sup>	$\frac{3}{5}$	$\frac{8}{45}$	$\frac{16}{45}$	$\frac{3}{5}$	$\frac{8}{45}$	$\frac{16}{45}$
$d^{10}$	Zn <sup>2+</sup>	0	0	0	0	0	0

<sup>a</sup>For  $d^n$  with  $n > 1$  the interelectron interaction is neglected.

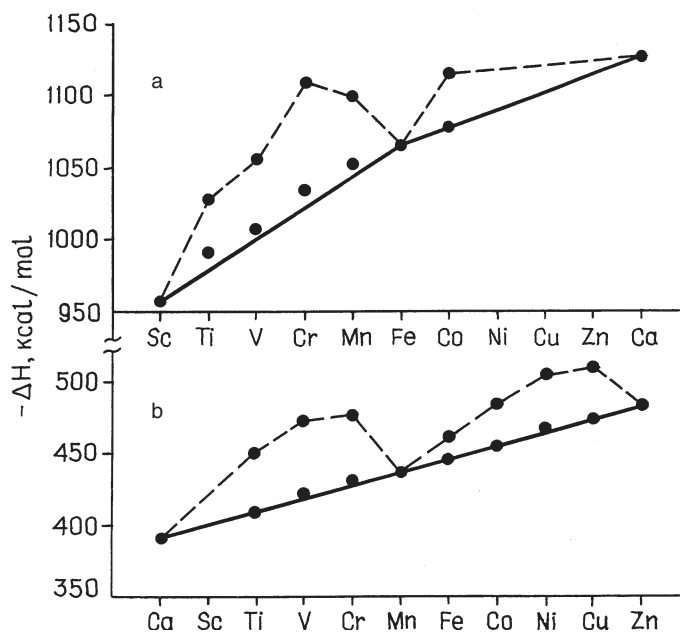


**FIGURE 4.14.** “Two-humped” dependence of the heat of formation  $\Delta H$  of aqua complexes of trivalent (a) and divalent (b) transition metals. The solid line links the values of  $\Delta H$  without extrastabilization.

**TABLE 4.10. Approximate Relative Values of  $d$  Orbital Energies (in  $\Delta$  Units) in Crystal Fields of Different Symmetries<sup>a</sup>**

Coordination Number	Mode of Coordination (Symmetry)	$d_{x^2-y^2}$	$d_{z^2}$	$d_{xy}$	$d_{xz}$	$d_{yz}$
1	—	-0.314	0.514	-0.314	0.057	0.057
2	Linear	-0.628	1.028	-0.628	0.114	0.114
3	Trigonal	0.546	-0.321	0.546	-0.386	-0.386
4	Tetrahedral	-0.267	-0.267	0.178	0.178	0.178
4	Square-planar	1.228	-0.428	0.228	-0.514	-0.514
5	Square pyramid	0.914	0.086	-0.086	-0.457	-0.457
5	Trigonal pyramid	-0.082	0.707	-0.082	-0.272	-0.272
6	Octahedral	0.600	0.600	-0.400	-0.400	-0.400
7	Pentagonal bipyramid	0.282	0.493	0.282	-0.528	-0.528

<sup>a</sup> $z$  is the axis of the highest symmetry.

vary for different numbers of electrons and ligands as well. These circumstances complicate the quantitative interpretation of the experimental data on  $\Delta H$  in CFT.

If the symmetry of the ligand field is lower than cubic, degenerate terms are subject to further splitting; its characterization requires additional parameters. For tetragonal distorted octahedra the additional parameters are  $D_s$  and  $D_t$ , given, respectively, by Eqs. (4.24) and (4.25) as functions of  $F_2(R)$  and  $F_4(R)$ . A rough simplification,  $F_2 \approx 2F_4$ , makes it possible to present approximately all the energy  $d$  levels as a function of one parameter  $\Delta$ . They are given in Table 4.10 for different types of ligand coordination to the CA. The data of this table can be used for qualitative estimations only. For more details on CFT parameters, see Ref. 4.23.

#### 4.6. LIMITS OF APPLICABILITY OF CRYSTAL FIELD THEORY

The limits of application of the CFT, as of any other approximate theory, are determined by its main assumptions (postulates), as well as by the additional simplifications introduced for their realization. Usually the limits of any theory can be established definitively when there is a more general theory for which the one under consideration can be considered as a particular case. In this sense the possibilities and limitations of the CFT are better understood when compared with the conclusions of the (in general) wider MO LCAO theory (Section 5.6).

As indicated above, the assumption of the pure electrostatic nature of the CA–ligand interaction with the ligands as point charges or dipoles a priori excludes the possibility of investigating, by means of CFT, such important problems as the nature of chemical binding and charge distribution in coordination compounds, as well as the phenomena that depend on the details of the electronic structure of the ligands (ligand activation, charge transfer spectra, reactivity, etc.).

The properties of coordination compounds that can be analyzed by CFT are limited by those originating from the electronic structure of the central atom influenced by the ligands. This excludes such important problems as complex formation (e.g.,  $\pi$  bonding), stereochemistry, reactivity, ligand activation, and hyperfine ESR spectra.

Even with these strong limitations, the range of CFT remains sufficiently wide. Indeed, it includes the origin of color (electronic absorption spectra in the visible and related regions, Section 8.2), magnetic susceptibility and ESR spectra (without ligand hyperfine structure; Section 8.4), relative stabilities in solutions, and some vibronic interaction effects (Chapter 7), and the number of such problems can be significantly increased by including covalence corrections (Section 5.2).

When analyzing the applicability of CFT, one should distinguish between its qualitative and quantitative aspects. The qualitative aspect of the theory (the analysis of term splitting, symmetry of states, relative energies, spin multiplicities, etc.) covers a much wider spectrum of problems and systems than do its quantitative treatments, which requires more accurate energy spectra and wavefunctions. Indeed, the qualitative conclusions of CFT are based mainly on the symmetry properties of the system that are independent of the nature of the bonding (and remain the same in all the theories), whereas the quantitative results are bound to the approximation of the electrostatic ligand fields, which is a priori invalid for many systems. Obviously, the qualitative conclusions of CFT not only have larger limits of application but are more reliable.

The CFT assumption that the ligands are point charges or dipoles at first sight seems to be rather rough. Nevertheless, the results obtained in this model, within the limits of its applicability, may be quite reasonable, due mainly to the compensation of the errors with opposite signs (Section 5.6). However, the semiempirical versions of CFT in which the main parameters are obtained from empirical data seem to be more useful. As mentioned in Section 4.4,  $f$  electrons in rare-earth complexes are strongly screened from the ligand field by the outer  $s$ ,  $p$ ,  $d$  electrons. For this reason the covalence with  $f$ -electron participation is rather weak, and study of  $f$ -electron states and related properties by CFT is quite acceptable also for quantitative calculations (see the case of weak covalence and AOM in Section 5.2). This conclusion is confirmed by experimental data [4.17, 4.18, 4.24, 4.25].

Finally, no less important is the fact that the CFT provided (and still provides) a simple introduction to (a tool for a better understanding of) more sophisticated theories discussed in the following chapters. The relative simplicity and stimulating power of the CFT allowed one of the most significant contributors to this theory, Professor Moffitt, to state [4.26]:

It will be a long time before a method is developed to surpass in simplicity, elegance and power that of crystal field theory. Within its extensive domain it has provided at very least a deep qualitative insight into the behavior of a many-electron system. No other molecular theory, to our knowledge, has provided so many useful numbers

which are so nearby correct. And none has a better immediate prospect of extending its chemical applications.

Although more than 50 years have passed since the time of this statement, only the last two sentences should be revised because of the impressive achievements in MO theories in more recent decades.

### SUMMARY NOTES

1. *Crystal field theory* (CFT) is a quantum extension of the prequantum electrostatic theory that assumed that the bonding in a transition metal system (TMS) is due to pure electrostatic interaction between the central atom (CA) and ligands. The CFT considers the electronic structure of the CA by means of quantum mechanics, while the ligands are treated as “structureless” sources of electrostatic (“crystal”) fields.
2. The main effect of ligand influence on the CA is splitting of its energy levels (Stark effect). This *crystal field splitting* explains a variety of optical, magnetic, and thermodynamic properties of TMS.
3. CFT allows one to *evaluate energy-level splitting* on either a qualitative level by means of group-theoretical considerations or by direct calculation of the splitting using quantum-mechanical perturbation theory. In the latter case the CFT is more reliable in its semiempirical approximation, in which some parameters are taken from experimental data.
4. When there is more than one electron in the *d* shell of the CA of the TMS, their distribution over the split energy levels may be different dependent on the splitting magnitude. If the splitting is sufficiently large, the electrons tend to occupy first the lowest levels (even if this is accompanied by pairing the spins of the electrons on the same level), thus resulting in *low-spin electronic configurations* in the ground state. In the other limit case of small CFT splitting the electrons occupy as much as possible levels with parallel spins producing *high-spin configurations* of the TMS.
5. In the general case of two or several *d* electrons, the energy terms of the corresponding electronic configuration can be obtained by numerical calculation of their energies as a function of the main parameter of the CFT splitting and the interelectron interaction, *Tanabe–Sugano diagrams*.
6. CFT *splitting of f-electron levels* of the CA is different from that of *d* electrons because they have different symmetry and bonding properties, and in many cases they are screened from the ligands by the outer *d* electrons.
7. The overall heuristic value of CFT lies mainly in its *qualitative results based on symmetry properties*. Its shortcomings are due to the neglect of electronic structure and quantum properties of the ligands. The angular overlap method in Chapter 5 is removing a part of this failure, but a full remedy is achieved in the MO theory.



**QUESTIONS**

*Answer the following questions with explanation:*

- 4.1. What are the main assumptions of CFT? What limitations are introduced by these assumptions in the study of TMS? Give examples of observable properties that cannot be explained by CFT.
- 4.2. Why are the energy levels of  $d$  electrons split in spite of symmetric arrangements of the ligands in octahedral and tetrahedral complexes? Are  $p$ -electron levels split in the same complexes?
- 4.3. According to Fig 4.3 and calculations, the destabilization energy produced by the averaged field of the ligands  $E_0$  is larger than the stabilization gained by the energy-level splitting. Why, then, are such complexes stable?
- 4.4. If the CA has several  $d$  electrons, which two types of octahedral or tetrahedral transition metal coordination systems are possible, dependent on the strength of the ligand field, and how do they relate to the number of  $d$  electrons and the total spin? Give examples.
- 4.5. Why do weakly influencing ligands (producing weak CFT splitting) generate electronic configurations with the highest possible total spin, whereas strongly influencing ligands form complexes with the lowest possible spin? Give three examples of low-spin complexes and three of high-spin ones with their electronic configurations.
- 4.6. From the term-splitting diagram in Fig. 4.7 for a system with the  $d^2$  electron configuration in octahedral crystal fields, can we judge as to whether the perturbation theory used for its calculation is applicable to this case?
- 4.7. Figures 4.8 and 4.11 show that some energy levels as a function of the crystal field parameter  $\Delta$  intersect while the others do not. What are the conditions for nonintersection?
- 4.8. In case of more than one  $d$  electron, what is the difference between crystal field destabilization (Fig. 4.9b) and electron interaction destabilization (Fig. 4.9d)? Should we expect that the former is larger than the latter in case of strong fields?
- 4.9. Why are low-spin tetrahedral complexes much rarer than octahedral ones?
- 4.10. Under equal ligand field strengths, what are the differences between  $d$ - and  $f$ -electron splittings?

**EXERCISES AND PROBLEMS**

- P4.1.** Similar to the calculation of the splitting of the energy levels of one  $d$  electron in different fields of ligands presented in Chapter 4 and Appendixes 1–3, calculate the energy-level splitting of one  $d$  electron in the field of eight ligands—point charges that form a square prism with the CA in its center, as a function of similar parameters.

- \*P4.2.** Find the energy-level splitting of (a) one  $d$  electron and (b) one  $f$  electron, in icosahedral crystal fields by means of group-theoretical analysis (Section 4.2).
- P4.3.** Check and ensure that in all the cases of crystal field splitting considered in this chapter the center of gravity of the split energy levels remains unchanged and equal to the energy level before splitting. Explain why this takes place.
- \*P4.4.** Determine whether  $\text{Cr}(\text{H}_2\text{O})_6^{2+}$ ,  $\text{Mn}(\text{H}_2\text{O})_6^{2+}$ ,  $\text{Mn}(\text{H}_2\text{O})_6^{3+}$ ,  $\text{Mn}(\text{en})_3^{2+}$ ,  $\text{Fe}(\text{H}_2\text{O})_6^{2+}$ ,  $\text{Fe}(\text{CN})_6^{4-}$ ,  $\text{Co}(\text{NH}_3)_6^{3+}$ , and  $\text{Co}(\text{CN})_6^{3-}$  are low-spin or high-spin complexes by estimating the pairing energy  $\Pi$  after Eq. (4.50) with Racah parameters from Table 4.7 and  $\Delta$  values from Table 8.2 in Chapter 8.
- \*P4.5.** On the basis of group symmetry rules, find the possible terms of electronic configurations  $(e_g)^2$  and  $(t_{2g})^3$  in octahedral and  $(e)^2$  and  $(t_2)^3$  in tetrahedral ligand fields. What are the ground-state terms in these cases according to Hund's rule?
- \*P4.6.** Using the Tanabe–Sugano diagrams and approximate  $\Delta$  values from Table 8.2 and spectrochemical series (8.24) (as well as literature data) find out existing transition metal coordination systems that can be expected to have coexisting low-spin and high-spin states important in the spin crossover phenomenon (Section 8.4).

## REFERENCES

- 4.1. J. H. Van Vleck, in *XXII International Congress of Pure and Applied Chemistry. Plenary Lectures*, London, Butterworths, 1970, p. 235.
- 4.2. H. Bethe, *Ann. Phys.* **3**, 133 (1928).
- 4.3. J. H. Van Vleck, *The Theory of Electronic and Magnetic Susceptibilities*, Oxford Univ. Press, London, 1965.
- 4.4. H. Hartmann, *Theorie der Chemischen Binding auf Quantum-Theoretische Grundlage*, Springer, Berlin, 1954.
- 4.5. L. E. Orgel, *An Introduction to Transition-Metal Chemistry. Ligand Field Theory*, Wiley, New York, 1960.
- 4.6. C. J. Ballhausen, *Introduction to Ligand Field Theory*, McGraw-Hill, New York, 1962.
- 4.7. H. L. Schlafer and G. Gliemann, *Basic Principles of Ligand Field Theory*, Wiley, New York, 1969.
- 4.8. C. K. Jorgensen, *Modern Aspects of Ligand Field Theory*, North-Holland, Amsterdam, 1971.
- 4.9. I. B. Bersuker and A. V. Ablov, *Chemical Bonding in Complex Compounds* (Russ.), *Stiinta* (Acad. Sci MoSSR), Kishinev, 1962; I. B. Bersuker, *Electronic Structure of Coordination Compounds* (Russ.), *Khimia*, Leningrad, 1971 (2nd ed., 1976; 3rd ed., 1986).
- 4.10. W. Kossel, *Ann. Phys. Lpz.* **44**, 229 (1916).

- 4.11. A. Magnus, *Z. Anorg. Chem.* **124**, 288 (1922).
- 4.12. H. H. Schmidtke, in H. A. O. Hill and P. Day, eds., *Physical Methods in Advanced Inorganic Chemistry*, Interscience, London, 1968, p. 107.
- 4.13. A. L. Companion and M. A. Komarynsky, *J. Chem. Educ.* **41**, 257 (1964).
- 4.14. M. Randic and Z. Maksic, *Theor. Chim. Acta* (Berlin) **4**, 145 (1966).
- 4.15. J. S. Griffith, *The Theory of Transition Metal Ions*, Cambridge Univ. Press, Cambridge, UK, 1962.
- 4.16. S. E. Harmung and C. E. Schafer, *Struct. Bonding* **12**, 201 (1972); *ibid.* **12**, 257 (1972).
- 4.17. B. G. Wyborne, *Spectroscopic Properties of Rare Earth*, Interscience, New York, 1965.
- 4.18. C. W. Nielson and G. F. Koster, *Spectroscopic Coefficients for the  $p^n$ ,  $d^n$ , and  $f^n$  Configurations*, MIT Press, Cambridge, MA, 1963.
- 4.19. S. Sugano and Y. Tanabe, *Multiplets of Transition Metal Ions in Crystals*, Academic Press, New York, 1970.
- 4.20. A. D. Lichr and C. J. Ballhausen, *Ann. Phys. (USA)* **6**, 134 (1959); A. D. Lichr, *J. Phys. Chem.*, **67**, 1314 (1963).
- 4.21. C. A. Coulson and G. R. Lester, *J. Chem. Soc.* 3650 (1956).
- 4.22. Z. Maksic and M. Randic, *Theor. Chim. Acta* **7**, 253 (1967).
- 4.23. M. Gerloch and R. S. Slade, *Ligand Field Parameters*, Cambridge Univ. Press, 1973.
- 4.24. M. A. El'ashevich, *Spectry Redkich Zemel'* (Russ.), Gostechteorizdat, 1953.
- 4.25. K. B. Yatsimirski, N. A. Kostromina, and Z. A. Sheka, *Chemistry of Rare Earth Complex Compounds* (Russ.), Naukova Dumka, Kiev, 1966.
- 4.26. W. Moffitt and C. J. Ballhausen, *Annu. Rev. Phys. Chem.* **7**, 107 (1956).

---

# 5

---

## METHOD OF MOLECULAR ORBITALS AND RELATED APPROACHES

*Molecular orbitals are the main electronic structural units for analysis and solution of chemical problems at the electronic level.*

Historically, application of the MO method to transition metal and rare-earth complexes began with the improvement of crystal field theory by means of including covalency effects, and in this aspect it was called *ligand field theory*. However, in its present form the MO method in application to coordination compounds basically does not differ from that widely used for organic and main-group systems, although practically the treatment of coordination system with this method is more complicated because of the presence of active *d* and *f* electrons.

In this chapter the main ideas and special features of the MO approach are presented in a form applicable to transition metal coordination compounds. The general presentation of the MO method is discussed together with the methods of numerical calculations (*ab initio*, nonempirical, semiquantitative, and semiempirical), as well as other related approaches, including density-functional methods. The application of these methods to the solution of the main problem of coordination chemistry—the origin of chemical bonding—is given in Chapter 6, while specific calculations of electronic structure using these methods are demonstrated in Chapters 6, 9, 10, 11, and Solutions to Problems.

## 5.1. BASIC IDEAS OF THE MO LCAO METHOD

### Main Assumptions

The basic idea behind the MO method, as compared with crystal field theory (CFT) discussed in Chapter 4, is to drop the main restricting CFT assumption that the electronic structure of the ligands can be ignored, and include explicitly all the electrons in the quantum-mechanical treatment of the molecular system. The MO approach makes no a priori assumptions about the nature of the chemical bonding. Unlike CFT, where the atoms or groups of atoms of the complex are assumed to preserve mainly their individual features, in the MO method the coordination system is considered, in principle, as an integral system in which separate atoms lose their individuality.

For example, the complex  $\text{Co}(\text{NH}_3)_6^{3+}$  is considered in the MO theory as having a skeleton of 6 nitrogen nuclei, 18 hydrogen nuclei, 1 cobalt nucleus, and 84 electrons that move in the field of the nuclei. The motion of each electron is determined by both the nuclear configuration (provided that the latter can be assumed to be fixed; Section 7.1) and the motions of the other 83 electrons. All these motions (including the nuclear motions) are determined by the Schrödinger equation (Section 1.1).

Exact solution of the Schrödinger equation (1.5) for a coordination system is hardly possible at present because of computation difficulties. So far, the only practically acceptable approaches are that based on the *adiabatic approximation* discussed in Section 7.1, and the *one-electron approximation*, which assumes that each electron can be considered as moving independently in the mean field created by the nuclei and the remaining electrons (Section 2.2). In the one-electron approximation, the coordination system is described by one-electron states that in general extend throughout the entire system; they are called *molecular orbitals* (MOs). The MO method was first suggested by Hund and Mulliken [5.1]; its applications to transition metal coordination compounds were developed by Van-Vleck, Orgel, Griffith, Ballhausen, and others (see in Refs. 5.2–5.6 and references cited therein).

In general, evaluation of one-electron MOs is still a complicated problem. Its solution requires further simplifications; the main one is the so-called LCAO approximation, in which the wavefunction of the MO is sought for in the form of a *linear combination of atomic orbitals* (LCAO):

$$\phi(\mathbf{r}) = c_1\psi_1(\mathbf{r}) + c_2\psi_2(\mathbf{r}) + \cdots + c_n\psi_n(\mathbf{r}) = \sum_i c_i\psi_i(\mathbf{r}) \quad (5.1)$$

where  $n$  is the number of atomic orbitals (note that each atom can be presented by more than one orbital),  $\psi_i$  is the  $i$ th one-electron atomic wavefunction, and  $c_i$  are variational coefficients to be evaluated as the best choice (see below). The set of  $\psi_i$ 's forms the *LCAO basis*. In fact, the LCAO approximation means that we assume that each MO electron can be found at each atom of the system with

a probability determined by the  $|c_i|^2$  value; when it is near the given atom, the MO electron moves as a usual atomic valence electron.

For coordination compounds with heavy atoms further simplifications may be needed. In particular, the inner electrons of atomic closed shells are often considered as localized near the nucleus and hence not participating directly in the bonding with other atoms. Hence only valence electrons remain in the MO LCAO treatment. However, the separation of inner-core electrons from the valence electrons is not straightforward and should be carried out with care, especially in ab initio calculations (see Section 5.4).

### Secular Equation

Following the variational principle, the coefficients  $c_i$  in the probe function (5.1) should satisfy the condition of minimum total energy of the system. Actually, calculation of the LCAO coefficients is one of the most important parts of the MO LCAO method, which is discussed in more detail in Section 5.3. Here we present some simple analytical relations that nevertheless have a basic meaning for all the versions of the method under consideration.

In the Hartree–Fock method (Section 2.2) each electron moves independently in an effective self-consistent field of nuclei and other electrons with the effective Hamiltonian  $H^k$  given by Eq. (2.55) (denoted there as  $F^k$ ). With this latter the energy of the MO electron (5.1) is (the  $k$  index is omitted)

$$E = \frac{\int \varphi^* H \varphi d\tau}{\int \varphi^* \varphi d\tau} \quad (5.2)$$

Substituting  $\varphi$  by its expression (5.1) and introducing the denotations

$$S_{ik} = \int \psi_i^* \psi_k d\tau \quad (5.3)$$

$$H_{ik} = \int \psi_i^* H \psi_k d\tau \quad (5.4)$$

we easily obtain

$$E \sum_{i,k} c_i^* c_k S_{ik} = \sum_{i,k} c_i^* c_k H_{ik} \quad (5.5)$$

As mentioned earlier (Section 2.1),  $S_{ik}$  is the overlap integral between the atomic functions  $i$  and  $k$  ( $S_{ii} = 1$  due to the normalization condition). The matrix elements (5.4) are discussed in Section 5.3; for  $i \neq k$ ,  $H_{ik}$  is called *the resonance integral*, and  $H_{ii}$  is *the Coulomb integral*. The condition of the energy minimum with respect to the  $c_i$  values means that the corresponding first

derivative must be zero:

$$\frac{\partial E}{\partial c_i} = 0 \quad i = 1, 2, \dots, n \quad (5.6)$$

This results in the following equations with respect to the  $c_i$ 's:

$$\sum_k c_k (H_{ik} - ES_{ik}) = 0 \quad i = 1, 2, \dots, n \quad (5.7)$$

This algebraic system of equations with respect to the unknown  $E$  is linear and uniform. It yields nonzero solutions provided that its determinant is zero:

$$\begin{bmatrix} H_{11} - E & H_{12} - ES_{12} & \dots & H_{1n} - ES_{1n} \\ H_{21} - ES_{21} & H_{22} - E & \dots & H_{2n} - ES_{2n} \\ \vdots & \vdots & \ddots & \vdots \\ H_{n1} - ES_{n1} & H_{n2} - ES_{n2} & \dots & H_{nn} - E \end{bmatrix} = 0 \quad (5.8)$$

or in the following compressed format, used later in this book:

$$\|H_{ik} - ES_{ik}\| = 0 \quad (5.8')$$

Condition (5.8) is in fact an algebraic equation of the  $n$ th power with respect to the unknown  $E$ . Such equations are usually called *secular equations*. In general, (5.8) gives  $n$  different solutions  $E_i$ ; for each of them a set of  $c_{ik}$  values,  $c_{i1}, c_{i2}, \dots, c_{in}$ , can be obtained from Eqs. (5.7). The uniform system (5.7) yields only  $n - 1$  constants  $c_{ik}$ ; one more is obtained from the condition of normalization  $\int \varphi^* \varphi d\tau = 1$ .

Thus, assuming that the one-electron wavefunctions have the form (5.1), that is, that they are linear combinations of  $n$  atomic functions, we get  $n$  MO energies  $E_i, i = 1, 2, \dots, n$ , and  $n$  sets of LCAO coefficients for each MO. Equations (5.7) and (5.8) form the basis of all the versions of the MO LCAO method. Calculations based on these equations are discussed in Section 5.3.

### Classification by Symmetry

One of the special features of coordination compounds concerning the use of the MO LCAO method is the importance of symmetry considerations. The latter usually reduce significantly the calculation difficulties. As compared with organic and some main-group inorganic compounds, TMSs acquire high-symmetry configurations much more often, especially in their active sites. Provided that one knows the symmetry group of the system (Section 3.2), the possible MOs can be a priori divided on symmetries, with each MO attributed to a certain IrRep.

Then, using the results of Section 3.5, one can construct the appropriate LCAO of the CA and ligand atomic functions that satisfy the required symmetry properties. With the known symmetry of the MOs, some of the matrix elements of the secular equation (5.8) vanish, thus reducing essentially the order  $n$  of this equation.

Let us first specify some notations. Figure 5.1 illustrates the choice of the general and local (ligand) coordinate systems, ligand numeration, and the orientation

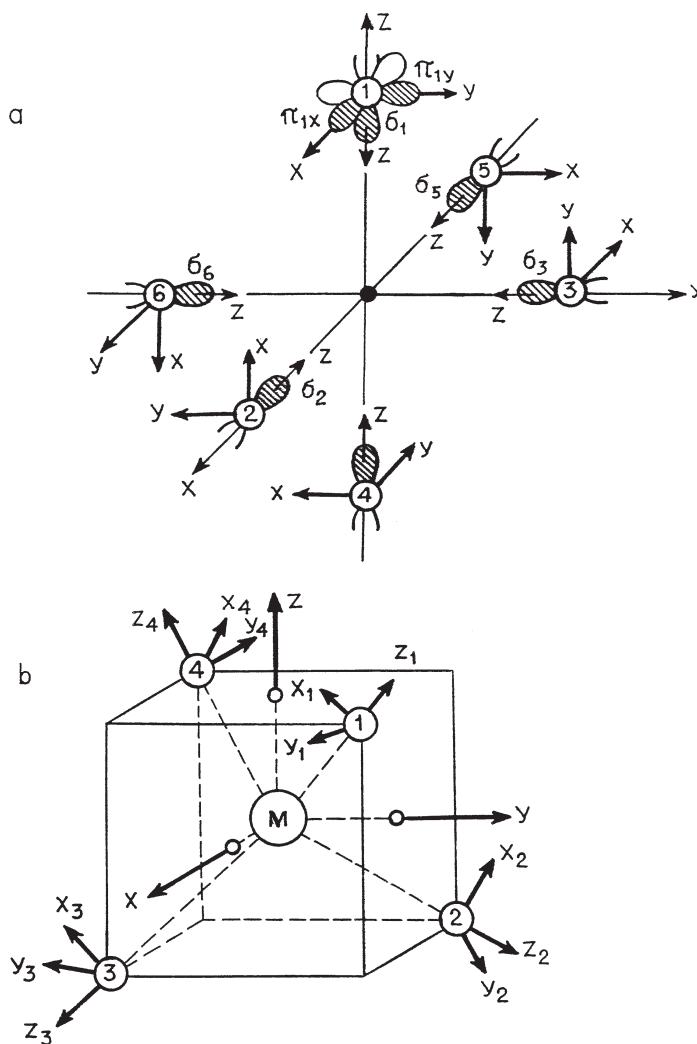


**FIGURE 5.1.** General and ligand local coordinate systems for octahedral (a) and tetrahedral (b) complexes. In the octahedral case the orientation of the  $\pi_{1x}$ ,  $\pi_{1y}$ , and  $\sigma_n$  ( $n = 1, 2, \dots, 6$ ) ligand orbitals is also demonstrated.



of their  $\sigma$  and  $\pi$  orbitals in octahedral and tetrahedral complexes. The  $z$  axes of the ligand coordinates are directed toward the central atom (for simplicity of overlap integral calculations), while the other axes are arbitrary. The  $\sigma$  orbitals have axial symmetry with respect to the ligand  $z$  axis, while the  $\pi$  orbitals lie in the plane that is perpendicular to this axis, and they are oriented along the local  $x$  or  $y$  axes. The ligand orbitals are also labeled according to their ligand number. For instance,  $\pi_{2x}$  means the  $\pi$  orbital of the second ligand oriented along the  $x$  axis of the local coordinate system.

As shown in Section 3.4, the symmetry of the system determines directly the classification of the MOs on the IrReps of the corresponding point group. For example, for an octahedral complex with six identical ligands that has  $O_h$  symmetry, the following MO types are possible (the degeneracy is indicated in parentheses):  $A_{1g}(1)$ ,  $A_{1u}(1)$ ,  $A_{2g}(1)$ ,  $A_{2u}(1)$ ,  $E_g(2)$ ,  $E_u(2)$ ,  $T_{1g}(3)$ ,  $T_{1u}(3)$ ,  $T_{2g}(3)$ , and  $T_{2u}(3)$  (see Tables 3.1 and A1.11). These symmetries restrict significantly the number of independent functions that describe the term under consideration (or the MO); it should be equal to the degeneracy (with the number in parentheses), and these functions should transform into each other under the symmetry transformations of the  $O_h$  group (Section 3.4).

Denote the wavefunction of the MO of corresponding symmetry of a transition metal coordination system by

$$\varphi(\mathbf{r}) = a\psi_0(\mathbf{r}) + b\Phi(\mathbf{r}) \quad (5.9)$$

where  $\psi_0$  is the atomic orbital of the CA or a linear combination of such orbitals [if there are two or several central atoms, the form (5.9) and the consequent results including Table 5.1, discussed below, should be modified], and  $\Phi$  is a molecular orbital—a linear combination of the ligand atomic functions  $\psi_i$  [cf. (5.1)]:

$$\Phi = c_1\psi_1 + c_2\psi_2 + \cdots + c_n\psi_n \quad (5.10)$$

and the LCAO coefficients  $a$ ,  $b$ ,  $c_1$ ,  $\dots$ ,  $c_n$  should be determined by calculations (from the condition of minimum energy and normalization).

Since the MO (5.9) must belong to one of the IrReps of the symmetry group of the system, both  $\psi_0$  and  $\Phi$  should belong to the same representation (or to the same line of the representation if it is degenerate), they must have the same symmetry properties. Such symmetrized linear combinations of atomic orbitals that transform after a given type of symmetry (IrRep) of the symmetry group of this system are called *group-symmetric orbitals*, or simply *group orbitals*, or else *symmetrized (symmetry-adapted) orbitals*. The possible group orbitals of the system are thus determined by its symmetry group (Appendix 1).

Note that, despite having quite understandable physical sense, MOs are not directly observable quantities. According to quantum mechanics, physical observables are determined by matrix elements of corresponding operators calculated with the *total* wavefunction  $\psi(\mathbf{r}_1, \mathbf{r}_2, \dots, \mathbf{r}_n)$  constructed by one-electron MOs  $\varphi(\mathbf{r})$  in the form of a determinant [Eq. (5.45)] or a combination of determinants. Charge distribution is given by  $|\psi(\mathbf{r}_1, \mathbf{r}_2, \dots, \mathbf{r}_n)|^2$  (see below).

### Symmetrized Orbitals

To determine the coefficients  $c_i$  in Eq. (5.10) that satisfy the necessary symmetry conditions for the wavefunction, one has to perform some relatively simple transformations described in Section 3.5. Using the method shown there, all the symmetrized MOs can be easily determined (Examples 3.3 and 3.4). The results for  $\sigma$ - and  $\pi$ -type symmetrized MOs of some important cases of octahedral ( $O_h$  symmetry), tetrahedral ( $T_d$ ), and bipyramidal-tetragonal ( $D_{4h}$ ) systems are given in Tables 5.1–5.3. Table 5.3 also contains the MO functions for square-planar complexes, for which one should put  $\sigma_1 = \sigma_4 = \pi_1 = \pi_4 = 0$  in the expressions of the functions for the bipyramidal system.

In all cases in Tables 5.1–5.3 it is assumed that the CA participates in the MO formation by its  $s$ ,  $p$ ,  $d$ , and  $f$  atomic orbitals, while the ligands participate by one  $\sigma$  (simple or hybridized) and two  $\pi$  orbitals each. It is seen that, for instance, in an octahedral system the  $s$  orbital of the central atom takes part in the MO  $A_{1g}$  type only, while the two  $e_g$  type orbitals,  $d_{z^2}$  and  $d_{x^2-y^2}$ , form a

**TABLE 5.1. Atomic Functions of the Central Atom  $\psi_0$  and Symmetrized Ligand  $\sigma$  and  $\pi$  Orbitals,  $\Phi_\sigma$  and  $\Phi_\pi$ , for Different Types of Symmetry of the  $O_h$  Group for Octahedral Complexes**

Type of Symmetry	$\psi_0$	$\Phi_\sigma$	$\Phi_\pi$
$A_{1g}$	$s$	$(1/\sqrt{6})(\sigma_1 + \sigma_2 + \sigma_3 + \sigma_4 + \sigma_5 + \sigma_6)$	—
$A_{2u}$	$f_{xyz}$	—	—
$T_{1u}$	$p_x, f_x$	$(1/\sqrt{2})(\sigma_2 - \sigma_5)$	$\frac{1}{2}(\pi_{1x} - \pi_{4y} - \pi_{3x} + \pi_{6y})$
	$p_y, f_y$	$(1/\sqrt{2})(\sigma_3 - \sigma_6)$	$\frac{1}{2}(\pi_{1y} - \pi_{4x} - \pi_{2y} + \pi_{5x})$
	$p_z, f_z$	$(1/\sqrt{2})(\sigma_1 - \sigma_4)$	$\frac{1}{2}(\pi_{2x} - \pi_{5y} + \pi_{3y} - \pi_{6x})$
$E_g$	$d_{x^2-y^2}$	$\frac{1}{2}(\sigma_2 + \sigma_5 - \sigma_3 - \sigma_6)$	—
	$d_{z^2}$	$(1/\sqrt{12})(2\sigma_1 + 2\sigma_4 - \sigma_2 - \sigma_5 - \sigma_3 - \sigma_6)$	—
$T_{2g}$	$d_{xy}$	—	$\frac{1}{2}(\pi_{2y} + \pi_{5x} + \pi_{3x} + \pi_{6y})$
	$d_{xz}$	—	$\frac{1}{2}(\pi_{1x} + \pi_{4y} + \pi_{2x} + \pi_{5y})$
	$d_{yz}$	—	$\frac{1}{2}(\pi_{1y} + \pi_{4x} + \pi_{3y} + \pi_{6x})$
$T_{1g}$	—	—	$\frac{1}{2}(\pi_{1y} + \pi_{4x} - \pi_{3y} - \pi_{6x})$
	—	—	$\frac{1}{2}(\pi_{2x} + \pi_{5y} - \pi_{1x} - \pi_{4y})$
	—	—	$\frac{1}{2}(\pi_{3x} + \pi_{6y} - \pi_{2y} - \pi_{5x})$
$T_{2u}$	$f_{x(y^2-z^2)}$	—	$\frac{1}{2}(\pi_{1x} - \pi_{4y} + \pi_{3x} - \pi_{6y})$
	$f_{y(z^2-x^2)}$	—	$\frac{1}{2}(\pi_{2y} - \pi_{5x} + \pi_{1y} - \pi_{4x})$
	$f_{z(x^2-y^2)}$	—	$\frac{1}{2}(\pi_{2x} - \pi_{5y} - \pi_{3y} + \pi_{6x})$

**TABLE 5.2. Atomic Functions of the Central Atom  $\psi_0$  and the Symmetrized Ligand  $\sigma$  and  $\pi$  Orbitals,  $\Phi_\sigma$  and  $\Phi_\pi$ , for Different Types of Symmetry of the  $T_d$  Group for Tetrahedral Complexes**

Type of Symmetry	$\psi_0$	$\Phi_\sigma$	$\Phi_\pi$
$A_1$	$s$	$\frac{1}{2}(\sigma_1 + \sigma_2 + \sigma_3 + \sigma_4)$	—
$A_2$	$f_{xyz}$	—	—
$T_2$	$p_x; d_{yz}; f_x$	$\frac{1}{2}(\sigma_1 - \sigma_2 + \sigma_3 - \sigma_4)$	$\frac{1}{4}(\pi_{4x} + \pi_{2x} - \pi_{1x} - \pi_{3x}) + (\sqrt{3}/4)(\pi_{4y} + \pi_{2y} - \pi_{1y} - \pi_{3y})$
	$p_y; d_{xz}; f_y$	$\frac{1}{2}(\sigma_1 + \sigma_2 + \sigma_3 - \sigma_4)$	$\frac{1}{2}(\pi_{1x} + \pi_{2x} - \pi_{3x} - \pi_{4x})$
	$p_z; p_{xy}; f_z$	$\frac{1}{2}(\sigma_1 - \sigma_2 - \sigma_3 - \sigma_4)$	$\frac{1}{4}(\pi_{3x} + \pi_{2x} - \pi_{1x} - \pi_{4x}) + (\sqrt{3}/4)(\pi_{4y} + \pi_{1y} - \pi_{2y} - \pi_{3y})$
$E$	$d_{x^2-y^2}$	—	$\frac{1}{4}(\pi_{1x} + \pi_{2x} + \pi_{3x} + \pi_{4x}) + (\sqrt{3}/4)(\pi_{1y} + \pi_{2y} + \pi_{3y} + \pi_{4y})$
	$d_{z^2}$	—	$\frac{1}{4}(\pi_{1x} + \pi_{2x} + \pi_{3x} + \pi_{4x}) - (\sqrt{3}/4)(\pi_{1y} + \pi_{2y} + \pi_{3y} + \pi_{4y})$
$T_1$	$f_{x(y^2-z^2)}$	—	$\frac{1}{4}(\pi_{2y} + \pi_{4y} - \pi_{3y} - \pi_{1y}) + (\sqrt{3}/4)(\pi_{1x} + \pi_{3x-2x} - \pi_{4x})$
	$f_{y(z^2-x^2)}$	—	$\frac{1}{2}(\pi_{1y} + \pi_{2y} - \pi_{3y} - \pi_{4y})$
	$f_{z(x^2-y^2)}$	—	$\frac{1}{4}(\pi_{2y} + \pi_{3y} - \pi_{1y} - \pi_{4y}) + (\sqrt{3}/4)(\pi_{2x} + \pi_{3x} - \pi_{1x} - \pi_{4x})$

twofold-degenerate  $\sigma$  MO of the type  $E_g$ , whereas three  $t_{2g}$ -type orbitals,  $d_{xy}$ ,  $d_{xz}$ , and  $d_{yz}$ , form only  $\pi$  MOs of  $T_{2g}$  type. On the contrary, in the tetrahedral system the  $E$  orbitals  $d_{z^2}$  and  $d_{x^2-y^2}$  form only  $\pi$  MOs, while the  $T_2$  orbitals can, in principle, participate in both  $\sigma$ - and  $\pi$ -type MO's. This is an example of the fact mentioned earlier (in Section 2.1) that the separation into  $\sigma$  and  $\pi$  MO's may be conventional for coordination compounds; the same atomic orbitals of the CA participate in the formation of MOs with both  $\sigma$  orbitals of (some) ligands and  $\pi$  orbitals of other ligands. Tables 5.1–5.3 also show other cases of “ $\sigma + \pi$ ” orbitals (the  $T_{1u}$  orbital in the  $O_h$  group,  $A_{2u}$ - and  $E_u$ -type orbitals in  $D_{4h}$  systems, etc.). Examples of such systems are discussed in Section 6.3.

Note also that some symmetry-adapted combinations of ligand atomic orbitals do not have corresponding parts on the CA (e.g.,  $T_{1g}$  states for  $O_h$  systems, as well as  $T_{2u}$  states for  $O_h$  and  $T_1$  for  $T_d$  systems in the absence of active  $f$

**TABLE 5.3. Atomic Functions of the Central atom and the Symmetrized Ligand  $\sigma$  and  $\pi$  Orbitals,  $\Phi_\sigma$  and  $\Phi_\pi$ , for Different Types of Symmetry of the  $D_{4h}$  Group for a Tetragonally Distorted Octahedron<sup>a</sup>**

Type of Symmetry	$\psi_0$	$\Phi_\sigma$	$\Phi_\pi$
$A_{1g}$	$s; d_{z^2}$	$(1/\sqrt{2})(\sigma_1 + \sigma_4);$ $\frac{1}{2}(\sigma_2 + \sigma_5 + \sigma_3 + \sigma_6)$	—
$B_{1g}$	$d_{x^2-y^2}$	$\frac{1}{2}(\sigma_2 + \sigma_5 - \sigma_3 - \sigma_6)$	—
$A_{2u}$	$p_z$	$(1/\sqrt{2})(\sigma_1 - \sigma_4)$	$\frac{1}{2}(\pi_{2x} - \pi_{5y} - \pi_{3y} - \pi_{5x})$
$E_u$	$p_x$	$(1/\sqrt{2})(\sigma_2 - \sigma_5)$	$(1/\sqrt{2})(\pi_{1x} - \pi_{4y})$
			$(1/\sqrt{2})(\pi_{3x} - \pi_{6y})$
	$p_y$	$(1/\sqrt{2})(\sigma_3 - \sigma_6)$	$(1/\sqrt{2})(\pi_{1y} - \pi_{4x})$ $(1/\sqrt{2})(\pi_{2x} - \pi_{5y})$
$B_{2g}$	$d_{xy}$	—	$\frac{1}{2}(\pi_{2y} + \pi_{5x} + \pi_{3x} + \pi_{6y})$
$E_g$	$d_{xz}$	—	$(1/\sqrt{2})(\pi_{1x} + \pi_{4y})$
			$(1/\sqrt{2})(\pi_{2x} + \pi_{5y})$
	$d_{yz}$	—	$(1/\sqrt{2})(\pi_{1x} + \pi_{4x})$ $(1/\sqrt{2})(\pi_{3y} + \pi_{6x})$

<sup>a</sup>For a square-planar  $D_{4h}$  system put  $\sigma_1 = \sigma_4 = \pi_{1x} = \pi_{1y} = \pi_{4x} = \pi_{4y} = 0$ .

states), and hence these states remain nonbonding. The same is true for the  $A_{2u}$  state in  $O_h$  systems when the central atom has active  $f$ -electron orbitals: the latter also remain nonbonding. Tables 5.1–5.3 contain all the possible group-symmetric combinations  $\Phi$  of 6  $\sigma$  and 12  $\pi$  ligand atomic orbitals of octahedral systems, and 4  $\sigma$  and 8  $\pi$  orbitals of the ligands of tetrahedral systems. The mutual overlap of the ligand AOs is ignored in the normalization coefficients of the ligand-symmetrized orbitals; they are included in the variational constants  $a$  and  $b$  in Eq. (5.9).

In Table 5.4 the *group overlap integrals*  $G_{0i}$  are also given:

$$G_{0i} = \int \psi_0^* \Phi_i d\tau = \sum_j c_{ij} \int \psi_0^* \psi_j d\tau = \sum_j c_{ij} S_{0j} \quad (5.11)$$

where  $S_{0j}$  are usual diatomic overlap integrals that can be easily expressed by the standard tabulated values of the type  $S(s, \sigma)$ ,  $S(p, \sigma)$ ,  $S(p, \pi)$ , ... (given as a function of interatomic distances), and the coefficients  $c_{ij}$  are those given in Tables 5.1–5.3 for symmetry-adapted combinations of the ligand functions. The group resonance integrals are defined quite similarly:

$$H_{0i}^G = \int \psi_0^* H \Phi_i = \sum_j c_{ij} \int \psi_0^* H \psi_j = \sum_j c_{ij} H_{0j} \quad (5.11')$$

**TABLE 5.4. Group Overlap Integrals  $G_{0\sigma}$  and  $G_{0\pi}$  for Different Types of Symmetry of Groups  $O_h$ ,  $T_d$ , and  $D_{4h}$  for Octahedral, Tetrahedral, and Tetragonally Distorted Octahedral Complexes, Respectively, Considered in Tables 5.1–5.3<sup>a</sup>**

Symmetry Group	Symmetry Type	$\psi_0$	$G_{0\sigma}$	$G_{0\pi}$
$O_h$	$A_{1g}$	$s$	$\sqrt{6S(s, \sigma)}$	—
	$T_{1u}$	$p_x$	$\sqrt{2S(p, \sigma)}$	$2S(p, \pi)$
		$f_x$	$\sqrt{2S(f, \sigma)}$	$2S(f, \pi)$
	$E_g$	$d_{x^2-y^2}$	$\sqrt{3S(d, \sigma)}$	—
	$T_{2g}$	$d_{xy}$	—	$2S(d, \pi)$
$T_{2u}$	$f_{x(y^2-z^2)}$	—	$2S(f, \pi)$	
$T_d$	$A_1$	$s$	$2S(s, \sigma)$	—
	$T_2$	$p_x$	$(2/\sqrt{3})S(p, \sigma)$	$-(\frac{8}{3})^{1/2} S(p, \pi)$
		$d_{xy}$	$(2/\sqrt{3})S(d, \sigma)$	$(\frac{8}{3})^{1/2} S(d, \pi)$
	$E$	$d_{x^2-y^2}$	—	$(\frac{8}{3})^{1/2} S(d, \pi)$
	$T_1$	$f_{x(y^2-z^2)}$	—	$(2/\sqrt{3})S(f, \pi)$
$D_{4h}$	$A'_{1g}$	$s$	$\sqrt{2S(s, \sigma_1)}$	—
		$d_{z^2}$	$\sqrt{2S(d, \sigma_1)}$	—
	$A''_{1g}$	$s$	$2S(d, \sigma_2)$	—
		$d_{z^2}$	$-S(d, \sigma_2)$	—
	$B_{1g}$	$d_{x^2-y^2}$	$\sqrt{3S(d, \sigma)}$	—
	$A_{2u}$	$p_z$	$\sqrt{2S(p, \sigma_1)}$	$2S(p, \pi_2)$
	$E_u$	$p_x$	$\sqrt{2S(p, \sigma_2)}$	$2S(p, \pi_1); \sqrt{2S(p, \pi_2)}$
	$B_{2g}$	$d_{xy}$	—	$2S(d, \pi)$
	$E_g$	$d_{xz}$	—	$\sqrt{2S(d, \pi_1)}; \sqrt{2S(d, \pi_2)}$

<sup>a</sup> $S(s, \sigma)$ ,  $S(p, \sigma)$ ,  $S(p, \pi)$ ,  $\dots$ , are the usual overlap integrals between the corresponding orbitals of two atoms.

### Simplification of the Secular Equation

With the symmetrized functions  $\psi_0$  and  $\Phi$  taken as a basis of the MO LCAO method, the secular equation (5.8) can be significantly simplified without reduction of accuracy. Indeed, as shown in Section 3.4, the integrals  $S_{ik}$  and  $H_{ik}$  after (5.3) and (5.4) are nonzero if and only if the two functions  $\psi_i$  and  $\psi_k$  have the same symmetry properties (i.e., belong to the same symmetry type). This means that in Eq. (5.8) all the off-diagonal elements for any  $\psi_i$  and  $\psi_k$  that belong to different IrReps are zero. After a corresponding grouping of the basic wavefunctions on their symmetries, Eq. (5.8) transforms to the following:

$$\begin{vmatrix}
 H_{ij} - ES_{ij} & & & 0 \\
 & H_{kl} - ES_{kl} & & \\
 & & \dots & \\
 0 & & & H_{md} - ES_{md}
 \end{vmatrix} = 0 \quad (5.12)$$

In this equation it is implied that the first, say,  $n_1$  functions labeled  $i$  and  $j$  belong to one and the same IrRep of the symmetry group, the next  $n_2$  functions labeled  $k$  and  $l$  belong to another IrRep, and so on, and that the last group of  $n_r$  functions belong to the  $r$ th representation. Hence the  $r$  quadratic matrices that occupy the diagonal positions in (5.12) belong to  $r$  IrReps of the symmetry point group of the systems, while the off-diagonal matrix elements between them are zero by symmetry.

As is well known, the determinant (5.12) equals the product of all the smaller determinants on the diagonal positions. This means that equation (5.12) of power  $n$  with respect to the MO energy  $E$  decomposes into  $r$  equations of much lower powers  $n_1, n_2, \dots, n_r$  ( $n_1 + n_2 + \dots + n_r = n$ ) that are much easier to solve, thus simplifying significantly the solution of the MO LCAO problem. Hence, when using symmetrized functions, the order of the equation that should be solved is reduced from the whole number of functions in the basis set  $n$  to the number of these functions in the partial groups belonging to the same IrRep.

For example, for an octahedral complex of  $O_h$  symmetry (without  $f$  electrons), in accordance with Table 5.1, the secular equation of the MO LCAO method, by using symmetrized functions, decomposes into one second-order equation for the  $A_{1g}$  representation [only two functions belong to  $A_{1g}$ :  $ns$  of the CA and  $\Phi_\sigma = (\frac{1}{6})^{1/2}(\sigma_1 + \sigma_2 + \dots + \sigma_6)$  of the ligands], three identical third-order equations for  $T_{1u}$ , two identical second-order equations for  $E_g$ , and three second-order equations for  $T_{2g}$ . One can see that for high-symmetry systems the order of the secular equation in the MO LCAO method is not very high. However, the problem as a whole with many valence electrons is still very complicated because of the interaction between the electrons, due to which, even in the one-electron HF approximation, the different square blocks in (5.12) are coupled via the integrals  $H_{ik}$  of the effective Hamiltonian (2.55), which contain LCAO coefficients of the MOs from all the other blocks. This problem is discussed in more detail in Section 5.3.

## 5.2. CHARGE DISTRIBUTION AND BONDING IN THE MO LCAO METHOD AND THE CASE OF WEAK COVALENCY

### Atomic Charges and Bond Orders

With the MO energies  $E_i$  and LCAO coefficients  $c_{ij}$  known, one can visualize the electronic structure. In particular, for the charge distribution the so-called Mulliken electron population analysis [5.7] is widely used. This analysis is based on the definition of electronic density. From the quantum-mechanical definition and statistical interpretation of the wavefunction in the coordinate representation,  $|\varphi(\mathbf{r})|^2 dv$  means the probability of finding the electron [that occupies the MO  $\varphi(\mathbf{r})$ ] within the volume  $dv$  near point  $\mathbf{r}$  (regardless of its spin value). Therefore the function  $\rho(\mathbf{r})$

$$\rho(\mathbf{r}) = |\varphi(\mathbf{r})|^2 \quad (5.13)$$

represents the probability density (or simply density) of electronic distribution along the MO  $\varphi(\mathbf{r})$ .

In a system with  $n$  electrons and wavefunction  $\Psi(\mathbf{r}_1, \mathbf{r}_2, \dots, \mathbf{r}_n)$ , the probability of finding an electron near  $\mathbf{r}_1$  is

$$\rho(\mathbf{r}_1) = n \int |\Psi(\mathbf{r}_1, \mathbf{r}_2, \dots, \mathbf{r}_n)|^2 dv_2 \cdots dv_n \quad (5.14)$$

The coefficient  $n$  is introduced because any of the  $n$  electrons can be at point  $\mathbf{r}_1$  and the density should be normalized:  $\int \rho(r_1) dv_1 = n$ . Thus the electronic density and hence the parameters of electronic distribution in the system are completely determined by its wavefunction.

The redistribution of the charge density by formation of molecules (chemical bonding) is determined by the function  $\Delta\rho$ :

$$\Delta\rho = \rho(\mathbf{r}) - \sum_{\mu} \rho_{\mu}(\mathbf{r}) \quad (5.15)$$

where  $\rho_{\mu}(\mathbf{r})$  means the electronic density function of the free atom in the position that it occupies in the molecule. By definition,  $\Delta\rho$  means the difference between the electronic density of the molecule and the free atoms, the *deformation density*, which indicates the changes in charge distribution that take place by the binding. The function  $\Delta\rho$  is usually presented by equal density curves which are more informative than the electron density diagrams (Section 8.6).

In the MO LCAO approximation where the MO wavefunction is presented by the LCAO (5.1), the electronic density  $\rho(\mathbf{r})$  can be expressed by the LCAO coefficients. Indeed, assume that the  $i$ th MO under consideration contains only two basis functions—AOs of two atoms  $A$  and  $B$ — $\psi_A$  and  $\psi_B$  [e.g., the atomic functions of the central atom and the ligand denoted in (5.9) as  $\psi_0$  and  $\Phi$ , respectively]:

$$\varphi_i(\mathbf{r}) = c_{iA}\psi_A + c_{iB}\psi_B \quad (5.16)$$

Then (we assume that the AOs and the LCAO coefficients are real)

$$|\varphi_i(\mathbf{r})|^2 = |c_{iA}|^2|\psi_A(\mathbf{r})|^2 + |c_{iB}|^2|\psi_B(\mathbf{r})|^2 + 2c_{iA}c_{iB}\psi_A\psi_B \quad (5.17)$$

In a more general case with  $\varphi_i(\mathbf{r})$  in (5.1)

$$|\varphi_i(\mathbf{r})|^2 = \sum_{\mu, \nu} c_{i\mu}c_{i\nu}\psi_{\mu}\psi_{\nu} \quad (5.17')$$

The first and second terms of expression (5.17) can be interpreted as the probabilities of finding the MO electron at the central atom and ligands, respectively, determined by the module square values of the corresponding LCAO coefficients. The last term has a more complicated nature. Denote the MO occupancy

by  $q_i$  and define it as the total charge on the MO:  $q_i = \int \rho_i(\mathbf{r})dv$ . Substituting  $\rho_i(\mathbf{r}) = q_i|\varphi_i(\mathbf{r})|^2$  and assuming that the AO functions are normalized, we have  $\left(\sum_{\mu,\nu} c_{i\mu}c_{i\nu}S_{\mu\nu} = 1\right)$

$$q_i = q_i \sum_{\mu,\nu} c_{i\mu}c_{i\nu}S_{\mu\nu} \quad (5.18)$$

in the two-center case under consideration

$$q_i = q_i|c_{iA}|^2 + q_i|c_{iB}|^2 + 2q_i c_{iA}c_{iB}S_{AB} \quad (5.18')$$

where  $S_{AB}$  is the overlap integral (or group overlap integral). It is seen from this expression that the whole charge  $q_i$  on the MO is divided into three parts: the part  $q_i|c_{iA}|^2$  originating from atom  $A$ , the  $q_i|c_{iB}|^2$  term contributed by atom  $B$ , and the third part  $p_i = q_i \cdot 2c_{iA}c_{iB}S_{AB}$ , called *overlap population* describing the contribution of the overlap area to the charge distribution.

Mulliken suggested [5.7] defining the electronic charge on the atom by including half of the overlap population into each of the two atomic charges:

$$\begin{aligned} q_{iA} &= q_i(|c_{iA}|^2 + c_{iA}c_{iB}S_{AB}) \\ q_{iB} &= q_i(|c_{iB}|^2 + c_{iA}c_{iB}S_{AB}) \end{aligned} \quad (5.19)$$

If atom  $A$  participates with its AOs in many MOs of the system, the *effective electronic charge* on the atom after Mulliken is

$$q_A = \sum_i q_{iA}$$

or in general

$$q_\mu = \sum_{i,\nu} q_i c_{i\mu} c_{i\nu} S_{\mu\nu} \quad (5.20)$$

The effective positive charge on the atom equals  $Z_A - q_A$ , where  $Z_A$  is the nuclear charge.

With the charges (5.20), *charge transfers*  $\Delta q$  can also be defined. Denoting the electronic charge on the free atom or group of atoms by  $q_\mu^0$ , we have

$$\Delta q_\mu = q_\mu - q_\mu^0 \quad (5.20')$$

Similarly, for *orbital charge transfer*  $\Delta q_i$  we get

$$\Delta q_i^A = q_{iA} - q_{iA}^0 \quad (5.20'')$$

where  $q_{iA}^0$  denotes the electronic charge on the  $i$ th orbital in the free atom or atomic group  $A$ .



Besides the atomic charges, the *bond orders*, or *density matrix*  $P_{\mu\nu}$

$$P_{\mu\nu} = \sum_i q_i c_{i\mu} c_{i\nu} \quad (5.21)$$

are used in characterization of the electronic charge distribution and binding.

The Mulliken definition of atomic charges is far from perfect: (1) the overlap population is equally divided into two parts for two interacting atoms  $A$  and  $B$ , which are, in general, different; and (2) the overlap population can be negative, resulting, if sufficiently large, in negative charge densities, or in orbital charges larger than 2. But the most significant fault of the Mulliken atomic charges is that they depend strongly on the basis set of LCAO calculations. It is obvious that the values  $c_{iA}^2$  characterize not so much the probability of location of the electron at atom  $A$  as the probability of its being *in the area where  $\psi_A$  has its maximum*. Depending on the nature of  $\psi_A$ , its maximum can be far outside atom  $A$ . This argument is especially important for transition metal compounds because their atomic functions are rather diffuse. Example 5.1 illustrates the inadequacy of Mulliken's definition of atomic charges in application to transition metal systems.

### EXAMPLE 5.1

#### Shortcomings of Mulliken's Definition of Atomic Charges in Molecules

Mulliken's definition of atomic charges in molecules may have some merit in application to organic and main-group compounds, but it fails for transition metal compounds because of the  $d$ -electron heterogeneity in the sense that usually the ligands have only  $sp$  electron configurations. Indeed, consider the radial distribution in the  $3d$  and  $4s$  Slater-type AOs (Section 2.1) shown in Fig. 5.2 for a typical transition metal system with respect to the positions of the central atom  $M$  and the ligand  $L$ . As one can see, while the  $3d$  distribution characterizes approximately the electron positions mainly on the CA, the  $4s$  AO is far beyond the atomic area, its maximum falling in the region of the ligand.

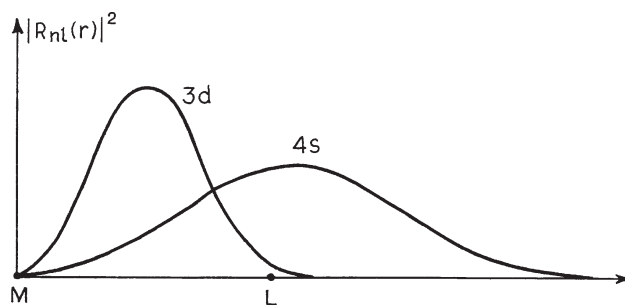


**FIGURE 5.2.** Typical radial distribution of atomic  $3d$  and  $4s$  electron densities of a transition metal  $M$  with respect to the position of the ligand  $L$ .

This means that in the atomic charge  $q_M$  calculated after (5.20), the contribution  $c_{4s}^2$  in fact characterizes not the charge on the central atom but that on the ligand L, thus revealing an incorrect notion about the real charge on M.

Nevertheless, the Mulliken analysis proved to be useful in many cases, especially when not absolute but relative values of charge distributions and their changes along a series of related compounds are considered.

Several other suggestions for more adequate calculations of atomic charges in molecules were made, and among them we note the one due to Politzer [5.8], in which the atomic charge is determined by direct integration of the electronic density function  $\rho(\mathbf{r})$  over the volume of the atom. Again, there is some uncertainty in the choice of borders of the atom in the molecule. In Section 8.6 we briefly discuss this problem in relation to the idea of Bader [8.107] to define the borders of the atom in the molecule as the surface  $S$ , where the gradient of the charge density is zero,  $\nabla\rho(\mathbf{r}_0) \cdot \mathbf{n}(\mathbf{r}_0) = 0$ ,  $\mathbf{r}_0 \in S$ , and  $\mathbf{n}$  is a unit vector normal to the surface  $S$ .

Another rule of calculation of atomic charges was suggested for coordination compounds by Noell [5.9] who proposed to use for the atomic charge on the atom  $\mu$  the following formula instead of (5.20):

$$q_\mu = \sum_{i,v} (F_\mu F_v)^{1/2} c_{i\mu} c_{iv} S_{\mu v} \quad (5.22)$$

where for the ligands  $F_\mu = F_v = 1$ , while for the CA  $F_\mu$  is defined by the following procedure. For the central AO

$$\int |\psi_\mu|^2 d\tau = 1 = I_\mu + L_\mu + R_\mu \quad (5.23)$$

where  $I_\mu$  is the portion within the covalent sphere of the metal with radius  $R_c$  ( $0 < r < R_c$ ),  $L_\mu$  is the ligand portion lying within the ligand cone [the volume with the radius vector  $r$  ( $R_c < r < \infty$ ) and angles  $\theta$  and  $\phi$  inside the cone of revolution with the apex at the metal and the base determined by the ligand dimensions], and  $R_\mu$  is the remaining part that enters neither the  $R_c$  sphere nor the ligand cone. Then  $F_\mu$  is defined as follows:

$$F_\mu = I_\mu + R_\mu \quad (5.24)$$

In other words, by introducing the  $F_\mu$  factor in the definition of the atomic charge of the central atom, one excludes the electronic cloud in the ligand region created by the central atom AO. For instance, for square-planar complexes of Pt and Pd the cones of revolution embracing the four ligands are taken as four  $90^\circ$  cones, while the covalent radius is chosen as  $R_c = 1.30 \text{ \AA}$  for both Pt and Pd [5.10]. For examples of calculations, see Sections 6.3, 6.4, and 11.3.

### Bonding, Nonbonding, and Antibonding Orbitals

To reveal the mechanism of chemical bonding in the MO LCAO scheme, consider first a simple example. Assume that for a given symmetry representation of the system there are only two basis functions that belong to this representation; one of them ( $\psi_0$ ) is an AO of the CA, while the other one ( $\Phi_1$ ) forms an appropriate linear combination of the ligand functions, as in (5.9). Such a case is realized, for instance, for the  $A_{1g}$  representation of an octahedral complex (Table 5.1). The secular equation for the two MOs,  $\Psi_1 = c'_0\psi_0 + c'_1\Phi_1$  and  $\Psi_2 = c''_0\psi_0 + c''_1\Phi_1$ , corresponding to this type of symmetry is

$$\begin{bmatrix} H_{00} - E & H_{01} - EG_{01} \\ H_{10} - EG_{10} & H_{11} - E \end{bmatrix} = 0 \quad (5.25)$$

where  $G_{01} = G_{10}$  is the group overlap integral given by Eq. (5.11) and in Table 5.4. This quadratic equation with respect to  $E$  can be solved directly. It yields two roots,  $E_1$  and  $E_2$ ,

$$E_{1,2} = [2(1 - G_{01}^2)]^{-1} \{H_{00} + H_{11} - 2H_{01}G_{01} \mp [(H_{00} - H_{11})^2 + 4[H_{01}^2 + H_{00}H_{11}G_{01}^2 - H_{01}G_{01}(H_{00} + H_{11})]^{1/2}]\} \quad (5.26)$$

From this expression it is seen, first, that in the absence of overlap between  $\psi_0$  and  $\Phi_1$ , that is, when  $G_{01} = H_{01} = 0$ , we have  $E_1 = H_{00}$ ,  $E_2 = H_{11}$ . This means that the two energy levels remain the same as in the atomic states  $\psi_0$  and  $\Phi_1$ . Substituting these energy values into Eq. (5.7), we obtain the  $c_i$  coefficients, which will enable us to easily find from Eqs. (5.1) and (5.9) that, indeed,  $\Psi_1 = \psi_0$  and  $\Psi_2 = \Phi_1$ ; that is, they remain purely atomic. The MOs corresponding to these states are called *nonbonding*. Such MOs, as mentioned above, are realized either when some atomic orbitals (or their linear combinations) have no counterparts of the same symmetry on other atoms (as, e.g., in the case of the  $T_1$  combination of ligand orbitals in a tetrahedral system of  $T_d$  symmetry in absence of  $f$  electrons; Table 5.2), or when the corresponding group overlap integrals  $G_{ij}$  and resonance integral  $H_{ij}$  are negligible.

In all other cases the values of the two roots (5.26) of Eq. (5.25) are beyond the area between  $H_{00}$  and  $H_{11}$ :  $E_1$  is smaller than the smallest value of  $H_{00}$  and  $H_{11}$ , while  $E_2$  is larger than the largest one (Fig. 5.3). It follows that one MO has the energy  $E_1$ , which is lower than the atomic energies of the free atoms, and hence this MO is *bonding*. On the contrary, the MO corresponding to the energy  $E_2$  increases the energy as compared with the free atoms; this MO is called *antibonding*. Since both  $G_{ij}$  and  $H_{ij}$  depend on the integral overlap between the  $\psi_0$  and  $\Phi_1$  functions, the bonding and antibonding magnitudes of the abovementioned MOs are also dependent on this overlap.

The wavefunctions of these two MOs, their LCAO coefficients  $c_0$  and  $c_1$  at  $\psi_0$  and  $\Phi_1$ , can be easily evaluated by substituting consecutively the values  $E_1$  and

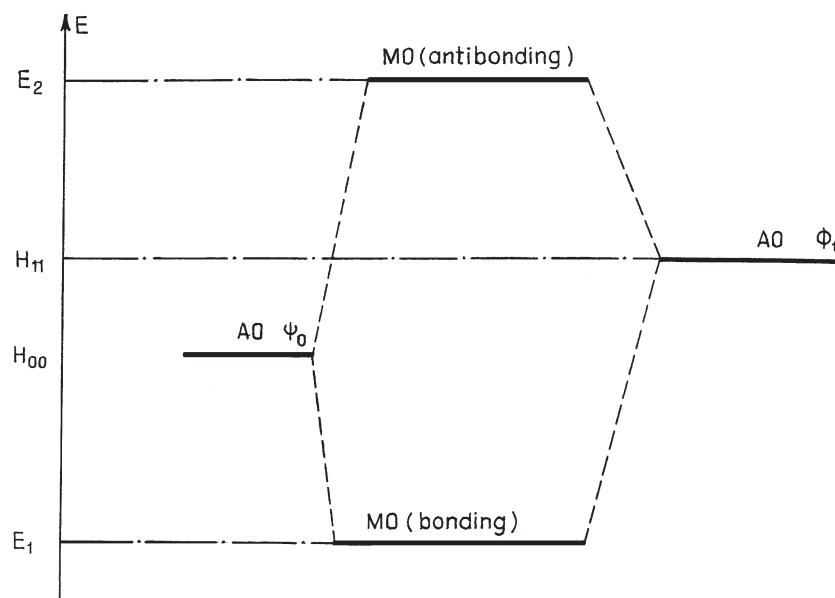


**FIGURE 5.3.** MO energy level scheme for two atomic states from two centers with AOs  $\psi_0$  and  $\Phi_1$  that produce bonding and antibonding MOs.

$E_2$  after (5.26) into Eq. (5.7) and calculating the corresponding coefficients  $c'_0, c'_1$  and  $c''_0, c''_1$  (also factoring in the normalization condition  $c_0^2 + c_1^2 + 2c_0c_1G_{01} = 1$  for each pair of  $c'_0, c'_1$  and  $c''_0, c''_1$  coefficients, respectively).

The bonding energy obviously depends on the number of electrons that occupy bonding (antibonding) MOs. Consider the case when each of the bonding parts, the central atom in the state  $\psi$  and the ligands in the state  $\Phi_1$ , are occupied by one electron. Then, after formation of the MOs that mix (collectivize) these states, the new two states, two MOs, should be populated by the same two electrons. Following the Pauli principle, in the ground state with the lowest energy the two electrons occupy the lowest MO with opposite spins. Neglecting the interelectron interaction, the bonding energy  $\Delta E$  is approximately

$$\Delta E = H_{00} + H_{11} - 2E_1 \quad (5.27)$$

where it is taken into account that in the nonbonding state the energies of the two electrons are  $H_{00}$  and  $H_{11}$ , respectively. Substituting  $E_1$  from (5.26), we have

$$\begin{aligned} \Delta E = & (1 - G_{01}^2)\{2H_{01}G_{01} - G_{01}^2(H_{00} + H_{11}) + [(H_{00} - H_{11})^2 \\ & + 4H_{01}^2 + 4H_{00}H_{11}G_{01}^2 - 4H_{01}G_{01}(H_{00} + H_{11})^{1/2}]\} \quad (5.28) \end{aligned}$$

Note that if there are four electrons, with two from each bonding part, they must occupy both the bonding and antibonding MOs in the ground state and

$$\begin{aligned}\Delta E &= 2(H_{00} + H_{11}) - 2(E_1 + E_2) \\ &= (1 - G_{01}^2)^{-1}[4H_{01}G_{01} - 2(H_{00} + H_{11})G_{01}^2] \cong 0\end{aligned}\quad (5.29)$$

Here it is noted that roughly  $H_{01} \cong \frac{1}{2}(H_{00} + H_{11})G_{01}$  (Section 5.5).

Equation (5.29) means that bonding and antibonding MOs approximately compensate each other, so there is almost zero bonding when they are both fully occupied by electrons. The compensation of bonding and antibonding MOs is also confirmed by more rigorous numerical calculations [5.11]. Hence the bonding in the MO scheme occurs only when there is no full compensation of the bonding MOs by the antibonding ones and the bonding is produced only by those electrons that occupy uncompensated bonding orbitals.

If the number of basis functions that transform according to the given symmetry type (and hence the order of the secular equation and the number of MOs) is larger than 2, the possibility of visual interpretation of the origin of the bonding features in the MO LCAO scheme decreases significantly, but the basic ideas of bonding, nonbonding, and antibonding MOs with respect to the corresponding free atomic states remain valid. Section 7.2 presents another criterion of MO bonding properties on the basis of their orbital vibronic constants.

It is clear that the total bonding energy equals the sum of the individual MO contributions (with corresponding corrections on changed interelectron interaction). Noting the almost exact compensation of the bonding MOs with the corresponding antibonding ones, we conclude that *the total bonding energy equals the summary contribution of the uncompensated bonding MOs* (see also Section 6.2). The number of the latter depends on the ordering of the bonding and antibonding MOs and their occupation numbers. *The highest occupied MO is usually abbreviated as HOMO, while the lowest unoccupied MO is LUMO.*

### Case of Weak Covalency

In transition metal coordination bonding (including solid-state lattice formation), the notion of *weak covalence* is very important. In fact this term is applicable to the cases when the bonds between the central atom and ligands are rather ionic and the covalence can be considered as a correction. Starting with ionic parts, let us define the condition of weak covalence by assuming that the magnitudes of the overlap integral  $S$  (or  $G$ ) and  $|H_{01}|/|H_{11} - H_{00}|$  are small as compared with a unity and that their squares can be neglected. This means that  $S \ll 1$  and  $|H_{01}| \ll |H_{11} - H_{00}|$  (we assume that  $|H_{11}| > |H_{00}|$ ). Then one can obtain from Eq. (5.26) the following relations for the energies of the bonding  $E_1$  and

antibonding  $E_2$  MO energies:

$$E_1 \cong H_{11} - \frac{H_{01} - H_{11}G_{01}}{H_{00} - H_{11}} \quad (5.30)$$

$$E_2 \cong H_{00} + \frac{H_{01} - H_{00}G_{01}}{H_{00} - H_{11}} \quad (5.31)$$

For the wavefunctions of these two MOs the following form seems to be convenient:

$$\Psi_1 = N_1(\psi_0 + \gamma\Phi_1) \quad (5.32)$$

$$\Psi_2 = N_2(\lambda\psi_0 - \Phi_1) \quad (5.33)$$

where  $N_1$  and  $N_2$  are the normalization coefficients,

$$N_1 = [1 + \gamma^2 + 2\gamma G_{01}]^{-1/2} \quad (5.34)$$

$$N_2 = [1 + \lambda^2 - 2\lambda G_{01}]^{-1/2}$$

The relation between  $\lambda$  and  $\gamma$  can be obtained from the condition of orthogonality  $\int \Psi_1^* \Psi_2 d\tau = 0$ :

$$\lambda = \frac{\gamma + G_{01}}{1 + \gamma G_{01}} \quad (5.35)$$

Within the approximation of weak covalence at hand, using Eq. (5.7) for the coefficients in Eqs. (5.32) and (5.33) and the energies (5.30) and (5.31), we get

$$\gamma = -\frac{H_{01} - H_{11}G_{01}}{H_{00} - H_{11}} \quad (5.36)$$

$$\lambda = -\frac{H_{01} - H_{00}G_{01}}{H_{00} - H_{11}} = \gamma + G_{01} \quad (5.37)$$

From these formulas it is seen first of all that the values  $\gamma$  and  $\lambda$  are also small because both  $G_{01}$  and  $H_{01}$  are small. Hence the bonding MO in Eq. (5.32) is mostly  $\Phi_1$ , mainly a ligand function with some contribution from the central atom, while the antibonding MO (5.33) is a CA function  $\psi_0$  with a smaller contribution of the ligand part. If  $\gamma = 0$ , then  $\Psi_1 = \Phi_1$ , and the bonding electron remains on the ligand. On the other hand,  $\gamma = 0$  is possible only when  $H_{01} = G_{01} = 0$ , and this means, following (5.37), that  $\lambda = 0$  and hence  $\Psi_2 = \psi_0$ , that is, the antibonding MO is of purely CA origin. Thus both the MOs in this case are nonbonding and the bond remains purely ionic.

If  $\gamma \neq 0$  and  $\lambda \neq 0$ , the bonding electrons become collectivized, and for  $\gamma = \lambda = 1$  the bonding state includes both the CA state  $\psi_0$  and the ligand state  $\Phi_1$

with equal probability. In this case the bonding by this MO can be considered as entirely covalent. Hence the constants  $\gamma$  (for the bonding MO) and  $\lambda$  (for the antibonding MO) may serve as a measure of covalence.

Note that if  $0 < \gamma < 1$ , then  $\lambda \neq \gamma$ , and hence the degree of covalence on the bonding and antibonding MOs may be different. If, in addition,  $G_{01} > 0$ , then  $\lambda > \gamma$ , and in the approximation above,  $N_2 > N_1$ . Consequently, in the state of the bonding MO the probability of the electron to remain on the ligand (determined by  $N_1^2$ ) and on the CA ( $N_1^2\gamma^2$ ) is always smaller than, respectively, on the ligands ( $N_2^2\lambda^2$ ) and at the central atom ( $N_2^2$ ) in the case of the antibonding MO (see numerical values in Problem 5.2).

This result is quite understandable if one considers that in the case of a bonding MO a part of the electronic cloud determined by the term  $2N_1^2\gamma G_{01}$  (the overlap population) is placed in between the bonding atoms (and in this position the electronic charge attracts the nuclei of both atoms, thus contributing to the bonding), whereas in the antibonding case the corresponding term  $-2N_2^2\lambda G_{01}$  is negative; the antibonding MO produces a "negative overlap density," a subtraction of the electronic cloud in between the bonding atoms. The energy stabilization on the bonding MO and its destabilization on the antibonding MO, as shown above, within the approximations employed, almost compensate each other.

### Angular Overlap Model

The case of weak covalence is rather widespread in coordination systems. In particular, almost all MOs formed by  $f$  electrons in coordination compounds of rare-earth elements belong to weak covalence. Indeed, as mentioned in Section 4.4, the  $f$  electrons are screened by the outer  $d$  electrons, and therefore they form weak covalent bonds with the ligands (but the outer  $d$  electrons still may form stronger covalent bonds). Even in  $d$  electron complexes in the case of high oxidation states the covalence is formed mainly by outer  $s$  and  $p$  orbitals, while the  $d$  electrons' participation in the overlap with ligands is much weaker (Section 6.1).

For compounds of weak covalence a qualitative and semiquantitative semiempirical method of determination of the main chemically active MO energies, called *the angular overlap model* (sometimes abbreviated as AOM) [5.4, 5.12] has been worked out.

To simplify Eqs. (5.30) and (5.31) let us employ again the proportionality between  $H_{01}$  and  $G_{01}$ . According to Eq. (5.100) (with  $k = 2$ ),  $H_{01} = (H_{00} + H_{11})G_{01}$ ; substituting this expression into Eqs. (5.30) and (5.31), we have

$$E_1 \cong H_{11} - \frac{H_{00}^2 G_{01}^2}{H_{00} - H_{11}} \quad (5.38)$$

$$E_2 \cong H_{00} + \frac{H_{11}^2 G_{01}^2}{H_{00} - H_{11}} \quad (5.39)$$

It is seen from these equations that within the approximation at hand the stabilization of the bonding MO  $H_{00} - E_1$  and the destabilization of the antibonding MO  $E_2 - H_{11}$  are proportional to the square of the overlap integral  $G_{01}$ . This statement is taken as the basic assumption of the AOM.

The destabilization of the antibonding  $d$  and  $f$  MO energy levels which is relatively easily observed in electronic spectra (especially in  $f$ -electron systems) can serve as a measure of covalence of the bonds and of the nephelauxetic effects (Section 8.2). However, the name of the method and its possibilities are concerned more with the presentation of the overlap integral  $G_{01}$  as a product of the radial  $G_{01}^*$  and angular  $\theta$  parts [5.12]:

$$G_{01} = G_{01}^* \theta_{01} \quad (5.40)$$

Substituting this expression into Eq. (5.39), one finds that the energy of destabilization of the  $d$ - and  $f$ -electron states,  $E^* = E_2 - H_{11}$ , is proportional to the square of the angular overlap  $\theta$ :

$$E^* = e_\lambda \theta_{01}^2 \quad (5.41)$$

where

$$e_\lambda = \frac{H_{00}^2 (G_{01}^*)_\lambda^2}{H_{11} - H_{00}} \quad (5.42)$$

and the index  $\lambda$  is introduced to distinguish among  $\sigma, \pi, \delta, \dots$  metal–ligand radial overlaps. From Eq. (5.41) the main conclusion of the AOM method follows: *The destabilization of the atomic states of the CA due to the formation of covalent bonds with the ligands is proportional to the square of the angular part of the overlap integral.* Since the radial part of the overlap integral  $G_{01}^*$  depends on the metal–ligand distance, and not on the angular position of the ligands, whereas the angular part  $\theta$  strongly depends on the angular positions of the latter, the angular overlap model may provide a good method for studying *relative* geometries of complexes with the same or similar CA and ligands.

In a more general treatment for molecular systems with low symmetries both  $\sigma$ - and  $\pi$ -type overlap can be active in the same bond, where the  $\pi$  overlap is of two types,  $\pi(s)$  and  $\pi(a)$ , respectively (symmetric and antisymmetric with respect to the reflection in the plane containing the  $z$  axis). Also, different types of ligand orbitals may overlap with the given CA orbitals. In these cases the formula for the destabilization energy of  $d$  and  $f$  orbitals (5.41) acquires the form

$$E^* = e_\sigma \sum_i k_{0i}^2(\sigma) + e_\pi(s) \sum_i k_{0i}^2[\pi(s)] + e_\pi(a) \sum_i k_{0i}^2[\pi(a)] \quad (5.43)$$

where  $k_{0i}^2$ , similar to  $\theta_{0i}^2$ , are the squares of the angular part of the overlap integral with the  $i$ th ligand and depend on the coordinates of the latter. Passing to symmetrized group orbitals that already include corresponding summation



over the ligands, one can simplify Eq. (5.43):

$$E^*(\Gamma) = e_\sigma k_{0\Gamma}^2(\sigma) + e_\pi(s) k_{0\Gamma}^2[\pi(s)] + e_\pi(a) k_{0\Gamma}^2[\pi(a)] \quad (5.44)$$

where  $k_{0\Gamma}^2$ , unlike  $k_{0i}^2$ , are the squares of the angular parts of the group overlap integrals for the  $\Gamma$  representation. Table 5.5 gives the formulas for the  $k_{0\Gamma}^2$  values for  $d$  orbitals.

As is seen from Table 5.5, the dependence of  $k_{0\Gamma}^2$  and hence  $E^*$  on the angular coordinates of the ligands  $\varphi$  and  $\phi$  is very strong.

Equation (5.44) shows that with a small number of parameters, three for each different ligand at most  $e_\sigma, e_\pi(s), e_\pi(a)$ , one can describe the destabilization of the metal orbitals that determine the spectroscopic properties of the complex in the visible and near-ultraviolet regions. Usually, the constants in Eq. (5.44) are considered as empirical parameters, then the relative destabilization energies for different geometries of the complex are well defined by this equation; the whole procedure is easily programmed for personal computers allowing direct estimation of CA orbital destabilization by different geometries of coordination (for more details, see Ref. 5.14).

So far the most useful applications of the model seem to be in spectroscopy of  $d-d$  transitions (Section 8.2), especially with  $f$ -electron participation. Compared with crystal field theory, AOM is more attractive because it considers partly the electronic structure of the ligands and introduces more realistic parameters. AOM occupies a position in between CFT and the MO LCAO method.

However, in general the AOM deficiencies are almost the same as those of CFT (Section 4.6). Indeed, although AOM factors in weak covalence, it does it for the CA states only. Hence in this model, similar to CFT, ligand electronic states are not involved explicitly, and the MOs of mainly ligand origin are excluded from consideration. This deprives us of the possibility of considering many important chemical phenomena, such as the origin of metal-ligand

**TABLE 5.5. Squared Angular Parts of Group Overlap Integrals with CA  $d$  States<sup>a</sup>**

$d$ States	$k_{0\Gamma}^2(\sigma)$	$k_{0\Gamma}^2[\pi(s)]$	$k_{0\Gamma}^2[\pi(a)]$
$d_{z^2}$	$N(\cos^2\theta - \sin^2\theta/2)^2$	$\frac{3}{4}N \sin^2 2\theta$	0
$d_{x^2-y^2}$	$\frac{3}{4} \sin^4\theta (\sum C_n \cos 2\phi_n)^2$	$\frac{1}{4} \sin^2 2\theta (\sum C_n \cos 2\phi_n)^2$	$\sin^2\theta (\sum C_n \sin 2\phi_n)^2$
$d_{xy}$	$\frac{3}{4} \sin^4\theta (\sum C_n \sin 2\phi_n)^2$	$\frac{1}{4} \sin^2 2\theta (\sum C_n \sin 2\phi_n)^2$	$\sin^2\theta (\sum C_n \cos 2\phi_n)^2$
$d_{xz}$	$\frac{3}{4} \sin^2 2\theta (\sum C_n \cos \phi_n)^2$	$\cos^2 2\theta (\sum C_n \cos \phi_n)^2$	$\cos^2\theta (\sum C_n \sin \phi_n)^2$
$d_{yz}$	$\frac{3}{4} \sin^2 2\theta (\sum C_n \sin \phi_n)^2$	$\cos^2 2\theta (\sum C_n \sin \phi_n)^2$	$\cos^2\theta (\sum C_n \cos \phi_n)^2$

<sup>a</sup> $N$  is the number of ligands,  $C_n$  is the LCAO coefficient of the  $n$ th ligand in the group orbital  $\Gamma$  (Tables 5.1–5.3), and  $\theta_n$  and  $\phi_n$  are the ligands' angular coordinates (all the sums should be taken from  $n = 1$  through  $n = N$ ).

bonding, charge transfer spectra, and the origin of configuration instability due to the vibronic mixing of CA states with ligand orbitals. In view of the essential progress in more accurate computational methods with user-friendly ready-made computer programs, described below, the AOM becomes less practical in use for solving coordination system problems. For the use of the weak covalence approximation see Problem 5.2.

### 5.3. METHODS OF CALCULATION OF MO ENERGIES AND LCAO COEFFICIENTS

#### SCF MO LCAO Approximation

Evaluation of the electronic structure of coordination compounds in the MO LCAO approximation, as shown above, can be reduced to the solution of the secular equation (5.8) that determines the MO energies  $E_i$  and Eqs. (5.7) for the LCAO coefficients for each  $E_i$  value. Equations (5.7) and (5.8) contain the overlap integrals  $S_{ij}$  (or the group overlap integrals  $G_{ij}$ ) and resonance integrals  $H_{ij}$ . Provided that the basis set of AOs is chosen, the  $S_{ij}$  (or  $G_{ij}$ ) values can be calculated directly, whereas evaluation of the  $H_{ij}$  magnitudes by Eq. (5.4) is rather difficult.

In Eq. (5.4)  $H$  is an effective Hamiltonian for the one-electron state; it describes the mean field of all the nuclei and other electrons in which the given electron moves. This field depends essentially on the states of the other electrons described by their MOs. The latter, in turn, depend on the MO of the electron under consideration. This situation, in the framework of the full separation of the variables of the electrons, is best described by the *Hartree–Fock (HF) method of self-consistent field* (SCF) described in Section 2.2. In application to molecules in a combination with the MO LCAO approximation, the corresponding equations were obtained first by Roothaan [5.15]; the joint method is abbreviated as *SCF MO LCAO*, or the *Hartree–Fock–Roothaan (HFR) method*.

Deduction of the HFR equations is relatively simple for closed-shell systems when each MO is occupied by two electrons (the total spin is zero) and there is no orbital degeneracy, but it becomes much more difficult when there are open shells, and for systems in excited states [5.16–5.19].

Following discussion of the Hartree–Fock method in Section 2.2, for a molecule with a closed-shell configuration of  $n$  electrons and  $n/2$  states occupied by two electrons each, the full wavefunction can be presented as a determinant of the type (2.28) formed by one-electron MOs (the spin functions for zero total spin are not shown):

$$\Psi_k = \left[ \left( \frac{n}{2} \right)! \right]^{-1/2} \det \| \varphi_1(\mathbf{r}_1) \cdot \varphi_2(\mathbf{r}_2) \cdots \varphi_{n/2}(\mathbf{r}_{n/2}) \| \quad (5.45)$$

where  $k$  indicates the electronic configuration under consideration. With this presentation of the wavefunction the self-consistent MOs  $\varphi_i(\mathbf{r}_i)$  are determined by Eq. (2.53). If the MOs are taken as LCAO (5.1), we come to the equations for the

MO energies and LCAO coefficients given by Eqs. (5.8) and (5.7), respectively. In the Hartree–Fock method the matrix elements of the effective Hamiltonian values  $H_{ij}$  of these equations are given by the matrix elements of the Fockian  $F^k$  [Eq. (2.55)]. Its more detailed form is as follows.

Denote the MOs and AOs by Greek and Latin labels, respectively. Then, for MOs of the type (5.1), we have (the asterisk denotes complex-conjugated magnitudes)

$$\begin{aligned}\varphi_\mu &= \sum_l^N c_{\mu l} \psi_l(\mathbf{r}) \\ \varphi_\mu^* &= \sum_k^N c_{\mu k}^* \psi_k(\mathbf{r})\end{aligned}\quad (5.46)$$

where  $N$  is the number of functions in the LCAO basis.

The matrix element of the effective Hamiltonian is

$$H_{ij} = F_{ij} = \int \varphi_i^* F^j \varphi_j d\tau \quad (5.47)$$

where the operator  $F^j$  (Fockian) [Eq. (2.55)] contains the functions (5.46). By substitution we get

$$\begin{aligned}H_{ij} &= H_{ij}^0 + \sum_{k,l} P_{kl} ([kl|ij] - \frac{1}{2}[kj|il]) \\ &= H_{ij}^0 + I_{ij} - K_{ij}\end{aligned}\quad (5.48)$$

Here, in accordance with Eq. (2.50), we have

$$H_{ij}^0 = T_{ij} - \sum_\alpha (U_\alpha)_{ij} \quad (5.49)$$

where the notations are the same as in Chapter 2;  $T$  is the operator of kinetic energy of the electron and  $U_\alpha$  is its potential energy of attraction to the  $\alpha$  nucleus, and

$$P_{kl} = \sum_{\mu=1}^{n/2} 2c_{\mu k}^* c_{\mu l} \quad (5.50)$$

is an important characteristic of the charge distribution in the system in the MO LCAO approximation—the matrix of bond orders, or density matrix, mentioned in Section 5.2 [Eq. (5.21)], and

$$I_{ij} = \sum_{k,l} P_{kl} [kl|ij] \quad K_{ij} = \frac{1}{2} \sum_{k,l} P_{kl} [kj|il] \quad (5.51)$$

are the abbreviated denotations for, respectively, the Coulomb and exchange interactions between the electrons. The notation  $[kl|ij]$  represents two-electron integrals (2.34).

Equations (5.48)–(5.50) show explicitly that in order to evaluate the  $H_{ij}$  values in Eqs. (5.7) and (5.8) of the MO LCAO method, one must know the sets of LCAO coefficients  $c_{\mu k}$  that are determined by the same equations. In other words, the equations determining the  $c_{\mu k}$  values are nonlinear [if one substitutes the expression (5.48) for  $H_{ij}$  into (5.7), the latter becomes cubic with respect to  $c_{\mu k}$ ]. In these cases the solution can be obtained by *the method of iterations* (similar to the atomic case in Section 2.2).

Assume that, from general knowledge about the system, we choose some reasonable values of the  $c_{\mu k}$  coefficients for all the MOs. With these coefficients the  $H_{ij}$  values after (5.48) can be calculated; then the MO energies  $E_{\mu}$  and new LCAO coefficients  $c'_{\mu k}$  can be evaluated for each MO after (5.8) and (5.7), respectively. With the new coefficients  $c'_{\mu k}$  one can calculate new  $H'_{ij}$  values and determine with them new  $c''_{\mu k}$  values, and so on, until the newly calculated MO energies  $E'_{\mu}$  and LCAO coefficients  $c''_{\mu k}$  coincide (within the required accuracy) with the previous ones. It is assumed that in this process of iterative calculations the solution converges to the *self-consistent values* of  $E_{\mu}$  and  $c_{\mu k}$  sought for.

For systems with unpaired electrons (open shells), the full wavefunction can be presented in the form of a linear combination of several determinants of the type (5.45) corresponding to the symmetry and spin of the molecular term under consideration. This results in an essential complication of the calculation procedure. However, in some cases the presentation with one determinant can be preserved. In particular, in the so-called *unrestricted Hartree–Fock (UHF) method* [5.16–5.19] it is assumed that the orbital parts of the wavefunctions of electrons with opposite spins,  $\alpha$  (up,  $\uparrow$ ) and  $\beta$  (down,  $\downarrow$ ), are different [in the *restricted Hartree–Fock (RHF) method* they are the same for the two electrons on a given one-electron orbital]. Then the expansion (5.46) should be written separately for the MOs with the spins  $\alpha$  and  $\beta$ ,  $\varphi_i^{\alpha}$  and  $\varphi_i^{\beta}$ , respectively, and hence the order of the secular equation (5.8) and the number of LCAO coefficients,  $c_{\mu k}^{\alpha}$  and  $c_{\mu k}^{\beta}$ , increase, becoming equal to the number of electrons in the system (in the RHF method for closed shells it is half the number of electrons).

Thus the calculations of electronic structure by the SCF MO LCAO (Roothaan) method can be performed by an iterative procedure in which each iteration consists of two important stages:

1. Calculation of the Coulomb integrals  $I_{ij}$  and exchange  $K_{ij}$  interactions between the electrons using Eq. (5.51), as well as the one-electron integrals of kinetic and potential energy (5.49) and overlap integrals  $S_{ij}$  (or  $G_{ij}$ )
2. Solution of Eqs. (5.7) and (5.8)

Each stage has its own difficulties, which increase with the number of electrons, but most of them are due to the calculation of integrals (stage 1). Indeed, in most

MO LCAO methods the number of integrals increases with the number of atoms (and hence the number of the basis functions  $n$ ) as  $n^4$  (see the discussion in Section 5.7). Many of these integrals are multicenter integrals; their evaluation requires the major part of computer time. However, the results of such calculations are far from being excellent. The reason is in the neglect of *correlation effects* and poor *basis sets*, discussed below.

Calculations by the abovementioned SCF MO LCAO methods employing neither empirical parameters nor restricting computational simplifications are called *ab initio*. When introducing some computational simplifications, they are also called *nonempirical*. These methods do not use any empirical parameters except the specification of the system by the number of nuclei and the nuclear charges, as well as the number of electrons (in the literature there may be some nonessential differences in this classification of methods). In the adiabatic approximation under consideration the Hamiltonian (Fockian)  $F^j$  in Eq. (5.47), taken after (2.55), also contains the nuclear configuration (geometry) of the molecular system, but this is not necessarily an empirical parameter. Indeed, in sufficiently full computations the electronic structure is calculated for different points of nuclear coordinates yielding the adiabatic potential energy surface (APES), and there are special procedures for reaching the minimum point on the APES sufficiently rapidly [5.18, 5.19]. The coordinates of this minimum are assumed to correspond to the equilibrium geometry of the molecule. Such calculations are termed *geometry optimization*. Some computer programs perform this procedure automatically.

### The Role of Basis Sets

The main assumption of the MO LCAO method—the presentation of the MO in the form of LCAO (5.1)—may be subjected to criticism. Indeed, in this presentation one tries to approximate the unknown function of the MO with a limited number of known atomic functions. Visually, the latter serve as molds, while the LCAO coefficients are a means for adapting the molds to the complicated MO surface. It is obvious that when the number of molds is small, and their form is rigid and does not fit the MO surface well, the MO in the form of (5.1) is not sufficient for presenting the real charge distribution (despite the best choice of LCAO coefficients by the variational method).

Mathematically, any function can be presented in the form of an expansion in a series of other functions, provided that the latter form a set that is complete from the mathematical perspective. The usual sets of valence atomic orbitals do not satisfy this condition. To be complete, the set of functions must include *all* the exact solutions of the Schrödinger equation for a given atom or any other polyatomic system.

This explains why the results of the calculation of the electronic structure of molecular systems obtained by the MO LCAO method depend on the choice of the basis set, larger (more complete) sets are preferable. However, as mentioned above, the increase in the number of basis functions sharply increases the

number of integrals to be calculated, making the problem much more difficult. Nevertheless, using modern computers this can be done for systems of moderate size. If the basis set is complete, the results are the same as if the prime Hartree–Fock equations (2.52) were solved exactly. Such results are called *Hartree–Fock limit solutions*.

In calculations of transition metal compounds performed so far, the basis set is far from being complete. Often the *minimal basis set* is used, which contains the AOs that are occupied by valence electrons in the ground state of the free atoms forming the molecule (the *valence basis*); the *extended basis* also includes unoccupied AOs of excited states. In general, three kinds of atomic functions can be used to present the AOs in the MO LCAO method: (1) *hydrogenlike orbitals* (Lagerr polynomials); (2) *Slater orbitals* (Section 2.1), and (3) *Gaussian functions*. For the region of interatomic orbital overlap where the chemical bonding is realized, Slater orbitals are most suitable, but they are not recommended for the region at the nuclei; hydrogenlike functions may be better for this region. In the MO LCAO problems the use of the basis of Slater orbitals or, more precisely, *Slater-type orbitals* (STOs), is most widespread.

Both Slater and hydrogenlike functions create many difficulties when used in calculations of molecular integrals. The problem is essentially simplified when the corresponding STOs are expressed by Gaussian function—Gauss-type orbitals (GTOs) [5.20–5.22]. The latter contain the exponential factor  $\exp(-\zeta r^2)$  with a  $r^2$  dependence on  $r$  [instead of  $\exp(-\zeta r)$  in the STO]; this allows for a much more simple evaluation of two-electron two-center integrals. On the other hand, the presentation of a given STO in the form of a sum of two or several ( $n$ ) GTOs with different coefficients is relatively simple and can be tabulated a priori. Such functions are termed STO- $n$ G. Usually  $n$  ranges from 2 to 6. The AOs (HF solutions)  $\psi_k$  in Eq. (5.46) can be approximated by one STOs [5.23], or by two or several STO [5.24, 5.25]. The notation STO- $n$ G refers to the latter case. The minimal basis set is usually STO-3G.

In general, several Gaussian functions represent each AO, and the question is whether they should all be presented by the same  $c_{\mu k}$  coefficient in the LCAO (one coefficient for the whole AO), or be grouped in two, three, ..., with two, three, ..., coefficients  $c_{\mu k}$ . In the former case the basis is an one-exponential one; in the case of two groups of orbitals for the same AO (with two variational coefficients  $c_{\mu k}$ ) the basis is named *two-exponential, or double-zeta* (DZ). Note that while the number of Gaussian functions in the AO determines the number of integrals to be calculated in the MO LCAO procedure, the number of  $c_{\mu k}$  coefficients determines the order of the secular equation (5.8).

The angular part of the AOs in all presentations remains the same; the  $s, p, d, f, \dots$  behavior is an important feature of the LCAO determining its classification on symmetry discussed in Section 5.1. But the radial part is not so strictly determined. In particular, the exponential parameter  $\zeta$  of the Slater orbital for free atoms is calculated to fit its charge distribution (atomic radii, interatomic distances, etc.). If the AO is given by several STOs, the latter could be chosen to fit, say, the HF solutions for the free atom.

Thus, to obtain the Gaussian basis set, one must perform several numerical calculation procedures: to obtain HF solutions, to fit them by STO, and then to fit the STO by a Gaussian function. Huzinaga [5.26] (see also Refs. 5.27–5.29) suggested avoiding all these lengthy intermediate calculations and determining the Gaussian basis set directly from the condition of the minimum of the ground-state energy of the atom. This can be done by means of a Roothaan procedure taking the AO as a linear combination of Gaussian orbitals and considering both the  $c_{ij}$  coefficients and the exponential parameters  $\zeta$  as variational parameters. Basis sets for many atoms were tabulated in this way [5.30, 5.31].

Obviously, the quality of the Huzinaga basis depends on how many individual Gaussian orbitals are taken to form the atomic orbitals of the type  $s, p, d, \dots$ . In this basis there is no sense in discriminating between  $1s, 2s, 3s, \dots$ , orbitals, because all of them have the same symmetry and enter in the same LCAO. However, different Gaussian  $s$  orbitals or groups of them can have different variational LCAO coefficients.

In total, the Gaussian basis set contains in general  $n_1$   $s$ -type functions,  $n_2$   $p$ -type ones,  $n_3$   $d$ -type ones, and so on. These are called *primitive functions* (PGTO), denoted as  $(n_1s \ n_2p \ n_3d)$ . In the LCAO they may be grouped (contracted) to  $N_1$   $s$ -type ( $N_1 < n_1$ ),  $N_2$   $p$ -type,  $N_3$   $d$ -type, and so on, AOs. This *contracted basis* is usually denoted in brackets as  $[N_1s \ N_2p \ N_3d]$ . For example, in the phrase “(9s5p3d) contracted to [4s3p2d],” (9s5p3d) means that the basis set contains nine primitive  $s$ -type Gaussian functions (nine different radial parts with the same  $s$ -type angular factor), five  $p$ -type and three  $d$ -type functions, while [4s3p2d] means that in the LCAO there are only four  $c_{ij}$  coefficients presenting the  $s$  functions (four groups of Gaussian functions with independent variational coefficients), three groups of  $p$  functions, and two groups for  $d$  functions; in total, there are 17 PGTOs with only nine LCAO coefficients.

In the presentation by Pople et al. [5.32] the notations for basis sets of first-row atoms contain several figures before the G letter denoting the numbers of Gaussian functions in the inner ( $1s$ ) state and in the split-valence states ( $2s$  and  $2p$ ). For example, 6-31G means that the inner  $1s$  function (for nonhydrogen atoms) is presented by six Gaussian functions, while the outer valenceshell functions are split into two groups ( $2s, 2p$  and  $2s', 2p'$ ), the first being of which is presented by a 3G (the same for  $2s$  and  $2p$ ) and the second by a single Gaussian function (one function for  $2s'$  and  $2p'$ ).

An extension of this basis set is achieved when the *polarization functions* are added to give additional flexibility to the description of the MOs. For  $s$  functions polarization additions are of the  $p$  type, and for  $p$  functions they are of the  $d$  type. If polarization functions are added for only nonhydrogen atoms, the basis set is denoted by one star (e.g., 6-31G\*), while additional polarization functions also for the hydrogen atoms ( $p$  functions) are indicated by adding a second star (6-31G\*\*). Krishnan et al. [5.32] give the parameters for an even more sophisticated basis set for first-row atoms, 6-311G\*\*. This means that the valence shell is split into three groups ( $2s, 2p; 2s', 2p'; 2s'', 2p''$ ) presented by three, one, and one Gaussian functions, respectively, and polarization functions for nonhydrogens



and hydrogens are included. In addition to polarization functions, the basis set may be improved by adding functions that are more extended in space, and more diffuse (usually hybridized  $sp$ ); such functions are especially important for anions. Diffuse basis functions are marked by “+,” for example, 4–31 + G.

In the case of transition metal compounds in the description ( $n_1s$   $n_2p$   $n_3d/n'_1s$   $n'_2p$   $n'_3d/\dots$ ) the slash usually divides different basis sets for different atoms of the same system; the first place is for the basis set of the CA, followed by one of the ligands of the first coordination sphere, and so on (the same notation is often used to separate hydrogen atoms after the slash). The use of different basis sets for the CA and ligands is quite reasonable, considering the difference in their electronic configuration, especially the essential role of  $d$  electrons, the *d-electron heterogeneity* introduced by the transition metal in the otherwise approximately *electronically homogeneous* system (in the sense that it contains electronically similar  $nsnp$  atoms). In homogeneous systems with generally electronically similar atoms, the use of different basis sets for different atoms is not recommended because this can result in an artifact of charge redistribution toward the region where a larger basis set is used.

In further development of computational methods the so-called *correlation consistent* (cc) basis sets were introduced [5.19] to accommodate the fact that in the contracted set the functions that contribute similar amounts of correlation energy should be included in the same group. For example, adding a polarization  $d$  function to an  $sp$  basis set significantly lowers the energy, but the contribution of the second  $d$  function will be less efficient and should be grouped together with the first  $f$  function. Similarly, the third  $d$  function should be grouped with the second  $f$  function and the first  $g$  function. Hence additional polarization functions should be given in the order  $1d, 2d1f, 3d2f1g$ , and so forth.

The size of the cc basis set is usually given in terms of the number of contracted functions: cc-pVDZ, cc-pVTZ, cc-pVQZ, cc-pV5Z, and cc-pV6Z, meaning *correlation consistent polarized double/triple/quadruple/quintuple/sextuple zeta* basis sets, respectively. Sometimes additional diffuse functions are added to these sets denoted by the prefix *aug-*. For instance, aug-cc-pVDZ means that functions  $1s, 1p$ , and  $1d$  are added to the cc-pVDZ basis set. In this way a sequence of basis sets can be generated that converges toward the basis set limit [5.19].

In choosing the best basis set for electronic structure calculation of configurationally unstable systems (e.g., transition states of chemical reactions) the pseudo-Jahn–Teller PJT origin of the instability (Chapter 7) should be factored in by choosing the additional basis functions to represent the excited electronic states that contribute to the instability of the ground state [5.33].

One common error introduced by the use of limited basis sets emerges in MO LCAO calculations of intermolecular interactions, for instance, in chemical reactions. If we calculate two molecular systems  $A$  and  $B$  separately with poor basis sets, their molecular properties will be evaluated with certain errors that, in principle, can be eliminated by extending the basis. When approaching  $A-B$  and calculating them together with the same two basis sets, the number of basis functions in the MO LCAO scheme becomes that of  $A + B$ , that is, much larger than



for  $A$  and  $B$  taken separately. This superposition of the basis sets, in addition to describing the  $A-B$  interaction, *improves the calculated intramolecular interactions in each of the two molecules*. Therefore, the energy of interaction between  $A$  and  $B$  ( $E_{\text{int}}$ ) is not equal to the difference between the energies of the joint system  $E(A-B)$  and the sum of the energies of the separate molecules  $E(A) + E(B)$ , because of the changes of  $E(A)$  and  $E(B)$  due to the superposition of the two basis sets. We have

$$E(A) + E(B) - E(A-B) = E_{\text{int}} + E_{\text{BSSE}}$$

where  $E_{\text{BSSE}}$  is the energy of the *basis set superposition error* (BSSE). The more complete the basis set, the less the  $E_{\text{BSSE}}$ . For example, for the interaction of  $\text{Li}^+$  with  $\text{C}_2\text{H}_5^-$ , ab initio calculations with STO-3G yield  $E_{\text{BSSE}} = 72.63$  kcal/mol, while with the 6-31+G basis  $E_{\text{BSSE}} = 0.20$  kcal/mol [5.34].

In summary, we see that the choice of a proper basis set for ab initio calculations is by itself nontrivial and may require significant effort. Fortunately, a great deal of experience is accumulated in this field, and there are ready-made basis sets for direct use in a variety of problems. For a variety of sources of basis sets aimed at electronic structure calculation of TMS, see Refs. 5.35.

### Electron Correlation Effects

Even when the best basis sets are used in MO LCAO calculations (functional complete sets) and the best possible HF (HF limit) solutions are obtained the results may be far from satisfactory. The discrepancy between full HF calculations and experimental data is due to the defect of the HF method mentioned above; it does not include the so-called electron correlation effects [5.18, 5.19].

The origin of electron correlation effects is as follows. In the one-electron approximations any given electron is assumed to move independently in the mean field created by all the other electrons and nuclei. Under this assumption the repulsion between the electrons is considered in average, but not at each moment. In particular, in this scheme there is a probability that two electrons meet at the same point in space, whereas actually this is impossible because of their repulsion, which keeps them as far away as possible from each other. Thus the motions of the electrons in time are not independent, but correlated.

For instance, in the simplest case of a helium atom the two correlated  $1s$  electrons at any instant occupy diametrically opposite positions on the  $1s$  sphere (Fig. 2.1), whereas in the HF description they can instantly be at the same point of the  $1s$  distribution. In the case of many electrons, the correlation around each electron produces a "hole" in the charge distribution of all the other electrons, sometimes called the *Fermi hole*.

A more detailed mathematical analysis shows that if the full wavefunction is taken in the one-determinant form (5.45) (thus obeying the Pauli principle), the probability of finding two electrons with parallel spins at the same point  $\mathbf{r}$  is zero. This means that the motions of spinlike electrons in the HF method are

correlated, and there are correlation Fermi holes in the charge distribution of such spinlike electrons. However, electrons with opposite spins remain uncorrelated. In particular, two electrons on the same MO have opposite spins, and hence they are uncorrelated.

The correlation energy  $E_{\text{corr}}$  of the system is determined as the difference between the exact nonrelativistic value  $E_{\text{ex}}$  and the Hartree–Fock limit  $E_{\text{HF}}$

$$E_{\text{corr}} = E_{\text{ex}} - E_{\text{HF}}$$

The importance of correlation effects for any molecular system is beyond doubt. Even in the case of small molecules it can be significant when important chemical characteristics are calculated. For instance, for the HF molecule (not to be confused with the HF method) the total energy calculated by the SCF MO LCAO method equals  $-2722.65$  eV, while the experimental value is  $-2734.16$  eV. At first sight the discrepancy is not very large, less than 1%. But if we calculate the dissociation energy as the difference between the energy of the whole molecule and the free atoms, we have (in eV)  $D = -2722.65 + 2718.54 = -4.11$ , whereas the experimental value is  $-6.08$  eV; the error is about 30%. Examples for coordination compounds are discussed in Sections 6.3 and 6.4.

The development of methods for calculating correlation effects was one of the most important and difficult problems of quantum chemistry [5.18, 5.19]. Presently there are several such methods well worked out. Most widespread are different versions of *configuration interaction* (CI), the main idea of which is to look for the full wavefunction of the system  $\Psi$  in the form of a linear combination of the wavefunctions  $\Psi_k$  constructed after (5.45) for different electronic configurations that have the same symmetry properties:

$$\Psi = \sum_k A_k \Psi_k \quad (5.52)$$

where the coefficients  $A_k$  are determined by the variational principle (similar to  $c_{\mu k}$  in the MO LCAO method). The inclusion of excited configurations into the search of the best fit to the real charge distribution in the system is certainly very helpful, allowing one to improve the HF results significantly. However, in practice the number of integrals and the size of determinants to be solved increase rapidly with the number of configurations in the expansion (5.52).

In general, the number of possible excited configurations equals the number of determinants of the form (5.45) that can be constructed from the basis set functions of the system. For example, if for the water molecule with 10 electrons one chooses a basis set of 14 AOs, which in the double-zeta approximation yield 28 orbitals in the LCAO, the number of possible configurations equals the number of combinations of 28 in 10 that equals  $\sim 1.3 \times 10^7$ . With such a large number

of excited configurations, the problem becomes extremely difficult. Fortunately, there are several ways to reduce the number of configurations in the CI procedure, based mostly on symmetry considerations. It is easily seen that only those excited configurations  $\Psi_k$  contribute to the CIs that have the same symmetry as the ground state. Indeed, since the Hamiltonian is totally symmetric, all its matrix elements are zero if the two functions, ground and excited, belong to different IrReps of the point group of the molecule (Section 3.4). For the example of the water molecule of  $C_{2v}$  symmetry with the ground state  $^1A_1$  described above, the effective excited configurations must be of orbital  $A_1$  symmetry and have the same number of  $\alpha$  and  $\beta$  (spinup and spindown) spin-orbitals.

But even after the essential reduction in the number of possible excited configurations by symmetry, it still remains too large to be manageable. Further reductions should be based on the analysis of the possible role of different configurations in order to make reasonable truncations of the expansion (5.52). The convergence of the latter is also dependent on the basis set. A detailed study of the problem [5.18, 5.19, 5.36] resulted in several versions of the CI method, including the *independent electron pair approximation* (IEPA), *single and double CI* (CISD), *cluster expansion of the wavefunction, many-electron theory* (MET), *coupled-pair many-electron theory* (CPMET), *coupled-electron pair approximation* (CEPA), and *coupled-cluster methods* (see below).

One extension of the CI method is to include the expansion (5.52) into the SCF MO LCAO scheme, that is, to vary the total energy with respect to  $c_{\mu k}$  and  $A_k$  simultaneously—in this case the method is called *multiconfiguration SCF* (MC SCF). More sophisticated (and time-consuming) is the *multireference CI* (MRCI), in which the configurations produced from the MCSFC states serve as the components of the expansion (5.52). Another method widely used now is *complete active space SCF* (CAS SCF), in which a full CI is included for a set of orbitals chosen as “active.” Quite a number of works are devoted to the use of approaches based on the many-body Rayleigh–Schrödinger perturbation theory (MB-RSPT, or simply PT) often called *Moeller–Plesset* (MP) *approximation*; MP2, MP3, . . . denote MP approximations of the second-, third-, and higher-order perturbation theory. Table 5.6 summarizes different classes of ab initio methods of electronic structure calculations [5.37]. Some of them are size-sensitive, meaning that they scale as the exact energy with the number of particles in the system [i.e., the energy  $E_{AB}(R \rightarrow \infty) = E_A + E_B$ , where  $A$  and  $B$  are two parts of the bonded system  $AB$  and  $R$  is the distance between them [5.18, 5.19]].

Coupled-cluster methods (CCMs) are more recent developments that compete with the CI methods. The idea of CCM is to include all electronic correlation corrections to infinite order. The wavefunction is taken as

$$\Psi_{\text{cc}} = e^T \Phi_0 \quad (5.53)$$

**TABLE 5.6. Summary of Basic Ab Initio Methods of Electronic Structure Calculations**

Method and Denotation	Choice of Variational $\Psi$	Characterization
Hartree–Fock (HF)	One determinant built from one-electron MO $\varphi(i)$	Labor $\sim n^4$ ; $\varphi(i)$ adjusted iteratively by the SCF procedure; the method is size extensive
Configuration interaction (CI)	Many determinants $\Psi = \sum_k A_k \Psi_k$	Labor $\sim n^5$ or greater, method converges slowly, not size extensive
Multiconfiguration SCF (MCSCF)	$\Psi$ is the same as in CI	Both CI and $\varphi(i)$ optimized simultaneously; not size extensive, convergence difficult
Multireference CI (MRCI)	$\Psi_k$ are produced from $\Psi$ in MCSCF	Truncated, not size extensive
Complete active space SCF (CAS SCF)	Special case of MCSCF	All determinants (full CI) within the chosen set of “active” orbitals in the MCSCF scheme; size extensive, CI expansion increases rapidly
Generalized valence bond (GVB)	Special case of MCSCF	VB functions (combinations of determinants) are used in the CI; simplest case, perfect pairing (two-electron bonds)
Many-body (Moller–Plesset) perturbation theory (MP2, MP3, etc.)	$\Psi$ same as in CI	$A_k$ is determined by perturbation theory; nonvariational, size extensive
Coupled cluster methods (CCD, CCDS, CCSD, IEPA, CEPA, etc.)	$\Psi$ same as in CI	$A_k$ determined by exponential cluster expansion; nonvariational, size extensive
Quantum Monte Carlo (QMC)	Quantum simulation HF or CI “guiding” functions	Small systems; difficult for excited states

Source: Adapted from Salahub and Zerner [5.37].

<sup>a</sup> $n$  denotes the number of atomic orbitals in the basis set.

where  $\Phi_0$  is a Slater determinant (5.45) and  $T$  is the cluster operator:

$$T = T_1 + T_2 + T_3 + \dots \quad (5.54)$$

The  $T_i$  operators, for instance, for  $T_1$  and  $T_2$  are

$$T_1 \Phi_0 = \sum_i^{\text{occ}} \sum_a^{\text{vir}} c_i^a \Phi_i^a \quad (5.55)$$

$$T_2 \Phi_0 = \sum_{i < j}^{\text{occ}} \sum_{a < b}^{\text{vir}} c_{ij}^{ab} \Phi_{ij}^{ab} \quad (5.56)$$

where  $\Phi_i^a$  and  $\Phi_{ij}^{ab}$  are excited-state determinants in which, respectively, one-electron and two-electron excitations are introduced (occ and vir denote occupied and virtual states, respectively). Thus, by expanding the exponential function in Eq. (5.53), we have

$$e^T = 1 + T + \frac{1}{2}T^2 + \frac{1}{6}T^3 + \dots \quad (5.57)$$

with  $T$  after (5.54)–(5.56).

By minimizing the total energy [calculated with the function (5.53)] with respect to the coefficients  $c_i^a$ ,  $c_{ij}^{ab}$ , and so on (in addition to the LCAO coefficients in the MOs in the  $\Phi$  determinants), one can get accurate values of energies and wavefunction (5.53). Obviously the expansions (5.54) and (5.57) should be truncated; this leads to different versions of CCM: CCD, CCSD, CCSD(T).

The ab initio methods of electronic structure calculations mentioned above and their computer program implementations are also aimed at determining the equilibrium geometry of the molecular systems [5.19]. The idea beyond such *geometry optimization* is to calculate the electronic energy at different (fixed) nuclear configurations and to find the minimum-energy one. The program starts with a reasonable configuration and chooses the steep slope as the shortest way to the minimum.

For all these methods there are commercial programs that perform in a user-friendly manner; some of them can be downloaded from the Internet free of charge. The most usable program packages are GAUSSIAN [5.38], GAMESS (generalized atomic and molecular electronic structure system) [5.39], and MOLPRO [5.40]. Examples 5.2 and 5.4 and Problems 5.4, 5.5, and 5.7 show in detail (step by step) how to perform ab initio calculations of electronic structure using programs that can be downloaded for free from the Internet.

**EXAMPLE 5.2*****Exercise: Ab Initio Calculation of CuF<sub>2</sub> Using Hartree–Fock and MP2 Methods***

Install GAMESS (available free of charge from the Internet (<http://classic.chem.msu.su/gran/gamess/index.html>) and read the manuals carefully. In order to prepare the input deck for an ab initio program, it is necessary to know a few basis facts about the molecule to be calculated.

- *Approximate Geometry of the Molecule or Possible Configurations.* In the case of CuF<sub>2</sub>, two reasonable geometries can be tried: (1) linear F—Cu—F and (2) angular (bent) F—Cu—F. An approximate initial value for the Cu—F distance can be obtained from ionic radii:  $d(\text{Cu—F}) \approx R(\text{Cu}^{2+}) + R(\text{F}^-) = 0.9 + 1.2 = 2.1 \text{ \AA}$ .
- *Total spin (S) of the Molecule.* Starting with the assumption that CuF<sub>2</sub> is an ionic molecule, one finds that fluorine is a closed-shell ion with  $S = 0$  and Cu<sup>2+</sup> is  $d^9$  ion with one unpaired electron so the total spin of CuF<sub>2</sub> is  $S = \frac{1}{2}$ .
- *An Adequate Basis Set to Represent the Wavefunction.* This is an advanced topic so we can just use a common basis set, 6-31G\*.

With these data we perform an initial run for a fixed geometry (usually called *single-point* in the literature) in the linear configuration using the simplest Hartree–Fock method. An appropriate input deck for GAMESS is given below:

```

$CONTRL SCFTYP=UHF  RUNTYP=ENERGY  UNITS=ANGS

          ICHARG=0    MULT=2  $END
$SYSTEM  TIMLIM=600  MEMORY=200000 $END
$SCF     DIRSCF=.True. $END
$GUESS   GUESS=HUCKEL  $END
$BASIS   GBASIS=N31  NGAUSS=6  NDFUNC=1 $END
$DATA
SP UHF/6-31G* Calculation of CuF2 - Linear
Dnh      4

COPPER   29.0    0.0    0.0    0.0
FLUORINE  9.0    0.0    0.0    1.2
$END

```

In the input above the 6-31G basis is introduced by the keywords GBA-SIS=N31 NGAUSS=6 while the extra polarization function that needs to be added to make it 6-31G\* is given by NDFUNC=1. Also note that the type of calculation is unrestricted Hartree–Fock (SCFTYP=UHF) because the system is not a spin singlet. Another important point is that very few ab initio programs handle full-symmetry groups and are usually restricted to Abelian symmetry. In GAMESS all linear molecules are treated using  $D_{4h}$  or  $C_{4v}$  symmetry groups (this does not damage the results). Also, many ab initio programs (GAMESS included) suppose that the density matrix is totally symmetric, and as a consequence of this restriction some problems can arise from calculating degenerate electronic states.

Read carefully the output of the program and ascertain the symmetry of the ground electronic state. Since the unpaired orbital is in an  $A_{1g}$  orbital (remember that GAMESS uses  $D_{4h}$  symmetry), the label for the ground state of  $\text{CuF}_2$  is  $^2 \sum_g^-$ . This state is not degenerate, and we can expect the program to run the calculations without difficulty.

Now it is time to calculate the equilibrium metal–ligand distance. Using the previous input deck change RUNTYP=OPTIMIZE and MEMORY=280000, run the calculation and find the metal–ligand distance. The solution is  $R = 1.713 \text{ \AA}$ .

Next check whether the molecule is linear or angular. In order to do so, write an input deck to optimize the angular configuration. Change the DATA block in the UHF (unrestricted Hartree–Fock) geometry optimization input to

```

$DATA
UHF/6-31G* optimization of CuF2 - Angular
Cnv      2

COPPER   29.0      0.0      0.0      0.0
FLUORINE  9.0       1.4      0.0      1.4
$END

```

In this input an initial angle of  $90^\circ$  has been introduced. Run the program and find the final geometry. The calculation should converge back to the linear configuration minimum.

In order to check the geometry, we perform MP2 calculations, which are much more accurate than the Hartree–Fock ones. This is done by adding the keyword MPLEVL=2 in the CONTRL section. The GAMESS program cannot calculate the gradients of unrestricted MP2 calculations, so we have to significantly modify our input to include non-gradient-geometry optimization. Check the manual to see how this is done and write the input deck. A possible solution is

```

$CONTRL SCFTYP=UHF MLEVEL=2 RUNTYP=TRUDGE UNITS=ANGS
      ICHARG=0   MULT=2   COORD=HINT $END

$SYSTEM TIMLIM=600 MEMORY=280000 $END

$SCF   DIRSCF=.True. $END

$GUESS GUESS=HUCKEL   $END

$BASIS GBASIS=N31 NGAUSS=6 NDFUNC=1 $END

$DATA

Nongradient UMP2/6-31G* optimization of CuF2 -
  Angular
Cnv      2

COPPER   29.0   LC   0.0   0.0   0.0   -   0   K
FLUORINE  9.0   PCC  1.7  45.0   0.0   +   0   K I

$END
$TRUDGE OPTMIZ=GEOMETRY NPAR=2 IEX(1)=21,22 $END

```

After running the calculation (which takes considerably longer than previous times), we finally obtain the metal–ligand distance as 1.693 Å and confirmation that the molecule is linear. Now, we can compare the total energy between UMP2 and UHF calculations in their respective minima. They are, respectively,  $-1838.19505$  and  $-1837.38058$  hartrees. The lower energy is an indication of more accurate results.

#### 5.4. SEMIQUANTITATIVE APPROACHES

Calculation of electronic structure of than those described in Example 5.1 by ab initio SCF MO more complex coordination compounds, LCAO methods is not a routine procedure yet for chemists who are not experts in this particular field. Each such calculation is in part a creative piece of work that requires from the researcher expert and intuitive knowledge of how to choose the method of calculation, the basis set, the iterative and CI procedures, the output, and so on, and to evaluate the meaning of the results. In addition, it requires considerable computer time, and is thus expensive, not to mention unmanageable for large molecules. Therefore there is a strong demand for simplifications of the methods of calculation to make them most accessible.



As mentioned above, the SCF version of the MO LCAO method, when carried out directly, is called *ab initio*, or *nonempirical* in the sense that it is not based on any assumptions about the parameters of the molecule except the nuclear charges and number of electrons (see Examples 5.2 and 5.4). This statement is not absolutely true because the calculation procedure is never purely mathematical; it requires a great deal of experience, knowledge of chemistry, and intuition. So far for coordination compounds, including heavy-metal atoms and polyatomic ligands, simplifications have been and are almost absolutely necessary. Some of them can be introduced without using empirical parameters, thus not violating very much the nonempirical character of the calculations. In these cases the method may be called *semiquantitative*.

An illustrative example of semiquantitative approaches aimed at transition metal systems is provided by the *Fenske–Hall method* [5.41], which employs some approximate presentation of the matrix elements of the effective Hamiltonian in the SCF MO LCAO method; it essentially simplifies the calculations without introducing empirical parameters. In the Fenske–Hall approximation these matrix elements are

$$\begin{aligned}
 H_{ii} &= \varepsilon_i^A - \sum_{\mu \neq A} \frac{e^2(Z_\mu - q_\mu)}{R_{A\mu}} \\
 H_{ij}^{AB} &= (\varepsilon_i^A + \varepsilon_j^B)S_{ij}^{AB} - T_{ij} - \frac{1}{2}e^2 S_{ij}^{AB} \sum_{\mu \neq A,B} \left( \frac{Z_\mu - q_\mu}{R_{A\mu}} + \frac{Z_\mu - q_\mu}{R_{B\mu}} \right) \quad (5.58) \\
 H_{ij}^{AA} &= 0
 \end{aligned}$$

where  $\varepsilon_i^A$  is the atomic orbital energy,  $R_{A\mu}$  is the distance from the CA to the atom  $\mu$  with the effective charge  $Z_\mu^* = Z_\mu - q_\mu$ ,  $Z_\mu$  is the nuclear charge,  $q_\mu$  is the electronic charge on the atomic center (5.20),  $q_\mu = \sum_{i,v} q_i c_{i\mu} c_{iv} S_{\mu\nu}$ , and  $S_{\mu\nu}$  is the overlap integral.

With the matrix elements (5.58) the HFR procedure of the MO LCAO method of calculation of the electronic structure is essentially simplified; instead of the matrix elements (5.48) including one-, two-, three- and four-center integrals (whose number is  $\sim n^4$ ), mainly one-center (in  $\varepsilon_i$ ), overlap ( $S_{ij}$ ), and kinetic energy integrals, as well as Mulliken charges (5.20) should be calculated. Unlike other methods that give similar simplicity (see below), the Fenske–Hall method does not involve any adjustable or empirical parameters, except the interatomic distances that are chosen in a nonarbitrary fashion. However, in general this approach is not rigorously founded, making the results of calculations with Eqs. (5.58) less credible than those obtained by *ab initio* and semiempirical methods. For examples of calculations using the Fenske–Hall method, see Section 11.3.

### Pseudopotentials or Effective Core Potentials (ECPs)

Among the semiquantitative methods of electronic structure calculations, the ones that use pseudopotentials are most widespread. To avoid all-electron calculations, various approximations were suggested, aimed at excluding the inner electrons. We present here one of the suggestions [5.42] that proved to be useful.

The idea in general is to assume that the inner electrons do not participate directly in the chemical bonding and hence can be accounted for in a simpler way as a source of a special potential for the outer (valence) electrons (in semiempirical methods it is assumed that the inner closed-shell electrons, together with the nucleus, form an effective nuclear charge). Provided that we know this potential exactly, the all-electron problem becomes a valence-electron problem, essentially simplifying the calculations. This potential is often called *pseudopotential*; in Ref. 5.42 it is termed *effective core potential* (ECP), or *relativistic ECP* (RECP) (when relativistic effects are included). ECP should be constructed in such a manner that it preserves all the features of interactions between the valence electrons and the core, at least in the valence area where chemical bonding is important. The procedure for doing this is as follows.

The electrons of the transition metal atom are divided into valence and core electrons. The core in the first-series transition elements is formed by the electrons with the Ar-like shell: [...  $3s^23p^6$ ] = [Ar]. For the second series they are [...  $3d^{10}4s^24p^6$ ] = [Kr], while for the third one the core is [...  $4d^{10}5s^25p^64f^{14}$ ] = [Xe ·  $4f^{14}$ ] with the exception of the La group, where the [Xe] core only is replaced by pseudopotentials. In some cases the outermost orbitals  $(ns)^2(np)^6$  cannot be replaced by ECP and should be treated on an equal footing with the valence  $nd$ ,  $(n+1)s$ , and  $(n+1)p$  electrons [5.42].

Each core electron with the angular momentum quantum number  $l$  creates an effective potential  $U_l$  for the valence electrons; the summary potential of the core electrons is

$$U(r) = U_L(r) + \sum_{l=0}^{L-1} [U_l(r) - U_L(r)] P_l^* \quad (5.59)$$

where  $L$  is a unity greater than the highest  $l$  of any core orbital and  $P_l^*$  is the so-called core projection operator:

$$P_l^* = |l\rangle \langle l| \quad (5.60)$$

where  $|l\rangle = \Phi_l$  ( $\langle l| = \Phi_l^*$ ) is an exact (relativistic or nonrelativistic) Hartree–Fock atomic function. Actually  $P_l^*$  means that in the equation for the valence electron wavefunction, for instance,  $|l'\rangle$ , the sum in the term emerging from the pseudopotential  $U$ , contains the expression  $\langle l|l'\rangle$ , due to which only those terms of  $U$  remain effective, for which the wavefunction  $|l\rangle$  is not orthogonal to  $|l'\rangle$ .

To obtain the effective potential  $U_l$ , a pseudo-Hartree–Fock function  $\Phi_l^p$  is introduced. It is assumed that  $\Phi_l^p$  follows  $\Phi_l$  as close as possible in the outer (valence) region of the atom, and that it is nodeless and smoothly going to zero inside the atom. More precisely,  $\Phi_l^p = \Phi_l$  in the region of  $r_e > r_c$ , where  $r_c$  is near to the outermost maximum of  $\Phi_l$ , while  $\Phi_l^p = r^b f(r)$  inside this region;  $f(r)$  is a fifth-degree polynomial and  $b = l + 3$  (in the relativistic case  $b$  is taken somewhat differently [5.42]). The coefficients of the polynomial are determined to satisfy the conditions of continuity, normalization, nodelessness, and so on.

Now, the potential  $U_l$  is obtained from the condition that, if inserted in the one-electron Hartree–Fock equation, it yields the pseudofunction  $\Phi_l^p$  with the same energy  $\varepsilon_l$ . This means that  $U_l(r)$  obeys the one-electron equation for the atomic radial wavefunction [5.43]:

$$\left[ -\frac{1}{2} \frac{d^2}{dr^2} + \frac{l(l+1)}{2r^2} - \frac{Z}{r} + U_l(r) + V_{\text{val}}(r) \right] \Phi_l^p = \varepsilon_l \Phi_l^p \quad (5.61)$$

where  $V_{\text{val}}(r)$  is the Hartree–Fock (Coulomb and exchange) interaction of the  $l$  electron with the valence electrons. If we relate this equation to that for the exact Hartree–Fock atomic orbital  $\Phi_l$ , we can extract the expression for  $U_l$  sought for:

$$U_l(r) = \varepsilon_l - \frac{l(l+1)}{2r^2} + \frac{Z}{r} + \frac{(\Phi_l^p)''}{2\Phi_l} - \frac{V_{\text{val}}\Phi_l^p}{\Phi_l} \quad (5.62)$$

Thus, to evaluate the one-electron ECP, the atomic Hartree–Fock one-electron functions  $\Phi_l$  and energies  $\varepsilon_l$ , as well as the pseudoorbitals  $\Phi_l^p$  after Eq. (5.61) and their second derivatives  $(\Phi_l^p)''$  should be calculated first.

Similar to basis wavefunctions (Section 5.3), the ECPs obtained by Eq. (5.62) are conveniently presented in the form of a sum of Gaussian functions with tabulated coefficients for all the important atoms up to Hg for both nonrelativistic and relativistic cases [5.42]. The latter are obtained from similar equations that include relativistic terms.

The pseudopotentials are thus generated from atomic data by adjustment to orbital energies and orbital densities. Another version of ECP can be obtained by adjustment to experimental data, for instance, to excitation and ionization energies [5.44]. This version of pseudopotentials has some advantages—the experimental data incorporate all the additional interactions not factored into the (necessarily approximate) calculations (e.g., relativistic and core–valence correlation effects). Calculations involving pseudopotentials are shown in Example 5.4.

### Density-Functional Approaches

Widely used methods of electronic structure calculations employ the *density-functional theory* (DFT) [5.45].

Modern DFT methods are based on the Hohenberg–Kohn (HK) theorem [5.46], which proves that there is a one-to-one correspondence between the

electronic density  $\rho(\vec{r})$  of the ground state and the potential  $V(r, Q)$  (which includes electron–nucleus and nucleus–nucleus interactions) under the assumption that  $V(r, Q)$  can be considered as an external potential to the electronic subsystem (see below). The definition of the electronic density is given by Eqs. (5.13) and (5.14), while the operator  $V(r, Q)$  ( $r$  and  $Q$  denote all the electronic and nuclear coordinates, respectively) is described in (7.3') [see also (1.5)]; the nucleus–nucleus interaction does not affect the electronic densities directly and may be excluded from the major part of the consideration below.

The  $\rho(\vec{r}) \Leftrightarrow V(r, Q)$  correspondence means that there is also a direct correspondence between  $\rho(\vec{r})$  and the energy and wavefunction of the system because the latter are defined by the Hamiltonian, which is a function of  $V(r, Q)$  and the number of electrons  $n$  [ $n$  also enters in  $\rho(\vec{r})$  by normalization; see Eq. (5.14)]. The density  $\rho(\vec{r})$  is a function of three space coordinates and spin, whereas the wavefunctions depend on  $3n$  coordinates and spin. Therefore it is very attractive (much simpler) to describe the system by electron densities instead of wavefunctions. Unfortunately, the HK theorem [5.46], as well as the consequent extensions [5.47], are just “theorems of existence” that give no recipes on how to find the explicit expression for the dependence of  $\rho(\vec{r})$  on  $V$ , or the energy  $E$  on  $\rho(\vec{r})$ .

Since  $\rho(\vec{r})$  is a function, the dependence of  $E$  on  $\rho(\vec{r})$  is a *functional* (a function of a function) denoted as  $E[\rho]$ . The expression for the ground-state energy  $E_0$  via this functional is straightforward:

$$E_0 = E[\rho] = F[\rho] + \int V(r, Q)\rho(\vec{r})\partial\tau \quad (5.63)$$

where  $F[\rho]$  is a “universal” functional in the sense that it does not depend on  $V$ , so it has the same form for all the systems

$$F[\rho] = \int \Psi^*(T + U)\Psi\partial\tau = T[\rho] + U[\rho] \quad (5.64)$$

where  $T$  and  $U$  are the operators of, respectively, the kinetic and potential energies in the electronic subsystem; the latter includes both electrostatic and exchange interactions between the electrons. In the second term of (5.64) the nuclear coordinates are assumed to be constants, and hence the nucleus–nucleus interactions, as mentioned above, may be excluded from further consideration.

The density  $\rho(\vec{r})$  was shown [5.47] to follow the variational principle, namely, that the true function  $\rho(\vec{r})$  minimizes the functional  $E[\rho]$ . But we are unable to perform this minimization procedure in order to get  $\rho(\vec{r})$  because we don't know the universal functional  $F[\rho]$ , namely, how the kinetic energy in (5.64) and the exchange energy in  $U$  depend on  $\rho(\vec{r})$ .

The next, more practical, step in realization of the DFT ideas was reached in the Kohn–Sham (KS) equations [5.48]. Consider an artificial system with  $n$  *noninteracting electrons*, each of which can be described by an orbital  $\varphi_i(\vec{r})$  that

is a solution of a simple one-electron Hartree-type equation (2.49) (Section 2.2):

$$\left[ \frac{-\hbar^2}{2\mu} \Delta + V_{\text{KS}}^{(i)}(\vec{r}) - \varepsilon_i \right] \varphi_i(\vec{r}) = 0 \quad (5.65)$$

where  $V_{\text{KS}}(\vec{r})$  is a local potential chosen in such a way that the density resulting from the summation of the one-electron densities equals exactly the ground-state density of the real system  $\rho_0(\vec{r})$ :

$$\rho_{\text{KS}}(\vec{r}) = \sum_{i=1}^n |\varphi_i(\vec{r})|^2 = \rho_0(\vec{r}) \quad (5.66)$$

The full wavefunction of the system is a Slater determinant (5.45) of  $\varphi_i(\vec{r})$  terms.

It was shown that such a noninteracting system that follows Eqs. (5.65) and (5.66) exists if the potential  $V_{\text{KS}}(\vec{r})$  is taken as follows:

$$V_{\text{KS}}(\vec{r}) = \int \frac{\rho(\vec{r}')}{|\vec{r} - \vec{r}'|} d\tau + V_{XC}(\vec{r}) - \sum_{\alpha} \frac{eZ_{\alpha}}{|\vec{R}_{\alpha} - \vec{r}|} \quad (5.67)$$

The first term in this expression represents the electrostatic interaction of the electron with all the other ones (including interaction with self), and the last term represents the electron–nuclei interaction, while the term  $V_{XC}(\vec{r})$ , called the *exchange–correlation potential* is assumed to include all the other interactions in the system, first the *exchange interaction* and *correlation effects*, as well as the compensation for the inaccuracies introduced by the presentation of the real system by the artificial model of noninteracting electrons, and for the self-interaction in the first term.

So far no approximations have been involved in derivation of the KS equations (5.66) and (5.67); hence, provided that the exchange–correlation potential  $V_{XC}(\vec{r})$  as a functional of  $\rho(\vec{r})$  is known (which is not the case!), we can relatively easily get the KS one-electron orbitals  $\varphi_i(\vec{r})$  and their energies  $\varepsilon_i$  from Eq. (5.65), as well as the total energy [5.19]. The full wavefunction of the system is a Slater determinant (5.45) of  $\varphi_i(\vec{r})$  values.

The KS equations are quite similar to the Hartree equation (2.49) and can be solved using a similar self-consistent approach (Section 2.2). For the multicenter molecular system the orbitals  $\varphi_i(\vec{r})$  can be sought for as a linear combination of atomic orbitals symmetrized to satisfy the initial conditions of the problem (see below), quite similar to the MO LCAO approach discussed in Sections 5.1 and 5.3 with the LCAO coefficients determined from the minimum-energy condition. With the first guess of  $\varphi_i(\vec{r})$ , one can calculate the approximate KS density and the potential  $V_{\text{KS}}(\vec{r})$  using, respectively, Eqs. (5.66) and (5.67). With this potential, new, more accurate orbitals  $\varphi_i(\vec{r})$  can be obtained from Eq. (5.60) to be used for the next iteration, and so on, until the newly obtained orbitals and energies coincide with the previous ones within a given tolerance. The simplicity

of this procedure as compared to the much more complicated ones in the wavefunction presentation is the most attractive feature of the DFT methods. It allows for calculation of electronic structure of relatively large molecular systems and crystals.

However, there are several major shortcomings of this approach that complicate its application. First, the exchange–correlation potential  $V_{XC}(\vec{r})$  is unknown, and there are no theoretical clues to its accurate evaluation. The choice of  $V_{XC}(\vec{r})$  is therefore necessarily approximate and may essentially reduce the accuracy of the results. Below we discuss suggestions for this potential. But even if the function  $V_{XC}(\vec{r})$  is known exactly (which is never the case), the physical meaning of the KS orbitals  $\varphi_i(\vec{r})$  and the orbital energies  $\varepsilon_i$  obtained for the artificial non-interacting system and their relation to the real system remains unclear. Without rigorous proof, some authors suggest that the KS orbitals approximately (qualitatively) reflect the situation in the real system, and there are at least two issues to indirectly support this point of view: (1) the sum of the orbital densities after Eq. (5.66) equals the density of the real system, and (2) the energy of the highest occupied orbital  $\varepsilon_{\max}$  equals the ionization potentials with the opposite sign. Although the KS orbitals cannot compete in accuracy and physical meaning with wavefunctions obtained in high-level correlated ab initio calculations, they are better than the HF ones that ignore correlation effects.

Other difficulties in DFT methods are related to spin multiplicity, excited states, and electronic degeneracy, all of which are most relevant to transition metal compounds considered in this book. The spin multiplicity and the excited-state symmetry can be predetermined by means of choosing appropriate spins and symmetries of the KS orbitals. In particular, in the *unrestricted Kohn–Sham* (UKS) approach (similar to the unrestricted HF approach), the total density (5.61) can be presented as a sum of two densities for electrons with the spinup  $\rho_\alpha(\vec{r})$  and spindown  $\rho_\beta(\vec{r})$ , respectively, choosing the number of electrons in these two groups to result in the required total spin and performing the procedure of self-consistency separately for each group with different exchange–correlation potentials  $V_{XC}^\alpha(\vec{r})$  and  $V_{XC}^\beta(\vec{r})$  (see below). Note that in this scheme the multiplicity is taken into account because of the KS approximation; in the rigorous DFT this is not possible because the electron density does not depend on the total spin [5.49]. Also, certain spin states cannot be accounted for with KS orbitals. Similarly, by choosing the  $\varphi_i(\vec{r})$  orbitals as transforming after corresponding IrReps of the symmetry group of the system, one can enforce the DFT minimization procedure to lead to the lowest state with a given symmetry that may be an excited state, provided that its symmetry is different from the ground-state one; excited states with the same symmetry as the ground state cannot be obtained in this way.

More difficulties emerge in application of DFT methods to degenerate and pseudodegenerate states [5.50]. From the very onset DFT assumes that the nuclei are fixed, and this allows one to consider their influence on the electronic system as an external potential. Although the nuclei are never fixed, in many cases their motions are limited to small vibrations, and in these cases the DFT assumption

seems to be a reasonable approximation (still the nuclear motions introduce some inaccuracy even in these cases). However, for degenerate and pseudodegenerate states (Chapter 7), the approach of fixed nuclei is unacceptable, in principle, and the DFT assumption does not hold [5.50]. Indeed, in these cases the adiabatic approximation is invalid (Section 7.1), the electronic and nuclear motions are not separable, and there is no way to present the electron–nucleus interaction as an external potential to the electronic subsystem. Attempts to formulate the HK theorem by presenting the total density as a product of electronic and nuclear densities [5.51] does not solve the problem because, for orbital degenerate states, the wavefunction cannot be presented as a product of the electronic and nuclear wavefunctions (their densities cannot be separated). In the wavefunction presentation the special coupling between the electronic and nuclear motions is considered in the system of coupled equations (7.6); the latter cannot be evaluated in the DFT because the coupling between different electronic states expressed by off-diagonal elements cannot be calculated in the density presentation.

For nondegenerate states that are well separated from the other electronic states, the KS approximation to DFT yields reasonably good results for energies and charge distributions (densities) with much less effort than in the conventional MO LCAO methods with CI (Section 5.3), provided that we know the exchange–correlation potential  $V_{XC}(\vec{r})$ . As mentioned above, the form of this potential is unknown (and, strictly speaking, not rigorously defined). In what follows it is shown how this potential has been approximately modeled.

First, it is convenient to present it as a derivative of the *exchange–correlation energy*  $E_{XC}[\rho]$ , which is a functional of the electron density:  $V_{XC}(\vec{r}) = \partial E_{XC}[\rho]/\partial \rho$ . The physical guess is that the main parts of  $E_{XC}[\rho]$  are the exchange  $E_X$  and correlation  $E_C$  energies with the former predominant. The first choices for the expressions of these energies in electron density approaches can be traced back to the Thomas–Fermi–Dirac (TFD) method applied to atomic and solid-state calculations [5.52]. The TFD method is based on the assumption that the electronic subsystem can be considered as a *uniform electron gas* moving on a positive background of nuclei, so the electron density is constant everywhere and equal to  $n/V$ , where  $V$  is the volume of the system.

For this model it is relatively easy to estimate the exchange and correlation energies (see below). One can approximately visualize constant electron density in an idealized crystal lattice with fixed nuclei and totally free electrons; less physical is the assumption of a uniform electron gas in atoms, and it is hardly acceptable for molecules. In further development of the TFD approach Slater et al. [5.53–5.55] suggested to separate the molecular system into congruent spheres around the atoms in the molecule, assuming different densities inside and outside these spheres, and sewing the in-sphere solutions at the borders between them for continuity. In view of the modern achievements this simple approach (termed  $X_\alpha$  methods) is no more widely used, but the simple idea of constant density is incorporated in the modern DFT methods as the *local density approximation* (LDA). For a variety of  $X_\alpha$  methods, see Refs. 5.54–5.58, including relativistic versions [5.58].



In the LDA the exchange–correlation energy is presented as

$$E_{XC}^{\text{LDA}}[\rho] = \int \rho(\vec{r}) \varepsilon_{XC}[\rho(\vec{r})] d\tau \quad (5.68)$$

where  $\varepsilon_{XC}[\rho(\vec{r})]$  is the exchange–correlation potential of a uniform electron gas of density  $\rho(\vec{r})$  per particle, weighted in Eq. (5.63) with the probability of finding the electron at point  $\vec{r}$ , which is equal to  $\rho(\vec{r})$ . In LDA  $\varepsilon_{XC}[\rho(\vec{r})]$  is presented approximately as a sum of exchange and correlation potentials,  $\varepsilon_{XC}[\rho(\vec{r})] = \varepsilon_X[\rho(\vec{r})] + \varepsilon_C[\rho(\vec{r})]$ , and the exchange part is taken as in the TFD model [5.53]:

$$\varepsilon_X[\rho(\vec{r})] = -\frac{3}{4} \left[ \frac{3\rho(\vec{r})}{\pi} \right]^{1/3} \quad (5.69)$$

With this simple exchange potential of a uniform electron gas  $\varepsilon_{XC}[\rho(\vec{r})]$ , the correlation part in  $\varepsilon_C[\rho(\vec{r})]$  can be evaluated numerically, and then conveniently parameterized and introduced in computer programs. In the UKS approach, mentioned above, the exchange–correlation energy should contain explicitly the densities  $\rho_\alpha(\vec{r})$  and  $\rho_\beta(\vec{r})$  for both spinup and spindown electrons, respectively:

$$E_{XC}^{\text{LDA}}[\rho_\alpha, \rho_\beta] = \int \rho(\vec{r}) \varepsilon_{XC}[\rho_\alpha(\vec{r}), \rho_\beta(\vec{r})] d\tau \quad (5.70)$$

In the LDA this method is then termed *local spin density approximation* (LSD). If  $\rho_\alpha \neq \rho_\beta$ , there is a nonzero total spin and the state is called *spin-polarized*. The spin polarization parameter is defined as

$$\xi = \frac{\rho_\alpha(\vec{r}) - \rho_\beta(\vec{r})}{\rho(\vec{r})} \quad (5.71)$$

It changes from zero (nonpolarized state) to one (fully polarized state) when all the electrons have the same spin.

The LDA seems to be a rough approximation as it is difficult to imagine that the electrons form a uniform gas assumed in the computation of the exchange–correlation potential. Nevertheless, it turns out that for many molecular problems the results obtained by LDA, and especially by LSD, are comparable to or better than those obtained by HF calculations. This is due to the fact that, although LDA employs a simplified exchange potential (5.69), it includes correlation effects that are fully ignored in the HF approximation. However, for such problems as bonding energies and reaction barriers, both HF and LDA are grossly inaccurate.

In further development of DFT methods, attempts were made to expand the presentation of the exchange–correlation energy by including terms that consider the variation in electron density along the molecule. This has been done in the *gradient expansion approximation* (GEA) or in the more advanced *generalized gradient approximation* (GGA) by including gradients of the density  $\nabla\rho$  in the



exchange–correlation potential. In the GGA the latter is taken as

$$E_{XC}^{\text{GGA}}[\rho_\alpha, \rho_\beta] = \int f(\rho_\alpha, \rho_\beta, \nabla\rho_\alpha, \nabla\rho_\beta) \partial\tau \quad (5.72)$$

By separating the exchange and correlation energies,  $E_{XC}^{\text{GGA}} = E_X^{\text{GGA}} + E_C^{\text{GGA}}$ , this leads to the following expression for the exchange potential:

$$E_X^{\text{GGA}} = E_X^{\text{LDA}} - \sum_{\alpha,\beta} \int F(s_{\alpha,\beta}) \rho_{\alpha,\beta}^{4/3}(\vec{r}) \partial\tau \quad (5.73)$$

with

$$s_{\alpha,\beta}(\vec{r}) = \frac{|\nabla\rho_{\alpha,\beta}(\vec{r})|}{\rho_{\alpha,\beta}^{4/3}(\vec{r})} \quad (5.74)$$

and different functions  $F(s)$  for different functionals. For instance, for the so-called Becke functional [5.59]

$$F(s) = \frac{as^2}{1 + 6as(\sinh^{-1} s)} \quad (5.75)$$

while for the Perdew functional [5.60]

$$F(s) = (1 + 1.29s^2 + 14s^4 + 0.2s^6) \quad (5.76)$$

with another function  $s(r)$ :

$$s(\vec{r}) = \frac{|\nabla\rho(\vec{r})|}{(24\pi)^{1/3} \rho^{4/3}(\vec{r})}$$

Many other functionals are used in DFT methods [5.19, 5.45]. In particular, the so-called LYP functional introduced by Lee, Yang, and Parr [5.61] is very popular, often used in combination with the Becke potential described above (the BLYP or B3LYP potential). Distinguished from the other potentials, the LYP one is not based on the uniform electron gas model; instead, it is derived from an expression for the correlation energy in the helium atom. This potential contains one empirical parameter.

It was also shown that time-domain DFT (TDDFT) [5.62], similar to the time-dependent Schrödinger equation (1.3), can handle optical (and other) transition probabilities in spectroscopy.

The most usable functionals are implemented in ready-made DFT programs for electronic structure calculations: ADF [5.63], Ab-init [5.64] (for solids), Siesta [5.65], or as a part of the software mentioned earlier such as Gaussian [5.38], GAMESS [5.39], and MOLPRO [5.40]. Example 5.3 and Problem 5.6 show in detail, step-by-step, how to use these programs to perform DFT calculations of specific TMS.

**EXAMPLE 5.3*****Exercise: Calculation of ZnCl<sub>2</sub> by the DFT Method***

Download and install Firefly (formerly PC-GAMESS) free of charge from the URL <http://classic.chem.msu.su/gran/gamess/index.html> and read the manuals carefully. In order to prepare the input file, it is necessary to know a few basic facts about the molecule to be calculated:

- *Approximate Geometry of the Molecule and Possible Configurations.* In the case of ZnCl<sub>2</sub>, two reasonable geometries can be tried: (1) linear Cl—Zn—Cl and (2) angular (bent) Cl—Zn—Cl. An approximate initial value for the Zn—Cl distance can be obtained from ionic radii:  $d(\text{Zn—Cl}) \approx R(\text{Zn}^{2+}) + R(\text{Cl}^-) = 0.7 + 1.8 = 2.5 \text{ \AA}$ .
- *Total Spin (S) of the Molecule.* Starting with the assumption that ZnCl<sub>2</sub> is an ionic molecule, one finds that both Cl<sup>-</sup> and Zn<sup>2+</sup> are closed-shell ions, so the total spin of ZnCl<sub>2</sub> is  $S = 0$ .
- *An Adequate Computational Model (i.e., a Combination of Method and Basis Set).* This is an advanced topic. As a demonstration, here we use the B3LYP hybrid density functional and relativistic effective core potential (RECP) double-zeta basis set SBKJC.

With these data we perform an initial run for a fixed geometry (usually called *single-point calculation* in the literature) in the linear configuration using the DFT method. An appropriate input deck for Firefly is given below:

```

--- ZnCl2: B3LYP/SBKJC-ECP
$CONTRL SCFTYP=RHF DFTTYP=B3LYP ICHARG=0 MULT=1
      ECP=SBKJC RUNTYP=ENERGY MAXIT=100
$END
$$SYSTEM TIMLIM=2000 MWORDS=20 $END
$GUESS GUESS=HUCKEL $END
$BASIS GBASIS=SBKJC $END

$DATA
--- ZnCl2: linear ---
Dnh 4

Zn      30.0      0.0      0.0      0.0
Cl      17.0      0.0      0.0      2.5
$END

```

(Note: there should be at least one space before each \$.)

In the input above the SBKJC basis is introduced by the keywords ECP=SBKJC (RECP part) and GBASIS=SBKJC (basis part). The type of calculation is restricted (SCFTYP=RHF) because the system is a closed-shell one. The functional is defined by DFTTYP=B3LYP. Another important point is that very few ab initio programs handle full-symmetry groups and are usually restricted to Abelian symmetry. In Firefly all linear molecules are treated using  $D_{4h}$  or  $C_{4v}$  symmetry groups (this does not deteriorate the results).

Read carefully the output of the program and find the symmetry of the ground electronic state. Since the molecule is closed-shell, the label for the calculated ground state of  $\text{ZnCl}_2$  is  $^1 \sum_g^+$ . The calculated energy is  $-256.020520800$  hartrees. It may somewhat differ from the B3LYP/SBKJC results by other programs. There are two reasons for this discrepancy:

- In some of the programs, the local correlation part of B3LYP is defined by VWN5 instead of VWN3. To use VWN5 in Firefly, please define \$DFT B3LYP=GAMESS \$END in the input above.
- Cartesian basis functions are used by default. To use spherical basis functions, just insert D5=.TRUE. into the \$CONTRL namelist.

Now it is time to calculate the equilibrium metal–ligand distance. Use the previous input deck but replace RUNTYP=ENERGY by RUNTYP=OPTIMIZE. Run the calculation and find the metal–ligand distance (you can search the phrase EQUILIBRIUM GEOMETRY LOCATED). The solution is  $R = 2.132 \text{ \AA}$ .

Next, we have to check whether the molecule is linear or angular. To do so, we write an input deck to optimize the angular configuration. Change the DATA block in the geometry optimization input given above to

```
$DATA
--- ZnCl2: bent ---
Cnv 2

Zn   30.0   0.0       0.0       0.0
Cl   17.0   0.0       1.7       1.7
$END
```

In this input an initial angle of  $90^\circ$  has been introduced. Run the program and find the final geometry. The calculation should converge back to the linear configuration minimum.

**EXAMPLE 5.4*****Exercise: Ab initio Calculation of the Electronic Structure of  $MnO_4^-$  Square-Planar, Tetrahedral, and Square-Based Pyramidal Configurations***

Download the programs from packages GAMESS (free of charge) or MOLPRO (trial version for one month free) aimed at electronic structure calculation and geometry optimization of molecular systems, and read the manuals. We perform here ab initio calculations of the ground state energies, wavefunctions, and equilibrium geometry (interatomic distances and angles) of  $MnO_4^-$  in square-planar, square-base pyramidal, and tetrahedral configurations in a simple, Hartree–Fock approximation with the basis set lan12dz. For similar calculations in other approximations see Problems 5.4–5.7.

The inputs for performing the requested tasks using MOLPRO are given below (they are similar in different programs). The input is built employing the following steps.

- *Geometry.* In order to input the geometry with adequate constraints for each case (square, tetrahedron, and pyramid) it is necessary to use a  $z$ -matrix. The  $z$ -matrix format ([http://en.wikipedia.org/wiki/Z-matrix\\_\(chemistry\)](http://en.wikipedia.org/wiki/Z-matrix_(chemistry)), <http://chemistry.umeche.maine.edu/Modeling/GGZmat.html>) allows us to introduce the geometry of the molecule without defining its position or orientation in space, which does not influence its internal energy in vacuum. The logic behind the  $z$ -matrix of each particular case is as follows:
- *Square-planar geometry.* Mn is placed first and then the oxygens are placed in turn. The first oxygen only requires the input of the metal–ligand distance (rml); the second one has the same (rml) and the O–Mn–O angle of  $90^\circ$ . The third and fourth oxygens are placed accordingly. In order to obtain a planar configuration, a dihedral angle of  $0^\circ$  or  $180^\circ$  for these ions is then used.
- *Tetrahedral geometry.* As in the previous case, Mn is placed first and then all oxygens are placed at the metal ligand distance (rml). For the first oxygen ion only the metal–ligand distance is needed. The other three will form a O–Mn–O angle (tang) with this oxygen equal to the tetrahedral angle,  $109.471^\circ$ . For the second oxygen only rml and tang are needed, while the third and fourth require dihedral angles (Mn–O1–O2–(O3, O4)) equal to  $+120^\circ$  and  $-120^\circ$ , respectively.

- *Pyramidal geometry.* For this geometry configuration it is convenient to define a *dummy atom*, as a reference point that does not affect the calculation in any other way. First we place the dummy atom with the Mn one at an arbitrary distance to it (rdummy). Then we place all oxygens forming a dummy–Mn–O angle (ang) that will be optimized during calculation and at a particular metal–ligand distance (rml). The dihedral atoms (dummy–Mn–Ox–Oy) will usually be  $+90^\circ$ ,  $-90^\circ$  or  $180^\circ$  depending on our particular definition.

We should properly define all the equivalent geometrical parameters (such as, the metal ligand distance) because this will be important in the performance of geometry optimization.

The next step is to include the basis set. Usually, ab initio programs internally store the most usable basis sets, but this is not always the case (e.g., MOLPRO does not have the Mn atom for the 6-31G\* basis set). For these cases the basis set can be retrieved from original papers or data bases on the internet (e.g., <https://bse.pnl.gov/bse/portal>).

It is then necessary to define the method of calculation and the assumed electronic state for the molecule. Check the manual of the program and include the method of calculation in the input. Different programs use different methods to define the electronic state of the molecule. In many cases only the total charge of the molecule and the spin multiplicity are needed (GAUSSIAN, GAMESS), while in other cases it is necessary to enter the number of electrons, the symmetry of the electronic state, and the total spin (MOLPRO). Depending on the program you are using, enter these quantities in the proper format. When counting the number of electrons in MOLPRO take into account that the lan12dz basis has a pseudopotential describing the core electrons; as a consequence, the Mn atom simulated in this basis set has fewer electrons than the real atom.

Finally, we should request that the program perform geometry optimization, that is to say, the program must look for the minimum energy under the geometry constraints of the input assumed in this problem. In a more general formulation, it is not necessary to input these geometry constraints and allow the program to find the global minimum of the APES (this requires longer computer time). From the results of the calculations below, the geometry optimization without constraint is expected to yield the pyramidal configuration.

*Input, square-planar geometry:*

```

***,MnO4-, HF/lanl2dz square planar
ro=1.52 Angstrom; ! the initial metal ligand distance
rdummy=1; ! this is an arbitrary number
ang=90.0; ! O-Mn-O angle
died=90.;

geometry={Q1;
          Mn,Q1,rdummy;
          O1,Mn,rml,Q1,ang;
          O2,Mn,rml,Q1,ang,O1,died;
          O3,Mn,rml,Q1,ang,O1,-died;
          O4,Mn,rml,Q1,ang,O2,died}
basis=lanl2dz; ! definition of the basis set
{rhf; ! the method employed for calculation
wf,46,1,0} ! the state definition, number of electrons
! (in lanl2dz there are less
electrons than in the real atom)
! irreducible representation of the
wavefunction
! Ag (closed shell) and S=0
{optg; ! geometry optimization
active,rml} ! only varies metal ligand and angle

```

*Input, tetrahedral geometry:*

```

***,MnO4-, HF/lanl2dz tetrahedral
rml=1.80 Angstrom; ! the initial metal ligand distance
tang=109.471; ! the tetrahedral
angle died=120.;
geometry={Mn;
          O1,Mn,rml;
          O2,Mn,rml,O1,tang;
          O3,Mn,rml,O1,tang,O2,died;
          O4,Mn,rml,O1,tang,O2,-died}
basis=lanl2dz;
{rhf; ! the method employed for calculation
wf,46,1,0} ! the state definition, number of electrons

! (in lanl2dz there are less
electrons than in the real atom)
! irreducible representation
of the wavefunction
! Ag (closed shell) and S=0
{optg; ! geometry optimization
active,rml} ! only varies metal ligand and angle

```

*Input, square-base pyramidal geometry:*

```

***,MnO4-, HF/lanl2dz pyramidal
rml=1.84 Angstrom; ! the initial metal ligand
                    distance
rdummy=1;          ! this is an arbitrary number
ang=130.0;         ! the initial rdummy-Mn-O angle
died=90.;         ! required to form a square-based pyramid
geometry={Q1;      ! dummy atom, useful to
                    generate the geometry
          Mn,Q1,rdummy;
          O1,Mn,rml,Q1,ang;
          O2,Mn,rml,Q1,ang,O1,died;
          O3,Mn,rml,Q1,ang,O1,-died;
          O4,Mn,rml,Q1,ang,O2,died}
basis=lanl2dz;    ! definition of the basis set
{rhf;            ! the method employed for
                  calculation
wf,46,1,0}       ! the state definition,
                  number of electrons
                  ! (in lanl2dz there are less
                  electrons than in the real
                  atom)
                  ! irreducible representation of
                  the wavefunction
                  ! Ag (closed shell) and S=0
{optg;          ! geometry optimization
active,rml,ang} ! only varies metal
                  ligand and angle

```

*Results:* Numerical results for the three configurations of MnO<sup>-</sup> obtained using MOLPRO are shown in the following table:

Configu- ration	Method	Basis	Angle		Energy (a.u.)
			rml (Å)	Dummy-Mn-O (degree)	
Square	Hartree- Fock	lanl2dz	1.839	—	-401.27643354
Tetrahedral	Hartree- Fock	lanl2dz	1.741	—	-401.42029498
Pyramidal	Hartree- Fock	lanl2dz	1.862	127.6	-401.48106362

The HF/1an12dz calculations predict that all three conformations are stable and that the pyramidal is significantly lower in energy. Further comparison with other methods/basis sets are given in Problems (solutions) 5.4–5.6.

In conclusion, we note that, strictly speaking, the DFT methods based on KS equations are just a form of MO LCAO methods in which the calculations are simplified by introducing special potentials instead of very complicated wavefunctions. This simplification is not without cost; part of the information about the properties of the system is lost. DFT methods are convenient, practical tools for essentially simplifying calculations of electronic structure of molecular systems, especially when the ground-state energy and electronic densities are sought for and the nuclear dynamics can be ignored. The scaling properties of DFT proportional to  $n^3$  instead of  $n^4$  in the wavefunction methods (Section 5.3) make it favorable for considering large molecular systems that cannot be treated by multideterminant methods. Less rigorous in general but still often practically acceptable are results on DFT calculations of some (restricted types of) excited states and spin multiplicities, while the whole approach is questionable (or unacceptable) in the presence of electron degeneracy or pseudo-degeneracy. Examples 5.2–5.4 are Problems (solutions) 5.4–5.7 provide further discussion and comparisons of different numerical methods of electronic structure calculation.

### Relativistic Approaches

One of the most essential differences between the methods of electronic structure calculation for transition metal heavy-atom compounds and those for organic or simple inorganic molecules is in the necessity to factor in the relativistic effects in the former, whereas they can often be neglected in the latter. For years relativistic effects were considered as relativistic correction to nonrelativistic calculations mainly by factoring in the spin–orbital interaction as a perturbation. This is unacceptable in more accurate calculations. For instance, for the atoms of the third transition period the spin–orbital interaction is of the same order of magnitude as or larger than the interelectron and interatomic (chemical) interactions. For this reason, in heavy-atom compounds there is no sense to calculate the electronic terms and chemical bonding without relativistic effects and/or to account for the spin–orbital interactions as a perturbation, as is done for most light-atom molecules. Extensive developments of relativistic electronic structure calculations in molecules began in the 1970s, although atomic systems were explored much



earlier. The latest achievements in this area can be found in several review publications [5.66–5.69].

Relativistic effects in chemical properties of atoms are considered in Section 2.1, and the results obtained there are also used in Section 6.5 in the discussion of chemical bonding. Here in this section we consider briefly some semiquantitative methods of relativistic electronic structure calculation of coordination compounds. In the next section semiempirical relativistic methods are also briefly discussed.

At present the relativistic calculations of transition metal compounds are rather semiquantitative. In a rigorous formulation the relativistic SCF MO LCAO equations are complicated. The main distinction from the nonrelativistic formulation lies in the use of the relativistic Dirac Hamiltonian for one-electron operators, in which the velocity of the electrons  $v$ , assumed to be comparable with the light velocity  $c$ , is taken into account explicitly. For the operator of the interelectron interactions the classical expression without relativistic effects is generally used; this does not introduce considerable inaccuracies except for small spin–spin interactions. Thus, for the Dirac Hamiltonian we have [5.43] (cf. Eq. (2.11))

$$H = \sum_i [\alpha_i c \mathbf{p}_i + mc^2 \beta_i + V(i)] + \sum_{i,j}' \frac{e^2}{r_{ij}} \quad (5.77)$$

where the summation is performed over all the electrons,  $m$  is the mass of the electron,  $\mathbf{p} = -i\hbar\nabla$  is the operator of the momentum;  $V(i) = -\sum_{\alpha} Z_{\alpha} e^2 / R_{i\alpha}$ ,  $\sum_{i,j} e^2 / r_{ij}$  are the Coulomb electron–nuclei and interelectron interactions, respectively; and  $\alpha_i$  and  $\beta_i$  are fourth-rank Dirac matrices given by Eqs. (2.12)–(2.14).

As indicated in Section 2.1, the relativistic Hamiltonian (5.77) has a matrix four-component form. The solutions of the Dirac equation with this Hamiltonian are also four-component one-electron functions—bispinors  $\Psi$  composed of two spinors [Eq. (2.15)]—and they obey the conditions (2.16) and (2.17). The fourth-rank matrix equation that determines the one-electron bispinor  $\Psi(i)$  is

$$\begin{aligned} \alpha_1 c \mathbf{p}_1 + mc^2 \beta_1 + V(1) + \sum_k \int \Psi_k^+(2) \frac{e^2}{r_{12}} (1 - P_{ik}) \Psi_k(2) d\tau_2 \Psi_i(1) \\ = E_i \Psi_i(1) \end{aligned} \quad (5.78)$$

where  $\Psi^+$  is the transposed bispinor  $\Psi$ .

Solving this equation by the MO LCAO self-consistent procedure, one can, in principle, obtain relativistic SCF MO LCAO ab initio solutions. However, this is a complicated procedure. A simplification can be reached in the *quasirelativistic approach* (QRA), where it is assumed that at least for the valence electrons

the relativistic effects can be accounted for approximately up to terms of the order  $(v/c)^2$ , inclusively. Simple estimates show that in the region of the valence electrons higher powers in  $v/c$  are small and can be neglected, confirming the validity of the QRA.

In the quasirelativistic approximation [5.43, 5.70] (see also Section 2.1) the wavefunction can be presented by only one two-component spinor  $\varphi_i(j)$  because the second one, in Eq. (2.15),  $\chi_i(j)$ , is of the order of  $(v/c)^2$  and hence yields higher-order smallness in the energy. In the MO LCAO approximation  $\varphi_i$  should be presented as a linear combination of the atomic spinors  $\Phi_j$  [5.71]

$$\varphi_i = \sum_j c_{ij} \Phi_j \quad (5.79)$$

Performing the calculations of the matrix elements  $H_{ij}$  of the secular equation (5.8) with the functions (5.79), one comes to the following formulas [cf. Eq. (5.48)]:

$$H_{ij}^R = H_{ij}^{0R} + I_{ij}^R - K_{ij}^R \quad (5.80)$$

where the quasirelativistic expressions for  $H_{ij}^{0R}$ ,  $I_{ij}^R$ , and  $K_{ij}^R$  are rather different from the nonrelativistic ones [5.76]:

$$H_{ij}^{0R} = H_{ij}^0 + \left\langle i \left| -\frac{p^4}{8m^3c^2} + \frac{\hbar^2 \Delta V}{8m^2c^2} + \frac{\hbar \sigma [\nabla V, \mathbf{p}]}{4m^2c^2} \right| j \right\rangle \quad (5.81)$$

$$I_{ij}^R = I_{ij} + \frac{\hbar}{2m^2c^2} \sum_{k,l} P_{kl} \langle \langle ik | \sigma_1 [\nabla_1 r_{12}^{-1}, \mathbf{p}_1] | lj \rangle \rangle \quad (5.82)$$

$$K_{ij}^R = K_{ij} + \frac{\hbar}{2m^2c^2} \sum_{k,l} P_{kl} \langle \langle ik | \sigma_1 [\nabla_1 r_{12}^{-1}, \mathbf{p}_1] | jl \rangle \rangle \quad (5.83)$$

Here  $\langle \langle ik | |lj \rangle \rangle$  means integration over  $r_1$  with the spinors  $k$  and  $l$ , and over  $r_2$  with the spinors  $i$  and  $j$ .

As one can see, the QR formula for the matrix elements in the MO LCAO method contains the usual nonrelativistic terms ( $H_{ij}^0$ ,  $I_{ij}$ , and  $K_{ij}$ , respectively) plus relativistic additions. The physical meaning of all these terms can be revealed by comparison with the relativistic terms which emerge in atomic calculations [5.43]. Similar to the atomic case, three types of relativistic corrections can be distinguished:

1. The term  $\sim p^4$ , the contribution of the *electron mass dependence on speed*
2. The term  $\sim \Delta V$ , the *Darwin interaction*, which has no classical interpretation
3. Terms proportional to the Pauli matrices  $\sigma$ , the *spin-orbital interaction*

As seen from Eqs. (5.81)–(5.83), the part  $H_{ij}^{0R}$  denoting the kinetic energy and the interaction with the core (nuclei), contains all three kinds of relativistic corrections, while the Coulomb  $I_{ij}^R$  and exchange  $K_{ij}^R$  interaction terms contain the correction on spin–orbital interaction only.

Note that the matrix elements (5.81)–(5.83) must be calculated by two-component spinors (all operators are  $2 \times 2$  matrices; where not explicitly noted, a  $2 \times 2$  unit matrix is implied). The latter depend on the basis set. The atomic basis function  $\Phi$  is an eigenfunction of the operator of the square of the total momentum  $J^2$  and its projection  $J_Z$ , and therefore  $\Phi$  is dependent on additional quantum numbers  $l, j, M$  (Sections 2.1 and 2.2):

$$\Phi_{l_j M}(\mathbf{r}, \beta) = \begin{pmatrix} \Phi_{l_j M}^1 \\ \Phi_{l_j M}^2 \end{pmatrix} = R_{l_j}(\mathbf{r}) Y_{l_j M}(\theta, \phi, \beta) \quad (5.84)$$

Here  $R_{l_j}(r)$  is a relativistic radial function, and  $Y_{l_j M}(\theta, \phi; \beta)$  is a spherical spinor that can be presented as an expansion over spherical functions  $Y_{lm}(\theta, \phi)$  [5.70]:

$$Y_{l_j M}(\theta, \phi, \beta) = \sum_{m, \mu} \langle l m \frac{1}{2} \mu | j M \rangle Y_{lm}(\theta, \phi) q_{\mu}(\beta) \quad (5.85)$$

where  $q_{\mu}(\beta)$  is the function of the spin argument  $\beta$ , its two values realizing the two components of the spinor, and  $\langle l m \frac{1}{2} \mu | j M \rangle$  is the corresponding Clebsh–Gordan coefficient. With the functions (5.84) and (5.85) the matrix elements (5.81)–(5.83) are reduced to linear combinations of integrals calculated by the usual spherical functions  $Y_{lm}(\theta, \phi)$  and relativistic radial functions  $R_{l_j}(\mathbf{r})$ .

Since in the relativistic case the spin-orbital interaction is strong and the  $j$ – $j$  coupling scheme is valid (Section 2.2), the multielectron states should be classified by the total momentum  $J$ , and *the MOs belong to the irreducible representations of the double point groups* (Section 3.5). The additional terms of relativistic corrections can be calculated in the same approximation as the non-relativistic terms. The QRA also allows semiempirical simplifications (see the next section).

At present several methods of relativistic electronic structure calculations are worked out and used in practice [5.66–5.69, 5.71–5.77], including all-electron fully relativistic ab initio calculations [5.73], ECP relativistic and quasirelativistic calculations and other pseudopotential approaches [5.74–5.77], relativistic and quasirelativistic density-functional approaches [5.78–5.80], as well as semiempirical realizations [5.71, 5.81] (see also Sections 5.5 and 6.5).

## 5.5. SEMIEMPIRICAL METHODS

Besides the semiquantitative approaches discussed in the previous section, semiempirical methods are widely used in practice in order to simplify electronic

structure calculations. In the semiempirical MO LCAO methods the main idea is to substitute as many as possible integrals in the matrix elements  $H_{ii}$  and  $H_{ij}$  of Eqs. (5.7) and (5.8) by empirical parameters. Among these methods one can distinguish two groups that differ as to whether they neglect the overlap integrals.

### Zero-Differential Overlap (ZDO)

The ZDO approach was first suggested independently by Pople, and Pariser and Parr for  $\pi$ -electron systems (see Refs. 5.82–5.88 and references cited therein). It assumes that the overlap of different atomic functions  $\psi_i$  and  $\psi_j$  for any elementary volume—the *differential overlap*—equals zero:

$$\psi_i(\mathbf{r})\psi_j(\mathbf{r})d\tau = 0 \quad i \neq j \quad (5.86)$$

In this approximation all integrals of the type  $[ij|kl]$  in Eqs. (5.48) and (5.51) are zero, except for  $i = j$  and  $k = l$ . This means that all the three- and four-center integrals are zero, the interelectronic interaction is described by the two-center integrals of the type  $[ii|kk]$ , and the overlap integrals

$$S_{ij} = \int \psi_i^*(\mathbf{r})\psi_j(\mathbf{r})d\tau = 0.$$

Logically, the assumption (5.86) leads to the conclusion that the resonance integral  $H_{ij}^0 = \int \psi_i^* H^0 \psi_j d\tau$  for  $i \neq j$  is also zero, but this gives completely unacceptable results. Therefore, in the ZDO methods, it is assumed that  $H_{ij}^0 \neq 0$  for  $i$  and  $j$  from the same or near-neighbor atoms.

At first sight the assumption (5.86) and its inconsistent repudiation when calculating  $H_{ij}^0$  seem to introduce rough approximations. Nevertheless, the ZDO approaches proved to be quite efficient in concrete calculations yielding satisfactory results for simple systems. Afterward the method was given additional grounds that also allowed one to clarify the nature of the assumption (5.86) and the limits of its validity, and to obtain quantitative relationships for the resonance integral [5.83]. It was shown that the ZDO formulas are valid when neglecting  $S^2$ , where  $S$  is the overlap integral. More accurate expressions in these methods can be obtained by using the so-called orthogonalized basis [5.84] for the calculation of matrix elements.

In electronic structure calculations of transition metal compounds, the ZDO method, called *complete neglect of differential overlap* (CNDO), may be useful. In this method in the secular equation (5.8):

- All the overlap integrals are zero.
- The diagonal matrix elements  $H_{ii}$  are taken from empirical data (see below).
- The off-diagonal core integrals  $H_{ij}^0$  with  $i \neq j$  are taken proportional to the overlap integrals  $S_{ij}$  when  $\psi_i$  and  $\psi_j$  are from near-neighbor atoms, and zero otherwise.

- The electron interaction integrals obey the condition

$$[ij|kl] = \gamma_{ik}\delta_{ij}\delta_{kl} \quad (5.87)$$

where hereafter the following denotation is used:

$$\gamma_{ik} = [ii|kk] \quad (5.88)$$

Under these conditions all the three- and four-center integrals vanish, and the matrix element of the SCF MO LCAO method (5.48) is significantly simplified.

However, as shown by direct calculations [5.82], in this approximation the results are not invariant with respect to the choice of the local coordinate systems on the atoms. In other words, the results of the calculations depend on the orientations of nonsymmetric atomic functions ( $p, d, f, \dots$ ) of a given atom with respect to the others (which is quite understandable because we neglect the angular dependent overlap between them), and this unacceptable feature is inherent to all the methods based on ZDO.

To overcome this principal difficulty, it was suggested [5.82] that all the electron repulsion integrals that depend on orientation be taken equal to each other and to the one calculated with spherical symmetric  $s$  functions that do not depend on orientation. In this approximation the repulsion integrals  $\gamma_{ij}$  depend on the type of atom, but not on its state. For instance, for the  $A$  atom  $\gamma_{ii} = \gamma_{AA}$  for all the  $i$  labels, and for diatomic integrals of the atoms  $A$  and  $B$   $\gamma_{ij} = \gamma_{AB}$  for all  $i$  and  $j$ . This results in further simplification of the matrix elements  $H_{ij}^0$  [recall Eq. (2.50):  $H^0 = H_A^0 - \sum_{B \neq A} U_B$  with  $H_A^0 = T_A - U_A$ , where  $T$  is the kinetic energy and  $U$  is the interaction with the nucleus):

$$\int \psi_{iA}^* H_A^0 \psi_{jA} d\tau = \varepsilon_i^A \delta_{ij} \quad (5.89)$$

$$\int \psi_{iA}^* U_B \psi_{jA} d\tau = U_B^A \delta_{ij} \quad (5.90)$$

and for near-neighbor atoms  $A$  and  $B$

$$\int \psi_{iA}^* H^0 \psi_{jB} d\tau = \beta_{AB}^0 S_{ij} \quad (5.91)$$

where  $\varepsilon_i^A$  characterizes the corresponding atomic orbital energy in the state  $\psi_i^A$  and  $\beta_{AB}^0$  is an empirical parameter. Denoting the valence electron density on the atom  $A$  by  $P_{AA} = \sum_k P_{kk}$  [cf. Eq. (5.21)], we obtain the following final expressions for the matrix elements of the CNDO method:

$$H_{ii}^{AA} = \varepsilon_i^A + \left( P_{AA} - \frac{P_{ii}}{2} \right) \gamma_{AA} + \sum_{B \neq A} (P_{BB} \gamma_{AB} - U_B^A) \quad (5.92)$$

$$H_{ij}^{AB} = \beta_{AB}^0 S_{ij} - \frac{P_{ij} \gamma_{AB}}{2} \quad (5.93)$$

$$H_{ij}^{AA} = -\frac{P_{ij}\gamma_{AA}}{2} \quad (5.94)$$

The empirical parameters  $\varepsilon_i^A$  and  $\beta_{AB}^0$  are taken as follows.  $\varepsilon_i^A$  is obtained from the relation

$$-I_{0i}^A = \varepsilon_i^A + (Z_A - 1)\gamma_{AA} \quad (5.95)$$

where  $I_{0i}^A$  is the corresponding ionization potential, while  $\beta_{AB}^0 = (1/2)(\beta_A^0 + \beta_B^0)$  [cf. Eq. (5.101)], and  $\beta_A^0$  and  $\beta_B^0$  are atomic parameters taken, for example, from the data of more accurate MO LCAO calculations for systems containing the corresponding atom.

Another choice of parameters is suggested in the modification of the CNDO method called CNDO/2 (as distinct from the abovementioned CNDO/1 method). In CNDO/2 it is assumed that  $U_B^A = Z_B\gamma_{AB}$ , while  $\varepsilon_i^A$  is taken from a relation that is somewhat different from (5.95):

$$-(I_{0i}^A + A_i) = \varepsilon_i^A + (Z_A - \frac{1}{2})\gamma_{AA} \quad (5.96)$$

where  $A_i$  is the corresponding electron affinity.

Thus in the CNDO methods only the overlap integrals  $S_{ij}$  and simple repulsion integrals with  $s$  functions,

$$\gamma_{AA} = e^2 \int s_A^2(\mathbf{r}_1)s_A^2(\mathbf{r}_2)r_{12}^{-1} d\tau_1 d\tau_2 \quad (5.97)$$

and

$$\gamma_{AB} = e^2 \int s_A^2(\mathbf{r}_1)s_B^2(\mathbf{r}_2)r_{12}^{-1} d\tau_1 d\tau_2 \quad (5.98)$$

should be calculated; in CNDO/1 the integral

$$U_B^A = Z_B e^2 \int s_A^2(\mathbf{r})|\mathbf{r} - \mathbf{R}|^{-1} d\tau \quad (5.99)$$

is also to be computed. The other magnitudes  $\varepsilon_i^A$  and  $\beta_{AB}^0$  are taken from empirical data.

The CNDO method, described above, contains some essentially restricting approximations that are especially significant in application to transition metal compounds. In particular, when the ZDO (5.86) is applied to two different orbitals of the same center, the integrals of exchange interactions between the intraatomic electrons is neglected. Meanwhile they may reach  $\sim 4-5$  eV.

If the basis of atomic functions contains no more than one function per atom (as, e.g., in  $\pi$ -electron approximation for conjugated organic molecules), there are no such integrals. But if there are several functions per atom in the basis set (for

a transition metal atom, as mentioned above, there are usually nine), the neglect of one-center repulsion integrals may be a source of considerable error. To avoid this, a version of ZDO can be employed, in which the approximation (5.86) is applied only to the pairs of orbitals from different atoms, whereas the product of functions  $\psi_{iA}(\mathbf{r})\psi_{jA}(\mathbf{r})$  from the same atom is considered nonzero, and the corresponding integrals with these products are calculated explicitly or approximated by parameters. This method of calculation, called *neglect of diatomic differential overlap* (NDDO), results in significant increase in the volume of calculations, as compared with CNDO.

Another difficulty with CNDO methods is the abovementioned necessity to introduce the same spherical symmetric (*s*-type) electronic cloud distribution for all the electrons (*p*, *d*, *f*, ...). For molecules containing only light (first-row) atoms, this circumstance is not very restricting because the averaged electron distribution in the  $2p$  state does not differ very much from that of the  $2s$  state. But for transition metals and rare-earth elements this simplification becomes unacceptable because of the significant differences in the electron distributions of *s*, *p*, *d*, and *f* orbitals.

In the *multicenter ZDO* (MCZDO) method [5.86], this difficulty is partly overcome while preserving the advantages of the NDDO method as compared with the CNDO one. Distinct from the latter, in the MCZDO method (1) the ZDO approximation (5.86) is not applied to the core integrals  $H_{ij}^0$  and to the one-center integrals of interelectron repulsion; (2) the ZDO approximation is applied to all the other multicenter electron repulsion integrals:  $[ij|kl] = \gamma_{ik}\delta_{ij}\delta_{kl}$  for *i* and *j* on different atoms; (3) averaged two-center repulsion integrals are different for different types of electrons; that is, instead of two integrals  $\gamma_{AA}$  and  $\gamma_{AB}$  of the CNDO method the following are introduced:  $\gamma_{ss}$ ,  $\gamma_{sp^*}$  (interaction of *s* cloud with the averaged *p* distribution denoted by  $p^*$ ),  $\gamma_{sd^*}$ ,  $\gamma_{p^*p^*}$ ,  $\gamma_{p^*d^*}$ ,  $\gamma_{d^*d^*}$ ,  $\gamma_{sf^*}$ , and so on.

There are also modified CNDO methods aimed at electronic structure calculations for systems with open shells. *Intermediate neglect of differential overlap* (INDO) [5.89] and *modified INDO* (MINDO) [5.90] methods, in the version for coordination compounds [5.88, 5.91], are based on the scheme of the unrestricted Hartree–Fock (UHF) method (Section 5.3), in which each electron is described by its own orbital function (the two electrons with opposite spins on the same orbital of the restricted HF method occupy different orbitals in the UHF method), and on the NDDO approximation, in which the interatomic overlap only is neglected (whereas the intraatomic one is included). However, unlike the NDDO method, the INDO approximation assumes the two-center integrals of interelectronic interaction  $[i^A j^A | k^B l^B] = 0$  if  $A \neq B$ ,  $i \neq j$ , and  $k \neq l$ . This simplifies the otherwise rather complicated calculations of the NDDO method, but it still accounts for the main part of electron interactions on each center (including the exchange interaction) that determine the spin states. The one-center interelectron interactions can be approximated by Slater–Condon parameters (Section 2.2).

Semiempirical methods of electronic structure calculations oriented toward TMS are implemented in a software package called ZINDO [5.91].

### Extended Hückel (Hoffmann) Method

The simplest *Hückel method*, where the overlap integrals  $S_{ij}$  in the secular equation of the MO LCAO method (5.8) are taken equal to zero and the matrix elements are substituted by empirical parameters, having some value in application to organic molecules, is invalid for coordination compounds. If ignoring  $S_{ij}$ , one loses the specific role of (the electron heterogeneity introduced by) the  $d$  electrons in the electronic structure. In ZDO methods targeting coordination compounds—for instance, in INDO, this deficiency is compensated for by the difference in the corresponding electron repulsion integrals. The *extended Hückel* (EH) and the related *iterative EH* (IEH), or the *self-consistent charge and configuration* (SCCC) *method*, avoid this fault by considering explicitly the overlap integrals in Eq. (5.8). On the other hand, these methods, unlike the ZDO ones, are completely semiempirical in the sense that all the matrix elements in (5.8) are substituted by empirical parameters and overlap integrals  $S_{ij}$ ; the latter are thus the only computed magnitudes.

In the EH approximation the empirical presentation of the matrix elements is as follows [5.92]:

$$H_{ii} = -I_i \quad (5.100)$$

$$H_{ij} = \frac{k}{2}(H_{ii} + H_{jj})S_{ij} \quad (5.101)$$

where  $k$  is a numerical coefficient, which in simple cases is taken equal to 1.67 for  $\sigma$  bonds and 2 for  $\pi$  bonds (see below), and  $I_i$  is the energy of ionization of the atomic  $i$ th state. The presentation of the diagonal matrix element  $H_{ii}$  by the corresponding ionization potential goes back to the simple Hückel method, while formula (5.101) for the off-diagonal element  $H_{ij}$  was first used in calculations of transition metal complexes by Wolfsberg and Helmholz [5.92] and widely demonstrated in calculations of organic molecules by Hoffmann [5.93].

It can be shown that Eqs. (5.100) and (5.101) are of the same level of approximation as the semiquantitative expressions (5.58) for the matrix element of the effective Hamiltonian; they differ mainly by the last term in (5.58), often called *crystal field corrections*. The latter improve the interatomic core interactions and were also introduced in the semiempirical calculations (see below).

Presentations (5.100) and (5.101) were significantly improved by introducing the dependence of the  $I_i$  values on the atomic and orbital charges and the requirement of self-consistency with respect to these charges [5.93]. Consider the diagonal element of the Hamiltonian starting with expression (5.58),  $H_{ii}^{AA} = \varepsilon_i^A - \sum_{\mu \neq A} e^2(Z_\mu - q_\mu)/R_{A\mu}$ . Here  $\varepsilon_i^A$  has the physical meaning of the orbital energy of the electron in the valence state of atom  $A$  in the molecule, that is, when the atom has a certain charge and electron population distribution over the atomic states participating in the formation of the MO. In other words,  $\varepsilon_i^A$  is the  $i$ th-state ionization energy in a specific configuration of other electrons, usually called *energy of ionization of the valence state* (EIVS):  $\varepsilon_i^A = -I_i[A]$ ,



where  $[A]$  denotes the corresponding electron configuration of  $A$  (a less accurate notation of this value is also in use: *valence orbital ionization potential* (VOIP)).

The effective charge of the other atoms is  $Z_\mu - q_\mu$ , where  $q_\mu = \sum_{i,v} q_i c_{i\mu} c_{iv} S_{\mu v}$  is the Mulliken total electronic charge on the  $\mu$  atom after Eq. (5.20). However, this formula does not account for the fact that the screening of the nuclei by the charge  $q_\mu$  is not complete. Therefore, the effective charges of the  $\mu$  atoms should be taken with a correction constant  $k_\lambda$  that depends on the kind of bonding between  $A$  and  $\mu$  produced by the  $i$ th function ( $\lambda = \sigma, \pi, \delta, \dots$ ). With this correction

$$H_{ii}^A = -I_i[A] - e^2 \sum_{\mu \neq A} \frac{Z_\mu - q_\mu + k_\lambda}{R_{\mu A}} \quad (5.102)$$

In general, EIVS is different from the corresponding ionization energy of the neutral atom because in the valence state the atom may have a considerable charge, and the population of the  $s, p, d, f$  orbitals are altered by MO formation. These effects are obviously much more significant for coordination compounds than for organic molecules. To account for the dependence of ionization energy on the atomic charge, Hoffmann suggested a linear correlation:

$$I_i^A = I_{0i}^A + aq^A \quad (5.103)$$

where  $I_{0i}^A$  is the ionization potential of the neutral atom and  $q^A$  is the atomic charge (the constant  $a$  can be obtained by comparison of  $I_i^A$  with one of the next ionization potentials; see below).

The crystal field corrections in the second term in (5.102) are also more important for coordination compounds than for organic molecules because the latter have much smaller atomic charges. These corrections are even more important when the coordination system is in a crystal lattice, where they are summarized into the *Madelung potential*, which includes the electrostatic field of all the ions of the lattice that influence the one under consideration.

Similar corrections should be introduced in the off-diagonal matrix elements (5.53). For semiempirical calculations, several other than (5.101), but generally equivalent, presentations of the off-diagonal element were suggested (Table 5.7). Numerical estimates show that very often all these presentations yield close results [5.99].

### Iterative Extended Hückel Method

The iterative EH (IEH) method [sometimes also called the *self-consistent charge and configuration* (SCCC) MO LCAO method] is an extension (improvement) of the EH approach important to calculation of electronic structure of coordination compounds. The essence of this improvement is to introduce a self-consistent procedure with respect to the atomic charges and electronic configuration. Indeed, the matrix elements  $H_{ii}$  and  $H_{ij}$  in Eqs. (5.100)–(5.102) contain those charges

**TABLE 5.7. Different Presentations of Off-Diagonal Matrix Element of Hamiltonian  $H_{ij}$  by Diagonal Elements ( $U_{ii}$  and  $H_{jj}$ ) and Overlap Integral  $S_{ij}$  in Semiempirical Methods**

Authors	$H_{ij}$
Wolfsberg and Helmholz	$kS_{ij}(H_{ii} + H_{jj})/2$
Ballhausen and Gray	$-kS_{ij}(H_{ii}H_{jj})^{1/2}$
Cussacs	$(2 -  S_{ij} )S_{ij}(H_{ii} + H_{jj})/2$
Erraneous	$kS_{ij} \cdot 2H_{ii}H_{jj}/(H_{ii} + H_{jj})$
Morokuma and Fukui	$S_{ij}[(H_{ii} + H_{jj})/2 + k]$
Neuton et al.	$T_{ij} + S_{ij}(U_{ii} + U_{jj})/2$

Source: McGlynn et al. [5.94].

<sup>a</sup> $U_{ii}$  is the matrix element of the potential energy; if the virial theorem holds,  $U_{ii} \approx 2H_{ii}$ .

and configurations that depend on LCAO coefficients, which, in turn, depend on  $H_{ii}$  and  $H_{jj}$ , and so on.

Assume that we calculated the matrix elements (5.101) [or (5.102)] and (5.100), and by solving Eqs. (5.7) and (5.8) we obtained a set of  $n$  MO energy levels of the system

$$\varepsilon_1, \varepsilon_2, \dots, \varepsilon_n \quad (5.104)$$

and for each of them a set of LCAO coefficients:

$$\begin{aligned} \varepsilon_1 &: c_{11}, c_{12}, \dots, c_{1n} \\ \varepsilon_2 &: c_{21}, c_{22}, \dots, c_{2n} \\ &\vdots \\ \varepsilon_n &: c_{n1}, c_{n2}, \dots, c_{nn} \end{aligned} \quad (5.105)$$

Each line of (5.105) corresponds to a certain ( $i$ th) MO, while each coefficient of the  $i$ th MO determines the contribution of the  $j$ th AO. By distributing all the electrons over the lowest energies  $\varepsilon_i$  following the Pauli principle, one finds the MO population numbers  $q_i$  equal to 2 (fully occupied MOs), 1 (half-occupied), or 0 (unoccupied) (in fragmentary calculations the charges may be fractional; see Section 5.6). With these data the atomic charges and, separately, the electronic charges on  $s, p, d, f, \dots$  orbitals, can be evaluated approximately by means of Mulliken population analysis [Section 5.2, Eq. (5.20)]. The electronic charges on the  $s, p,$  and  $d$  orbitals (in units of the electron charge)—*occupation numbers*—are

$$q_s^A = \sum_{i,j} q_i c_{is}^A c_{ij} S_{sj} \quad (5.106)$$

$$q_p^A = \sum_{i,j} \sum_{pA} q_i c_{ip}^A c_{ij} S_{pj} \quad (5.107)$$

$$q_d^A = \sum_{i,j} \sum_{dA} q_i c_{id}^A c_{ij} S_{dj} \quad (5.108)$$

where the label  $A$  in combination with  $s$ ,  $p$ , and  $d$  means that the latter are denoting the corresponding orbitals of atom  $A$ . The total (positive) atomic charge  $Z_A^*$  is ( $m^A$  is the number of valence electrons on the AOs of the reference neutral atom or ion included in the LCAO)

$$Z_A^* = m^A - (q_s^A + q_p^A + q_d^A) \quad (5.109)$$

The dependence of the atomic ionization energy on the atomic charge for a given electronic configuration  $I_i[A]$  can be well approximated by a three-term square dependence, as follows:

$$I_i[A] = A_i Z^2 + B_i Z + C_i \quad (5.110)$$

The constants  $A_i$ ,  $B_i$ , and  $C_i$  can be found if one knows the ionization potentials  $I_i$  for three  $Z$  values, for instance, for the neutral ( $Z = 0$ ), ionized ( $Z = +1$ ), and double-ionized ( $Z = +2$ ) states. These data can be obtained from the analysis of the energy terms and ionization potentials of free atoms in the given electronic configuration  $[A]$  [5.95]. The ionization potential is taken equal to the weighted-average energy value for all the terms formed by this configuration (Section 2.2). For instance, the  $d$  energy of the configuration  $d^2$  (see Table 2.6) is

$$I_d[d^2] = \frac{1}{45}[9E(^1A) + 21E(^3F) + 5E(^1D) + 9E(^3P) + E(^1S)] \quad (5.111)$$

where the coefficients at the term energies  $E(^{2S+1}L)$  equal the term degeneracy  $(2S+1)(2L+1)$ , while the term energies are known from spectroscopic data. The EIVS and constants  $A$ ,  $B$ , and  $C$  for some most usable atoms obtained in this way are given in Refs. 5.94–5.97.

However, the atomic orbital charge distribution  $d^{q_d} s^{q_s} p^{q_p}$  is, in general, fractional ( $q_d$ ,  $q_s$ , and  $q_p$  are not integers). For fractional configurations there are no empirical data on ionization energies. They can be approximated by linear combinations of the known values for integer–number configurations with fractional coefficients, which are chosen to make the summary electronic configuration equal to the fractional one.

Let us present the configuration  $d^{q_d} s^{q_s} p^{q_p}$  with  $q_s + q_p + q_d = n(1 - \Delta)$  [where  $n$  is integer and  $\Delta = 1 - (q_s + q_p + q_d)/n$  is a small fractional number], as a linear combination of integer–number configurations  $d^n$ ,  $d^{n-1}s$ ,  $d^{n-1}p$  (meaning that we present the fractional configuration as a sum of integer ones):

$$d^{q_d} s^{q_s} p^{q_p} = a d^n + b d^{n-1} s + c d^{n-1} p \quad (5.112)$$

Then, by equalizing the populations on the same orbitals, we get  $c = q_p$ ,  $b = q_s$ , and  $a = 1 - q_p - q_s - \Delta$ . Consequently, the EIVS of a fractional electronic

configuration in the case under consideration is

$$I_i[d^{q_d} s^{q_s} p^{q_p}] = (1 - q_p - q_s - \Delta) I_i[d^n] + q_s I_i[d^{n-1} s] + q_p I_i[d^{n-1} p] \quad (5.113)$$

Thus the procedure of self-consistent solutions in the IEH (SCCC) MO LCAO method is as follows. With the LCAO coefficients  $c_{ij}$  obtained from Eqs. (5.7) and (5.8), one calculates the atomic and configuration charges after (5.106)–(5.108), and then determines new EIVS by Eq. (5.113) and new matrix elements  $H_{ii}$  and  $H_{ij}$  by Eqs. (5.100)–(5.102), which allow one to determine new  $c_{ij}$  values, new charges, and so on. Provided that this process converges, each new iteration yields more precise results than the previous one, and this process can be continued until the new atomic charges and configuration, within the accuracy required, coincide with the previous ones, that is, are self-consistent.

The crystal field corrections can be included in the computation program directly. However, in some cases they are omitted. The reason is that usually the atomic charges on the central (metal) atom and ligands have opposite signs with the positive charge on the CA. Hence, for the metal, the EIVS value is larger than that for the neutral atom, and the crystal field corrections after Eq. (5.102) increase the absolute value of  $H_{ii}$ . On the contrary, EIVS is smaller for the ligand than for the corresponding neutral atom, and the crystal field of the positive central atom increases the absolute value of  $H_{ii}$ , making it closer to the neutral atom value. Therefore, one can assume that when the ligand charges are not very large, the charge dependence of EIVS of ligand atoms is compensated for by the crystal field corrections. Hence the self-consistent procedure can be carried out only on the central atom charges and configurations, keeping the  $H_{ii}$  values for the ligands constant and equal to their neutral atom values.

As to the correction constants  $k_\lambda$  in Eq. (5.102), they remain almost arbitrary, although their choice, within reasonable limits, does not strongly influence the results. Bash and Gray [5.98] suggested two sets of  $k_\lambda$  values: (1)  $k_\sigma = 0.6$ ,  $k_\pi = 0.40$ ,  $k_\delta = 0.2$  and (2)  $k_\sigma = 0.5$ ,  $k_\pi = 0.4$ ,  $k_\delta = 0.3$ .

Extended Hückel calculations of the octahedral  $\text{TiF}_6^{3-}$  complex are presented in more detail in Example 5.5.

### EXAMPLE 5.5

#### *$A_{1g}$ -Type MOs of Octahedral $\text{TiF}_6^{3-}$ Calculated Using the Extended Hückel (Wolfsberg–Helmholz) Approximation*

A reasonable approach is to present  $\text{TiF}_6^{3-}$  as  $\text{Ti}^{3+}(\text{F}^-)_6$  with one  $d$  electron above the closed shells of  $\text{Ti}^{4+}$  and six  $\text{F}^-$  ions. Then taking as a basis set the Ti atomic orbitals  $3d$ ,  $4s$ , and  $4p$ , and one  $\sigma$  and two  $\pi$  orbitals from each  $\text{F}^-$  ion, we come to the symmetry-adapted LCAOs

for octahedral complexes given in Table 5.1. Two AOs belong to the  $A_g$  symmetry,  $\psi_0 = 4s$  and  $\Phi_\sigma = (1/\sqrt{6})(\sigma_1 + \sigma_2 + \sigma_3 + \sigma_4 + \sigma_5 + \sigma_6)$  (the latter is a group orbital), forming two MOs,  $\psi = c_{4s}\psi_0 \pm c_\sigma\Phi_\sigma$ . The secular equation (5.8) or (5.12) with respect to the MO energies  $E$  and wavefunctions is thus [cf. Eq. (5.25)]

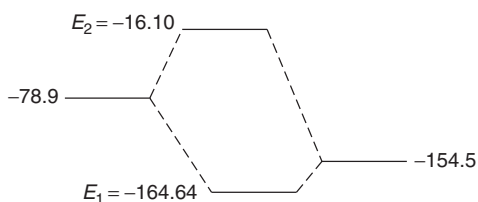
$$\begin{vmatrix} H_{4s4s} - E & H_{4s\sigma}^G - EG(4s, \sigma) \\ H_{4s\sigma}^G - EG(4s, \sigma) & H_{\sigma\sigma} - E \end{vmatrix} = 0 \quad (5.114)$$

where, according to Table 5.4, the group integral  $G(4s, \sigma) = \sqrt{6}S(4s, \sigma)$ , and similarly the group resonance integral  $H_{4s,\sigma} = \sqrt{6}H_{4s,\sigma}$  [see Eq. (5.11')]. Equation (5.114) is a quadratic equation with respect to the energy  $E$  with solutions given by Eq. (5.26). Following the Wolfsberg–Helmholz formula (5.101) with  $K = 2$  we get  $H_{4s,\sigma} = (H_{4s4s} + H_{\sigma\sigma})S(4s, \sigma)$ , and for the diagonal element we should take the ionization energy of the valence state (EIVS) with the opposite sign. Preliminary estimations by an iterative procedure [5.99] for the electronic configuration of the Ti site in this complex yield  $\text{Ti}^{0.51+}(3d^{2.6}4s^{0.37}4p^{0.50})$  with  $H_{4s4s} = -78.90$  kK ( $1\text{kK} = 10^3 \text{ cm}^{-1}$ ) and for the hybridized ligand  $\sigma$  state  $H_{\sigma\sigma} = -154.5$  kK. For the overlap integral calculations [5.99] at  $R(\text{Ti}-\text{F}) = 2.05 \text{ \AA}$  yield  $S(4s, \sigma) = 0.175$ . With these data we obtain the following from Eq. (5.26):

$$E_1 = -164.64 \text{ kK}$$

$$E_2 = -16.10 \text{ kK}$$

The energy diagram for these MOs is thus (numeric values in kilocalories):



with  $E_1$  bonding and  $E_2$  antibonding.

With these energies we estimate the LCAO coefficients from Eq. (5.7). For  $E_1$ ,  $c_{4s} = 0.289$ ,  $c_\sigma = 0.841$ , and hence the bonding MO is  $\psi_1 = 0.289|4s\rangle + 0.841 \cdot (1/\sqrt{6})(\sigma_1 + \sigma_2 + \sigma_3 + \sigma_4 + \sigma_5 + \sigma_6)$ . For the antibonding MO we get  $\psi_2 = 0.289|4s\rangle - 0.841 \cdot (1/\sqrt{6})(\sigma_1 + \sigma_2 + \sigma_3 + \sigma_4 + \sigma_5 + \sigma_6)$ .

Higher-energy MOs can be estimated in the same manner (see Problem 5.1).

One of the main deficiencies of the extended Hückel method, described above, is that it does not apply to molecular geometry optimization. Indeed, the Wolfsberg–Helmholz formula (5.101) or its analogs in Table 5.8 do not correctly account for the (nonoverlap) electrostatic interactions, especially between the atomic cores, and therefore it cannot apply for potential energy curves for stretching modes. Anderson and Hoffmann [5.100] attempt to overcome this difficulty by adding a two-body electrostatic interaction to the energy term in the EH approximation, while Calzaferri et al. [5.101] improved this presentation significantly and implemented it in a computer program (called ICONC).

With the two-body electrostatic terms included, it is possible to derive the corresponding geometries by energy optimization. The results obtained in this way strongly depend on the parameterization of the additional terms [5.101]. Appropriate parameters have been suggested for some organometallic compounds [5.102]. However, in general, in application to coordination compounds with center-delocalized bonds and nontransferable metal–ligand bond properties the parameterization based only on two-body interactions should be handled with much caution. Apparently, such parameters could be applied to compounds for which the metal–ligand bonds in question are mainly localized. The situation here is very similar to that arising in the problem of molecular mechanics, where intramolecular interactions are approximated by two-body atom–atom potentials with appropriate transferable parameters (see Section 5.6). The merit of empirical methods is discussed further in Section 5.7.

### Quasirelativistic Parameterization

Quasirelativistic (QR) semiempirical versions are based on the general QR approaches to the MO LCAO scheme, discussed in Section 5.4. Additional difficulties in QR parameterization of the calculations emerge, in particular, owing to the two-component spinor presentation of the wavefunction, and the classification of MO states on the IrReps of the double groups of symmetry required by the  $j-j$  coupling between the electrons (Sections 2.1, 3.6, and 5.4).

For the ZDO methods described above, the QR expressions for the matrix elements formally remain the same as in the nonrelativistic case [5.103], but the

**TABLE 5.8. Ionization Energies of  $s$ ,  $p$ , and  $d$  Electrons from Several Valence States (EIVS) of Pt Atom**

Ionized State	Ionization Process	EIVS ( $\text{cm}^{-1}$ )
$s_{1/2}$	$D^9(^2D_{5/2})s_{1/2} \rightarrow D^9(^2D_{5/2}) + e$	71,976
$p_{1/2}$	$D^9(^2D_{5/2})p_{1/2} \rightarrow D^9(^2D_{5/2}) + e$	38,803
$p_{3/2}$	$D^9(^2D_{5/2})p_{3/2} \rightarrow D^9(^2D_{5/2}) + e$	33,648
$d_{3/2}$	$(d_{5/2}^6 d_{3/2}^4)_0 \rightarrow (d_{5/2}^6 d_{3/2}^3)_{3/2} + e$	74,578
$D_{5/2}$	$(d_{5/2}^6 d_{3/2}^4)_0 \rightarrow (d_{5/2}^5 d_{3/2}^4)_{5/2} + e$	66,160

Source: Bersuker et al. [5.103].

meaning of the parameters is relativistic. In particular, in the CNDO methods the overlap integrals and the interelectron repulsion integrals (5.97) and (5.98) must be calculated by QR spinors, while the empirical parameters in (5.96), the ionization potential, and the electron affinity should be taken for atomic states classified in the  $j-j$  scheme.

Consider in more detail the QR IEH (or SCCC) MO LCAO parameterization. As in the nonrelativistic version, the diagonal matrix elements  $H_{ii}$  are given by EIVS expressed in terms of atomic charges and fractional configuration occupation numbers (5.113). But unlike the nonrelativistic case, for which the electron configuration is taken in the form  $s^x p^y d^z f^u$ , in the QR analog the electronic configuration must be taken after the  $j-j$  coupling scheme as  $s_{1/2}^a p_{1/2}^b p_{3/2}^c d_{3/2}^l d_{5/2}^k f_{7/2}^m$  (etc.), where  $x, y, \dots, a, b, c, \dots$  are the fractional occupation numbers.

To illustrate the procedure for EIVS evaluation, consider a simple case of a two-electron system in a  $sp$  configuration. For the free atom two relativistic valence configurations are possible (Section 2.1):  $s_{1/2}p_{1/2}$  and  $s_{1/2}p_{3/2}$ . Their energy-level scheme is shown in Fig. 5.4. Similar to (5.111), the mean energy

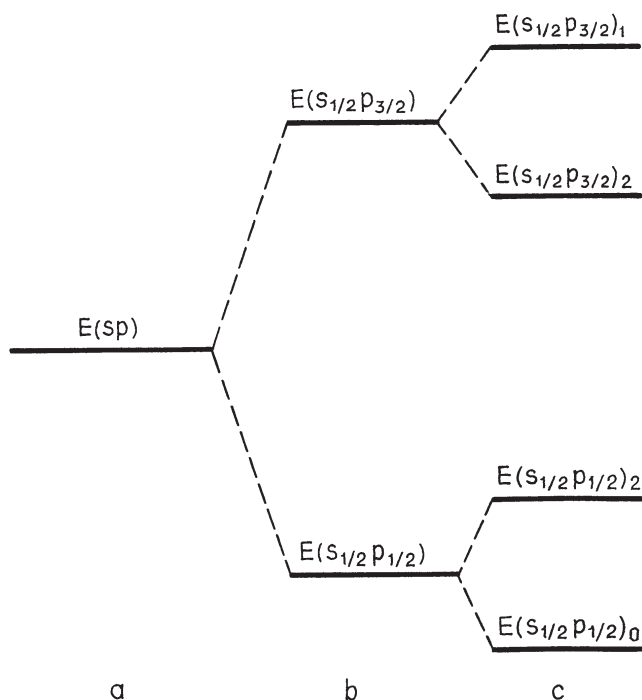


**FIGURE 5.4.** Energy-level diagram for a two-electron atom in the  $sp$  configuration and  $j-j$  coupling scheme: (a) averaged (“spherical”) interelectron interaction; (b) spin-orbital interaction added; (c) nonspherical (“local”) interelectron interaction added (classification of the total momentum  $J = 0, 1, 2$ ).

of these two configurations can be taken as averaged over the energy terms with different total momentum quantum numbers  $J$ :

$$E(s_{1/2}p_{1/2}) = \frac{1}{4}[E(s_{1/2}p_{1/2})_0 + 3E(s_{1/2}p_{1/2})_1] \quad (5.115)$$

$$E(s_{1/2}p_{3/2}) = \frac{1}{8}[5E(s_{1/2}p_{3/2})_2 + 3E(s_{1/2}p_{3/2})_1] \quad (5.116)$$

For the ionized atom that has only one valence electron there are three possible states:  $s_{1/2}$ ,  $p_{1/2}$ , and  $p_{3/2}$  (Fig 5.5). Then, for the EIVS, we have

$$\begin{aligned} -I_{p_{1/2}}[sp] &= I_0 + E(s_{1/2}) - E(s_{1/2}p_{1/2}) \\ -I_{p_{3/2}}[sp] &= I_0 + E(s_{1/2}) - E(s_{1/2}p_{3/2}) \\ -I_{s_{1/2}}[sp] &= I_0 + E(p_{1/2}) - E(s_{1/2}p_{1/2}) \end{aligned} \quad (5.117)$$

where  $I_0 = E_1 - E_0$  is the energy difference between the ground-state energies of the ion and the atom, respectively, from which the configuration energies  $E(s_{1/2})$ ,  $E(s_{1/2}p_{1/2})$ ,  $\dots$ , are read off. In particular, when the ground state of the ion is  $s_{1/2}$ , then  $E(s_{1/2}) = 0$  (its  $p_{1/2}$  state is not shown in Fig. 5.5). Another example including  $d$  electrons (for Pt compounds [5.103]) is illustrated in Fig. 5.6 in Example 5.6.

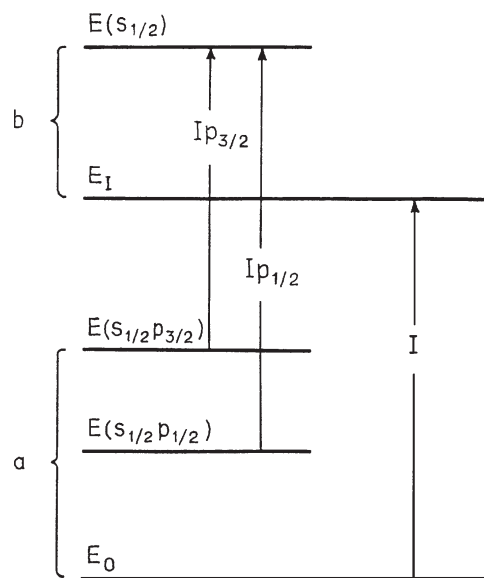


**FIGURE 5.5.** Energy-level scheme for a two-electron atom in the  $sp$  configuration (a) and its ion (b) (the energies are term-averaged). The ionization potentials are shown by arrows.



**EXAMPLE 5.6*****Quasirelativistic Evaluation of Energies of Ionization of Several Valence States (EIVS) of s, p, and d Electrons of the Pt Atom***

Figure 5.6 shows several experimental energy levels of the neutral and ionized Pt atom that are taken as the basis for evaluation of the EIVS used in semiempirical relativistic IEH calculation of the electronic structure of  $\text{PtCl}_6^{2-}$  [5.103]. The numerical values are given in Table 5.8. The results obtained for this complex are discussed in Section 6.5.

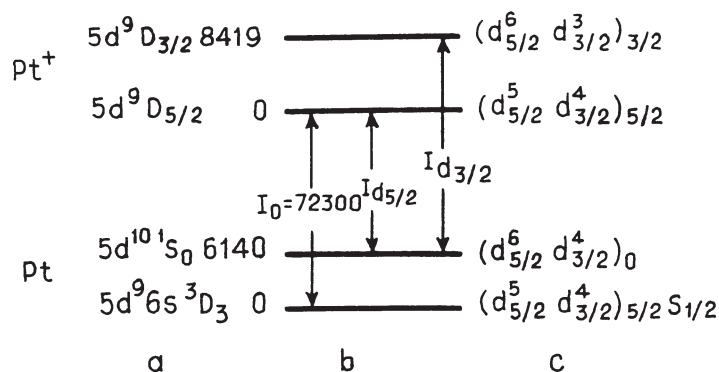


**FIGURE 5.6.** Illustration to evaluation of EIVS  $d_{3/2}$  and  $d_{5/2}$  of the Pt atom in the quasirelativistic approximation to the IEH (SCCC) MO LCAO method ( $I_0$  is the first ionization potential): (a) electron configurations and terms of Pt and Pt<sup>+</sup>; (b) energy-level values (in cm<sup>-1</sup>); (c) electron configurations in the strong coupling scheme.

The dependence of QR EIVS on the fractional charges  $a, b, c, \dots$ , can be determined in the same way as for the nonrelativistic case (5.113). Pykko et al. [5.104] give semiempirical parameterization for  $5f$  elements. For reviews of other possibilities, see Refs. 5.66–5.69, 5.81, and 5.105.

## 5.6. FRAGMENTARY CALCULATIONS, MOLECULAR MECHANICS, AND COMBINED QUANTUM/CLASSICAL (QM/MM) MODELING

Despite the impressive speed and efficiency reached in modern computers, relatively large (e.g., biological) molecular systems are still unattainable in electronic structure calculations by high-level MO LCAO or DFT methods and are expected to remain refractory to treatment by these methods in the near future (see also

the discussion in Section 5.7). On the other hand, there is the permanent controversy between the quantum local properties of molecular systems and the classical properties of macroscale systems that contain large numbers of such molecules. The description of macro properties based on microscopic molecular mechanisms includes a hierarchy of methods from quantum mechanics (QM) to classical molecular mechanics (MM), to molecular dynamics (MD), statistics, and so on, which involves a transition from quantum to classical methods. Therefore, with the increase in size of molecular systems that can be treated by QM methods, there will still remain the interaction with the larger environment to be treated by classical methods. In this hierarchy of methods the next-to-pure QM calculations are fragmentary calculations, classical MM, and combined QM/MM methods.

### Fragmentary Calculations

The importance of fragmentary calculations is increasing continuously together with demands for molecular modeling and its applications in various fields, especially in biology and drug design. To avoid bulky calculations of the electronic structure of large molecular systems, it may be useful to expand the molecule into smaller fragments that can be calculated separately, and then to construct the solution for the system as a whole as a combination of fragment solutions. Note that in the main versions of MO LCAO calculations, computation time is approximately proportional to  $n^4$ , where  $n$  is the number of basis functions, and for  $r$  fragments  $n = n_1 + n_2 + \cdots + n_r$ ,  $n^4 \gg n_1^4 + n_2^4 + \cdots + n_r^4$ , meaning significant savings in fragmentary computation. The latter are also important in the above mentioned realization of interfaces between quantum-mechanical description of local properties in large molecular systems and classical treatment of the system as a whole (see below).

For nonempirical calculations of large organic molecules with closed shells, molecular fragments can be calculated first, and then their wavefunctions can be used as the basis set for a full MO LCAO calculation of the system as a whole [5.106]. For instance, to calculate the ethane molecule in this way, the methane molecule is calculated first, and then the solution for the ethane molecule is presented as a linear combination of two solutions for two methane molecules at a certain distance from each other. In so doing, it is assumed that the elimination of two hydrogen atoms between them is counter balanced in the basis set by formation of the C—C bond. The method was extended to large organic molecules.

Fragmentary calculations used for organic molecules cannot be transferred directly to transition metal coordination compounds because of the  $d$ -electron delocalization properties (Sections 1.2 and 6.1) and significant charge transfers between the fragments (see below). A special analysis of the conditions when this separation is valid (at least approximately) yields the following results [5.107, 5.108].

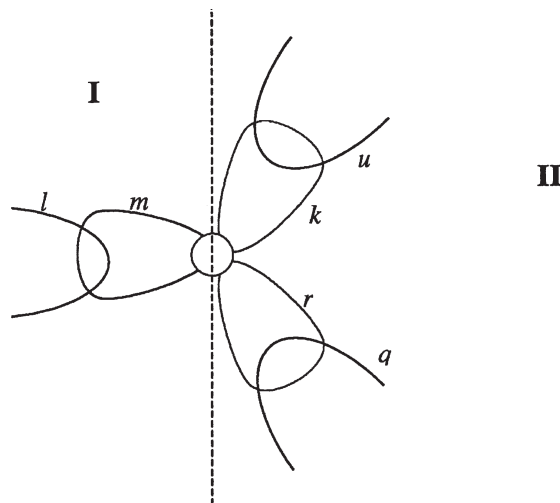


**FIGURE 5.7.** The border atom (BA) cut by the border surface (dashed line) into two fragments I and II, and its  $sp^2$  hybridized orbitals  $m$ ,  $k$ , and  $r$ . The near-neighbor orbitals  $l$ ,  $u$ , and  $q$  realize the intrafragment bonding to the BA.  $\pi$ -bonding (allowed to only one of the fragments) can be formed via the remaining  $p$  orbital of the BA.

It is obvious that the separation of a molecule into fragments is possible when the interfragment interaction is much smaller than the intrafragment one. To formulate this condition quantitatively, consider an arbitrary molecule cut into two fragments in such a way that there is only one border atom (BA), the borderline between the fragments crosses this atom (Fig. 5.7), and the BA does not form  $\pi$  bonds with at least one of the two fragments. Assume that  $sp^2$  hybridization of the BA atomic orbitals takes place and denote the  $\sigma$  functions directed to fragments I by  $m$  and II by  $k$  and  $r$ , respectively, the corresponding  $\sigma$  orbitals of nearest-neighbor atoms in the fragments being  $l$ ,  $u$ , and  $q$  (for simplicity, the possible  $\pi$  bond with one of the fragments is omitted).

With these basis functions the secular equation (5.8) contains two types of integrals  $H_{ij}$ : intrafragment of the type  $H_{mm}$  and  $H_{ml}$  and interfragment of the type  $H_{mk}$  and  $H_{mu}$  ( $H_{lu}$ -type integrals are assumed to be negligibly small). If the interfragment integrals are smaller than the intrafragment ones, they can be neglected in the zeroth-order approximation, and then the secular equation decomposes into two independent equations for the two fragments. A similar picture can be drawn for other cases of  $sp^n$  hybridization.

The four types of integrals can be estimated from the general formulas for  $sp^n$  hybridization (Section 2.1). They are given in Table 5.9.

Comparing the integrals in Table 5.9, we see that if the BA is a carbon atom (for which the  $2s$  and  $2p$  orbitals are very close in energy), the differences

**TABLE 5.9. Intrafragment and Interfragment Integrals that Should Be Compared in Validation of the Proposed Fragmentation**

Hybridization	Intrafragment Integrals		Interfragment Integrals	
	$H_{mm}$	$H_{ml}$	$H_{mk}$	$H_{mu}$
$sp^n$				
$sp$	$\frac{1}{2}(H_{ss} + H_{pp})$	$(1/\sqrt{2})(H_{s\sigma} + H_{p\sigma})$	$\frac{1}{2}(H_{ss} - H_{pp})$	$(1/\sqrt{2})(H_{s\sigma} - H_{p\sigma})$
$sp^2$	$\frac{1}{3}(H_{ss} + 2H_{pp})$	$(1/\sqrt{3})(H_{s\sigma} + \sqrt{2}H_{p\sigma})$	$\frac{1}{3}(H_{ss} - H_{pp})$	$1/\sqrt{3}[H_{s\sigma} - (\sqrt{2}/2)H_{p\sigma}]$
$sp^3$	$\frac{1}{4}(H_{ss} + 3H_{pp})$	$\frac{1}{2}(H_{s\sigma} + \sqrt{3}H_{p\sigma})$	$\frac{1}{4}(H_{ss} - H_{pp})$	$\frac{1}{2}[H_{s\sigma} - (\sqrt{3}/3)H_{p\sigma}]$

Sources: Bersuker [5.107, 5.108].

$H_{ss} - H_{pp}$  and  $H_{s\sigma} - H_{p\sigma}$  are, respectively, much smaller than the sums  $H_{ss} + H_{pp}$  and  $H_{s\sigma} + H_{p\sigma}$ . For instance, for saturated carbon in organic compounds,  $H_{2p2p}/H_{2s2s} \sim 0.7$  and hence the ratio  $H_{mk}/H_{mm} \sim 0.15$ . This value changes with the charge on the atom; for  $C^+$ ,  $H_{mk}/H_{mm} \sim 0.09$ . Similar estimates can be given for comparison of other integrals; the interfragment/intrafragment integrals ratios decrease with the power  $n$  of the  $sp^n$  hybridization. For N, O, and F the ratios  $H_{mk}/H_{mm}$  are similar to that of carbon with a slight increase along this series. Thus  $2s2p$  atoms C, N, O, and F are the best BA for fragmentation of large molecular systems that obey the necessary conditions of fragmentation, provided that they do not serve as  $\pi$ -electron bridges between the fragments.

If the BA forms active  $\pi$  orbitals with both fragments, there are no grounds for separating the latter by this BA, because the off-diagonal intrafragment and interfragment matrix elements  $H_{ik}$  are of the same order of magnitude. Therefore, *the first rule of fragmentation is that the border atom between any two fragments must have only localized  $\sigma$  bonds with at least one of the two fragments* [5.107, 5.108].

In any fragmentation of the molecule (even when the abovementioned rule is fulfilled and  $H_{ik}$  is small), the solution obtained differs from the true one for the molecule as a whole, and the problem is to find some criteria of the inaccuracy introduced by such fragmentary calculations. Fortunately, there is a mathematical theorem regarding localization of the characteristic numbers of matrices (in our case values of energies  $\varepsilon$ ) proved by Gershgorin [5.109] that contributes significantly to the solution of this problem. Following this theorem, the interval of localization of the roots of the secular equation (5.8) of the order  $n$  (i.e., the MO energies  $\varepsilon$  in the MO LCAO method with a basis of  $n$  functions) is limited by the following inequalities:

$$|H_{ii} - \varepsilon| \leq \sum_{j \neq i} |H_{ij}| \quad (5.118)$$

(In complex-conjugated numbers these intervals become circles on the complex plane and are termed—*Gershgorin circles*.) It is seen from this expression that localization of the MO energies  $\varepsilon$  with respect to the diagonal element (Coulomb integral)  $H_{ii}$  is determined by the sum of absolute values of all the off-diagonal elements (resonance integrals)  $H_{ij}$  of the  $i$ th row. Therefore, neglect of one of the matrix elements  $H_{ik}$  reduces two intervals of localization of the MO energies in the two fragments [the radii of the  $i$ th and  $k$ th Gershgorin circles in (5.118)], making them closer to the atomic values  $H_{ii}$  and  $H_{kk}$ . The effect is thus determined by the magnitude  $|H_{ik}|$ , as compared with the sum of all the other values  $|H_{ij}|$  (in the first fragment) or  $|H_{kj}|$  (in the second fragment). From these results the second rule of fragmentation emerges: *the greater the intrafragment delocalization (the larger the sum of  $|H_{ij}|$ ) as compared with interfragment interaction ( $H_{ik}$ ), the less the error of fragmentation.*

For small  $H_{ik}$  values the fragmentary solutions can be improved by considering  $H_{ik}$  as a small perturbation. In the case of  $n$  interacting MOs from the two fragments, the value of the new MO energy level  $\varepsilon_\alpha$  with respect to the unperturbed one  $\varepsilon$  is given by the following inequality, which is similar to (5.118) [5.107, 5.108]:

$$|\varepsilon_\alpha - \varepsilon| \leq v |c_{\alpha i} H_{ik}| \quad (5.119)$$

where  $2v^2 = [(4n+1)^{1/2} - 1]$ , and  $c_{\alpha i}$  is the LCAO coefficient in the intrafragment MO formed by the BA orbital. It is seen that the deviation of  $\varepsilon_\alpha$  from  $\varepsilon$  under the influence of the nearest-neighbor fragment is proportional to both  $H_{ik}$  and  $c_{\alpha i}$ . The latter is the smaller, the more delocalized the intrafragment MO. Hence, again, *the electron delocalization inside the fragment reduces the influence of the neighbor fragments*. In Ref. 5.107 (see also Ref. 5.108), a procedure for double (intrafragment and interfragment) self-consistent calculations is worked out; it takes into account the influence of interfragment interactions on both the energy levels and charge distribution. The latter is of special importance to transition metal systems due to significant charge transfers between the fragments; in these cases the interface between the fragments should be electronically transparent (see below).

In application to coordination compounds, the results presented above allow one to conclude that the central metal atom cannot be used as a BA to perform the fragmentation procedure, due to the rather delocalized nature of the electronic distribution created by the  $d$  or  $f$  electrons. However, the ligands can be calculated fragmentary, if the above mentioned conditions are obeyed.

Also, in multinuclear (multi-metal-center) coordination compounds the separations into one-center fragments may be quite necessary in order to perform the calculations.

For multicenter coordination compounds or coordination compounds in ionic crystals, some one-center atomic groups (or a limited number of centers in crystals) can be selected for electronic structure calculations, with the cut bonds substituted by some boundary conditions that simulate the influence of the cluster environment in the real systems. This can be done, for example, by setting some pseudoatoms on the broken bonds [5.110] (sometimes called “dummy atoms”), or by using cyclic border condition for clusters in crystals [5.111] in which the broken bonds on the border are linked to the equivalent bonds on the other border (see below). The discussion of fragmentary calculations is continued below together with QM/MM methods.

### Molecular Mechanics

Before discussing the more relevant (to transition metal systems) combined quantum–classical methods of molecular modeling we briefly discuss the purely classical method of *molecular mechanics* (MM). The MM method [5.112] is presently widely employed in *molecular modeling*, especially in conformational analysis of organic compounds, including biological systems. In its modern versions (computer programs MM2 and MM3), and used within the limits of validity, MM proved to be very useful [5.112–5.116]. MM methods gained even more interest because of their application in *molecular dynamics*, which considers the classical (driven by the Newton law) motions of atoms or molecules (e.g., in liquids) along the APES produced by MM interaction between them [5.19].

*The main assumption of the MM method is that there are well-defined parameters of interaction (bonding) between given pairs of atoms that are transferable from one molecular system to another.* With this assumption the purpose of the MM method is to represent the total energy of the molecular system as a function of its geometry given by interatomic distances and angles between the bonds, and to find the equilibrium geometry from the condition of energy minimum. Unlike quantum-chemical methods in which the total energy is obtained from electronic structure calculations, in the method of MM the total energy is computed as a sum of bond contributions calculated in a classical way by means of empirical parameters. The total energy is presented as follows:

$$E_{\text{total}} = E_s + E_b + E_{\text{tors}} + E_{\text{vdw}} + E_{\text{elec}} \quad (5.120)$$

where  $E_s$  is the bond-stretching energy,  $E_b$  is the angle-bending energy,  $E_{\text{tors}}$  is the energy of torsional distortion,  $E_{\text{vdw}}$  is Van der Waals interaction of nonbonded atoms, and  $E_{\text{elec}}$  is their electrostatic interaction energy. Figure 5.8 gives the denotation of the coordinates used in the definition of the energies (5.120).

The potential of stretching energy (of deformation along the bond) is given by a harmonic term, a parabola with a minimum at the equilibrium (unstrained)

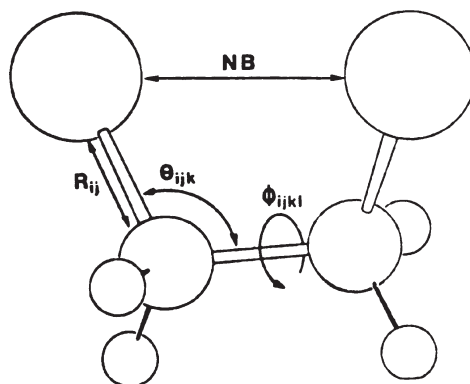


**FIGURE 5.8.** Illustration to the choice of coordinates of intramolecular interactions determining the geometry of molecules in molecular mechanics (NB denotes nonbonded atoms).

interatomic distance  $R^0$ :

$$E_s(R_{ij}) = \frac{1}{2}K_{ij}(R_{ij} - R_{ij}^0)^2 \quad (5.121)$$

where  $K_{ij}$  is the stretching force constant of the  $i$ — $j$  bond. This equation contains two constants,  $K_{ij}$  and  $R_{ij}^0$  (sometimes called force-field constants), which in the MM method are considered identical for all  $i$ — $j$  bonds between atoms  $i$  and  $j$ , and are taken equal to some values for the free, unstrained bond (unaffected by other bonds).

For the bending interaction potential a similar quadratic dependence on the bending angle  $\theta_{ijk}$  between the two bonds  $i$ — $j$  and  $j$ — $k$  (Fig. 5.8) is suggested:

$$E_b(\theta_{ijk}) = \frac{1}{2}K_{ijk}(\theta_{ijk} - \theta_{ijk}^0)^2 \quad (5.122)$$

In a similar way the other terms in (5.120) are presented by classical interaction formulas with constants to be obtained from empirical data [5.112–5.116].

In application to coordination compounds, this method raises some questions and concerns [5.108, 5.117, 5.118]. As stated elsewhere in this book (Sections 1.2, 6.1, etc.), because of the three-dimensional delocalization of the coordination bond, there are no constant values of the type  $K_{ij}$  and  $R_{ij}^0$  for specific metal–ligand M—L bonds which could be used for any complex independent of the other M—L' bonds formed by the same metal M. For instance, as seen from Table 9.10, the Cu—O bond length varies from 1.8 to 3.0 Å depending on the other Cu—ligand bonds. Therefore, in general, there are no fixed transferable parameters for the metal–ligand bonds to be employed in the molecular force field of MM.

Another implication emerges from the charge redistribution (discussed in Section 6.3) in the ligands by coordination to a transition metal center, which

**TABLE 5.10. Interaction Constants  $K_{ij}$  and  $R_{ij}^0$  for Bond Length Deformation  $E_s(R_{ij}) = \frac{1}{2}K_{ij}(R_{ij} - R_{ij}^0)^2$  in Some Coordination Compounds**

Bond Type		$K_{ij}$ (mdyn/Å)	$R_{ij}^0$ (Å)
$i$	$j$		
Co(III)	N	2.25	1.95
Co(III)	O	2.25	1.93
Co(III)	Cl	1.68	2.30
Ni(II)	N	0.68	2.10
Cu(II)	S	0.50	2.38
Cu(II)	N=	0.89	2.00
Cu(II)	O	0.89	2.00

Source: Brubaker and Johnson [5.113].

makes the former electronically excited. The ligand ground state HOMO is depopulated, while its excited MOs become populated as a result of the *backdonation* from the metal (see Fig. 6.6). Therefore, the ligands in transition metal systems *should be modeled in their partially excited state*, with the measure of excitation determined by the coordination center.

Attempts to use the MM method for transition metal systems in a similar way as done for organic compounds may have some grounds for specific cases that allow for sidestepping the difficulties mentioned above. For instance, for quite similar coordination centers with the same first coordination sphere and weak influence of the next coordination spheres, one can assume that the force constants for the same metal–ligand bonds are approximately the same. For example, the Co(III)—N bond parameters in all the octahedral complexes with six almost equivalent Co(III)—N bonds that differ slightly in the second and next coordination spheres can be considered approximately transferable within this set of systems.

Table 5.10 provides some force-field constants for metal–nitrogen interactions, as well as some other constants for comparison [5.113]. Example 5.7 shows an application of molecular modeling to macrocycle complexes.

### EXAMPLE 5.7

#### *Application of Molecular Modeling to Transition Metal Complexes with Macrocycles*

An example illustrating the possibilities of the MM method in the limits of its applicability is demonstrated by the results of the calculations for some macrocycle complexes [5.114]. Figure 5.9 shows the three most probable conformations of transition metal tetraaza macrocycle complexes, and in Fig. 5.10 the total strain energy is given calculated



by Eq. (5.117) for two conformers, *trans*-I and *trans*-III, of  $[M(12\text{-aneN}_4)]^{n+}$  as a function of the M—N— length. The nature of the metal M is not considered since it is shown that the results are not sensitive to the assumed M—N force constant, provided that the bond is sufficiently weak.

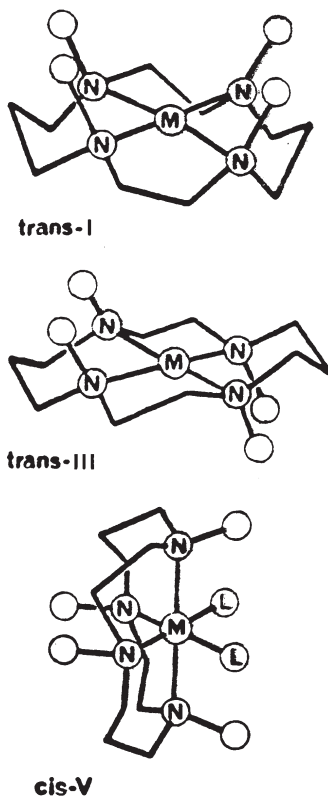


**FIGURE 5.9.** Three conformers of metal complexes with 14-aneN<sub>4</sub> tetraaza macrocycles. The open circles are hydrogen atoms, while L is another ligand. (After Hancock [5.114].)

From the results of MM calculations presented in Fig. 5.10 several conclusions emerge: (1), the energy of the *trans*-III conformation with the 12-aneN<sub>4</sub> macrocycle is much higher than that of *trans*-I, and hence the former is not likely to occur; and (2) the best-fit M—N bond length for the more stable conformer is 2.11 Å. Finally, the curvature of the APES at the minimum of the *trans*-I conformer is much smaller than that of *trans*-III, meaning that the former is much more tolerant to the variation of the metal ion size.

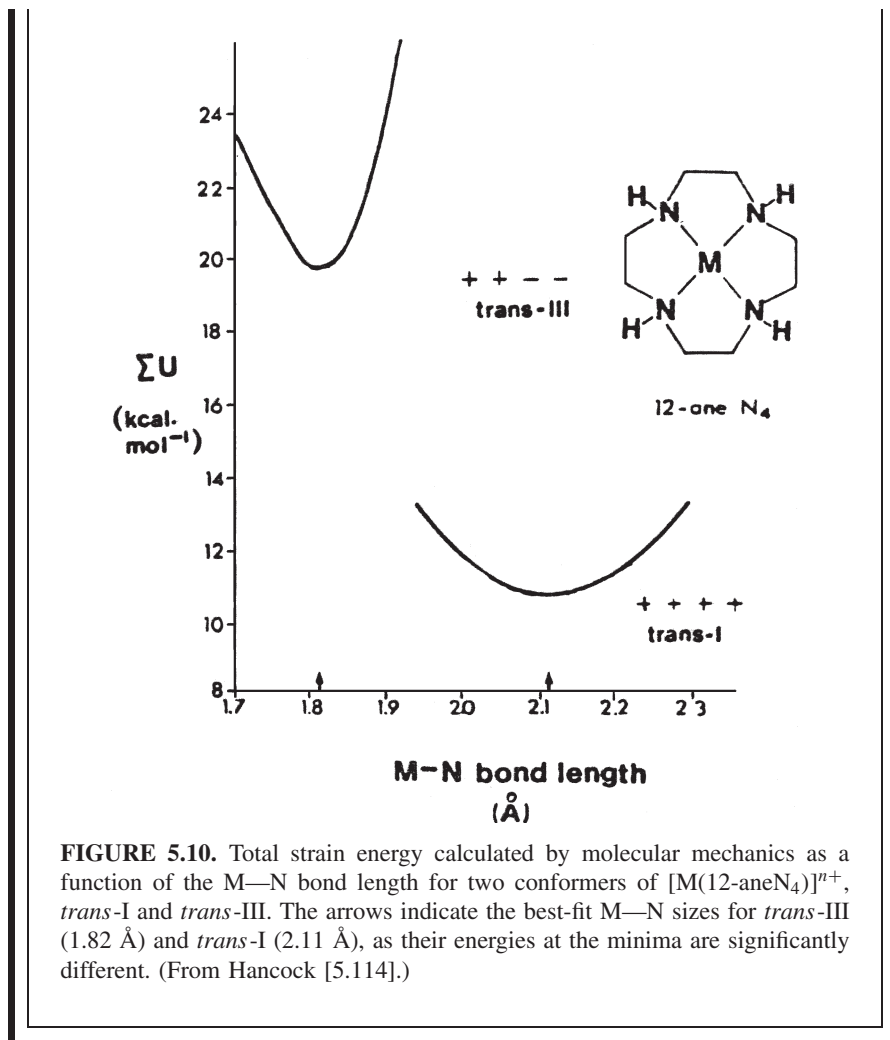


**FIGURE 5.10.** Total strain energy calculated by molecular mechanics as a function of the M—N bond length for two conformers of  $[M(12\text{-ane}N_4)]^{n+}$ , *trans*-I and *trans*-III. The arrows indicate the best-fit M—N sizes for *trans*-III (1.82 Å) and *trans*-I (2.11 Å), as their energies at the minima are significantly different. (From Hancock [5.114].)

The relatively good results obtained in some of the simple MM calculations of transition metal systems (see Example 5.7) show that they are based on a reasonable sidestepping of the difficulties of the MM method, mentioned above. This could be done, in particular, due to the homoligand complexes considered in this example. Attempts to consider heteroligand systems in a similar way, that is, to use the same constants of the force field (5.117) for a M—L<sub>1</sub> bond in different systems in which other M—L<sub>n</sub> bonds are different, have been shown to be ungrounded [5.108, 5.117, 5.118]. This statement can be

illustrated by a series of specific effects important to transition metal systems but not evolved in the MM method. For example, the well-known effects of mutual influence of ligands (*cis* and *trans* effects; Section 9.3) indicate directly that the local metal–ligand bond in these systems is not specific and cannot be characterized by the same parameters when other bonds are different. Similarly, the Jahn–Teller and pseudo-Jahn–Teller effects (Sections 7.3 and 7.4), for instance, the off-center position of the CA (Section 9.2), the plasticity effect (Section 9.4), and so on, are completely beyond the possibilities of the MM methods (note the abovementioned diversity in Cu–L bond lengths illustrated in Tables 9.10–9.12, which obviously cannot be described by fixed parameters).

Some combined quantum mechanical/molecular mechanics (QM/MM) method of modeling transition metal compounds, including organometallics and metallo-biochemical systems, are devoid of the failures of the MM methods mentioned above, but preserve the simplicity and visualization achieved in modeling organic compounds.

#### Combined Quantum/Classical (QM/MM) Methods

The idea underlying methods of combined quantum-mechanical (QM) calculations with simple molecular mechanics (MM) treatment is based on the understanding that in large molecular systems the quantum effects usually take place in the *active centers*, often metal centers (e.g., in metallobiochemical systems), while the large organic environment mostly changes its conformation without essential electronic changes. In these conditions it is reasonable to divide the system into two (or more) fragments, one of which contains the metal center, the others sharing the remaining organic part. The geometry of the metal fragment can be optimized using QM methods (Section 5.5), while the configuration of the huge organic part can be evaluated by the MM methods. Then the use of a special interface between QM and MM, discussed below, allows for a self-consistent description of the system as a whole.

The advantage of this fragmentary approach with QM for the metal center and classical description (MM) for the organic ligands is that in the more explicit treatment of the former the special effect produced by the *d* electrons (including nontransferability, mutual influence of ligands, Jahn–Teller effects, etc.) are factored in, while the MM treatment of the ligands preserves the simplicity achieved in modeling organic compounds. A full QM optimization of the entire system may be beyond the practical possibilities of the modern computers and programs; the *ab initio* methods are unavailable for large molecules, while semiempirical methods, although affordable for larger (but not very large) systems, are not sufficiently accurate in treating intramolecular nonbonding interactions (Section 5.7). In general, as mentioned above, when passing from *microscopic* description to

*macroscale* properties, an interface between quantum description and classical treatment may be inevitable.

Before discussing the conditions of QM/MM division of a molecular system and treatment of the QM and MM regions with different methods, we give a summarized formulation of the main requirements to this approach that follow from quantum mechanics [5.108]:

- *Condition of Fragmentation.* In dividing the molecular system into fragments, there should be significant theoretical grounds to assume that the main electronic features are not lost in the proposed fragmentation; that is, the fragmentary description may serve as a zeroth-order approximation (this condition is discussed above together with fragmentary calculations).
- *Condition of Interfragment Self-Consistency.* If the fragments are calculated separately, it should be possible to converge (with a criterion for convergence of) the results to those of the system as a whole that includes charge redistribution between the fragments.
- *Condition of QM-MM Continuity.* If some of the fragments are calculated by QM methods while the others are considered by MM, there should be a QM/MM interface that allows for a smooth transition between the QM (quantum) and MM (classical) description of nearest-neighbor fragments. Since quantum and classical descriptions have different basic equations, this condition is not trivial and may cause significant difficulties in the implementation of the QM/MM approaches and interpretation of the results.

The main condition of fragmentation follows directly from the QM formulation of the problem. Assume that our polyatomic system is divided in two regions, QM and MM (Fig. 5.11), with the intention of performing combined QM/MM treatment of its properties. In some cases it is useful to divide the QM region into two (or more) layers to be treated at different computation levels and/or to introduce a third region around the QM/MM one, the boundary region (BR), in order to account for the interaction with the remaining environment (which is always present, in principle).

The full Hamiltonian  $H$  of the system can be presented as a sum of terms that belong to the QM and MM regions ( $H_{\text{QM}}$  and  $H_{\text{MM}}$ , respectively) and the interaction between them  $H_{\text{QM/MM}}$ :

$$H = H_{\text{QM}} + H_{\text{MM}} + H_{\text{QM/MM}} \quad (5.123)$$

In many studies on the QM/MM approach it is assumed that by means of the Hamiltonian (5.123) we obtain the following expression for the partition of energy directly:  $E = E_{\text{QM}} + E_{\text{MM}} + E_{\text{QM/MM}}$ , where  $E_{\text{QM}}$  and  $E_{\text{MM}}$  are the energies of the QM and MM regions, respectively, and  $E_{\text{QM/MM}}$  is the energy of

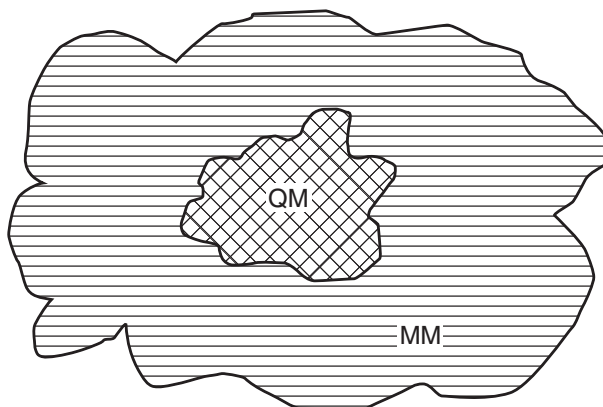


**FIGURE 5.11.** Schematic representation of the division of a large molecular system in QM and MM regions. BR (boundary region) denotes the remaining environment.

their interaction. In general, *this assumption is invalid* [5.108]; it may take place approximately if, and only if, the interaction between the two fragments is small and can be considered as a perturbation to the solutions of the two fragments taken separately; only in this case the total wavefunction of the system in the zeroth approximation may be taken in a multiplicative form to result in the above partition of the energy.

In some earlier publications devoted to solute–solvent systems the QM region contains the solute (which includes the molecules that undergo a chemical transformation), while the MM region is just the solvent (or a chemically nonbonded enzyme environment). In such cases the interaction between the two regions can intuitively be assumed to be small, perturbationlike. But even in solute–solvent interactions of TMS [5.119] (and even for organic compounds, for example, in enzyme–water interaction [5.120]) the QM–MM interaction may significantly involve charge transfer.

Charge transfer between the QM and MM regions creates a major problem for the QM/MM approach. Orbital charge transfers (Section 5.2) between the metal center (QM region) and ligands (MM region) are especially important for a TMS, where they determine the main properties of the system. If the orbital charge transfers are factored in, the simple separation of the energy in fragments is not valid. A more elaborate approach deemed to manage both the condition of fragmentation and the charge transfer problem is discussed below.

One QM/MM method aimed at TMS, available in commercial packages of computer programs, is called ONIOM (our own *N*-layered integrated molecular orbital and molecular mechanics) method [5.121] (a previous simpler version was called IMOMM: integrated MO+MM). The main idea of this method is to

divide the system under consideration in two or several ( $N$ ) layers that can be treated at a different level of QM calculations down to MM. The most important points in this approach is how to present the total energy of all  $N$  layers when each is treated differently, how to handle the interface between them, and how to satisfy the condition of interlayer self consistency.

For the energy, the authors [5.121–5.123] suggest the following scheme of calculations. Consider the three-layer system. Denote by, respectively, H, M, and L the high, medium, and low levels of approximation in the calculations, and by S, I, and R, the small (central layer), intermediate (central plus next layer), and real (all three layers) systems, respectively. Then the total energy of the three-layer system  $E(3)$  is presented by the following equation:

$$E(3) = E(H;S) + E(M;I) + E(L;R) - E(M;S) - E(L;I) \quad (5.124)$$

where  $E(H;S)$  means the energy of the small system calculated by the highest level,  $E(M;I)$  is the energy of the intermediate (two-layer) system calculated at the medium level, and  $E(L;R)$  is the energy of the real system with all the three layers calculated in the lowest (MM) level. In fact, Eq. (5.124) means that only the smallest (most active) part of the system (S) is calculated at the highest level (H), while for the next layer the energy is presented as  $E(M;I) - E(M;S)$ , that is, the energy of the two-layer intermediate system calculated at the medium level minus the energy of the small system calculated at the same (medium) level. Similarly, for the third layer the energy is presented as the difference between the whole (real) three-layer system and the two-layered intermediate system, both calculated at the lowest level of theory (e.g., MM).

To explain how the interface between the layers is handled, consider a two-layer system [5.122] in which the real system is  $M(P(CH_3)_3)_2$  and the smaller one (model system) to be treated by the ab initio method is  $M(PH_3)_2$ . As seen from Fig. 5.12, four sets of atoms can be distinguished according to their roles in the two-layer calculations. The carbon atoms in set 3 of the real system are substituted by hydrogen atoms in the model system, where they form set 2. Therefore, when considering the real system by MM after ab initio calculating the model system, we can take the coordinates of the atoms in set 3 (denoted in general as  $\mathbf{R}_3$ ) as functions of  $\mathbf{R}_1$  and  $\mathbf{R}_2$  of the atoms in set 1 and set 2, respectively:

$$\mathbf{R}_3 = \mathbf{R}_3(\mathbf{R}_1, \mathbf{R}_2) \quad (5.125)$$

With this in mind, we obtain the following expressions for the energies  $E$ :

For the model system:

$$E_{QM} = E_{QM}(\mathbf{R}_1, \mathbf{R}_2) \quad (5.126)$$

For the real system:

$$E_{MM} = E_{MM}(\mathbf{R}_1, \mathbf{R}_3, \mathbf{R}_4) = E_{MM}(\mathbf{R}_1, \mathbf{R}_2, \mathbf{R}_4) \quad (5.127)$$

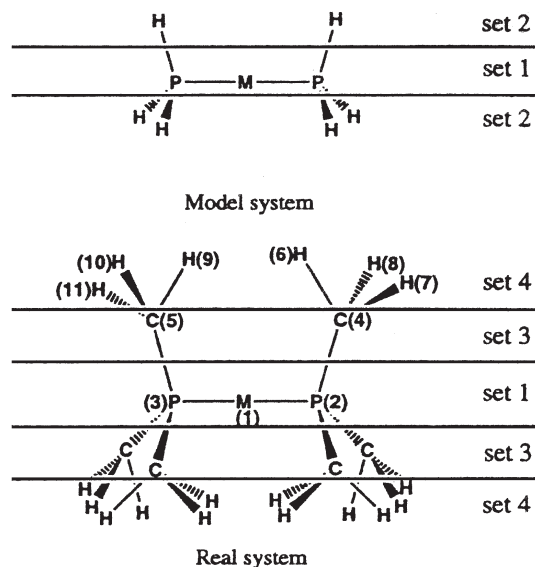


**FIGURE 5.12.** The IMOMM two-layer system with four sets of atoms for  $M(P(CH_3)_3)_2$ . The model system to be calculated ab initio is  $M(PH_3)_2$ . (After Maseras and Morokuma [5.122].)

For the combined QM+MM description:

$$E = E_{QM} + E_{MM} = E(\mathbf{R}_1, \mathbf{R}_2, \mathbf{R}_4) \quad (5.128)$$

Equations (5.124)–(5.128), together with the corresponding equations for the energy gradients with respect to  $R_i$  coordinates, solve, in principle, the combined problem of electronic structure and geometry optimization (for more details, see Refs. 5.121–5.123). Example 5.8 shows how this procedure works in application to the reaction of oxidative addition of  $H_2$  to  $Pt(t-Bu)_3)_2$ .

### EXAMPLE 5.8

#### *Oxidative Addition of $H_2$ to $Pt(t-Bu)_3)_2$ Treated by ONIOM Version of QM/MM Methods*

The treatment [5.121] of oxidative addition of  $H_2$  to  $Pt(P(t-Bu)_3)_2$  may serve as an example to illustrate the ONIOM method applied to a three-layer system. Figure 5.13 illustrates the choice of the three parts in the calculations: real, intermediate, and small.

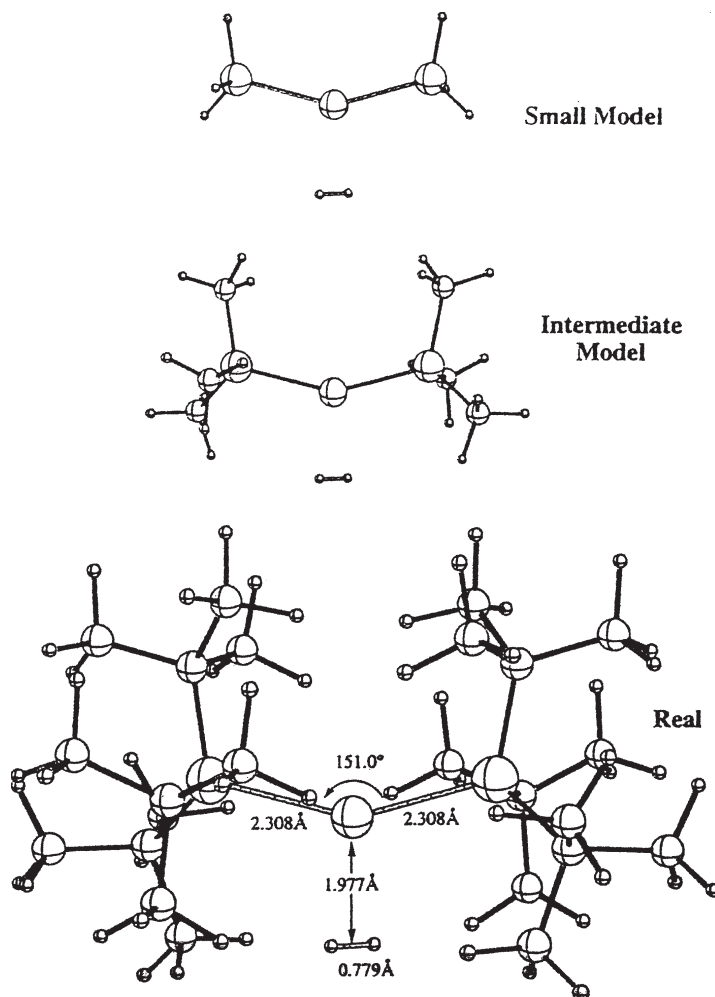


**FIGURE 5.13.** ONIOM three-layer system (real system, intermediate model, and small model) for oxidative addition of  $\text{H}_2$  to  $\text{Pt}(\text{P}(t\text{-Bu})_3)_2$ . (After Svenson et al. [5.121].)

Table 5.11 shows the results obtained by different three-level calculations for this system. The geometry was optimized at the IMOMM level with MP2 for the QM part and MM3 for the MM treatment (MP2:MM3) [5.123]. It is seen that reasonable results for the activation energy of the reaction are obtained in the ONIOM (B3LYP:HF:MM3) calculations at a much lower cost than the DFT(B3LYP:B3LYP:B3LYP) calculations of the whole system.



**TABLE 5.11. Activation Barriers  $E_a$ , Energies of Reaction  $E_r$  (in kcal/mol), and Their Errors  $\Delta E$  with Respect to the Pure DFT(B3LYP) Method for Oxidative Addition of  $H_2$  to  $Pt(P(t-Bu)_3)_2$  Calculated with Various ONIOM Schemes**

Scheme	$E_a$	$\Delta E_a$	$E_r$	$\Delta E_r$	Computer Time (s)
B3LYP:B3LYP:B3LYP	18.3	0.0	10.5	0.0	1207
HF:HF:HF	24.6	6.3	18.7	8.2	438
B3LYP:B3LYP:HF	19.1	0.8	14.9	4.4	586
B3LYP:B3LYP:MM3	16.8	-1.5	7.0	-3.5	148
B3LYP:HF:HF	19.8	1.5	14.0	3.4	453
B3LYP:HF:MM3	17.5	-0.8	6.1	-4.4	51
B3LYP:MM3:MM3	16.4	-1.9	8.0	-2.5	15
CCSD(T):MP2:MM3	14.2	—	4.1	—	500

Source: Svenson et al. [5.121].

Analyzing the ONIOM method from the perspective of the general theory outlined above, we note that the requirements of the theory are not well satisfied in at least two essential points. First, the total energy of the system is taken as a sum of the QM and MM fragment energies [Eq. (5.124)]. As emphasized above, this additive presentation of the energies is valid if and only if there is a separation of variables of the fragments that would allow for the total wavefunction to be taken as a product of wavefunctions of each fragment taken separately. The authors [5.121–5.123] do not discuss the validity of Eq. (5.124) based on this requirement.

In the oxidative addition of  $H_2$  to  $Pt(P(t-Bu)_3)_2$  in Example 5.8, such separation of variables means that the delocalization over the whole (real) system electronic states (the MOs) may be approximately presented as a multiplicative combination of MOs localized on the small, intermediate, and real systems, taken separately. This is not possible, or at least it has not been proved that it is possible. In view of the conditions of such separation discussed below, the relatively good results of QM/MM calculation of the energy of this system (Table 5.1) is seemingly due in part to saturated  $\sigma$  bonds formed by the atoms (carbons) at the border between the fragments (see next section).

The neglect of the general condition of division in fragments is more evident in other applications of this method to TMS [5.108]. In particular, in a two-layer (DFT:MM) treatment of several large organometallic palladium complexes [5.124] the division into the QM and MM regions cuts double bonds. Such a separation of the two regions violates the basic requirements of the fragmentation theory.

The total energy is an “average” characteristic of the system that is less sensitive to the approximation used in its calculation than with charge distribution

determined by the local values of the wavefunction. Since electronic structure calculations are carried out on the QM fragment only, it is implicitly assumed that the charge distribution in the fragment will remain the same as in the real system. In case of TMS, as emphasized above, this may not be the case. It brings us to the second requirement of the general theory, the condition of interfragment self-consistency, which is not satisfied in the ONIOM approach. In other words, ONIOM does not account for (and does not predict) charge transfer between the QM and MM parts of the system.

Returning to the Example 5.8, Fig. 5.13, we see that, according to Eq. 5.124, we should perform five calculations, including one for the whole (real) system at the lower MM level and another for the intermediate model system at the same MM level. However, as discussed above in this section, there are no reliable force-field parameters for transition metals, and the MM approach is in general not applicable to TMS. These comments apply to all the metal-containing systems treated by the ONIOM method.

Another method, the *QM/MM method with charge transfer between the QM and MM parts* (the QM/MM/CT method) [5.108, 5.117, 5.118], is based on fragmentation of polyatomic systems discussed at the beginning of this section, and it is aimed directly at TMS. It satisfies all the fragmentation requirements of the general theory and includes the main distinguished feature of TMS: charge transfer between its constituent fragments.

As shown above, the fragmentation condition can be obeyed if the interfragment interactions are much stronger than the intrafragment ones. On the basis of the fragmentation procedure discussed above, consider the two fragments, I and II, of Fig. 5.7 and choose the border borderline between the fragments to cut an  $2s2p$  atom that is not a bridge of  $\pi$ -electron delocalization; in other words, the border atom (BA) should not form  $\pi$  bonds with at least one of the two fragments. As above, assume that some of its  $sp^n$ -hybridized orbitals belong to fragment I, while the others pertain to fragment II. This partitioning method, in which the borderline between the fragments cuts an atom (not a bond), has the advantage of (1) satisfying the condition of fragmentation, outlined above, and (2) allowing for direct charge transfers between the fragments, which is most important when there is strong electron heterogeneity, for example, when some of the fragments contain transition metals.

For evaluation of the charge transfer between the fragments and with interfragment self-consistency the *double-self-consistency (DSC) procedure* was suggested [5.108, 5.117, 5.118]. It allows one to correct both the energy-level positions and orbital charge distribution of the zeroth-order solutions due to the interfragment interaction.

In semiempirical MO-LCAO calculations of any type, for instance, the iterative extended Hückel (IEH) approximation (Section 5.5), the charges on atoms, and more specifically their in-molecule electronic configurations, are usually calculated by means of a Mulliken population analysis (other population schemes can be involved and similar procedures can be realized in *ab initio* calculations).

For instance, for the  $p$ -electron density on atom  $A$  according to Eq. (5.18), we have

$$q_p^A = \sum_{i,v} \sum_{p \in A} n_i c_{ip} c_{iv} S_{pv} \quad (5.129)$$

where  $c_{ip}$  and  $c_{iv}$  are the  $i$ th MO LCAO coefficients of the orbitals  $p$  and  $v$ , respectively,  $S_{pv}$  is their overlap integral, and  $n_i$  is the occupancy number of the  $i$ th MO. These orbital densities determine the ionization energy of the valence state and the matrix elements  $H_{ii}$  and  $H_{ij}$  for the next iteration in the self-consistent calculations. In other methods these matrix elements are determined by the density matrix  $P_{\mu\nu}$  [Eq. (5.21)]:

$$P_{\mu\nu} = \sum_i n_i c_{\mu i} c_{\nu i}^*$$

For the border atoms, as for the others, the atomic orbital charges and the density matrix are determined by the LCAO coefficients of all the AOs of the atoms that participate in the corresponding MO. In iteration procedures the charges on the border atoms that determine the ionization energy of the valence state or the density matrix (which, in turn, form the matrix elements of the secular equation) depend on the results of the previous calculation of *both fragments*. If as a result of the zeroth-order calculations with separate fragments and arbitrary distribution of electrons (first iteration), there is no balance of charge between the fragments, i.e. the atomic charges (or density matrix) for the BA were underestimated in one of the fragments and overestimated in the other one, the density matrix evaluation for the next iteration should increase the corresponding matrix elements in the first fragment and decrease them in the second fragment.

Denote the atomic charge on the BA obtained after (5.129) by separate self-consistent-field calculations of fragments I and II by  $q^{\text{BA}}(\text{I})$  and  $q^{\text{BA}}(\text{II})$ , respectively. Then the difference

$$\Delta q^{\text{BA}} = q^{\text{BA}}(\text{I}) - q^{\text{BA}}(\text{II}) \quad (5.130)$$

may serve as a measure of interfragment self-consistency. In the next iteration the BA charges on fragments should be changed to

$$q^{\text{BA}'}(\text{I}) = q^{\text{BA}}(\text{I}) - k \Delta q^{\text{BA}} \quad (5.131)$$

and

$$q^{\text{BA}'}(\text{II}) = q^{\text{BA}}(\text{II}) + k \Delta q^{\text{BA}} \quad (5.132)$$

respectively, where  $k$  is an arbitrary coefficient introduced for speeding convergence:  $q^{\text{BA}}$  is the charge on *one* atom (BA), while the charge transfer goes to the whole fragment.

The BAs thus serve as *channels of charge transfer from one fragment to another*, and the final solution of such fragmentary calculations yields MO energies and density matrices that are self-consistent with respect to both intrafragment and interfragment charge distribution (*double self-consistency*). In this way *an electronically transparent interface* between the fragments is realized; it factors in all effects of charge transfer, excitation by coordination, and so on, mentioned above. We calculate the fragments in parallel and independently, but in fact they are strongly interdependent since after each iteration the charges, or the density matrix, that determine the matrix elements of the Hamiltonian for each fragment are calculated on the basis of the results of the previous iteration obtained from both fragments.

This implementation of the condition of interfragment self-consistency implies that both neighboring fragments are calculated quantum-mechanically. If one of these fragments is to be optimized by MM as stipulated by the QM/MM method, both conditions of interfragment self-consistency and QM/MM quantum-to-classical continuity can be satisfied simultaneously by an additional procedure in which, in addition to the smaller part of the system, which is given a full QM treatment, and its larger part, which is optimized by MM, an intermediate fragment between them (a part of the MM site) is separated and treated by both QM (electronic structure) and MM (geometry optimization), the QM+MM fragment. This allows one to reach double self-consistency at the border atom using the electronic structure data from both fragments, and to realize a smooth transition from the quantum site to the classical MM description of the organic ligands.

For real molecular systems, especially (but not only) organometallics, appropriate fragmentation results in more than two fragments, some of them having more than one BA (see the example below). This complicates the DSC procedure mainly because the charge transfer to a given fragment via one of the BAs should be balanced with that from other fragments (via other BAs). A procedure is suggested [5.108, 5.117] to expedite the DSC convergence in this case, and the geometry optimization problem should be handled at each iteration accordingly.

A major problem emerges in geometry optimization when unsaturated valences remain at the border of the fragments. For instance, in the fragmentation method, discussed above, when the BA participates with some of its orbitals in one of the fragments, with its other orbitals engaged in the other fragment, the BA has unsaturated valences when included in any one of the fragments. There are several approximate procedures for handling this problem; the most useful one is the so-called method of link atoms (or dummy atoms). The essence of this method is simply to substitute the free valence by a bond to a hydrogen atom. This means, for example, that the cut single bond C—N in —C—N< is substituted by H—N< in the right fragment, and —C—H in the left one. If an atom is cut in the fragmentation, the valences can be substituted by either link atoms, as above, or link groups, as illustrated in Fig 5.14. While intuitively the scheme of link atoms seems to be reasonable,

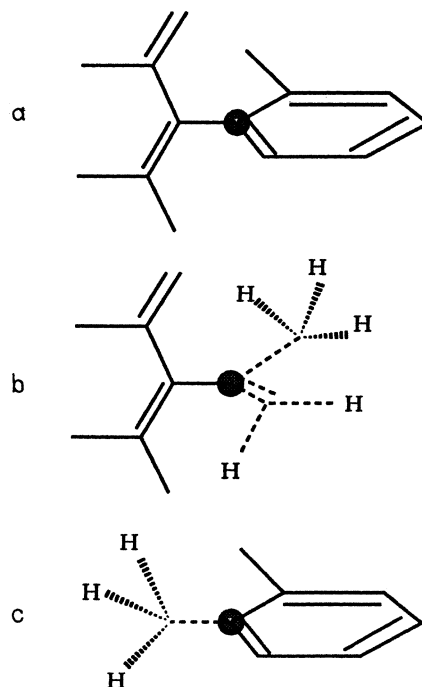


**FIGURE 5.14.** Link groups for one of the border atoms (carbon) in the fragmentation of iron picket-fence porphyrin (Fig. 5.15): (a) the real bonds formed by the border atom (the latter is shown by encircled dots); (b) the link groups (shown by dashed lines) in calculations for the central fragment; (c) the link groups for the ligand fragment.

the computational details may be complicated [5.108, 5.117]. Example 5.9 shows the results of application of the QM/MM/CT method to iron picket-fence porphyrin.

### EXAMPLE 5.9

#### *Iron Picket-Fence Porphyrin Treated by the QM/MM Method with Charge Transfer (QM/MM/CT)*

By way of example we show here some results obtained by QM/MM/CT calculations of *iron picket-fence porphyrin* [5.117, 5.108]. Figure 5.15 shows the chemical structure of this system [5.125]; dashed lines indicate the fragmentation used in the calculations [5.117]. The BA (four carbon atoms at four “fence” ligands and the nitrogen of the axial ligand) do not form  $\pi$  bonds with the central fragment because of steric restrictions (the corresponding two molecular groups from both sides of the BA are not coplanar).

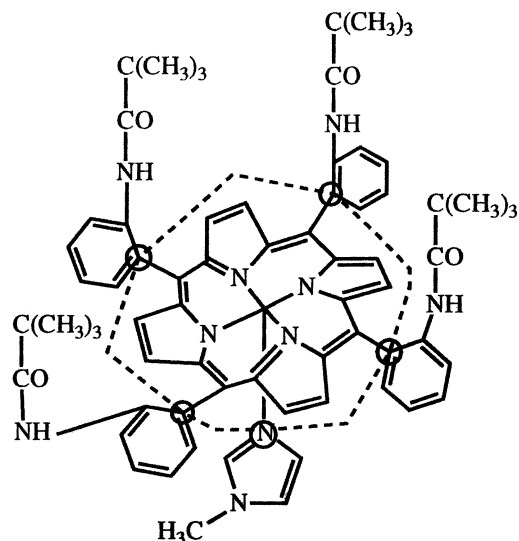


**FIGURE 5.15.** Structure of iron picket-fence porphyrin. The dashed line separates the central fragment; the border atoms are encircled.

The choice of link atomic groups is shown in Fig. 5.14. The authors [5.117] tried also a simpler version with just one hydrogen atom for each free valence with not very significant changes in the results. The central fragment was optimized using INDO/1 from the ZINDO package [5.91, 5.126] reprogrammed to include the fractional MO occupancy numbers following Eqs. (5.130)–(5.132). The MM treatment was realized by using the Tripos force field [5.127] within the SYBYL molecular modeling package.

The optimization procedure for the central fragment is rather fast (several minutes) for the initial (closed-shell low-spin configuration) fragment and becomes much slower for the open-shell calculations after fractional charge transfers. The results reproduce the out-of-plane position of the iron atom with respect to the porphyrin ring at a distance  $h = 0.45 \text{ \AA}$ ; the experimental value is  $0.40 \text{ \AA}$  [5.128], which is usual for the group of similar porphyrins [5.129]. This out-of-plane position of the central atom is an important feature of some iron (and other metal) porphyrins that is due to the vibronic mixing of the occupied  $a_{2u}(\pi)$  MO of the porphyrin ring with the unoccupied  $a_{1g}(d_{z^2})$  MO of (mainly) the iron atom by the out-of-plane displacement of the iron atom (see Section 9.2). It is one of the effects that cannot be accounted for properly without QM treatment: MM does not involve electronically excited states. The authors used INDO/1 [5.91, 5.126] for geometry optimization and ICONC [5.130] for calculation of charge distribution and

redistribution after charge transfer. Interfragment self-consistency was reached after eight or nine cycles. The convergence process together with the DSC charge redistribution between the fragments is illustrated in Fig. 5.16.

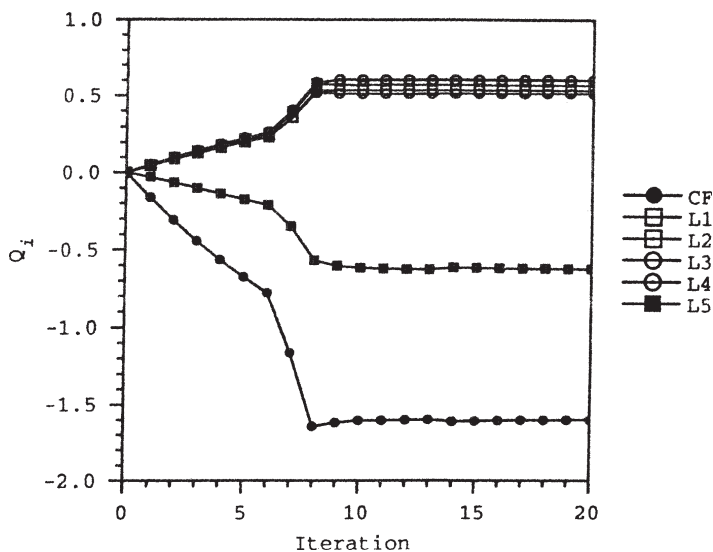


**FIGURE 5.16.** Charge redistribution between the six fragments (CF is the central fragment and  $L_n$  is the  $n$ th ligand fragment) in the DSC procedure versus iteration. It is seen that self-consistency is achieved after the 8th iteration.

It is seen that each of the four “fence” fragments loses approximately 0.5–0.6 electron, while the axial ligand gains about 0.6 electron, transferred via the central fragment; the balance of the latter is thus approximately about  $-1.6$  electrons. This substantial charge transfer between the fragments confirms that the non-charge-transfer models of QM/MM treatment, discussed above, may be invalid for TMS. The size of these charge transfers seems to be correct in order of magnitude. A ligand-to-metal transfer of 0.5–1.0 electron is not unexpected, and the large total transfer to the metal fragment may be reasonable in view of the high “charge capacitance” of the porphyrin ring (Section 10.1, Example 10.1). The optimized geometry agrees quite well with the experimental data available, in particular with X-ray results [5.128].

For QM/MM/CT calculations for other systems, see Refs. 5.117, 5.118 and 5.131.

## 5.7. GENERAL COMPARISON OF METHODS

Discussion of the advantages and disadvantages of the methods of electronic structure calculations and their mutual comparison is an extensive subject for entire monographs [5.17, 5.37, 5.132–5.134]. The goal of this section is to provide a general brief outline of the problem for a better understanding and rough estimation of the relative value of semiempirical and nonempirical MO methods, as well as DFT and QM/MM methods in their application to transition metal compounds.

The modern state of the art in the MO LCAO and related methods discussed in this section is rather advanced and, in principle, makes it possible to compute numerically the electronic structure of any molecular system of reasonable size. This statement does not mean that there are no problems in the realization of such computations. Concerning *ab initio* and nonempirical methods, these problems are created by *reasons of cost* and difficulties in the *rationalization of the results*.

The cost reasons are due to the increased computer time required for the calculations with an increased number of atoms in the system. For the calculation of a moderate seven-atom octahedral complex of a  $3d$  transition metal using a minimal Gaussian basis set, one must compute about  $10^9$  integrals that can be reduced to  $10^7$  by preliminary contraction of the basis set (Section 5.3), and the number of integrals usually increases as  $n^4$ , where  $n$  is the number of functions in the basis set, which is larger than the number of atoms (in the DFT methods the number of integral is proportional to  $n^3$ ). For instance, for a 30-atom molecular system the number of integrals and hence the computer time increase more than 250 times as the basis set increases 4 times. Obviously, there is a limit of economic expediency of such calculations. Note also that in the calculation of fine details (small effects) of electronic structure different versions of highly sophisticated methods may yield different (sometimes conflicting) results, which complicate their reliable interpretation [5.135].

Another difficulty with nonempirical calculations is that for large systems the computer output information, the wavefunction, spread in thousands of determinants is so vast that without additional rationalization it is useless. Fortunately, modern computer programs are aimed at yielding final physical quantities without revealing the wavefunction explicitly. As mentioned in Section 1.2, numerical results of electronic structure calculations, taken as such, are rather experimental data relevant to the specific system for which the calculations were performed, and only when accumulated for series of somewhat similar compounds, they can be used for comparisons and theoretical generalizations based on *analytical models*.

From this perspective the semiquantitative and semiempirical methods are more advantageous. First, with these methods the computer time is essentially reduced. For instance, for the  $\text{MnO}_4^-$  complex with a valence basis set of  $3d$ ,  $4s$ , and  $4p$  AOs of Mn and only  $p$  AOs of the oxygen atoms, the number of repulsion integrals to be computed in the nonempirical method is 26,796, while in the NDDO method it is reduced to 2415, and in the semiempirical CNDO method



there are only 15 [5.86]. In the semiempirical methods the results of numerical computation, as distinct from the ab initio data, are quite understandable in terms of visual MOs built up from atomic valence states, the picture of the electronic structure is thus more acceptable for chemists.

However, semiquantitative and especially semiempirical methods have other faults, mainly *insufficient theoretical foundation, limited quantitative reliability, and low credibility*. As to the theoretical foundation, it is certainly reduced in semiempirical methods as compared with the nonempirical ones. For instance, in the extended Hückel method (Section 5.5) the coefficient  $k$  in the presentation of the off-diagonal matrix element of the Hamiltonian  $H_{ij}$  by the diagonal elements,  $H_{ij} = \frac{1}{2}k(H_{ii} + H_{jj})$ , is usually taken as  $k = 2$  for  $\pi$  bonds and  $k = 1.67$  for  $\sigma$  bonds, which, theoretically, are almost arbitrary (for further criticism of such methods, see Refs. 5.85–5.87). Therefore, one cannot expect the energies and wavefunctions obtained with such coefficients to be sufficiently trustworthy.

For absolute values of semiempirically calculated quantities, the credibility is low, but increases when there are nonempirical results that can be used as calibration points. When used with the same  $k$  value for series of compounds, this method yields much *more reliable relative values* in which the systematic error introduced by the arbitrary choice of the basic formula is mostly excluded. As stated by Hoffmann [5.136], the extended Hückel theory “has the merit of being of the low end of a quality scale of approximate MO calculations. Since all other methods are superior to it, it inculcates in its user a feeling of humility and forces him or her to think about why the calculations come out the way they do. The method is widely applicable and transparent but it has limited quantitative reliability.”

On another occasion, as Pyykko put it [5.105]: “it is said that when no such results were yet available, some of the earliest semiempirical conclusions [5.71, 5.103] suggesting that relativistic effects might be important in chemistry, were met with derision.” This derision was ungrounded because in these studies the semiempirical approach was used only for *comparison* of relativistic and non-relativistic results obtained with the same method for the same compounds. The consequent developments confirmed the importance of relativistic effects in chemistry (see Section 6.5).

The low credibility in semiempirical methods is often based also on their inappropriate use and the ignorance of *limits of applicability*. All the methods of calculation of electronic structure of molecules have limits of applicability determined by the principles on which they are based and the additional assumptions made when the calculations are carried out. The main limitations of the MO and density-functional methods are mentioned in Sections 5.3–5.5. The DFT methods as simplified ab initio MO LCAO approaches gained significant attention in the last two decades.

In view of the variety of existing methods of calculation, the user may have problems choosing the method that is adequate to the problem at hand. It is clear that *the method of calculation of the electronic structure of a given molecular system should satisfy the requirement of minimum labor compatible with the*

*problem to be solved and the accuracy required.* For instance, to calculate the expected  $g$  factors in the ESR spectra of transition metal and rare-earth complexes (Section 8.4), the crystal field theory (Chapter 4) may be sufficient, whereas the superhyperfine structure cannot be estimated without taking into account the covalence effects, that is, without using one of the MO approximations (Section 5.2). If the spin density distribution over a larger ligand system is sought for, a more complete MO LCAO approach should be employed (semiempirical, semiquantitative, nonempirical, *ab initio*, and their different versions) depending on the required quantitative reliability and accuracy.

The problem of *accuracy of the results* of quantum-chemical calculations is not trivial. Although quantum chemistry is, in general, a theoretical discipline based on the stone background of quantum mechanics, unlike the majority of mathematical disciplines, it has no mathematically rigorous internal criterion of calculations accuracy. This statement emerges from the basic approximations of quantum chemistry, mentioned in Section 1.3, which are inevitable and have no exact quantitative measure of the error they introduce that can be easily evaluated.

As a measure of accuracy of the calculations, the *quantum-mechanical limit*—calculations in which all the interactions are taken into account exactly as required by quantum mechanics—could be used. However, strictly speaking, the *exact* quantum-mechanical limit cannot be reached, not only because of technical problems, but also, in principle, because of the lack of exact Hamiltonians that include the relativistic interaction between the electrons (Section 5.4). Although the latter is important only for some relatively weak magnetic properties, it is a matter of principle that, strictly speaking, the exact quantum-mechanical limit does not exist.

Practically, the quantum-mechanical limit cannot be reached for more prosaic reasons that are discussed in Sections 1.3, 5.3, and 5.4. For the MO and DFT methods they are: (1) use of limited basis sets and neglect of (a part of) electron correlation effects, (2) adiabatic and nonadiabatic coupling to nuclear motions, and (3) relativistic effects. Extension of the basis set leads to the Hartree–Fock limit. Including the correlation effects (e.g., by CI), one moves significantly to the quantum-mechanical limit, but still remains far from it. Exact calculations, including nuclear motions and relativistic effects, are beyond the practical possibilities not only for coordination compounds, but also for much smaller molecules.

Thus in electronic structure calculations in general we are far from the quantum-mechanical limit, and there are no quantitative estimates of the remaining distance to this limit in each specific case. Therefore, the only practically acceptable criterion of accuracy of the results of calculations is the *comparison with experimental data*.

Concerning the comparison with experiments, in some cases the less laborious and less quantitatively reliable semiempirical results may be closer to the experimental data than the nonempirical calculations. This better agreement with experiments is reached not by more accurate calculations, but by introducing appropriate empirical and other (sometimes arbitrary, adjustable) parameters.

With adjustable parameters, one can obtain results that are more adequate to the experimental data, but they cannot be classified as more accurate results of calculations in the sense of approaching the quantum-mechanical limit.

Table 5.12 compares nonempirical and semiempirical calculations from the perspective of their relative advantages and disadvantages denoted by “+” and “-,” respectively.

The nonempirical methods are ahead in determining the progress in the area as a whole. The more recent achievements in solving chemical problems (Sections 6.3–6.5, 11.3) based in major part on the use of modern computers, show the increasing ability of these methods. As mentioned above, nonempirical methods are also used to obtain calibrating points for semiempirical methods and other model approximations, thus influencing their development and serving them as a test.

On the other hand, semiempirical methods have many advantages of simplicity, visualization, and flexibility; they are less labor-intensive and computer-time-consuming and enable calculations for much larger systems than do nonempirical methods. These advantages are of particular importance to coordination compounds with heavy atoms and large ligands (e.g., metallobiochemical compounds). Special attention should also be paid to better visualization and more direct relevance to analytical models that allow for a better understanding and contribute significantly to the formation of intuitive thinking (Section 1.1). Analytical models also contribute to the rationalization of numerical results and development of the general theory of electronic structure.

As for coordination compounds, some additional remarks are in order on comparison of MO LCAO approaches with crystal field theory (CFT). CFT provides a satisfactory qualitative description of one of the main effects of coordination: CA term splitting. The MO LCAO scheme, in the part concerning the CA states,

**TABLE 5.12. Comparison of Nonempirical and Semiempirical MO LCAO Methods in Terms of Relative Advantages and Disadvantages Denoted by “+” and “-,” Respectively**

Characteristic	Nonempirical Methods	Semiempirical Methods
Theoretical foundation	+	-
Accuracy of results	+	-
Quantitative reliability (credibility)	+	-
Labor consumption	-	+
Calculative molecular size	-	+
Flexibility (e.g., the possibility of fragmentary calculations)	-	+
Visualization of results	-	+
Relation to analytical models	-	+

results in qualitatively the same energy level splitting (Section 6.2). But the absolute value of the main CFT parameter  $\Delta$  can be correctly calculated only in the MO LCAO approaches.

In the late 1950s–early 1960s there was intensive discussion of whether the CFT gives a correct order of magnitude for  $\Delta$  calculated in the point charge model, and it was concluded that for predominant ionic compounds the covalence contribution to  $\Delta$  is about 10–20% [5.11]. If covalence corrections are introduced, for instance, in the AOM approximation of weak covalence (Section 5.2), the results on energy-level splitting may be quite satisfactory. A more detailed theoretical comparison between CFT, AOM, and MO LCAO methods is given by Gerloch [5.134].

However, as discussed in Section 8.4, the CFT cannot, in principle, consider phenomena that depend on the details of electronic structure of ligands, including the detailed description of the bonding,  $\pi$ -bond formation, backdonation, charge transfer spectra, and ligand activation by coordination, and the AOM is also strongly limited to phenomena that take place within the  $d$ -electron shell (Section 5.2). All these problems should be treated by MO LCAO or density-functional methods.

The possibilities of quantum chemistry increase significantly when reasonable combinations of quantum-mechanical, semiclassical, and classical methods are employed. For instance, Clementi and Corongiu [5.137] have shown that very large systems with thousands of atoms can be described by using nonempirical quantum-chemical calculations of electronic structure for a part of the system followed by a hierarchy of models, including molecular mechanics, statistical physics, and fluid mechanics, as well as molecular dynamics. The DNA in solutions (more than 4000 atoms) was used as an example. This and many other similar works shows that the possibilities of theoretical chemistry using electronic structure calculations as a basic element is practically unlimited and may reach the level of macrosystems, provided that the theory is used with a proper understanding of its possibilities.

An essential problem here is to work out appropriate interfaces between different parts of the polyatomic system that are treated by significantly different methods. This brings us to the classical and quantum–classical methods considered in Section 5.6. Notwithstanding their limitations, these approaches may serve as a basis for further progress in understanding and prediction of properties of transition metal systems when more accurate electronic structure calculations are practically inaccessible. The QM/MM methods provide also for an interface between (microscopic) quantum and (macroscale) classical treatments that may be unavoidable in the interpretation of observable properties of matter.

The majority of combined QM/MM methods are aimed at organic systems and do not include the option of charge transfers between its fragments; hence they are inapplicable to transition metal systems for which such charge transfers are most important. The QM/MM/CT method, described above, is aimed at large TMS: it performs QM calculation and geometry optimization of the metal-containing fragment and MM treatment of the organic ligands with an electronically transparent

interface based on a double (intrafragment and interfragment) self-consistent procedure that allows for the interfragment charge transfers.

## SUMMARY NOTES

1. The *one-electron approximation* in electronic structure calculations is the most widely used one; it assumes that each electron is moving independently in the averaged field of the nuclei and all the other electrons, and its motion can be described by *molecular orbitals* (MOs).
2. The presentation of MOs by *linear combinations of atomic orbitals* (LCAO), originally introduced to reflect approximately the real motion of the electron along the atomic valence states of the molecular system, was extended to include as much as possible excited atomic states (in the *basis set*); this allows one to mathematically approach the *SCF Hartree–Fock limit* to the exact solution in the one-electron approximation (which still lacks correlation effects).
3. Symmetry considerations allow one to employ group-theoretical methods to classify MOs on symmetry (to obtain *symmetry-adapted MOs*) that essentially simplify the description of the electronic structure and reduce numerical calculations.
4. *Charge distribution* in MOs renders them either bonding, or nonbonding, or antibonding. When pairwise populated with electrons, bonding and antibonding MOs approximately counterbalance each other in bonding energy. The notion of Mulliken atomic charges is roughly approximate and may be misleading in application to TMS.
5. *Numerical calculations* of energies and wavefunctions (LCAO coefficients) with MO LCAO methods are central in quantitative evaluation of electronic structure. In the one-electron approximation, mentioned above, the results may be unsatisfactorily inaccurate (even with the best basis sets) because of neglect of *electron correlation effects*—the difference between instant and averaged interelectron repulsion.
6. Various *methods of electronic structure calculations* factor in electron correlation effects, most of them based on configuration interaction and perturbation theory. Approved by multiple applications, these methods are available in user-friendly computer programs (some of them downloadable online free of charge).
7. By calculating the electronic energy as a function of nuclear coordinates—the *adiabatic potential energy surface* (APES)—one can reveal the nuclear configuration at the minimum of this function, the equilibrium geometry; modern software packages perform such *geometry optimization* automatically. This procedure is based essentially on the adiabatic approximation. Important deviations from this approximation are considered in Chapter 7.

8. *Ab initio methods* are limited by labor and computer time required for electronic structure calculation of large molecular systems. Therefore, *semi-quantitative and semiempirical methods* remain in widespread use. Among them approaches based on *density functional theory* (DFT) are most usable for large molecular systems and crystals.
9. Among the various semiempirical methods, which are much simpler than *ab initio* and semiquantitative methods, the *iterative extended Hückel* (IEH) method with charge and configuration self-consistency (SCCC method) is often used for coordination systems.
10. Fragmentary calculations and *combined quantum–classical methods* in which the active site of the system is treated by quantum mechanics, while the rest of the system is considered by classical molecular mechanics, are unavoidable in the study of large coordination (e.g., metallobiochemical) systems.

## EXERCISES AND PROBLEMS

- \*P5.1.** Following Example 5.4, in which calculations of  $A_g$ -type MOs of  $\text{TiF}_6^{3-}$  are carried out using the Wolfsberg–Helmholz-type semiempirical IEH approximation, calculate in the same way both  $\sigma$ - and  $\pi$ -type MOs of  $E_g$  and  $T_{2g}$  symmetry of this system and construct its MO energy diagram. Use the following numerical values of the empirical parameters [5.99] (in kK: 1 kK =  $10^3 \text{ cm}^{-1}$ ):  $H_{dd} = -91.382$ ,  $H_{ss} = -78.898$ ,  $H_{pp} = -46.060$ ,  $H_{\sigma\sigma} = -154.5$ ,  $H_{\pi\pi} = -177.2$ ,  $S(s, \sigma) = 0.175$ ,  $S(p, \pi) = 0.135$ ,  $S(p, \sigma) = 0.198$ ,  $S(d, \sigma) = 0.180$ , and  $S(d, \pi) = 0.101$ .
- \*P5.2.** For the same problem of evaluating the two  $A_{1g}$ -type MOs in  $\text{TiF}_6^{3-}$  solved in Example 5.4 by the semiempirical IEH method, use the approximation of weak covalence of Section 5.4, in particular, Eqs. (5.38) and (5.39), to obtain the same MO energies, and Eqs. (5.34)–(5.37) for the wavefunctions, and compare the results with those of the IEH method. Analyze the differences between the two methods and indicate your preferences.
- P5.3.** Formulate the relative advantages and disadvantages of DFT methods in application to TMS. Since the charge density does not depend on spin explicitly, can we evaluate the spin of the system by DFT methods? Can we calculate excited states by these methods? Can we treat degenerate states by DFT?
- \*P5.4.** (Carefully repeat the exercises in Examples 5.2 and 5.4 before solving this problem.) Quite similar to Example 5.4, download the program GAMESS (free of charge) or MOLPRO (trial version free for one month), aimed at electronic structure calculation and geometry optimization of molecular systems, carefully read the manuals, and calculate ground-state energies, wavefunctions, and equilibrium geometry (interatomic distances

and angles) of  $\text{MnO}_4^-$  in square-planar, pyramidal, and tetrahedral configurations in the Hartree–Fock approximation with the basis set 6-31G\*. Compare the energies of the three configurations, as well as all the other results with those obtained for the same system in the next three problems.

- \*P5.5.** The same as in Problem 5.4 but calculated using the MP2 approximation with the 6-31G\* basis set with the same comparisons as in Problem 5.4.
- \*P5.6.** The same as in Problem 5.4 but calculated in the DFT approximation using LDA and B3LYP exchange–correlation functionals and the 6-31G\* basis set with all comparisons as in Problem 5.4; compare the results also with DFT- $X_\alpha$  calculations in Ref. 5.138.
- \*\*5.7.** (Carefully repeat the exercises in Examples 5.2–5.4 and Problems 5.4–5.6 before solving this problem.) Download the program GAMESS (free of charge) or MOLPRO (trial version free for one month) aimed at electronic structure calculation and geometry optimization of molecular systems, carefully read the manuals, and calculate ground-state energies, wavefunctions, and equilibrium geometry (interatomic distances and angles) of  $\text{FeF}_6^{4-}$  in high-spin and low-spin configurations using the CASSCF method. Compare their energies with those in the corresponding Tanabe–Sugano diagram in Section 4.3. Can this TMS be used as a temperature-dependent spin crossover system (Section 8.4)?

## REFERENCES

- 5.1. R. S. Mulliken, in *XXII Int. Congress of Pure and Applied Chemistry, Plenary Lectures*, Butterworths, London, 1970, p. 203.
- 5.2. L. E. Orgel, *An Introduction to Transition-Metal Chemistry*, Wiley, New York, 1960.
- 5.3. K. Ballhausen, *Introduction to Ligand Field Theory*, McGraw-Hill, New York, 1962; *Molecular Electronic Structure of Transition Metal Complexes*, McGraw-Hill, New York, 1979.
- 5.4. C. K. Jorgensen, *Modern Aspects of Ligand Field Theory*, North-Holland, Amsterdam, 1971.
- 5.5. I. B. Bersuker, *Electronnoe Stroenie i Svoistva Koordinatsionnykh Soedinenii* (Russ.), 3rd ed., Khimia, Leningrad, 1986.
- 5.6. A. Veillard, ed., *Quantum Chemistry: The Challenge of Transition Metals and Coordination Chemistry*, NATO ASI Series C: Math. Phys. Sci., Vol. 176, Reidel, Dordrecht, 1986.
- 5.7. R. S. Mulliken, *J. Chem. Phys.* **23**, 1841 (1955).
- 5.8. P. Politzer and R. R. Harris, *J. Am. Chem. Soc.* **92**, 6541 (1970); P. Politzer, *Theor. Chim. Acta* **23**, 203 (1971).
- 5.9. J. O. Noell, *Inorg. Chem.* **21**, 11 (1982).
- 5.10. P. J. Hay, *J. Am. Chem. Soc.* **103**, 1390 (1981).
- 5.11. R. E. Watson and A. J. Freeman, *Phys. Rev. A* **134**, 1526 (1964); E. Simanek and Z. Sroubek, *Phys. Stat. Sol.* **4**, 251 (1964).



- 5.12. C. K. Jorgensen, R. Pappalardo, and H. H. Schmidtke, *J. Chem. Phys.* **39**, 1422 (1963); C. E. Schaffer, *Struct. Bond.* **14**, 69 (1973).
- 5.13. D. W. Smith, *Struct. Bond.* **12**, 49 (1972).
- 5.14. A. B. P. Lever and E. I. Solomon, in E. I. Solomon and A. B. P. Lever, eds., *Inorganic Electronic Structure and Spectroscopy*, Vol. 1, Wiley, New York, 1999, p. 1.
- 5.15. C. C. Roothaan, *Rev. Mod. Phys.* **23**, 69 (1951); **32**, 179 (1960).
- 5.16. J. C. Slater, *Electronic Structure of Molecules*, McGraw-Hill, New York, 1963.
- 5.17. J. A. Pople and R. K. Nesbet, *J. Chem. Phys.* **22**, 571 (1954); A. T. Amos and G. G. Hall, *Proc. Roy. Soc. (Lond.)* **A263**, 483 (1961).
- 5.18. R. McWeeny, *Methods of Molecular Quantum Mechanics*, 2nd ed., Academic Press, London, 1989; R. McWeeny, *Ab Initio Methods in Quantum Chemistry*, Academic Press, London, 1989; A. Szabo and N. Ostlund, eds., *Modern Quantum Chemistry*, McGraw-Hill, New York, 1989.
- 5.19. F. Jensen, *Introduction to Computational Chemistry*, Wiley, New York, 2002.
- 5.20. R. McWeeny, *Nature* **166**(4209), 21 (1950).
- 5.21. S. F. Boys, *Proc. Roy. Soc. (Lond.)* **A200**, 542 (1950).
- 5.22. E. Clementi and D. R. Davis, *J. Comput. Phys.* **1**, 223 (1966)
- 5.23. E. Clementi and D. C. Raimondi, *J. Chem. Phys.* **38**, 2686 (1963).
- 5.24. J. W. Richardson, W. C. Nieuwoort, R. R. Powell, and W. F. Edgell, *J. Chem. Phys.* **36**, 1057 (1962).
- 5.25. E. Clementi, *IBM Res. Devel. Suppl.* **9**, 2 (1965).
- 5.26. S. Huzinaga, *J. Chem. Phys.* **42**, 1293 (1965).
- 5.27. A. Veillard, *Theor. Chim. Acta* **12**, 405 (1968).
- 5.28. B. Roos, A. Veillard, and G. Vinit, *Theor. Chim. Acta* **20**, 1 (1971).
- 5.29. B. Roos and K. Siegbahn, *Theor. Chim. Acta* **17**, 209 (1970)
- 5.30. S. Huzinaga, *Approximate Atomic Wave Functions*, Vols. I, II, Dept. Chem. Report, Edmonton, Alberta (Canada), Univ. Alberta, 1971.
- 5.31. E. Clementi and C. Roetti, *Atomic Data and Nuclear Data Tables*, Vol. 14, 1974, pp. 177–478.
- 5.32. R. Krishnan, J. S. Binkley, R. Seeger, and J. A. Pople, *J. Chem. Phys.* **72**, 650 (1980).
- 5.33. I. B. Bersuker, *The Jahn-Teller Effect*, Cambridge Univ. Press, Cambridge, UK, 2006.
- 5.34. S. M. Bachrach and A. Streitwieser, Jr., *J. Am. Chem. Soc.* **106**, 2283 (1984).
- 5.35. (a) <http://tyr0.chem.wsu.edu/~kipeters/basissets/basis.html>;  
(b) N. B. Balabanov and K. A. Peterson, *J. Chem. Phys.* **123**, 064107 (2005); (c) <ftp://ftp.chemie.uni-karlsruhe.de/pub/basen/>; (d) <http://www.emsl.pnl.gov/forms/basisform.html>.
- 5.36. J. Almlof, in B. Ross, ed., *Lecture Notes in Quantum Chemistry II*, Lecture Notes in Chemistry, Vol. 64, Springer, Berlin, 1994, p. 1; P. R. Taylor, *ibid.*, p. 125; P. Carsky and M. Urban, *Ab Initio Calculations. Methods and Applications in Chemistry*, Lecture Notes in Chemistry, Vol. 16, Springer-Verlag, Berlin, 1980; W. Kutzelnig, in H. F. Schaefer III, ed., *Modern Theoretical Chemistry*, Vol. 3, Plenum, New York, 1977.



- 5.37. D. R. Salahub and M. C. Zerner, in D. R. Salahub and M. C. Zerner, eds., *The Challenge of d and f Electrons. Theory and Computation*, Eds. ACS Symposium Series 394, Washington, DC, 1989, p. 1.
- 5.38. GAUSSUAN03: M. J. Frisch, G. W. Trucks, H. B. Schlegel, et al., Gaussian, Inc., Pittsburg PA, 2003.
- 5.39. GAMESS: M. W. Schmidt et al., distributed by M. W. Schmidt, Dept. Chemistry, Iowa State Univ., Ames.
- 5.40. MOLPRO: H.-J. Werner, P. J. Knowles, et al., School of Chemistry, Univ. Birmingham, Edgbaston, Birmingham, B15 2TT, UK.
- 5.41. M. B. Hall and R. F. Fenske, *Inorg. Chem.* **11**, 768 (1972)
- 5.42. P. J. Hay and W. R. Wadt, *J. Chem. Phys.* **82**, 270, 299 (1985); W. R. Wadt and P. J. Hay, *J. Chem. Phys.* **82**, 284 (1985)
- 5.43. H. A. Bethe and E. E. Salpeter, *Quantum Mechanics of One- and Two-electron Atoms*, Springer, Berlin, 1957.
- 5.44. U. Weding, M. Dolg, H. Stoll, and H. Preuss, in A. Veillard, ed., *Quantum Chemistry: A Challenge of Transition Metals and Coordination Chemistry*, NATO Series C., Vol. 176, 1986, p. 79.
- 5.45. R. G. Parr and W. Yang, *Density Functional Theory of Atoms and Molecules*, Oxford Univ. Press, New York, 1989; J. K. Labanowski and J. Andzelm, eds., *Density Functional Methods in Chemistry*, New York, 1991; J. Weber, ed., *Applications of Density Functional Theory in Chemistry and Physics*, in *New J. Chem.* **17**(12) (1992); N. H. March, *Electron Density Theory of Atoms and Molecules*, Academic Press, New York, 1992; N. C. Handy, in B. Ross, ed., *Lecture Notes in Quantum Chemistry II, Lecture Notes in Chemistry*, Vol. 64, Springer, Berlin, 1994, p. 91; D. R. Salahub, in D. R. Salahub and N. Russo, eds., *Metal-Ligand Interaction: From Atoms, to Clusters, to Surfaces*, Kluwer, Dordrecht, 1992.
- 5.46. P. C. Hohenberg and W. Kohn, *Phys. Rev.* **136**, B846 (1964); P. C. Hohenberg, W. Kohn, and L. J. Sham, *Adv. Quant. Chem.* **21**, 7 (1990).
- 5.47. M. Levy, *Proc. Natl. Acad. Sci. USA* **76**, 6062 (1979); *Phys. Rev.* **A26**, 1200 (1982); E. Lieb, *Int. J. Quantum Chem.* **24**, 243 (1983).
- 5.48. W. Kohn and L. J. Sham, *Phys. Rev.* **140**, A1133 (1965).
- 5.49. I. G. Kaplan, *J. Mol. Struct.* **838**, 39 (2007).
- 5.50. I. B. Bersuker, *J. Comput. Chem.* **18**, 260 (1997).
- 5.51. J. F. Capitani, R. F. Nalewajski, and R. G. Parr, *J. Chem. Phys.* **76**, 568 (1982).
- 5.52. P. A. M. Dirac, *Proc. Cambridge Phys. Soc.* **26**, 376 (1930).
- 5.53. J. C. Slater, *Adv. Quant. Chem.* **6**, 1 (1972); J. C. Slater and K. H. Johnson, *Phys. Rev. B* **5**, 844 (1972).
- 5.54. K. H. Johnson, *Adv. Quant. Chem.* **7**, 143, (1973); K. H. Johnson and F. C. Smith, Jr., *Phys. Rev. B* **5**, 813 (1972); K. H. Johnson, J. C. Norman, Jr., and J. W. D. Connolly, in F. Herman, A. D. McLean, and R. K. Nesbet, eds., *Computational Method for Large Molecules and Localized States in Solids*, Plenum, New York, 1973, p. 161; K. H. Johnson, *Annu. Rev. Phys. Chem.* **26**, 39 (1975).
- 5.55. H. Chermette, in B. Ross, ed., *Lecture Notes in Quantum Chemistry II*, Lecture Notes in Chemistry, Vol. 64, Springer, Berlin, 1994, p. 1081.
- 5.56. A. Rosen, D. E. Ellis, H. Adachi, and F. W. Averill, *J. Chem. Phys.* **65**, 3629 (1976).

- 5.57. J. Q. Snijders and E. J. Baerends, *Mol. Phys.* **33**, 1651 (1977).
- 5.58. A. Rosen and D. E. Ellis, *J. Chem. Phys.* **62**, 3039 (1975); D. E. Ellis and G. L. Goodman, *Int. J. Quantum Chem.* **25**, 185 (1984).
- 5.59. A. D. Becke, *Phys. Rev. B* **38**, 3098 (1988).
- 5.60. J. D. Perdew and Y. Wang, *Phys. Rev. B* **33**, 8800 (1986).
- 5.61. C. Lee, W. Yang, and R. G. Parr, *Phys. Rev. B* **37**, 785 (1988).
- 5.62. R. Sratmann, G. Scuseria, and M. Frish, *J. Chem. Phys.* **109**, 8218 (1998).
- 5.63. ADF: <http://www.scm.com/Doc/Doc2008.01/Background/References/page1.html>.
- 5.64. Ab-Init: X. Gonze, J.-M. Beuken, R. Caracas, et al., *Comput. Mater. Sci.* **25**, 478 (2002).
- 5.65. Siesta: [http://www.icmab.es/siesta\\_new/index.php?option=com\\_content&task=view&id=9&Itemid=15](http://www.icmab.es/siesta_new/index.php?option=com_content&task=view&id=9&Itemid=15).
- 5.66. P. Pyykko, *Chem. Rev.* **88**, 563 (1988).
- 5.67. S. Wilson, ed., *Methods in Computational Chemistry*, Vol. 2, *Relativistic Effects in Atoms and Molecules*, Plenum, New York, 1988.
- 5.68. D. R. McKelvey, *J. Chem. Educ.* **60**, 112 (1983).
- 5.69. G. L. Mali, ed., *Relativistic Effects in Atoms, Molecules and Solids*, Plenum, New York, 1983.
- 5.70. A. I. Akhiezer and V. B. Berestetskii, *Quantum Electrodynamics* (Russ.), Nauka, Moscow, 1969.
- 5.71. I. B. Bersuker, S. S. Budnikov, and B. A. Leizerov, *Int. J. Quant. Chem.* **6**, 849 (1972); *Teor. Exp. Khim.* **4**, 586 (1974).
- 5.72. D. A. Case, *Annu. Rev. Phys. Chem.* **33**, 151 (1982).
- 5.73. L. Visscher, P. J. C. Aerts, and W. C. Nieuwport, *J. Chem. Phys.* **96**, 2910 (1992).
- 5.74. L. A. La John, P. A. Christiansen, R. B. Ross, T. Atashroo, and W. C. Ermler, *J. Chem. Phys.* **87**, 2812 (1987).
- 5.75. Y. Sakai, E. Miyoshi, M. Klobukowski, and S. Huzinaga, *J. Comput. Chem.* **8**, 226 (1987); *ibid.* **8**, 256 (1987).
- 5.76. M. Dolg, H. Stoll, and H. Preuss, *J. Chem. Phys.* **90**, 1730 (1989); Kuechle, M. Dolg, and H. Preuss, *J. Chem. Phys.* **100**, 7535 (1994).
- 5.77. T. R. Cundari and W. Stevens, *J. Chem. Phys.* **98**, 5555 (1993).
- 5.78. H. Chermette and A. Goursot, in J. P. Dahl and J. Avery, eds., *Local Density Approximation in Quantum Chemistry and Solid State Physics*, Plenum, New York, 1984, p. 353.
- 5.79. E. J. Baerends, J. A. Snijders, C. A. de Lange, and G. Jonkers, in J. P. Dahl and J. Avery, eds., *Local Density Approximation in Quantum Chemistry and Solid State Physics*, Plenum, New York, 1984, p. 415.
- 5.80. E. K. U. Gross and R. M. Dreizler, in J. P. Dahl and J. Avery, eds., *Local Density Approximation in Quantum Chemistry and Solid State Physics*, Plenum, New York, 1984, p. 353.
- 5.81. P. Pyykko, *Report HUKI 1-86*, Univ. Helsinki, 1986.
- 5.82. J. A. Pople, D. P. Santry, and G. A. Segal, *J. Chem. Phys.* **43**, 129 (1965).

- 5.83. M. G. Veselov and M. M. Mestechkin, *Litovskii Fiz. Sbornik* **3**, 269 (1963); I. J. Fisher-Hjalmars, *J. Chem. Phys.* **42**, 1962 (1965); *Adv. Quant. Chem.* **2**, 25 (1965).
- 5.84. P. O. Lowdin, *Adv. Quant. Chem.* **5**, 185 (1970)
- 5.85. J. P. Dahl and C. J. Ballhausen, *Adv. Quant. Chem.* **4**, 170 (1969).
- 5.86. D. A. Brown, W. I. Chambers, and N. I. Fitzpatric, *Inorg. Chim. Acta Rev.* **6**, 7 (1972); R. D. Brown and K. R. Roby, *Theor. Chim. Acta (Berlin)* **16**, 175, 194 (1970).
- 5.87. P. G. Burton, *Coord. Chem. Rev.* **12**, 37 (1974).
- 5.88. M. Zerner in K. B. Lipkowitz and D. B. Boyd, eds., *Reviews in Computational Chemistry*, Vol. 2, VCH, New York, 1991, p. 313.
- 5.89. J. A. Pople, D. L. Beveridge, and P. A. Dobosh, *J. Chem. Phys.* **47**, 2026 (1967); M. S. Gordon and J. A. Pople, *J. Chem. Phys.* **49**, 4643 (1968).
- 5.90. N. C. Baird and M. J. S. Dewar, *J. Am. Chem. Soc.* **91**, 352 (1969).
- 5.91. A. D. Bacok and M. C. Zerner, *Theor. Chim. Acta* **53**, 21 (1979).
- 5.92. M. Wolfsberg and L. Helmholz, *J. Chem. Phys.* **20**, 837 (1952).
- 5.93. R. Hoffmann, *J. Chem. Phys.* **39**, 1397 (1963).
- 5.94. S. P. McGlynn, L. G. Vanquickenborne, L. G. Kinoshita, and D. G. Carroll, *Introduction to Applied Quantum Chemistry*, Holt, Rinehart and Winston, New York, 1972.
- 5.95. C. J. Ballhausen and H. Gray, *Molecular Orbital Theory*, Benjamin, New York, 1964.
- 5.96. H. Bash, A. Viste, and H. B. Gray, *J. Chem. Phys.* **44**, 10 (1966).
- 5.97. V. I. Baranovski and A. B. Nikolski, *Theor. Eksp. Khim.* **3**, 527 (1967).
- 5.98. H. Bash and H. B. Gray, *Inorg. Chem.* **6**, 630 (1967).
- 5.99. H. D. Bedon, S. M. Horner, and S. Y. Tyree, *Inorg. Chem.* **3**, 647 (1964).
- 5.100. A. B. Anderson and R. Hoffmann, *J. Chem. Phys.* **60**, 4271 (1974).
- 5.101. G. Calzaferri, L. Forss, and I. Kamber, *J. Phys. Chem.* **93**, 5366 (1989); M. Brandle and G. Calzaferri, *Helv. Chim. Acta* **76**, 924, 2350 (1993).
- 5.102. F. Savary, J. Weber, and G. Calzaferri, *J. Phys. Chem.* **97**, 3722 (1993).
- 5.103. I. B. Bersuker, S. S. Budnikov, and B. A. Leizerov, *Int. J. Quant. Chem.* **11**, 543 (1977).
- 5.104. P. Pyykko, L. J. Laakkonen, and K. Tatsumi, *Inorg. Chem.* **28**, 1801 (1989).
- 5.105. P. Pyykko, in S. Wolson, ed., *Methods in Computational Chemistry*, Vol. 2, Plenum, New York, 1988, p. 137.
- 5.106. R. E. Christoffersen, *Adv. Quantum Chem.* **6**, 333 (1972).
- 5.107. I. B. Bersuker, *Teor. Eksp. Khim.* **9**, 3 (1973) (Engl. transl.: *Theoretical and Experimental Chemistry*).
- 5.108. I. B. Bersuker, in J. Leszczynski, ed., *Computational Chemistry: Reviews of Current Trends*, Vol. 6, World Scientific, Singapore, 2001, p. 69.
- 5.109. S. A. Gershgorin, *Izvestia AN SSSR, Ser. VII, OFMN*, **6**, 749 (1931).
- 5.110. F. P. Larkins, *J. Phys. Chem.* **4**, 3065 (1971).
- 5.111. J. K. Burdett, *Molecular Shapes. Theoretical Models of Inorganic Stereochemistry*, New York, Wiley, 1980.

- 5.112. U. Burkert and A. L. Allinger, *Molecular Mechanics*, ACS Monograph 177, ACS, Washington, DC, 1982; J. P. Bowen and N. L. Allinger, in K. B. Lipkowitz and D. B. Boyd, eds., *Reviews in Computational Chemistry*, Vol. 2, VCH, New York, 1991, p. 81; U. Dinur and A. T. Hagler, *ibid.*, p. 99.
- 5.113. G. R. Brubaker and D. W. Johnson, *Coord. Chem. Rev.* **53**, 1 (1984)
- 5.114. R. D. Hancock, *Progr. Inorg. Chem.* **37**, 187 (1989).
- 5.115. A. K. Rappe, K. S. Colwell, and C. J. Casewit, *Inorg. Chem.* **32**, 3438 (1993); B. P. Hay, *Coord. Chem. Rev.* **126**, 177 (1993); G. Wipff, *J. Coord. Chem.* **27**, 7 (1992); H. Marques, *J. Am. Chem. Soc.* **114**, 7218 (1992).
- 5.116. P. Comba and T. W. Hambley, *Molecular Modeling of Inorganic Compounds*, VCH, New York, 1995; C. R. Landis, D. M. Root, and T. Cleveland, in K. B. Lipkowitz and D. B. Boyd, eds., *Reviews in Computational Chemistry*, VCH, New York, 1995, Vol. 6, p. 73.
- 5.117. I. B. Bersuker, M. K. Leong, J. E. Boggs, and R. S. Pearlman, *Int. J. Quant. Chem.* **63**, 1051 (1997).
- 5.118. I. B. Bersuker, M. K. Leong, J. E. Boggs, and R. S. Pearlman, in J. Gao and M. Thompson, eds., *Combined Quantum and Molecular Mechanics Methods*, ACS Symposium Series 712, American Chemical Society, Washington, DC, 1998, p. 66.
- 5.119. K. K. Stavrev and M. C. Zerner, *J. Am. Chem. Soc.* **117**, 8684 (1995)
- 5.120. G. Nadiy, L. C. Van Zant, L. Dixon, and K. Merz, *J. Am. Chem. Soc.* **120**, 5593 (1998).
- 5.121. M. Svenson, S. Humbel, R. D. J. Froese, T. Matsubara, S. Sieber, and K. Morokuma, *J. Phys. Chem.* **100**, 19357 (1996).
- 5.122. F. Maseras and K. Morokuma, *J. Comput. Chem.* **16**, 1170 (1995); S. Humbel, S. Sieber, and K. Morokuma, *J. Chem. Phys.* **105**, 1959 (1996).
- 5.123. T. Matsubara, F. Maseras, N. Koga, and K. Morokuma, *J. Phys. Chem.* **100**, 2573 (1996); S. Dapprich, I. Kamamori, K. S. Byun, K. Morokuma, and M. J. Frisch, *J. Mol. Struct. (THEOCHEM)* **462**, 1 (1999).
- 5.124. T. K. Woo, G. Pioda, U. Rothlisberger, and A. Togni, *Organometallics* **19**, 2144 (2000).
- 5.125. J. P. Collman, J. I. Brauman, E. Rose, and K. S. Suslick, *Proc. Natl. Acad. Sci. USA* **75**, 1052 (1978); K. Kim, J. Fettinger, J. L. Sessler, M. Cyr, J. Hugdahl, J. P. Collman, and J. A. Ibers, *J. Am. Chem. Soc.* **111**, 403 (1989); J. P. Collman, J. I. Brauman, K. M. Doxsee, T. R. Halbert, E. Bunnenberg, R. E. Linder, G. N. LaMar, J. Del Gaudio, G. Lang, and K. Spartalian, *J. Am. Chem. Soc.* **102**, 4182 (1980).
- 5.126. M. Zerner, in K. B. Lipkowitz and D. B. Boyd, eds., *Reviews in Computational Chemistry*, Vol. 2, VCH, New York, 1991, p. 313; *ZINDO, A General Semiempirical Program Package*, Dept. Chemistry, Univ. Florida, Gainesville, 1995; M. Zerner, in D. R. Salahub and N. Russo, eds., *Metal-Ligand Interactions: From Atoms, to Clusters, to Surfaces*, Kluwer, Dordrecht, 1992, p. 101.
- 5.127. M. Clark, R. D. Cramer III, and N. Van Opdenbosch, *J. Comput. Chem.* **10**, 982 (1989); Distributed by Tripos, Inc., 1699 S. Hanley Road, Suite 303, St. Louis, MO 63144.

- 5.128. G. B. Jameson, F. S. Molinaro, J. A. Ibers, J. P. Collman, J. I. Brauman, E. Rose, and K. S. Suslick, *J. Am. Chem. Soc.* **102**, 3224 (1980).
- 5.129. W. R. Sheidt and M. Gouterman, in A. B. P. Lever and H. B. Gray, eds., *Iron Porphyrins* (Part I), Addison-Wesley; London, 1983, p. 89.
- 5.130. G. Calzaferri and M. Brandle, *ICONC & INPUTC; QCPE* **12**, 73 (1992); M. Brandle and G. Calzaferri, *Helv. Chim. Acta* **76**, 924 (1993).
- 5.131. I. B. Bersuker, M. K. Leong, J. E. Boggs, and R. S. Pearlman, *Proc. 32nd Int. Conf. Coord. Chem., Bol. Soc. Chil. Quim.* **42**, 226 (1997).
- 5.132. E. R. Davidson, in D. R. Salahub and M. C. Zerner, eds., *The Challenge of d and f Electrons. Theory and Computation*, ACS Symposium Series, Vol. 394, Washington, DC, 1989, p. 153.
- 5.133. M. C. Zerner, in D. R. Salub and N. Russo, eds., *Metal-Ligand Interaction: From Atoms, to Clusters, to Surfaces*, Kluwer, Dordrecht, 1992, p. 101.
- 5.134. M. Gerloch, *Progr. Inorg. Chem.* **31**, 371 (1984).
- 5.135. Y. Liu, W. Zou, I. B. Bersuker, and J. E. Boggs, *J. Chem. Phys.* **130**, 184305 (2009).
- 5.136. R. Hoffmann, *Pure Appl. Chem.* **50**, 55 (1978).
- 5.137. E. Clementi and G. Corongiu, in N. Tanaka, H. Ohtaki, and R. Tamamushi, eds., *Studies in Physical and Theoretical Chemistry*, Vol. 27: *Ions and Molecules in Solutions*, Elsevier, Amsterdam, 1982, p. 397.
- 5.138. K. H. Johnson, J. C. Norman, Jr., and J. W. D. Connolly, in F. Herman, A. D. McLean, and R. K. Nesbet, eds., *Computational Methods for Large Molecules and Localized States in Solids*, Plenum, New York, 1973, p. 161.

---

# 6

---

## ELECTRONIC STRUCTURE AND CHEMICAL BONDING

*Chemical bonding predetermines the very existence of chemical substances and their specific structure and properties. Knowledge of origin and control of chemical bonding underlies purposeful synthesis of new compounds.*

This chapter is devoted to the origin of chemical bonding in transition metal coordination compounds as a feature of their electronic structure.

### 6.1. CLASSIFICATION OF CHEMICAL BONDS BY ELECTRONIC STRUCTURE AND ROLE OF *d* AND *f* ELECTRONS IN COORDINATION BONDING

Following the electronic nature of chemical bonding, defined in Section 1.2 as resulting from collectivization of the electrons of interacting atoms, electronic structure should play a key role in the classification of chemical bonds and definition of coordination bonding. Analysis of this problem in terms of the achievements and modern understanding of the origin of chemical bonding has not received due attention in the literature [6.1]. In fact, the commonly used attribution of compounds to different classes is based on the historically established classification carried out when our knowledge about the electronic structure was rather poor, and therefore it creates controversies and misunderstandings. In this chapter we discuss the classification of covalent bonds; as mentioned in Section 1.2, pure ionic compounds do not exist (in spite of the fact that the ionic model may be useful in particular cases).

---

*Electronic Structure and Properties of Transition Metal Compounds: Introduction to the Theory,*  
Second Edition By Isaac B. Bersuker  
Copyright © 2010 John Wiley & Sons, Inc.

### Criticism of the Genealogical Classification

The traditional (“classical”) classification of chemical bonds is based on the idea of atomic valence. Following this idea, it is assumed that there is a large class of *valence compounds* in which the chemical bonds have a localized diatomic nature similar to that of the H—H bond in the H<sub>2</sub> molecule. The main assumption is that *the valence bond is formed by the pairing of two electrons supplied by one from each of the binding atoms*. The development of this concept led to the notions of *multiple bonds* and *bond saturation*, as well as to the presentation of a complex molecule by its *valence structure* with single, double, and triple bonds. For many classes of compounds, their presentation in the form of one valence structure proved to be invalid, and in order to preserve the concept of valence, the idea of *superposition of two or several valence structures* was employed.

In addition to this traditional valence system, there is a large class of compounds in which the chemical bonding can be presented as formed by two atoms or atomic groups which (one or both) have no unpaired electrons. For these cases it is assumed, following the valence scheme, that the two electrons needed for formation of the bond are supplied by one of the bonding groups (the electrons donor), while the other group participates as an acceptor of electrons. Here we have the *donor–acceptor bond*, or *coordination bond*, with the two notions thus assumed identical.

It is seen that in the traditional classification two main types of bonds—valence bonds and donor–acceptor (coordination) bonds—are distinguished according to the possibility to reduce them to local diatomic and two-electron bonding. More precisely, the whole difference between these two types of bonds is reduced to *the genealogy* (origin) of the two bonding electrons in the diatomic bond; in valence compounds (bonds) the bonding electrons are provided by two atoms, or they occur as a superposition of several such possibilities, whereas in donor–acceptor bonds the two electrons are supplied by only one atom, the donor. Therefore *this classification can be called genealogical*. It is based entirely on the concept of valence (Table 6.1).

Data accumulated from many years of study of chemical compounds show that the genealogical classification does not correlate with their electronic structure and properties. Indeed, two simple systems, CH<sub>4</sub> and NH<sub>4</sub><sup>+</sup>, are isoelectronic and quite similar in the distribution of the  $\Psi$  cloud of electrons determining the bonding and properties (in both systems there are four tetrahedral two-electron bonds [6.2]). The difference between them is that in NH<sub>4</sub><sup>+</sup> there is an additional proton in the nucleus of the CA, rendering the hydrogen atoms more electropositive than in CH<sub>4</sub>. However, following the genealogical classification, one must assume that CH<sub>4</sub> is a valence compound, while NH<sub>4</sub><sup>+</sup> is a coordination (donor–acceptor) system (NH<sub>3</sub> is the donor and H<sup>+</sup> is the acceptor). On the other hand, between NH<sub>4</sub><sup>+</sup> and, for example, CuCl<sub>4</sub><sup>2-</sup>, there is almost nothing in common in either electronic structure or properties. The genealogical classification, however, puts them in the same class of coordination compounds.



**TABLE 6.1. Classification of Chemical Bonds**

Type of Bond	Origin of Bonding Electrons (a) and Electronic Structure (b)	Examples	Characteristic Properties
<i>a. By Origin (Genealogy) of Bonding Electrons</i>			
Valence	Each of the two bonding atoms supplies one unpaired electron, or a superposition of several such possibilities (several valence schemes) is considered	CH <sub>4</sub> , C <sub>6</sub> H <sub>6</sub> , diamond, graphite, NO	No characteristic properties in common
Coordination	Both unpaired electrons are supplied by one of the atoms	CuCl <sub>4</sub> <sup>2-</sup> , NH <sub>4</sub> <sup>+</sup> , BF <sub>3</sub> · NH <sub>3</sub>	No characteristic properties in common
<i>b. By Electronic Structure and Properties</i>			
Valence	The one-electron bonding states are localized between the pairs of bonding atoms and are occupied by two paired electrons	CH <sub>4</sub> , NH <sub>4</sub> <sup>+</sup> , diamond	Approximate additive and transferable bond energies, vibrational frequencies, dipole moments
Orbital or conjugated	The one-electron bonding states are delocalized over many atoms along the line of bonding with possible ramifications	C <sub>6</sub> H <sub>6</sub> , graphite	Conductivity along the bond, aromaticity
Coordination	The one-electron bonding states are three-dimensionally delocalized in space around a center	CuCl <sub>4</sub> <sup>2-</sup> , Cr(CO) <sub>6</sub>	Nonadditive and nontransferable bond features, strong mutual influence of CA–ligand bonds, specific color, magnetic, thermodynamic, reactivity properties

These deficiencies of the genealogical classification have not been criticized, nor critically studied and analyzed, because the classification of compounds after their origin (their past history) in many cases reflects the real process of the synthesis of the compounds; in the absence of details of electronic structure the genealogical classification was quite reasonable.

Presently the subjects of investigation in modern chemistry are real compounds with their properties determined by the *actual electronic structure* regardless of the preparation method and history (genealogy). As mentioned in Section 1.2,



the domination of preparative chemistry in the past is rapidly changing to structural chemistry. From the structural perspective, the classification according to the genealogy of the bonding electrons that attributes compounds with quite different (sometimes opposite) properties to the same class is unacceptable. The genealogical classification is also not acceptable as a matter of principle because it is based entirely on the concept of valence, which is not a comprehensive characteristic of all the chemical properties of atoms, especially transition metals.

### Classification by Electronic Structure and Properties

In most cases the description of the electronic structure of polyatomic systems is given by one-electron MOs, which in general are delocalized over the entire system (Chapter 5). The total wavefunction is composed of MOs by means of an appropriate symmetrization procedure (Section 2.2). It was shown by Lenard-Jones [6.3] that in some special cases, discussed below, there is a possibility to transform the full wavefunction to the so-called equivalent orbitals. The latter are occupied by two electrons with the electronic charge concentrated mainly in the space between the corresponding pairs of nearest-neighbor atoms. In this presentation the total energy equals approximately the sum of the bonding energies between the pairs of atoms described by the equivalent orbitals.

This description of electronic structure can serve as a theoretical foundation for the existence of valence bonds. However, description of the system by equivalent orbitals is restricted by specific conditions, in particular, by the requirement that the number of bonding electrons be exactly equal to the doubled number of bonds [6.3]. Chemical bonds in such (and only such) compounds are valence bonds, indeed. By this definition, *valence compounds include all the systems that can be described by one valence scheme* (without conjugation): saturated hydrocarbons,  $\text{CH}_4$  and  $\text{NH}_4^+$ , as well as  $\text{BH}_4^-$ ,  $\text{BF}_3\text{—NH}_3$  (electronic analog of  $\text{CF}_3\text{—CH}_3$ ), and so on.

Similar electronic structure determines similar characteristic features. For valence compounds they are approximate *additivity* with respect to the bonds properties (e.g., the dipole moments, polarizabilities, bond energies, etc.), and *transferability*, that is, relatively minor changes in the properties of a given bond (dipole moments, vibrational frequencies, and energies) by passing from one compound to another (Table 6.1). The transferability property implies that comparisons are made between the bonds of the same type (the same type of hybridization and bond order), in the first approximation. As compared with the case of delocalized bonds—conjugated and coordination bonds (see below)—the changes in the properties of localized valence bonds when passing to other compounds are much smaller and are influenced mainly by the nearest-neighbor atoms only.

All the other compounds cannot be described by localized (between pairs of atoms) two-electron bonds, and hence they cannot be considered as valence compounds. In nonvalence compounds, the one-electron MOs remain essentially delocalized; conjugated systems form a major part of them. The bonds in these

systems can be characterized as *orbital or conjugated (or metallic) bonds* created by delocalized electrons. In fact, *this definition includes all compounds that cannot be described by one valence scheme, except coordination compounds.*

In the nonvalence, conjugated bonds, delocalization of electrons takes place along one dimension or one plane of conjugation (as, e.g., in benzene) with possible ramifications (as, e.g., in naphthalene). Beside these is a large class of nonvalence compounds in which *the electronic states are three-dimensionally delocalized around some centers.* These compounds can be reasonably called *coordination compounds.* Thus we define them as *compounds with high coordination and three-dimensional delocalization.* This characteristic is novel; it differentiates the coordination system from other donor–acceptor compounds.

In this description two factors determine the coordination bond: high coordination, which implies the presence of a center of coordination and its environment, and three-dimensional delocalization, that is, several collectivized (nonlocalized) bonds CA–ligand. It can be shown that the latter condition is obeyed when *d (or f) orbitals* of the central atom (which have a multilobe form) are actively involved in the bonding; pure *s* and *p* orbitals cannot provide the required combination of high coordination and delocalization. Indeed, by means of *s* and *p* orbitals one can obtain, at the most, tetrahedral coordination on behalf of  $sp^3$  hybridization. But hybridization implies localization (Section 2.1), and hence hybridized states are attributed to localized (valence) bonds and not to delocalized coordination bonds. This is the main cause for the differences in electronic structure and properties between the valence compound  $\text{CH}_4$  ( $sp^3$  hybridization, localized C–H bonds) and the coordination system  $\text{CuCl}_4^{2-}$  (participation of *d* electrons delocalized over all four Cu–Cl bonds). The participation of *d* (or *f*) orbitals in the formation of coordination bonds is thus most important.

The notion of *s, p, d, f, ...* atomic orbitals in molecules is not rigorous and may be misleading. Indeed, as mentioned in Section 2.1, these atomic states originate from the spherical symmetry of the free atom. Within the molecule the spherical symmetry is necessarily lowered, and partition of the orbitals into *s, p, d, ...* is, strictly speaking, no longer valid. However, one can find a region near the nuclei of the atoms where the influence of the atomic environment is smaller than that of the spherical symmetric nuclear field, and in this region the concept of *s, p, d, f* orbitals in molecules is approximately valid. Therefore, the statement of participation of *d* (or *f*) orbitals in the formation of coordination bonds should be understood in the sense that there are occupied one-electron states which in the region near the nucleus of the CA are of *d* (or *f*) nature, and at greater distances they become modified by the environment. In fact, the statement that *d* or *f* electrons participate in the bonding implies that they participate in occupied MOs of *corresponding* (to these *d* or *f* states) *symmetry* that are delocalized over the CA and all (or several) ligands.

Note also that in coordination compounds of nontransition elements there may be significant influence of *virtual d states* (see below). The measure of *d* participation in the bonding in various systems may be rather different [6.4]; it

determines a large variety of special properties and the extent to which these systems are coordination compounds.

Although, in terms of the CA, the coordination bond seems delocalized (it does not allow accurate partition of the bonding into separate metal–ligand bonds), from the ligand perspective the bond may be quite localized and directed to the CA. However, this will not be a ligand–metal bond, but a ligand–“remaining-complex” bond; any change of other ligands, owing to the three-dimensional delocalization, influences the ligand–complex bond under consideration.

The bonds classification does not necessarily coincide with the classification of compounds. Indeed, some compounds may have different types of bonds in their different parts. Some localized valence bonds become delocalized by excitation. There are atoms which in different conditions can form different types of bonds, especially when there are low-lying unoccupied *d* orbitals (see discussion below on the coordination bonding by pre- and posttransition elements). It is reasonable to consider the molecular system as a transition metal coordination compound if it possesses at least one coordination center (coordination bond). Similarly, the compound is a conjugated system, if it has at least one conjugated region but no coordination centers, and the molecule is a valence compound if it has neither coordination centers nor planar delocalized bonds, but only localized bonds.

Coordination compounds include many classes of transition metal and rare-earth compounds: complexes, chelates, clusters, organometallic compounds including metallobiochemical systems, crystals, alloys and solid solutions, chemisorbed surface states, and so on.

Thus based on electronic structure and properties, one can distinguish three main types of chemical bonds (Table 6.1): *valence bonds*, *orbital (or conjugated) bonds*, and *coordination bonds*. There are no strict demarcation lines between these types of bonds, and in this respect the above classification is conventional; however, outside the border regions it is quite definitive.

### Features of Coordination Bonds

The classification of chemical bonds discussed above and the definition of the coordination bond based on this classification enable us to differentiate some general features of coordination compounds listed in Table 6.2. As mentioned in Section 1.2, the presence of a coordination center allows one to denote the coordination system in a general way as  $ML_n^p$ , where M is the *d* (or *f*) central atom and L are the *n* ligands; the latter are either single atoms or groups of atoms, equal or different, and *p* is the total charge.

First, the role of *d* (*f*) electrons determines the *increasing tendency to form coordination systems when passing from light and main-group atoms to transition and rare-earth elements*. Further, *CA–ligand bonds are delocalized, collectivized, and hence strongly interdependent*. Each M–L bond may depend strongly on all the other bonds in the system formed by M. Therefore, in general, the bond properties should be considered either for group of bonds M–L<sub>1</sub>, M–L<sub>2</sub>, M–L<sub>3</sub>, and so on, or for the bond M–L<sub>1</sub> in the presence of M–L<sub>2</sub>, M–L<sub>3</sub>, . . . , M–L<sub>*n*</sub>.

**TABLE 6.2. Correlation between the Features of Electronic Structure and Properties of Coordination Compounds**

Features of Electronic Structure	Properties
Increasing activity of <i>d</i> and <i>f</i> atomic states when moving down along the periodic table of elements	Increasing tendency to form coordination compounds in same direction: almost complete absence of this tendency in second period, intermediate position in third period, and full manifestation in fourth and lower periods
Three-dimensional delocalization of the bonding electron density	Strong interdependence of CA–ligand bonds and nontransferability of their properties: energy, bond length, vibrational frequency, dipole moment, polarizability, reactivity, and so forth
High symmetry and large coordination numbers, high capacity of <i>d</i> and <i>f</i> orbitals and hence close-in-energy (degenerate and pseudodegenerate) states	Two types of magnetic behavior: high-spin and low-spin, characteristic colors, thermodynamic properties, multiorbital bonds, strong vibronic effects, and so on, in spectroscopy, stereochemistry, crystal chemistry, reactivity, and chemical activation in catalysis

Thus *the coordination metal–ligand bonds, in general, are essentially nontransferable*, and this feature is confirmed by many experimental data. For instance, one of the main bond characteristics, the bond length M–L, where M is a transition metal, and L = N,O,C,Br, . . . , is heavily dependent on the nature of other bonds formed by M (e.g., the Cu–O bond length varies between 1.8 and 3.0 Å; Table 9.10), whereas the bond length C–L in different valence compounds is almost constant. This feature, formulated in general, does not mean that there are no *particular cases* where some transferability is possible within a limited group of similar compounds (see molecular modeling in Section 5.6), but it means that any assumption of transferability should be specially substantiated.

The third main feature includes the *characteristic properties caused by the participation of *d* (or *f*) orbitals of the CA*: characteristic color (electronic absorption in the visible and related regions of the spectrum, Section 8.2), magnetic (low-spin and high-spin complexes; Sections 4.3, 6.2, and 8.4), thermodynamic (two-humped dependence of the thermodynamic stability on the number of *d* electrons, Section 4.5), and stereochemical (Chapter 9), reactivity (Chapters 10 and 11), and special nuclear dynamics properties (Chapter 7). The latter feature is due to the fact that the usually open shell of *d* (or *f*) electrons (formally closed shells but with low-energy excited states have similar properties, Sections 7.3 and 7.4) in combination with high coordination (high symmetry) creates *degenerate or pseudodegenerate energy terms*, ground or excited, which, in turn, results in a series of special effects and phenomena [6.5].

### Coordination Bonding by Pre- and Posttransition Elements

From the definition of coordination systems given above, a question emerges as to how to explain the fact that some compounds of posttransition elements are similar in properties to coordination systems. In the definition of coordination bonding, the CA must have active  $d$  or  $f$  electrons. Nontransition elements have no such electrons in *the free noncoordinated state*. This does not mean that active  $d$  or  $f$  states cannot occur in the corresponding *oxidation state*, or in the chemical bonding—in the so-called *valence state* of the atom-in-molecule. As emphasized in Sections 6.3 and 11.2, *coordination often results in excitation of the coordinated atoms or group of atoms* (see Fig. 6.6 in Section 6.3). Hence by coordination the electronic configuration of the bonding groups changes, and in certain conditions these changes may lead to the activation of  $d$  (or  $f$ ) electrons of the CA.

Any element has excited  $d$  states, but if they are very high in energy, they cannot be activated by the bonding. On the other hand, there may be occupied  $d$  states that are deep in energy as compared with the HOMO, and hence they cannot be excited simply by the bonding. We come to the conclusion that *potential coordination centers of nontransition elements can be found among the immediate pretransition or posttransition elements*.

In pretransition elements of the third period there are active  $s$  and  $p$  states and higher-energy inactive  $d$  orbitals. To make the  $d$  states active, that is, to lower their energy and to populate them with electrons, strong oxidizing ligands are required that simultaneously are good  $\pi$  donors to the unoccupied  $d$  states of the CA (see the interdependence of  $\sigma$ -acceptor and  $\pi$ -donor properties, Section 6.3). For example, oxygen, sulfur, and chlorine can activate the  $d$  states of Al, Ga, Ge, In, Sn, and so on, making them good coordination centers.

For posttransition elements, which are simultaneously pretransition elements for the next transition group, there are two possibilities for  $d$ -electron activation. The first is the same as for pretransition elements: oxidizing ligands with  $\pi$ -donor abilities. The second possibility is to activate the inner occupied  $d$  states. For instance, the inactive  $d$  electrons of the  $d^{10}$  closed shell of  $\text{Zn}^{2+}$  or  $\text{Ga}^{3+}$  may become active under the influence of ligands that have significant  $\sigma$ -donor and  $\pi$ -acceptor properties. The former render the  $d$  states more diffuse in space, due to the additional interelectron repulsion (see the nephelauxetic effect, Section 8.2), while the latter allow for  $\pi$  backdonation.

In both cases the  $d$  orbitals are involved in the bonding. The measure of  $d$  participation is dependent on the nature of the ligands and can vary greatly. In this sense *there are no sharp borders between coordinating and noncoordinating elements*. In principle, *any element can serve as a center of coordination bonding provided the ligands induce significant  $d$  participation*.

Note that even within the transition metal group the extent to which  $d$  electrons participate in the coordination bonding may be quite different [6.4]. In high oxidation states the metal  $nd$  electrons are strongly attracted to the nucleus, and hence their overlap with the ligand orbitals is very small; the bonding, for the most

part, is realized via  $(n + 1)s$  and  $(n + 1)p$  orbitals. Donation of electrons from the ligands renders the  $d$  states more diffusive, increasing their participation in the bonding. In low oxidation states (e.g., in carbonyls) the  $d$  states are most active in the bonding. This tendency for  $d$  participation in the coordination bonding varies stepwise by moving from early to late transition elements.

Thus *the ability to form coordination compounds with  $d$  (or  $f$ ) participation changes gradually when moving from pretransition to transition elements, from early to late transition elements, and then to posttransition elements, with strong dependence on the nature of the ligands and without sharp borders between transition and immediate pre- and posttransition elements.*

Following the definition of coordination systems based on the electronic structure given above, pre- and posttransition element compounds are coordination compounds to the extent of  $d$ -electron participation in the bonding, which makes them similar in properties to the  $d$ -electron compounds. Experimental data confirm the  $d$ -orbital participation in the bonding of nontransition elements [6.6]. In many cases the possible (in principle)  $d$ -electron participation is in fact minor [6.7, 6.8].

Direct calculations of the electronic structure to confirm the  $d$  electron participation are not always unambiguous; the most reliable results of nonempirical calculations are dependent on the choice of the basis set, which, in fact, predetermines the  $d$ -orbital occupation sought for (the more  $d$  functions included, the greater the  $d$  occupation numbers). As stated in Section 5.3, expansion of the wavefunction in basis set functions is a mathematical procedure and cannot be used directly to relate the electron distribution to the atomic functions. However, the  $d$  character of the electron distribution is reflected in the symmetry of the MOs, and in this sense the participation of atomic  $d$  states (which makes the bonding three-dimensionally delocalized) is demonstrated indirectly. The charge distribution may also confirm the experimentally observable specific features of coordination compounds (Table 6.2), including the interdependence (mutual influence; Section 9.3) of different metal–ligand bonds in the same compound and *nontransferability* of their characteristics to other compounds. Thus, when discussing  $d$  orbitals in molecules the  *$d$  origin* of the corresponding MO symmetry is implied. In this meaning the classification of chemical bonds by their electronic structure is also genealogical, but it is based on the genealogy of the electronic structure of the compound under consideration with respect to its atoms or atomic groups, and *not on its way of preparation*.

## 6.2. QUALITATIVE ASPECTS AND ELECTRONIC CONFIGURATIONS

### Most Probable MO Schemes

Consider a transition metal of the  $3d$  group as a CA. Its outer orbitals  $3d$ ,  $4s$ , and  $4p$  in the valence (oxidation) state in complexes form the following sequence of



energy levels:

$$E(3d) < E(4s) < E(4p) \quad (6.1)$$

Overlap of the wavefunctions of these orbitals with ligand functions is larger for  $4s$  and  $4p$  orbitals, and smaller for the  $3d$  functions. Considering the dependence of the bonding (antibonding) properties of the MOs on the magnitude of the overlap integral [Section 5.1, Eq. (5.26)], we conclude that the  $3d$  orbitals form weaker bonding (and antibonding) MOs than do the  $4s$  and  $4p$  functions.

Consider an octahedral complex of  $O_h$  symmetry. The  $4s$  orbital belongs to the  $A_{1g}$  representation (symmetry) (Table 5.1),  $4p$  belongs to  $T_{1u}$ , and the five  $3d$  orbitals form two groups: two  $3d(e_g)$  orbitals ( $d_{z^2}$  and  $d_{x^2-y^2}$ ) belonging to the  $E_g$  representation, and three  $3d(t_{2g})$  orbitals ( $d_{xy}$ ,  $d_{xz}$ , and  $d_{yz}$ ) that belong to  $T_{2g}$ . The  $e_g$  orbitals are directed with their lobes of charge distribution toward the ligands and form  $\sigma$  bonds (Table 5.1), whereas the  $t_{2g}$  orbitals can form only  $\pi$  bonds. Hence the overlap of the  $3d(t_{2g})$  orbitals with the corresponding ligand functions are smaller than that of  $3d(e_g)$ . It follows that the largest splitting into bonding and antibonding orbitals is expected in the formation of MOs by the  $4s$  and  $4p$  orbitals of the CA, smaller splitting comes from the  $3d(e_g)$  orbitals, and the smallest one is due to the  $3d(t_{2g})$  orbitals. Note also that according to Eqs. (5.26)–(5.29) these splittings are determined by the group overlap integrals  $G_{0i}$  in Table 5.4, not  $S_{0i}$ .

With these ideas, we come to the most probable MO energy-level scheme given in Fig. 6.1 for an octahedral coordination compound of  $O_h$  symmetry formed by a  $3d$  transition metal CA and ligands that have only  $s$  and  $p$  active orbitals. By comparison, one can easily ensure that this scheme corresponds to the data in Table 5.1. It is seen that the lowest MOs  $a_{1g}$ ,  $t_{1u}$ ,  $e_g$ , and  $t_{2g}$  are bonding, the  $t'_{1u}$ ,  $t_{2u}$ , and  $t_{1g}$  MOs are nonbonding, while the remaining MOs (marked by asterisks) are antibonding (the  $t'_{1u}$  orbitals may become bonding in the presence of  $f$  electrons). For numerical calculations revealing such MO energy levels and wavefunctions, see Example 5.5 and Problems 5.1 and 5.2.

For a tetrahedral system of  $T_d$  symmetry, on the contrary, the  $3d(e_g)$  orbitals of the central atom are less overlapped with the ligand orbitals than  $3d(t_{2g})$ , their role thus changing as compared with the octahedral case; by forming MOs the energy levels of the  $e_g$  orbitals are less split than the  $t_{2g}$  orbitals (Fig. 6.2, Table 5.2).

In systems with lower symmetries the degenerate MO energy levels are further split by the ligand field, and the splitting magnitude is dependent on the nature of the ligand. Here the MO energy-level scheme becomes complicated and no general ideas or solutions can be suggested; the corresponding problems should be solved by calculations.

### Electronic Configurations in Low- and High-Spin Complexes

The next stage in determining the electronic structure of coordination compounds in the MO approximation is to find the electron distribution over the one-electron MOs, the *electronic configuration* of the system. In accordance with the Pauli

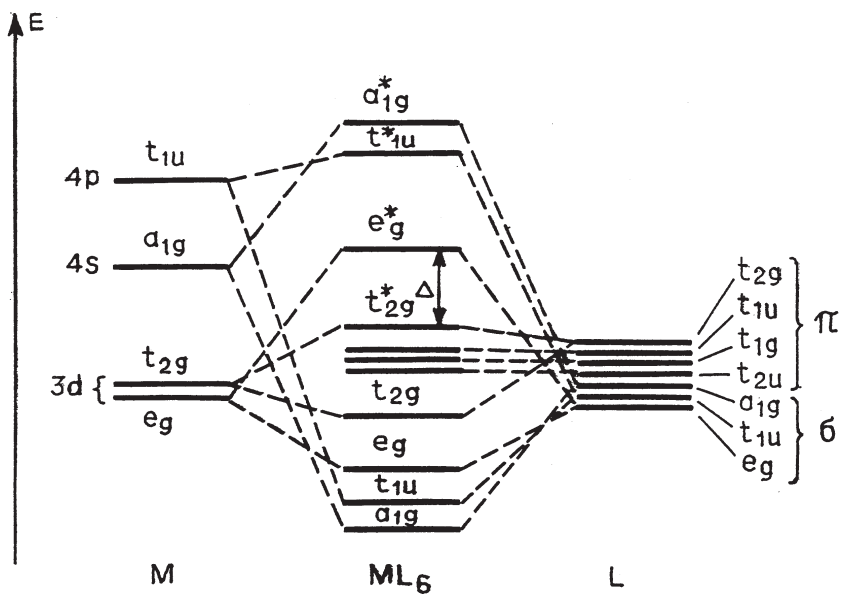


FIGURE 6.1. Most probable MO energy-level scheme for regular octahedral complexes  $ML_6$  of  $3d$  transition metals  $M$  with ligands  $L$  that have one  $\sigma$  and two  $\pi$  active AOs each.

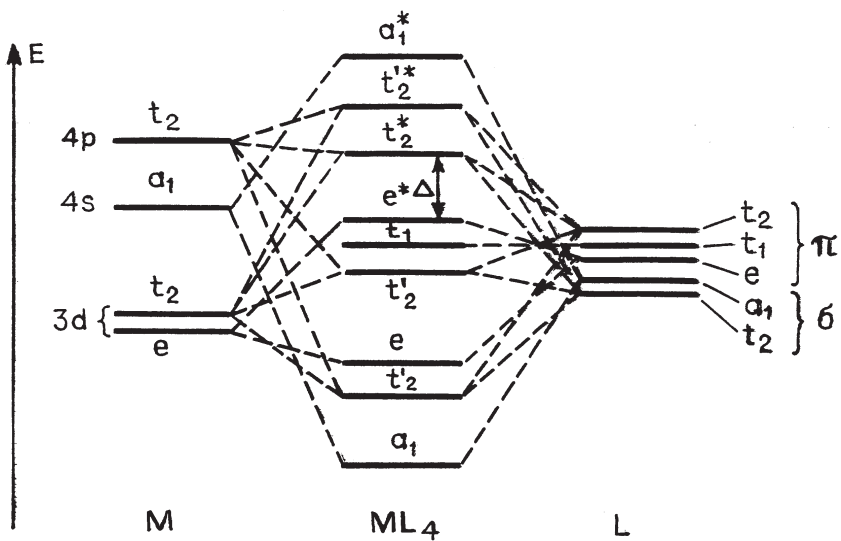


FIGURE 6.2. Most probable MO energy-level scheme for regular tetrahedral complexes  $ML_4$  of  $3d$  transition metals  $M$  with ligands  $L$  that have one  $\sigma$  and two  $\pi$  active AOs each.



principle, in the ground state the electrons occupy the lowest-energy MOs, in groups of two with opposite spins on each MO. The number of electrons to be distributed on the MOs equals the number of electrons that occupy the AOs used in the formation of these MOs. For instance, in the  $\text{TiCl}_6^{3-}$  complex the valence AOs used in the formation of MOs are as follows: one  $\sigma$  hybridized  $sp$  and two  $\pi$ -type  $3p$  orbitals from each  $\text{Cl}^-$  ion and  $3d$ ,  $4p$ , and  $4s$  orbitals of  $\text{Ti}^{3+}$ , a total of  $3 \times 6 + 9 = 27$  AOs that form 27 MOs occupied by  $6 \times 6 + 1 = 37$  electrons. The number of MOs equals the number of AOs used for their formation, and hence not all MOs will be occupied by two electrons in the ground state.

One can imagine the following picture (Fig. 6.1): the  $6 \times 6 = 36$  electrons from the six  $\text{Cl}^-$  ions occupy the following orbitals (the electron occupation numbers are indicated in parentheses):  $a_{1g}(2)$ ,  $t_{1u}(6)$ ,  $e_g(4)$ ,  $t_{2g}(6)$ ,  $t'_{1u}(6)$ ,  $t_{2u}(6)$ , and  $t_{1g}(6)$ , and hence the  $3d$  electron from  $\text{Ti}^{3+}$  occupies the antibonding  $t_{2g}^*$  orbital. This representation has reasonable physical meaning; as shown by calculations, the bonding orbitals  $a_{1g}$ ,  $t_{1u}$ ,  $e_g$ , and  $t_{2g}$  are basically (and the nonbonding orbitals are completely) ligand orbitals. Of course, the MO occupation scheme remains the same when one starts not from  $\text{Cl}^-$  and  $\text{Ti}^{3+}$  ions, but from neutral atoms.

Thus the electronic configuration of the complex  $\text{TiCl}_6^{3-}$  is  $(a_{1g})^2(t_{1u})^6(e_g)^4(t_{2g})^6(t'_{1u})^6(t_{1g})^6(t_{2g}^*)^1 - ^2T_{2g}$ , or by denoting the “closed shell” (including all the bonding and nonbonding orbitals fully occupied by electrons) by  $M$  in square brackets:  $[M](t_{2g}^*)^1 - ^2T_{2g}$ . The full multielectron term  $^2T_{2g}$  is determined here simply by one unpaired electron in a MO of  $t_{2g}$  symmetry, but in more complicated cases it should be determined by multielectron wavefunction rules (Section 2.2).

The result obtained here is qualitatively the same as it emerges from the more simple treatment of crystal field theory (Section 4.2), where the electronic configuration of the complex at hand is  $[A](3d)^1 - ^2T_{2g}$  (Table 4.5). Indeed, the antibonding  $t_{2g}^*$  orbital is localized mostly on the CA, and its difference from the  $3d$  orbital of the  $\text{Ti}^{3+}$  ion is in a small admixture of the  $\pi$  functions of the  $\text{Cl}^-$  ions. Note that the first excited state in the abovementioned MO scheme is  $[M](e_g)^1 - ^2E_g$ , which coincides with that obtained in crystal field theory, as well. Hence the long-wavelength electronic transition  $^2T_{2g} \leftrightarrow E_g$  is analogous to that expected in the crystal field theory. However, the energy gap  $\Delta = E(^2E_g) - E(^2T_{2g})$ , which determines the corresponding absorption band position, may be quite different in these two theories.

For more than one  $d$  electron above the closed shell  $[M]$  (e.g., in an octahedral complex of  $\text{V}^{3+}$  with two  $d$  electrons), one encounters complications caused by the interaction between the electrons. Indeed, the approximate MO schemes of Figs. 6.1 and 6.2 are one-electron schemes in which the interelectron interaction is not accounted for explicitly. For two  $d$  electrons several possibilities of the one-electron MO occupation arise:

1. Two of three different  $t_{2g}^*$  orbitals are occupied by the two electrons with parallel spin orientations resulting in the configuration  $(t_{2g}^* \uparrow)(t_{2g}^* \uparrow)$  with a total spin  $S = 1$ .

2. The same two orbitals are occupied by two electrons with opposite spin orientations,  $(t_{2g}^* \uparrow)(t_{2g}^* \downarrow)$ ,  $S = 0$ .
3. One  $t_{2g}^*$  orbital is occupied by two electrons with opposite spin orientations,  $(t_{2g}^* \uparrow\downarrow)$ ,  $S = 0$ .
4. One electron is in  $t_{2g}^*$ , the other is in the excited orbitals  $e_g$ , and so on.

Obviously, the electrostatic and exchange interactions between the electrons in these distributions differ, resulting in different energy terms. The ground-state configuration and spin will be that of lowest energy. Similar situations in free atoms and with ligand crystal fields are considered in detail in Sections 2.2 and 4.3, respectively. Several terms of the same electronic configuration may occur, and all of them can be determined by taking into account the interelectron interactions.

The procedure of distribution of the  $d$  electrons of the CA on the antibonding  $t_{2g}^*$  and  $e_g^*$  MOs with consequent inclusion of the interelectron interactions in each of these distributions is quite similar to that employed in crystal field theory (CFT) for the strong-field limit (Section 4.3). In particular, for two electrons, three electronic configurations— $(t_{2g}^*)^2$ ,  $(t_{2g}^*)^1(e_g^*)^1$ , and  $(e_g^*)^2$ —are possible with the same two energy gaps between them equal to the  $t_{2g}^* - e_g^*$  separation  $\Delta$  for a single electron. The energy splitting of these configurations by the interelectron interaction results in electronic terms similar in spacing to that obtained in the crystal field approximation (4.47) in which the Racah constants  $A$ ,  $B$ , and  $C$  should be substituted by the parameters of interelectron repulsions on the MOs, not AOs, with MO wavefunctions instead of AOs in the integrals of the type (2.32).

Corrections to the formulas of atomic energy term formation in ligand fields that account for the transformation of the AOs into MOs can be introduced [6.9]. For antibonding orbitals these corrections are negative, which means that the Racah parameters for antibonding MOs are smaller than for AOs. This result can be easily understood; when passing from AOs to MOs, the electronic cloud diffuses over a larger volume in which the interelectron repulsion is obviously reduced.

Thus in the case under consideration the MO energy scheme of a coordination compound remains the same as in CFT with a different meaning of the Racah constants  $A$ ,  $B$ , and  $C$  that become dependent on the covalence parameters (LCAO coefficients). As in the crystal field approximation, the  $(t_{2g}^*)^2$  configuration yields four terms,  ${}^3T_{1g}$ ,  ${}^1T_{2g}$ ,  ${}^1E_g$ , and  ${}^1A_{1g}$  (see Problem 3.9), with relative energies given in Eq. (4.47). The largest splitting between them is  $\Delta = E({}^1A_{1g}) - E({}^3T_{1g}) = 15B + 5C$ . Hence the limit of strong ligand field in which these configurations can be considered separately is valid if  $15B + 5C \ll \Delta$ . If this condition is not fulfilled, and in the opposite limit case of weak ligand field ( $\Delta < 15B + 5C$ ), the terms of the same symmetry from different configurations are strongly mixed and all the configurations should be considered simultaneously (Section 4.3).

Of special note are cases where, owing to the interelectron interactions, the electronic configuration of the ground state changes when passing from the limit

of strong fields to that of weak fields, and vice versa. Let us elucidate this situation by the example of an octahedral complex of a  $d^4$  transition metal atom or ion. The first three (of the four)  $d$  electrons, in accordance with Hund's rule, occupy the three  $t_{2g}^*$  orbitals with parallel spin orientations; their total spin hence is  $S = \frac{3}{2}$ . The fourth electron has two main possibilities. One of them is to occupy one of the already half-populated orbitals with an opposite orientation of the spin, and then the electronic configuration of the complex becomes  $[M](t_{2g}^* \uparrow)^3(t_{2g}^* \downarrow)^1$  with a total spin  $S = 1$  and ground state  ${}^3T_{2g}$ . Note that the total energy of the system is significantly increased here not only by the interelectron repulsion of the electrons (two of them are now on the same orbital) but also by the reduction of the negative energy of exchange interaction (per electron), which is non-zero for the electrons with parallel spins only.

The second possibility is to occupy the  $e_g$  orbital that is higher in energy by  $\Delta$  (Fig. 6.1), but with the same spin orientation as in the three  $t_{2g}$  orbitals. Then the configuration becomes  $[M](t_{2g}^* \uparrow)^3(e_g^* \uparrow)^1$  with a total spin  $S = 2$ ; the ground state is  ${}^5E_g$ . Here we have less interelectron repulsion (the electrons are in different orbitals and hence occupy different regions in space), and more negative contribution of the exchange interaction (all the electrons have parallel spin orientations), but one electron is higher in orbital energy by  $\Delta$ . These two possibilities result in two essentially different electronic configurations with different spin values. The latter is a convenient indicator of the differences. Therefore, the two possibilities are usually called *low-spin and high-spin configurations*, respectively, quite similar to the CFT treatment (Section 4.3).

As in Section 4.3, the energy difference between the two configurations, the pairing energy, can be denoted by  $\Pi$ ; it can be estimated by the same formulas (4.50) in which, as above, the Racah parameters  $A$ ,  $B$ , and  $C$  should be calculated by MO (not AO) functions; that is, they should be taken as modified by covalence. Provided the pairing energy  $\Pi$  is known, the question of whether the low-spin or high-spin configuration is realized can be solved directly; if  $\Pi < \Delta$ , the low-spin case is realized, and if  $\Pi > \Delta$ , the high-spin configuration is preferable. Since  $\Delta$  characterizes the strength of the ligand field, these two cases can also be called *strong-field and weak-field limits*, respectively. As in the crystal field approximation, the two possible configurations become important in  $d^n$  complexes for  $n = 4, 5, 6, 7$  in octahedral environments, and  $n = 3, 4, 5, 6$  for tetrahedral systems, resulting in different (high-spin or low-spin) ground states. Tables 6.3 and 6.4 illustrate these results for octahedral and tetrahedral complexes, respectively.

### Covalence Electrons and Ionization Potentials

As shown in Section 5.2, in the MO method the bonding occurs as a result of electronic redistribution in the bonding MOs because the electronic cloud is concentrated mainly in the space between the nuclei welding them together (another source of bonding is the reduction of the electron kinetic energy). The electronic energy on these orbitals is lower than on the corresponding AOs. On the

**TABLE 6.3. Electronic Configurations and Ground States of Coordination Compounds of  $d^n$  Metals with Octahedral  $O_h$  Symmetry<sup>a</sup>**

$d^n$ Example	High Spin (Weak Field)		Low Spin (Strong Field)	
	Electronic Configuration	Ground State	Electronic Configuration	Ground State
$d^1$ Ti <sup>3+</sup>	$(t_{2g}^* \uparrow)^1$	${}^2T_{2g}$	$(t_{2g}^* \uparrow)^1$	${}^2T_{2g}$
$d^2$ V <sup>3+</sup>	$(t_{2g}^* \uparrow)^2$	${}^3T_{1g}$	$(t_{2g}^* \uparrow)^2$	${}^3T_{1g}$
$d^3$ Cr <sup>3+</sup>	$(t_{2g}^* \uparrow)^3$	${}^4A_{2g}$	$(t_{2g}^* \uparrow)^3$	${}^4A_{2g}$
$d^4$ Mn <sup>3+</sup>	$(t_{2g}^* \uparrow)^3(e_g^* \uparrow)^1$	${}^5E_g$	$(t_{2g}^* \uparrow)^3(t_{2g}^* \downarrow)^1$	${}^3T_{1g}$
$d^5$ Mn <sup>2+</sup>	$(t_{2g}^* \uparrow)^3(e_g^* \uparrow)^2$	${}^6A_{1g}$	$(t_{2g}^* \uparrow)^3(t_{2g}^* \downarrow)^2$	${}^2T_{2g}$
$d^6$ Fe <sup>3+</sup>				
$d^6$ Fe <sup>2+</sup>	$(t_{2g}^* \uparrow)^3(e_g^* \uparrow)^2(t_{2g}^* \downarrow)^1$	${}^5T_{2g}$	$(t_{2g}^* \uparrow)^3(t_{2g}^* \downarrow)^3$	${}^1A_{1g}$
$d^6$ Co <sup>3+</sup>				
$d^7$ Co <sup>2+</sup>	$(t_{2g}^* \uparrow)^3(e_g^* \uparrow)^2(t_{2g}^* \downarrow)^2$	${}^4T_{1g}$	$(t_{2g}^* \uparrow)^3(t_{2g}^* \downarrow)^3(e_g^* \uparrow)^1$	${}^2E_g$
$d^8$ Ni <sup>2+</sup>	$(t_{2g}^* \uparrow)^3(e_g^* \uparrow)^2(t_{2g}^* \downarrow)^3$	${}^3A_{2g}$	$(t_{2g}^* \uparrow)^3(t_{2g}^* \downarrow)^3(e_g^* \uparrow)^2$	${}^3A_{2g}$
$d^9$ Cu <sup>2+</sup>	$(t_{2g}^* \uparrow)^3(e_g^* \uparrow)^2(t_{2g}^* \downarrow)^3(e_g^* \downarrow)^1$	${}^2E_g$	$(t_{2g}^* \uparrow)^3(t_{2g}^* \downarrow)^3(e_g^* \uparrow)^2(e_g^* \downarrow)^1$	${}^2E_g$
$d^{10}$ Zn <sup>2+</sup>	$(t_{2g}^* \uparrow)^3(e_g^* \uparrow)^2(t_{2g}^* \downarrow)^3(e_g^* \downarrow)^2$	${}^1A_{1g}$	$(t_{2g}^* \uparrow)^3(t_{2g}^* \downarrow)^3(e_g^* \uparrow)^2(e_g^* \downarrow)^2$	${}^1A_{1g}$

<sup>a</sup>The inner closed shells are omitted.**TABLE 6.4. Electronic Configurations and Ground States of Coordination Compounds of  $d^n$  Metals with Tetrahedral  $T_d$  Symmetry<sup>a</sup>**

$d^n$ Example	High Spin (Weak Field)		Low Spin (Strong Field)	
	Electronic Configuration	Ground State	Electronic Configuration	Ground State
$d^1$ Ti <sup>3+</sup>	$(e^* \uparrow)^1$	${}^2E$	$(e^* \uparrow)^1$	${}^2E$
$d^2$ V <sup>3+</sup>	$(e^* \uparrow)^2$	${}^3A_2$	$(e^* \uparrow)^2$	${}^3A_2$
$d^3$ Cr <sup>3+</sup>	$(e^* \uparrow)^2(t_2^* \uparrow)^1$	${}^4T_1$	$(e^* \uparrow)^2(e^* \downarrow)^1$	${}^2E$
$d^4$ Mn <sup>2+</sup>	$(e^* \uparrow)^2(t_2^* \uparrow)^2$	${}^5T_2$	$(e^* \uparrow)^2(e^* \downarrow)^2$	${}^1A_1$
$d^5$ Mn <sup>2+</sup>	$(e^* \uparrow)^2(t_2^* \uparrow)^3$	${}^6A_1$	$(e^* \uparrow)^2(e^* \downarrow)^2(t_2^* \uparrow)^1$	${}^2T_2$
$d^5$ Fe <sup>3+</sup>				
$d^6$ Fe <sup>2+</sup>	$(e^* \uparrow)^2(t_2^* \uparrow)^3(e^* \downarrow)^1$	${}^5E$	$(e^* \uparrow)^2(e^* \downarrow)^2(t_2^* \uparrow)^2$	${}^3T_1$
$d^6$ Co <sup>3+</sup>				
$d^7$ Co <sup>2+</sup>	$(e^* \uparrow)^2(t_2^* \uparrow)^3(e^* \downarrow)^2$	${}^4A_2$	$(e^* \uparrow)^2(e^* \downarrow)^2(t_2^* \uparrow)^3$	${}^4A_2$
$d^8$ Ni <sup>2+</sup>	$(e^* \uparrow)^2(t_2^* \uparrow)^3(e^* \downarrow)^2(t_2^* \downarrow)^1$	${}^3T_1$	$(e^* \uparrow)^2(e^* \downarrow)^2(t_2^* \uparrow)^3(t_2^* \downarrow)^1$	${}^3T_1$
$d^9$ Cu <sup>2+</sup>	$(e^* \uparrow)^2(t_2^* \uparrow)^3(e^* \downarrow)^2(t_2^* \downarrow)^2$	${}^2T_2$	$(e^* \uparrow)^2(e^* \downarrow)^2(t_2^* \uparrow)^3(t_2^* \downarrow)^2$	${}^2T_2$
$d^{10}$ Zn <sup>2+</sup>	$(e^* \uparrow)^2(t_2^* \uparrow)^3(e^* \downarrow)^2(t_2^* \downarrow)^3$	${}^1A_1$	$(e^* \uparrow)^2(e^* \downarrow)^2(t_2^* \uparrow)^3(t_2^* \downarrow)^3$	${}^1A_1$

<sup>a</sup>The inner closed shells are omitted.

contrary, on the antibonding MOs the electron does not screen the repulsion between the nuclei; hence its MO energy is higher than in the corresponding atomic states. Obviously, the chemical bonding takes place when the occupancy of bonding orbitals predominates that of the antibonding MOs. Therefore, it is

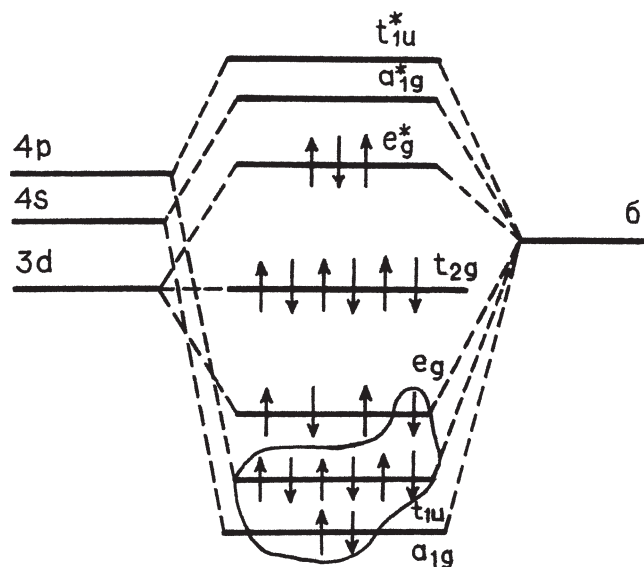


**FIGURE 6.3.** Scheme of mutual compensation of bonding and antibonding orbitals. The noncompensated bonding orbitals are shown enveloped by a line.

worthwhile to consider the question of what electrons (more precisely, what occupied one-electron states) are responsible for the covalent bonding in coordination compounds. Since each bonding orbital is accompanied by an antibonding MO so that their contributions to the binding are approximately mutually compensated for [6.10] (Section 5.2), the chemical bond is formed by only those bonding MOs that remain uncompensated by the antibonding orbitals.

In Fig. 6.3 the MO energy scheme for a Cu(II) complex is given with an indication of the MO occupancies (for simplicity, only  $\sigma$  bonds are shown). It is seen that in the ground state the uncompensated bonding MO are  $a_{1g}$  (two electrons),  $t_{1u}$  (six electrons), and  $e_g$  (one electron). Thus, not the valence one-electron states, but *the inner bonding MOs, which are not compensated for by the outer antibonding MOs, produce the chemical bonding*. In particular, it is ungrounded to try to describe the covalence in coordination compounds, for instance, by ESR data or by spin density distribution (Sections 8.4 and 8.6). These data characterize the covalence of the one-electron states of the unpaired electrons, whereas the bonding is formed by many inner electrons.

Another important MO problem is to determine the ionization potentials equal to the energy of ionization from a given state of the system (see also Section 6.4). These quantities are especially important for interpretation of the experimental data on photoelectron spectra (Section 8.3). As mentioned in Section 2.2, in the one-electron case the ionization energy, following the Koopmans theorem [6.11], equals the energy of the MO state (with opposite sign) calculated by the self-consistent method. Indeed, in these calculations the MO energy includes

the interaction of a given electron with the nuclei and all the other electrons, which apparently is the energy that should be applied to remove the electron from this MO.

This consideration (and the Koopmans theorem) is rigorously true in the one-electron case only. When there are two or many electrons in the system, the ionization of one of them changes the one-electron states of the others. Indeed, the reduction of the number of electrons by one reduces their interelectron repulsion, and the one-electron MOs “relax” to new self-consistent states. As a result of these electron relaxations, their energy decreases, and hence the absolute value of the ionization potential also decreases by the same amount (the decrease of the interelectron repulsion promotes the ionization).

If the relaxation energy is small, the Koopmans theorem predicts the correct consequence of ionization potentials corresponding to the MO energy level positions. This is true in many cases, especially for very stable closed-shell molecules for which the electronic energy-level spacing is sufficiently large. However, as shown by calculations, the Koopmans theorem is far from being valid for other systems, including many coordination compounds (see the discussion in the following sections of this chapter).

The deviations from the prediction of the Koopmans theorem depend on the state to be ionized and change from state to state. For instance, one can expect that the ionization of a (predominantly) *d* electron from a strong covalent metal-ligand complex results in much stronger reorganization (relaxation) of the other electrons than in the case of the ionization of a ligand nonbonding electron. The exact value of ionization energy should be calculated as the difference between the total energies of the initial (un-ionized) and final (ionized) systems evaluated with the interelectron interaction included. This problem is discussed further in Section 6.4.

### 6.3. LIGAND BONDING

#### General Considerations: Multiorbital Bonds

The origin of ligand bonding is one of the most important problems in coordination chemistry. It provides a basic understanding of a series of properties and processes that involve ligand coordination. To reveal the origin of ligand bonding means to elucidate the electronic structure of the bond, determined by the electronic features of the ligand and the remaining complex, and to establish direct correlations between the bonding properties and electronic structure parameters.

As emphasized in Section 6.1, due to the three-dimensional center-delocalized nature of the coordination bond, all metal–ligand bonds are, in general, strongly interdependent. Therefore, when considering ligand bonding, one has to investigate not just the metal–ligand bond but also the *complex–ligand bond*. From the ligand side the bond is mostly localized. In other words, ligand bonding means chemical interaction (electron collectivization, Section 1.2) between a ligand and a coordination center, which may be strongly dependent on the bonding

of the latter to other ligands. This circumstance, together with the significant difference in electronic structure of the metal ( $d$  electrons) and the ligand ( $sp$  electrons)—*the  $d$ -electron heterogeneity*—makes the metal–ligand bond essentially different from those in organic (and main-group element) compounds.

In the MO LCAO scheme the metal–ligand bond is determined by the overlap of the metal and ligand valence orbitals, which, in turn, depends on the valence state of the ligand and the metal and *the mode (geometry) of ligand coordination*. The valence orbitals of transition metals and rare-earth elements are given in Section 2.1. Assume that, with respect to the ligand under consideration, the complex is characterized by  $\sigma$  and  $\pi$  orbitals formed by a transition metal  $nd$ ,  $(n+1)s$ , and  $(n+1)p$  valence orbitals (which, in the presence of other ligands, transform into corresponding MOs).

Depending on the oxidation state and the nature of other ligands bound to the coordination center, the valence orbitals of the metal are differently populated by electrons, and hence they have different bonding abilities. A characteristic case is shown in Fig. 6.4 when the lowest  $\pi$  level of the metal (e.g.,  $d_{xz}$ ) is occupied, while its  $\sigma$  AO is unoccupied; the metal (complex) is thus a  $\sigma$  acceptor and a  $\pi$  donor. Of course, this picture is rather simplified; in real cases the complex may have several  $\sigma$  and  $\pi$  levels (see below) and may be both  $\sigma$  and  $\pi$  donor and acceptor on different orbitals, but usually one or two of them are most active in the ligand bonding.

As simple examples of ligands in metal–ligand bonding, free atoms or diatomics formed by the atoms of the second row of the periodic table can be suggested. Figure 6.5 illustrates a typical MO scheme for such a diatomic

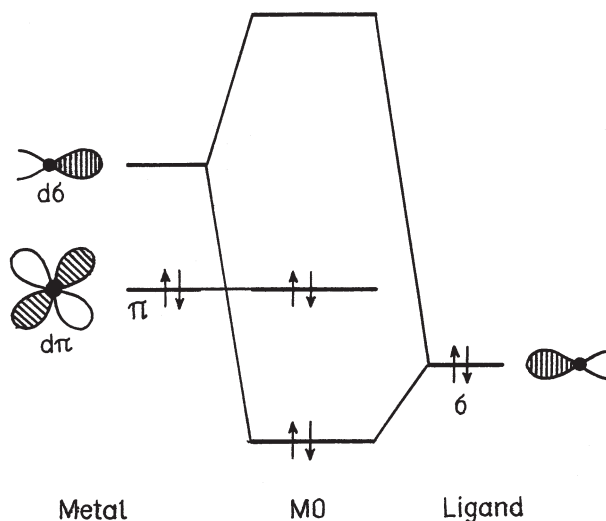


**FIGURE 6.4.**  $\sigma$  and  $\pi$  AOs of the metal in a monoorbital MO bonding with the ligand that has only one active  $\sigma$  orbital.



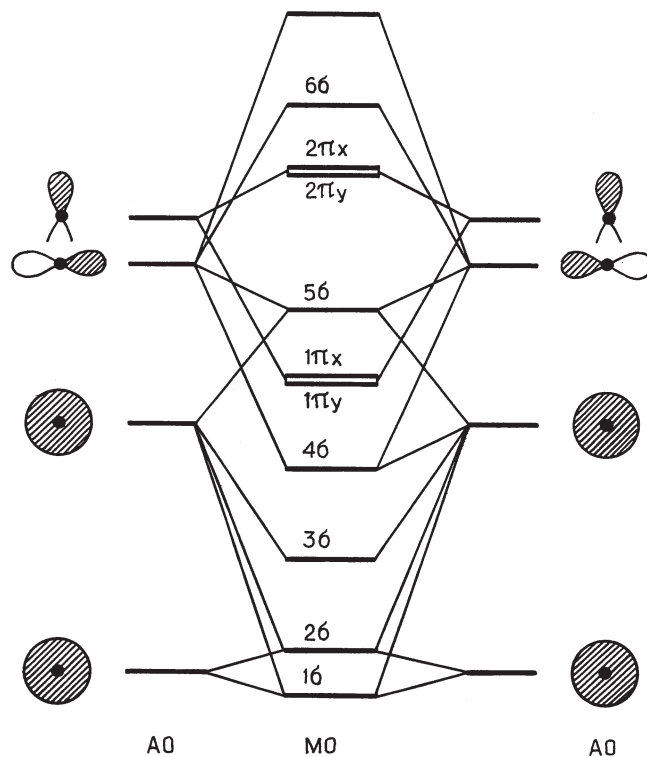


FIGURE 6.5. Atomic orbitals and MOs for diatomics of second-row atoms.

molecule. The  $1s$  orbitals, owing to their deep bedding and hence poor overlap, form very weak bonding  $1\sigma$  and antibonding  $2\sigma$  MOs (in the case of identical atoms they are  $\sigma_g$  and  $\sigma_u$ , respectively), which, because they are both occupied, do not contribute to the bonding between the atoms.

The  $2s$  orbitals form much stronger bonding and antibonding MOs. The close-in-energy  $2p_\sigma$  orbitals of the two atoms have the same  $\sigma$  symmetry and strong overlap with each other and with the  $2s$  orbitals. Therefore all four orbitals become mixed (hybridized), forming the  $3\sigma, 4\sigma, \dots$  MOs (all the  $\sigma$  orbitals are mixed; the  $1s$  orbital contribution is usually negligible).

In addition to the  $\sigma$  orbitals,  $2p_\pi$  AOs also overlap (although less than do the  $\sigma$  AOs), forming bonding  $1\pi$  and antibonding  $2\pi$  MOs. Depending on the nature of the atoms in the diatomic molecule, the mutual position of the close-in-energy MOs  $4\sigma, 1\pi$ , and  $5\sigma$  can vary, and this is important when considering their bonding to the coordination center.

The main features that make the local metal–ligand bond distinct from the corresponding organic bonds are due to the relatively strong asymmetry of the overlapping orbitals produced by the  $d$ -electron heterogeneity; this causes relatively large orbital charge transfers, which are often mutually compensated for



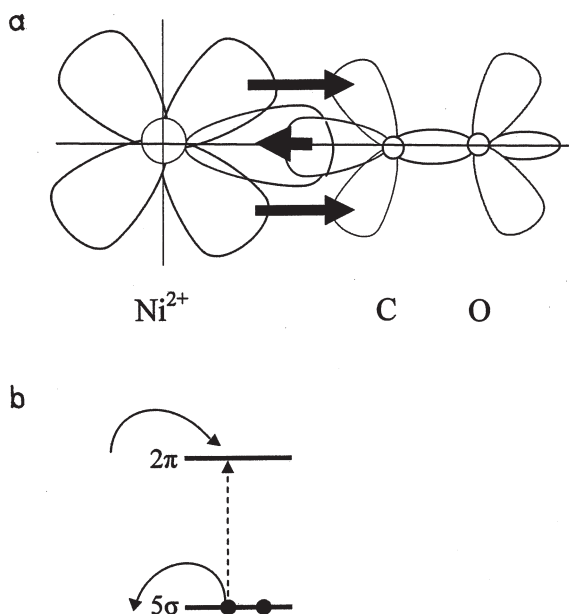


**FIGURE 6.6.** Mutual compensation of the ligand's  $\sigma$ -donor and  $\pi$ -acceptor charge transfers results in its partial excitation; in case of  $\text{Ni}^+ - \text{CO}$  the  $5\sigma \rightarrow 2\pi$  excitation amounts to  $\sim 0.3$  electron.

in the diorbital and multiorbital bonds (see below). Together with the fact that the ligand is bound by the entire complex, rather than only by the CA, these distinctions render the usual ideas of multiple bonds insufficient for a full characterization of the bond. For a better description of ligand bonding, MO-based definition of bond multiplicity is suggested, in which *monoorbital, diorbital, and multiorbital metal–ligand bonds are distinguished*.

*In the MO definition, the multiplicity of the orbital bonding (mono-, di-, and multiorbital) equals the number of complex–ligand bonding MOs uncompensated by the antibonding orbitals* (Section 6.2). These types of bonds, as shown below, differ significantly from and are complementary to the well-known single, double, and triple bonds in organic (or main-group) compounds by both definition and effect. The simple multiple bonds are particular cases of the defined multiorbital bonds.

By definition, the number of orbitals that participate in the bonding does not coincide with the bond multiplicity. In the usual definition the multiplicity of the bond equals the number of pairs of electrons that participate in the bonding, whereas the number of bonding orbitals may be smaller, since some of them may be degenerate. In particular, in the triple bond with one  $\sigma$  and two  $\pi$  bonds the latter may be degenerate, and hence the bond is diorbital with one  $\sigma$  MO and one double-degenerate  $\pi$  MO. Besides, the bonding (antibonding) orbital can be

occupied by one electron. The advantage of the MO terminology is seen from the treatment of ligand bonding given below in this section.

An important feature of diorbital and multiorbital metal–ligand bonding is *the mutual compensation of orbital charge transfers*. Consider a diorbital M–L bond in which one of the bonding MOs is a  $\sigma$  MO while the other is of the  $\pi$  type. The orbital charge transfers  $\Delta q_i$  defined in Section 5.2, Eq. (5.20'), may be both negative and positive. Usually the orbital charge transfers along the  $\sigma$  MO go from the ligand to the metal:  $\Delta q_\sigma < 0$  (*negative* transfer means reduction of the ligand electronic charge), while for the  $\pi$  MO  $\Delta q_\pi > 0$  (backdonation). The total charge transfer is thus

$$\Delta q = \Delta q_\sigma + \Delta q_\pi \quad (6.2)$$

It is known that  $\Delta q$  cannot be very large because of thermodynamic restrictions (cf. the Pauling electroneutrality principle [6.12]). In monoorbital binding  $\Delta q$  coincides with the orbital charge transfer, and hence they are both small. Distinct from (and contrary to) the monoorbital bonds, for diorbital bonds *the total charge transfer  $\Delta q$  may be small, while the orbital charge transfers are large*, because they may have opposite signs for which  $\Delta q = |\Delta q_\pi| - |\Delta q_\sigma|$ . This is a specific feature of the diorbital (multiorbital) bond, as compared with monoorbital (single) bonds, and it has far-reaching consequences for both bonding energy and charge distribution, which changes the properties of the coordinated ligands. In particular, while the orbital charge transfers compensate each other, their effect on ligand activation may be additive with respect to their absolute values (Section 11.2).

This enhanced coordination by mutually compensated charge transfers is in general not directly related to the usual double bonds in organic compounds. Indeed, in the latter the orbital charge transfers are relatively small and not mutually compensating. Therefore, the usual terminology of single and double bonds that is most useful for organic and main-group systems may not be sufficiently informative for coordination compounds. In the case of diorbital bonding, the scheme of mutually compensating charge transfers is qualitatively the same as in backdonation, first suggested by Dewar [6.13] and Chatt and Duncanson [6.14].

The charge compensation in the  $\sigma$ -donor and  $\pi$ -dative interactions in the ligand bonding also generates another important effect: the interdependence and mutual enhancement of the two types of charge transfers,  $\Delta q_\sigma$  and  $\Delta q_\pi$ : *the  $\pi$ -dative charge transfer to the ligand enhances its donor properties on the  $\sigma$  bond because of the increased interelectron repulsion, and vice versa* [6.4, 6.17].

On the other hand, *changes in the occupancies of the ligand MOs may result in its partial excitation*. Indeed, as a result of coordination, the unoccupied excited  $\pi$  MO of the free diatomics becomes populated, while its ground-state  $\sigma$  MO depopulates, which is qualitatively equivalent to full or partial excitation (Fig. 6.6). *The two effects, orbital charge transfers in opposite directions and partial excitation, strongly influence the properties of the ligands coordinated by diorbital or multiorbital bonds* (Section 11.2).

Note that neither of these two effects can be characterized by simply the total charge transfer to the ligand  $\Delta q = |\Delta q_\pi| - |\Delta q_\sigma|$ ; only both orbital charge transfers reflect the coordination properties. Therefore, attempts to interpret experimental data on coordinated ligands by the  $\Delta q$  value, often reported in publications (e.g., to consider coordinated oxygen in the state of superoxide according to its stretching vibration frequency, Section 11.2), are ungrounded.

In the qualitative treatment above, it is assumed that the orbital charge transfers  $\Delta q_i$  can be calculated by Eq. (5.20''). In so doing one should note the discussion in Section 5.2 and Example 5.1 concerning the restricted physical meaning of charge distribution given in terms of atomic orbitals, and its strong dependence on the basis set employed in the calculations. In many cases the results of sophisticated numerical calculations cannot be visualized in terms of free metal and ligand atomic orbitals, *in terms of origin of ligand bonding*, as is done in the qualitative treatment. This is a general feature of exact numerical data on electronic structure discussed in Section 5.6; *the more sophisticated mathematical methods used in accurate numerical calculations of electronic structure, the less visual the possible treatment in terms of atomic orbitals* (Section 5.3).

In some cases the valence AOs (ground and excited) emerge in the resulting MOs with considerable weight, which can be approximately interpreted as a measure of participation of the corresponding orbitals in the bonding. If extended basis sets and/or a superposition of many configurations are used in the calculations, the direct correlation of the results with certain ligand AOs becomes very difficult. However, the MOs can be differentiated by symmetry properties ( $\sigma$ ,  $\pi$ ,  $\delta$ , etc.), and this allows one to calculate orbital charge transfers for such MOs.

### **Monoorbital Bonds: Coordination of NH<sub>3</sub> and H<sub>2</sub>O**

The case of monoorbital bonds is the simplest. As a rule, the monoorbital bond is realized when the ligand has only one active orbital that is able to bond to the complex. In this case only one  $\sigma$  metal–ligand bond is usually formed. A simple example of this kind is the bonding of ammonia, in which the lone pair of electrons of the nitrogen atom occupies its hybridized  $sp^3$  orbital, which can be taken as the ligand  $\sigma$  orbital. Figure 6.4 illustrates the MO scheme for this simple case of ligand bonding (cf. Fig. 5.3).

The charge distribution in this bond is not symmetric with respect to the metal and ligand; under the assumption that the metal is a  $\sigma$  acceptor and the ligand is a  $\sigma$  donor, a typical donor–acceptor bond is obtained. This type of ligand bonding takes place mostly when either the ligand has no active  $\pi$  orbitals that can form bonds with the metal (meaning unoccupied or too high in energy) or the metal  $\pi$  orbitals are weakly active. The former possibility is more probable. In addition to NH<sub>3</sub> that has no active  $\pi$  orbitals, many similar ligands can be suggested (e.g., PH<sub>3</sub>, CH<sub>3</sub><sup>−</sup>, H<sup>−</sup>). However, under certain conditions phosphines (e.g., PF<sub>3</sub>), as well as similar compounds of other pretransition elements, may exhibit  $\pi$ -accepting abilities [6.15].

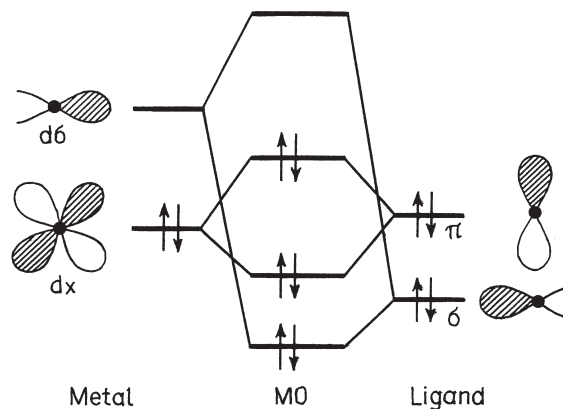


**FIGURE 6.7.** Monoorbital bonding with ligands that have active but occupied  $\pi$  orbitals.

Monoorbital bonds can also be realized when both the ligand and metal active  $\pi$  orbitals are occupied. Halogen ions and water can be indicated as examples of ligands that have such  $\pi$ -donor orbitals. In these cases both  $\pi$ -type MOs formed by the ligand and metal orbitals, bonding and antibonding, are occupied by electrons (Fig. 6.7), and hence their total contribution to the bonding is very small because of mutual compensation (Sections 5.2 and 6.2). In principle, there is a possibility that within this combination of two  $\sigma$  and two  $\pi$  MOs with six electrons the antibonding  $\sigma$  and  $\pi$  MOs are inverted, and the  $\sigma$  MO is occupied instead of the  $\pi$  MO. As a result, the bond remains monoorbital, but of  $\pi$  type. Practically, other MO energy levels may interfere in this region becoming occupied, but then diorbital or multiorbital bonds should be considered.

In monoorbital bonds the influence of the complex on the ligand is relatively simple: *polarization*. Indeed, as a result of the bonding, a donor–acceptor shift of the electronic cloud from the ligand to the metal takes place with all the consequences for the properties of the coordinated ligand and the complex as a whole. This effect can also be described in the simpler models of crystal field theory (CFT, Chapter 4) and angular overlap method (AOM, Section 5.2), provided that the effective charge and polarization of the ligand are taken into account. Therefore, analysis of some properties of coordination compounds with simple ligands that form only monoorbital (single) bonds can often be carried out within the approximations of CFT or AOM.

Monoorbital bonding, as a rule, does not change radically the properties of the ligands but modifies them, sometimes significantly. For instance, in the case of coordination of the ammonia molecule mentioned above, the donor–acceptor shift of the electronic charge to the metal weakens the N—H bonds, lowers their stretching vibration frequencies, and increases the acidity of the coordinated molecule. Example 6.1 demonstrates calculations of the electronic structure of some monoorbital bonds.

**EXAMPLE 6.1*****Ab Initio Numerical SCF-CI Calculations of the Electronic Structure of Monoorbital Bonds: Ni(H<sub>2</sub>O)<sub>n</sub> and Ni(PH<sub>3</sub>)<sub>n</sub>, n = 1, 2 [6.16]***

In the case of Ni—OH<sub>2</sub>, the Ni—O bond, as expected, is a mono-orbital of the second kind when the ligand has active  $\pi$  orbitals but they are occupied by electrons (Fig. 6.7). The results of CASSCF (Section 5.3) calculations yield  $\Delta q_\sigma = -0.13$ ,  $\Delta q_\pi = -0.03$  (the charges on the atoms are  $q_{\text{Ni}} = -0.17$ ,  $q_{\text{O}} = -0.69$ ,  $q_{\text{H}} = 0.43$ ). For H<sub>2</sub>O—Ni—OH<sub>2</sub> (linear configuration) the orbital charge transfers are practically the same as in the Ni—OH<sub>2</sub> case:  $\Delta q_\sigma = -0.14$ ,  $\Delta q_\pi = -0.04$  ( $q_{\text{Ni}} = -0.36$ ,  $q_{\text{O}} = -0.70$ ,  $q_{\text{H}} = +0.43$ ). This confirms that the Ni—O bond is mono-orbital and localized (the small  $\Delta q_\pi$  value characterizes the slightly asymmetric charge distribution in the mutual compensating bonding and antibonding  $\pi$  MO in H<sub>2</sub>O).

To verify the abovementioned approximate validity of the CFT in mono-orbital bonding in this case, the authors [6.16] also calculated the interaction of the Ni(<sup>1</sup>D) atom with the dipoles OH<sub>2</sub>; the dipole moment was taken equal to 2.4 D formed by two charges:  $-0.860$  at a distance of 3.79 au (from the Ni atom) and  $+0.860$  at 4.873 au. The resulting bonding energy is 16.0 kcal/mol, which is in good agreement with the more detailed calculations given above.

Another example of expected mono-orbital bonding is the Ni—P bond in Ni—PH<sub>3</sub>. The calculations [6.16] yield  $\Delta q_\sigma = -0.32$ ,  $\Delta q_\pi = 0.07$  ( $q_{\text{Ni}} = -0.24$ ,  $q_{\text{P}} = 0.14$ ,  $q_{\text{H}} = 0.03$ ). Although the PH<sub>3</sub> molecule at first sight has no active  $\pi$  orbitals, there is a small  $\pi$  backdonation from the Ni atom to PH<sub>3</sub>. This indicates that, unlike the NH<sub>3</sub> case, where there is no backdonation, in PH<sub>3</sub> the  $d$  orbitals may become weakly active (see also Ref. [6.15] and Section 6.1). The dissociation energy (in the <sup>1</sup>A<sub>1</sub> state) is  $D_e = 13.7$  kcal/mol.

For the linear H<sub>3</sub>P—Ni—PH<sub>3</sub> system the charge transfers are almost the same as in Ni—PH<sub>3</sub>:  $\Delta q_\sigma = -0.26$ ,  $\Delta q_\pi = 0.10$  ( $q_{\text{Ni}} = -0.32$ ,  $q_{\text{P}} = 0.10$ ,  $q_{\text{H}} = 0.02$ ), which confirms that the bonding is approximately localized and mono-orbital.

**Diorbital Bonds: Coordination of the N<sub>2</sub> Molecule**

More widespread and rich in content are *diorbital bonds*. As explained above, this term is used to denote the presence of two types of uncompensated bonding MOs involved in metal–ligand bonding. The diorbital bond is realized when the

ligand possesses, in addition to the  $\sigma$  orbital, a free  $\pi$  orbital that can form an additional  $\pi$  bond with the metal. In the more usual terminology diorbital bonding may result in single, double, triple, and higher-multiplicity bonds, as well as semibonds, depending on the number of electrons on the bonding MOs. The single bond is realized when two bonding electrons occupy one of the two bonding MOs; four electrons on the latter form a double bond. Higher bond multiplicities may occur if one or both bonding MOs are degenerate, for instance, in the case of metal–metal bonds (see below).

As simple examples of ligands in diorbital bonds, the diatomics seem to be most informative. Consider first the most stable diatomic molecule of the series under consideration, the  $N_2$  molecule. Figure 6.8 shows its MO energy levels and their wavefunction symmetries with indication of the electron occupancy [6.18]. It is seen that the HOMO is  $5\sigma$ , while the LUMO is  $2\pi$ . By comparison with the symmetries of the valence orbital of the metal (Fig. 6.4), one can easily

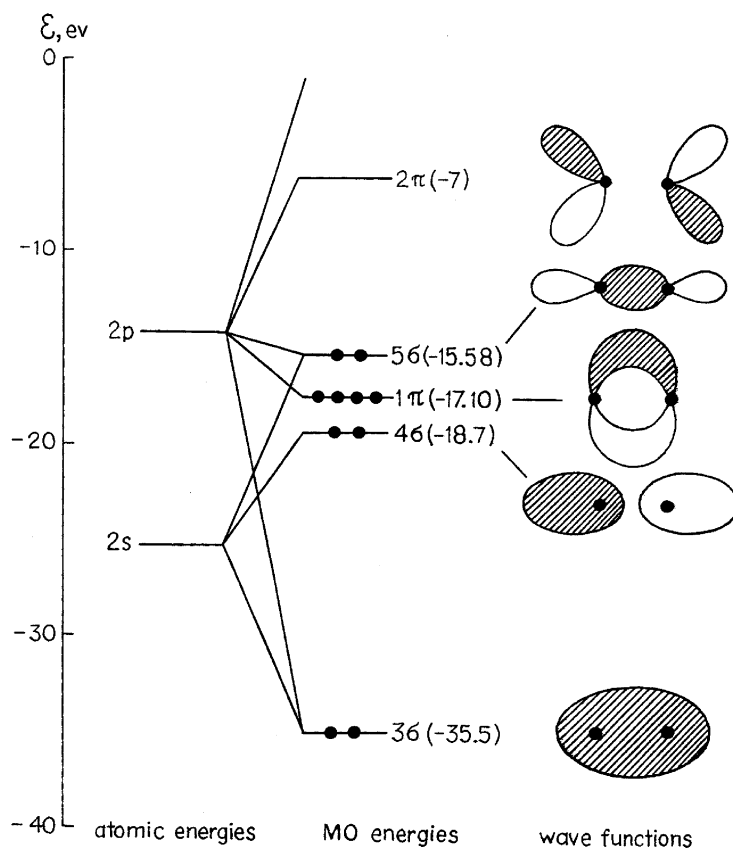


**FIGURE 6.8.** MO energy-level scheme (energies in eV are indicated in parentheses) and wavefunction symmetries for the dinitrogen molecule.

conclude that the possibility of a nonzero orbital overlap and bonding depends on the *geometry of coordination*.

For *linear end-on coordination* when the axis of the  $N_2$  molecule coincides with the line of the bond to the metal, the  $5\sigma$  MO of  $N_2$  can form further  $\sigma$  MOs with the  $\sigma$  orbital of the metal, while the  $2\pi$  MO forms  $\pi$  MOs with the metal  $\pi$  orbital. Taking into account the extension of these orbitals in space, one can see that at large distances a better overlap and bonding is achieved with the  $\sigma$  MO, while shorter distances are required for a good  $\pi$  overlap.

For *side-on coordination* when the axis of the molecule is perpendicular to the line of the bond to the metal, the overlap with the  $5\sigma$  MO of  $N_2$  (and hence the possibility of formation of a corresponding  $\sigma$  bond) deteriorates. In this geometry the  $1\pi$  MO has the required  $\sigma$  symmetry with respect to the bond, and despite being deeper in energy, it may become significant. Note that if the metal is a  $\pi$  acceptor, the only possibility for accepting  $\pi$  electrons from the ligand  $N_2$  is provided by the  $1\pi$  MO in the linear end-on coordination, and by the antibonding  $4\sigma$  MO in the case of side-on coordination. This illustrates the general statement of a *strong dependence of ligand bonding on the details of their electronic structure and geometries of coordination*.

If the metal has occupied  $\pi$  and free  $\sigma$  orbitals, dinitrogen coordination produces a diorbital bond with one  $\sigma$ -bonding MO and one  $\pi$ -bonding MOs in both end-on and side-on geometries, provided the small contributions of the inner orbitals are neglected (Fig. 6.9). Example 6.2 illustrates these conclusions by considering the specific case of  $N_2$  bonding in  $FeN_2$  [6.19].

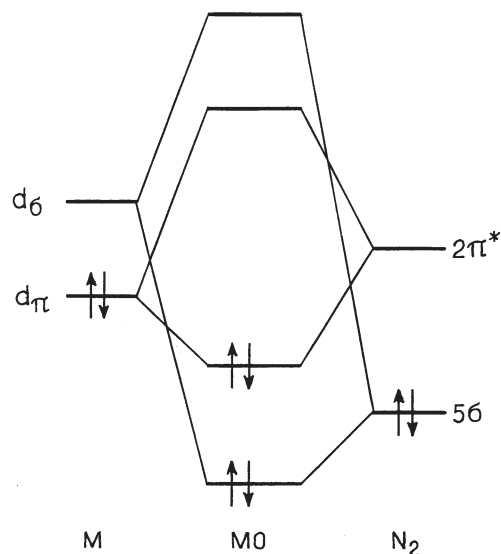


**FIGURE 6.9.** Diorbital MO bonding of the  $N_2$  molecule to a  $\sigma$ -acceptor ( $\pi$ -donor) metal  $M$  in the linear end-on coordination.

**EXAMPLE 6.2*****Electronic Structure and Bonding in FeN<sub>2</sub>*** [6.19]

The ab initio calculations were carried out in the CASSCF version of MO LCAO (Section 5.3). The basis set is taken as (14s11p6d)/[8s6p4d] for the iron atom and (9s6p)/[4s4p] for N. For FeN<sub>2</sub> with side-on coordination, the main orbital charge transfers to the N<sub>2</sub> molecule are  $\Delta q_{\sigma} = -0.13$ ,  $\Delta q_{1\pi} = -0.19$ , and  $\Delta q_{2\pi} = 0.68$ . Compared with end-on coordination, the transfer from the 5 $\sigma$  MO is lower, while the transfer from the bonding 1 $\pi$  MO is significant, and the backdonation to the antibonding 2 $\pi$  MO is predominant.

Because of opposite signs the  $\Delta q_i$  values compensate each other in the total charge transfer, but they contribute additively toward weakening of the N—N bond discussed above and in Section 11.2 (except in special cases where it is important, the multiplicities of the bonds are not indicated). The increase of the interatomic distance  $\Delta R(\text{N—N})$  and the decrease in frequency of stretching vibration  $\Delta\omega$  by coordination are calculated to be  $\Delta R = 0.162$  au and  $\Delta\omega = -671$  cm<sup>-1</sup> (in a larger CASSCF version they are  $\Delta R = 0.165$  au and  $\Delta\omega = -467$  cm<sup>-1</sup>). This bond weakening is very important in chemical activation of molecules by coordination. In particular, in the case of N<sub>2</sub> this bond weakening is the major factor in nitrogen fixation [6.20]. For other examples of N<sub>2</sub> coordination, see Table 11.2.

**Coordination of Carbon Monoxide**

The CO molecule is isoelectronic to N<sub>2</sub> [6.18] and can be characterized by qualitatively the same MO scheme (Fig. 6.10). But unlike N<sub>2</sub>, carbon monoxide has other MO energy-level positions and bonding features and nonsymmetric electronic charge distribution between the C and O atoms; the electronic charge is attracted more to the oxygen atom and it is more diffusive in the carbon side.

The coordination of CO to the metal atom results in a diorbital bonding with one  $\sigma$  MO and one  $\pi$  MOs, quite similar to the N<sub>2</sub> case, but the effect of coordination is different. In particular, the 5 $\sigma$  orbital of CO is slightly antibonding (in N<sub>2</sub> it is bonding), and therefore the charge transfer from this orbital to the metal strengthens the C—O bond. On the other hand, the 2 $\pi$  MO in CO is stronger antibonding than in N<sub>2</sub> (Sections 7.2 and 11.2), and hence the charge transfer to this MO gives a stronger destabilization effect than in N<sub>2</sub>. Again, the orbital charge transfers themselves also differ in these two cases. Various metal—CO bonding properties are illustrated by numerical calculations in Examples 6.3–6.5.



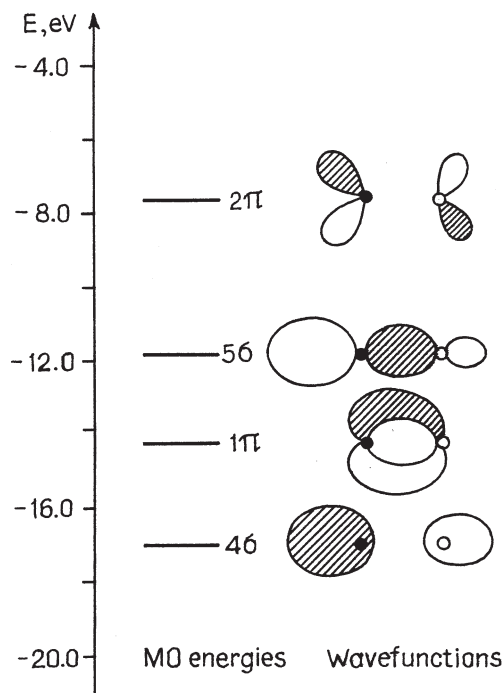


**FIGURE 6.10.** MO energy-level scheme and wavefunction symmetries for the CO molecule (compare with that of  $N_2$  in Fig. 6.8).

### EXAMPLE 6.3

#### Bonding and Charge Transfer in the Pt—CO Complex [6.21]

Many studies are devoted to analysis of CO coordination based on electronic structure calculations. For the system Pt—C—O, with linear end-on coordination, calculations were carried out in approximation of the effective core potential with a large basis set including electronic correlation energy by means of configuration interactions (Section 5.3). In the ground singlet state  $^1\Sigma^+$ , which corresponds to dissociation of the system into the Pt atom in the excited singlet state  $5d^{10}(^1S)$  and the CO molecule in the ground state, Pt—CO bonding is rather strong ( $\sim 70.4$  kcal/mol), while the equilibrium distance Pt—C is  $R_e = 1.707$  Å. With respect to the cleavage into the Pt atom in the ground-state configuration  $5d^96s^1$  and CO in the ground state the bonding energy is smaller, 43.8 kcal/mol; in the triplet states  $^3\Sigma^+$  and  $^3\Delta$  it is 19.4 kcal/mol and 18.2 kcal/mol with equilibrium distances  $R_e = 1.820$  Å and  $R_e = 1.895$  Å, respectively (Fig. 6.11).

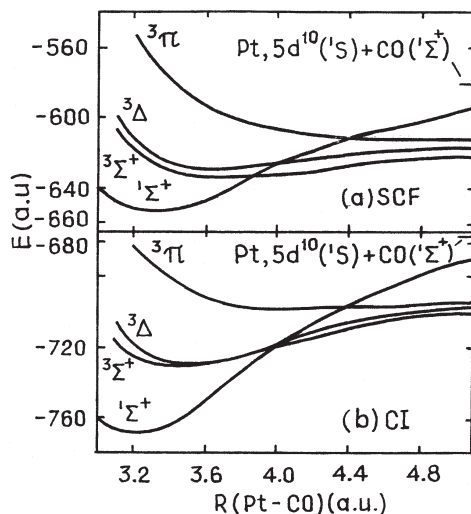


**FIGURE 6.11.** Binding energy curves for  $^1\Sigma^+$ ,  $^3\Sigma^+$ ,  $^3\Delta$ , and  $^3\Pi$  states of the linear system Pt—C—O calculated in the SCF MO LCAO approximation without (a) and with (b) CI (energies are given relative to  $-48$  au). (After Bash and Cohen [6.21].)

In the  $^3\Pi$  state obtained from the electronic configuration of the Pt atom with a hole (vacancy) in the  $d_\pi$  orbitals ( $d_{xz}$  or  $d_{yz}$ ), the  $\pi$ -donor properties of Pt are weakened, and there is no Pt—CO bond (Fig. 6.11). This result confirms the considerations, given above, about the role of the diorbital (multiorbital) nature of the bond in the mutual enhancing  $\sigma$ -donor and  $\pi$ -acceptor interactions: the weakening of the  $\pi$  dative interaction Pt—CO reduces the  $\sigma$ -donor properties of CO, making bonding impossible.

The orbital charge transfers calculated for the ground state are [6.21]  $\Delta q_{5\sigma} = -0.25$ ,  $\Delta q_{2\pi} = 0.38$  (total for two  $\pi$  MOs), and the total transfer  $\Delta q = 0.13$ , as expected, is not very large. This additional electronic charge on the CO molecule is concentrated mainly on the carbon atom. Calculated in the same approximation, the charges on the atoms in the free CO molecule are  $q(\text{C}) = 0.12$  and  $q(\text{O}) = -0.12$ , while after coordination they become  $q'(\text{C}) = 0.02$  and  $q'(\text{O}) = -0.14$ .

The Pt—C bond can be characterized by the overlap population  $P(\text{Pt—C})$ . It follows from the results of the calculations that, as expected, the major contribution to the Pt—C bonding is due to the  $\sigma$  MO,  $P_\sigma(\text{Pt—C}) = 0.66$ . This includes the contribution of the  $5\sigma(\text{CO})$  orbital,  $P_{5\sigma} = 0.25$ , while that of  $5d$  orbitals from the Pt atom is  $P_{d\sigma} = 0.41$ . For the  $\pi$  MOs, contribution to the overlap population comes entirely from the Pt atom (the  $2\pi$  MO of the free CO molecule is unoccupied) and equals  $P_\pi(\text{Pt—C}) = 0.42$ , in 0.21 on each of the two  $\pi$  MOs.

Again, the absolute values of charges in different regions of the molecular system (e.g., the atomic charges) in the presence of strong covalent bonds are, in a sense, conventional and depend on the mode of separation of the system into parts and the choice of the wavefunction basis set in the Mulliken population analysis (see the discussion in Section 5.2).

#### EXAMPLE 6.4

##### *Bonding in M—CO with M = Cr, Fe, Co, Ni* [6.21]

The calculations for these systems are quite similar to that of Pt—CO since they are carried out in the same nonempirical approximation with an effective core potential, but with a smaller basis set and for the metal electronic configuration  $M(3d^{n-1}4s)$  only. The main bonding features in M—CO are the same as in the case of Pt—CO, namely, the integral charge transfer from the metal to the CO molecule is relatively small,  $\Delta q \approx 0.1-0.3$ , while the orbital charge transfers  $\Delta q_\sigma$  from CO to the metal and  $\Delta q_\pi$  from the metal to CO are much larger.

This is also seen from the data in Table 6.5, where the changes of one-electron energy levels by coordination are shown [6.7]. In particular, the energy of the  $5\sigma$  level is significantly lowered by coordination, and this confirms once more the antibonding nature of the  $5\sigma$  MO. Because of the different basis sets used in the calculations, the absolute values of the atomic charges differ from those obtained by Bash and Cohen [6.21]. This is seen explicitly from the comparison of the data for the free CO molecule; Itoh and Kunz [6.22] noted charges on C and O of  $q = \pm 0.33$ , whereas from the Bash–Cohen study [6.21] it follows that they are  $q = \pm 0.12$ .

**TABLE 6.5. Shifts of MO Energy Levels of the CO Molecule by Coordination to Transition Metals M (in eV)**

MO	Free CO	M			
		Cr	Fe	Co	Ni
$5\sigma$	-15.12	-16.47	-16.67	-17.11	-17.64
$1\pi$	-18.15	-17.43	-17.64	-18.07	-18.54
$4\sigma$	-21.74	-21.12	-21.25	-21.73	-22.23
$3\sigma$	-42.41	-41.26	-41.47	-42.01	-42.57

Source: From Korol'kov [6.7].

**EXAMPLE 6.5****Bonding in Sc—CO, Ni—CO, and Ni(CO)<sub>2</sub>**

The calculations for Sc—CO [6.23] was carried out by the multireference single- and double-CI method employing the pseudopotential approximation. Reasonable results were obtained under the assumption that the starting configuration of the Sc atom is  $3d^3$  (term  $^4F$ ) and the ground state of linear Sc—CO is  $^4\Sigma^-$ . The SCF one-electron MO energies are shown in Fig. 6.12. The orbital charge transfers are  $\Delta q_\sigma = -0.22$ ,  $q_{2\pi} = 0.52$ , and the total charge transfer from Sc to CO is  $\Delta q = 0.30$  ( $q_C = 0.07$ ,  $q_O = 0.23$ ). The orbital charge distribution obtained for the  $2\sigma$ ,  $3\sigma$ ,  $4\sigma$ , and  $2\pi$  MOs seem to be very expressive (Fig. 6.13). The dissociation energy for the reaction  $\text{ScCO}(^4\Sigma^-) \rightarrow \text{Sc}(3d^3, ^4F) + \text{CO}(X^1\Sigma^+)$  is 1.14 eV (26.30 kcal/mol).

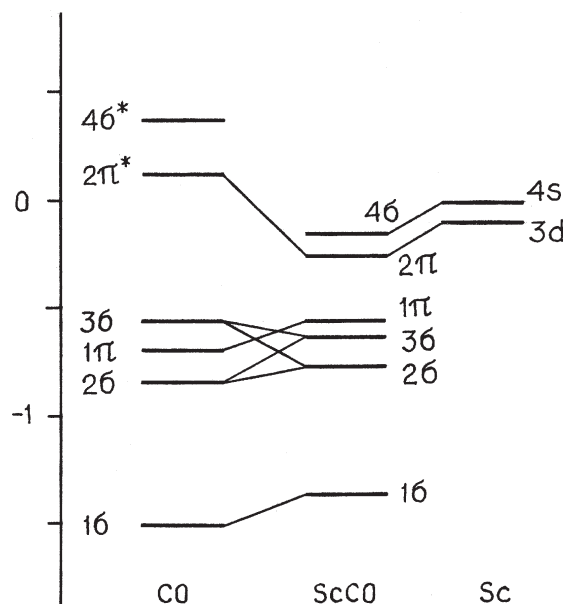


**FIGURE 6.12.** Correlation diagram for the SCF one-electron energies in the  $^4\Sigma^-$  state of ScCO (in atomic units; the numeration of  $\sigma$  levels in Ref. 6.23 differs from that of Fig. 6.10 because the inner levels are not indicated).

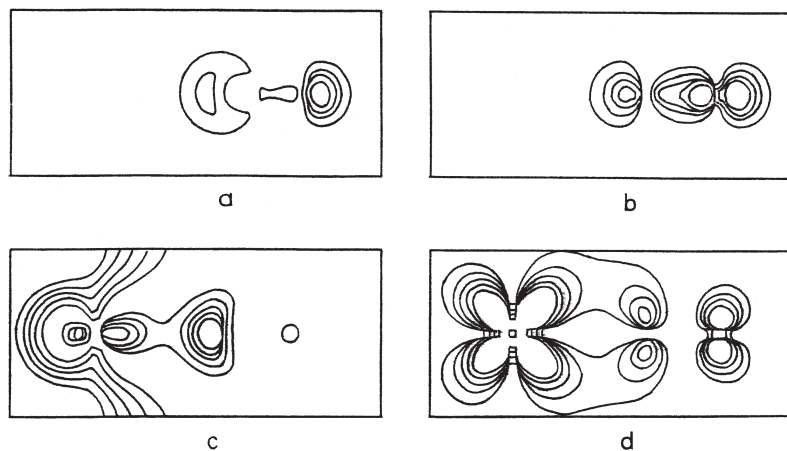


**FIGURE 6.13.** Electron density contour maps for the orbitals of Sc—CO in the  $^4\Sigma^-$  state:  $2\sigma$  (a),  $3\sigma$  (b),  $4\sigma$  (c),  $2\pi$  (d).  $R(\text{C—O})=2.2$  Bohr,  $R(\text{Sc—C})=4$  Bohr. (From Jeung [6.23].)

These data can be compared with similar ab initio SCF CI calculations for Ni—CO [6.23]. For the  $^1\Sigma^+$  state  $\Delta q_\sigma = -0.15$ ,  $\Delta q_\pi = 0.45$ ,  $\Delta q = 0.30$  ( $q_{\text{Ni}} = 0.30$ ,  $q_{\text{C}} = 0.14$ ,  $q_{\text{O}} = -0.43$ ), and the dissociation energy into singlet nickel, Ni( $^1D$ ), is 29.9 kcal/mol. In the case of two ligands Ni(CO) $_2$  in the linear configuration the charge transfers change:  $\Delta q_\sigma = -0.24$ ,  $\Delta q_\pi = 0.29$  ( $q_{\text{Ni}} = 0.11$ ,  $q_{\text{C}} = 0.33$ ,  $q_{\text{O}} = -0.39$ ), while the energy of dissociation into Ni( $^1D$ ) + 2CO is  $D_e = 57.1$  kcal/mol. These changes could be expected since the Ni—CO bonds are delocalized.

### $\sigma + \pi$ Bonding

So far we have tried to interpret the results of numerical calculations of CO bonding in terms of the diorbital ( $\sigma$  and  $\pi$ ) bond. In the cases of M—CO, where M is a metal atom, such interpretation does not encounter difficulties. However, in more complicated cases of ligand bonding this description may become evidently inadequate. In the general case of complex—ligand bonds, in addition to the  $\sigma$  and  $\pi$  MOs, other MOs of the multielectron system may be involved, making the bonding multiorbital. Let us illustrate this statement by the example of formation of the “ $\sigma + \pi$ ” MO in metal carbonyls in addition to the pure “ $\sigma$ ” and “ $\pi$ ” MO’s [6.24].

Consider the octahedral complex Cr(CO) $_6$  (a general MO scheme and possible electronic configurations for such complexes are given in Sections 6.1 and 6.2). Let us analyze the ligand—complex bond (CO) $_5$ Cr—CO. The CO molecule takes part in the end-on coordination by the same  $5\sigma$  and  $2\pi$  MOs as in the simpler

system M—CO, and the main bonding  $\sigma$  and  $\pi$  MOs can be found by considering their overlap with the corresponding orbitals of the complex, that is, with the orbitals of the metal modified by the influence of other ligands. As shown below, the presence of the latter is a matter of principle leading to a new type of bonding.

Figure 6.14 is a schematic representation of the cross section of the system in the  $xz$  plane comprising the CA and four CO ligands, illustrating the symmetries of the wavefunctions  $5\sigma$  of the two ligands on the  $z$  axis and  $1\pi$  of the other two ligands on the  $x$  axis, as well as the  $p_z$  function of the CA. As one can see, the  $p_z$  function of the Cr atom has nonzero overlap with both the  $\sigma$  MOs of the two ligands on the  $z$  axis and the  $\pi$  MOs of the ligands on the  $x$  axis, thus forming a common MO that is a  $\sigma$  MO for the former ligands and a  $\pi$  MO for the latter. (Two more CO ligands on the  $y$  axis participate with their  $1\pi$  MOs in this common MO.) Obviously, an equivalent MO is formed by the  $\sigma$  MOs of the two CO ligands on the  $x$  axis and the MOs of the four CO ligands on the  $z$  and  $y$  axes, overlapping with the  $p_x$  orbital of CA, and a third orbital of this kind formed quite similarly by the  $p_y$  orbital of the Cr atom. These three MOs belong to the threefold-degenerate  $T_{1u}$  representation of the  $O_h$  group. The chemical bonding realized by these MOs mixes the  $\sigma$  bonds of some ligands with the  $\pi$  bonds of others and vice versa; the bonding thus is  $\sigma + \pi$ . Example 6.6 illustrates such an MO obtained by numerical calculations of  $\text{Cr}(\text{CO})_6$ .

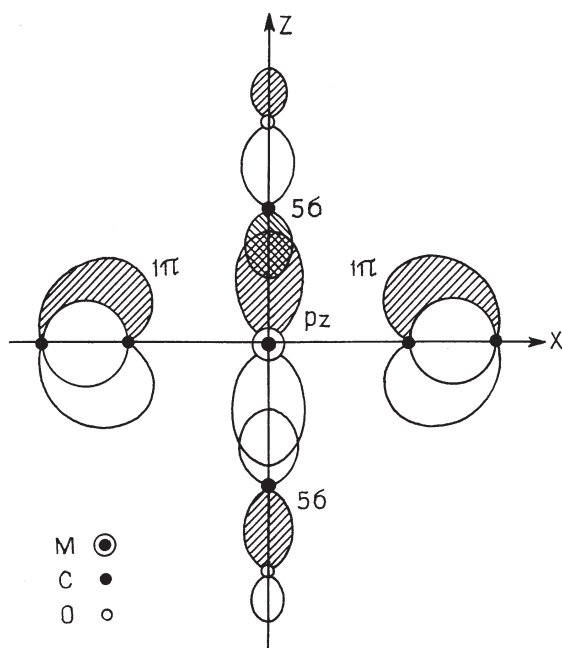


**FIGURE 6.14.** Illustration of  $\sigma + \pi$  bonding: the  $xz$  cross section of the  $t_{1u}$  function in transition metal carbonyls.

**EXAMPLE 6.6****Electronic Structure of Transition Metal Hexacarbonyls  $M(\text{CO})_6$** 

Figure 6.15 shows an outline of a  $\sigma + \pi$  ( $t_{1u}$ ) wavefunction (more precisely, of its  $\Gamma_8$  component after the spin-orbital splitting) obtained by numerical calculations of the  $\text{Cr}(\text{CO})_6$  system in the DFT relativistic  $X_\alpha$  approximation (Section 5.5) [6.24]. Since in the linear combination

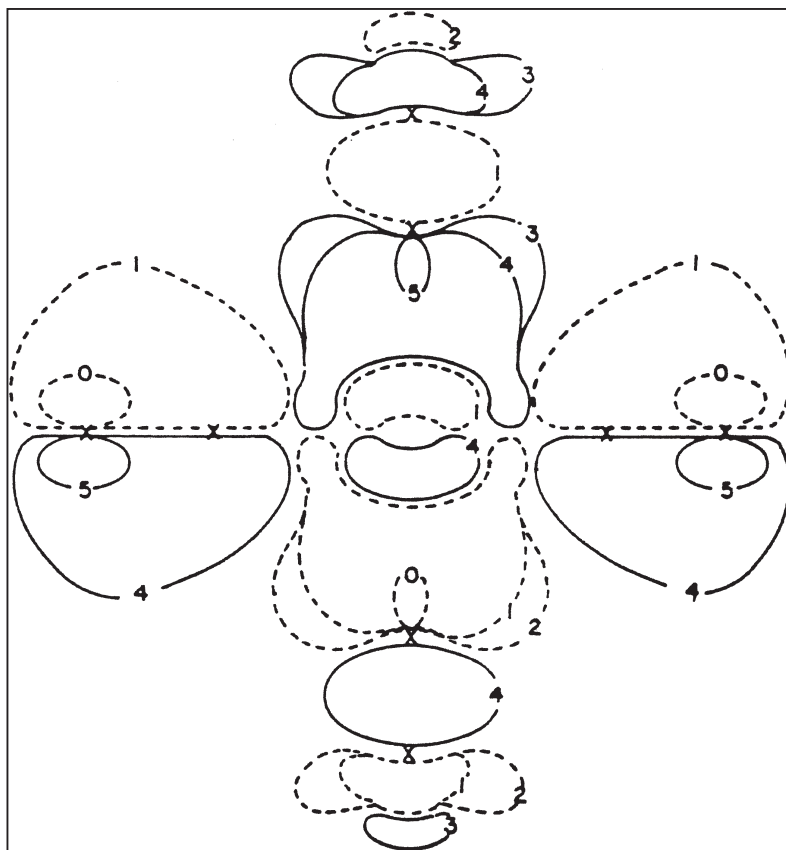


**FIGURE 6.15.** Contour lines for the  $t'_{1u}$  MO of  $\text{Cr}(\text{CO})_6$  in the  $xy$  plane containing Cr and four CO ligands slightly modified by spin-orbital interaction ( $\Gamma_8$  component). The  $\sigma + \pi$  nature of the MO is seen explicitly; the CA forms simultaneously  $\sigma$  bonds with two ligands on the  $Oy$  axis and  $\pi$  bonds with the other two ligands on the  $Ox$  axis (cf. Fig. 6.14). (After Arratia-Perez and Yang [6.24].)

resulting in the  $\sigma + \pi$  MO, three starting functions are used (one  $p$  orbital, one combination of the  $5\sigma$  function of two CO ligands on the same axis, and one combination of the  $1\pi$  functions of four remaining ligands, with all the combinations  $t_{1u}$  symmetrized), three types of  $t_{1u}$  MOs ( $t'_{1u}$ ,  $t''_{1u}$ , and  $t'''_{1u}$ ) emerge from the LCAO calculations [6.24].

The numerical data show that bonding by the  $\sigma + \pi$  MO is rather important; in  $\text{Cr}(\text{CO})_6$  it has the same order of magnitude as the “pure”  $\sigma$  and  $\pi$  MOs. This is seen also from comparison of the orbital charge transfers:  $\Delta q_{5\sigma} = -0.54$ ,  $\Delta q_{2\pi} = 0.27$  (for each of the  $2\pi$  MOs), and  $\Delta q_{\sigma+\pi} = -0.31$ . The last figure contains the transfer of 0.22 electron from the  $5\sigma$  MO and 0.09 from the  $1\pi$  MO of each CO ligand to the  $p$  orbital of the CA, its integral occupation becoming 1.89. Furthermore, in addition to the antibonding HOMO  $5\sigma$  and LUMO  $2\pi$ , the bonding  $4\sigma$  and  $1\pi$  MOs take part in the CO binding. In Table 6.6 the orbital charge transfers to and from these orbitals are shown [6.24]. The metal–ligand integral charge transfers may be different (or even of opposite direction) from those obtained in the simplified diorbital scheme (here again the dependence of the local charges on the method of calculation should be considered).

**TABLE 6.6. Orbital Charge Transfers  $\Delta q_i$  in Hexacarbonyls of Cr, Mo, and W (in electronic charge units per ligand)**

$\Delta q_i$	$\text{Cr}(\text{CO})_6$	$\text{Mo}(\text{CO})_6$	$\text{W}(\text{CO})_6$
$\Delta q_{1\pi}$	-0.07	-0.08	-0.06
$\Delta q_{5\sigma}$	-0.54	-0.56	-0.53
$\Delta q_{4\sigma}$	-0.17	-0.11	-0.18
$\Delta q_{2\pi}$	0.27	0.28	0.31

The existence of  $\sigma + \pi$  MO confirms the statement about the three-dimensional delocalization of the electronic cloud around the CA in coordination compounds. Moreover, as seen from the electron distribution in these orbitals, there is a significant ligand–ligand interaction, which is antibonding in the higher MO (Fig. 6.15) and bonding in the lower one [6.24]. This also shows that, strictly speaking, the ligand bonding is not of purely local ligand–metal nature from the ligand perspective either; it is combined ligand–metal, ligand–ligand, and so on, although the local ligand–metal contribution is predominant.

With respect to the complex as a whole, the  $t_{1u}$  orbital is a usual MO, its possible formation resulting from the general MO scheme for octahedral complexes with  $O_h$  symmetry (Fig. 6.1 and Table 5.1). The  $\sigma + \pi$  description emerges when one tries to consider the metal–ligand bond separately (as a local property). Such a description is useful in revealing the properties of coordinated ligands and ligand–ligand mutual interactions.



The orbital charge transfers are important to the analysis of the properties of coordinated ligands and their activation by coordination (Section 11.2). In the case of CO, the donation of electrons from the slightly antibonding  $5\sigma$  MO strengthens the C—O bond, while the backdonation to the strongly antibonding  $2\pi$  MO weakens this bond. Since the  $5\sigma$  MO is more extended in space than the  $2\pi$  MO, we conclude that in the approach of CO to M, at large distances where the  $\sigma$  overlap becomes essential (while the  $\pi$  one is still small), the C—O bond is expected to be strengthened (and the interatomic distance shortened), as compared with the free molecule. By further approaching the metal, the increase in the occupancy of the antibonding  $2\pi$  orbital weakens the bond C—O. It is this process that was observed in the detailed calculations of the  $(\text{CO})_5\text{Cr—CO}$  bonding [6.25]. The strengthening of the C—O bond by increasing the M—C distance is also confirmed experimentally in X-ray analysis. For instance, in the compound  $\text{Rh}_2(\text{O}_2\text{CCH}_3)_4(\text{CO})_2$  the Rh—C distance is unusually long (2.092 Å), while the C—O one (1.120 Å) is shorter than in the usual cases [6.26].

It follows from the calculations [6.25] that the energy of the process  $\text{Cr}(\text{CO})_6 \rightarrow \text{Cr}(\text{CO})_5 + \text{CO}$  equals 49.8 kcal/mol, which is larger than the mean dissociation energy  $I_{\text{av}} = 29.5$  kcal/mol per ligand ( $I_{\text{av}} = \{E[\text{Cr}(\text{CO})_6] - E[\text{Cr}+6\text{CO}]\}/6$ ). This result can be easily understood in view of the delocalized nature of the coordination bond and hence the dependence of each local M—CO bond on the presence of other bonds. It confirms again the nontransferability of metal–ligand bond parameters discussed in Section 5.6.

We conclude this subsection by noting that when there are strong relativistic effects, even monoorbital local diatomic bonds as shown in Section 6.3, may be of mixed  $\sigma + \pi$  nature.

### CO Bonding on Surfaces

Ligand bonding on surfaces (chemisorption) now forms a part of solid-state chemistry. The electronic structure of solids has some distinct features, including the *density of states*, which occurs instead of the MO energy levels in the molecular case. However, solid-state systems are beyond the scope of this book (an introduction to this field is given by Hoffmann [6.27]).

In what follows we consider some local features of ligand bonding on surfaces. One of these features is that, depending on the surface structure, several types of bonding may occur, including simultaneous bonding to several coordination centers on the surface: *multicenter bonding*. Similar multicenter bridge bonding takes place in multicenter transition metal complexes (Section 11.2). Depending on the nature of the multicenter bonding, the charge transfers and hence ligand activation may be rather different.

The CO bonding on surfaces may be of *one-center*, *two-center*, or *tricenter type* (Fig. 6.16), often denoted by  $\mu_1$ ,  $\mu_2$ , and  $\mu_3$ , respectively. Let us compare first some results of one-center coordination on different faces of different metals, Ti(0001), Cr(110), Fe(110), Co(0001), Ni(100), and Ni(111) [6.28], obtained by the extended Hückel method (Section 5.5). In these calculations it is assumed that

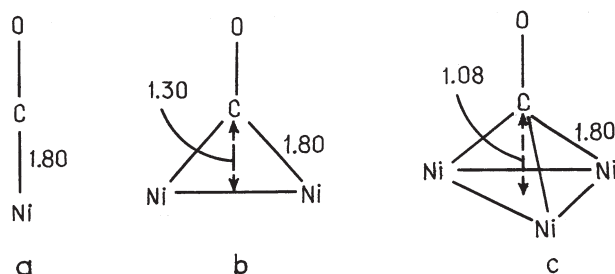


**FIGURE 6.16.** Three types of possible CO coordination to the Ni surface: one-center (a), two-center (b), and tricenter (c). In cases (b) and (c) the C—O distance is assumed equal to the one-center case (a).

**TABLE 6.7. Ligand Bonding Energies  $\Delta E$  (in eV per one CO ligand), Orbital Charge Transfers  $\Delta q_{5\sigma}$  and  $\Delta q_{2\pi}$ , and Bond Order Changes  $\Delta P(M-C)$  and  $\Delta P(C-O)$  by One-Center Coordination of the CO Molecule to Different Metals and Surfaces<sup>a</sup>**

	Ti(0001)	Cr(110)	Fe(110)	Co(0001)	Ni(100)	Ni(111)
$\Delta q_{5\sigma}$	-0.27	-0.33	-0.38	-0.40	-0.40	-0.41
$\Delta q_{2\pi}$	1.61	0.74	0.54	0.43	0.39	0.40
$\Delta P(M-C)$	1.11	0.93	0.91	0.83	0.78	0.75
$\Delta P(C-O)$	-0.78	-0.34	-0.25	-0.20	-0.18	-0.19
$\Delta E$ (eV)	-6.77	-3.44	-2.64	-1.98	-1.97	-1.66

<sup>a</sup>In the free CO molecule  $P(C-O) = 1.21$ .

the CO molecules are linear end-on coordinated and each center on the surface bounds one CO molecule. The last assumption is not restrictive, since it was shown that the dependence of the coordination properties of CO on its filling on the surface is very weak (reduction of the surface filling in half does not change the charge transfers).

In Table 6.7 CO bonding energies and the orbital charge transfers to the  $2\pi$  MO and from the  $5\sigma$  MO of CO by coordination to the metals, listed above, as well as the changes in M—C and C—O bond orders  $\Delta P$  as compared with the noncoordinated case (for which  $P = 0$  and 1.21, respectively), are given (in the table  $\Delta q_{2\pi}$  means the charge transfer to one of the two  $2\pi$  MOs; the total transfer thus is twice that in the table). As one can see, by moving along this series from right to left, the C—O bond weakens [following these data, the bond is hardly possible in the case of Ti(0001)], mostly because of the increase in the population of the antibonding  $2\pi$  MO and the reduction of  $\Delta q_{5\sigma}$ . On the other hand, the M—C bond is strengthening; this is seen from both the bonding energy and bond orders  $P(M-C)$ .

For bridged two-center and tricenter coordination, the problem of adequate choice of interatomic distances arises. In Table 6.8 compares charge transfers,

**TABLE 6.8. Orbital Charge Transfers  $\Delta q_{5\sigma}$  and  $\Delta q_{2\pi}$ , Bond Order Changes  $\Delta P(\text{Ni—C})$  and  $\Delta P(\text{C—O})$ , and Bonding Energies  $\Delta E$  (in eV per one CO ligand) in One-Center ( $\mu_1$ ), Two-Center ( $\mu_2$ ), and Three-Center ( $\mu_3$ ) Bonding to the Ni(111) Face for Two Sets of Interatomic Distances**

	$R(\text{Ni—C}) = 1.80 \text{ \AA}$			$R_N = 1.80 \text{ \AA}$	
	$\mu_1$	$\mu_2$	$\mu_3$	$\mu_2$	$\mu_3$
$\Delta q_{5\sigma}$	-0.41	-0.43	-0.44	-0.43	-0.46
$\Delta q_{2\pi}$	0.40	0.54	0.64	0.41	0.41
$\Delta P(\text{Ni—C})$	0.76	0.57	0.41	0.31	0.16
$\Delta P(\text{C—O})$	-0.19	-0.24	-0.28	-0.19	-0.19
$\Delta E$	-1.66	-2.72	-3.24	-0.89	-0.71

bond populations, and bonding energies of CO coordinated to the Ni surface [6.28] for two cases: (1) the distance  $R(\text{Ni—C}) = 1.80 \text{ \AA}$  to all the centers (to two centers in the two-center coordination  $\mu_2$ , and to three centers in the tri-center coordination  $\mu_3$ ; Fig. 6.16) is the same as in the one-center coordination  $\mu_1$ —here the distance from the carbon atom to the surface is smaller, specifically,  $R_N = 1.30 \text{ \AA}$  in two-center bonding, and  $R_N = 1.08 \text{ \AA}$  in tricenter case; and (2) the distance from the carbon atom to the surface  $R_N = 1.80 \text{ \AA}$ , while the distance  $R(\text{Ni—C})$  is  $2.19 \text{ \AA}$  in two-center bonding, and  $2.30 \text{ \AA}$  in tricenter bonding. Case 1 seems to be more appropriate, since a considerable increase in the Ni—C distance associated with a corresponding bond weakening (Table 6.8) in the absence of steric hindrance is thermodynamically inconvenient.

As one can see, when passing from one-center coordination to  $\mu_1$  to  $\mu_2$  and  $\mu_3$  in case 1, *ceteris paribus*, the orbital charge transfer to the  $2\pi$  MO increases, while the C—O bond population decreases [the negative  $\Delta P(\text{C—O})$  increases]. In other words, with increase in the number of bonding centers for each CO molecule its activation by coordination increases. This multicenter effect in chemical activation by coordination is discussed also in Section 11.2.

### Bonding of NO

In the CO bonding considered above, it has been assumed that the linear end-on geometry of coordination is realized, although, in principle, other geometries can also be important. This problem is discussed in Section 9.2 in terms of its influence on stereochemistry of ligand coordination. The electronic structures of the NO and CO molecules differ in two respects: (1) the  $\sigma$  and  $\pi$  MO energy-level positions (Fig. 6.17; cf. Fig. 6.10) are lower in the NO case (the lower  $2\pi$  MO makes the NO molecule a good  $\pi$  acceptor), and (2) the population of the (unoccupied in CO)  $2\pi$  MO differs by one electron. Example 6.7 shows how these features of the NO molecule affect its coordination properties.

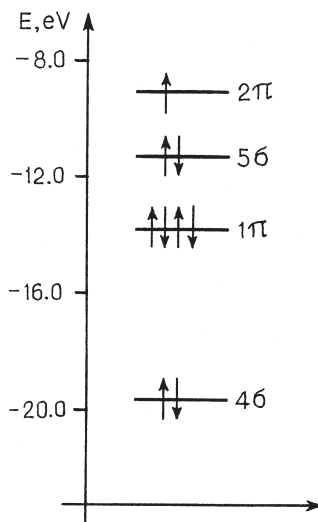


**FIGURE 6.17.** MO energy levels of the NO molecule. The wavefunction symmetries (not shown) are quite similar to the CO case in Fig. 6.9 (see also Figs. 6.7 and 6.8).

### EXAMPLE 6.7

#### *Coordination of NO on the Ni(111) Surface* [6.29]

Omitting many details of the calculations for this case [6.29], we mention here that if the surface is filled in less than (or about)  $\frac{1}{3}$  and the coordination is linear end-on normal to the surface, the electronic interaction of the NO molecule with the surface is approximately the same, as in the absence of other NO molecules on the surface. Table 6.9 gives the orbital charge transfers  $\Delta q_i$  and changes of bond orders  $\Delta P(\text{Ni—N})$  and  $\Delta P(\text{N—O})$  for one-, two-, and tricenter coordination of NO. The calculations were carried out in the extended Hückel approximation [6.29] (Section 5.5) with interatomic distances  $R(\text{Ni—N}) = 1.680 \text{ \AA}$  for all the cases.

As compared with CO, these calculations are more accurate; the charge transfers from the deeper  $4\sigma$  and  $1\pi$  MOs are not neglected, and it is assumed that for the two-center coordination the two  $2\pi$  MOs  $\pi_x$  and  $\pi_y$  are not degenerate (the interaction with two Ni atoms in the plane of the  $\pi$  MO and perpendicular to this plane are no longer equal; see Fig. 6.16). We see that in this case, as in the CO one, the increase in the number of coordination centers per each coordinated NO molecule increases its bonding to the surface and decreases the N—O bond order (increases the NO activation). The dependence of the bonding on the angle  $\phi$  between the N—O line and the normal to the surface was also considered [6.29].

**TABLE 6.9. Orbital Charge Transfers  $\Delta q_i$ , Bond Order Changes, and Bonding Energies  $\Delta E$  (in eV per one NO ligand) for One-Center ( $\mu_1$ ), Two-Center ( $\mu_2$ ), and Tricenter ( $\mu_3$ ) Bonding of the NO Molecule to the Ni(111) Face<sup>a</sup>**

$\Delta q_i$	$\mu_1$	$\mu_2$	$\mu_3$
$\Delta q_{4\sigma}$	-0.156	-0.199	-0.215
$\Delta q_{1\pi x}$	-0.016	-0.097	-0.101
$\Delta q_{1\pi y}$	-0.016	-0.043	-0.101
$\Delta q_{5\sigma}$	-0.276	-0.263	-0.242
$\Delta q_{2\pi x}$	0.408	0.765	0.671
$\Delta q_{2\pi y}$	0.408	0.391	0.671
$\Delta P(\text{Ni-N})$	0.822	0.583	0.483
$\Delta P(\text{NO})$	-0.197	-0.263	-0.308
$\Delta E$	-3.067	-4.130	-4.240

<sup>a</sup>  $P(\text{N-O}) = 1.231$ ,  $P(\text{Ni-N}) = 0$ .

### Coordination of $\text{C}_2\text{H}_4$

When polyatomic ligands are coordinated, the bonding picture becomes complicated. However, in some particular cases the problem can be simplified and approximately reduced to coordination of diatomics. Let us consider the coordination of olefines, for instance, ethylene, from this perspective. Simplification is possible in the case of bonding in the scheme of a  $\pi$  complex when the  $\text{C}=\text{C}$  bond line is perpendicular to the line of the bonding to the metal.

In the planar configuration of  $\text{C}_2\text{H}_4$  the  $\text{C}=\text{C}$  bond has one  $\sigma$ - and one  $\pi$ -bonding MOs with the latter lying in the plane perpendicular to that of the molecule (Fig. 6.18). In the  $\pi$  complex, since the  $\text{C}-\text{H}$  bonds do not take part in the chemical interaction with the metal directly, one can conclude that the metal–ligand bond in  $L_n\text{M}-\text{C}_2\text{H}_4$  is approximately diorbital. However, this bond is different from those of  $\text{N}_2$  and  $\text{CO}$  coordination: in the last two cases the HOMO is of  $\sigma$  type (bonding in  $\text{N}_2$  and weakly antibonding in  $\text{CO}$ ), whereas in  $\text{C}_2\text{H}_4$  it is a bonding  $\pi$  MO. The LUMO is an antibonding  $2\pi$  MO in all the cases, but in  $\text{N}_2$  and  $\text{CO}$  there are two MOs of this kind ( $\pi_x$  and  $\pi_y$ ), whereas in  $\text{C}_2\text{H}_4$  there is only one.

In the bonding of  $\text{C}_2\text{H}_4$  to the metal in the form of a  $\pi$  complex, both its bonding orbitals (either  $\sigma$  or  $\pi$ ) act as  $\sigma$  donors, while only one antibonding  $\pi^*$  MO (and less probably the antibonding  $\sigma^*$  MO) takes part in the metal–ligand diorbital bond. This determines the stronger  $\sigma$ -donor and weaker  $\pi$ -acceptor interaction of ethylene with the metal atom, as compared with  $\text{CO}$  and  $\text{NO}$ . Hence one can expect that the weakening of the  $\text{C}=\text{C}$  bond of an olefin by coordination is promoted by good  $\sigma$ -acceptor properties of the metal. In particular, one can anticipate that the  $\text{C}=\text{C}$  bond will be less weakened if the  $\sigma$ -acceptor orbitals of the metal are occupied by electrons. Examples 6.8 and 6.9 provide more details on  $\text{C}_2\text{H}_4$  coordination to metal centers.

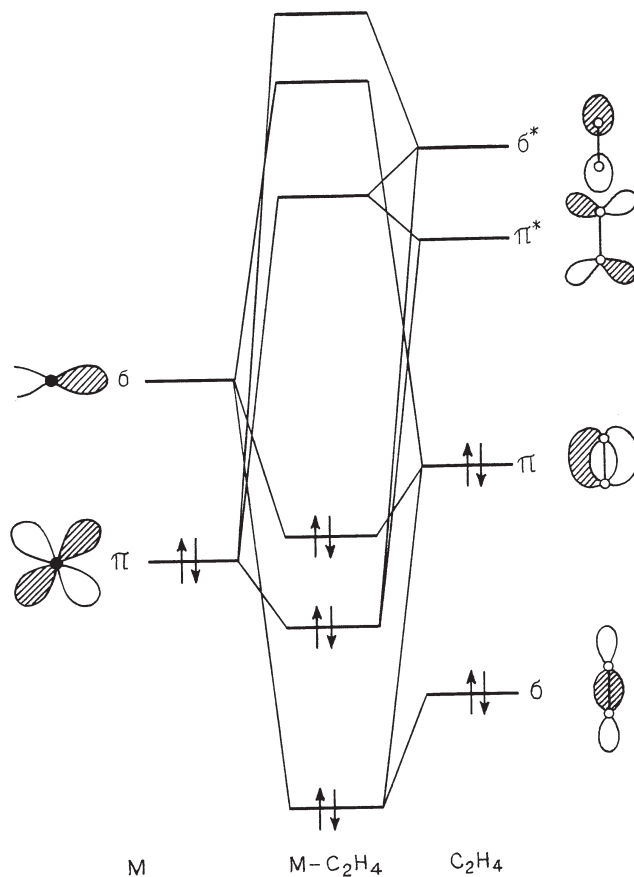


**FIGURE 6.18.** MO energy-level scheme for the M-C<sub>2</sub>H<sub>4</sub> bonding in the  $\pi$ -type coordination of ethylene to the metal ( $\pi$  complex). Two orbitals of C<sub>2</sub>H<sub>4</sub>  $\sigma + \pi$  form  $\sigma$  bonds with M, while the other two  $\sigma^* + \pi^*$  produce the  $\pi$  bonding to the  $d_{\pi}$  orbital of M.

### EXAMPLE 6.8

#### *Ethylene Bonding to Transition Metal Centers* [6.30–6.35]

One of the first well-studied systems of this kind was  $\text{Ag}^+ - \text{C}_2\text{H}_4$ ; its electronic structure was calculated and first reported in 1972 [6.30], and then repeated in 1977 [6.31] using another AO basis set and comparing the results with those of the valence basis set approximation (i.e., when the valence orbitals only are taken as a basis set; Section 5.3). Qualitatively, the results of these two studies coincide. The C<sub>2</sub>H<sub>4</sub> molecule is assumed planar, and coordination of the Ag<sup>+</sup> ion placed on the twofold C<sub>2</sub> axis perpendicular to the plane of the molecule is

energetically more convenient than on a similar axis in the molecular plane [6.30]. The bonding energy (in kcal/mol) is 27.6 [6.30], or 28.9 [6.31] or in the abovementioned valence approximation, 38.3 [6.31]. The main contribution to the bonding is due to the  $\sigma$ -donor charge transfer from the bonding  $\pi$  MO of the ethylene molecule to the  $\sigma$  orbital of the metal (formed mainly by the 5s orbital of the Ag atom with additions from its 5p orbital). A much smaller contribution to the bonding is due to the dative charge transfer to the antibonding  $\pi^*$  MO of ethylene from the  $3d_{\pi}$  orbital of Ag. In the valence approximation the charge on the Ag atom equals +0.85 [6.31], and the orbital charge transfers to  $C_2H_4$  is  $\Delta q_{(\sigma+\pi)} = -17$  and  $\Delta q_{(\sigma^*+\pi^*)} = 0.02$ , respectively.

In the semiempirical CNDO calculations [6.32] the charge transfers are larger and the charge on Ag is +0.71, while the C=C bond order is reduced by coordination from 0.96 to 0.88. Approximately half of the  $Ag^+ - C_2H_4$  binding ( $\sim 15$  kcal/mol [6.30]) is due to electrostatic polarization of the C=C bond by the  $Ag^+$  ion. The separation of this component of bonding is partly conventional, though.

The calculations of  $PdC_2H_4$ ,  $Pd(C_2H_4)_3$ , and  $Pd(C_2H_4)_4$  carried out by the same method as  $Ag^+ - C_2H_4$ , yield similar results [6.31]. In the case of  $Pd - C_2H_4$ ,  $R(Pd - C) = 2.2 \text{ \AA}$ ,  $R(C = C) = 1.37 \text{ \AA}$ , and with the planar  $C_2H_4$  molecule coordinated to Pd in the same way as in  $Ag^+ - C_2H_4$ , the bonding energy (62.8 kcal/mol) is much larger than in the latter case despite the absence of pure electrostatic polarization. The bonding is more covalent and multiorbital with orbital charge transfers (see Fig. 6.18)  $\Delta q_{(\sigma+\pi)} = -0.14$ ,  $\Delta q_{(\sigma^*+\pi^*)} = 0.33$ . The total transfer to  $C_2H_4$   $\Delta q = 0.19$  is positive, in contrast to the  $Ag^+ - C_2H_4$  case, where  $\Delta q = -0.15$ . With the increase in the number of ligands  $n$  in the complex  $Pd(C_2H_4)_n$ , the bonding energy per ligand  $\Delta E_n$  decreases (in kcal/mol):  $\Delta E_1 = 62.8$ ,  $\Delta E_3 = 53.6$ , and  $\Delta E_4 = 45.5$ . With electronegative substituents in ethylene (as in  $C_2F_4$ ), the energy of its antibonding MO lowers and the corresponding metal-ligand charge transfer increases.

### EXAMPLE 6.9

#### Ethylene Bonding in $PtCl_3(C_2H_4)^-$ and $PdCl_3(C_2H_4)^-$

More complete calculations of ethylene bonding were carried out for the Zeise salt  $PtCl_3(C_2H_4)^-$  (I) and its Pd analog  $PdCl_3(C_2H_4)^-$  (II) [6.33] using nonempirical methods with extended basis sets and relativistic corrections. Figures 6.19 and 6.20 illustrate the results for these two systems in different geometries, including the upright and planar

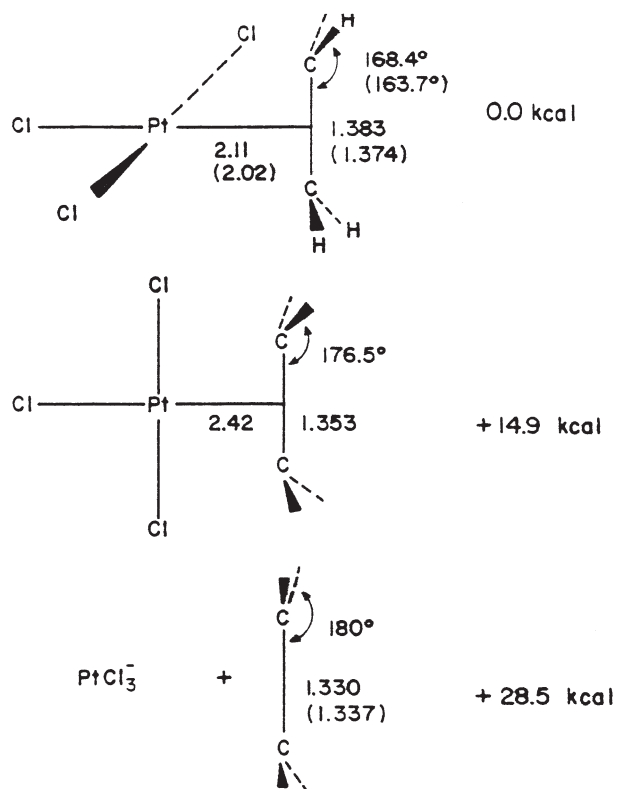


**FIGURE 6.19.** Calculated geometries for  $\text{PtCl}_3(\text{C}_2\text{H}_4)^-$  for the upright and planar forms of coordinated ethylene along with uncoordinated ethylene (experimental values are indicated in parentheses). (From Hay [6.33].)

coordination (when the  $\text{C}=\text{C}$  bond is perpendicular to the plane and in the plane of the complex, respectively) and the dissociated state. The experimental data for I obtained by neutron diffraction are in good agreement with these calculations. The  $\text{Pt}-\text{C}_2\text{H}_4$  distance  $R = 2.06 \text{ \AA}$  (calculated with a basis set that includes the  $3d$  function of the carbon atom) is close to the experimental value  $R = 2.02 \text{ \AA}$ .

The planar configuration in Zeise salt I is by 15 kcal/mol higher in energy than the upright one; the bonding energy for the latter is 28.5 kcal/mol. It follows that internal rotation of the ethylene molecule is possible with a rotation barrier of 15 kcal/mol. Such barriers are observed experimentally for related complexes in the region of 10–16 kcal/mol [6.34]. Comparison of these results with those obtained by the extended Hückel method [6.34] shows that the latter correctly predicts that the upright coordination is more stable, but it overestimates the barrier height: 35 kcal/mol in the case when the



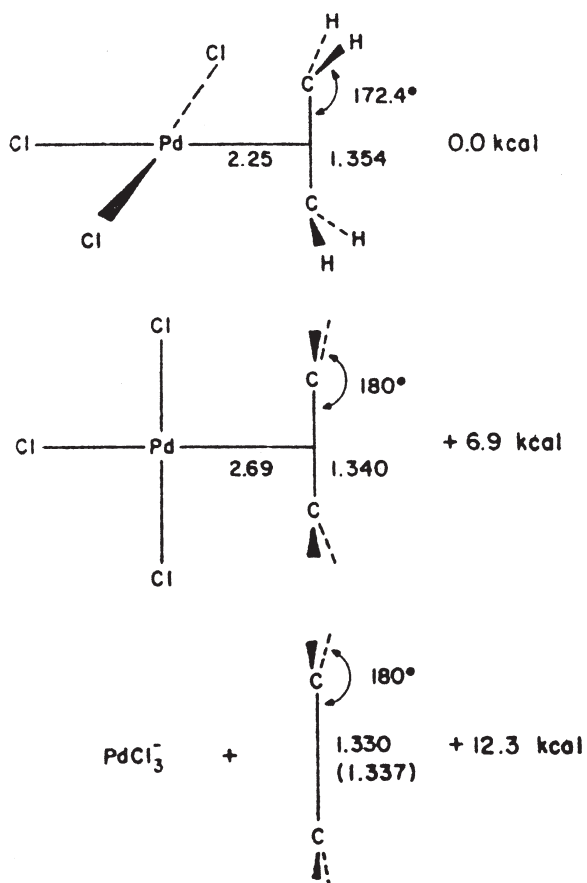


**FIGURE 6.20.** Calculated geometries for  $\text{PdCl}_3(\text{C}_2\text{H}_4)^-$  for the upright and planar forms of coordinated ethylene along with uncoordinated ethylene. (From Hay [6.33].)

geometry of the  $\text{PtCl}_3$  group remains in the planar configuration, and 22 kcal/mol if two Cl atoms deviate from the initial in-plane position by seven degrees ( $7^\circ$ ).

Note that in the calculations with geometry optimization the possible out-of-plane displacements of the Cl atoms is not taken into account: a stronger effect that allows for relaxation of the stressed planar configuration is achieved by increasing the  $\text{Pt}-\text{C}_2\text{H}_4$  distance from  $R = 2.11$  Å to  $R = 2.42$  Å (for the latter distance the out-of-plane displacements of the Cl atoms are no longer important). Albright et al. [6.35] consider other cases of coordination of olefins to metals in detail and discuss the possibility of internal rotations of olefins. The main contribution to the barrier of rotations is due to the steric repulsion between the  $\text{CH}_2$

groups of the olefins and the chlorine atoms in the planar configuration. This result is confirmed by more accurate calculations [6.34].

For the  $\text{PdCl}_3(\text{C}_2\text{H}_4)^-$  complex the bonding energy of the ethylene molecule is 12.3 kcal/mol, and the energy barrier of internal rotations (6.9 kcal/mol) is much smaller than in the Zeise salt [6.33]. The deformation of the complex due to the ethylene coordination is also smaller. The author [6.33] believes that this result explains why the Pd complex is more active in olefin oxidation; although the  $\text{C}=\text{C}$  bond is more activated in the Pt complex, the rather strong  $\text{Pt}-\text{C}_2\text{H}_4$  bond decelerates the reaction at the stage of cleavage of the oxidation product.

The orbital charge transfers  $\Delta q_\sigma$  and  $\Delta q_\pi$  are given in Table 6.10, in which the values obtained by means of the more accurate Noell method [Section 5.2, Eq. (5.22)] are also shown. At first sight the differences in the orbital charge transfers calculated by these two methods are not very large, but the resulting charges on the metal are much different. Indeed, in the Zeise salt the atomic charge on the Pt atom after Mulliken is  $q(\text{Pt}) = 0.02$ , whereas after Noell  $q'(\text{Pt}) = 1.40$  [similarly, for the Pd complex  $q(\text{Pd}) = 0.20$  and  $q'(\text{Pd}) = 1.27$ ].

**TABLE 6.10. Orbital Charge Transfers  $\Delta q_\sigma$  and  $\Delta q_\pi$  to Ethylene in  $\text{PtCl}_3(\text{C}_2\text{H}_4)^-$  and  $\text{PdCl}_3(\text{C}_2\text{H}_4)^-$  Calculated by Mulliken Populations Analysis<sup>a</sup>**

	$\text{PtCl}_3(\text{C}_2\text{H}_4)^-$	$\text{PdCl}_3(\text{C}_2\text{H}_4)^-$
$\Delta q_\sigma$	-0.37 (-0.24)	-0.18 (-0.12)
$\Delta q_\pi$	0.23 (0.22)	0.07 (0.07)

Source: From Hay [6.33].

<sup>a</sup>The modified values after Noell are given in parentheses.

Ethylene coordination is also discussed in Section 11.3 as the main feature in olefin insertion reactions and polymerization with Ziegler–Natta catalysts.

### Metal–Metal Bonds and Bridging Ligands

The metal–metal bond may be regarded formally as ligand bonding in which the ligand is a metal. However, in fact the metal–metal bond is very different from that of the usual ligands [6.36–6.46]. There may be several metal ligands in the case of multicenter (polynuclear) cluster compounds.

Consider the  $\text{M}-\text{M}$  bond, where  $\text{M}$  is a transition metal that can participate in the bonding with its  $s$ ,  $p$ , and  $d$  orbitals. One distinct feature of the  $d$  states is that they can produce  $\delta$  bonds (Section 2.1, Fig. 2.7) in addition to  $\sigma$  and  $\pi$

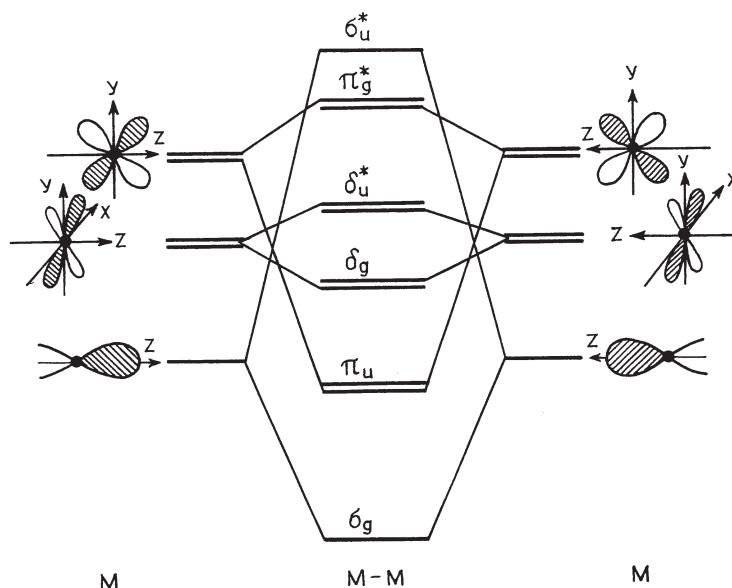


**FIGURE 6.21.** Illustration to the  $\sigma$ ,  $\pi$ , and  $\delta$  MOs formed by the  $d$  orbitals in the M—M bond: bonding  $\sigma$  and antibonding  $\sigma^*$  (produced by the two  $d_{z^2}$  AOs of the two atoms), twofold degenerate  $\pi$  and  $\pi^*$  (formed by the two  $d_{xz}$  and two  $d_{yz}$  AOs, respectively), and twofold degenerate  $\delta$  and  $\delta^*$  (emerging from the overlap of, respectively, the two  $d_{xy}$  and two  $d_{x^2-y^2}$  AOs).

bonds. Figure 6.21 illustrates the main types of MOs that are built up from the  $d$  AOs of the transition metal M. The  $\sigma$  MO can be formed by  $s$ ,  $p_\sigma$ , and  $d_{z^2}$  AOs, and hence there may be three AOs of  $\sigma$  type (or even more when M has ligands) which produce three bonding and three antibonding MOs instead of one  $\sigma$  and one  $\sigma^*$  as shown in Fig. 6.21. The  $\pi$  bonds are formed by the doubly degenerate  $d_\pi$  ( $d_{xz}$ ,  $d_{yz}$ ) AOs with possible admixture of  $p_\pi$ . The  $\delta$  bond is also doubly degenerate since it is produced by the two degenerate  $d_\delta$  AOs,  $d_{xy}$  and  $d_{x^2-y^2}$ . The qualitative scheme in Fig. 6.21 is based on the well-known fact that the  $\sigma$  overlap is the strongest possible, producing the largest energy splitting between the bonding and antibonding MOs; the  $\pi$  overlap is smaller, while the  $\delta$  overlap is the smallest.

As follows from this MO scheme, there are rich possibilities for multiorbital bonding in M—M depending on the number of electrons  $n$  that occupy the MOs. With one or two electrons, we have a monoorbital single bond. Up to six electrons give one  $\sigma$  and two  $\pi$  bonds (a diorbital triple bond). With more electrons we get triorbital fourfold and fivefold bonds. The last two possibilities are a special feature of M—M bonds that is unknown for other bonds [6.36]. For larger  $n$  the number of uncompensated bonding MOs decreases, provided that the additional  $\sigma$  orbitals from the  $s$  and  $p$  AOs are high in energy and not occupied (see below). Example 6.10 illustrates the M—M bonding in specific systems.

**EXAMPLE 6.10****Multiple Metal–Metal Bonds in  $[\text{Re}_2\text{Cl}_8]^{2-}$  and  $[\text{Mo}_2\text{Cl}_8]^{4-}$** 

The first identification of a fourfold bond was obtained in 1964 for the Re—Re bond in the  $[\text{Re}_2\text{Cl}_8]^{2-}$  anion in different compounds (e.g., in  $\text{K}_2\text{Re}_2\text{Cl}_8 \cdot 2\text{H}_2\text{O}$ ) [6.36, 6.40]). This anionic complex is diamagnetic and has the structure shown in Fig. 6.22 [6.41]. Its important feature is that the eight chlorine atoms form a square prism (eclipsed structure), not an antiprism (staggered structure) as expected from the repulsion of the negative  $\text{Cl}^-$  ions. But the most significant result of these studies is that the interatomic Re—Re distance in this complex is very short, about 2.22 Å, shorter than in the metallic state.

The explanation for these data was given qualitatively [6.40] on the basis of the MO scheme of Re—Re bonding shown in Fig. 6.21. The eight electrons that remain after the formation of the eight  $\text{Cl}^-$  ions in the  $[\text{Re}_2\text{Cl}_8]^{2-}$  system occupy one  $\sigma$ , two  $\pi$ , and one  $\delta$  bonding orbitals, resulting in the configuration  $\sigma^2\pi^4\delta^2$  with a fourfold bond. The  $\delta$  bond between the two  $d_{xy}$  AOs of the Re atoms also explains the origin of the eclipsed structure of the  $[\text{Re}_2\text{Cl}_8]^{2-}$  anion; in the alternative staggered structure, formation of the  $\delta$  bond is impossible (the  $d_{x^2-y^2}$  orbitals are engaged in the Re—Cl bonds), and it can be assumed that the energy gain in this  $\delta$  bond is larger than the increase in  $\text{Cl}^-$ — $\text{Cl}^-$  repulsions in the eclipsed structure.

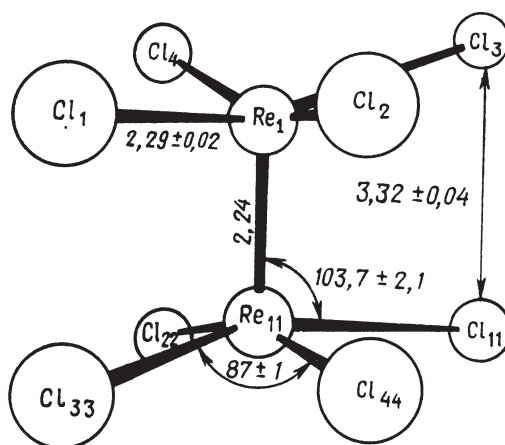


**FIGURE 6.22.** Atomic structure of the  $[\text{Re}_2\text{Cl}_8]^{2-}$  ion. (From Kuznetsov and Koz'min [6.41].)

This qualitative explanation of the Re—Re fourfold bond was confirmed afterward by semiempirical and nonempirical calculations. The first DFT- $X_\alpha$  computations (Section 5.4) were carried out for  $[\text{Mo}_2\text{Cl}_8]^{4-}$  [6.42] and  $[\text{Re}_2\text{Cl}_8]^{2-}$  [6.43]. The presence of other AOs of the metal and ligands may complicate the pure  $d$ -orbital M—M MO energy-level scheme of Fig. 6.21. In particular, the additional  $\sigma$  and  $\pi$  MOs formed by the (next to  $d$ )  $s$  and  $p$  orbitals of the metal with the ligands and in the M—M bond may occur in between the  $d$ — $d$  levels. However, the calculations show that in the oxidation states under consideration, +2 and +3, the additional electronic states are too

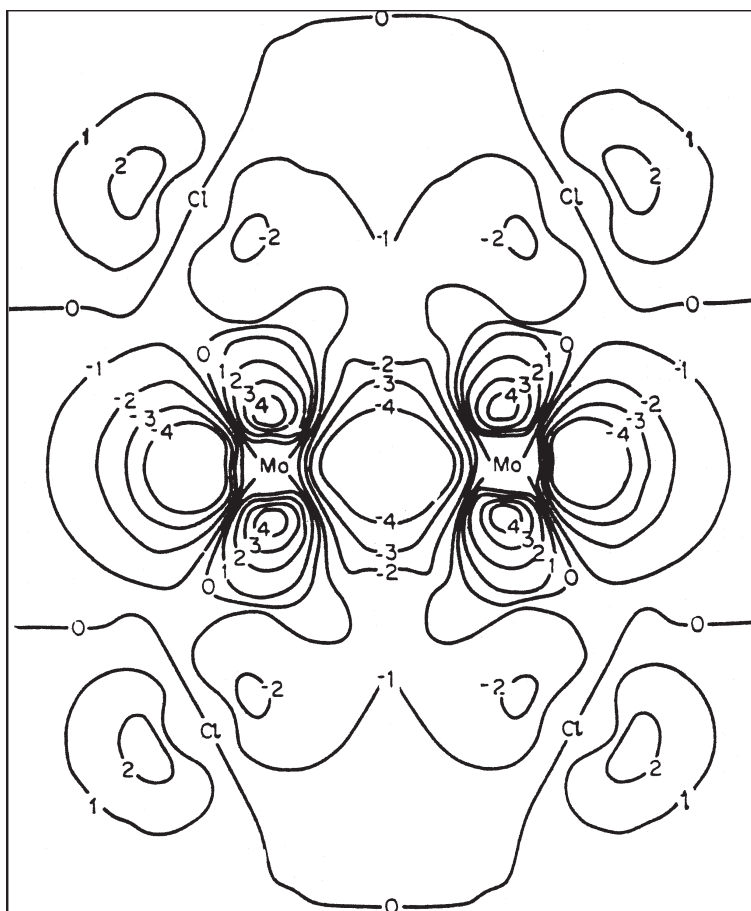


**FIGURE 6.23.** Contour diagram of the wavefunction of the Mo—Mo  $\sigma$ -bonding MO of  $[\text{Mo}_2\text{Cl}_8]^{4-}$ ; the cross section including the two Mo and four Cl atoms is shown. (After Norman and Kolari [6.42].)

high in energy and do not interfere with the levels of the scheme in Fig. 6.21.

Visual presentations of the corresponding wavefunctions by the contour diagrams in Figs. 6.23, 6.24, and 6.25 for  $\sigma$ ,  $\pi$ , and  $\delta$  MOs, respectively, illustrate their M—M bonding nature; the calculations [6.42, 6.43] confirm the qualitative electronic configuration  $\sigma^2\pi^4\delta^2$  with a fourfold bond M—M in  $[\text{Mo}_2\text{Cl}_8]^{4-}$  and  $[\text{Re}_2\text{Cl}_8]^{-2}$ . A qualitatively similar result was obtained [6.44] in the MO LCAO

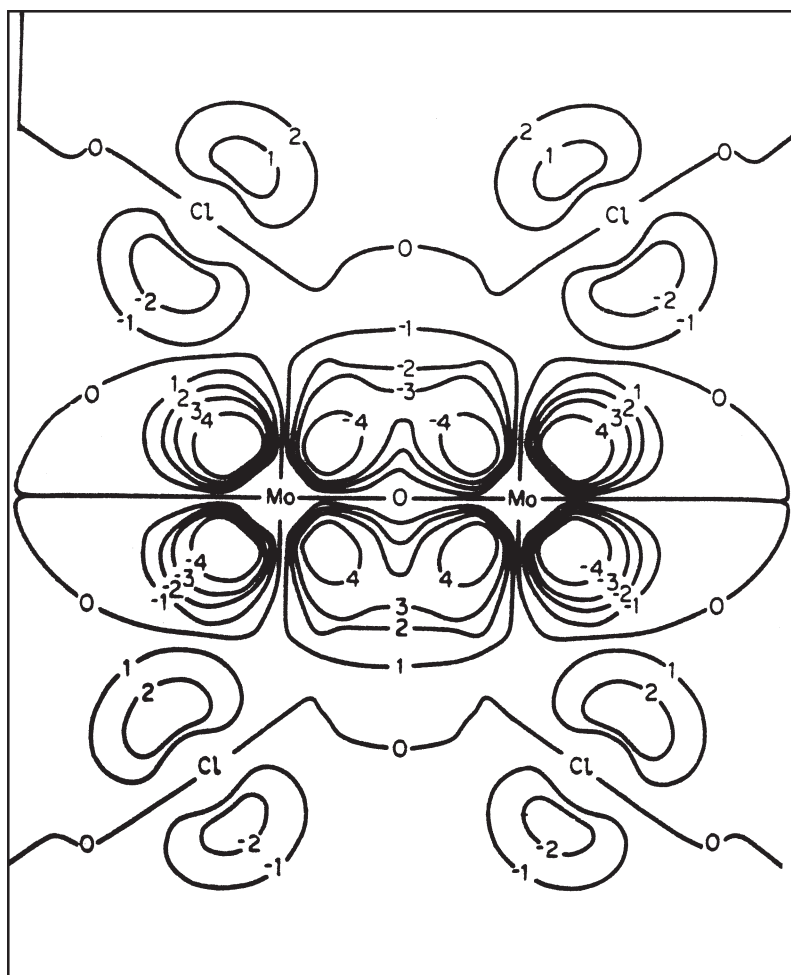


**FIGURE 6.24.** Contour diagram of the wavefunction of the Mo—Mo  $\pi$ -bonding MO in  $[\text{Mo}_2\text{Cl}_8]^{4-}$  shown in the same cross section as in Fig. 6.23. (From Norman and Kolari [6.42].)

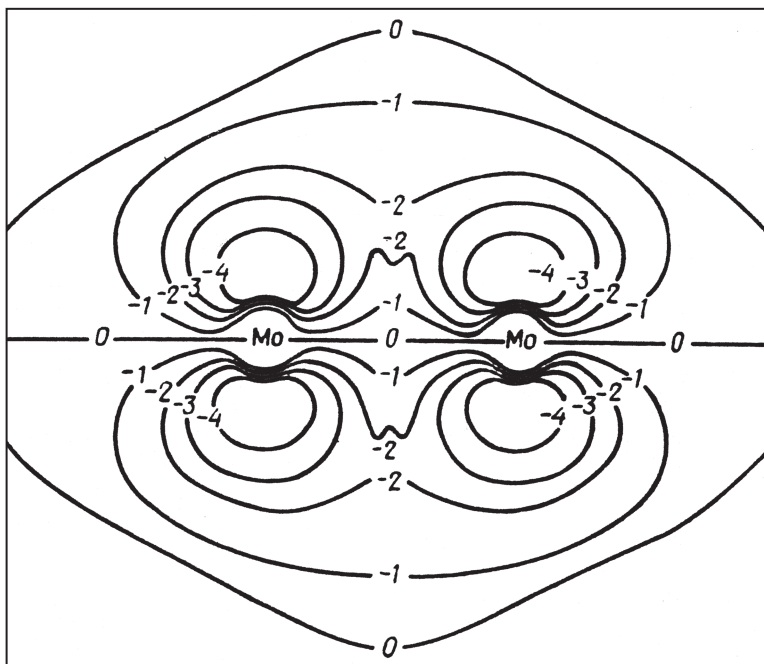


**FIGURE 6.25.** Contour diagram of the wavefunction of the Mo—Mo  $\delta$ -bonding MO of  $[\text{Mo}_2\text{Cl}_8]^{4-}$ ; the cross section containing the two Mo atoms and the positive lobes of their  $d_{xy}$  AO (i.e., bisecting two opposite Cl—Mo—Cl right angles in each of the  $\text{MoCl}_4$  groups) is shown. (After Norman and Kolari [6.42].)

Hartree–Fock (HF) approximation, but the DFT approach gives better results (lower energies) because it includes a part of the correlation energy (Section 5.4). The latter can also be factored into the HF approximation by adding CI (Section 5.3) with higher-energy configurations  $\sigma^2\pi^4\sigma^{*2}$ ,  $\sigma^2\pi^2\delta^2\pi^{*2}$ , ...,  $\sigma^{*2}\pi^4\delta^{*2}$ . Without CI the results may yield erroneous conclusions. For instance, a HF single-determinant calculation gives no Cr—Cr bonding in  $\text{Cr}_2(\text{O}_2\text{CH})_4(\text{H}_2\text{O})_2$  (electronic configuration  $\sigma^2\delta^2\delta^{*2}\sigma^{*2}$  with no uncompensated bonding MOs), whereas CI calculations result in the correct fourfold bonding with an interatomic distance of 2.27 Å [6.45].

Many other M—M bonds in coordination systems were studied and different bond multiplicities revealed, including the fourfold bond W—W in  $[\text{W}_2(\text{CH}_3)_8]^{4-}$ , the 3.5-fold bond Tc—Tc in  $[\text{Tc}_2\text{Cl}_8]^{3-}$  with the configuration  $\sigma^2\pi^4\delta^2\delta^*$ , and Mo—Mo in  $[\text{Mo}_2(\text{SO}_4)_4]^{3-}$  with the configuration  $\sigma^2\pi^4\delta$ , the

**TABLE 6.11. Calculated Electronic Structure of Metal–Metal Bonds in Dimer  $M_2$  Systems<sup>a</sup>**

$M_2$	Ground State	Electronic Configuration	Bond Order	$R_0$ (Å)	Method of Calculation
Sc <sub>2</sub>	$^5\Sigma^-$	$s\sigma_g^2 d\sigma_g^1 \pi_u^2 s\sigma_u^1$	2	2.57	SCF CI
	$^1\Sigma_g^+$	$s\sigma_g^2 d\sigma_g^2 s\sigma_u^2$	1	3.05	SCF
Ti <sub>2</sub>	$^1\Sigma_g$	$\sigma_g^2 d\sigma_g^2 \pi_u^4$	4	1.87	SCF
V <sub>2</sub>	$^1\Sigma_g$	$s\sigma_g^2 d\sigma_g^2 s\sigma_u^2 \pi_u^4$	3	1.96	SCF
		$\pi_u^4 d\sigma_g^2 s\sigma_g^2 \delta_g^2$	5	1.78	$X_\alpha$ -DV
Mn <sub>2</sub>	$^1\Sigma_g$	$d\sigma_g^2 \pi_u^4 \delta_g^4 s\sigma_g^2 \delta_u^2$	5	1.69	$X_\alpha$ -DV
		$d\sigma_g^2 s\sigma_g^2 s\sigma_u^2 \pi_u^4 \delta_u^4$	5	1.52	SCF
Fe <sub>2</sub>	$^7\Delta_u$	$d\sigma_g^{1.57} \pi_u^{3.06} \delta_g^{2.53} \delta_u^{2.47} \times$ $d\sigma_u^{1.49} \pi_g^{2.89} s\sigma_g^2$	1.3	2.40	SCF CI
Co <sub>2</sub>	$^5\Sigma_g^+$	$d\sigma_g^2 \pi_u^{3.09} \delta_g^{3.02} \delta_u^{2.98} \times$ $\pi_g^{2.91} d\sigma_u^2 s\sigma_g^{1.94} s\sigma_u^{0.06}$	1.1	2.40	SCF CI
		$d\sigma_g^2 \pi_u^4 \delta_g^4 s\sigma_g^2 s\sigma_u^1 \pi_g^3$ $1\sigma_g^2 \sigma_u^2 2\sigma_g^2 \pi_u^4 \pi_g^4 \delta_g^3 \delta_u^3$	2	2.16	$X_\alpha$ -SW
Ni <sub>2</sub>	$^3\Pi_u$			2.26	SCF CI
Nb <sub>2</sub>	$^1\Sigma_g$	$\sigma_g^2 \pi_u^4 \delta_g^4$	5	1.97	$X_\alpha$ -DV
Tc <sub>2</sub>	—	$d\sigma_g^2 \pi_u^4 \delta_g^4 s\sigma_g^2 \delta_u^2$	5	1.92	$X_\alpha$ -DV
Ru <sub>2</sub>	$^1\Sigma_g$	$d\sigma_g^2 \pi_u^4 \delta_g^4 \delta_u^4 s\sigma_g^2$	4	1.94	$X_\alpha$ -DV
	$^7\Delta_u$	$d\sigma_g^{1.67} \pi_u^{3.31} \delta_g^{2.73} \delta_u^{2.42} \pi_g^{2.60} \times$ $d\sigma_u^{1.27} s\sigma_g^{1.94} s\sigma_u^{0.06}$	1.7	2.71	SCF CI

Source: From Kl'agina and Gutsev [6.46].

<sup>a</sup>Notations  $s\sigma_g, d\sigma_g, \pi_u, \delta_g, \dots$  represent the corresponding  $\sigma, \pi, \delta, \dots$ , MOs formed by  $s, d, \dots$ , AOs;  $u$  and  $g$  orbitals of the same type approximately compensate each other

triple bond Re—Re in  $\text{Re}_2\text{Cl}_5(\text{dth})_2$  and  $\text{Re}_2\text{Cl}_4(\text{PR}_4)_4$  ( $\sigma^2 \pi^4 \delta^2 \delta^{*2}$ ), the shortest fourfold bond Cr—Cr in  $\text{Cr}_2(\text{C}_3\text{H}_4)_4$ , and others [6.36, 6.46].

For the Cr—Cr bond with a very short bond length,  $R = 1.68$  Å in  $\text{Cr}_2(\text{C}_3\text{H}_4)_4$  (cf.  $R = 2.55$  Å in the metallic state) and apparently the shortest metal–metal bond Mo—Mo with  $R = 1.93$  Å (metallic  $R = 2.76$  Å), it has been assumed [6.46] that the bond is sixfold; that is, in addition to the triorbital fivefold (one  $\sigma$ , two  $\pi$ , and two  $\delta$ ) bond, a  $\sigma$  bond from the  $ns$  orbitals occurs. The DFT- $X_\alpha$  calculations [6.47, 6.48] apparently confirm this point of view.

Table 6.11 lists a series of electronic structure calculations of metal–metal bonds in  $M_2$  systems which indicate the ground state, electron configuration, bond order, bond length  $R_0$ , and the calculation method [6.46].

In some cases the calculations disprove the assumptions made on a qualitative basis. For example, the Rh—Rh bond in  $\text{Rh}_2(\text{OCCH}_3)_4(\text{H}_2\text{O})_2$  was found to be shorter ( $\sim 2.39$  Å) than in  $\text{Rh}_2(\text{dmg})_4(\text{PPh})_2$  ( $\sim 2.94$  Å), and this led to the



assumption [6.49] that in the acetate dimer the Rh—Rh bond is a triple bond with the configuration  $\sigma^2\pi^4\delta^2\sigma_n^2\sigma_n'^2\delta^{*2}$ , where  $\sigma_n$  and  $\sigma_n'$  are some nonbonding orbitals comprising essentially 5s and 5p<sub>σ</sub> AOs of Rh. Both semiempirical [6.50] and DFT- $X_\alpha$  [6.51] (see also Ref. 6.52) calculations show that in these and some other similar  $d^7-d^7$  Rh dimers the 14 electrons produce the electronic configuration  $\sigma^2\pi^4\delta^2\pi^*4\delta^{*2}$  leaving only one uncompensated orbital  $\sigma$ . Hence the Rh—Rh bond is monoorbital (single), and the  $\sigma_n, \sigma_n'$ -type orbitals are not active.

An important problem related to metal–metal bonds is the role of *bridging and semibridging ligands*. In the presence of ligands that occupy a position close to both metals (or to several metals in polynuclear cluster compounds), a question arises as to whether there is direct metal–metal bonding, or whether it is realized completely through the nearest-neighbor ligands, which thus serve as bonding bridges. An example of this kind is briefly discussed in Section 8.4 for the dimeric copper acetate hydrate and other copper carboxylates (Examples 8.11 and 8.12). The semiempirical IEH (SCCC) MO LCAO calculations (Section 5.5) show [6.53] that in these cases Cu—Cu bonding is realized via the carboxylate bridges, and there is no direct Cu—Cu bonding.

More accurate calculations of the electronic structure of dimers were carried out more recently to reveal the role of bridging ligands. An interesting example is provided by the  $\text{Co}_2(\text{CO})_8$  complex. The Co—Co interatomic distance in this complex, although not very short, allows one to propose that there is a direct Co—Co single bond, and this assumption is also supported by the *18-electron rule* [6.54] (a closed shell with 18 electrons, similar to [Ar] configuration, is assumed to be most stable; see the inert-gas rule in Section 9.1). If this is true, the bond can be either linear, or bent. The latter possibility is enhanced by the symmetry of the system. Figure 6.26 shows these two possibilities together with a third one when there is no direct M—M bond.

Calculations in the IEH approximation [6.55] show that there is no direct Co—Co bond, whereas the CNDO approach yields such a bond [6.56]. This controversy stimulated more accurate ab initio SCF computations [6.57]. A detailed analysis of the deformation density (Section 8.6) with respect to two  $\text{Co}(\text{CO})_3$  fragments and two CO molecules and additional topological investigation of the electronic density in the region between the Co atoms shows that there is no direct Co—Co bond in this compound. For related calculations of  $\text{Fe}_3(\text{CO})_{12}$  and  $\text{MoCr}(\text{O}_2\text{CH})_4$ , see the articles by Rosa and Baerends and Wiest et al. [6.58].

To conclude this subsection, we briefly comment on *semibridging ligands*. This term is generally used to denote a ligand (often a carbonyl, thiocarbonyl) that is asymmetrically coordinated to two metal centers between which there is a direct bonding. Figure 6.27 illustrates this possibility for the CO molecule as a semibridging ligand between two metals (usually M and M' are different). The question under discussion in a series of papers concerns the nature of the bonding to the secondary metal M'. The position of the CO molecule with respect to M' enables its four bonding electrons on the  $\pi$  orbitals to be  $\sigma$  donors to M' (see Fig. 6.9). On the other hand, its antibonding  $\pi^*$  MO can serve as a good acceptor

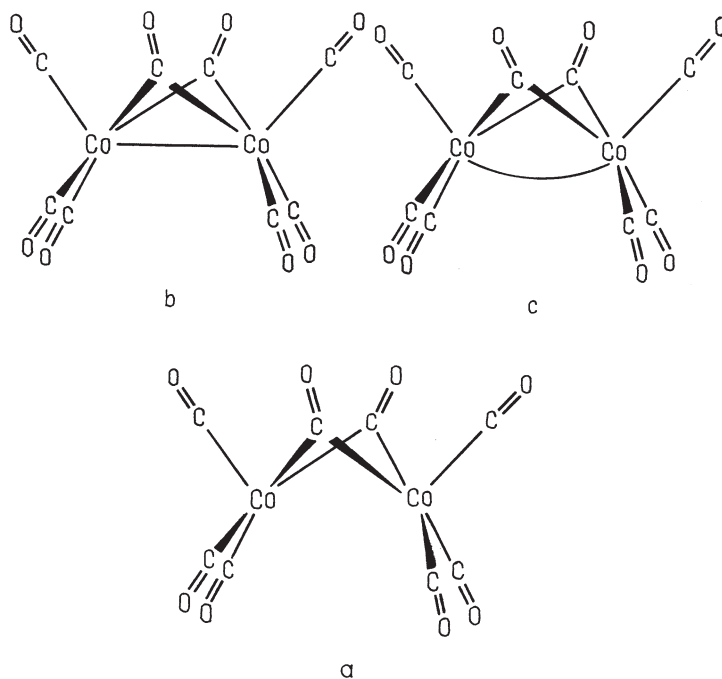


**FIGURE 6.26.** Structure of the  $\text{Co}_2\text{CO}_8$  complex without (a) and with a linear (b) and bent (c) direct Co—Co bond.

of electrons. Hence there are two possibilities of charge transfer from CO to  $M'$  and from  $M'$  to CO as shown in Fig. 6.27.

It is clear that the actual charge transfers depend essentially on the nature of the metals  $M'$ ,  $M$ , and the other ligands coordinated to these metals. For instance, if  $M'$  is a good  $\sigma$  acceptor and  $\pi$  donor, significant orbital charge transfer to the antibonding  $\pi^*$  MO of CO can be expected, as long as the metal  $M$  does not occupy this  $\pi^*$  MO in the bonding with CO; this, in turn, depends on the nature of  $M$  and its other ligands. Obviously, the problem should be solved by reliable electronic structure calculations.

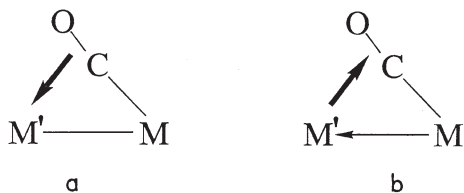


**FIGURE 6.27.** Semibridging CO ligand with indication of two possible situations of charge transfer: (a) from and (b) to the ligand.

Concerning carbonyl complexes, three different types of semibridging ligand bonding can be distinguished: (1) the secondary metal atom  $M'$  is an early transition metal (I), (2)  $M'$  is an atom from the middle of the series (II), and (3) it is a late transition or posttransition element (III). It was shown in a series of electronic structure calculations carried out for several systems of types II and III that in these cases the CO ligand is a  $\pi$  acceptor (Fig. 6.27b).

For example, for the dimer  $(\text{NH}_3)_2\text{CuCo}(\text{CO})_4$  the electronic structure calculations [6.59] in the Fenske–Hall approximation (Section 5.4) performed for the system as a whole and separately for the two fragments,  $(\text{H}_3\text{N})_2\text{Cu}$  and  $\text{Co}(\text{CO})_4$ , show explicitly that in the system  $(\text{H}_3\text{N})\text{Cu}—\text{Co}(\text{CO})_4$  one of the CO ligands is semibridging and accepts an electronic charge transfer of  $\sim 0.14$  to its antibonding  $\pi^*$  MO from the copper  $d_{xz}$  orbital.

In early transition elements  $M'$  (complexes of group I) the  $d_{xz}$ -type orbitals are unoccupied and cannot be electron donors to CO. Detailed calculations of  $\text{CpCo}(\mu\text{-CO})_2\text{ZrCp}_2$  ( $\text{Cp} = \eta^5\text{-C}_5\text{H}_5$ ) in the same Fenske–Hall approximation [6.58] show that in the interaction of the two groups,  $\text{Cp}_2\text{Zr}$  and  $\text{Co}(\text{CO})_2\text{Cp}$ , the semibridging CO ligand is a four-electron  $\pi$  donor to the electron-deficient Zr atom.

#### 6.4. ENERGIES, GEOMETRIES, AND CHARGE DISTRIBUTIONS

This section continues the discussion of electronic structure and bonding in coordination compounds by revealing some further features closely related to those of ligand bonding: total and ionization energies, charge distributions, and geometries of coordination.

##### Ionization Energies

As noted in Section 6.2, one should be careful when relating the one-electron MO energies to observable spectroscopic properties (ionization potentials, optical, photoelectron, X-ray, etc., spectra; Sections 8.1–8.3). In particular, for the ionization potentials  $I$  the Koopmans theorem (mentioned earlier multiple times) states that the energy of ionization of an electron from a given electronic state equals the energy of the corresponding MO taken with opposite sign (Sections 2.2 and 6.2). This means that the order and position of the consequent  $I$  values or the positions of the peaks of photoelectron spectra, observed experimentally, should correspond to the consequence of the MO energy-level positions from top to bottom. This correspondence takes place indeed in some cases, for example, in  $\text{Ni}(\text{CO})_4$  [6.60, 6.61].

However, in many cases, for instance, in organometallic compounds and complex anions, the Koopmans theorem does not hold. As emphasized in Sections 2.2 and 6.2, the Koopmans approach does not account for the fact that when one removes the electron from a given one-electron state, all the other electronic states change; the electrons relax to new self-consistent states in which the

interelectron repulsion is reduced. This relaxation, which may be small or even negligible when the state to be ionized is well localized, becomes very important in the case of coordination compounds where the ionization takes place from MOs containing  $d$  states with essentially delocalized charge distribution.

For instance, in the case of ferrocene  $\text{Fe}(\text{Cp})_2$  the calculations yield the following order of MO energy-level positions [6.62]:

$$\begin{aligned} a_{1g}(3d) < e_{2g}(\sigma - \text{Cp}) \sim a_{2u}(\pi - \text{Cp}) \sim e_{2u}(\sigma - \text{Cp}) \\ < e_{2g}(3d) < e_{1g}(\pi - \text{Cp}) \sim e_{1u}(\pi - \text{Cp}) \end{aligned} \quad (6.3)$$

The order of ionization potentials  $I$  determined experimentally from the photoelectron spectra is different from sequence (6.3) [6.63]. If one negates the Koopmans theorem, then the  $I$  values should be calculated as a difference between the energies of the ground state of the  $\text{Fe}(\text{Cp})_2$  molecule and the final state after ionization  $\text{Fe}(\text{Cp})_2^+$  (both calculated with full account for interelectron interactions). The calculations carried out in this way [6.62] give another consequence of ionization potentials  $I$ :

$$I(e_{2g}) < I(a_{1g}) < I(e_{1u}) < I(e_{1g}) \quad (6.4)$$

in agreement with the experimental data.

Similarly, for complex anions the HOMO energy levels are often of ligand type ( $p$  levels of halogens,  $\pi$  levels of CN, etc.), whereas the first ionization potential calculated as the energy difference between the initial complex and its ionized state corresponds to elimination of the  $3d$  electron of the metal in accordance with the experimental data. In *ab initio* calculations the difference between the self-consistent (SCF) energies of two systems, initial and ionized, is often denoted by  $\Delta\text{SCF}$ .

Another and sometimes no less important reason for the observed deviations from the Koopmans theorem lies in the difference in electron correlation energy (Section 5.3) in these two states. A sufficiently full calculation of ionization energies in photoelectron (X-ray) spectra must include the correlation energies (e.g., by means of CI) in both states, before and after ionization; the corresponding energy difference is then denoted by  $\Delta\text{SCF-CI}$ .

For coordination compounds, as distinct from more simple systems, such a full calculation of the  $\Delta\text{SCF-CI}$  values may be difficult. A modified Green function method—two-particle-hole Tamm–Dancoff approximation (2phTDA) [6.65] has been suggested for these problems and proved to be more convenient and less computer-time-consuming than CI. The results are illustrated by calculations for a series of coordination systems:  $\text{Ni}(\text{C}_3\text{H}_5)_2$ ,  $\text{Ni}(\text{CN})_4^{2-}$ ,  $\text{Co}(\text{CN})_6^{3-}$ ,  $\text{Fe}(\text{CN})_6^{4-}$  [6.64, 6.66]. Example 6.11 illustrates in more detail the results obtained for  $\text{Ni}(\text{C}_3\text{H}_5)_2$ .

**EXAMPLE 6.11*****Ab Initio Calculations of Ni(C<sub>3</sub>H<sub>5</sub>)<sub>2</sub>***

Ni(C<sub>3</sub>H<sub>5</sub>)<sub>2</sub> was one of the first coordination systems calculated ab initio [6.67, 6.68]. Rohmer and Veillard [6.68] illustrated explicitly the need to account for the relaxation of electrons by ionization. Then it occurred to them that the calculated SCF MO energies are also not adequate and give an incorrect order of ionization states. In Table 6.12 the ionization energies for the valence states of this system obtained by ab initio calculations after Koopmans and by  $\Delta$ SCF,  $\Delta$ SCF-CI, and 2eh-DTA methods are listed [6.64, 6.66]. The experimental data were taken from the photoelectron spectra [6.69] (Section 8.3). The notations of the MOs are given after the irreducible representations of the symmetry group  $D_{2h}$ .

The HOMO  $7a_u$  is a pure ligand  $\pi$  MO originating from its  $a_2 \pi$  MO. The next one,  $6b_g$ , is a mixing of an appropriate combination of this  $a_2$  MO with the  $d_{xz}$  orbitals of the metal and gives the largest contribution to the bonding. The  $11b_u$  MO is a nonbonding, antisymmetric mixing of the ligand  $\pi$  MOs of  $b_1$  type. Their symmetric combination overlaps with the Ni  $d_{xy}$  orbital, yielding the  $9a_g$  and  $13a_g$  MOs. The  $10a_g$ ,  $5b_g$ , and  $11a_g$  MOs contain, respectively, the metallic  $3d_{z^2}$ ,  $3d_{xy}$ , and  $3d_{x^2-y^2}$  orbitals and are mainly nonbonding. The remaining valence MOs are related to the  $\sigma$  core of the ligands.

As shown by the numerical data of the calculations with CI, the contribution of the basic Hartree–Fock (HF) configuration to the wavefunction of the ground state is 83%, which is significantly less than for compounds without transition metals (where it is greater than 95%). In other words, CI is more important in calculations of the electronic structure of transition metal compounds than for organic compounds. The largest contribution to the CI comes from excited states formed by one-electron and two-electron excitations  $6b_g \rightarrow 7b_g$  and  $6b_g^2 \rightarrow 7b_g^2$ , where  $7b_g$  is the antibonding metal–ligand MO (corresponding to the  $6b_g$  bonding MO). In the  $7b_g$  MO the contribution of the Ni  $3d$  orbital is 43%, while in  $6b_g$  it is 38%. Therefore, by including correlation effects, more electronic charge is transferred to the metal.

As seen from Table 6.12, the Koopmans theorem gives not only incorrect values of ionization energies but also wrong sequences of the latter beginning from the third band of the spectrum. The discrepancies are larger for states that include the metal  $d$  orbitals (as anticipated) and much less for pure ligand states. The  $\Delta$ SCF calculation improves essentially the results, but still it gives an incorrect sequence of the ionization bands. The inclusion of correlation effects by the CI method

gives a further improvement in the results, while the 2ph-TDA method gives the best fit to the experimental data.

**TABLE 6.12. Calculated Ionization Energies of Valence MOs of Ni(C<sub>3</sub>H<sub>5</sub>)<sub>2</sub> (in eV)**

MO	Origin <sup>a</sup>	Koopmans Theorem	Method of Calculation		Extended 2ph-TDA	Experiment <sup>b</sup>
			ΔSCF	ΔSCF-CI		
7a <sub>u</sub>	π(L)	7.5	6.7	6.7	6.4	7.7(1)
6b <sub>g</sub>	3d <sub>xz</sub> ; π(L)	9.0	5.6	6.6	7.7	8.1(2)
11b <sub>u</sub>	π(L)	11.8	11.0	10.8	10.3	10.3(5)
13a <sub>g</sub>	3d <sub>xy</sub> ; π(L)	11.7	5.5	6.4	7.6	8.1(2)
12a <sub>g</sub>	σ(L)	14.0	—	—	13.5	12.7(7)
5b <sub>g</sub>	3d <sub>yz</sub>	14.0	—	—	8.5	
11a <sub>g</sub>	3d <sub>x<sup>2</sup>-y<sup>2</sup></sub>	14.2	—	—	8.2	8.5(3)
6a <sub>u</sub>	σ(L)	14.6	—	—	13.3	
10b <sub>u</sub>	σ(L)	14.6	—	—	13.4	12.7(7)
4b <sub>g</sub>	σ(L)	15.0	—	—	13.7	
10a <sub>g</sub>	3d <sub>z<sup>2</sup></sub>	15.3	—	—	8.8	9.4(4)
9a <sub>g</sub>	3d <sub>xy</sub> ; π(L)	16.4	—	—	11.5	11.5(6)
5a <sub>u</sub>	σ(L)	16.5	—	—	14.9	
3b <sub>g</sub>	σ(L)	17.3	—	—	15.1	14.2(8)
9b <sub>u</sub>	σ(L)	18.0	—	—	16.2	
8a <sub>g</sub>	σ(L)	19.0	—	—	16.5	15.6(9)

Source: Guest [6.64] and Hillier [6.66].

<sup>a</sup>L denotes ligand.

<sup>b</sup>The order numbers of the bands in the photoelectron spectra are indicated in parentheses.

Reasonable results for ionization energies (photoelectron spectra) were obtained by density functional methods. Some earlier works on  $X_{\alpha}$  calculations are reviewed by Johnson and others [6.70, 6.71]. Decleva et al. [6.72] calculated a series of transition metal systems, including Ni(CO)<sub>4</sub>, Cr(NO)<sub>4</sub>, Fe(CO)<sub>2</sub>(NO)<sub>2</sub>, bis(π-allyl)nickel, and bis(π-allyl)palladium using DFT methods, and compared the results with those of other methods and with experimental data. A more complicated system, ruthenocene, is calculated in the ground and excited states [6.73] by so-called linear combinations of Gauss-type orbitals–model core potential–density-functional (LCGTO-MCP-DF) method [6.74] (Section 5.4). The authors also addressed the issue of term multiplicity (one of the difficult problems in density-functional methods, Section 5.4) and obtained absorption and emission frequencies in good agreement with experimental data.

### Total and Bonding Energies, Geometries, and Other Properties

Ab initio calculations of relatively simple coordination compounds became possible about three decades ago. Table 6.13 lists some examples of earlier nonempirical computations of the electronic structure and properties of a series of coordination systems [6.70–6.72]. It includes the total energy (for fixed nuclei), bonding energy (with respect to either the metal in the corresponding oxidation state and the ligands, or the atoms), and the formal charge on the central atom after Mulliken (Section 5.2).

Besides the data presented in Table 6.13, the calculations cited there allow one to determine the electronic distribution in the system, the relative stability of different electronic and geometric configurations (where these configurations were calculated), the one-electron energy-level ordering for the outer electrons, potentials of ionization from different states (expected photoelectron spectra), electron affinities, frequencies and probabilities of electronic transitions with absorption and emission of light, and so on. For example, Fig. 6.28 illustrates the electronic charge distribution along the Ni—C—N bond in the  $\text{Ni}(\text{CN})_4^{2-}$  complex [6.61].

Several examples are devoted to relative stability of different geometries. For  $\text{CuCl}_4^{2-}$  the configuration of a compressed (flattened) tetrahedron of  $D_{2d}$  symmetry with a Cl—Cu—Cl angle of  $120^\circ$  is most stable (in Table 6.13, the data obtained by the same basis set should be compared) in accordance with the Jahn–Teller effect (Section 7.3).

In the  $\text{NiCl}_4^{2-}$  complex, the high-spin (triplet) state  ${}^3T_1$  is more stable (by 65 kcal/mol) than the low-spin state  ${}^1T_2$  in agreement with the experimental data. Nonempirical calculations of five-coordinated complexes  $\text{CuCl}_5^{3-}$ ,  $\text{Cu}(\text{H}_2\text{O})_5^{2+}$ , and  $\text{Fe}(\text{CO})_5$  [6.88] in the configurations of a square pyramid and of a trigonal bipyramid show that the energies of these two configurations are very close (the difference is of the order of several kcal/mol). This explains their stereochemical softness and the Jahn–Teller pseudorotation [6.89]; these effects are discussed in Section 9.2. A full SCF calculation with geometry optimization for  $\text{Cu}(\text{H}_2\text{O})_6^{2+}$ ,

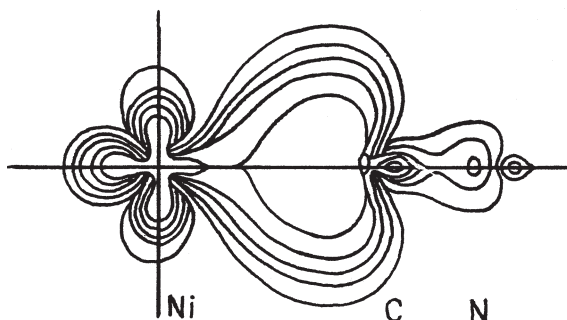


**FIGURE 6.28.** Contour map of electronic charge distribution along the Ni—C—N coordinate in  $\text{Ni}(\text{CN})_4^{2-}$  obtained by nonempirical calculations. (After Demuyne and Veillard [6.61].)

**TABLE 6.13. Some Results on Earlier Nonempirical Calculations of Coordination Systems**

System	Symmetry Group	Electronic State	Total Energy (au)	Bonding Energy (kcal/mol)	Charge on CA	Ref.
Cr(CO) <sub>6</sub>	<i>O<sub>h</sub></i>	<sup>1</sup> A <sub>1g</sub>	-1702.613	240 <sup>a</sup>	+0.703	[6.60]
NiF <sub>6</sub> <sup>4-</sup>	<i>O<sub>h</sub></i>	<sup>3</sup> A <sub>2g</sub>	-2084.4339	—	—	[6.79]
			-2099.1291 <sup>b</sup>	—	—	[6.80]
NiCl <sub>4</sub> <sup>2-</sup>	<i>D<sub>4h</sub></i>	<sup>1</sup> A <sub>1g</sub>	-3334.454	—	—	[6.78]
	<i>T<sub>d</sub></i>	<sup>1</sup> T <sub>2</sub>	-3334.446	—	—	[6.78]
	<i>T<sub>d</sub></i>	<sup>3</sup> T <sub>1</sub>	-3334.5497	—	—	[6.78]
Ni(CN) <sub>4</sub> <sup>2-</sup>	<i>D<sub>4h</sub></i>	<sup>1</sup> A <sub>1g</sub>	-1872.496	608 <sup>a</sup>	+0.46	[6.61]
Ni(CO) <sub>4</sub>	<i>T<sub>d</sub></i>	<sup>1</sup> A <sub>1</sub>	-1953.949	86 <sup>a,c</sup>	+0.24	[6.61]
			-1939.436	144 <sup>a,d</sup>	+0.466	[6.60]
CuF <sub>4</sub> <sup>2-</sup>	<i>D<sub>4h</sub></i>	<sup>2</sup> B <sub>1g</sub>	—	—	—	[6.79]
CuCl <sub>4</sub> <sup>2-</sup>	<i>D<sub>4h</sub></i>	<sup>2</sup> B <sub>1g</sub>	-3470.577	588 <sup>a</sup>	+1.28	[6.81]
			-3472.284 <sup>b</sup>	606 <sup>a</sup>	—	[6.81]
	<i>T<sub>d</sub></i>	<sup>2</sup> T <sub>2</sub>	-3470.606	—	—	[6.81]
	<i>D<sub>2d</sub></i>	<sup>2</sup> B <sup>2</sup>	-3470.608	—	—	[6.81]
VO <sub>4</sub> <sup>3-</sup>	<i>T<sub>d</sub></i>	<sup>1</sup> A <sub>1</sub>	-1229.9361	—	-0.07	[6.82]
CrO <sub>4</sub> <sup>2-</sup>	<i>T<sub>d</sub></i>	<sup>1</sup> A <sub>1</sub>	-1329.9148	—	+0.58	[6.82]
MnO <sub>4</sub> <sup>-</sup>	<i>T<sub>d</sub></i>	<sup>1</sup> A <sub>1</sub>	-1435.4853	-186 <sup>e</sup>	+0.93	[6.82]
			-1448.7571	-167 <sup>e</sup>	—	[6.83]
CrO <sub>8</sub> <sup>3</sup>	<i>D<sub>2d</sub></i>	<sup>2</sup> B <sub>1</sub>	-1598.188	4 <sup>e</sup>	—	[6.84]
			-1628.4862	93 <sup>e</sup>	+2.58	[6.85]
Fe(C <sub>5</sub> H <sub>5</sub> ) <sub>2</sub>	<i>D<sub>5h</sub></i>	<sup>1</sup> A <sub>g</sub>	-1643.1252	—	+1.23	[6.62]
Fe(C <sub>5</sub> H <sub>5</sub> ) <sub>2</sub> <sup>+</sup>	<i>D<sub>5h</sub></i>	<sup>2</sup> E <sub>2g</sub>	-1642.821	—	—	[6.62]
Co(C <sub>5</sub> H <sub>5</sub> ) <sub>2</sub>	<i>D<sub>5h</sub></i>	<sup>2</sup> E <sub>1g</sub>	-1761.8221	—	—	[6.68]
		<sup>2</sup> E <sub>2g</sub>	-1761.5607	—	—	[6.68]
		<sup>2</sup> E <sub>2u</sub>	-1761.5084	—	—	[6.68]
Mn(C <sub>5</sub> H <sub>5</sub> ) <sub>2</sub>	<i>D<sub>5h</sub></i>	<sup>2</sup> E <sub>2g</sub>	-1526.7099	—	—	[6.68]
		<sup>2</sup> A <sub>1g</sub>	-1526.6521	—	—	[6.68]
Mn(CO) <sub>5</sub> H	<i>C<sub>4v</sub></i>	<sup>1</sup> A <sub>1</sub>	—	—	—	[6.86]
Mn(CO) <sub>5</sub> CH <sub>3</sub>	<i>C<sub>4v</sub></i>	<sup>1</sup> A <sub>1</sub>	—	—	—	[6.86]
Ag(C <sub>2</sub> H <sub>4</sub> ) <sup>+</sup>	<i>C<sub>2v</sub></i>	<sup>1</sup> A <sub>1</sub>	-6272.1673	28 <sup>c</sup>	+0.10	[6.30]
Ni(C <sub>3</sub> H <sub>5</sub> ) <sub>2</sub>	<i>C<sub>2h</sub></i>	<sup>1</sup> A <sub>g</sub>	-1723.8044	—	—	[6.68]
Co(NH <sub>3</sub> ) <sub>6</sub> <sup>3+</sup>	<i>O<sub>h</sub></i>	<sup>1</sup> A <sub>1g</sub>	-189.092 <sup>f</sup>	654	+1.6	[6.87]

<sup>a</sup>With respect to the metal and ligands.

<sup>b</sup>By the extended basis.

<sup>c</sup>With respect to Ni<sup>0</sup> in the <sup>1</sup>S state.

<sup>d</sup>With respect to Ni<sup>0</sup> in the <sup>3</sup>F state.

<sup>e</sup>With respect to the atoms.

<sup>f</sup>Valence orbitals only.



$\text{Cr}(\text{H}_2\text{O})_6^{2+}$ ,  $\text{Mn}(\text{H}_2\text{O})_6^{3+}$ ,  $\text{Cu}(\text{H}_2\text{O})_6^+$ , and  $\text{Mn}(\text{H}_2\text{O})_6^{2+}$  with the correlated pair functional method for the former two was carried out [6.90]. The results confirm the Jahn–Teller distortions in the first three complexes (and absence of distortions in the last two systems) as predicted by the general theory for orbital degenerate  $E$  terms (Sections 7.3 and 9.2).

Bonding energies are given in Table 6.13 for some cases only. Their comparison with experimental data encounters difficulties, because in many cases it is not clear what should be considered as bonding agents: neutral ligands, their ions, separate atoms, and so on. For instance, the calculated bonding energy in  $\text{Ni}(\text{CO})_4$  with respect to the ligands and the neutral atom  $\text{Ni}^\circ$  in the singlet state  $^1S$  equals 86 kcal/mol [6.61], whereas in another calculation the bonding energy with respect to the neutral  $\text{Ni}^\circ$  atom in the triplet state  $^3F$  equals 144 kcal/mol [6.60]. The experimental value for the gas phase is 140 kcal/mol.

In  $\text{Ni}(\text{CN})_4^{2-}$  the bonding energy with respect to the cleavage into ions  $\text{Ni}^{2+}$  and  $\text{CN}^-$  is 608 kcal/mol. The largest part of it comes from the electrostatic interaction of the ions [6.61], and therefore it cannot be compared with the experimental estimate (43 kcal/mol) obtained under conditions when the ions are solvated. Note that in the case of  $\text{Ag}^+ - \text{C}_2\text{H}_4$  discussed in Section 6.3, the largest part of the bonding energy, 15 to 28 kcal/mol, is also due to the electrostatic interaction [6.30].

Further advances in computer technology made it possible to calculate the electronic structure of more complicated systems, including metalloporphyrins and other active sites and models of biological systems [6.91–6.95]. For metalloporphyrins [6.91–6.93] the calculations yield the order of the HOMO and LUMO energy levels, ionization potentials, distribution of electronic charge, metal positions with respect to the porphyrin plane, conformation of the porphyrin ring, and so on. Using a method that combines INDO with RHF SCF (Sections 5.3 and 5.5), parameterized to include transition metals, the electronic structure of a series of heme complexes in model compounds and intact proteins was studied with emphasis on the spin states and spectroscopic properties [6.91, 6.92]. For such important biological systems as cytochrome P-450, peroxidase, catalase, and metmyoglobin, some unresolved questions regarding the resting states have been addressed and interesting features of their functionality elucidated [6.91].

Most difficulties occur in geometry optimization of transition metal systems. A relatively accurate and compact basis set ( $11s7p4d/5s3p2d$ ) that proved to yield bond lengths with an accuracy of 0.03–0.08 Å for  $\text{Cr}(\text{CO})_6$ ,  $\text{HMn}(\text{CO})_5$ ,  $\text{Fe}(\text{CO})_5$ ,  $\text{Cr}(\text{C}_6\text{H}_6)_2$ ,  $\text{Fe}(\text{C}_5\text{H}_5)_2$ ,  $\text{Ni}(\text{C}_4\text{H}_4)_2$ ,  $(\text{C}_5\text{H}_5)\text{Mn}(\text{CO})_3$ , and  $(\text{C}_6\text{H}_6)\text{Cr}(\text{CO})_3$  was suggested [6.97] [for  $\text{Ni}(\text{CO})_4$  and  $\text{Cr}(\text{NO})_4$  the basis set used is ( $19s9p6d/10s4p4d$ )]. The calculations were carried out by the program GAMESS [6.96] (Section 5.3). In Table 6.14, the calculated parameters of the geometric structure of a series of 14 coordination compounds obtained using the computer program GAMESS are given together with the experimental data available [6.64]. The calculations were carried out by two basis sets: minimal STO-3G and double-zeta (DZ).

From Table 6.14, the following conclusions emerge:

1. The results of the calculations, in general, describe correctly the geometry of the compounds under consideration and, with a few exceptions discussed below, predict quantitatively the interatomic distances and angles for these compounds.
2. The better basis set DZ in the overwhelming majority cases yields better geometry parameter values.
3. In some cases significant discrepancies between the calculated and experimental interatomic distances still remain. For instance, in the mixed carbonyls and nitrosyls the calculated M—N distance is shorter by 0.1–0.2 Å and the M—C bond is longer by 0.1 Å than the experimental values. The calculated Fe—C distance in  $\text{Fe}(\text{CO})_2(\text{NO})_2$  is completely wrong (by 0.40 Å longer than the experimental value). The Ni—C distance in bis(allyl)nickel is also incorrect.

The analysis [6.64] shows that these discrepancies are caused by the neglect of electron correlation effects in the HF calculations of the electronic structure. In particular, the short distance M—N in mixed carbonyls and nitrosyls can be corrected by including CI [6.98, 6.99]. The HF calculated electronic configuration in  $\text{Co}(\text{CO})_3\text{NO}$  is  $[\text{core}](11e)^4(17a_1)^2(12e)^4$ , where  $11e$ ,  $17a_1$ , and  $12e$  are the HOMOs;  $11e$  and  $17a_1$  are mainly of  $d$  origin (75% and 66%, respectively), and  $12e$  represents the  $\pi$ -bonding cobalt–nitrosyl.

By taking into account the CI, one has to include additional terms from excited configurations of the same symmetry, the main one of which corresponds to the excitation of electrons from the  $12e$  to the  $13e$  MO. The latter is a  $\pi$  antibonding cobalt–nitrosyl MO, and hence its superposition to the ground state factors in the electronic correlation along the M—N bond. The calculations show that the configuration  $13e$  has a high weight (–0.52), and this explains directly the failure of the pure HF calculations; they do not include the antibonding MO  $13e$  (which represents the corresponding correlation effects), thus making the distance Co—N shorter than the experimental value.

Similar difficulties were encountered in calculations of other types of coordination compounds [6.100–6.105, 6.88]:  $\text{Ni}(\text{CO})_4$  [6.101], sandwich compounds (in ferrocene [6.102] the calculated metal–ligand distance is longer by 0.23 Å than the experimental value, whereas in manganocene [6.104] this distance is correct),  $\text{Fe}(\text{CO})_5$  [6.105], and so on. In most cases the calculated distances are longer than observed. In calculations including electron correlation effects these discrepancies were eliminated. For instance, the HF calculation of the distances to the two axial ligands in  $\text{Fe}(\text{CO})_5$  [6.88] in its bipyramidal configuration yields a value that is longer by 0.17 Å, than the experimental bond length, whereas there is no discrepancy for the equatorial distances. The calculation [6.105] including large-scale CI with all possible excited configurations (a total of 592,000 configurations compressed in a special way to 7750) and its comparison with the pure HF calculation [6.88] shows that the electron correlation effects increase the

**TABLE 6.14. Calculated and Experimental Parameter Values for the Equilibrium Geometry of Various Transition Metal Coordination Compounds<sup>a</sup>**

System	Point Group	Geometry Parameter	Calculation Basis Set Minimal STO-3G	DZ	Experimental Values
ScF <sub>3</sub>	<i>D</i> <sub>3h</sub>	<i>R</i> (Sc—F)	1.845	1.879	1.91
TiCl <sub>4</sub>	<i>T</i> <sub>d</sub>	<i>R</i> (Ti—Cl)	2.167	2.214	2.17
VF <sub>5</sub>	<i>D</i> <sub>3h</sub>	<i>R</i> (V—F <sub>ax</sub> )	1.641	1.744	1.734
		<i>R</i> (V—F <sub>eq</sub> )	1.608	1.702	1.708
VOCl <sub>3</sub>	<i>C</i> <sub>3v</sub>	<i>R</i> (V—O)	1.468	1.518	1.570
		<i>R</i> (V—Cl)	2.107	2.177	2.142
		<(Cl—V—Cl)	109.9	110.5	111.3
Cr(NO) <sub>4</sub>	<i>T</i> <sub>d</sub>	<i>R</i> (Cr—N)	1.576	1.689	1.79
		<i>R</i> (N—O)	1.218	1.160	1.16
Cr(CO) <sub>6</sub>	<i>O</i> <sub>h</sub>	<i>R</i> (Cr—C)	1.786	1.975	1.92
		<i>R</i> (C—O)	1.167	1.142	1.16
Ni(CO) <sub>4</sub>	<i>T</i> <sub>d</sub>	<i>R</i> (Ni—C)	1.579	1.900	1.836
Fe(CO) <sub>2</sub> (NO) <sub>2</sub>	<i>C</i> <sub>2v</sub>	<i>R</i> (Fe—C)	1.708	2.198	1.8
		<i>R</i> (Fe—N)	1.518	1.822	1.77
		<i>R</i> (C—O)	1.154	1.127	1.15
		<i>R</i> (N—O)	1.221	1.202	1.12
		<(C—Fe—C)	107.7	92.2	—
		<(N—Fe—N)	111.8	129.6	—
Co(CO) <sub>3</sub> NO	<i>C</i> <sub>3v</sub>	<i>R</i> (Co—N)	1.478	1.593	1.76
		<i>R</i> (Co—C)	1.664	1.938	1.83
		<i>R</i> (N—O)	1.231	1.197	1.10
		<i>R</i> (C—O)	1.155	1.132	1.14
		<(C—Co—N)	111.9	114.3	—
Mn(NO) <sub>3</sub> CO	<i>C</i> <sub>3v</sub>	<i>R</i> (Mn—C)	1.751	1.921	1.83
		<i>R</i> (Mn—N)	1.513	1.658	1.76
		<i>R</i> (C—O)	1.154	1.133	1.14
		<i>R</i> (N—O)	1.222	1.164	1.10
		<(N—Mn—C)	106.1	104.8	—
(C <sub>2</sub> H <sub>5</sub> )NiNO	<i>C</i> <sub>5v</sub>	<i>R</i> (Ni—C)	2.084	2.211	2.11
		<i>R</i> (Ni—N)	1.420	1.571	1.626
		<i>R</i> (C—C)	1.420	1.424	1.43
		<i>R</i> (N—O)	1.271	1.165	1.165
		<i>R</i> (C—H)	1.078	1.067	1.09
HMn(CO) <sub>5</sub>	<i>C</i> <sub>4v</sub>	<i>R</i> (Mn—C <sub>ax</sub> )	1.725	1.960	1.823
		<i>R</i> (Mn—C <sub>eq</sub> )	1.717	1.982	1.823
		<i>R</i> (Mn—H)	1.628	1.684	1.50
		<i>R</i> (C—O <sub>ax</sub> )	1.162	1.137	1.139
		<i>R</i> (C—O <sub>eq</sub> )	1.163	1.137	1.139
		<(H—Mn—C <sub>eq</sub> )	72.3	82.3	83.6
		<(Mn—C—O <sub>eq</sub> )	171.2	172.8	—

TABLE 6.14. (Continued)

System	Point Group	Geometry Parameter	Calculation Basis Set Minimal STO-3G	DZ	Experimental Values
Mn(CO) <sub>5</sub> CN	C <sub>4v</sub>	R(Mn—C—CN)	2.045	—	1.98
		R(Mn—CO <sub>ax</sub> )	1.825	—	1.822
		R(Mn—CO <sub>eq</sub> )	1.804	—	1.853
		R(C—O <sub>eq</sub> )	1.162	—	1.134
		R(C—O <sub>ax</sub> )	1.152	—	1.134
		R(C—N)	1.156	—	1.16
Ni(C <sub>3</sub> H <sub>5</sub> ) <sub>2</sub>	C <sub>2h</sub>	R(Ni—C)	1.744	2.088	—
		R(Ni—C <sub>t</sub> )	2.183	2.253	2.10
		R(C <sub>t</sub> —C)	1.405	1.399	1.41
		R(C <sub>t</sub> —H)	1.074	1.076	1.08
		R(C—H)	1.094	1.073	1.08
		<(C <sub>t</sub> —C—C <sub>t</sub> )	128.5	124.0	—

Source: Guest [6.64].

<sup>a</sup>Distances are given in angstroms (Å); angles, in degrees (°).

orbital charge transfers  $q_i$  both from the ligand to the metal along the  $\sigma$  bond and from the metal to the ligand on the  $\pi$  MO, thus improving the metal–ligand bond and decreasing its length (cf. Section 6.3). This result is quite understandable since the  $\sigma$  and  $\pi$  orbitals occupy different space regions and expansion of the charge over a larger space decreases the interelectron repulsion.

This effect takes place for all the bonds, but in Fe(CO)<sub>5</sub> it is much stronger for axial than for equatorial ligands. Figure 6.29 illustrates this statement by means of electron deformation densities (Section 8.6) obtained by calculations with and without correlation effects in the planes of the axial (Fig. 6.29a) and equatorial (Fig. 6.29b) ligands [6.105]. It is seen that the electron correlation effects strongly increase the population of the  $d_{z^2}$  orbital of the iron atom at the expense of the  $5\sigma$  orbitals of the axial CO ligands, as well as the  $2\pi^*$  orbitals of the axial and equatorial CO ligands that overlap with the metallic  $d_{xz}$ ( $d_{yz}$ ) orbitals (Fig. 6.29a); the population of the in-plane  $2\pi^*$  MOs of the equatorial CO ligands is increased about 4 times less, and the donation from the latter is almost unchanged (Fig. 6.29b). That is why, by including the correlation effects the axial ligands, experience a much larger reduction in the distance to the metal than do the equatorial ligands.

The conclusions from these examples have a general meaning. If the ligands possess active  $\pi$  orbitals, the competition between the tendency to form metal–ligand  $\pi$  bonds, which shortens the distance between them, and the opposite tendency to increase this distance caused by the increasing repulsion on the  $\sigma$  bond for which the equilibrium distance is larger (Section 6.3), is solved in favor of a shorter distance when the correlation effects are included, because the latter reduce the interelectron repulsion [see also the geometry calculations for Fe(CO)<sub>5</sub> and Ni(CO)<sub>4</sub> carried out by the DFT method [6.106]]. Examples 5.2 and 5.4 and

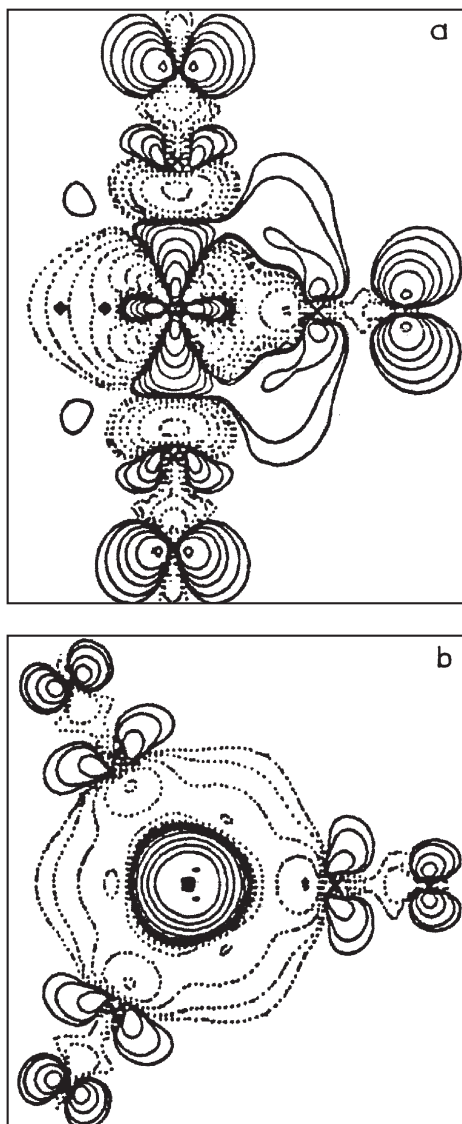


**FIGURE 6.29.** Fe(CO)<sub>5</sub> total electron density difference calculated ab initio with and without correlation effects: (a) in the plane containing the threefold axis and (b) in the equatorial plane. Dotted lines indicate negative values (domains of higher density without correlation effects). Contours are at 0.0001, 0.0002, 0.0010, 0.0020, 0.0050, 0.0100, 0.0200, and 0.0500e/(au)<sup>3</sup>. Crosses indicate the positions of the nuclei; the iron atom is in the center of the plot. (After Lüthi et al. [6.105].)

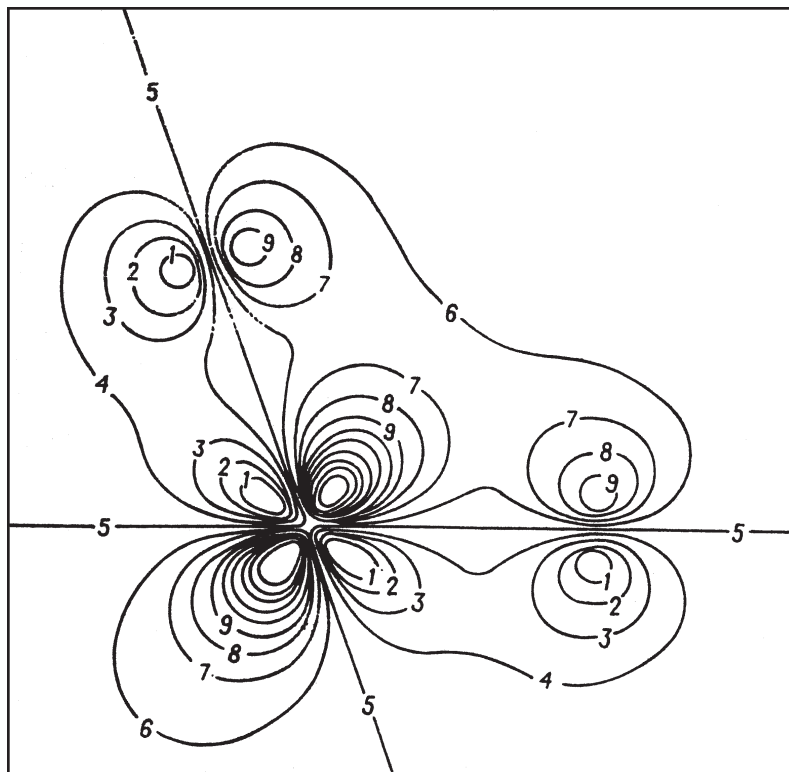


**FIGURE 6.30.** Contour map of the  $1e$  one-electron wavefunction in the O—Mn—O plane of the tetrahedral  $\text{MnO}_4^-$  system obtained by DFT- $X_\alpha$  calculations. The contours are given with a spacing of 0.05 from  $-0.2(N = 1)$  to  $+0.2(N = 9)$ . Along the  $N = 5$  line there is the node of the  $\pi$  function. The Mn—O distance is 3.00 au. (After Johnson et al. [6.71].)

Problems 5.4–5.7 in Section 5.3 show how the available program packages can be used to perform electronic structure calculations with geometry optimization including correlation effects.

Density-functional calculations compete with the MO LCAO methods in energy calculations and less so in geometries. Figure 6.30 shows the  $1e$  one-electron wavefunction in the O—Mn—O plane of the tetrahedral  $\text{MnO}_4^-$  system obtained in one of the early DFT- $X_\alpha$  calculations [6.71]. From other coordination systems calculated by the DFT- $X_\alpha$  method, note  $\text{TiCl}_4$ ,  $\text{NiF}_6^{4-}$ ,  $\text{CuCl}_4^{2-}$ ,  $\text{PtCl}_4^{2-}$ ,  $\text{Ni}(\text{CO})_4$ ,  $\text{Cr}(\text{CO})_6$ ,  $\text{Fe}(\text{CO})_5$  [6.71], and carbonyls [6.107]. One advantage of DFT methods is that they are applicable to solid-state clusters and polyatomic formations on surfaces. For instance, the cluster  $\text{NiO}_6^{10-}$  that models the Ni site in the NiO crystal was calculated by considering explicitly all its 86 electrons and the influence of the (very strong in this case)

crystal field of the environment (the Madelung potential) [6.108]. Besides the good agreement of the results with the photoelectron spectra [6.109], the calculations allow one to address the problem of adsorbed oxygen on metallic nickel surfaces. Comparison of the results of the calculations [6.108] with the photoelectron spectra of adsorbed oxygen and its concentration dependence shows that for sufficiently large concentrations the oxygen atoms penetrate the metal lattice, forming clusters  $\text{NiO}_6^{10-}$  on the surface [6.110].

The density-functional calculations allow one to consider the effect of spin polarization, that is, the difference in the energies of orbitals with spinup and spindown (Section 5.4), which may be significant in complexes with unpaired electrons. For instance, for  $\text{MnCl}_4^{2-}$  ( $d^5$ ) and  $\text{CoCl}_4^{2-}$  ( $d^7$ ) even the consequence of the  $t_2$ ,  $e$ , and  $a_1$  energy levels is different for the orbitals with unpaired electrons with spinup and spindown [6.111]. For  $\text{CuCl}_4^{2-}$  with  $T_d$  symmetry the orbitals with opposite spin orientation have the same order of consequence but different energies. More recent works illustrate the advantages of the density-functional methods in energy calculations of systems with increasing complexity. These include model systems for homogeneous and heterogeneous catalysis [6.112, 6.113], metal–ligand interactions on surfaces [6.114, 6.115], transition metal clusters [6.116], and biological systems [6.117]. Example 5.3 in Section 5.4 and Problem 5.6 show how DFT calculations can be performed using available program packages for electronic structure calculations.

## 6.5. RELATIVISTIC EFFECTS

The discussion of relativistic effects (REs) in chemical bonding is given in a separate section for two reasons: (1) the topic is of special interest for transition metal coordination compounds, and (2) the area as a whole in application to molecular problems is relatively new. The relativistic Dirac equation (Section 2.1) was used for studies of atoms beginning in the 1930s, whereas its direct application to molecular bonding phenomena (MO theories) started in the late 1960s and early 1970s. This delay was due mainly to the complication of relativistic molecular calculations (Section 5.4), although some reluctance in the study of REs in molecules was also induced by the authoritative statement of Dirac that the REs are not important in chemical bonding because the average speed  $v$  of valence electrons is small with respect to the speed of light  $c$ . In view of more recent achievements in this area (see below), this remark is only partly true.

Formally,  $v$  is small only when the electrons are moving in the valence area. However,  $s$  electrons (even valence  $s$  electrons) spend a considerable amount of time near the nuclei where their speed is very high, thus being influenced by relativity directly, and all the other electrons are also influenced indirectly because of the interaction with the  $s$  electrons. Again, the spin–orbital splitting

of energy levels, essential for any spectroscopic studies, is a purely relativistic effect.

In this section a brief discussion of the main REs relevant to transition metal compounds is given. Relativistic atomic states are considered in Section 2.1, while relativistic approaches to electronic structure calculations are discussed in Sections 5.4 and 5.5. For some reviews, see Refs. 6.118–6.121.

### Orbital Contraction and Valence Activity

To understand the origin of REs, let us begin with heavy-atom features. One of the most essential REs in atoms, important to chemical properties, is the *relativistic contraction of  $s$  and  $p_{1/2}$  orbitals*. The Bohr radius of the  $1s$  electron is  $R_0 = 4\pi\hbar^2/me^2$ , where  $m$  is the electron mass. The latter, following the theory of relativity, is dependent on its speed:  $m = m_0[1 - (v/c)^2]^{-1/2}$ , where  $m_0$  is the rest mass. This means that the relativistic mass is greater than the rest mass of the electron, and hence the radius of its orbital motion becomes smaller owing to REs. In atomic units  $c \cong 137$  and for  $1s$  electrons  $v = Z$ , where  $Z$  is the atomic number. Thus, for instance, for gold  $v/c = \frac{79}{137} = 0.58$ , and its  $1s$  electron radius  $R_0$  is relativistically contracted by about 19%.

This relativistic orbital contraction of the inner  $1s$  electrons modifies the orbital states of all the other electrons, including the outer valence electrons. Indeed, the higher  $s$  orbitals, although having a lower average speed, must be orthogonal to the inner  $s$  states, and therefore their radial distribution undergoes a similar contraction (the  $p$ ,  $d$ ,  $f$  orbitals are orthogonal to the  $s$  orbitals by the angular parts). The calculations show that the relativistic contraction of the valence electrons owing to these effects is, in general, not smaller (it can be even a percentile or so larger), than for the  $1s$  electrons.

Figure 6.31 [6.122] illustrates the relativistic contraction of the  $6s$  shell of atoms from Cs to Fm obtained from numerical data of relativistic Dirac–Fock (Section 5.4) and Hartree–Fock calculations. Interestingly, it is seen from this figure that the largest relativistic contraction is inherent to the ground state of Au with the electronic configuration  $5d^{10}6s^1$ . It makes gold a unique element and explains its *redox nobility*. A similar relativistic radial contraction is expected for  $p_{1/2}$  states (see below).

On the contrary, the  $d$  and  $f$  electrons are subject to a *radial expansion* and destabilization due to the RE. Indeed, the  $d$ - and  $f$ - electron densities are zero at the nuclei (Section 2.1, Table 2.3, and Fig. 2.3). Hence these electrons are not expected to have relatively high speeds and direct relativistic reduction of their radii. On the other hand, they are automatically orthogonal to the  $s$  orbitals by symmetry (by the angular parts) and hence are not subject to indirect contraction, as are the valence  $s$  electrons. However, because of the relativistic contraction of the  $s$  and  $p$  shells, the  $d$  and  $f$  electrons are more efficiently screened, and hence they go up in energy and outward radially [6.123].



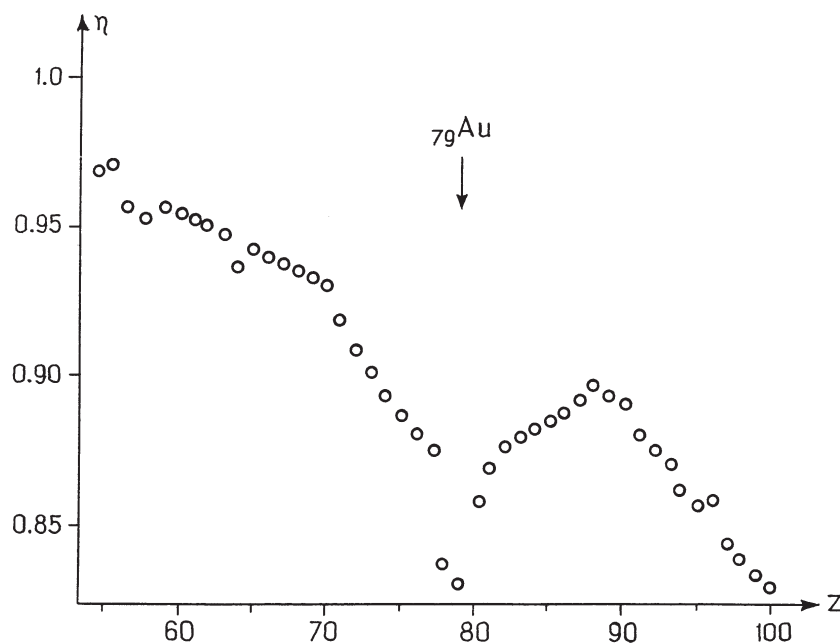


**FIGURE 6.31.** The relativistic contraction  $\eta = \langle r \rangle_{\text{rel}} / \langle r \rangle_{\text{nonrel}}$  of the 6s shell in the elements from Cs ( $Z = 55$ ) to Fm ( $Z = 100$ ). (After Pyykko and Desclaux [6.122].)

Thus the main RE in heavy atoms (besides the spin-orbital splitting) is the *radial contraction and stabilization of s and  $p_{1/2}$  electrons and the radial expansion and destabilization of d and f electrons*. These effects directly influence the possible electronic configurations and *valence states* of heavy atoms [6.124, 6.125]. Indeed, stabilization of the s shells and destabilization of d shells in transition metals obviously favors electronic configurations with more s than d contribution. In particular, this becomes important in the comparison of ground-state configurations of the period 5 and period 6 elements in the same group. Table 6.15 illustrates such a comparison for groups 5–10.

**TABLE 6.15. Electronic Configurations of Ground-State 4d and 5d Elements in Groups 5–10 of the Periodic Table**

Row	Group					
	5	6	7	8	9	10
5	Nb $d^4s^1$	Mo $d^5s^1$	Tc $d^5s^2$	Ru $d^7s^1$	Rh $d^8s^1$	Pd $d^{10}$
6	Ta $d^3s^2$	W $d^4s^2$	Re $d^5s^2$	Os $d^6s^2$	Ir $d^7s^2$	Pt $d^9s^1$

Source: From Pyykko [6.119].

As seen from this table, the period 6 elements have more  $s$  electrons in the electronic configuration of the free atom than do the isoelectronic period 5 elements, explicitly demonstrating the increasing relativistic contraction (stabilization) of the  $s$  states, as compared with the  $d$  states, when passing to heavier atoms. In Tc the configuration is  $d^5s^2$  (and hence it does not change when passing to Re) because of the additional stability of half-filled  $d^5$  configurations. Similarly, for Pd  $d^{10}$  is more stable than  $d^9s^1$ , whereas in Pt  $d^9s^1$  is more stable because of the stronger  $s$  contraction.

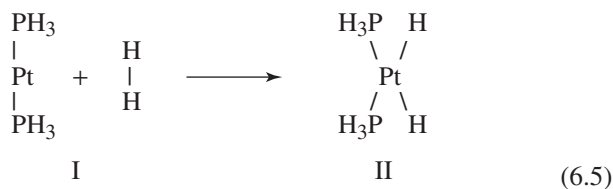
Similar REs were noted in other atoms and ions [6.119]. For instance, the configuration of  $\text{Mo}^+$  is  $4d^5$ , whereas that of  $\text{W}^+$  is  $5d^46s$ , the ground state of Lr is  $7s^27p_{1/2}^1$  and not  $7s^26d^1$ , as assumed earlier, the  $^3\text{P}_0$  ground state of Pb is in 92.5%  $(p_{1/2})^2$ , and so on.

The change in the ground-state electronic configuration of atoms is definitely very important in their chemical behavior. First, *the formal valence of the atom changes* [cf. Ag(I) and Au(III)]. Although the physical meaning of the notion of valence in case of coordination compounds is far from its prime definition (Sections 6.1 and 1.2), the general understanding of the *activity of valence electrons* that underlies a variety of chemical properties is certainly determined by the electronic configuration, and hence the REs change the valence activity. Example 6.12 shows how the relativistic effects influence the catalytic activity of transition metal complexes.

### EXAMPLE 6.12

#### Relativistic Effects in Catalytic Activity of Pt and Pd Complexes

A visual example of RE in valence activity is the difference in chemical behavior of  $\text{Pd}(4d^{10})$  and  $\text{Pt}(5d^96s^1)$ , especially in their catalytic activity. Consider, for instance, the following oxidative addition and reductive elimination reaction:



It was shown [6.126] that system I is favored by the configuration  $\text{Pt}-5d^{10}$ , while II requires  $5d^96s^1$ . Therefore, the barrier of the transformation (6.5), following Table 6.15, is low (2.34 kcal/mol). On the contrary, in the case of Pd this reaction is unknown because Pd prefers the configuration  $4d^{10}$ .

### Bond Lengths, Bond Energies, and Vibrational Frequencies

Relativistic effects in bond lengths are not determined entirely by the  $s$ -orbital contraction and  $d$ ,  $f$ -orbital expansion, discussed above, although both the former and latter significantly influence the bonding features. Indeed, the bond formation changes the charge distribution in the area between and around the bonding atoms, which is very dependent on their orbitals' overlap and consequent changes in interelectron interaction effects. The attempt to correlate these effects with the RE shows that relativistic contraction of orbitals and relativistic contraction of bond lengths are two parallel but largely independent effects [6.119, 6.127].

A more detailed analysis [6.120] shows that the main effect of relativity is the reduction in kinetic energy of the electrons involved in the bonding. In Section 5.4, general expressions for the contributions of REs to the bonding are given. In particular, as seen from Eq. (5.81), the first relativistic correction to the electron–core interaction  $H^0$  in the quasirelativistic approximation  $\Delta T^R = -p^4/8m_0^3c^2$  is in fact a correction of the order of  $(v/c)^2$  to the nonrelativistic kinetic energy  $T = p^2/2m_0$  [note that the rigorous expression for the kinetic energy is  $T^R = (p^2c^2 + m_0^2c^4)^{1/2} - m_0c^2$ , with  $p = m_0v$ ]. Because it is negative, this relativistic correction reduces the kinetic energy. The next term in (5.80), the Darwin interaction (5.82), is positive [6.127] and increases the energy, but its value is smaller than the kinetic energy correction; the latter is always predominant. The third correction, spin–orbital splitting, is discussed below.

The relativistic decrease in kinetic energy is important to many chemical effects, including bond length, bond energy, and vibrational frequency. It was shown [6.127] that the negative relativistic contribution increases with the decrease in the interatomic distance, and hence *this RE stabilizes and contracts the chemical bond*. This effect becomes important when the RE is strong enough to overcome the increase in nonrelativistic kinetic energy with decrease in the interatomic distance. The latter is proportional to  $v^2$ , whereas the relativistic correction is  $v^4$ , and hence for sufficiently high speeds  $v$  a contraction and stabilization of the chemical bond takes place. Example 6.13 illustrates this effect.

#### EXAMPLE 6.13

##### *Relativistic Effects in Metal Hydrides*

The simplest heavy-atom compounds studied to confirm the abovementioned RE are the metal hydrides MH. Table 6.16 [6.120] illustrates some Hartree–Fock (Section 5.3) relativistic calculations of the M–H bond length  $R_0$ , dissociation energy  $D$ , and vibrational frequency  $\omega$ , in comparison with the corresponding HF nonrelativistic (NR) calculations and experimental data [6.128]. As one can see from this table, all the bonds become relativistic contracted and stabilized by moving

toward heavier atoms, and this trend is confirmed by the corresponding experimental data. The RE are strong in Au and Hg; for them, the NR calculations are inadequate. For more complex hydrides the bond contraction is similar. For instance, for CrH<sub>6</sub>, MoH<sub>6</sub> and WH<sub>6</sub>,  $\Delta R$  (in picometers) equals 0.6, 1.6, and 5.4, respectively [6.130].

**TABLE 6.16. Comparison of Relativistic (R) and Nonrelativistic (NR) Calculations of Bond Lengths  $R_0$ , Dissociation Energies  $D$ , and Vibrational Frequencies  $\omega$  with Experimental Data (Exp) for Some Metal MH Hydrides, MH<sup>+</sup> Ions, and M<sub>2</sub> Molecules (after [6.120])**

System	$R_0$ (Å)			$D$ (kcal/mol)			$\omega$ (cm <sup>-1</sup> )		
	NR	R	Exp	NR	R	Exp	NR	R	Exp
Cu—H	1.51	1.50	1.46	59	61	66 ± 2	1884	1905	1940
Ag—H	1.71	1.61	1.61	39	47	53 ± 2	1605	1709	1760
Au—H	1.78	1.55	1.52	37	68	74 ± 3	1704	2241	2305
Zn—H <sup>+</sup>	1.58	1.58	1.52	58	58	65 ± 9	1803	1810	1916
Cd—H <sup>+</sup>	1.78	1.74	1.68	46	48	48 ± 9	1665	1669	1775
Hg—H <sup>+</sup>	1.88	1.64	1.59	41	62	53 ± 10	1267	2156	2034
Cu <sub>2</sub>	2.26	2.24	2.22	51	53	45 ± 2	268	274	266
Ag <sub>2</sub>	2.67	2.52	—	40	47	37 ± 2	184	203	192
Au <sub>2</sub>	2.90	2.44	2.47	27	58	52 ± 2	93	201	191

From general considerations it is known that all REs increase as some powers of  $Z$ . For simple hydrides of metals of groups 11, 13, and 14, the bond contraction was shown to be proportional to  $Z^2$  [6.129]:

$$R = R_{NR} - R_R = 17(6) \times 10^{-4} Z^2 \text{ pm} \quad (6.6)$$

(1pm =  $10^{-12}$  m =  $10^{-2}$  Å). For other groups the bond contraction is different and follows roughly the  $s$ -orbital contraction (Fig. 6.31), going from a minimum for the groups 1 through a “gold maximum” at the group 11 and further decreases for higher groups.

Similar bond contraction and stabilization were revealed for metal diatomics Cu<sub>2</sub>, Ag<sub>2</sub>, and Au<sub>2</sub> (Table 6.16). The NR stability row Cu<sub>2</sub> > Ag<sub>2</sub> > Au<sub>2</sub> changes to Cu<sub>2</sub> > Ag<sub>2</sub> < Au<sub>2</sub> when the REs are taken into account. Similarly, the REs increase the bonding in W<sub>2</sub> by 25 kcal/mol changing the NR inequality Mo<sub>2</sub> > W<sub>2</sub> to W<sub>2</sub> > Mo<sub>2</sub> [6.131]. This trend in bond strength is observed in various organometallic compounds of groups 6 (Cr > Mo < W), 8 (Fe > Ru < Os), 9 (Co > Rh < Ir), 10 (Ni > Pd < Pt), and 11 (Cu > Ag < Au), and it is attributed to the RE [6.132].

On the other hand, multiple metal–metal bonds in binuclear complexes of the types M<sub>2</sub>Cl<sub>4</sub>(PR<sub>3</sub>)<sub>4</sub> and M<sub>2</sub>X<sub>6</sub>, where the bonding involves mostly  $nd$  orbitals,

**TABLE 6.17. Some Experimental Interatomic Distances (in pm) in 4*d* and 5*d* Metal MX<sub>6</sub> and MX<sub>4</sub> Complexes**

Compound	M	$R(4d)$	$R(5d)$	$R(4d) - R(5d)$
MF <sub>6</sub>	Ru, Os	187.75	183.3	4.7
MF <sub>6</sub>	Rh, Ir	187.38	183.0	4.4
MF <sub>6</sub>	Pd, Pt	187	182.9	4.1
MCl <sub>4</sub>	Zr, Hf	232	231.6	0
MBr <sub>4</sub>	Zr, Hf	246.5	245	1.5
MI <sub>4</sub>	Zr, Hf	266.0	266.0	0

rather than  $(n+1)s$  orbitals, are much less affected by relativistic corrections (the latter are of the order of 6–10 kcal/mol for the 5*d* homologues). In these cases, as well as in similar cases of metal–ligand  $\sigma$  bonds (involving mostly *d* orbitals) the bonding energy is determined mainly by the orbital overlap with minor RE influence.

Other examples of bond contraction by passing from 4*d* to 5*d* metals in MX<sub>6</sub> and MX<sub>4</sub> compounds are seen from the experimental data in Table 6.17. Note that the relativistic contractions  $R = R_{NR} - R_R$  are larger than the observed (or calculated) differences  $R(4d) - R(5d)$  because the former also compensates for the difference in atomic radii: in the absence of the RE the atomic radii of the 5*d* metals are larger than those of the 4*d* ones. It is seen from the table that by passing from complexes of the 4*d* triad Ru, Rh, and Pd, to the 5*d* triad Os, Ir, and Pt, with the same ligands, the bond shortens by about 4 pm (despite the considerable increase in atomic radii) [6.133]. The experimental contraction for the Zr–Hf pairs is about zero, meaning a considerable relativistic contraction, but smaller than for the abovementioned triad.

In  $M(\text{CH}_3)_2(\text{PR}_3)_2$  compounds with  $M = \text{Pd, Pt}$ , the Pt–C bond is longer by 3 pm than the Pd–C bond, whereas the Pt–P bond is shorter by 4 pm than Pd–P. This is difficult to explain within the context of nonrelativistic ideas, while relativistic pseudopotential calculations reproduce this trend [6.134]. The Pt–P bond is more relativistically contracted than the Pt–C one because the former is softer than the latter, and hence the same “contraction force” produces a larger effect on the softer Pt–P bond. For linear  $M(\text{PH}_3)_2$  complexes the Pd–P interatomic distance is 241 pm, while for Pt–P it is 232 pm [6.134], demonstrating a strong relativistic contraction.

Several examples are available for illustration of REs in compounds involving actinides. Table 6.18 shows the results of quasirelativistic calculations (Sections 5.4 and 5.5) of bond energies in compounds  $\text{AMCl}_3$  with  $M = \text{Th, U}$  and  $A = \text{H, CH}_3$  in comparison with corresponding nonrelativistic calculations and experimental data [6.120].

It is seen that the relativistic corrections here are very large (50–60 kcal/mol) and absolutely necessary to reproduce experimental data. On the other hand, the lanthanoid contraction, the contraction of the ionic radii in the lanthanoid series of isostructural crystals with the coordination number 8 by 18.3 pm when

**TABLE 6.18. Calculated Relativistic (R) and Nonrelativistic (NR) Bond Energies  $D(M-A)$  in  $AMCl_3$  Complexes and Experimental Data (Exp) (in kcal/mol)**

Compound	$D(M-A)$		Exp
	NR	R	
HThCl <sub>3</sub>	30.1	76.0	~ 80
CH <sub>3</sub> ThCl <sub>3</sub>	35.8	79.8	~ 80
HUCl <sub>3</sub>	10.5	70.1	76
CH <sub>3</sub> UCl <sub>3</sub>	16.8	72.2	72

Source: From Ziegler et al. [6.120].

passing from La<sup>III</sup> ( $4f^0$ ) to Lu<sup>III</sup> ( $4f^{14}$ ), is shown to be only 10%, due to the RE [6.119]. Other examples of relativistic bond contraction and stabilization have been provided in several review articles [6.119–6.121, 6.132]. Comparative studies of electronic structure with and without REs demonstrating the significance of the latter have been carried out to reveal the origin of specific geometry and color in Bi(C<sub>6</sub>H<sub>5</sub>)<sub>5</sub> as compared with Sb(C<sub>6</sub>H<sub>5</sub>)<sub>5</sub>, P(C<sub>6</sub>H<sub>5</sub>)<sub>5</sub>, and As(C<sub>6</sub>H<sub>5</sub>)<sub>5</sub> (semiempirical calculations) [6.135], as well as for BiPh<sub>5</sub>, PbCl<sub>6</sub><sup>2-</sup>, and WS<sub>4</sub><sup>2-</sup> (DFT- $X_\alpha$  approximation) [6.136]. Nuclear quadrupole coupling and isomer shifts in neptunyl compounds were calculated in the relativistic extended Hückel approximation [6.137].

### Correlation Between Spin–Orbital Splitting and Bonding

Relativistic spin–orbital interaction corrections enter directly the matrix elements of the quasirelativistic MO LCAO approximation in calculation of the electronic structure [Section 5.4, Eqs. (5.80)] and indirectly in the basis set of the LCAO that should be formed by relativistic atomic functions that follow the  $j-j$  coupling scheme and double-group representations (Section 2.1; see also Section 5.5 for quasirelativistic parameterization). In the  $j-j$  scheme each electron is characterized by its momentum  $\mathbf{j}_i = \mathbf{l}_i + \mathbf{s}_i$  ( $\mathbf{l}_i$  and  $\mathbf{s}_i$  are the orbital and spin momenta, respectively) with quantum numbers  $j_i = l_i \pm \frac{1}{2}$ ; the total momentum of the atom is  $\mathbf{J} = \sum_i \mathbf{j}_i$  with the quantum number  $J = j_1 + j_2, j_1 + j_2 - 1, \dots, |j_1 - j_2|$ . Thus in the valence basis set the states  $p_{1/2}, p_{3/2}, d_{3/2}, d_{5/2}$ , and so on should be employed in the relativistic calculations instead of the NR functions  $p, d, f$ .

However, the energy differences between the pairs of atomic states  $p_{1/2}$  and  $p_{3/2}, d_{1/2}$  and  $d_{3/2}$ , and so on are determined by spin–orbital splitting. If this splitting is zero, the corresponding pairs of orbitals are degenerate and there is no reason to differentiate them [see Eq. (2.20)]. The same is true when the spin–orbital splitting is small, as compared with the interatomic interaction, because in this case the two component functions may become largely intermixed.

In the case of strong spin–orbital interaction the two atomic functions with the same orbital quantum number  $l$  but different  $j$  values,  $l + \frac{1}{2}$  and  $l - \frac{1}{2}$  ( $l \neq 0$ ), become quite independent also from the chemical perspective. This statement

is especially important for  $p$  functions. Consider an atom with one  $p$  electron. In case of strong RE (large spin-orbital splitting) the corresponding relativistic states are  $p_{1/2}(\frac{1}{2})$ ,  $p_{3/2}(\frac{1}{2})$ ,  $p_{1/2}(\frac{3}{2})$ , and  $p_{3/2}(\frac{3}{2})$ , where the values  $j = \frac{1}{2}, \frac{3}{2}$  are shown in parentheses, while their projections values  $\frac{1}{2}, \frac{3}{2}$  are indicated as indices. The total momentum in the  $p(\frac{1}{2})$  states ( $j = \frac{1}{2}$ ) is smaller than that of nonrelativistic  $p$  electrons ( $l = 1$ ), but larger than that for  $s$  electrons ( $l = 0$ ), which have spherical symmetric distribution. The  $p(\frac{1}{2})$  state (more correctly, its larger spinor; see Section 2.1) can be visually presented as having a spherical form (Fig. 6.32) that consists of the usual  $\sigma$ -like part (dashed area) and a  $\pi$ -like contribution (dotted area) that supplements the former to a sphere. The two functions  $p_{1/2}(\frac{1}{2})$  and  $p_{3/2}(\frac{1}{2})$  differ in their projections on the  $z$  axis, that is, by their orientation in space with respect to the axis of quantization.

If two  $p_{1/2}(\frac{1}{2})$  functions from two bonding atoms overlap, they form  $\frac{1}{3}$  of  $\sigma$  bonding and  $\frac{2}{3}$  of  $\pi$  antibonding MOs (Fig. 6.32b), or vice versa for opposite signs:  $\frac{1}{3}\sigma$  antibonding and  $\frac{2}{3}\pi$  bonding. The two  $p_{3/2}(\frac{1}{2})$  functions form  $\frac{1}{3}\pi$  bonding and  $\frac{2}{3}\sigma$  antibonding, or vice versa [6.138, 6.139]. The  $p_{1/2}(\frac{3}{2})$  and  $p_{3/2}(\frac{3}{2})$  functions form normal  $\sigma$  and  $\pi$  bonds.

It is evident that in any combination the bonding between two relativistic  $p_{1/2}$  states is weaker than in the nonrelativistic case. This weakening is compensated when all the  $p$  states are occupied by electrons. Accordingly, the weakening does not occur when all the  $p$  states are degenerate or strongly mixed by external influence. Therefore, if not all the  $p$  states of the bonding atoms participate with their electrons in the bonding, that is, not all the bonding MOs originating from  $p$  states are occupied, *the spin-orbital splitting of  $p$  states weakens the bonding in which  $p(\frac{1}{2})$  states are involved.*

Several experimental facts can be attributed to this RE. For instance, in the series of isostructural ( $p$  “isoelectronic”) compounds  $\text{Sb}_4$ ,  $\text{BiSb}_3$ , ...,  $\text{Bi}_4$ , the dissociation energy decreases systematically from 9.04 to 6.03 eV [6.140].

On the other hand, there is a backward influence of the bonding on the spin-orbital splitting. Indeed, there are two reasons for changes (reduction) of the spin-orbital splitting by the chemical bonding: (1) the symmetry of the field in which the electron moves lowers and hence the orbital moment of the electron becomes, in general, reduced (Section 8.4); and (2) when there is a covalent bonding between a heavy atom with a light atom, the relativistic electron of the former becomes delocalized over the region, including also the light atom, and this delocalization reduces the speed of the electron [6.141].

Consider a heavy-atom hydride  $\text{MH}$  and assume that the  $\text{M}-\text{H}$  bonding is realized through overlap of the  $ns$  orbital of  $\text{M}$  (e.g., in the case of  $\text{Au}$  this orbital is  $6s$ ) with the  $1s$  orbital of  $\text{H}$ . Then the bonding orbital is  $N(\psi_{ns}^{\text{M}} + \lambda\psi_{1s}^{\text{H}})$  with  $\lambda$  as a covalence parameter and  $N$  as the normalization constant (Section 5.2). The latter is less than unity,  $N < 1$ , and decreases with increase in  $\lambda$ . Since hydrogen is almost nonrelativistic, the weight of the relativistic wavefunction in the MO is reduced (times  $N$ ), as compared with the AO. In this way all the RE become reduced by covalence.

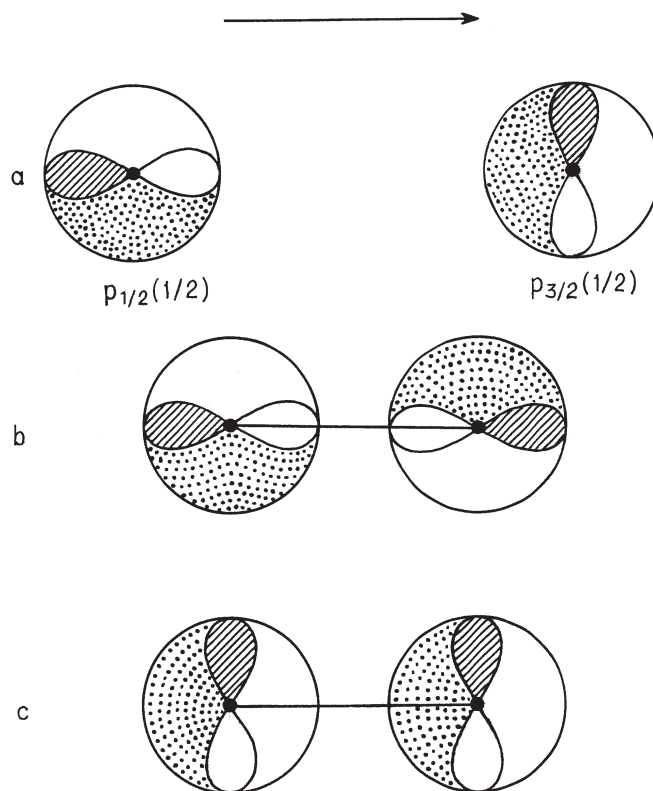


**FIGURE 6.32.** Schematic illustrations of the bonding between two atoms with relativistic  $p_{1/2}$  orbitals: (a) visual presentation of the  $p_{1/2}(\frac{1}{2})$  and  $p_{3/2}(\frac{1}{2})$  orbitals; (b)  $p_{1/2}(\frac{1}{2}) - p_{1/2}(\frac{1}{2})$  overlap representing  $\frac{1}{3}\sigma$  bonding and  $\frac{2}{3}\pi$  antibonding [ $p_{1/2}(\frac{1}{2}) + p_{1/2}(\frac{1}{2})$  is  $\frac{1}{3}\sigma$  antibonding and  $\frac{2}{3}\pi$  bonding]; (c)  $p_{3/2}(\frac{1}{2}) + p_{3/2}(\frac{1}{2})$  overlap yielding  $\frac{1}{3}\pi$  bonding and  $\frac{2}{3}\sigma$  antibonding (the arrow indicates the axis of quantization).

The most observable (easiest) reduction of RE is spin-orbital splitting since it can be, in principle, observed in both the atom and the molecules. However, there may be some difficulties concerning the spectroscopic classification of energy levels in the relativistic case. Example 6.14 elucidates the RE in a platinum complex by means of numerical calculation of its electronic structure.

#### EXAMPLE 6.14

##### *Relativistic Semiempirical Calculation of $\text{PtCl}_6^{2-}$ [6.141]*

The free Pt atom has a relatively moderate spin-orbital splitting ( $8.418 \times 10^3 \text{ cm}^{-1}$ ). The quasirelativistic (QR) calculations of



the electronic structure of  $\text{PtCl}_6^{2-}$  were performed [6.141] in the semiempirical IEH (SCCC) approximation (Section 5.5), while the corresponding nonrelativistic (NR) calculations used here for comparison were carried out much earlier [6.142].

The comparison allows one to follow, at least qualitatively, how the spin-orbital splitting in the Pt atom is modified under the influence of the bonding to chlorine atoms. Figure 6.33 illustrates this effect. Figure 6.33a shows the  $d_{3/2}$ - $d_{5/2}$  spin-orbital splitting in the free Pt atom. The crystal field of the ligands and the bonding with the corresponding ligand orbitals result in quasirelativistic MO LCAO energy levels given in Fig. 6.33b. Note that the relativistic classification of the MOs is given after the double-group representations (Section 3.6). For

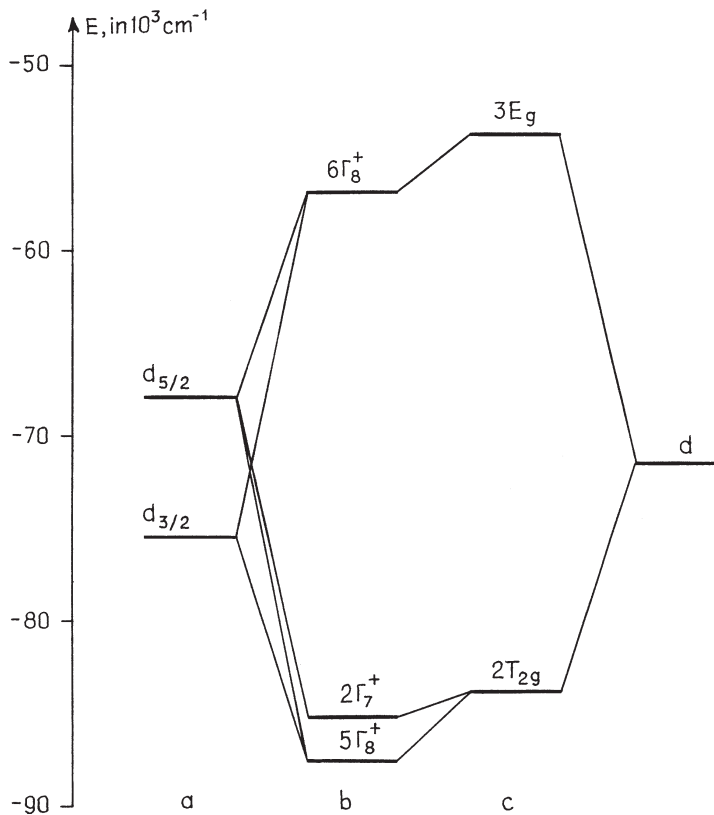


**FIGURE 6.33.** Reduction of spin-orbital splitting by bonding [6.141]: (a) spin-orbital  $d_{3/2}$ - $d_{5/2}$  splitting in the free Pt atom; (b) the MOs formed by these  $d$  orbitals with the corresponding ligand counterparts in  $\text{PtCl}_6^{2-}$ ; (c) the same MOs in the nonrelativistic calculation [6.142].

comparison, the corresponding nonrelativistic  $d$ -orbital splitting into  $T_{2g}$  and  $E_g$  is also shown (Fig. 6.33c).

From these data one can see that, as far as the MO energy levels under consideration are concerned, when passing from the NR to QR calculations (1) all the energy levels lower and (2) the  $T_{2g}$  level splits into  $5\Gamma_8^+$  and  $2\Gamma_7^+$ . While effect 1 can be attributed to the contraction and stabilization, discussed above, effect 2 is obviously due to the spin-orbital interaction. However, its magnitude,  $1.9 \times 10^3 \text{ cm}^{-1}$ , is much smaller than the spin-orbital splitting in the free atom,  $8.418 \times 10^3 \text{ cm}^{-1}$ . Thus there is an obvious *reduction of the spin-orbital splitting by bonding*. The two sources of this effect, mentioned above, are seen from the calculations explicitly; the octahedral crystal field splitting into  $E_g$  and  $T_{2g}$  mixes the  $d_{3/2}$  and  $d_{5/2}$  levels of the free atom, and hence the spin-orbital splitting  $T_{2g} \rightarrow 5\Gamma_8^+ + 2\Gamma_7^+$  includes both the orbital reduction and covalent delocalization over nonrelativistic atoms (the RE in the Cl atoms are neglected [6.141]).

Spin-orbital splitting in heavy atoms also reduces the dissociation limit  $D_e$  in diatomics  $\text{BiH}^+$ ,  $\text{Pb}_2$ ,  $\text{PbO}$ ,  $\text{PbH}$ , and  $\text{Tl}_2$  (for references, see Pyykko's article [6.119]). Figure 6.34 explains the origin of this reduction. With zero spin-orbital splitting in the  $\text{Bi}^+$  ion (i.e., in the NR approximation), the dissociation of  $\text{BiH}^+$  into  $\text{Bi}^+$  and H yields the  $\text{Bi}^+$  ion in the  $^3P$  state, whereas with respect to the spin-orbital interaction, its ground-state energy  $^3P_0$  is lower by 2.3 eV. There are also cases when the REs increase the  $D_e$  values [6.119].

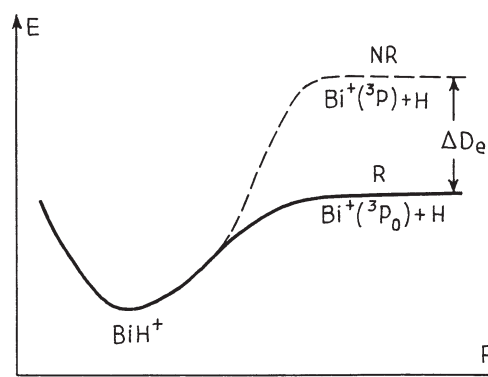


**FIGURE 6.34.** Reduction  $\Delta D_e$  of the dissociation energy limit  $D_e$  in  $\text{BiH}^+$  due to spin-orbital splitting in the free ion  $\text{Bi}^+$ . In the NR case the dissociation results in  $\text{Bi}^+$  in the state  $^3P$ , which is 2.3 eV higher than the relativistic ground state  $^3P_0$ .

### Other Relativistic Effects

Quite a number of relativistic (mostly quasirelativistic) calculations of electronic structure and properties of heavy-atom coordination compounds are listed and reviewed in several publications [6.118–6.121, 6.132, 6.138]. Many studies are concerned with photoelectron spectra and bonding. Relativistic and quasirelativistic DFT- $X_\alpha$  calculations for this purpose are reported, for instance, in Refs. 6.143 and 6.144. The effect of the central atom “inert lone pair” on the coordination compound stereochemistry, discussed in Section 9.2, (originally suggested by Sidgwick [6.145]) has also some important relativistic aspects. Indeed, since the  $s$  states are contracted and stabilized, due to relativistic effects, the  $(6s)^2$  inert pair effect should increase for heavy metals. This explains the tendency of the  $6s^2$  electron pair to remain formally unoxidized in compounds of Tl(I), Pb(II), Bi(III), and so on [6.146]. However, the problem of stereochemistry induced by lone pairs is much more complicated, since it involves excited states via vibronic coupling (Section 9.2).

The essential influence of RE can be easily seen in spectroscopic and optical properties. First of all is the well-known spin–orbital splitting. Concerning the special optical properties induced by RE, one of them is the yellow color of gold [6.147]. The observed refractivity responsible for the color is due to the transition from the valence  $5d$  band to the mainly  $6s$  Fermi level [6.148]. Its sudden onset falls at  $h\nu = 2.4$  eV in accordance with the relativistic calculations. The nonrelativistic calculations move this absorption border much higher in energy, out of the visible region. Thus, in the nonrelativistic approach, gold is white, and only the relativistic effect makes it yellow. Note that for silver the corresponding relativistic rising of  $5d$  orbitals and stabilization of the  $6s$  states is much smaller than for gold, and the absorption border occurs in the ultraviolet region at 3.7 eV, making it white. The absorption itself is a solid-state effect (the transition  $5d^9 6s \rightarrow 5d^8 6s^2$  in atoms is forbidden).

Relativistic calculations of  $f$ -element systems have been reviewed [6.149]; for relativistic calculations of solid-state systems, see Refs. 6.150–6.153.

### SUMMARY NOTES

1. Chemical bonding is an electronic phenomenon. The bonding between two atoms is due to the electrostatic interaction between the (collectivized) electrons and nuclei that move in accordance with the laws of quantum mechanics stipulating wave properties of the electrons and their constructive interference in the area between the nuclei.
2. Differences in chemical bonds should be related to and classified on the basis of their varied electronic structure. The specific features of coordination bonding are due to the participation of the atomic  $d$  or  $f$  electrons which produce three-dimensionally delocalized electronic states,

- resulting in mutually dependent (and nontransferable) metal–ligand bond properties.
3. In molecular orbital description the binding is due to the occupied bonding MOs that are not compensated for by the antibonding ones.
  4. Ligand bonding is characterized by  $\sigma$ ,  $\pi$ , and  $\sigma + \pi$  mono-, di-, and multi-orbital bonds. Uncompensated MOs of di- and multi-orbital bonds produce multiple bonds. A characteristic feature of di- and multi-orbital bonds is the partial mutual compensation of their orbital charge transfers.
  5. Metal–metal bonds may be multi-orbital, producing  $\sigma$ ,  $\pi$ , and  $\delta$  binding.
  6. Modern electronic structure calculations reveal the MOs and total energies, charge distributions, and geometries of coordination systems in good agreement with experimental data.
  7. Relativistic effects are important for heavy-atom transition metal systems producing, in addition to spin–orbital splittings, orbital contraction and other effects, which results in changes in interatomic distances, valence activities, dissociation energies, vibrational frequencies, and other parameters.

### EXERCISES AND PROBLEMS

- 6.1. Formulate the main differences between valence, orbital, and coordination bonding in the classification on electronic structure. What are the shortcomings of the alternative genealogical classification, and why is it inappropriate?
- 6.2. In classification of electronic structure the distinguished features of coordination bonding are due to the participation of  $d$  and/or  $f$  electrons. List these features and show how they are related to the  $d$  and/or  $f$  electronic states. Give examples.
- 6.3. Subject to the ligand influence, pre- and posttransition (and some other) elements with apparently no active  $d$  or  $f$  electrons may form coordination systems with such ligands with properties similar to those of transition metal systems provided the ligands are chosen appropriately. What are the required ligand features that produce  $d$ - or  $f$ -electron properties in nontransition elements?
- 6.4. The most probable MO LCAO energy-level scheme for an octahedral system  $ML_6$  with M as a  $3d$  transition element in Fig. 6.1 is constructed under the assumption that the group overlap integrals  $G(3d, \pi) < G(3d, \sigma) < G(4p, \sigma) < G(4s, \sigma)$ . Use the numerical data in Problems 5.1 and 5.2 to verify whether these inequalities are valid for the complex  $TiF_6^{3-}$ .
- P6.5. Construct an MO energy-level diagram for the case when  $G(3d, \sigma) < G(3d, \pi) < G(4s, \sigma)$ . What essential differences in the properties of systems with such MO diagrams are expected as compared with those having the usual MO scheme in Fig. 6.1?

- 6.6. State the differences between multiorbital bonding in coordination systems and multiple bonds in organic and main-group compounds. Give examples.
- 6.7. Electron spin resonance (ESR) methods allow one to estimate the distribution of the unpaired electrons over the CA and ligands and hence the covalence produced by these electrons (Section 8.4). Can this information serve as a measure of covalence of the CA–ligand bonds?
- 6.8. In di- and multiorbital metal–ligand bonding orbital charge transfer compensation is an important electronic effect. Explain why and how it takes place and what observable properties are influenced by this effect. Give specific examples. Is a similar effect possible in the approximately uniform (nonheterogenic) multiple bonds of organic compounds?
- 6.9. In the examples of ligand bonding 6.1–6.9, the simplest case of H<sub>2</sub> bonding to a metal center is not considered. Explore this case qualitatively. Is the CA–H<sub>2</sub> side-on bonding mono- or diorbital? Find all possible donor and acceptor  $\sigma$  and  $\pi$  orbitals, and relate the results to the case of H<sub>2</sub> coordination to Pt(PH<sub>3</sub>)<sub>2</sub> shown in Example 11.6.
- 6.10. In Example 6.2 the N<sub>2</sub> bonding to the iron atom in FeN<sub>2</sub> is explored numerically. Involving Fig. 6.8, explain why end-on and side-on coordination yield different orbital charge transfers and how the latter affect the properties (bond length, vibrational frequency, and reactivity) of the coordinated molecule.
- 6.11. Referring to the discussion in Example 6.9, explore qualitatively which derivatives of the Zeise salt X<sub>3</sub>Pt(C<sub>2</sub>H<sub>4</sub>)<sup>−</sup>, X = F, Cl, or Br, should weaken the C=C bond in the ethylene  $\pi$  complex.
- 6.12. In Chapter 2, where  $\sigma$  and  $\pi$  bonds are introduced, we emphasized that these two kinds of bonding orbitals have different symmetry. On the other hand, only functions with the same symmetry can be combined to form an MO. How, then, can  $\sigma + \pi$  MOs occur in coordination systems?
- 6.13. At the end of the subsection on  $\sigma + \pi$  bonding in Section 6.3, it is stated and in Section 6.3 it is explained, how, in the presence of strong relativistic effects, the monoorbital, single bond between two atoms may be a mixture of  $\sigma$  and  $\pi$  contributions. Doesn't this result violate the symmetry and angular momentum considerations based on which  $\sigma$  and  $\pi$  bonding are differentiated in Chapter 2?
- 6.14. The three transition metals Cu, Ag, and Au occupy the same column in the periodic table of elements but have significantly different properties: Au is a noble metal, Ag is seminoble, while Cu is very reactive, and the color of these metals is different as well. Explain these differences on the basis of relativistic effects.

## REFERENCES

- 6.1. I. B. Bersuker, in *Brief Chemical Encyclopedia* (Russ.), Vol. 5, Soviet Encyclopedia, Moscow, 1967, p. 627.
- 6.2. R. F. W. Bader and M. E. Stephen, *J. Am. Chem. Soc.* **97**, 7391 (1975).
- 6.3. J. E. Lenard-Jones, *Proc. Roy. Soc. A* **198**, 1 (1949).
- 6.4. M. Gerloch, *Coord. Chem. Rev.* **99**, 117 (1990).
- 6.5. I. B. Bersuker, *The Jahn-Teller Effect*, Cambridge Univ. Press, Cambridge, UK, 2006.
- 6.6. H. Kwart and K. King, *d-Orbitals in the Chemistry of Silicon, Phosphorus and Sulphur*, Springer, Berlin, 1977.
- 6.7. D. V. Korol'kov, *Electronic Structure and Properties of Compounds of Non-transition Elements* (Russ.), Khimia, St. Peterburg, 1992.
- 6.8. W. Kutzelnig, *Angew. Chem. Int. Ed.* **23**, 272 (1984).
- 6.9. B. P. Martinenas, K. K. Eringis, and R. S. Dagis, in *The Theory of Electronic Shells of Atoms and Molecules* (Russ.), Mintis, Vilnius, 1971, p. 294.
- 6.10. R. E. Watson and A. J. Freeman, *Phys. Rev. A* **134**, 1526 (1964); E. Simanek and Z. Sroubek, *Phys. Stat. Solidi* **4**, 251 (1964).
- 6.11. T. Koopmans, *Physica* **1**, 104 (1933).
- 6.12. L. Pauling, *J. Chem. Soc.* 1461 (1948); *Proc. Symp. Coord. Chem.*, Copenhagen, 1953, p. 256.
- 6.13. M. J. C. Dewar, *Bull. Soc. Chim. Fr.* 79 (1951).
- 6.14. J. Chatt and L. A. Duncanson, *J. Chem. Soc.* 2939 (1953).
- 6.15. D. S. Marynick, *J. Am. Chem. Soc.* **106**, 4064 (1984).
- 6.16. M. R. A. Blomberg, U. B. Brandemark, P. E. M. Siegbahn, K. B. Mathisen, and G. Karlström, *J. Phys. Chem.* **89**, 2171 (1985).
- 6.17. I. B. Bersuker, *Zh. Struct. Khim.* **4**, 461 (1963).
- 6.18. P. A. Christiansen and E. A. McCulloch, Jr., *J. Chem. Phys.* **67**, 1877 (1977).
- 6.19. C. W. Bauschlicher, Jr., L. G. M. Pettersson, and E. M. Siegbahn, *J. Chem. Phys.* **87**, 2129 (1987).
- 6.20. C. Veeger and W. E. Newron, eds., *Advances in Nitrogen Fixation*, Nijhoff, Boston, 1991.
- 6.21. H. Bash and D. Cohen, *J. Am. Chem. Soc.* **105**, 3856 (1983).
- 6.22. H. Itoh and A. B. Kunz, *Chem. Phys. Lett.* **64**, 576 (1979).
- 6.23. G. M. Jeung, in A. Veillard, ed., *Quantum Chemistry: The Challenge of Transition Metals and Coordination Chemistry*, NATO ASI Series, Vol. 176, Reidel, Dordrecht, 1986, p. 101.
- 6.24. R. Arratia-Perez and C. Y. Yang, *J. Chem. Phys.* **83**, 4005 (1985).
- 6.25. D. E. Sherwood and M. B. Hall, *Inorg. Chem.* **22**, 93 (1983).
- 6.26. Y. B. Koh and G. G. Christoph, *J. Am. Chem. Soc.* **101**, 1422 (1979).

- 6.27. R. Hoffmann, *Solids and Surfaces: A Chemist's View of Bonding in Extended Structures*, VCH, New York, 1988.
- 6.28. S. Sung and R. Hoffmann, *J. Am. Chem. Soc.* **107**, 578 (1985).
- 6.29. S. Sung, R. Hoffmann, and P. A. Thiel, *J. Phys. Chem.* **90**, 1380 (1986).
- 6.30. H. Bash, *J. Chem. Phys.* **56**, 441 (1972).
- 6.31. J. N. Murrell and C. E. Scollary, *J. Chem. Soc. Dalton Trans.* 1034 (1977).
- 6.32. S. Sakaki, *Theor. Chim. Acta* **30**, 159 (1973).
- 6.33. P. J. Hay, *J. Am. Chem. Soc.* **103**, 1390 (1981).
- 6.34. A. A. Bagatur'ants, O. V. Gritsenko, and I. I. Moiseev, *Koord. Khim.* **4**, 1779 (1978).
- 6.35. T. A. Albright, R. Hoffmann, J. C. Thibeault, and D. L. Thorn, *J. Am. Chem. Soc.* **101**, 3801 (1979).
- 6.36. F. A. Cotton and R. A. Walton, *Multiple Bonds between Metal Atoms*, Clarendon Press, Oxford, 1993.
- 6.37. W. C. Trogler, *J. Chem. Educ.* **57**, 424 (1980).
- 6.38. M. Moscovitz, ed., *Metal Clusters*, Wiley, New York, 1986.
- 6.39. G. P. Kostikova and D. V. Korol'kov, *Uspekhi Khim.* **54**, 591 (1985).
- 6.40. F. A. Cotton, N. F. Curtis, C. B. Harris, B. F. G. Johnson, S. J. Lippard, J. T. Mague, W. R. Robinson, and J. S. Wood, *Science* **145**, 1305 (1964); F. A. Cotton, *Inorg. Chem.* **3**, 334 (1964); F. A. Cotton, in A. F. Williams, C. Floriani, and A. E. Merbach, eds., *Perspectives in Coordination Chemistry*, VCH, New York, 1992, pp. 321–332.
- 6.41. V. G. Kuznetsov and P. A. Koz'min, *IY Conf. Cryst. Chem., Abstracts*, Stiintsa, Kishinev, 1961, p. 74; *Zh. Struct. Khim.* **4**, 55 (1963); F. A. Cotton and C. B. Harris, *Inorg. Chem.* **4**, 330, (1965).
- 6.42. J. G. Norman, Jr. and H. J. Kolari, *J. Chem. Soc. Chem. Commun.* 303 (1974); *J. Am. Chem. Soc.* **97**, 33 (1975).
- 6.43. A. P. Mortola, J. W. Moskowitz, and N. Roch, *Int. J. Quantum Chem., Symp.* **8**, 1974, p. 161; A. P. Mortola, J. W. Moskowitz, N. Roch, C. D. Cowman, and H. B. Gray, *Chem. Phys. Lett.* **32**, 283 (1964).
- 6.44. M. Bernard, *J. Am. Chem. Soc.* **100**, 2354 (1978).
- 6.45. M. B. Hall, in A. Veillard, ed., *Quantum Chemistry: The Challenge of Transition Metals and Coordination Chemistry*, NATO ASI Series, Vol. 176, Reidel, Dordrecht, 1986, p. 391.
- 6.46. A. P. Kl'agina and A. A. Levin, *Koord. Khim.* **10**, 579 (1984).
- 6.47. B. Delley, A. J. Freeman, and D. E. Ellis, *Phys. Rev. Lett.* **50**, 488 (1983).
- 6.48. A. P. Kl'agina, G. L. Gutsev, V. D. Lutatskaya, and A. A. Levin, *Zh. Neorg. Khim.* **29**, 2834 (1984).
- 6.49. F. A. Cotton, *Acc. Chem. Res.* **2**, 240 (1969).
- 6.50. L. Dubicki and R. L. Martin, *Inorg. Chem.* **9**, 673 (1970).
- 6.51. J. G. Norman and H. J. Kolari, *J. Am. Chem. Soc.* **100**, 791 (1978).
- 6.52. B. E. Bursten and F. A. Cotton, *Inorg. Chem.* **20**, 3042 (1981).
- 6.53. I. B. Bersuker and Yu. G. Titova, *Teor. Exp. Khim.* **6**, 469 (1970).
- 6.54. P. S. Braterman, *Struct. Bond.* **10**, 57 (1972).

- 6.55. D. L. Thorn and R. Hoffmann, *Inorg. Chem.* **17**, 126 (1978); R. H. Summerville and R. Hoffmann, *J. Am. Chem. Soc.* **101**, 3821 (1979).
- 6.56. H.-J. Freund and G. Hohlneicher, *Teor. Chim. Acta* **51**, 145 (1979); H.-J. Freund, B. Dick, and G. Hohlneicher, *ibid.* **57**, 181 (1980).
- 6.57. A. A. Low, K. L. Kunze, P. J. MacDougall, and M. B. Hall, *Inorg. Chem.* **30**, 1079 (1991); *ibid.* **32**, 3880 (1993).
- 6.58. A. Rosa and E. J. Baerends, *New J. Chem.* **15**, 815 (1991); R. Wiest, A. Strich, and M. Benard, *ibid.* **15**, 801 (1991).
- 6.59. B. J. Morris-Sherwood, C. B. Powell, and M. B. Hall, *J. Am. Chem. Soc.* **106**, 5079 (1984); A. L. Sargent and M. B. Hall, *ibid.* **111**, 1563 (1989).
- 6.60. I. H. Hillier and V. R. Saunders, *Mol. Phys.* **22**, 1025 (1971).
- 6.61. J. Demuynck and A. Veillard, *Theor. Chim. Acta* **28**, 241 (1973).
- 6.62. M. Coutiere, J. Demuynck, and A. Veillard, *Theor. Chim. Acta* **27**, 281 (1972).
- 6.63. D. W. Turner, in H. A. O. Hill and P. Day, eds., *Physical Methods in Advanced Inorganic Chemistry*, Interscience, Oxford, 1968, p. 79.
- 6.64. M. F. Guest, in M. Dupuis, ed., *Supercomputer Simulation in Chemistry*, Lecture Notes in Chemistry, Vol. 44, Springer-Verlag, Heidelberg, 1986, p. 98.
- 6.65. J. Schirmer and L. S. Cederbaum, *J. Phys. B* **11**, 1889 (1978); J. Schirmer, L. S. Cederbaum, and O. Walter, *Phys. Rev.* **28**, 1237 (1983).
- 6.66. I. M. Hillier, in A. Veillard, ed., *Quantum Chemistry: The Challenge of Transition Metals and Coordination Chemistry*, NATO ASI Series, Vol. 176, Reidel, Dordrecht, 1986, p. 143.
- 6.67. A. Veillard, *Chem. Commun.* 1022 (1969); 1427 (1969).
- 6.68. M.-M. Rohmer, and A. Veillard, *J. Chem. Soc. Chem. Commun.* 250 (1973).
- 6.69. C. D. Batich, *J. Am. Chem. Soc.* **98**, 7585 (1976).
- 6.70. K. H. Johnson, *Adv. Quant. Chem.* **7**, 143 (1973); *Annu. Rev. Phys. Chem.* **26**, 39 (1975).
- 6.71. K. H. Johnson, J. C. Norman, Jr., and J. W. D. Connolly, in F. Herman, A. D. McLean, and R. K. Nesbet, eds., *Computational Methods for Large Molecules and Localized States in Solids*, Plenum, New York, 1973, p. 161.
- 6.72. P. Decleva, G. Fronzoni, and A. Lisini, in J. K. Labanowski and J. W. Andzelm, eds., *Density Functional Methods in Chemistry*, Springer, New York, 1991, p. 323.
- 6.73. C. Daul, H.-H. Gudel, and J. Weber, *J. Chem. Phys.* **98**, 4023 (1993).
- 6.74. D. R. Salahub, *Adv. Chem. Phys.* **69**, 447 (1987).
- 6.75. D. A. Brown, W. I. Chambers, and N. I. Fitzpatrick, *Inorg. Chim. Acta Rev.* **6**, 7 (1972).
- 6.76. P. G. Burton, *Coord. Chem. Rev.* **12**, 37 (1974).
- 6.77. E. J. Baerends and P. Ros, *Mol. Phys.* **30**, 1735 (1975).
- 6.78. A. Veillard, in XV ICCO (Internat. Conf. Coord. Chem.) Moscow, 1973, Section Lecture (preprint).
- 6.79. J. A. Tossel and W. N. Lipscomb, *J. Am. Chem. Soc.* **94**, 1505 (1972).
- 6.80. J. W. Moskowitz, C. Hollister, C. J. Hornback, and H. Bash, *J. Chem. Phys.* **53**, 2570 (1970).
- 6.81. J. Demuynck, A. Veillard, and U. Wahlgren, *J. Am. Chem. Soc.* **95**, 5563 (1973).



- 6.82. J. A. Connor, I. H. Hillier, V. R. Saunders, M. H. Wood, and M. Barber, *Mol. Phys.* **24**, 497 (1972).
- 6.83. H. Johansen, *Chem. Phys. Lett.* **17**, 569 (1972).
- 6.84. P. D. Dacre and H. Elder, *J. Chem. Soc (Dalton)* **13**, 1426 (1972).
- 6.85. J. Fischer, A. Veillard, and R. Weiss, *Theor. Chim. Acta* **24**, 317 (1972).
- 6.86. M. B. Hall, M. F. Guest, and I. H. Hillier, *Chem. Phys. Lett.* **15**, 592 (1972).
- 6.87. B. L. Kalman and W. Richardson, *J. Chem. Phys.* **55**, 4443 (1971).
- 6.88. J. Denmynck, A. Strich, and A. Veillard, *Nouv. J. Chim.* **1**, 217 (1977).
- 6.89. D. Reinen and C. Friebe, *Inorg. Chem.* **23**, 791 (1984); D. Reinen and M. Atanasov, *Chem. Phys.* **136**, 27 (1989).
- 6.90. R. Akeson, L. G. M. Pettersson, M. Sandstrom, and U. Wahlgren, *J. Phys. Chem.* **96**, 150 (1992).
- 6.91. A. Veillard, A. Dedieu, and M.-M. Rohmer, in K. Fukui and P. Pullman, eds., *Horizons of Quantum Chemistry*, Reidel, Dordrecht, 1980, p. 197; M.-M. Rohmer, A. Dedieu, and A. Veillard, *Chem. Phys.* **77**, 449 (1983).
- 6.92. G. Loew, in E. I. Solomon and A. B. P. Lever, eds., *Inorganic Electronic Structure and Spectroscopy*, Vol. II, *Applications and Case study*, Wiley, New York, 1999, p. 451.
- 6.93. K. Ohno, in K. Fukui and P. Pullman, eds., *Horizons of Quantum Chemistry*, Reidel, Dordrecht, 1980, p. 245; H. Kashiwagi and S. Obara, *Int. J. Quant. Chem.* **20**, 843 (1981).
- 6.94. F. U. Axe, L. Chantranupong, A. Waleh, J. Collins, and G. H. Loew, in *The Challenge of d and f Electrons. Theory and Computation*, ACS Series 394, Washington, DC, 1989, p. 339.
- 6.95. A. Strich and A. Veillard, *Theor. Chim. Acta* **60**, 379 (1981); *Nouv. J. Chim.* **7**, 347 (1983).
- 6.96. GAMESS: M. W. Schmidt et al., distributed by M. W. Schmidt, Dept. Chemistry, Iowa State Univ., Ames.
- 6.97. R. L. Williamson and M. B. Hall, *Int. J. Quant. Chem. Symp.* **21**, 503 (1987).
- 6.98. R. F. Fenske and J. R. Jensen, *J. Chem. Phys.* **71**, 3374 (1979).
- 6.99. M. F. Guest, I. H. Hillier, A. A. McDowel, and M. Berry, *Mol. Phys.* **41**, 519 (1980).
- 6.100. T. E. Taylor and M. B. Hall, *Chem. Phys. Lett.* **114**, 338 (1985).
- 6.101. K. Faegri and J. Almlof, *Chem. Phys. Lett.* **107**, 121 (1984).
- 6.102. H. P. Lüthi, J. H. Ammeter, J. Almlöf, and K. Faegri, Jr., *J. Chem. Phys.* **77**, 2002 (1982).
- 6.103. J. Almlof, K. Faegri, Jr., B. E. R. Schilling, and H. P. Lüthi, *Chem. Phys. Lett.* **106**, 266 (1983).
- 6.104. K. Faegri, Jr., J. Almlöf, and H. P. Lüthi, *J. Organomet. Chem.* **249**, 303 (1983).
- 6.105. H. P. Lüthi, P. E. M. Siegbahn, and J. Almlöf, *J. Phys. Chem.* **89**, 2156 (1985).
- 6.106. N. Rösch, H. Jörg, and B. I. Dunlap, in A. Veillard, ed., *Quantum Chemistry: The Challenge of Transition Metals and Coordination Chemistry*, NATO ASI Series C, Vol. 176, Reidel, Dordrecht, 1986, p. 179.

- 6.107. T. Ziegler and V. Tschinke, in J. K. Labanowski and J. W. Andzelm, eds., *Density Functional Methods in Chemistry*, Springer, New York, 1991, p. 139.
- 6.108. J. W. D. Connolly, *Solid State Commun.* **12**, 313 (1973).
- 6.109. G. K. Wertheim and S. Hufner, *Phys. Rev. Lett.* **28**, 1028 (1972).
- 6.110. R. P. Messmer, C. W. Tucker, and K. H. Johnson, *Surf. Sci.* **42**, 341 (1974).
- 6.111. M. Barber, J. Clark, A. Hinchliffe, and D. S. Urch, *J. Chem. Soc. Faraday Trans. 2* **74**, 681 (1978).
- 6.112. D. R. Salahub, in D. R. Salahub and N. Russo, eds., *Metal-Ligand Interaction: From Atoms, to Clusters, to Surfaces*, Kluwer, Dordrecht, 1992, p. 311.
- 6.113. N. Russo, *ibid.*, p. 341.
- 6.114. T. Ziegler, *ibid.*, p. 367.
- 6.115. A. J. Freeman, S. Tang, S. H. Chou, Y. e Ling, and B. Delley, in J. K. Labanowski and J. W. Andzelm, eds., *Density Functional Methods in Chemistry*, Springer, New York, 1991, p. 61.
- 6.116. L. Noodleman, D. A. Case, and E. J. Baerends, *ibid.* p. 109.
- 6.117. L. Noodleman and D. A. Case, *Adv. Inorg. Chem.* **38**, 423 (1992); E. I. Solomon, F. Tuczek, D. E. Root, and C. A. Brown, *Chem. Rev.* **94**, 827 (1994).
- 6.118. D. A. Case, *Annu. Rev. Phys. Chem.* **33**, 151 (1982).
- 6.119. P. Pyykko, *Chem. Rev.* **88**, 563 (1988).
- 6.120. T. Ziegler, J. G. Snijders, and E. J. Baerends, in D. R. Salahub and M. C. Zerner, eds., *The Challenge of d and f Electrons. Theory and Computation*, ACS Symposium Series 394, Washington, DC, 1989, p. 322.
- 6.121. G. L. Malli, ed., *Relativistic Effects in Atoms, Molecules and Solids*, Plenum, New York, 1983.
- 6.122. P. Pyykko and J. P. Desclaux, *Acc. Chem. Res.* **12**, 276 (1979).
- 6.123. R. G. Boyd, A. C. Larson, and J. T. Waler, *Phys. Rev.* **129**, 1629 (1963).
- 6.124. B. Fricke, *Struct. Bond. (Berlin)* **21**, 89 (1975).
- 6.125. D. M. Bylander and L. Kleiman, *Phys. Rev. Lett.* **51**, 889 (1983).
- 6.126. J. J. Low and W. A. Goddard III, *J. Am. Chem. Soc.* **106**, 6928 (1984); **108**, 6115 (1986); *Organometalics* **5**, 609 (1986).
- 6.127. P. Pyykko, J. G. Snijders, and E. J. Baerends, *Chem. Phys. Lett.* **83**, 432 (1981).
- 6.128. K. S. Krasnov, V. S. Timoshinin, T. G. Danilova, and S. V. Khandozhko, *Handbook of Molecular Constants of Inorganic Compounds*, Israel Program for Scientific Translations, Jerusalem, 1970.
- 6.129. P. Pyykko, *J. Chem. Soc. Faraday Trans. 2* **75**, 1256 (1979).
- 6.130. P. Pyykko and J. P. Desclaux, *Chem. Phys.* **34**, 261 (1978).
- 6.131. T. Ziegler, V. Tschinke, and A. Becke, *Polyhedron* **6**, 685 (1987).
- 6.132. P. Pyykko, in S. Willson, I. P. Grant, and B. L. Gyorffy, eds., *The Effects of Relativity in Atoms, Molecules and the Solid-State*, Plenum, New York, 1991.
- 6.133. A. V. Dzhalavyan, E. G. Rakov, and A. S. Dudin, *Russ. Chem. Rev. (Engl. transl.)* **52**, 960 (1983).
- 6.134. J. M. Wisner, T. J. Bartczak, J. A. Ibers, J. J. Low, and W. A. Goddard, *J. Am. Chem. Soc.* **108**, 347 (1986).

- 6.135. A. Schmuck, P. Pyykko, and K. Seppelt, *Angew. Chem. Int. Ed. Engl.* **29**, 213 (1990).
- 6.136. B. D. El-Issa, P. Pyykko, and H. M. Zanati, *Inorg. Chem.* **30**, 2781 (1991).
- 6.137. P. Pyykko and J. Jove, *New J. Chem.* **15**, 717 (1991).
- 6.138. K. S. Pitzer, *Acc. Chem. Res.* **12**, 271 (1979).
- 6.139. K. S. Pitzer, *J. Chem. Phys.* **63**, 1032 (1975); *Chem. Commun.*, 760 (1975).
- 6.140. D. Schield, R. Pflaum, K. Sattler, and E. Recknagel, *J. Phys. Chem.* **91**, 2649 (1987).
- 6.141. I. B. Bersuker, S. S. Budnikov, and B. A. Leizerov, *Int. J. Quant. Chem.* **11**, 543 (1977).
- 6.142. F. A. Cotton and C. D. Harris, *Inorg. Chem.* **6**, 369 (1967).
- 6.143. R. Arratia-Perez and G. L. Mali, *Chem. Phys. Lett.* **125**, 143 (1986); *J. Chem. Phys.* **84**, 5891 (1986); F. Zuloaga, R. Arratia-Perez, and G. L. Mali, *J. Phys. Chem.* **90**, 4491 (1986).
- 6.144. H. Chermette and A. Goursot, in J. P. Dahl and J. Avery, eds., *Local Density Approximation in Quantum Chemistry and Solid State Physics*, Plenum, New York, 1984, p. 635.
- 6.145. N. V. Sidgwick, *The Covalent Link in Chemistry*, Cornell Univ. Press, Ithaca, NY, 1933.
- 6.146. M. L. Cohen and V. Heine, *Solid State Phys.* **24**, 37 (1970).
- 6.147. S. Kupratakal, *J. Phys. C: Solid State Phys.* **3**, S109 (1970).
- 6.148. N. E. Christensen and B. O. Seraphin, *Phys. Rev. B* **4**, 3321 (1971).
- 6.149. P. Pyykko, *Inorg. Chim. Acta* **139**, 243 (1987).
- 6.150. G. Trinquier and R. Hoffmann, *J. Phys. Chem.* **88**, 6696 (1984).
- 6.151. L. Visscher, P. J. C. Aerts, and W. C. Nieuwport, *J. Chem. Phys.* **96**, 2910 (1992); L. Visscher and W. C. Nieuwport, *Theor. Chim. Acta* **88**, 447 (1994).
- 6.152. M. Dolg, H. Stoll, and H. Preuss, *J. Chem. Phys.* **90**, 1730 (1989); Kuechle, M. Dolg, and H. Preuss, *J. Chem. Phys.* **100**, 7535 (1994).
- 6.153. T. R. Cundari and W. Stevens, *J. Chem. Phys.* **98**, 5555 (1993).

---

# 7

---

## **ELECTRONIC CONTROL OF MOLECULAR SHAPES AND TRANSFORMATIONS VIA VIBRONIC COUPLING**

*Vibronic coupling conveys a bridge between electronic structure and nuclear configurations realizing electronic influence on the formation and transformation of molecular shapes, as well as their spontaneous symmetry breaking. The mechanism of vibronic coupling is one of the modern problems of theoretical chemistry which has many applications.*

In the development of quantum chemistry the main problem was electronic structure calculations at fixed nuclei, while the backward influence of electrons on the nuclear configurations received much less attention. Meanwhile many important chemical phenomena, including chemical transformations, are determined by nuclear displacements induced by electron rearrangements. Any changes of molecular systems under external influence, including the influence of another molecule involved in collisions (chemical reactions), begin with perturbations in the less inertial electronic structure which affects the heavy nuclear framework via vibronic coupling. The latter thus plays an important role in the description of molecular and condensed matter properties.

We begin this chapter with a discussion of pure vibrations and proceed to vibronic coupling, orbital vibronic coupling, and the Jahn–Teller effect, as well as one of the important consequences—the proof that nuclear configuration changes involve necessarily at least two electronic states (the TEST paradigm).

## 7.1. MOLECULAR VIBRATIONS

### Adiabatic Approximation

The idea of molecular vibrations is based on the assumption that nuclear and electronic motions can be approximately separated and that there exists a nuclear framework in which each nucleus has a stable (energy minimum) position. For stable systems and in the absence of electronic degeneracy or pseudodegeneracy this assumption can be proved in the *adiabatic approximation*. In view of its general importance, we consider this approximation in some detail and disclose the criterion of its validity [7.1–7.6].

The adiabatic approximation is based on the strong inequality of the masses and velocities of electrons and nuclei. Since the nuclear mass  $M$  is about 2000 times that of the electron  $m$ , the velocity of the latter is much greater than that of the former. Therefore, it can be assumed that at every instant position of the nuclei, the electronic distribution is stationary. In other words, because of the relatively slow motions of the nuclei, the electronic state is in time to relax instantly to the changing nuclear positions (i.e., the electrons follow the nuclei *adiabatically*), and the motions of the nuclei are determined by the instant averaged field of the electrons. Mathematically this means that the electron distribution in space is determined by the nuclear coordinates, not by their speed.

This assumption enables us to solve the overall problem of electron and nuclear motions in two steps: (1) solving the problem of electronic motion for fixed nuclei and then (2) using the obtained in this way electronic energy as a function of nuclear coordinates as the potential energy of nuclear motions. This procedure ignores the nonadiabatic changes of the electronic structure under nuclear displacements (meaning the dependence of electronic states not only on the nuclear positions but also on their speed, acceleration, etc.), and this is the most restrictive feature of the adiabatic approximation.

Let us refer to a more rigorous consideration. The Schrödinger equation (1.5) for the system as a whole that includes  $n$  electrons and  $N$  nuclei can be written as follows:

$$H\Psi(r, Q) = E\Psi(r, Q) \quad (7.1)$$

where (as elsewhere in this book)  $r$  and  $Q$  denote the entire set of coordinates of the electrons  $r_i, i = 1, 2, \dots, n$  and nuclei  $Q_\alpha, \alpha = 1, 2, \dots, N$ , respectively.

Divide the total Hamiltonian  $H$  into three parts:

$$H = H_r + H_Q + V(r, Q) \quad (7.2)$$

where  $H_r$  is the electronic part including the kinetic energy of the electrons and the interelectron electrostatic interaction,  $H_Q$  is the kinetic energy of the nuclei,  $H_Q = -\sum_{\alpha} (\hbar^2/2M_{\alpha})\Delta_{\alpha}$  (where  $M_{\alpha}$  are the nuclear masses), and  $V(r, Q)$  is the energy of the interaction of the electrons with the nuclei plus the internuclear

repulsion:

$$V(r, Q) = - \sum_{i, \alpha} \frac{e^2 Z_\alpha}{|\mathbf{r}_i - \mathbf{R}_\alpha|} + \frac{1}{2} \sum'_{\alpha, \beta} \frac{e^2 Z_\alpha Z_\beta}{|\mathbf{R}_\alpha - \mathbf{R}_\beta|} \quad (7.3)$$

Here  $\mathbf{R}_\alpha$  are the vector coordinates of the nuclei; their relation to the  $Q_\alpha$  coordinates is clarified below (the coefficient  $\frac{1}{2}$  in the last sum is introduced to offset double summation, while the prime indicates that the terms with  $\alpha = \beta$  should be excluded).

The operator  $V(r, Q)$  can be expanded in a series of small displacements of the nuclei about the point  $Q_\alpha = Q_{\alpha 0} = 0$  chosen as the origin:

$$V(r, Q) = V(r, 0) + \sum_{\alpha} \left( \frac{\partial V}{\partial Q_\alpha} \right)_0 Q_\alpha + \frac{1}{2} \sum'_{\alpha, \beta} \left( \frac{\partial^2 V}{\partial Q_\alpha \partial Q_\beta} \right)_0 Q_\alpha Q_\beta + \dots \quad (7.3')$$

Considering the first term of this expansion as the potential energy of the electrons in the field of fixed nuclei, one can solve the electronic part of the Schrodinger equation, the *electronic equation*

$$[H_r + V(r, 0) - \varepsilon'_k] \varphi_k(r) = 0 \quad (7.4)$$

and obtain a set of energies  $\varepsilon'_k$  and wavefunctions  $\varphi_k(r)$  for the given nuclear configuration corresponding to the point  $Q_{\alpha 0}$ . In order to see how these solutions vary under nuclear displacements, the full Schrödinger equation (7.1) must be solved. Rigorously, the total wavefunction  $\Psi(r, Q)$  can be sought for in the form of an expansion over the set of electronic functions  $\varphi_k(r)$ :

$$\Psi(r, Q) = \sum_k \chi_k(Q) \varphi_k(r) \quad (7.5)$$

where the expansion coefficients  $\chi_k(Q)$  depend on the nuclear coordinates. Substituting (7.5) into Eq. (7.1) and taking into account Eq. (7.4), we obtain, after some simple transformations, the following infinite system of coupled equations for the functions  $\chi_k(Q)$  (the prime at the sum means that the term with  $m = k$  is excluded):

$$[H_Q + \varepsilon_k(Q) - E] \chi_k(Q) + \sum'_m W_{km}(Q) \chi_m(Q) = 0 \quad k = 1, 2, \dots \quad (7.6)$$

where  $W_{km}(Q)$  denotes the electronic matrix element of the *vibronic interaction*  $W$  [7.2, 7.3], that is, the part of the electron–nucleus interaction  $V(r, Q)$  in

Eq. (7.3') that depends on  $Q$ :

$$\begin{aligned} W(r, Q) &= V(r, Q) - V(r, 0) \\ &= \sum_{\alpha} \left( \frac{\partial V}{\partial Q_{\alpha}} \right)_0 Q_{\alpha} + \frac{1}{2} \sum_{\alpha, \beta} \left( \frac{\partial^2 V}{\partial Q_{\alpha} \partial Q_{\beta}} \right)_0 Q_{\alpha} Q_{\beta} + \dots \end{aligned} \quad (7.7)$$

and

$$\varepsilon_k(Q) = \varepsilon'_k + W_{kk}(Q) \quad (7.8)$$

is the electronic energy as a function of nuclear coordinates called *adiabatic potential energy surface* (APES). In the absence of electronic degeneracy or pseudodegeneracy the APES equals the potential energy of the nuclei in the mean field of the electrons in the state  $\varphi_k(r)$ .

It is seen from the system of coupled equations (7.6) that if the vibronic mixing of different electronic states is ignored [ $W_{km}(Q) = 0$  for  $k \neq m$ ], the coupling between these states vanishes and the system of equations decomposes into a set of simple equations for given  $k$ :

$$[H_Q + \varepsilon_k(Q) - E]\chi_k(Q) = 0 \quad (7.9)$$

Each of these equations represents the Schrödinger equation for the nuclei that move in the mean field of electrons in the state  $\varphi_k(r)$ , *the equation of nuclear motions*. In other words, the motions of the nuclei and electrons are separated and the problem as a whole can be solved in the two stages mentioned above. In the first stage the electronic states  $\varphi_k(r)$  are determined as solutions of Eq. (7.4) and used to calculate the potential energy of the nuclei  $\varepsilon_k(Q)$  by Eq. (7.8). In the second stage the wavefunctions  $\chi_k(Q)$  and energies  $E$  of the nuclei are evaluated after Eq. (7.9); the total wavefunction is  $\Psi(r, Q) = \varphi_k(r)\chi_k(Q)$ . This is the *simple adiabatic approximation, or the Born–Oppenheimer approximation*.

Thus the simple adiabatic approximation is valid if and only if the terms of the vibronic mixing of different electronic states in Eq. (7.6) can be ignored. It can be shown [7.1–7.5] that this is possible if the energy spacing of the vibrations, the vibrational quanta  $\hbar\omega$  in the state under consideration, are much smaller than the electronic energy gap to the other states:

$$\hbar\omega \ll \varepsilon'_k - \varepsilon'_j \quad (7.10)$$

This inequality can be considered as a *criterion of the adiabatic approximation*; it remains the same in more rigorous treatments [7.1]. The physical meaning of criterion (7.10) becomes clear when one considers that approximately the vibrational frequency  $\omega$  characterizes the speed of nuclear motion, while  $\varepsilon'_k - \varepsilon'_j$  reflects the “speed” of electronic motion.

In a fuller treatment of the adiabatic approximation, all the terms of  $V(r, Q)$  from Eq. (7.3') are introduced into the electronic Eq. (7.4):

$$[H_r + V(r, Q) - \varepsilon_k(Q)] \varphi_k(r, Q) = 0 \quad (7.11)$$

Here the solutions  $\varepsilon_k(Q)$  and  $\varphi_k(r, Q)$  depend on  $Q$  as parameters, and in the system of coupled equations (7.6)  $W_{km}(Q)$  are replaced by matrix elements of the so-called operator of nonadiabacity, which is also determined by the vibronic interactions  $W$ . In this version of the adiabatic approximation separation of motions of the electrons and nuclei is ultimately determined by the same type of simplification as in the previous one—by ignoring the vibronic mixing of different electronic states.

However, in detail, this approach, called *the adiabatic approximation* (or *full adiabatic approximation*) is somewhat different from the Born–Oppenheimer (or *simple adiabatic*) approximation. The full adiabatic approximation, if applicable [i.e., when criterion (7.10) is satisfied], yields more accurate results than the simple approach. Some estimates of orders of magnitudes may be obtained using the *order of smallness* (or *parameter of smallness*)  $a = (m/M)^{1/4} \approx 0.15$ . It can be shown [7.5] that the neglected terms in the simple adiabatic approximation, *provided that the criterion (7.10) is satisfied*, are of the order of  $a^2 \approx 2.3 \times 10^{-2}$ , while those of the full adiabatic approximation are of the order of  $a^3 \approx 3.4 \times 10^{-3}$ , and the ratio of averaged velocities of the nuclei and electrons is also of the order of  $a^3$ . Thus the simple adiabatic approximation is less accurate than the full one.

However, when criterion (7.10) is *not* satisfied, Eq. (7.6), based on the simple adiabatic approximation, is a more suitable starting point to consider the role of the electronic states in the origin of special nuclear nonadiabatic (and/or nonvibrational) motions.

The adiabatic approximation is of great importance to chemistry. *Without the adiabatic approximation even the notion of nuclear configuration (molecular shape) cannot be defined rigorously.* Therefore, when a specific molecular configuration is considered, the validity of the adiabatic approximation is implied. However, in many cases this approximation is not valid (Sections 7.3 and 7.4).

### Normal Coordinates and Harmonic Vibrations

For stable molecular systems in nondegenerate states Eq. (7.9), for the nuclear motions, describes molecular vibrations. Indeed, a stable system means that the APES  $\varepsilon(Q)$  has a minimum at a certain point  $Q = Q_0$ ; the solution of Eq. (7.9) with such a potential, as shown below, yields nuclear vibrations at this point.

Significant simplification of Eq. (7.9) allowing for its direct solution is reached in the harmonic approximation by means of *normal coordinates*. With  $N$  nuclei, (7.9) is an equation of  $3N$  coordinates  $\mathbf{R}_\alpha(X_\alpha, Y_\alpha, Z_\alpha)$ ,  $\alpha = 1, 2, \dots, N$ ; after excluding the coordinates describing the rotation and translation of the system as a whole, it transforms into an equation of  $3N - 6$  variables. If the APES as a



function of these variables has only one absolute minimum at  $\mathbf{R}_\alpha = \mathbf{R}_{\alpha 0}$ , then the function  $\varepsilon(\mathbf{R}_\alpha)$  near this point can be approximated by a paraboloid (quadratic function of  $R_\alpha$ ). This is the *harmonic approximation*.

In the harmonic approximation the function  $\varepsilon(\mathbf{R}_\alpha)$ , which is a quadratic form of the variables, can be reduced to the so-called canonical form. The latter means that the variable  $\mathbf{R}_\alpha$  can be transformed (by unitary transformations, Section 3.1) such that in the new variables there are only quadrates of coordinates and no cross-terms in the potential. In other words, the possibility of reducing the quadratic function  $\varepsilon(\mathbf{R}_\alpha)$  to its canonical form means that there are new coordinates  $Q_\alpha$ , instead of  $\mathbf{R}_\alpha(X_\alpha, Y_\alpha, Z_\alpha)$ , such that in the new coordinates the potential energy  $U$  is

$$U(Q_\alpha) = \frac{1}{2} \sum_{\alpha} K_{\alpha} Q_{\alpha}^2 \quad (7.12)$$

that is,  $U$  does not contain crossing terms of the type  $Q_{\alpha} Q_{\beta}$ , and in this case the constant  $K_{\alpha} = M_{\alpha} \omega_{\alpha}^2$  is the force constant. If in the new coordinates realizing the canonical form of the APES (7.12), the operator of kinetic energy of the nuclei [see (7.2)]  $-\sum_{\alpha} (\hbar^2/2M_{\alpha}) \partial^2/\partial Q_{\alpha}^2$  is also an additive function of  $Q_{\alpha}$  (i.e., it has no cross-terms  $\partial^2/\partial Q_{\alpha} \partial Q_{\beta}$ ), then the  $Q_{\alpha}$  coordinates are *normal coordinates*.

Thus in normal coordinates  $Q_{\alpha}$  Eq. (7.9) decomposes into  $3N-6$  equations, each of which is the *equation of the harmonic oscillator*

$$\frac{-\hbar^2}{2M_{\alpha}} \frac{d^2 \chi_{\alpha}}{dQ_{\alpha}^2} + \frac{1}{2} M_{\alpha} \omega_{\alpha}^2 Q_{\alpha}^2 \chi_{\alpha} = E_{\alpha} \chi_{\alpha} \quad (7.13)$$

where  $M_{\alpha}$  is the *reduced mass* of the normal vibration  $\alpha$  and  $\omega_{\alpha}$  is its frequency. Quantum mechanics gives a direct solution of this equation with eigenvalues:

$$E_{n\alpha} = \hbar \omega_{\alpha} (n_{\alpha} + \frac{1}{2}) \quad (7.14)$$

where  $n_{\alpha} = 0, 1, 2, \dots$  is the vibrational quantum number and eigenfunctions  $\chi_{n\alpha}(Q_{\alpha})$  (the index  $\alpha$  is omitted below for simplicity) are

$$\chi_n(Q) = \left( \frac{a}{2^n n! \pi^{1/2}} \right)^{1/2} \exp\left( -\frac{a^2 Q^2}{2} \right) H_n(aQ) \quad (7.15)$$

where  $H_n(y)$  is a Hermitian polynomial

$$H_n(y) = (-1)^n \exp(y^2) \frac{d^n \exp(-y^2)}{dy^n} \quad (7.16)$$

and

$$a = \left( \frac{M\omega}{\hbar} \right)^{1/2} \quad (7.17)$$

In particular, for the ground state  $n = 0$

$$E_0 = \frac{\hbar\omega}{2} \quad (7.18)$$

$$\chi_0(Q) = \left(\frac{M\omega}{\hbar\pi}\right)^{1/4} \exp\left(\frac{-M\omega Q^2}{2\hbar}\right) \quad (7.19)$$

It is important that  $\omega_\alpha$  is the same frequency as in mechanical vibration with the potential energy  $\frac{1}{2}M_\alpha\omega_\alpha^2 Q_\alpha^2$  of the assumed harmonic approximation. This means that  $\omega_\alpha$  is a solution of the equation of mechanical vibrations:

$$\frac{d^2 Q_\alpha}{dt^2} + \omega_\alpha^2 Q_\alpha^2 = 0 \quad (7.20)$$

In other words, if one approximates the APES by a quadratic term  $U(Q) = \frac{1}{2}K_\alpha Q_\alpha^2$ , then, taking  $K_\alpha = M_\alpha\omega_\alpha^2$ , one obtains directly the frequency of normal vibrations  $\omega_\alpha$ . To do this, knowledge of the normal coordinates  $Q_\alpha$ , the curvature  $K_\alpha$  of the APES at the point of the minimum in the direction  $Q_\alpha$ , and the reduced mass  $M_\alpha$  is needed.

The methods of determination of normal coordinates are described in detail in manuals on vibrational spectra [7.7–7.9]. In coordination compounds with high local symmetry the group-theoretical rules considered in Section 3.4 can be very useful. Indeed, the Hamiltonian in the Schrödinger equation (7.9) for the nuclear motions has the same symmetry as the molecular framework. Therefore, its eigenvalues and eigenfunctions transform as (belong to) the IrReps (types of symmetry) of the group of symmetry of the system (Appendix 1). In the harmonic approximation Eq. (7.13) describes normal vibrations (vibrations in normal coordinates), and hence the IrReps of the group determine the possible types of symmetry of these vibrations, the shape of the normal coordinates, the degeneracy of the vibrational frequencies, and so on. As shown in Section 3.5, using the methods of group theory, one can relatively easily determine the normal vibrations and their symmetry characteristics (see Example 3.5 and Problem 8.3).

Figures 7.1–7.3 show the form of the most important normal vibrations of octahedral, tetrahedral, triangular, and square-planar complexes, while Table 7.1 gives the expressions of normal coordinates  $Q_\alpha$  in Cartesian coordinates  $X_\alpha, Y_\alpha, Z_\alpha$ .

Similar to wavefunctions of degenerate states that have the same energies, degenerate vibrational modes (vibrations that belong to irreducible representations  $E, T, \dots$ ) have the same frequency, and each normal coordinate of the degenerate set is undefined in the sense that any of their linear combinations is also a normal coordinate. In particular, the shape of twofold  $E(Q_2, Q_3)$  (called *tetragonal*) and threefold  $T_2(Q_4, Q_5, Q_6)$  (called *trigonal*) vibrations given in Table 7.1 and Figs. 7.1 and 7.2, although most usable, are conventional within any linear combination of the two and three degenerate vibrations, respectively.

If there are two or more normal coordinates of the same symmetry (e.g.,  $T_2'$  and  $T_2''$  in a tetrahedron, Table 7.1), they interact, mix (similar to the case of

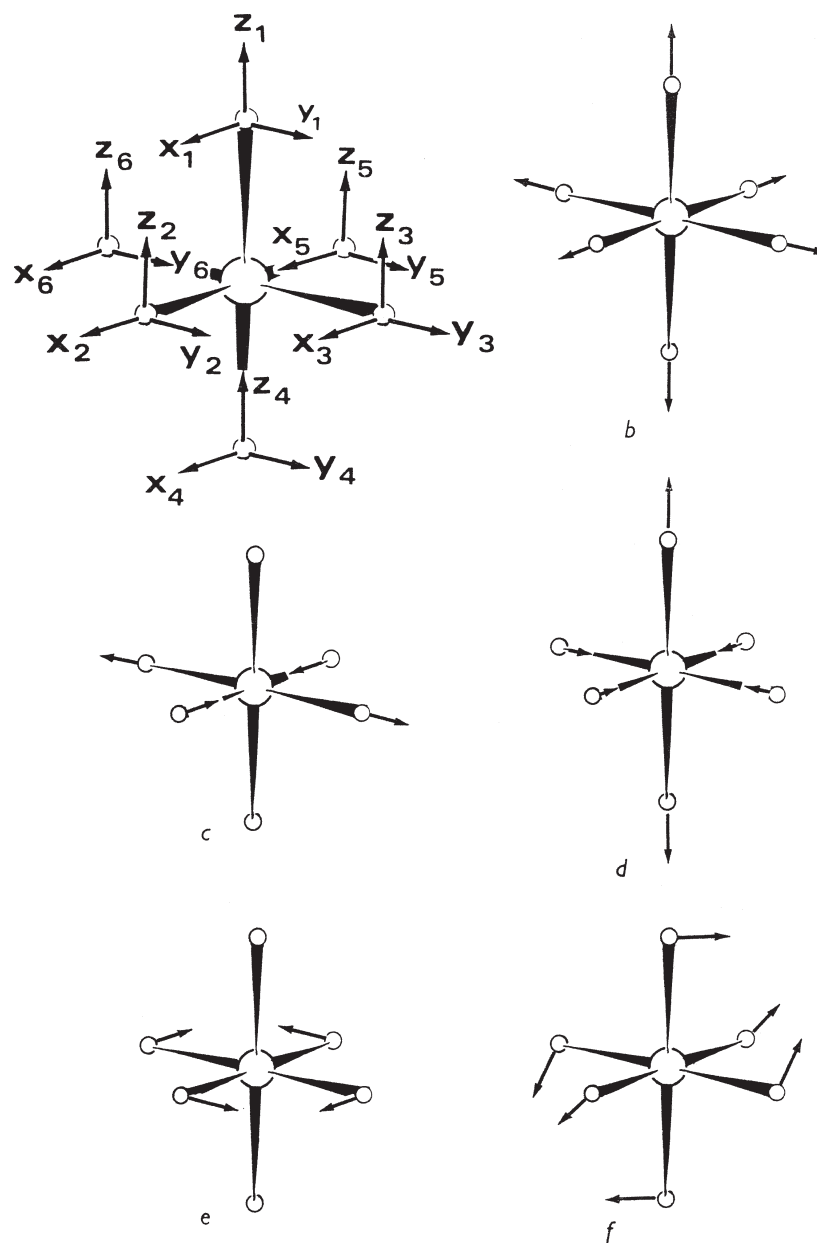


**FIGURE 7.1.** Shapes of symmetrized displacements of atoms in an octahedral complex  $ML_6$ : (a) numbering and orientation of Cartesian displacements; (b) totally symmetric  $A_{1g}$ , (c)  $E_g$ -type  $Q_\epsilon$ , (d)  $E_g$ -type  $Q_\theta$ , and (e)  $T_{2g}$ -type  $Q_\xi$  displacements. For degenerate displacements, any linear combination of these can be realized, for example,  $(Q_\zeta + Q_\eta + Q_\xi)/\sqrt{3}$  for  $T_{2g}$  (f) (note that the ligand local coordinates selected differ from those of Fig. 5.1).

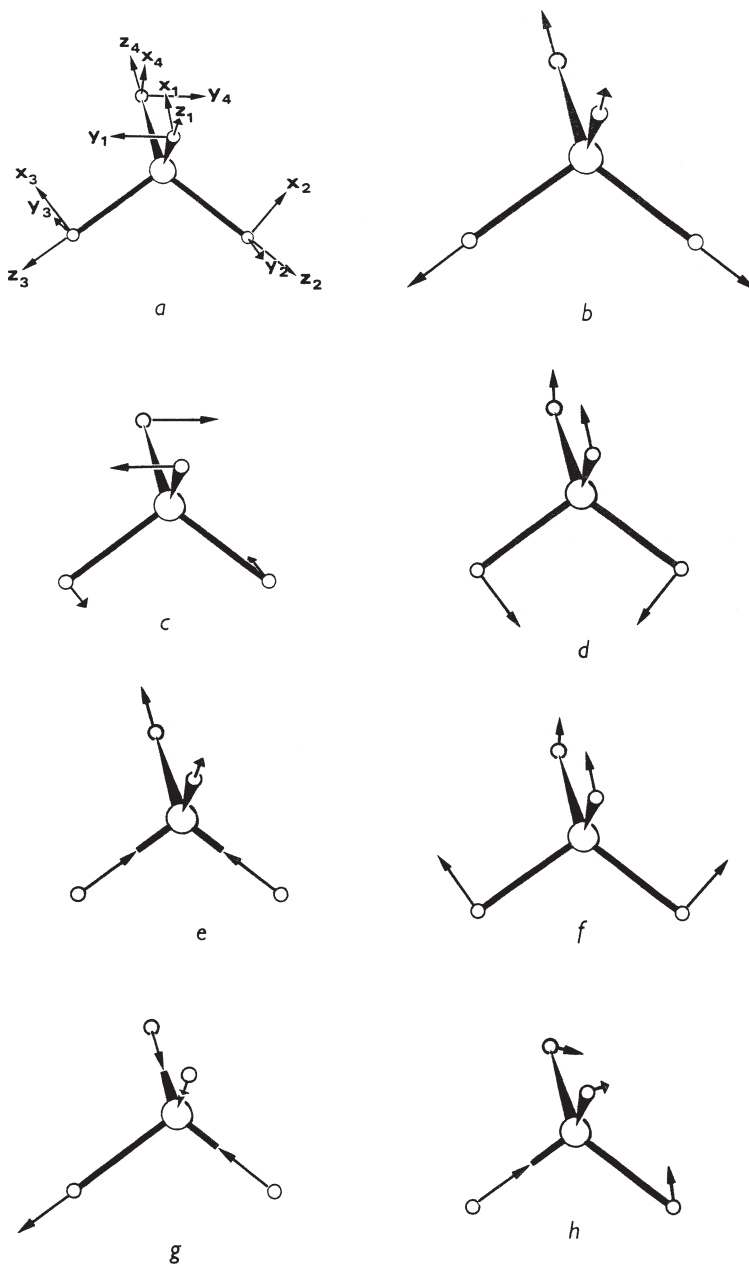


**FIGURE 7.2.** Shapes of symmetrized displacements of atoms in a tetrahedral complex: (a) numbering and orientation of Cartesian coordinates, (b) totally symmetric  $A_1$ , (c)  $E$ -type  $Q_\epsilon$ , (d)  $E$ -type  $Q_\theta$ , (e)  $T_2$ -type  $Q_\xi$ , (f)  $T_2'$ -type  $Q_{\xi^*}$  displacements. In the case of degeneracy any combination of component displacements can be realized, such as,  $(Q_\zeta + Q_\eta + Q_\xi)/\sqrt{3}$  (g),  $(Q_{\zeta^*} + Q_{\eta^*} + Q_{\xi^*})/\sqrt{3}$  (h).

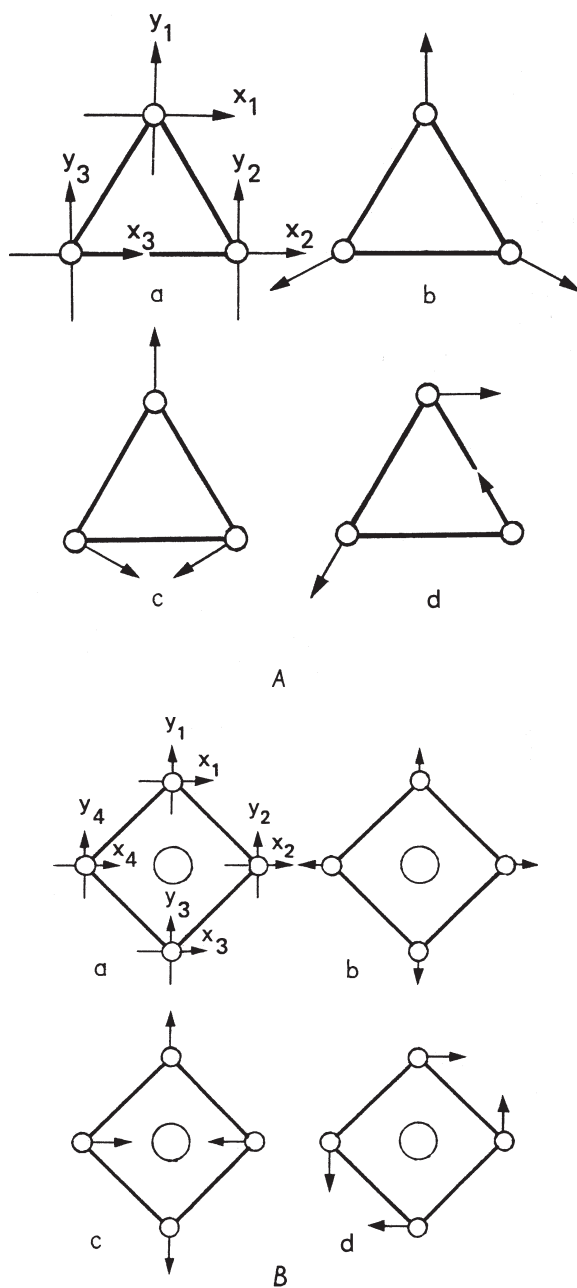


**FIGURE 7.3.** Symmetrized displacements of atoms in triangular (A) and square-planar (B) molecular systems: (a) labeling of Cartesian displacements; (b) totally symmetric displacements of type  $A_1$ ; (c)  $E'$ -type  $Q_y$  in (A) and  $B_{1g}$  in (B) displacements; (d)  $E'$ -type  $Q_x$  in (A) and  $B_{2g}$  in (B) displacements.

**TABLE 7.1. Symmetrized Displacements  $Q$  (Normal Coordinates) Expressed by Cartesian Coordinates (Figs. 7.1–7.3) for Some Trigonal, Tetragonal, Tetrahedral, and Octahedral Systems**

$Q$	Symmetry Type	Transformation Properties	Expressions by Cartesian Coordinates
<i>Trigonal Systems <math>X_3</math>; Symmetry <math>D_{3h}</math></i>			
$Q_x^{(t)}$	$E'$	$x$	$(X_1 + X_2 + X_3)/\sqrt{3}$
$Q_y^{(t)}$	$E'$	$y$	$(Y_1 + Y_2 + Y_3)/\sqrt{3}$
$Q_{a2}^{(r)}$	$A_2'$	$S_z^a$	$(2X_1 - X_2 - \sqrt{3}Y_2 - X_3 + \sqrt{3}Y_3)/\sqrt{12}$
$Q_a$	$A_1'$	$x^2 + y^2$	$(2Y_1 + \sqrt{3}X_2 - Y_2 - \sqrt{3}X_3 - Y_3)/\sqrt{12}$
$Q_x$	$E'$	$2xy$	$(2X_1 - X_2 + \sqrt{3}Y_2 - X_3 - \sqrt{3}Y_3)/\sqrt{12}$
$Q_y$	$E'$	$x^2 - y^2$	$(2Y_1 - \sqrt{3}X_2 - Y_2 + \sqrt{3}X_3 - Y_3)/\sqrt{12}$
<i>Square-Planar Systems <math>ML_4</math>; Symmetry <math>D_{4h}</math></i>			
$Q_a$	$A_{1g}$	$x^2 + y^2$	$\frac{1}{7}(Y_1 + X_2 - Y_3 - X_4)$
$Q_1$	$B_{1g}$	$x^2 - y^2$	$\frac{1}{7}(Y_1 - X_2 - Y_3 + X_4)$
$Q_2$	$B_{2g}$	$xy$	$\frac{1}{7}(X_1 + Y_2 - X_3 - Y_4)$
$Q'_a$	$A_{2g}$	$S_z$	$\frac{1}{7}(X_1 - Y_2 - X_3 + Y_4)$
$Q_x$	$E_{1u}$	$x$	$\frac{1}{7}(X_1 + X_2 + X_3 + X_4)$
$Q_y$	$E_{1u}$	$y$	$\frac{1}{7}(Y_1 + Y_2 + Y_3 + Y_4)$
$Q'_x$	$E'_{1u}$	$x$	$X_0^b$
$Q'_y$	$E'_{1u}$	$y$	$Y_0$
<i>Tetrahedral Systems <math>ML_4</math>; Symmetry <math>T_d</math></i>			
$Q_a$	$A_1$	$x^2 + y^2 + z^2$	$\frac{1}{7}(Z_1 + Z_2 + Z_3 + Z_4)$
$Q_\theta$	$E$	$2z^2 - x^2 - y^2$	$\frac{1}{7}(X_1 - X_2 - X_3 + X_4)$
$Q_\varepsilon$		$\sqrt{3}(x^2 - y^2)$	$\frac{1}{7}(Y_1 - Y_2 - Y_3 + Y_4)$
$Q'_\xi$	$T_2'$	$x, yz$	$\frac{1}{7}(Z_1 - Z_2 + Z_3 - Z_4)$
$Q'_\eta$	$T_2'$	$y, xz$	$\frac{1}{7}(Z_1 + Z_2 - Z_3 - Z_4)$
$Q'_\zeta$	$T_2'$	$z, xy$	$\frac{1}{7}(Z_1 - Z_2 - Z_3 + Z_4)$
$Q''_\xi$	$T_2''$	$x, yz$	$\frac{1}{4}(-X_1 + X_2 - X_3 + X_4) +$ $(\sqrt{3}/4)(-Y_1 + Y_2 - Y_3 + Y_4)$
$Q''_\eta$	$T_2''$	$y, xz$	$\frac{1}{4}(-X_1 - X_2 + X_3 + X_4) +$ $(\sqrt{3}/4)(Y_1 + Y_2 - Y_3 - Y_4)$
$Q''_\zeta$	$T_2''$	$z, xy$	$\frac{1}{2}(X_1 + X_2 + X_3 + X_4)$
$Q_x$	$T_2$	$x$	$X_0^b$
$Q_y$	$T_2$	$y$	$Y_0$
$Q_z$	$T_2$	$z$	$Z_0$
<i>Octahedral Systems <math>ML_6</math>; Symmetry <math>O_h</math></i>			
$Q_a$	$A_{1g}$	$x^2 + y^2 + z^2$	$(X_2 - X_5 + Y_3 - Y_6 + Z_1 - Z_4)/\sqrt{6}$
$Q_\theta$	$E_g$	$2z^2 - x^2 - y^2$	$(2Z_1 - 2Z_4 - X_2 + X_5 - Y_3 + Y_6)/2\sqrt{3}$
$Q_\varepsilon$	$E_g$	$\sqrt{3}(x^2 - y^2)$	$\frac{1}{2}(X_2 - X_5 - Y_3 + Y_6)$
$Q_\xi$	$T_{2g}$	$yz$	$\frac{1}{2}(Z_3 - Z_6 + Y_1 - Y_4)$

TABLE 7.1. (Continued)

$Q$	Symmetry Type	Transformation Properties	Expressions by Cartesian Coordinates
$Q_\eta$	$T_{2g}$	$xz$	$\frac{1}{2}(X_1 - X_4 + Z_2 - Z_5)$
$Q_\zeta$	$T_{2g}$	$xy$	$\frac{1}{2}(Y_2 - Y_5 + X_3 - X_6)$
$Q'_x$	$T'_{1u}$	$x$	$\frac{1}{2}(X_1 + X_3 + X_4 + X_6)$
$Q'_y$	$T'_{1u}$	$y$	$\frac{1}{2}(Y_1 + Y_2 + Y_4 + Y_5)$
$Q'_z$	$T'_{1u}$	$z$	$\frac{1}{2}(Z_1 + Z_3 + Z_5 + X_6)$
$Q''_x$	$T''_{1u}$	$x$	$(X_2 + X_5)/\sqrt{2}$
$Q''_y$	$T''_{1u}$	$y$	$(Y_3 + Y_6)/\sqrt{2}$
$Q''_z$	$T''_{1u}$	$z$	$(Z_1 + Z_4)/\sqrt{2}$
$Q_x$	$T_{1u}$	$x$	$X_0^b$
$Q_y$	$T_{1u}$	$y$	$Y_0$
$Q_z$	$T_{1u}$	$z$	$Z_0$
$Q'_\xi$	$T_{2u}$	$x(y^2 - z^2)$	$\frac{1}{2}(X_3 + X_6 - X_1 - X_4)$
$Q'_\eta$	$T_{2u}$	$y(z^2 - x^2)$	$\frac{1}{2}(Y_1 + Y_4 - Y_2 - Y_5)$
$Q'_\zeta$	$T_{2u}$	$z(x^2 - y^2)$	$\frac{1}{2}(Z_2 + Z_5 - Z_3 - Z_6)$

<sup>a</sup> $S_z \equiv R_z$  is an axial vector that describes *rotations* around the  $z$  axis.

<sup>b</sup> $X_0, Y_0, Z_0$  are the Cartesian displacements of the central atom; the three  $T_{1u}$  coordinates in the octahedral  $ML_6$  system (and  $E'_{1u}$  and  $T_2$  ones in  $ML_4$ ) are not independent, and each of them separately does not preserve the center of mass; their correct linear combinations depend on the ratio of the M and L masses.

terms with the same symmetry, Section 4.3). Hence their frequencies are no longer independent, and the corresponding coordinates are *symmetrized, but not normal*. To obtain the normal vibrations, the corresponding perturbation problem must be solved to diagonalize the matrix of interacting coordinates [7.7–7.9] (cf. Section 4.3, Eq. (4.55)).

Not all the types of symmetry of the group can be realized as types of vibrations. For instance, in the octahedral  $O_h$  system there are no  $A_{1u}, A_{2u}, A_{2g}, E_u$ , and  $T_{1g}$  vibrations, in the tetrahedron there are no  $A_2$  and  $T_1$  vibrations, and so on. Table 7.2 lists some results on classification of the normal vibrations on symmetry for some most usable types of coordination system obtained as shown in Section 3.5, Example 3.5, and Problems 3.8 and 8.8.

To conclude this subsection, it is necessary to emphasize that the idea of normal vibrations is essentially based on the harmonic approximation, in which cubic and higher terms in the expansion of the APES in a power series can be neglected. This implies that the APES has one (deep) minimum; at its bottom the amplitude of vibrations is small, provided that only low vibrational states are populated (low temperatures). The deviation from the harmonic approximation occurs as a result of either large amplitudes of vibrations involving cubic terms in the Hamiltonian of the nuclear motions in (7.12) or the mixing with low-lying excited electronic states, *the vibronic anharmonicity*, discussed in Section 7.4. For anharmonicity corrections to the vibrational frequencies, see Refs. 7.7–7.12.

**TABLE 7.2. Classification of Symmetrized Displacements  $\Gamma$  for Several Types of Molecules with  $N$  Atoms**

$N^a$	Symmetry	Example, Shape	$\Gamma$
4(6)	$C_{3v}$	NH <sub>3</sub> , pyramid	$A'_1, A''_1, E', E''$
5(9)	$T_d$	MnO <sub>4</sub> <sup>-</sup> , tetrahedron	$A_1, E, T'_2, T''_2$
7(15)	$O_h$	CrF <sub>6</sub> <sup>3-</sup> , octahedron	$A_{1g}, E_g, T_{2g}, T_{2u}, T'_{1u}, T''_{1u}$
7(15)	$D_{4h}$	MA <sub>4</sub> B <sub>2</sub> , tetragonally distorted octahedron	$A_{1g}, A''_{1g}, A'_{2u}, A''_{2u}, B_{1g}, B_{2g}, B_{2u}, E_g, E_u, E'_u, E''_u$
9(21)	$O_h$	CsF <sub>8</sub> , cub	$A_{1g}, A_{2u}, E_g, E_u, T_{2u}, T'_{1u}, T''_{1u}, T'_{2g}, T''_{2g}$

<sup>a</sup>The number of normal vibrations  $3N-6$  is indicated in parentheses.

### Special Features of Vibrations of Coordination Systems

The prediction of the number of possible frequencies and shapes of vibrations based on symmetry properties of the system is the more informative, the higher the symmetry. This circumstance forms the basis of the qualitative identification of infrared (IR) and Raman spectra of coordination compounds (Section 8.2). The higher the symmetry, the easier the identification of the spectra and the analysis of the electronic structure based on these spectra.

For instance, in a regular octahedral system with seven atoms there is a total of  $3 \times 7 - 6 = 15$  vibrations, which, following Table 7.2, are divided into one  $A_{1g}$  vibration, two  $E_g$ , and four types of threefold vibrations:  $T_{2g}, T_{2u}, T'_{1u}, T''_{1u}$ . Since degenerate vibrations have the same frequency, only six different frequencies are expected in the vibrational spectra of such systems. For systems with an inversion center, selection rules stipulate that odd vibrations may be observed in the IR absorption, while even vibrations manifest themselves in the Raman scattering of light (Section 8.2). Therefore, three frequencies ( $T_{2u}, T'_{1u}$ , and  $T''_{1u}$ ) are seen in the IR spectra and the other three ( $A_{1g}, E_g$ , and  $T_{2g}$ ) in the Raman spectra [7.9–7.12].

For further analysis and identification it may be useful to consider the splitting of degenerate frequencies in fields of lower symmetry. These splittings are quite similar in nature to the term splitting discussed in Chapter 4. Sections 3.4 and 4.2 illustrate how to determine the splitting of high-symmetry terms (vibrations) under perturbations of lower symmetry, and Tables 4.2 and 4.3 provide some results. If one knows how the degenerate frequencies split in the fields of lower symmetry, vibrational spectroscopy can be used to study the influence of the environment on (or ligand substitution in) the coordination system. Special applications of external uniaxial stress and its influence on the IR line splitting are also employed.

Another important feature of IR spectra is related to the three-dimensional center-delocalized coordination bond (Section 6.1). This delocalization renders the metal–ligand bonds non-specific and nontransferable. It means that in general, in the presence of different ligands there is no way to differentiate individual metal–ligand vibrations and to consider that their frequencies remain the same (even approximately) by passing to another complex with the same metal–ligand



bond but with other ligands changed. The three-dimensional delocalization of the bonding electrons makes all the metal–ligand bonds collectivized, and the vibrations, as a rule, are related to the system as a whole. This is one of the main distinctions of vibrational spectroscopy in application to coordination compounds, as compared with organic valence (not conjugated) compounds with localized bonds (Section 6.1) for which the vibrational frequencies of given atom–atom bonds are approximately constant.

Finally, the vibrations in coordination compounds are characterized by a wide variety of frequencies ranging from infrared to several tens of wavenumbers ( $\text{cm}^{-1}$ ). More detailed analyses of IR and Raman vibrational spectra of transition metal compounds are given in Section 8.2 and in special monographs [7.8–7.12].

## 7.2. VIBRONIC COUPLING

### Vibronic Constants

As stated above, molecular changes under external influence begin with alterations of the less inertial electronic shells, while molecular transformations (and many other properties) are determined by the changes in nuclear motions. *The bridge from electronic to nuclear motions is conveyed by vibronic coupling* [7.1–7.4].

The expression for the operator of vibronic coupling  $W$  is given in the previous section, Eq. (7.7). It describes the interaction of the electrons with the nuclear displacements from the initial configuration hereafter called *reference configuration*. The latter is usually taken as the molecular configuration of the stable ground state, or any other high-symmetry configuration (see the discussion in Ref. 7.1). With the reference configuration known, one can use symmetrized or normal coordinates in the expansion of  $V(r, Q)$  in  $Q$  (7.3'), which simplifies further treatment.

In Bethe's notations the  $f$ -fold-degenerate IrRep  $\Gamma_i$  has  $f$  rows denoted by  $\gamma$  (Section 3.3). For instance, the twofold-degenerate representation  $\Gamma_3 = E$  has two lines  $\gamma = \vartheta, \varepsilon$ , while the threefold representation  $\Gamma_5 = T_2$  has three lines  $\gamma = \xi, \eta, \zeta$ . Denoting the symmetrized coordinates that belong to a certain row of IrRep  $\Gamma$  by  $Q_{\Gamma\gamma}$ , one can rewrite the operator of vibronic coupling (7.7) in these coordinates (the reference configuration is taken at  $Q_{\Gamma\gamma} = 0$ ):

$$W(r, Q) = \sum_{\Gamma\gamma} \left( \frac{\partial V}{\partial Q_{\Gamma\gamma}} \right)_0 Q_{\Gamma\gamma} + \frac{1}{2} \sum_{\Gamma\gamma} \sum_{\Gamma'\gamma'} \left( \frac{\partial^2 V}{\partial Q_{\Gamma\gamma} \partial Q_{\Gamma'\gamma'}} \right)_0 Q_{\Gamma\gamma} Q_{\Gamma'\gamma'} + \dots \quad (7.21)$$

Consider the meaning of the coefficients of this expansion which are derivatives of the electron–nucleus and nucleus–nucleus interaction  $V$ . The matrix

elements of these coefficients are *the constants of vibronic coupling, or vibronic constants*. They are very important in vibronic interaction effects; *vibronic constants characterize the measure of coupling between the electronic states and nuclear displacements*. In other words, vibronic constants characterize the influence of the nuclear displacements on the electron distribution or, conversely, the effect of the changes in the electronic structure on the nuclear configuration and dynamics. The problem of *how electrons control molecular configurations* can be formulated and approximately solved by means of vibronic constants.

Denote the electronic states by the corresponding IrReps  $\Gamma, \Gamma', \dots$  of the symmetry group of the molecular system and assume first that the states  $\Gamma$  and  $\Gamma'$  are not degenerate. The matrix element

$$F_{\Gamma^*}^{(\Gamma\Gamma')} = \langle \Gamma | \left( \frac{\partial V}{\partial Q_{\Gamma^*}} \right)_0 | \Gamma' \rangle \quad (7.22)$$

is called the *linear vibronic constant*. Following the rules of group theory,  $F_{\Gamma^*}^{(\Gamma\Gamma')}$  is nonzero if and only if  $\Gamma \times \Gamma' = \Gamma^*$ . If  $\Gamma, \Gamma'$ , or both are degenerate (in this case  $\Gamma^*$  may also be degenerate), a set of linear vibronic constants corresponding to all the lines  $\gamma$  and  $\gamma'$  of the two representations  $\Gamma$  and  $\Gamma'$  and their combinations  $F_{\Gamma^*\gamma^*}^{(\Gamma\gamma\Gamma'\gamma')}$  should be introduced instead of one vibronic constant for nondegenerate states. This can be easily done because the matrix elements within a degenerate term differ solely in (tabulated) numerical coefficients (see the Wigner–Eckart theorem in Section 3.4).

Some of the linear vibronic constants have a clear-cut physical meaning. *The diagonal constant of the linear coupling*  $F_{\Gamma^*\gamma^*}^{(\Gamma\gamma\Gamma'\gamma')} \equiv F_{\Gamma^*\gamma^*}^{\Gamma\gamma}$  has the sense of the force with which the electrons in the state  $\Gamma\gamma$  act on the nuclei in the direction of symmetrized displacements  $Q_{\Gamma^*\gamma^*}$ . For instance,  $F_{E\vartheta}^{(E\varepsilon)}$  means the force with which the electron in the  $E\varepsilon$  state distorts the nuclear configuration in the direction of  $E\vartheta$  displacements (see Fig. 7.1).

For degenerate states  $\Gamma$ , according to the group-theoretical rules, the diagonal matrix element  $F_{\Gamma^*}^{\Gamma}$  is nonzero if the symmetric product  $[\Gamma \times \Gamma]$  contains  $\Gamma^*$ :  $\Gamma^* \in [\Gamma \times \Gamma]$  (compare with the condition for off-diagonal elements  $\Gamma^* \in \Gamma \times \Gamma'$ ). For nondegenerate states  $[\Gamma \times \Gamma] = \Gamma \times \Gamma = A_1$ , where  $A_1$  is the totally symmetric representation. It follows that in nondegenerate states  $\Gamma = A_1$ , and the electrons can distort the nuclear configuration only in the direction of totally symmetric displacements, for which the symmetry of the system does not change. In this case there is no distortion but changes in interatomic distances (see, however, the possible implication of the pseudo-JTE, Sections 7.3 and 7.4). If the electronic state  $\Gamma$  is degenerate, the symmetric product  $[\Gamma \times \Gamma]$  contains nontotally symmetric (along with totally symmetric) representations. Indeed, for cubic symmetry  $[E \times E] = A_1 + E$ ,  $[T \times T] = A_1 + E + T$ ; for  $D_{4h}$  symmetry  $[E \times E] = A_1 + B_1 + B_2$ , and so on. In these cases  $\Gamma^*$  may be nontotally symmetric (degenerate  $E, T$ , or nondegenerate  $B_1, B_2$ , etc.). Thus, under the influence of the electrons in degenerate states, the nuclear configuration

undergoes distortions that are not totally symmetric. It is just these distortions that are predicted by the Jahn–Teller theorem discussed in Section 7.3.

The quadratic (or second-order) vibronic constants can be introduced similarly to the linear constants, although there are some complications [7.1]. The second derivatives in Eq. (7.21) (which are terms of the type  $\partial^2 V / \partial Q_{\Gamma_1} \partial Q_{\Gamma_2}$ ) can be grouped into a totally symmetric combination and nontotally symmetric parts. The diagonal matrix element of the totally symmetric combination

$$K_{0\Gamma^*} = \langle \Gamma | \left( \frac{\partial^2 H}{\partial Q_{\Gamma^*}^2} \right)_0 | \Gamma \rangle \quad (7.23)$$

is the *nonvibronic contribution* to the curvature of the APES, or the *primary force constant*. The full curvature  $K_{\Gamma^*}^{\Gamma}$  (Section 7.4), which at the minimum of the APES coincides with the *force constant*, is

$$K_{\Gamma^*}^{\Gamma} = K_{0\Gamma^*}^{\Gamma} - \sum_{\Gamma'}' \frac{|F_{\Gamma^*(\Gamma\Gamma')}|^2}{\Delta_{\Gamma'\Gamma}} \quad (7.23')$$

where  $\Delta_{\Gamma'\Gamma} = \frac{1}{2}(\varepsilon_{\Gamma'} - \varepsilon_{\Gamma})$  is the energy semidifference between states  $\Gamma'$  and  $\Gamma$ . The diagonal matrix elements of the nontotally symmetric part of the second derivatives in (7.21) are the *diagonal quadratic* (or *second-order*) *vibronic constant*  $G_{\Gamma^*}^{\Gamma}(\Gamma_1 \times \Gamma_2)$ . The off-diagonal matrix elements are the *off-diagonal quadratic vibronic constants*  $G_{\Gamma^*}^{(\Gamma\Gamma')}(\Gamma_1 \times \Gamma_2)$ , where  $\Gamma^* \in \Gamma_1 \times \Gamma_2$  and  $\Gamma_1$  and  $\Gamma_2$  are IrReps of the corresponding two displacements [7.1].

### Orbital Vibronic Constants

The orbital vibronic constants [7.3, 7.13, 7.14] enable us to consider approximately the influence of each electron (separately) on the nuclear framework and its dynamics. On the other hand, the introduction of orbital vibronic constants creates a bridge between the idea of vibronic coupling and the MO approach to the investigation of molecular structure and properties. The one-electron MOs supplemented by vibronic coupling constants result in *vibronic molecular orbitals*. The latter, as shown below, present a more refined picture of molecular structure, which includes parameters of nuclear dynamics.

Denote the one-electron MO energies by  $\varepsilon_i$  and their wavefunctions by  $\varphi_i(r) = |i\rangle$ . Taking into account the additivity of the electron–nucleus interaction operator  $V(r, Q)$  with respect to electronic coordinates (7.3), we have

$$V = \sum_k V'(\mathbf{r}_k) \quad (7.24)$$

$$V'(\mathbf{r}) = - \sum_{\alpha} \frac{e^2 Z_{\alpha}}{|\mathbf{r} - \mathbf{R}_{\alpha}|} + \frac{1}{n} \frac{1}{2} \sum_{\alpha, \beta}' \frac{e^2 Z_{\alpha} Z_{\beta}}{|\mathbf{R}_{\alpha} - \mathbf{R}_{\beta}|} \quad (7.24')$$

where  $n$  is the total number of electrons (the second term in (7.24'), the evenly distributed internuclear repulsion per electron, does not depend on electronic coordinates; it is introduced for convenience). On the basis of these notations, the orbital vibronic constants can be introduced similarly to the vibronic constants for the system as a whole (7.22). In contradistinction to the orbital vibronic constants, the usual vibronic constants may be called *integral vibronic constants*.

For the *linear orbital vibronic constants* we have

$$f_{\Gamma^*}^{(ij)} = \langle i | \left( \frac{\partial V'}{\partial Q_{\Gamma^*}} \right)_0 | j \rangle \quad (7.25)$$

Similarly to the integral case, the totally symmetric part ( $\Gamma^* = A_1$ ) of the orbital diagonal matrix elements of the quadratic terms of vibronic interactions  $k_{0\Gamma^*}^{(ii)} = k_{0\Gamma^*}^i$  ( $\Gamma^* = \Gamma_1 = \Gamma_2$ ) contributes to the orbital force constant  $k_{\Gamma^*}^i$  (see below); the nontotally symmetric parts, which are nonzero for degenerate MOs only, form the diagonal second-order orbital vibronic constants  $g_{\Gamma^*}^i(\Gamma_1 \times \Gamma_2)$ , and the off-diagonal matrix elements of these terms are the off-diagonal orbital vibronic constants  $g^{(ij)}(\Gamma_1 \times \Gamma_2)$ .

The physical meaning of the orbital vibronic constants can be clarified by means of the addition theorem: the linear diagonal integral vibronic constant equals the sum of linear diagonal orbital vibronic constants multiplied by the appropriate MO occupation numbers  $q_i^\Gamma$ ,

$$F_{\Gamma^*\gamma^*}^\Gamma = \sum_i q_i^\Gamma f_{\Gamma^*\gamma^*}^i \quad (7.26)$$

The proof of this theorem [7.13] is based on the additivity properties of the vibronic constants mentioned above. Presenting the total wavefunction in the expression of  $F_{\Gamma^*}^\Gamma$ , Eq. (7.22), by the determinant (or a linear combination of determinants) of the one-electron MO functions  $\varphi_i(r_i)$  and factoring in the expressions (7.24) for  $V$  and (7.25) for  $f_{\Gamma^*}^i$ , one can deduce Eq. (7.26).

It is seen from Eq. (7.26) that the distorting influence of the electrons on the nuclear framework with a force  $F_{\Gamma^*\gamma^*}^\Gamma$  is produced additively by all the corresponding MO single-electron effects  $f_{\Gamma^*\gamma^*}^i$ . A clear-cut physical meaning of the latter follows immediately: *The linear diagonal orbital vibronic constant  $f_{\Gamma^*\gamma^*}^i$  equals the force with which the electron of the  $i$ th MO distorts the nuclear configuration in the direction of the symmetrized displacements  $Q_{\Gamma^*\gamma^*}$ .*

For quadratic vibronic constants, quite similar to Eq. (7.26), we obtain the following addition formula:

$$G_{\Gamma^*\gamma^*}^\Gamma(\Gamma_1 \times \Gamma_2) = \sum_i q_i^\Gamma g_{\Gamma^*\gamma^*}^i(\Gamma_1 \times \Gamma_2) \quad (7.27)$$

Deduction of similar expressions for off-diagonal vibronic constants is more difficult because they involve excited states for which calculation of the contribution of the one-electron MOs is complicated. The analysis can be simplified in the

“frozen orbital” approximation equivalent to the approximation of the Koopmans theorem in quantum chemistry (Sections 2.2 and 6.4). In this approximation the one-electron excitation of the system  $\Gamma \rightarrow \Gamma'$  is realized by the substitution of only one MO, for instance,  $i$  by  $j$ , while the changes of the other MOs due to alteration of the interelectron repulsion are neglected. In this case there are simple relations between integral and orbital off-diagonal linear vibronic constants:

$$F_{\Gamma^* \gamma^*}^{(\Gamma \Gamma')} = f_{\Gamma^* \gamma^*}^{(ij)} \quad \Gamma \neq \Gamma' \quad (7.28)$$

For fractional charge transfers, important in applications to chemical problems, the difference in the corresponding electron population numbers  $q_i$  and  $q_j$  of the two mixing MOs determines the magnitude of the off-diagonal vibronic mixing (Sections 10.3 and 11.2):

$$F_{\Gamma^* \gamma^*}^{(\Gamma \Gamma')} = f_{\Gamma^* \gamma^*}^{(ij)} (q_i - q_j) \quad (7.28')$$

Using this relation, the APES curvature (or the force constant)  $K_{\Gamma^*}^\Gamma$  can be presented as a sum of orbital contributions  $k_{\Gamma^*}^i$

$$K_{\Gamma^*}^\Gamma = \sum_i q_i k_{\Gamma^*}^i \quad (7.29)$$

$$k_{\Gamma^*}^i = k_{0\Gamma^*}^i - \sum_j' \frac{|f_{\Gamma^*}^{(ij)}|^2}{\Delta_{ji}}$$

where  $\Delta_{ij} = \frac{1}{2}(\varepsilon_i - \varepsilon_j)$ . The proof of these relations is analogous to that of Eq. (7.27) [7.13].

In the MO approach, the electronic structure of a molecule with fixed nuclei is presented approximately by the one-electron MO charge distributions and energies in the field of the nuclei. This picture is static; it does not characterize sufficiently well the backward influence of the electrons on the nuclear framework. If the electronic structure is determined without geometry optimization, the static picture does not indicate whether the chosen (reference) nuclear configuration will be stable for the electronic structure under consideration. More important, the static picture does not allow us to predict how the nuclear configuration and its dynamics will change under electronic structure alterations.

This deficiency of the MO approach can be overcome by means of the vibronic constants that characterize the forces (and force constants, anharmonicities, etc.) with which the electrons influence the nuclei. The orbital vibronic constants are of special interest. If the orbital vibronic constants and the orbital contributions to the force constants are known, the behavior of the nuclear configuration (changes in stable configuration, force constants, anharmonicities) under small changes of the electronic structure (changes of electronic MO occupation numbers) can be predicted. These effects can be used to predict changes of the molecular reactivity by electronic rearrangements (Section 11.2). Thus *the orbital vibronic constants complement the static picture of the electronic structure in terms of*

*MOs with dynamic parameters of their coupling to the nuclear displacements.* In Example 7.1 the main features of orbital vibronic constants are illustrated by their numerical values for  $N_2$  and CO.

### EXAMPLE 7.1

#### Vibronic MO Description of Electronic Structure of $N_2$ and CO

In Fig. 7.4 the new parameterization of the molecular structure based on orbital vibronic constants is illustrated for the HOMO  $5\sigma$  and the

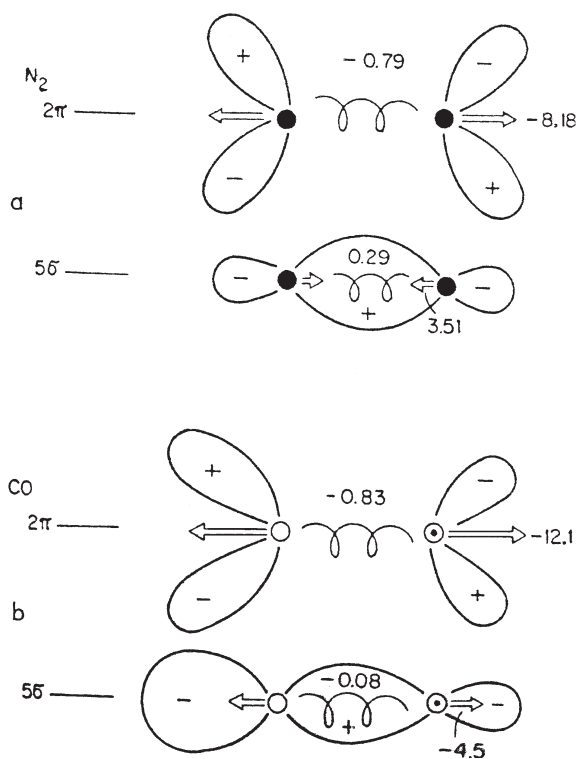


**FIGURE 7.4.** Vibronic molecular orbital description of electronic structure. In addition to the MO energies and wavefunctions, the orbital vibronic constants characterize the contribution of the orbital electron to the distorting force  $f$  (shown by arrows; values are given in  $10^{-4}$  dyn) and force constant coefficient  $k$  (shown by springs; values are given in  $10^6$  dyn/cm); (a) HOMO and LUMO of the nitrogen molecule—the HOMO  $5\sigma$  is bonding ( $f > 0$ ), whereas the LUMO  $2\pi$  is antibonding ( $f < 0$ ); (b) HOMO and LUMO of carbon monoxide—the HOMO is weakly antibonding, whereas the LUMO is strongly antibonding.

LUMO  $2\pi$  of two molecules  $N_2$  and CO, taken as examples (the numerical values are obtained in Section 11.2). In addition to the usual MO energy and wavefunction, it is shown that the electron of the HOMO  $5\sigma$  in the  $N_2$  molecule tightens the nuclei with the force  $f_R^{5\sigma}(N_2) = 3.51 \times 10^{-4}$  dyn (where  $R$  denotes the distance between the nuclei), while in the CO molecule the electron of the analogous MO pushes them away with force  $f_R^{5\sigma}(CO) = -4.5 \times 10^{-4}$  dyn [more precisely, the binding of the nuclei by the electron is less than the corresponding one-electron portion of their repulsion by this amount; see Eq. (7.24')].

The electron of the LUMO  $2\pi$  pushes away the nuclei in both the  $N_2$  and CO molecules with the forces  $f_R^{2\pi}(N_2) = -8.18 \times 10^{-4}$  dyn and  $f_R^{2\pi}(CO) = -12.1 \times 10^{-4}$  dyn, respectively. For the corresponding one-electron MO contribution to the force constant  $k^{(i)}$  shown in Fig. 7.4 by a spring, we have [Eq. (11.34)]  $k_R^{5\sigma}(N_2) = 0.29 \times 10^{-6}$  dyn/cm,  $k_R^{2\pi}(N_2) = -0.79 \times 10^{-6}$  dyn/cm,  $k_R^{5\sigma}(CO) = -0.08 \times 10^{-6}$  dyn/cm, and  $k_R^{2\pi}(CO) = -0.83 \times 10^{-6}$  dyn/cm.

It follows from these data that the orbital  $5\sigma$  is bonding in  $N_2$  and antibonding in CO, whereas the  $2\pi$  MO is antibonding in both cases.

In general, we have:

For bonding MO:

$$f_{\Gamma^*}^{(i)} > 0, \quad k_{\Gamma^*}^{(i)} > 0$$

For antibonding MO:

$$f_{\Gamma^*}^{(i)} < 0, \quad k_{\Gamma^*}^{(i)} < 0$$

For non-bonding MO:

$$f_{\Gamma^*}^{(i)} \approx 0, \quad k_{\Gamma^*}^{(i)} \approx 0$$

and the absolute values of  $f^{(i)}$  and  $k^{(i)}$  follow approximately the measure of the MO contribution to the bonding or antibonding.

These relations are not trivial. Indeed, when there are several orbitals of the same type (as, e.g.,  $5\sigma$ ,  $4\sigma$ ,  $3\sigma$ , ... MOs in diatomics), it is difficult to reveal the bonding nature of each of them, even qualitatively, from MO calculations only. The orbital vibronic constants provide a semiquantitative measure of the MO bonding or antibonding quality and its contribution to the distorting force, force constants, and anharmonicity constants, serving thus as parameters of electronic control on nuclear configuration and dynamics (Sections 7.4 and 11.2). As mentioned above, the MO complemented by orbital vibronic coupling constants can be termed *vibronic molecular orbital* (VMO).

Vibronic MOs are of special importance for the analysis of the influence of electronic rearrangements on the nuclear configuration. They are also used in studying intervalence electron transfer [7.15] and can be significant for many other problems in which the details of electronic structure and vibronic coupling are important (see, e.g., Ref. 7.16, where they are used in discussion of the origin of high- $T_c$  superconductivity in fullerenes). In polyatomic molecules, there are more than one possible symmetrized direction of distortion and softening, and therefore the orbital vibronic constants and the orbital contributions to the force constants and anharmonicity constants contain additional information about molecular distortions (cleavage) by electronic rearrangements.

From the group theory rules (Section 3.4) the linear orbital vibronic constant  $f_{\Gamma}^{(ij)} = \langle i | (\partial V / \partial Q_{\Gamma^*})_0 | j \rangle$  is nonzero if the direct product of the IrReps  $\Gamma_i$  and  $\Gamma_j$  of the  $i$  and  $j$  MOs contains the  $\Gamma^*$  representation of the symmetrized displacements  $Q_{\Gamma^*}$ . Different  $\Gamma_i$  and  $\Gamma_j$  yield  $\Gamma^*$  that may be of any type allowed in the symmetry group of the system under consideration. For the diagonal constant  $f_{\Gamma^*}^i$ ,  $\Gamma^*$  must be the component of the symmetric product  $[\Gamma_i \times \Gamma_i]$  [Eq. (3.34)]. Therefore (quite similarly to the case of vibronic constants considered above), if  $\Gamma_i$  is nondegenerate,  $\Gamma^*$  is totally symmetric. In other words, the electrons of nondegenerate MOs distort (displace) the nuclear configuration  $A_1$  along  $Q_{A_1}$  that leaves its symmetry unchanged (again, see the possible implications of the pseudo-JTE in Section 7.3).

For degenerate MOs the product  $[\Gamma_i \times \Gamma_i]$  contains nontotally symmetric representations (in addition to the  $A_1$  representation). Hence the electrons of degenerate MOs distort the nuclear framework, changing its symmetry in accordance with (and in directions determined by) the Jahn–Teller effect (Section 7.3). In addition to this distortion the orbital electron softens, or hardens the nuclear framework according to Eq. (7.29). This equation contains the off-diagonal orbital vibronic constant  $f_{\Gamma^*}^{(ij)}$ , for which  $\Gamma$  may be of any type, and therefore the softening or hardening may be in any direction depending on the mixing orbitals. For further discussion and applications of orbital vibronic constants, see Section 11.2.

### 7.3. THE JAHN–TELLER EFFECT

#### The Jahn–Teller Theorem

In the formulation of the problem given in the previous section the vibronic mixing of different electronic states by nuclear displacements is described by an infinite system of coupled equations (7.6) for the nuclear motions with the APES  $\varepsilon_k(Q)$  determined by Eq. (7.8). For an  $f$ -fold-degenerate electronic term that is well separated from other terms, the number of equations can be approximately reduced to  $f$ . Qualitatively, many features of the nuclear motions and related experimental observables can be obtained from the APES shapes without solving the vibronic equations. Some general special features of the APES of electronically degenerate states are outlined by the Jahn–Teller (JT) theorem [7.17]. Similar effects in nondegenerate states are considered in Section 7.4.



The JT theorem is based on the group-theoretical analysis of the behavior of the APES of a polyatomic system near the point of electronic degeneracy. Similar to other group-theoretical statements, the JT theorem allows one to deduce qualitative results without performing specific calculations, or essentially reduces the extent of such calculations. However, unlike the usual situations in quantum chemistry, in which the group-theoretical treatment is introduced to simplify the calculations, the proof of the JT theorem preceded the calculations of APES and stimulated such calculations.

Suppose that by solving the electronic Schrödinger equation (7.4) for the nuclei fixed at the point  $Q_{\Gamma\gamma} = Q_{\Gamma\gamma}^0 = 0$ , we obtain an  $f$ -fold-degenerate electronic term, that is,  $f$  states  $\varphi_k(r)$ ,  $k = 1, 2, \dots, f$ , with equal energies  $\varepsilon'_k = \varepsilon_0$ . How do these energy levels change under nuclear displacements  $Q_{\Gamma\gamma} \neq 0$ ? To answer this question, the variation in APES in the space of the coordinates  $Q_{\Gamma\gamma}$  near the point of degeneracy must be determined. This can be done by estimating the effect of vibronic interaction terms  $W(r, Q)$  in Eq. (7.21) on the energy levels  $\varepsilon'_k$  using perturbation theory.

For sufficiently small nuclear displacements  $Q_{\Gamma\gamma}$ , the APES  $\varepsilon_k(Q)$  can be obtained as solutions of the secular equation of perturbation theory:

$$\begin{bmatrix} W_{11} - \varepsilon & W_{12} & \dots & W_{1f} \\ W_{21} & W_{22} - \varepsilon & \dots & W_{2f} \\ \vdots & \vdots & \dots & \vdots \\ W_{f1} & W_{f2} & \dots & W_{ff} - \varepsilon \end{bmatrix} = 0 \quad (7.30)$$

where  $W_{ij}$  are the matrix elements of the vibronic interaction operator (7.21) calculated with the wavefunctions of the degenerate term. Since the degeneracy is assumed to be caused by the high symmetry of the system, the totally symmetric displacements  $Q_A$  (that do not change the symmetry) do not remove the degeneracy and are not considered in this section. Again, because of the assumed small values of  $Q_{\Gamma\gamma}$ , we restrict the consideration (in the first-order approximation) with only linear nontotally symmetric terms  $W_{ij} = \sum_{\Gamma\gamma} \langle i | (\partial V / \partial Q_{\Gamma\gamma}) | j \rangle Q_{\Gamma\gamma}$  (this important limitation is discussed below). If at least one of these terms (e.g., for  $Q_{\Gamma^*\gamma^*}$ ) is nonzero, then at least one of the roots  $\varepsilon$  of Eq. (7.30) contains linear terms in  $Q_{\Gamma^*\gamma^*}$ , and hence the APES  $\varepsilon_k(Q)$  has no minimum at the point  $Q_{\Gamma^*\gamma^*}^0 = 0$  with respect to these displacements.

On the other hand, the question as to whether the vibronic constant  $F_{\Gamma^*}^\Gamma = \langle \Gamma | (\partial V / \partial Q_{\Gamma^*})_0 | \Gamma \rangle$  is zero may be easily answered by means of the well-known group-theoretical rule:  $F_{\Gamma^*}^\Gamma$  is nonzero if and only if the symmetric product  $[\Gamma \times \Gamma]$  contains the representation  $\Gamma^*$  of the symmetrized displacement  $Q_{\Gamma^*}$ . For instance, for a usual  $E$  term,  $[E \times E] = A_1 + E$  and thus, if the system under consideration has  $E$  vibrations (see the classification of vibrations given in Table 7.2), it has no minimum at the point of degeneracy with respect to the  $E$  displacements.

Jahn and Teller [7.17] examined all types of degenerate terms of all symmetry point groups and showed that for any orbital degenerate term of any molecular

system, there are nontotally symmetric displacements with respect to which the adiabatic potential of the electronic term (more precisely, at least one of its branches) has no minimum; molecules with linear arrangement of atoms are exceptions from this proof (see below). A similar statement is also valid in the case of spin degeneracy, with the exception of twofold degeneracy for systems with  $S = \frac{1}{2}$  (*Kramers doublets*) which can be split only by magnetic fields. The statement regarding the absence of extremum at the point of degeneracy is just *the Jahn–Teller theorem* [7.17], which may be formulated more rigorously as follows [7.3]. *If the adiabatic potential of a nonlinear polyatomic system has several ( $f > 1$ ) branches that coincide at one point ( $f$ -fold degeneracy), at least one of them has no extremum at this point; Kramers doublets are exceptions.* A more general formulation of the JT theorem is given below.

The variation of the adiabatic potential in the simplest case of an orbitally double-degenerate electronic term in the space of only one coordinate  $Q$  is shown schematically in Fig. 7.5. It is seen that the two curves intersect at the point of degeneracy. Away from this point the energy term splits, and the degeneracy is removed. As a result, the energy is lowered so that the small nuclear displacements  $Q$  are advantageous. For larger  $Q$  values the quadratic, cubic, and higher-order terms become important and further distortion of the system may be energetically disadvantageous (Section 7.4).

The exclusion of linear molecules from the JT statement needs clarification. For linear molecules the nontotally symmetric displacements are of odd type with respect to reflections in the plane comprising the molecular axis, whereas the product of any two wavefunctions of degenerate states (which have the same parity) is always even with respect to such reflections. This means that the corresponding vibronic constant equals zero, and hence the adiabatic potential at the

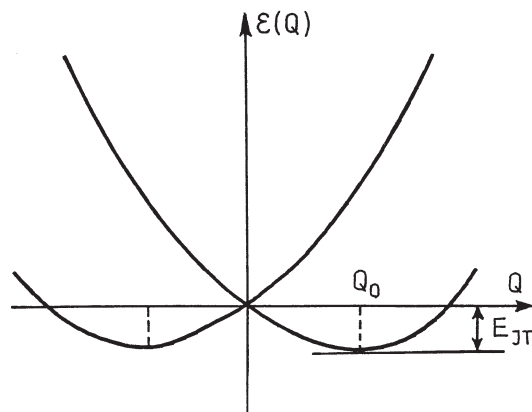


**FIGURE 7.5.** Variation of the adiabatic potential of a molecular system in a twofold orbitally degenerate electronic state with respect to one active coordinate  $Q$ . At the point of degeneracy  $Q = 0$  there is no minimum.  $E_{JT}$  is the Jahn–Teller stabilization energy.

point of linear configuration, as opposed to nonlinear molecules, has no terms of linear displacements; it is extremal.

However, if the linear terms of the vibronic interactions  $W(r, Q)$  are zero, the quadratic terms become of primary importance [see Eq. (7.7)]. They are even, their matrix elements in the case of linear molecules in degenerate states are nonzero, and the solution of the secular equation (7.30) results in a splitting of the energy term and possible instability. This is the *Renner–Teller effect* (RTE) [7.18]. This effect is discussed further below and in Section 7.4.

The proof of the JT theorem by examination of all the types of degenerate terms for all the symmetry point groups, one by one [7.17], although rigorous, cannot be considered as sufficiently elegant from the mathematical perspective. More general proofs have been obtained in later studies [7.19] (see also Ref. 7.1). However, the search over all the possible cases has its advantages, one of which is to reveal the *Jahn–Teller active modes*, that is, the nuclear displacements  $Q$  for which the vibronic constant  $F_{\Gamma^*}^{\Gamma}$  is nonzero. These active modes (active vibrations) are important basic components of the JT problem, because they form the space of nontotally symmetric nuclear displacements in which the JT theorem is operative and show the possible directions of distortions in specific cases.

If the types of possible vibrations of the system under consideration are known (Table 7.2), the JT active nuclear displacements  $Q_{\Gamma^*}$  may be obtained easily. As indicated above,  $F_{\Gamma^*}^{\Gamma}$  is nonzero if the symmetric product  $[\Gamma \times \Gamma]$  contains  $\Gamma^*$ . Hence the nontotally symmetric components of this product are just the representations  $\Gamma^*$  of the active displacements  $Q_{\Gamma^*}$ . For instance, for a  $E_g$  term in an octahedral system  $[E_g \times E_g] = A_{1g} + E_g$ , and hence the JT active displacements are of  $E_g$  type. Similarly, for a  $T$  term in a tetrahedral system  $[T \times T] = A_1 + E + T_2$ , and both  $E$ - and  $T_2$ -type displacements are JT active. The JT active displacements for all important point groups can be found in Refs. 7.1 and 7.3.

The lack of minimum of the APES at the point of electronic degeneracy is usually interpreted as instability of the nuclear configuration at this point. Therefore the formulation of the JT theorem is often given as follows: a nonlinear polyatomic system in the nuclear configuration with a degenerate electronic term is unstable. This statement of instability is often treated in the sense that the system distorts itself spontaneously so that the electronic term splits and the ground state becomes nondegenerate. Such interpretation of the JT theorem initiated by its authors [7.17] now appears in monographs and handbooks and has widespread use in general treatments of experimental results. Meanwhile, as shown in a number of publications (see Refs. 7.1–7.4), the actual situation in systems with electron degeneracy is much more complicated than implied by the simple statement of instability. Moreover, taken literally without additional explanation of terminology, this statement is not true and may lead to misunderstanding [7.20].

The conclusion about the lack of a minimum of the APES  $\varepsilon_k(Q)$  at the point of degeneracy was reached as a consequence of the solution of the electronic part of the Schrödinger equation (7.4), and therefore, strictly speaking, it cannot

be attributed to the nuclear behavior that in case of degeneracy (or pseudodegeneracy) is determined by the nuclear motion equations (7.6). The absence of a minimum of the function  $\varepsilon_k(Q)$  may generally be interpreted as proper instability only when there is no degeneracy or pseudodegeneracy. Indeed, in the absence of degeneracy (or in the areas far from the point of degeneracy), the electronic and nuclear motions can be separated in the adiabatic approximation, so that the APES  $\varepsilon_k(Q)$  has the meaning of the potential energy of the nuclei in the mean field of the electrons, and hence the derivative  $(d\varepsilon_k/dQ)_0$  means the force acting on the nuclei at the point  $Q_{\Gamma\gamma}^0$ . Here the condition  $(d\varepsilon_k/dQ)_0 \neq 0$  may be interpreted as a nonzero distorting force that makes the nuclear configuration unstable in the  $Q$  direction.

However, in the presence of electronic degeneracy and at the points near the degeneracy, the APES  $\varepsilon_k(Q)$  loses the meaning of the potential energy of the nuclei in the mean field of the electrons, since the motions of the electrons and nuclei at these points cannot be separated. In this area the notion  $\varepsilon_k(Q)$  becomes formal with no definitive physical meaning and hence the reasoning given above about distorting force and instability is, strictly speaking, invalid. In these cases the term “instability” should be taken formally as an indication of the *lack of minimum of the APES* but not as a nuclear feature. The latter, as indicated above, must be deduced from the solutions of equations (7.6) of nuclear dynamics.

Distortions of the nuclear configuration of free JT systems are, in general, of dynamic nature in which the quantum-mechanically averaged nuclear coordinates remain unchanged [7.20]. *It is not the simple nuclear configuration distortion, but special nuclear dynamics that are predicted by the Jahn–Teller theorem in free (unperturbed) molecular systems.* In the majority of cases the degeneracy is not removed, either; with vibronic interactions included, the electronic degeneracy transforms into vibronic degeneracy. Nevertheless, the lack of minimum of the APES indicates that various novel effects and properties may occur, jointly termed the *Jahn–Teller effect* (JTE), and the JT theorem predicts if and when such effects take place. The dynamic distortions become static and quite observable under external perturbations or as a cooperative effect in crystals (see the following chapters for further discussion of the observable consequences of the JTE).

The specific JT behavior of the APES due to the electronic degeneracy or pseudodegeneracy, similar to many other features of electrostatic origin, can be explained by simple images. In the general case of electronic degeneracy, two or more different electronic states with the same energy are necessarily nontotally symmetric with respect to the nuclear framework. Therefore, if only a part of them are occupied by electrons, the charge distribution is nontotally symmetric and distorts the nuclear configuration. Consider, for example, the case of one electron in one of three equivalent  $p$  orbitals ( $p_x$ ,  $p_y$ , or  $p_z$ ) of the CA of a hexacoordinated molecular system  $\text{MX}_6$  (term  $T_{1u}$ ) with the ligands X bearing negative charges (Fig. 7.6). It is clear that if the electron is on the  $p_x$  orbital, it interacts more strongly with the nearest ligands 1 and 3 and repels them. As a result, the octahedral complex becomes tetragonally distorted along the  $x$  axis.

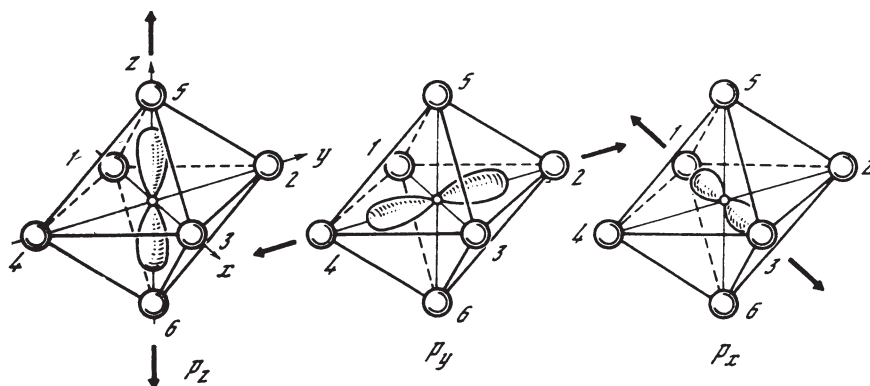


**FIGURE 7.6.** Rough illustration of the electrostatic origin of Jahn-Teller distortions of the nuclear configuration of an octahedral  $ML_6$  complex in a threefold degenerate electronic state. If the electron of the CA falls into one of the three equivalent states, it repels (or attracts) the corresponding pair of ligands, resulting in a tetragonal distortion. The three equivalent directions of distortion are shown by arrows.

Similarly, the electron on the  $p_y$  orbital repulses ligands 2 and 4, distorting the complex equivalently to the previous case, but along the  $y$  axis, and for the electron on the  $p_z$  orbital the distortion is along  $z$ . It follows that the APES of the system has three minima, corresponding to the three directions of distortions, and no minimum in the high-symmetry octahedral configuration due to obvious electrostatic forces. (Note that the degeneracy of the three  $p$  states is lifted by these distortions.) The same result emerges from the MO description with the atomic  $p$  orbitals taking part in the corresponding antibonding MOs (for bonding orbitals the distortions have opposite sign).

A question emerges from the discussion above as to whether the nonadiabatic JT effects are related to the exact degeneracy of the electronic states, or the latter may be just close in energy. The answer is that electronic states with sufficiently close energy levels may be similar (in the sense of instability) to exact degenerate states [7.21]; they have no minimum of the ground-state adiabatic potential at the point of the closest energies, and the nuclear motions are described by coupled equations such as (7.6), instead of (7.9). For reasons given below, the case of sufficiently close energy states is called *the pseudo Jahn–Teller effect* (PJTE), and the corresponding set of energy levels are considered as *pseudodegenerate* (or *quasidegenerate*). The pseudo JT (PJT) nonadiabacity follows directly from condition (7.11), which is not satisfied for sufficiently close energy levels  $\varepsilon'_k \approx \varepsilon_j$ . For these latter, the coupling terms in (7.6) containing the matrix elements of the vibronic interaction  $W_{km}$  cannot be neglected and the adiabatic approximation is invalid.

The similarity with the JTE is also extended to the behavior of the APES near the point of pseudodegeneracy. Detailed calculations and discussion of this point are given in Section 7.4; the simple case of two coupled pseudodegenerate

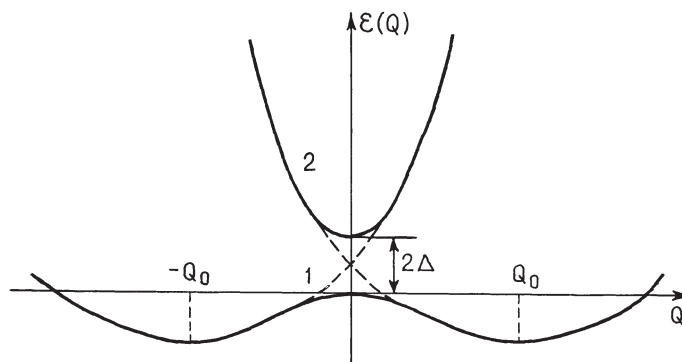


**FIGURE 7.7.** Variation of the adiabatic potential of a molecular system with two sufficiently close energy levels that mix under the  $Q$  displacements. The picture is similar to that of “avoided crossing” (pseudodegeneracy) shown by dashed lines. The lack of minimum of the ground state at  $Q = 0$  (pseudo Jahn–Teller instability) is similar to the Jahn–Teller case in Fig. 7.5, but with quadratic dependence on  $Q$  (dynamic instability), which causes differences in observable properties.

terms and one active coordinate is illustrated in Fig. 7.7. If the pseudocrossing of the two terms shown by dashed lines is taken into account, the analogy with the JTE becomes quite visual. But as distinguished from the JT case, the PJT lack of minimum in the ground state takes place only when a specific inequality is satisfied (Section 7.4).

It follows from formulation of the JT theorem that it does not refer to linear molecules. The reason is mentioned above; linear (first-order) low-symmetry (bending) distortions of linear molecules are of odd type, and hence the matrix elements  $W_{ij}$  of the linear terms of the vibronic coupling with  $i$  and  $j$  of the same symmetry type are zero, due to the selection rules. However, the quadratic terms of  $W$  give nonzero matrix elements, since the second-order distortions are even. Hence, when quadratic terms of the vibronic interaction (7.7) are factored in, linear molecules are subject to effects similar to those described for nonlinear systems. Linear molecules in this respect were first discussed by Renner [7.18], and the vibronic instability in linear systems is known as *the Renner–Teller effect* (RTE).

However, the Renner-type instability is similar but not identical to the JT one. Indeed, quadratic dependence on  $Q_{\Gamma^*}$  means that there is no intersection (only splitting) of the adiabatic potentials  $\varepsilon(Q)$  at the point of degeneracy  $Q_{\Gamma^*} = 0$  (Fig. 7.8). The behavior of  $\varepsilon(Q)$  at this point strongly depends on the strength of the vibronic coupling given by the quadratic vibronic constant  $G_{\Gamma^*}^{(\Gamma\Gamma')}$  (Section 7.2). There are two cases:

1. *Weak Renner–Teller effect*—the quadratic vibronic coupling  $G$  is small and the splitting of the APES does not result in the instability of the ground state (Fig. 7.8a)

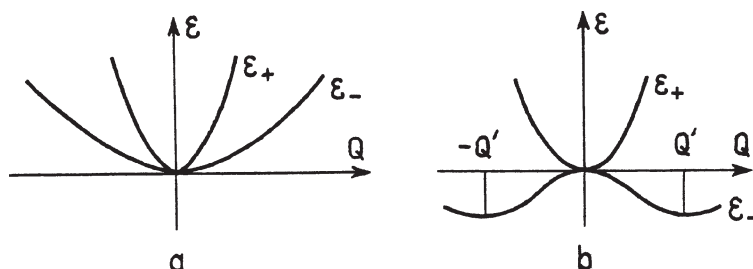


**FIGURE 7.8.** Variation of the adiabatic potential of a linear molecular system with respect to odd displacements  $Q$  in the case of the Renner–Teller effect: (a) weak coupling—term splitting without instability; (b) strong coupling—dynamic instability of the ground state.

2. *Strong Renner–Teller effect*—as a result of the vibronic splitting the ground state becomes unstable (Fig. 7.8b) [the increase in  $\varepsilon(Q)$  at larger  $Q$  values is provided by the higher-order terms in (7.7)].

Thus, for linear molecules with electronic degeneracy and strong quadratic vibronic coupling, the adiabatic potential of the ground state has no minimum at the point of degeneracy. However, in contrast to the JT case, the first derivative  $(d\varepsilon/dQ_{\Gamma^*})_0 = 0$ , that is, the point of degeneracy is extremal in the  $Q_{\Gamma^*}$  direction, but  $(d^2\varepsilon/dQ_{\Gamma^*}^2)_0 < 0$ , which means that it is a maximum in this direction. In terms of instability both PJT and RT systems are dynamically (quadratically) unstable, as opposed to the linear instability in the JT case. For further details on the RT effect, see Refs. 7.3, 7.22, and 7.23.

All the observable effects related to the special features of the adiabatic potential predicted by the JT theorem are called *the Jahn–Teller effects* [7.1–7.3]. For simplicity this term usually also includes the PJT and RT effects. The most widespread cases of the JTE are given below in this section, while the pseudo-JTE is given special attention in Section 7.4. Various applications of these effects to specific problems are considered in different sections of this book; many more examples can be found in Refs. 7.1–7.4 and references cited therein.

### The Jahn–Teller Effect in a Twofold-Degenerate Electronic State

The JT problems—the typical cases of electronic degeneracies that strongly influence the nuclear configurations and nuclear motions in molecular systems—are considered in detail in special monographs and books (see Refs. 7.1–7.4 and references cited therein). In this section we briefly review some results important for the study of coordination compounds and partly used in the next sections. Most widespread are orbitally double-degenerate  $E$  terms for systems that have at least one axis of symmetry of the third-order  $C_3$ , threefold-degenerate  $T$  terms (systems with cubic symmetry), and fourfold-degenerate  $G'$  (or  $\Gamma_8$ ) terms for



cubic systems with strong spin–orbital coupling; fivefold-degenerate terms of icosahedral systems are inherent mostly in organic compounds (e.g., fullerenes). Two-level and many-level PJTE are considered in Section 7.4.

To solve a JT problem means to find the JT active coordinates for the given  $f$ -fold degenerate electronic term, determine the APES in the space of these coordinates, and solve the system of  $f$  coupled equations (7.6). The resulting solution includes the energy-level spectrum and wavefunctions that allow one to calculate physical magnitudes. However, each of the abovementioned stages of the problem has an independent meaning and gives some qualitative insight into the problem. In particular, the JT active coordinates indicate the space of possible distortions of the system, while the APES describes the possible nuclear motions in the semiclassical approach.

In polyatomic systems with a large number of atoms ( $N$ ) and hence a large number of possible vibrations ( $3N-6$ ) there can be more than one, or even a large (in crystals—infinite) number of JT active coordinates. For instance, for a twofold-degenerate  $E$  term the JT active coordinates are also of  $E$  type, and the JT problem is  $E \otimes e$  (the active vibrations are indicated by small letters). But for large numbers  $N$  many  $E$  vibrations ( $E_1, E_2, \dots$ ) may be JT active. Then we have a *multimode problem* [denoted as  $E \otimes (e_1 + e_2 + \dots)$ ], distinct from the *ideal problem* for which there is only one active vibration of given symmetry.

The multimode problem is usually significant for coordination compounds with polyatomic ligands or multicenter systems, although even a simple five-atom tetrahedral complex  $MA_4$  has two types of vibrations with the same symmetry,  $T_2'$  and  $T_2''$  (Table 7.2), and hence its *Jahn–Teller* problem for a  $T$  term interacting with  $T_2$  vibrations is a two-mode one [ $T \otimes (t_2' + t_2'')$ ]. Under some restrictions, the multimode problem can be reduced to the ideal problem. Only ideal problems will be considered in this section. Discussion of multimode problems and solutions are given elsewhere (see Ref. 7.1 and references cited therein).

For an  $f$ -fold-degenerate term the  $f$  branches of the APES  $\varepsilon_k(Q_{\Gamma\gamma})$ ,  $k = 1, 2, \dots, f$ , are determined by Eq. (7.8) with the corrections  $W_{kk}(Q_{\Gamma\gamma})$  obtained from the solutions of the secular equation (7.30) taking  $W$  from (7.21). As mentioned in Section 7.2, there is a totally symmetric combination of the matrix elements of the coefficients at the quadratic terms in  $W$  that is equal to the primary force constant  $K_{0\Gamma}$ ; the corresponding terms can be grouped in expressions of the strain energy  $\frac{1}{2} \sum_{\Gamma\gamma} K_{0\Gamma} Q_{\Gamma\gamma}^2$ . The matrix elements of the remaining quadratic term coefficients are quadratic vibronic constants. Therefore, we can present the APES (7.8) in the form

$$\varepsilon_k(Q_{\Gamma\gamma}) = \frac{1}{2} \sum_{\Gamma\gamma} K_{0\Gamma} Q_{\Gamma\gamma}^2 + \varepsilon_k^v(Q_{\Gamma\gamma}) \quad (7.31)$$

where the vibronic corrections to the electronic term are the roots of the secular equation

$$\|W_{\gamma\gamma'}^v - \varepsilon^v\| = 0 \quad \gamma, \gamma' = 1, 2, \dots, f \quad (7.32)$$



and  $W_{\gamma\gamma'v}$ , as distinct from the similar Eq. (7.30), contains matrix elements of vibronic coupling terms only (without the elasticity term separated in (7.31)).

For a twofold orbitally degenerate  $E$  term, the JT active coordinates are either  $A_1 + E$  [in cases when  $(E \times E) = A_1 + E$ ], or  $A_1 + B_1 + B_2$  [for  $(E \times E) = A_1 + B_1 + B_2$ ]. The latter case is realized only in systems containing symmetry axes of the order multiple with four ( $C_4, C_8, \dots$ ). The totally symmetric vibrations  $A_1$  do not distort the system and can be eliminated by a special choice of the coordinate origin (however, see below). Hence the  $E$  term generates either *the  $E \otimes e$  problem*, which is more widespread, or *the  $E \otimes (b_1 + b_2)$  problem* for systems with  $4k$ -fold symmetry axes, where  $k$  is an integer.

Consider *the  $E \otimes e$  problem*. The two electronic wavefunctions of the  $E$  term may be denoted by  $|\vartheta\rangle$  and  $|\varepsilon\rangle$  with symmetry properties of the well-known functions  $\vartheta \sim 3z^2 - r^2$  and  $\varepsilon \sim x^2 - y^2$  (more often denoted as  $\vartheta \sim d_{z^2}$  and  $\varepsilon \sim d_{x^2-y^2}$ ). The two components of the normal  $E$ -type (tetragonal) displacements  $Q_\vartheta$  and  $Q_\varepsilon$  are illustrated in Fig. 7.1 (see also Fig. 9.20), while their expressions in Cartesian coordinates of the nuclei are given in Table 7.1. Accordingly, the matrix elements  $W_{\gamma\gamma'v}$  and hence  $\varepsilon_k^v(Q_{\Gamma\gamma})$  in Eq. (7.32) are dependent on these two coordinates only, and the APES in all the other coordinates after Eq. (7.31) retains a simple parabolic form:

$$\varepsilon_k(Q_{\Gamma\gamma}) = \frac{1}{2} \sum' K_\Gamma Q_{\Gamma\gamma}^2 \quad (\Gamma \neq E) \quad (7.33)$$

With regard to active  $E$  displacements, the vibronic interaction acquires a simple form if we employ the vibronic constants introduced in Section 7.2. Denote

$$F_E = \langle \vartheta | \left( \frac{\partial V}{\partial Q_\vartheta} \right)_0 | \vartheta \rangle \quad (7.34)$$

$$G_E = \frac{1}{2} \langle \vartheta | \left( \frac{\partial^2 V}{\partial Q_\vartheta \partial Q_\varepsilon} \right)_0 | \varepsilon \rangle \quad (7.35)$$

Then, keeping only the linear and second-order vibronic interaction terms, we obtain the explicit form of Eq. (7.32) for the  $E$ - $e$  problem:

$$\begin{vmatrix} F_E Q_\vartheta + G_E(Q_\vartheta^2 - Q_\varepsilon^2) - \varepsilon^v & -F_E Q_\varepsilon + 2G_E Q_\varepsilon Q_\vartheta \\ -F_E Q_\varepsilon + 2G_E Q_\vartheta Q_\varepsilon & -F_E Q_\vartheta - G_E(Q_\vartheta^2 - Q_\varepsilon^2) - \varepsilon^v \end{vmatrix} = 0 \quad (7.36)$$

This equation can be solved directly. In polar coordinates

$$Q_\vartheta = \rho \cos \phi \quad Q_\varepsilon = \rho \sin \phi \quad (7.37)$$

the two roots of (7.36) are

$$\varepsilon_\pm^v(\rho, \phi) = \pm \rho [F_E^2 + G_E^2 \rho^2 + 2F_E G_E \rho \cos 3\phi]^{1/2} \quad (7.38)$$

Inserting these values into Eq. (7.31), we obtain the following expression for the APES in the space of the  $Q_\vartheta$  and  $Q_\varepsilon$  Jahn–Teller active coordinates transformed into  $(\rho, \phi)$ :

$$\varepsilon_{\pm}(\rho, \phi) = \frac{1}{2}K_E\rho^2 \pm \rho[F_E^2 + G_E^2\rho^2 + 2F_E G_E \rho \cos 3\phi]^{1/2} \quad (7.39)$$

In particular, in the linear approximation (i.e., when quadratic terms may be neglected,  $G_E = 0$ ), this surface is simplified:

$$\varepsilon_{\pm}(\rho, \phi) = \frac{1}{2}K_E\rho^2 \pm |F_E|\rho \quad (7.40)$$

Here the adiabatic potential is independent of  $\phi$ ; it has the form of a surface of revolution often called the “Mexican hat” (Fig. 7.9). The radius  $\rho$  of the circle at the bottom of the trough and its depth reckoned from the degeneracy point at  $\rho = 0$ —the Jahn–Teller stabilization energy  $E_{JT}$ —are given by the following relationships:

$$\rho_0 = \frac{|F_E|}{K_E}, \quad E_{JT} = \frac{F_E^2}{2K_E} \quad (7.41)$$

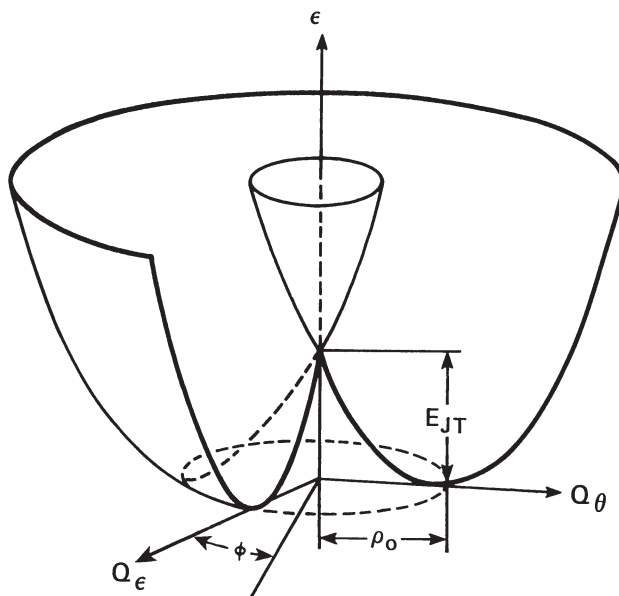


**FIGURE 7.9.** The APES for a twofold degenerate  $E$  term interacting linearly with the twofold degenerate  $E$ -type vibrations described by  $Q_\vartheta$  and  $Q_\varepsilon$  coordinates [linear  $E \otimes e$  problem, the “Mexican hat” (sombbrero)].  $E_{JT}$  is the Jahn–Teller stabilization energy.

If the quadratic terms of vibronic interaction are taken into account, this surface warps and three wells occur along the bottom of the trough of the Mexican hat, alternating regularly with three humps (the “tricorn,” Figs. 7.10 and 7.11).

The extremal points of the surface  $(\rho_0, \phi_0)$  are

$$\begin{aligned}\rho_0 &= \frac{\pm F_E}{K_E \mp (-1)^n 2G_E} \\ \phi_0 &= \frac{n\pi}{3} \quad n = 0, 1, \dots, 5\end{aligned}\quad (7.42)$$

with the upper and lower signs corresponding to the cases  $F_E > 0$  and  $F_E < 0$ , respectively. If  $F_E G_E > 0$ , the points of  $n = 0, 2, 4$  are minima, and those of  $n = 1, 3, 5$  are saddle points, whereas for  $F_E G_E < 0$  the two types of extremal points interchange. For the Jahn–Teller stabilization energy  $E_{JT}$  we have

$$E_{JT} = \frac{F_E^2}{K_E - 2|G_E|} \quad (7.43)$$

and the (minimal) barrier height between the minima is

$$\Delta = \frac{4E_{JT}|G_E|}{K_E + 2|G_E|} \quad (7.44)$$

In the linear approximation the curvature of the surface along the trough  $K_\phi = 0$ , and in the perpendicular (radial) direction  $K_\rho = K_E$  (note that in the absence of vibronic interactions  $K_\phi = K_\rho = K_E$ ). Taking into account the quadratic terms, one can obtain

$$K_\rho = K_E - 2|G_E| \quad K_\phi = \frac{9|G_E|(K_E - 2|G_E|)}{K_E - |G_E|} \quad (7.45)$$

It follows that if  $2|G_E| > K_E$ , the system has no minima at the point  $\rho_0$  and it decomposes, provided that the higher terms in  $Q$  of the vibronic interactions, neglected above, do not stabilize it at larger distances. At the minima points the curvature equals the force constant.

The two wavefunctions  $\Psi_\pm$  that correspond to the two sheets of Eq. (7.39) are

$$\begin{aligned}\Psi_- &= \cos \frac{\Omega}{2} |\vartheta \rangle - \sin \frac{\Omega}{2} |\varepsilon \rangle \\ \Psi_+ &= \sin \frac{\Omega}{2} |\vartheta \rangle + \cos \frac{\Omega}{2} |\varepsilon \rangle\end{aligned}\quad (7.46)$$

where

$$\tan \Omega = \frac{F_E \sin \phi - |G_E| \rho \sin 2\phi}{F_E \cos \phi + |G_E| \rho \cos 2\phi} \quad (7.47)$$

It is often assumed that  $\Omega \equiv \phi$ , which is true only in the absence of quadratic terms,  $G_E = 0$ .

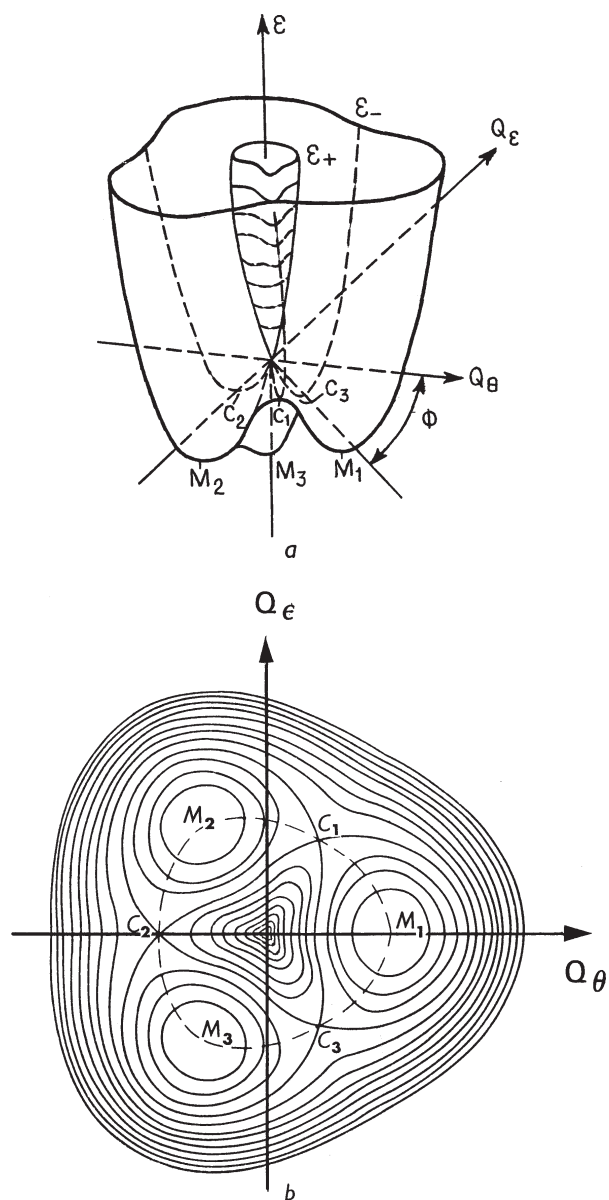


**FIGURE 7.10.** The APES for the  $E \otimes e$  problem with both the linear and quadratic terms of the vibronic interaction taken into account: (a) general view and (b) equipotential sections of the lower sheet  $\epsilon_-$ . Three minima ( $M_1, M_2, M_3$ ) and three saddle points ( $C_1, C_2, C_3$ ) are linked by the dashed line of the steepest slope from the latter to the former.

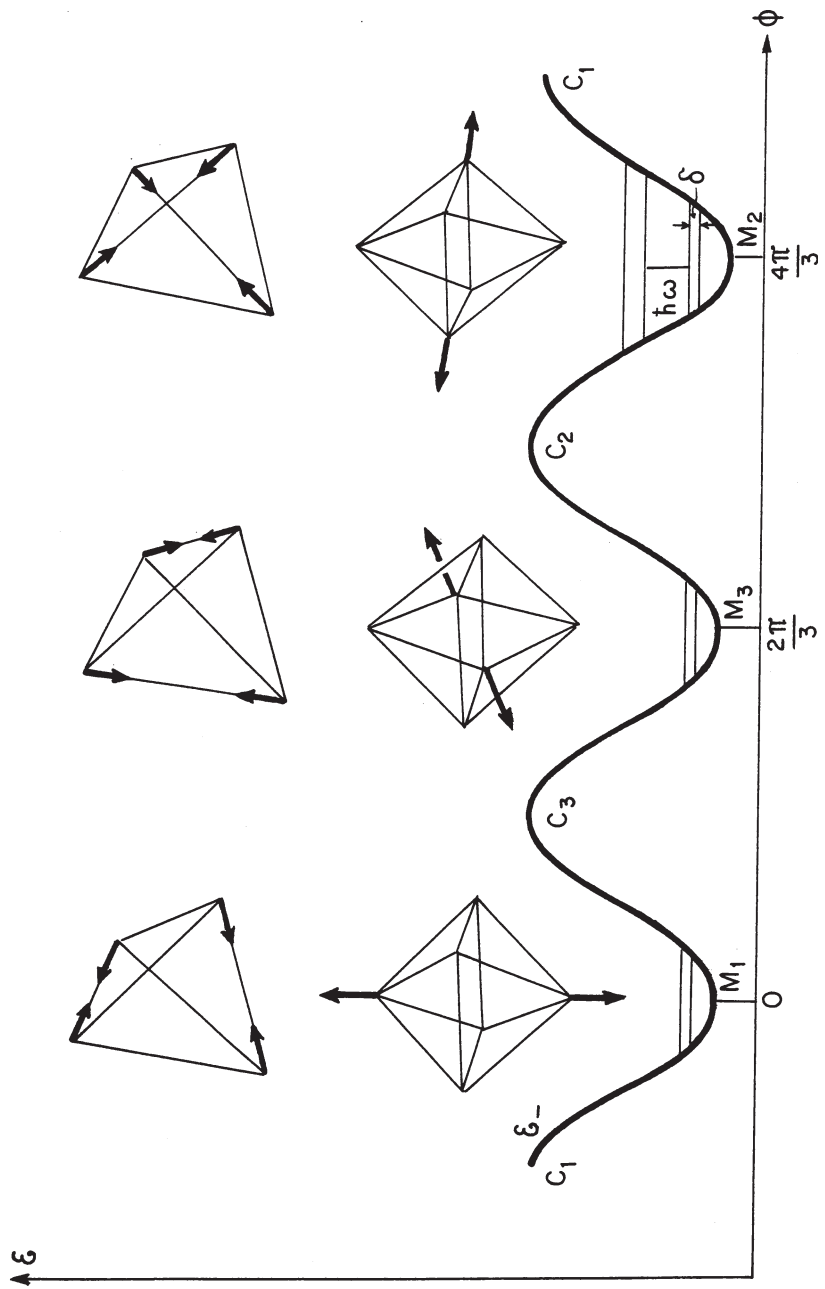
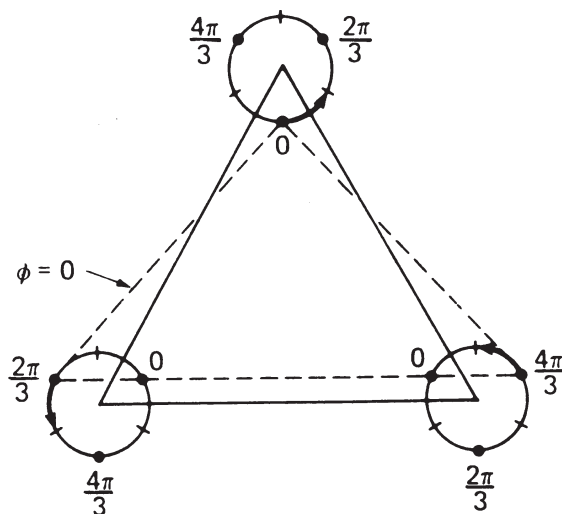


FIGURE 7.11. The section of the lowest sheet  $\epsilon_-$  of the APES of the quadratic  $E \otimes e$  problem along the angle  $\phi$  at the bottom of the trough of Fig. 7.9 (dashed line in Fig. 7.10) with illustration of the distortions of octahedral and tetrahedral systems at the points of minima.

With the shapes of the symmetric displacements  $Q_\vartheta$  and  $Q_\varepsilon$  and their values at the minima points known, one can evaluate the corresponding Jahn–Teller distortions for different types of molecules [7.3].

If the APES is known, some qualitative features of the nuclear behavior can be evaluated in the *semiclassical approach*, that is, considering the nuclei moving along the APES. This approximation is valid when the energy gap between different sheets of the APES is sufficiently large. This is realized for strong vibronic coupling and for nuclear configurations near the minima of the lowest sheet where the energy gap is the largest (in case of the  $E$  term this gap equals  $4E_{JT}$ ). If only the linear terms are accounted for and hence the lowest sheet of the APES has the shape of a Mexican hat, *the nuclear configuration performs free rotations in the space of the  $Q_\vartheta$  and  $Q_\varepsilon$  coordinates along the circle of minima in the trough*. In this case each atom, for instance, in a triangle molecule  $X_3$  describes a circle with radius equal to  $\rho_0\sqrt{3}$ . The circular motions of these atoms are correlated; the vectors of their displacements are shifted in phase through an angle of  $2\pi/3$  (Fig. 7.12). In any instant the equilateral triangle  $X_3$  is distorted to an isosceles triangle, and *the distortion travels as a wave around the geometric center performing specific internal rotations often called pseudorotations*.

In an octahedral molecule, which in the trigonal projection resembles two equivalent triangles, the two waves of deformations, traveling around each of



**FIGURE 7.12.** Distortions of a triatomic molecule  $X_3$  due to movement along the bottom of the trough of the lowest sheet of the APES in the linear  $E \otimes e$  problem. Each of the three atoms moves along a circle; their phases are deferred by  $2\pi/3$  from each other. The bold points indicate the minima positions when quadratic terms are taken into account. The dashed triangle corresponds to the point of minimum in Fig. 7.10 (the case of compressed triangles is shown; with the opposite sign of the vibronic constant, they are elongated).

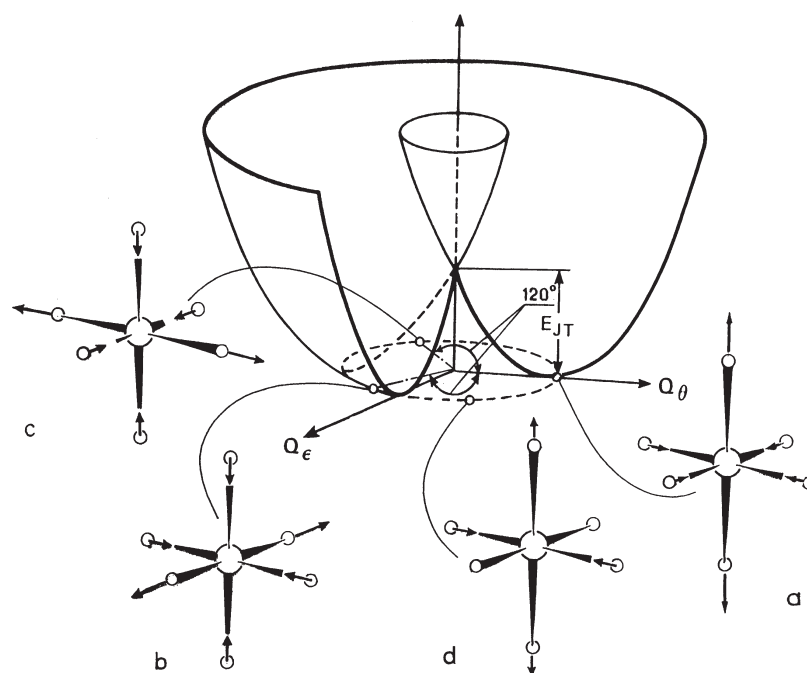


**FIGURE 7.13.** Distortions of an octahedral system  $ML_6$  at different points  $\varphi$  along the bottom of the trough of the “Mexican hat” in the linear  $E \otimes e$  problem. At points  $\varphi = 0, 2\pi/3, 4\pi/3$ , the octahedron is tetragonally distorted along the three fourfold axes, respectively (a, b, c). In between these points the configuration has  $D_{2h}$  symmetry (d) and varies continuously from one tetragonal configuration to another.

the triangles, are opposite in phase. As a result, the octahedron becomes elongated (or compressed) alternatively along each of the three fourfold axes and simultaneously compressed (elongated) along the remaining two axes (Fig. 7.13).

If the quadratic terms of the vibronic interactions are factored in, the lowest sheet of the adiabatic potential has three minima, in each of which the octahedron is elongated (or compressed) along one of the three axes of order 4 (Fig. 7.11); when allowing for quantum effects, *the nuclear motions along the adiabatic potential surface are likewise hindered rotations and tunneling transitions between the minima*, which may be presented by way of illustrations as “pulse” motions.

As indicated earlier, since  $[E \times E] = A_1 + E$ , the totally symmetric displacements  $A_1$  are also JT active in the  $E$  state (as in all the other cases): strictly speaking, the  $E-(e + a_1)$  problem should be solved instead of the  $E \otimes e$  one, considered above. However, the totally symmetric displacements do not change the molecular symmetry; they change proportionally only the interatomic distances. Therefore, in many cases, it may be assumed that the origin is taken in the new minimum position with regard to  $A_1$  coordinates, so that the interaction

with the  $A_1$  displacements, as with all the other JT modes, may be set apart. This cannot be done when one has to compare the vibronic effects in different systems or in a series of systems for which the  $A_1$  displacement contributions may be different (Section 9.4). For this (and other) reasons, the more rigorous expressions for the APES, including the interaction with all the active modes, may be useful [7.3].

To obtain the energy spectra and wavefunction in the JT  $E \otimes e$  problem the system of two equations (7.6) should be solved with the potential (7.39) or (7.40). For arbitrary parameter values this can be done numerically. However, for limiting values of strong and weak vibronic coupling, Eq. (7.6) can be solved analytically. Define the quantitative criterion of weak and strong coupling by comparing the JT stabilization energy  $E_{JT}^\Gamma$ , (7.41) or (7.43), with the energy of the  $n_\Gamma$ -fold zero-point vibration  $n_\Gamma \hbar \omega_\Gamma / 2$  (in the case under consideration  $\Gamma = E$  and  $n_\Gamma = 2$ ). Denote  $\lambda_\Gamma = 2E_{JT}^\Gamma / n_\Gamma \hbar \omega_\Gamma$ . Then, if  $\lambda_\Gamma \ll 1$  ( $E_{JT}^\Gamma \ll n_\Gamma \hbar \omega_\Gamma / 2$ ), the vibronic coupling is regarded as weak, and if  $\lambda_\Gamma \gg 1$  ( $E_{JT}^\Gamma \gg n_\Gamma \hbar \omega_\Gamma / 2$ ), the coupling is strong.  $\lambda_\Gamma$  is the dimensionless vibronic constant.

In the limit of weak vibronic coupling the depth of the vibronic minima are smaller than the zero-vibration energies, and therefore there are no local states in the minima. On the contrary, in the strong coupling limit there are such local states. Nevertheless, in both cases the system is delocalized into all the equivalent minima, provided that the stationary states of the free system (not instantaneous or specially prepared states) are considered. Therefore, the terms *dynamic Jahn–Teller effect* for weak coupling and *static Jahn–Teller effect* for strong coupling are unsuitable because, strictly speaking, in the absence of external perturbations both cases are dynamic. However, the term *static JTE* may be still meaningful if used to indicate situations when, in the limit of very deep minima, the one-minimum state is manifest in the experiment; this state may be regarded as a quasistationary one for the given process of measurement (see the relativity rule concerning the means of observation, Section 9.1).

Consider first the weak coupling limit, when  $\lambda \ll 1$  and the vibronic interaction  $W$  can be considered as a perturbation. The energy levels obtained in the second-order perturbation theory (with respect to linear in  $W$  terms) are

$$\begin{aligned} E_{nlm} &= \hbar \omega_E [n + 1 + 2\lambda_E (l^2 - m^2 - \frac{3}{4})] \\ l &= n, n-2, \dots, -n+2, -n \\ m &= \pm \frac{1}{2}, \pm \frac{3}{2}, \dots, \pm [n + \frac{1}{2}] \end{aligned} \quad (7.48)$$

where  $\lambda_E = (E_{JT}^E / \hbar \omega_E) = F_E^2 / 2\hbar \omega_E K_E$ . Since  $l$  and  $m$  are not independent, the energy  $E_{nlm}$  depends on only two quantum numbers, say,  $n$  and  $l$ ,  $E_{nl} = \hbar \omega_E [n + 1 + 2\lambda_E (\pm l - 1)]$ . Hence the  $2(n+1)$ -fold-degenerate level with a given  $n$  splits in  $n+1$  components ( $l$  may have  $n+1$  values). Each level remains twofold-degenerate owing to the independence of the energy (7.48) on the sign of  $m$ . The ground state is also twofold-degenerate,  $E_{00, \pm 1/2} = \hbar \omega_E (1 - \lambda_E) = \hbar \omega_E - 2E_{JT}$ . However, some of these levels, namely, those with quantum numbers



$m = \pm\frac{3}{2}, \pm\frac{9}{2}, \pm\frac{15}{2}, \dots$  pertain to the symmetry  $A_1 + A_2$ , which indicates that they are accidentally degenerate (the others are of E symmetry and therefore regularly degenerate).

In the other limit  $E_{JT} > \hbar\omega_E$  the quadratic terms of vibronic coupling may be important. The corresponding APES has the shape given in Fig. 7.10. If the barrier between the minima is not very large,  $\Delta \ll \hbar\omega_E$ , a separation between radial (along  $\rho$ ) and angular (along  $\phi$ ) motions is possible; it results in the following equation of motion along  $\phi$  [7.24]:

$$\left(-\frac{\alpha}{\hbar^2} \frac{\partial^2}{\partial \phi^2} + \beta \cos 3\phi - E_m\right) \Phi(\phi) = 0 \quad (7.49)$$

where  $\alpha = \hbar^2/3M\rho_0^2$  and  $\beta = G_E\rho_0^2$ .

This equation has been solved numerically. The energy levels obtained as functions of the ratio  $\beta/\alpha$  are illustrated in Fig. 7.14. It is seen that some of

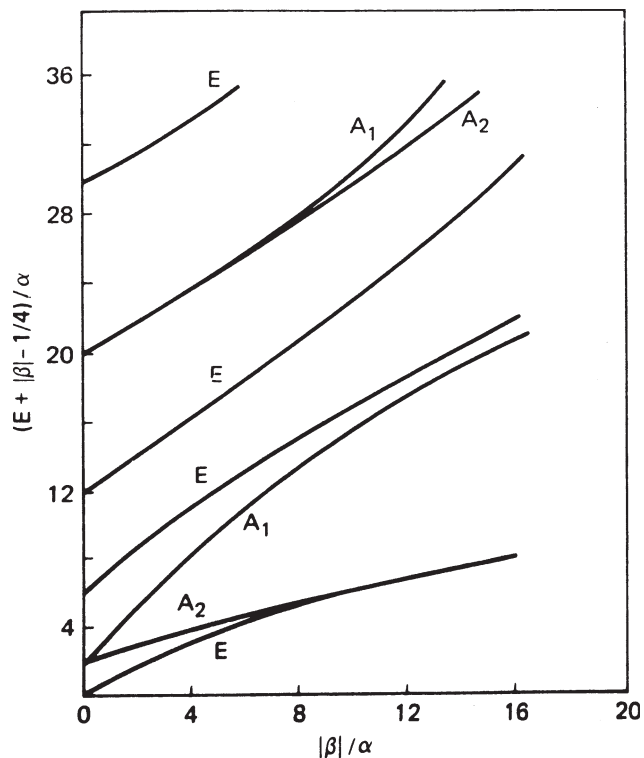


**FIGURE 7.14.** Energy levels for the quadratic  $E \otimes e$  problem—solutions of Eq. (7.49)—as functions of the ratio of the quadratic to linear vibronic constants,  $\beta/\alpha$ . (After O'Brien [7.24].)

the doublet rotational levels for  $\beta = 0$  (discussed above), namely, those transforming after the irreducible representations  $A_1 + A_2$  [i.e., accidental degenerate, cf. (7.48)], are split when the quadratic terms of vibronic interactions are taken into account, that is, when  $\beta \neq 0$ .

If the quadratic terms are nonzero, the motions in the circular trough, as distinct from the linear case, are no longer free rotations. At every point of the trough, as in the linear case, the distorted system performs rapid vibrations with the frequency  $\omega_E$ . When moving along the trough, the distortion of the nuclear configuration changes slowly assuming a continuous set of geometric figures in the space of  $E$  displacements illustrated in Fig. 7.13. However, unlike the linear case for which the motion of the distorted configuration along the bottom of the trough is uniform, in the presence of quadratic vibronic coupling the abovementioned changes of the nuclear configurations are hindered (or even reflected) by the adiabatic potential barriers. As a result, the system remains longer at the minima rather than at the barriers' maxima. *The picture as a whole can be characterized as hindered internal rotations of the Jahn–Teller distortions.*

For sufficiently large quadratic terms, when the quadratic barrier  $\Delta$  in Eq. (7.44) is of the order of or larger than the vibrational quanta  $\hbar\omega_E$  ( $\Delta > \hbar\omega_E$ ), the  $E \otimes e$  problem becomes complicated with three minima of the adiabatic potential and with high barriers between the minima. In this case the separation of the variables  $\rho$  and  $\phi$  is not valid, so the problem should be solved by another technique. Since the minima of the adiabatic potential are deep enough, local quasistationary states arise in each of them. Therefore, as far as the lowest vibronic states are concerned, the local states in the three minima can be taken as a starting approximation and then modified by their interactions by means of perturbation theory. As a result, the local vibrational states in the minima split, and the phenomenon as a whole resembles a quantum-mechanical *tunneling splitting*; it is a special case of tunneling splitting when the electronic and nuclear motions are coupled by the vibronic interaction and the minima are not purely vibrational.

The problem of tunneling splitting in Jahn–Teller systems was solved in different approximations for different cases [7.25] (see also Refs. 7.1–7.4 and 7.26 and references cited therein). The number of tunneling energy levels equals the number of minima (or more precisely, the number of vibrational states in the minima that interact, resulting in the splitting). For the splitting magnitude  $\delta$  in different states, see Ref. 7.3.

Visually, the *transitions between differently oriented distorted configurations may be imagined as pulsating deformations (distortions)*. Assume that as a result of synthesis or external perturbation the system happens to fall into the Jahn–Teller distorted configuration of one of the equivalent minima of the APES. Then, after a time  $\tau$ —the lifetime of the system in the minimum (which equals the inverse to the tunneling frequency or the tunneling splitting)—during which the system performs ordinary vibrations, it occurs in the equivalent state of another minimum, at which the distortion is similar but otherwise oriented

(Fig. 7.12). Then again, after time  $\tau$ , the system jumps (tunnels) into the third equivalent minimum configuration (or back to the first), and so on.

If the system is octahedral and is tetragonally distorted in the minimum (as in the  $E \otimes e$  problem), for instance, elongated along the fourfold axis, the pulsations of these deformations result in periodic (with a period  $\tau$ ) elongations along each of the three fourfold axes, alternatively. Since  $\delta \ll \hbar\omega$ , the frequency of pulsating distortions of the molecule is much less than the frequency of the vibrations in the distorted configuration, and the lifetime  $\tau$  of the latter is much greater than the period of vibrations.

Thus there are three types of Jahn–Teller dynamics: *free internal rotation* (pseudorotation), *hindered rotation*, and *pulsating Jahn–Teller deformations*.

*Tunneling splitting* in JT systems has received additional attention more recently in conjunction with the *topological (Berry) phase problem*. The latter started with the  $E \otimes e$  JT problem and is now widespread in treatments of a variety of physical and chemical phenomena. The issue is as follows. The wavefunction of the two ground vibronic states (7.46) are not single-valued (!); they change sign when transferred along the trough of the Mexican hat on a full circle around the conical intersection:  $\Psi_{\pm}(\phi + 2\pi) = -\Psi_{\pm}(\phi)$ . Since the total wavefunction should be single-valued, an additional phase factor  $e^{im\phi}$  with half-integer  $m$  values from (7.48) (for which  $e^{im(\phi+2\pi)} = -e^{im\phi}$ ) should be added to the nuclear wavefunction to compensate for the unphysical sign change. Berry [7.27] generalized this result and showed that this wavefunction phase property is due to the presence of the conical intersection and is of general importance to many physical and chemical properties [7.28]. For JT problems it is this topological phase factor that makes the quantum number  $m$  semiinteger and the ground vibronic state double-degenerate.

However, this phase factor occurs when there is only one or an odd number of conical intersections encircled by the nuclear motion. For an even number  $n$  of conical intersections the phase factor is  $2\pi n$ , and it does not influence the system in this respect [ $\Psi_{\pm}(\phi + 2\pi n) = \Psi_{\pm}(\phi)$ ]. In the  $E \otimes e$  problem with strong quadratic coupling and weak linear coupling there are three additional conical intersections that come near the central one, and the nuclear motion encircles four conical intersections. In this case the topological phase influence vanishes, the quantum numbers  $m$  for the vibronic energy levels become integers, and the ground state is nondegenerate  $A$  instead of the degenerate  $E$  when there is only one conical intersection [7.29].

One important effect of vibronic coupling is the reduction in ground-state physical quantities of electronic nature (*vibronic reduction*). It originates from the backward influence of the JT nuclear dynamics on the electronic structure and properties. In the majority of solutions of the vibronic problems, obtained above, the ground vibronic state possesses the same type of symmetry, degeneracy, and multiplicity as the initial electronic term in the high-symmetry configuration. The coincidence of the symmetry of the ground-state terms with and without the vibronic coupling allows one to simplify the calculations of many properties. It was shown [7.30] that if, taking into account the vibronic

coupling, the spin–orbital splitting of the ground state is proportional not only to the spin–orbital coupling constant, as in the usual nonvibronic cases, but also to this constant multiplied by the overlap integral between the vibrational functions of different minima. Since overlap integrals are always smaller than 1, the vibronic coupling reduces the spin–orbital splitting, sometimes by several orders of magnitude. Ham [7.31] generalized this idea and showed that such a reduction occurs for any physical magnitude, provided that its operator depends on electronic coordinates only. This reduction is sometimes called the *Ham effect*.

Reduction factors are denoted as  $K_\Gamma(\Gamma^*)$ ; they depend only on the degenerate electronic term under consideration  $\Gamma$ , the symmetry  $\Gamma^*$  of the physical property (operator) to be reduced, and the JT stabilization energy  $E_{JT}$ . For the linear  $E \otimes e$  problem approximate analytic expressions for the vibronic reduction factors  $K_E(A_2)$  and  $K_E(E)$ , often denoted by  $p$  and  $q$ , respectively, can be derived directly from the approximate solutions of the problem. For ideal linear  $E \otimes e$  problems  $2q - p = 1$ . In case of weak coupling  $p \approx \exp(-4E_{JT}/\hbar\omega_E)$ . For arbitrary coupling the  $p$  value can be derived from numerical solutions; for  $0.1 < E_{JT}/\hbar\omega_E < 3.0$ , the  $p$  value obeys the following relation [7.31]:

$$p = \exp \left[ -1.974 \left( \frac{E_{JT}}{\hbar\omega_E} \right) 0.761 \right] \quad (7.50)$$

and  $q = \frac{1}{2}(1 + p)$ . For sufficiently strong vibronic coupling  $p = 0$  and  $q = \frac{1}{2}$ .

Vibronic reduction factors and their manifestation in specific problems see are discussed in further detail in Ref. 7.3.

### Threefold-Degenerate Electronic States

Threefold orbital degenerate terms are possible for molecular systems that belong to the cubic or icosahedral symmetry point groups ( $T$ ,  $T_d$ ,  $T_h$ ,  $O$ ,  $O_h$ ,  $I$ ,  $I_h$ ). There are two types of orbital triplets:  $T_1$  and  $T_2$ . Since the vibronic effects in these two cases are similar, the consideration of only one of them, say,  $T_2$ , is sufficient. Denote the three wavefunctions, transforming as the coordinate products  $yz$ ,  $xz$ ,  $xy$ , by  $|\xi\rangle$ ,  $|\eta\rangle$ , and  $|\zeta\rangle$ , respectively. In the  $T$ -term case, unlike the  $E$  term, there are five Jahn–Teller active nontotally symmetric coordinates: two tetragonal  $Q_\vartheta$  and  $Q_\varepsilon$  ( $E$  type) and three trigonal  $Q_\xi$ ,  $Q_\eta$ , and  $Q_\zeta$  ( $T_2$  type) (see Figs. 7.1 and 7.2 and Table 7.1). For all the other coordinates the adiabatic potential remains parabolic [i.e., they provide no vibronic contributions  $\varepsilon_k^v$  in Eq. (7.31)]. *The problem is  $T \otimes (e + t_2)$ .*

The secular equation (7.32), which determines the vibronic parts of the APES  $\varepsilon_k^v(Q)$ , is of the third order. The matrix elements  $W_{\gamma\gamma'}^v$  contain two linear vibronic constants,  $F_E$  and  $F_T$ , and several quadratic constants  $G_\Gamma(\Gamma_1 \times \Gamma_2)$  [7.1–7.3].

Consider first the linear approximation for which  $G_\Gamma = 0$ . Denote

$$F_E = \langle \zeta | \left( \frac{\partial V}{\partial Q_\vartheta} \right)_0 | \zeta \rangle, \quad F_T = \langle \eta | \left( \frac{\partial V}{\partial Q_\xi} \right)_0 | \zeta \rangle \quad (7.51)$$

According to Eq. (3.44), all the matrix elements of the linear terms of the vibronic interactions can be expressed by means of these two constants, and secular equation (7.32) for  $\varepsilon_k^v(Q)$  takes the following form:

$$\begin{vmatrix} F_E(-Q_\vartheta + \sqrt{3}Q_\varepsilon) - 2\varepsilon^v & 2F_T Q_\zeta & 2F_T Q_\eta \\ 2F_T Q_\zeta & F_E(-Q_\vartheta - \sqrt{3}Q_\varepsilon) - 2\varepsilon^v & 2F_T Q_\xi \\ 2F_T Q_\eta & 2F_T Q_\xi & 2F_E Q_\vartheta - 2\varepsilon^v \end{vmatrix} = 0 \quad (7.52)$$

The three roots of this equation  $\varepsilon_k^v(Q)$ ,  $k = 1, 2, 3$ , are surfaces in the five-dimensional space of the coordinates  $Q_{\Gamma\gamma}$ ,  $\Gamma\gamma = E\vartheta, E\varepsilon, T\xi, T\eta, T\zeta$ . Together with the parabolic (nonvibronic) parts in Eq. (7.31), they determine the three sheets of the adiabatic potential (in the space of these coordinates), crossing at  $Q_{\Gamma\gamma} = 0$ :

$$\varepsilon_k(Q) = \frac{1}{2}K_E(Q_\vartheta^2 + Q_\varepsilon^2) + \frac{1}{2}K_T(Q_\xi^2 + Q_\zeta^2 + Q_\eta^2) + \varepsilon_k^v(Q) \quad k = 1, 2, 3 \quad (7.53)$$

However, the analytical solution of Eq. (7.52) is difficult. Opik and Pryce [7.21] worked out a procedure to determine the extremal points of the surface (7.53) without solving Eq. (7.52). In the particular case when  $F_T = 0$ ,  $F_E \neq 0$  (*the  $T \otimes e$  problem*) Eq. (7.52) can be solved directly:

$$\begin{aligned} \varepsilon_1^v(Q_\vartheta, Q_\varepsilon) &= -F_E Q_\vartheta \\ \varepsilon_2^v(Q_\vartheta, Q_\varepsilon) &= \frac{1}{2}F_E Q_\vartheta + \frac{\sqrt{3}}{2}F_E Q_\varepsilon \\ \varepsilon_3^v(Q_\vartheta, Q_\varepsilon) &= \frac{1}{2}F_E Q_\vartheta - \frac{\sqrt{3}}{2}F_E Q_\varepsilon \end{aligned} \quad (7.54)$$

Substitution of these solutions into Eq. (7.53) yields the APES consisting of a set of paraboloids; among them, the minima of only those containing the tetragonal  $Q_\vartheta$  and  $Q_\varepsilon$  coordinates are displaced from the origin. In these coordinates the surface has the shape of three equivalent paraboloids intersecting at the point  $Q_\vartheta = Q_\varepsilon = 0$  (Fig. 7.15). The positions of the three minima are given by the coordinates

$$(Q_0^E, 0) \quad \left(\frac{1}{2}Q_0^E, \frac{\sqrt{3}}{2}Q_0^E\right) \quad \left(\frac{1}{2}Q_0^E, -\frac{\sqrt{3}}{2}Q_0^E\right) \quad (7.55)$$

where

$$Q_0^E = \frac{F_E}{K_E} \quad (7.56)$$

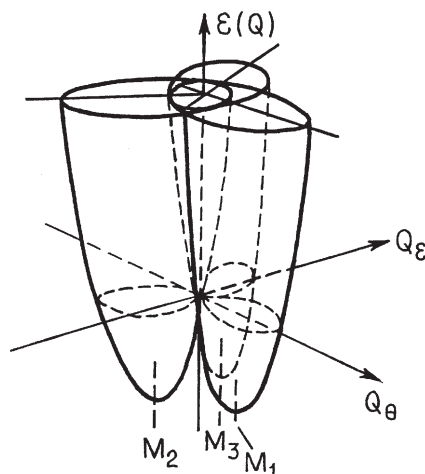


**FIGURE 7.15.** The APES surface for the Jahn–Teller  $T \otimes e$  problem. Three paraboloids intersect at  $Q_\theta = Q_\epsilon = 0$ ;  $M_1$ ,  $M_2$ , and  $M_3$  are the three minima.

For the depth of the minima, the Jahn–Teller stabilization energy, we have

$$E_{JT}^E = \frac{F_E^2}{2K} \quad (7.57)$$

Note that the relief of the surface sheets near the point of degeneracy (Fig. 7.15) is different from that of the  $E$  term (Figs. 7.9 and 7.10); in the case of the  $T$  term there is a real intersection of the surface sheets at the point  $Q_\theta = Q_\epsilon = 0$ , whereas for the  $E$  term there is a conical intersection, a branching instead of an intersection at this point. The wavefunction for the three paraboloids,  $|\zeta\rangle \sim yz$ ,  $|\eta\rangle \sim xz$ , and  $|\xi\rangle \sim xy$ , as distinct from the  $E \otimes e$  problem, are mutually orthogonal; they do not mix by the tetragonal displacements, and there is no tunneling splitting.

In the other particular case when  $F_E = 0$ ,  $F_T \neq 0$  (the  $T \otimes t_2$  problem) the third-order Eq. (7.52) cannot be solved directly. Using the method of Opik and Pryce [7.21], one can determine the extremal points of the adiabatic potential without solving Eq. (7.52). For the case in question the surface  $\varepsilon(Q_\zeta, Q_\eta, Q_\xi)$  in the space of trigonal coordinates has four minima lying on the  $C_3$  axes of the cubic system at the points  $(m_1 Q_0^T, m_2 Q_0^T, m_3 Q_0^T)$ , where the four sets of the numbers  $(m_1, m_2, m_3)$  are  $(1, 1, 1)$ ,  $(-1, 1, -1)$ ,  $(1, -1, -1)$ ,  $(-1, -1, 1)$ , and  $Q_0^T = -2F_T/3K_T$ .

At these minima the system is distorted along the trigonal axes. The displacements of the atoms corresponding to this distortion for an octahedral system are illustrated in Fig. 7.16. The six ligands, in two sets of three ligands each, move on the circumscribed cube toward two apexes that lie on the corresponding  $C_3$  axes. The depth of the minima, the Jahn–Teller stabilization energy, is

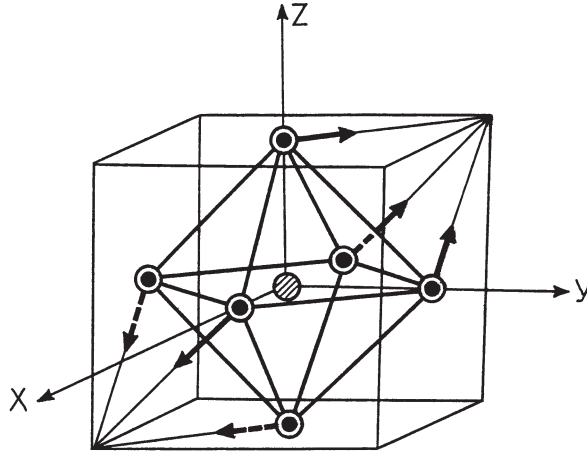


**FIGURE 7.16.** Trigonal distortion of an octahedron in an electronic  $T$  state (compare with the  $Q_\xi + Q_\eta + Q_\zeta$  displacement in Fig. 7.2).

$$E_{JT}^T = \frac{2F_T^2}{3K_T} \quad (7.58)$$

In this case the frequency  $\omega_T$  of the trigonal  $T_2$  vibrations splits into two [7.1, 7.3]:

$$\omega_A = \omega_T \quad K_A = K_T \quad (7.59)$$

$$\omega_E = \left(\frac{2}{3}\right)^{1/2} \omega_T \quad K_E = \frac{2}{3} K_T \quad (7.60)$$

The electronic wavefunctions in the minima are given by the relation

$$\Psi = \frac{1}{\sqrt{3}}(m_1|\xi\rangle + m_2|\eta\rangle + m_3|\zeta\rangle) \quad (7.61)$$

with the values of  $m_1$ ,  $m_2$ , and  $m_3$ , given above.

In the  $T \otimes (e + t_2)$  problem when the simultaneous interaction with both the tetragonal ( $F_E \neq 0$ ) and trigonal ( $F_T \neq 0$ ) displacements is taken into account, the APES in the five-dimensional space of the five coordinates  $Q_{\Gamma\gamma}$  is rather complicated, but the extremal points may be obtained using the Opik–Pryce procedure [7.21]. The APES for the linear  $T \otimes (e + t_2)$  problem has three types of extremal points:

1. Three equivalent tetragonal points, at which only tetragonal coordinates  $Q_\vartheta$  and  $Q_\varepsilon$  are displaced (from the origin  $Q_{\Gamma\gamma} = 0$ ). The coordinates of the minima and their depths are the same as in the linear  $T \otimes e$  problem, and are given by Eqs. 7.55–7.57.

2. Four equivalent trigonal points at which only the trigonal coordinates  $Q_\xi$ ,  $Q_\eta$ , and  $Q_\zeta$  are displaced (Fig. 7.15). The coordinates at the minimum coincide with those obtained in the  $T \otimes t_2$  problem [see Eq. (7.58)].
3. Six equivalent orthorhombic points, at each of which one trigonal and one tetragonal coordinate are displaced, and the minima depth is

$$E_{JT}^0 = \frac{1}{4}E_{JT}^E + \frac{3}{4}E_{JT}^T \quad (7.62)$$

If  $E_{JT}^E > E_{JT}^T$ , the trigonal points are minima and the tetragonal ones are saddle points, and vice versa, tetragonal points are minima while trigonal ones are saddle points when the opposite inequality holds. The orthorhombic extremal points are always saddle points in the linear approximation (compare with the quadratic case described below). In particular, when  $E_{JT}^E = E_{JT}^T$ , all the extremal points (including the orthorhombic ones) have the same depth; in this case a continuum of minima is realized, forming a two-dimensional trough on the five-dimensional surface of the APES (in a sense similar to the Mexican hat in the  $E$ -term case) [7.32].

If  $K_E = K_T$ , the classical motion of an octahedral system along the trough corresponds to the motions of the ligands around identical spheres centered at the apexes of the octahedron [7.1–7.3]. The displacements of different ligands are correlated; at every instant their radius vectors drawn from the center of the sphere, if shifted to a common origin, form a star whose apexes produce a regular octahedron rotating around its geometric center.

In the quadratic approximation the vibronic  $T \otimes (e + t_2)$  problem is rather complicated [7.33]. As in the  $E$ -term case, the quadratic terms of the vibronic interactions produce significant changes in the shape of the adiabatic potential of the  $T$  term. As in the case of linear coupling, there may be either trigonal or tetragonal minima, but in addition to these, under certain conditions, the orthorhombic extremal points (which are always saddle points in the linear approximation) may become minima. Moreover, there is also a possibility that the orthorhombic minima coexist with either the tetragonal, or the trigonal minima [7.1, 7.3]; this was confirmed experimentally.

Similar to the  $E \otimes e$  problem, the quadratic vibronic coupling influences essentially the topology of the APES in the  $T \otimes e$  and  $T \otimes (e + t_2)$  problems [7.34], but the latter are much more complicated, with several lines of conical intersections instead of just several points as in the  $E \otimes e$  problem.

An important feature of the orbital  $T$  terms, as distinct from those of the  $E$  terms, is the large splitting caused by the spin–orbital interaction (in the first order of perturbation theory). Therefore, if the system has unpaired electrons or, more generally, if the total spin  $S$  of the state under consideration is nonzero, the problem should be considered for the components that result from spin–orbital splitting of the  $T$  term. For instance, the spin doublet  ${}^2T$  (one unpaired electron) under spin–orbital interaction splits into two components:  ${}^2T = \Gamma_8 + \Gamma_6$ , from which the first  $\Gamma_8$  is a spin quadruplet and the second  $\Gamma_6$  is a spin doublet. The latter can be treated as a usual doublet, considered above, whereas the quadruplet term  $\Gamma_8$  requires additional treatment. Since  $[\Gamma_8 \times \Gamma_8] = A_1 + E + T_2$ , the



Jahn–Teller active displacements for the  $\Gamma_8$  state are  $E$  and  $T_2$ , and *the problem is*  $\Gamma_8 \otimes (e + t_2)$ , analogous to  $T \otimes (e + t_2)$ . Many features of the former are similar to those of the latter, but there are also some distinctions. Vibronic reduction factors for these terms, as well as other JT problems and applications to specific molecular systems and crystals, are discussed further in Refs. 7.1–7.4.

#### 7.4. PSEUDO-JAHN–TELLER EFFECT AND THE TWO-LEVEL PARADIGM

As mentioned in the previous Section 7.3, the *pseudo Jahn–Teller effect* (PJTE) takes place in the presence of pseudodegeneracy and may lead to configuration instability, which is similar (but not identical) to the JT one. *Pseudodegeneracy* means a nondegenerate ground state interacting (mixing) with a relatively low-energy excited state under nuclear displacements. Later in this section we show that there are limitations on symmetry, but not on the energy gap to such excited states; moreover, *vibronic (PJT-type) mixing of the ground electronic state with the excited states is the only possible source of high-symmetry configuration instability*. This statement can serve as a general tool for considering *how electrons control molecular configurations*. It creates a paradigm—*nuclear configuration changes necessarily involve the mixing of two or more electronic states*.

##### Pseudo-Jahn–Teller (PJT) Instability

Consider first an easy case of two nondegenerate states  $\Gamma$  and  $\Gamma'$  separated by an energy interval of  $2\Delta$  [7.21]. In order to obtain the adiabatic potential of these states, the vibronic contributions  $\varepsilon_k^v$  should be evaluated from the solutions of the secular equation (7.32). Assuming that only one coordinate  $Q = Q_{\Gamma^*}$ ,  $\Gamma^* = \Gamma \times \Gamma'$ , mixes the two states (in principle, there may be more than one coordinate of the type  $\Gamma^*$ ), and, taking into account only linear terms in the vibronic interaction  $W$  in Eq. (7.21), we obtain (the energy is read off from the middle of the  $2\Delta$  interval between the initial levels):

$$\begin{vmatrix} -\Delta - \varepsilon^v & FQ \\ FQ & \Delta - \varepsilon^v \end{vmatrix} = 0 \quad (7.63)$$

where  $F = \langle \Gamma | (\partial V / \partial Q_{\Gamma^*})_0 | \Gamma' \rangle$  is the off-diagonal linear vibronic constant. Inserting the solutions of Eq. (7.63)

$$\varepsilon^v = \pm [\Delta^2 + F^2 Q^2]^{1/2} \quad (7.64)$$

into Eq. (7.31) and assuming that the force constant is the same in both states  $K_0 = K_{0\Gamma} = K_{0\Gamma'}$ , we have

$$\varepsilon_{\pm} = \frac{1}{2} K_0 Q^2 \pm [\Delta^2 + F^2 Q^2]^{1/2} \quad (7.65)$$

or, after expanding the second term in  $Q$ ,

$$\varepsilon_{\pm}(Q) = \pm\Delta + \frac{1}{2} \left( K_0 \pm \frac{F^2}{\Delta} \right) Q^2 \mp \frac{1}{8} \frac{F^4}{\Delta^3} Q^4 \pm \dots \quad (7.66)$$

It is seen from these expressions that as a result of the vibronic coupling the two adiabatic potential curves change in different ways: in the upper sheet the curvature (the force constant) increases, whereas in the lower one it decreases. If  $\Delta > (F^2/K_0)$ , the minima of both states remain at the point  $Q = 0$  as in the absence of vibronic mixing. This is the case of *weak PJTE* (Fig. 7.17a). It contributes only to the change in curvatures (vibrational frequencies) at the minima of the two APES.

However, if

$$\Delta < \frac{F^2}{K_0} \quad (7.67)$$

the curvature of the lower sheet of the adiabatic potential becomes negative and the system is unstable with respect to the  $Q$  displacements. This is the case of *strong PJTE* (Fig. 7.17b). It is convenient to denote  $(F^2/K_0) = M$ . Then the points of minima of the adiabatic potential are given by  $\pm Q_0$

$$Q_0 = \left( \frac{M^2 - \Delta^2}{K_0 M} \right)^{1/2} \quad (7.68)$$

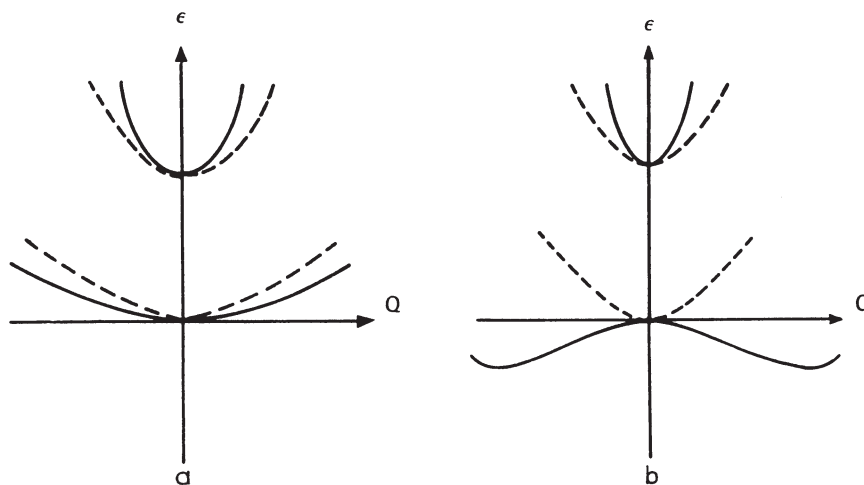


**FIGURE 7.17.** The APES behavior in the cases of (a) weak pseudo-Jahn–Teller effect (the ground state is softened but remains stable) and (b) strong pseudo-Jahn–Teller effect (the ground state becomes unstable at  $Q = 0$ ). The terms without vibronic coupling are shown by dashed lines.

$$M = \frac{F^2}{K_0}$$

with the curvature at the minima points

$$K = K_0 \left( 1 - \frac{\Delta^2}{M^2} \right) \quad (7.69)$$

If  $\Delta < M$  [see (7.67)], the curvature  $K$  of the APES at the minima (Eq. (7.69)), is positive (not to be confused with that at the high-symmetry configuration, which is negative), and hence distorted configurations may be stable.

Consider now a more complicated case of a transition metal complex with the electron configuration  $d^0$ , for instance, four-valence titanium in an octahedral coordination of oxygen atoms as in the cluster  $[\text{TiO}_6]^{8-}$  in  $\text{BaTiO}_3$  [7.3, 7.35]. For an approximate treatment, one may restrict the problem by considering the vibronic mixing of a group of close-in-energy electronic terms that are well separated from the other terms. The typical qualitative scheme of the MO energy levels and electron occupation numbers for this complex is shown in Fig. 7.18. It is seen that for a sufficiently comprehensive consideration at least nine MOs,  $t_{2g}$ ,  $t_{1u}$ , and  $t_{2g}^*$  (occupied by 12 electrons in the  $\text{TiO}_6^{8-}$  cluster) must be factored in. With allowance for interelectron repulsion, these states form the ground one,  ${}^1A_{1g}$ , and the excited states, from which those of the same multiplicity (singlets) are  ${}^1A_{2u}$ ,  ${}^1E_u$ ,  ${}^1T_{1u}$ ,  ${}^1T_{2u}$ ,  ${}^1A_{2g}$ ,  ${}^1E_g$ ,  ${}^1T_{1g}$ , and  ${}^1T_{2g}$ .

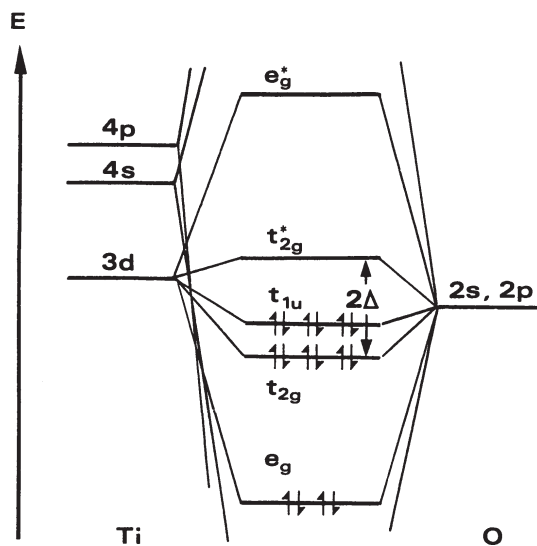


**FIGURE 7.18.** Schematic presentation of the HOMO and LUMO for the  $\text{TiO}_6^{8-}$  cluster in the  $\text{BaTiO}_3$ -type crystal.

In most cases of practical use the energies and wavefunctions, as well as covalence parameters for the MOs, are unknown. For a qualitative analysis of the vibronic effects the vibronic interaction may be considered at an earlier stage before covalence and the multielectron term formation. Then the nine atomic functions, three  $3d_\pi$  functions of the  $\text{Ti}^{4+}$  ion ( $d_{xy}$ ,  $d_{xz}$ ,  $d_{yz}$ ) and six combinations of the  $2p_\pi$  functions of the  $\text{O}^{2-}$  ions (forming the abovementioned nine MO  $t_{2g}$ ,  $t_{1u}$ , and  $t_{2g}^*$ ) may be taken as a basis of the vibronic treatment. These states mix by the  $T_{1u}$ -type displacements, which have three components,  $Q_x$ ,  $Q_y$ , and  $Q_z$ , one of which is shown in Fig. 7.19. The problem is thus  $(A_{1g} + T_{1u}) \otimes t_{1u}$ .

According to the Wigner–Eckart theorem (Section 3.4), the matrix elements of the ninth-order secular equation of perturbation theory in the linear approximation with respect to the vibronic coupling contain only one vibronic constant

$$F = \langle 2p_y | \left( \frac{\partial V}{\partial Q_x} \right)_0 | 3d_{xy} \rangle \quad (7.70)$$

Omitting the equation itself, we present its solutions [7.3, 7.35] ( $2\Delta$  is the energy interval between the  $3d_{xy}$  and  $2p_y$  states):

$$\begin{aligned} \varepsilon_{1,2}^v &= \pm [\Delta^2 + F^2(Q_x^2 + Q_y^2)]^{1/2} \\ \varepsilon_{3,4}^v &= \pm [\Delta^2 + F^2(Q_y^2 + Q_z^2)]^{1/2} \\ \varepsilon_{5,6}^v &= \pm [\Delta^2 + F^2(Q_x^2 + Q_z^2)]^{1/2} \\ \varepsilon_{7,8,9}^v &= -\Delta \end{aligned} \quad (7.71)$$

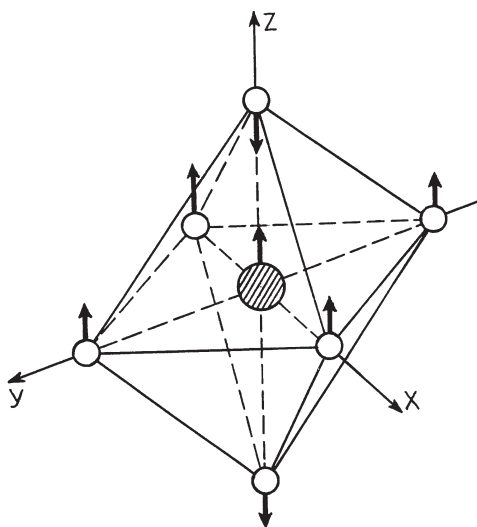


FIGURE 7.19. One component of the  $T_{1u}$  displacement in the octahedral  $\text{TiO}_6$  cluster.

From these nine levels only the lower six are occupied by the 12 electrons (mentioned above) in the ground state. Substituting  $\varepsilon_1^v$ ,  $\varepsilon_3^v$ , and  $\varepsilon_5^v$  from (7.71) into Eq. (7.31), we obtain the following expression for the ground-state adiabatic potential ( $\varepsilon_{7,8,9}$  are independent of  $Q$  and can be excluded from further consideration):

$$\begin{aligned} \varepsilon(Q_x, Q_y, Q_z) = & \frac{1}{2}K_0(Q_x^2 + Q_y^2 + Q_z^2) - 2\{[\Delta^2 + F^2(Q_x^2 + Q_y^2)]^{1/2} \\ & + [\Delta^2 + F^2(Q_y^2 + Q_z^2)]^{1/2} + [\Delta^2 + F^2(Q_x^2 + Q_z^2)]^{1/2}\} \end{aligned} \quad (7.72)$$

The shape of this surface depends on the relation between the constant  $\Delta$ ,  $F$ , and  $K_0$ . Denoting  $Z = 4F^2/K_0$ , we can see that if  $\Delta > Z$ , the surface has one minimum at the point  $Q_x = Q_y = Q_z = 0$ , and the system remains undistorted. This is the weak pseudo-Jahn–Teller effect (Fig. 7.19a). However, if

$$\Delta < Z \quad (7.73)$$

the surface (7.72) acquires a rather complicated shape with four types of extremal points:

1. One maximum at  $Q_x = Q_y = Q_z = 0$  (dynamic instability).
2. Eight minima at points  $|Q_x| = |Q_y| = |Q_z| = Q_0^{(1)}$

$$Q_0^{(1)} = \left(2 \frac{Z^2 - \Delta^2}{K_0 Z}\right)^{1/2} \quad (7.74)$$

with the Jahn–Teller stabilization energy

$$E_{\text{JT}}^{(1)} = \frac{3(Z - \Delta)^2}{Z} \quad (7.75)$$

At these minima the Ti atom is displaced along the trigonal axes, equally close to three oxygen atoms and removed from the other three.

3. Twelve saddle points at  $|Q_p| = |Q_q| \neq 0$ ,  $Q_r = 0$ ,  $p, q, r = x, y, z$  (with a maximum in section  $r$  and minima along  $p$  and  $q$ ). At these points the Ti atom is displaced toward two oxygen atoms lying on the  $p$  and  $q$  axes, respectively.
4. Six saddle points at  $Q_p = Q_q = 0$ ,  $Q_r = Q_0^{(2)}$

$$Q_0^{(2)} = 2 \left(\frac{Z^2 - \Delta^2}{K_0 Z}\right)^{1/2} \quad (7.76)$$

with a depth

$$E_{\text{JT}}^{(2)} = \frac{2(Z - \Delta)^2}{Z} \quad (7.77)$$

With covalence and multielectron term formation included, these results, especially their quantitative expression, are modified, but the main qualitative conclusions do not alter.

The origin of the instability of the position of the  $\text{Ti}^{4+}$  ion in the center of the octahedron can be given a visual treatment similar to that in Fig. 7.20, discussed below. When the Ti atom is in the central position exactly, the overlap of its  $d_{xy}$  AO with the appropriate ( $T_{1u}$ ) combination of the oxygen  $p_y$  AO is zero on symmetry (positive overlaps are counterbalanced for by negative ones). However, if the Ti atom is shifted toward any of the oxygen atoms resulting in its off-center position (Fig. 7.19), the overlap becomes nonzero and produces a new covalent bonding that lowers the energy of such distortions.

Similar treatment is possible for tetrahedral complexes of the type  $MA_4$ . For them, in the strong vibronic coupling limit and under certain vibronic mixing conditions four equivalent minima are expected. In each of these minima one bond M—A is longer or shorter than the other three, which remain identical.

In stereochemistry and reactivity problems, as well as in spectroscopy and crystal chemistry (Sections 9.2, 9.4, 11.2, etc.), other cases of pseudo-Jahn–Teller effects may be significant. In particular, the vibronic mixing of  $E$  and  $A_1$  terms under  $E$ -type displacements [the  $(E + A) \otimes e$  problem] is often encountered. We consider here this type of mixing for a system with  $C_{4v}$  symmetry [7.36]. The two wavefunctions of the  $E$  term transform as the  $x$  and  $y$  coordinates. If we denote the two components of the  $E$  mode by  $Q_x$  and  $Q_y$  and the energy gap between the  $E$  and  $A_1$  levels by  $2\Delta$ , the secular Eq. (7.32) in the linear approximation takes the following form:

$$\begin{vmatrix} -\Delta - \varepsilon^v & 0 & FQ_x \\ 0 & -\Delta - \varepsilon^v & FQ_y \\ FQ_x & FQ_y & \Delta - \varepsilon^v \end{vmatrix} = 0 \quad (7.78)$$

In polar coordinates (7.37) the roots of this equation are

$$\varepsilon_{1,3}^v = \pm[\Delta^2 + F^2\rho^2]^{1/2} \quad \varepsilon_2^v = -\Delta \quad (7.79)$$

and for the APES of the ground state, we get

$$\varepsilon(\rho, \phi) = \frac{1}{2}K_E\rho^2 - [\Delta^2 + F^2\rho^2]^{1/2} \quad (7.80)$$

It is seen that in the linear approximation the APES is independent of the angle  $\phi$ —it is a surface of revolution. Similar to the two-level case considered at the beginning of this subsection with  $M = F^2/K_E$ , we find that if  $\Delta < M$ , the

surface has a maximum at the point  $\rho = 0$  (dynamic instability), and a circular trough at  $\rho = \rho_0 = [(M^2 - \Delta^2)/K_E M]^{1/2}$ . The depth of the trough [read off the point  $\varepsilon(0) = -\Delta$ ] is

$$E_{\text{PJT}} = \frac{M^2 - \Delta^2}{2M} \quad (7.81)$$

If quadratic terms of the vibronic interaction are taken into account, two quadratic constants,  $G_1$  and  $G_2$ , must be introduced. The secular equation complicates and the adiabatic potential, unlike the linear case, becomes dependent on the angle  $\phi$  (acquiring the initial symmetry  $C_{4v}$ ); four minima regularly alternating with four saddle points occur on the adiabatic potential as a function of  $\phi$  [along the trough (7.80)]. At the extremal points  $\phi = n\pi/4$ , where  $n = 0, 1, 2, \dots, 7$ . If  $G_1 > G_2$ , the minima are given by  $\phi_0(\text{min}) = n\pi/4$ ,  $n = 1, 3, 5, 7$ , and the saddle points are at  $n = 0, 2, 4, 6$ . In the opposite case,  $G_1 < G_2$ , the minima and saddle points interchange, and if  $G_1 = G_2$ , the surface preserves the trough of the linear approximation.

These examples show that for relatively close-in-energy electronic terms (pseudodegeneracy) *the adiabatic potential as a result of the PJTE acquires features similar to those obtained in the JTE: instability of the high symmetry configuration and several equivalent (or a continuum of) minima*. The criterion of the strong effect of PJT instability (7.67) or (7.73) (in other cases this condition appears similar) contains three parameters:  $\Delta$ ,  $K_0$ , and  $F$ , and therefore it may be “soft” for any of them taken apart. In particular, a strong effect may occur for large values of the energy gap  $\Delta$ , if the force constant  $K_0$  is sufficiently small and the vibronic constant  $F$  is large.

Cases when the criterion of strong PJT effect is not satisfied,  $\Delta > (F^2/K)$ , are also important. Indeed, although the configuration is stable (the APES has a minimum in this configuration), the curvature of the ground state, as indicated above, is lowered, *the nuclear configuration is softened* in the  $Q$  direction, and it is further softened when  $F$  is larger and  $\Delta$  is smaller (for a given  $K_0$  value). This situation is significant, for instance, in investigation of chemical reaction mechanisms (Section 11.2).

*Along with strong similarities, there are essential differences between the Jahn–Teller and pseudo Jahn–Teller effects.* An important feature of the pseudo effect is that the two (or more) mixing electronic states  $\Gamma$  and  $\Gamma'$  may belong to different IrReps of the point group of the system, whereas in the JT case they belong to the same representation. Consequently, in the PJTE the direction of distortion may have any symmetry that is possible in the symmetry group of the system under consideration, whereas in the JTE these directions are limited by JT active modes (Section 7.3). In particular, for systems with an inversion center the two mixing states  $\Gamma$  and  $\Gamma'$  in the PJTE may possess opposite parity. Then the vibronic constant  $F_{\Gamma^*}^{(\Gamma\Gamma')}$  is nonzero for odd nuclear displacements  $Q$ , which remove the inversion center and form a dipole moment (*dipolar instability*). As a result, the system in its minima configurations has a dipole moment. This

dipolar instability is impossible in JT systems with inversion centers since the mixing electronic terms have the same symmetry  $\Gamma = \Gamma'$  and hence the active modes can be only even.

Similarly to JT distortions, the origin of instability of the high-symmetry configuration and its distortion due to the strong PJTE can be illustrated in simple images. Consider, for instance, a square-planar complex of the type  $MA_4$  with  $D_{4h}$  symmetry and suppose that the  $d_{z^2}$  orbital of the metal M (the  $A_{1g}$  orbital) is the HOMO, while the LUMO of  $A_{2u}$  symmetry is formed by the four  $p_z$  orbitals of the ligands (Fig. 7.20) (or vice versa, the  $d_{z^2}$  orbital is the LUMO and  $A_{2u}$  is the HOMO). In the planar configuration these two MOs do not mix, since the overlap integral  $S$  is zero (Fig. 7.20a).

However, if the atom M displaces out of and transversely to the plane (in the  $A_{2u}$  direction), a nonzero overlap occurs and the two orbitals mix to form a  $\pi$  bond between the metal and the ligands (Fig. 7.20b). As a result, the energy of the ground state is lowered (as compared with that without mixing) and the curvature of the adiabatic potential in the direction of the  $A_{2u}$  displacement decreases (weak effect; Fig. 7.17a), or becomes negative (strong effect; Fig. 7.17b). The latter case takes place when the covalence of the new bond formed is superior to the changes in strain energy. For further discussion of the origin of vibronic instability, see Eqs. (7.88)–(7.91) and Table 7.4 (in Example 7.3).

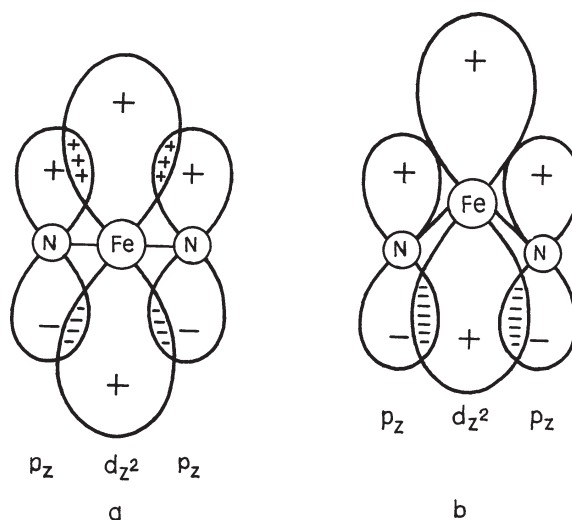


**FIGURE 7.20.** Visual treatment of the origin of the pseudo-Jahn–Teller effect using the N—Fe—N fragment of the square-planar  $FeN_4$  group as an example (cf. iron porphyrin, Section 9.2): (a) when Fe is in the  $N_4$  plane (on the N—Fe—N line), the  $d_{z^2}$ – $p_z$  overlap between the HOMO (nitrogen  $p_z$ ) and LUMO (iron  $d_{z^2}$ ) orbitals is zero; (b) the out-of-plane displacement of the Fe atom results in nonzero  $d_{z^2}$ – $p_z$  overlap and bond formation, which lowers the curvature of the adiabatic potential in the direction of such a displacement.



### Uniqueness of the Vibronic Mechanism of Configuration Instability: The Two-Level Paradigm

Consider in more detail the criterion of the strong PJTE given by the inequality (7.67). The three parameters ( $\Delta$ , the energy gap between the ground and excited state;  $F$ , the vibronic coupling constant; and  $K_0$ , the primary force constant) can acquire arbitrary values (or at least a wide range of values), which means that condition (7.67) can be obeyed for any value of one of these parameters, if the other two are appropriate. It follows that *the PJTE can be operative for any polyatomic system without a priori restrictions*.

Note that in the PJT case all the electrostatic (attraction and repulsion) forces in the reference nuclear configuration are equilibrated; that is, the first derivative of the APES in the given direction  $Q$  is zero. Thus the pseudo-Jahn–Teller effect is rather a case of *unstable equilibrium, or dynamic instability*, as distinct from the static instability in the Jahn–Teller effect when the Coulomb forces are not compensated. In both cases the term *configuration instability* means instability of the reference nuclear configuration with respect to certain distortions, which does not necessarily imply absolute instability of the molecular system with respect to its component parts; the system may be stable in the distorted configuration.

*The PJTE provides a mechanism of electronic control of nuclear configuration instability via vibronic coupling.* In this mechanism any two electronic states of a given nuclear configuration, ground 1 and excited 2, can cause its instability in a certain (symmetrized) direction  $Q$ , provided that inequality (7.67) is satisfied. From this statement an important question emerges: Is this vibronic mechanism of dynamic instability (unstable equilibrium) the only possible one, or do other mechanisms control this instability? In other words, *is the condition of instability (7.67) both necessary and sufficient, or is it only sufficient?*

To state this question more rigorously, consider the expression for the curvature of the adiabatic potential of the system at the point  $Q_{\Gamma^*} = 0$  in the direction of the symmetrized coordinate  $Q_{\Gamma^*}$  (7.23) (hereafter for simplicity the index  $\Gamma^*$  is omitted):

$$K^{\Gamma} = K_0^{\Gamma} + K_v^{\Gamma} \quad (7.82)$$

where (note that  $\partial H/\partial Q = \partial V/\partial Q$ )

$$K_0^{\Gamma} = \langle \Gamma | \left( \frac{\partial^2 H}{\partial Q^2} \right)_0 | \Gamma \rangle \quad (7.83)$$

$$K_v^{\Gamma} = - \sum_{\Gamma'} \frac{|F^{\Gamma\Gamma'}|^2}{\Delta_{\Gamma\Gamma'}} \quad (7.84)$$

and  $F^{\Gamma\Gamma'}$  and  $\Delta_{\Gamma\Gamma'}$  are as denoted above. Equation (7.82) can be obtained by means of second-order perturbation theory, but it is an exact expression for the curvature as the coefficient at  $\frac{1}{2}Q^2$  in the dependence of the APES on  $Q$  at the

minimum point; it was discussed first by Bader [7.37]. The first term  $K_0^\Gamma$ , after (7.83), the mean value of the curvature operator in the ground state, has the meaning of the contribution (to  $K^\Gamma$ ) from the  $Q$  displacement of the nuclei in a fixed (frozen) electronic distribution. The second term,  $K_v^\Gamma$ , after (7.84), gives the negative contribution to  $K^\Gamma$  that arises because the electrons follow the nuclei (at least partly), and hence the electronic states change under nuclear displacements. This is *the relaxation term*.

On the other hand, this term describes the contribution of vibronic mixing of the ground state with excited states to the  $K^\Gamma$  value of the former. A similar contribution to  $K$  from one excited state as a result of the PJTE is given by Eq. (7.66). As distinct from this two-level PJTE, Eq. (7.84) gives the pseudo-Jahn–Teller contribution to the ground-state curvature arising from *all* the excited states (*multilevel PJTE*).  $K_v^\Gamma$  is therefore the *vibronic contribution* to the curvature, as opposed to  $K_0^\Gamma$ , which is the proper, or *ground-state, contribution* (often called the *primary force constant*).

Since  $K_v^\Gamma$  is negative, it always lowers the curvature of the ground state; the vibronic coupling destabilizes the system (in the ground state). If  $K_0^\Gamma > 0$  and  $|K_v^\Gamma| > K_0^\Gamma$ , the system possesses a negative total curvature  $K^\Gamma < 0$ , and hence the vibronic coupling to the excited states causes instability of the ground state. The condition

$$\sum_{\Gamma'} \frac{|F^{(\Gamma\Gamma')}|^2}{\Delta_{\Gamma'\Gamma}} > K_0^\Gamma \quad (7.85)$$

is thus a multilevel analogy of the criterion of the two-level PJT instability (7.67). In the infinite sum in (7.85) only several terms (in most cases one to three) are significant; the others are negligible because of either selection rules ( $\Gamma^* \in \Gamma \times \Gamma'$ ), or large denominators  $\Delta_{\Gamma'\Gamma}$ .

Now, if  $K_0^\Gamma < 0$ , the system is unstable without vibronic coupling. But if  $K_0^\Gamma > 0$ , then condition (7.85) becomes necessary for the instability. Thus if one proves that

$$K_0^\Gamma > 0 \quad (7.86)$$

then the condition of vibronically induced dynamic instability is both necessary and sufficient and the vibronic mechanism of instability is the only possible one in polyatomic systems.

There are several particular proofs of the inequality  $K_0^\Gamma > 0$  for different types of polyatomic systems. First, the formulation of the problem and a general but not very rigorous proof was given [7.38]. Then this proof was significantly improved and expanded [7.39]. Mathematically rigorous proofs of the inequality  $K_0 > 0$  was obtained for diatomics [7.40], and for cubic systems (crystals) and some linear chains [7.41, 7.42] (see also Refs. 7.1 and 7.3). The proofs are most general with the restriction that the first derivative  $\langle \Gamma | (\partial H / \partial Q)_0 | \Gamma \rangle = 0$ , meaning that

at the nuclear configuration under consideration the Coulomb forces are equilibrated so there is either a maximum or a minimum on the APES (we call this a *high-symmetry configuration*), and the condition  $K_0^\Gamma > 0$  means that without the pseudo-JTE there is always a minimum. Example 7.2 demonstrates explicitly that  $K_0 > 0$  in unstable configurations by means of numerical calculations, while Example 7.3 shows some results of ab initio calculations of pseudo-JT instabilities in TMS.

### EXAMPLE 7.2

#### *Numerical Confirmation of PJT Origin of Instability of High-Symmetry Configurations*

To confirm the analytical deductions and to reveal the excited states that cause the instability of the ground state, ab initio calculations were performed for a series of molecular systems in unstable configuration with  $K < 0$  [7.39]. Some results are presented in Table 7.3. The  $K_0$  values

**TABLE 7.3. Ab Initio Calculations of Vibronic Constants ( $F^{0i}$ ), Nonvibronic ( $K_0$ ), and Vibronic ( $K_v$ ) Contributions to the Force Constant ( $K$ ) for Some Molecular Hydrides in the Unstable Configuration with Respect to Hydrogen Displacements<sup>a</sup>**

System, Symmetry	Coordinate of Instability	$F^{(0i)}$ $10^{-4}$ dyn	$\Delta_{i0}$ eV	$K_0$ (mdyn/Å)	$K_v = \Sigma_i K_v^i$ (mdyn/Å)	$K = K_0 + K_v$ (mdyn/Å)
H <sub>3</sub> , $D_{\infty h}$	$\Pi_u$	4.84	12.0	0.13	-0.24	-0.11
NH <sub>3</sub> , $D_{3h}$	$A_2''$	8.76	14.0	0.43	-0.68	-0.25
BH <sub>4</sub> , $D_{4h}$	$B_{2u}$	6.04	6.8	0.83	-1.34	-0.51
		8.99	22.8			
CH <sub>4</sub> , $D_{4h}$	$B_{2u}$	6.98	11.1	0.69	-1.27	-0.58
		11.45	25.8			
NH <sub>4</sub> <sup>+</sup> , $D_{4h}$	$B_{2u}$	6.32	14.2	0.44	-0.87	-0.43
		10.55	33.4			
OH <sub>4</sub> <sup>2+</sup> , $D_{4h}$	$B_{2u}$	5.14	16.0	0.29	-0.51	-0.22
		9.30	36.4			
AlH <sub>4</sub> <sup>-</sup> , $D_{4h}$	$B_{2u}$	5.34	8.7	1.06	-1.18	-0.12
		9.48	19.8			
SiH <sub>4</sub> , $D_{4h}$	$B_{2u}$	5.04	7.3	0.71	-1.15	-0.44
		9.15	23.4			
PH <sub>4</sub> <sup>+</sup> , $D_{4h}$	$B_{2u}$	4.53	4.6	0.48	-1.11	-0.63
		8.96	27.2			
SH <sub>4</sub> <sup>2+</sup> , $D_{4h}$	$B_{2u}$	3.85	8.4	0.37	-0.66	-0.30
		9.02	25.5			

<sup>a</sup>Two values of  $F^{(0i)}$  and  $\Delta_{i0}$  correspond to two excited states that contribute to the instability.

were calculated directly by Eq. (7.83) with the ground-state wavefunctions obtained by numerical calculations in the 3G-STO approximation (Section 5.3). In Table 7.3 the vibronic coupling parameters are also given.

For the systems in this table the distortions (indicated by symmetry in column 2) involve displacement of the hydrogen atoms for which, as follows from the analytical deductions [7.39], the inequality  $K_0 > 0$  is less favorable than for more heavy atoms. Nevertheless, the results of the calculations (column 5) show explicitly that indeed  $K_0 > 0$  in these cases, too, as follows from the general theory.

### EXAMPLE 7.3

#### *Numerical Calculations Confirming the PJT Origin of Configuration Instability of Coordination Systems [7.43]*

Table 7.4 shows the results of ab initio calculations of the negative contribution of the PJTE  $K_v$  to the curvature  $K = K_0 + K_v$  of the ground-state APES in the direction of  $T_{1u}$  distortions for three isoelectronic transition metal fluorides [7.43]. We see that for  $\text{XeF}_6$  the  $K$  value, due to the PJTE, becomes negative, and its configuration is thus accordingly distorted in agreement with the experimental data;  $\text{TeF}_6^{3-}$  and  $\text{IF}_6^-$  are not distorted. In all three systems the main contribution to the instability is due to the excited states formed by the one-electron transition  $25a_{1g} \rightarrow 28f_{1u}$  [7.43].

**TABLE 7.4. Ground-State Interatomic M—F Distance  $R_e$  (in bohrs), Energy  $E$  (in hartrees), Nonvibronic  $\tilde{K}_0$ , and PJT  $\tilde{K}_v$  Contributions to the Curvature  $K$  of the APES of Three Isoelectronic Octahedral Fluorides  $\text{MF}_6$  with Respect to Odd Trigonal  $T_{1u}$  Distortions ( $K_0$ ,  $K_v$ , and  $K$  in hartrees/bohr<sup>2</sup>)**

Parameter	$\text{TeF}_6^{3-}$	$\text{IF}_6^-$	$\text{XeF}_6$
$R_e$ (Å)	2.0740	1.9450	1.8765
$E$ (hartree)	-151.513252	-154.742296	-158.339908
$\tilde{K}_0$	1.20720	1.72396	2.26929
$\tilde{K}_v$	-1.17385	-1.72277	-2.28941
$K = \tilde{K}_0 + \tilde{K}_v$	0.03345	0.00119	-0.02011

A fundamental consequence of the uniqueness of the vibronic instability is that it lies in the base of all structural symmetry breakings in molecular systems and condensed matter [7.44]. It was shown that the spontaneous breakdown of space symmetry of molecular systems and solids (distortions, conformation changes, phase transitions, including melting and vaporization, together with formation of molecules from atoms, molecular transformations, etc.) is always triggered by Jahn–Teller-type vibronic interactions between two or more electronic states [7.44]. It is interesting (and exciting) that a similar statement of uniqueness of symmetry breakings exists in particle physics: “Symmetry breaking is always associated with a degeneracy” [7.45], and degeneracy in particle physics means equal masses; this includes also pseudodegenerate particles that have sufficiently close values of mass. Together with the spontaneous symmetry breaking in molecular systems and condensed matter due to electronic degeneracy or pseudodegeneracy we may draw the conclusion that *nature tends to avoid degeneracies* [7.46]. This statement is not trivial and may have influence on general understanding of the origin of “driving forces” in natural phenomena.

On the other hand, the “philosophy” of this chapter as a whole is of special interest to understanding the mechanisms of molecular transformations as they are triggered by the electronic structure. As elucidated above, changes in any given (reference) nuclear configuration *necessarily* require the mixing of at least two of its electronic states, degenerate or non-degenerate. This means that the presence of such two or more electronic states is *crucial* in understanding the origin of changes in nuclear configuration. In other words, to investigate and predict molecular distortions and transformations, one should start with finding the two or more electronic states that trigger corresponding nuclear configuration changes. This is a *novel paradigm*, which provides a higher level of theory and understanding of the origin of chemical phenomena on the electronic level, for the first time outlined in this book—the *paradigm of vibronic mixing of two or more electronic states in initiating nuclear configuration changes*, or more compactly, the “two electronic states in chemical transformations” (TEST) paradigm. The JTE, PJTE, and RTE are particular cases of this paradigm.

### Further Insight into the Pseudo-JTE and Hidden JTE

The proof that  $K_0 > 0$  means that configuration instability with  $K < 0$  is due only to the vibronic coupling to the excited states. For simplicity, consider the case when only one excited state contributes significantly to the inequality (7.85), while the others are negligible. In this case the formulation of the problem is reduced to that of a usual two-level pseudo Jahn–Teller effect considered above in this section. According to Eq. (7.66), the curvatures of the adiabatic potentials of the two states at the point of instability are

$$K_{1,2} = K_0 \pm \frac{F^2}{\Delta} \quad (7.87)$$

Because  $K_0 > 0$ , the curvature of the excited state  $K_0 + F^2/\Delta$  is positive, while that of the ground state  $K_0 - F^2/\Delta$ , under condition (7.67), is negative. Thus *instability of the ground state is accompanied by a stable excited state* the coupling with which produces the instability [7.38]. This result, namely, *the prediction of the existence of stable excited states in dynamically unstable ground-state configurations*, is one consequence of the TEST paradigm, formulated above; it has interesting physical and chemical applications (Chapters 9–11).

If more than one excited state contributes to the instability of the ground state in Eq. (7.85), the relation between the  $K$  values of all these states becomes more complicated, but the general idea is the same—the negative contribution to the curvature of the ground state that makes it unstable equals the sum of positive contributions to the excited states. *As a result of the vibronic mixing the excited states become stabilized*. If the excited state that causes the instability of the ground state is occupied by electrons, the instability disappears: Eq. (7.87) shows that the total change of curvature of the two interacting states equals zero. Therefore, vibronic coupling between fully occupied MOs does not contribute to the instability.

For a further understanding of the origin of the vibronic instability, the terms in the sum  $K_v$  after (7.84) may be divided into two groups:

1. The basis wavefunctions  $|0\rangle$  and  $|i\rangle$  in the matrix element  $F^{(0i)}$  are mainly from the same atom. In this case the term  $-|F^{(0i)}|^2/\Delta_{0i}$  can be interpreted as the contribution of the polarization of this atom by the displacements of other atoms. For instance, for the instability of the central position of the Ti ion in the octahedron of oxygens in the  $\text{TiO}_6^{8-}$  cluster of  $\text{BaTiO}_3$  with respect to off-center displacements, discussed above, the contribution of the polarization of the oxygen atom by the off-center displacement of the titanium ion is given by the mixing of the oxygen  $2p$  and  $3s$  atomic function under this displacement [7.35b, 7.47]:

$$K_v^{\text{pol}} = -\frac{|\langle 2p_{\sigma z}(\text{O}) | (\partial V / \partial Q_z)_0 | 3s(\text{O}) \rangle|^2}{\Delta_{2p3s}} \quad (7.88)$$

Since the integrals  $F^{(0i)} = \langle 0 | (\partial V / \partial Q)_0 | i \rangle$  are calculated with the orthogonal (ground and excited) wavefunctions of the same atom, then, transforming the symmetrized coordinate  $Q$  into Cartesian coordinates and taking the corresponding derivative of the Coulomb potential  $V = e^2/|\mathbf{r} - \mathbf{R}_\beta|^{-1}$ , we come to integrals of the type  $I_x = \langle 0 | (x - X_\beta) / |\mathbf{r} - \mathbf{R}_\beta|^3 | i \rangle$ , where  $x$  are the electronic coordinates of the polarizing atom and  $X_\beta$  are the nuclear coordinates of the displacing atoms. If we assume that approximately  $R_\beta$  is much larger than the atomic size (which is already true for the second coordination sphere), then  $T_x \approx R_\beta^{-3} \langle 0 | x | i \rangle$ , and the polarization contribution is

$$K_v^{\text{pol}} \sim \frac{e^2 \alpha_x}{R_\beta^6} \quad (7.89)$$

where, according to quantum mechanics

$$\alpha_x = \frac{e^2 | \langle 0|x|i \rangle |^2}{\Delta_{0i}} \quad (7.90)$$

is the part of the atomic polarizability in the  $x$  direction that is due to the contribution of the  $i$ th excited state (the summation over  $i$  gives the full atomic polarizability in this direction).

2. The two functions in  $F^{(0i)}$  are from two different (nearest-neighbor) atoms. In this case the vibronic contribution is due to new covalency produced by the distortion. Indeed, in the reference configuration the overlap of these two electronic states is zero (they are orthogonal), hence their vibronic mixing means that a nonzero overlap occurs under the low-symmetry displacements  $Q$ .

For the Ti ion off-center displacements with respect to the oxygen octahedron the covalent contribution is due to the new overlap of the ground-state  $t_{1u}$  combination of the highest occupied  $2p_{\pi z}$  functions of the oxygen atoms with the lowest unoccupied  $d_{xz}$  function of the titanium ion:

$$K_v^{\text{cov}} = - \frac{| \langle 2p_{\pi z}(\text{O}) | (\partial V / \partial Q_x)_0 | 3d_{xz}(\text{Ti}) \rangle |^2}{\Delta_{2p3d}} \quad (7.91)$$

The new overlap (which is forbidden by symmetry in the reference configuration) produces new (additional) covalence. The inequality (7.85), made possible by this term, means that with the new covalence the energy is lower than that of the reference configuration, resulting in instability.

Both kinds of vibronic contribution to instability, new covalence and atomic polarization, may be significant, but the numerical calculations performed so far show that the covalence contribution is an order of magnitude larger than the polarization. Example 7.4 demonstrates this statement by numerical data.

The prediction of possible existence of stable excited states that cause the instability of the ground state in a two-level problem, discussed above, may have applications in different fields of chemistry. For instance, it predicts the possible existence of stable excited states for the unstable transition states of chemical reactions [7.38] (Sections 11.1 and 11.2). In stereochemistry (Section 9.2) it means that the low-symmetry configurations of molecular systems may have higher symmetry in some excited states (e.g., bent triatomic molecules are expected to be linear in the excited state, which is coupled to the ground one via bending displacements, and vice versa [7.3]).

**EXAMPLE 7.4****Comparison of Covalence versus Polarization Contributions to PJT Instability**

Table 7.5 shows three examples of numerical calculations of covalence and polarization contributions to the pseudo-JTE in three essentially different systems [7.47]: the instability of  $\text{NH}_3$  in the planar configuration with respect to out-of-plane displacements of the nitrogen atom (toward the stable pyramidal  $C_{3v}$  configuration) [7.39];  $\text{CuCl}_5^{3-}$  in the trigonal-bipyramidal configuration with respect to  $E'$  displacements (toward a square pyramid) [7.48]; and the  $\text{TiO}_6^{8-}$  cluster in  $\text{BaTiO}_3$  with respect to  $T_{1u}$  (Ti off-center) displacements initiating the spontaneous (ferroelectric) polarization of the crystal [7.35, 7.42]. In all these examples the new covalence contribution to the instability is much more significant, by at least one order of magnitude.

**TABLE 7.5. New Covalence  $K_v^{\text{cov}}$  versus Polarization  $K_v^{\text{pol}}$  Contributions to Instability of the High-Symmetry Configuration of Several Polyatomic Systems**

	$\text{NH}_3$	$\text{CuCl}_5^{3-}$	$\text{TiO}_6$ in $\text{BaTiO}_3$
Reference configuration	Planar $D_{3h}$	Trigonal bipyramidal $D_{3h}$	Octahedral $O_h$
Instability coordinate	$A_2''$	$E'$	$T_{1u}$
Ground state <sup>a</sup>	${}^1A_1'[2p_z(\text{N})]$	${}^2A_1'[3d_{z^2}(\text{Cu})]$	${}^1A_{1g}[2p(\text{O})]$
Excited state—cov <sup>b</sup>	${}^1A_2''$	${}^2E'$	${}^1T_{1u}$
	$2p_z(\text{N}) \rightarrow 1s(\text{H})$	$3s(\text{Cl}) \rightarrow 3d(\text{Cu})$	$2p(\text{O}) \rightarrow 3d(\text{Ti})$
$K_v^{\text{cov}}$	$-0.62 \text{ mdyn/\AA}$	$-2.85 \cdot 10^{28} \text{ s}^{-2c}$	
Excited state—pol <sup>b</sup>	${}^1A_2''$	${}^2E'$	${}^1T_{1u}$
	$2p_z(\text{N}) \rightarrow 3s(\text{N})$	$3d_{xy}(\text{Cu}) \rightarrow 3d_{z^2}$	$2p(\text{O}) \rightarrow 3s(\text{O})$
$K_v^{\text{pol}}$	$-0.06 \text{ mdyn/\AA}$	$-0.05 \cdot 10^{28} \text{ s}^{-2c}$	
$K_v^{\text{cov}}/K_v^{\text{pol}}$	$1.03 \times 10$	$5.7 \times 10$	$1.1 \times 10$

<sup>a</sup>The main contributing AOs are indicated in brackets.

<sup>b</sup>The corresponding one-electron excitations are shown.

<sup>c</sup>In mass-weighted units.

Considering the symmetries of the corresponding MO's, *one can control (manipulate) the geometry (configuration instability) of molecular systems by means of electronic rearrangements: excitation, ionization, MO population changes by coordination, redox processes, and so on.* This is directly related to chemical activation by coordination (Section 11.2), photochemical



reactions (Section 11.3), internal pseudorotations (Section 9.2), structural phase transformations in condensed media (Section 9.4), and other factors.

As mentioned earlier, in addition to instability of the high-symmetry configuration, vibronic mixing of the ground state with excited states causes anharmonicity in the nuclear motions of the former [7.3] (*vibronic anharmonicity*). In some cases vibronic anharmonicity is more important than the proper anharmonicity caused by the higher-order terms in the expansion (7.3).

The JTE is presently a powerful general approach to (a tool for) solving problems in physics, chemistry, and biology. Many examples confirming this statement are given in the literature (see, e.g., Ref. 7.3); some examples are discussed in the Chapters 8–11. Example 7.5 illustrates how the JTE approach works in evaluation of the origin of structural properties of relatively simple molecules  $ML_2$ .

### EXAMPLE 7.5

#### *Why Some $ML_2$ Molecules ( $M = Ca, Sr, Ba$ ; $L = H, F, Cl, Br$ ) are Bent While Others Are Linear*

This problem is solved by means of the PJTE [7.49]. Indeed, consider the linear configuration  $L-M-L$ . Its general MO energy-level scheme is shown in Fig. 7.21, where it is seen that the occupied MOs are formed mainly by the ligand orbitals, while the lowest unoccupied ones are

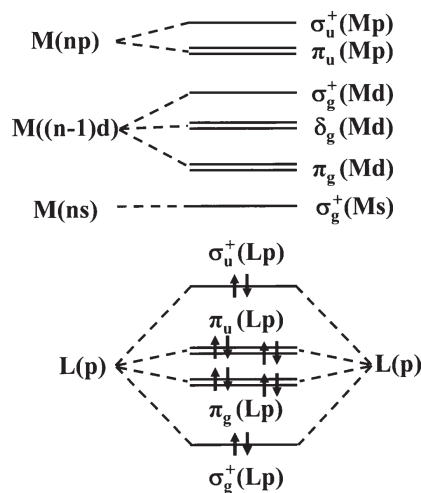


**FIGURE 7.21.** Molecular orbital (MO) scheme of the valence states in the  $ML_2$  molecules ( $M = Ca, Sr, Ba$ ;  $L = H, F, Cl, Br$ ). The main atomic orbital contributions to the MOs are shown in parentheses.

formed mainly by excited  $d$  orbitals of the M atom. The bending of the linear configuration is an odd  $E_u$ -type distortion that can be realized by the PJT mixing of an occupied even ( $g$ ) state with unoccupied odd ( $u$ ) one, or vice versa. Analyzing the MO scheme in Fig. 7.21, we see that the PJT mixing of the HOMO  $\sigma_u$  (which produces the term  $\sum_u$ ) formed mainly by the ligand orbitals with the unoccupied  $\Pi_g$  orbitals (term  $\Pi_g$ ) formed mainly by central atomic  $d$  orbitals may produce the odd (*bending*) nuclear distortion.

This  $(\sum_u + \Pi_g) \otimes e_u$  PJTE takes place in all the  $ML_2$  molecules above; however, depending on the energy gap between these states  $\Delta$  and the vibronic coupling constant  $F$ , which are specific for the atoms M and L, in some of the molecules, the condition of instability (7.71) is not obeyed (the PJTE is weak, see Fig. 7.17a), and these molecules remain linear (albeit softened by the PJTE), while in others the PJTE is strong enough to produce the observed instability and distortion. Calculations [7.47] not only explain fully the origin of the distortions and answer the question above, but also show that the previous attempts to explain this situation based on qualitative models (orbital hybridization, VSEPR, polarization, etc.; see Section 9.1) are either just particular cases of the PJTE or produce negligible effects.

It is remarkable that if in the same  $ML_2$  molecule M is substituted by a transition metal, the  $d$ -containing orbitals are occupied and the PJTE vanishes (other excited states that are appropriate in symmetry are too high in energy and hence produce very small contributions to the instability). Indeed, direct calculations of the  $CuF_2$  molecule show that it is linear (see Example 5.2).

An interesting development termed a *hidden JTE* has emerged more recently [7.50]. Numerous molecular systems have a ground-state geometry that is distorted as compared with the nearby possible higher symmetry configuration, and the latter has neither degenerate state (no JTE), nor low-lying excited states to assume a PJTE. On the other hand, we stated above that *all* the instabilities and distortions from high-symmetry configurations are of JT, PJT, or RT origin. How is this controversy solved?

It was shown [7.50, 7.51] that in all the cases when the JTE is not seen explicitly, it is “hidden” in the excited states. There are two kinds of hidden JTE: (1) one of the excited states is degenerate and its JTE is so strong that its stabilization energy is larger than the energy gap to the ground state, thus producing a global minimum with a distorted configuration (an example of this type is the ozone molecule [7.52]); (2) another, more widespread, possibility emerges when there is a strong PJTE on two excited states that causes the lower one to cross the ground state and become the global minimum with a distorted configuration. This case of hidden JTE is demonstrated by ab initio calculations of  $CuF_3$  in Example 7.6.

**EXAMPLE 7.6*****Hidden JTE in CuF<sub>3</sub>: Ab Initio Calculations***

The CuF<sub>3</sub> molecule has a planar obtuse-triangular configuration in the ground state with the Cu atom displaced from the center (the two angles F—Cu—F are about  $\alpha \sim 93^\circ$ ) and a singlet  $^1A'_1$  ground electronic state. In the high-symmetry regular triangular configuration  $D_{3h}$  with the Cu atom in the center, the electronic configuration of the system is  $e^2$  originating from Cu<sup>3+</sup> ( $d^8$ ), and it has a triplet ground state  $^3A'_2$  and two excited states  $^1A'_1$  and  $^1E'$  (see Example 3.2 in Section 3.4). Hence there is no JTE in the ground state  $^3A'_2$ , nor is there a PJT mixing with the excited states as they have different spin states (the vibronic coupling does not mix states with different spins). So why is the real (global) ground-state configuration distorted?

This is a typical example of a hidden PJTE of the second type. Ab initio calculations [7.50], including the ground and the abovementioned two excited states, fully confirmed this statement. Figure 7.22 illustrates some of the results. In the cross section along the  $\alpha$  angle we see that a strong PJTE of the type  $(^1A'_1 + ^1E') \otimes e$  (Section 7.4) that mixes the two excited states, pushes down the lower  $^1A'_1$  state, and the effect is so strong that the latter crosses the  $^3A'_2$  state and produces the global minimum with a distorted configuration of an obtuse triangle with  $\alpha \sim 93^\circ$ .

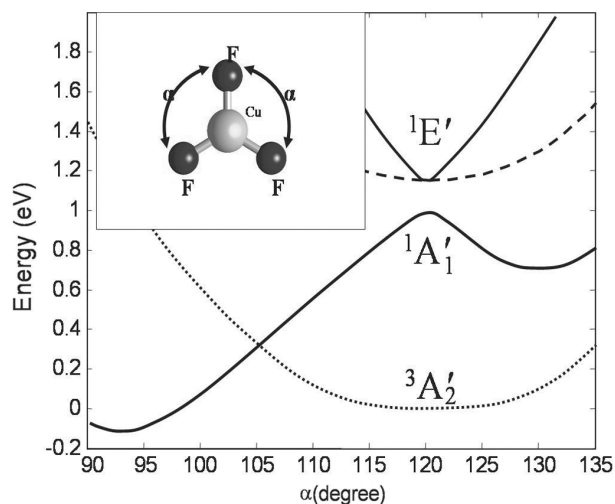


**FIGURE 7.22.** Cross-section of the APES of CuF<sub>3</sub> along the angle  $\alpha$  (F-Cu-F) showing a strong PJTE between the two excited  $E$  and  $A$  states that leads to the formation of a global minimum in which the high-symmetry configuration is distorted ( $\alpha \sim 93^\circ$ ) [7.50]. The inset shows the molecular geometry.

There are additional important effects accompanying this distortion, including *orbital disproportionation* when the initial, orbitally totally symmetric electronic configuration  $|e_{\vartheta} \uparrow; e_{\varepsilon} \uparrow\rangle$  transforms into a spin singlet  $|e_{\vartheta} \uparrow; e_{\vartheta} \downarrow\rangle$  with a charge distribution corresponding to the distortion [7.50]. In the distorted configuration this molecule has a dipole moment, but no magnetic moment, whereas in the undistorted geometry the magnetic moment is nonzero (the spin  $S = 1$ ), but there is no dipole moment. This coexisting magnetic and dipolar bistability (“multiferroic” effect) makes such molecules important and possible novel materials for electronics.

### SUMMARY NOTES

1. *Nuclear configurations and dynamics* are central to chemical problems such as stereochemistry, chemical reactions, and conformational transitions. Nuclear motions are controlled by electronic distributions via vibronic coupling.
2. *Orbital vibronic coupling* (OVC) creates a bridge between static MO description of the electronic structure and nuclear displacements providing for the contribution of each MO to the latter. OVC is especially important in evaluation of changes in nuclear configuration and dynamics produced by changes in electronic structure.
3. The overwhelmingly widespread *adiabatic approximation*, which essentially simplifies the description of electronic and nuclear motions by separating their variables (assuming that the heavy nuclei may be considered fixed when the electronic motion is calculated, and the nuclei move in the averaged field of the electrons), is not always valid for transition metal coordination systems.
4. Special effects triggered by instabilities and distortions of high-symmetry configurations (*Jahn–Teller effects*) may occur when there are two or more degenerate or close-in-energy electronic states. They are present in the overwhelming majority of transition metal coordination systems.
5. The *pseudo-JTE* for systems in nondegenerate states is of special interest as it is relevant to any polyatomic system. The JTE (including proper JTE, pseudo-JTE, and the Renner–Teller effect) is the only source of instability and distortions (symmetry breaking) of high-symmetry configurations of molecular systems and solids.
6. It is proved that at least two electronic states must be involved in any changes of molecular configurations, including chemical and physical transformations (e.g., formation of molecular shapes and crystal lattices, conformational changes and phase transitions, chemical activation and

mechanisms of chemical reactions, etc.). This leads to the paradigm of *two electronic states in transformations* (TEST).

## EXERCISES AND PROBLEMS

- 7.1. Transition metal coordination systems often possess degenerate and/or close-in-energy electronic states that do not satisfy the criterion (7.10) of the adiabatic approximation. What experimentally observable effects of such nonadiabaticity are expected in these cases?
- 7.2. In Figs. 7.1–7.3 (and Table 7.1) the shape of possible symmetrized nuclear displacements are shown for several kinds of systems. Are they real atomic displacements during molecular vibrations? For degenerate vibrations two or more equivalent displacement shapes are shown. Which of them is real?
- 7.3. Define linear and quadratic vibronic coupling constants, diagonal and off-diagonal, and explain their physical meaning. Also define force constants and relate them to vibronic coupling constants.
- 7.4. Diagonal linear orbital vibronic coupling constants (DLOVCCs) have the physical meaning of the force with which an electron on a given MO acts on the nuclei in the direction of symmetrized displacements. Consider examples for which we can predict the changes in nuclear configuration and dynamics based on known DLOVCC (some examples are given in Chapters 10 and 11).
- 7.5. The Jahn–Teller effect is a quantum phenomenon that occurs as a result of the nontotally symmetric charge distribution on any of the two or more degenerate states. Since the latter complement each other to form a totally symmetric distribution, why is the one-state distribution (that produces distortion) preferred over the all-state average one without distortion?
- 7.6. Figure 7.13 shows changes in the shape of an octahedral complex during motion of the system along the bottom of the trough of the Mexican-hat-like APES inherent to twofold electronic degenerate states. Can these changes be observed experimentally, directly, or indirectly? How?
- 7.7. It can be easily verified that in the JT  $E \otimes e$  problem the wavefunctions (7.46) of the electronic states as a function nuclear coordinates are not single-valued, they change sign under the transformation  $\phi \rightarrow \phi + 2\pi$ , forming a full circle along the bottom of the trough that brings the system back to its initial configuration. On the other hand, quantum mechanics requires that wavefunctions be single-valued. How is this controversy solved in the JTE theory?
- 7.8. The statement that the JTE (including proper JTE, pseudo-JTE, and the Renner–Teller effect) is the only source of structural instability and distortion of polyatomic systems refers to “high-symmetry configurations.” What does this mean? For example, if a system of two atomic ionic groups, both charged positive (or both negative), is unstable and undergoes distortion, is it a consequence of the JTE? Explain your answer and give examples.

## REFERENCES

- 7.1. I. B. Bersuker and V. Z. Polinger, *Vibronic Interactions in Molecules and Crystals*, Springer, New York, 1989.
- 7.2. R. Englman, *The Jahn-Teller Effect in Molecules and Crystals*, Wiley, London, 1972.
- 7.3. I. B. Bersuker, *The Jahn-Teller Effect*, Cambridge Univ. Press, Cambridge, UK, 2006.
- 7.4. I. B. Bersuker, *Chem. Rev.* **101**, 1067 (2001).
- 7.5. S. Sugano, Y. Tanabe, and H. Kamimura, *Multiplets of Transition Metal Ions in Crystals*, Academic Press, New York, 1970.
- 7.6. L. D. Landau and E. M. Lifshitz, *Quantum Mechanics. Non-relativistic Theory*, Pergamon Press, Oxford, 1977.
- 7.7. E. B. Wilson, Jr., J. G. Decius, and P. C. Cross, *Molecular vibrations. The Theory of Infrared and Raman Spectra*, McGraw-Hill, New York, 1958.
- 7.8. G. Gerzberg, *Infrared and Raman Spectra of Polyatomic Molecules*, Van Nostrand, New York, 1945.
- 7.9. M. V. Vol'kenshtein, L. A. Gribov, M. A. El'yashevich, and B. I. Stepanov, *Molecular Vibrations* (Russ.), 2nd ed., Nauka, Moscow, 1972.
- 7.10. K. Nakamoto, *Infrared and Raman Spectra of Inorganic and Coordination Compounds*, 4th ed., Wiley, New York, 1986.
- 7.11. Yu. Ya. Khariton, ed., *Vibrational Spectra in Inorganic Chemistry* (Russ.), Nauka, Moscow, 1971.
- 7.12. D. M. Adams, *Metal-Ligand and Related Vibrations*, London, 1967.
- 7.13. I. B. Bersuker, *Kinet. Katal.* **18**, 1268 (1977); *Chem. Phys.* **31**, 85 (1978); *Teor. Exp. Khim.* **14**, 3 (1978); in D. Banerjee, ed., (*IUPAC*) *Coordination Chemistry-20*, Pergamon Press, Oxford and New York, 1980, p. 201.
- 7.14. S. S. Stavrov, I. P. Decusar, and I. B. Bersuker, *New J. Chem.* **17**, 71 (1993).
- 7.15. S. B. Piepho, *J. Am. Chem. Soc.* **110**, 6319 (1988); in K. Prassides, ed., *Mixed-Valency Systems: Applications in Chemistry, Physics and Biology*, Kluwer, Dordrecht, 1991, p. 329.
- 7.16. T.-X. Lu, *Chem. Phys. Lett.* **194**, 67 (1992); J. C. R. Faulhaber, D. Y. K. Ko, and P. R. Briddon, *Phys. Rev. B* **48**, 661 (1993-I).
- 7.17. H. A. Jahn and E. Teller, *Proc. Roy. Soc.* **161**, 220 (1937).
- 7.18. R. Renner, *Z. Phys.* **92**, 172 (1934).
- 7.19. E. Ruch and A. Schonhofer, *Theor. Chim. Acta* **3**, 291 (1965); E. L. Blount, *J. Math. Phys.* (NY), **12**, 1890 (1971).
- 7.20. I. B. Bersuker, *Teor. Exp. Khim.* **2**, 518 (1966).
- 7.21. U. Opik and M. H. L. Pryce, *Proc. Roy. Soc.* **A238**, 425 (1957).
- 7.22. H. Sponer and E. Teller, *Rev. Mod. Phys.* **13**, 75-170 (1941).
- 7.23. H. C. Longuet-Higgins, in *Advances in Spectroscopy*, Vol. 2, New York, 1961, p. 429.
- 7.24. M. C. M. O'Brien, *Proc. Roy. Soc. (Lond.)* **A281**, 323 (1964).
- 7.25. I. B. Bersuker, *Opt. Spectrosc.* **11**, 319 (1961); *Zh. Eksp. Teor. Fiz.* **43**, 1315 (1962) (Engl. transl.: *Sov. Phys.—JETP*).

- 7.26. I. B. Bersuker, ed., *The Jahn-Teller Effect. A Bibliographic Review*, IFI/Plenum, New York, 1984.
- 7.27. M. V. Berry, *Proc. Roy. Soc. A* **392**, 45 (1984).
- 7.28. A. Shapere and F. Wilczek, eds., *Geometric Phases in Physics*, World Scientific, Singapore, 1989.
- 7.29. H. Koizumi and I. B. Bersuker, *Phys. Rev. Lett.* **83**, 3009 (1999).
- 7.30. I. B. Bersuker and B. G. Vekhter, *Fiz. Tverdogo Tela* **5**, 2432–2440 (1963) (English transl.: *Sov. Phys—Solid State*).
- 7.31. F. S. Ham, *Phys. Rev.* **A138**, 1727 (1965); in S. Geschwind, ed., *Electron Paramagnetic Resonance*, Plenum, New York, 1972, pp. 1–484.
- 7.32. M. C. M. O'Brien, *Phys. Rev.* **187**, 407 (1969).
- 7.33. I. B. Bersuker and V. Z. Polinger, *Phys. Lett.* **44A**, 495 (1973); *Sov. Phys. JETP* **66**, 2078 (1974).
- 7.34. H. Koizumi, I. B. Bersuker, J. E. Boggs, and V. Z. Polinger, *J. Chem. Phys.* **112**, 8470 (2000).
- 7.35. (a) I. B. Bersuker, *Phys. Lett.* **20**, 589 (1966); (b) *Ferroelectricity* **164**, 75 (1995).
- 7.36. I. B. Bersuker and S. S. Stavrov, *Chem. Phys.* **54**, 331 (1981).
- 7.37. R. F. W. Bader, *Mol. Phys.* **3**, 137 (1960); *Can. J. Chem.* **40**, 1164 (1962); R. F. W. Bader and A. D. Bandrauk, *J. Chem. Phys.* **49**, 1666 (1968).
- 7.38. I. B. Bersuker, *Nouv. J. Chim.* **4**, 139 (1980); *Teor. Eksp. Khim.* **16**, 291 (1980).
- 7.39. I. B. Bersuker, N. N. Gorinchoi, and V. Z. Polinger, *Theor. Chim. Acta* **66**, 161 (1984).
- 7.40. T. K. Rebane, *Teor. Eksp. Khim.* **20**, 532 (1984).
- 7.41. I. B. Bersuker, *Pure Appl. Chem.* **60**(8), 1167 (1988); *Fiz. Tverdogo Tela* **30**, 1738 (1988).
- 7.42. I. B. Bersuker, *J. Coord. Chem.* **34**, 289 (1995).
- 7.43. I. B. Bersuker, N. B. Balabanov, D. M. Pekker, and J. E. Boggs, *J. Chem. Phys.* **117**, 10478 (2002).
- 7.44. I. B. Bersuker, *Adv. Quant. Chem.* **44**, 1 (2003).
- 7.45. S. Weinberg, *Quantum Theory of Fields*, Cambridge Univ. Press, Cambridge, UK, 1995, Chapter 11.
- 7.46. I. B. Bersuker, in P. Piecuch et al., eds. *Progress in Theoretical Chemistry and Physics*, vol. 19, Springer, 2009, 343.
- 7.47. I. B. Bersuker, *New J. Chem.* **17**, 3 (1993).
- 7.48. V. Z. Polinger, N. N. Gorinchoy, and I. B. Bersuker, *Chem. Phys.* **159**, 75 (1992).
- 7.49. P. Garcia-Fernandez, I. B. Bersuker, and J. E. Boggs, *J. Phys. Chem. A* **111**, 10409 (2007).
- 7.50. P. Garcia-Fernandez, I. B. Bersuker, and J. E. Boggs, *J. Chem. Phys.* **125**, 104102\$ (2006).
- 7.51. I. B. Bersuker, in I. B. Bersuker et al., eds., *Proc XIX Symp. Jahn-Teller Effect, J. Mol. Struct.* **838**, 44, (2007).
- 7.52. P. Garcia-Fernandez, I. B. Bersuker, and J. E. Boggs, *Phys. Rev. Lett.* **96**, 163005 (2006).

---

# 8

---

## ELECTRONIC STRUCTURE INVESTIGATED BY PHYSICAL METHODS

*Physical methods of investigation provide very powerful sources of information about the electronic structure of transition metal compounds, and the problem is to ascertain direct correlations between the observables and electronic parameters.*

The variety of physical methods aimed at experimental study of the electronic structure of coordination compounds can be divided into two groups: *resonance methods*, including all-range spectroscopy from radio- through  $\gamma$ -ray frequencies; and *nonresonance methods*, which consist of diffraction (X-ray, electron, and neutron diffraction) and polarization (measurements of magnetic and electric susceptibilities) methods. An important distinction between these two types of methods is that the observables in the resonance methods carry information about at least two states of the system, initial and final, between which a transition takes place (induced by the resonance interaction), whereas the nonresonance method describes, in principle, one electronic state, although the field response in this case may also include other states admixed by the external perturbation to the one being considered.

This chapter is not devoted to the systematic presentation of all these methods and their technical realization; for a detailed study, the reader is referred to corresponding monographs and textbooks [8.1–8.10]. Instead, we present here an introduction to *the theory of electronic origin of observables in the physical methods of investigation* with emphasis on features related to other properties of transition metal compounds considered in this book. Attention is paid to electronic visible, ultraviolet, Raman, and photoelectron spectra; infrared, ESR, EXAFS, and  $\gamma$ -resonance spectroscopy; magnetic and electric susceptibilities;

---

*Electronic Structure and Properties of Transition Metal Compounds: Introduction to the Theory,*  
Second Edition By Isaac B. Bersuker  
Copyright © 2010 John Wiley & Sons, Inc.



and related methods, as well as diffraction methods in electron deformation and spin densities.

## 8.1. BAND SHAPES OF ELECTRONIC SPECTRA

### Qualitative Interpretation of Vibrational Broadening

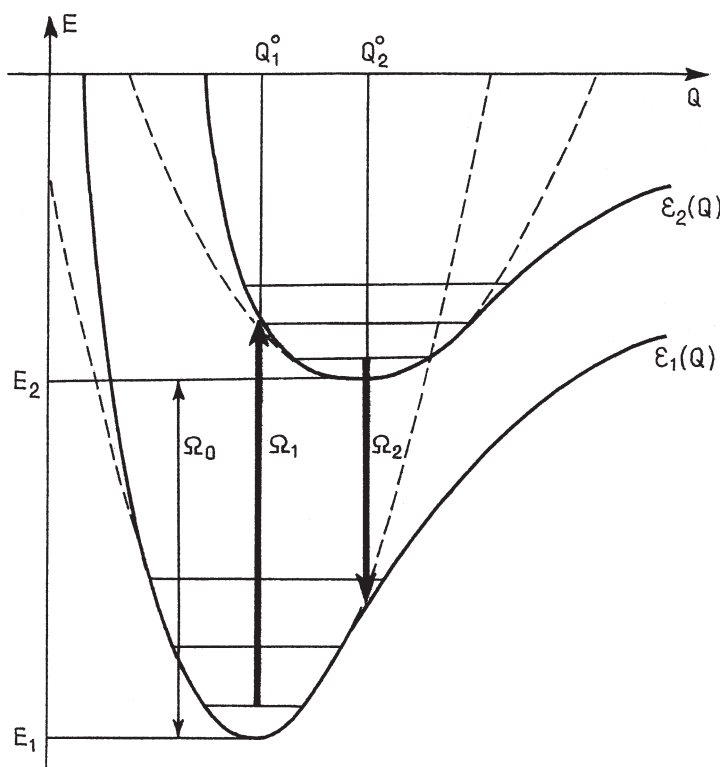
Electronic spectra result from electronic transitions between two states of the system and carry information about these states. One important special feature relevant to coordination compounds (as well as to many other molecular systems) is the strong dependence of electronic energies on interatomic distances. For this reason the stationary states of the system are not purely electronic but electron-vibrational. For free molecular systems in the gas phase, rotational states are also important.

Figure 8.1 is a schematic representation of the electronic energies of two nondegenerate states as functions of symmetrized coordinates: cross sections of APES (Section 7.1). This simple presentation by APES enables us to obtain many important qualitative features related to the electronic structure. First, consider the *Franck–Condon principle* due to which the nuclear configuration does not (is not in time to) change during the electron transition, and hence the latter takes place at the unchanged nuclear configuration of the initial state. Indeed, the electronic transitions are much faster than the vibrational motion; the time of transition  $\tau$  is approximately inversely proportional to the light frequency  $\Omega$ , and for visible light  $\tau \sim \Omega^{-1} = 10^{-15}$  s, while for vibrations  $\omega^{-1} = 10^{-10} - 10^{-12}$  s.

In terms of the Franck–Condon principle, the transitions between the electronic states in Fig. 8.1 are described by vertical arrows starting from the vibrational state in the minimum of the APES of the initial electronic state. It is seen that for most cases when the minima points of the two electronic states do not coincide, the transition is not purely electronic; it also changes the vibrational states. The transition frequency  $\Omega$  (the energy of the absorbed or emitted quantum  $\hbar\Omega$ ) also depends on the initial vibrational state. It changes approximately from  $\Omega_1$  to  $\Omega_2$  depending on the number of vibrational quanta of the ground and excited states involved in the transition. The probability of such transitions that include vibrational components is proportional to the *Franck–Condon factor*, the overlap of the vibrational wavefunctions of the initial and final states.

With the thermal population of different vibrational states and the proper width of each transition, the molecular spectra appear as rather wide bell-shaped bands (*vibrational broadening*), distinct from the narrow lines of atomic spectra. The *half-width* (the width at the half intensity) of the bands is about  $\Omega_1 - \Omega_2$ . In Fig. 8.1 one can see that the width of the band is directly related to the difference in the minima positions  $Q_1^0$  and  $Q_2^0$  on the two APES, that is, to *the shift of equilibrium position by excitation*  $\Delta Q = Q_1^0 - Q_2^0$ . The larger  $\Delta Q$ , the wider the transition band.

On the other hand, the difference in the equilibrium interatomic distances in different electronic states that determines  $\Delta Q$  is strongly dependent on the



**FIGURE 8.1.** AP curves (APES cross-sections), vibrational states, and “vertical” transition between two electronic states.  $\Omega_0$ ,  $\Omega_1$ , and  $\Omega_2$  are the pure electronic, absorption, and emission frequencies, respectively.

differences in their electronic configurations. In coordination compounds the ionic radii that determine approximately the interatomic distances depend strongly on the occupation numbers  $n$  and  $m$  of different  $d$  orbitals of the electronic configuration  $(t_2)^n(e)^m$  (Sections 4.3 and 6.2). Therefore, the changes in these occupation numbers,  $\Delta n$  and  $\Delta m$ , may be used for qualitative estimates of the changes of the equilibrium interatomic distances by the transition from one electronic state to another. Two groups of electronic transitions can be distinguished:

1. Transition for which  $\Delta n \neq 0$  and  $\Delta m \neq 0$  with significant changes in the electronic configuration resulting in *broad bands* of light absorption and luminescence. These bands remain broad down to low temperatures. The calculations (see below) give an estimate of the bandwidth to be from one thousand to several thousand wave numbers ( $\text{cm}^{-1}$ ).
2. Transitions with  $\Delta n = 0$ ,  $\Delta m = 0$  for which the electronic configuration remains unchanged (as in spin-forbidden transitions) resulting in *narrow lines* with a width of the order of  $100 \text{ cm}^{-1}$ .

Note that in systems with  $f$ -electron configurations the dependence of interatomic equilibrium distances on the number of different  $f$  electrons is very weak because their participation in the bonding is low. Therefore, the transitions that involve changes of only  $f$ -electron occupation numbers yield mostly narrow lines.

A semiquantitative (but still not very rigorous) description of the vibrational broadening under consideration can be obtained if one knows the energy diagrams  $E = f(\Delta)$  of the energy levels as a function of the crystal field parameter  $\Delta$  (see Tanabe–Sugano diagrams in Section 4.3). As mentioned above and shown in Fig. 8.1, the transition frequency  $\hbar\Omega = E_2 - E_1$  depends on the minima shift  $\Delta Q$ ; the larger  $\Delta Q$ , the greater the dependence of  $\Omega$  on  $Q$ , and the larger the derivative  $d(\hbar\Omega)/dQ = (dE_2/dQ) - (dE_1/dQ)$ . This magnitude can serve as a rough measure of the bandwidth. On the other hand, the derivative  $dE/d\Delta$  characterizes the relative sensitivity of the energy level  $E$  to the ligand influence, which in turn depends on the (symmetrized) metal–ligand distance  $Q$ . Although the changes in  $\Delta$  may not be in direct proportion to changes in  $Q$ , for the sake of simplicity one can assume that in the first (linear) approximation  $d(\hbar\Omega)/dQ \sim d(\hbar\Omega)/d\Delta$ , and hence

$$\frac{d(\hbar\Omega)}{dQ} \sim \frac{d(\hbar\Omega)}{d\Delta} = \frac{dE_2}{d\Delta} - \frac{dE_1}{d\Delta} \quad (8.1)$$

Provided that this relation holds, the division of the electronic transition bands described above into two groups can be obtained directly using the results of crystal field theory for the functions  $E = f(\Delta)$ . Approximately (without accounting for electron interactions explicitly), for the  $(t_2)^m(e)^n$  configuration, we have (Sections 4.3 and 4.5)

$$\begin{aligned} E_1 &= \text{const} - m_1 \frac{2}{5} \Delta + n_1 \frac{3}{5} \Delta \\ E_2 &= \text{const} - m_2 \frac{2}{5} \Delta + n_2 \frac{3}{5} \Delta \end{aligned}$$

and

$$\frac{d(\hbar\Omega)}{d\Delta} = \frac{2}{5}(m_1 - m_2) + \frac{3}{5}(n_2 - n_1) \quad (8.2)$$

If the electronic configuration is not changed by the transition, then  $m_1 = m_2$ ,  $n_1 = n_2$ , and the derivative that determines the vibrational broadening is zero—the bands are expected to be narrow. For transitions that change the electronic configuration the derivative  $dE/d\Delta$  is nonzero. For example, for the most frequently studied  $t_2 \rightarrow e$  transition ( $d \leftrightarrow d$ ):  $\Delta m = m_1 - m_2 = 1$ ,  $\Delta n = n_1 - n_2 = -1$ ,  $d(\hbar\Omega)/d\Delta = 1$ , and the band is broad.

This qualitative reasoning, which explains the origin of two groups of electronic bands, relatively broad and narrow, can be regarded as the first stage in the interpretation of the origin of electronic spectra in coordination complexes.

Although it is only a rough approximation, it contains possibilities for revealing some important features. Example 8.1 illustrates this statement.

### EXAMPLE 8.1

#### *Broad and Narrow Bands in Light Absorption and Emission by Transition Metal Complexes*

Consider some examples of the theoretical predictions above. Complexes  $[\text{TiA}_6]^{3+}$  with one  $d$  electron are expected to manifest one  $d-d$  transition  ${}^2T_{2g} \rightarrow {}^2E_g$  accompanied by a change in electronic configuration  $(t_{2g})^1 \rightarrow (e_g)^1$  with  $\Delta m = 1$ ,  $\Delta n = -1$  that yields a broad band of absorption in accordance with experimental data [8.11a]. The transitions  ${}^1A_{1g} \rightarrow {}^1T_{1g}$  and  ${}^1A_{1g} \rightarrow {}^1T_{2g}$ , as well as the spin-forbidden transitions  ${}^1A_{1g} \rightarrow {}^3T_{1g}$  and  ${}^1A_{1g} \rightarrow {}^3T_{2g}$  in low-spin octahedral complexes with electron configuration  $d^6$  [e.g.,  $[\text{Co}(\text{NH}_3)_6]^{3+}$ ], are associated with a change in electronic configuration  $(t_{2g})^6 \rightarrow (t_{2g})^5(e_g)^1$ . Hence the absorption bands should be and they are broad [8.11b]. On the contrary, spin-forbidden transitions with spin-only changes  $(t_{2g} \downarrow)^3 \rightarrow (t_{2g} \downarrow)^2(t_{2g} \uparrow)$ , for which  $\Delta S = 1$  but  $\Delta n = \Delta m = 0$  [e.g., the transition  ${}^4A_{2g} \rightarrow {}^2E_g$  in  $[\text{Cr}(\text{H}_2\text{O})_6]^{3+}$ ] yield narrow lines of absorption. A more detailed differentiation of bandwidths is given by the theory below.

#### Theory of Absorption Band Shapes

This subject has been presented and discussed in a variety of publications (see Refs. 8.1–8.4, 8.13–8.15, and references cited therein). The energy  $E$  of the main interaction of matter with electromagnetic radiation that results in spectroscopic dipolar transitions is given by the expression

$$E = -(\mathbf{M}, \mathcal{E}) \quad (8.3)$$

where  $\mathbf{M}$  is the dipole moment of the system and  $\mathcal{E}$  is the intensity of the electric field of the electromagnetic wave; the expressions for quadrupole interactions and interaction between the magnetic dipole moment and the magnetic field, as well as interaction between polarization of the system with the field  $\mathcal{E}$  in light scattering, are similar (see below). As proved in quantum theory, the probability of transition between two states of the system described by the wavefunctions  $\psi_1$  and  $\psi_2$  under the influence of perturbation (8.3) is proportional to the square of the matrix element  $M_{12}$  (the *moment of transition*)

$$\mathbf{M}_{12} = \int \psi_1^* \mathbf{M} \psi_2 d\tau \quad (8.4)$$

where  $\mathbf{M}$  is the operator of electric dipole moment above, but depending on the type of perturbation, it can also be the magnetic, polarization dipole, or quadrupole (multipole) moment of the system. The *moment* (8.4) contains the main information about the system that can be extracted from the spectra. For electric dipole transitions  $\mathbf{M} = \sum_i q_i \mathbf{r}_i$ , where  $q_i$  and  $\mathbf{r}_i$  are the charges and radius vectors of the particles, respectively.

The integral (8.4) depends on the wavefunctions  $\psi_1$  and  $\psi_2$  that also include vibrational and rotational states involved in the transition. This can be characterized by the dependence of  $M_{12}(\Omega)$  on the transition frequency  $\Omega$ . Provided that  $M_{12}(\Omega)$  is known, one can easily evaluate the *coefficient of light absorption*  $K_{12}(\Omega)$ . Experimentally it can be obtained from the relation  $I = I_0 \exp[-K_{12}(\Omega)l]$ , where  $I_0$  and  $I$  are the intensities of the incident and transmitted light, respectively, and  $l$  is the thickness of the absorbing layer of the substance. Then [8.1, 8.13, 8.14]

$$K_{12}(\Omega) = \frac{4\pi^2 N \Omega}{3\hbar c} |M_{12}(\Omega)|^2 \quad (8.5)$$

where  $N$  is the number of absorbing centers in a unit volume and  $c$  is the speed of light.

If there are close vibrational energy levels with an almost continuous function  $M_{12}(\Omega)$  as in coordination systems in solid states or liquids, it is convenient to introduce the *spectral density of absorption*  $k(\Omega)$ , such as the integral coefficient of absorption is given by  $K = \int k(\Omega) d\Omega$ , where the integration is performed over the width of the spectral line or band. To calculate  $K$  we have to summarize the transition probabilities to all vibrational states  $\nu'$  of the final (excited) term and average them over the different vibrational states  $\nu$  of the initial (ground) term using the Boltzmann occupation probability  $\rho_{1\nu}$  of the latter (which is a function of temperature). This leads to the following equation [8.14, 8.15], introduced here without the details of mathematical transformations [definition of the  $\delta$  function is similar to that of the  $\delta$  index (2.46):  $\delta(x) = 1$  if  $x = 0$  and  $\delta(x) = 0$  if  $x \neq 0$ ; in the expression below it provides for the condition of resonance transitions]:

$$K = \sum_{\nu, \nu'} \rho_{1\nu} K_{\nu, \nu'}(\Omega_{\nu, \nu'}) = \sum_{\nu, \nu'} \rho_{1\nu} \int K_{\nu, \nu'}(\Omega) \delta(\Omega - \Omega_{\nu, \nu'}) d\Omega \quad (8.6)$$

Then, for the spectral density  $k(\Omega)$ , we get

$$k(\Omega) = \frac{8\pi^2 \Omega N}{3\hbar c n} F(\Omega) \quad (8.7)$$

where

$$F(\Omega) = \sum_{\nu, \nu'} \rho_{1\nu} |\langle 1\nu | \vec{M}(\Omega_{\nu, \nu'}) | 2\nu' \rangle|^2 \delta(\Omega - \Omega_{\nu, \nu'}) \quad (8.8)$$

is the so-called *form function of the band* [8.13–8.15]. The function  $\Omega F_{12}(\Omega)$  determines the dependence of the light absorption coefficient (8.7) on the frequency  $\Omega$  and hence the shape of the absorption curve.

In the *semiclassical approximation* (at sufficiently high temperatures) when the APES has the physical meaning of the potential energy of the nuclei and hence the latter can be assumed to move along the APES,  $F_{12}(\Omega)$  can be calculated analytically. Indeed, in this approximation the vibrational functions in the matrix elements in Eq. (8.8) can be substituted by the APES functions of the symmetrized coordinates and the summation by integration over the latter. For instance, taking the two APES of Fig. 8.1 as parabolas (i.e., ignoring anharmonicity), we have

$$\begin{aligned}\varepsilon_1(Q) &= \frac{1}{2}K Q^2 \\ \varepsilon_2(Q) &= \hbar\Omega_0 + \frac{1}{2}K'(Q - Q_0)^2\end{aligned}\quad (8.9)$$

where  $\Omega_0$  is the frequency of the pure electronic transition, and neglecting the *Dushinski effect* [8.16], that is, taking the force constant  $K$  [not to be confused with the absorption coefficient  $K_{12}(\Omega)$ ] the same in the two states,  $K = K'$ , we obtain the following expression for the form function of the absorption band:

$$F_{12}(\Omega) = \frac{|\mathbf{M}_{12}|^2}{Q_0(2\pi K kT)^{1/2}} \exp\left[\frac{-\hbar^2(\Omega_1 - \Omega)^2}{2Q_0^2 K kT}\right] \quad (8.10)$$

where  $\mathbf{M}_{12} = \mathbf{M}_{12}(\Omega_0)$  is the pure electronic transition dipole moment,  $\Omega_1$  is the frequency at the band maximum (Fig. 8.1), and  $k$  is the Boltzmann constant [not to be confused with spectral density  $k(\Omega)$ ].

Expression (8.10) shows that in the semiclassical approximation the absorption band has a Gaussian shape (exponential dependence on the square of the frequency deviations from the maximum value  $\Omega_1$ ), and it is strongly temperature-dependent. However, the integral intensity of the band (the area under the absorption curve) is independent of temperature; this can be shown by integrating expression (8.10) over  $\Omega$ .

A more exact expression for the band shape form function  $F_{12}(\Omega)$  can be obtained by renouncing the semiclassical approximation and performing a full quantum-mechanical calculation. The latter was carried out under the assumption that only one vibrational frequency  $\omega$  is active in the vibrational broadening; it yields the following formula [8.14]:

$$\begin{aligned}F_{12}(\Omega) &= |\mathbf{M}_{12}|^2 \exp\left(-\frac{a}{2} \coth \frac{\beta}{2} + p\beta\right) I_p(Z) \\ Z &= \frac{a}{2sh(\beta/2)}\end{aligned}\quad (8.11)$$

where  $p = (\Omega - \Omega_0)/\omega$ ,  $\beta = \hbar\omega/kT$ ,  $I_p(Z)$  is a Bessel function, and  $a$  is the *parameter of heat release* determined by the summary shift of the minima positions  $Q_{1\alpha}^0 - Q_{2\alpha}^0$  of the ground and excited states for all the normal vibrations

$Q_{1\alpha}$  involved in the transition. In dimensionless units of oscillator coordinates

$$a = \sum_{\alpha} (Q_{1\alpha}^0 - Q_{2\alpha}^0)^2 \quad (8.11')$$

If only one coordinate is active in the broadening, as in Eq. (8.11) and Fig. 8.1, then  $a = (\Delta Q)^2$ .

### Band Shapes of Electronic Transitions between Nondegenerate States; Zero-Phonon Lines

The expressions for the form function  $F_{12}(\Omega)$  obtained above enable us to analyze the expected band shape of electronic absorption of light by transitions between nondegenerate electronic terms. The Bessel function  $I_p(Z)$  is nonzero for integer values  $p$  only. Hence  $F_{12}(\Omega)$  in (8.11) and the absorption coefficient  $K_{12}(\Omega)$  in (8.5) have the form of a set of equidistant lines with a spacing equal to  $\omega$  and an envelope that [following the behavior of the exponent in (8.11)] is a slightly asymmetric bell-shaped curve (Fig. 8.2). If one takes into account the natural width of the individual lines  $\gamma$  and the influence of the crystal or liquid environment, these lines coalesce into a continuous band that has the form of the envelope.

Following Eq. (8.11), the position of the absorption maximum of the band under the condition of only one type of vibrations involved in the electronic transition is determined by the relation

$$\Omega_{\max}^{\text{abs}} = \Omega_0 + \frac{a\omega}{2} \quad (8.12)$$

An important conclusion emerges from this formula: *the band maximum, in general, does not coincide with the frequency of the pure electronic transition  $\Omega_0$ .*

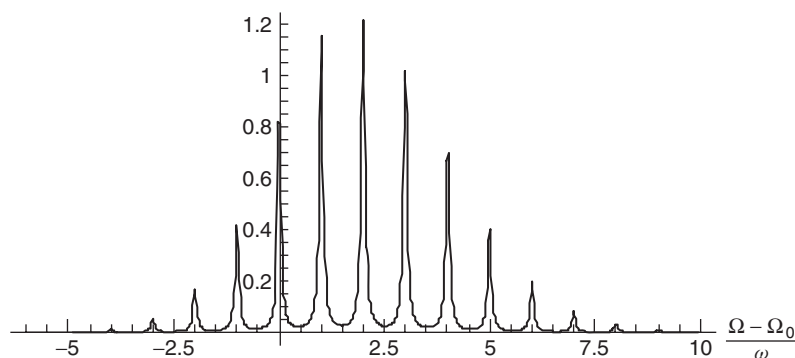


**FIGURE 8.2.** Electron transition band as a function of  $p = (\Omega - \Omega_0)/\omega$  calculated by Eq. (8.11) with  $a = 4$ ,  $kT/\hbar\omega = 1$ , and the broadening parameter of the individual vibrational lines  $\gamma = 0.05\omega$ . The envelope of the vibrational components has a slightly asymmetric Gaussian form.

The temperature dependence of the band shape is also important. At sufficiently high temperatures when the relations  $\hbar\omega < 2kT$  and  $a \gg sh(\hbar\omega/2kT)$  hold, the absorption band acquires a symmetric Gaussian form (8.10). Hence at these temperatures the semiclassical approximation is valid. The half-width  $\delta\Omega$  of the band is proportional to  $\sqrt{T}$ :

$$\delta\Omega = 2\omega \left( \frac{2akT \ln 2}{\hbar\omega} \right)^{1/2} \quad (8.13)$$

In the opposite limit case, at sufficiently low temperatures when  $kT \ll \hbar\omega$  and  $a \ll 2sh(\hbar\omega/2kT)$ , the band is asymmetric and the half-width is independent of temperature:

$$\delta\Omega = 2\omega(a \ln 2)^{1/2} \quad (8.14)$$

Equations (8.10)–(8.14) play a significant role in the interpretation of electronic spectra and allow one to reveal interesting parameters of electronic structure. For example, following (8.13) and (8.14), the band half-width  $\delta\Omega$  is proportional to  $a^{1/2}$ . Hence, when there are no large minima shifts and  $a$  is small, the absorption bands are narrow, in accordance with the qualitative considerations given above. For most coordination compounds the vibrational frequencies  $\omega$  are sufficiently large and obey the low-temperatures criterion at room (and lower) temperatures; hence Eq. (8.14) is valid for these compounds. By combining (8.14) with (8.12), we obtain

$$\Omega_{\max}^{\text{abs}} = \Omega_0 + \frac{(\delta\Omega)^2}{5.5\omega} \quad (8.15)$$

Hence the shift in band maximum with respect to the frequency of the pure electronic transition depends on the band half-width squared and can be relatively large. For example, with  $\delta\Omega \sim 3000 \text{ cm}^{-1}$  and  $\omega \sim 600 \text{ cm}^{-1}$ , the shift is  $\sim 3000 \text{ cm}^{-1}$ , the same as the half-width. Note that from the exact formula (8.11) (as is also seen from Fig. 8.1)

$$\Omega_{\max}^{\text{abs}} = \Omega_1 \quad (8.16)$$

which means that the frequency at the maximum of absorption coincides with that of the Franck–Condon (vertical) transition from the ground-state vibrational level. It follows that *the frequencies of the band maxima of electronic absorption are determined by the energy gaps between the electronic terms calculated for the equilibrium configuration of the ground state*. This important conclusion means that, for interpretation of the origin of the band maxima positions in transitions between nondegenerate states, the simple energy-level scheme obtained in crystal field theory (Chapter 4) or in the MO LCAO approach (Chapter 5) yield, in principle, correct results, but in general *the maximum absorption frequencies is*



not equal to the energy difference between the ground and excited states, each at their equilibrium positions.

In the case of *light emission* (luminescence or fluorescence) the maximum of the band corresponds to the vertical transition from the minimum of the excited state to the ground state, that is, to  $\Omega_2$  (Fig. 8.1). One can easily find that

$$\Omega_2 = \Omega_0 - \frac{a \cdot \omega}{2} \quad \Omega_1 - \Omega_2 = a \cdot \omega \quad (8.17)$$

Thus the frequency difference between the absorption and luminescence (or fluorescence) band maximum (*the Stocks shift*) is due to the difference in the equilibrium configuration of the ground and excited states (Section 8.4). If the Stocks shift is not very large, there may be an overlap between the absorption and fluorescence bands, resulting in *resonance fluorescence*.

Note that the transition from the excited electronic state to the ground state (or to another lower-energy excited state) can also take place as a *radiationless transition* without light emission. The radiationless transition is a kind of relaxation when the excitation energy is transformed into vibrations, and it is strongly temperature-dependent.

An important feature of electronic spectra of polyatomic systems, especially at low temperatures, is the *zero-phonon line* [8.14, 8.15]. It occurs as an additional acute (resonance) peak at the pure electronic frequency  $\Omega_0$  on the background of the broad band, provided that the parameter of heat release  $a$  is not very large. In electronic transitions the operator of the dipole moment in the matrix element  $M_{1v2v'}$  in Eq. (8.8), which determines the transition probabilities, contains only electronic coordinates, hence  $M_{1v2v'} = \langle 1|M|2\rangle\langle v|v'\rangle$  and the vibrational contribution will be presented by the overlap integral between the vibrational wavefunctions of the two combining vibrational states  $\langle v|v'\rangle$  (the *Franck–Condon factor*). The smaller is this overlap, the larger is  $a$ . As seen from Fig. 8.1, if  $a$  (or  $Q_1^0 - Q_2^0$ ) is small, the pure electronic transition with vibrational quantum numbers 0 in both states ( $0 \rightarrow 0$ , or *zero-phonon transition*) becomes most probable. Moreover, the transitions  $1 \rightarrow 1$ ,  $2 \rightarrow 2$ , and so on, which in the absence of anharmonicity have the same frequency  $\Omega_0$  as the  $0 \rightarrow 0$  line, are also most probable. The sum of all these transitions with the same frequency yields a narrow line of great intensity (the *zero-phonon line*) on the background of the less intensive one-, two-, ..., phonon satellites. The latter are much broader and coalesce into a broad phonon wing (mostly of higher frequency). This result emerges from the general formula (8.11) for the form function of the band if one substitutes  $p = 0$  and  $a \rightarrow 0$ . The distinct feature of zero-phonon lines is that their frequencies  $\Omega_0$  are the same in absorption and luminescence and hence may be observed as a line of *resonance fluorescence*. Figure 8.3 illustrates this observation together with the demonstration of an example spectrum with a zero-phonon line [8.14].

The zero-phonon line carries interesting information about the electronic structure of the system. In particular, it gives the exact value of the energy difference between two electronic terms at their equilibrium nuclear configurations. The zero-phonon line of transitions between nuclear states lies in the base of the

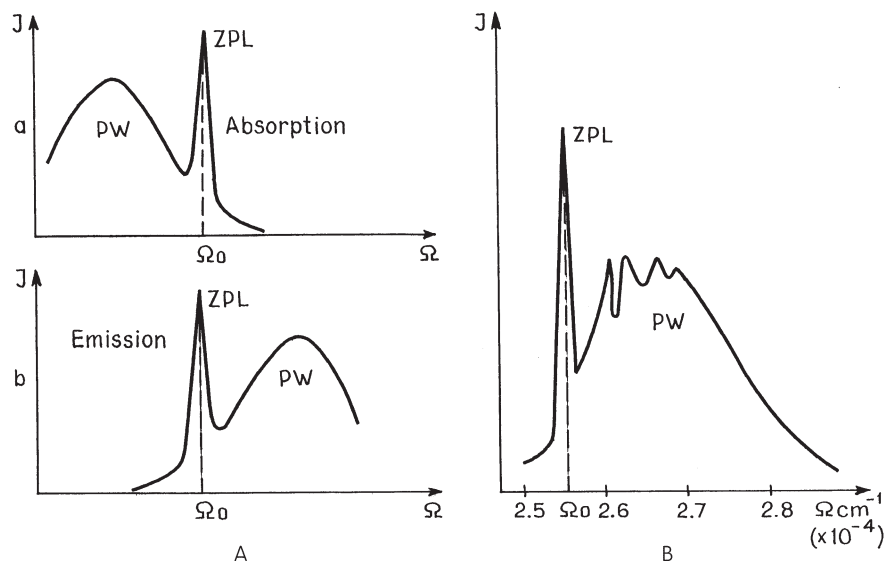


**FIGURE 8.3.** (A) absorption (a) and emission (b) band shapes in the presence of a zero-phonon line (ZPL) (PW is the phonon wing); (B) example of experimentally observed absorption spectrum with a ZPL for color centers in NaF (see descriptions in Refs. 8.13 and 8.14).

Mossbauer effect (Section 8.5). The role of orbital degeneracies in optical band shapes is discussed in Section 8.2.

### Types of Electronic Transitions on Intensity

In expressions for the form function of the band shapes of electronic transition and hence in the absorption coefficient, the square of the pure electronic matrix element  $|M_{12}(\Omega_0)|^2$  determines the band absolute intensities. They vary by several orders of magnitude, dividing the observable spectra into different types differentiated according to intensity.

First, the *selection rules* for the transition moment  $M_{12}$  after (8.4) must be taken into account. Since  $\mathbf{M}$  is a vector or a tensor, the selection rules can be obtained directly using group-theoretical procedures, as shown in Section 3.4. The matrix element  $M_{12}$  is nonzero if and only if the product of the IrReps (Appendix 1) of the wavefunctions  $\psi_1$  and  $\psi_2$  and the operator  $\mathbf{M}$  contains the unity (totally symmetric) representation.

The transitions for which the integral (8.4) is zero, called *forbidden transitions*, can be evaluated in a general way. For electric-dipole transitions in systems with an inversion center the integral (8.4) is zero when states 1 and 2 have the same parity because  $\mathbf{M}$  changes its sign by inversion. Hence electric-dipole transitions are forbidden as  $g \leftarrow / \rightarrow g$  and  $u \leftarrow / \rightarrow u$  (*parity forbidden transitions*), and may be allowed as  $g \leftrightarrow u$  ( $g$  and  $u$ , as above, denote even and odd parity,

respectively). Another general case is provided by the *spin-forbidden transitions*, sometimes called *intersystem combinations*, when the two states have different spin multiplicities. If the spin-orbital mixing of these states with other states is not accounted for (see below), the integral (8.4) is zero, due to the orthogonality of the spin functions ( $\mathbf{M}$  is independent of spin).

For a given transition the three components of  $M_{12}$

$$M_{12}^x = \int \psi_1^* M_x \psi_2 d\tau \quad M_{12}^y = \int \psi_1^* M_y \psi_2 d\tau \quad M_{12}^z = \int \psi_1^* M_z \psi_2 d\tau$$

may be subject to different selection rules. Therefore, if the coordination system is in an anisotropic crystal state where all the absorbing centers have the same orientation with respect to the electric (or magnetic) vector of the electromagnetic wave of light, the absorption (emission, reflection) of polarized light may vary with the direction or orientation of the crystal (*dichroism or polychroism*). Related phenomena of circular dichroism and magnetic circular dichroism are discussed in Section 8.4. Methods of group-theoretical evaluation of selection rules are given in Section 3.4 and Problems 3.3 and 8.2. Example 8.2 shows how to determine the selection rules of polarized absorption using  $\text{PtCl}_4^{2-}$  as a specific case.

### EXAMPLE 8.2

#### Selection Rules for Polarized Light Absorption by the $\text{PtCl}_4^{2-}$ Complex

$\text{PtCl}_4^{2-}$  is a square-planar complex with  $D_{4h}$  symmetry. Its ground state is  $^1A_{1g}$ , and the most intensive bands are associated with the one-electron ligand  $\rightarrow$  metal *charge transfer transitions* (see below in this section)  $b_{2u} \rightarrow b_{1g}$ ,  $e_u \rightarrow b_{1g}$ , and  $a_{2u} \rightarrow b_{1g}$  from the MOs  $b_{2u}$ ,  $e_u$ , and  $a_{2u}$  (formed mainly by the four  $p_z$  AOs of the chlorine atoms) to the MO  $b_{1g}$  (which is mainly the Pt AO  $d_{x^2-y^2}$ ) resulting in the excited  $^1A_{2u}$ ,  $^1E_u$ , and  $^1B_{2u}$  states, respectively ( $b_{2u} \times b_{1g} = A_{2u}$ ,  $e_u \times b_{1g} = E_u$ ,  $a_{2u} \times b_{1g} = B_{2u}$ ). In the  $D_{4h}$  point group  $M_z$  transforms as a  $z$  component of a vector and belongs to  $A_{2u}$ , while  $M_x$  and  $M_y$  belong to  $E_u$  (Appendix 1, Table A1.8), so we have the following for the transition  $^1A_{1g} \rightarrow ^1A_{2u}$ :

$$A_{1g} \times A_{2u} \times A_{2u} = A_{1g} \quad \text{for } z \text{ component}$$

$$A_{1g} \times E_u \times A_{2u} = E_g \quad \text{for } x \text{ and } y \text{ components}$$

Similarly, for the transition  $^1A_{1g} \rightarrow ^1E_u$ :  $A_{1g} \times A_{2u} \times E_u = E_g$ ,  $A_{1g} \times E_u \times E_u = A_{1g} + B_{1g} + E_g$ , and for  $^1A_{1g} \rightarrow ^1B_{2u}$ :  $A_{1g} \times A_{2u} \times B_{2u} = B_{1g}$ ,  $A_{1g} \times E_u \times B_{2u} = E_g$ . From all these transitions, the only ones allowed are those for which the abovementioned

products of IrReps contain the totally symmetric one  $A_{1g}$ . It follows that the transition  ${}^1A_{1g} \rightarrow {}^1A_{2u}$  is possible only for light polarized in the  $z$  direction, whereas in the  $x$  and  $y$  directions it is forbidden. On the contrary, the transition  ${}^1A_{1g} \rightarrow {}^1E_u$  is allowed when the light is polarized in the  $x$  or  $y$  direction (in any direction in the  $xy$  plane) but is forbidden in the  $z$  direction. The transition  ${}^1A_{1g} \rightarrow {}^1B_{2u}$  is forbidden in any direction (in this approximation). Another example of polarized spectra is considered in Problem P8.2.

While the selection rules for the matrix elements (8.4) obtained by group-theoretical considerations are exact, the matrix element itself (i.e., the wavefunctions of the initial and final states and the operator of interaction of the system with light) are defined approximately within a certain model. Therefore, when the matrix element  $M_{12} = 0$  by symmetry considerations, this does not mean that the corresponding transition is absolutely forbidden; *it is forbidden within the approximation employed*, and hence it can become allowed in the next approximation.

For instance, forbidden electric-dipole transitions can become allowed as magnetic-dipole transitions, and if the latter are also forbidden, they can become possible as quadruple transitions. Transitions that are forbidden by parity restrictions become allowed by interaction with odd vibrations, while spin-forbidden transitions are allowed as intersystem combinations when the spin-orbital interaction removes the prohibition, and so on. Depending on the approximation in which the electronic transition becomes allowed, the corresponding intensities of the band have quite different orders of magnitude. Each approximation that enables the otherwise forbidden transition can be related to a specific interaction with an order of magnitude determined by the interaction constant. This enables us to estimate the order of magnitude of the intensity of the corresponding transitions.

To characterize the intensities quantitatively, the *oscillator strength*  $f_{12}$  can be employed. The definition of  $f$  (not to be confused with  $f$  electrons) is expressed as follows:

$$f_{12} = \frac{mc}{N\pi^2e^2} \int k(\Omega)d\Omega \quad (8.18)$$

It reflects the strength of the transition as compared with that of an electron oscillating harmonically in three dimensions. For absorptions in solutions the following presentation may be more convenient:

$$f_{12} = 4.32 \cdot 10^{-9} \text{ L}^{-1} \cdot \text{mol cm}^2 * \gamma_{12}(\sum) d \sum \quad (8.19)$$

where  $\gamma_{12}(\sum)$  is the *extinction coefficient* or *molar absorption coefficient* (defined in  $\text{L} \cdot \text{mol}^{-1} \text{cm}^{-1}$ ), determined from the relation  $I = I_0 10^{-\epsilon C_0 l}$  with  $C_0$  as the molar concentration (cf.  $I = I_0 e^{-kl}$  used above);  $N_A$  is the Avogadro number.

Note that  $f$  is a dimensionless number and cannot be larger than one: the sum of the oscillator strengths for all one-electron transitions from a given state equals one. For the different types of transitions mentioned above, the  $f$  value varies from 1 to  $10^{-10}$  and less. Most intensive are the transitions allowed through the electric-dipole mechanism, that is, between states with opposite parity ( $g \leftrightarrow u$  in the case of systems with an inversion center) but with the same spin multiplicity. The oscillator strength of electric-dipole bands  $f \sim 1$  to  $10^{-2}$ . In transition metal coordination compounds such transitions are known mostly as *charge transfer bands* (see next section).

*Parity-forbidden transitions* (transitions forbidden by the parity rule  $g \leftarrow / \rightarrow g$  and  $u \leftarrow / \rightarrow u$ ) become allowed through the interaction between the electronic states and odd vibrations, which mix odd electronic states with even ones (Section 8.2). For these transitions  $f \sim 10^{-4}$ – $10^{-5}$ . They can also be allowed as *magnetic-dipole transitions* with  $f \sim 10^{-6}$ . Parity-forbidden transitions constitute the majority of observable electronic transitions in coordination compounds in the visible and related regions of light; the most frequently studied are the  $d$ - $d$  transitions, considered in the next section.

The next type of “forbidden” transitions is formed by the abovementioned *spin-forbidden, or intersystem combination, transition*. These are transitions between electronic states with different spin multiplicities, for which the integral (8.4) is zero because of the orthogonality of the spin functions of the two states. Spin-forbidden transitions become allowed when the spin-orbital interaction, which mixes the states with different spin multiplicities, is factored in. Perturbation theory estimates show that the mixing terms are of the order of  $(\lambda/\Delta)^2$ , where  $\lambda$  is the spin-orbital coupling constant (Section 2.1) and  $\Delta$  is the energy gap between the mixing states. These terms are of the order of  $10^{-3}$ – $10^{-5}$ , and hence this is the order of the oscillator strength  $f$  expected for such spectra.

If the transition is forbidden by both the parity rule and the spin difference, then  $f \sim 10^{-6}$ – $10^{-7}$  when the transition is enabled by the interaction with odd vibrations, and  $f \sim 10^{-9}$  and  $f \sim 10^{-10}$  for magnetic-dipole and electric quadrupole transitions, respectively.

Table 8.1 lists the most important types of electronic transitions in coordination compounds, with indication of their oscillator strengths (by order of magnitude) and coefficients of molar extinction at the maximum band intensity  $\varepsilon(\Omega_{\max})$  [Eq. (8.19)]; the  $\varepsilon$  values are determined from the relation  $f = 4.32 \times 10^{-9} \varepsilon(\Omega_{\max}) \delta\Omega$ , which is approximately true for symmetric Gaussian bands.

## 8.2. $d$ - $d$ , CHARGE TRANSFER, INFRARED, AND RAMAN SPECTRA

With respect to their origins related to electronic structure, the following main types of absorption and emission spectra of coordination systems in the visible and adjacent spectral regions can be distinguished: metal  $d$ - $d$ , metal-ligand, and

**TABLE 8.1. Orders of Magnitudes of Oscillator Strengths  $f$  and Extinction Coefficients in the Maximum of the Band  $\varepsilon(\Omega_{\max})$  for Different Types of Electronic Transitions**

Type of Electronic Transition	$f$	$\varepsilon(\Omega_{\max})$
Electric-dipole	$1-10^{-2}$	$10^5-10^3$
Parity-forbidden, allowed by odd vibrations	$10^{-4}-10^{-5}$	$10^3-10^1$
Magnetic-dipole	$10^{-6}$	1
Electric-quadrupole	$10^{-7}$	$10-1$
Spin-forbidden (intersystem combination)	$10^{-3}-10^{-5}$	$100-10$
plus parity-forbidden:		
Allowed by vibrations	$10^{-6}-10^{-7}$	$1-10^{-1}$
Magnetic-dipole	$10^{-9}$	$10^{-3}$
Electric-quadrupole	$10^{-10}$	$10^{-4}$

intraligand charge transfer, as well as vibrational infrared and Raman. Intraligand transitions are less interesting in terms of the electronic structure of the coordination center, but may be important in the study of chemical activation by coordination (Chapter 10).

### Origin and Special Features of $d-d$ Transitions

In accordance with the role of  $d$  and  $f$  electrons of the CA in the formation of coordination bonding (Section 6.1), optical transitions that involve these electrons are most important for the study of the electronic structure of transition metal compounds. Of particular interest are the transitions between the states originating from  $d^n$  configuration, often called  $d-d$  transitions. These transitions fall into the visible and related regions of the optical spectrum, thus determining the color of the compound. The  $d-d$  spectra were studied intensively beginning with the 1920s and, together with the magnetic properties (Section 8.4), served as an experimental basis for the creation of crystal field theory (Chapter 4).

Consider the energy levels of  $d^n$  configurations obtained in CFT (Sections 4.2 and 4.3; in the MO LCAO approach the qualitative description is similar; see Section 6.2). A general picture of  $d^n$  energy-level splitting in the cubic field of ligands as a function of the ligand field parameter  $\Delta$  is given by the Tanabe–Sugano diagrams (Fig. 4.11). These diagrams provide the most important parameter of the spectrum—the positions of the band maxima. To determine the latter, draw a vertical line on the diagram through the point  $\Delta = \Delta_0$  relevant to the complex under consideration. Following the conclusions of Section 8.1, the expected band maxima positions  $\Omega_i$  are given by the ordinates of the points of intersection of this vertical line with the curves  $E_i(\Delta) : \Omega_i = E_i(\Delta_0)$ . The  $\Delta_0$  value can be found from the experimentally observed position of the maximum of one of the bands. Example 8.3 illustrates this statement.

**EXAMPLE 8.3*****d-d Transitions in the Absorption Spectrum of  $Mn(H_2O)_6^{2+}$*** 

Consider the diagram of the  $d^5$  energy-level splitting for the  $Mn^{2+}$  ion in a cubic weak field, calculated by Orgel [8.17] (Fig. 8.4), and compare it with the experimental absorption spectrum of this hydrated ion (Fig. 8.5) [8.18].

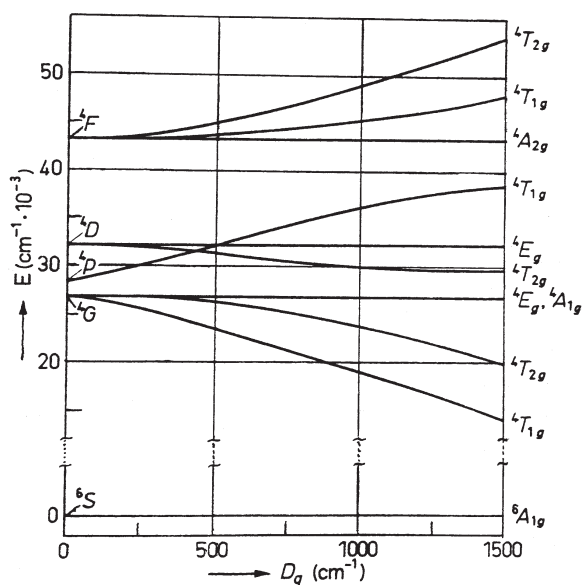


**FIGURE 8.4.** Energy-level diagram of the  $Mn^{2+}(d^5)$  ion in a cubic crystal field as a function of the parameter  $\Delta = 10D_q$ . (After Orgel [8.17].)

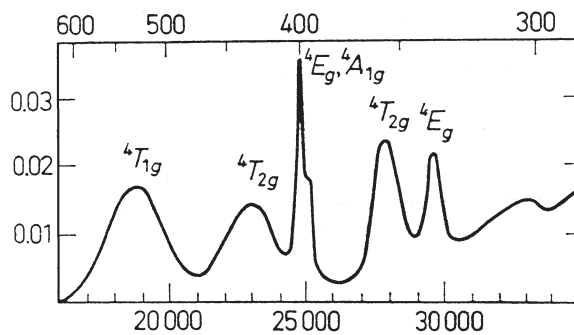


**FIGURE 8.5.** The absorption spectrum of the aqua complex  $Mn(H_2O)_6^{2+}$  in  $cm^{-1}$  (lower figures) and  $\mu m$  (upper figures).

From Fig. 8.4, taking the vertical line at  $\Delta_0 \approx 9000\text{--}10000\text{ cm}^{-1}$ , we get the maxima positions of all bands of the spectrum, which can thus be interpreted as corresponding to the electronic transitions from the ground state  ${}^6A_{1g}$  to the excited states  ${}^4T_{1g}$ ,  ${}^4T_{2g}$ ,  ${}^4E_g$ ,  ${}^4A_{1g}$ ,  ${}^4T_{2g}$ ,  ${}^4E_g$ , and so on, as indicated in Fig. 8.5; there is relatively good quantitative agreement between the theoretical predictions and experimental values of the maxima frequencies.

The relative bandwidths of this spectrum can also be explained using the theoretical conclusions obtained in the previous section. Indeed, the ground state  ${}^6A_{1g}$  originates from the half-filled  $d$  shell with the configuration  $(t_{2g})^3(e_g)^2$  in the octahedral field. Therefore the transitions  ${}^6A_{1g} \rightarrow {}^4T_{1g}[(t_{2g})^4(e_g)^1]$  and  ${}^6A_{1g} \rightarrow {}^4T_{2g}[(t_{2g})^4(e_g)^1]$  with  $\Delta m = 1$ ,  $\Delta n = -1$ , following (8.3), are expected to yield broad bands in accordance with the experimental data.

On the contrary, the next excited terms,  ${}^4E_g$ ,  ${}^4A_{1g}$ ,  ${}^4T_{2g}$ , and  ${}^4E_g$ , originate from the same electronic configuration  $(t_{2g})^3(e_g)^2$  as the ground state, and hence the transitions to them are expected to produce more narrow lines. This is indeed the case (Fig. 8.5), but the bandwidths of these transitions differ significantly from each other, indicating that a more refined analysis is required. It can be performed using the derivatives  $d\Omega/d\Delta$  introduced in Section 8.1, Eq. (8.1), as an approximate relative measure of the width. Since the ground state is taken as an energy readoff,  $dE_1/dQ = 0$  and  $d\Omega/d\Delta = dE_2/d\Delta$ . The latter can be estimated directly from the slope of the curves  $E_i = f(\Delta)$  at  $\Delta = \Delta_0$ . For the octahedral aqua complex of  $\text{Mn}^{2+}$  the relative values of  $dE_2/d\Delta$  for the sequence of excited states can be estimated roughly from Fig. 8.4, as follows: 1; 0.8; 0; 0; 0.2;  $< 0.1$ ; 0.9, for the terms  ${}^4T_{1g}$ ,  ${}^4T_{2g}$ ,  ${}^4E_g$ ,  ${}^4A_{1g}$ ,  ${}^4T_{2g}$ ,  ${}^4E_g$ , and  ${}^4T_{1g}$ , respectively. As one can see from Fig. 8.5, the observed bandwidths follow approximately (although not exactly proportionally) the sequence of predicted values.

An important feature of electric-dipole  $d-d$  transitions is that they are parity-forbidden; that is, they originate from the transitions between two states that have the same parity (Section 8.1). In atoms  $d-d$  transitions are strongly forbidden, but in molecular systems there are several additional interactions that remove this prohibition. Since the parity rule is operative when the system has an inversion center, low-symmetry ligand fields that remove the inversion symmetry make the  $d-d$  transition allowed. If there are no low-symmetry fields, the vibronic coupling of the electronic states to odd vibrations that produce the required off-center distortions may induce the  $d-d$  transitions (*vibration-induced transitions*). This vibronic mechanism is most operative except at very low temperatures.



In Section 3.4 it is shown how the inclusion of odd vibrations allow for otherwise forbidden  $g \leftrightarrow g$  and  $u \leftrightarrow u$  transitions. Quantitative estimates of the intensity, band shapes, and temperature dependence of the spectrum can be obtained by taking into account the vibronic coupling to the odd vibrations explicitly (Section 7.2). Consider a parity-forbidden transition between two even states  $\Psi_1^g$  and  $\Psi_2^g$  (the same result is valid for two odd states) in a system with inversion symmetry for which the matrix element  $\mathbf{M}_{12}$  in (8.4) is zero. Factoring in the vibronic coupling terms (7.3) with odd vibrations  $Q_u$ , the wavefunction  $\Psi^g$  receives an admixture of an odd function  $\Psi^u$  of the excited state:

$$\Psi_1(r, Q_u) = \Psi_1^g + \frac{F^{(gu)}}{\Delta_{ug}} Q_u \Psi^u \quad (8.20)$$

where, for simplicity, only one (odd) linear term of the vibronic interaction (7.3) is accounted for, and only one excited state  $\Psi^u$  is included;  $F^{(g,u)}$  is the constant of vibronic coupling between the two states (7.22) (not to be confused with the form function  $F_{12}$ ), and  $\Delta_{ug}$  is the energy gap between them.

The additional term in (8.20) that contains the odd wavefunction gives a nonzero contribution of the order  $(F/\Delta)Q$  (hereafter the labels  $g$  and  $u$  are omitted) to the integral (8.4), placing the corresponding form function  $F_{12}(\Omega)$  on the order of  $(F/\Delta)^2$ , and modifying the band shape and its temperature dependence. Calculations similar to those resulting in Eq. (8.11) yield an appropriate expression for the form function  $F_{12}(\Omega)$  in this case:

$$F_{12}(\Omega) = \left(\frac{F}{\Delta}\right)^2 |M_{12}|^2 \exp\left(\frac{a \coth \beta - a' \coth \beta'}{2}\right) \times [(n+1) \exp(-p_1\beta) I_{p_1}(z) + n \exp(-p_2\beta) I_{p_2}(z)] \quad (8.21)$$

where, in addition to the notation in (8.11)  $a' = (F/\hbar\omega')^2$  (in dimensionless units),  $p_1 = (\Omega - \Omega_1 + \omega')/\omega$ ,  $p_2 = (\Omega - \Omega_1 - \omega')/\omega$ ,  $\beta' = \hbar\omega'/2kT$ ,  $n = [\exp(\hbar\omega'/kT) - 1]^{-1}$  is the Boltzmann occupation number of the odd vibrations,  $\omega'$  is their frequency, and  $\Omega_1$ , the frequency of the band maximum, is

$$\Omega_1 = \Omega_0 - \frac{F^2}{2} \frac{(2n+1)\Delta - \hbar\omega'}{\Delta^2 - (\hbar\omega')^2} \quad (8.22)$$

It follows from (8.21) that the odd vibrations that make the bands allowed influence significantly their maximum positions and intensities, as well as the temperature dependence of the absorption. In particular, if  $\omega'$  is not very large, one can assume that for many points of the band,  $p_1 \approx p_2$ , which yields in (8.21) the factor  $n + \frac{1}{2}$  (this factor also remains after integration over  $\Omega$ ). This means that the integral intensity of the band increases with increase in occupation of the odd vibrations  $n$ , that is, with temperature. This is an important conclusion that enables us to discriminate electronic *d-d* transitions that are

allowed by vibrations from other possible mechanisms; *the increase in oscillator strength with temperature is inherent to only these vibrationally induced transitions*. Example 8.4 demonstrates this effect in experimentally observed spectra of specific systems.

#### EXAMPLE 8.4

##### Temperature-Dependent Absorption Spectra of $K_2NaCrF_6$ and Emerald [8.19]

Figure 8.6 shows the  $d-d$  absorption spectrum of the  $Cr^{3+}$  ion at two temperatures, 77 and 300 K, in a centrosymmetric environment in  $K_2NaCrF_6$ , and in a noncentrosymmetric environment in emerald [beryl mineral  $Be_3Al_2(SiO_3)_6$  with Cr impurities] [8.19]. It is seen that in the first case when the transitions are allowed as assisted by the vibrations, the intensity increases with temperature significantly, while in emerald, where the transitions are allowed mainly because of the noncentrosymmetric ligand field contributions, the intensity of the spectrum is almost independent of temperature, even somewhat lower at higher temperature.

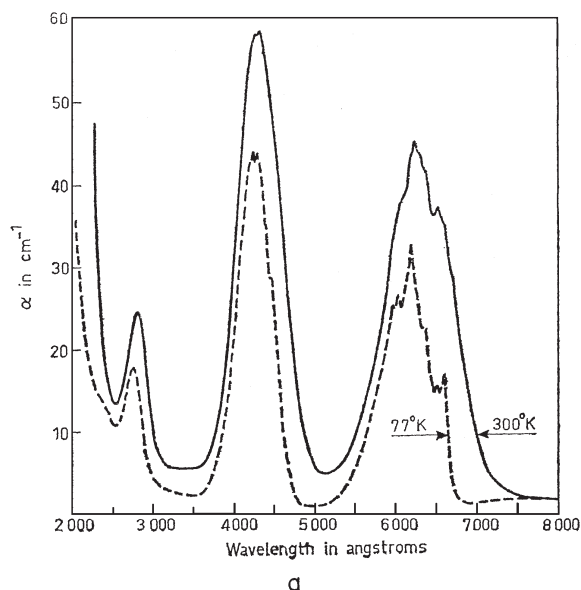
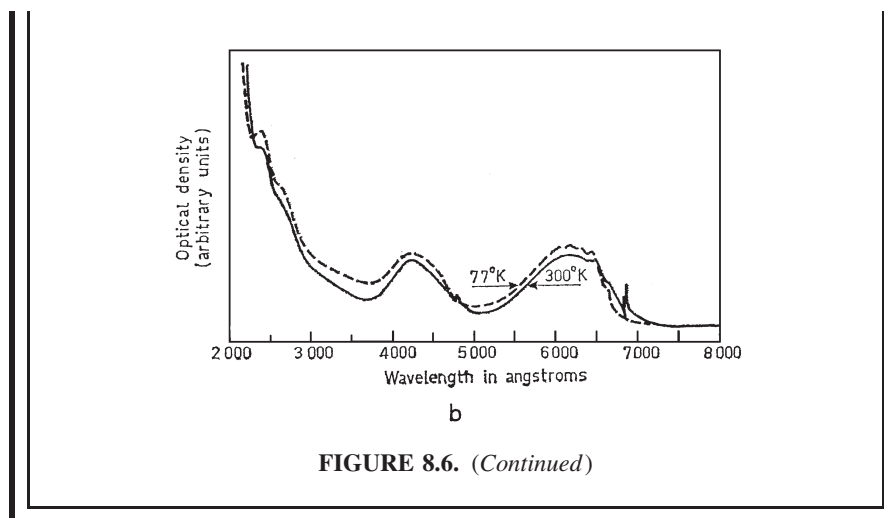


**FIGURE 8.6.** Temperature dependence of intensities in absorption spectra of two systems: (a)  $K_2NaCrF_6$ , with chromium position centrosymmetric (the intensity increases with temperature); and (b) emerald,  $Cr : Be_3Al_2(SiO_3)_6$ , with chromium position noncentrosymmetric (the intensity decreases with temperature). (From Wood et al. [8.19].)



For non-center-symmetric (e.g., tetrahedral) ligand fields, mixing of the even and odd atomic states of the central atom takes place without involvement of vibrations. Here the static ligand field makes a much stronger contribution to the  $d-d$  transition intensity than do odd vibrations, but in this case *the intensity does not increase with temperature*. As mentioned above,  $d-d$  transitions are also allowed through the magnetic-dipole and electric-quadrupole mechanisms (with  $f \sim 10^{-6}$  and  $f \sim 10^{-7}$ , respectively) which are practically independent of temperature. These mechanisms may be effective in rare cases when the coupling between the electronic states and odd vibrations is very weak.

### Spectrochemical and Nephelauxetic Series

As far as  $d-d$  transitions are concerned, two main parameters determine the optical band positions in cubic complexes:  $\Delta$ , the main parameter of ligand field splitting, and  $B$ , the Racah parameter of interelectron repulsion in  $d$  states. This can be seen directly from the Tanabe-Sugano diagrams (Fig. 4.11) in which the calculated energy levels of  $d^n$  configurations are given as a function of  $\Delta/B$ . Indeed, if  $\Delta$  and  $B$  are known, all the band frequencies can be estimated from these diagrams, and the  $\text{Mn}^{2+}$  complex considered in Example 8.3 shows that this description of the spectrum is satisfactory for such systems. Let us consider some general rules in the dependence of these two parameters on the nature of the CA and ligands.

The dependence of  $\Delta$  on the properties of the central atom is briefly discussed in Section 4.5. First,  $\Delta$  strongly increases with the charge (oxidation state) of the CA, that is, it increases in the series  $\text{M(II)} < \text{M(III)} < \text{M(IV)}$ . For the same oxidation state  $\Delta$  increases with the principal quantum number of the  $d$  electrons:  $3d < 4d < 5d$ . For  $3d$  elements  $\Delta$  is of the order of  $\sim 10,000 \text{ cm}^{-1}$  for  $\text{M}^{2+}$ ,

**TABLE 8.2. Numerical Values of the Crystal Field Parameter  $\Delta$  (in  $10^2 \text{ cm}^{-1}$ ) for  $d^n$  Transition Metal Complexes with Different Ligands**

$d^n$	Ion	Ligand <sup>a</sup>							
		6Br <sup>-</sup>	6Cl <sup>-</sup>	3Ox <sup>2-</sup>	6H <sub>2</sub> O	Enta <sup>4-</sup>	6NH <sub>3</sub>	3En	6CN <sup>-</sup>
3d <sup>1</sup>	Ti <sup>3+</sup>	—	—	—	203	184	—	—	—
3d <sup>2</sup>	V <sup>3+</sup>	—	—	165	177	—	—	—	—
3d <sup>3</sup>	V <sup>2+</sup>	—	—	—	126	—	—	—	—
	Cr <sup>3+</sup>	—	136	174	174	184	216	219	263
4d <sup>3</sup>	Mo <sup>3+</sup>	—	192	—	—	—	—	—	—
3d <sup>4</sup>	Cr <sup>2+</sup>	—	—	—	139	—	—	—	—
	Mn <sup>3+</sup>	—	—	201	210	—	—	—	—
3d <sup>5</sup>	Mn <sup>2+</sup>	—	—	—	78	68	—	91	—
	Fe <sup>3+</sup>	—	—	—	137	—	—	—	—
3d <sup>6</sup>	Fe <sup>2+</sup>	—	—	—	104	97	—	—	330
	Co <sup>3+</sup>	—	—	180	186	204	230	233	340
4d <sup>6</sup>	Rh <sup>3+</sup>	189	203	263	270	—	339	344	—
5d <sup>6</sup>	Ir <sup>2+</sup>	231	249	—	—	—	—	412	—
	Pt <sup>4+</sup>	240	290	—	—	—	—	—	—
3d <sup>7</sup>	Co <sup>2+</sup>	—	—	—	93	102	101	110	—
3d <sup>8</sup>	Ni <sup>2+</sup>	70	73	—	85	101	108	116	—
3d <sup>9</sup>	Cu <sup>2+</sup>	—	—	—	126	136	151	164	—

<sup>a</sup>Ox, oxalate; Enta = ethylenetetramine, En = ethylenediamine.

Source: Jorgensen [8.20].

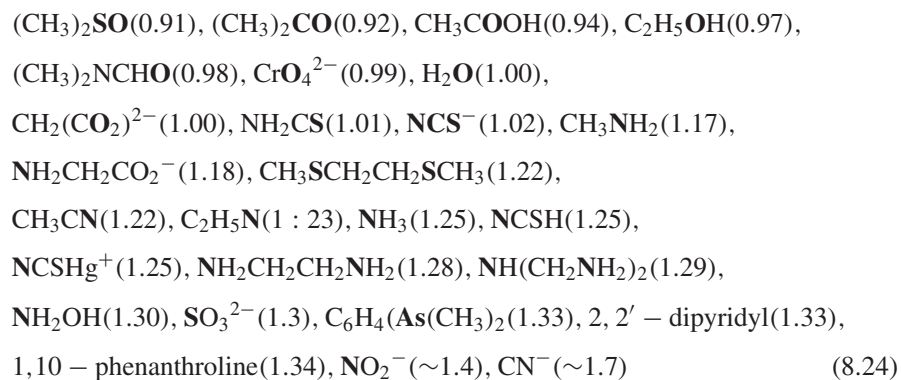
and  $\sim 20,000 \text{ cm}^{-1}$  for  $M^{3+}$ . Passing to 4d and 5d electrons,  $\Delta$  increases and reaches  $\sim 40,000 \text{ cm}^{-1}$ . The dependence of  $\Delta$  on the ligands is weaker but much more diversified.

Table 8.2 shows some examples of  $\Delta$  values for different ions and ligands (data collected from Ref. 8.20). An interesting general feature emerging from these data is that  $\Delta$  increases when passing from one ligand to another from left to right for all the CAs. This allows one to formulate the spectrochemical rule, or the *spectrochemical series*, that characterizes the increase of ligand influence by the increase of  $\Delta$ :

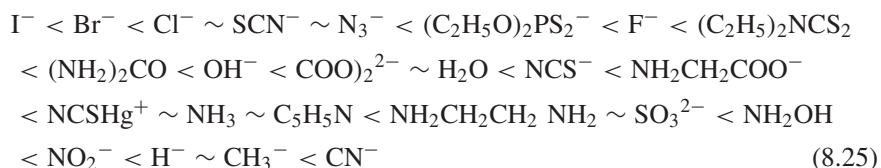
$$\text{Br}^- < \text{Cl}^- < \frac{1}{2}\text{Ox}^{2-} < \text{H}_2\text{O} < \text{NH}_3 < \frac{1}{2}\text{En} < \text{CN}^- \quad (8.23)$$

A more complete spectrochemical series with indication (in parentheses) of the relative  $\Delta$  values (in units of that for  $\text{H}_2\text{O}$ ) is as follows [8.20] (the coordinating atom is indicated in boldface letters):

**Br**<sup>-</sup> (0.72), (C<sub>2</sub>H<sub>5</sub>)<sub>2</sub>**PSe**<sup>-</sup> (0.74), **SCN**<sup>-</sup> (0.75), **Cl**<sup>-</sup> (0.78),  
 (CrH<sub>5</sub>)<sub>2</sub>**PS**<sub>2</sub><sup>-</sup> (0.78), (CrH<sub>5</sub>)<sub>2</sub>**PSe**<sub>2</sub><sup>-</sup> (0.8), **POCl**<sub>3</sub> (0.82), **NNN**<sup>-</sup> (0.83),  
 (CrH<sub>5</sub>O)<sub>2</sub>**PS**<sub>2</sub><sup>2-</sup> (0.83), (CrH<sub>5</sub>)<sub>2</sub>**NCS**<sub>2</sub><sup>-</sup> (0.85), **F**<sup>-</sup> (0.9), (C<sub>2</sub>H<sub>5</sub>)<sub>2</sub>**NCS**<sub>2</sub><sup>-</sup> (0.90),



Along with the spectrochemical series, there is a *hypsochromic series* in which the ligands are arranged following the increase in shift of the first absorption band to higher frequencies (ultraviolet shift):



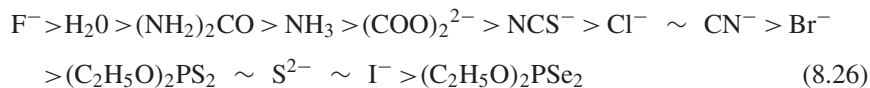
Note that these two series, although somewhat similar, are not identical. Indeed, the ultraviolet band shift coincides with the increase of  $\Delta$  only when the band results from a simple  $t_2 \rightarrow e$  transition. In more complicated cases with more than one  $d$  electron, as is seen from the Tanabe–Sugano diagrams (Fig. 4.11), the frequency of some transitions may either increase or decrease with the increase of  $\Delta$ . In particular, in the cubic complex of  $\text{Mn}^{2+}(d^5)$ , discussed in Example 8.3, the frequency of the first band,  ${}^6A_g \rightarrow {}^4T_{1g}$  [originating from the transition  $(t_{2g})^3(e_g)^2 \rightarrow (t_{2g})^4(e_g)^1$ ], decreases with  $\Delta$  (Fig. 8.4).

Besides, in the region of the breaks of the curves  $E_1 = f(\Delta)$  in the Tanabe–Sugano diagrams, a transition from high- to low-spin spectra takes place (spin crossover, Section 8.4), which completely changes the type of the first transition. Therefore, the hypsochromic series, in general, does not mean that the parameter  $\Delta$  increases by the corresponding ligand substitutions from left to right. The rule of hypsochromic increase with  $\Delta$  is valid approximately only for simple  $t_2 \leftrightarrow e$  transitions without changing the spin state.

The other parameter of the  $d-d$  transitions, the Racah parameter  $B$  (2.43), is also dependent on the nature of the ligands. If one compares the  $B$  value of the free ion with that in the complex, one finds that the latter is always smaller than the former. This reduction of  $B$  by complex formation, meaning the reduction of the interelectron repulsion in the  $d$  states, is obviously caused by the delocalization (expansion) of the electron cloud on larger regions, due to the formation of MO, and this interpretation is confirmed quantitatively by

calculations. The effect of ligand influence on interelectron repulsion in  $d$  states characterized by  $B$  was first studied by Jorgensen [8.21] (see also Ref. 8.20), and it was named *nephelauxetic effect*, which in translation from Greek means the effect of “cloud-expanding.”

The  $B$  values for some free ions and their complexes obtained from spectroscopic data are given in Table 8.3 (for the free ions some of them are slightly different from those in Table 4.7). Introducing the *nephelauxetic ratio*  $\beta = B_{\text{complex}}/B_{\text{ion}}$ , one can arrange the ligands in a series of decreasing  $\beta$  values for the same CA in the same oxidation state, the *nephelauxetic series*:



An important feature of the nephelauxetic effect is that it is directly related to covalence. Indeed, the delocalization of the  $d$  electrons in the complex is caused by the formation of covalent bonds and MOs. Hence the measure of the  $B$  reduction in the complex is simultaneously a measure of covalence. This means that the nephelauxetic series (8.26), following the decrease of  $\beta$  from left to right, reflects the increase of covalence in this direction (in the complexes formed by the corresponding ligands). From this perspective the nephelauxetic effect is more informative with respect to chemical bonding than the spectrochemical effect, although they both are rough qualitative properties.

Only one nephelauxetic ratio  $\beta$  may be insufficient to characterize the nephelauxetic effect in some complexes with many  $d$  electrons. Indeed, the value  $B_{\text{complex}}$  is determined from spectroscopic data (Section 2.2), and it can vary for different  $d-d$  transitions. Therefore, in a more detailed description of complexes with  $(t_2)^m(e)^n$  configurations, three values of  $B$  can be introduced:  $B(e \rightarrow e)$ ,  $B(e \rightarrow t_2)$ , and  $B(t_2 \rightarrow t_2)$ , where  $e \rightarrow e$ ,  $e \rightarrow t_2$ , and  $t_2 \rightarrow t_2$

**TABLE 8.3. Numerical Values (in  $\text{cm}^{-1}$ ) of the Racah Parameter  $B$  for Free  $d^n$  Ions of Transition Metals and Their Complexes with Different Ligands**

$d^n$	Ion	Ligand <sup>a</sup>								
		Free Ion	6Br <sup>-</sup>	6Cl <sup>-</sup>	3Ox <sup>2-</sup>	6H <sub>2</sub> O	Enta <sup>4-</sup>	6NH <sub>3</sub>	3En	6CN <sup>-</sup>
3d <sup>3</sup>	Cr <sup>3+</sup>	950	—	510	640	750	720	670	620	520
3d <sup>5</sup>	Mn <sup>2+</sup>	850	—	—	—	790	760	—	750	—
3d <sup>5</sup>	Fe <sup>3+</sup>	~1000	—	—	—	770	—	—	—	—
3d <sup>6</sup>	Co <sup>3+</sup>	~1050	—	—	560	720	660	660	620	440
4d <sup>6</sup>	Rh <sup>3+</sup>	~800	300	400	—	500	—	460	460	—
5d <sup>6</sup>	Ir <sup>3+</sup>	660	250	300	—	—	—	—	—	—
3d <sup>7</sup>	Co <sup>2+</sup>	1030	—	—	—	~970	~940	—	—	—
3d <sup>8</sup>	Ni <sup>2+</sup>	1130	760	780	—	940	870	890	840	—

<sup>a</sup>Ox = oxalate, Enta = ethylenetetraamine, En = ethylenediamine.

Source: Jorgensen [8.20].

indicate the type of spectroscopic transition data from which the *B* value is extracted. In the notations of Bethe  $E = \Gamma_3$  ( $e = \gamma_3$ ) and  $T_2 = \Gamma_5$  ( $t_2 = \gamma_5$ ) and the corresponding nephelauxetic ratios are denoted by  $\beta_{33}$ ,  $\beta_{35}$ , and  $\beta_{55}$ , respectively. It can be shown that approximately [8.20]

$$\frac{\beta_{33}}{\beta_{35}} = \frac{\beta_{35}}{\beta_{55}} \tag{8.27}$$

With this relation only two nephelauxetic parameters remain independent, for instance,  $\beta_{55}$  and  $\beta_{35}$ . Table 8.4 presents some of these parameters for a series of hexafluorides.

For further details, the number of such parameters can be increased but this hardly makes sense; the larger the number of parameters required for the interpretation of experimental data, the less informative this interpretation. Therefore attempts to improve the spectrochemical and nephelauxetic series seem to be useless.

### Charge Transfer Spectra

As noted above, the *d-d* transitions depend on the ligand environment in a generalized way, mostly on the symmetry and magnitude of the crystal field

**TABLE 8.4. Racah's Parameters of Interelectronic Repulsion  $B_{55}$  and  $B_{35}$  (in  $\text{cm}^{-1}$ ) and the Corresponding Nephelauxetic Ratios  $\beta_{55}$  and  $\beta_{35}$  for Some Hexafluoride Complexes of  $d^n$  Transition Metals**

$d^n$	Complex	$B_{55}$	$\beta_{55}$	$B_{35}$	$\beta_{35}$
$3d^3$	$\text{CrF}_6^{3-}$	860	0.93	820	0.89
	$\text{MnF}_6^{2-}$	815	0.77	600	0.56
$3d^5$	$\text{MnF}_6^{4-}$	—	—	845	0.94
	$\text{FeF}_6^{3-}$	—	—	845	0.78
$3d^6$	$\text{NiF}_6^{2-}$	—	—	450	0.36
$3d^8$	$\text{NiF}_6^{4-}$	—	—	960	0.92
	$\text{CuF}_6^{3-}$	—	—	650	0.54
$4d^2$	$\text{RuF}_6$	300	0.37	—	—
$4d^3$	$\text{TcF}_6^{2-}$	560	0.79	530	0.76
	$\text{RuF}_6^-$	480	0.61	—	—
$4d^6$	$\text{RhF}_6^{3-}$	—	—	460	0.64
	$\text{PdF}_6^{2-}$	—	—	340	0.42
$4d^8$	$\text{AgF}_6^{3-}$	—	—	460	0.60
$5d^2$	$\text{OsF}_6$	380	0.52	—	—
$5d^3$	$\text{ReF}_6^{2-}$	540	0.83	—	—
	$\text{OsF}_6^-$	530	0.73	—	—
$5d^4$	$\text{IrF}_6$	380	0.43	—	—
	$\text{PtF}_6$	260	0.30	—	—
$5d^6$	$\text{PtF}_6^{2-}$	—	—	380	0.51

Source: Jorgensen [8.20].

splitting. Different ligands in the same position and with similar field strengths produce the same  $d-d$  spectra. A more adequate reflection of the nature of the ligands is given in the metal–ligand *charge transfer transitions* mentioned above. In the MO LCAO scheme they correspond to the transitions between bonding and antibonding MOs, which in systems with inversion symmetry are of opposite parity. These two types of orbitals are described by Eqs. (5.32) and (5.33), and in case of  $\gamma < 0$  they are localized mainly on different atomic groups of the system (e.g., the bonding MO is on the ligands, while the antibonding one is on the CA), the electronic transition between them (transitions of the type  $\pi \leftrightarrow d$ ,  $\sigma \leftrightarrow d$ ,  $d \leftrightarrow \pi^*$ , where  $\sigma$ ,  $\pi$ ,  $\pi^*$ , ... are mainly ligand orbitals) are associated with charge transfer from one of these groups to another justifying the above denotation of the transition. Charge transfer spectra may be either ligand  $\rightarrow$  metal or metal  $\rightarrow$  ligand. Example 8.5 shows specific cases.

### EXAMPLE 8.5

#### *Some Ligand $\rightarrow$ Metal or Metal $\rightarrow$ Ligand Charge Transfer Spectra*

A charge transfer transition in  $\text{PtCl}_4^{2-}$  was considered in Example 8.3. Another metal  $\rightarrow$  ligand resonance Raman charge transfer band is considered in Example 8.6. The transitions  $\pi \rightarrow d_{z^2}$  (band I) and  $\sigma \rightarrow d_{z^2}$  (band II) in the spectra of the complexes  $[\text{Co}(\text{NH}_3)_5\text{X}]^{2+}$ ,  $\text{X} = \text{F}, \text{Cl}, \text{Br}, \text{I}$  may serve as more examples of such spectra. Some other ligand  $\rightarrow$  metal and metal  $\rightarrow$  ligand charge transfer bands are shown in Tables 8.5 and 8.6. An azide  $\rightarrow$  Cu charge transfer band in  $[\text{py}_2\text{Cu}(\text{NO}_3)\text{N}_3]$  is shown in Fig. 8.7 [8.27]. Many other examples are given in special monographs (see Refs. 8.1–8.4 and references cited therein).

**TABLE 8.5. Examples of Some Ligand  $\rightarrow$  Metal Charge Transfer Bands in Octahedral Halogen Complexes of Ru, Os, and Pt**

Ion ( $d^n$ )	Frequency Ranges (in $\text{cm}^{-1}$ ) for Transitions		
	$\sigma \rightarrow e_g$	$\pi \rightarrow e_g$	$\pi \rightarrow t_{2g}$
$\text{RuCl}_6^{2-}$ ( $4d^4$ )	—	36,000–41,000	17,150–24,600
$\text{PtCl}_6^{3-}$ ( $4d^5$ )	—	43,600	25,600–32,400
$\text{PtBr}_6^{3-}$ ( $4d^5$ )	—	35,000	19,300–27,200
$\text{OsCl}_6^{2-}$ ( $5d^4$ )	—	47,000	23,900–30,000
$\text{OsBr}_6^{2-}$ ( $5d^4$ )	—	35,700–40,800	17,000–25,000
$\text{OsI}_6^{2-}$ ( $5d^4$ )	—	26,800–35,600	11,600–18,600
$\text{PtCl}_6^{2-}$ ( $5d^6$ )	—	38,200	—
$\text{PtBr}_6^{2-}$ ( $5d^6$ )	44,200	27,000–33,300	—
$\text{PtI}_6^{2-}$ ( $5d^6$ )	39,800–43,500	20,250–29,150	—

Sources: From Jorgensen [8.20, 8.21].



**TABLE 8.6. Examples of Metal → Ligand Charge Transfer Bands in Some Six-Coordinate Complexes**

Complex	Frequencies at Band Maximum (in $\text{cm}^{-1}$ ) for Transitions	
	$e_g \rightarrow \pi^*$	$t_{2g} \rightarrow \pi^*$
Mn(picO) <sub>2</sub> 2H <sub>2</sub> O	24,700	—
Fe(picO) <sub>2</sub> 2H <sub>2</sub> O	—	21,050
Co(picO) <sub>2</sub> 2H <sub>2</sub> O	—	23,800
Ni(picO) <sub>2</sub> 2H <sub>2</sub> O	—	24,400
Cu(picO) <sub>2</sub> 2H <sub>2</sub> O	26,700	—
Fe(bipyz) <sub>3</sub> <sup>2+</sup>	—	19,673, 21,000
Co(bipyz) <sub>3</sub> <sup>2+</sup>	—	26,400
Ni(bipyz) <sub>3</sub> <sup>2+</sup>	—	27,600

Source: From Lever et al. [8.22].

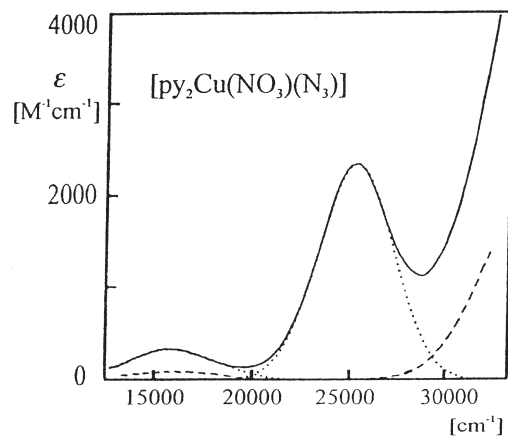


**FIGURE 8.7.** Ligand → metal (azide → Cu) charge transfer band in the absorption of  $[\text{py}_2\text{Cu}(\text{NO}_3)(\text{N}_3)]$  (dotted line). The dashed line shows the absorption of the non-azide-containing analog in this region. (From Pate et al. [8.27]).

### Infrared Absorption and Raman Scattering

While infrared (IR) and Raman spectra belong to different regions of radiation frequencies (IR and visible or ultraviolet, respectively), we consider them in the same section because they both carry information mainly about the vibrational properties of the system.

In Section 7.1 we introduced harmonic vibrations, vibrational frequencies, wavefunctions [Eqs. (7.13)–(7.15)] and shapes of symmetrized displacements (Table 7.1, Figs. 7.1–7.3), as well as the types of allowed vibrations for several

of the most usable symmetry groups (Table 7.2). Group-theoretical methods of classification and evaluation of normal vibrations are described in Section 3.5 and Example 3.5.

Similar to electronic transitions, IR absorption and emission occur as a result of transitions between the vibrational states. The absorption coefficient is given by the same equation [Eq. (8.5)], in which the matrix element  $M_{12}$  should be calculated by Eq. (8.4) with the vibrational wavefunctions (7.15) for the two combining states with different quantum numbers  $n$  and  $n'$ , respectively. Since these functions are orthogonal by definition, the integral (8.4) is nonzero only if the moment  $M$  depends on nuclear coordinates and changes during the vibration. If  $M$  is the dipole moment (dipolar transitions), the active vibration should be polar. For systems with inversion symmetry polar vibrations belong to odd-symmetry IrReps.

For small (vibrational) nuclear symmetrized polar displacements  $Q$ , we have

$$M = M_0 + \left( \frac{\partial M}{\partial Q} \right)_0 Q + \frac{1}{2} \left( \frac{\partial^2 M}{\partial Q^2} \right)_0 Q^2 + \dots \quad (8.28)$$

where  $M_0$  is the dipole moment at the point of equilibrium and the derivatives are taken at the same point. With the linear term of (8.28) and odd coordinates  $Q$ , the matrix element (8.4) yields  $(\partial M / \partial Q)_0 \langle n | Q | n' \rangle$ , which, with the wavefunctions  $|n\rangle$  and  $|n'\rangle$  after (7.15), is nonzero only when  $n' = n \pm 1$ . In other words, dipolar vibrational transitions are allowed only between nearest-neighbor states of polar vibrations that differ in energy by one vibrational quantum,  $E_{n'} - E_n = \pm \hbar\omega$ , where  $\omega$  is the *fundamental frequency* of vibrations [see Eq. (7.14)].

With the quadratic term in Eq. (8.28), the matrix element of the transition  $n \rightarrow n'$  yields  $\frac{1}{2} (\partial^2 M / \partial Q^2)_0 \langle n | Q^2 | n' \rangle$ , which is nonzero when  $n' = n \pm 2$ . These are the *overtone transitions* involving two vibrational quanta. They are weaker than the fundamental transitions because quadratic terms of small displacements are smaller than linear terms. With higher terms in Eq. (8.28), higher overtone quanta are involved.

Following Eq. (8.5), the intensity of the fundamental IR absorption lines is direct proportional to  $|(\partial M / \partial Q)_0|^2$ , which, as mentioned above, is nonzero for polar displacement  $Q$  only. This means that only polar vibrations are manifest in IR spectra. In particular, if the system has a center of inversion, only odd vibrations of the type  $\Gamma_u$  (see Table 7.2) are active in the IR spectra.

What about the even vibrations  $\Gamma_g$  or, in general, nonpolar vibration? Can they be seen in the spectra? It turns out that nonpolar vibrations are active in nonelastic light scattering called the *Raman effect*. Indeed, as mentioned in Section 8.1, in addition to the interaction of the proper dipole moment  $M$  of the system with the electric field  $\mathcal{E}$ ,  $E = -(\mathbf{M}, \mathcal{E})$ , there is a similar interaction  $E = (\mathbf{P}, \mathcal{E})$ , where  $\mathbf{P}$  is the *induced dipole moment*. The latter occurs under the action of the electric field  $\mathcal{E}$ , which moves the electrons and nuclei in opposite directions, thus polarizing the system,  $\mathbf{P} = \alpha \mathcal{E}$ , where  $\alpha$  is the polarizability. The energy of this interaction is thus  $E = \alpha \mathcal{E}^2$  (there are higher powers in  $\mathcal{E}$ , and hence

weaker terms in the interaction with radiation that cause a variety of *nonlinear effects* in optics). In general, the polarizability depends on the direction of  $\mathcal{E}$  with respect to the axes of the molecule. In other words,  $\alpha$  is a tensor with the components  $\alpha_{xx}, \alpha_{xy}, \alpha_{xz}, \alpha_{yy}, \alpha_{yz},$  and  $\alpha_{zz}$ , which coincide in systems with spherical symmetry, thus reducing the tensor to a constant.

With the interaction  $E = \alpha \mathcal{E}^2$ , the matrix element (8.4) for the transition between two electronic states,  $|1\rangle$  and  $|2\rangle$ , accompanied by the vibrational states  $|n\rangle$  and  $|n'\rangle$ , respectively, yields  $\langle 1n|\alpha \mathcal{E}^2|2n'\rangle = \langle 1|2\rangle \langle n|\alpha|n'\rangle \mathcal{E}^2$ , where we note that  $\mathcal{E}$  is a constant and  $\alpha$  does not depend on electronic coordinates (it is a constant for a given nuclear configuration). Since the two electronic functions are orthonormalized, the integral  $\langle 1|2\rangle$  is nonzero (and equal to 1) only when  $|1\rangle \equiv |2\rangle$ . This means that under the polarization effect there are no electronic transitions—light is not absorbed, just scattered. On the other hand, the polarization  $\alpha$  does depend on nuclear displacements, and hence the integral  $\langle n|\alpha|n'\rangle$  may be nonzero, meaning that the vibrational states may change during the scattering. Hence the energy of the scattered photon may differ from the incident one by vibrational quanta. This is the *Raman effect*.

To ascertain when the Raman effect takes place, we first consider the selection rules. Tensor components  $\alpha_{ij}$ ,  $i, j = x, y, z$  transform as corresponding products of Cartesian coordinates  $x^2, xy,$  and so on, or their linear combinations (compare with vectors that transform as the coordinates  $x, y, z$ ). Tables of characters of symmetry groups (see Appendix 1) usually also indicate the IrReps to which the components of a tensor (product of coordinates) belong. Then, with known transformation properties of the vibrational functions, one can reveal the nonzero matrix elements  $\langle n|\alpha|n'\rangle$  using the group theory rules (Chapter 3). This will reveal directly the symmetry type of the vibrations that may be involved in the Raman scattering.

Examining the character tables in the Appendix 1, we can see that in the majority of cases vectors and tensors belong to different representations. In particular, if the system has a center of inversion, the vector components (Cartesian coordinates) belong to odd representations  $\Gamma_u$ , whereas the tensor components transform as even representations  $\Gamma_g$ . This means that when the matrix elements of the former are zero, those of the latter are nonzero, and vice versa. In other words, in systems with an inversion center the vibrations seen in IR and Raman spectra are mutually complementary.

The intensity of the Raman scattering depends on how rapidly the polarizability changes during nuclear displacements in the allowed vibration. For small nuclear displacement  $Q$  [cf. Eq. (8.28)], we obtain

$$\alpha = \alpha_0 + \left(\frac{\partial \alpha}{\partial Q}\right)_0 Q + \frac{1}{2} \left(\frac{\partial^2 \alpha}{\partial Q^2}\right)_0 Q^2 + \dots \quad (8.29)$$

The first term  $\alpha_0$  is independent of  $Q$ , hence the matrix element  $\langle n|\alpha_0|n'\rangle \neq 0$  only when  $|n'\rangle = |n\rangle$ , that is, when, in addition to the unchanged electronic state, the vibrational state does not change as well. This is termed *Rayleigh*

scattering, for which the frequency of the scattered light coincides with the incident frequency  $\Omega_0$ . The linear  $Q$  term in Eq. (8.29) yields the matrix element  $(\partial\alpha/\partial Q)_0 \langle n|Q|n'\rangle$ , which, similar to dipolar transitions in IR spectra, is nonzero when  $n' = n \pm 1$ . This is the *fundamental Raman transition* for which the frequency of the scattered light is either  $\Omega_0 - \omega$  (Stokes Raman scattering) or  $\Omega_0 + \omega$  (anti-Stokes Raman scattering);  $\omega$  is the frequency of Raman-allowed vibration. Similar to the IR case above, the next terms in Eq. (8.29) produce scattered overtones with  $n' = n \pm 2$ ,  $n' = n \pm 3$ , and so on, of, respectively,  $\Omega_0 \pm 2\omega$ ,  $\Omega_0 \pm 3\omega$ , and so on, frequencies. Scattering with combined vibrational frequencies  $\omega_i + \omega_j$  is also possible provided that they obey the selection rules on symmetry.

Figure 8.8 is a schematic representation of the corresponding transitions. In Raman scattering there is no real excited electronic state, so the spectrum can be obtained with any frequency of the incident light. The spectrum contains the most intensive central line corresponding to the Rayleigh scattering plus satellites at the fundamental and overtone Raman frequencies. The satellites are less intensive than the central line [because of the falling magnitude of the terms in the expansion (8.29)], and the anti-Stokes lines are less intensive because the corresponding transitions start from the excited vibrational state (Fig. 8.8) which

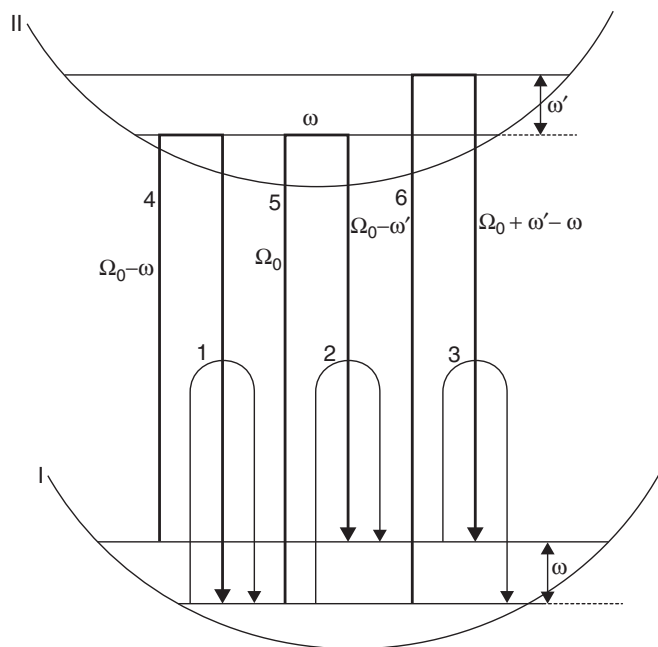


**FIGURE 8.8.** Schematic illustration of Rayleigh (line 1), Raman (lines 2 and 3), and resonance Raman (thick lines 4, 5, and 6) transitions and their Stokes (2, 5, and 6) and anti-Stokes (3 and 4) satellites in light scattering. The electronic states are denoted by I and II. In Rayleigh and Raman scattering there are no real excited electronic states involved, so the incident light frequency is arbitrary.

is less populated, the ratio of their intensities is [8.23]

$$\frac{I_{aS}}{I_S} = \frac{(\Omega_0 + \omega)^4}{(\Omega_0 - \omega)^4} \exp\left(-\frac{\hbar\omega}{kT}\right) \quad (8.30)$$

Because of the exponential dependence on temperature, the anti-Stokes intensity vanishes at low temperatures [the relation (8.30) is valid for  $\Omega_0 \gg \omega$ ].

A special case of Raman spectroscopy widely used in the study of coordination systems is provided by *resonance Raman transitions*. Normal Raman scattering takes place when the incident light falls in the region where the system is transparent and no direct absorption takes place. This can be interpreted as a two-photon process in which one photon excites the system to a virtual (nonexistent in the absence of light) state created as a result of polarization; the other is emitted, bringing the system back to the same electronic, but different vibrational state. In resonance Raman scattering the two photons are real as the intermediate state is a real excited electronic state of the system (Fig. 8.8). The process appears as if the system were to absorb a photon of resonance frequency  $\Omega_0$  and emit it instantly with another frequency  $\Omega_0 \pm n\omega$ . The scattering thus takes place in the region where the system is absorbing and hence not transparent. Because of the resonance, this scattering is much more intensive than in the normal case.

Both processes, absorption and emission, in the resonance Raman scattering seem similar to the usual (real) absorption followed by fluorescence, but in essence they are different; in the real absorption there is a lifetime of the excited state ( $\sim 10^{-7}$ – $10^{-8}$  s) and possible vibrational relaxation to lower vibrational states of the excited electronic state, as well as radiationless transition to the ground or intermediate state, whereas in resonance scattering the emission takes place instantly (on the timescale of  $\sim 10^{-14}$  s) and without any change in the excited state. The Raman spectra of a specific coordination system is considered in Example 8.6. For further reading, see Refs. 8.23 and 8.25.

### EXAMPLE 8.6

#### *Resonance Raman Spectrum of Red $K_2[Ni(dto)_2]$ in Solid State*

Figure 8.9 shows the spectrum of resonance Raman scattering from the crystal  $K_2[Ni(dto)_2]$  (dto = dithiooxalato) at frequency  $\Omega_0 = 488.0$  nm, which is in resonance with the  $Ni(II) \rightarrow S_2C_2O_2^-$  metal  $\rightarrow$  ligand charge transfer transition [8.24]. The Raman satellites can be separated into two progressions as shown in the figure. One of them is a multiple  $n_1\nu_1$  (overtones) of the fundamental Raman frequency  $\nu_1 = 1085$   $cm^{-1}$ , which is mainly a combination of C—C and C—S stretching displacements. The other is this series combined with another vibrational frequency  $\nu_2 = 1602$   $cm^{-1}$  resulting in  $n_1\nu_1 + \nu_2$ , which reflects

mainly the combined C—O and C—C stretching. The high overtones up to  $n_1 = 6$  observed in this case are unusual for such complexes; they allowed the authors to extract more information about the spectral properties of this systems, in particular, the anharmonicity of the vibrations.

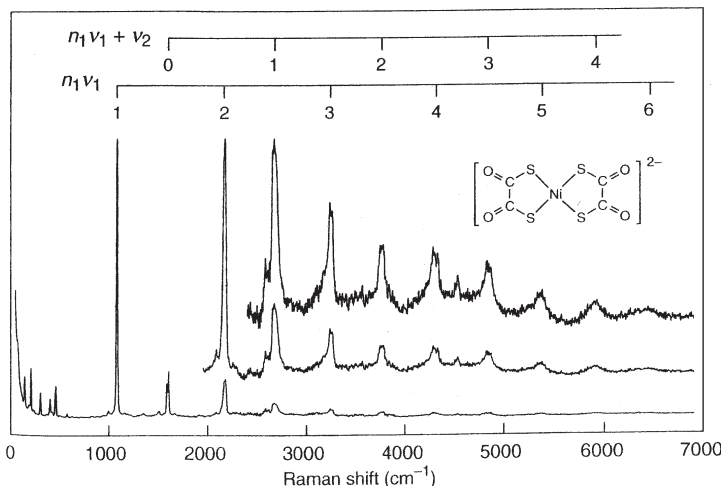


**FIGURE 8.9.** Resonance Raman spectrum of  $\text{K}_2[\text{Ni}(\text{dto})_2]$  (dto = dithiooxalato) in solid state with indication of the separated two progressions. (From Czernuszewicz et al. [8.24]).

### Transitions Involving Orbitally Degenerate States

Most  $d-d$  transitions involve orbitally degenerate electronic terms as initial or final states. As compared with nondegenerate terms, degenerate states may yield quite different types of spectra. Indeed, the band shapes and frequencies are strongly dependent on the APESs (Section 8.1), which for degenerate terms are much more complicated [8.15, 8.26] (Section 7.3).

Consider first the case when one of the combining states is an orbitally double-degenerate  $E$  term and the other is nondegenerate ( $A \rightarrow E$  and  $E \rightarrow A$  transitions). The energy spectrum for the  $E$  term can be obtained approximately by solving the linear  $E \otimes e$  problem (Section 7.3), while for the nondegenerate electronic  $A$  the vibrational states are usual harmonic oscillators (Section 7.1). Calculating the energy-level differences and transition probabilities for each transition from the oscillator states to the vibronic levels of the  $E$  state ( $A \rightarrow E$  transition) or vice versa ( $E \rightarrow A$  transition), one can obtain all the lines of the expected spectrum. The data shown in Fig. 8.10 were obtained numerically in this way [8.28]. They illustrate the relative intensities of the vibrational components

of the bands  $A \rightarrow E$  and  $E \rightarrow A$  for several values of the dimensionless vibronic coupling constant  $\lambda = E_{JT}/\hbar\omega$  (Section 7.3).

It is seen from Fig. 8.10 that the  $A \rightarrow E$  band, the envelope of the vibrational components, has a two-humped form. Compared with the band of transitions to a nondegenerate term given in Fig. 8.2, the two maxima can be interpreted as the Jahn–Teller splitting of the nonvibronic band. For transitions  $E \rightarrow A$  such a splitting does not occur, but this is due to the neglect of the temperature population of the excited vibrational states, which is valid only for  $T = 0$ .

A more general picture of the band shape (although less accurate in detail) can be obtained in the semiclassical approximation discussed in Section 8.1 (which is not valid for very low temperatures). Substituting the APES expressions (8.7) for the  $A$  term and (7.40) for the  $E$  term into the expression of the form function

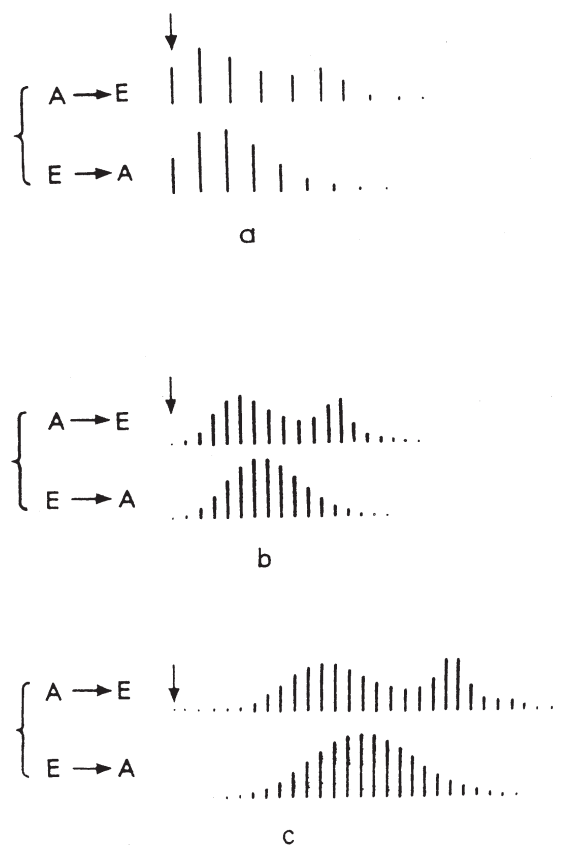


**FIGURE 8.10.** Frequencies and relative intensities of vibronic components and the band shape (envelope) for  $A \rightarrow E$  and  $E \rightarrow A$  transitions calculated at  $T = 0$  for the following values of the dimensionless vibronic constant: (a)  $\lambda = 2.5$ ; (b)  $\lambda = 7.5$ ; (c)  $\lambda = 15$ . The position of the zero-phonon line is shown by an arrow. (After Longuet-Higgins et al. [8.28].)

$F_{12}(\Omega)$ , and performing appropriate integrations, we obtain for  $Q_0 = 0$  [8.15, 8.26]:

$$F_{12}(\Omega) = \frac{M_{12}^2 K \hbar |\Omega - \Omega_0|}{F^2 2kT} \exp \left[ \frac{-K \hbar^2 (\Omega - \Omega_0)^2}{F^2 2kT} \right] \quad (8.31)$$

The function (8.31) is presented graphically in Fig. 8.11a. It has a symmetric shape with two humps and a dip at  $\Omega = \Omega_0$ . Similar to the numerical results presented above, this band shape can be attributed to Jahn–Teller splitting of the nonvibronic band. The splitting (the distance between the two maxima) equals  $(8E_{JT}kT)^{1/2}$ . If we account for the contribution of the totally symmetric vibrations to the broadening, the “acute elements” of the curve in Fig. 8.11a are smoothed, and the curve assumes the form given in either Fig. 8.11b or Fig. 8.11c, depending on whether the coupling with the totally symmetric vibrations is stronger than that with the  $e$  vibrations. The strength of coupling and the influence of thermal population of the corresponding vibrations is given by the quantities  $X_A = F_A^2 \coth(\hbar\omega_A/2kT)$  and  $X_E = F_E^2 \coth(\hbar\omega_E/2kT)$ , where  $F_A$  and  $F_E$ , and  $\omega_A$  and  $\omega_E$ , are the corresponding vibronic constants and vibrational frequencies, respectively (see Problem 8.10).

Thus, if the totally symmetric vibrations predominate ( $X_A > X_E$ ), the dip in the curve is completely filled up and disappears (Fig. 8.11c). For comparison, the temperature dependence of the  $A \rightarrow E$  band as determined by the numerical solution [8.29] is given in Fig. 8.12. Further details on  $A \rightarrow E$ ,  $E \rightarrow A$ , and  $E \rightarrow E$  transitions, see Refs. 8.26 and 8.30.

The  $A \rightarrow T$  transitions also have complicated band shapes except when in the  $T$  state the coupling to  $t_2$  vibrations is negligible and the vibronic problem is  $T \otimes e$  (Section 7.3). In the latter case no splitting of the  $A \rightarrow T$  band occurs despite the split adiabatic potential of the  $T$  term (Fig. 7.15). This shows how carefully visual presentations should be used in the analysis of complicated phenomena. In general, we can say that for absorption transitions from nondegenerate to degenerate terms the band does not split if the point of degeneracy on the APES is a point of actual crossing of the surfaces, as in the  $T \otimes e$  problem (Fig. 7.15). This is in contrast to the case when the point of degeneracy is a branching point of the surface, as in the  $E \otimes e$  problem (Figs. 7.9 and 7.10), for which the band is split. The zero-phonon line of transitions involving degenerate states may also be split because of the tunneling between equivalent minima [8.26].

If the coupling to  $t_2$  vibrations is predominant, the  $A \rightarrow T$  absorption curve in simple cases has three humps, the band is split into three components, but the temperature dependence and other parameters render them rather nonequivalent. For examples of such and other related transitions and more detailed considerations of transitions between degenerate states, see Refs. 8.15, 8.26, 8.30, and 8.31.

The brief discussion in this subsection allows us to conclude that *vibronic effects strongly influence the band shapes of electronic  $d-d$  transition* that involve degenerate terms, and that the frequently used *interpretation of electronic spectra disregarding vibronic interactions may be invalid* if the ground or excited state,



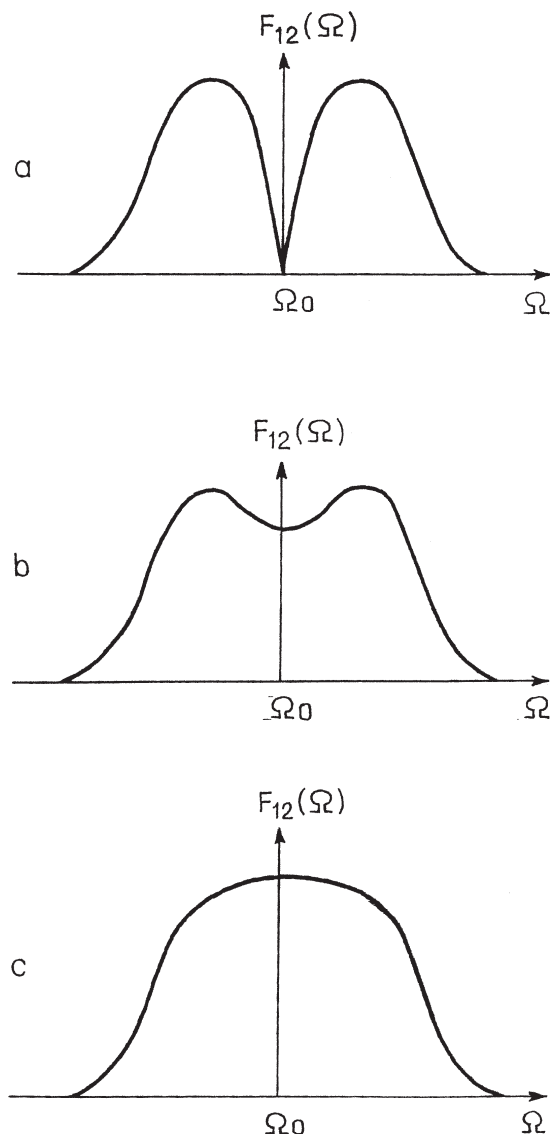


**FIGURE 8.11.** Schematic presentation of the band shape of the  $A \rightarrow E$  transition calculated in the semiclassical approximation including the linear coupling with  $E$  and  $A$  vibrations: (a) coupling with totally symmetric vibrations  $A$  is neglected; (b) the  $A$  vibrations are included, but the coupling to  $E$  vibrations is predominant; (c) the coupling to  $A$  vibrations is predominant.

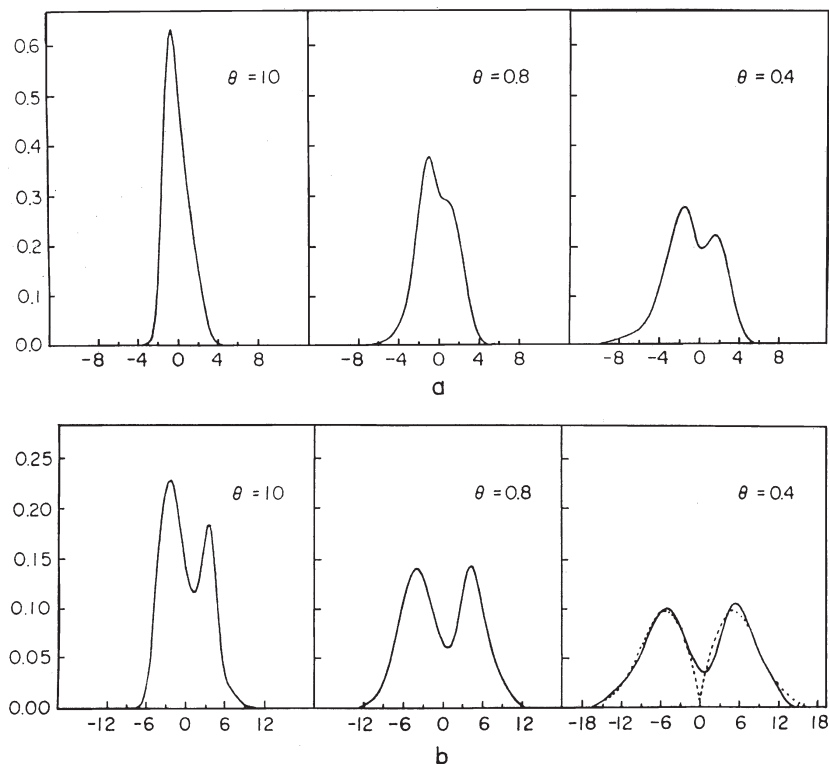


**FIGURE 8.12.** Temperature dependence of the absorption band shape of the  $A \rightarrow E$  transition obtained by numerical solution of the linear  $E \otimes e$  problem including the coupling with  $E$  and  $A$  vibrations with  $\lambda_A = 0.5$  and  $\lambda_E = 0.5$  (a) and  $\lambda_E = 5.0$  (b). The frequency with respect to the pure electronic transition  $\Omega = 0$  is given in  $\omega_E$  units, and  $\theta = \hbar\omega_E/kT$ . For strong vibronic coupling and at higher temperatures the absorption curve approaches the semiclassical limit shown by dashed line (cf. Fig. 8.11). (From Muramatsu and Sakamoto [8.29].)

or both, are degenerate, or if at least one of them is vibronically coupled to a third state with sufficient strength.

### 8.3. X-RAY AND ULTRAVIOLET PHOTOELECTRON SPECTRA; EXAFS

#### General Ideas

Photoelectron spectroscopy is based on the photoelectric effect; its principle was disclosed by Einstein in a paper that is one of the cornerstones of quantum mechanics. The energies of quanta of light (photons) are determined by their

frequency,  $E = \hbar\Omega$ . Hence there is a minimum-threshold frequency  $\Omega_c$  at which the photon is able to overcome the minimum energy  $e\phi$  required for removing an electron from a metal to the vacuum,  $\hbar\Omega = e\phi$  ( $\phi$  is called the *workfunction*). For photoemission of electrons from atoms or molecules in the gas phase, the minimum energy that creates the threshold equals the binding energy  $E_B$ , or the ionization potential  $I_i$  from state  $i$ ,  $\hbar\Omega_c^i \approx I_i$ .

If the frequency of the photon  $\Omega$  exceeds that of  $\Omega_c$ , the emitted electron has a nonzero kinetic energy  $E_k = \hbar\Omega - I_i$ , and

$$I_i = \hbar\Omega - E_k \quad (8.32)$$

Thus, if the experiment on photoemission is carried out with sufficiently large (fixed) frequencies of light, the kinetic energy spectrum of the emitted electrons is a replica of the energy distribution of occupied bond states. Photoelectron spectroscopy then becomes a method for direct determination of the electronic states of atoms, molecules, and solids. Obviously, for inner electron (core) states the frequency  $\Omega$  corresponds to X rays.

The method was suggested for the optical region by Vilesov et al. [8.32], and Turner and Al-Joboury [8.33] and for the X-ray region by Ziegahn and coworkers (see Refs. 8.5, 8.34, and references cited therein). It was developed and gained widespread use only when some significant difficulties in exact and high-resolution measurements of electron kinetic energies was overcome. At present the accuracy of electron energy measurements is about  $10^{-2}$  eV in the optical region and  $10^{-1}$  eV in the X-ray region.

In fact, there are several closely related photoemission and X-ray processes illustrated in Fig. 8.13 that form the basis for four related methods of photoelectron spectroscopy:

1. *Ultraviolet photoelectron spectroscopy (UPS)*—the light photon ejects the electron from the atomic valence shell or MO to the continuous spectrum (Fig. 8.13a).
2. *X-ray photoelectron spectroscopy (XPS)*—the X-ray photon ejects the electron from the inner shell (core) states of the system (Fig. 8.13b).
3. *Auger electron spectroscopy (AES)*—after formation of a hole in the core shell a radiationless transition of an electron from levels higher than that of the hole takes place, and the excess energy is transferred to another electron that is thus emitted with a corresponding kinetic energy (Fig. 8.13c) (after P. Auger, who first observed such electrons).
4. *X-ray emission spectroscopy (XES)*—after formation of a hole in the inner shell, a transition from the excited one-electron states to the hole state with irradiation of an X-ray photon takes place (Fig. 8.13d).

Unlike the UPS and XPS cases, where the kinetic energy of the electrons is a direct consequence of the photoeffect, in AES the emitted electrons emerge

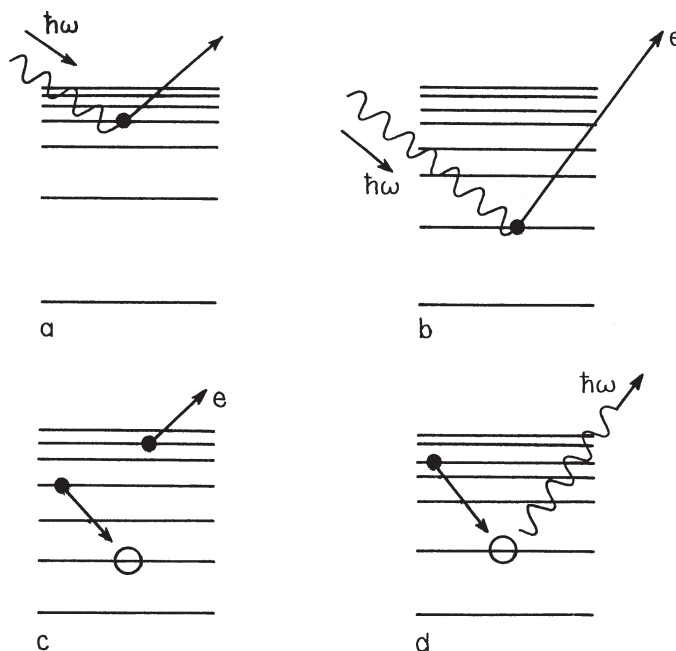


**FIGURE 8.13.** Schematic presentation of four types of photoelectron spectroscopy: (a) the photon ejects an electron from the valence shell MO of the system (UPS); (b) the photon ejects an electron from the inner (core) states (XPS); (c) the hole created by the photon is radiationless, populated by an electron from higher states, with another electron emitted (AES); (d) the inner shell hole is occupied by a higher-energy electron, with an X-ray quantum emitted (XEP).

from a postphotoeffect process of radiationless relaxation of the excited state in competition with possible radiation transitions. Photoelectron spectra are registered in the form of the number (counting rate) of photoelectrons as a function of their kinetic energies or the ionization potential  $I_i$  following Eq. (8.32).

The examples below demonstrate the main trends of applications of photoelectron spectroscopy:

1. Determination of one-electron energy levels of the system from the positions of photoelectron peaks and their intensities
2. Evaluation of the parameters of electron density distribution from photoelectron chemical shifts

Both these trends advanced essentially during the last several decades, and new possibilities for studying electronic structures were elucidated. Several illustrative photoelectron spectra are presented and briefly discussed in Example 8.7.

**EXAMPLE 8.7*****Photoelectron Spectra of Specific Coordination Systems and Their Interpretation***

Figures 8.14, 8.15, and 8.16 illustrate, by way of examples, a part of the UPS of ferrocene [8.35], two lines of XPS of metallic Pt and Pt in  $K_2PtCl_6$  [8.5a], and the AES of  $TiO_2$  [8.5a], respectively. In Fig. 8.14 one can see two peaks of the outer  $3d(t_{2g})$  orbitals of iron (occupied by six electrons) split in ferrocene by the ligand field of  $D_{5h}$  symmetry into  $a_{1g}$  and  $e_g$  (in fact, these orbitals are MOs, not AOs). The occupation number of the  $e_g$  orbitals is twice that of  $a_{1g}$  [the outer electron's configuration is  $(a_{1g})^2(e_g)^4$ ], and the intensity of the photoelectron band (the area under the curve) of the former is approximately 2 times larger than the latter.

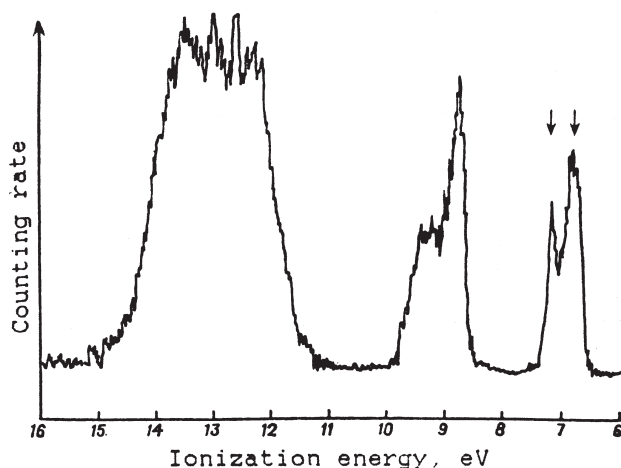


**FIGURE 8.14.** A part of the PES of ferrocene. The arrows indicate the  $3d$  orbitals of iron. (After Turner [8.35].)

Figure 8.15 illustrates the effect of inner-shell line shift in the XPS due to chemical bonding, the *chemical shift* (see below). Indeed, the positions of the two lines of photoelectrons from the  $N$  shell ( $N_{YI}N_{VII}$  or  $4f_{5/2}4f_{7/2}$ ; don't confuse the atomic shell  $N$  with the nitrogen atom) of the Pt atom in  $K_2PtCl_6$  is displaced with respect to the same lines in metallic Pt by more than 2 eV toward higher binding energies (lower kinetic energies of the photoemitted electrons). This means that in the chloroplatinate ion the  $N$ -shell electrons of the Pt atom are more strongly bonded to the nucleus than in metallic Pt. This is understandable because of the charge redistribution in  $K_2PtCl_6$ : the

increasing electron density on the chlorine atoms and its decrease on Pt with respect to the metallic phase (in the XPS spectra the source of X rays ( $MgK_{\alpha}$ ) is indicated).

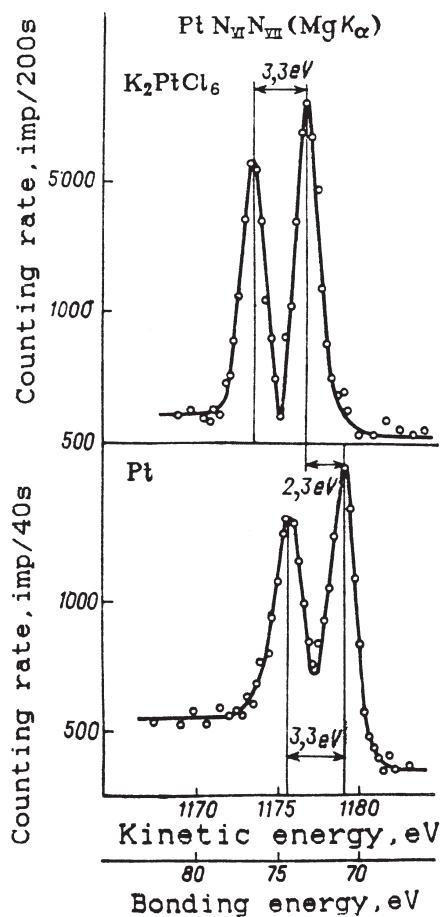
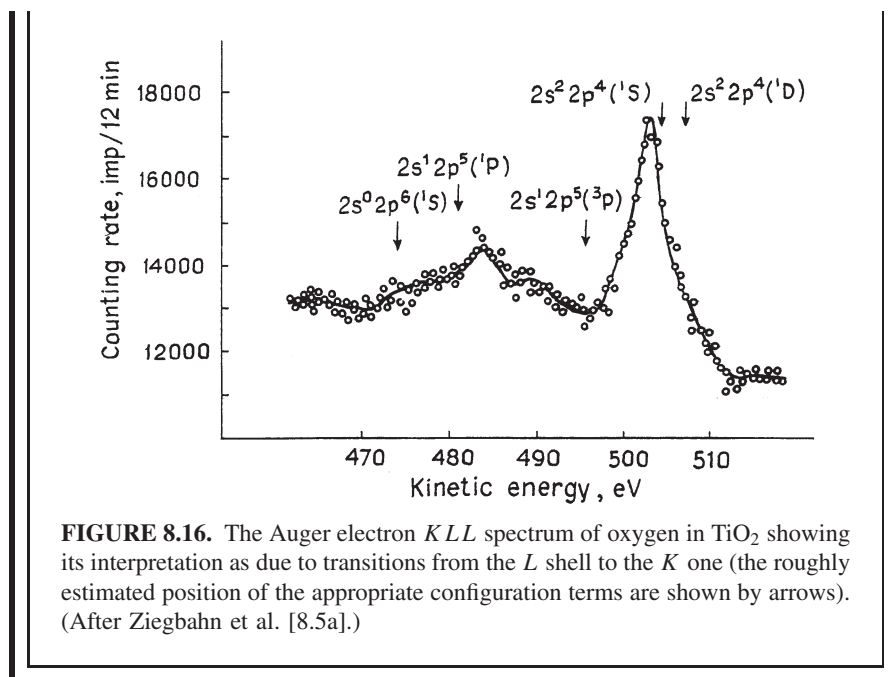


**FIGURE 8.15.** Two lines of XPS of the N shell of the Pt atom in  $K_2PtCl_6$  and in metallic platinum. (From Ziegbahn et al. [8.5a].)

The AES of the *KLL* transitions in oxygen in  $TiO_2$  (*K* and *L* denote the respective electronic shells) in Fig. 8.16 shows the excited configuration terms from which the radiationless transition produces the emitted electron. In combination with the X-ray photoemission that preceded the Auger effect, the AES determines the energy-level positions of the excited states of inner electrons.



### Electron Relaxation; Shakeup and CI Satellites

Interpretation of the photoelectron spectra is not always straightforward. To begin with, the attribution of the photoelectron peak positions to electronic energy levels is complicated by several side effects: electron relaxation, shakeup and shakeoff satellites, multiplet splitting, and final-state configuration interaction. Let us consider them sequentially.

The relaxation process is discussed in Section 6.2. In accordance with the Koopmans theorem (Section 2.2), the binding energy of the electron in the given  $i$ th MO equals the potential of ionization  $I_i$  of this electron taken with the opposite sign:

$$I_i = -\varepsilon_i \quad (8.33)$$

However, the Koopmans theorem does not account for the fact that when the  $i$ th electron is ionized, all the *other electrons relax to new self-consistent states* in which the interelectron repulsion is reduced by the removal of one electron (Sections 2.2, 6.2, and 6.4). The relaxation energy may be significant, thus reducing the observed ionization potentials as compared with those predicted by the Koopmans theorem and, what is even more important, sometimes changes the

order of their occurrence in the series of photoelectron peaks. To calculate the ionization potential with sufficient accuracy, one must discard the Koopmans theorem and define  $I_i$  as the difference between the self-consistent energies of the initial and ionized states calculated independently (see Table 6.12 in Section 6.4).

Even when calculations of  $I_i$  are performed with the highest accuracy, there is no a priori evidence that the calculated photoelectron peak positions coincide with the observed peaks because of the *shakeup and shakeoff processes*. Their physical meanings are as follows. The electron relaxation during (or after) the photoionization takes place not instantly, but within a certain timescale  $\tau$  estimated as about  $\tau \sim 10^{-17}$  s (cf. the vibrational relaxation time  $\sim 10^{-12}$ , which allows for the Franck–Condon transitions; see Section 8.1). Therefore, if the photoeffect process has a shorter timescale  $\tau'$ ,

$$\tau' < \tau \quad (8.34)$$

the electronic subsystem does not manage to relax during the photoionization, and hence the relaxation energy will not be incorporated (at least not completely) into the kinetic energy of the emitted electron. Then, what will be seen in the photoelectron experiments under the condition (8.34), and how to relate the observed spectrum to the electronic structure of the system? Quantum mechanics enables us to answer this question.

The nonrelaxed state of the ionized system produced by a very short time-dependent *sudden perturbation* is not a stationary solution of the Schrödinger equation. The theory of sudden perturbations shows that the final nonstationary state  $\Psi_f$  can be expanded into a series of the stationary states of the ion  $\Psi_k$ :

$$\Psi_f = \sum_k C_k \Psi_k \quad (8.35)$$

Because  $\Psi_k$  are mutually orthonormalized, the probability  $P_k$  of the system falling into one of them is

$$P_k = |C_k|^2$$

$$C_k = \int \Psi_k^* \Psi_f d\tau \quad (8.36)$$

Thus, in the case of incomplete relaxation under the condition (8.34), there is a probability for the system to occur in one of several stationary states  $\Psi_k$  producing several peaks of the photoemission electron spectrum (*shakeup satellites*) instead of only one peak as expected following calculations of the unperturbed system. Visually, the process behaves as if the system during the photoionization to a nonstationary state were shaken up to one of the stationary states that are excited states of the ion (usually outer-shell excitations). Equation (8.35) also includes, of course, the ground state of the ion. If  $\Psi_k$  is an ionized state, then we have a *shakeoff process*.



The shakeup transitions described by the transition probability (8.36) are monopole transitions in the sense that the transition operator is scalar (cf. dipolar transitions in Section 8.1). This means that all the states  $\Psi_k$  that produce the satellite lines in the spectrum must be of the same symmetry and multiplicity [otherwise the integral (8.36) is zero].

For the shakeup satellites, there are some interesting relations (sometimes called *the sum rules*) estimating their possible positions and intensities. Denoting the latter by  $I_k^0$  (not to be confused with the ionization potential  $I_k$ ) and their peak energies by  $E_k$  (while the Koopmans energies are  $\varepsilon_i$ ), we can introduce the *n*th moment of the distribution in the set of quantities  $I_k^0$ :

$$\sum_k I_k^0 (E_k - \varepsilon_i)^n \quad n = 0, 1, 2, \dots \quad (8.37)$$

Each of these moments has some physical sense. For the zero moment (summary value) we get

$$\sum_k I_k^0 (E_k - \varepsilon_i)^0 = \sum_k I_k^0 = I_i^0 \quad (8.38)$$

where  $I_i^0$  is the initially expected Koopmans intensity. For the first moment (center of gravity of the set), this yields

$$\sum_k I_k^0 (E_k - \varepsilon_i)^1 = 0 \quad (8.39)$$

In other words, the zero moment of the set, the sum of intensities of the shakeup satellites, equals the initially expected (Koopmans) intensity, while their center of gravity (the first moment) coincides with the Koopmans peak. On the other hand, Eq. (8.38) implies that the shakeup satellites borrow intensities from the main line, while (8.39) shows that the Koopmans peak can be easily obtained by finding the center of gravity of the main line plus satellites. Note that the deviation of the satellite line  $E_k - \varepsilon_i$  cannot be larger than the relaxation energy. It can be shown that for large deviations the probability  $P_k = |C_k|^2$  is small.

Concerning the characteristic time of the photoemission  $\tau'$ , it is strongly dependent on the photoelectron speed and hence on the photon frequency; the larger the latter, the smaller the  $\tau'$  and the more favorable the satellite occurrence. These considerations allow one to formulate some qualitative rules for shakeup satellites given in Table 8.7.

The shakeup satellites are somewhat related to the final-state *configuration interaction satellites*. Configuration interaction (CI) is discussed in Section 5.3 in connection with the problem of correlation effects. Since different electronic configurations may yield energy terms with the same symmetry and multiplicity, their linear combination of the type (5.62) [or a quite similar one (8.35)] must be taken as the most general form of the possible final state of the photoelectron transition. This means that more than one final state of the same symmetry

**TABLE 8.7. Some Qualitative Rules for the Occurrence of Shakeup Satellites in PES**

Types of Energy Levels	Ionization Potentials (eV)	Relaxation Energies (eV)	Expected Shakeup Satellites
Outer valence	<~15	0.5–5.0	No intensive satellites
Inner valence	15–50	~2–5	Intensive and relatively close satellites
Inner core	>50	>10	Weak and extended satellite structure

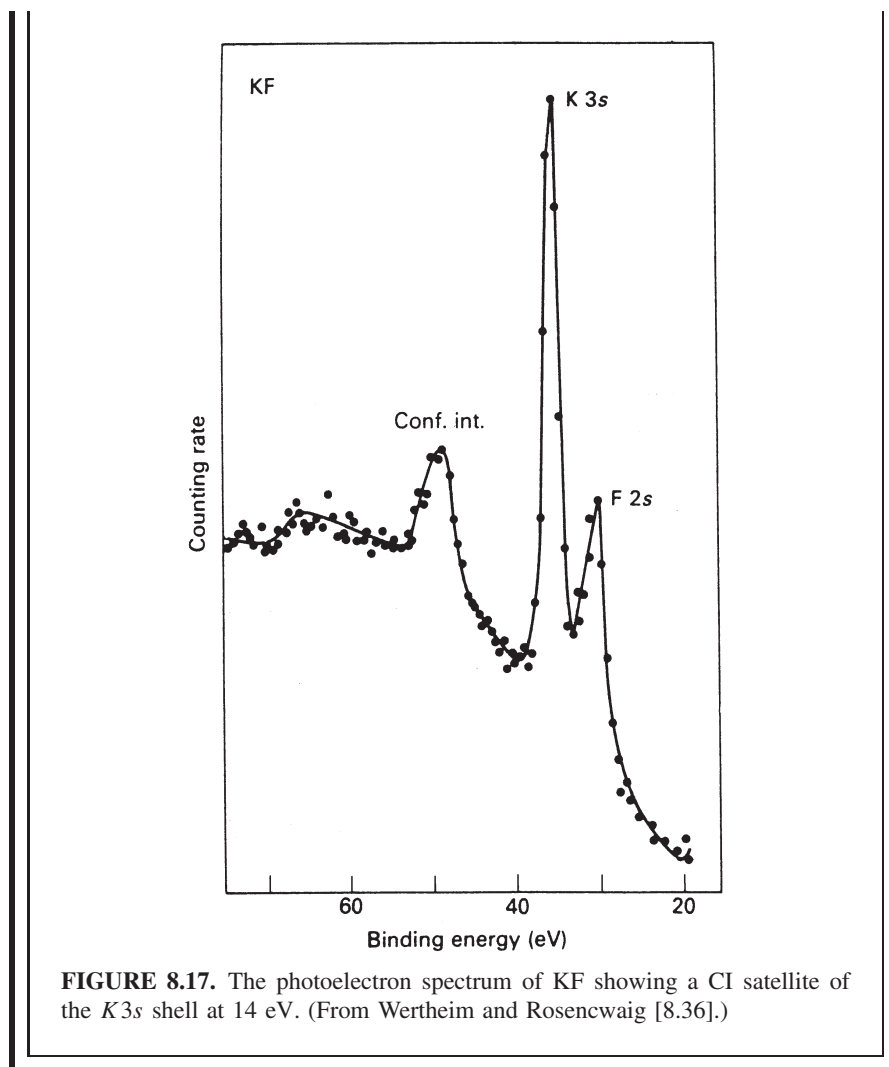
may take part in the transition. However, to be observable, the CI states must be comparable in energy and in transition probability as determined by the  $C_k$  coefficients of the CI expansion. Therefore, only the outer-shell ionized configurations produce observable CI satellites.

The shakeup satellites are similar to the CI ones in both nature and appearance. There are still some possibilities for differentiating between the former and the latter. Both types of satellites can be regarded as outer-shell excitations, but the CI satellites are unique only to the given outer-shell configuration and will not be repeated in other (inner-shell or core) configurations, whereas the same shakeup satellites, which are monopole transitions, occur in any (outer, inner, core) photoemission of the system whenever the electron relaxation energy must be compensated. Example 8.8 demonstrates a CI satellite spectrum.

### EXAMPLE 8.8

#### *Configuration Interaction Satellite to the $K^+$ 3s Emission Line in the UPS Spectrum of KF*

Figure 8.17 illustrates the case of a CI satellite to the  $K^+$  3s electron emission line in the UPS of KF, at 14 eV toward greater binding energies [8.36]. The  $K^+$  ion has a ground state  $S$  produced by the electronic configuration  $[\text{Ne}]3s^23p^6$ . The photoemission from the 3s shell produces an  $^2S$  state with the  $[\text{Ne}]3s^13p^6$  configuration. There are several other relatively close-in-energy configurations that produce the same  $^2S$  term at about 14 eV:  $[\text{Ne}]3s^23p^43d^1$ ,  $[\text{Ne}]3s^23p^44s^1, \dots$ , but the calculation shows that only transitions to the  $M$  shell have appreciable probabilities, and the observed satellite is identified as the  $[\text{Ne}]3s^23p^43d^1$  final state [8.36]. In this photoemission of  $K^+$  in KF the core lines have no 14-eV satellites ruling out an interpretation based on the monopole mechanism.



Another complication in the interpretation of photoelectron line positions is created by the *multiplet structure* of the core electron energy levels. Consider, for instance, the simple case of the  $\text{Mn}^{2+}$  ( $3d^5$ ) ion with the sextet ground state  $^6S$  that has no angular momentum ( $L = 0$ ). The core  $s$ -electron photoeffect creates a hole spin  $\frac{1}{2}$ , which couples to the outer electron spins, producing two terms,  $^7S$  and  $^5S$ . They are split by the spin-orbital interaction, and hence two  $s$ -core lines are expected instead of one. The two lines were found, indeed, and they have the intensity ratio 7–5, as required by the theory: transition probabilities are proportional to occupancies which, in turn, are proportional to degeneracies. Another example is shown in Fig. 8.15 of Example 8.7, where two lines of the

Pt  $N$ -shell photoelectrons (from  $f_{5/2}$  and  $f_{7/2}$ , respectively) are well resolved. For a nonzero orbital momentum (open shells) the multiplet structure becomes much more complicated.

Sometimes the interpretation of photoelectron spectra is facilitated by studying the *angular dependence of the intensity* (or cross section  $\sigma$ ) of photoionization. The differential cross section of photoionization of a given energy level with polarized light is

$$I_{\theta} = \frac{\sigma_t}{4\pi} \left[ 1 + \frac{\beta}{2}(3 \cos^2 \theta - 1) \right] \quad (8.40)$$

where  $\sigma_t$  is the total cross section of photoionization,  $\theta$  is the angle between the electric vector of the photon and the direction of the outgoing electron, and  $\beta$  is the *parameter of asymmetry*. If the light is not polarized, then

$$I_{\theta} \sim 1 + \frac{\beta}{2} \left( \frac{3}{2} \sin^2 \theta - 1 \right) \quad (8.41)$$

where  $\theta$  is the angle between the radiation beam and outgoing electrons.

The asymmetry parameter  $\beta$  is an unknown function of both the wavefunction of the ionized state and the photoelectron energy. It changes from  $-1$  to  $+2$ . So far this function has been studied for simple molecules [8.37], not for coordination compounds. Nevertheless, using Eq. (8.40) or (8.41) and experimental  $I_{\theta}$  values, one can separate the overlapping bands (components), provided that they have different  $\beta$  values.

As for the band shapes of UPS and XPS, all the results obtained in Sections 8.1 and 8.2 for electronic transitions are valid. Indeed, the ionization process is also an electronic transition in which the final state belongs to the continuous spectrum. The two states can be described by the same APESs as in the case of optical transitions (Fig. 8.1), and hence the resulting band shapes and intensities are those discussed in Sections 8.1 and 8.2. In particular, because of the change in the number of electrons, the photoelectron transition is always a spin-forbidden transition (Section 8.1), and in most systems it involves orbitally degenerate states, which result in JT splitting (Section 8.2).

Photoelectron band shapes were evaluated by calculating the vibronic states in degenerate and pseudodegenerate excited (ionized) states performed by the Green's function method [8.38]. The results agree well with the experimental data (see, e.g., the theoretical interpretation of the UPS of  $\text{BF}_3$  obtained by calculation of the PJTE in  $\text{BF}_3^+$  [8.39]). Other examples are available in the article by Koppel et al. [8.40].

### Chemical Shift

This notion is widespread in chemistry, determining the shift of energy levels due to chemical bonding, and as such it appears in many physical methods of

investigation (Mossbauer spectroscopy, NMR, etc.). In the UPS, XPS, and XES under consideration in this section, the chemical shift denotes the shift of the corresponding inner-shell spectral lines caused by change in the local chemical environment by passing from one compound to another. The shift of the two  $f$ -electron lines ( $f_{5/2}$  and  $f_{7/2}$ ) of Pt in  $K_2PtCl_6$  with respect to their positions in metallic Pt (Fig. 8.15) is an example of this kind of chemical shift.

A widespread explanation of the origin of chemical shifts  $\Delta E$  of inner energy levels is that the formation of chemical bonds redistributes the electronic charge and changes the interelectron repulsion and screening of the nucleus. The effective atomic charge  $q^A$  of atom  $A$  in its valence state in the molecule (Section 5.2) can serve as a rough measure of this charge redistribution. The idea is to use the calculated dependence of the inner energy-level positions in free atoms (ions) as a function of their charges  $\Delta E = f(q^A)$  (interpolated from ionized states) to estimate the atomic charges from chemical shifts in the spectra.

However, as stated in Section 5.2, the effective atomic charge is not directly observable, and the result of its calculation depends on the definitions and approximations used. For instance, as calculated after Mulliken [Eq. (5.20)], the atomic charges depend on the basis set, while after Politzer [cf. (5.22)], they depend on the assumed atomic border in the molecule. Besides, the integral charge effect may be not sufficiently informative. Indeed, the contributions of different atomic orbitals to the chemical shift may be quite different (even different in sign, see below), and they may be differently affected by the bonding. This is a general property of TMS that is due to  $d$ -electron participation leading to backdonation and ligand excitation (see Section 6.3, Fig. 6.6). Because of this specific TMS property, dependence of the chemical shift on the integral charge of the atom in the molecule may even be misleading; the chemical shift may be large even when the integral charge is not changed.

The MO LCAO scheme gives a much more refined possibility for linking the observed chemical shifts  $\Delta E$  with the electronic structure. Consider the orbital charge transfers  $\Delta q_i$  [Eq. (5.20'')], which characterize the electronic charge transferred to ( $\Delta q_i > 0$ ) or removed from ( $\Delta q_i < 0$ ) each one-electron orbital, and assume that the chemical shift produced by removing one electron from the  $i$ th orbital of the atom, the *orbital chemical shift*  $\Delta \varepsilon_i$  (the shift per unit charge), is known. Then, assuming that  $\Delta q_i$  are not very large, we have approximately

$$\Delta E = - \sum_i \Delta q_i \Delta \varepsilon_i \quad (8.42)$$

The  $\Delta q_i$  values are more significant for the valence electrons that participate in the bonding, and they can be obtained from calculations. The orbital chemical shifts can be obtained relatively easily from empirical data, for instance, from the photoelectron or X-ray emission spectra of free atoms and ions. For the chemical shift of the  $K\alpha_1$  line in heavy-atom compounds ( $30 < Z < 75$ ), the authors [8.41], using XES data, obtained the following values of orbital contributions

$\Delta\varepsilon_i$  for the valence electrons  $s, p, d, f$  (in meV):

$$\begin{aligned}\Delta\varepsilon_s &= \Delta\varepsilon_p = 80 \pm 10 \\ \Delta\varepsilon_d &= -115 \pm 10 \\ \Delta\varepsilon_f &= -570 \pm 30\end{aligned}\tag{8.43}$$

These data are interesting in several aspects. First, they show the most essential differentiation between the contributions of different types of valence electrons to the  $K\alpha_1$  line shift; while for  $s$  and  $p$  electrons it is positive, meaning that they increase the X-ray emission frequency, for  $d$  and  $f$  electrons it is negative. Second, the absolute values of the effect are also different; they are significantly larger for  $d$  and  $f$  electrons.

Now consider the chemical shift of the  $K\alpha_1$  line in the XES of a nontransition atom in a molecule, which participates in the bonding with its valence  $s$  and  $p$  orbitals ( $\Delta q_d \approx \Delta q_f \approx 0$ ). Provided that the relation  $\Delta\varepsilon_s \approx \Delta\varepsilon_p$  is valid [see (8.43)], we get from (8.42) the following equation for  $sp$  elements:

$$\Delta E = -(\Delta q_s + \Delta q_p)\Delta\varepsilon_s = -q^A \Delta\varepsilon_s\tag{8.44}$$

where  $q^A = \Delta q_s + \Delta q_p$  is the effective charge of the atom under consideration. It is seen that in this case the chemical shift is proportional to the effective charge, in accordance with the abovementioned widespread interpretation.

However, for transition metals and rare-earth elements in coordination compounds the participation of  $d$  electrons in the bonding is most essential, and Eq. (8.44) does not hold. Indeed, with  $d$  electron participation

$$\Delta E = -(\Delta q_s + \Delta q_p)\Delta\varepsilon_s - \Delta q_d \Delta\varepsilon_d$$

and it is seen that the effective charge  $q^* = \Delta q_s + \Delta q_p + \Delta q_d$  does not characterize the chemical shift  $\Delta E$  accurately. On the contrary, if for illustration we take  $|\Delta\varepsilon_s| \approx |\Delta\varepsilon_d|$ , then (since  $\Delta\varepsilon_d < 0$ )

$$\Delta E \approx -(\Delta q_s + \Delta q_p - \Delta q_d)\Delta\varepsilon_s$$

As discussed in Section 6.3, in transition metal compounds there are diorbital bonds in which the  $\sigma$  and  $\pi$  bindings give orbital charge transfers  $\Delta q_\sigma$  and  $\Delta q_\pi$  of opposite signs ( $\Delta q_\sigma < 0$ ,  $\Delta q_\pi > 0$ ; Fig. 6.6). If, as usual, the  $\sigma$  bonds are realized by  $s$  and  $p$  orbitals, while the  $\pi$  bonds involve  $d$  orbitals, then the atomic charge  $q^A = |\Delta q_s + \Delta q_p| - |\Delta q_d|$  may be very small, even zero, while

$$\Delta E = -(|\Delta q_s + \Delta q_p|\Delta\varepsilon_s + |\Delta q_d|\Delta\varepsilon_d)\tag{8.45}$$

can be very large; *there is no direct correlation between the effective charge on the transition metal atom and the chemical shift*. Example 8.9 demonstrates the variety of chemical shifts of the same atom  $N$  in different compounds. For many

other examples of applications of UPS, XPS, AES, and XES, see the literature [8.5, 8.6, 8.25, 8.34, 8.41–8.43].

### EXAMPLE 8.9

#### *The 1s Line of Nitrogen in the XPS of Different Coordination Systems Reflecting the Variety of Its Bonding in Different Groups*

The sensitivity of chemical shifts to the chemical environment improves the efficiency of the photoelectron method in structural investigations. Figure 8.18 illustrates an example [8.42]. It is seen that the position of the line of the nitrogen 1s state in the XPS depends essentially on the chemical bonds with this atom and allows one to distinguish between coordinated and outer-sphere positions. In the AES the chemical shifts are significantly larger than those of core levels.

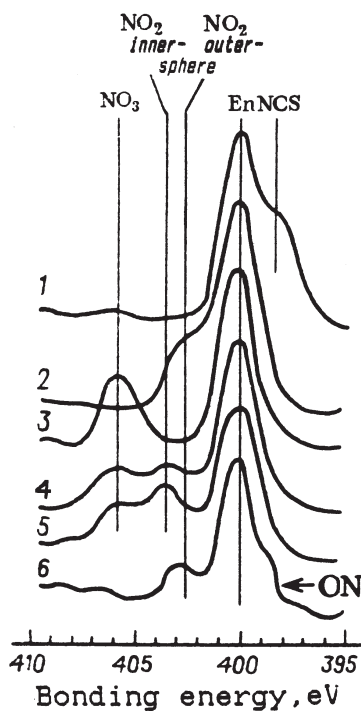


**FIGURE 8.18.** Dependence of the position of the XPS 1s line of the nitrogen atom in different groups on the near and distal structures of the molecular environment in (1)  $[\text{Ir}(\text{en})_3](\text{NCS})_2$ ; (2)  $[\text{Ir}(\text{en})_3](\text{NO}_2)_3$ ; (3)  $[\text{Ir}(\text{en})_3](\text{NO}_3)_3$ ; (4)  $[\text{Ir}(\text{en})_2\text{ClNO}_2]\text{NO}_3$ ; (5)  $[\text{Ir}(\text{en})_2](\text{NO}_2)_2\text{NO}_3$ ; (6)  $[\text{Co}(\text{NH}_3)_5\text{CN}](\text{NO}_2)_2$ . (From Nefedov [8.42].)

### EXAFS and Related Methods

*Extended X-ray absorption fine structure (EXAFS)* became, during the last several decades, a widespread structural tool (see Refs. 8.44–8.48, 8.25, and references cited therein). The phenomenon of additional modulated absorption beyond the *K* or *L* edge of the X-ray absorption spectrum has been known for more than 50 years. It is caused by the interference processes that the photoelectron wave undergoes by scattering from the environment of the absorbing atom; the outgoing photoelectron waves propagate to neighboring atoms and scatter back; then the interference of the initial and scattered waves produce corresponding modifications of the final state of the X-ray transition, resulting in modulated absorption intensity. Figure 8.19 illustrates this effect. A modification of EXAFS is known as *X-ray absorption near-edge structure (XANES)*.

However, the EXAFS effect remained unused until it was shown [8.44] that the information regarding the interatomic distances to neighboring atoms contained in the modulated absorption intensity can be relatively easily extracted by means of *Fourier transform*, which allows one to extract the interatomic distance from the observed wave of interference (Fig. 8.20). On the other hand, synchrotron radiation in the X-ray range has become available and proved to be an ideal source for XAFS measurements. Other usual sources of X-rays are less effective because the extended absorption is weak.

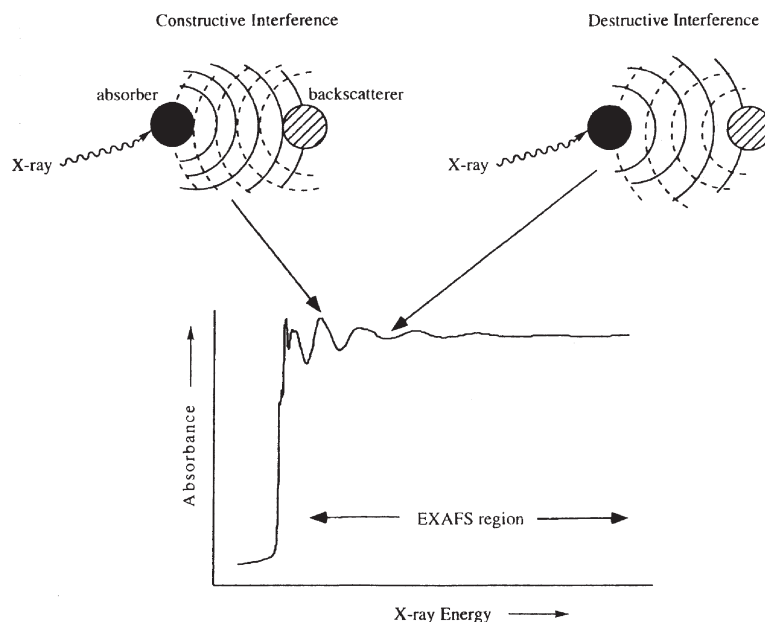


**FIGURE 8.19.** Illustration of the constructive (mutually enhancing) and destructive (mutually compensating) interference of the outgoing and incoming electromagnetic waves resulting in EXAFS. (From [8.47].)



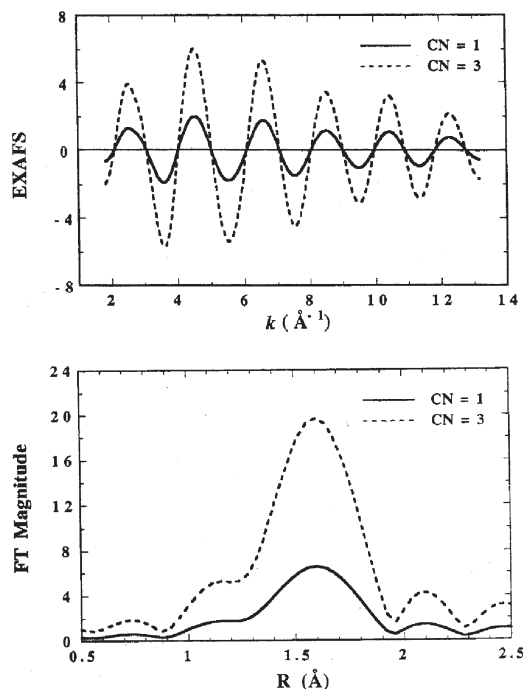


**FIGURE 8.20.** EXAFS signal and its Fourier transform (FT) showing the main and additional interatomic distances that produce the X-ray interference. The amplitude of the signal and its FT also depend on the number of equivalent neighbors (CN). (From [8.47].)

The main advantage of the EXAFS method is that it enables one to determine the interatomic distances from the absorbing to neighboring atoms of the first and second coordination spheres also *in the noncrystalline state*. This makes the method distinct from X-ray diffraction and unique when nonsolid and/or irregular structures are investigated. At present the EXAFS method is applied to study structural features of coordination centers in solutions and on surfaces [surface EXAFS (SEXAFS)], including supported and homogeneous catalysts, biological systems, disordered solids, thin films, and intercalated systems. Example 8.10 shows applications of EXAFS to a variety of chemical problems.

Another somewhat related method is the *electron energy loss spectroscopy* (EELS) [8.55]. In this method a high-energy electron beam (hundreds of kiloelectronvolts) is sent through a thin foil (several hundred angstroms thick) and the electrons scattered in a given direction are energy analyzed. The spectrum of energy loss corresponds to excitation of core and valence electronic states, as well as vibrational states. Despite the limitations created by demands for sample preparation (thin films), unless the  $Z$  elements are very large, the EELS method may have some advantages such as better signal-to-noise ratio, as compared with synchrotron absorption, but so far not very many coordination systems have been studied by this technique.

**EXAMPLE 8.10*****Applications of EXAFS Spectroscopy to a Variety of Problems***

Consider some examples. The dimerization of Mo(IV) in HCl solution was revealed by EXAFS that also allowed one to evaluate the Mo—Mo bond lengths at 2.51 Å [8.49]. In addition, two short Mo—O distances at 1.95 Å and four long ones at 2.15 Å were detected.

For  $\text{Cu}(\text{H}_2\text{O})_6^{2+}$  and  $\text{Cr}(\text{H}_2\text{O})_6^{2+}$  in solutions the problem was to determine whether the JT tetragonal distortions of the octahedron with an electronic  $E$  ground state (Section 7.3) can be detected by EXAFS. It confirmed the prediction of the vibronic theory; for the axial  $R_L$  and equatorial  $R_S$  metal–ligand distances the following values were obtained (in Å):  $R_L(\text{Cr—O}) = 2.30$ ,  $R_S(\text{Cr—O}) = 1.99$ ,  $R_L(\text{Cu—O}) = 2.60$ ,  $R_S(\text{Cu—O}) = 1.96$  [8.50]. For hydrated ions with nondegenerate terms there is no distortion.

The next example is related to the spin crossover phenomenon (Section 8.4). The transition high spin  $\rightarrow$  low spin is expected to contract the metal–ligand bond. The EXAFS experiments [8.51] show that in  $\text{Fe}(\text{phen})_2(\text{NCS})_2$  the transition  $S = \frac{5}{2} \rightarrow S = \frac{1}{2}$  with a spin change  $\Delta S = 2$  yields a mean contraction  $\langle \Delta R \rangle = 0.24$  Å. In  $\text{Co}(\text{H}_2\text{fsa}2\text{en})\text{L}_2$ , where  $\text{H}_4\text{fsa}2\text{en} = N, N'$ -ethylenebis(3-carboxysalicylaldimine) and  $L = \text{H}_2\text{O}$ , pyridine, the transition  $S = \frac{3}{2} \rightarrow S = \frac{1}{2}$  ( $\Delta S = 1$ ) gives  $\langle \Delta R \rangle = 0.09$  Å.

In biologic systems the EXAFS technique allows one to solve some very complicated problems. For nitrogenase [8.52], it was shown that the local environment of Mo is S and Fe (as distinct from another Mo enzyme, sulfite oxidase, where O and S are nearest neighbors). For hemoglobin the EXAFS data [8.53] rule out the large-scale lengthening (as postulated by Perutz and Hoard) of the Fe—N bond when passing from oxyhemoglobin to its deoxy form; in both cases this distance is almost the same,  $2.055 \pm 0.01$  Å and  $1.98 \pm 0.01$  Å, respectively. The discussion of the iron atom position in hemoglobin and other metal enzymes is given in Sections 9.2 and 10.3.

A series of interesting results were obtained in EXAFS measurements for ferroelectric crystals that undergo the so-called displacive phase transitions ( $\text{BaTiO}_3$ ,  $\text{KNbO}_3$ ,  $\text{PbTiO}_3$ , see Table 9.15 and references cited therein). These experiments confirmed that the distortions of the crystal lattice are of local origin, as predicted by the PJTE theory, and the phase transitions are of the order–disorder type rather than displacive (Section 9.4).

## 8.4. MAGNETIC PROPERTIES

### Magnetic Moment and Quenching of Orbital Contribution

Magnetic properties of any substance can be characterized by its response to the external magnetic field intensity  $\mathcal{H}$ . This response is best described by the magnetic induction  $\mathbf{B}$ , defined as the magnetic field intensity inside the matter:

$$\mathbf{B} = \mathcal{H} + \mu_0 \mathbf{M} \quad (8.46)$$

where  $\mathbf{M}$  is the *magnetization*, the effective sum of elementary magnetic moments per unit volume, and  $\mu_0$  is a constant called *permeability of vacuum* introduced to simplify the units; if the magnetic field  $\mathcal{H}$  and induction  $\mathbf{B}$  are given in *Tesla* units T (not to be confused with temperature;  $T = NA^{-1} \text{ m}^{-1}$ , where  $N$  is Newton, A is Ampere),  $\mu_0 = 4\pi \times 10^{-7} NA^{-2}$ .  $\mathbf{M}$  also depends on the magnetic field  $\mathcal{H}$ , and for isotropic media in not very strong fields

$$\mu_0 \mathbf{M} = \chi \mathcal{H} \quad (8.47)$$

where  $\chi$  is the *magnetic susceptibility* (defined here in dimensionless units); in stronger fields there may be quadratic and higher-order terms in  $\mathcal{H}$ , meaning that  $\chi$  may be dependent on the magnetic field [see Eqs. (8.57) and (8.58)]. In anisotropic substances  $\chi$  is not a scalar, but a tensor; provided that the appropriate axes are chosen, it has three components,  $\chi_x$ ,  $\chi_y$ , and  $\chi_z$ , which characterize the magnetic susceptibilities in different directions, the *magnetic anisotropy* [for a powder the averaged value  $\chi = (\chi_x + \chi_y + \chi_z)/3$  is observed].

The magnetic susceptibility is one of the most important magnetic properties of matter that is directly related to its electronic structure [8.3, 8.7, 8.25, 8.56–8.64]. The magnetization  $\mathbf{M}$  of the substance is determined by the magnetic moments  $\mu$  of its elementary units (its molecules or other magnetic centers) and their cooperative behavior in the magnetic field. If  $\mu \neq 0$ , the magnetic moments of free molecules tend to orient along the external magnetic field  $\mathcal{H}$  (*paramagnetism*), but their chaotic collisions in the gas phase (which increase with temperature  $T$ ) destroy the orientation and do not allow for full ordering; the magnetization becomes temperature-dependent. The Langeven theory predicts that in this case (quite similar to the polarization of electric dipoles) the magnetic susceptibility  $\chi$  is inversely proportional to the temperature

$$\chi = \frac{N\mu_0\mu^2}{3kT} \quad (8.48)$$

where  $N$  is the number of magnetic moments: per unit volume [for molar susceptibility  $(\chi_{\text{mol}})N = N_A$  and  $\chi_{\text{mol}} = (M/\rho)\chi$ , where  $M$  is the molar mass and  $\rho$  is the density, so it has the dimensionality of  $\text{m}^3 \text{ mol}^{-1} = 10^6 \text{ cm}^3 \text{ mol}^{-1}$ ].

If there is a strong magnetic interaction between the magnetic units  $\mu$  (usually in crystals), then their orientations are no longer free, and at sufficiently low temperatures an ordering of these magnets (a magnetic phase transition) takes place (cf. Section 9.4). There are several main types of magnetic ordering: *ferromagnetic*, when all the magnets are parallel and the magnetization is maximal; *antiferromagnetic*, when the nearest-neighbor elementary magnets occupy alternating opposite directions, and the macroscopic total magnetization is zero; *ferrimagnetic*, when in the antiferromagnetic ordering the values of the elementary magnetic moments of opposite orientation are different and the net magnetic moment is non-zero); and others (see Table 8.8). Compared with paramagnets,  $\chi$  for ferromagnetic materials can be larger by several orders of magnitude, while the antiferromagnets may have the same order of  $\chi$  magnitude as paramagnets. Table 8.8 lists the diversity of possible magnetic behavior of substances.

In addition to the magnetization based on the orientation of the elementary magnets, there is also induced magnetization (*diamagnetism*) when, under the influence of the external magnetic field  $\mathcal{H}$ , a local circular current occurs with its own magnetic field opposite to  $\mathcal{H}$ . The diamagnetic susceptibility is thus negative; its absolute value is smaller by orders of magnitude than the paramagnetic susceptibility. The diamagnetic behavior (repulsion from the magnetic field), although weak, is apparently the only possible response to the magnetic influence on systems with  $\mu = 0$  (however, see Van Fleck paramagnetism below).

Information about the electronic structure of molecules consists in its magnetic moment  $\mu$ . It is known from quantum mechanics that each momentum of the microsystem is associated with a proportional magnetic moment. For the free electron with a spin momentum  $\mathbf{S}$ , its associated magnetic moment is

$$\mu = \frac{e\hbar}{mc}\mathbf{S} \quad (8.49)$$

while the magnetic moment of its orbital motion with an orbital momentum  $\mathbf{L}$  (Section 2.2) is

$$\mu_L = \beta\mathbf{L} \quad (8.50)$$

where  $\beta = e\hbar/2mc$  is the elementary magnetic moment, called *Bohr magneton*,  $\beta = 9.274 \times 10^{-24}$  erg/tesla. Hence the total magnetic moment of the system is

$$\mu = \beta(\mathbf{L} + 2\mathbf{S}) \quad (8.51)$$

This expression is, in fact, the operator of the magnetic moment, while the observable moments are determined as quantum-mechanical averaged values of the operator  $\mu$  over the states under consideration. In particular, for a free atom with a total momentum  $\mathbf{J} = \mathbf{L} + \mathbf{S}$ , taking the projection of  $\mu$  on  $\mathbf{J}$  and the average  $\langle J^2 \rangle = J(J + 1)$ , we have (see Problem 8.3)

$$\mu_J = g\beta[J(J + 1)]^{1/2} \quad (8.52)$$

**TABLE 8.8. The Main Types of Magnetic Response of Substances**

Type of Magnetism	Origin <sup>a</sup>	$\sim\chi$ at 20°C	Temperature Dependence	Examples
<b>Diamagnetism</b>				
	Proper MM equals zero; induced MM is opposite to the external field	$-10^{-6}$	None	KCl, C <sub>6</sub> H <sub>6</sub>
<b>Paramagnetism</b>				
Atomic, ionic, and molecular	Electronic orbital and/or spin MM is nonzero	$(1-20) \times 10^{-6}$	$1/T$ or $1/(T + \theta)$	H, Ti <sup>3+</sup> NO, K <sub>3</sub> Fe(CN) <sub>6</sub>
Nuclear	Nuclear MM is nonzero	$10^{-9}$	None	H in hydrids
Free electrons	Electronic gas MM is nonzero	$10^{-8}$	Weak	Metallic K or Na
Van-Vleck, or T-independent	Excited states with other MM lay higher than $kT$	$10^{-6}$	None	KMnO <sub>4</sub> Co <sup>III</sup> amines
<b>Cooperative magnetism (ordered systems)</b>				
Ferromagnetism	Crystal lattice with parallel MM of the centers	$1-10^2$	Complicated; decreases at $T_c$	Metallic iron
Antiferromagnetism	Two ferromagnetic sublattices with antiparallel mutual compensating spins	$10^{-4}-10^{-5}$	A maximum at Neel $T$	KNiF <sub>3</sub> , MnSe
Ferrimagnetism	Partial compensated antiparallel spins of different sublattices	$10^{-5}$	Similar	Fe <sub>3</sub> O <sub>4</sub>
Metamagnetism	A kind of ferrimagnetism with complicated ordering of sublattices	$10^{-5}$	Similar	NiCl <sub>2</sub> at liquid H <sub>2</sub>

<sup>a</sup>MM denotes magnetic moment.

where

$$g = 1 + \frac{J(J+1) + S(S+1) - L(L+1)}{2J(J+1)} \quad (8.53)$$

The coefficient  $g$ , *the g factor, or Landé factor* (see Landé intervals (2.15)), plays a significant role in molecular magnetism. For a free electron  $L = 0$ ,  $J = S$ , and  $g = 2$ . In fact, however, a more correct value for the free-electron  $g$  factor is  $g = 2.0023$ .

Equation (8.52) is valid when there is a single energy level with a given  $J$  value, well separated from other levels, that is, when there is a sufficiently strong spin-orbital coupling ( $\lambda \gg kT$ ). This case may take place in heavy atoms. In the other limit case when  $\lambda \ll kT$  [light atoms and transition metals of the first (and even second) row at not very low temperatures] the energy levels of the same  $LS$  term with different  $J$  values are almost equally populated, and hence the effective measured magnetic moment, averaged over all the  $J$  values, is [8.63]

$$\mu_{\text{eff}} = \beta[4S(S+1) + L(L+1)]^{1/2} \quad (8.54)$$

If the atom or ion is placed in the field of ligands, its electronic structure changes and expressions (8.52) and (8.54), in general, are no longer valid. In particular, the orbital moment is subject to significant changes. Experimental data show that in most cases the magnetic properties of transition metal ions in complexes are as if the orbital contribution vanished,  $L = 0$ :

$$\mu_{\text{eff}} \approx 2\beta[S(S+1)]^{1/2} \quad (8.55)$$

that is, the orbital momentum is reduced to zero and the magnetic moment has a spin-only value.

This *quenching of the orbital contribution to the magnetic moment by the ligand field* can be explained as follows. The effective orbital magnetic moment is due to additional magnetization of the substance (additional magnetic susceptibility), which occurs as a result of free orientation of the magnetic moment (of the orbital motion) along the external magnetic field. This free orientation is possible in the free atom because for  $L \neq 0$  the energy term is degenerate, and in absence of external perturbation there is no fixed direction of the orbital moment—all directions are equivalent.

Now, the main effect of the ligand field on the CA is the splitting of its degenerate energy terms (Section 4.2), as a result of which the orbital motion in the ground state becomes fixed or limited in orientation, and it cannot freely follow the magnetic field. Therefore, although the orbital momentum of the CA electrons in the field of ligands can be nonzero ( $L \neq 0$ ), it may not be manifest (or may be manifest only partly) in the magnetic behavior of the electrons. Hence the magnetic orbital momentum is completely or partially quenched by the ligand field.

The partial quenching of the orbital magnetic moment takes place when the crystal field splitting is not complete, and there are still some possibilities for the orbital magnetic moment to rotate and follow the external magnetic field. These cases are well known from symmetry considerations. Indeed, for the electronic state of a cubic system  $\Psi_\Gamma$  that belongs to the IrRep  $\Gamma$  (Section 3.4), the average orbital momentum is determined by the integral

$$\int \Psi_\Gamma^* \mathbf{L} \Psi_\Gamma d\tau \quad (8.56)$$

Since the orbital momentum  $\mathbf{L}$  in cubic groups belongs to the  $T_1$  representation, the integral (8.56) is nonzero if and only if the symmetric product  $[\Gamma]^2$  contains  $T_1$  [see Eq. (3.34) in Section 3.4]. It can be easily shown that for cubic symmetries this is possible only when  $\Gamma = T_1$ , or  $\Gamma = T_2$  (for icosahedral symmetry there are more possibilities). In all other cases, namely, for nondegenerate or double-degenerate terms in cubic groups, the orbital magnetism is completely quenched and the magnetic moment is determined by the spin-only formula (8.55).

The electronic configurations and the ground-state terms of coordination compounds with different coordination geometries are given in Table 6.3. From the data in that table, one can state that for octahedral complexes with  $d^3, d^8, d^9, d^{10}$  as well as high-spin  $d^4, d^5$  and low-spin  $d^6, d^7$  configurations, the spin-only magnetic behavior in Eq. (8.55) is expected, while for  $d^1, d^2$ , high-spin  $d^6, d^7$ , and low-spin  $d^4, d^5$  configurations, an orbital contribution to the magnetic moment can be significant. Experimental data [8.63] confirm these expectations.

The orbital contribution to the magnetic moment is also nonzero when the  $T$  term is split by low-symmetry crystal fields or spin-orbital interaction, and the splitting magnitude is not very large as compared with  $kT$ . If it is of the order of  $kT$ ,  $\mu_{\text{eff}}$  becomes temperature-dependent.

### Paramagnetic Susceptibility

The magnetic moments  $\mu$  of molecular systems can be determined from the measured magnetic susceptibility  $\chi = \mu_0 M / \mathcal{H}$  [Eq. (8.47)], provided that the relation between  $\mu$  and  $\chi$  is known. The simple expression (8.48) for  $\chi$  obtained from the Langeven theory is valid when all the freely rotating elementary molecular magnets have the same magnetic moments. This means that there are no thermally accessible magnetic excited states with  $\mu' \neq \mu$ .

However, in most cases, especially in transition metal coordination compounds, there are many close-in-energy states (created by the spin-orbital and crystal field splitting) that have different spins and orbital moments and hence different magnetic moments  $\mu_i$ . If these states are thermally populated, the effective magnetic moment in  $\chi$  equals the averaged moment taken as a sum of Boltzmann distributed elementary magnets  $\mu_i$ . The theory of paramagnetic susceptibility for

this case was developed by Van Vleck [8.56]; it yields

$$\chi = N \sum_{n,m} \left( \frac{(\varepsilon_{n,m}^{(1)})^2}{kT} - 2\varepsilon_{n,m}^{(2)} \right) \frac{\exp(-\varepsilon_n^0/kT)}{\sum_{n,m} \exp(-\varepsilon_n^0/kT)} \quad (8.57)$$

where  $\varepsilon_{n,m}^{(1)}$  and  $\varepsilon_{n,m}^{(2)}$  are the first- and second-order corrections to the energy level  $\varepsilon_n^0$  in the magnetic field, that is

$$\varepsilon_{n,m} = \varepsilon_n^{(0)} + \varepsilon_{n,m}^{(1)}\mathcal{H} + \varepsilon_{n,m}^{(2)}\mathcal{H}^2 \quad (8.58)$$

and it is assumed that the energy splitting in the magnetic field (the Zeeman effect; see below) are much smaller than  $kT$  [in the absence of the magnetic field  $\varepsilon_{n,m} = \varepsilon_n^{(0)}$  is degenerate with respect to  $m$ ].

If the excited states with  $n > 1$  are not thermally populated,  $\varepsilon_n^0 - \varepsilon_1^0 \gg kT$ , Eq. (8.57) can be essentially simplified:

$$\chi = N \left\{ \sum_m \frac{[\varepsilon_{1,m}^{(1)}]^2}{kT} - 2 \sum_m \varepsilon_{1,m}^{(2)} \right\} \quad (8.59)$$

The first term here is the usual paramagnetic susceptibility, which obeys the *Curie law*:  $\chi = C/T$ . From the Zeeman effect (see below) it is known that the term that is linear in  $\mathcal{H}$  in (8.58) is simply related to the effective magnetic moment of the system:  $\sum_m [\varepsilon_{1,m}^{(1)}]^2 = \mu_{\text{eff}}^2/3$ , and hence this part of  $\chi$  coincides with Eq. (8.48) given by Langeven's theory. However, the second term in (8.58), in contrast to the first one, is independent of temperature. Its contribution is *temperature-independent*, or *Van Vleck, paramagnetism*. Since the second-order perturbation correction in (8.59) is of the order of  $\sum_n |(1|W|n)|^2/(\varepsilon_n^0 - \varepsilon_1^0)$ , where  $W$  is the energy of interaction of the magnetic moment (8.50) with the external field,  $\varepsilon_1^{(2)}$  is the larger, the more low-lying excited states are admixed to the ground state by the magnetic field. Typical values of Van Vleck paramagnetism for 3d metals range from  $60 \times 10^{-6} \text{ cm}^3 \cdot \text{mol}^{-1}$  for Cu(II) to  $400 \times 10^{-6} \text{ cm}^3 \cdot \text{mol}^{-1}$  for Co(II) [8.63] and reach about  $10^{-3} \text{ cm}^3 \cdot \text{mol}^{-1}$  for some rare-earth ions.

Calculations of the paramagnetic susceptibilities using the Van Vleck formula (8.57) require knowledge of the thermally populated energy levels in the magnetic field. Thermal population is significant if the energy spacing of these levels is about or smaller than  $kT$ . Usually this means that they are spin sublevels of the same electronic term split by the low-symmetry ligand field and external magnetic field. In this case the spin energy levels can be obtained by means of the *spin Hamiltonian* method [8.57].

The idea of the spin Hamiltonian is as follows. Provided that the expected spin states emerge from the same electronic term (i.e., no excited electronic states are admixed by the magnetic field), one can average the full Hamiltonian of the system (including all the interactions with the magnetic field) over the



electronic and nuclear coordinates to obtain a Hamiltonian that contains explicitly only spin  $\mathbf{S}$  and magnetic field  $\mathcal{H}$  operators and some averaged electronic (and nuclear) parameters. In a general form (without nuclear spins) the spin Hamiltonian appears as follows [8.57]:

$$H = \sum_{i,j} [D_{ij}S_iS_j + \beta g_{ij}\mathcal{H}_iS_j] \quad (8.60)$$

where  $i, j = x, y, z$ ,  $D_{ij}$  and  $g_{ij}$  are the tensors of zero field splitting and  $g$  factor, respectively. These parameters contain all the information about the electronic structure of the system and can be calculated, provided that the wavefunction of the term under consideration is known. On the other hand, the  $D_{ij}$  and  $g_{ij}$  values can be obtained from experimental data by comparing the magnetic properties with those predicted by the spin Hamiltonian (8.60).

The procedure for evaluating the energy levels  $\varepsilon_i$  by means of the spin Hamiltonian is to consider  $\mathcal{H}$  as a perturbation to the  $(2S + 1)$ -fold-degenerate spin multiplet. By solving the secular equation of perturbation theory [the matrix elements of the spin operators are determined as in Eqs. (2.22)–(2.25)]

$$\|H_{ij} - \varepsilon\delta_{ij}\| = 0 \quad (8.61)$$

we get the  $2S + 1$  energy levels sought for.

The number of independent parameters in the spin Hamiltonian (8.60) depends on the symmetry of the system. *Kramers doublets*, that is, spin doublet states with  $S = \frac{1}{2}$ , are not split by crystal fields (they split only in magnetic fields). In the crystal field of lower than cubic symmetry the spin Hamiltonian can be written as follows:

$$H = D[S_z^2 - \frac{1}{3}S(S + 1)] + E(S_x^2 - S_y^2) + \beta(g_x\mathcal{H}_xS_x + g_y\mathcal{H}_yS_y + g_z\mathcal{H}_zS_z) \quad (8.62)$$

where  $D$  and  $E$  are the parameters of axial and rhombic distortions, respectively. Depending on the spin value  $S$ , this magnetic field Hamiltonian yields a series of energy levels that contribute to  $\chi$ . In particular, in the case of an axial field  $D \neq 0$ ,  $E = 0$ ,  $g_z = g_l$ ,  $g_x = g_y = g_n$ , there are two values of  $\chi$ :  $\chi_l$  and  $\chi_n$ , parallel and perpendicular to the axis of symmetry, respectively. Their temperature dependence after (8.57) (without the temperature-independent magnetism) for different total spin  $S$  values is given in Table 8.9 [8.64].

### Electron Spin Resonance (ESR)

The ESR method is based on resonance absorption of electromagnetic irradiation in the radio and microwave regions associated with transitions between the energy levels of the electronic term split by the external magnetic field. The splitting

**TABLE 8.9. Temperature Dependence of the Magnetic Molar Susceptibility**  
 $\chi/C$ ,  $C = N_A \mu_0 g^2 \beta^2 / kT$  ( $g = g_l$  for  $C_l$  and  $g = g_n$  for  $C_n$ ) for Several Spin States  
 $S$  of One-Center Coordination Compounds with Axial Symmetry;  $x = D/kT$

$S$	$\chi_l/C_l, \chi_n/C_n$
	$\chi_l/C_l$
1	$2e^{-x}/(1 + 2e^{-x})$
$\frac{3}{2}$	$(1 + 9e^{-2x})/4(1 + e^{-2x})$
2	$(2e^{-x} + 8e^{-4x})/(1 + 2e^{-x} + 2e^{-4x})$
$\frac{5}{2}$	$(1 + 9e^{-2x} + 25e^{-6x})/4(1 + e^{-2x} + e^{-6x})$
	$\chi_n/C_n$
1	$(2/x)(1 + e^{-x})(1 + 2e^{-x})$
$\frac{3}{2}$	$[4 + (3/x)(1 - e^{-2x})]/4(1 + 2e^{-2x})$
2	$[(6/x)(1 - e^{-x}) + (4/3x)(e^{-x} - e^{-4x})]/(1 + 2e^{-x} + 2e^{-4x})$
$\frac{5}{2}$	$[9 + (8/x)(1 - e^{-2x}) + (9/2x)(e^{-2x} - e^{-6x})]/4(1 + e^{-2x} + e^{-6x})$

of the energy levels in magnetic fields is known as the *Zeeman effect*. Zeeman splitting can be evaluated using the spin Hamiltonian [Eqs. (8.60) and (8.62)] and solving the secular equation (8.61).

In the simplest case, if the total momentum of an atom  $\mathbf{J} = \mathbf{L} + \mathbf{S}$  is described by the quantum number  $J$  and its projection  $m = J, J - 1, \dots, -J$ , the energy levels in the magnetic field  $\mathcal{H}$  are given by the simple Zeeman splitting:

$$\varepsilon_m = g\beta\mathcal{H}m \quad (8.63)$$

where  $g$  is the Landé factor (*g factor*) given by Eq. (8.53) (see also Problem 8.1).

Electromagnetic transitions between these levels are allowed as magnetic-dipole transitions obeying the selection rule  $\Delta m = \pm 1$ . This is accompanied by absorption of a quantum of electromagnetic irradiation

$$\hbar\omega = \varepsilon_{m+1} - \varepsilon_m = g\beta\mathcal{H} \quad (8.64)$$

which, for a given external field  $\mathcal{H}$ , is completely determined by the  $g$  factor. It is seen from Eq. (8.53) that if the spin  $S = 0$ , but the orbital momentum  $L \neq 0$ , then  $J = L$  and  $g = 1$ , while for  $L = 0, S \neq 0$ , we have  $J = S$  and  $g_s = 2$  (as mentioned above, a more precise value is  $g_s = 2.0023$ ).

If the atom is in a transition metal compound, the ligand influence changes the  $g$  factor drastically. To begin with, the orbital contribution to the momentum  $J$ , as shown above, may become completely or partially quenched. This reduction of the orbital contribution is determined by the symmetry of the crystal field. Several other parameters of the electronic structure also contribute significantly to the ESR spectrum: spin-orbital admixing of excited states; symmetry and strength of

the ligand fields, yielding *anisotropic g factors*; admixture of ligand states (*covalence contribution*); splitting of the line due to the splitting of the spin states (*fine structure*); further splitting due to the interaction with the nuclear spin (*hyperfine splitting*); splitting due to the ligand nuclear spin (*superhyperfine splitting*); *g-factor reduction* due to orbital degeneracy (*vibronic reduction*); dependence of the line shape on temperature via interactions with vibrations (*paramagnetic relaxation*); and so on. Thus *the ESR spectra carry very rich information about the electronic structure of transition metal compounds*.

The origin of the covalence contribution can be clarified by considering the widespread case of tetragonally distorted  $\text{Cu}^{2+}$  complexes of  $D_{4h}$  symmetry. In the approximation of crystal field theory (Section 4.1) the energy levels of the  $d^9$  configuration in the ligand field are as shown in Fig. 8.21 (cf. Fig. 4.4 and note that a hole in the  $d^{10}$  configuration has an energy-level diagram inverse to that in  $d^1$ ). The  $B_{1g}$  ground state corresponds to the atomic orbital  $d_{x^2-y^2}$ . This state originates from the  $E$  term in a cubic field and hence its orbital contribution is quenched, thus having a pure spin  $g$  factor  $g = 2.0023$ . However, the spin-orbital interaction mixes this ground state with the excited states  $B_{2g}$  and  $E_g$ ; the latter emerge from the  $T_{2g}$  term of the cubic system, which has an orbital contribution.

Denote the wavefunctions of the mixing antibonding states  $B_{1g}$ ,  $B_{2g}$ , and  $E_g$  by  $\Psi_{0i}$  with  $i = 1, 2, 3$ , respectively. In the weak-covalence model, following Eq. (5.33), these wavefunctions are

$$\Psi_i = N_i(\Psi_{0i} - \gamma\Phi_i) \quad (8.65)$$

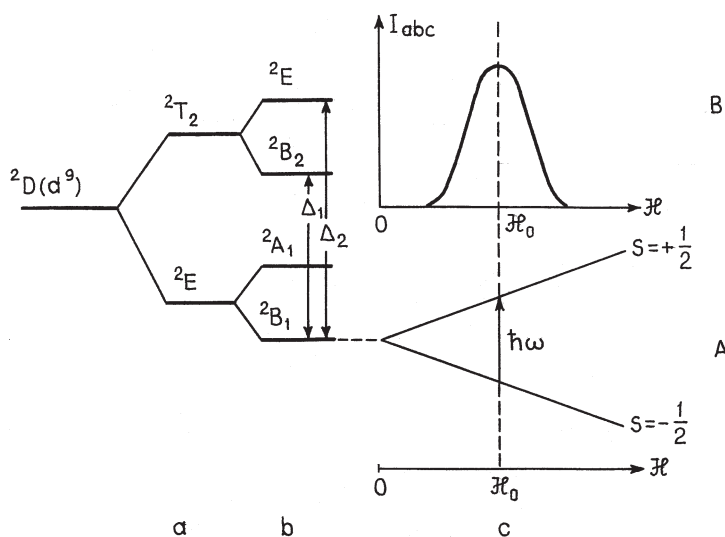


**FIGURE 8.21.** The  $\text{Cu}^{2+} {}^2D(3d^9)$  term splitting in tetrahedral (a) and tetragonally elongated tetrahedral (b) crystal fields, and in the external magnetic field  $\mathcal{H}$  (c, A). At  $\beta\mathcal{H}_0 = \hbar\omega$  there is a resonance absorption (B) that changes the spin state.

where  $\Phi_i$  is the ligand group orbital,  $\gamma$  is the covalence constant,  $N_i = [1 + \gamma_i^2 - 2\gamma_i S_i]^{-1}$  is the normalization constant, and  $S_i$  is the overlap integral:  $S_i = \langle \psi_{0i} | \Phi_i \rangle$ . Then, considering the spin-orbital interaction  $\lambda(L, S)$  as a perturbation [Eq. (2.23);  $\lambda$  is the spin-orbital coupling constant], one can obtain the following in the second-order perturbation theory for the longitudinal ( $l$ ) and normal ( $n$ ) components:

$$\begin{aligned} g_l = g_{zz} &= 2 - \frac{8\lambda}{\Delta_1} N_1^2 N_2^2 \\ g_n = g_{xx} = g_{yy} &= 2 - \frac{2\lambda}{\Delta_2} N_1^2 N_3^2 \end{aligned} \quad (8.66)$$

Here  $\Delta_1$  and  $\Delta_2$  are the energy gaps to the excited states (Fig. 8.21), and terms of the order of  $\gamma_i \gamma_j$  and  $\gamma_i S_j$  are ignored.

For pure CA states  $N_1 = N_2 = N_3 = 1$ , and the orbital contributions to  $g_l$  and  $g_n$  are  $-8\lambda/\Delta_1$  and  $-2\lambda/\Delta_2$ , respectively. Note that for Cu,  $\lambda < 0$ , and hence these contributions are positive increasing the  $g$  factors. For nonzero covalence  $N_i < 1$ , so the orbital contributions to the  $g$  factors are reduced  $k_1^2 = N_1^2 N_2^2$  and  $k_2^2 = N_1^2 N_3^2$  times for  $g_l$  and  $g_n$ , respectively. This reduction can be presented as if the spin-orbital constant  $\lambda$  were reduced to  $\lambda' = k^2 \lambda$ . If  $\Delta_1$  and  $\Delta_2$  are known (e.g., from spectroscopic data or calculations), one can evaluate  $\lambda'$  from the measured  $g$  factors and estimate  $k^2$ , the covalence reduction.

The covalence reduction of the spin-orbital constant  $\lambda$  (or the orbital contribution to the  $g$  factor) is similar to the nephelauxetic effect (discussed in Section 8.2), which results from reduction of the interelectron interaction Racah parameter  $B$  by formation of covalence bonds. Both these parameter reductions (and some others) are due to the quite understandable effects of electron delocalization on larger volumes by coordination. The spin-orbital interaction may also be reduced as a result of special relativistic effects of ligand coordination (Section 6.5).

The two components of the  $g$  factor in Eq. (8.66),  $g_l$  and  $g_n$ , may differ significantly following the anisotropy of the tetragonal system. For an arbitrary direction of the magnetic field  $\mathcal{H}$  with an angle  $\theta$  to the tetragonal axis, we obtain

$$g_\theta = [g_l^2 \cos^2 \theta + g_n^2 \sin^2 \theta]^{1/2} \quad (8.67)$$

For lower symmetries all the three components of the  $g$  factor are different.

In cubic fields the three components of the  $g$  factor are equivalent, and hence no angular dependence of the ESR spectrum is expected. However, in many cases, as in the preceding example of  $\text{Cu}^{2+}$  complexes, the ground state in cubic fields is orbitally degenerate. This creates quite new circumstances, due to which the ESR spectrum complicates significantly [8.26]. Indeed, according to the JTE and other vibronic interaction effects (Sections 7.3 and 7.4), the electronic degeneracy causes a special coupling between the electronic and nuclear

motions, which renders invalid the direct application of the spin Hamiltonian approach.

In particular, for the  $E$  term of the example of  $\text{Cu}^{2+}$  octahedral complexes with strong vibronic coupling, presented above, there are three APES minima in which the octahedron is elongated along one of the three fourth-order axes (one for each minimum) (Figs. 7.10 and 7.11). In each of these minima the  $g$  factor corresponds to the tetragonally distorted octahedron.

On the other hand, the system performs pulsating motions with relatively high-frequency transitions between the equivalent minima. As shown in Section 7.3, these pulsating distortions result in the *tunneling splitting* of the vibrational energy levels. When it is sufficiently small (with strong vibronic coupling) the tunneling levels are mixed by the external magnetic field, resulting in a special Zeeman splitting that yield a complicated ESR spectrum with a characteristic dependence on temperature and irradiation frequency [8.26]. If the tunneling splitting is larger than the Zeeman splitting ( $\sim\beta H$ ), the ESR spectrum is determined by the ground level only. In this case the  $g$  factor is subject to vibronic reduction (Section 7.3).

Set  $g_1 = g_s - (4\lambda/\Delta)$ ,  $g_2 = -(4\lambda/\Delta)$ , and let  $l$ ,  $m$ , and  $n$  represent the direction cosines of the magnetic field vector  $\mathcal{H}$ . Then it can be shown that, by taking into consideration the vibronic reduction factor  $q = K_E(E)$  after Eqs. (7.50), the angular dependence of the  $g$  factor is [8.57]:

$$g_{1,2} = g_s - g_2 \pm qg_2 f \quad (8.68)$$

$$f = [1 - 3(l^2m^2 + l^2n^2 + m^2n^2)]^{1/2}$$

For very strong vibronic coupling (with deep minima of the adiabatic potential and high barriers between them)  $q = \frac{1}{2}$ , while in the absence of the reduction  $q = 1$ . The angular dependence of  $g$  for these two limit cases is shown in Fig. 8.22 together with experimental data obtained for  $\text{Cu}^{2+}$  ions as impurities in  $\text{MgO}$  at  $T = 1.2$  K (see, e.g., in Ref. 8.26). As one can see, the difference between the two spectra (with and without vibronic coupling) is rather significant and the experimental data confirm unambiguously the importance of the vibronic reduction. For the vibronic implications in the ESR spectra of other terms and other conditions see [8.15, 8.26, 8.30].

So far we have considered a single ESR line, especially its  $g$  factor. As mentioned above, the fine, hyperfine, and superhyperfine structures of the ESR spectrum may also be important. Consider the  $\text{Cr}^{3+}(d^3, {}^4F)$  ion in the ligand field of trigonal symmetry  $D_{3h}$  resulting in the orbitally nondegenerate ground-state spin quadruplet  ${}^4A_{2g}$  ( $S = \frac{3}{2}$ ,  $m_s = \pm\frac{1}{2}, \pm\frac{3}{2}$ ). The spin-orbital interaction splits this term into two doublets with  $m_s = \pm\frac{1}{2}$  and  $m_s = \pm\frac{3}{2}$ , respectively (e.g., for chromium alum the splitting is  $2D = 0.15 \text{ cm}^{-1}$ ), which are further split by the external magnetic field  $\mathcal{H}$ , as shown in Fig. 8.23. As a result, there are three values of  $\mathcal{H}$  ( $\mathcal{H}_1, \mathcal{H}_2$ , and  $\mathcal{H}_3$ ) for which the resonance absorption of the same quantum of irradiation takes place, each thus having its own  $g$  factor (fine structure).

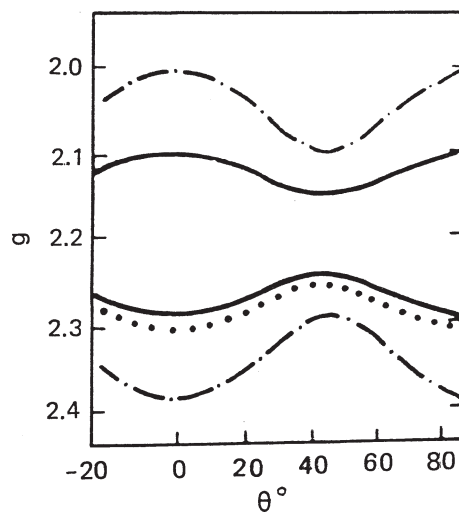


**FIGURE 8.22.** Two limiting cases of angular dependence of the  $g$  factor for the Jahn–Teller linear  $E \otimes e$  problem with strong ( $q = \frac{1}{2}$ , solid line) and without ( $q = 1$ , dashed line) vibronic coupling. Experimental data are shown by points.

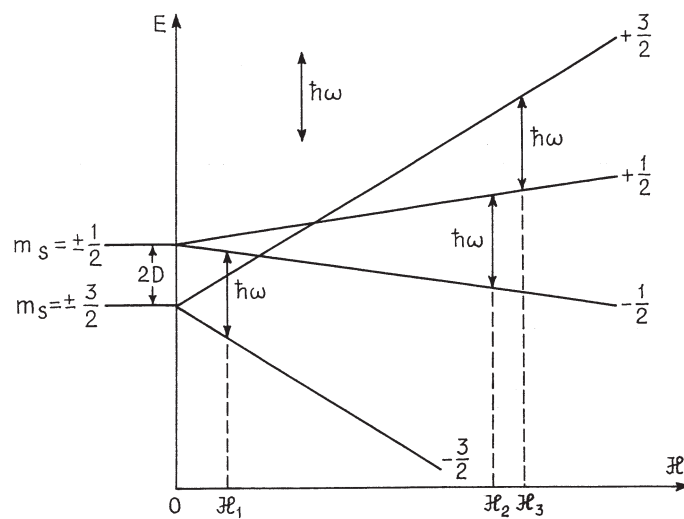


**FIGURE 8.23.** Zeeman splitting and ESR transitions for a  ${}^4F(D^3)$  ( $\text{Cr}^{3+}$ -type) term in magnetic fields. The  $\mathcal{H}_1$ ,  $\mathcal{H}_2$ , and  $\mathcal{H}_3$  values indicate the magnetic field intensities for three possible resonance transitions with the same quantum of irradiation  $\hbar\omega$ .

The hyperfine structure is described by additional terms  $H^N$  in the spin Hamiltonian that include the interaction between the electron (**S**) and nuclear (**I**) spins:

$$H^N = \sum_{ij} [A_{ij} S_i I_j + P_{ij} I_i I_j] - g_N \beta_N (\mathbf{I}, \mathcal{H}) \quad (8.69)$$

Here  $A_{ij}$  are the constants of the spin–spin (dipole–dipole) magnetic interaction between the electrons and nuclei,  $P_{ij}$  are the constants of the quadrupole interactions, and the last term describes the interaction between the nuclei and the external magnetic field;  $g_N$  and  $\beta_N$  are the nuclear  $g$  factor and Bohr magneton, respectively ( $\beta_N \cong \beta/1840$ ).

While the last term in (8.69) is important for nuclear magnetic resonance (NMR) spectra (for a review of NMR spectroscopy in coordination compounds, see Ref. 8.65), the quadrupole splitting is most important in Mossbauer spectroscopy (Section 8.5). For the spin–spin interaction that yields the hyperfine structure of the ESR spectra the number of independent constants  $A_{ij}$  depends on the symmetry of the system. In cubic systems there is only one constant  $A$ , while in axial symmetry there are two,  $A$  and  $B$ :

$$H^N = A S_z I_z + B(S_x I_x + S_y I_y) \quad (8.70)$$

The constants of hyperfine interaction contain the nuclear magnetic moment proportional to  $g_N \beta_N$ , which is about 1840 times smaller than the electronic magnetic moment. Therefore, hyperfine splitting is accordingly smaller than fine-structure splitting. In a sufficiently strong magnetic field each line of the fine structure splits into  $2I + 1$  lines, which are equally spaced when  $B = 0$  (cubic symmetry). Magnetic-dipole transitions are allowed between any two levels with  $\Delta m_s = \pm 1$  and  $\Delta M = 0$  (as above,  $M$  is the nuclear magnetic quantum number).

The electron–nucleus dipole–dipole interaction is nonzero only if the electron has an orbital moment  $L \neq 0$  [8.57]. However, there is another term of electron–nucleus interaction not included in (8.69), the *contact Fermi interaction*, which is nonzero for only  $s$  electrons that have nonzero electron density  $|\Psi(0)|^2$  at the nuclei. The contact interaction is much stronger than the dipole–dipole one, and it is less dependent on the ligands. Therefore, even when there is no dipole–dipole interactions ( $L = 0$ ) and no direct  $s$ -orbital participation, the hyperfine structure can still be observed because of the configuration interaction (Section 5.3) with  $s$ -containing configurations of the same symmetry and multiplicity (*s-configuration interaction*). The observed hyperfine structure in  $\text{Mn}^{2+}$  salts ( $d^5$ ,  $L = 0$ ) is an example of this kind.

The hyperfine constants are also linked to the covalence. In particular, for  $N_1$  of Eq. (8.65), which is a measure of CA participation in the covalent MO, the following approximate relation holds for systems with axial symmetry:

$$N_1^2 = \frac{-A}{P} + (g_l - 2) + \frac{3}{7}(g_n - 2) + 0.04 \quad (8.71)$$

where  $P = 2g_N\beta_N\beta\langle r^{-3} \rangle$  is the constant of the electron–nucleus interaction [8.57]. For  $\text{Cu}^{2+}$ ,  $P = 0.36 \text{ cm}^{-1}$ .

The superhyperfine structure is due to the interaction between the unpaired electrons and the nuclear spin of the ligands, which can be described by an additional term in the spin Hamiltonian:

$$H^{N'} = \sum_{N'} A'_{ij} S_i I'_j \quad (8.72)$$

Here  $N'$  denotes the ligand nuclei that have nonzero spin  $I'$  and  $A'_{ij}$  are mostly *contact Fermi interaction* constants (the ligands participate in the bonding by mostly  $s$  or  $s$ -hybridized orbitals). Usually, the unpaired electron remains on the ligands for a relatively shorter time than on the CA. Therefore,  $A'_{ij}$  are smaller than  $A_{ij}$  and describe further splitting of the hyperfine lines. For comparison of orders of magnitude, examples of ESR spectra constants for some  $\text{Cu}^{2+}$  and  $\text{V}^{4+}$  complexes in solutions are given in Table 8.10.

Interestingly, the number of superhyperfine lines and their relative intensities are determined by the number of equivalent ligand nuclei  $n$ . In particular, for  $I' = \frac{1}{2}$  the line intensities follow exactly the binomial coefficients:  $1, n, n(n-1)/2, \dots, n, 1$ ; the number of lines thus is  $n + 1$ . Similar rules are established for other values of  $I'$  [8.57].

**TABLE 8.10. ESR Spectra Parameters for Some Chelate Cu(II) and V(IV) Compounds in Solutions**

Compound	Solvent <sup>a</sup>	$g_l$	$g_n$	$A \times 10^4$ ( $\text{cm}^{-1}$ )	$B \times 10^4$ ( $\text{cm}^{-1}$ )	$A' \times 10^{4b}$ ( $\text{cm}^{-1}$ )
Bis(acetylacetonato)- Cu(II)	I	2.264	2.036	145.5	29	—
Bis(dimethyldithio- carbomato)Cu(II)	I	2.098	2.035	154 <sup>c</sup>	40	—
				165 <sup>c</sup>	43	—
	II	2.121	2.040	134 <sup>c</sup>	25	—
Bis(salicylaloxymato)- Cu(II)	III	2.171	2.020	146.5 <sup>c</sup>	27	—
				183	41	14
Bis(salicylaldimino)- Cu(II)	III	2.14	2.08	168	16	—
Bis(8 chinolinato)Cu(II)	III	2.172	2.042	162	25	10
Dichlorophenantroline- Cu(II)	III	2.22	2.08	119	29	—
Oxo(bis- acetylacetonato)V(IV)	III	1.944	1.996	173.5	63.5	—

<sup>a</sup>I, 60% toluol, 40% chloroform; II, 40% pyridine, 60% chloroform; III, 40% toluol, 60% chloroform.

<sup>b</sup>Superhyperfine structure from the ligand nitrogen atoms.

<sup>c</sup>Results for two copper isotopes: <sup>63</sup>Cu and <sup>65</sup>Cu.



An extension known as *electron nuclear double resonance* (ENDOR) is often used to obtain more resolved information. Since the energy gap between the Zeeman levels in ESR is relatively small, the difference in their thermal (Boltzmann) population at nonzero temperatures is small as well. Therefore, if the microwave power is sufficiently high and the relaxation process is slow, the ESR signal will be lost because of the rapid saturation of the transition as the populations of the two levels become equalized. Under these conditions, an additional irradiation of the system with a much lower (radio-) frequency that is in resonance with the Zeeman splitting of the nuclear spin levels produces transitions between them seen as additional absorption at that frequencies. This simultaneously improves the ESR signal because it serves as an additional channel of relaxation. Figure 8.24 illustrates the ENDOR spectra for the case of electron spin  $S = \frac{1}{2}$  and nuclear spin  $I = \frac{1}{2}$  (relevant to protons) when the nuclear Zeeman splitting is larger than the hyperfine interaction. For other cases and more details, see Ref. 8.25.

The magnetic resonance methods are among the most powerful means of investigating electronic structure of coordination compounds. The main limitations of the ESR method lie in the requirement of unpaired electrons ( $S \neq 0$ ) and relatively slow paramagnetic relaxations that make it impossible to observe the ESR spectrum and its resolution. Note also that *most of the information from the ESR spectra refers solely to the states of the unpaired electrons*. In particular, the conclusions about covalence drawn from ESR data [Eq. (8.66)] refer to orbital covalence on the MOs of the unpaired electrons, whereas the covalence of the bond as a whole, as discussed in Section 6.2, is produced by other electrons, namely, by those on uncompensated bonding MOs (Fig. 6.3).

### Magnetic Exchange Coupling

One of the most important and up-to-date applications of magnetic measurements is for the study of the magnetic exchange interactions in multicenter (polynuclear) coordination compounds [8.7, 8.58, 8.60]. The interaction of two atoms with unpaired spins is a typical problem of covalent bonding. As mentioned in Section 1.2, for the hydrogen molecule this was solved by Heitler and London in 1927, and this solution forms the basis of the *valence bond theory*. In the Heitler–London treatment the  $H_2$  molecule has two states: bonding spin singlet (the two spins are antiparallel ( $\uparrow\downarrow$ ,  $S = 0$ ) and antibonding spin triplet ( $\uparrow\uparrow$ ,  $S = 1$ ). The energy gap between these two states is dependent on the two-electron exchange integral  $K$  given by Eq. (2.36) (Section 2.2). In the case of  $H_2$ ,  $K < 0$ ; if  $K > 0$ , the triplet state is lower than the singlet state. The interaction resulting in the high-spin ground state is called *ferromagnetic interaction* (because it is analogous to the parallel spin ordering in ferromagnets, mentioned in Section 8.1), while that resulting in zero or the lowest spin is the *antiferromagnetic interaction*.

If the two centers with nonzero spins are bonded not directly but via intermediate (bridging) groups, the spin–spin interaction between them becomes more complicated, involving the electrons of the intermediate centers (*indirect*,

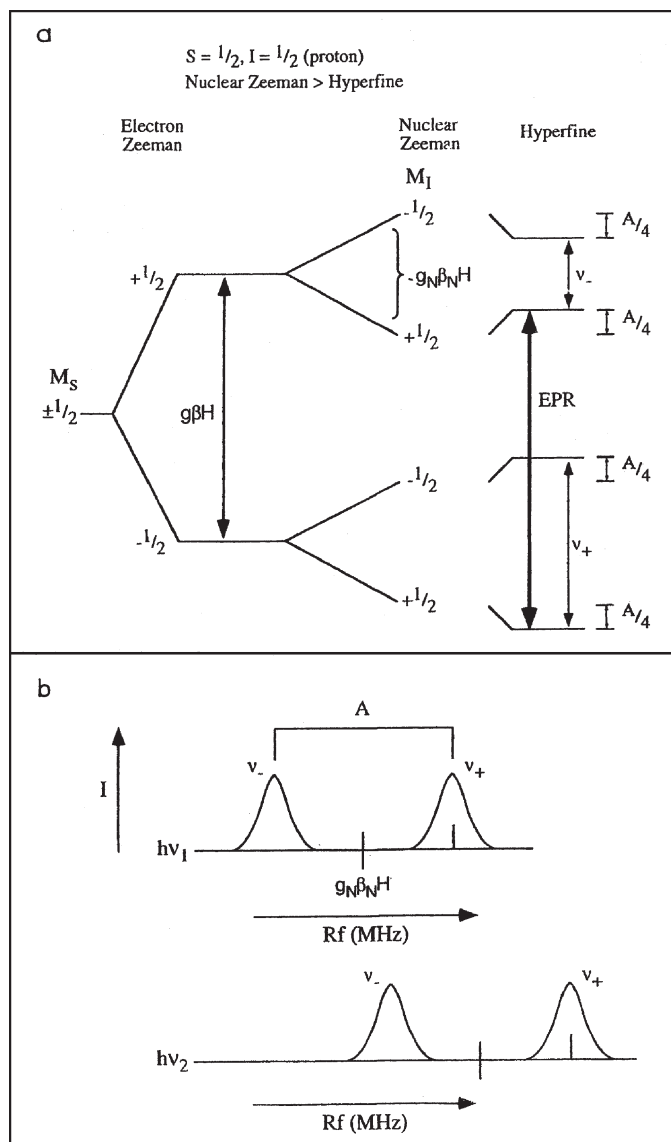


**FIGURE 8.24.** Illustration of the ENDOR on protons ( $I = \frac{1}{2}$ ) and the electronic spin  $S = \frac{1}{2}$  in the case of nuclear Zeeman splitting larger than hyperfine splitting  $A$ : (A) Zeeman splitting and ESR,  $\Delta M_S = 1$ ,  $\Delta M_I = 0$  (full arrow), and ENDOR,  $\Delta M_S = 0$ ,  $\Delta M_I = 1$  ( $v_+$  and  $v_-$ ); (B) the two ENDOR lines separated by hyperfine splitting  $A$  and centered at the Larmor frequency. Larger microwave frequencies  $\nu_2$  shift the ENDOR absorption to higher radiofrequencies  $R_f$ . (From [8.4].)

or superexchange). Heisenberg and Dirac suggested a simple spin Hamiltonian model for the magnetic interactions between two centers  $i$  and  $j$  later modified by Van Vleck (*the HDVV model*), which has the form

$$H = -2J_{ij}S_iS_j \quad (8.73)$$

where  $J_{ij}$  is the *isotropic exchange coupling constant*. The HDVV model assumes that the intracenter interactions (that produce, respectively, the spins  $S_i$  and  $S_j$  on the two centers) are much stronger than the interaction between the centers. This assumption holds for all superexchange situations, but may be violated in direct metal–metal multiple bonding.

The eigenvalues of the Hamiltonian (8.73) are

$$E(S) = -J[S(S+1) - S_i(S_i+1) - S_j(S_j+1)] \quad (8.74)$$

where the total spin  $S$  is determined, as usual, following the rule of addition of moments:

$$S = S_i + S_j, S_i + S_j - 1, \dots, |S_i - S_j| \quad (8.75)$$

The energy intervals between the levels (8.74) (the Landé intervals; Section 2.2) are

$$\Delta_S = E(S) - E(S-1) = -2J_{ij}S \quad (8.76)$$

In particular, for two centers with one unpaired electron on each of them (omitting indices at  $J$ ), we obtain

$$\Delta_1 = E(1) - E(0) = -2J \quad (8.77)$$

and hence the exchange constant  $J$  characterizes the energy gap  $\Delta$  between different spin states. Its sign determines the type of interaction: ferromagnetic for  $J > 0$  and antiferromagnetic for  $J < 0$ . Calculations show that for two directly bonded spin centers  $a$  and  $b$  (as in the molecule  $H_2$ )

$$J = \frac{2(I_{ab}S_{ab}^2 - K_{ab})}{1 - S_{ab}^4} \quad (8.78)$$

where  $I_{ab}$  and  $K_{ab}$  are, respectively, the Coulomb and exchange integrals given by Eqs. (2.35) and (2.36), and  $S_{ab}$  is the overlap integral. For superexchange and for larger spin values on the centers the expressions for  $J$  become much more complicated. Anderson [8.66] first suggested that exchange interaction between metallic ions can be presented as a sum of ferromagnetic  $J_F$  and antiferromagnetic  $J_{AF}$  contributions

$$J = J_F + J_{AF} \quad (8.79)$$

where

$$J_F = 2K_{ab}$$

and

$$J_{AF} = 4H_{ab}S_{ab} \quad (8.80)$$

where  $H_{ab}$  is the resonance integral (5.4).

Note that while the ferromagnetic contribution (which is proportional to the Coulomb interelectron repulsion) is always nonzero and positive, the antiferromagnetic term is proportional to the overlap integral  $S_{ab}$ , and hence it is nonzero for nonorthogonal orbitals only and can be either positive or negative. Kahn and coworkers [8.62] extended this idea to indirect superexchange interactions in multicenter coordination compounds. In a binuclear complex, as distinct from two metallic atoms, the two one-electron orbitals of the unpaired spins are no longer pure AOs, but *magnetic orbitals* defined as single occupied MOs centered, respectively, on the two sites  $a$  and  $b$ , and partially delocalized toward the terminal and bridging ligands. If the overlap between these two magnetic orbitals is nonzero, they form two MOs with an energy gap  $\Delta = -2H_{ab}$ . Therefore for equivalent centers

$$J_{AF} = -2\Delta S_{ab} \quad (8.81)$$

while for nonequivalent centers

$$J_{AF} = -2(\Delta^2 - \Delta_0^2)^{1/2} S_{ab} \quad (8.82)$$

where  $\Delta_0$  is the energy gap between the reference magnetic (often atomic) orbitals.

A somewhat different suggestion for  $J_{AF}$  was given by Hoffmann [8.67]:

$$J_{AF} = \frac{-\Delta^2}{I_{aa} - I_{ab}} \quad (8.83)$$

Since  $\Delta \sim S_{ab}$ , the two expressions (8.81) and (8.83) are qualitatively similar.

The main conclusion drawn from these formulas is that the antiferromagnetic contribution  $J_{AF}$  to the exchange coupling constant  $J$  is strongly dependent on the overlap integral between the magnetic orbitals of the interacting centers ( $\sim S_{ab}^2$ ). This explains the dependence of the observed magnetic properties of multicenter compounds on small structural changes [8.68]. In particular, if  $S_{ab} = 0$  (orthogonal magnetic orbitals), then  $J_{AF} = 0$ , and the magnetic coupling is expected to be ferromagnetic with a high-spin ground state. On the other hand, the ferromagnetic contribution  $J_F$  is also dependent on structural features, mostly on charge density distribution [8.62, 8.68]. Examples 8.11 and 8.12 give further insight into the details of metal–metal exchange-coupled interaction.

**EXAMPLE 8.11*****Magnetic Exchange Coupling in Binuclear Copper Acetate Hydrate***

An interesting example that contributed significantly to the understanding of exchange coupling in coordination compounds is the binuclear copper(II) acetate hydrate  $[\text{Cu}(\text{OAc})_2\text{H}_2\text{O}]_2$ . Intensive investigation of this system began in 1952, when Bleaney and Bowers [8.69] showed that its magnetic susceptibility  $\chi$  and ESR spectrum are unusual for  $\text{Cu}^{2+}$  complexes (its dimeric structure was not known at that time). Indeed, the temperature dependence of  $\chi$  has a maximum at  $T_{\text{max}} = 255 \text{ K}$  [8.70] (for the dehydrated complex  $T_{\text{max}} = 270 \text{ K}$ ) and decreases almost to zero at lower temperatures as shown in Fig. 8.25. Although the  $g$  factors of the ESR spectrum are similar to those of other copper(II) salts, its intensity decreases with temperature and becomes zero at  $T = 20 \text{ K}$ , exhibiting a small zero-field absorption at  $D = 0.34 \pm 0.03 \text{ cm}^{-1}$ . This magnetic behavior is somewhat like that of Ni(II) compounds with  $S = 1$ ; therefore, the authors [8.69] assumed that the system is dimeric with two exchange-coupled  $\text{Cu}^{2+}$  centers in each molecule. The X-ray structural investigation confirmed this assumption [8.71] (Fig. 8.26).

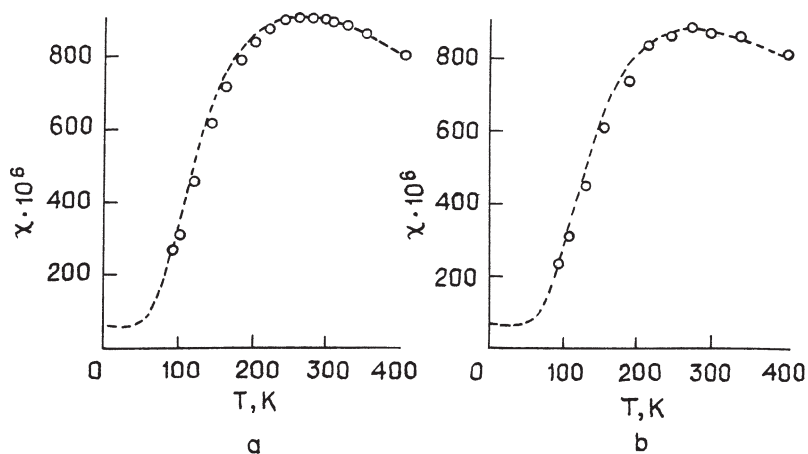


**FIGURE 8.25.** Temperature dependence of the magnetic susceptibility of  $[\text{Cu}(\text{OAc})_2\text{H}_2\text{O}]_2$  (a) and its dehydrated analog  $[\text{Cu}(\text{OAc})_2]$  (b) calculated by Eq. (8.84) (dashed line) and obtained from experimental data (points). (From Figgis and Martin [8.70].)

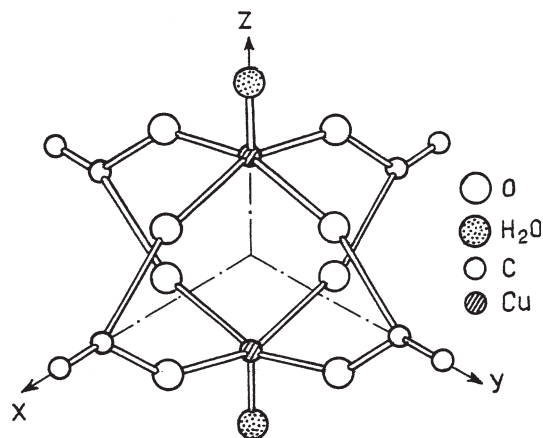


FIGURE 8.26. Molecular structure of  $[\text{Cu}(\text{OAc})_2\text{H}_2\text{O}]_2$ . (From Martin [8.71].)

For the dimeric binuclear  $\text{Cu}^{2+}$  system with two equivalent spin  $S = \frac{1}{2}$  magnetic centers, the HDVV Hamiltonian (8.73) yields two energy levels with  $S = 0$  and  $S = 1$ , respectively. To explain the experimental data, one must assume that the ground state is singlet  $S = 0$ , which means that  $J < 0$  and the magnetic exchange coupling is antiferromagnetic. The magnetic susceptibility is then determined by the Van Vleck equation (8.57) which for a two-center system under consideration with  $S = 1$  and  $J < 0$  yields (cf. Table 8.9 for one-center systems):

$$\chi = \frac{(2Ng^2\beta^2/kT)}{3 + \exp(-2J/kT)} \quad (8.84)$$

This is the *Bleaney–Bowers equation* [8.69]. With  $-2J/k = 480$  K ( $2J = -334 \text{ cm}^{-1}$ ) it fits well the experimental data in Fig. 8.25.

### EXAMPLE 8.12

#### *The Nature of Metal–Metal Bonding in Binuclear Copper Acetate Hydrate*

The revealed dimeric structure and magnetic exchange coupling between the two copper centers in acetate and related compounds raised several hypotheses about the electronic structure of these

compounds and possible direct Cu—Cu interaction in view of their rather large interatomic distance 2.64 Å: direct  $\delta$  bonding between the two  $d_{x^2-y^2}$  orbitals (Sections 2.1 and 6.3) [8.70],  $\sigma$  bonding between their  $d_{z^2}$  orbitals [8.72], superexchange through the bridging carboxyl ions [8.73], and others.

Semiempirical calculations [8.74] in the IEH approximation (Section 5.5) show that the bonding in the copper(II) acetate is much more complicated. The unpaired electron in the triplet state occupies the  $d_{x^2-y^2}$  orbital, as indicated by the ESR spectrum (and in this sense the exchange coupling is realized through the two orbitals of  $\delta$  bonding), but the mechanism of coupling involves the oxygen atoms, hence it is a rather indirect superexchange coupling through the carboxyl bridges. This conclusion agrees well with the weak dependence of the  $2J$  constant on the Cu—Cu interatomic distance in different compounds with similar structure [8.75].

The calculations [8.74] show also that when the electronic charge is reduced from the binuclear binding area the bonding between the two centers deteriorates; this result can serve as a qualitative explanation of the fact that mono- and dichloroacetates of copper form dimers, whereas trichloroacetates do not. With fluorine, monofluoroacetate only gives dimers. Many other copper dimers were studied from this perspective [8.7]. For a review of magnetic properties of polynuclear carboxylates, see the article by Moreland and Doedens [8.76].

For coordination compounds with more than two magnetic centers, the magnetic properties can be revealed in a similar way. Let us consider some examples. For a trinuclear cluster the HDVV Hamiltonian is

$$H = -2J_{12}S_1S_2 - 2J_{13}S_1S_3 - 2J_{23}S_2S_3 \quad (8.85)$$

For equivalent centers in an equilateral triangle, such as in the heteropolycuster  $[\text{SiV}_3^{\text{IV}}\text{W}_9\text{O}_{40}]^{-10}$ ,  $J_{12} = J_{13} = J_{23} = J$ , and for  $S(\text{V}^{\text{IV}}) = \frac{1}{2}$  the temperature dependence of the magnetic susceptibility is [8.77]

$$\chi = \frac{Ng^2\beta^2}{4kT} \frac{1 + 5 \exp(3J/kT)}{1 + \exp(3J/kT)} \quad (8.86)$$

This agrees well with the experimental data. For a similar tetrahedral cluster with equivalent centers with  $S = \frac{1}{2}$  and an isotropic exchange  $J$ , the energy level splitting and the Van Vleck formulas yield the following for  $\chi$  [8.64]:

$$\chi = \frac{2Ng^2\beta^2}{kT} \frac{(5 + 3e^{-2J/kT})}{5 + 9e^{-2J/kT} + 2e^{-3J/kT}} \quad (8.87)$$

However, the magnetic behavior of some of the tetrahedral clusters of the type  $\text{Cu}_4\text{OL}_4\text{X}_6$  with  $\text{X} = \text{Cl}, \text{Br}$  and  $\text{L} = \text{Cl}, \text{Br}, \text{pyridine}, \text{OPR}_3, \text{ONR}_3$ , does not coincide with the predictions of this formula. Indeed, some of these clusters exhibit a nonmonotonous behavior of the magnetic moment  $\mu(T)$  with a maximum that cannot be explained by internal isotropic exchange with equal  $J_{ij}$  parameters ( $i, j = 1, 2, 3, 4$ ); some of these clusters do not have such a maximum of  $\mu(T)$ . The assumption of static distortions [8.78] explains the presence of the maximum in  $\chi(T)$ , but it is in contradiction with the ESR measurements.

The solution to the problem was obtained [8.79] on the basis of the JTE in a tetrahedral four-center system. Using the results of the vibronic theory (Sections 7.3 and 7.4), it was shown that the dynamic JT (PJT) distortions on each of the four Cu(II) centers are coupled to each other in such a way that the magnetic moment of the system is that of distorted centers with a maximum on the  $\mu(T)$  curve, whereas the ESR spectra correspond to undistorted centers (see the relativity rule concerning the means of observation in Section 9.1).

The isotropic magnetic exchange interaction model represented by the HDVV spin Hamiltonian (8.73), although covering most cases of transition metal coordination compounds, is not the only possible one and is not sufficient for the description of all the magnetic properties of multicenter systems [8.60]. If  $S > \frac{1}{2}$  and if the paramagnetic centers are not symmetry related, additional terms of the spin Hamiltonian may be required for description of the magnetic exchange interaction, in particular, the *biquadratic exchange* term:

$$H_{bij} = j_{ij}(S_i S_j)^2 \quad (8.88)$$

Although the constant  $j_{ij}$  is much smaller than the isotropic exchange constant  $J$  ( $j \sim 10^{-2}J$ ), the biquadratic exchange (8.88) produces new observable effects. In particular, it violates the rule of Landé intervals in spin-level splitting (8.76). The biquadratic term is most important in polynuclear compounds with more than two magnetic centers in a high-symmetry arrangement because it splits the otherwise accidentally degenerate spin levels [8.60].

Another term, the *Dzyaloshinsky–Moriya interaction, or antisymmetric exchange* [8.60–8.64]

$$H_{DM} = \mathbf{D}_{ij}[\mathbf{S}_i \times \mathbf{S}_j] \quad (8.89)$$

explains the origin of the *spin canting phenomenon* observed in many compounds. The essence of this effect is that the interacting spins in the ordered state (especially in crystals) are not collinear. As seen from Eq. (8.89), because of the vector product  $[\mathbf{S}_i \times \mathbf{S}_j]$ , which is zero for collinear spins, to lower the energy the latter attempt to occupy noncollinear positions. There are symmetry restrictions on this interaction—no inversion center, and at least one magnetic center must have an anisotropic spin component. Again, the constant of antisymmetric exchange  $|D| \approx (|g - 2|/g)J$  is much smaller than  $J$ .



Finally, the *anisotropic Ising Hamiltonian*

$$H_I = -2J^{ab}S_{az}S_{bz} \quad (8.90)$$

may be significant, especially in multicenter compounds. Its constant  $J^{ab}$  is also small:

$$|J^{ab}| \sim \left(\frac{g-2}{g}\right)^2 J \quad (8.91)$$

but it characterizes the dependence of the magnetic properties on the direction of the magnetic field  $\mathcal{H}$ . For binuclear copper carboxylates in Example 8.11 the Hamiltonian (8.90) allows one to obtain for the anisotropic susceptibility

$$\chi_{\parallel} = \frac{Ng^2\beta^2/2kT}{1 + e^{-J/kT}} \quad (8.92)$$

which differs from the Bleaney–Bowers equation (8.84).

For comprehensive reviews of different aspects of the theory of magnetochemistry and ESR in different systems, see the literature [8.6, 8.7, 8.57–8.64, 8.68, 8.71, 8.76]. The problem of *molecular magnets* [8.62, 8.80] seems to be one of the most challenging among the modern applications of magnetochemistry.

### Spin Crossover

Among many other effects and applications of magnetic properties of coordination compounds we discuss briefly the *spin crossover phenomenon* (see Refs. 8.81–8.87 and references cited therein). It follows directly from the Tanabe–Sugano diagrams for electronic  $d^n$  energy-level dependence on the ligand field parameter  $\Delta$  (Section 4.3, Fig. 4.11). It is seen from these diagrams that for the electronic configurations  $d^4$ ,  $d^5$ ,  $d^6$ , and  $d^7$  in the cubic symmetry environment, there is a certain value of  $\Delta = \Delta_0$  for which the ground-state symmetry and multiplicity change. The energies on the Tanabe–Sugano diagrams are read off from the ground state, and therefore the intersection of the excited term with the ground one produces an energy-level break.

The two types of ground states resulting in two types of complexes, high-spin (HS) and low-spin (LS), are discussed in Section 4.3 in the approximation of crystal field theory, and in Section 6.2 in the MO scheme. The HS state is the ground one when the inequality (4.49) (Section 4.3) takes place:

$$\Delta < \Pi \quad (8.93)$$

where  $\Pi$  is the electron pairing energy, that is, the electron interaction energy difference between the LS and HS states per electron, while for  $\Delta > \Pi$  the LS state is lower. This means that the crossing of the two spin terms, *the spin crossover* takes place at  $\Delta_0 = \Pi$ .

In the approximation of crystal field theory the  $\Pi$  values for different electronic  $d^n$  configurations are given by Eqs. (4.50). In more precise calculations [8.87] [ $B$  and  $C$  are the Racah parameters given by Eqs. (2.43)], we obtain

$$\begin{aligned}\Delta_0(d^5) &= 6.347B + 4.897C \\ \Delta_0(d^6) &= 2.195B + 3.708C \\ \Delta_0(d^7) &= 5.051B + 3.594C\end{aligned}\tag{8.94}$$

Equations (8.94) were derived for cubic-symmetry complexes, but a small reduction of symmetry does not significantly influence the qualitative results of the spin crossover phenomenon; hereafter the deviation from cubic symmetry is ignored. In tetrahedral complexes the two possible spin states occur in  $d^3$ ,  $d^4$ ,  $d^5$ , and  $d^6$  configurations. However, because of the smaller  $\Delta$  values ( $\Delta_T = -\frac{4}{9}\Delta_0$ ), the LS state is rarely realized in these cases.

The point of exact intersection between the two terms, HS and LS, is a point of accidental degeneracy. At this point the two states coexist with fast transitions  $\text{HS} \leftrightarrow \text{LS}$ . In fact, there is a whole region of coexistence due to vibrations ( $\hbar\omega$ ) and thermal population. It includes the  $\Delta$  values for which the energy difference between the two terms is  $\sim (kT + \hbar\omega)$ . Out of this region the excited state may also be populated, and its population is strongly (exponentially) temperature-dependent. The increase in temperature always enhances the spin transition ( $\text{HS} \rightarrow \text{LS}$  if  $\Delta < \Delta_0$ , and  $\text{LS} \rightarrow \text{HS}$  if  $\Delta > \Delta_0$ ). In free complexes (gas-phase or dilute solution) when the interaction between them is weak, there is a Boltzmann equilibrium between the LS and HS states with continuous dynamic interconversions



where the rate constants  $k$  and  $k_{-1}$ , for instance, for Fe(II) complexes vary between  $4 \times 10^5$  and  $2 \times 10^7 \text{ s}^{-1}$  [8.89].

If the interaction between the complexes is sufficiently strong, as it is in crystals, the cooperative effects become most significant. It is important that the  $\text{HS} \leftrightarrow \text{LS}$  transition is accompanied by a change in the interatomic distances. An example of this is mentioned in Example 8.10, where contraction of the bond length measured by EXAFS is given [8.51]. The spin transition changes the electronic configuration and the degeneracy of the ground state [e.g.,  ${}^1A_1 \rightarrow {}^5T_2$  in Fe(II) complexes]. This, in turn, produces distortions in the local environment of the transition center that may be subject to cooperative interactions in the crystal (Section 9.4). The latter favor an ordered state, but the entropy effects (which increase with temperature) destroy this ordering. Hence, for sufficiently strong interactions a phase transition at a certain temperature  $T_c$  may be expected [8.90].

Among the spin crossover systems in the crystalline state, two kinds of spin transition can be distinguished: (1) *discontinuous (abrupt) transitions*, which occur at a well-defined temperature  $T_c$ ; and (2) *continuous (gradual) transitions*, which take place over an extended range of temperatures; in this case  $T_c$  is defined as the temperature for which the fraction of HS systems is half:  $n_{HS} = 0.50$ .

To distinguish between the two types of spin transitions and to disclose their nature, many experimental methods of investigation were applied, including magnetic, spectroscopic, Mossbauer, X-ray diffraction, EXAFS, and other measurements (see, e.g., Refs. 8.86, 8.89, 8.91, and references cited therein). The main general conclusion is that the abrupt transitions are associated with a structural phase transition, while the continuous transition, gradually converting the system from one state to another, does not change the structural phase.

Figure 8.27 illustrates [8.92] an abrupt HS  $\leftrightarrow$  LS,  $S = \frac{3}{2} \leftrightarrow S = \frac{1}{2}$ , transition in a Co(II)( $3d^7$ ) compound,  $\text{Co}(\text{H}_2\text{fsa}_2\text{en})(4-t\text{-Bipy})_2$  shown in the magnetic susceptibility curve  $\chi \cdot T$  versus  $T$ . The LS state is realized at low temperature, while the HS state is stable at high temperature, and this is the usual situation in spin crossover transitions [8.85]. One of the features seen in Fig. 8.27 is *hysteresis*; the transition takes place at slightly different temperatures by heating ( $\uparrow$ ) and cooling ( $\downarrow$ ), respectively. The hysteresis is due to cooperative effects (Section 9.4) and it has interesting applications, mentioned below.

Numerous spin crossover systems studied so far are mainly iron(II), iron(III), and cobalt(II) complexes, but the phenomenon was also observed in many other metal complexes of Mn(II), Mn(III), Co(III), Ni(II), and Mo(II), as well as in

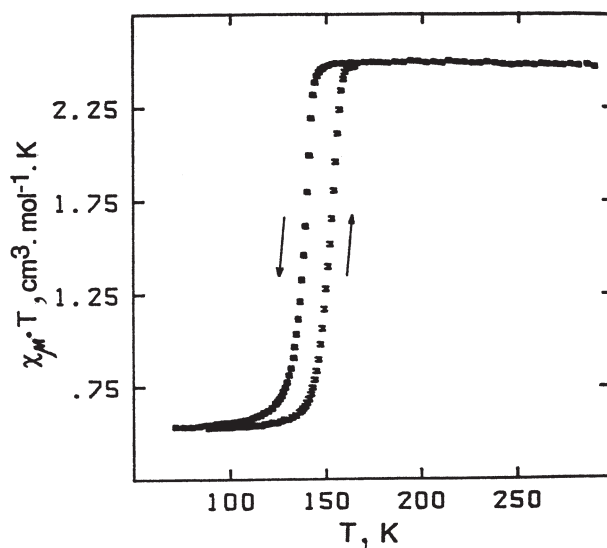


**FIGURE 8.27.** Temperature dependence of  $\chi_{\mu} \cdot T$  for  $\text{Co}(\text{H}_2\text{fsa}_2\text{en})(4-t\text{-Bipy})_2$ . Falling and rising arrows indicate decreasing and increasing temperatures. (From Thuery and Zarembowitch [8.92].)

systems of the type  $\text{Nb}_6\text{I}_{11}$ . For  $\text{Fe(II)}(3d^6)$  the two spin states involved in the spin transition are  ${}^1A_1(t_2^6)$  and  ${}^5T_2(t_2^4e^2)$ , while for  $\text{Fe(III)}(3d^5)$  they are  ${}^2T_2(t_2^5)$  and  ${}^6A_1(t_2^3e^2)$ . For  $\text{Co(II)}(3d^7)$  the transition occurs between  ${}^2E(t_2^6e)$  and  ${}^4T_1(t_2^5e^2)$ . In  $\text{NbI}_{11}$  the transition is  $S = \frac{1}{2} \leftrightarrow S = \frac{3}{2}$ . Besides the temperature dependence (thermally induced spin crossovers), spin transition can also be produced by variation of external pressure [8.85] and irradiation with light [8.81]. The pressure retains the smaller interatomic distances in the LS state, thus increasing  $T_c$ ; for uniaxial stress an opposite effect may be expected in degenerate HS states that produces low-symmetry distortions. Light absorption accompanied by an allowed electronic transition from the LS(HS) state to an excited state can be followed by radiationless transitions to the HS(LS) state. This is the effect of *light-induced excited spin-state trapping* (LIESST) [8.81, 8.84], and it was shown to be reversible.

The interest in spin crossover systems has increased following suggestions for using them as electronic microdevices in information storage and molecular signal processing employing their property of bistability [8.85]. The two spin states differ essentially in their magnetic properties, and there are possibilities for controlling the switch from one state [e.g., the nonmagnetic state  ${}^1A_1$  in  $\text{Fe(II)}$  complexes] to another (magnetic  ${}^5T_2$ ), provided that it occurs sufficiently abruptly. On the other hand, the hysteresis of the HS  $\leftrightarrow$  LS transition may serve for information storage [8.85].

#### Magnetic Circular Dichroism (MCD)

Magnetic circular dichroism is widely used in the studies of coordination compounds, especially in biological systems. In Section 8.1 the effect of dichroism (polychroism)—the dependence of the absorption of polarized light on the direction of polarization with respect to the anisotropic (crystal) system—is mentioned. A related effect, widespread in chemistry, is the *rotation of the plane of polarization* [8.93], called *optical activity*.

The plane-polarized wave of light can be presented as a sum of two circular polarized (*cp*) waves: right (*rcp*) and left (*lcp*) [8.93]. If the absorption coefficients of the right and left circular polarized waves  $K_l$  and  $K_r$  are different ( $K$  is determined from the relation  $I = I_0 \times 10^{-Kl}$ , Section 8.1), then it is said that there is *circular dichroism*. The quantity

$$\varepsilon_l - \varepsilon_r = \frac{K_l - K_r}{c} \quad (8.96)$$

where  $c$  is the speed of light, is taken as a measure of circular dichroism.

Both the optical activity and circular dichroism are due to the asymmetry in charge distribution and polarizability of the compound under consideration. The angle of rotation of the plane of polarized light is

$$\alpha = \frac{n_l - n_r}{\lambda} \quad (8.97)$$

where  $n_l$  and  $n_r$  are the coefficients of refraction of the *lcp* and *rcp* light, respectively, and  $\lambda$  is the wavelength. While  $\alpha$  may be nonzero in the region of transparency,  $\varepsilon_l - \varepsilon_r$  is related to the absorption. In the region of absorption all optically active compounds exhibit circular dichroism. An important feature of both optical activity and circular dichroism is thus their *dispersion*, that is, the dependence on light frequency. The curves of dispersion of optical rotation and circular dichroism are used to study molecular structures [8.1].

However, for transition metal compounds the method of *magnetic circular dichroism* (MCD) is more usable. This method does not demand that the compound to be studied be optically active; it becomes active under the influence of the external magnetic field. Figure 8.28 illustrates this effect. Consider, for simplicity, an atomic system with a nondegenerate ground state  $^1S$  and excited threefold-degenerate  $^1P$  state (analogous states in a cubic coordination systems are  $^1A_1$  and  $^1T_1$ ). In the magnetic field  $\mathcal{H}$  the degenerate  $P$  state splits into three components  $\varepsilon_m = mg\beta H$  [Eq. (8.63)] with  $m = 0, \pm 1$  (Fig. 8.28a).

Now we take into account the selection rules, according to which the absorption of the *lcp* wave is allowed if  $\Delta m = -1$ , while  $\Delta m = +1$  for the *rcp* one. Hence the maxima of absorption coefficients  $K_l$  and  $K_r$  are displaced by  $2g\beta H$  (Fig. 8.28b), and the  $\varepsilon_l - \varepsilon_r$  dispersion curve is as shown in Fig. 8.28c. This is a typical MCD dispersion curve with zero absorption at the zero-field frequency  $\Omega_0$ ; it is called *term A*. Term *A* is realized when the ground state is nondegenerate while the excited state is degenerate.

Another MCD spectrum, *term C*, is seen when the ground state is degenerate and the excited state is not (Fig. 8.29). The *rcp* component with  $\Delta m = +1$  corresponds to the transition from the ground state with  $m = -1$ , while the *lcp* with  $\Delta m = -1$  starts from the excited state  $m = +1$  (Fig. 8.29a). Therefore, at extremely low temperatures  $T \approx 0$  when the state  $m = +1$  is not populated, the *rcp* transition only is observed, and a small *lcp* component occurs when rising the temperature (Fig. 8.29b). The summary spectrum, unlike term *A*, has no nodal behavior, but the position of its maximum of absorption with respect to  $\Omega_0$  is a measure of the magnetic field splitting, which is proportional to  $\mathcal{H}$ .

The third case of MCD, *term B*, occurs when there is no orbital degeneracy in the two combining states, and one of the MCD components results from mixing of the ground electronic state with the excited states by the magnetic field. It is precisely this mixing that results in the Van Vleck temperature-independent paramagnetism in Eq. (8.59). Therefore, this MCD spectrum, which is formally similar to the nodeless term *C*, is distinct from the latter by being independent of temperature. An example of *B*-term MCD can be found, for instance, in a study by Jaw and Mason [8.94], where the MCD spectrum of the  $\text{Au}_9(\text{PPh}_3)_8^{3+}$  and its interpretation in terms of the MO LCAO model is given. The book by Piepho and Schatz [8.95] contains many useful standard definitions and conventions used in the MCD method.

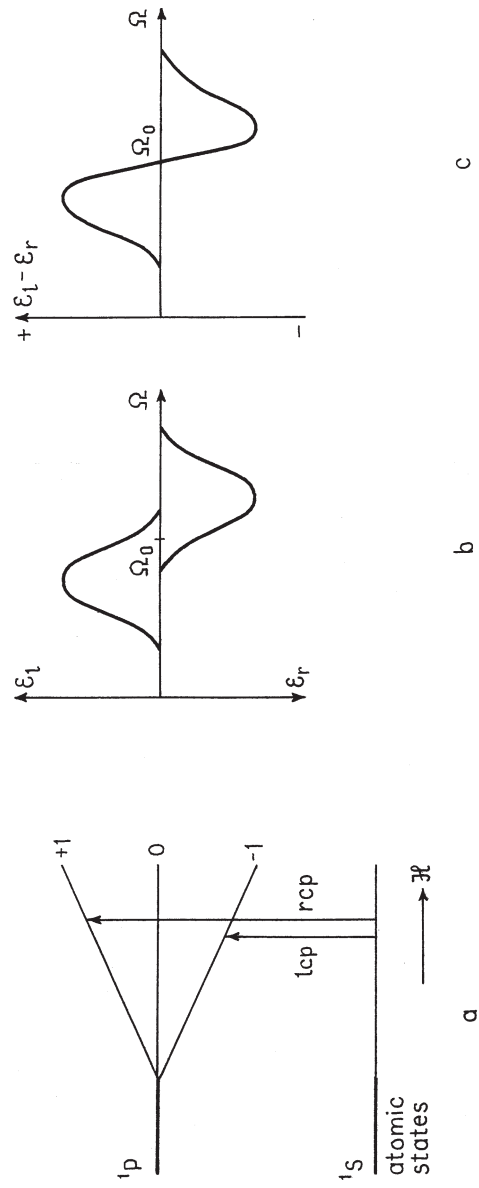


**FIGURE 8.28.** Illustration to the origin of MCD spectrum, term A: (a) atomic  $1S$  (ground) and  $1P$  (excited) term splitting in the magnetic field  $\mathcal{H}$ , and  $rcp$  and  $lcp$  transitions; (b)  $lcp$  and  $rcp$  absorption versus light frequency  $\Omega$  ( $\Omega_0$  is the zero-field frequency); (c) summary MCD spectrum.

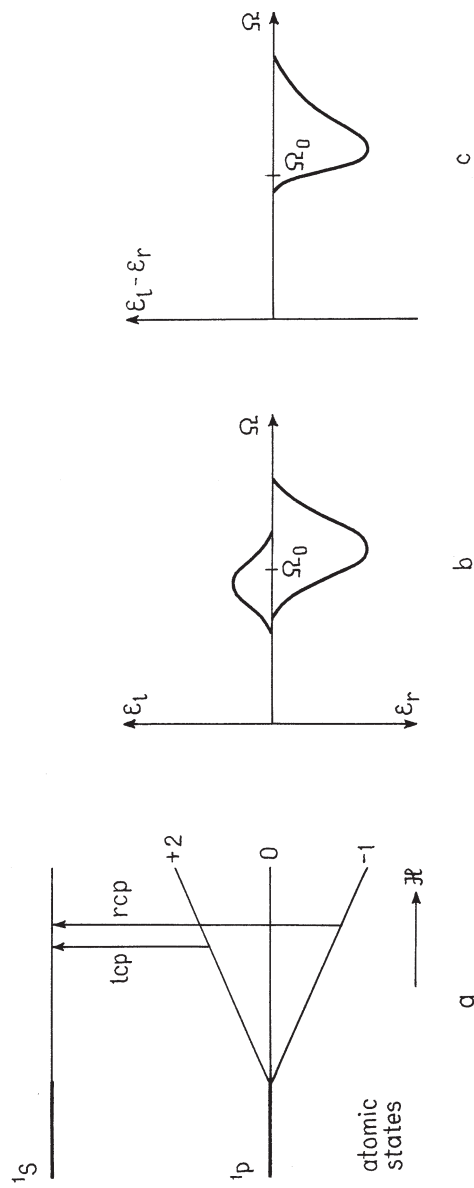


**FIGURE 8.29.** Illustration to the origin of the MCD spectrum, term C: (a) atomic  $1p$  (ground) and  $1s$  (excited) term splitting in the magnetic field  $\mathcal{H}$ , and  $rcp$  and  $lcp$  transitions; (b)  $lcp$  and  $rcp$  absorptions versus light frequency  $\Omega$  ( $\Omega_0$  is the zero-field frequency); (c) summary MCD spectrum.

### 8.5. GAMMA-RESONANCE SPECTROSCOPY

Among the variety of physical methods for investigating electronic structure and properties of transition metal compounds,  $\gamma$ -resonance spectroscopy (GRS) occupies an honorable place (see Refs. 8.8, 8.9, 8.96–8.98, and references cited therein). It is based on the possibility of observing resonance transitions between the energy levels of the nuclei first realized half a century ago by Rudolph Mossbauer [8.96]. Since the energy gap between the nuclear energy levels ranges from tenths to hundreds of kiloelectronvolts, the Mossbauer effect can be achieved only by means of very-high-frequency electromagnetic irradiation,  $\gamma$ -quanta.

#### The Mossbauer Effect

To understand the principles of  $\gamma$ -resonance transitions between nuclear states, we refer to the notions of zero-phonon line and resonance fluorescence (Section 8.2), which take place when there is an overlap between the frequencies in the absorption  $\Omega_1$  and emission  $\Omega_2$  bands (Figs. 8.1 and 8.3). Denoting  $\Omega_1 - \Omega_2 = \delta\Omega$  and the bandwidth by  $\Gamma$ , we have the following condition of resonance fluorescence:

$$\Gamma > \hbar\delta\Omega \quad (8.98)$$

With respect to this inequality the nuclear parameters are very different from the electronic ones. For “fixed” nuclei the absorption band with frequency  $\Omega_0$  at the maximum has the natural bandwidth  $\Gamma$  related to the lifetime of the excited state  $\tau$ :  $\Gamma = \hbar/\tau$ . For nuclear states  $\tau$  is the same as for atoms,  $\tau \sim 10^{-7} - 10^{-8}$  s, and hence  $\Gamma \sim 10^{-8} - 10^{-7}$  eV. The ratio  $\Gamma/\hbar\Omega_0$  serves as a measure of accuracy of “tuning” required for obtaining resonance absorption. Because of the drastic difference in the  $\Omega_0$  values, we have  $\Gamma/\hbar\Omega_0 \sim 10^{-7} - 10^{-8}$  for atoms and molecules, whereas for nuclei  $\Gamma/\hbar\Omega_0 \sim 10^{-11} - 10^{-12}$ . Hence, to obtain a resonance in nuclear transitions, one needs an accuracy of fine tuning that is several orders higher in magnitude than that for atoms.

For such a fine tuning even small losses of energy (that are ignored in electronic and vibrational transitions) can destroy the resonance. For a free nucleus the *recoil energy* is most important in this respect, all the more so because it differs in absorption and emission. Indeed, in the latter the recoil is an energy loss, while in the former it is a gain. Using the preservation laws for energy and momentum, it can be shown that with including the recoil corrections the emission  $\Omega'$  and absorption  $\Omega''$  frequencies are (where  $M$  is the mass of the nucleus and  $c$  is the speed of light):

$$\begin{aligned} \hbar\Omega' &= \hbar\Omega_0 \left( 1 - \frac{\hbar\Omega_0}{2Mc^2} \right) \\ \hbar\Omega'' &= \hbar\Omega_0 \left( 1 + \frac{\hbar\Omega_0}{2Mc^2} \right) \end{aligned} \quad (8.99)$$



From these relations we obtain for the emission–absorption band shift:

$$\hbar\delta\Omega = \frac{(\hbar\Omega_0)^2}{Mc^2} \quad (8.100)$$

Obviously  $\hbar\delta\Omega \gg \Gamma$  because of very large  $\Omega_0$  values, and hence the observation of resonance fluorescence of  $\gamma$  quanta in free nuclei is impossible. To exclude the recoil phenomenon, the nucleus should be “fixed.” This can be done by means of its location in a crystal lattice. Mossbauer was the first to realize this idea [8.96].

For the nuclei in the crystal lattice, the recoil is associated with excitation of vibrations of the lattice (phonons), quite similar to that of the electronic transition (Section 8.1), but with nuclear vibration coupling parameters instead of electron-vibration (vibronic) coupling. Of particular interest here is the zero-phonon line discussed in Section 8.2, the absorption and emission of the pure nuclear frequency  $\Omega_0$ , which is equivalent to a *recoilless transition* ( $\Omega' = \Omega'' = \Omega_0$ ).

The probability  $f$  of nuclear zero-phonon transitions, according to Eqs. (8.10) and (8.17), is strongly dependent on the vibrational spectrum of the crystal and the shift  $a$  between the equilibrium positions of the ground and excited states [Eq. (8.11)], which is much smaller for nuclear states than for electronic ones. Approximate calculations, factoring in the possible anisotropy of the crystal, shows that

$$f \sim \exp\left(-\frac{\langle X_\lambda^2 \rangle}{\lambda^2}\right) \quad (8.101)$$

where  $\langle X_\lambda^2 \rangle$  is the average squared projection of the amplitudes of the vibrations of the absorbing nucleus in the direction of propagation of the  $\gamma$  quanta and  $\lambda$  is their wavelength.

Thus *the Mossbauer effect is a resonance fluorescence of  $\gamma$  quanta realized by zero-phonon (recoilless) transitions between nuclear energy levels in crystals [nuclear  $\gamma$  resonance, (NGR)].*

### $\gamma$ -Resonance Spectra

Most important to application of the Mossbauer effect is its abovementioned high tuning accuracy,  $\Gamma/\hbar\Omega_0 \sim 10^{-11} - 10^{-12}$ , due to which a very small change in frequency of the  $\gamma$  quanta destroys the resonance fluorescence. This enables one to observe very fine effects that influence the position and shape of the zero-phonon line; it forms the basis for the method of  *$\gamma$ -resonance spectroscopy (GRS)*.

The essence of the GRS method is as follows. Consider a source of  $\gamma$  quanta—a set of nuclei (of the same element) in their excited state in a given crystal lattice, and an absorber of these quanta—the same nuclei in their ground state, but in another lattice, for instance, in another compound. Because of the influence of the local chemical environment on the position of the zero-phonon line, discussed below, the differences in frequencies of absorption  $\Omega'$  and

emission  $\Omega''$  of the nucleus may be sufficient to destroy the resonance, and the  $\gamma$  quanta emitted by the source may not be absorbed by the absorber.

The frequency of the absorption (emission) can be slightly corrected by means of the *linear Doppler effect*—the dependence of the wave frequency on the speed  $v$  of relative displacement of the emitter and the absorber. According to this effect the absorption frequency  $\Omega'$  is dependent on the projection  $v$  of the relative speed on the direction of propagation of the  $\gamma$  quanta:

$$\Omega' = \Omega_0 \left( 1 + \frac{v}{c} \right) \quad (8.102)$$

For some value of  $v = v_0$ ,  $\Omega' = \Omega''$ , and the quanta of the emitter are absorbed by the substance of the absorber. Therefore, by measuring the dependence of the intensity of absorption on the relative speed  $v$ , we obtain the curve  $I(v)$  which is called  $\gamma$ -resonance spectrum (GRS). The principle of installation for these measurements is illustrated in Fig. 8.30. The intensity  $I$  is usually measured by the number of  $\gamma$  quanta transmitted by the sample, so the spectrum in its simplest form appears as shown in this figure.

Not all the nuclei meet the requirements of NGR to be used as subjects of GRS investigation. For light nuclei the combination of very high frequencies ( $\Omega_0 \sim 300$  keV) with their small mass makes the probability of this effect negligibly small. On the other hand, heavy-atom nuclei with about 100 nuclear transitions for which NGR is possible are mostly transition metal elements that form coordination systems, and this makes the GRS method especially useful in their investigation [8.8, 8.9, 8.97, 8.98].

### Isomer Shift and Quadrupole Splitting in GRS

Unlike the electron–vibration (vibronic) interaction (Chapter 7), meaning interaction of electronic states with nuclear displacements, the electron–nucleus interaction in GRS represents the influence of electronic charge distribution and spin

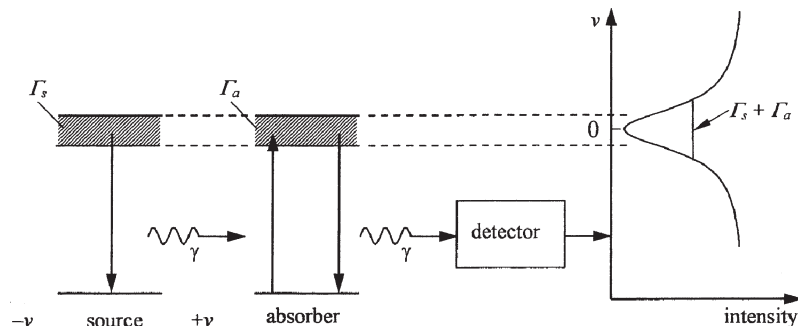


**FIGURE 8.30.** Schematic diagram of an experiment illustrating the Mossbauer effect: the  $\gamma$  quanta from the source modulated by the Doppler effect ( $v$  motion) fall in resonance with the absorber and produce a dip in the number of detected quanta as a function of  $v$ .

on the energy levels of the nucleus and resonance transitions between them. Electron–nucleus interaction can be divided into two parts: electrostatic and magnetic. *Electrostatic interactions* are determined by two main parameters of electronic structure: the electronic density on the nucleus,  $\rho_e = e|\psi(0)|^2$ , which produces the Fermi contact interaction (Section 8.4), and the *electric field gradient* (EFG) on the nucleus created by the environment.

On the other hand, the nucleus has finite dimensions, positive charge distribution with density  $\rho_N$ , spin  $\mathbf{I}$ , quadrupole moment  $Q$  for  $I \geq 1$ , and no dipole moment. If we assume that the nuclear positive charge is distributed uniformly in a sphere of radius  $R$ , then  $\rho_N = 3Ze/4\pi R^3$ , and the calculation shows that the direct electrostatic interaction of the electronic and nuclear densities shifts the nuclear energy levels by

$$\delta' = \frac{2\pi}{5} e^2 Z R^2 |\Psi(0)|^2 \quad (8.103)$$

This electrostatic energy shift is of the order of  $\sim 10^{-4}$  eV.

Since the radius  $R$  in different nuclear states is different, the shifts in the ground  $\delta'_{\text{gr}}$  and excited  $\delta'_{\text{ex}}$  states of the nuclear transition are different too, resulting in the shift of the NGR line:

$$\delta'' = \delta'_{\text{ex}} - \delta'_{\text{gr}} = \frac{4\pi}{5} e^2 Z R \Delta R |\Psi(0)|^2 \quad (8.104)$$

where we assumed that approximately  $R_{\text{ex}}^2 - R_{\text{gr}}^2 = (R_{\text{ex}} + R_{\text{gr}})(R_{\text{ex}} - R_{\text{gr}}) \cong 2R \Delta R$ ;  $\delta''$  is called *isomer shift* (or *chemical shift*) of the NGR line.

In the GRS the nucleus in the substances of the emitter and the absorber may have different environments, and hence the isomer shift of the GRS line is equal to the difference of their contributions:

$$\delta = \delta''_{\text{abs}} - \delta''_{\text{em}} = \frac{4\pi}{5} e^2 Z R \Delta R [|\Psi_{\text{abs}}(0)|^2 - |\Psi_{\text{em}}(0)|^2] \quad (8.105)$$

This is one of the basic equations that relate the line position in GRS to the electronic structure of the nucleus environment. To analyze this equation, we note that nonzero  $\psi(0)$  is caused by the contribution of the atomic *ns* orbitals only (the wavefunctions of *p, d, f, ...* states equal zero at the nucleus) and *p*<sub>1/2</sub> states in the case of very strong relativistic effects (Sections 2.1, 5.4, and 6.5). Other electrons contribute indirectly by screening the s states from the nuclei, thus reducing their  $\psi(0)$  values. Hence the chemical difference between the emitter and absorber is manifested in the isomer shift  $\delta$  only when the chemical bonds involving s electron states are different.

The second important feature of the electronic structure that influences the nuclear energy levels and the GRS, the electric field gradient (EFG)  $q^G$ , is a tensor with three components,  $q_{xx}^G$ ,  $q_{yy}^G$ , and  $q_{zz}^G$ , for which  $q_{xx}^G + q_{yy}^G + q_{zz}^G = 0$ . For a cubic environment  $q_{xx}^G = q_{yy}^G = q_{zz}^G = 0$ . In the most widespread case of axial

symmetry  $q_{zz}^G = -2q_{xx}^G = q^G$ , and the calculations yield the following equation for the shift  $W_q$  of the NGR line due to the quadrupole interaction of the EFG with the quadrupole moment of the nucleus  $Q$  [8.98]:

$$W_q = e^2 q^G Q \frac{3M^2 - I(I+1)}{4I(2I-1)} \quad (8.106)$$

Here  $M$  is the quantum number of the projection of the nuclear spin  $I$ ,  $M = I, I-1, \dots, -I$ , and  $Q = 0$  for  $I = 0, \frac{1}{2}$ . Since this quadrupole shift of the nuclear energy levels is different for different spin projections  $M$ , it leads to *quadrupole splitting*. For instance, the nuclear state with a spin  $I = \frac{3}{2}$  has four component states with  $M = \frac{3}{2}, \frac{1}{2}, -\frac{1}{2}, -\frac{3}{2}$ . Their quadrupole shift is

$$\begin{aligned} W_q^{\pm 1/2} &= -\frac{1}{4} e^2 q^G Q \\ W_q^{\pm 3/2} &= \frac{1}{4} e^2 q^G Q \end{aligned}$$

Hence the nuclear term  $I = \frac{3}{2}$  under the EFG influence of the electronic environment with axial symmetry is split into two components (Fig. 8.31); the splitting  $\Delta$  is

$$\Delta = W_q^{\pm 3/2} - W_q^{\pm 1/2} = \frac{1}{2} e^2 q^G Q \quad (8.107)$$

The quadrupole splitting  $\Delta$  is of the order of  $\sim 10^{-7}$  eV.

For many of the NGR transitions studied, the ground-state spin is  $I = \frac{1}{2}$  and the excited one is  $I = \frac{3}{2}$  (this is the situation in the  $^{57}\text{Fe}$  nucleus, which is most widespread in GRS). As mentioned above, the state  $I = \frac{1}{2}$  has no quadrupole moment; hence only the excited state  $I = \frac{3}{2}$  is split in the field of axial symmetry. This quadrupole splitting can be observed in the absorption of  $\gamma$  quanta as two lines at a distance  $\Delta$  from each other (Fig. 8.31). If the symmetry is lower than axial, then  $q_{xx}^G \neq q_{yy}^G \neq q_{zz}^G$ , and the quadrupole splitting is ( $q$  is the largest component):

$$\Delta = \frac{1}{2} e^2 |q^G Q| \left(1 + \frac{1}{3} \eta^2\right) \quad (8.108)$$

where  $\eta = (q_{yy}^G - q_{xx}^G)/q_{zz}^G$  is the *asymmetry constant*.

Equations (8.106)–(8.108) show that the quadrupole splitting in GRS is related to the electronic structure of the system via the EFG produced by the latter on the nucleus. Unlike  $s$  electrons, which create an isotropic density on the nucleus and zero EFG, each of the  $p, d, f, \dots$  electrons separately produces a nonzero EFG with three components for which, as above,  $q_{xx}^G + q_{yy}^G + q_{zz}^G = 0$ . Equivalent electrons in the same shell have the same three absolute EFG values, but they are differently oriented in space with respect to the three axes; in a closed shell they complement each other to form a spherical symmetric distribution with a zero EFG. In lower symmetry produced by other atoms of the environment, the

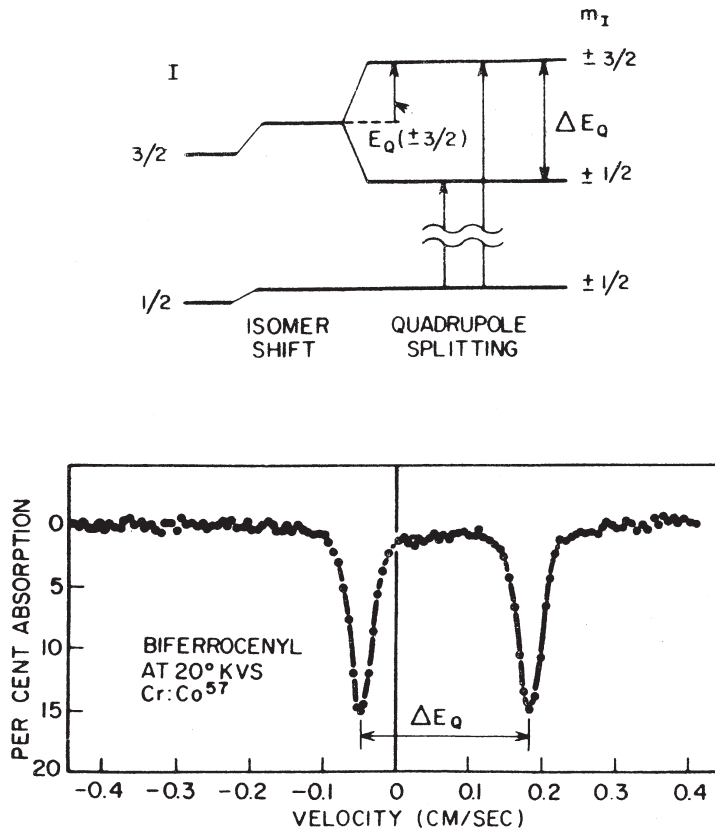


**FIGURE 8.31.** Isomer shift and quadrupole splitting of the nuclear ground ( $I = \pm \frac{1}{2}$ ) and excited ( $I = \pm \frac{3}{2}$ ) energy levels of  $^{57}\text{Fe}$  and the  $\gamma$ -resonance absorption of biferrocenyl.

equivalence of the electrons in the same shell is destroyed (even when it is a closed shell) because they participate in the formation of different MOs, thus acquiring different occupation numbers  $g_{ik}$ . The following approximate formula accounts for this:

$$q^G = \sum_{i,k} g_{ik} q_i^G (1 - R_i) \tag{8.109}$$

where  $q_i^G$  is the EFG produced by the electron on the  $i$ th AO, and  $R_i$  is the so-called Sternheimer antiscreening parameter ( $1 > R_i > 0$ ); it takes into account the polarization of the inner shell by the  $i$ th electron, which lowers the EFG value. As for the atomic electron with quantum numbers  $n, l, m$ , (Section 2.1), the EFG is shown to be as follows:

$$q_{lm}^G = 2e\langle r^{-3} \rangle_{nl} \frac{3m^2 - l(l+1)}{(2l+1)(2l-1)} \tag{8.110}$$

where

$$\langle r^{-3} \rangle_{nl} = \int R_{nl}^2(r) r^{-3} d\tau \quad (8.111)$$

In particular, for a  $p$  electron  $q_{11}^G = 2e\langle r^{-3} \rangle_{np}$ , while for a  $d$  electron  $q_{22}^G = (4e/5)\langle r^{-3} \rangle_{nd}$ , and  $\langle r^{-3} \rangle_{np}$  is much larger than  $\langle r^{-3} \rangle_{nd} \approx 4.8$  au ( $\langle r^3 \rangle_{np}$  is much smaller than  $\langle r^3 \rangle_{nd}$ ).

Equation (8.106) does not include the EFG produced by the atomic charges of other atoms in the environment, the crystal field corrections. The latter are usually small and can be ignored if the main contribution (8.106) is nonzero; otherwise they are of first order. Note also that the probability of the Mossbauer effect (8.101) for the two components of the quadrupole splitting may be different, resulting in asymmetric spectra.

For systems in degenerate electronic states with strong vibronic coupling resulting in several equivalent minima of the APES and tunneling between them (Section 7.4), the quadrupole splitting is subject to further complications [8.26].

### Hyperfine Splitting

The magnetic influence of the electronic shell on the nuclear energy levels  $W_H$  is, in fact, a nuclear Zeeman effect (Section 8.4). Considering the magnetic field of the electronic motion  $\mathcal{H}$  as an external (to the nucleus) field,  $W_H$  can be written as

$$W_H = -g_N \beta_N (\mathcal{H}, \mathbf{I}) \quad (8.112)$$

where  $g_N$  and  $\beta_N$  are the nuclear  $g$  factor (Section 8.4) and nuclear Bohr magneton, respectively. The operator of the magnetic field  $\mathcal{H}$  can also be presented in a general way [8.57]:

$$\mathcal{H} = \frac{-8\pi}{3} |\psi(0)|^2 \mathbf{S} - \frac{\beta \mathbf{L}}{r^3} - \frac{3(\mathbf{r}, \mathbf{S})\mathbf{r}}{r^5} + \frac{\mathbf{S}}{r^3} \quad (8.113)$$

The first term represents the Fermi contact interaction (cf. Section 8.4) of the electron spin  $\mathbf{S}$  with the nuclear spin, the second term gives the magnetic influence of the orbital motion with the moment  $\mathbf{L}$ , and the last two terms describe the magnetic dipole–dipole (spin–spin) influence.

Under the influence of the interaction (8.112) considered as a small perturbation, the nuclear energy levels  $E_M$  (which are degenerate with respect to the magnetic quantum number  $M$ ) split under the Zeeman effect (quite similar to the electronic Zeeman splitting):

$$E_M = \frac{\mu}{I} M \mathcal{H} \quad M = I, I-1, \dots, -I \quad (8.114)$$

where  $\mu = g_N \beta_N I$  is the magnetic moment of the nucleus. This splitting ( $\sim 2 \times 10^{-7}$  eV) results in the *magnetic hyperfine structure* of the GRS.

Obviously, the observation of the magnetic hyperfine structure is possible only if the line spacing  $\mu \mathcal{H}/I$  is larger than the line width  $2\Gamma$ . The latter rapidly increases with temperature, due to fast *relaxation transitions*. In the intensity of the magnetic field of the nucleus environment given by Eq. (8.113), the Fermi contact term (originating from the atomic *s* states with unpaired electrons or spin-polarized *s* pairs with decompensated spin) gives the largest contribution to the magnetic hyperfine interaction. The dipole-dipole interaction depends on the direction of the spin **S**. In free molecular systems there is no definite direction of **S**. In paramagnetic substances the spin may perform rapid relaxations (changes of spatial orientation), leading to a corresponding reduction in the averaged field. Since relaxation rates increase with temperature, the spectrum is temperature-dependent, and the hyperfine structure may appear at lower temperatures. Example 8.13 illustrates this effect in GRSs of iron complexes.

### EXAMPLE 8.13

#### *Magnetic Hyperfine Structure in GRS of Coordination Compounds with a $^{57}\text{Fe}$ Nucleus*

As mentioned above, the ground state of  $^{57}\text{Fe}$  has spin  $I = \frac{1}{2}$  with two levels with  $M = \pm \frac{1}{2}$ , and the excited state  $I = \frac{3}{2}$  has four levels with  $M = \pm \frac{1}{2}, \pm \frac{3}{2}$ . The spacing of these levels  $(\mu/I)\mathcal{H}$  depends on the magnetic moment of the nucleus  $\mu$ , which may be different in the ground ( $\mu_1$ ) and excited ( $\mu_2$ ) states. The magnetic dipole transitions are allowed for  $\Delta M = 0, \pm 1$ . Therefore, when  $\mu_1 \neq \mu_2$ , there are six transitions with different frequencies (Fig. 8.32), whereas for  $\mu_1 = \mu_2$  there are only three, and for  $\mu_1 = -\mu_2$  the number of lines is five. In an isotropic polycrystalline sample the intensities of the six lines for  $\mu_1 \neq \mu_2$  emerge in the ratio 3 : 2 : 1 : 1 : 2 : 3, where from left to right the two groups of three lines of emission transitions to the ground states  $I = \frac{1}{2}$  and  $I = -\frac{1}{2}$ , respectively, are listed. Figure 8.33 shows a typical spectrum of this kind obtained for iron dithiocarbamate, in which the dependence of the hyperfine splitting on temperature is seen explicitly [8.99].

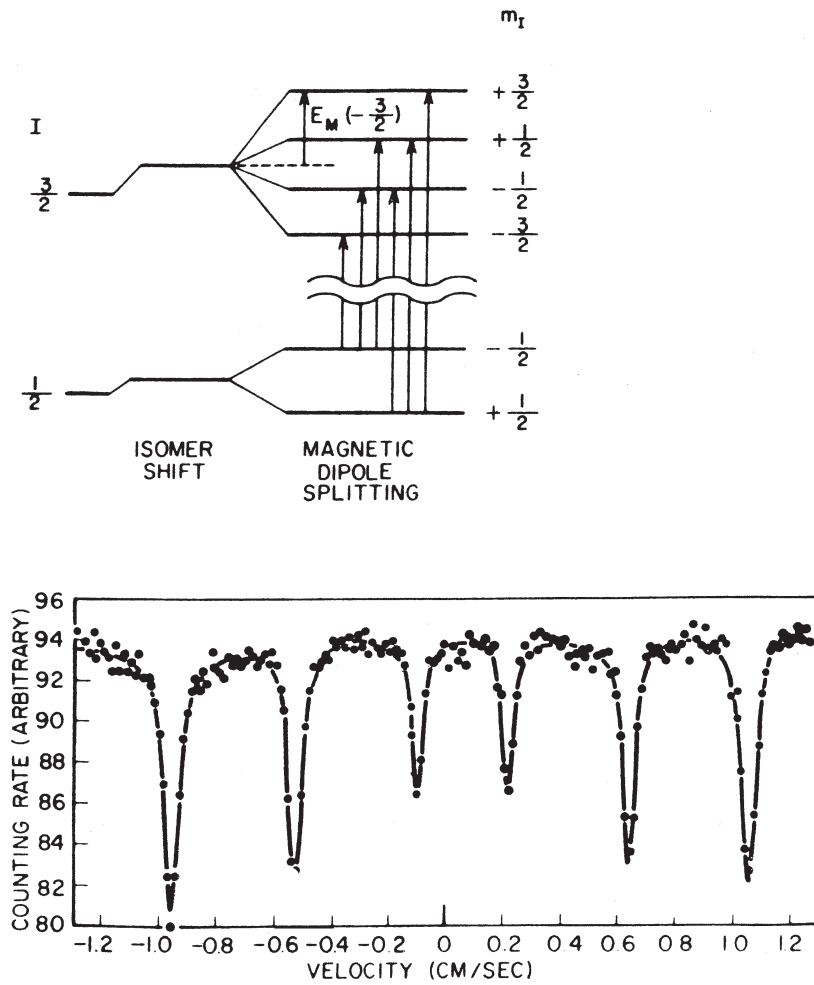


**FIGURE 8.32.** Hyperfine splitting of the nuclear ground state with  $I = \frac{1}{2}$  and excited state with  $I = \frac{3}{2}$  of  $^{57}\text{Fe}$  in magnetic fields and the corresponding  $\gamma$ -resonance absorption spectrum. The six magnetic-dipole allowed transitions with  $\Delta m = \pm 1$  are shown by arrows.



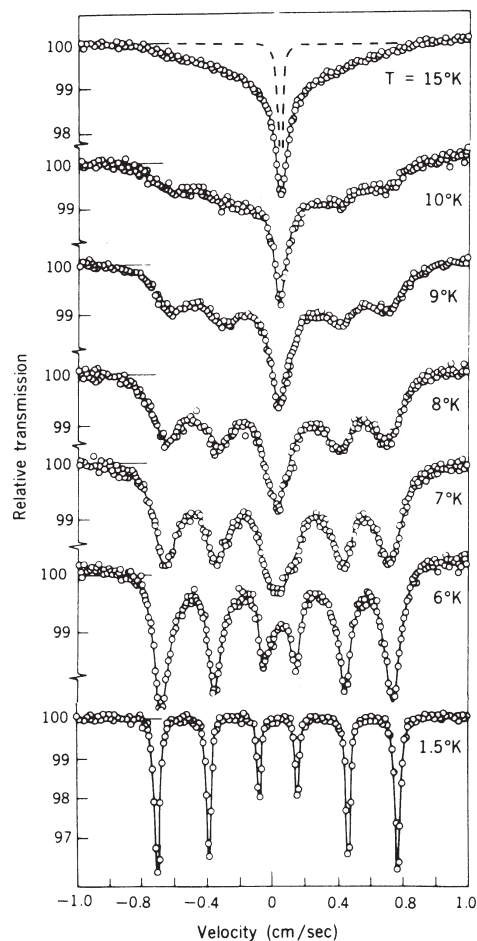


**FIGURE 8.33.**  $\gamma$ -resonance absorption spectrum of  $\text{Fe}^{57}$  in a high-spin dithiocarbamate at different temperatures from 1.5 to 15 K. At low temperatures the spin relaxation is slow and the six lines of the spectrum are well resolved, as in a static external field (Fig. 8.32). At higher temperatures the rapid fluctuations of the spin average out the hyperfine pattern and only one broad line is seen. The dashed line shows the expected absorption without hyperfine broadening.

The spin  $S$  has a fixed orientation in spin-ordered systems (with ferromagnetic, antiferromagnetic, ferrimagnetic, etc., ordering; Section 8.4); hence the hyperfine splitting can be observed at any temperature in such systems, provided that the inequality  $(\mu\mathcal{H}/I) > 2\Gamma$  holds.

Example 8.14 demonstrates applications of GRS to the study of spin crossover in coordination systems.

**EXAMPLE 8.14****Observation of Spin Crossover in the  $\gamma$ -Resonance Spectrum of  $[\text{Fe}(\text{phen})_2(\text{NCS})_2]$** 

Figure 8.34 shows several GRS of  $[\text{Fe}(\text{phen})_2(\text{NCS})_2]$  (phen = phenanthroline) in the crystal phase obtained at different temperatures

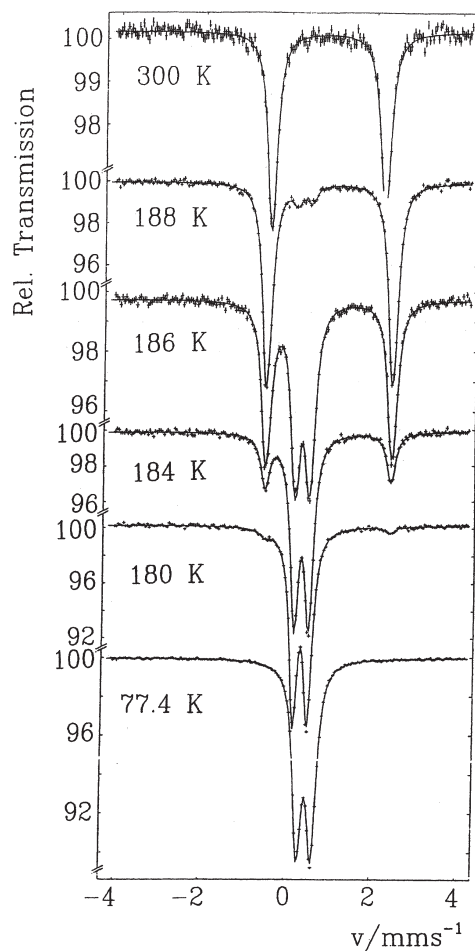


**FIGURE 8.34.**  $\gamma$ -resonance absorption spectrum of  $\text{Fe}^{57}$  in a spin crossover system  $[\text{Fe}(\text{phen})_2(\text{NCS})_2]$  at several temperatures from 77.4 to 300 K showing an abrupt change of the quadrupole splitting due to the LS  $\rightarrow$  HS spin transition at 185 K (in the HS configuration the quadrupole splitting is larger). Between  $\sim 184$  and 186 K the two spin states coexist. From [8.97].)

from 77 to 300 K [8.97]. At low temperatures a small quadrupole splitting is seen, which at approximately 185 K almost abruptly changes to a much larger one. Together with magnetic measurements this proves that at this temperature a spin crossover (Section 8.4) takes place from the electronic low-spin state [the  $^1A_1$  state of the valence  $(t_{2g})^6$  configuration of Fe(II)] to the high-spin state ( $^5T_2$  state of the  $(t_{2g})^4(e_g)^2$  configuration), and this crossover takes place in the form of a phase transition like that shown in Fig. 8.27. A small hysteresis of several kelvins (where the two phases coexist) is also seen in the spectra near the transition at 185 K.

## 8.6. ELECTRON CHARGE AND SPIN DENSITY DISTRIBUTION IN DIFFRACTION METHODS

Experimental determination of electron density distribution in molecular solids has reached a high level of accuracy. For molecules containing only light atoms, the charge densities observed are in good agreement with sophisticated theoretical calculations. For organic and main-group compounds the densities can be predicted, at least qualitatively, from simple valence bond models. This is not the case for transition metal compounds, where the participation of  $d$  electrons and their three-dimensional delocalization about the CA (Sections 1.2 and 6.1) makes the expected electron density distribution far less obvious. Therefore, the experimental evaluation of electron distribution, together with its theoretical interpretation, is an important approach to investigation of the electronic structure of transition metal coordination compounds.

Electron densities are usually determined by X-ray or neutron scattering. The technical problems in the experiment itself lie beyond the scope of this book; they can be found elsewhere [8.10, 8.100]. Here it is worthwhile to emphasize that in transition metal complexes, as distinct from light-atom compounds, the valence electron distribution contributes a smaller fraction to the total X-ray scattering, thus decreasing the accuracy of the experimental results. Also, experimental problems, such as errors in the corrections for absorption and extinction, become more significant when transition metal or other heavy atoms are present. Nevertheless, the accuracy of such experiments improves continuously.

### The Method of Deformation Density

The data of high-resolution X-ray intensity measurements are usually presented by a set of experimental *structure factors*  $F_{\text{obs}}$  with phases obtained from a model structure. The structure factors  $F(\mathbf{S})$  are defined as a Fourier transform of the

charge density  $\rho(\mathbf{r})$  (Section 5.2) [8.10]:

$$F(\mathbf{S}) = \int \rho(\mathbf{r}) \exp[2\pi i(\mathbf{S} \cdot \mathbf{r})] d\mathbf{r} \quad (8.115)$$

where the integration is expanded over the unit cell,  $\mathbf{S}$  is the scattering vector perpendicular to the diffraction plane,  $S = 2 \sin \theta / \lambda$ ,  $\theta$  is the scattering angle, and  $\lambda$  is the X-ray wavelength. If the structure factors  $F_{\text{obs}}$  are known, the inverse transform allows one to determine the charge density:

$$\rho(\mathbf{r}) = \frac{1}{V} \sum_{\mathbf{S}} F_{\text{obs}}(\mathbf{S}) \exp[-2\pi i(\mathbf{S} \cdot \mathbf{r})] \quad (8.116)$$

Here the integral is replaced by a summation over the amplitudes of all diffraction beams allowed by Bragg's law. In simple centrosymmetric structures the phases in (8.116) are known, whereas in more complicated (acentric) structures they can be obtained from a model structure; in this case the densities  $\rho(\mathbf{r})$  remain model-dependent.

The electron density redistribution produced by the chemical bonding can be characterized by the *deformation density* (DD), defined as the difference  $\Delta\rho$  between the density of the compounds under consideration  $\rho(\mathbf{r})$  and that of the free atoms that occupy the same position as in the compounds  $\rho_{\text{ref}}(\mathbf{r})$ ,  $\Delta\rho = \rho(r) - \rho_{\text{ref}}(r)$  [Section 5.2, Eq. (5.15)]. In terms of the X-ray experiments the DD is

$$\Delta\rho = \frac{1}{V} \sum_{\mathbf{S}} (F_{\text{obs}} - F_{\text{ref}}) \exp 2\pi i(\mathbf{S} \cdot \mathbf{r}) \quad (8.117)$$

where  $F_{\text{ref}}$  are the structure factors of a superposition of neutral, usually spherical atoms (however, see below).

The DD  $\Delta\rho(\mathbf{r})$  can also be obtained by calculations. In this case both  $\rho(\mathbf{r})$  and  $\rho_{\text{ref}}(\mathbf{r})$  are computed using the methods described in Section 5.3. The densities  $\rho_{\text{ref}}$  of the free atoms in ground states are known (and tabulated), and the accuracy of  $\Delta\rho$  is determined completely by the approximations employed in the calculation of  $\rho(\mathbf{r})$  after (5.13). The  $\Delta\rho$  values are usually illustrated by means of *deformation density maps*, in which the lines of equal density are given with a definite spacing, and with the full lines for positive  $\Delta\rho$  values and dashed lines for negative ones.

The knowledge of the DD  $\Delta\rho$  allows one to reveal, at least in principle, the electron redistribution due to the formation of the compound, and to relate it to the bonding. However, to do so in practice, many difficulties emerge. Most of them are related to the inaccuracy of the measurements and/or calculations. As mentioned above, in coordination compounds  $\Delta\rho$  is a small difference between two large quantities [Eqs. (8.117), (5.15)], and hence to determine  $\Delta\rho$  with a high degree of accuracy, the value  $\rho(\mathbf{r})$  must be obtained with a much higher accuracy.

Meanwhile, the experimental resolution in diffraction methods is limited, and so are the calculation possibilities [8.101].

The experimental limitations are due to side effects in intensity measurements (absorption, extinction, multiple scattering, etc.), scaling of intensities, phasing of structure amplitudes, series truncation, and so on. The theoretical calculations are usually constrained by the adiabatic approximation (Section 7.1), neglect of relativistic effects, finite basis set, and correlation effects (Chapter 5). Additional errors are introduced by the neglect of molecular and crystal vibration (temperature smearing).

The results on DD  $\Delta\rho$ , as mentioned above, are usually given in deformation density maps. Information on electronic structure can be extracted from these maps by three approaches: (1) direct inspection, (2) modeling with deformation functions, and (3) comparison with theoretical calculations.

*Direct inspection* of the experimental DD map enables us to make some qualitative conclusions about the bonding features. In general, positive DD (increase in density as compared with nonbonded atoms) are expected in the region of covalent bonds and strong electronegative atoms. Often, density peaks are associated with bonding and nonbonding lone pairs. In many cases sharp peaks are also observed around transition metals with partially filled  $d$  orbitals because their electron distribution, matching the occupied  $d$  states, is nonspherical. Example 8.15 provides for some further details.

### EXAMPLE 8.15

#### *Deformation Density in Sodium Nitroprusside (Direct Inspection)*

As a simple example we consider the qualitative conclusions from direct inspection of the DD maps for the slightly distorted octahedral anion  $[\text{Fe}(\text{CN})_5\text{NO}]^{2-}$  of sodium nitroprusside [8.102]. Figure 8.35 shows the main features of the DD in two sections including the axial (CN—Fe—NO) (Fig. 8.35a) and equatorial (CN—Fe—CN) (Fig. 8.35b) coordinates. First we note the maxima *A* near the CA situated in between the ligand coordinates. These maxima correspond to the occupied  $d_{xy}$  orbital; in the crystal field approximation the high-spin  $3d$  orbital configuration in the tetragonally distorted octahedron is (Section 4.3, Fig. 4.5):  $d_{xy}^2 d_{xz}^1 d_{yz}^1 d_{z^2}^1 d_{x^2-y^2}^1$ . The decreasing density along *B* near the CA and the maxima in between Fe and C indicate the  $\sigma$  bonds between the iron AO  $d_{x^2-y^2}$  and carbon. The minimum of DD ( $\sim -0.30 \text{ e } \text{\AA}^3$ ) at point *C* near the Fe atom extended to about  $2 \text{ \AA}$  in the  $z$  direction toward the NO ligand is due to the bonding of the  $d_{z^2}$  AO with the axial ligands, which is stronger for NO (the atom Fe is  $0.185 \text{ \AA}$  out of plane toward NO). Along all the ligands and beyond the distal nitrogen there are maxima of the DD indicating

the bonding areas and lone pairs, respectively (beyond oxygen there is no lone pair). This picture of bonding is in qualitative agreement with electronic structure calculations and Mossbauer spectra.

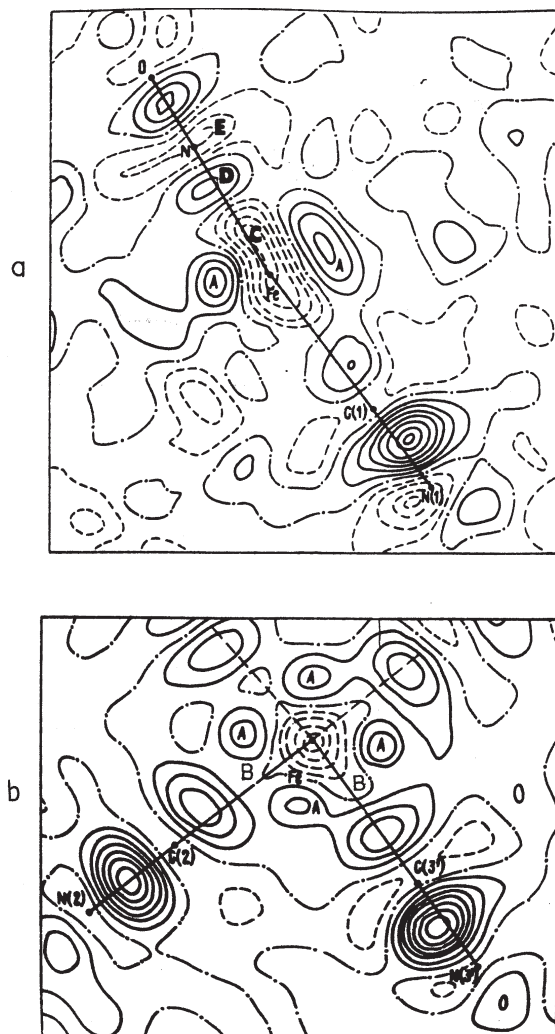


**FIGURE 8.35.** DD maps for Na<sub>2</sub>[Fe(CN)<sub>5</sub>NO]: (a) section in the plane comprising the CA Fe and the axial ligands NO and CN; (b) section in the equatorial plane of Fe and CN groups (only two CN groups are shown). Dashed lines show  $\Delta\rho < 0$ , while dotted-dashed lines correspond to  $\Delta\rho = 0$ . Line spacing is equal to  $0.1 e \text{ \AA}^{-3}$  (From Antipin and Struchkov [8.102].)

However, in general, a direct correlation between density accumulation and bonding may be wrong, especially when a negative DD is attributed to the absence of bonding. To understand this statement, consider a simple example of the diatomic molecule  $F_2$ . In the free atoms all the valence  $p$  states have the same occupation,  $\frac{5}{3}$  electrons each. Through interaction, the two  $p_\sigma$  orbitals from the two atoms form one bonding MO and one antibonding MO; the former only being occupied by two electrons in the ground state. Hence the DD value in the bonding region is approximately  $2 - 2\left(\frac{5}{3}\right) = -\frac{4}{3}$  electrons.

Thus, *despite the two-electron bonding, the deformation density in the bonding region is negative!* This misleading presentation emerges in all the cases when there is a bond between atoms with almost completed electronic shells. In particular, this is expected in the case of metal–metal bonds when the metal  $d$  shell is occupied in more than half.

These misleading conclusions about the DD method are obviously due to the wrong idea that before entering the bonding the atoms are spherical symmetric. To understand the situation, consider again the abovementioned example of the  $F_2$  molecule. The free fluorine atom has the electronic configuration  $1s^2 2s^2 2p^5$  with a  $p$  hole in the spherical symmetric electron distribution that can occupy any of the three  $p$  states:  $p_x, p_y, p_z$ . Provided that there are no external perturbations, these three one-electron states are equivalent (threefold degeneracy), the hole can occupy any of them or their linear combination with the same probability. As stated in Section 2.1, in the case of degeneracy the real charge distribution remains uncertain until there is an external perturbation that removes the degeneracy (such perturbation is also created by any attempt to observe the charge distribution).

However, *uncertainty (arbitrariness) of the  $p$ - (or other one-electron) state orientation in space does not mean averaged spherical symmetric distribution*, although sometimes such a model can be justified. For atoms in molecules the uncertain atomic degenerate orbital orientation becomes quite definitive before the bonding. The threefold-degenerate  $p$  states of the fluorine atom in the axial field of the other atom split into two levels,  $\Sigma$  and  $\Pi$  (in  $C_{\infty v}$  symmetry), and it can be easily shown that the ground state is  $\Sigma$ , which corresponds to the  $p_\sigma$  hole (the  $p_\sigma$  orbital occupied by one electron). This is the *correct zeroth-order function in the case of degeneracy* [8.103].

These zeroth-order states are just a *correct presentation of the interacting atoms before any density redistribution*. They correspond to the lowest energy configuration of the atom in a given field symmetry. Hence there are only two electrons in the two atomic  $p_\sigma$  states of the two free atoms that form the  $F_2$  molecule, instead of the  $2\left(\frac{5}{3}\right) = \frac{10}{3}$  electrons in the approximation of averaged spherical symmetric charge distribution. As a result of the MO bonding produced by these two  $p_\sigma$  AOs, the charge density increases in the bonding area (Section 5.2), and the deformation density in between the atoms increases, as anticipated. It can be shown that when the atomic shell is less than half-full, the spherical density approximation overestimates the deformation density in the bonding area.

It follows that the approximation of spherical densities of free atoms with open shells is ungrounded and may be misleading. For these systems the correct

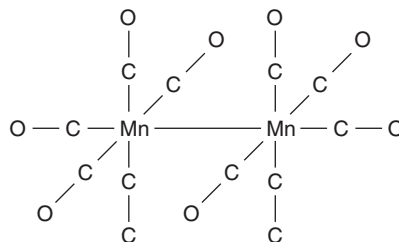
zeroth-order states should be obtained first (this can be done easily by symmetry considerations, as in the example above), and then the free-atom densities can be defined from these states. In other words, the free-atom densities  $\rho_{\text{ref}}$  should be prepared before being subtracted from the measured densities to result in DD.

The failure of the spherical density assumption is a part of a more general failure of the DD approach when used to clarify the origin of chemical bonding without *specification of the reference density*, with respect to which the deformation density is determined. As discussed in Section 6.1, coordination bonds are seldom localized, and each metal–ligand bond is strongly dependent on the other bonds formed by the metal. Therefore, atom deformation densities are not sufficiently informative for each metal–ligand bond taken apart. To examine such a bond, the *fragment deformation density*, that is, the difference between the total density and the densities of the ligand and the fragment taken as a whole (including the metal with the other ligands), should be studied instead of atom deformation densities. An example of fragment DD study is given in Example 8.16.

### EXAMPLE 8.16

#### *Metal–Metal Bonding in $\text{Mn}_2(\text{CO})_{10}$ ; Fragment Deformation Density [8.104]*

This is an example of *calculated DD* which, in addition to elucidation of the electronic origin of the metal–metal bond, demonstrates the advantages of the fragment deformation density studies. The structure of  $\text{Mn}_2(\text{CO})_{10}$  in the eclipsed configuration is



(although the staggered conformer was found in the solid state, the energy difference and the rotation barrier between the two conformers, staggered and eclipsed, is very small [8.104]). For this configuration, the electron density distribution, as well as atomic deformation density (total density minus spherical atoms) and fragment deformation density (total minus two fragments) were calculated by the Fenske–Hall method (Section 5.4). The results are presented in Fig. 8.36.



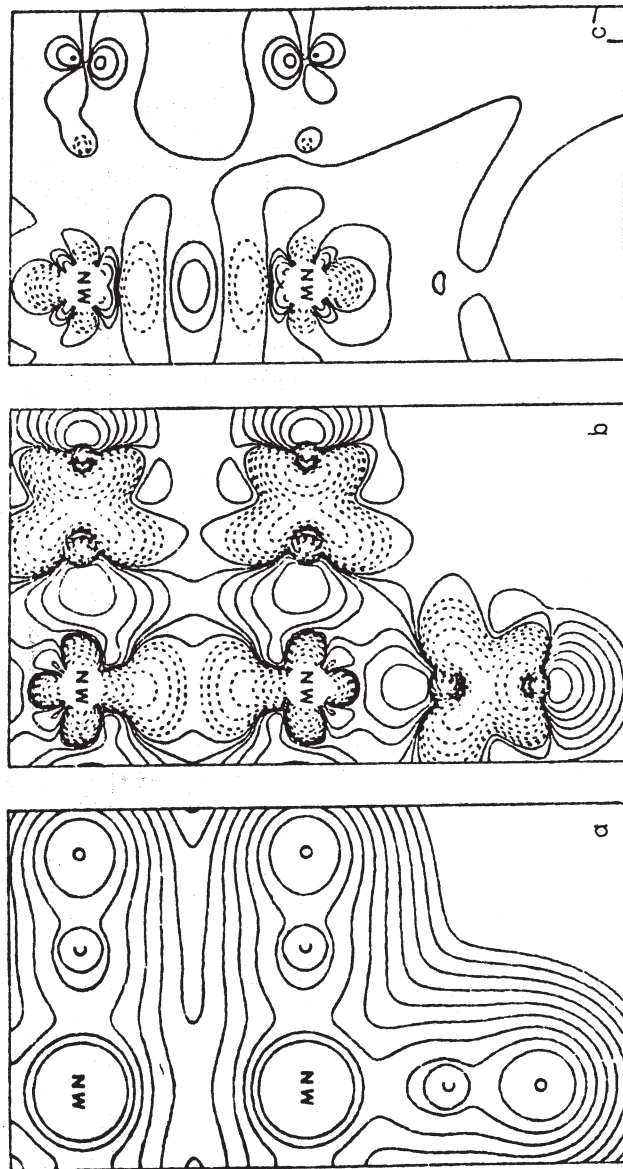


**FIGURE 8.36.**  $\text{Mn}_2(\text{CO})_{10}$  density maps: (a) total density; (b) atom deformation density; (c) fragment deformation density. (After Hall [8.104].)

The fragment DD is equal to the difference between the total density and the density of the two  $\text{Mn}(\text{CO})_5$  fragments. As mentioned above, owing to the three-dimensional center-delocalized nature of the coordination bond discussed in Section 6.1, the atom deformation density may be less informative with respect to the metal–metal bond than the fragment deformation density. Figure 8.36 confirms this expectation. Indeed, the atomic deformation density (Fig. 8.36b) shows a net loss of density between the two manganese atoms where we expect to find the Mn–Mn bond. In the fragment deformation density (Fig. 8.36c) there is a definitive density accumulation along the Mn–Mn line demonstrating the formation of the metal–metal bond between the two prepared fragments.

This example confirms that, as discussed above, to ensure an adequate answer about the bonding origin from DD data the question must be correctly formulated and the bonding species, atoms or fragments, should be properly prepared. As seen from Fig. 8.36b, the deformation density in the region between the atoms C and O is also negative. This may be due to the approximation of spherical free atoms (the atomic shell of oxygen is more than half occupied). Another reason is the minimal basis set used in calculations of the electronic density, which is known to overemphasize the lone pairs beyond the bond [8.104]. Formation of the Mn–C bonds is also seen.

The fact that charge accumulation in the region between the bonding atoms is not the only cause of chemical bonding (the other one is the reduction of the kinetic energy) is of general importance for the deformation density methods. It means that if there is accumulation of charge (positive  $\Delta\rho$ ) in the bonding region, it can serve as an indication of bonding, but  $\Delta\rho \sim 0$  (or even  $\Delta\rho < 0$ ) does not indicate that there is no bonding at all, especially in cases of delocalized bonds. For coordinated ligands, multiorbital bonds and orbital charge transfers in opposite directions are important (Sections 6.3 and 11.2).

Unfortunately, in many (perhaps most) studies on DD these important ideas, especially the failure of the atomic spherical densities, are not paid due attention, and interpretation of the results thus are not sufficiently informative or may even be misleading.

For quantitative interpretation of the experimental results on DD, the method of *density modeling* can be used. The idea is to present the electron density  $\rho(\mathbf{r})$  approximately by a finite number of analytical probing functions  $g_i(\mathbf{r})$ , with corresponding coefficients  $C_i$  (populations)

$$\rho(\mathbf{r}) = \sum_i C_i g_i(\mathbf{r}) \quad (8.118)$$

where the  $C_i$  values are determined by least-squares refinement of the X-ray data along with the usual crystallographic parameters (scale factor, positions, thermal parameters, extinctions, etc.). In particular, if the functions  $g_i(\mathbf{r})$  have an explicit physical meaning, the model presentation (8.118) allows one to reveal some features of the electron distribution.

For coordination compounds, it is reasonable to model the electron density by  $d$ -electron distributions, which means taking the corresponding  $d$ -electron spherical harmonics  $Y_{lm}$  as the probing functions  $g_i(\mathbf{r})$ . A simple consideration [8.105] shows that in the crystal field approximation the metal density  $\rho_M$  can be presented as

$$\rho_M = \rho_{\text{core}} + C_{4s}\rho_{4s} + R(r) \sum_{l,m} C_{lm} Y_{lm} \quad (8.119)$$

where  $\rho_{\text{core}}$  includes the density of  $K$ ,  $L$ , and  $M$  shells;  $C_{4s}$  is the population of the  $4s$  orbital; and the last term denotes the  $d$  densities  $\rho_d$ . On the other hand, the latter densities can be represented by the sum of the squares of the atomic  $d$  functions with appropriate occupancies  $q_m$ :

$$\rho_d = [(R_2(r))]^2 \sum_m q_m (Y_{lm})^2 \quad (8.120)$$

Determining the  $C_{lm}$  coefficients from the experimental data and using the known decomposition  $(Y_{lm})^2 = \sum_{l'm'} A_{lm'l'm'} Y_{l'm'}$ , one can evaluate the occupancy numbers  $q_m$ . Example 8.18 illustrates the application of density modeling to some iron and cobalt systems.

### EXAMPLE 8.17

#### *Density Modeling for Fe(II)–Phthalocyanine and Co(II)–Tetraphenylporphyrin*

These examples are given to demonstrate the possibilities of density modeling in the study of electronic structure and bonding by the DD method. The DD for these two compounds have been obtained from diffraction experiments and then presented as fractions of the  $d$ -orbital densities using the formulas in the text.

In Fe(II)–phthalocyanine [8.106] and Co(II)–tetraphenylporphyrin (CoTPP) [8.105] the polyhedron around the CA is square-planar for which the  $d$ -orbital ordering is  $d_{yz}d_{xz}d_{z^2}d_{xy}d_{x^2-y^2}$  (Sections 4.2 and 4.3, Fig. 4.5). In the spherical atom high-spin configuration these orbitals are equally occupied by 1.2 electrons each in the iron complex, and 1.4 in the cobalt complex. In the low-spin configuration the spherical atoms have the configurations  $d_{yz}^2 d_{xz}^2 d_{z^2} d_{xy}^0 d_{x^2-y^2}^0$  and  $d_{yz}^2 d_{xz}^2 d_{z^2} d_{xy}^{0.5} d_{x^2-y^2}^{0.5}$  for Fe(II) and Co(II), respectively.

However, the prepared oriented (nonspherical) atoms that have the lowest energy in the square planar field are  $d_{yz}^{1.5}d_{xz}^{1.5}d_{z^2}^1d_{xy}^1d_{x^2-y^2}^1$  for Fe(II) and  $d_{yz}^2d_{xz}^2d_{z^2}^1d_{xy}^1d_{x^2-y^2}^1$  for Co(II). The DD analysis should be carried out with respect to these prepared atom densities. Tables 8.11 and 8.12 illustrate the relevant data, including spherical atom reference densities for comparison. It is seen that there is a considerable orbital charge transfer from the field-oriented  $d_{xz}$ ,  $d_{yz}$ ,  $d_{x^2-y^2}$  orbitals of the iron ion (0.3–0.4 electron from each) to the phthalocyanine and a backdonation of  $\sim 0.7$  electron to the planar  $d_{xy}$  orbital; similar charge transfers but smaller in magnitude also occur in the case of CoTPP. Larger charge transfers to and from the CA in iron phthalocyanine as compared with CoTPP can be understood if one takes into account the larger *redox capacitance* (Section 10.1) of phthalocyanine, as compared with the TPP system.

**TABLE 8.11. *d*-Orbital Occupancies  $q_m$  and the Deformation Density (DD) of Fe(II)–Phthalocyanine as Determined from X-Ray Electron Densities in Comparison with Those in the Free Spherical (SPH) Ion Model and the Field-Oriented (OR) One<sup>a</sup>**

<i>d</i> AOs	$q_m$ , exp (Molecule)	$q_m$ (Atom, SPH)	DD (Incorrect)	$q_m$ (Atom, OR)	DD (Correct)
$d_{yz} + d_{xz}$	2.12	2.40	−0.28	3.00	−0.88
$d_{z^2}$	0.93	1.20	−0.27	1.00	−0.07
$d_{xy}$	1.68	1.20	0.48	1.00	0.68
$d_{x^2-y^2}$	1.70	1.20	0.50	1.00	0.70

<sup>a</sup>The  $q_m$  values in the SPH model of the free ions are taken for the high-spin configuration. The incorrect DD values in this case are due to the (rather widespread) wrong presentation of the orbital occupancies before the charge redistribution by bonding.

**TABLE 8.12. *d*-Orbital Occupancies  $q_m$  and the Deformation Density (DD) of Co(II)–Tetraphenylporphyrin as Determined from X-Ray Electron Densities in Comparison with Those in the Free Spherical (SPH) Ion Model and the Field-Oriented (OR) One<sup>a</sup>**

<i>d</i> AOs	$q_m$ , exp (Molecule)	$q_m$ (Atom, SPH)	DD (Incorrect)	$q_m$ (Atom, OR)	DD (Correct)
$d_{yz} + d_{xz}$	3.7	2.80	0.90	4.00	−0.30
$d_{z^2}$	1.0	1.40	−0.40	1.00	0.00
$d_{xy}$	1.3	1.40	−0.10	1.00	0.30
$d_{x^2-y^2}$	1.00	1.40	−0.40	1.00	0.00

<sup>a</sup>The  $q_m$  values in the SPH model of the free ions are taken for the high-spin configuration. The incorrect DD values in this case are due to the (rather widespread) wrong presentation of the orbital occupancies before the charge redistribution by bonding.

Note that density modelling (8.119) is based on the crystal field theory and hence is rather qualitative. Therefore, the values of the charge transfers in Table 8.11 in Example 8.17 cannot pretend to quantitative interpretation of the DD data. This interpretation is also complicated by the low accuracy of the X-ray density measurement, mentioned above.

The idea of electronic densities was used to specify the notion of the *atom in molecules*. It is obvious that by formation of chemical bonds a significant part of the atomic electrons become collectivized (Section 1.2) and the atom loses its individual properties. Therefore, the notion “atom in molecules,” strictly speaking, only has sense as indicating the genealogy and nuclear composition of the molecule. However, some features of atoms in molecules are important. For instance, atomic charges in molecules are of widespread use in specification of charge distribution. In Section 5.2 the difficulties of defining such atomic charges are discussed: they are due mainly to the lack of atomic borders in molecules.

Bader [8.107] suggested that the atomic borders in molecules should be defined as the surface  $S$  at which the gradient of the charge density  $\nabla\rho(\mathbf{r})$  equals zero; that is,  $\nabla\rho(\mathbf{r})$  changes its sign when moving along the bonding vector:

$$\nabla\rho(\mathbf{r}_0) \cdot \mathbf{n}(\mathbf{r}_0) = 0 \quad \mathbf{r}_0 \in S \quad (8.121)$$

where  $\mathbf{n}$  is the unit vector normal to  $S$  [ $\nabla\rho(\mathbf{r})$  is also a vector]. On the basis of this presentation, a whole trend of electron density topology has been worked out [8.107].

In addition to some applications of the deformation density method illustrated in Examples 8.15–8.17, see other examples in Refs. 8.10, 8.101, 8.105, and references cited therein.

### Spin Densities from Neutron Scattering

Unlike X-ray scattering, *polarized neutron diffraction* experiments reveal *magnetization densities, or spin densities*, that is, the density of distribution of magnetic moments created by orbital motion and spin of electrons. *The magnetic structure factor*  $\mathbf{M}(\mathbf{S})$  can be presented in the same way as the charge density (8.116) [8.108]:

$$\mathbf{M}(\mathbf{S}) = \sum_n f_n(\mathbf{S})\mathbf{M}_n \exp[-2\pi i(\mathbf{S} \cdot \mathbf{r}_n)] \quad (8.122)$$

where  $\mathbf{M}_n$  is the magnetic moment of the atom  $n$  positioned at  $\mathbf{r}_n$  and  $f_n(\mathbf{S})$  is the magnetic form factor for this atom

$$f(\mathbf{S}) = \frac{\int m(\mathbf{r}) \exp(i\mathbf{S} \cdot \mathbf{r}) d\tau}{\int m(\mathbf{r}) d\tau} \quad (8.123)$$

and  $m(\mathbf{r})$  is the magnetization density of the atom.

For a single atomic shell the form factor can be presented as

$$f(\mathbf{S}) = \sum_l A_l(\mathbf{S}) \int R_{nl}^2(r) j_l(Sr) r^2 dr \quad (8.124)$$

where  $j_l(Sr)$  is a Bessel function of the order  $l$ ,  $R_{nl}^2(r)$  is the radial part of the electron wavefunction, and  $A_l$  are expansion coefficients that have been tabulated for many transition metal ions [8.109]. On the basis of these formulas, the observed spin densities, by means of some least-squares procedures, can be attributed to certain  $d$  state and other MO populations in the system. For more practical details, see Example 8.18.

### EXAMPLE 8.18

#### *Spin Distributions in Some Coordination Systems Obtained from Neutron Scattering*

From the experimentally measured magnetic structure factors of  $\text{KNa}_2\text{CrF}_6$ , the spin populations were found to be as follows [8.110]:  $t_{2g}^{2.66} e_g^{-0.06} 4s^{0.4}$  for  $\text{Cr}^{3+}$  and  $2p_{\pi x}^{0.02} 2p_{\pi y}^{0.02} 2p_{\sigma}^{-0.02}$  at fluorine. For the  $\text{Co}^{2+}$  ion in phthalocyaninatocobalt [8.111] the spin populations are  $3d_{xy}^{0.40} 3d_{xz,yz}^{0.17} 3d_{z^2}^{0.79} 3d_{x^2-y^2}^{-0.21} 4s^{-0.44}$  with a total spin of  $-0.17$  on the phthalocyanine. In a similar manganese complex the spin populations are different:  $3d_{xy}^{0.74} 3d_{xz}^{1.17} 3d_{z^2}^{0.83} 3d_{x^2-y^2}^{-0.15} 4s^{-0.44}$  with  $-0.31$  on the ligand atoms [8.108].

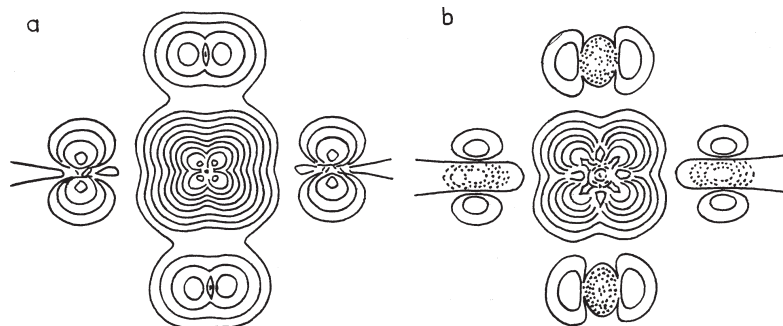


**FIGURE 8.37.** Spin density map for  $\text{Co(II)}$ -phthalocyanine in the plane of the molecule (a) and in the section  $0.25 \text{ \AA}$  above (and parallel to) this plane (b). The  $n$ th contour is at the  $\pm 2^{n-1} \cdot 10^{-3} e \text{ \AA}^{-3}$  density level from the zero (first continuous) line. (From Williams et al. [8.111].)

An example of spin density maps is shown in Fig. 8.37 for phthalocyaninatocobalt(II) [8.111]. Given in two sections, in the molecular plane (Fig. 8.37a) and 0.25 Å above (Fig. 8.37b), the lines of equal spin densities with a spacing of  $\pm 2^{n-1} \cdot 10^{-3} \text{ e } \text{Å}^{-3}$  show the variation of the spin distribution in space. From the lineshapes it is seen that the unpaired electrons occupy antibonding (or nonbonding) orbitals (the spin density is lower in the bonding region), despite the high covalence of the bonds as a whole. This result confirms the statements in Section 6.2 (Fig 6.3; see also Section 8.4) that the covalence is realized by the uncompensated bonding MO, which are not necessarily related to the HOMO and LUMO usually occupied by the unpaired electrons.

The conclusion in Example 8.18 is a part of a general feature of the spin density maps; the spin density contributions are not necessarily related directly to the chemical bonding, but they are related directly to ESR spectra (Section 8.4), and the spin density method reveals some important features of the origin of these spectra [8.111]. It is also seen from Fig. 8.37b that nitrogen  $\pi$  orbitals have negative spin densities.

#### SUMMARY NOTES

1. *Physical methods of investigation* of electronic structure and properties of transition metal systems (TMSs) consist of resonance (spectroscopic) and nonresonance (diffraction, polarization) methods that provide direct correlations between observable properties and structural parameters.
2. *Optical band shapes* of absorption and/or emission of light contain information of the energy gap between the corresponding electronic states and relative equilibrium positions of the nuclei in these states, as well as vibrations involved in the electronic transition. Broad bands are related to electronic transitions that change the electronic configuration of the TMS, while narrowband transitions take place within the same configuration.
3. *Band shape form functions* can be evaluated approximately in the semi-classical approximation. More accurate quantum calculations provide for specific relation between the bandwidth and the shift in equilibrium position (interatomic distances) by excitation, and show that the absorption frequency at the maximum of the band coincides with the energy gap between the electronic states calculated at the configuration of the initial state (Frank–Condon vertical transitions).
4. For sufficiently small changes of nuclear configuration by the electronic transition, *zero-phonon lines* that don't involve vibrations may occur in the spectrum. Zero-phonon lines are especially important for solid-state TMS spectra; they also explain the origin of the Mossbauer effect.

5. *Intensities* of electronic transitions vary in a wide range with oscillator strengths from 1 to  $10^{-10}$  dependent on the allowed mechanism from electric-dipole and parity-forbidden electric-dipole to magnetic-dipole, electric-quadrupole, spin-forbidden, and so on.
6. Spectra that emerge because of the transition between the  $d$  electronic states of the CA ( $d \rightarrow d$  transitions) are specific for TMS. They explain the origin of the color and many other optical, magnetic, and thermodynamic properties. The variety of  $d \rightarrow d$  spectra is well characterized by empirical *spectrochemical and nephelauxetic series*.
7. The ligand influence is best presented in metal  $\rightarrow$  ligand and ligand  $\rightarrow$  metal *charge transfer spectra*, which are due to electronic transitions between bonding and antibonding (nonbonding) MOs of the TMS. Vibrational properties are reflected in the vibrational structure of electronic spectra, as well as in *IR, Raman, and resonance Raman spectra*.
8. If the electronic transition involves *orbitally degenerate states*, the band structure of the optical spectrum under certain conditions becomes more complicated with two or three humps possible for transitions to twofold- and threefold-degenerate terms, respectively. The zero-phonon line may also be split by the tunneling between equivalent minima.
9. *Ultraviolet and X-ray photoelectron spectra* occupy an honorable place in the investigation of electronic structure of TMS. Chemical shift, shakeup, and configuration interaction satellites in photoelectron spectra represent some important structural features of the system. EXAFS is an outstanding version of these spectra as it allows one to determine interatomic distances in liquid and other disordered states of matter.
10. *Magnetic properties* of TMS are studied mainly via magnetic susceptibility measurements. The ligand field may quench (reduce) the orbital contribution of the CA electrons to the magnetic moment. Magnetic susceptibility is usually temperature-dependent, but there may be a temperature-independent component. Cooperative effects in solid state, dependent on the interaction details, may result in paramagnetic, ferromagnetic, ferrimagnetic, diamagnetic, and other forms of magnetism.
11. *Electron spin resonance (ESR)* is a powerful method of investigation of electronic structure of TMSs in the presence of unpaired electrons showing the symmetry, covalence, and degeneracy of their orbitals; splitting of orbital and spin terms; and influence of the environment and nuclear spins. It is effective in any phase state of the matter.
12. *Exchange and superexchange magnetic coupling* between different centers is very important in electronic structure investigation of polycenter TMSs. In a simple Heisenberg–Dirac–Van Vleck (HDVV) model the indirect coupling between the local center states (magnetic orbitals) is described by one parameter that can be estimated approximately. Exchange-coupled TMS clusters are especially important in molecular magnets. Spin crossover is another application of magnetic phenomena in TMSs.



13. *Optical activity, circular dichroism, and magnetic circular dichroism* are in widespread use in TMS, especially in metallobiochemical systems.
14. *Gamma-resonance spectroscopy (GRS)* based on the Mossbauer effect is yet another powerful method of electronic structure investigation of many TMSs. It allows one to reveal their electronic features as they influence the isomer shift, quadrupole splitting, and magnetic fine structure of the spectral lines produced by the transitions between the states of the nuclei. The majority of nuclei suitable for GRS are those of transition metal elements. Most widely studied are iron compounds.
15. *X-ray, electron, and neutron diffraction methods* are very useful tools for TMS studies, including electronic structure studies. Electron charge deformation densities (DD) provide a visual picture of the bonding features; their analysis using the electronic structure theory allows for a better understanding of the origin of the bonding. The spin DD obtained by neutron scattering serves the same purpose.

## EXERCISES AND PROBLEMS

- \*P8.1.** From the light absorption curve of  $\text{K}_2\text{NaCrF}_6$  at 77 K given in Fig. 8.6 one finds that there is a maximum of a  $d \rightarrow d$  absorption band at  $\Omega_1 \cong 4300 \text{ \AA}$  ( $23,300 \text{ cm}^{-1}$ ) with a bandwidth at half intensity  $\delta\Omega \sim 530 \text{ \AA}$  ( $2800 \text{ cm}^{-1}$ ). Using these data and assuming that the maximum of the luminescence band is at  $\Omega_2 \cong 19900 \text{ cm}^{-1}$ , evaluate the following:
- (a) The frequency  $\omega$  of the vibration that broadens the band (assuming that mainly one vibration contributes to the broadening and the condition of  $\hbar\omega \gg kT$  is obeyed)
  - (b) The shift  $a$  in minimum positions (equilibrium configurations) of the excited state with respect to the ground state one
  - (c) The frequency at the pure electronic transition  $\Omega_0$ .
- P8.2.** The  $d \rightarrow d$  transition  ${}^4A_{2g} \rightarrow {}^2E_g$  in  $[\text{Cr}(\text{H}_2\text{O})_6]^{3+}$  yields a narrow band in the absorption spectrum. Explain why this line is narrower than in other  $d \rightarrow d$  transitions and find three other examples with similar narrow bands in TMS spectra.
- \*P8.3.**  $d \rightarrow d$  transitions in TMS are transitions between the states of  $d^n$  configurations split by the crystal field of the ligands. In TMSs with an inversion center these states have the same parity (as, e.g., in the  ${}^4A_{2g} \rightarrow {}^2E_g$  transition in Problem P8.2). On the other hand, according to selection rules (Section 3.4), such transitions are forbidden. How is this controversy solved? Explain in detail and indicate experimental support of your explanation.
- P8.4.** What is the difference between the three quantitative characteristics of spectral intensity: absorption coefficient, extinction coefficient, and

oscillator strength? Are there relationships between them? Indicate approximately their observable minimum and maximum values.

- 8.5. Explain the origin of the zero-phonon line and formulate the conditions under which it can be observed in the absorption and emission spectra. What information about the electronic structure of the system can be obtained from the zero-phonon line position and its intensity?
- \*8.6. The two series of ligands, *spectrochemical* and *nephelauxetic*, extracted from experimental spectroscopic data [Eqs. (8.23)–(8.26)] describe two apparently independent kinds of properties: while the former characterizes the crystal field strength of the ligands ignoring covalence, the nephelauxetic series indicates just the covalence changes. Meanwhile by comparison of these two series one can see some pattern. For instance, in the series F, Cl, Br, I the parameters increase from left to right in both spectrochemical and nephelauxetic series. What does it mean, and how would you explain this correlation between the two series?
- \*8.7. On Fig. 8.38 the low-temperature polarized absorption spectrum of  $(\text{Naem})\text{CuCl}_4$  [Naem: *N*-(2-ammonioethyl)morpholinium] in the visible and near-IR region is shown. The two bands are attributed to two  $d-d$  transitions in the distorted (compressed tetrahedral)  $\text{CuCl}_4^{2-}$  units that have  $D_{2d}$  symmetry [8.112].

Draw a qualitative scheme of the  $d$  energy levels of this complex and explain the origin of the observed polarizations of the two bands, similar to how it is done in Example 8.2. Note that the low frequency band is polarized along the  $[8.101]$  direction of the crystal that is parallel to the  $z$  axis of the complex. (*Hint*: Compare your  $d$ -level diagram with that in Figs. 4.5 and 8.21.)

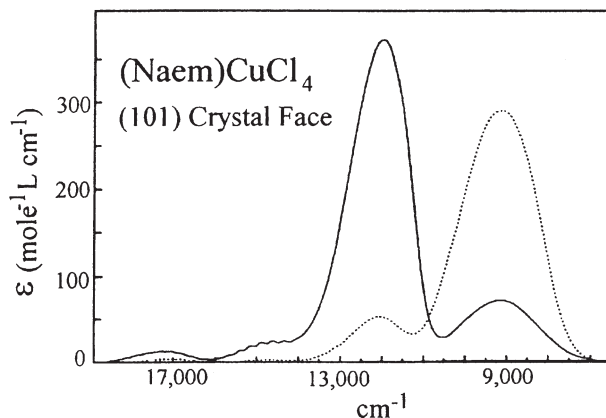


FIGURE 8.38. Polarized spectra of the crystalline  $(\text{Naem})\text{CuCl}_4$  at  $\sim 12$  K [Naem=*N*-(2-ammonioethyl)morpholinium], with the electric vector along  $[101]$  (solid line) and parallel to the  $b$  axis (dashed line).

- \*P8.8.** Using the method described in Section 3.5, Example 3.5, and Problem 3.8, find the allowed and forbidden normal vibrations in IR and Raman spectra for the following molecular systems: planar triangular  $\text{CuF}_3$  with symmetry  $D_{3h}$ , tetrahedral  $\text{CoCl}_4^{2-}$  with  $T_d$  symmetry, octahedral  $\text{UF}_6$  with symmetry  $O_h$ , and cubic  $\text{OsF}_8$  with symmetry  $O_h$ . Are there normal vibrations that can be seen in both IR and Raman spectra?
- P8.9.** What is the difference between Raman scattering and resonance Raman scattering? Are the vibrational frequencies obtained from the Raman spectra different from those in IR spectra? If vibrational shifts in the Raman scattering do not depend on the frequency of incident light, can we obtain them with IR irradiation? How can we increase the intensity of the Stokes and anti-Stokes lines in the Raman spectra?
- \*P8.10.** The constants of vibronic coupling of the  $E$  state of  $\text{VF}_3$  to degenerate  $e$  and totally symmetric  $a$  vibrations equal (in dimensionless units)  $F_E = k_E = 0.78$  and  $F_A = k_A = 0.52$ , respectively, while the corresponding vibrational frequencies are  $\omega_E = 784 \text{ cm}^{-1}$  and  $\omega_A = 692 \text{ cm}^{-1}$ . Use the semiclassical approximation to determine whether the optical band of the  $A \rightarrow E$  transition will be two-humped at room temperatures. How does this condition change with temperature?
- P8.11.** Do the peaks of photoelectron spectra (PES) or X-ray photoelectron spectra (XPS) coincide with MO energy levels? Explain your answer. What kind of satellites may be observed in the PES and XPS and why do they occur?
- P8.12.** Chemical shifts in XPS are attributed to the shift of the inner energy levels of the atom due to the change in effective atomic charge by the bonding to other atoms. Can we estimate effective atomic charges from the chemical shifts? What more accurate bonding characteristics determine the chemical shift, and how do they relate to the general understanding of backdonation and excitation by coordination as discussed in Section 6.3 (Fig. 6.6)?
- \*P8.13.** Use the definition of the magnetic moment  $\mu$ , the expression for quantum-mechanical averages of momenta  $\langle \mathbf{M} \rangle = M(M+1)$ , and Eq. (2.24) to prove that for free atoms the component of the magnetic moment is given by Eq. (8.52):  $\mu_J = g\beta[J(J+1)]^{1/2}$ , where the  $g$  factor follows the Landé formula (8.52).
- P8.14.** The magnetic moment of a free transition metal atom is formed by orbital (for  $L \neq 0$ ) and spin ( $S \neq 0$ ) contributions of comparable value. When the same atom is the CA of some TMS, its orbital contribution almost completely vanishes (this is also seen from the  $g$ -factor values in ESR spectra, which, for instance, for the Cu(II) TMS are near the spin-only value  $g \approx 2$ ). When and why does this quenching of the orbital magnetic moment by the ligands take place? Give three examples of when the magnetic orbital contribution does not vanish. Are there cases when the orbital quenching depends on temperature?

- \*P8.15.** Following the formulas in Table 8.9, calculate the axial and equatorial molar magnetic susceptibility values at room temperature for  $[\text{Fe}(\text{urea})_6]\text{Cl}_3$  with  $D = 0.130 \text{ cm}^{-1}$  and  $g_n = g_l = 2.002$ , noting that in the octahedral environment in this TMS the iron atom has a high-spin configuration.
- P8.16.** What electronic structure characteristics can be obtained from ESR spectra? In cases when the orbital contribution to the magnetic moment is quenched (for nondegenerate terms or twofold degenerate  $E$  terms) the  $g$  factor is still not exactly equal to the spin-only value; what is the origin of nonspin contributions? Does the covalence derived from the ESR spectra characterize the whole chemical bonding?
- P8.17.** As stated in Example 8.12, the semiempirical calculations show that in the binuclear copper(II) acetate hydrate  $[\text{Cu}(\text{OAc})_2\text{H}_2\text{O}]_2$  the exchange coupling between the two unpaired electrons on the  $d_{x^2-y^2}$  orbitals of the two Cu(II) centers ( $\delta$  bonding) is not via direct Cu—Cu interaction (not via direct  $d_{x^2-y^2} - d_{x^2-y^2}$  overlap), but indirect, via the oxygens of the ligands. How can this conclusion be drawn from the obtained in the calculations MO LCAO diagram with MO populations? (*Hint*: Employ the condition of bonding in the MO LCAO scheme discussed in Chapters 5 and 6.)
- P8.18.** What are the conditions of antiferromagnetic coupling between indirect interacting magnetic centers?
- P8.19.** Formulate the main conditions for application of  $\gamma$ -resonance spectroscopy to studies of TMS. What main structural and electronic information about TMS can be obtained from  $\gamma$ -resonance spectra (GRS)? Do GRS depend on temperature? If so, explain why.
- P8.20.** *Deformation density* (DD) in electron diffraction methods is usually defined as the difference between the density of the electronic cloud in the molecular system obtained experimentally (or by calculations) and the spherical symmetric densities of free atoms in the positions that they occupy in the molecule, while positive DD is directly related to the bonding. Does this definition of DD correctly describe the changes in electronic density by the bonding? Explain your answer and give examples.

## REFERENCES

- 8.1. G. Herzberg, *Electronic Spectra and Electronic Structure of Polyatomic Molecules*, Van Nostrand, New York, 1966.
- 8.2. G. Herzberg, *Vibrational and Rotational Spectra of Polyatomic Molecules*, Van Nostrand, New York, 1945.
- 8.3. E. I. Solomon and A. B. P. Lever, eds., *Inorganic Electronic Structure and Spectroscopy, Vol. I, Methodology*, Wiley, New York, 1999.
- 8.4. E. I. Solomon and A. B. P. Lever, eds., *Inorganic Electronic Structure and Spectroscopy, Vol. II, Applications and Case Studies*, Wiley, New York, 1999.

- 8.5. (a) K. Ziegahn, C. Nordling, A. Fahlman, R. Nordberg, K. Hamrin, J. Hedman, G. Johansson, T. Bergmark, S. E. Karlsson, I. Lindgren, and E. Lindberg, *ESCA. Atomic, Molecular and Solid State Structure Studied by Means of Electron Spectroscopy*, Nova Acta Regial Societatis Scieintarum Upsaliensis, Series IV, Vol. 20, Uppsala, 1967; (b) D. W. Turner, C. Baker, A. D. Baker, and C. R. Brundle, *Molecular Photoelectron Spectroscopy*, Wiley, New York, 1970; (c) S. Hufner, *Photoelectron Spectroscopy*, Springer, Heidelberg, 1996.
- 8.6. A. K. Cheetham and P. Day, eds., *Solid State Chemistry. Techniques*, Clarendon Press, Oxford, 1988.
- 8.7. R. L. Carlin, *Magnetochemistry*, Springer, Berlin, 1986.
- 8.8. V. I. Goldanskii and R. H. Herber, eds., *Chemical Applications of Mossbauer Spectroscopy*, Academic Press, New York, 1968; G. J. Long and F. Grandjean, eds., *Mossbauer Spectroscopy Applied to Inorganic Chemistry*, Vol. 3, Plenum, New York, 1989; D. P. E. Dickson and F. J. Berry, eds., *Mossbauer Spectroscopy*, Cambridge Univ. Press, 1986.
- 8.9. A. G. Maddock, *Mossbauer Spectroscopy Principles and Applications*, Harwood, Chichester, UK, 1997.
- 8.10. P. Coppens, "Concepts of charge density analysis: The experimental approach" in P. Coppens and H. B. Hall, eds., *Electron Distribution and Chemical Bond*, Plenum, New York, 1982, p. 3.
- 8.11. (a) H. Hartman, H. L. Schlafer, and K. H. Hansen, *Z. Anorg. Chem.* **289**, 40 (1957); (b) M. Linhard, *Z. Electrochem.* **50**, 224 (1944).
- 8.12. G. M. Pearl, M. C. Zerner, A. Broo, and J. McKelvey, *J. Comput. Chem.* **19**, 781 (1988); I. P. Mercier, I. R. Gold, and D. A. Klug, *J. Phys. Chem.* **B103**, 7720 (1999); R. C. Walker and D. A. Klug, *J. Phys. Chem.* **B106**, 11658 (2002).
- 8.13. S. Sugano, Y. Tanabe, and H. Kamimura, *Multiplets of Transition-Metal Ions in Crystals*, Academic Press, New York, 1970.
- 8.14. Yu. E. Perlin and B. S. Tsukerblat, in Yu. E. Perlin and M. Wagner, eds., *The Dynamical Jahn-Teller Effect in Localized Systems*, North-Holland, Amsterdam, 1984, p. 251.
- 8.15. I. B. Bersuker and V. Z. Polinger, *Vibronic Interactions in Molecules and Crystals*, Springer, Heidelberg, 1989.
- 8.16. F. Dushinsky, *Acta Physicochim. URSS* **7**, 551 (1937).
- 8.17. L. E. Orgel, *An Introduction to Transition Metal Chemistry*, Methuen, London, 1960.
- 8.18. C. K. Jorgensen, *Acta Chem. Scand.* **8**, 1502 (1954).
- 8.19. D. L. Wood, J. Ferguson, K. Knox, and J. F. Dillon, *J. Chem. Phys.* **39**, 890 (1963).
- 8.20. C. K. Jorgensen, *Oxidation Numbers and Oxidation States*, Springer, Berlin, 1969; C. K. Jorgensen, *Modern Aspects of Ligand Field Theory*, North-Holland, Amsterdam, 1971.
- 8.21. C. K. Jorgensen, *Progr. Inorg. Chem.* **4**, 73 (1962); *Adv. Chem. Phys.* **5**, 33 (1963).
- 8.22. A. B. P. Lever, J. Lewis, and R. S. Nyholm, *J. Chem. Soc.* 5262 (1962); 1187 (1964).

- 8.23. R. S. Czernuszewicz and T. Spiro, in E. I. Solomon and A. B. P. Lever, eds., *Inorganic Electronic Structure and Spectroscopy, Vol. I, Methodology*, Wiley, New York, 1999, p. 353.
- 8.24. R. S. Czernuszewicz, K. Nakamoto, and D. P. Strommen, *J. Am. Chem. Soc.* **104**, 1515 (1982).
- 8.25. E. I. Solomon and M. A. Hanson, in E. I. Solomon and A. B. P. Lever, eds., *Inorganic Electronic Structure and Spectroscopy, Vol. II, Applications and Case Studies*, Wiley, New York, 1999, p. 1.
- 8.26. I. B. Bersuker, *The Jahn-Teller Effect*, Cambridge Univ. Press, Cambridge, UK, 2006.
- 8.27. J. E. Pate, P. K. Ross, T. J. Thamann, C. A. Reid, K. D. Karlin, T. N. Sorrell, and E. I. Solomon, *J. Am. Chem. Soc.* **111**, 5198 (1989).
- 8.28. H. C. Longuet-Higgins, U. Opic, M. H. L. Pryce, and R. A. Sack, *Proc. Roy. Soc. Lond.*, **A244**, 1 (1958).
- 8.29. S. Muramatsu and N. Sakamoto, *J. Phys. Soc. Jpn.* **36**, 839 (1971).
- 8.30. I. B. Bersuker, ed., *The Jahn-Teller Effect. A Bibliographic Review*, IFI Plenum, New York, 1984.
- 8.31. I. B. Bersuker, *Chem. Rev.* **101**, 1067 (2001).
- 8.32. F. I. Vilesov, B. Kurbatov, and A. I. Terenin, *Dokl. Acad. Nauk SSSR* **138**, 1329 (1961).
- 8.33. D. W. Turner and M. I. Al-Joboury, *J. Chem. Phys.* **37**, 3007 (1962); M. I. Al-Joboury and D. W. Turner, *J. Chem. Soc.* 5141 (1963).
- 8.34. G. M. Bancroft and Y. F. Hu, in E. I. Solomon and A. B. P. Lever, eds., *Inorganic Electronic Structure and Spectroscopy, Vol. I, Methodology*, Wiley, New York, 1999, p. 443.
- 8.35. D. W. Turner, in H. A. O. Hill and P. Day, eds., *Physical Methods in Advanced Inorganic Chemistry*, Interscience, New York, 1968.
- 8.36. G. K. Wertheim and A. Rosencwaig, *Phys. Rev. Lett.* **26**, 1179 (1971).
- 8.37. L. N. Mazalov, *X-ray Emission and Electronic Spectroscopy of Molecules (Theoretical Bases)* (Russ.), Nauka, Novosibirsk, 1979.
- 8.38. L. S. Cederbaum and W. Domske, *Adv. Chem. Phys.* **36**, 205 (1977).
- 8.39. E. Haller, H. Koppel, and L. S. Cederbaum, *J. Chem. Phys.* **78**, 1359 (1983)
- 8.40. H. Koppel, W. Domske, and L. S. Cederbaum, *Adv. Chem. Phys.* **53**, 59 (1984)
- 8.41. O. I. Sumbaev, E. B. Petrovich, Yu. P. Smirnov, I. M. Band, and A. I. Smirnov, *Uspekhi Fyz. Nauk* **113**, 360 (1974).
- 8.42. V. I. Nefedov, *Application of X-ray Electron Spectroscopy in Chemistry* (Russ.), in *Reviews of Science and Technique*, Ser. Molecular Structure and Chemical Bond, Vol. 1, VINITI, Moscow, 1973.
- 8.43. T. A. Carlson, *Photoelectron and Auger Spectroscopy*, Plenum, New York, 1975.
- 8.44. D. E. Sayers, E. A. Stern, and F. W. Lytle, *Phys. Rev. Lett.* **27**, 1204 (1971); E. A. Stern, *Contemp. Phys.* **19**, 289 (1978).
- 8.45. *EXAFS and Near Edge Structure (IV)*, Vol. 2, *J. Phys.* 47 (Colloque C8, N 12) (1986); B. K. Teo, ed., *EXAFS: Basic Principles and Data Analysis, Inorg. Chem. Concepts*, Vol. 9, Springer, Berlin, 1986.

- 8.46. D. C. Koningsberger and R. Prins, eds., *X-ray Absorption: Principles, Applications, Techniques of EXAFS, SEXAFS, XANES* (Chem. Analysis, Vol. 92), Wiley, New York, 1988; S. S. Husuain, ed., *X-ray Absorption Fine Structure (Proc. 6th Int. Conf. EXAFS and XANES)*, Harwood, New York, 1991.
- 8.47. H. H. Zhang, B. Hedman, and K. O. Hodgson, in E. I. Solomon and A. B. P. Lever, eds., *Inorganic Electronic Structure and Spectroscopy, Vol. I, Methodology*, Wiley, New York, 1999, p. 513.
- 8.48. S. P. Cramer, H. Wang, C. Bryant, M. Legros, C. Horn, D. Patel, C. Ralston, and X. Wang, in I. Solomon and O. Hodgson, eds., *Spectroscopic Methods in Bioinorganic Chemistry*, ACS Symp. Series 692, ACS, Washington, DC, 1998, p. 154.
- 8.49. S. P. Cramer, H. B. Gray, Z. Dori, and A. Binu, *J. Am. Chem. Soc.* **101**, 2770 (1979).
- 8.50. T. K. Sham, J. B. Hastings, and M. L. Perlman, *Chem. Phys. Lett.* **83**, 391 (1981).
- 8.51. C. Cartier, P. Thuery, M. Verdaguer, Z. Zarembowitch, and A. Michailowicz, *J. Phys.* **47**, C8, 563 (1986).
- 8.52. S. P. Kramer and K. O. Hodgson, *Progr. Inorg. Chem.* **25**, 1 (1979).
- 8.53. P. M. Eisenberger and B. M. Kinkaid, *Science* **200**, 1441 (1978).
- 8.54. O. Hanske-Petitpierre, Y. Yacoby, J. Mustre de Leon, E. A. Stern, and J. J. Rehr, *Phys. Rev. B* **44**, 6700 (1992); N. Sicron, B. Ravel, Y. Yacoby, E. A. Stern, F. Dogan, and J. J. Rehr, *Phys. Rev. B* **50**, 13168 (1994—II).
- 8.55. H. Froitzheim, "Electron energy loss spectroscopy," in H. Ibach, ed., *Electron Spectroscopy for Surface Analysis*, Springer, Berlin, 1977.
- 8.56. J. H. Van Vleck, *The Theory of Electric and Magnetic Susceptibility*, Oxford Univ. Press, Oxford, UK, 1932.
- 8.57. A. Abraham and B. Bleaney, *Electron Paramagnetic Resonance of Transition Ions*, Clarendon Press, Oxford, 1970.
- 8.58. A. Bencini and D. Gatteschi, in E. I. Solomon and A. B. P. Lever, eds., *Inorganic Electronic Structure and Spectroscopy, Vol. I, Methodology*, Wiley, New York, 1999, p. 93.
- 8.59. F. E. Mabbs and D. Collison, *Electron Paramagnetic Resonance of Transition Metal Compounds*, Elsevier, Amsterdam, 1992.
- 8.60. B. S. Tsukerblat and M. I. Belinski, in M. Vol'pin, ed., *Soviet Scientific Reviews. Chemistry Reviews*, Harwood, Amsterdam, 1987, p. 209.
- 8.61. V. T. Kalinikov and Yu. V. Rakitin, *Introduction to Magnetochemistry. The Method of Static Magnetic Susceptibility in Chemistry* (Russ.), Nauka, Moscow, 1980.
- 8.62. O. Kahn, "Magnetism of the heteropolymetallic systems," *Struct. Bond.* **68**, 89 (1987).
- 8.63. A. Earnshaw, *Introduction to Magnetochemistry*, Academic Press, New York, 1968.
- 8.64. C. J. O'Connor, "Magnetochemistry—advances in theory and experimentation," *Progr. Inorg. Chem.* **29**, 203 (1982).
- 8.65. P. S. Pregosin, ed., *Transition Metal Nuclear Magnetic Resonance*, Elsevier, Amsterdam, 1991.



- 8.66. P. W. Anderson, in G. T. Rado and H. Suhl, eds., *Magnetism*, Vol. 1, Academic Press, New York, 1963, p. 25.
- 8.67. P. J. Hay, J. C. Thibault, and R. Hoffmann, *J. Am. Chem. Soc.* **97**, 4884 (1975).
- 8.68. O. Kahn and M.-F. Charlot, in R. Daudel, A. Pullman, L. Salem, and A. Veillard, eds., *Quantum Theory of Chemical Reactions*, Vol. 2, Reidel, Dordrecht, 1980, p. 215.
- 8.69. B. Bleaney and K. D. Bowers, *Proc. Roy. Soc. (Lond.)* **A214**, 451 (1952).
- 8.70. B. N. Figgis and R. L. Martin, *J. Chem. Soc.* 3837 (1956).
- 8.71. R. L. Martin, in E. A. V. Ebsworth, A. G. Maddock, and A. G. Sharpe, eds., *New Pathways in Inorganic Chemistry*, Cambridge Univ. Press, 1968, Chapter 9.
- 8.72. L. S. Forster and C. J. Ballhausen, *Acta Chem. Scand.* **16**, 1385 (1962).
- 8.73. T. Watanabe, *J. Phys. Soc. Jpn.*, **16**, 1677 (1961).
- 8.74. I. B. Bersuker and Yu. G. Titova, *Teor. Exp. Khim.* **6**, 469 (1970).
- 8.75. M.-F. Charlot, M. Verdaguer, Y. Journaux, P. de Loth, and J. P. Dandey, *Inorg. Chem.* **23**, 3802 (1984); M. Julve, M. Verdaguer, A. Gleizes, M. Philoche-Levisalles, and O. Kahn, *ibid.* 3808 (1984).
- 8.76. J. A. Moreland and R. J. Doedens, *J. Am. Chem. Soc.* **97**, 508 (1974).
- 8.77. M. M. Mossova, C. J. O'Connor, M. T. Pope, E. Sinn, G. Herve, and A. Teze, *J. Am. Chem. Soc.* **102**, 6864 (1980).
- 8.78. D. H. Jones, J. R. Sams, and R. C. Thompson, *J. Chem. Phys.* **79**, 3877 (1983).
- 8.79. I. B. Bersuker, V. Z. Polinger, and L. F. Chibotaru, *Mol. Phys.* **52**, 1271 (1984).
- 8.80. D. Gatteschi, R. Sessoli, and J. Villain, *Molecular Nanomagnets*, Oxford Univ. Press, 2006.
- 8.81. P. Gutlich, H. S. Spiering, and A. Hauser, in E. I. Solomon and A. B. P. Lever, eds., *Inorganic Electronic Structure and Spectroscopy*, Vol. II, *Applications and Case Studies*, Wiley, New York, 1999, p. 575.
- 8.82. O. Kahn, J. Krober, and C. Jay, *Adv. Mater.* **4**, 718 (1992).
- 8.83. O. Kahn and C. J. Martinez, *Science* **279**, 5347 (1998).
- 8.84. A. Hauser, *Top. Curr. Chem.* **234**, 155 (2004).
- 8.85. J. Zarembowitch and O. Kahn, *New J. Chem.* **15**, 181 (1991); J. Zarembowitch, *New J. Chem.* **16**, 255 (1992).
- 8.86. E. Konig, *Progr. Inorg. Chem.* **35**, 527–622 (1987).
- 8.87. T. Mallah, S. Thiebaut, M. Verdaguer, and P. Veillet, *Science* **262**, 1554 (1993).
- 8.88. E. Konig and S. Kremer, *Theor. Chim. Acta* **23**, 12 (1971).
- 8.89. E. Konig, G. Ritter, and S. K. Kullshreshtha, *Chem. Rev.* **85**, 219 (1985).
- 8.90. T. Kambara, *J. Chem. Phys.* **70**, 4199 (1979); N. Sasaki and T. Kambara, *ibid.* **74**, 3472 (1981).
- 8.91. M. Bacci, *Coord. Chem. Rev.* **86**, 245 (1988); P. Gutlich, *Struct. Bond.* **44**, 83 (1981); C. N. R. Rao, *Int. Rev. Phys. Chem.* **4**, 19 (1985).
- 8.92. P. Thuery and J. Zarembowitch, *Inorg. Chem.* **25**, 2001 (1986).
- 8.93. S. F. Hason, *Molecular Optical Activity and the Chiral Discrimination*, Cambridge Univ. Press, Cambridge, UK, 1982.
- 8.94. H.-R. C. Jaw and W. R. Mason, *Inorg. Chem.* **30**, 275 (1991).



- 8.95. S. B. Piepho and P. N. Schatz, *Group Theory in Spectroscopy with Applications to Magnetic Circular Dichroism*, Wiley-Interscience, New York, 1983.
- 8.96. R. Mossbauer, *Z. Phys.* **151**, 124 (1958).
- 8.97. P. Gutlich and J. Ensling, in E. I. Solomon and A. B. P. Lever, eds., *Inorganic Electronic Structure and Spectroscopy, Vol. I, Methodology*, Wiley, New York, 1999, p. 161.
- 8.98. (a) G. K. Wertheim, *Mossbauer Effect: Principles and Applications*, Academic Press, New York, 1964; (b) G. M. Bancroft, *Mossbauer Spectroscopy. An Introduction for Inorganic Chemists*, McGraw-Hill, New York, 1973.
- 8.99. H. H. Wickman and C. F. Wagner, *J. Chem. Phys.* **51**, 435 (1969).
- 8.100. G. H. Stout and L. H. Jensen, *X-ray Structure Determination*, Macmillan, New York, 1968.
- 8.101. M. B. Breitenstein, H. Dannohl, H. Meyer, A. Schweig, and W. Zittlau, in P. Coppens and M. B. Hall, eds., *Electron Distribution and the Chemical Bond*, Plenum, New York, 1982, p. 255.
- 8.102. M. Yu. Antipin and Yu. T. Struchkov, *Metalloorganich. Khim.* **2**, 128 (1989).
- 8.103. W. Kauzmann, *Quantum Chemistry. An Introduction*, Academic Press, New York, 1957.
- 8.104. M. B. Hall, in P. Coppens and M. B. Hall, eds., *Electron Distribution and the Chemical Bond*, Plenum, New York, 1982, p. 205.
- 8.105. E. D. Stevens, in P. Coppens and M. B. Hall, eds., *Electron Distribution and the Chemical Bond*, Plenum, New York, 1982, p. 331.
- 8.106. P. Coppens and L. Li, *J. Chem. Phys.* **81**, 1983 (1984).
- 8.107. R. F. W. Bader, in B. M. Deb, ed., *The Force Concept in Chemistry*, Van Nostrand; R. F. W. Bader, T. T. Nguyen Dang, and Y. Tal, *Rep. Progr. Phys.* **44**, 893 (1981).
- 8.108. R. Mason, in P. Coppens and M. B. Hall, eds., *Electron Distribution and the Chemical Bond*, Plenum, 1982, p. 351.
- 8.109. R. J. Weiss and A. J. Freeman, *J. Phys. Chem. Solids* **10**, 147 (1959).
- 8.110. B. N. Figgis, P. A. Reynolds, and G. A. Williams, *J. Chem. Soc. Dalton* 2348 (1980).
- 8.111. G. A. Williams, B. N. Figgis, and R. Mason, *J. Chem. Soc. Dalton* 734 (1981).
- 8.112. R. G. McDonald, M. J. Riley, and M. A. Hitchman, *Inorg. Chem.* **27**, 894 (1988).

---

# 9

---

## STEREOCHEMISTRY AND CRYSTAL CHEMISTRY

*Stereochemistry underlies chemical intelligence; without assumptions of molecular shapes, there is no way to rationalize molecular structure and chemical transformations.*

During a relatively short period stereochemistry and crystal chemistry of transition metal compounds changed from a (charge) ball-packing treatment to a complicated electronic and vibronic problem.

### 9.1. DEFINITIONS. SEMICLASSICAL APPROACHES

#### The Notion of Molecular Shape

Stereochemistry deals with spatial arrangement of atoms in molecules: *molecular shapes*. It occupies one of the most important places in the hierarchy of the basic ideas of modern chemistry [9.1–9.5]. Therefore, it is worthwhile to discuss in some more detail the physical understanding that underlies the definition of molecular shapes.

The usual assumption that a molecule has a fixed spatial (volume) arrangement of atoms with small vibrations near some equilibrium positions is not always valid. It excludes some isomers, tautomers, nonrigid molecules, alterdentate ligands, and conformers—quite a number of situations when there are large-amplitude nuclear dynamics or intramolecular transformations. In many

---

*Electronic Structure and Properties of Transition Metal Compounds: Introduction to the Theory,*  
Second Edition By Isaac B. Bersuker  
Copyright © 2010 John Wiley & Sons, Inc.

cases the latter cannot be presented as distinct transitions from one nuclear configuration (conformation) to another.

As stated in Section 1.2, *any rigorous definition of a physical quantity should contain, explicitly or implicitly, an indication of the means of its observation.* This statement follows from the understanding that the quantities that cannot be observed can only pretend to be virtual, but not real. To observe a molecular system in a given configuration, it should have a “lifetime”  $\tau$  that is larger than the characteristic “time of measurement”  $\tau'$  determined by the means of observation:

$$\tau > \tau' \quad (9.1)$$

The lifetime of a given molecular configuration is directly related to the shape of its APES (Section 7.1). If the molecular configuration under consideration corresponds to a sufficiently deep minimum of the APES and there are no other equivalent (or comparable in energy) minima, then  $\tau$  can be assumed to be sufficiently large to define rigorously the molecular shape. If the opposite inequality  $\tau \leq \tau'$  holds, the molecular (nuclear) configuration becomes uncertain.

By way of example, consider a model of two isomers of a rhodium compound shown in Fig. 9.1 [9.6] (the existence of these isomers is questionable, but this does not influence the discussion below). The two minima corresponding to the two configurations are expected to be different in depths, and we assume that there is an energy barrier between them  $\Delta E$ . The essential feature required for the isomers to exist is that *there be localized states in the minima*. The condition for localized states follows from quantum mechanics; the depth of the minimum well should be larger than the kinetic energy of the motions within the well.

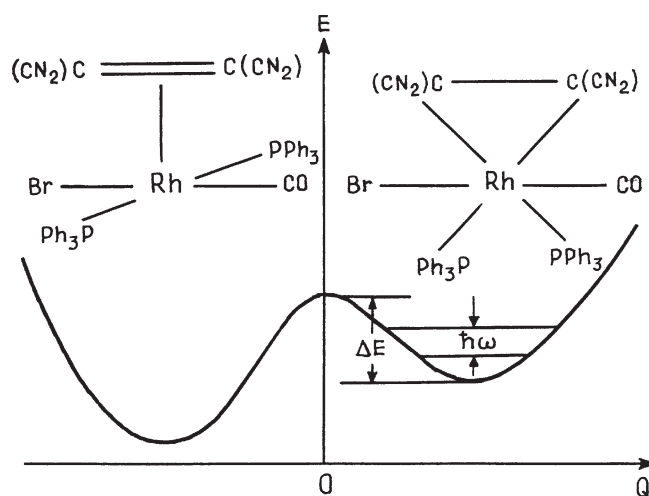


**FIGURE 9.1.** Adiabatic potential curve for two feasible isomers of a Rh complex (Ph = phenyl) along the coordinate of their interconversion. The isomers may exist (can be detected) if and only if  $\Delta E > \hbar\omega$ .

If there are localized states in the wells, the system performs vibrations with a frequency  $\omega$  that can be observed, say, by IR spectra. The characteristic time of measurement  $\tau'$  is then no less than  $T = 2\pi/\omega$ . On the other hand, in the presence of other minima the finite barrier height between them  $\delta$  allows the system to transfer from one configuration to another with a rate determined by either overcoming the barrier thermally (at sufficiently high temperatures), or tunneling through the barrier. In the latter instance the lifetime of the system at the minimum is determined by the tunneling rate, which is exponentially dependent on the ratio  $\delta/\hbar\omega$ . In general, the observation of a certain configuration is possible when at least

$$\delta > \hbar\omega \quad (9.2)$$

Thus, when there are two or several APES minima, the nuclear configurations in each of them may be considered as the corresponding molecular shape if and only if the energy barriers between them are sufficiently high. Otherwise, when  $\delta < \hbar\omega$ , there are no isomers, and the system performs only large-amplitude vibrations involving the above configurations.

A similar treatment relates to tautomers. It is generally believed that tautomers differ by electronic distribution only. However, according to the adiabatic approximation (Section 7.1), any change in electronic structure is associated with alterations in the nuclear configuration. Tautomer transformations are thus also transitions between the APES minima that are, from this perspective, similar to isomer conversion.

The APES minimum position that determines the molecular shape can be evaluated by means of direct electronic structure calculations with geometry optimization. Many examples of such calculations are given elsewhere in this book, especially in Sections 6.3–6.5 and 11.3. The modern state of the art in numerical quantum chemistry allows one to obtain molecular (including coordination) system equilibrium configurations that agree fairly well with experimental data. However, as discussed in Section 5.7, any full numerical quantum-chemical calculation, although contributing significantly to understanding of the origin of molecular shapes, is in fact a computer experiment, and its results belong almost entirely to the specific system that is subject to experimentation. The numerical results are, in general, not directly transferable to other systems, and hence they cannot serve as a basis for the formulation of general laws of stereochemistry. Therefore, *general models and qualitative results remain most important to the understanding and prediction of stereochemistry*, along with quantitative electronic structure calculations with geometry optimization.

### **Directed Valences, Localized Electron Pairs, and Valence Shell Electron Pair Repulsion (VSEPR)**

The existing qualitative models in stereochemistry are based on some assumptions about electronic charge distribution that determines the nuclear configuration. The simplest model employs *hybridized atomic orbitals* (Section 2.1). The idea was developed successfully by Pauling [9.7].

According to the assumption of hybridized orbitals, the atomic pure  $s$ ,  $p$ ,  $d$ , ... orbitals under external influence become mixed. The mixed (hybridized) orbitals, dependent on the mixing coefficients, are spatially oriented and, if they are occupied by one electron, form *directed valences*. Table 2.4 of Section 2.1 and Fig. 2.8 show some examples of  $sp$  and  $spd$  hybridization with indication of the directions of the valences. Kimball [9.8] considered the possible  $spd$  hybridizations resulting in various geometries of directed valences for coordination numbers from 2 to 8. Formally these assumed hybridizations include almost all the observed geometries of coordination compounds; for reasons given below, we do not discuss them in more detail (the majority of such hybridizations are listed in Burdett's book [9.1]).

As emphasized in Section 2.1, *hybridization of atomic orbitals, which determines their spatial orientation, does not mean that free atoms possess such directed orbitals; they are formed as a result of the bonding* (coordination). In the absence of ligands the free atom has spherical symmetry for which  $s$ ,  $p$ ,  $d$ , ... orbitals are well separated in energy and orthogonal in space. Under the influence of ligand fields that destroy the spherical symmetry, a specific type of hybridized orbital with orientations toward the ligands is produced, provided that the energy gained by the better overlap and bonding by hybridized orbitals is greater than the energy lost in the promotion of electrons from lower to higher orbitals required by the hybridization.

The picture of bonding with hybridized orbitals implies that there are localized metal–ligand bonds realized by corresponding electron pairs, that is, that there is a *localized electron pair bonding*. As discussed in Section 6.1, this type of bonding is relevant to *valence bonds* in *valence compounds*. The valence pair bonding model is most successful in organic chemistry and main-group compounds, but it fails in coordination chemistry. As shown by rigorous analysis, the more general MO presentation of electronic states may be reduced to localized orbitals if and only if the valence electrons form a closed shell, and their number is twice the number of bonds in the system. Neither of these conditions is fulfilled, in general, in transition metal coordination compounds. On the contrary, the latter differ from simple valence compounds just by their open-shell delocalized bonds, which are due to the participation of  $d$  electrons (Section 6.1).

Nevertheless, there are systems, especially among coordination compounds of nontransition elements (not very strong  $d$  participation, Section 6.1), for which the description with localized electron pairs is approximately valid. In stereochemistry of these systems the approach of *valence shell electron pair repulsion* (VSEPR) may be useful. This approach can be traced back to the earlier works of Lewis, Sidgwick and Powel, and Gillespie and Nyholm [9.1, 9.2]. The main idea is that, as long as all the bonds in the system are formed by localized electron pairs, their mutual repulsion determines the molecular shape.

An important additional circumstance is that some of the localized pairs of electrons may be unshared by the ligands; that is, they are “lone pairs” (analogies of nonbonding orbitals in the MO presentation; see below). The lone pairs,

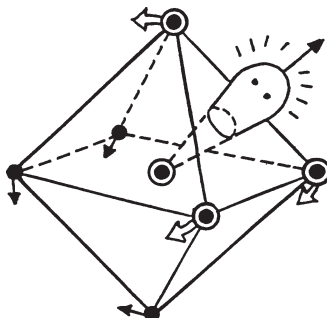


**FIGURE 9.2.** Schematic representation of the distortion of the octahedral complex  $\text{XeF}_6$  produced by the repulsive lone pair in the VSEPR model. (From Bartell and Gavin [9.10].)

although not participating in the bonding, are nevertheless important for stereochemistry because they participate actively in the electron pair repulsion. Usually lone pairs distort the otherwise more symmetric arrangement of the localized bonds.

Again, only limited cases of coordination compounds may be subject to such treatments. An example of these is the system  $\text{XeF}_6$  [9.9, 9.10]. Figure 9.2 shows how the lone pair (which remains after the formation of six Xe—F localized electron pair bonds) distorts the otherwise octahedral arrangement of six fluorine atoms (it is also assumed that the lone pair is *sp*-hybridized under the ligand field). The lone pair thus occupies a coordination place and the complex becomes seven-coordinated, somewhat similar to  $\text{IF}_7$ . This situation is discussed in more detail in the next section.

The approaches of the VSEPR type are *semiclassical* because they try to avoid the due microscopic (quantum-chemical) treatment of the electronic structure by means of introducing generalized classical parameters that allow one to reduce the problem of stereochemistry to electrostatic interactions. The simplicity of the VSEPR model, on one hand, and the complexity of quantum-chemical calculation, on the other hand, explain the attempts to improve this model, or to work out more sophisticated versions based on the same principles, despite the deficiencies of such approaches (especially for coordination compounds) in competition with *ab initio* calculations.

One improvement in the VSEPR model was suggested by Kepert [9.4]. Each metal–ligand bonding pair and lone pair is presented as being located at a point in space. The interaction between two electron pairs  $u_{ij}$  is taken as a Born type repulsion:

$$u_{ij} = \frac{a_{ij}}{r_{ij}^n} \quad (9.3)$$

where  $r_{ij}$  is the distance between the pairs,  $a_{ij}$  is a coefficient, and  $n$  is an integer, usually between 1 and 12;  $n = 6$  is considered as most adequate to the electron density repulsions (in most cases the results are given in comparison for  $n = 1$ ,

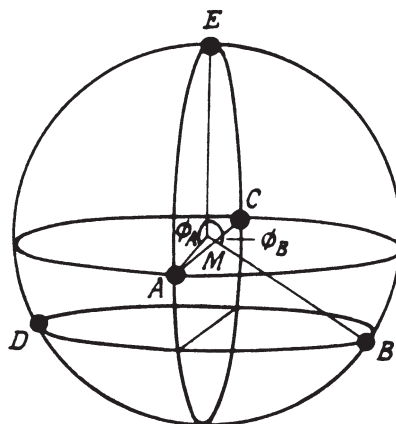


**FIGURE 9.3.** General presentation of the possible configurations of five-coordinated complexes  $[MX_5]^{n-}$  of  $C_{2v}$  symmetry described in a spherical model by two angles,  $\phi_A$  and  $\phi_B$ . (From Kepert [9.4].)

6, and 12). If all the pairs (the bonds) are equivalent, then  $r_{ij} = r$ , the points of the pair location are on a sphere as in the simple VSEPR model, and the total interaction energy

$$U = \sum_{ij} u_{ij} = a_n X_n r^{-n} \quad (9.4)$$

where  $X_n$  is the coefficient of repulsion that depends on  $n$  and the geometry of the coordination polyhedron. For a given  $n$ ,  $X_n$  is obtained from the condition of energy minimization (minimum of  $U$ ). For different ligands additional parameters are introduced, some of them taken from empirical data; others are variational.

The problem was considered for many coordination systems [9.4]. By way of example, the scheme for five-coordinated complexes of the type  $[MX_5]^{n-}$  is shown in Fig. 9.3. The most regular polyhedron for this system is either a trigonal bipyramid (TBP) with  $\phi_A = 90^\circ$  and  $\phi_B = 120^\circ$ , or a square pyramid (SP) with  $\phi_A = \phi_B$ . Calculations [9.4] of the energy [Eq. (9.4)] as a function of  $\phi_A$  and  $\phi_B$  with the parameters  $n = 6$  and the ratio  $X_{ax}/X_{eq} = 1.21$  for the axial and equatorial ligands, respectively, show that there are two minima corresponding to the TBP configurations with  $\phi_A = 90^\circ$ ,  $\phi_B = 120^\circ$  and  $\phi_A = 120^\circ$ ,  $\phi_B = 90^\circ$ , respectively, but the energy barrier between them is negligible. Thus the system can easily convert from one TBP configuration through the SP one to another TBP configuration (*Berry pseudorotation* [9.11]; see Section 9.2), and all these configurations (including the intermediates along a specific pathway) are equivalent.

In fact, crystal structure data on various systems containing  $MX_5$  polyhedra show a large variety of mainly fixed angles  $\phi_A$  and  $\phi_B$  from  $90^\circ$  to  $120^\circ$  [9.4], and this obviously results from the plasticity effect discussed in Section 9.4.

The electronic structure of the  $\text{MX}_5^{n-}$  systems and electronic control of their nuclear configuration and dynamics, as well as the possible pseudorotation in such systems, is discussed in Section 9.2. In particular, it is shown that the pseudorotation in  $\text{MX}_5^{n-}$  systems does not follow the Berry rotations scheme of  $\text{TBP} \rightarrow \text{SP} \rightarrow \text{TBP}$  interconversion.

### Nonbonding Orbitals and Nodal Properties

As seen from the discussion of the VSEPR model above, lone pairs of electrons are important for the geometry of coordination because they occupy a significant region of repulsion (Fig. 9.2), which can be even larger than that for metal–ligand bonds. Each lone pair thus acts stereochemically as a virtual additional ligand, essentially distorting the otherwise more symmetric polyhedron. However, in practice the picture may be more complicated since it turns out that not all the lone pairs are stereochemically active; this circumstance is discussed in more detail in Section 9.2. Nevertheless, the problem of how many and what kind of lone pairs are expected in a given coordination compounds is of significant interest.

In a more rigorous MO LCAO formulation, lone pairs—that is, pairs of electrons unshared by the ligands (or unshared by the CA for ligand lone pairs)—are formed by two electrons that occupy a nonbonding MO (“unshared by ligands” means nonbonding). It can be occupied by one electron only producing stereochemical influence that is qualitatively similar to that of the lone pair (and this is one advantage of the MO description).

In addition to this important property of nonbonding orbitals in stereochemistry, which is similar to that of lone pairs in the VSEPR model, the MO description formulates this feature more precisely; *the ligands are always located on the nodal lines, planes, or cones of occupied nonbonding orbitals*. Obviously, this orbital effect is due to the same electron repulsion of nonbonding electrons as in the VSEPR model, but it gives a more accurate indication of the possible ligand geometry; it is determined by the nodal properties of the nonbonding orbitals that can be relatively easily established.

The possible number of nonbonding orbitals in coordination compounds of the type  $\text{ML}_n$  and their role in stereochemistry is discussed by Mingos and Zhenyang [9.12]. It is assumed that the Coulomb integrals  $\alpha_i = H_{ii}$  [Eq. (5.4)] for the  $s$ ,  $p$ ,  $d$  electrons are equal to each other:  $\alpha_s = \alpha_p = \alpha_d$ , but the results remain valid qualitatively when they are different. An interesting  $m-n$  rule was formulated: provided that only  $\sigma$  bonds are considered, the number of nonbonding orbitals in a  $\text{ML}_n$  coordination system equals  $|m - n|$ , where  $m$  is the number of valence orbitals of  $M$ . Table 9.1 gives some information about nonbonding orbitals in different coordination systems of transition elements that participate in coordination with  $m = 9$  (one  $s$ , three  $p$ , and five  $d$ ) orbitals.

Different types of nonbonding orbitals influence the geometry of coordination differently. Example 9.1 illustrates several important cases.



**TABLE 9.1. Nonbonding Orbitals of the CA in  $ML_n$  Complexes with Nine AOs from the CA and One  $\sigma$  Orbital from Each Ligand Nine**

Geometry	$p$	$d$	Hybridized
Linear $ML_2$	$p_x, p_y$	$d_{x^2-y^2}, d_{xy}, d_{xz}, d_{yz}$	$s - \lambda d_z$
Trigonal $ML_3$	$p_z$	$d_{xz}, d_{yz}$	$s + \lambda d_z,$ $d_{x^2-y^2} + \lambda_2 p_x,$ $d_{xy} + \lambda_3 p_y$
Square-planar $ML_4$	$p_z$	$d_{xy}, d_{xz}, d_{yz}$	$s + \lambda d_z$
Trigonal bipyramidal $ML_5$	—	$d_{xz}, d_{yz},$	$d_{x^2-y^2} + \lambda p_x,$ $d_{xy} + \lambda p_y$
Octahedral $ML_6$	—	$d_{xy}, d_{xz}, d_{yz}$	—
Trigonal prismatic $ML_6$	—	—	$s + \lambda_1 d_z,$ $d_{x^2-y^2} + \lambda_2 p_x,$ $d_{xy} + \lambda_3 p_y$
Pentagonal bipyramidal $ML_7$	—	$d_{xz}, d_{yz}$	—
Square antiprismatic $ML_8$	—	—	$s + \lambda d_z$
Dodecahedral $ML_8$	—	$d_{x^2-y^2}$	—

Source: Mingos and Zhenyang [9.12].

### EXAMPLE 9.1

#### *Influence of Nonbonding MOs on Coordination Geometry*

Consider first pure CA nonbonding orbitals, with respect to which the ligands are located either on their nodal planes as in  $BH_3$  where the hydrogens are in the nodal plane of the  $p_z$  orbital (Fig. 2.2), or in the nodal cones formed by, for instance, the nonbonding  $d_{xy}, d_{xz}, d_{yz}$  orbitals in octahedral complexes  $ML_6$  (Fig. 2.3).

Nonbonding hybridized orbitals  $sp, sd, dp, \dots$  are of another type. Mainly owing to these orbitals, the system avoids higher symmetries in  $C_{nv}$  groups. For example,  $SF_4$  has  $C_{2v}$  symmetry instead of the higher ones  $C_{4v}, D_{4h}$ , or  $T_d$ . In many cases this effect can be presented as resulting from the tendency to avoid occupying metal–ligand strong antibonding orbitals instead of the nonbonding states at lower symmetries; the additional repulsions in the distorted system may be smaller than the energy loss by occupation of antibonding MOs. For instance, in  $SH_4$  two electrons prefer the nonbonding  $p_x - d_{xy}$  orbital, resulting in  $C_{2v}$  symmetry than the antibonding  $a_1$  MO in the tetrahedral  $T_d$  symmetry;  $CH_4$  is exactly tetrahedral since the critical two antibonding electrons are lacking.

Another example of this kind is provided by some “sandwich” compounds. In the high-symmetry configurations (e.g.,  $D_{5h}$  or  $D_{6h}$ ) the overlap of the CA  $d$  orbitals with the ring  $\pi$  MOs of the type

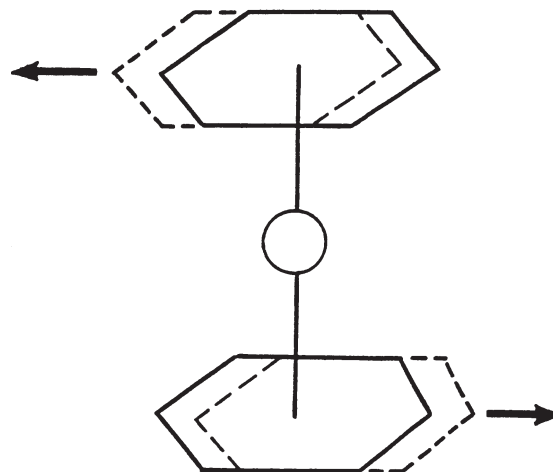


**FIGURE 9.4.** Slip distortion of the high-symmetry  $D_{6h}$  configuration of sandwich compounds that reduces the AO overlap and antibonding character of the  $d_{xz} - e_1^\pi(x)$  MO.

$d_{xz} - e_1^\pi(x)$  produces occupied antibonding orbitals that can be reduced by a simple “slip” distortion (Fig. 9.4). Again, this effect is realized when the antibonding nature of the MOs under consideration is sufficiently strong. Therefore, the first-row metallocenes, for instance,  $\text{Co}(\eta\text{-C}_2\text{H}_5)_2$  and  $\text{Ni}(\eta\text{-C}_5\text{H}_5)_2$ , are not distorted [9.13], whereas the second- and third-row sandwich compounds, where the overlap and hence antibonding character of the corresponding MOs are much larger [e.g., in  $\text{Ru}(\eta^6\text{-C}_6\text{Me}_6)(\eta^4\text{-C}_6\text{Me}_6)$ ], undergo a slip distortion as shown in Fig. 9.4 [9.14].

In many other systems the corresponding MO in the high-symmetry configuration is not sufficiently strongly antibonding, and these systems are not distorted, despite of the presence of two additional electrons that might be considered as a lone pair. For example, the complexes  $\text{SbX}_6^{3-}$ ,  $\text{X} = \text{Cl}, \text{Br}, \text{I}$ ,  $\text{MX}_6^{2-}$ ,  $\text{M} = \text{Se}, \text{Te}$ , have seven electron pairs but remain octahedral, and  $\text{XeF}_8^{2-}$  has nine electron pairs, but it is a square antiprism. In these cases it is said that the lone pairs are stereochemically inactive (inert). A more rigorous treatment of these effects based on the PJTE is given in Section 9.2.

### Complementary Spherical Electron Density Model

A stereochemical model, quite similar in spirit to those discussed above in this section, was suggested by Mingos [9.15–9.17]. The essence of the model is as follows. Consider an  $\text{ML}_n$  complex as a CA surrounded by a sphere of ligand

electron densities that are localized into distinct regions of the sphere. In the MO LCAO approximation (Section 5.1) the AOs are taken in appropriate symmetry-adapted linear combinations, separately for the CA and ligands (Table 5.1), and then the linear combinations of the functions of the same symmetry from both parts are combined by the corresponding LCAO coefficients into a MO (5.9). While the AOs  $\psi_0$  of the CA are well-known spherical harmonics  $Y_{lm}(\theta, \phi)$  [see Eq. (2.2)], which can be classified as  $s, p, d, \dots$  functions (Section 2.1), Mingos attracted attention to the fact that the linear combinations of ligand functions  $\Phi$  can also be presented as spherical harmonics, provided that *the radial distribution is considered the same for all the ligands*, namely, as concentrated on the same sphere with M in the center. This is the most limiting assumption of the model.

Under this assumption both the AOs of the CA and ligands are presented as spherical harmonics  $Y_{lm}$  with the same quantum numbers  $l$  (azimuthal;  $l = 0, 1, 2, \dots$ ) and  $m$  (magnetic,  $m = 0, \pm 1, \pm 2, \dots$ ). In order to deal with real functions, the degenerate states with  $m > 0$  are taken in the corresponding real linear combinations as shown in Section 2.1:  $Y_{l,m\pm} = c^\pm(Y_{l,m} \pm Y_{l,m-})$ .

For example, in  $MH_4$  with spherically distributed hydrogen atoms about M the corresponding linear combinations of the hydrogen  $\sigma$  function forming spherical harmonics can be presented as follows:

$$\Phi_{lm} = \sum_i^n c_i \sigma_i = N \sum_i Y_{l,m}(\theta_i, \varphi_i) \sigma_i \quad (9.5)$$

where  $N$  is the normalization factor and  $\theta_i, \varphi_i$  are the angular coordinates of the  $i$ th ligand on the sphere. For  $l = 0$  and  $m = 0$ ,  $Y_{00}$  is independent of  $\theta$  and  $\varphi$ , and hence  $\Phi_{00}$  is the sum of  $\sigma_i$ . If  $l = 1$ , there are three functions,  $\Phi_{1,0}$ ,  $\Phi_{1,1+}$ , and  $\Phi_{1,1-}$ , which can be easily found from (9.5) by substituting the corresponding ligand coordinates. To distinguish between the harmonics  $\Phi_{lm}$  and that of the CA, the notations  $S, P, D, \dots$  are introduced. These indicate that the  $\Phi_{00}$  function is  $S^\sigma$  (the superscript  $\sigma$  indicates the assumed  $\sigma$  functions of the hydrogen atoms), while  $\Phi_{10}$ ,  $\Phi_{1,1+}$ ,  $\Phi_{1,1-}$  mean  $P_0^\sigma, P_+^\sigma, P_-^\sigma$ , respectively. There are also five  $D$  functions:  $D_0^\sigma, D_{1+}^\sigma, D_{1-}^\sigma, D_{2+}^\sigma, D_{2-}^\sigma$ , seven  $F^\sigma$  functions, and so on.

The ligand spherical harmonics (9.5) can be found relatively easily, provided that the ligand geometry (the  $\theta_i, \varphi_i$  coordinates) is known. In the spherical electron density model under discussion it is assumed that the ligand arrangement should form either the best covering, or the best packing polyhedron on the sphere, or both. The two types of polyhedrons are found as solutions of the following problems [9.17]:

“If  $n$  oil supply depots are available on the surface of the sphere, what is their best arrangement to give the most efficient utilization of oil resources?” (Covering problem.)

“If  $n$  inimical dictators control the planet, how could they be located on the surface of the sphere, so as to maximize the distances between them?” (Packing problem.)

**TABLE 9.2. Best Covering and Packing Polyhedrons  $ML_n$  in the Spherical Ligand Electron Density Model**

$n$	Best Covering Polyhedron	Best Packing Polyhedron
3	Triangle	Triangle
4	Tetrahedron	Tetrahedron
5	Trigonal bipyramid	Square pyramid
6	Octahedron	Octahedron
7	Pentagonal bipyramid	Capped octahedron
8	Dodecahedron	Square antiprism
9	Tricapped trigonal prism	Capped square antiprism

Source: Mingos [9.16].

The results of the solution of covering and packing problems for some most usable coordination numbers  $n$  are listed in Table 9.2 (capped polyhedron means a regular polyhedron with an additional capping atom located on a face). If the geometry of the complex is known, the ligand spherical harmonics can be found directly from Eq. (9.5).

One of the most interesting applications of the spherical density model is in the confirmation of the *inert-gas rule*, which states that *coordination systems and main-group molecules with the valence electron configuration of the appropriate inert gas* (configurations with 8, 18, 32, etc., valence electrons) *are most stable*. The inert-gas rule is widely used in discussion of qualitative molecular structure, but little attention has been paid to its theoretical foundation.

First, consider a hypothetical system in which the ligands form an exact spherical distribution of charge about the CA. It can be shown that in this instance the ligand states, that is, the solutions for a charged ball that has spherical symmetry, are also spherical harmonics  $\Phi_{nim}(\theta, \varphi)$  of the type  $S$ ,  $P$ ,  $D$ , with the same symmetry and nodal properties as  $s$ ,  $p$ ,  $d$ , and with the energy consequence  $S < P < D, \dots$ . If there is a considerable overlap of the CA functions with the ligand sphere functions, appropriate bonding MOs of the type (5.9) or (5.32) are formed:

$$\Psi_{lm} = N_{lm}(\psi_{lm} + \lambda\Phi_{lm}) \quad (9.6)$$

Because of the exact spherical symmetry of the system, the functions  $\psi_{lm}$  and  $\Phi_{l'm'}$  with different quantum numbers are orthogonal and do not form MOs. Hence the number of bonding MOs equals the number of active valence orbitals of the CA. For example, if the CA has valence  $s$ ,  $p_x$ ,  $p_y$ ,  $p_z$  orbitals, then they overlap in pairs with  $S$ ,  $P_0$ ,  $P_+$ ,  $P_-$  spherical shell functions to form four bonding MOs that can accommodate 8 valence electrons. If the five  $d$  electron states are also involved, then there are 9 bonding MOs with 18 electrons (with  $f$  states added there will be 16 bonding MOs with 32 electrons).

If the number of electrons is less than 8, 18, and 32, respectively, then not all the bonding MOs are occupied, and the stability of the system is expected to decrease. If the number of electrons is larger, the stability of the system, again,

decreases since all the bonding MOs are occupied and the excess electrons occupy antibonding MOs. In *sp* systems the electrons in excess of 8 could, in principle, occupy *D* states, but they are much higher in energy than are *S* and *P*. Thus the numbers of electrons of the inert gas are indeed optimal for the stability of the spherical shell system.

This result is hardly surprising in view of the assumed spherical symmetry of the system. The complex of the CA with a spherical shell charge distribution of ligands is just an extended atom that has qualitatively the same atomic distributions as the free atom. Therefore, in this system the inert-gas closed-shell stability rule, well known in free atoms, is obeyed, and for the same reasons as for free atoms; in the dependence of the energy on the hydrogenlike quantum numbers the configurations with  $\sum_{l=0}^{l=l^*} 2(2l+1)$  ( $l^* = 0, 1, 2, \dots$ ) valence electrons are most stable.

In the spherical density model described above the ligand charges occupy distinct places on the same sphere, and hence their charge distribution is not spherically symmetric. It means that the orthogonality of the CA and ligand spherical harmonics with different quantum numbers  $\psi_{lm}$  and  $\Phi_{l'm'}$  does not hold, and the MO scheme employed above should be reconsidered. However, if the nonorthogonality arising because of the nonuniform (not exactly spherical) distribution of the ligand charges on the sphere is not very large, one can assume that the qualitative features of the abovementioned spherical charge distribution are approximately valid, and this approximation is the better, the more spherical the ligand arrangement about the central atom. Thus the inert-gas rule is expected to hold approximately, and it is more acceptable for a larger number of more identical ligands.

In the complementary spherical electron density model under consideration, this inert-gas rule is considerably extended to what can be called a *generalized inert-gas rule* [9.16, 9.17]. If the coordination number *n* is less than 9, then the number of ligand spherical harmonics is reduced, and the  $D^\sigma$  functions are successively lost (their number becomes  $n - 4$ ). As a result, the pseudo-spherical electron distribution assumed for the occupied one *S*, three *P*, and five *D* functions is also lost because of the holes in the  $D^\sigma$  shell formed by the lack of corresponding electron pairs. However, if the missing  $D^\sigma$  states are compensated for by matching *d* states occupied by the electrons of the CA, then a more spherical electron distribution is attained. Example 9.2 provides for illustration of this consideration.

### EXAMPLE 9.2

#### *The Inert-Gas Rule in Stereochemistry of Some Coordination Compounds*

A classical example of the inert-gas rule is provided by the system  $[\text{ReH}_9]^{2-}$ . In the tricapped trigonal prism configuration of the best covering polyhedron (Table 9.2) there are nine ligand spherical harmonics

TABLE 9.3. The Generalized Inert-Gas Rule<sup>a</sup>

<i>n</i> Structure	<i>S</i>	<i>P</i> <sub>0</sub>	<i>P</i> <sub>+</sub>	<i>P</i> <sub>-</sub>	<i>D</i> <sub>0</sub>	<i>D</i> <sub>1+</sub>	<i>D</i> <sub>1-</sub>	<i>D</i> <sub>2+</sub>	<i>D</i> <sub>2-</sub>	Examples
9 Tricapped trigonal prism	+	+	+	+	+	+	+	+	+	[ReH <sub>9</sub> ] <sup>2-</sup>
8 Square antiprism	+	+	+	+	<i>d</i> <sub>z<sup>2</sup></sub>	+	+	+	+	H <sub>4</sub> [W(CN) <sub>8</sub> ]
8 Dodecahedron	+	+	+	+	+	+	+	<i>d</i> <sub>x<sup>2</sup>-y<sup>2</sup></sub>	+	K <sub>4</sub> [W(CN) <sub>8</sub> ], [MoH <sub>4</sub> (PMe <sub>2</sub> Ph) <sub>4</sub> ]
7 Pentagonal bipyramid	+	+	+	+	+	<i>d</i> <sub>xz</sub>	<i>d</i> <sub>yz</sub>	+	+	[OsH <sub>4</sub> (PMe <sub>2</sub> Ph) <sub>3</sub> ]
7 Capped octahedron	+	+	+	+	+	+	<i>d</i> <sub>x<sup>2</sup>-y<sup>2</sup></sub>	<i>d</i> <sub>xy</sub>		[W(CO) <sub>4</sub> Br <sub>3</sub> ]
7 Capped trigonal prism	+	+	+	+	+	+	<i>d</i> <sub>yz</sub>	<i>d</i> <sub>x<sup>2</sup>-y<sup>2</sup></sub>	+	[Mo(CNbut) <sub>7</sub> ] <sup>2</sup>
6 Octahedron	+	+	+	+	+	<i>d</i> <sub>xz</sub>	<i>d</i> <sub>yz</sub>	+	<i>d</i> <sub>xy</sub>	[Mo(CO) <sub>6</sub> ]
5 Trigonal bipyramid	+	+	+	+	+	<i>d</i> <sub>xz</sub>	<i>d</i> <sub>yz</sub>	<i>d</i> <sub>x<sup>2</sup>-y<sup>2</sup></sub>	<i>d</i> <sub>xy</sub>	[Fe(CO) <sub>5</sub> ]
5 Square pyramid	+	+	+	+	<i>d</i> <sub>z<sup>2</sup></sub>	<i>d</i> <sub>xz</sub>	<i>d</i> <sub>yz</sub>	+	<i>d</i> <sub>xy</sub>	[Ni(CN) <sub>5</sub> ] <sup>3-</sup>
4 Tetrahedron	+	+	+	+	<i>d</i> <sub>z<sup>2</sup></sub>	<i>d</i> <sub>xz</sub>	<i>d</i> <sub>yz</sub>	<i>d</i> <sub>x<sup>2</sup>-y<sup>2</sup></sub>	<i>d</i> <sub>xy</sub>	[Ni(CO) <sub>4</sub> ]

<sup>a</sup>The rule states that the ligand spherical harmonics (*S*, *P*, *D*) of the ML<sub>*n*</sub> complex, together with the indicated compensating *d* orbitals of the CA, form a complete set for a closed-shell 18-electron configuration.

Source: Mingos [9.16].

(Table 9.3) that fit exactly the nine CA functions forming nine bonding MOs with an 18-electron closed shell (assuming that the above-mentioned nonorthogonality is neglected). A ligand arrangement in a capped square-antiprism also generates a complete set of *S*<sup>σ</sup>, *P*<sup>σ</sup>, and *D*<sup>σ</sup> functions providing an alternative stereochemistry that satisfies the requirement of inert-gas formulation (other polyhedrons are nonfit). This means that the configuration of the complex may be flexible within these two polyhedra, and this result is consistent with the observed stereochemical nonrigidity of [ReH<sub>9</sub>]<sup>2-</sup> [9.18]. DFT-*X*<sub>α</sub> calculations [9.19] of this system show that the radial distribution of the hydrogens around the CA emulates that of an inert gas.

In another example, a dodecahedral MH<sub>8</sub> system misses one ligand spherical harmonic *D*<sub>2+</sub><sup>σ</sup> (Table 9.3). The remaining eight bonding orbitals with 16 electrons do not fit the inert-gas rule that requires 18 bonding electrons. However, if the *d*<sub>x<sup>2</sup>-y<sup>2</sup></sub> AO of the CA, which matches approximately the *D*<sub>2+</sub> orbital by space distribution, is occupied by two electrons, the spherical symmetry is regained and the generalized inert-gas rule of stability is obeyed. For this system a square-antiprism arrangement of the hydrogens misses the *D*<sub>0</sub><sup>σ</sup> ligand function, which can be compensated for by the occupied CA *d*<sub>z<sup>2</sup></sub> orbital. Other arrangements, such as a cube or hexagonal bipyramid, require *f* functions for the compensation that are not available. Hence the generalized inert-gas rule serves as a tool for stereochemistry treatments. Table 9.3 shows other examples illustrating the efficiency of the generalized inert-gas rule.

To summarize, the complementary spherical electron density model shows that the inert gas rule is valid when there is a complementary interaction between the ligand and central atom electronic states in which the CA nonbonding  $d$  electrons compensate for the missing ligands, resulting in pseudospherical electron distribution. Those polyhedra that give the best covering and/or packing of the ligands on the sphere are most effective in emulating the required spherical distribution by generating the corresponding set of contiguous  $S^\sigma$ ,  $P^\sigma$ ,  $D^\sigma$ , ... functions. The nonbonding  $d$  orbitals of the CA that compensate for the missing  $9 - n$  ligands (ligand spherical harmonics) can experience an additional stabilization through  $\pi$ -bonding effects [9.18]. Other examples and extensions of the complementary spherical electron density model, in particular, to cluster compounds, can be found in the literature [9.15–9.17].

In overlap with these semiclassical ideas in stereochemistry are the methods of *molecular modeling* discussed in Section 5.6.

## 9.2. VIBRONIC EFFECTS IN STEREOCHEMISTRY

### **Nuclear Motion Effects: Relativity to the Means of Observation and Vibronic Amplification of Distortions**

In terms of quantum mechanics, the methods used in the previous Section, as mentioned above, are semiclassical in the sense that the electron distribution is considered as resulting from approximate (even qualitative) quantum-chemical treatments, while the interaction between localized bonds or lone pairs (nonbonding states) is taken into account as a pure electrostatic repulsion. In so doing, many quantum features of the phenomenon, in particular, vibronic coupling effects, are omitted.

A more rigorous formulation of the problem should be based on quantum mechanics involving the vibronic interaction theory given in Chapter 7. In the adiabatic approximation (Section 7.1) the stable nuclear configuration corresponds to the absolute minimum of the APES. The latter is directly influenced by the vibronic coupling between different electronic states, ground and excited (see the TEST paradigm in Section 7.4). Therefore, the vibronic coupling theory enables us to formulate some general stereochemistry rules, thus serving as an analytical model for the theory of stereochemistry (*vibronic stereochemistry*).

The theory of vibronic coupling is in essence a perturbational approach, and therefore the vibronic effects are most general (no exceptions) and of utmost significance in APES behavior at the extrema points and points of degeneracy. First, as stated by the JT theorem (Section 7.3), at the points of electronic degeneracy, that is, at the nuclear configurations for which the electronic state is degenerate, the adiabatic potential has no minimum. A similar situation emerges in the PJTE. Following the simplified formulation, the lack of APES minimum means that the system is unstable in this configuration. In general, this conclusion is not sufficiently rigorous and not always valid (Section 7.3); a more general conclusion is



that in these cases *there is a special coupling between the electronic and nuclear motions and they cannot be separated.*

The lack of minimum of APES at the point of electronic degeneracy or pseudodegeneracy due to the JTE usually means that there are two or several (or an infinite number of) equivalent minima, at each of which the system is distorted along one of the equivalent symmetry axes (or along a trough, Section 7.3). In case of a limited number of minima, if the energy barriers between them are sufficiently high, the distorted configurations of the system may be observable, provided that the condition (9.1),  $\tau > \tau'$ , for the means of measurement is satisfied.

The "time of measurement"  $\tau'$  varies for different physical methods of measurement. Usually  $\tau'$  is inversely proportional to the frequency of external perturbations in the resonance methods of investigation (Sections 8.1–8.5). Hence  $\tau'$  can be quite different in different methods of investigation, whereas  $\tau$ , the lifetime of the system in one of the equivalent minima, is constant for the given system. This means that for some of the measurements the condition (9.1) is obeyed,  $\tau' < \tau$ , whereas for others,  $\tau' > \tau$ . In other words, in a free JT or PJT system with strong vibronic coupling, *the observable nuclear configurations depend on the means of observation and may vary by changing the method of measurement* [9.20].

The relevance of this *relativity rule* concerning the means of observation of molecular shapes is actually rather widespread, but sometimes not given due attention. Note that in this rule the distorted configuration is expected to be seen in the measurement with higher frequencies ( $\tau' < \tau$ ). This means that one can observe the distorted configuration, say, in optical experiments, and the undistorted configuration (averaged over all the equivalent minima) in the ESR spectra, but *not vice versa*. Sometimes this rule allows one to understand the origin of contradictory empirical data obtained from different experiments. X-ray diffraction measurements (long exposure) [e.g., in  $\text{K}_2\text{PbCu}(\text{NO}_2)_6$ ] show that the octahedrons around Cu(II) are compressed, whereas ESR spectra (with much shorter  $\tau'$ ) yield antiferrodistortively ordered elongated octahedrons (Section 9.4). Further examples of this kind can be found in other chapters of this book and in the literature (see, e.g., Ref. 9.20 and references cited therein).

The situation changes significantly when there are small perturbations slightly lowering the symmetry of the system (differences in the ligands or ligand substituents, or small external fields, including small crystal fields). If these perturbations are sufficiently strong to produce a distortion larger than the JT one, they remove the JTE as such. For smaller perturbations the JTE is not removed but modified with interesting consequences for stereochemistry.

Consider a system with a JT  $E \otimes e$  problem (a double-degenerate electronic  $E$  term interacting with  $e$  vibrations; Section 7.3) in the linear approximation, in which APES assumes the form of a Mexican hat (Fig. 7.9). For the free system the averaged picture displayed in the experiment is an undistorted nuclear configuration. Under the influence of a small distorting perturbation, say, elongating in the  $Q_\theta$  direction, the circular trough becomes distorted, namely, an additional



potential well in the  $Q_\theta$  direction (and a hump in the opposite  $-Q_\theta$  direction) appears. If the depth of the well is greater than the kinetic energy of the circular motion in the trough, then the nuclear motions are localized in this well and the corresponding distorted nuclear configuration can be observed in the experiments.

The most exciting result in this picture is that *the magnitude of the distortion is determined mainly by the vibronic effects and may be independent of the (small) perturbation magnitude* [9.20]. Indeed, the additional well is formed at a point of the circular trough with coordinates  $(\rho_0, \varphi_0)$ , where  $\varphi_0$  only depends significantly on the perturbation, as the magnitude of the  $\rho_0$  value is less affected (in fact the perturbation slightly distorts the trough circle, too; see below). This  $\rho_0$ -value distortion is often called the *static limit* of the Jahn–Teller effect.

Thus, a small perturbation  $W$  acting on a JT system produces a perturbation that is determined by the static limit  $\rho_0$  of the JTE, which stabilizes the static distortions. Since the kinetic energy of the motion along the trough  $E_k$  is of the order of several wavenumbers ( $\text{cm}^{-1}$ ) [9.20], the condition  $W \geq E_k$  is fulfilled even for small perturbations. Meanwhile, the static distortions  $\rho_0$  may be rather large. Hence we obtain the “*amplification rule*” in Jahn–Teller distortions; *a small distorting perturbation may be amplified by vibronic effects*.

Let us make some qualitative (or semiquantitative) estimations of the coefficient of vibronic amplification  $P_a$ . In the absence of vibronic coupling the distortion magnitude  $Q_0$  can be found from the fact that the perturbation energy  $W$  transforms into strain energy:  $W = (\frac{1}{2}) K_E Q_0^2$ , where  $K_E$  is the force constant for the  $E$  distortions under consideration (Section 7.3); hence  $Q_0 = (2W/K_E)^{1/2}$ . If the vibronic effects are taken into account,  $Q_0^{\text{JT}} = \rho_0 + Q_0$ , and the amplification coefficient, equal to the ratio of the corresponding distortions, is  $P_a = Q_0^{\text{JT}}/Q_0 = 1 + (E_{\text{JT}}/W)^{1/2}$ , where the relationship  $\rho_0 = (2E_{\text{JT}}/K_E)^{1/2}$  [see Eq. (7.41)] has been used. The maximum amplification is attained when  $W = E_k$ :

$$P_a^{\text{max}} = 1 + 4 \frac{E_{\text{JT}}}{h\omega_E} = 1 + 4\lambda_E \quad (9.7)$$

It follows that the vibronic amplification may be very large, since the  $\lambda_E$  value may be substantial. For example, if we assume [as expected for octahedral compounds of Cu(II), Mn(III), Cr(II)] that  $\lambda_E$  is about 5–10, then  $P_a^{\text{max}} \sim 20$ –40.

In the quadratic  $E \otimes e$  problem with a more complicated APES that has three equivalent tetragonal minima (Section 7.3, Figs. 7.10 and 7.11), a low-symmetry perturbation renders them nonequivalent, and the system becomes “locked” at that minimum, which is deeper. Consequently, the pulsating system under small perturbations becomes strongly distorted statically. Such effects are encountered in many perturbation investigations of Jahn–Teller systems [9.20].

Temperature dependence of the amplification effect was also explored approximately. It was shown [9.20] that for a JT system with a threefold-degenerate  $T$  term interacting with  $t_2$  nuclear distortions (the  $T \otimes t_2$  problem, Section 7.3) at not very low temperatures, the temperature dependence of the vibronic amplification of external distortions  $P_a$  is  $P_a \approx E_{\text{JT}}^T/kT$ , where  $E_{\text{JT}}^T$  is the JT stabilization energy. For instance, for moderate JTE,  $E_{\text{JT}} \sim 10^3 \text{ cm}^{-1}$ ,  $P_a \sim 10$  even at

room temperatures. These numbers are approximate, but the conclusion about an uncommonly large *susceptibility of vibronic systems to distortions* due to vibronic amplification seems to be quite general.

The notion of vibronic amplification contributes to a better understanding of the JTE on the expected molecular shapes. In particular, it rejects the incorrect statements (often encountered in the literature) that the JTE is not expected in systems where differences in the ligands or other low-symmetry perturbations formally eliminate the electronic orbital degeneracy. On the contrary, we emphasize in this section that to observe JT distortions directly, some low-symmetry perturbations that trap the system in one of its equivalent APES minima are necessary. These perturbations may be very weak, often the influence of the next coordination sphere (such perturbations can also be created by the process of measurement when  $\tau' < \tau$ ), and even more often cooperative effects in crystals (Section 9.4). *In the absence of these perturbations the Jahn–Teller distortions are of dynamic nature and do not manifest themselves in an absolute way in stereochemistry and crystal chemistry.*

#### **Qualitative Stereochemical Effects of Jahn–Teller and Pseudo-Jahn–Teller Distortions**

Provided that the conditions for experimental observation of molecular shapes corresponding to the minima of the adiabatic potential are fulfilled, the distortions of high-symmetry configurations predicted by the vibronic coupling theory (Sections 7.3 and 7.4) have a direct impact on stereochemistry. At present, Jahn–Teller distortions in stereochemistry are widely employed in current investigations (see Refs. [9.1, 9.20–9.26], and references cited therein). Many works are devoted to  $\text{Cu}^{2+}$  stereochemistry that may serve as a reference example of vibronic stereochemistry. Since it is determined mainly from crystal structures, the stereochemistry of  $\text{Cu}^{2+}$  is discussed in Section 9.4.

In the JTE the distorted configurations are determined by the Jahn–Teller active coordinates. More rigorously, the symmetry of the Jahn–Teller distorted system can be predicted in a general way by means of group-theoretical considerations using the *epikernel principle* [9.21]. An *epikernel* of  $\Gamma$  in  $G$ , denoted  $E(G, \Gamma)$ , is defined as the subgroup of  $G$  that contains all the symmetry elements for which at least one basis function of  $\Gamma$  remains totally symmetric. The epikernels can easily be found directly from the character tables of the corresponding point groups:  $E(T_d, E) = D_{2d}$ ,  $E(T_d, T_2) = C_{3v}, C_{2v}, C_s$ ;  $E(T_d, E + T_2) = D_{2d}, D_2, C_{3v}, C_{2v}, C_2, C_s$ . In the last case it is assumed that the  $E$  and  $T_2$  vibrations have the same frequency, forming a fivefold-degenerate Jahn–Teller active space. For the octahedral  $O_h$  group  $E(O_h, E) = D_{4h}, C_{4v}$ ;  $E(O_h, T_2) = D_3, C_{3v}$ , and so on.

The epikernel principle can be formulated as follows [9.39]. *Extrema points on a Jahn–Teller surface prefer epikernels; they prefer maximal epikernels to lower-ranking ones. Stable minima are to be found with the structures of maximal epikernel symmetry.* This statement implies that, although forced to distort in

order to remove the electronic degeneracy, the system prefers nuclear configurations with higher symmetry compatible with this requirement. In this formulation the epikernel principle is related to the more general statement of Pierre Curie given in 1894 [9.27]: “The symmetry characteristic of a phenomenon is the maximal symmetry compatible with the existence of this phenomenon.” In relation to the statement in Section 7.4 that *nature tends to avoid degeneracy*, this Curie formula means that nature keeps the highest possible symmetry compatible with avoiding degeneracy.

The distortions that are predicted by the epikernels described above coincide with those that are well known from the general formulation of the vibronic effects in Section 7.3. As further illustration, some specific examples may be mentioned:  $\text{Ni}^{2+}(d^8)$  and  $\text{Cu}^{2+}(d^9)$  four-coordinated complexes usually have the  $D_{2d}$  structure compatible with an electronic  $T$  term and  $E$  distortions (similar  $\text{Zn}^{2+}$  complexes are undistorted tetrahedrons);  $\text{Fe}(\text{CO})_4$  exhibits  $C_{2v}$  distortions, as if resulting from a  $T-(e + t_2)$  problem (see the discussion below), while the  $\text{Co}(\text{CO})_4$  fragment shows trigonal geometry.

However, the proof of the epikernel principle is based on the assumption of only linear vibronic coupling, meaning that, in general, the epikernel principle can be violated. In particular, this can take place when the higher-order vibronic interaction terms in Eq. (7.21) are important and/or the PJTE is efficient. The influence of PJTE on stereochemistry is even greater than that of JTE. For systems with the PJTE the electronic ground state is nondegenerate, but the strong vibronic mixing with the excited states renders the system unstable with respect to low-symmetry (nontotally symmetric) nuclear displacements. Following the statement (theorem) about the uniqueness of the vibronic mechanism of instability, discussed in Section 7.4, the only source of instability (unstable equilibrium) of high-symmetry configurations of molecular systems with a nondegenerate ground state is the vibronic mixing with the excited states by nuclear displacements of lower symmetry. If one starts with a high-symmetry configuration of the system, its possible instability and directions of distortions are controlled by, and only by strongly admixing excited states. The number of the latter, that are active in causing the instability of the ground state, is limited by selection rules and not very large energy gaps.

The condition of PJT instability in the direction of the symmetrized coordinate  $Q$  is given by Eq. (7.85). This equation reveals the specific excited electronic states that produce the configuration instability in the ground state in a certain direction. Relations similar to (7.82) [which leads to (7.85)] were discussed by Bader [9.28] and further developed in application to instability problems by Pearson [9.26]. In this Bader–Pearson treatment the reduction in curvature of the ground-state APES resulting from its vibronic mixing with the excited states is given as one possible explanation for the softening and instability of the ground state. In the vibronic approach, as distinct from the Bader–Pearson treatment, the vibronic mixing of the ground and excited electronic states is *the only possible source of any configuration instability* (see the TEST paradigm, Section 7.4). This also means that if there is instability, there should be excited states that cause

the distortion. Since the PJTE is the only source of distortions of high-symmetry configurations in nondegenerate states, the observed geometry of molecular systems can be explained (predicted) by direct estimation of the corresponding JTE and/or PJTE parameters and the contribution of the excited states to the instability of the ground state under consideration.

Example 9.3 illustrates this statement by considering the stereochemistry of  $\text{MX}_4$  and  $\text{MX}_6$  systems, and Example 9.4 shows how the differences in observed geometries of some Cu(II) and Zn(II) complexes can be rationalized using numerical estimations of the PJTE. The role of the PJTE in the formation of molecular shapes is elucidated also in Examples 7.2–7.4 by means of ab initio calculations. Quite a number of other examples of JT- and PJT-induced distortions in coordination systems are considered in Ref. 9.20.

### EXAMPLE 9.3

#### *Stereochemistry of $\text{MX}_n$ Systems Controlled by Electronic Structure and Vibronic Coupling*

Consider  $\text{MX}_n$  systems where M is a transition element. In a planar  $\text{MX}_4$  system the typical electronic configuration is (Section 6.2):

$$\dots(a_{1g})^2(b_{1g})^2(e_u)^4\{(b_{2g})(e_g)(2a_{1g})(2b_{1g})\}(a_{2u})^0(3a_{1g})^0$$

where the MOs in braces should be populated by the  $d$  electrons. The distortion of the square-planar configuration toward  $D_{2d}$  and/or tetrahedral  $T_d$  symmetry is a  $B_{2u}$  nuclear displacement. Hence, if the ground electronic state is nondegenerate and totally symmetric, this distortion may take place because of its strong mixing with an excited state  $B_{2u}$ . The latter can be obtained by one of the following one-electron excitations:  $e_u \rightarrow e_g$ ,  $b_{1g} \rightarrow a_{2u}$ , or  $b_{2u} \rightarrow 2a_{1g}$  ( $b_{2u}$  is an inner MO not shown above). Therefore, if the  $e_g$  and  $2a_{1g}$  MOs are fully occupied by  $d$  electrons, but the  $2b_{1g}$  MO is unoccupied, the square-planar configuration is stable. In other words, low-spin  $\text{MX}_4$   $d^8$  complexes of Ni(II), Pd(II), and Pt(II) are expected to be square planar. On the contrary, high-spin  $d^5$  and  $d^{10}$  complexes with an occupied  $2b_{1g}$  MO may be unstable in the planar configuration because of the strong mixing with the low-lying  $B_{2u}(2b_{1g} \rightarrow a_{2u})$  term.

Passing on to octahedral  $\text{MX}_6$  systems, let us consider the example of  $\text{XeF}_6$  [9.9, 9.10]. Nonempirical calculations of the electronic structure of this molecule [9.29] show that the outer MOs are arranged in the following sequence:  $(t_{2g})^6(t_{2u})^6(t_{1u})^6(t_{1g})^6(e_g)^4(a_{1g})^2(2t_{1u})^0$  with an energy gap of about 3.7 eV between the  $a_{1g}$  and  $t_{1u}$  MOs. This results in instability of the system with respect to  $T_{1u}$  displacements. For comparison, the calculations [9.30] performed for a similar system  $\text{SF}_6$  yield the

following sequence of MOs:  $(t_{2g})^6(e_g)^4(t_{1u})^6(t_{2u})^6(t_{1g})^6(a_{1g})^0(2t_{1u})^0$ . Here the  $a_{1g}$  MO (distinct from  $\text{XeF}_6$ ) is unoccupied, and since the energy gap between the highest occupied  $t_{1g}$  and unoccupied  $t_{1u}$  MOs is sufficiently large, the  $O_h$  symmetry configuration of  $\text{SF}_6$  is stable with respect to odd (dipolar) displacements. A series of investigations of the vibronic effects in the  $\text{XeF}_6$  system, including electronographic and spectral measurements and MO LCAO calculations [9.9, 9.10, 9.31], confirm the PJT origin of the instability with respect to the odd  $T_{1u}$  displacements (dipolar instability).

#### EXAMPLE 9.4

##### *Pseudo-JT Origin of Distortions in $\text{CuCl}_5^{3-}$ versus $\text{ZnCl}_5^{3-}$*

An example of a PJTE application in stereochemistry is provided by the comparison of instabilities of two pentacoordinated complexes  $\text{CuCl}_5^{3-}$  (I) and  $\text{ZnCl}_5^{3-}$  (II) with respect to the two possible types of distortion:  $E'$ , toward a square-pyramidal (SP) configuration, and  $A_2''$ , toward a distorted tetrahedron with an additional ligand on the axis of distortion shown in Fig. 9.5. These two systems, I and II, are very similar, with the distinction that in II there is an additional  $d$  electron of the CA (and an additional proton in the nucleus) making its electron configuration  $d^{10}$ , instead of  $d^9$  as in I. In terms of electronic structure and vibronic coupling, this difference is most important.

The structure of II in the crystal state also differs radically from that of I. The  $\text{CuCl}_5^{3-}$  ion in the  $[\text{Co}(\text{NH}_3)_6][\text{CuCl}_5]$  crystal is unstable with respect to  $E'$ -type distortions describing the conversion TBP  $\rightarrow$  SP (Fig. 9.5a); it has three equivalent (almost) SP configurations and performs rapid conversions between them: molecular pseudorotations [9.32] (see below in this section). The  $\text{ZnCl}_5^{3-}$  ion in a quite similar crystal  $[\text{Co}(\text{NH}_3)_6][\text{ZnCl}_5]$  is also not TBP, but it forms a distorted tetrahedron plus one chlorine ion on (almost) the trigonal axis [9.33], and there are no pseudorotations. This configuration can be regarded as produced by the  $A_2''$  distortion of the TBP configuration, as shown in Fig. 9.5b.

An explanation for these experimental observations was given [9.34] on the basis of the pseudo-JTE using approximate semiempirical IEH (SCCC) calculations of the electronic structure (Section 5.5) and vibronic coupling constants to numerically confirm the vibronic origin of the distortion. The idea was to compare the negative pseudo-JT contribution  $K_v$  [Section 7.4, Eq. (7.84)] of the relevant excited

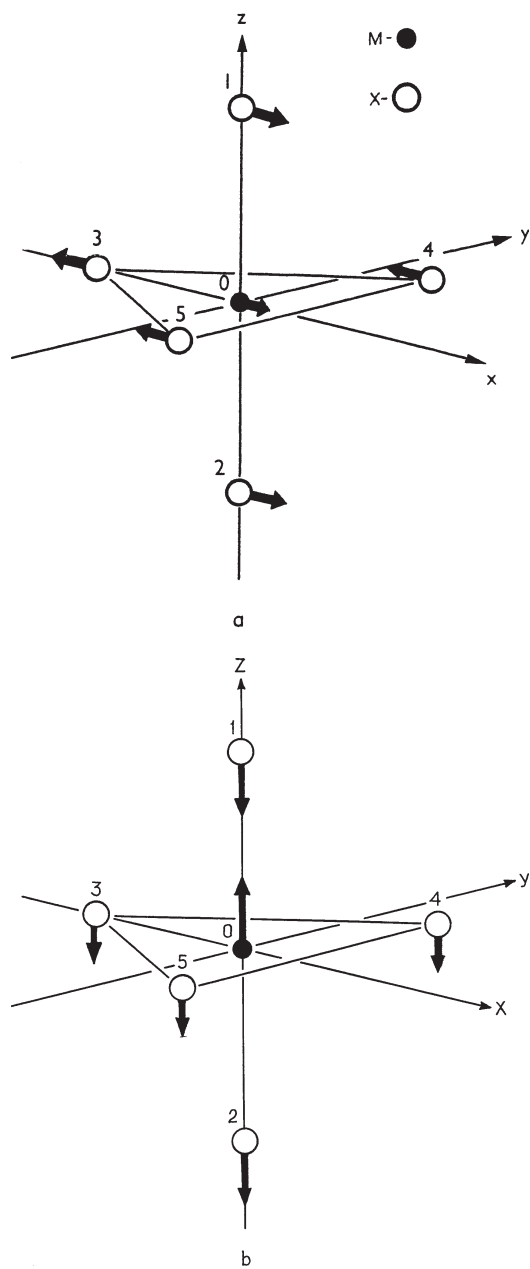


**FIGURE 9.5.** Ligand numeration and the main symmetrized distortions in pentacoordinated complexes  $MX_5^{n-}$ : (a)  $E'$ -type displacements realizing TBP  $\rightarrow$  SP conversion; (b)  $A_2''$ -type displacement realizing the transformation  $MX_5(\text{TBP}) \rightarrow MX_4(\text{tetrahedron}) + X$ .

states to the instability of the ground state with respect to  $E'$  and  $A''$  distortions, respectively, and to reveal in this way the expected distortions (largest  $K_v$ ) in each of the two systems I and II.

The ground state of  $\text{CuCl}_5^{3-}$  in the TBP geometry is  ${}^2A'_1$  with the MO configuration  $\dots(3e'')^4(5e')^4(5a'_1)^1$ . The highest single occupied MO  $5a'_1$  is an antibonding linear combination of the copper AO  $3d_{z^2}$  and chlorine AOs  $3p_\sigma$ . The relevant excited states of required symmetry (for which the PJT vibronic coupling constant is nonzero) are produced by corresponding one-electron excitations. Because of different occupation numbers the contributing excited states in  $\text{ZnCl}_5^{3-}$  differ from those in  $\text{CuCl}_5^{3-}$ , and the numerical contributions to  $K_v$  of similar excited states also differ.

The semiempirical method [9.34] does not allow one to calculate accurately the  $K_0$  values that depend on the wavefunction at the nuclei, but the data on the pseudo-Jahn–Teller contribution of the excited states obtained by calculations allow one to estimate the relative instabilities induced by the vibronic coupling in different symmetrized directions of the same system, for which the  $K_0$  value, in its part depending on  $\Psi(0)$ , can be assumed to be the same. In this way the relative instabilities of the same system with respect to the two possible distortions,  $E'$  and  $A''_2$ , are estimated for I and II. The contribution of the closed-shell core electrons (and all the  $ns$  electrons) that make the  $\Psi(0)$  quantity nonzero may be assumed to be the same for both distortions, whereas the contributions of the  $d$  hole to these two displacements are different. The  $d$ -state contributions  $K_0^d$  to  $K_0$  can be easily calculated. The hole in the  $d^{10}$  configuration is  $d_{z^2}$ , and the contribution is negative for  $E'$  distortions and positive for  $A''_2$  (the opposite signs are due to the field gradient created by the  $d_{z^2}$  hole, which is positive in the  $z$  direction and negative in the  $xy$  plane).

The numerical data in Ref. 9.34 show explicitly that the  $\text{CuCl}_5^{3-}$  complex is more unstable with respect to the  $E'$  distortion that transforms the TBP configuration into SP (or near SP) (Fig. 9.5a), whereas in  $\text{ZnCl}_5^{3-}$  the instability is stronger with respect to the  $A''_2$  distortion that describes the transformation of the TBP configuration toward a distorted tetrahedron plus one ligand on the trigonal axis at a greater distance (Fig. 9.5b), in full qualitative agreement with the experimental data mentioned above. Indeed, for  $\text{CuCl}_5^{3-}$  (in  $\text{mdyn}/\text{\AA}$ )  $K_v(E') = -263$ , while  $K_v(A'') = -220$ , whereas for  $\text{ZnCl}_5^{3-}$ , we have  $K_v(E') = -130$  and  $K_v(A'') = -151$ . These examples show in detail how the electronic structure, ground and excited states, control the nuclear configuration (via vibronic coupling), making it, under certain conditions, unstable with respect to nuclear displacements of specific symmetry.



### Off-Center Position of the Central Atom

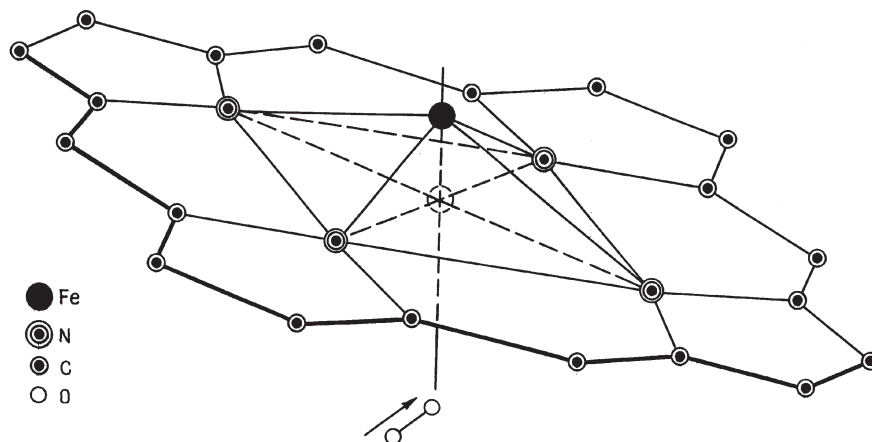
Displacement of the CA from its geometric center in coordination compounds is a special case of vibronic effects in stereochemistry. An example of this effect is considered in Section 7.4 for the  $\text{TiO}_6^{8-}$  cluster in perovskites, where it is shown that, as a result of the PJTE (vibronic mixing of the ground state  $A_{1g}$  with the excited  $T_{1u}$  term), the Ti atom may be displaced from the inversion center resulting in dipole moment formation. This displacement, as shown in Section 9.4, produces the spontaneous polarization of the lattice and ferroelectric phase transitions, provided that cooperative effects in crystals are taken into account. Similar effects are well known for impurity centers in crystals [9.20].

Consider another illustrative example: the out-of-plane displacements of the iron atom, as well as other metal atoms, in metal porphyrins and hemoproteins [9.35]. Besides being of special interest in biology, this example has general significance. It reflects the situation in a great number of corresponding classes of organometallic compounds with close-in-energy states of the metal  $d$  electrons and porphyrin (or a similar ligand)  $\pi$  electrons. The mixing of these states under nuclear displacements, which shifts the metal atom out of and transverse to the porphyrin ring plane, renders the system soft or even unstable with respect to such displacements. Visually, the out-of-plane displacement of the metal atom with regard to the porphyrin ring is due to the additional  $\pi$  binding of the  $d$  orbitals of the metal and  $\pi$  orbitals of the ligands, illustrated in Fig. 7.20.

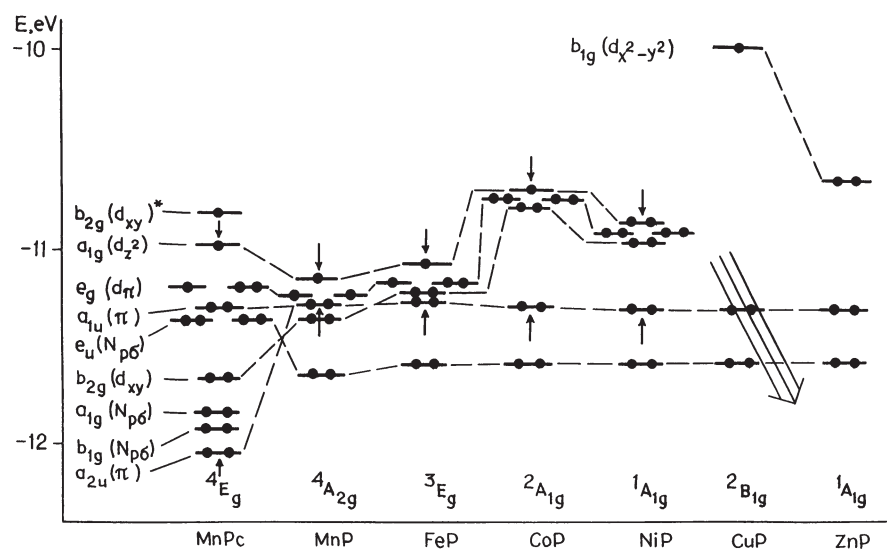
According to Eq. (7.67) or (7.85), the softening and instability of the high-symmetry configuration due to the PJTE is determined by the value of  $F^2/\Delta$ , where  $F = \langle 1 | \partial V / \partial Q | 2 \rangle$  is the vibronic constant of mixing states 1 and 2 by the nuclear displacements  $Q$ , and  $2\Delta$  is the energy gap between them. As a result of the pseudo-Jahn–Teller effect the force constant changes from  $K_0$  to  $K_0 - (F^2/\Delta)$ , and if  $(F^2/\Delta) > K_0$ , the system becomes unstable with respect to the  $Q$  displacements. For metal porphyrins (MP) of  $D_{4h}$  symmetry the out-of-plane displacement is of  $A_{2u}$  symmetry (Fig. 9.6), which means that  $F$  is nonzero if and only if the product of the representations of the mixing states 1 and 2 contains the  $A_{2u}$  representation.

Figure 9.7 shows several HOMO and LUMO energy levels of Mn, Fe, Co, Ni, Cu, and Zn porphyrins, as well as Mn phthalocyanine (MnPc) obtained from calculations for the planar configuration [9.36]. It is seen that in FeP, for instance, the calculated ground state is  ${}^3E_g$ ; hence the excited state that couples with the ground one by the  $A_{2u}$  displacements must be  ${}^3E_u$  (because in the  $D_{4h}$  group  $E_g \times A_{2u} = E_u$ ). In MnP, MnPc, and CoP the corresponding excited states are  ${}^4A_{2u}$ ,  ${}^4E_g$ , and  ${}^4A_{2u}$ , respectively. All of them correspond to a one-electron excitation from the  $a_{2u}(\pi)$  MO (predominantly from the porphyrin ring) to the empty  $a_{1g}(d_{z^2})$  (predominantly from the metal), and the excitation energy  $2\Delta = \varepsilon(a_{1g}) - \varepsilon(a_{2u})$  is relatively small. In the remaining metal porphyrins NiP, CuP, and ZnP, the  $a_{1g}$  MO is occupied, whereas the next MO of the same symmetry is very high (not shown in Fig. 9.7). It follows that in the last three MePs there





**FIGURE 9.6.** Structure of metalloporphyrins. In the  $D_{4h}$  symmetry group the out-of-plane displacement of the CA has  $A_{2u}$  symmetry. The nondisplaced position of the iron atom is shown by dashed line. The approaching oxygen molecule is also shown.



**FIGURE 9.7.** HOMO and LUMO energy levels for some metal porphyrins (MPs) and manganese phthalocyanine (MnPc) with indication of the ground state for the in-plane position of the metal. The two MOs forming the energy gap  $2\Delta$  between the ground and excited states that mix under the  $A_{2u}$  displacement are shown by arrows.

is practically no PJT instability with regard to the out-of-plane displacement of the metal atom, whereas for other cases the effect may be important.

For an estimate of the effect, the calculated values of  $2\Delta$  can be used; they are approximately equal to 0.15, 0.20, 0.6, and 1.0 eV in MnP, FeP, CoP, and MnPc, respectively. The vibronic constant was roughly estimated as  $F \approx 10^{-4}$  dyn for FeP (for other MePs with approximately the same wavefunctions  $F$  has the same order of magnitude), while the  $K_0$  value for the  $A_{2u}$  displacements can be taken as  $K_0 \sim 10^4$  dyn/cm. We have  $(F^2/K) \sim 0.1$  eV, that is,  $F^2/K$  and  $\Delta$  are of the same order of magnitude and this confirms that the PJTE may soften the ground state. In MnP and FeP ( $\Delta \sim 0.08$  and 0.1 eV, respectively)  $\Delta < (F^2/K)$  and the softening transforms into instability, while in CoP and MnPc ( $\Delta \sim 0.3$  and 0.5 eV, respectively) only a softening but no instability of the metal position may be expected. These results are in qualitative agreement with the empirical data available.

The metal atom position with respect to the porphyrin ring is significant in determining some biologic functions of hemoproteins (Section 10.3). The first explanation of the origin of the out-of-plane position of the iron atom was that in the high-spin configuration the atomic radius of Fe(II) is too large to fit the cavity in the porphine ring [in the low-spin configuration the Fe(II) ion occupies an in-plan position; Section 10.3]. Such "nonquantum" explanations, in general, may not work, especially when there are nonlocalized bonds as in transition metal compounds. Indeed, the cavity in phthalocyanine is considerably smaller than in porphine. Nevertheless, MnPc is planar, whereas MnP is non-planar. Again, a series of porphyrins of other metals, such as Sn(IV) and Mo(IV), with ionic radii larger than Fe(II), are planar [9.35].

### Geometry of Ligand Coordination

Another important problem in stereochemistry of coordination compounds is the mode of coordination of small ligands to the central atom. This problem, too, can be successfully considered by means of the vibronic approach. Consider, for example, the O<sub>2</sub>, CO, and NO molecules coordinated to metal porphyrins or the heme in hemoproteins (for the coordination of NO to other systems, see Ref. 9.37 and references cited therein). Four modes of coordination are observed experimentally (Fig. 9.8): linear end-on, bent end-on, bent side-on, and symmetric side-on. The study of the mode of coordination with metalloporphyrins (MeP) in model compounds shows that, depending on the metal, the linear end-on coordination is characteristic for NO and CO, while the bent end-on coordination is usually observed for NO or O<sub>2</sub>, and the O<sub>2</sub> ligand can also be in symmetric side-on geometry. The origin of these geometries has aroused intensive discussions [9.35].

Consider this problem using the vibronic approach. This approach implies that the bent end-on configuration appears as a consequence of the pseudo-JT instability of the linear end-on and symmetric side-on geometries. In metal porphyrins of  $D_{4h}$  symmetry with a linear end-on coordination of diatomics at the

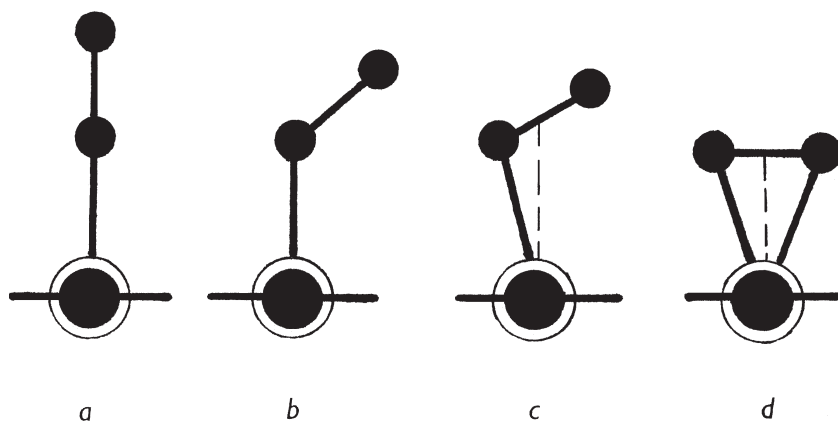


**FIGURE 9.8.** Four types of geometry of coordination of diatomics to a transition metal center: (a) linear end-on, (b) bent end-on, (c) bent side-on, (d) symmetric side-on.

fifth coordinate, bending of the ligand is an  $E$ -type displacement (for the influence of the imidazole ligand at the sixth coordinate position, e.g., in Hb, see Ref. 9.35). Therefore, the PJT instability with respect to the bending of the diatomic ligand may take place if the product of representations of the ground and (not very high in energy) excited states contains the  $E$  representation.

Several HOMO and LUMO energy levels for the MeP—CO, MeP—NO, and MP—O<sub>2</sub> systems calculated assuming linear end-on coordination [9.37, 9.38] are given in Fig. 9.9. The qualitative changes of some of these levels due to their vibronic mixing with the excited states formed by one-electron transition from the  $e(d_\pi - \pi^*)$  or  $e(d_\pi + \pi^*)$  MOs to the  $a_1(d_z)$  MO are illustrated in Fig. 9.10. In fact, only the most essential mixing orbitals with sufficiently large vibronic constants should be considered. Large vibronic constants occur when the mixing states contribute substantially to the bonding that is strongly influenced by the  $E$  displacements (by the ligand bending). For example, the  $E$  displacements formally mix the MO  $e(P)$  with  $a_1(d_{z2})$ , but since  $e(P)$  is the state of the porphine ring not involved in the metal—diatomic bond, the vibronic constant  $F = \langle e(P) | (\partial V / \partial Q_E) | a_1(d_{z2}) \rangle$  ranges from small to zero.

Denoting the corresponding energy intervals in Fig. 9.9 and vibronic constants by  $2\Delta_1$  and  $2\Delta_2$  and  $F_1$  and  $F_2$ , respectively, and considering the vibronic mixing of each pair of MOs,  $e(d_\pi - \pi^*)$  with  $a_1(d_{z2})$ , and  $e(d_\pi + \pi^*)$  with  $a_1(d_{z2})$ , we conclude, using Eq. (7.85), that each of these mixing lowers the force constant  $K_E$  by an amount dependent on the respective MO occupation numbers. Denoting the latter by  $q_1$ ,  $q_2$ , and  $q_3$ , respectively, for levels 1, 2, 3 marked with arrows in Fig. 9.9, we obtain the following condition for the instability of the linear end-on configuration:

$$\frac{(q_1 - q_3)F_1^2}{\Delta_1} + \frac{(q_2 - q_3)F_2^2}{\Delta_2} > K_E \quad (9.8)$$

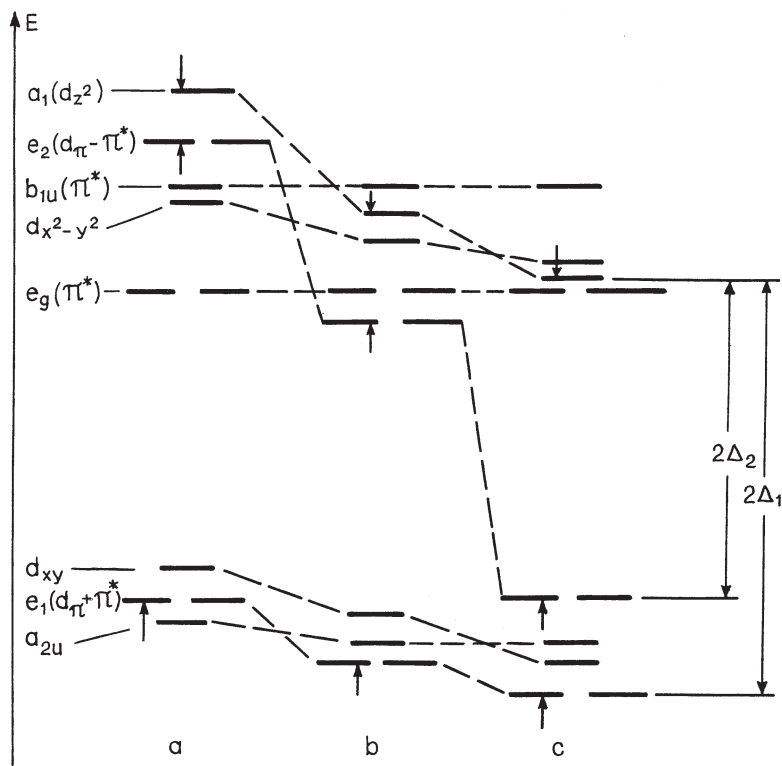


**FIGURE 9.9.** MO energy-level diagrams for linear end-on coordination of diatomics to metalloporphyrins: (a) CO, (b) NO, (c) O<sub>2</sub>. The arrows indicate the energy gaps  $2\Delta_1$  and  $2\Delta_2$  between the  $e$  and  $a_1$  MOs that mix under the bending ( $E$ -type) displacement of the ligand.

If this condition is satisfied, the adiabatic potential of the system with respect to the  $E$  displacement in question has a maximum for the linear end-on coordination and a continuum of minima, forming a circular trough (7.79) [9.35]. Each point of the latter corresponds to bent end-on coordination at a certain angle to the linear end-on line with arbitrary orientation around this line. If the quadratic terms of the vibronic interaction are included in the calculation, four additional minima (7.85) are formed along the bottom of the trough, regularly alternating with four saddle points. In this case the bent end-on coordination of diatomics has four preferable orientations with respect to the pyrrole ring: either toward the nitrogen atoms or between them, depending on the sign of the quadratic vibronic constant (see discussion of the  $E-A$  mixing problem in Section 7.4).

Consider now the MeP—CO system, for which  $2\Delta_1 = 4.0$  eV,  $2\Delta_2 = 0.3$  eV [9.38, 9.39] (Fig. 9.9). Using the known order of magnitudes of  $F$  and  $K_E$ , we conclude that if only the lower  $e(d_{\pi} + \pi^*)$  state is occupied by electrons and contributes to softening of the system (i.e.,  $q_2 = q_3 = 0$ ), inequality (9.8) is not

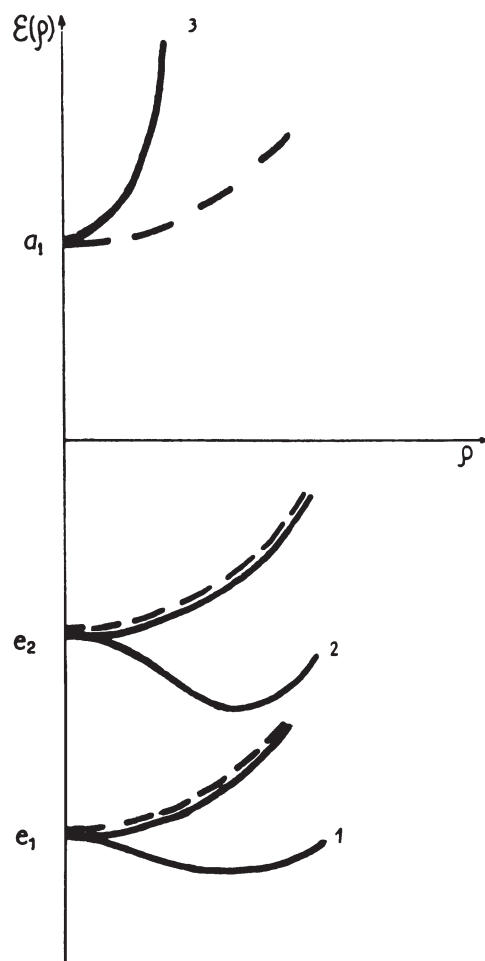


**FIGURE 9.10.** MO energies of some of the (active) levels of Fig. 9.9 as a function of the bending angle  $\rho$  with strong (solid line) and without (dashed line) pseudo-Jahn-Teller mixing  $e - a_1$ .

satisfied ( $\Delta_1$  is large) and the linear coordination is stable. If the higher MO  $e(d_\pi - \pi^*)$  is occupied, inequality (9.8) is satisfied, due to the small value  $\Delta_2$ , and the linear end-on coordination becomes unstable. In MeP—CO with linear end-on geometry the state  $e(d_\pi - \pi^*)$  remains unoccupied for all  $3d^n$  metals, including  $3d^{10}$ . Hence, in  $3d^n$  transition metal porphyrins, the CO molecule is expected to be linearly end-on-coordinated. This prediction of the vibronic theory agrees well with the abovementioned experimental data.

For the MeP—NO system, the values  $2\Delta_1$  and  $2\Delta_2$  have the same orders of magnitude as in the previous instance of MeP—CO, but the energy-level ordering

is different (Fig. 9.9); the  $e(d_\pi - \pi^*)$  MO becomes occupied when the number of  $d$  electrons plus the antibonding  $\pi^*$  electrons of the NO molecule exceeds six. Thus, in the  $3d^n$  metal porphyrins the NO molecule in the linear end-on configuration is stable for  $n+1 \leq 6$  and unstable for  $n+1 > 6$ . This conclusion also agrees with the experimental data.

Finally, in MeP—O<sub>2</sub> both  $e$  MO levels are at about the same distance from the  $a_1$  level (Fig. 9.9) ( $2\Delta_1 = 3$  eV and  $2\Delta_2 = 2.5$  eV) and may give a comparable contribution to the softening of the linear geometry Me—O—O with respect to the  $E$  bending. Therefore, it can be assumed that the cumulative effect suffices to provide essential softness or even instability of the linear coordination. The softening is expected to be approximately doubled when the number of  $d$  electrons plus two antibonding  $\pi^*$  electrons of the O<sub>2</sub> molecule exceed six. This result also agrees qualitatively with the experimental data.

Stability of the symmetric side-on coordination of small ligands can be considered similarly. The displacements toward bent coordination are of  $B_1$  (or  $B_2$ ) symmetry, for which the nonzero vibronic constant corresponds to the mixing of the  $b_1(d_{xz})$  [or  $b_2(d_{yz})$ ] with the  $a_1$  MO. Both these MOs are nondegenerate, and hence the PJT instability can be obtained directly using Eq. (9.8). Estimations for the Me—O<sub>2</sub> system show that the criterion  $(F^2/\Delta) > K_E$  is not satisfied, and the symmetric side-on coordination of O<sub>2</sub> is expected to be stable.

Another feature directly related to the geometry of ligand coordination is the change in geometry (distortion) of the ligand itself by coordination. The only possible distortion in diatomics is the change in interatomic distance. It takes place, indeed, and this topic is discussed in more detail in Section 11.2, together with chemical activation by coordination. For ligands with three or more atoms, distortion of the nuclear configuration that lowers its symmetry may take place as a result of the electronic rearrangement induced by coordination.

Consider, for example, the C<sub>2</sub>H<sub>4</sub> molecule coordinated as a ligand to a transition metal complex (cf. Sections 6.3 and 11.3). The free molecule in the ground state is planar and has a nondegenerate ground state  $^1A_{1g}$  (valence electron configuration  $\pi^2\pi^{*0}$ ), while in the first excited state  $^1B_u(\pi^1\pi^{*1})$  it is nonplanar, with the two CH<sub>2</sub> groups in mutual perpendicular planes. By coordination as a  $\pi$  complex to transition metals in low oxidation states, an orbital charge transfer from the bonding  $\pi$  orbital of C<sub>2</sub>H<sub>4</sub> to the metal together with a strong  $\pi$  backdonation to the free  $\pi^*$  orbital of C<sub>2</sub>H<sub>4</sub> take place, and the local charge distribution in C<sub>2</sub>H<sub>4</sub> becomes similar to  $\pi^{2-\delta}\pi^{*\delta}$ . The population of the  $\pi^*$  orbital distorts the ground-state planar configuration of the molecule, making it similar to the excited state. The experimental data show that, indeed, the geometry of coordinated C<sub>2</sub>H<sub>4</sub> is intermediate between those of the ground (planar) and excited states, the latter having the configuration with two mutually perpendicular CH<sub>2</sub> groups [9.40].

For other examples, refer to the literature [9.1, 9.20, 9.23, 9.26, 9.37]. In Section 11.2 other aspects of ligand coordination are considered in connection with their activation.

### Stereochemically Active and Inert Lone Pairs

In Section 9.1 the stereochemistry of lone pairs is considered in the semiclassical approximation in which the lone pairs are treated as repulsion units alongside the bond pairs, and as such they occupy a coordination place, distorting the otherwise symmetric coordination polyhedron. However, in some systems the polyhedron is not distorted, despite the presence of a lone pair, and in these cases the latter is called *inactive* or an *inert lone pair* [9.41].

Very often the lone pair originates from the CA  $(ns)^2$  configuration, with  $n = 4, 5, 6$ ; the posttransition elements In(I), Tl(I), Pb(II), Sb(III), Te(IV), Xe(VI), and so on, are of this type. In  $\text{SbBr}_6^{3-}$  and  $\text{TeCl}_6^{2-}$ , for example, the  $(ns)^2$  lone pair is stereochemically inert (the octahedron is not distorted), whereas in  $\text{XeF}_6$ ,  $\text{InCl}_6^{5-}$ , and other compounds the octahedron is distorted. The  $(ns)^2$  pair itself is spherical symmetric and does not cause distortions. Hence, using the VSEPR model (Section 9.1) in order to explain the origin of distortion, one has to assume that there is a strong hybridization of the  $ns$  states with the  $np$  ones resulting in a directed lone pair (Fig. 9.2) [9.42, 9.43].

On the other hand, as stated above (Section 2.1 and 9.1), hybridization is, in fact, not the cause of the distortions but rather its consequence. It is mentioned in Section 9.1 that in the more general MO LCAO scheme the distortion may occur if in the high-symmetry configuration the two electrons occupy a strongly antibonding MO that under the distortion, transforms to a lone pair. These considerations are qualitatively true, but they give no rigorous general solution of the problem that would contribute to a more general understanding. Such a solution was obtained on the basis of the vibronic approach [9.44].

Consider the general MO LCAO scheme (Fig. 9.11) for an undistorted octahedral system  $\text{MX}_6$ , which, in the representation of local M—X bonds, has a  $(ns)^2$  electron pair above the six bonding pairs (in fact, each M—X bond may have more than one bonding electron pair, as in the case of multiple bonds). In this scheme the two  $ns$  electrons occupy the antibonding MO  $a_{1g}$  ( $\pi$  MOs and ligand nonbonding MOs are not indicated). The ground state of the system as a whole  $A_{1g}$  is nondegenerate, but relatively close in energy are the excited  $T_{1u}$  states formed by one-electron excitations  $a_{1g}^* \rightarrow t_{1u}^*$ .

In the vibronic approach the stability or instability of the regular octahedral configuration is determined by Eq. (7.85) or (7.67), which gives the relationship of the parameters for which the system is stable or unstable, and the direction of instability in the latter case. The PJT mixing of the ground  ${}^1A_{1g}$  state with the excited  ${}^1T_{1u}$  by  $T_{1u}$ -type nuclear displacements results in instability of the ground state with respect to  $T_{1u}$  distortions (Section 7.4), provided that the condition of instability is satisfied. This distortion is somewhat similar to the dipolar instability produced by the same  $A_{1g}-T_{1u}$  mixing in the  $\text{TiO}_6^{8-}$  octahedron (Section 7.4), but the change from  $d$  electrons in Ti to  $sp$  electrons in the  $\text{MX}_6$  systems introduces significant alterations. It can be shown that in the linear approximation with respect to the vibronic coupling terms in the Hamiltonian, the  $s-p$  ( $A_{1g}-T_{1u}$ ) vibronic mixing [ $(A_{1g} + T_{1u}) \otimes t_{1u}$  problem] results in a trough of minima in the space of  $T_{1u}$  distortions [i.e., all the distortions corresponding to any combination

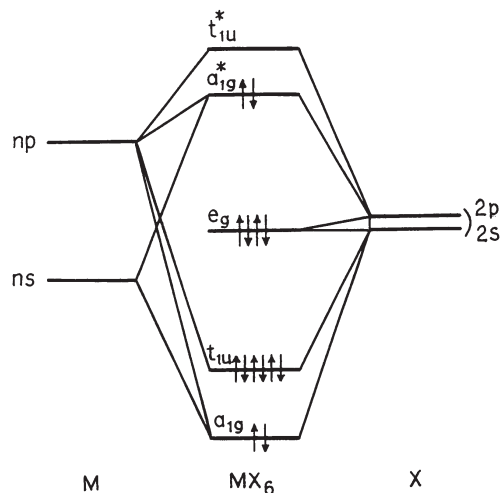


**FIGURE 9.11.** The MO LCAO energy-level scheme for an  $\text{MX}_6$  system with a lone pair—a  $(ns)^2$  configuration above the closed shells of M and X. Six ligand  $\sigma$  ( $sp$ ) AOs form with the CA  $ns$  and  $np$  AOs the bonding  $a_{1g}$  and  $t_{1u}$  MOs and the nonbonding  $e_g$  MOs occupied by 12 electrons, while the antibonding MO  $a_{1g}^*$  is occupied by the two  $(ns)^2$  electrons ( $\pi$  MO and ligand nonbonding MO are not shown).

of the three  $T_{1u}$  coordinates (Table 7.1) have the same energy], but inclusion of the second-order terms makes the eight (equivalent) trigonal directions preferable.

However, this problem may be complicated by the fact that the excited  $T_{1u}$  term is degenerate and hence is subject to the Jahn–Teller  $T_{1u} \otimes (e_g + t_{2g})$  effect [9.44]. If the latter is taken into account, the vibronic problem as a whole is a combined pseudo Jahn–Teller and Jahn–Teller problem  $(A_{1g} + T_{1u}) \otimes (t_{1u} + e_g + t_{2g})$ , meaning that there may be distortions of three types:  $T_{1u}$ ,  $E_g$ , and  $T_{2g}$ . The solutions obtained in the linear approximation with respect to the vibronic coupling show that, depending on the vibronic coupling constants and the energy gap  $4\Delta$  between the ground  $A_{1g}$  and excited  $T_{1u}$  states, several possibilities emerge. Assume that  $F$ ,  $F_E$ , and  $F_T$  are the coupling constants to, respectively, the  $T_{1u}$ ,  $E$ , and  $T_{2g}$  displacements;  $K_0$ ,  $K_0^E$ , and  $K_0^T$  are the respective primary force constants (Section 7.4); and the energies of the two mixing terms are taken as  $E(^1A_{1g}) = -3\Delta$  and  $E(^1T_{1u}) = \Delta$ .

Denote

$$\begin{aligned}
 f &= \frac{F^2}{K_0 \Delta} \\
 e &= \frac{F_E^2}{K_E \Delta} \\
 t &= \frac{F_T^2}{3K_T \Delta}
 \end{aligned}
 \tag{9.9}$$



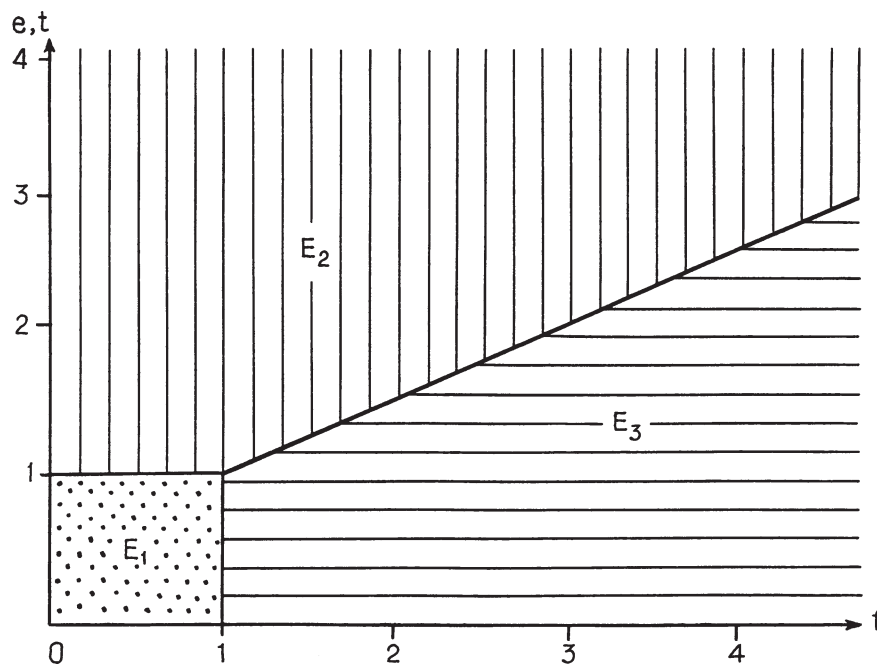


**FIGURE 9.12.** Three domains of existence of different Jahn–Teller and pseudo-Jahn–Teller distortions in  $MX_6$  systems with  $(ns)^2$  lone pairs in each of the two  $e-f$  and  $t-f$  planes:  $E_1$ —no distortions (inert lone pair);  $E_2$ —combined dipolar  $T$  and either tetragonal  $E_g$  (in the  $e-f$  plane), or trigonal  $T_{2g}$  (in the  $t-f$  plane) distortions;  $E_3$ —pure Jahn–Teller either tetragonal (in the  $e-f$  plane) or trigonal (in the  $t-f$  plane) distortions.

These constants have the physical meaning of the corresponding Jahn–Teller stabilization energies in units of  $\Delta$ , taken from the reference position.

In these denotations the expected distortions of the regular octahedron in  $MX_6$  systems under consideration can be evaluated analytically (in Ref. 9.44 totally symmetric distortion are also included). The results are illustrated in Fig. 9.12, which, in fact, comprises two coinciding schemes, one for  $e$  versus  $f$ , and the other for  $t$  versus  $f$ . The meaning of these schemes is as follows. The area delimited by the axes  $e$  and  $f$  (or  $t$  and  $f$ ) is divided into three domains,  $E_1$ ,  $E_2$ , and  $E_3$ , that have different kinds of adiabatic potential minima. In the first domain (dotted-line area), where  $f < 1$ ,  $e < 1$ , and  $t < 1$ , the JT and pseudo-JT stabilization energies are smaller than the corresponding threshold given by Eq. (7.89), and hence there are neither JT nor PJT distortions. This is the case of *inert lone pairs*.

In the area where  $f > 1$ , the PJT  $T_{1u}$  (dipolar) distortion becomes operative, but the admixing of the excited  $T_{1u}$  term involves JT  $T_{2g}$  and  $E_g$  distortions as well. According to the calculations [9.44], the relative energies of the minima in

the three domains in Fig. 9.12 are (in  $\Delta$  units):

$$\begin{aligned} E_1 &= -6 \\ E_2 &= -6 - \frac{2(f-1)^2}{f-t} \\ E_3 &= 2 - 8t \end{aligned} \quad (9.10)$$

and the same relations with  $e$  instead of  $t$  for the  $e-f$  plane. Therefore, the trigonal dipolar (pseudo-Jahn–Teller) distortions  $T_{1u}$  with admixture of either  $E_g$  or  $T_{2g}$  distortions are preferable when  $E_2 < E_3$ , which yields, in addition to  $f > 1$ , the following equations, respectively:

$$f + 1 > 2t \quad (9.11)$$

$$f + 1 > 2e \quad (9.12)$$

If the opposite inequalities hold, then

$$2e > f + 1 \quad (9.13)$$

or

$$2t > f + 1 \quad (9.14)$$

and then the tetragonal  $D_{4h}$  or trigonal  $D_{3h}$  JT minima of the excited state  $T_{1u}$  are lower (than the assumed ground-state one), and they are active in stereochemistry. The preference between tetragonal or trigonal minima is the same as in the usual JT  $T_{1u} \otimes (e + t_{2g})$  problem (Section 7.3): the trigonal distortions are preferable if  $t > e$ , and the tetragonal ones occur for the opposite inequality,  $e > t$ .

All these distorted geometries of  $\text{MX}_6$  systems with  $(ns)^2$  lone pair configurations are found in different systems [9.1–9.4, 9.10–9.12, 9.15, 9.20, 9.41]. Moreover, the combined distortions described above explain the origin of complicated (helical) crystal structures (Section 9.4). In particular, in the  $\text{InCl}$  crystal ( $\text{InCl}_6^{5-}$  units) both types of distortion in the  $E_2$  area of Fig. 9.12, trigonal  $T_{2g}$  plus dipolar  $T_{1u}$ , and tetragonal  $E_g$  plus dipolar  $T_{1u}$ , are observed in two phases of the crystal, yellow and red, respectively [9.45].

A similar treatment, in principle, is possible for many other types of systems. For instance, in multicenter transition metal clusters the change of geometry from regular tetrahedral in 60-electron tetraclusters to butterfly geometry in similar 62-electron clusters was subject to discussion with respect to a vibronic problem on two electronic terms,  $T_1 + T_2$ , mixing via  $e_g + t_{2g}$  distortions [9.21, 9.46]. Many observed cluster geometries can be explained in this way.

### Pseudorotations in Coordination Systems

As shown in Sections 7.3 and 7.4, the JTE [including proper JT, pseudo-JT, and RT (Renner–Teller) effects] in the high-symmetry configuration of a molecular system may result in the formation of two or several (or an infinite number of) equivalent minima of its APES that correspond to equivalently distorted polyhedrons. If the energy barriers between these minima are not very high (or even zero, as in the cases of a trough of minima), the free system performs continuous transitions between the minima. These transitions are classified in Section 7.3 as internal *free rotations*, *hindered rotations*, and *pulsating motions*.

As emphasized above, the transitions between the configurations of equivalent minima are never real rotations, although outwardly the equivalent configurations may appear to rotate from one to another. For instance, for tetragonal distortion of the octahedron in the quadratic  $E \otimes e$  problem, the transition from the configuration elongated along the  $Z$  axis to that elongated along the  $X$  axis (Figs. 7.11 and 7.13), owing to the identity of the ligands, resembles a rotation on  $\pi/2$  along the  $Y$  axis. In fact, however, such a rotation does not take place, the nuclear motions in in this transition are more complicated [9.20] (Fig. 7.13). They can be observed experimentally in the NMR spectra, isotopic substitutions experiments, central atom GRS spectra, tunneling splitting (Section 7.3), and other spectroscopic

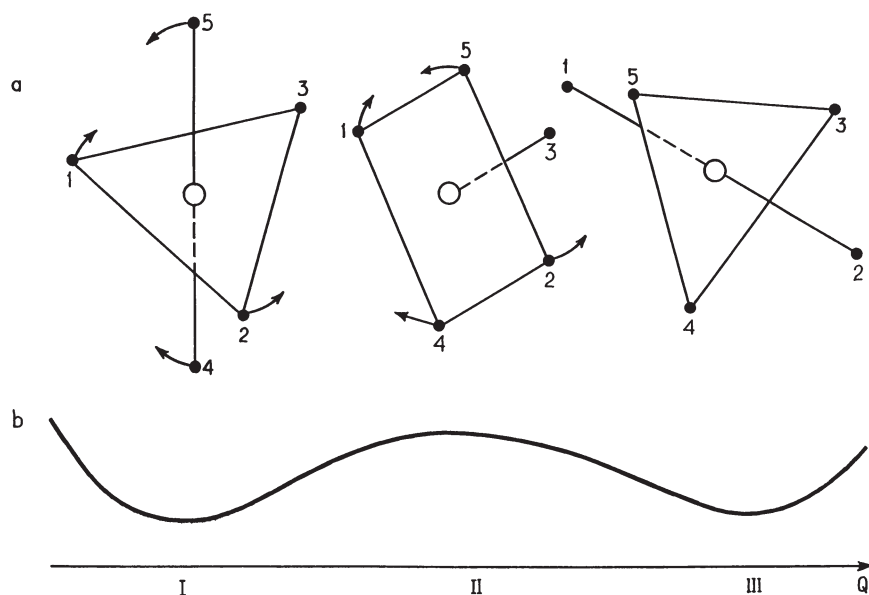


**FIGURE 9.13.** Berry pseudorotation of a trigonal bipyramidal molecule: (a) the distortions shown by arrows (combined  $E$  type) convert the configuration I into an equivalent III via the intermediate square-pyramidal structure II that has a higher energy; (b) the APES curve along the distortion coordinate on the APES.

measurements. These internal motions are called *pseudorotations*. Of course, the free molecular system may also perform regular (traditional) rotations.

In coordination compounds, pseudorotations are sometimes called *flexional behavior* [9.47]. As seen from the examples, considered below, in many cases the JT and pseudo-JT dynamics can be interpreted visually as a continuously changing “flexional” configuration. One of the first observations of such behavior relates to Cu(II) compounds [9.48]. Another kind of flexionality takes place in coordination compounds with the *alterdentate ligands*; the latter offer to the metal ion two or more equivalent coordination sites, and hence under certain conditions the metal can resonate between them (e.g., in the alloxan radical anion) [9.5, 9.49].

Pseudorotations in molecular systems, in general, were known for a long time. Berry [9.11] (not the author of the Berry phase problem in Section 7.3) assumed that the APES of such systems has several equivalent minima (without specifying their origin) with small energy barriers between them, and the observed pseudorotations are due to the transitions between the minima. For instance, the pseudorotation molecule  $PF_5$  is assumed to have an energy minimum in trigonal-bipyramidal (TBP) configuration I with the F atoms 4 and 5 in axial positions (Fig. 9.13a), and as a result of the displacement of the type  $Q$  (combined  $E$  displacements) transforms into square-pyramidal (SP) configuration II. By further transformation, II converts again into TBP configuration III, but with other atoms F on the threefold axis (1 and 2 instead of 4 and 5). With identical F atoms this transformation looks like a  $90^\circ$  rotation of the threefold axis.

Another example is the  $SF_4$  molecule with minima at  $C_{2v}$  symmetry, which can be considered as either a strongly distorted tetrahedron or a less distorted square with two angles F—S—F of  $183^\circ$  and  $104^\circ$ . Here the Berry rotation consists of transitions between two equivalent distorted configurations via the intermediate unstable square-planar geometry; this mechanism of interconversion in  $SF_4$  is confirmed by dynamic NMR experiments [9.50] and by direct electronic structure calculations [9.51].

In both examples the intermediate configuration has a maximum of the APES of the nondegenerate ground state with respect to a specific symmetrized direction  $Q$ . According to the conclusions of the vibronic theory, the instability of the high-symmetry intermediate configuration is due to the vibronic mixing of its electronic ground state with some excited states of appropriate symmetry determined by the nonzero vibronic constant. The Berry rotations under consideration are thus pseudorotations caused by a strong PJTE.

It is important that in *Jahn–Teller distortions (orbitally degenerate ground states) pseudorotations do not follow Berry rotations*. Indeed, consider an  $MX_5$  system in the TBP configuration outwardly similar to the Berry  $PF_5$  molecule, but with a double-degenerate electronic  $E$  term (an example of such systems,  $CuCl_5^{3-}$ , is discussed in Example 9.3). According to the general solution of the  $E \otimes e$  problem (Section 7.3), in a  $D_{3h}$  system there are three minima of the adiabatic potential in the space of two  $E$ -type displacements (Fig. 7.10). In the case under consideration, these minima correspond to three SP (or near to

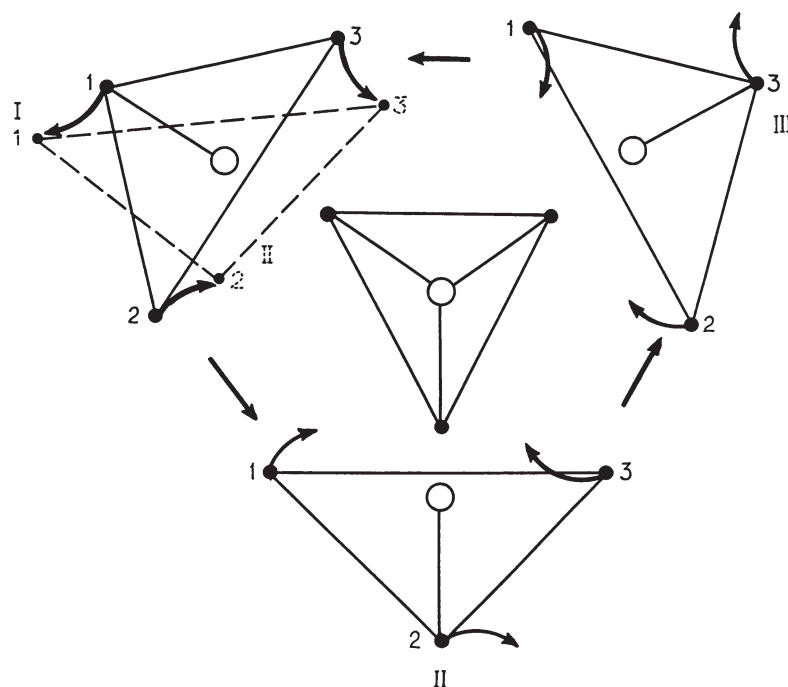


**FIGURE 9.14.** Pseudorotation in the  $E \otimes e$  Jahn–Teller  $\text{CuCl}_5^{3+}$ -type system with three equivalent equilibrium configurations of SP (or near-SP) symmetry (top view); the interconversion between them goes beyond the TBP configuration. The arrows show (schematically) the displacements of the equatorial ligands transforming one configuration into another (the axial ligand displacements are not shown).

SP) configurations, shown in Fig. 9.14, and this result is confirmed by many experimental and theoretical investigations [9.32–9.34].

The pseudorotations here are simply interconversions between the three SP configurations. Direct examination of the APES surfaces in the  $E \otimes e$  problems (Figs. 7.10 and 7.12) shows that the lowest pathway to overcome the barriers between the minima goes around (not through) the high-symmetry TBP configuration  $D_{3h}$ , and hence the latter is not involved in the pseudorotation; the coordinates of interconversion do not include the point  $Q_\theta = Q_\varepsilon = 0$  (which is a conical intersection). Thus the JT pseudorotation cannot be reduced to the direct TBP  $\longleftrightarrow$  SP interconversions, as in the Berry mechanism.

Apparently, a similar situation takes place in the  $\text{MoCl}_5$  complex, which in the TBP configuration has the ground electronic  $E$  term. The fact of pseudorotation in this complex emerges from its electron diffraction spectra [9.52]; the authors interpreted the experimental data as compatible with a picture in which  $\sim 56\%$  of the molecules have the SP configuration  $C_{4v}$ , while the remaining have  $D_{3h}$  (TBP) symmetry with large amplitudes of the corresponding vibrations (if normal

vibrations are assumed, 18% of the molecules must be considered as dimers). This explanation ignores the vibronic effects and the consequent pseudorotation. The experimental results [9.52] are well understood as pseudorotations based on the vibronic coupling scheme discussed above; the percentage of different configurations extracted from the experimental data may even allow one to estimate the barrier height between the SP configurations.

The situation for tetrahedral systems is similar; the pseudorotation that results from the JT distortions is different from that predicted by the Berry mechanism. Indeed, in the  $\text{Fe}(\text{CO})_4$  complex taken as an example [9.53, 9.54], the ground-state electronic term  $T$  is threefold-degenerate and the JT problem is  $T \otimes (e + t_2)$ . As mentioned above, if both types of displacement,  $E$  and  $T_2$ , are active (this is determined by the corresponding vibronic constants), the epikernel of the problem is  $C_{2v}$ , and this is the symmetry of the six minima for the distorted tetrahedron. The experimental data confirm these distortions; the configuration of the  $\text{Fe}(\text{CO})_4$  complex is similar to that of  $\text{SF}_4$  with the two angles C—Fe—C at  $\sim 145^\circ$  and  $\sim 120^\circ$  (Fig. 9.15).

In the Berry rotation scheme the interconversion between two  $C_{2v}$  configurations proceeds via the intermediate high-symmetry square-planar  $D_{4h}$  or

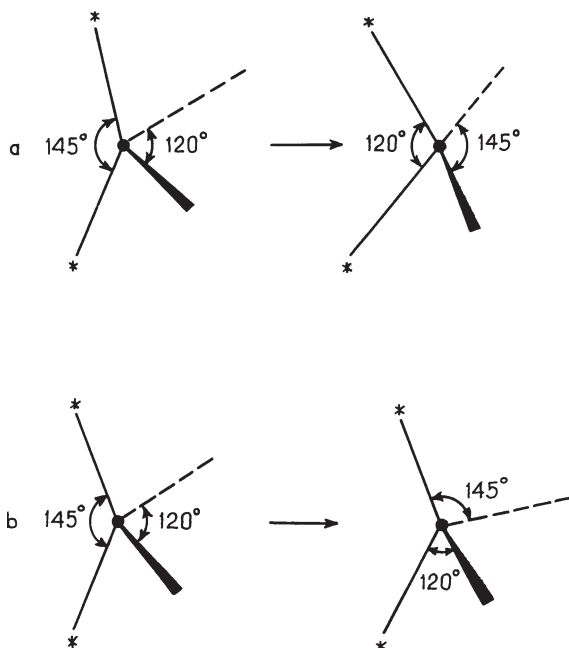


**FIGURE 9.15.** Pseudorotation in  $\text{Fe}(\text{CO})_4$ . The interconversion between two distorted  $C_{2v}$  configurations: (a) predicted by the Berry mechanism, (b) observed experimentally. The two isotope  $^{13}\text{C}$  and  $^{18}\text{O}$  ligands are marked by stars (the complex studied experimentally [9.53] is  $\text{Fe}(\text{CO})_2(^{13}\text{C}^{18}\text{O})_2$ ).

tetrahedral  $T_d$  configurations. The latter seem to be more appropriate for  $\text{Fe}(\text{CO})_4$  in view of the relatively large angles between the bonds (as compared with that of  $\text{SF}_4$ ). However, the experimental data do not confirm such a pathway in the mechanism of interconversion of equivalent distorted configurations in  $\text{Fe}(\text{CO})_4$ . The pseudorotation in this system was studied experimentally by means of ligands marked by  $^{13}\text{C}$  and  $^{18}\text{O}$  isotopes [9.53]. If in the system  $\text{Fe}(\text{CO})_2(^{13}\text{C}^{18}\text{O})_2$  an isomerization is induced by means of an infrared laser that excites the C—O bond, the expected Berry interconversion is that shown in Fig. 9.15a. The observed interconversion is illustrated in Fig. 9.15b; it does not reduce to the Berry rotations. Meanwhile, by examining the APES of the  $T \otimes (e + t_2)$  problem (see Section 7.3 and Ref. 9.20 for more details), one can see that the observed experimental isomerization (Fig. 9.15b) corresponds directly to the pathway via the lowest energy barrier between two nearest-neighbor minima of  $C_{2v}$  symmetry. As in the JT  $E \otimes e$  problem for  $\text{MX}_5$  complexes, considered above, *the pathway of the transition between two equivalent minima via the lowest energy barrier does not cross the configuration of highest symmetry.*

The difference between the Berry (PJT) and JT mechanisms of pseudorotation has an even more important reason than that of energy barriers. To make this statement clear, consider a simple case of the  $E \otimes b_1$  PJT problem, which is of general interest (see, e.g., Section 9.4). The twofold degenerate electronic  $E$  term, for instance, in square-planar systems, interacts with one Jahn–Teller active coordinate  $Q(B_{1g})$ , resulting in two minima at  $+Q_0$  and  $-Q_0$ , respectively, as shown in Fig. 9.16. It is important that the electronic functions of these two minima configurations are mutually orthogonal, and therefore in the absence of additional perturbations *no transitions between these two configurations are possible*; they are strictly forbidden. If additional interactions are nonzero [e.g., the interaction with  $b_{2g}$  displacements in the  $E \otimes b_{1g}$  problem that renders it as

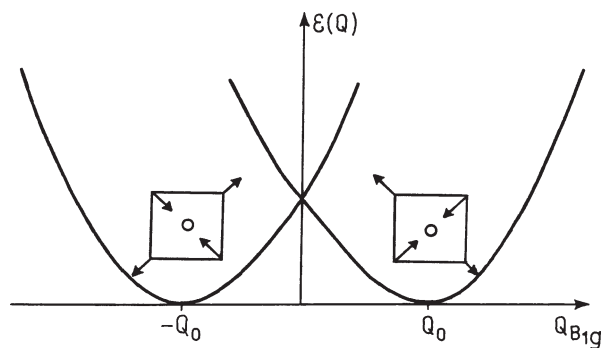


**FIGURE 9.16.** The APES of the  $E \otimes b_{1g}$  problem with two equivalent minima in the space of  $B_{1g}$  displacements  $Q_{B_{1g}}$  of a square configuration  $D_{4h}$ . The intersection at the high-symmetry configuration means that the states in the two minima are exactly orthogonal and no direct interconversions between the two distorted configurations via the square intermediate is possible.

$E \otimes (b_{1g} + b_{2g})$ ], then there is a nonzero probability of transitions between the two configurations via  $b_{2g}$  coordinates, but not directly along  $b_{1g}$ .

In the JT systems discussed above the situation is much the same as in the  $E \otimes b_1$  problem. Indeed, the Berry rotation in Fig. 9.15b is a transition between two  $C_{2v}$  minima of the APES of the tetrahedral  $T \otimes (e + t_2)$  problem. In the cross section of this APES along the  $Q_\zeta$  coordinate the configurations in these minima can be regarded as tetrahedra distorted, respectively, to  $+Q_{0\zeta}$  and  $-Q_{0\zeta}$  from the regular configuration. As in Fig. 9.16, regarding the  $E \otimes b_1$  problem, the electronic wavefunctions of these two configurations are orthogonal to each other, and hence direct transition between them is forbidden. However, *the transitions via other coordinates is not forbidden*.

In the  $\text{PF}_5$  and  $\text{SF}_4$  systems discussed above, the ground state is nondegenerate and hence the electronic states in the minima are not orthogonal. If the excited state producing the instability of the ground state is also nondegenerate, there is only one coordinate of interminimum conversion, the coordinate that mixes the two states. Here the Berry mechanism is the only possible one. If the excited state is degenerate, there may be more than one coordinate of interconversion of the minima configurations, and hence both the Berry and non-Berry mechanisms of pseudorotation may be possible.

### 9.3. MUTUAL INFLUENCE OF LIGANDS

#### The Model: *trans* and *cis* Influences in Stereochemistry

There is a large amount of experimental and correlation data on the mutual influence of ligands in transition metal coordination compounds. The trend began in the mid-1920s with the work of Chernyaev [9.55], who showed convincingly that in the substitution reactions with square-planar Pt(II) complexes,  $\text{PtXYZV} + \text{U} \rightarrow \text{PtXYZU} + \text{V}$ , the ligand V to be substituted first is determined by the properties of that located in the *trans* position to V (*trans influence*), and all the ligands can be arranged in a series according to their *trans*-influence power (Section 11.3). Later it was established that not only the *trans* effect, but also the *cis* effect, as well as other mutual influence of ligands, is manifest in many properties of transition metal compounds, including stereochemistry.

The data on mutual influence of ligands are usually divided into two groups: (1) *static mutual influence*, in which structural parameters (bond lengths, vibrational frequencies, magnetic resonance parameters, etc.) as functions of mutual influence are discussed, and (2) *kinetic mutual influence*, in which reactivity effects (activation energies and rates of substitution reactions) are considered. Sometimes the static effects are called *trans* (or *cis*) *influence*, while the kinetic consequences are called *trans* (or *cis*) *effect*. Obviously, group 1 of mutual influence (structural effects) is important for stereochemistry and is considered in this section, whereas the reactivity effects are discussed in Section 11.3.

Stereochemical effects of mutual influence of ligands were discussed repeatedly [9.56–9.60]. Illustrative examples of *trans* and *cis* influence are given in



**TABLE 9.4. Influence of the Ligand in *trans* Position (*trans* Influence) on Bond Lengths R(Pt—Cl) in some Pt(II) Compounds**

Complex	<i>trans</i> Atom (Ligand)	R(Pt—Cl) (Å)
K[Pt(acac) <sub>2</sub> Cl]	O	2.28(1)
<i>trans</i> -[(PEt <sub>3</sub> ) <sub>2</sub> PtCl <sub>2</sub> ]	Cl	2.30(1)
<i>cis</i> -[(p-C <sub>6</sub> H <sub>4</sub> S) <sub>2</sub> PtCl <sub>2</sub> ]	S (of RS <sup>-</sup> )	2.30
<i>trans</i> -[(PEt <sub>3</sub> ) <sub>2</sub> Pt(CO)Cl]	CO	2.30
<i>cis</i> -[(PEt <sub>2</sub> PH)Pt(CNEt)Cl <sub>2</sub> ]	RNC	2.314(10)
K <sub>2</sub> [PtCl <sub>4</sub> ]	Cl	2.316
[Pt(L-methionine H)Cl <sub>2</sub> ]	S (of R <sub>2</sub> S)	2.32
K[Pt(NH <sub>3</sub> )Cl <sub>3</sub> ]H <sub>2</sub> O	N	2.321(7)
K[Pt(C <sub>2</sub> H <sub>4</sub> )Cl <sub>3</sub> ]H <sub>2</sub> O	C=C	2.327(7)
[Pt(H <sub>3</sub> NCH <sub>2</sub> CH=CHCH <sub>2</sub> NH <sub>3</sub> )Cl <sub>3</sub> ]	C=C	2.342(2)
<i>cis</i> -[(PMe <sub>3</sub> ) <sub>2</sub> PtCl <sub>2</sub> ]	P	2.37(1)
<i>cis</i> -[(PEt <sub>2</sub> Ph)Pt(CNEt)Cl <sub>2</sub> ]	P	2.390(8)
<i>trans</i> -[PMe <sub>2</sub> Ph) <sub>2</sub> Pt(CH <sub>2</sub> SiMe <sub>3</sub> )Cl]	C (of alkyl)	2.415(5)
<i>trans</i> -[(PPH <sub>2</sub> Et) <sub>2</sub> PtHCl]	H	2.42(1)
<i>trans</i> -[PMe <sub>2</sub> Ph) <sub>2</sub> Pt(SiMePh <sub>2</sub> )Cl]	Si	2.45(1)

Source: From Hartley [9.56].

**TABLE 9.5. Influence of the Ligand in *cis* Position (*cis* Influence) on Bond Lengths R(Pt—Cl) in Some Pt(II) Complexes**

Complex	<i>cis</i> Atom (Ligand)	R(Pt—Cl), (Å)
<i>trans</i> -[(PEt <sub>3</sub> ) <sub>2</sub> PtCl <sub>2</sub> ]	P	2.29
[Pt( <i>cis</i> -MeCH=CHCH <sub>2</sub> NH <sub>3</sub> )Cl <sub>3</sub> ]	C=C	2.297(6)
K[Pt(C <sub>2</sub> H <sub>4</sub> )Cl <sub>3</sub> ]H <sub>2</sub> O	C=C	2.305
K[Pt(NH <sub>3</sub> )Cl <sub>3</sub> ]H <sub>2</sub> O	N	2.315
K <sub>2</sub> [PtCl <sub>4</sub> ]	Cl	2.316
<i>trans</i> -[Pt(NH <sub>3</sub> ) <sub>2</sub> Cl <sub>2</sub> ]	N	2.32(1)

Source: Hartley [9.56].

Tables 9.4–9.7. The data in Table 9.4 show explicitly that in compounds of Pt(II) with square-planar coordination the *trans* ligand strongly influences the bond length Pt—Cl. Substitution of the *trans* ligand changes the Pt—Cl bond length from 2.28 to 2.45 Å. The *cis* influence (Table 9.5) is less informative. In comparison with Table 9.4, it is seen that *cis*-influence is much weaker than *trans* influence.

The data in Table 9.6 allow us to follow the variation of one of the most informative parameters of the *trans* influence: the *trans* elongation  $\Delta = R(\text{M}—\text{X}_{\text{trans}}) - R(\text{M}—\text{X}_{\text{cis}})$  in a series of MOX<sub>5</sub> complexes with *d*<sup>0</sup>, *d*<sup>1</sup>, and *d*<sup>2</sup> configurations [9.61]. It is seen that there is an essential decrease in *trans* influence along the series *d*<sup>0</sup> > *d*<sup>1</sup> > *d*<sup>2</sup>. Note, however, that in Table 9.6 the change in *d*<sup>n</sup> configuration is associated with a change in CA itself. Table 9.7 shows some

**TABLE 9.6. Comparison of *cis* and *trans* Bond Lengths,  $R(\text{M}-\text{X}_{cis})$  and  $R(\text{M}-\text{X}_{trans})$ , and the *trans*-Elongation  $\Delta = R(\text{M}-\text{X}_{trans}) - R(\text{M}-\text{X}_{cis})$  in Some  $\text{MOX}_5$  Complexes with  $d^0$ ,  $d^1$ , and  $d^2$  Configurations**

Compound	$d^n$	$R(\text{M}-\text{X}_{trans})$ (Å)	$R(\text{M}-\text{X}_{cis})$ (Å)	$\Delta$ (Å)
MoOF <sub>5</sub>	$d^0$	2.29	1.86	0.43
K <sub>2</sub> [NbOF <sub>5</sub> ]	$d^0$	2.06	1.84	0.22
K <sub>2</sub> [MoOF <sub>5</sub> ]H <sub>2</sub> O	$d^1$	2.03	1.87	0.16
OsOF <sub>5</sub>	$d^2$	1.72	1.78	-0.06
(NH <sub>4</sub> ) <sub>2</sub> [MoOBr <sub>5</sub> ]	$d^1$	2.83	2.55	0.28
K <sub>2</sub> [MoOCl <sub>5</sub> ]	$d^1$	2.587	2.39	0.20
K <sub>2</sub> [ReOCl <sub>5</sub> ]	$d^2$	2.47	2.39	0.08

Source: After Porai-Koshitz and Atovmean [9.61].

**TABLE 9.7. Comparison of Structural Parameters in *cis*- and *trans*-PtCl<sub>2</sub>(PR<sub>3</sub>)<sub>2</sub> Compounds**

Quantity	<i>cis</i>	<i>trans</i>
$R(\text{Pt}-\text{Cl})$ (Å)	2.37	2.29
$R(\text{Pt}-\text{P})$ (Å)	2.25	2.30
$\nu(\text{Pt}-\text{Cl})$ (cm <sup>-1</sup> )	294	340
$\nu(\text{Pt}-\text{P})$ (cm <sup>-1</sup> )	435	419
$J(\text{Pt}-\text{P})$ (Hz)	3520	2400
$J(\text{P}-\text{P})$ (Hz)	-18.7	510
$\nu'(^{35}\text{Cl})$ (MHz)	~18.0	20.99
$\delta(^{31}\text{P})$ , 10 <sup>6</sup> $d$	24.0	15.8
$E_b(\text{Cl}, 2p)$ (eV)	198.2	198.6

other structural characteristics for *trans*- and *cis*-PtCl<sub>2</sub>(PR<sub>3</sub>)<sub>2</sub> (don't confuse the substituent R, here mainly Et and sometimes Me, with the interatomic distance  $R$ ): bond lengths  $R(\text{Pt}-\text{Cl})$  and  $R(\text{Pt}-\text{P})$ , vibrational frequencies  $\nu(\text{Pt}-\text{Cl})$  and  $\nu(\text{Pt}-\text{P})$ , the constants of nuclear spin-spin interaction  $J(\text{Pt}-\text{P})$  and  $J(\text{P}-\text{P})$ , NMR chemical shift  $\delta(^{31}\text{P})$  with respect to H<sub>3</sub>PO<sub>4</sub>,  $NQR$  frequency  $\nu'(^{35}\text{Cl})$ , and the  $2p$ -electron bonding energy  $E_b$  in Cl determined from X-ray photoelectron spectra. Comparison of these data shows that the bonds Pt-Cl in the *trans* complex and Pt-P in the *cis* complex are stronger than the same bonds in the *cis* and *trans* complexes, respectively. This means that PR<sub>3</sub> is a stronger *trans* influencing ligand than Cl, and this *trans* influence is reflected in a number of structural characteristics.

### Electronic Factors

The effects of mutual influence of ligands are obviously of electronic and vibronic origin, and the problem is to formulate some general rules that correlate the

observed influences with specific electronic features of the ligands and the CA. There have been many attempts to contribute to the solution of this problem; we consider here some general and more recent achievements.

The first attempts to explain the origin of *trans* influence were based on comparison of  $\sigma$ -donor and  $\pi$ -acceptor properties of the ligands. To begin with, consider a complex  $\text{MX}_n$  in which the possible  $\pi$  bonding is neglected. If one ligand X is substituted by some better  $\sigma$  donor Y, the positive charge on M decreases and, in general, all the other  $\sigma$  bonds M—X weaken. This inductive effect, due to special properties of the wavefunctions of M involved in the bonding and charge transfer, is angle-dependent; that is, it has special predominant directions. In a square-planar  $\text{MX}_4$  complex, for instance,  $\text{PtX}_4$  with  $d^8$  configuration, four equivalent bonds are formed by the Pt  $d_{x^2-y^2}$  orbital, and the directed influence of Y is realized through the MOs that involve the unoccupied  $p$  orbitals of Pt. The two ligands Y and X in the *trans* positions to each other are strongly interrelated via these MOs.

A simple expression of this *trans* influence was obtained [9.1, 9.62] by means of the angular overlap model (AOM) (Section 5.2). In this model, the difference in stabilization energy  $\Delta E$  of the bond M—X when passing from the *trans* coordinate system X—M—X to the Y—M—X one is proportional to  $e_\sigma$  and the difference  $\Delta e_\sigma = e_\sigma(\text{X}) - e_\sigma(\text{Y})$ :

$$\Delta E \sim e_\sigma(\text{X})[e_\sigma(\text{X}) - e_\sigma(\text{Y})] \quad (9.15)$$

where  $e_\sigma(\text{X})$  and  $e_\sigma(\text{Y})$  are the AOM parameters for ligands X and Y, respectively [Eq. (5.42)].

It follows from Eq. (9.15) that if ligand Y has a larger  $e_\sigma$  value than that of X,  $e_\sigma(\text{Y}) > e_\sigma(\text{X})$ , then  $\Delta E < 0$ , and the bond in the *trans* position is weakened (elongated). On the contrary, if  $e_\sigma(\text{Y}) < e_\sigma(\text{X})$ , then  $\Delta E > 0$  and the *trans* bond M—X is strengthened. Hence the *trans* elongation increases with the  $e_\sigma(\text{Y})$  values. If one assumes that the  $e_\sigma$  value increases with the  $\sigma$ -donor properties (decreases with Pauling electronegativities), then the *trans* influence (elongation) increases with increasing  $\sigma$ -donor properties or decreasing electronegativities of the ligand Y. Figure 9.17 shows that the experimental data, in general, confirm this trend [9.62, 9.1] (note that the  $\sigma$ -donor effect on the *trans* influence was suggested much earlier [9.63, 9.66]).

Moreover, Eq. (9.15) also predicts that the largest *trans* influence is expected not only when the difference  $e_\sigma(\text{Y}) - e_\sigma(\text{X})$  is large, but also when  $e_\sigma(\text{X})$  is large. Thus the ligands with larger  $e_\sigma$  values are both larger *trans*-influencing and more strongly susceptible to the *trans* influence of other ligands. Indeed, the best *trans*-influencing ligands are often also most easily influenced by stronger *trans*-influencing ligands.

The presence of  $\pi$  bonds may be essential for the mutual influence of ligands. The role of  $\pi$  donation in the *trans* effect was first revealed by Chatt, Duncanson, and Venanzi [9.64] and independently by Orgel [9.65], and it is discussed in more detail in Section 11.3. Here we consider some aspects at the  $\pi$  bonding that have

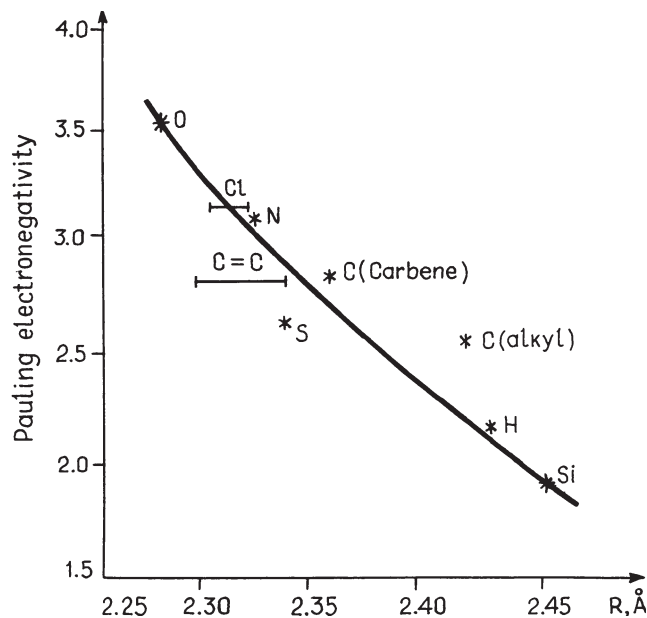


FIGURE 9.17. The Pt—Cl bond length in square-planar Pt(II) complexes (Table 9.4) versus the Pauling electronegativities of the *trans* ligand.

direct stereochemical effect. This is, first of all, the interrelation between  $\sigma$  and  $\pi$ -orbital charge transfers.

In Section 6.3 the diorbital bonding of the ligand, including one  $\sigma$  and one  $\pi$  bond, is considered (with two  $\pi$  bonds, the effect is similar). It is emphasized there that the total charge transfer  $\Delta q = \Delta q_{\pi} + \Delta q_{\sigma}$  to the CA ( $\Delta q < 0$ ) or to the ligand ( $\Delta q > 0$ ) may be small, while the orbital charge transfers,  $\Delta q_{\pi}$  and  $\Delta q_{\sigma}$ , can be relatively large, because they may have opposite signs (usually  $\Delta q_{\sigma} < 0$ , and  $\Delta q_{\pi} > 0$ : backdonation; see Fig. 6.6). Note that small  $\Delta q$  values are required by thermodynamic conditions; large total charge transfers are energetically inconvenient due to electron correlation effects.

For this reason in the absence of  $\pi$  bonding ( $\Delta q_{\pi} = 0$ ),  $\Delta q_{\sigma}$  cannot be very large. In the presence of a  $\pi$  backdonation  $\Delta q_{\pi} > 0$ ,  $\Delta q_{\sigma}$  can be much larger. The  $\pi$  backdonation enhances  $\sigma$ -donor properties of the ligands. But the  $\sigma$ -donor properties, as shown above, are directly related to the *trans* influence. Hence the formation of  $\pi$  bonds, enhancing  $\sigma$ -donor properties, increases the *trans* influence [9.66]. This conclusion explains many experimental data on *trans* elongation and other *trans* influences.

At the early stages of discussion the statement about the role of  $\pi$  bonding in *trans* influence was very stimulating. For example, it was observed that the  $\text{NO}_2^-$  group which is able to form strong  $\pi$  bonds with the CA, is relatively weak *trans*-influencing: the Pt—Cl bond length  $R \approx 2.34 \text{ \AA}$  in the *trans* position to

$\text{NO}_2^-$  in *cis*- $\text{K}_2 [\text{Pt}(\text{NO}_2)_3 \text{Cl}_3]$  is the same as for the  $\text{C}=\text{C}$  *trans* group in square-planar Pt(II) compounds (Table 9.4), whereas the  $\pi$ -acceptor properties of  $\text{NO}_2^-$  are much stronger. To explain this discrepancy, it was assumed that the position of the  $\text{NO}_2^-$  group in the case where it is weak *trans*-influencing is bent with respect to the position in which it forms good  $\pi$  bonds [9.66, 9.67]. The X-ray experiments carried out to verify this assumption confirmed the bent position of  $\text{NO}_2^-$  in the above complex [9.67].

As stated above, directed (*trans*)  $\sigma$  influence is possible when there are such atomic states of the CA (e.g., *p* states), which, as they are involved in the bonding, transfer the influence mainly in the *trans* direction. However, this does not mean that the *cis* ligands do not participate in the mutual influence. Indeed, since the charge transfer to the CA is limited, all the ligands compete in this process, which means that strong  $\sigma$ -donor ligands in the *cis* position reduce the  $\sigma$ -donor ability of the given ligand [9.66], and hence its *trans* influence. In other words, strong *trans*-influencing (i.e., *trans*-weakening) ligands reduce the similar effect on the *cis* coordinate, thus producing an opposite *cis* influence (*cis*-strengthening). Thus, in this model *the trans and cis influences of the same ligand have opposite signs*.

This effect is seen explicitly from the data in Table 9.5. Indeed, compare the Pt—Cl bond lengths in two complexes, *trans*- $[\text{Pt}(\text{PEt}_3)_2\text{Cl}_2]$  and *trans*- $[\text{Pt}(\text{NH}_3)_2\text{Cl}_2]$ , that differ by the linear fragment in the *cis* position (P—Pt—P and N—Pt—N, respectively) to the *trans* coordinate Cl—Pt—Cl. Since the latter is the same in both complexes, the difference in the Pt—Cl bond lengths is due entirely to the *cis* influence. From Table 9.4 it is seen that the *trans* influence of P is stronger than that of N, and hence the *cis* influence, following the abovementioned qualitative treatment, should be opposite. Thus the Pt—Cl bond length is expected to be shorter in the  $[\text{Pt}(\text{PEt}_3)_2\text{Cl}_2]$  complex than in  $[\text{Pt}(\text{NH}_3)_2\text{Cl}_2]$ , in agreement with the experimental data in Table 9.5 (2.29 and 2.32 Å, respectively).

The problem of the CA orbitals that promote the directed *trans* and *cis* influences is one of the most important in the prediction of the CA that are effective in the mutual influence of ligands. Its full solution requires numerical calculations, including all possible active orbitals. However, in general, the results of numerical calculations are not transferable and cannot be related directly to specific properties of the CA and ligands (Section 6.1); qualitative or semiquantitative treatments remain rather important. More exact but less general results of numerical calculations and more general but less exact results of analytical (qualitative and semiquantitative) treatments are complementary to each other.

### Vibronic Theory of Ligand Mutual Influence

In a more rigorous treatment the TEST (two electronic states in transformation) paradigm (Section 7.4) can be invoked to consider the mutual influence of ligands as a vibronic effect. Indeed, the substitution of one ligand in the complex by another can be regarded as a change in the electronic structure (substitution

perturbation mixing the unperturbed states) which produces changes in the nuclear configuration via vibronic coupling. In Section 11.2 a detailed consideration of the vibronic effects in ligand coordination is given, which also evaluates the changes of interatomic distances by coordination, and in Section 9.2 the distortion of ligand geometry induced by the coordination is briefly discussed. A somewhat similar idea is used here in this Section to consider the mutual influence of ligands or, more precisely, the change in mutual influence by changing ligands [9.59].

Consider a homoligand coordination system of the type  $\text{MX}_n$  with a nondegenerate electronic ground state. Following Section 7.1, its Hamiltonian can be presented as

$$H = H_{\text{el}} + W \quad (9.16)$$

where  $H_{\text{el}}$  is the electronic part of the Hamiltonian for fixed nuclei [see Eq. (7.4)] and  $W$  is the vibronic coupling (7.7). In the stable configuration  $Q_\alpha = 0$ ,  $\alpha = 1, 2, \dots, N$ , the adiabatic potential  $\varepsilon(Q_\alpha)$  has a minimum with respect to all symmetrized coordinates  $Q_\alpha$ , and in the harmonic approximation  $\varepsilon(Q_\alpha)$  has the usual quadratic form (7.12) with  $K_\alpha$  given by Eqs. (7.82)–(7.84).

On substitution of ligands X by Y, the change of the Hamiltonian (9.16) can be presented just by adding the so-called substitution Hamiltonian  $H_S$  equal to the difference between the Hamiltonians of the  $\text{MX}_{n-1}\text{Y}$  and  $\text{MX}_n$  systems:

$$H = H_{\text{el}} + W + H_S \quad (9.17)$$

Now we assume that  $H_S$  can be considered as a perturbation. This implies that changes in energy states induced by  $H_S$  are small. Then, to obtain the APES of the  $\text{MX}_{n-1}\text{Y}$  system with the Hamiltonian (9.17), one must consider two perturbations,  $H_S$  and  $W$ , instead of  $W$  only in the  $\text{MX}_n$  system. With the two perturbations the adiabatic potential  $\varepsilon'(Q_\alpha)$  in the first approximation is [9.59]

$$\varepsilon'(Q_\alpha) = \varepsilon(Q_\alpha) + h_{00} - \sum_j \frac{h_{0j}^2}{\Delta_{j0}} - 2 \sum_{\alpha,j} \frac{h_{0j} F_\alpha^{0j}}{\Delta_{j0}} Q_\alpha \quad (9.18)$$

where we denoted

$$h_{0j} = \langle 0 | H_S | j \rangle \quad (9.19)$$

$F_\alpha^{0j} = \langle 0 | \partial H / \partial Q_\alpha | j \rangle$  are the vibronic constants (7.22), and  $\Delta_{ij}$  is the energy gap between the states  $|0\rangle$  and  $|j\rangle$ . From Eq. (9.18) one can see that in addition to the constant terms  $h_{00}$  and  $-\sum h_{0j}^2 / \Delta_{j0}$ , which shift the energy levels, there is a term that is linear in  $Q_\alpha$ . Added to the quadratic terms in  $\varepsilon(Q_\alpha)$  after (7.31), this linear term displaces the minimum position in the  $Q_\alpha$  (or  $-Q_\alpha$ ) directions;

the sign of this displacement is determined by the sign of the product  $h_{0j}F^{0j}$ . The new equivalent positions are

$$Q_{\alpha}^0 = 2 \sum_j \frac{h_{0j}F_{\alpha}^{0j}}{\Delta_{j0}K_{\alpha 0}} \quad (9.20)$$

where  $K_{\alpha 0}$  is as given by Eq. (7.83).

Thus the idea of vibronic mutual influence of ligands is that if we substitute one of the ligands, the changes in electronic structure are no more consistent with the previous geometry, and other ligands relax to new equilibrium positions (new minima of the APES). To find them, the vibronic constants  $F^{0j}$  and the substitution operator  $h_{0j}$  should be analyzed. This can be done by a model description for more specific types of systems.

Consider, for example, the MO LCAO model for octahedral  $\sigma$ -bonded complexes  $MX_6$  of the following three basic types:

- (i) M is a transition element, and there are 12 electrons in the valence  $\sigma$  MOs.
- (ii) M is a nontransition element in a low oxidation state, and there are 14 electrons in the  $\sigma$  MOs (i.e., there is an electron lone pair in addition to the 12 electrons on  $6\sigma$  orbitals).
- (iii) M is a nontransition element in a higher oxidation state.

The typical MO energy-level schemes for these systems are illustrated in Fig. 9.18. By populating the one-electron MOs with the number of valence electrons available, we easily find the HOMO and LUMO. For group (i) the HOMO is  $t_{1u}$ , while the LUMO is  $e_g^*$ , for (ii) the HOMO and LUMO are  $a_{1g}^*$  and  $t_{1u}^*$ , respectively, and so on (Table 9.8).

Thus, by restricting the problem in the HOMO–LUMO approximation we get the coordinate of distortion. In particular, the  $Q'' = (Z_1 + Z_4)/\sqrt{2}$  coordinate describes the displacements of the two atoms, 1 and 4, in *trans* positions (both in the same direction), with the sign of this displacement dependent on the product  $hF^0$ . Following Eq. (9.18),  $h \sim \langle 0|H_s|1 \rangle$ , and the operator  $H_s$  of the substitution  $X \rightarrow Y$  can be taken approximately proportional to the difference between their Coulomb integrals  $\alpha$ :  $h \approx \Delta\alpha = \alpha(Y) - \alpha(X)$ . On the other hand,  $\alpha(Y)$  and  $\alpha(X)$  characterizes the  $\sigma$ -donor properties of Y and X, respectively (such approximations are quite usual in organic chemistry [9.68]). Some qualitative conclusions from this approximation are as follows.

Assume that by substitution  $X \rightarrow Y$  the  $\sigma$ -donor properties increase,  $\Delta\alpha = \alpha(Y) - \alpha(X) > 0$ . Then [9.59] for octahedral  $\sigma$ -bonded coordination compounds of group (i) (transition metals with 12 electrons on the six MOs)  $h < 0$ ,  $F > 0$ , and hence for these systems  $Q_z'' < 0$ . This distortion is equivalent to *trans* elongation because in  $Q_z'' = (Z_1 + Z_4)/\sqrt{2}$ ,  $Z_1 = Z_4$ , and hence  $Z_4 < 0$ . For  $\Delta\alpha < 0$  the *trans* elongation changes to *trans* shortening. Note that in this approximation the *cis* ligands are not involved in the mutual influence.

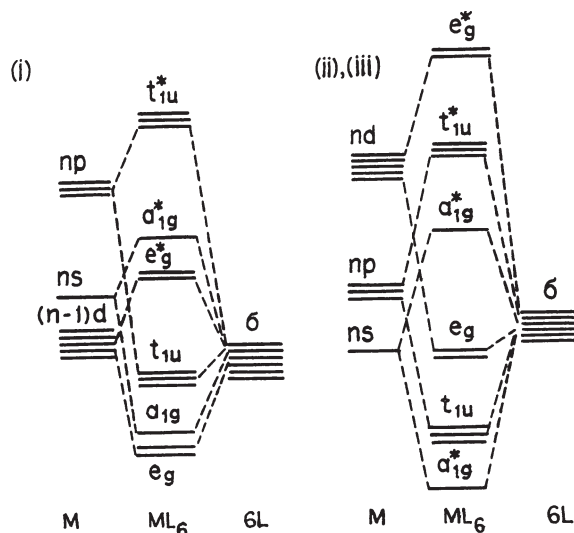


**FIGURE 9.18.** Typical  $\sigma$  MO energy-level schemes for octahedral  $\text{MX}_6$  complexes of transition (i) and nontransition (ii,iii) elements. The HOMO are (i)  $t_{1u}$ , (ii)  $a_{1g}^*$ , (iii)  $e_g$  [cf. Fig. 6.1; for denotations (i), (ii), and (iii) see the text].

**TABLE 9.8. Parameters Characterizing the Distortions in  $\sigma$ -Bonded Complexes of Transition and Nontransition Elements Produced by Substitutions  $\text{MX}_6 \rightarrow \text{MX}_5\text{Y}$  in Octahedral and  $\text{MX}_4 \rightarrow \text{MX}_3\text{Y}$  in Square-Planar Complexes**

Type of Complex	HOMO	LUMO	Distortion Mode for AOs of CA for which $F_\alpha \neq 0$	Distortion Coordinate for AOs of CA for which $h \neq 0$	Distortion Coordinate $Q_\alpha$
Octahedral					
(i)	$t_{1u}$	$e_g^*$	$T_{1u}, T_{2u}$	$p_z, d_{z^2}$	$Q_z'' = (Z_1 + Z_4)/\sqrt{2}$
(ii)	$a_{1g}^*$	$t_{1u}^*$	$T_{1u}$	$s; p_z$	$Q_z'' = (Z_1 + Z_4)/\sqrt{2}$
(iii)	$e_g$	$a_{1g}^*$	$E_g$	$d_{z^2}; s$	$Q_\theta = (2Z_1 - 2Z_4 - X_2 + X_5 - Y_3 + Y_6)/2\sqrt{3}$
Square-planar					
(i)	$e_u$	$b_{1g}^*$	$E_u$	$p_x; d_{x^2-y^2}$	$Q_x = (X_2 + X_4)/\sqrt{2}$
(ii)	$a_{1g}^*$	$e_u^*$	$E_u$	$s; p_x$	$Q_x = (X_2 + X_4)/\sqrt{2}$

Source: From Levin [9.59].

In complexes of type (ii)  $F < 0$  and  $h > 0$ , and hence  $Q_z'' < 0$ . Thus, in octahedral  $\sigma$ -bonded complexes of nontransition elements with 14 electrons on the  $\sigma$  MOs (one lone pair), the distortion by ligand substitution is similar to that expected for group (i): *trans* elongation for increasing  $\sigma$ -donor properties,  $\Delta\alpha > 0$ , and *trans* shortening when the opposite inequality  $\Delta\alpha < 0$  holds. Many examples in the literature confirm these conclusions [9.56–9.58].



In compounds of type (iii), posttransition element complexes in high oxidation states, the situation is more complicated, but some further differentiation of the ligands with respect to their  $\sigma$ -donor properties allows one to obtain some qualitative results that explain the origin of many observed geometries [9.59].

For square-planar  $\sigma$  complexes of the type  $\text{MX}_4$ , the typical HOMO and LUMO, as well as the coordinates of distortion for two types of systems, (i) and (ii), are given in Table 9.8:

- (i) M is a transition metal, and there are 8 valence electrons on the  $\sigma$  MOs (typical example  $[\text{Pt}^{\text{II}}\text{X}_4]$ ).
- (ii) M is a posttransition element in a low oxidation state (typical example  $[\text{Te}^{\text{II}}\text{X}_4]$ ).

For  $\Delta\alpha > 0$ , a procedure quite similar to that used above for octahedral complexes yields  $F > 0$ ,  $h < 0$  in case (i) and  $F < 0$ ,  $h > 0$  in case (ii), thus in both cases the product  $F \cdot h < 0$ , and hence the coordinate of distortion  $Q_x < 0$ , which indicates *trans* elongation [9.59]. This is the typical *trans* influence well known for square-planar complexes, in particular, for Pt(II).

If the ligands produce  $\pi$  bonds, they enhance the *trans* influence, but its sign depends significantly on the coordination center M. Interesting examples of this kind are provided by actinides, where the participation of  $f$  electrons in the bonding is important. In complexes of the type  $\text{MX}_6$ , where M is an actinide, the HOMO  $t_{1u}$  contains both  $\sigma$  and  $\pi$  bonding ( $\sigma + \pi$  bonds), while the LUMO is  $T_{2u}^*$  (a  $\pi$  MO). The coordinate of distortion by the  $\text{MX}_6 \rightarrow \text{MX}_5\text{Y}$  substitution is  $Q_\theta$ , and its sign proved to be negative [9.59],  $Q_\theta < 0$ . This means that the distortion due to the mutual influence is *trans*-shortening and *cis*-elongating. The experimental data (Table 9.9) confirm this prediction. Note that in quite similar complexes of transition metals the mutual influence of ligands results in *trans* elongation. For instance [9.61], in  $\text{K}_2[\text{MoOCl}_5]$  (I) and  $\text{K}_2[\text{ReOCl}_5]$  (II)  $R(\text{M}-\text{X}_{\text{trans}})$  is significantly larger than  $R(\text{M}-\text{X}_{\text{cis}})$  (in angstroms): 2.587 and 2.39 in (I) and 2.47 and 2.39 in (II), respectively. This illustrates the fact that the electronic structure (ground and excited states) of the coordinating element M that transfers the mutual influence is most important.

**TABLE 9.9. Experimental Data on *cis* Elongation and *trans* Shortening in Some Actinide  $\text{MOX}_5$  Compounds**

Compound	$R(\text{M}-\text{O})$ (Å)	$R(\text{M}-\text{X}_{\text{trans}})$ (Å)	$R(\text{M}-\text{X}_{\text{cis}})$ (Å)
$\text{UCl}_6$	—	2.47	2.47
$(\text{PPh}_4)[\text{UOCl}_5]$	1.76	2.43	2.53
$(\text{NEt}_4)_2[\text{PaOCl}_5]$	1.74	2.42	2.64
$(\text{NEt}_4)_2[\text{UOCl}_4]$	1.75	—	2.67

Source: From Levin [9.59].

#### 9.4. CRYSTAL STEREOCHEMISTRY

In stereochemistry of transition metal compounds the crystalline state is most important because it provides for the possibility (often the unique possibility) of direct observation of molecular shapes. Indeed, these compounds rarely exist as free molecules in the gas phase, and the study of molecular shapes by other (e.g., spectroscopic) methods is a rather indirect observation.

On the other hand, the crystal environment influences significantly the local stereochemistry. One of the main differences between crystal chemistry of organic and inorganic compounds is that the organic crystals are (mostly) molecular crystals containing conveniently packed organic molecules, whereas inorganic crystals may have nothing to do with molecules, and the whole crystal may be just one giant molecule (compare  $\text{CH}_4$  and  $\text{NaCl}$  crystals). In terms of the electronic structure considered in this book, the interaction between organic molecules in crystals is mainly nonvalence in nature and can be described by some empirical parameters. This cannot be done in many cases of inorganic compounds in which the details of the electronic structure of the crystal components play a key role in crystal lattice formation and stereochemistry (see also the discussion in the last subsection of Section 9.1).

Coordination compounds of transition metals occupy an intermediate place between the two extremes described above. The coordination system enters the crystal state mostly as a whole entity and preserves many of its molecular features, but the interaction between the coordination centers in the lattice is relatively strong, and it is determined by electronic factors that may be more significant than nonvalence (steric) interactions.

Classical crystal stereochemistry is based on the ideas of "ball packing," or its significantly advanced form, the VSEPR model, which can be considered as a kind of "charge packing" (Section 9.1). The crystal structure of coordination compounds is rather complicated, and in most cases it cannot be reduced to "charge packing" because of the primary importance of quantum effects. As mentioned in Section 9.2, the vibronic approach provides a further insight into the problem [9.69]. In particular, it allows one to separate the contribution of local (chemical) forces from that of the long-range interactions in the lattice (cooperative effects), and to show that the local forces are most essential in determining the polyatomic stereochemistry. In the remainder of this section, we emphasize the main nonclassical aspects of stereochemistry in the crystal state.

##### The Plasticity Effect

As mentioned in Section 9.2, the distortions induced by the JT, PJT, and RT effects in free coordination systems are of dynamic nature; they were classified in Section 7.4 as free rotations, hindered rotations, and pulsating motions. Some of these motions can be observed as pseudorotations, provided that certain conditions considered in Sections 9.1 and 9.2 are satisfied.

In Section 9.1 we discussed the role of small external perturbations that quench the dynamics of the distortions and make them static, so that a very small perturbation may result in strong distortion (vibronic amplification of external perturbations). The symmetry of this static distortion corresponds to that of the external influence, provided that it is uniaxial in the direction of one of the JT active coordinates. It follows that among the many possible equivalent distortions of a coordination system predicted by the vibronic theory (Section 7.3 and 7.4), only those in the crystal state that correspond to the symmetry of the environment are realized, and in a measure allowed by this environment. Hence *the same coordination polyhedron may have significantly different shapes in different crystals*. This phenomenon seems to imply that the coordination polyhedron has a soft (plastic) coordination sphere that in the crystal state assumes the form of the crystal environment; it is called *the plasticity effect* [9.20, 9.25] (see also the “flexional behavior” mentioned in Section 9.2 [9.47]). The first observation of this effect is due to Fackler and Pradilla-Sorzano [9.48] (see also [9.70]).

The best examples illustrating the plasticity effect are octahedral coordination compounds with a twofold-degenerate  $E$  term [Cu(II), Mn(III), Cr(II), etc.]. For them the APES in the case of weak quadratic terms (small  $G_E$  constants; Section 7.3) has the form of a Mexican hat that allows for any distortion of the coordination sphere along the symmetrized  $Q_\theta$  and  $Q_\varepsilon$  displacements within the limits  $Q_\theta^2 + Q_\varepsilon^2 = \text{const}$  (Fig. 7.13). If the quadratic vibronic terms are significant, only three directions of tetragonal distortions along the fourth-order axes remain equally probable (Fig. 7.10). In other systems with other degenerate terms distortions with three tetragonal, six orthorhombic, and so on, equivalent directions, as well as continuous sets of distortions (a trough), are possible (see Section 7.3 and Ref. 9.20).

These predictions of the theory are confirmed by a large amount of experimental data. X-ray analysis shows that the six-coordinated systems with a degenerate  $E_g$  term are not regular octahedrons even when all the ligands are identical, and in the majority of known cases the octahedron is tetragonally distorted. In Tables 9.10–9.13 the crystallographic distances to the two axial ( $R_L$ ) and four equatorial ( $R_S$ ) ligands in a series of  $\text{CuO}_6$  (Table 9.10),  $\text{CuN}_6$  (Table 9.11), and other  $\text{CuX}_6$  (Table 9.12) polyhedra, as well as in similar octahedral Mn(II) and Cr(II) systems (Table 9.13) in different compounds, are given [9.25, 9.71].

It follows from these tables (and many other sources of empirical data) that the six-atom polyhedra around the Cu(II), Mn(III), and Cr(II) centers in different crystals are mainly elongated octahedra  $R_L > R_S$ , with two ligands on the long axis and four on the short axes. For some of the tabulated compounds, although the atoms from the second and next coordination spheres are different (and in the crystal state the interatomic distances also depend on the packing of the molecules in the lattice), the large number of these compounds confirms statistically that the deformation of the coordination sphere around Cu(II), Mn(III), and Cr(II) is due to internal forces, that is, to the  $E$ -term JTE. The fact that elongated octahedra are observed confirms the assumption of strong vibronic coupling and

**TABLE 9.10. Equatorial  $R_S$  and Axial  $R_L$  Interatomic Distances Cu—O in Cu(II) Compounds Containing  $\text{CuO}_6$  Clusters**

Compound <sup>a</sup>	$R_S$ (Å)	$R_L$ (Å)
$\text{Cu}(\text{C}_6\text{H}_4\text{OHCOO})_2 \cdot 4\text{H}_2\text{O}$	1.88	3.00
$\text{Cu}(\text{glycollate})_2$	1.92	2.54
$\text{Cu}(\text{acac})_2$	1.92	3.08
$\text{Na}_2\text{Cu}(\text{CO}_3)_2$	1.93	2.77
$\text{Na}_2\text{Cu}(\text{PO}_3)_4$	1.94	2.52
$\text{Cu}(\text{meso-tartrate}) \cdot \text{H}_2\text{O}$	1.94	2.54
$\text{Cu}(\text{OMPA})_2(\text{ClO}_4)_2$	1.94	2.55
$\text{Cu}(\text{OH})_2$	1.94	2.63
$\text{Cu}_2\text{P}_4\text{O}_{12}$	1.95	2.38
$\text{Cu}(\text{C}_8\text{H}_5\text{O}_4)_2 \cdot 2\text{H}_2\text{O}$	1.95	2.68
$\text{CuO}$	1.95	2.78
$\text{Ca}(\text{Cu,Zn})_4(\text{OH})_6(\text{SO}_4)_2 \cdot 3\text{H}_2\text{O}$	1.96	2.43
$\text{PbCuSO}_4(\text{OH})_2$	1.96	2.53
$\text{CuSO}_4 \cdot 5\text{H}_2\text{O}$	1.97	2.41
$\text{Cu}(\text{NaSO}_4)_2 \cdot 2\text{H}_2\text{O}$	1.97	2.41
$\text{Cu}_6(\text{Si}_6\text{O}_{19}) \cdot 6\text{H}_2\text{O}$	1.97	2.68
$\text{Cu}(\text{C}_2\text{H}_5\text{OCH}_2\text{COO})_2 \cdot 2\text{H}_2\text{O}$	1.98	2.38
$\text{CuWO}_4$	1.98	2.40
$\text{Ti}_2[\text{Cu}(\text{SO}_3)_2]$	1.99	2.44
$\text{Ba}_2\text{Cu}(\text{HCOO})_6 \cdot 4\text{H}_2\text{O}$	2.00	2.18
$\text{Cu}(\text{HCOO})_{12} \cdot 2\text{H}_2\text{O}$	2.01	2.37
$[\text{C}_{14}\text{H}_{19}\text{N}_2]\text{Cu}(\text{hfacac})_3$	2.02	2.18
$\text{CdCu}_3(\text{OH})_6(\text{NO}_3)_2 \cdot \text{H}_2\text{O}$	2.03	2.43
$\text{K}_2\text{BaCu}(\text{NO}_2)_6$	2.04	2.29
$\text{Cu}_4(\text{NO}_3)_2(\text{OH})_6$	2.04	2.34
$\text{Ca}(\text{Cu,Zn})_4(\text{OH})_6(\text{SO}_4)_2 \cdot 3\text{H}_2\text{O}$	2.06	2.23
$\text{Cu}(\text{OMPA})_3(\text{ClO}_4)_2$	2.07	2.07
$\text{Cu}(\text{H}_2\text{O})_6\text{SiF}_6$	2.07	2.07
$\text{Cu}(\text{IPCP})_3(\text{ClO}_4)_2$	2.07	2.11
$\text{Cu}(\text{NO}_3)_2\text{HgO} \cdot 3\text{H}_2\text{O}$	2.10	2.10
$\text{Cu}(\text{PCP})_3(\text{ClO}_4)_2$	2.11	2.04
$\text{Ca}(\text{Cu,Zn})_4(\text{OH})_6(\text{SO}_4)_2 \cdot 3\text{H}_2\text{O}$	2.11	2.11
$\text{Cu}(\text{ClO}_4)_2 \cdot 6\text{H}_2\text{O}$	2.13	2.28
$(\text{NH}_4)\text{Cu}(\text{SO}_4)_2 \cdot 6\text{H}_2\text{O}$	2.15	1.97

<sup>a</sup>Abbreviations: acac = acetoacetate; OMPA = octamethylpyrophosphoramidate; hfacac = hexafluoroacetylacetonate; IPCP = tetraisopropylmethylene-diphosphonate; PCP = octamethylmethylene-diphosphonic diamide.

Sources: From Bersuker et al. [9.20, 9.25].

**TABLE 9.11. Equatorial  $R_S$  and Axial  $R_L$  Interatomic Cu—N Distances in Cu(II) Compounds Containing  $\text{CuN}_6$  Clusters**

Compound <sup>a</sup>	$R_S$ (Å)	$R_L$ (Å)
$\text{Cu}(\text{C}_4\text{H}_7\text{N}_5\text{O})_2(\text{ClO}_4)_2$	1.97	3.14
$\text{Cu}(\text{NH}_3)_4(\text{NO}_2)_2$	1.99	2.65
$\text{Cu}(\text{NH}_3)_2(\text{N}_3)_2$	2.01	2.62
$\text{Na}_4\text{Cu}(\text{NH}_3)_4\text{Cu}(\text{S}_2\text{O}_3)_2\cdot\text{NH}_3$	2.01	2.88
$\text{Cu}(\text{phen})_3(\text{ClO}_4)_2$	2.05	2.33
$\text{Cu}(\text{dien})_2\text{Br}_2\cdot\text{H}_2\text{O}$	2.04	2.43
$\text{Cu}(\text{N},\text{N}'\text{-(CH}_3)_2\text{en})_2(\text{NCS})_2$	2.06	2.52
$[\text{Cuen}_2]\text{Hg}(\text{SCN})_4$	2.08	2.58
$\text{Cu}(\text{l-pn})_3\text{Br}_2\cdot 2\text{H}_2\text{O}$	2.09	2.31
$\text{K}_2\text{PbCu}(\text{NO}_2)_6$	2.11	2.11
$\text{Cu}(\text{dien})_2(\text{NO}_3)_2$	2.22	2.01
$\gamma\text{-K}_2\text{PbCu}(\text{NO}_2)_6$	2.23	2.05

<sup>a</sup>Abbreviations: phen = *o*-phenanthroline; en = ethylenediamine; pn = 1,2-propanediamine; dien = diethylenetriamine.

Sources: From Bersuker et al. [9.20, 9.25].

**TABLE 9.12. Equatorial  $R_S$  and Axial  $R_L$  Interatomic Distances Cu—X in Cu(II) Compounds Containing  $\text{CuX}_6$  Clusters, where X = F,Cl,Br**

Compound	$R_S$ (Å)	$R_L$ (Å)
$\text{Ba}_2\text{CuF}_6$	1.85; 1.94	2.08
$\text{Na}_2\text{CuF}_4$	1.91	2.37
$\text{CuF}_2$	1.93	2.27
$\text{K}_2\text{CuF}_4$	1.92	2.22
$\text{KCuF}_3$	1.96; 1.89	2.25
$\text{CuCl}_2$	2.30	2.95
$(\text{NH}_4)_2\text{CuCl}_4$	2.30; 2.33	2.79
$\text{CsCuCl}_3$	2.28; 2.36	2.78
$\text{CuBr}_2$	2.40	3.18

Sources: From Bersuker et al. [9.20, 9.25].

strong quadratic vibronic interaction; one of the three adiabatic potential minima is stabilized by the crystal environment.

The octahedron of the first coordination sphere is regular for several compounds, which means that the distortions are not stabilized by the crystal environment or cooperative effects considered below. In other words, the phase transition to lower-symmetry structures due to cooperative effects has not taken place at the temperatures of the X-ray measurements in question; they could be expected at lower temperatures. For some of these compounds [ $\text{CuSiF}_6 \cdot 6\text{H}_2\text{O}$ ,  $\text{KPbCu}(\text{NO}_2)_6$ , etc.], this assumption has been confirmed by ESR and other

**TABLE 9.13. Equatorial  $R_S$  and axial  $R_L$  Interatomic Distances Me—X in Some Compounds Containing  $MX_6$  Clusters, where M = Mn(III), Cr(II) and X = O, S, F, Cl, I**

Compound	$R_S$ (Å)	$R_L$ (Å)
$K_2MnF_5 \cdot H_2O$	1.83	2.07
$(NH_4)_2MnF_5$	1.85	2.10
$K_2NaMnF_6$	1.86	2.06
$MnF_3$	1.79–1.91	2.09
$Cs_2KMnF_6$	1.92	2.07
$Mn(trop)_3$ , I	1.94	2.13
$Mn(trop)_3$ , II	1.94–1.99	2.09
$CrF_2$	1.99	2.43
$Mn(acac)_3$	2.00	1.95
$KCrF_3$	2.14	2.00
$Mn(Et_2dtc)_3$	2.38–2.43	2.55
$CrCl_2$	2.40	2.92
$CrI_2$	2.74	3.24

Sources: From Bersuker et al. [9.20, 9.25].

direct measurements. Systems reported with tetragonally compressed octahedra in  $(NH_4)_2Cu(SO_4)_2 \cdot 6H_2O$ ,  $Cu(PCP)_3(ClO_4)_2$ ,  $Cu(dien)_2(NO_3)_2$ ,  $Cu(en)_3SO_4$ ,  $Mn(acac)_3$ , and  $Ba_2CuF_6$  need additional investigation. In similar compounds [e.g., in nitrate of bis(terpyridin)Cu(II),  $Cu(en)_3Cl_2$ ,  $K_2CuF_4$ ,  $K_2PbCu(NO_2)_6$ ] a more careful study shows that in fact the octahedrons are tetragonally elongated and antiferrodistortively ordered, which gives an average picture of diffraction similar to that for ferrodistoritively ordered compressed octahedra. A similar conclusion about elongated octahedra instead of the compressed ones emerges from the ESR investigation [9.72].

In some cases the tetragonally compressed octahedral polyhedron around Cu(II) is presumably controlled by the crystal structure:  $CuF_6$  polyhedra in the  $Ba_2ZnF_6$  crystal may serve as an example [9.73]. Indeed, in  $Ba_2ZnF_6$  the octahedral environment around Zn is compressed because of crystalline effects, and the substitution  $Ba_2Zn_{1-x}Cu_xF_6$  with  $x < 0.3$  does not change the crystal structure and the compressed octahedral environment of Cu(II). One may speculate that in these cases the crystal influence is sufficiently strong; it changes the sign of the quadratic vibronic constant  $G_E$  (Section 7.3).

The origin of elongated octahedra (and lack of compressed ones) in Cu(II) compounds was attributed [9.74] to the contribution of configuration interaction (Section 5.3) with the excited state, which includes the  $4s$  orbital of the copper atom. This negative contribution to the energy in the  ${}^2B_{1g}$  state (elongated octahedron) was shown to be twice that in the  ${}^2A_{1g}$  state (tetragonally compressed octahedron). Another conclusion derived from the data in Tables 9.10–9.13 concerns the diversity of Cu—O and Cu—N distances, which vary greatly from one system to another, preserving some relationship between  $R_L$  and  $R_S$ . This confirms that the characteristics of metal–ligand bonds in coordination systems are,

in general, not transferable from one compound to another and cannot be used for classical molecular modeling similar to organic compounds (Section 5.6).

### Distortion Isomers

In the diversity of crystal environments, there may be cases when not one, but two or several configurations of the coordination sphere are stabilized. If these configurations are sufficiently close in energy, but differ in distortion magnitude and direction, they may be observed as different crystal isomers. The so-called distortion isomers of Cu(II) originally synthesized and studied by Gazo et al. [9.25, 9.71] may serve as an example of this kind. These isomers have the same total composition and the same Cu(II) ligand environment, but differ in the interatomic metal–ligand distances in the distorted coordination sphere. Distortion isomers also differ in their properties, such as color, appearance, crystal form, chemical behavior, solubility, and spectroscopic data. They pass from one to another under the influence of pressure, heating, or long-term storage. In some cases, besides the two principal isomers (usually called  $\alpha$  and  $\beta$ ), a series of intermediate species have been obtained.

One of the simplest compounds that has distortion isomers is  $\text{Cu}(\text{NH}_3)_2\text{X}_2$ , where  $\text{X} = \text{Cl}, \text{Br}$ . Their possible Jahn–Teller origin was suggested when the isomers were discovered, but the true understanding of their local PJT and cooperative crystal nature was reached later [9.25, 9.69]. The results of Section 7.4 give quite a natural explanation for the origin of distortion isomers as being due to the vibronic properties of the Cu(II) center accompanied by the stabilizing influence of the crystal lattice. Example 9.4 explains the origin of distortion isomers of some specific compounds.

#### EXAMPLE 9.5

##### *Origin of Distortion Isomers in $\text{Cu}(\text{NH}_3)_2\text{X}_2$ , $\text{X} = \text{Cl}, \text{Br}$*

The crystals  $\text{Cu}(\text{NH}_3)_2\text{X}_2$  constitute mutually parallel chains, each of which is arranged as illustrated in Fig. 9.19a, where all the X atoms occupy equivalent bridge positions. There is a strong interaction between the Cu(II) centers inside the chain through bridging atoms, while the bonding between the chains realized by Van der Waals interactions and/or hydrogen bonds is weak. Each copper atom is surrounded by four X atoms in the plane of the square and by two  $\text{NH}_3$  groups in the axial *trans* positions. The degeneracy of the ground Cu(II) state in the octahedron is removed as a consequence of the difference between X and  $\text{NH}_3$ , and the  ${}^2E_g$  term is split in  ${}^2A_{1g}$  and  ${}^2B_{1g}$ . Denote the splitting by  $2\Delta$ .

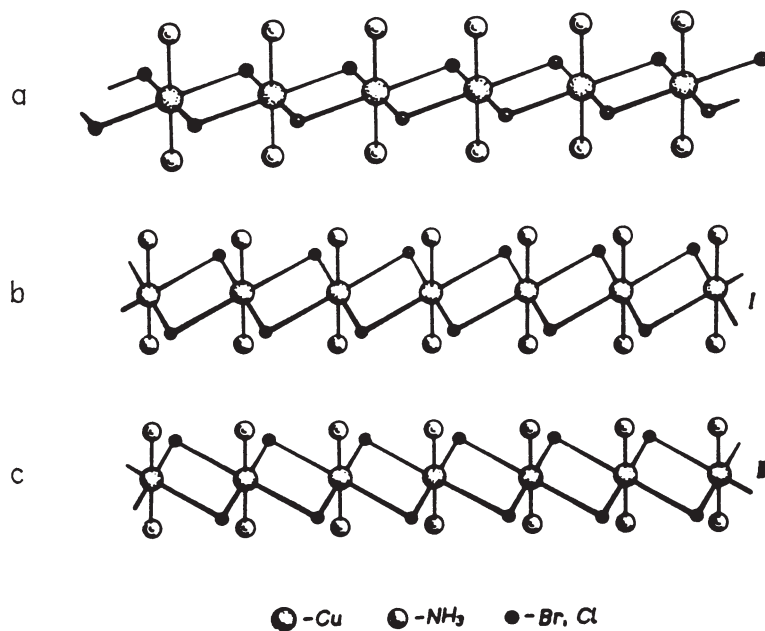


**FIGURE 9.19.** Chain structure of the crystal  $\text{Cu}(\text{NH}_3)_2\text{X}_2$  in the cubic undistorted unstable  $\beta$  isomer (a) and in two equivalent configurations of the  $\alpha$  isomer, I and II (b and c), resulting from the in-chain cooperative pseudo Jahn-Teller effect. (After Bersuker et al. [9.20, 9.25].)

If we assume that the X atoms in the plane form a regular square, the polyhedron  $\text{Cu}(\text{NH}_3)_2\text{X}_4$  is a tetragonally distorted octahedron that belongs to  $D_{4h}$  symmetry. The two close-in-energy  $A_{1g}$  and  $B_{1g}$  terms are subject to the PJTE. This case fully corresponds to the two-level system considered in Section 7.4, so the results obtained there may be applied directly. In particular, the normal coordinate  $Q$ , which mixes the states  $A_{1g}$  and  $B_{1g}$ , transforms according to  $B_{1g}$  ( $A_{1g} \times B_{1g} = B_{1g}$ ) and the corresponding  $B_{1g}$  displacements in the  $D_{4h}$  group coincide with the  $Q_e$  displacement of the  $O_h$  group given in Fig. 7.1 and Table 7.1 and shown here in Fig. 9.20.

The vibronic constant of the mixing of the two electronic states is  $F = \langle A_{1g} | \partial H / \partial Q | B_{1g} \rangle$ , and the APES in the space of the  $Q$  coordinate has the form given by Eq. (7.65). If the instability condition (7.67),  $\Delta < F^2/K_0$ , is satisfied, we obtain two minima on the lower sheet of the adiabatic potential at  $\pm Q_0$ , determined by Eq. (7.68).

Thus, the pseudo-Jahn-Teller effect at each center distorts the bipyramidal environment: the equatorial square with four atoms X at the apexes transforms to a rhombus with the major diagonal along  $Q_x$  corresponding to the minimum I in Fig. 9.21, or along  $Q_y$  (minimum II).



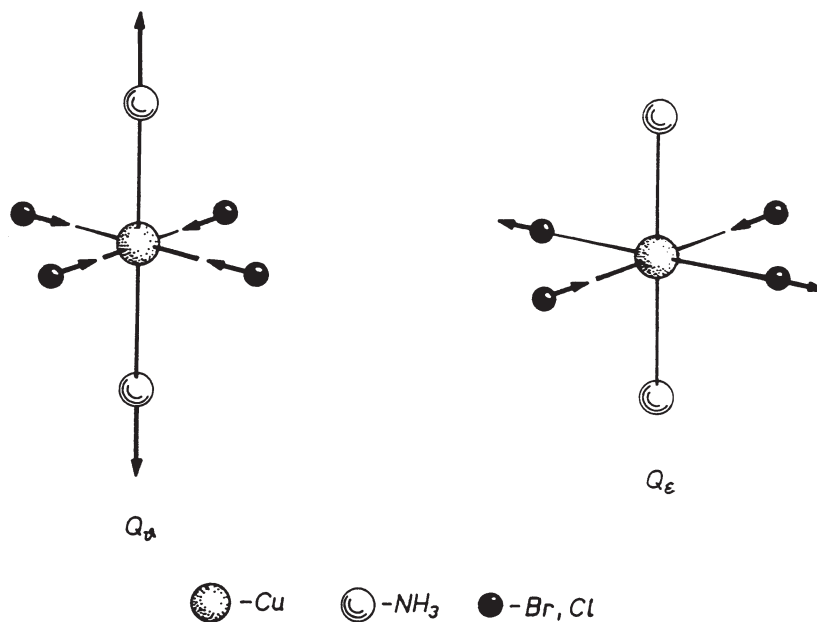


**FIGURE 9.20.**  $Q_\theta$  and  $Q_\epsilon$  displacements in the octahedral  $\text{Cu}(\text{NH}_3)_4\text{X}_2$  cluster. The  $Q_\epsilon$  distortion has  $B_{1g}$  symmetry and mixes the  $A_{1g}$  and  $B_{1g}$  electronic states.

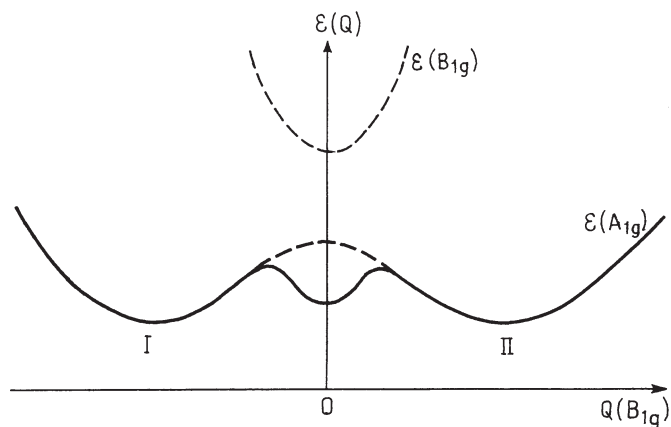


**FIGURE 9.21.** Energy curve for the  $\text{Cu}(\text{NH}_3)_2\text{X}_2$  crystal as a function of the cooperative ferrodistorptive intrachain distortion, which is of  $B_{1g}$  symmetry on each center. Curves I and II indicate the two pseudo-Jahn–Teller minima, while the additional minimum at  $Q(B_{1g}) = 0$  corresponds to the best-fit interchain interactions of undistorted chains (dashed lines).

As a result of the strong interaction between the distortions of neighboring centers in the chain via the ligands X in common, a ferrodistorptive ordering of these distortions along the chain takes place, and

this ordering remains unchanged up to high temperatures, so it can be assumed that at room temperatures each chain has two stable configurations I and II of Fig. 9.19 [parts (b) and (c), respectively], that correspond to the two minima in Fig. 9.21 (I and II, respectively).

As for the interaction between the chains, the analysis indicates that it is optimal when the chains are not distorted and the entire crystal is cubic. In this cubic state the intermolecular distances (between the strongest interacting atoms of different chains) are minimal, and they increase with intrachain distortions toward configuration I or II. Hence the interchain interaction in the crystal results in a minimum at  $Q = 0$  (Fig. 9.21), where  $Q$  is the coordinate of the cooperative intrachain distortion corresponding to the  $B_{1g}$  distortion at each center. Thus the total energy of the crystal has three minima (Fig. 9.21): besides two minima I and II for the stable distorted configurations of the chains, there is a third minimum for the cubic crystal with undistorted chains.

It can be shown that this description explains qualitatively the origin of all the main features of the distortion isomers in  $\text{Cu}(\text{NH}_3)_2\text{X}_2$ . The  $\alpha$  isomer corresponds to the deepest minimum of the APES (I or II) with the structures illustrated in Figs. 9.19b and 9.19c. The unstable  $\beta$  isomer with the cubic structure corresponds to the shallower minimum at  $Q = 0$ , and the intermediate preparations with noncubic structures correspond to the additional relative minima for the uncorrelated chain distortions. This interpretation agrees well with the experimental features of the isomers, including their behavior under stress and temperature, the dependence on conditions of their preparation, spectral properties, and transitions from one isomer to another [9.25, 9.71].

The PJT origin of the intrachain distortions was confirmed by approximate calculations of the distortions of the  $\text{Cu}(\text{NH}_3)_2\text{X}_4$  polyhedron. The electronic energy as a function of the  $Q(B_{1g})$  distortions was estimated by means of the angular overlap model (Section 5.2). Using empirical data for the value  $K_0$ , the minima positions (I and II) on the APE curve (7.65) were estimated [9.75]. The results confirm that the distortion is of the PJT origin:  $Q(B_{1g})(\text{calculated}) \approx 0.5 \text{ \AA}$ , while  $Q(B_{1g})(\text{experimental}) \cong 0.4 \text{ \AA}$ .

### Temperature-Dependent Solid-State Conformers

The dynamic JT and PJT distortions, under the influence of the crystal environment, may be reduced to static distortions in different ways, resulting in a variety of possible configurations, including temperature-dependent configurations. One of them may be called *temperature-dependent solid-state conformers* [9.76]. They occur when there are two or several rapidly converting distorted configurations

that are slightly nonequivalent because of the crystal influence, and the observed Boltzmann averaged configuration is thus temperature-dependent.

Consider the system  $[\text{Cu}(\text{bpy})_2(\text{ONO})]\text{NO}_3$  ( $\text{bpy}$  = bipyridine) with the copper polyhedron  $\text{cis-CuN}_4\text{O}_2$ . In the high-symmetry configuration of  $[\text{Cu}(\text{bpy})_3]^{2+}$  the system has  $D_3$  symmetry with a twofold-degenerate  ${}^2E$  ground state. The substitution of one of the  $\text{bpy}$  groups by  $\text{ONO}$  reduces the symmetry to  $C_2$  and splits the  ${}^2E$  term in  ${}^2A$  and  ${}^2B$ . Similar to the distortion isomers discussed in Example 9.4, there is a possibility for a PJTE and consequent instability of the ground state  ${}^2A$  with respect to  $B$  displacements ( $A \times B = B$ ), provided that the vibronic coupling constant  $F = \langle A | \partial H / \partial Q_B | B \rangle$  is sufficiently large and inequality (7.85) or (7.67) holds. The  $B$  displacements emerge from  $Q_e$  (Fig. 9.20, Table 7.1) and have the same geometry.

Assuming that (7.67) is satisfied, we obtain for the APE curve, as a function of the coordinate  $Q(B)$ , the picture shown in Fig. 7.17b and reproduced here in Fig. 9.22 together with the indication of the modes of distortion of the  $\text{CuN}_4\text{O}_2$  polyhedron in the minima. The value of the distortion coordinate  $Q$  (the

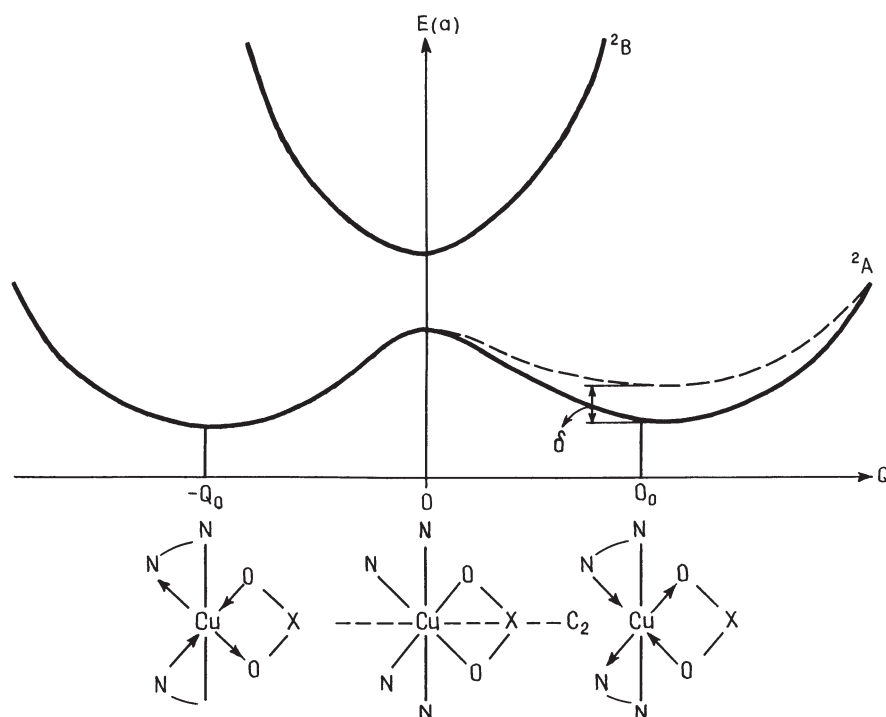


**FIGURE 9.22.** Two minima of the adiabatic potential in the  $[\text{Cu}(\text{bpy})_2(\text{ONO})]\text{NO}_3$  crystal with a strong pseudo Jahn–Teller effect on each center and slightly different minima depths ( $\sim\delta$ ) due to the crystal environment (influence of the next coordination sphere).

coordinate  $Q_\varepsilon = (\frac{1}{2})(X_2 - X_5 - Y_3 + Y_6)$ , Table 7.1) in our denotations for the *cis*- $\text{CuN}_4\text{O}_2$  polyhedron is

$$Q = (\frac{1}{2}) [\Delta R(\text{Cu}-\text{N}_1) + \Delta R(\text{Cu}-\text{O}_1) - \Delta R(\text{Cu}-\text{N}_2) - \Delta R(\text{Cu}-\text{O}_2)] \quad (9.21)$$

where  $\text{N}_1$ ,  $\text{N}_2$ ,  $\text{O}_1$ , and  $\text{O}_2$  are the two nitrogen and two oxygen atoms in the plane containing the  $C_2$  axis (Fig. 9.22), and  $\Delta R$  denotes the elongation of the bond with respect to that in the high-symmetry configuration. It is seen that for linear distortions  $\Delta R(\text{Cu}-\text{N}_1) - \Delta R(\text{Cu}-\text{N}_2) = R(\text{N}_1) - R(\text{N}_2)$  and  $\Delta R(\text{Cu}-\text{O}_1) - \Delta R(\text{Cu}-\text{O}_2) = R(\text{O}_1) - R(\text{O}_2)$ , where  $R(\text{X})$  means the bond length  $\text{Cu}-\text{X}$ . Hence

$$Q = (\frac{1}{2}) [R(\text{N}_1) - R(\text{N}_2) + R(\text{O}_1) - R(\text{O}_2)] \quad (9.22)$$

In the unstable high-symmetry configuration  $Q = 0$ , while in the two minima  $Q = \pm Q_0 \neq 0$ . If the energy barrier between the minima (i.e., the PJT stabilization energy) is not very large, the system converts rapidly between the minima configurations, and in some experimental measurements (say, by X-ray diffraction methods) the averaged undistorted configuration will be observed (if the minima are shallow and there are no local states in them, the averaged configuration will be observed in all the methods, Section 9.1).

The situation changes when, in response to the crystal environment, the two minima become slightly nonequivalent, as shown in Fig. 9.22 by dashed lines, but the energy difference  $\delta$  between the minima is smaller than the barrier height (otherwise the second minimum disappears). In this case there is no complete averaging over the two configurations because the two minima are not equally populated. Denote the relative populations of the two configurations by  $n_1$  and  $n_2$ , respectively. According to Boltzmann's thermal populations

$$n_2 = n_1 \exp \frac{-\delta}{kT} \quad (9.23)$$

with the normalization  $n_1 + n_2 = 1$ . Then the observed thermal averaged distortion is

$$Q_{\text{av}} = (n_1 - n_2) Q_0 \quad (9.24)$$

or

$$Q_{\text{av}} = Q_0 \frac{1 - \exp(-\delta/kT)}{1 + \exp(-\delta/kT)} \quad (9.25)$$

Thus the observable averaged distortion  $Q_{\text{av}}$  is temperature dependent, its absolute value being determined by both  $Q_0$  and  $\delta$ .

These distorted configurations of the same compound, which change gradually with temperature, can be called *temperature-dependent solid-state*

*conformers*. At high temperature when  $kT \gg \delta$ , in the first order with respect to  $\delta/kT$ ,  $\exp(-\delta/kT) \approx 1 - (\delta/kT)$  and

$$Q_{\text{av}} = \frac{Q_0 \delta}{2kT} \quad (9.26)$$

In the opposite limit case when  $kT \ll \delta$ ,  $\exp(-\delta/kT) \approx 0$ , and  $Q_{\text{av}} \approx Q_0$ .

The observed distortions in  $[\text{Cu}(\text{bpy})_2(\text{ONO})]\text{NO}_3$  and similar systems [9.76] follow these rules rather well. The atomic structure of this compound has been determined in four temperature regions: 20, 100, 165, and 296 K. Table 9.14 shows the corresponding interatomic distances and the value  $Q_{\text{av}}$  calculated by Eq. (9.21) for different temperatures, as well as the same data for  $[\text{Zn}(\text{bpy})_2(\text{ONO})]\text{NO}_3$  at 295 K, for comparison. In the Zn compound there is no PJTE of the kind present in  $[\text{Cu}(\text{bpy})_2(\text{ONO})]\text{NO}_3$  and hence no temperature-dependent conformers are expected.

The data in Table 9.14 are very illustrative for temperature-dependent solid-state conformers; the temperature dependence of  $Q_{\text{av}}$  closely follows the pattern seen in Eq. (9.25). In particular, if we assume that at  $T = 20$  K  $Q_0 \approx Q_{\text{av}} = 0.3$ , while at  $T = 296$  K Eq. (9.26) holds, we obtain the following value directly:  $\delta = (Q_{\text{av}}/Q_0)2kT \approx 69 \text{ cm}^{-1}$ . The author [9.76] performed a more exact estimation:  $\delta = 74 \text{ cm}^{-1}$ . Note that in the Zn(II) compound  $Q_{\text{av}}$ , as expected, ranges from small to zero, and the absence of conformers in the Zn(II) compound is also seen from the temperature factor in X-ray experiments [9.76].

The solid-state conformers under consideration differ from each other in interatomic distances, and in this sense they are similar to distortion isomers, discussed above. However, the latter coexist at the same temperature, whereas different conformers are observed at different temperatures, and the larger the temperature difference, the larger the structural differences of the conformers. Also important is the fact that the structural changes with temperature in conformers take place gradually, in contrast to structural phase transitions, which take place abruptly, at a certain temperature (see below).

**TABLE 9.14. Bond Lengths  $R(X) = R(\text{M}-\text{X})$  (in Å) and Distortion Coordinate Values  $Q_{\text{av}}$  in the  $\text{MN}_4\text{O}_2$  Polyhedra of  $[\text{M}(\text{bpy})_2(\text{ONO})]\text{NO}_3$  with  $\text{M} = \text{Cu}$  at Different Temperatures  $T$  (K), and for  $\text{M} = \text{Zn}$**

	M = Cu				M = Zn
	20 K	100 K	165 K	296 K	295 K
$R(\text{N}_1)$	2.142(2)	2.110(2)	2.098(2)	2.085(2)	2.085(2)
$R(\text{N}_2)$	2.028(2)	2.060(2)	2.071(2)	2.074(4)	2.082(3)
$R(\text{O}_1)$	2.536(2)	2.414(2)	2.351(3)	2.320(5)	2.204(3)
$R(\text{O}_2)$	2.051(2)	2.155(2)	2.204(3)	2.230(5)	2.223(3)
$Q_{\text{av}}$	0.299	0.155	0.087	0.050	0.008

### Cooperative Effects: Order–Disorder and “Displacive” Phase Transitions and Helicoidal Structures

Cooperative effects are very important in crystal stereochemistry of transition metal compounds. In this section we consider first briefly a general picture of ordering of local distortions in crystals (cooperative vibronic effects), followed by a discussion of the relative role of long-range (lattice) and short-range (chemical) forces in local stereochemistry and lattice formation, using the problem of origin of ferroelectricity as an example.

If the crystal is formed from ready-made entities (molecules) that interact by stericlike forces, the energy of their interaction in the lattice  $U$  depends on the mutual orientation of these entities. In such cases the minimum of free energy  $F = U - TS$  (where  $S$  is the entropy) requires at  $T = 0$  an ordering of the interacting molecules in which their mutual orientations make  $U$  minimal. At higher temperatures the entropy term  $TS$  becomes large, and at a certain temperature  $T = T_c$  (Curie point) a phase transition to the disordered state takes place for which the entropy is a maximum (*order–disorder transitions*).

In inorganic and coordination compounds, in addition to such order–disorder transitions, *displacive phase transitions* may take place. In them, as distinct from the order–disorder transitions, the atomic arrangement in the coordination center itself changes. Displacive transitions are directly related to the electronic structure, demonstrating the fact that in crystal stereochemistry of transition metal coordination compounds the electronic structure of the coordination center plays a key role and cannot be ignored or taken into account by means of empirical parameters.

Local distortions in crystals and distortion-related structural phase transitions can be considered by means of the vibronic coupling theory (Chapter 7). Let us begin with a simple case when the JT centers in the crystal possess a twofold orbital degenerate  $E$  term vibronically coupled to  $B_1$  vibrations, which results in the  $E \otimes b_1$  problem mentioned in Section 9.2 (Fig. 9.16). Such a situation may occur, for example, when the crystal  $E$  term centers in question possess local  $D_{4h}$  symmetry. For simplicity, assume that the JT centers are square-planar. The adiabatic potential curve with two equivalent minima and the rhombic distortions ( $B_{1g}$  displacements) of the square at each of the minima are illustrated in Fig. 9.16. In the absence of interaction between the centers, the two configurations [which we denote here by (+) and (–)] are equally probable and the JTE has the dynamic nature discussed above: the averaged distortion equals zero and the initial symmetry is preserved. Note that in the case in question the averaging becomes possible as a result of other perturbations involved; without them the transition (+)  $\rightarrow$  (–) is forbidden (see the remark at the end of Section 9.2).

The picture changes when the interactions between the centers are taken into account. Let us consider two interacting centers. In each of them the  $E \otimes b_1$  problem is realized. Under the assumption of parallel orientations of their squares, there may be four configurations in which the two one-center distortions are correlated: (++) , (––) , (+–) , and (–+) (Fig. 9.23). It is clear that if the interaction

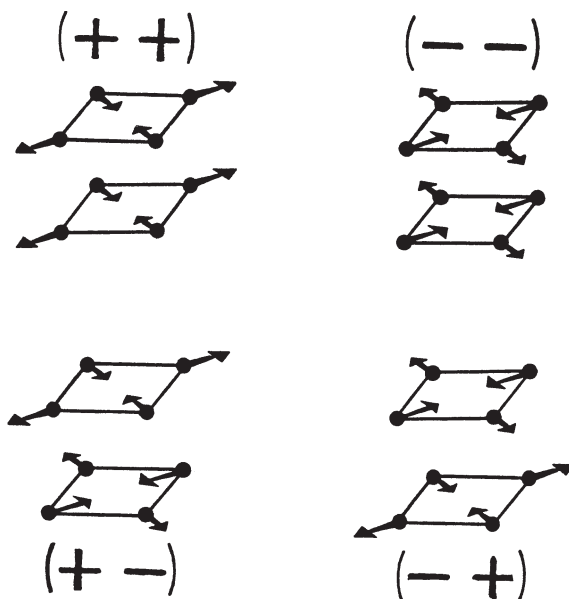


**FIGURE 9.23.** Four types of possible packing of two interacting Jahn–Teller centers. For each of them the  $E \otimes b_1$  problem of a square-planar system with  $B_{1g}$  distortions (Fig. 9.16) is assumed.

lowers the energy for parallel orientations of the distortions (*ferrodistortive interactions*), the energy of the configurations  $(++)$  and  $(--)$  is lower than that of  $(+-)$  and  $(-+)$ . On the other hand, if the antiparallel distortions are preferable (*antiferrodistortive interactions*), the configurations  $(+-)$  and  $(-+)$  are lower in energy. In both cases the two configurations “+” and “–” of each center are no longer equivalent. This conclusion can be generalized to many interaction centers and in the limit, to the entire crystal.

It is evident that at suitably low temperature, the minimum free-energy configuration is realized in which the crystal has statically distorted and distortion-correlated centers. For ferrodistortive interactions such an ordering of the local distortions (*ferrodistortive ordering*) leads to a macrodeformation of the crystal as a whole. New properties of the crystal arising from the correlation (ordering) of the JT (PJT) local distortions, including the formation of new crystal structures and structural phase transitions, are called, respectively, the *cooperative Jahn–Teller effect (CJTE)* or the *cooperative pseudo-Jahn–Teller effect (CPJTE)*.

In the example above, the two correlated configurations  $(++)$  and  $(--)$  are equivalent and, in principle, the pair of correlated centers may resonate between the  $(++)$  and  $(--)$  states, dynamically preserving the initial symmetry. However, in the macroscopic crystal with a large number of centers, the barriers between the equivalently distorted configurations of the entire crystal  $(+++ \dots)$  and  $(--- \dots)$  become so high that the transitions between them are practically

impossible, and the crystal remains in one of them for an infinitely long period. The situation here is quite similar to that found in ferromagnetics, in which there are also different equivalent directions of magnetization, but no spontaneous inversion of the magnetic moment.

In these cases, as distinct from the one-center problem, the symmetry of the ground-state configuration of the crystal is lower than that of the Hamiltonian; this is sometimes called the *effect of "broken symmetry."* Strictly speaking, such a crystal state is not stationary, but, owing to the very large height of the barriers, it may remain there for infinitely long time.

It is clear that the lattice vibrations and temperature fluctuations tend to destroy the correlation between the JT distortions. With the increase of temperature  $T$  the second term in the abovementioned free energy  $F = U - TS$  becomes significant, while the entropy  $S$  increases with disorder. Therefore, in principle, for any given energy of interactions of the ordered distortions there is a certain temperature  $T_c$  at which the free energies of the two phases coincide,  $U_1 - T_c S_1 = U_2 - T_c S_2$ ; above  $T_c$  the ordering is destroyed and the lattice acquires a more symmetric structure with independent (uncorrelated) dynamic distortions at each center (provided that the crystal does not melt at lower temperature). This temperature dependent breakdown (disordering) of the correlations of the distortions is merely a *structural phase transition*. The larger the distortion at each center and the energy of interactions of the distorted units, the higher the temperature of the phase transition to the disordered state. *The structural phase transition to the crystal state with disordered JT or PJT local distortions is one of the most important features of the cooperative vibronic effects* [9.20, 9.77, 9.78].

At present, structural phase transitions in many classes of crystals have been attributed to cooperative vibronic effects. In particular, in a series of tetragonal rare-earth zircons of general formula  $RXO_4$ , where R is rare earth and X = V, As, P, a direct correspondence between electronic structure parameters of the JT rare-earth ion  $R^{3+}$  (R = Tm, Dy, Tb) and the temperatures of structural phase transitions in the cooperative JT approach was established. Other crystals, such as spinel (e.g.,  $NiCr_2O_4$ ,  $FeCr_2O_4$ ,  $CuCr_2O_4$ ,  $FeV_2O_4$ ,  $FeCr_2S_4$ ,  $Mn_3O_4$ ,  $CuFe_2O_4$ ,  $FeTiO_4$ ), perovskites ( $KCuF_3$ ,  $KMnF_3$ ,  $PbFeF_3$ ), other structures [ $CsCuCl_3$ ,  $K_2CuF_4$ ,  $(NH_4)_2CoCl_2$ ,  $Copy_2Cl_2$ ,  $UO_2$ ,  $A_2BCu(NO_2)_6$ ,  $Cu(ONC_5H_6)_6X_2$ ], were also treated by the vibronic approach (see Refs. 9.20, 9.77, 9.78, and references cited therein).

Consider now the displacive mechanism of lattice formation (*displacive phase transitions*) taking *ferroelectricity and ferroelectric phase transitions* in perovskite-type crystals as an example. In ferroelectric crystals, at certain temperatures, structural phase transitions to a spontaneous polarized (ferroelectric) state take place [9.79]. If there are molecular groups with proper dipole moments in the initial crystal structure, the transition to the ferroelectric phase may be regarded as an ordering of rigid dipoles (order-disorder transitions). However, in perovskite ferroelectrics (e.g., barium titanate,  $BaTiO_3$ ) there are no such dipoles: the lattice is assumed to have cubic symmetry in the paraphase



(the Ti site local symmetry is  $O_h$ ), while the dipole moment is supposed to emerge as a result of the displacive phase transition.

It is evident that if there are no rigid dipole groups in the elementary cells of the crystal, but such groups might occur as a result of the JT or PJT distortions, *ferroelectric phase transition may take place as a result of the ordering of JT and/or PJT dipolar distorted centers*. As noted in Section 7.4, the JTE cannot result in dipolar distortions in systems that have an inversion center, but these distortions can occur as a result of the PJTE. Again, most ferroelectrics are dielectrics that have no degenerate ground states, and hence they are not subject to the JTE.

The PJT mechanism of spontaneous polarization and ferroelectric phase transitions was suggested more than four decades ago [9.80]; it led to the vibronic theory of ferroelectricity [9.20, 9.77, 9.80, 9.81] (see review article [9.81]). Rigorous versions of the problem were solved by modern methods of theoretical physics. The qualitative aspect of the problem, mainly the electronic features that lead to a physically visual picture of the microscopic origin of ferroelectricity, can be revealed by investigation of the APES obtained from the PJTE.

For the the  $\text{BaTiO}_3$  crystal, the PJTE in the octahedral cluster  $\text{TiO}_6^{8-}$  is considered in Section 7.4, where it is shown that the vibronic mixing of the ground  $A_{1g}$  term with the nearest excited term  $T_{1u}$  by odd displacements of  $T_{1u}$  type (dipolar displacements) under certain conditions results in an APES with eight equivalent minima along the trigonal axes of the octahedron, 12 saddle points along the twofold axes, and six higher-energy saddle points along the tetragonal axes. At the minima and saddle points the cluster has nonzero dipole moments. Allowing for strong correlation between these clusters in  $\text{BaTiO}_3$  through common ligands, the cooperative PJTE results in a structural phase transition to the spontaneously polarized ferroelectric state of the lattice in which all the local dipole moments have the same orientation. Depending on the sign of the interacting distortions, an antiferroelectric ordering with alternating directions of the dipoles is also possible.

With this APES, a semiclassical approach qualitatively reproduces all the observed ferroelectric phases in barium titanate, including the consequence of their occurrence with temperature, the symmetry of the crystal, and the direction and relative value of polarization in each phase. Moreover, it follows from this theory that only one of the three ferroelectric phases in  $\text{BaTiO}_3$ —the low-temperature rhombohedral phase—is completely ordered. The other two, orthorhombic and tetragonal, are partly disordered, the former along one direction and the latter along two directions, while the paraphase is completely disordered in all directions. This conclusion is fundamentally novel and does not follow from any other theories of ferroelectricity. It has been confirmed by quite a number of experiments on diffuse scattering of X rays [9.82], light scattering [9.83], refined ESR measurements with probe ions [9.84], XAFS experiments [9.85, 9.86], and so on. Table 9.15 lists some of such publications. Similar order–disorder effects are observed in  $\text{K}_2\text{PbCu}(\text{NO}_2)_6$  [9.92].

**TABLE 9.15. Experimental Evidence of Local Origin of Distortions and Order–Disorder Nature of Phase Transitions in “Displacive” Ferroelectrics**

Author(s), Year	Method, System	Main Result
Comes et al., 1968 [9.82]	X-ray, diffuse scattering, BaTiO <sub>3</sub>	Qualitative confirmation of main predictions of the vibronic theory for BaTiO <sub>3</sub>
Quitet et al., 1973 [9.83]	Raman spectra, BaTiO <sub>3</sub> , KNbO <sub>3</sub>	Polar distortions in the cubic paraphase
Burns and Dacol, 1981 [9.87]	Optical refractive index, BaTiO <sub>3</sub>	Nonvanishing component ( $P^2$ ) in the cubic phase
Gervais, 1984 [9.88]	Infrared reflectivity, BaTiO <sub>3</sub>	Nonvanishing component ( $P^2$ ) in the cubic phase
Ehses et al., 1981 [9.89]	X-ray, BaTiO <sub>3</sub>	Strong order–disorder component in cubic phase
Itoh et al., 1985 [9.90]	X-ray, BaTiO <sub>3</sub>	[111] displacement of Ti in paraphase up to 180 K above $T_c$
Muller, 1986 [9.84]	ESR with probing ion BaTiO <sub>3</sub> , KNbO <sub>3</sub>	[111] displacements in rhombohedral phase; reorientations in orthorhombic phase, $10^{-10} < \tau < 10^{-9}$ (s)
Hanske-Petitpierre et al., 1992 [9.85]	XAFS, KNb <sub>x</sub> Ta <sub>1-x</sub> O <sub>3</sub>	[111] displacements in all three phases for any $x > 0.08$ ; mean-square displacements much smaller due to dynamics
Dougherty et al., 1992 [9.91]	Femtosecond resolution of light scattering, BaTiO <sub>3</sub> , KNbO <sub>3</sub>	No relaxational modes that might exclude the distortion model
Sicron et al., 1994 [9.86]	XAFS, PbTiO <sub>3</sub>	Ti and Pb ions are displaced in the paraphase up to 200 K above $T_c$

It was also shown [9.81] that *the long-range forces themselves cannot result in instability of the high-symmetry configuration of the lattice*. Together with the very convincing experimental confirmation (Table 9.15), *this result casts doubts on the very existence of displacive phase transitions* meaning phase transitions induced by long-range forces only. In case of weak PJTE on the centers the local distortions are of dynamic nature, so they became observable only after their ordering in the crystal. In such cases the phase transitions look displacive, but it is still triggered by the local PJTE. Many other details in ferroelectric properties are revealed and explained in the vibronic theory [9.81].

If the local distortions in crystals do not create dipole moments, the picture of cooperative vibronic interactions and structural phase transitions is the same

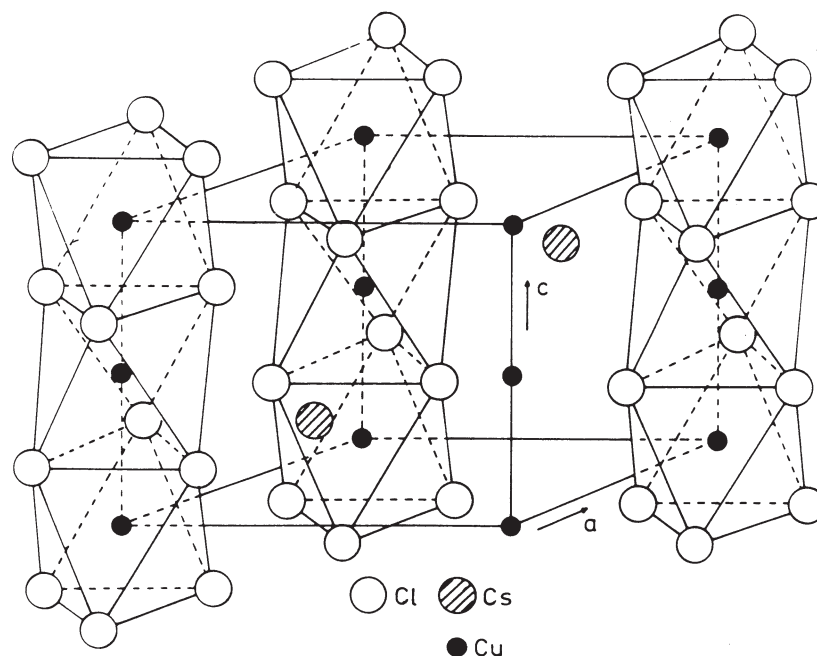
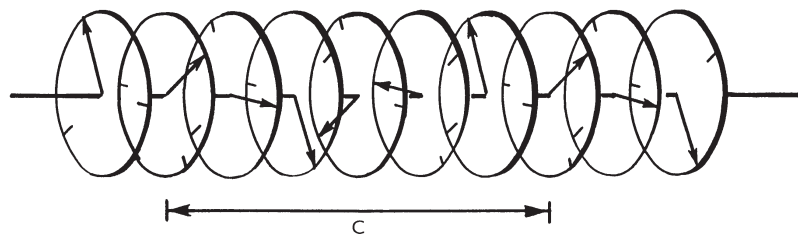


FIGURE 9.24. The crystal structure of  $\text{CsCuCl}_3$ .

as considered above, with the distinction that nonpolar distortions produce not ferroelectric, but *ferroelastic, phase transition*. Since any local distortion from the high-symmetry configuration is of vibronic nature (Section 7.4), all the structural phase transitions in crystals can be explained in this way.

One interesting feature of structural phase transitions is the formation of *helicoidal structures*. Consider the crystal  $\text{CsCuCl}_3$  [9.93]. Its parallel chains in the lattice contain  $\text{CuCl}_6$  octahedral polyhedra that are interlinked by triple bridges produced by three chlorine atoms, the latter thus forming a common triangular face for two nearest-neighbor polyhedra (Fig. 9.24). Each Cu(II) center, due to the JTE, requires a tetragonally distorted octahedron of six chlorine atoms, and there are three equivalent directions of distortions corresponding to three fourfold axes. However, because of the common ligands, the distortions of the nearest-neighbor octahedra are correlated. In particular, if the direction of distortion for a given polyhedron is, say, along the  $z$  axis, its neighbor should distort along either the  $x$  or the  $y$  axis. From the perspective of the trigonal axis along which the Cu atoms are located in the chain, the directions of the distortions of the two neighboring octahedrons are rotated by an angle  $\phi = 60^\circ$  (from one apex of the interfacing triangle to the next). This is shown schematically in Fig. 9.25. As one can see, the period of the lattice in the distorted helicoidal screwlike configuration is 6 times larger than in the undistorted one.



**FIGURE 9.25.** Schematic illustration to the helicoidal structure of the  $\text{CsCuCl}_3$  crystal. The  $\text{CuCl}_3$  chain is shown conventionally; the Cu atoms are on the trigonal axis of the local octahedral polyhedron (Fig 9.24), and are shown in a circle with an arrow indicating the direction of the Jahn–Teller tetragonal local distortion. Because of the common shared Cl ligands, the latter are shifted in phase by  $\phi = 60^\circ$  for any two nearest-neighbor Cu atoms in the chain, and the lattice period along the chain is 6 times larger than in the undistorted crystal.

Another example of helicoidal structure is mentioned in Section 9.2, the  $\text{InCl}$  crystal [9.94]. It has a rock-salt structure in the high-symmetry configuration, but the vibronic interaction of the lone pair  $(5s)^2$  with the excited states produces a combined PJT off-center distortion associated with the excited state JT  $e_g$  or  $t_{2g}$  distortion [9.44], discussed in Section 9.2 in more detail. This distortion, owing to the common ligands of the nearest-neighbor polyhedra, for reasons similar to those considered above, produces the helicoidal structure [9.94].

In the example of  $\text{CsCuCl}_3$  above, as is seen from Fig. 9.25, the new period of the helicoidal distorted lattice is exactly 6 times that of the undistorted lattice. However, in certain cases the ratio of the lattice period in the new phase to that of the higher-symmetry phase is not an integer. In these cases the new structure is described as being *incommensurate* with the previous one, and the phase transition takes place to an *incommensurate phase*. An interesting example of incommensurate phases is provided by  $\text{K}_2\text{PbCu}(\text{NO}_2)_6$  [9.20, 9.92]. A related phenomenon, important for transition metal compounds, is *structural magnetic transitions* [9.20, 9.92].

## SUMMARY NOTES

1. *Stereochemistry* deals with molecular shapes. *Molecular shape* can be defined as the nuclear configuration that corresponds to a sufficiently deep minimum of the APES.
2. *Nuclear configurations* are controlled by electronic structure. APES for specific TMS can be obtained by quantum-chemical calculations. The theory of stereochemistry should be based on more general models that incorporate such specific calculations.
3. *Earlier approaches* explaining the origin of stereochemistry are mostly semiclassical. They include directed valencies, valence shell electron pair

repulsion, complementary electron density distribution, and other related models. *Semiclassical models* assume that there are localized charge distributions that interact electrostatically to produce a certain configuration of the nuclear framework. With regard to TMS, semiclassical models are unable to take into account the inherent *d*- and *f*-electron delocalization and vibronic coupling effects.

4. The *vibronic coupling* produces new, unexpected (from the classical perspective) configurations, including JT, PJT, and RT distorted (from high-symmetry) polyhedrons, off-center displaced CA, peculiar geometry of ligand coordination, origin of inactivity of some lone pairs, and specific pseudorotations in TMS.
5. Vibronic mixing of at least two electronic states under nuclear displacements is *crucial* in initiating any nuclear configuration changes, including configuration distortions, conformation transitions, chemical transformations, phase transitions, structural symmetry breaking, and so on. This *novel paradigm*—the two electronic states in transformations (TEST) paradigm—provides for a higher level of theory and a better understanding of chemical and physical phenomena.
6. *Mutual influence of ligands*, in particular, *cis*- and *trans* influences, explain some special features of TMS stereochemistry, especially in crystalline state (*cis*- and *trans* effects in chemical reactivity are considered in Section 11.3). It can be presented as the influence of electronic changes accompanying a given ligand substitution on *trans* (*cis*) ligand position (and reactivity) via the vibronic coupling mechanism.
7. Vibronic coupling is also important in *formation of the crystal lattices* and their transformations (phase transitions). Several illustrative examples confirm this statement, including the plasticity effect, distortion isomers, and temperature-dependent conformers; no classical or semiclassical approach can explain these unusual crystal chemistry phenomena.
8. *Ferroelectricity* in perovskite-type crystals is due to the PJTE that displaces the transition metal from the center forming local dipole moments, their partial and full ordering explain the origin of different phases. In this explanation three phases out of four (including the cubic paraphrase) are disordered, and this is fully confirmed experimentally.
9. The vibronic theory also explains the origin of other *unusual crystal formations*, such as helicoidal structures.

## EXERCISES AND PROBLEMS

- P9.1.** How can we define rigorously molecular shapes? Give examples of when the experimentally observed molecular geometry differs when obtained with different methods of measurement.

- P9.2.** Why is the method of directed valences not good enough in determining the stereochemistry of TMS?
- P9.3.** The VSEPR model assumes that a pair of electrons occupying a non-bonding atomic orbital (a lone pair) is a source of electrostatic repulsion that destroys the otherwise symmetric arrangement of the ligands around the CA. Many TMSs with lone pairs are distorted, but certain systems are not distorted despite the presence of a lone pair. Can the VSEPR model explain this controversy? (See Problem P9.6.)
- P9.4.** Following the “gas rule,” complexes with 2, 8, 18, 32, and more electrons should be most stable. For atoms these “magic numbers” of stability follow directly from quantum theory of system with spherical symmetry, they correspond to closed-shell configurations. TMSs have no spherical symmetry, so how does the gas rule happen to be approximately valid in many systems?
- P9.5.** Example 9.3 shows how the electronic configuration (the several highest occupied and lowest unoccupied MOs and their symmetries) may serve as a basis for qualitative stereochemical predictions. What numerical parameters do you need for more rigorous predictions of molecular shapes?
- P9.6.** The vibronic approach solves, in principle, the problem of origin of active and inert lone pairs. What electronic structure parameters do we need to predict the lone-pair activity, and how can we get them from experimental data and/or calculations?
- P9.7.** What is the difference between Berry-type and JT-type pseudorotations? How can we observe this difference experimentally? Give examples.
- P9.8.** According to the three-dimensional delocalization of  $d$  electrons in TMSs (Section 6.1), we could expect the changes in a given ligand to affect all the other ligands that take part in the delocalization of the affected orbitals. Why, then, do such changes influence mostly *trans*-ligands (*trans* influence)? What main parameters characterize the *trans*-influence power? (*Hint*: Involve the discussion in Section 11.3 and Fig. 11.11 in your answer.)
- P9.9.** The plasticity effect is employed in understanding the origin of a variety of crystal lattices of TMS and explanation of their properties. What transition metals are most appropriate for producing the plasticity effect in TMS, and why? Explain your answer and give examples from the literature. (*Hint*: Literature data can be obtained from the *Science Citation Index* by revealing papers that cite the original publications on the plasticity effect.)
- P9.10.** Phase transitions in solid TMS are most important also because of their applications. What is the driving force of nuclear displacements in such transitions? What are the necessary conditions of dipolar displacements that lead to local dipole moment formation and their cooperative

interaction to produce ferroelectricity? (*Hint*: Utilize the discussion in Section 7.4 and/or Section 8.3 of Ref. 9.20.)

- P9.11.** Show how the TEST paradigm (Section 7.4) works in explanation of off-center positions of CA and geometry of ligand coordination. Give examples.

## REFERENCES

- 9.1. J. K. Burdett, *Molecular Shapes. Theoretical Models of Inorganic Stereochemistry*, Wiley-Interscience, New York, 1980.
- 9.2. R. G. Gillespie, *Molecular Geometry*, Van Nostrand, Reinhold, London, 1972; R. G. Gillespie and I. Hargittai, *The VSEPR Model of Molecular Geometry* (Int. Student ed.), Allyn & Bacon, London, 1991.
- 9.3. J. E. Fergusson, *Stereochemistry and Bonding in Inorganic Chemistry*, Prentice-Hall, Englewood Cliffs, NJ, 1974.
- 9.4. D. L. Kepert, *Inorganic Stereochemistry*, Springer, Berlin, 1982.
- 9.5. A. von Zelewsky, *Stereochemistry of Coordination Compounds*, Wiley, New York, 1996.
- 9.6. Yu. S. Varshavskii, T. G. Cherkasova, and M. M. Singh, *Zh. Neorg. Khim.* **15**, 2746 (1970).
- 9.7. L. Pauling, *The Nature of the Chemical Bond and the Structure of Molecules and Crystals*, 3rd ed., Cornell Univ. Press, Ithaca, NY, 1960.
- 9.8. D. J. Kimball, *J. Chem. Phys.* **8**, 188 (1940).
- 9.9. R. M. Gavin and L. S. Bartell, *J. Chem. Phys.* **48**, 2460 (1968).
- 9.10. L. S. Bartell and R. M. Gavin, *J. Chem. Phys.* **48**, 2466 (1968).
- 9.11. R. S. Berry, *J. Chem. Phys.* **32**, 933 (1960).
- 9.12. D. M. P. Mingos and L. Zhenyang, *Struct. Bond.* **71**, 1 (1989).
- 9.13. P. Seiver and J. D. Dunitz, *Acta Cryst.* **B36**, 2255 (1980).
- 9.14. S. Lange and G. Huttner, *Acta Cryst.* **B28**, 2049 (1972).
- 9.15. M. R. Mingos, *Introduction to Cluster Chemistry*, Prentice-Hall, Hertfordshire, UK, 1990.
- 9.16. D. M. P. Mingos, *Pure Appl. Chem.* **59**, 145 (1987).
- 9.17. D. M. P. Mingos and J. C. Hawes, *Struct. Bond.* **63**, 1 (1985).
- 9.18. S. C. Abrahams, A. P. Ginsberg, and K. Knox, *Inorg. Chem.* **3**, 538 (1964).
- 9.19. A. P. Ginsberg, *Transition Metal Hydrides*, Advances in Chemistry Series Vol. 167, Academic Press, 1978, p. 201.
- 9.20. I. B. Bersuker, *The Jahn-Teller Effect*, Cambridge Univ. Press, Cambridge, UK, 2006.
- 9.21. A. Ceulemans and L. G. Vanquickenborne, *Struct. Bond.* **71**, 125 (1989).
- 9.22. A. Ceulemans, D. Beyens, and L. G. Vanquickenborne, *J. Am. Chem. Soc.* **106**, 5824 (1984).
- 9.23. I. B. Bersuker, ed., *The Jahn-Teller Effect. A Bibliographic Review*, IFI Plenum, New York, 1984.



- 9.24. B. J. Hathaway, *Struct. Bond.* **57**, 55 (1984).
- 9.25. J. Gazo, I. B. Bersuker, J. Garaj, M. Kabesova, J. Kohout, H. Langfelderova, M. Melnik, M. Serator, and F. Valach, *Coord. Chem. Rev.* **19**, 253 (1976).
- 9.26. R. G. Pearson, *Symmetry Rules for Chemical Reactions, Orbital Topology and Elementary Processes*, Wiley, New York, 1976.
- 9.27. P. Curie, *Oeuvres de Pierre Curie*, Gauthiers-Villars, Paris, 1908, p. 118.
- 9.28. R. F. W. Bader and A. D. Bandrauk, *J. Chem. Phys.* **49**, 1666 (1968).
- 9.29. H. Bash, J. W. Moskowitz, C. Holister, and D. Hankin, *J. Chem. Phys.* **55**, 1922 (1971).
- 9.30. F. A. Gianturco, C. Quidotti, and U. Lamanna, *J. Chem. Phys.* **57**, 840 (1972).
- 9.31. L. S. Bartell, *J. Chem. Phys.* **73**, 375 (1981).
- 9.32. D. Reinen and C. Friebel, *Inorg. Chem.* **23**, 792 (1984); D. Reinen and M. Atanasov, *Chem. Phys.* **136**, 27 (1989); D. Reinen and M. Atanasov, *Chem. Phys.* **155**, 157 (1991); M. Atanasov, W. Koenig, M. Craupner, and D. Reinen, *New J. Chem.* **17**, 115 (1993).
- 9.33. D. W. Meek and J. A. Ibers, *Inorg. Chem.* **9**, 405 (1970).
- 9.34. V. Z. Polinger, N. N. Gorinchoy, and I. B. Bersuker, *Chem. Phys.* **159**, 75 (1992); N. N. Gorinchoy, I. B. Bersuker, and V. Z. Polinger, *New J. Chem.* **17**, 125 (1993).
- 9.35. I. B. Bersuker and S. S. Stavrov, *Coord. Chem. Rev.* **88**, 1 (1988).
- 9.36. M. Zerner and M. Gouterman, *Theor. Chim. Acta* **4**, 44 (1966); M. Gouterman, in D. Dolphin, ed., *The Porphyrins*, ed., Vol. III, Academic Press, 1978, p. 1.
- 9.37. J. H. Enemark and R. D. Feltham, *Coord. Chem. Rev.* **13**, 339 (1974).
- 9.38. M. Zerner and M. Gouterman, *Theor. Chim. Acta* **6**, 363 (1966).
- 9.39. W. A. Eaton, L. K. Hanson, P. J. Stephens, J. C. Sutherland, and B. R. Dunn, *J. Am. Chem. Soc.* **100**, 4991 (1978).
- 9.40. R. Rericha, *J. Mol. Struct. (THEOCHEM)*, **227**, 305–310 (1991).
- 9.41. A. F. Wells, *Structural Inorganic Theory*, Clarendon, Oxford, 1984.
- 9.42. L. E. Orgel, *J. Chem. Educ.* 3815 (1959).
- 9.43. S. Y. Wang and L. L. Lohr, Jr., *J. Chem. Phys.* **60**, 3901 (1974); **61**, 4110 (1974).
- 9.44. W. J. A. Maaskant and I. B. Bersuker, *J. Phys. Condens. Matt.* **3**, 37 (1991).
- 9.45. W. J. A. Maaskant, *New J. Chem.* **17**, 97 (1993).
- 9.46. A. Ceulemans, *J. Chem. Phys.* **84**, 6442 (1986).
- 9.47. B. J. Hathaway, *Struct. Bond.* **57**, 55 (1984).
- 9.48. J. Pradilla-Sorzano and J. P. Fackler, *Inorg. Chem.* **12**, 1182 (1973).
- 9.49. A. von Zelewsky, *Inorg. Chem.* **20**, 4448 (1981).
- 9.50. W. G. Klemperer, D. D. Traficante, and G. M. Whitesides, *J. Am. Chem. Soc.* **97**, 7023 (1975).
- 9.51. M. M. L. Chen and R. Hoffmann, *J. Am. Chem. Soc.* **98**, 1651 (1976).
- 9.52. J. Brunvoll, A. A. Ischenko, V. P. Spiridonov, and T. G. Strand, *Acta Chem. Scand.* **A38**, 115 (1984).
- 9.53. B. Daines, A. McNeish, M. Poliakoff, and J. J. Turner, *J. Am. Chem. Soc.* **99**, 7573 (1977).
- 9.54. M. Poliakoff and A. Ceulemans, *J. Am. Chem. Soc.* **106**, 50 (1984).



- 9.55. I. I. Chernyaev, in *Selected Works: Complex Compounds of Platinum* (Russ.), Nauka, Moscow, 1973.
- 9.56. F. R. Hartley, *Chem. Soc. Rev.* **2**, 163 (1973).
- 9.57. E. M. Shustorovich, M. A. Porai-Koshitz, and Iu. A. Buslaev, *Coord. Chem. Rev.* **17**, 1 (1975).
- 9.58. V. I. Nefedov and M. M. Hofman, *Mutual Influence of Ligands in Inorganic Compounds* (Russ.), in *Itoghi Nauki i Techniki, Series Inorganic Chemistry*, Vol. 6, VINITI, Moscow, 1978.
- 9.59. A. A. Levin, in *Sov. Sci. Rev. B, Chem. Rev.* **9**, 279–335 (1987); A. A. Levin, *New J. Chem.* **17**, 31 (1993).
- 9.60. J. Gazo, R. Boca, E. Jona, M. Kabesova, L. Macaskova, J. Sima, P. Pelikan, and F. Valach, *Coord. Chem. Rev.* **43**, 87 (1982).
- 9.61. M. A. Porai-Koshitz and L. A. Atovmean, *Crystal Chemistry and Stereochemistry of Molybdenum Coordination Compounds* (Russ.), Nauka, Moscow, 1974.
- 9.62. J. K. Burdett and T. A. Albright, *Inorg. Chem.* **18**, 2112 (1979).
- 9.63. A. A. Grinberg, *Zh. Neorg. Khim.* **4**, 1517 (1959).
- 9.64. J. Chatt, L. A. Duncanson, and L. M. Venanzi, *J. Chem. Soc.* 4456 (1955).
- 9.65. L. E. Orgel, *J. Inorg. Nucl. Chem.* **2**, 137 (1956).
- 9.66. I. B. Bersuker, *Zh. Neorg. Khim.* **9**, 36 (1964); *Zh. Struct. Khim.* **4**, 461 (1963).
- 9.67. G. B. Bokii and I. B. Bersuker, *Zh. Struct. Khim.* **4**, 934 (1963).
- 9.68. M. J. S. Dewar, *The PMO Theory of Organic Chemistry*, Plenum Press, New York, 1975.
- 9.69. I. B. Bersuker, *Zh. Struct. Khim.* **16**, 935 (1975).
- 9.70. J. P. Fackler and A. Avdeev, *Inorg. Chem.* **13**, 1864 (1974).
- 9.71. J. Gazo, *Pure Appl. Chem.* **38**, 279 (1974).
- 9.72. C. Friebel and D. Reinen, *Z. Anorg. Allgem. Chem.* **407**, 193 (1974).
- 9.73. J. K. Burdett, *Inorg. Chem.* **20**, 1959 (1981).
- 9.74. H. Yamatera, *Acta Chem. Scand.* **A33**, 107 (1979).
- 9.75. T. Obert and I. B. Bersuker, *Proc. XIX ICCO*, Prague, 1978, Vol. 2, p. 94; *Czech. J. Phys. B* **33**, 568 (1983).
- 9.76. C. J. Simmons, *New J. Chem.* **17**, 77 (1993).
- 9.77. I. B. Bersuker and V. Z. Polinger, *Vibronic Interactions in Molecules and Crystals*, Springer, Berlin, 1989.
- 9.78. G. A. Gehring and K. A. Gehring, *Rep. Progr. Phys.* **38**, 1 (1975).
- 9.79. M. E. Lines and A. M. Glass, *Principles and Applications of Ferroelectrics and Related Materials*, Clarendon Press, Oxford, 1977.
- 9.80. I. B. Bersuker, *Phys. Lett.*, **20**, 586 (1966); I. B. Bersuker and B. G. Vekhter, *Ferroelectrics* **19**, 137 (1978); I. B. Bersuker, *Fiz. Tverdogo Tela (Sov. Phys. Solid State)* **30**, 1738 (1988).
- 9.81. I. B. Bersuker, *Ferroelectrics* **164**, 75 (1995).
- 9.82. R. Comes, M. Lambert, and A. Guinier, *Solid State Commun.* **6**, 715 (1968).
- 9.83. A. M. Quittet, M. Lambert, and A. Guinier, *Solid State Commun.* **12**, 1053 (1973); R. Comes, R. Currat, F. Denoyer, M. Lambert, and M. Quittet, *Ferroelectrics* **12**, 3 (1976).

- 9.84. K. A. Muller, *Helv. Phys. Acta* **59**, 874 (1986); in A. R. Bishop, ed., *Nonlinearity in Condensed Matter*, Springer, Heidelberg, 1986, p. 234.
- 9.85. O. Hanske-Petitpierre, Y. Yacoby, J. Mustre de Leon, E. A. Stern, and J. J. Rehr, *Phys. Rev. B* **44**, 6700 (1992).
- 9.86. N. Sicron, B. Ravel, Y. Yacoby, E. A. Stern, F. Dogan, and J. J. Rehr, *Phys. Rev. B* **50**, 13168 (1994—II); B. Ravel and E. A. Stern, *Physica B* **208/209**, 316 (1995).
- 9.87. G. Burns and F. Dacol, *Ferroelectrics* **37**, 661 (1981).
- 9.88. F. Gervais, *Ferroelectrics* **53**, 91 (1984).
- 9.89. K. H. Ehses, H. Bock, and K. Fischer, *Ferroelectrics* **37**, 507 (1981).
- 9.90. K. Itoh, L. Z. Zeng, E. Nakamura, and N. Mishima, *Ferroelectrics* **63**, 29 (1985).
- 9.91. T. P. Dougherty, G. P. Wiederrecht, K. A. Nelson, M. H. Garrett, H. P. Jensen, and C. Warde, *Science* **258**, 770 (1992).
- 9.92. D. Reinen and C. Friebel, *Struct. Bond.* **37**, 1 (1979).
- 9.93. W. J. A. Maaskant and W. G. Haye, *J. Phys. C* **19**, 5295 (1986).
- 9.94. C. P. J. M. Van der Vorst, W. J. A. Maaskant, *J. Solid State Chem.* **34**, 301 (1980); W. J. A. Maaskant, *New J. Chem.* **17**, 97 (1993).

---

# 10

---

## **ELECTRON TRANSFER, REDOX PROPERTIES, AND ELECTRON-CONFORMATIONAL EFFECTS**

*Chemical interaction begins with electronic charge redistribution, which initiates nuclear displacements resulting in chemical transformations.*

In chemical processes with transition metal participation charge transfer by coordination, intra- and intermolecular electron transfer, and *electron-conformational effects* (conformation changes due to charge transfer) are of primary importance. Charge transfer by coordination is a unique property of TMS controlled by *d*- and *f*-electron heterogeneity (Chapter 6). Electron transfer in mixed-valence multicenter TMS determines their main features. Conformational transitions triggered by charge transfer are most important in both chemistry and biology. Examples of these phenomena as controlled by the electronic structure are briefly discussed in this chapter.

### **10.1. ELECTRON TRANSFER AND CHARGE TRANSFER BY COORDINATION**

#### **Intramolecular Charge Transfer and Intermolecular Electron Transfer**

As stated in Section 1.2, chemical bonding is an electronic phenomenon based mostly on collectivization of the electrons of interacting atomic groups. Any chemical interaction of atoms is thus associated with electronic charge redistribution, which generates further transformations. Charge transfers are especially

important in coordination compounds because of the heterogeneity introduced by  $d$  and  $f$  states, distinguished from the almost (electronically) homogeneous organic and main-group systems (in the sense that they contain only  $nsnp$ -electron atoms).

Section 5.2 discusses methods of quantum-chemical calculation of charge redistribution and integral and orbital charge transfer, and Sections 6.3, 6.4, and 11.2 provide many examples of such calculations. Here we try to give a more general understanding of the origin of electron transfer and charge transfer by coordination, and to correlate these quantities with the electronic structure of the coordinating subunits.

The problem is to find *a measure of ability of the molecular system to donate or accept electronic charge*, based on its electronic structure. Many attempts have been made to solve this problem, beginning with those based on Pauling's *electronegativity* [10.1]. Its explicit formulation states that the ability to transmit electronic charge is directly related to the ionization energy  $E_I$ , while the acceptance of electrons can be linked to the *electron affinity*  $E_A$ . The possibility of charge transfer by coordination is characterized by some combinations of  $E_I$  and  $E_A$  of the interacting atomic groups. A more flexible treatment of this phenomenon is based on the empirical conception of *hard and soft acids and bases* [10.2]; some more accurate quantitative estimates and formulas are given below.

The charge transfer between two molecular fragments within the stable coordination system is an *intramolecular charge transfer*. Also, there is much interest in *intermolecular electron transfer*. The latter takes place when there are two weakly interacting (almost independent) systems between which an electron instantly transfers from one system to another by collision. Such electron transitions are most important for *electron transfer reactions* and for various *electron-conformational effects* (Section 10.3). The possibility of intermolecular electron transfer and its rate are directly related to the electronic structure of the interacting molecules.

Consider two weakly interacting systems that can be conventionally called the *donor* (D) and the *acceptor* (A). Fig. 10.1 shows a simplified scheme of the highest occupied and lowest unoccupied molecular orbitals (HOMO and LUMO, Section 6.2) of D and A. If there is no significant bonding between D and A, the electron transfer  $D \rightarrow A$  (the reaction  $D + A \rightarrow D^+ + A^-$ ) is energetically convenient in case I (Fig. 10.1a) when the ionization energy  $E_I$  of D is smaller than the electron affinity  $E_A$  of A,  $E_I < E_A$ . In case II the electron transfer is formally not convenient (Fig. 10.1b) since  $E_I > E_A$ , but the electron transfer can still take place when promoted by some excitation process, as shown in Fig. 10.1c.

This picture of electron transfer between a noninteracting DA pair is rather oversimplified in many aspects. First, the absolute value of the ionization energy is taken to be equal to the HOMO energy; this is in accordance with the Koopmans theorem, which has limited applicability and is unacceptable in a number of cases (Sections 6.2, 6.4, and 8.3). The accurate value  $E_I$  can be calculated as

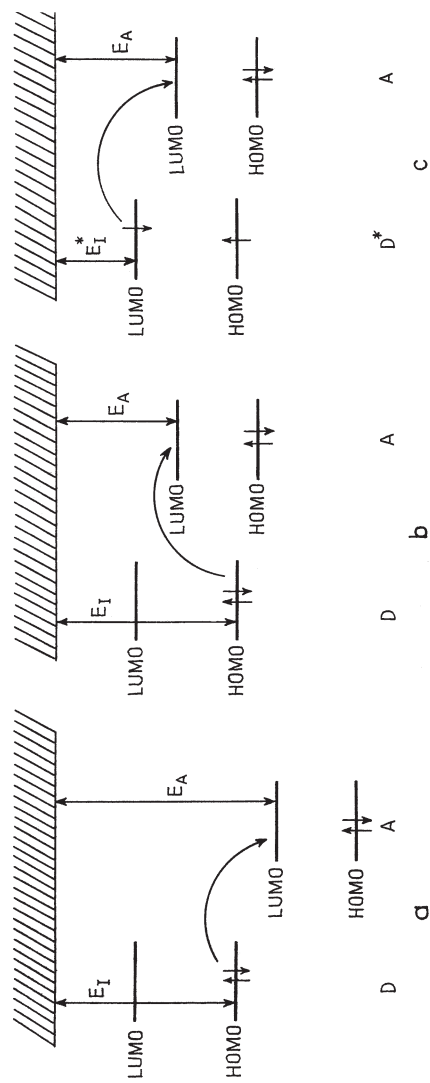


**FIGURE 10.1.** Simple scheme of HOMO–LUMO energy levels of a donor–acceptor pair DA: (a) the ionization energy  $E_I$  of  $D$  is smaller than the electron affinity  $E_A$ ; (b)  $E_I > E_A$ ; (c) for the excited state  $D^*$  of the case (b)  $E_I^* < E_A$ .

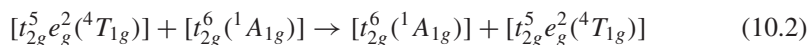
the difference between the total ground-state energies of D and D<sup>+</sup> and, accordingly,  $E_A$  is the difference between the total energies of A<sup>-</sup> and A. Hence the scheme of Fig. 10.1 remains valid if one substitutes  $\varepsilon(\text{HOMO})$  and  $\varepsilon(\text{LUMO})$  of the donor and acceptor by total energies  $E(\text{D})$ ,  $E(\text{D}^*)$ ,  $E(\text{A})$ , and  $E(\text{A}^-)$ , respectively (D\* denotes the corresponding excited state).

The HOMO–LUMO energies or, more precisely, the total energies of D, D\*, A, and A<sup>-</sup>, are directly related to the *standard electron potentials*  $E_{\text{ox}}^0$  and  $E_{\text{red}}^0$  and/or to the (approximately the same) *half-width potentials*  $E_{1/2}^{\text{ox}}$  and  $E_{1/2}^{\text{red}}$  in polarography (for details, see the text by Chanon et al. [10.3]). Thus the above mentioned electronic structure parameters (sometimes roughly the HOMO and LUMO energies) characterize the redox properties of the systems under consideration.

Electron transfer in DA pairs in which D and A are coordination systems have been studied in many cases but mostly by experimental methods. In coordination DA pairs D is generally an anion and A is a cation. An example of a well-studied series of ion pairs is  $\text{M}(\text{CN})_6^{4-}$  anions (M = Fe, Ru, Os) with  $\text{Ru}(\text{NH}_3)_5\text{L}^{3+}$  cations (L = pyridine or substituted pyridine) [10.4]. The rate of electron transfer depends on the energy barrier between the DA pair, which, in turn, is determined by the orbitals involved in the D–A orbital overlap during the instant interaction that realizes the electron tunneling. Newton [10.5] provides an example of ab initio calculations of such electron transfer process,



which can be presented as the transition between corresponding electronic configuration (Section 6.2):



It is seen that in this electron transfer each of the two complexes undergoes electron configuration and spin transition ( $^4T_{1g} \rightarrow ^1A_{1g}$  and  $^1A_{1g} \rightarrow ^4T_{1g}$ , respectively). As in the spin crossover phenomenon described in Section 8.4, these transitions produce changes in the ligand geometry via vibronic coupling.

The electron transfer reaction (10.1) is symmetric (D<sup>+</sup>  $\equiv$  A, A<sup>-</sup>  $\equiv$  D); the direct and inverse reactions have the same probability. Electron transfer also takes place between asymmetric pairs of coordination systems, including those mentioned above. For them the products of electronic transfer, D<sup>+</sup> and/or A<sup>-</sup>, may be unstable initiating secondary reactions. For example, consider the following two cases (where sep = sepulchrate):



Only case I produces a secondary reaction of dissociation into Co, NH<sub>3</sub>, and Ru<sup>III</sup>(CN)<sub>6</sub><sup>3-</sup>; as distinct from Co<sup>II</sup>(NH<sub>3</sub>)<sub>6</sub><sup>2+</sup>, Co<sup>II</sup>(sep)<sup>2+</sup> with cage-type ligands is rather stable; it does not decompose easily and the decomposition rate cannot compete with the backward electron transfer process.

If the bonding between coordinated groups that participate in the electron transfer is sufficiently strong, so that they can be considered as one molecule, the electron transfer is of the aforementioned intramolecular nature. However, in large systems there may be electron transfers between molecular sites that are not bonded directly. Figure 10.2 illustrates the absorption spectrum of electron transfer in the complex *cis*-(NH<sub>3</sub>)<sub>5</sub>Ru<sup>II</sup>NCRu<sup>II</sup>(bpy)<sub>2</sub>CNRu<sup>III</sup>(NH<sub>3</sub>)<sub>5</sub><sup>7+</sup> [10.6], which is, in fact, a mixed-valence compound (Section 10.2). Owing to the large distances (and hence weak coupling) between different sites of this system, the spectrum appears to have resulted from electron transfer reactions. The authors [10.6] succeeded in decomposing the integral absorption curve into components, each corresponding to a certain site-to-site electron transfer (similar to intervalence transfer in Section 10.2), shown in Fig. 10.2 by arrows.

A large subject of *outer-sphere electron transfer* between metal complexes in solution is not considered here in detail. In these cases the rate of electron transfer is determined by the nonadiabatic process in which the sluggish motion of solvent structure and/or counterions is important [10.7]. Quite relevant to electron

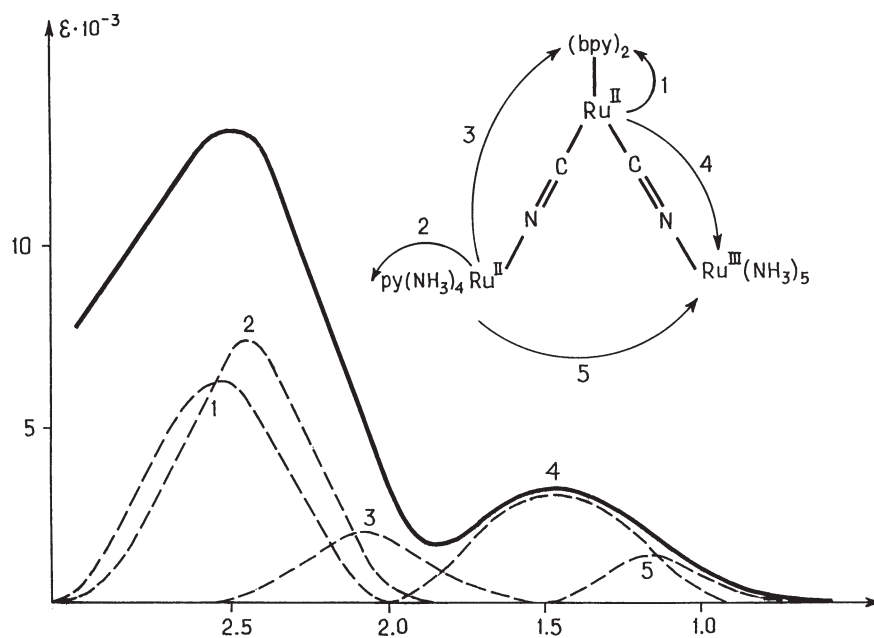


**FIGURE 10.2.** Absorption spectrum of the shown tricenter mixed-valence complex (Section 10.2) approximately resolved into component bands corresponding to the various site-to-site electron transfer transitions. (From Balzani and Scandola [10.6].)

transfer is also the more general topic of *tunneling phenomena in chemistry*, which include, in addition to *electron tunneling* of different origins, *the tunneling of heavy particles*, atoms, and atomic groups [10.8].

### Redox Capacitance

We begin the discussion of intramolecular charge transfer with a simple picture of charge transfer by coordination. Consider two coordinating systems, 1 and 2, and denote their HOMO and LUMO energy levels by  $\varepsilon_1^0$ ,  $\varepsilon_2^0$ ,  $\varepsilon_1''$ , and  $\varepsilon_2''$ , respectively. As mentioned above, in the Koopmans approximation (Sections 2.2, 6.2, and 6.4) the energies of the HOMO are equal to the corresponding ionization potentials taken with the opposite sign. The LUMO energies  $\varepsilon_1''$  and  $\varepsilon_2''$  under the same assumptions could be attributed to the electron affinities  $E_{Ai}$ , but this is a rough approximation: the addition of an electron to or removal from the system changes significantly the  $\varepsilon''$  and  $\varepsilon^0$  levels and may change even the sign of  $\varepsilon''$  (since the latter is nearer to zero than  $\varepsilon^0$ ).

As discussed above, if  $\varepsilon_1^0 > \varepsilon_2''$ , the electronic charge from the HOMO of 1 transfers to the LUMO of 2, following the principle of minimum energy, and if  $\varepsilon_2^0 > \varepsilon_1''$ , a charge transfer in the opposite direction takes place. How large will the charge transfer  $\Delta q$  be in these cases? To answer this question, a characteristic of the system that gives the measure of its *charge storage capacity* is needed [10.9, 10.10]. It is well known that MO energy levels are dependent on the total charge in the system,  $\varepsilon = \varepsilon(q)$ , and these functions are used in many semiempirical versions of self-consistent calculations of electronic structure of coordination compounds (Section 5.5). In particular, following the IEH method, the function  $\varepsilon(q)$  can be approximated by a three-term polynomial [cf. Eq. (5.107)]:

$$\varepsilon(q) = aq^2 + bq + c \quad (10.3)$$

Thus, when the charge of the system changes from the initial value of  $q = q_0$  to  $q = q_0 + \Delta q$ , the MO energy level changes by  $\Delta\varepsilon = (d\varepsilon/dq)_0 \Delta q = 2aq_0 \Delta q + b \Delta q$ . The derivative

$$C = \left( \frac{dq}{d\varepsilon} \right)_0 \quad (10.4)$$

which is equal to the amount of charge that increases the HOMO energy level of the system by a unity, can be called *redox capacitance* [10.9]. As seen from Eq. (10.3), at  $q_0 = 0$ ,  $C = (dq/d\varepsilon)_0 = 1/b$ . It characterizes the ability of the system to donate or accept charge with less change of its HOMO energy (or chemical potential  $\mu$ ; see below).

Provided that the redox capacitances of the two coordinating systems are known, the charge transfer can be calculated directly. Indeed, by coordination, the MOs of the two systems are collectivized and the coordinated system acquires a common HOMO energy level  $\varepsilon^0$  (another, similar, requirement is that the chemical potentials of the two coordinated system equalize; see below). The



charge transfers for the two subsystems are equal in absolute value and opposite in sign (we assume that  $\varepsilon_1^0 > \varepsilon_2^0$ ):

$$-\Delta q_1 = \Delta q_2 = \Delta q \quad (10.5)$$

Hence

$$\varepsilon_1^0(-\Delta q) = \varepsilon_2^0(\Delta q) = \varepsilon^0 \quad (10.6)$$

Then, in the linear approximation with respect to  $\Delta q$ , which is valid when either  $\Delta q$  is sufficiently small or  $C$  is constant (or both), we have (Fig. 10.3):

$$\begin{aligned} \Delta q &= C_1(\varepsilon_1^0 - \varepsilon^0), \\ -\Delta q &= C_2(\varepsilon_2^0 - \varepsilon^0) \\ \Delta q &= \frac{\varepsilon_1^0 - \varepsilon_2^0}{C_1^{-1} + C_2^{-1}} \end{aligned} \quad (10.7)$$

$$\varepsilon_1^0 - \varepsilon^0 = \frac{\varepsilon_1^0 - \varepsilon_2^0}{1 + C_1/C_2} \quad (10.8)$$

$$\varepsilon_2^0 - \varepsilon^0 = \frac{(\varepsilon_1^0 - \varepsilon_2^0)}{1 + C_2/C_1} \quad (10.9)$$

$$\frac{\varepsilon_1^0 - \varepsilon^0}{\varepsilon_2^0 - \varepsilon^0} = \frac{-C_2}{C_1} \quad (10.10)$$

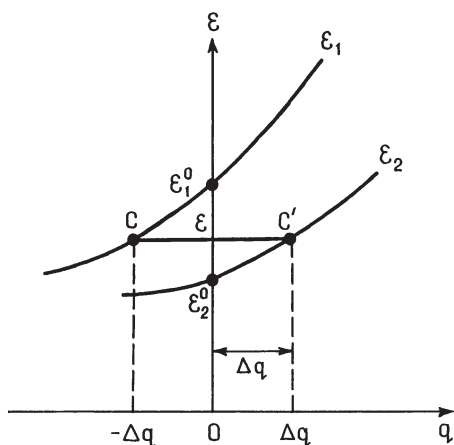


**FIGURE 10.3.** Graphic solution of the equation of charge transfer in the linear approximation. In the coordinated system  $\varepsilon_1^0(-\Delta q) = \varepsilon_2^0(\Delta q) = \varepsilon^0$ . The curves  $\varepsilon_1^0(q)$  and  $\varepsilon_2^0(q)$  after (10.3) are taken to be arbitrary.

If  $\varepsilon_2'' > \varepsilon_1^0$ , the sign of  $\Delta q$  changes to the opposite. There may be also other combinations of energy spectra leading to similar formulas [10.10]; a formula for charge transfer, somewhat similar to (10.7), was derived by Huheey [10.11].

Equations (10.7)–(10.10) show that the energy-level difference and redox capacitance determine the main important features of the charge transfer by coordination. In particular, if the capacitance of one of the systems is much larger than the other one,  $C_2 \gg C_1$ , then

$$\Delta q \approx C_1(\varepsilon_1^0 - \varepsilon_2'') \quad (10.11)$$

$$\varepsilon_2'' \approx \varepsilon^0 \quad (10.12)$$

and the charge transfer is determined by the relative value of the energy level and capacitance of system 1. This is often the case with catalysts (see below).

Consider in more detail the physical meaning of redox capacitance. By definition, Eq. (10.4)  $C$  is a measure of the ability to accept or transmit charge with smaller changes in energy levels. It is clear that this property depends on electronic structure, particularly on the possibility of the excess charge to delocalize over larger regions of space, thus reducing the additional interelectron repulsion. The larger the delocalization, the higher the capacitance  $C$ . The latter becomes especially large for conjugated systems for which the addition of an electron results in the population of the next energy level in the valence band that is close in energy. In this case the redox capacitance can be estimated using approximate expressions for the energy levels calculated in the model of a potential box [10.12]:

$$\varepsilon_n \approx \frac{n^2 \pi^2}{2mN^2 l^2} \quad (10.13)$$

where  $N$  is the number of chain members,  $l$  is their linear dimension, and  $m$  is the mass of the electron. Population of the first  $N/2$  levels (for simplicity,  $N$  is even) by  $N$  electrons (by one electron from each chain member) yields the ground state with  $n = N/2$  and an energy gap  $\varepsilon_{(N/2)+1} - \varepsilon_{N/2} = \Delta\varepsilon$  to the first excited state with  $n = (N/2)+1$ . To occupy the latter, one should add a two-electron charge,  $\Delta q = 2e$ . Consequently, we obtain

$$C \approx \frac{\Delta q}{\Delta\varepsilon} \sim \frac{4mel^2}{\pi^2 \hbar^2} \frac{N^2}{N+1} \quad (10.14)$$

Or approximately, for  $N \gg 1$

$$C \sim aN \quad (10.15)$$

with  $a = 4mel^2/\pi^2 \hbar^2$ .

It is seen that the redox capacitance is approximately proportional to the number of chain members  $N$  in the conjugated system. Note that the same energy

gap  $\Delta\varepsilon$  to the excited states determines the polarizability of the system, and hence larger capacitance means larger polarizabilities. On the other hand,  $\Delta\varepsilon$  equals the quantum of the first longwave optical transition with the wavelength  $\lambda_m$ ,  $\Delta\varepsilon = \hbar c/\lambda_m$  (where  $c$  is the speed of light), and hence  $C = 2e\lambda_m/\hbar c$ . Thus the redox capacitance for conjugated molecules can also be estimated using empirical data on light absorption. In Example 10.1 the charge transfer by coordination of peroxide to iron porphyrin is estimated in this model.

### EXAMPLE 10.1

#### *Charge Transfer by Coordination of Peroxide to Iron Porphyrin*

By way of illustration, consider the charge transfer by coordination of hydrogen peroxide (system 1) to iron porphyrin (system 2) [10.9]. Semiempirical calculations of  $\text{H}_2\text{O}_2$  in different charge states allow one to estimate the curve  $\varepsilon_1(q)$  from which the approximate value of  $C_1$  follows directly:  $C_1 = 0.02 \text{ e/kK}$  ( $1 \text{ kK} = 10^3 \text{ cm}^{-1}$ ), while for iron porphyrin  $C_2 = 0.6 \text{ e/kK}$ . This means that  $C_2 \gg C_1$ , and the simplified formulas (10.11) and (10.12) can be applied. For the HOMO-LUMO energy-level difference we have  $\varepsilon_2^0 - \varepsilon_1^u = 55 \text{ kK}$ . Hence the charge transfer from the porphyrin to hydrogen peroxide is  $\Delta q \approx C_1(\varepsilon_2^0 - \varepsilon_1^u) \approx 1.1e$ . This transfer to the antibonding orbital of the  $\text{H}_2\text{O}_2$  molecule strongly activates its O—O bond.

The notion of redox capacitance is important, first, to the problems of redox catalysis. It also contributes significantly to the understanding of the origin of high oxidation states (e.g., phthalocyanins can accept several electrons simultaneously [10.13]). This property is of special interest to ferredoxins that play an important role in a series of biological processes, where they serve for both electron transfer and electron storage, the latter allowing for synchrony multielectron processes. In accordance with the results discussed above, the ferredoxins realize these functions owing to their high redox capacitance. This is confirmed experimentally. For instance, for the cluster  $\text{Fe}_4(\eta^5 - \text{C}_5\text{H}_5)_4(\mu_3 - \text{S})_4^n$ , four inverse stages of one-electron charge transfers corresponding to the cluster states with  $n = -1, 0, 1, 2, 3$  have been revealed by means of the cyclic voltamperimetric method [10.14]. For calculation of redox capacitance for such systems, see Ref. 10.15.

#### **Hard and Soft Acids and Bases**

The necessity to introduce a property of molecular systems that characterizes their ability to act as an acid or base (i.e., as above, the ability to donate or

accept electronic charge) was recognized by chemists long ago on the basis of chemical intuition. Pearson [10.2] introduced the term *hard and soft acids and bases* (HSAB) for this reason.

According to the definition of HSAB, molecular systems are divided into four groups [10.2]:

- (1) soft acid—the acceptor atom is of low positive charge, large size and has polarizable outer electrons; (2) hard acid—the acceptor atom is of high positive charge, small size and has not easily polarized outer electrons; (3) soft base—the donor atom is of low electronegativity, easily oxidized, highly polarizable and with low-lying empty orbitals; (4) hard base—the donor atom is of high electronegativity, hard to oxidize, of low polarizability and with only high energy empty orbitals.

On the basis of this definition, an empirical rule was formulated: Hard acids prefer to coordinate with hard bases and soft acids prefer to coordinate with soft bases. Hard–hard coordination represents a more ionic bonding, while the soft–soft one is more covalent.

This rather qualitative formulation contains many uncertainties that have been subjected to criticism. More quantitative formulations based on the electronic structure were reached later [10.16]. On the basis of the density functional theory (Section 5.2), the authors [10.16] defined the *chemical potential*  $\mu$  as a derivative of the total energy of the system  $E$  with respect to the electronic charge produced by  $N$  electrons, while the nuclear charge  $Z$  is fixed:

$$\mu = \left( \frac{\partial E}{\partial N} \right)_Z = \left( \frac{\partial E}{\partial q} \right)_Z \quad (10.16)$$

In the finite-difference approximation the  $\mu$  value can be derived from the curve  $E = E(\mu)$  and roughly expressed by known parameters as follows:

$$-\mu \approx \frac{I + A}{2} = \chi_\mu \quad (10.17)$$

where  $I$  is the ionization potential and  $A$  is the electron affinity, while  $\chi_\mu$  is the Mulliken definition of electronegativity of the molecular system (Section 6.4).

The quantity  $\mu$  is, in fact, of significant importance to different topics in chemistry. In particular, if two molecular systems that have different chemical potentials  $\mu_1$  and  $\mu_2$  coordinate, the joint system acquires a common value of

$$\mu = \mu_1(-\Delta q) = \mu_2(\Delta q) \quad (10.18)$$

Now, the *chemical hardness* of an acid or base denoted by  $\eta$  (the softness is  $\sigma = 1/\eta$ ) is defined as follows [10.16, 10.2]:

$$\eta = \frac{1}{2} \frac{\partial \mu}{\partial q} = \frac{1}{2} \frac{\partial^2 E}{\partial q^2} \quad (10.19)$$

Similar to (10.17), in the same finite-difference approximation

$$\eta = \frac{I - A}{2} \quad (10.20)$$

It is seen from definition (10.19) that the chemical hardness equals half the change of the chemical potential, due to the increase of the charge on the system by unity. In other words, chemical hardness characterizes the resistance of the chemical potential  $\mu$  to the change of electronic charge.

Consider two coordinated systems, 1 and 2, and denote their chemical potentials and hardness values by  $\mu_1$  and  $\mu_2$ , and  $\eta_1$  and  $\eta_2$ , respectively. In the linear approximation with respect to the charge transfer  $\Delta q = \Delta q_1 = -\Delta q_2$ , we obtain

$$\begin{aligned} \mu_1 &= \mu_1^0 + 2\eta_1 \Delta q \\ \mu_2 &= \mu_2^0 - 2\eta_2 \Delta q \end{aligned}$$

and

$$\begin{aligned} \Delta q &= \frac{\mu_2^0 - \mu_1^0}{2(\eta_1 + \eta_2)} \\ &= \frac{\chi_1^0 - \chi_2^0}{2(\eta_1 + \eta_2)} \end{aligned} \quad (10.21)$$

Surprisingly, Eq. (10.21) for molecular systems with well-spaced energy levels coincides *exactly* with Eq. (10.7) (derived in Refs. 10.9 and 10.10), based on the notion of redox capacitance (Note the 16-year interval between the publications in 1967 [10.9] (or [10.10]) and in 1983 [10.16]; the latter does not cite the former). Indeed, for systems with discrete energy levels  $\varepsilon_n$  the chemical potential  $\mu$  is defined by the well-known statistical formula of the temperature dependence of the population  $n(T)$  of the  $\varepsilon_n$  level:

$$n(T) = \left[ 1 + \exp\left(\frac{\varepsilon_n - \mu}{kT}\right) \right]^{-1} \quad (10.22)$$

At  $T = 0$ ,  $n(0) = 1$  for  $\varepsilon_n < \mu$ , and  $n(0) = 0$  for  $\varepsilon_n > \mu$ . This means that for any system at  $T = 0$ ,  $\mu$  coincides with the highest occupied energy level  $\varepsilon^0$ , introduced above [see (10.6)]. The equality  $\mu = \varepsilon^0$  also holds for all the much higher temperatures, for which the excited states are not significantly thermally populated. For the electronic energy levels under consideration, this condition is obeyed, provided that there are no degenerate or pseudodegenerate electronic states.

With  $\mu = \varepsilon^0$ , Eq. (10.18) coincides with (10.6), the hardness  $\eta$  after definition (10.19) coincides with the inverse of redox capacitance (10.4) (with a factor  $\frac{1}{2}$ ):  $\eta = \left(\frac{1}{2}\right) C^{-1}$ , and  $\Delta q$  after (10.21) coincides exactly with  $\Delta q$  after (10.7).

**TABLE 10.1. Electronegativities  $\chi^0$  in the Low-Spin Valence State of Transition Metals M, Their Hardness  $\eta$ , Charge Transfers  $\Delta q$  by Coordination M + CO, and Activation Enthalpies  $\Delta H$  for Dissociation of the First CO Ligand from  $M(\text{CO})_6$**

Transition Metal	$\chi^0$ (eV)	$\eta$ (V)	$\Delta q$ ( <i>e</i> )	$\Delta H^\ddagger$ (kcal)
V	2.24	1.24	0.211	V(CO) <sub>6</sub> stable
Cr	2.47	1.58	0.196	40
Mn	3.10	2.19	0.149	37
Fe	2.55	1.55	0.188	42
CO	4.12	3.04	0.091	22
Ni	3.50	2.30	0.128	22
Cu	5.84	4.61	0.110	Very unstable
Mo	3.18	1.98	0.148	40
Ru	3.54	2.34	0.125	28
Pd	4.45	3.89	0.070	Unstable
Ag	6.87	5.57	-0.029	Very unstable
Pt	5.30	2.90	0.037	Unstable
Au	6.70	4.40	-0.026	Very unstable

Source: Pearson [10.2].

The two coinciding formulas, (10.21) and (10.7), as well as all the others based on them, are certainly rather qualitative or semiquantitative and reflect the tendency of charge transfers by coordination, giving a general understanding of the origin and mechanism of this process. Taken as approximate relations aimed at qualitative understanding, it does not make very much sense to improve these relations at the expense of their further complication. For more exact calculations of charge transfers, approved quantum-chemical methods and computer programs should be employed (Sections 5.3–5.6). Nevertheless, attempts to improve the expressions for the hardness  $\eta$  as a function of electronic structure parameters are continuing, and some of the results seem to be relevant [10.2, 10.17].

It is clear that soft acids and soft bases, as well as hard acids and hard bases, are more compatible than are soft acids and hard bases or hard acids and soft bases. This statement can be confirmed using perturbation theory for chemical interactions (Section 11.1). In many cases the HSAB concept correlates with the metal–ligand bonding energy  $\Delta H$ . For illustration, the values of hardness  $\eta$  and charge transfers  $\Delta q$  in the coordination M + CO for a series of transition metals M and their correlation with experimental  $\Delta H$  values are shown in Table 10.1 [10.2]. The values  $\chi^0$  and  $\eta$  are estimated for the low-spin valence states of M (as they are expected to appear in the coordination with CO), and the  $\Delta q$  values are calculated by Eq. (10.22) (for CO  $\chi^0 = 6.1$  eV and  $\eta = 7.9$  eV [10.2]).

It is seen that the values  $\Delta q$  in Table 10.1 follow roughly the stability of corresponding complexes, the value  $\Delta H$  of dissociation of the first ligand in  $M(\text{CO})_6$ ; for small and negative values of  $\Delta q$  the complexes are unstable and very unstable, respectively. Note that, in general, a full quantitative correlation between the total charge transfers  $\Delta q$  and bonding energies is not expected.

Indeed, as stated elsewhere in this book (see, e.g., Sections 5.2, 6.3, and 11.2), the total charge transfer  $\Delta q$  results from orbital charge transfers  $\Delta q_i$  that may have opposite signs, and hence  $\Delta q$  can be small for large absolute values of  $\Delta q_i$  that determine the bonding.

## 10.2. ELECTRON TRANSFER IN MIXED-VALENCE COMPOUNDS

### Mixed-Valence Compounds as Electronic Systems; a Two-Level Dimer

Mixed-valence (MV) compounds represent one of the most interesting examples of intramolecular electron transfer [10.18–10.20]. The increasing importance of these compounds is due to their applications such as redox catalysts, models of metalloenzymes [10.21, 10.22], local centers in superconducting ceramics [10.23, 10.24], molecular magnets [10.25], and other molecular electronic devices [10.26].

In a larger definition [10.27], MV compounds contain ions of the same element in two different formal states of oxidation. These ions can be regarded as having the same oxidation state, but with additional (excess) electrons that can either occupy one of the ions changing its oxidation state and causing it to differ from the others, or be delocalized over all (or a part of) the centers.

With respect to the excess electron delocalization, Robin and Day [10.27] suggested the following classification. All the MV compounds are divided into three classes, I, II, and III, with an additional division of class III into IIIA and IIIB. In class I the metal ions of the MV system are in ligand fields of different symmetry and/or strength (e.g., tetrahedral vs. octahedral). In this case no active MOs are formed by the AOs occupied by the excess electron at different centers because of the large difference in their energies and very small resonance integral  $w$  [see Section 5.1 and below, Eq. (10.26)]. Hence the excess electron is firmly trapped at one of the centers, making the latter essentially nonequivalent.

Class II contains metal ions in ligand fields of nearly identical symmetry differing from one another by distortions of only a few tenths of an angstrom. In these systems  $w \neq 0$ , and hence there are MOs in common formed by the AOs of the centers and occupied by the excess electron, but the valencies are still distinguishable with slight delocalization on the MO. In class IIIA the metal ions are grouped into polynuclear clusters within which they are equivalent; inside the cluster  $w$  is maximal, and the excess electron can be either localized or delocalized, depending on the bridging group. Finally, in class IIIB all the ions in the lattice are equivalent (complete delocalization over the cation sublattice).

Following this classification, coordination MV compounds belong mainly to class IIIA (polynuclear MV clusters) with a few exceptions, which could be attributed to class II, for instance, when the small structural differences between the centers are of molecular or vibronic origin. The other cases are MV solids (mostly ionic solids); Table 10.2 illustrates some examples [10.28].

In what follows in this section, we consider only transition metal MV compounds. By definition, they contain two or more equivalent coordination centers

**TABLE 10.2. Illustration (Examples) of Different Classes of MV Solids with the Classification after Robin and Day**

Example	Classification	Remarks
Pb <sub>3</sub> O <sub>4</sub>	I	Red lead
Sb <sub>2</sub> O <sub>4</sub>	I	Mineral cervantite
Fe <sub>4</sub> [Fe(CN) <sub>6</sub> ] <sub>3</sub> · 4H <sub>2</sub> O	II	Prussian blue
Li <sub>x</sub> Ni <sub>1-x</sub> O	II	Hopping semiconductor
La <sub>1-x</sub> Sr <sub>x</sub> MnO <sub>3</sub>	II	Ferromagnetism
BaBi <sub>1-x</sub> Pb <sub>x</sub> O <sub>3</sub>	III	Superconductivity
LiTi <sub>2</sub> O <sub>4</sub>	III	Superconductivity
K <sub>2</sub> Pt(CN) <sub>4</sub> Br <sub>0.30</sub> · 3H <sub>2</sub> O	III	Molecular metal; Pailer's instability
Na <sub>x</sub> WO <sub>3</sub>	III	Bronze luster; metallic at high <i>x</i>
M <sub>x</sub> Mo <sub>6</sub> S <sub>8</sub>	III	Superconductivity
Fe <sub>4</sub> S <sub>4</sub> (ferredoxins)	III	Enzymes

Sources: Robin and Day [10.27] and Rao [10.28].

divided by some bridging atomic groups with one or more excess electrons, the number of which is smaller than the number of centers. If the excess electron is localized at one of the equivalent centers, the latter have different valence (oxidation) states, and this explains the origin of the name of these compounds.

The equivalence of the centers means that the excess electron can occupy any of the centers with equal probability. In terms of quantum mechanics, in the stationary state the excess electron should be uniformly distributed (delocalized) over all the centers. However, if the energy barrier for the electron transfer between the centers (created by the bridging groups) is sufficiently large, the excess electron can remain trapped at one center for a relatively long time, with its possible delocalization controlled by the barrier height and temperature.

In these cases there is a lifetime of the electron at each center, and the observable properties of the MV compound depend on the method of observation, more precisely on the ratio of the "time of measurement" to the lifetime of electron localization (cf. the relativity rule concerning the means of observation, Section 9.2). Hence the notions of "localized" and "delocalized" electron may be to a certain extent conventional, in general, but quite definitive for specific systems and conditions. *The localization–delocalization alternative is the main problem of MV compounds.*

To formulate the problem quantitatively, consider a MV dimer with two equivalent electronic closed-shell centers, 1 and 2, and one excess electron [10.29, 10.30]. Assume that the one-electron states at each center,  $\varphi_1$  and  $\varphi_2$ , are non-degenerate. This means that when the excess electron is localized at one of the centers, it distorts its nearest-neighbor environment along the totally symmetric coordinate. The corresponding local distortion (breathing) coordinates can be



denoted by  $Q_1$  and  $Q_2$ , respectively (they are similar to the coordinates producing the polaron effect in crystals). The coupling of the electronic state to these distortions is described by the vibronic constant  $F$  (Section 7.2):

$$F = \langle \varphi_1 | \left( \frac{\partial H}{\partial Q_1} \right)_0 | \varphi_1 \rangle = \langle \varphi_2 | \left( \frac{\partial H}{\partial Q_2} \right)_0 | \varphi_2 \rangle \quad (10.23)$$

where  $H$  is the Hamiltonian.

For the system as a whole, presentations of the wavefunctions

$$\Phi_{\pm} = \left( \frac{1}{2} \right)^{1/2} (\varphi_1 \pm \varphi_2) \quad (10.24)$$

and coordinates

$$Q_{\pm} = \left( \frac{1}{2} \right)^{1/2} (Q_1 \pm Q_2) \quad (10.25)$$

are more convenient.  $Q_+$  is a totally symmetric coordinate of the system describing the simultaneous (synchronous) breathing distortion of both centers, while  $Q_-$  gives the asymmetric, antiphase breathing distortion of the two centers produced by the electron localization on one center.

If there is an overlap between the two states  $\varphi_1$  and  $\varphi_2$ , they form bonding  $\Phi_+$  and antibonding  $\Phi_-$  states with an energy gap  $2w$ , where  $w$  is the resonance integral (Section 5.1):

$$w = \langle \varphi_1 | H | \varphi_2 \rangle \quad (10.26)$$

This parameter is most important for the MV theory characterizing the strength of the intercenter interaction and hence the electron transfer rate.

With the notations (10.23)–(10.26), the problem of the excess electron in the MV dimer under consideration can be formulated as a vibronic problem (Section 7.4). Indeed, the two states  $\Phi_{\pm}$  at  $Q_1 = Q_2 = 0$  ( $Q_{\pm} = 0$ ) mix under the nuclear displacements  $Q_-$  and shift under  $Q_+$ . For the problems considered in this section the shift  $Q_+$  is not important and can be excluded by an appropriate choice of the energy readoff (Section 7.4). Mixing of the two electronic states by the nuclear displacements  $Q_-$  taken as a perturbation results in the PJT problem (7.63) with the solution—the APES along the  $Q_-$  coordinate—given in Eq. (7.65) ( $K_0$  is the force constant of the  $Q_1$  or  $Q_2$  distortions):

$$\varepsilon_{\pm}(Q_-) = \left( \frac{1}{2} \right) K_0 Q_-^2 \pm (w^2 + F^2 Q_-^2)^{1/2} \quad (10.27)$$

These two curves are analyzed in Section 7.4. For  $|w| > F^2/K_0$  both have a minimum at  $Q_- = 0$ . However if [cf. (7.67)]

$$|w| < \frac{F^2}{K_0} \quad (10.28)$$

the lowest curve has a maximum at  $Q_- = 0$  and two minima at  $Q_- = \pm Q^0$ :

$$Q^0 = \left( \frac{F^2}{K_0^2} - \frac{w^2}{F^2} \right)^{1/2} \quad (10.29)$$

The two curves  $\varepsilon_{\pm}(Q)$  for this case are illustrated in Fig. 7.19 for the pseudo-Jahn–Teller effect. It is seen that if condition (10.28) is obeyed, that is, if the contribution to the energy due to the localization distortion  $Q_-$  is larger than that of the electron transfer  $w$ , the minimum energy (and the wavefunction) corresponds to the localization of the excess electron at one of the two centers. In the opposite case, when  $|w| > F^2/K_0$ ,  $Q_- = 0$  and there are no localization minima; the electron is uniformly delocalized over the two centers. Thus, for MV dimers the inequality (10.28) serves as the condition of localization of the excess electron. Example 10.2 elucidates further details of electronic structure that control the charge transfer between coordination centers in mixed-valence compounds using the Creutz–Taube ion as an object of specific calculations.

### EXAMPLE 10.2

#### *The Creutz–Taube (CT) Ion as a Mixed-Valence System* [10.20, 10.32]

The CT ion  $[(\text{NH}_3)_5\text{Ru}(\text{pyz})\text{Ru}(\text{NH}_3)_5]^{5+}$ , where  $\text{pyz} = \text{pyrazine}$ , became a classical object of polynuclear MV system studies. Its relatively simple composition and structure makes it possible to discriminate between different factors influencing the intramolecular electron transfer. In the CT ion the two  $\text{Ru}^{3+}$  centers have  $4d^5$  low-spin configuration with one excess electron that occupies the hole in the  $(t_{2g})^6$  closed-shell configuration of each center or its corresponding MOs (see below). Distinguished from the case of one excess electronic state on each center considered above, the CT ion has several such states.

The structure of the CT ion and the chosen coordinate system is shown in Fig. 10.4. Note that the  $X$  axis lies in between the nitrogen atoms; hence the three  $t_{2g}$  orbitals are  $d_{xz}$ ,  $d_{yz}$ , and  $d_{x^2-y^2}$  (the last one substitutes  $d_{xy}$  in the more usual cases; Section 4.2). The direct overlap between the  $d$  states of the two Ru centers is negligible. Therefore their MO combinations of appropriate symmetry in the  $C_{2v}$  group of the system as a whole are simple linear combinations of the corresponding atomic functions shown in Fig. 10.5 (actually the shown  $d$  orbitals are MOs that they form with the ligands on each center). From these MOs only one, the  $b_{2g}$  type, overlaps with the empty  $\pi^*$  orbital of the pyrazine bridge, forming the corresponding bonding and antibonding MOs. The resulting MO energy scheme including these

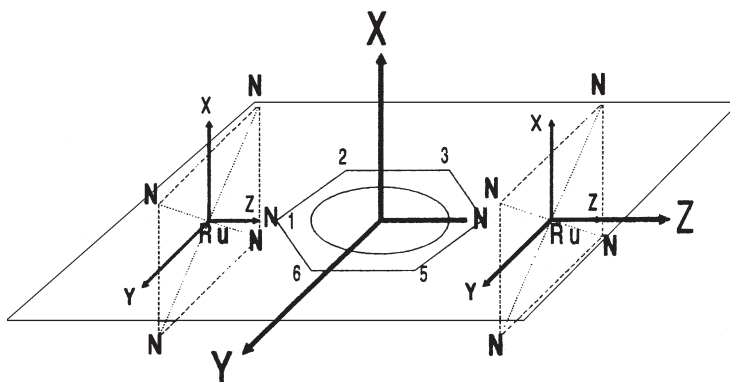


FIGURE 10.4. Structure and the coordinate system of the Creutz-Taube ion.

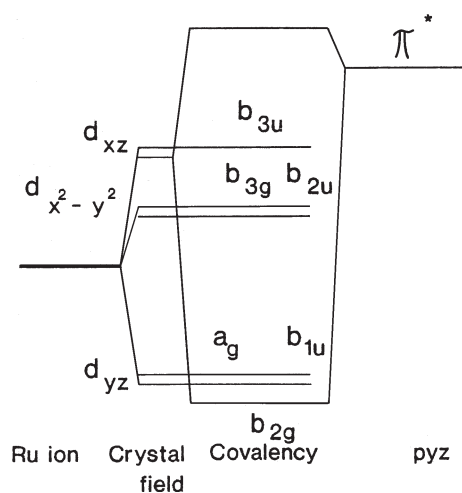
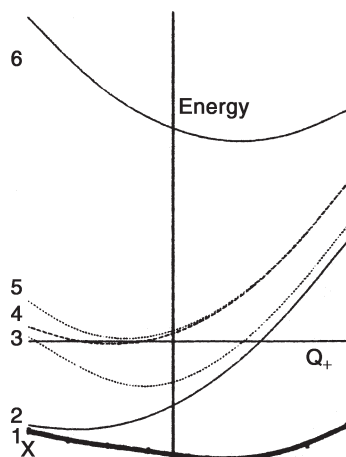


FIGURE 10.5. Schematic presentation of the valence MO energy scheme of the Creutz-Taube ion.

states is shown in Fig. 10.5. The relative positions of the energy levels were obtained from the electronic structure calculations performed in the DFT- $X_\alpha$  approximation [10.31].

The population of the six one-electron MOs by 11 electrons results in the ground-state spin doublet  ${}^2B_{3u}$  and five relatively close-in-energy excited doublets  ${}^2B_{3g}$ ,  ${}^2B_{2u}$ ,  ${}^2B_{1u}$ ,  ${}^2A_g$ , and  ${}^2B_{2g}$  formed by the one-electron excitation from the corresponding one-electron MOs to the  $b_{3u}$  MO. These states are subject to further modification under the spin-orbital interaction, which is significantly strong in the Ru ion (the spin-orbital constant  $\xi \approx 10^3 \text{ cm}^{-1}$ ). Only three of these states,  $A_g$ ,  $B_{2g}$ , and  $B_{3g}$ , participate in the electron transfer. Their coupling to the  $Q$  coordinates (10.25) is determined by three vibronic constants,



**FIGURE 10.6.** Extremal crosssection  $Q_- = 0$  of the APES of the Creutz-Taube ion. X is a saddle point between two minima at  $Q_- \neq 0$ .

which were estimated from empirical data [10.32]:  $F_1 = 1.44$ ,  $F_2 = -1.19$ , and  $F_3 = 0.76$  (in dimensionless units).

With these  $F_i$  values, the six adiabatic potential surfaces were computed [10.32]. Their cross sections at  $Q_- = 0$  are shown schematically in Fig. 10.6. Ground state 1 has a minimum at  $Q_+ \neq 0$  ( $Q_- = 0$  in the entire section), which corresponds to the electron delocalization. The optical intervalence band originates from the transition from the ground state to state 6. In the semiclassical approximation, the calculated maximum of the band is at  $6600 \text{ cm}^{-1}$ , in good agreement with the experimental value,  $6200 \text{ cm}^{-1}$  [10.35].

One observable property of MV systems is the *intervalence transition* (IT) *band of light absorption* produced by the transition from the minimum (localized) ground state to the excited (delocalized) state. An example of such an IT band is given in Fig. 10.2. Both the frequency and the probability (band shape) of the IT are dependent on the parameters of electron transfer  $w$  and vibronic coupling  $F$ . To calculate the band shape more accurately, one has to compute the vibronic states of the system with the potential (10.27), individual transitions between them, and the envelope band shape [10.20, 10.29, 10.30].

The simplest model of the MV dimer, discussed above, may be insufficient for describing real systems. The main complications may be caused by (1) more than one electronic state on each center that can be occupied by the excess electron, (2) influence of low-symmetry crystal fields and spin-orbital interactions, and (3) open-shell (non-zero-spin) cores resulting in magnetic exchange coupling

between them and with the excess electron [10.20]. The influence of some of these important factors on the electron transfer effects are discussed briefly below.

In the presence of several active electronic states on each center, one of the additional effects is the pseudo Jahn–Teller effect (PJTE). In the case of the CT ion in Example 10.2 this effect is neglected, which is justified by the fact that the excess electron is delocalized, and the alternative “localization–delocalization” is not critical. In other cases the one-center PJTE may be more significant. In particular, it provides an additional channel of localization of the excess electron [10.20]; in addition to the totally symmetric distortions at each center caused by the localized electron [polaron effect described by each of the  $Q_i$  coordinates in (10.25)], it also produces low-symmetry distortions due to the pseudo-JT mixing with the excited states. Therefore, even when the usual polaron effect is weak (ranging from small vibronic coupling  $F$  to totally symmetric distortions, rigid environment) and does not localize the excess electron (because  $|w| > F^2/K_0$ ), it can be localized by the PJT distortion, which has a different coupling constant  $F$  and other rigidity  $K_0$  (Section 7.4). Other implications of the PJTE are important to the problem of electron delocalization in mixed-valence compounds [10.20, 10.36].

### Magnetic Properties

Another complication of the simple model mentioned above is that many MV compounds have open-shell centers with nonzero spins besides that of the excess electron. In these cases additional magnetic interactions between the latter and each of the centers and between the centers themselves complicate the process of electron transfer. The usual formulas of magnetic exchange coupling between the centers (Section 8.4) do not apply here because the migrating excess electron participates simultaneously in the formation of the magnetic moments of both centers, ventering invalid the Heitler–London approach, on which the HDVV model (8.80) is based. For open-shell (magnetic) centers with excess electrons, the concept of *double exchange* initially developed for crystals is very useful.

The idea of double exchange is as follows (see also Ref. 10.37). In the ground state, the spin  $S'$  of the excess electron localized at the magnetic center is parallel to the spin  $S_1$  of the latter because of the strong intraatomic exchange interaction  $J_0$  [cf. Hund’s rule, Section 2.2; for simplicity the electronic shell of each center is assumed to be filled in less than a half]. Because of the equivalence of the centers and the electron transfer, the excess electron spin  $S'$  interacts similarly with the spin of the second center  $S_2$ . Therefore, the energy gain via exchange interaction is maximal when the spins of the two centers are parallel (the resonance interaction determining the electron transfer  $w$  is independent of the spin). Thus *the electron transfer favors ferromagnetic ordering of the spin centers*.

In application to MV compounds the idea of double exchange is different in some aspects from the crystal case [10.20]. First, consider a simple case of a

three-electron problem in a MV dimer with  $S_1 = S_2 = S = \frac{1}{2}$  and two nondegenerate one-electron states on each center  $\varphi_1, \varphi'_1$  and  $\varphi_2, \varphi'_2$ , respectively [this case corresponds, e.g., to the Ni(I)—Ni(II) dimer]. In the ground state the two orbitals  $\varphi_1$  and  $\varphi_2$  contain two electrons, one in each orbital, while the third (excess) electron can occupy either of the orbitals  $\varphi'_1$  and  $\varphi'_2$  with equal probability. If, in addition to the intraatomic exchange integral  $J_0$ , mentioned above [an integral of type (2.36) calculated by the functions  $\varphi_1$  and  $\varphi'_1$ , see Ref. 10.20], we introduce the intercenter exchange integral  $J$  (calculated by the functions  $\varphi_1$  and  $\varphi_2$ , or  $\varphi'_1$  and  $\varphi_2$ , or  $\varphi_1$  and  $\varphi'_2$ ), then the energy levels as a function of the total  $S$  are as follows [10.20]:

$$E\left(S = \frac{3}{2}\right) = -(J_0 + 2J) \pm w \quad (10.30)$$

$$E\left(S = \frac{1}{2}\right) = \pm[(J_0 - J)^2 + w^2 \pm (J_0 - J)w]^{1/2} \quad (10.31)$$

Equations (10.33) and (10.34) can be generalized to the case when the core spin is larger than  $\frac{1}{2}$  using the method suggested by Anderson and Hasegawa [10.38]. Denoting the total spin of each magnetic center without the excess electron by  $S_0$  and the maximum spin  $S_{\max} = 2S_0 + \frac{1}{2}$ , we have [10.20]

$$E(S < S_{\max}) = \frac{J_0}{2} + J\left(S_0 + \frac{1}{2}\right) - JS(S+1) \\ \pm \left[ \left(S_0 + \frac{1}{2}\right)^2 (J_0 - J)^2 + w^2 \pm (J - J_0)w \left(S + \frac{1}{2}\right) \right]^{1/2} \quad (10.32)$$

and

$$E(S_{\max}) = -J_0S_0 + J(2S_0 + 1) - JS(S+1) \pm w \quad (10.33)$$

For transition metal compounds the orders of magnitude of the parameters entering Eqs. (10.32) and (10.33) are as follows:  $J_0 \sim 1-10$  eV,  $W \leq 1$  eV, and  $J \sim 10^{-1}-10^{-3}$  eV, and the  $w$  values can be comparable in magnitude with  $J$  (see below).

It can be seen that Eq. (10.32) contains two pairs of states with an energy separation of about  $2J_0$ . The states of the upper pair are often called *non-Hund-state* because they arise from the states with a local spin of  $S_0 - \frac{1}{2}$ , in contrast to the Hund rule. In most cases the non-Hund states can be neglected. Then, expanding Eq. (10.32) in powers of  $w/J_0$  and keeping linear terms in  $w$  only, we obtain for the energies of the Hund states as functions of  $S$ :

$$E(S) = -JS(S+1) \pm \frac{w\left(S + \frac{1}{2}\right)}{2S_0 + 1} \quad (10.34)$$

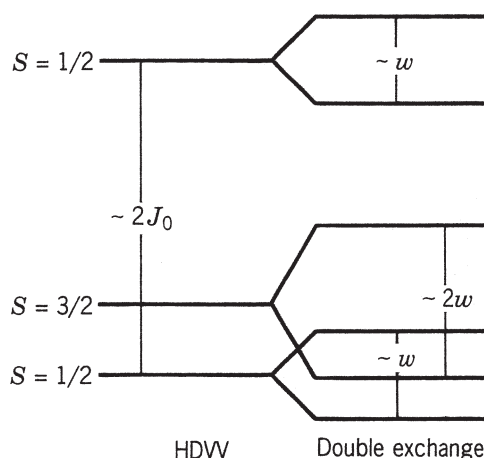


**FIGURE 10.7.** Electronic energy levels of a  $d^1 - d^2$  exchange-coupled MV dimer (the ratios between  $J_0$ ,  $J$ , and  $w$  are not obeyed numerically).

Here the terms not containing  $S$  are omitted, and hence the energy readoff is changed as compared with (10.32) and (10.33). This equation is also valid in the states of a more-than-half-filled electronic shell that have no non-Hund states and no terms containing  $J_0$ .

Equation (10.34) emerges from other theories of energy spectra of MV dimers as well. Although approximate, the energy spectrum calculated by these formulas agrees qualitatively with that obtained in quantum-chemical computations for specific MV dimers [e.g., Fe(II)–Fe(III) pairs in ferredoxin and in oxides]. It allows one to obtain a qualitative picture of the energy spectrum of the systems under consideration using the relation between  $w$  and  $J$ . For each value of the total spin  $S$  there are two resonance states  $E(S)$ . The spacing of the centers of gravity of these doublets is determined by the intercenter exchange, while their splitting is linear dependent on the spin value (Fig. 10.7).

It follows that the double exchange favors the ferromagnetic spin ordering. However, unlike the HDVV ferromagnetic exchange interaction, the double exchange does not necessarily result in a ground state with a maximal spin when  $J < 0$ . The condition for such a ground state is more complicated:  $w > (2n + 1)(n + 1)J$ , where  $n$  is the number of electrons in the ionic core. In general, it is clear that the migration of the electron results in an energy spectrum that is essentially different from that expected in the simple exchange scheme of the HDVV model (Section 8.4). In molecular crystals MV dimers are coupled to the other dimers by dipole–dipole interaction, which may produce phase transitions to charge-ordered states [10.39] in which the excess electron is localized at one of the centers producing a dipole moment.

Since the vibronic coupling constant  $F$  does not depend on the spin states, one can assume that  $F$  is the same for all spin states, provided that there is

only one orbital state on each center that is occupied by the excess electron ( $\varphi'_1$  or  $\varphi'_2$ ). In these cases each pair of states with the same spin mixes under the nuclear displacements  $Q_-$ , producing a pseudo-Jahn–Teller adiabatic potential, quite similar to the one-electron case (10.27) with  $Q_-$  in Eq. (10.25). Following (10.34), the energy gap  $2\Delta_S$  between the two mixing states with a given spin  $S$  is

$$2\Delta_S = \frac{w(2S+1)}{2S_0+1} \quad (10.35)$$

and the APES is

$$\varepsilon_S(Q_-) = \left(\frac{1}{2}\right) K_0 Q_-^2 \pm [\Delta_S^2 + F^2 Q_-^2]^{1/2} - JS(S+1) \quad (10.36)$$

If the inequality  $\Delta_S < F^2/K_0$  is satisfied, the lowest curve in (10.36) has two minima at  $\pm Q_-^0$  (Fig. 7.19), each corresponding to localization of the excess electron at one of the centers. For  $\Delta_S > F^2/K_0$ ,  $Q_-^0 = 0$ , and the electron is delocalized over the two centers. According to Eq. (10.35), since  $\Delta_S$  increases with the total spin, a situation is possible when the excess electron is localized in the states with small total spins and delocalized in the states with larger spins.

More exact predictions of the magnetic behavior (and other properties) can be made on the basis of detailed calculations of the vibronic energy states  $E_n$  with the potential (10.36). With the values  $E_n$  known, the magnetic moment  $\mu$  is estimated by the following formula (Section 8.4):

$$\mu^2 = \frac{g^2 \beta^2 \sum_{n,S} S(S+1)(2S+1) \exp[-E_n(S)/kT]}{\sum_{n,S} (2S+1) \exp[-E_n(S)/kT]} \quad (10.37)$$

Some results of such calculations are illustrated in Fig. 10.8 [10.20] for a  $d^1-d^2$  MV dimer with an antiferromagnetic exchange coupling  $J < 0$ . It is seen that in the absence of vibronic coupling ( $F = 0$ , curve 1) the two centers, owing to the double exchange and large  $w$ , are ferromagnetically ordered with a maximum magnetic moment of three unpaired electrons ( $S = \frac{3}{2}$ ). The vibronic interaction changes the magnetic behavior, and for  $F = 3$  the ground state, becomes  $S = \frac{1}{2}$  instead of  $S = \frac{3}{2}$  (see Fig. 10.8, curve 3). This phenomenon is formally similar to the spin crossover (Section 8.4) where the ground-state spin changes as a function of the ligand field parameter; in the case under consideration the latter is played by the vibronic coupling.

The quantity of *electron transfer probability*  $P$  may also be important, especially for applications. It can be calculated directly from the vibronic energy spectrum of the system [10.20]:  $P$  is dependent on the spin  $S_0$  and exchange parameters. In particular, for two systems with the same  $S$ ,  $w$ , and  $|J|$ , but opposite signs of  $J$ , that is, for ferromagnetic  $P_F$  and antiferromagnetic  $P_{AF}$  systems (states), we obtain

$$\frac{P_F}{P_{AF}} = (2S_0 + 1)^2 \quad (10.38)$$



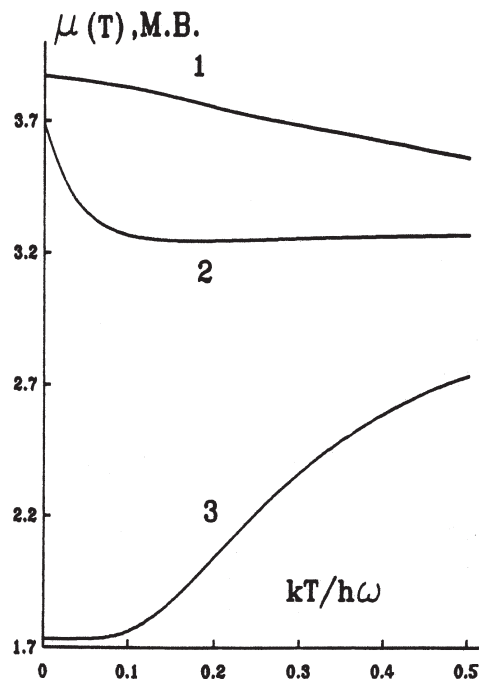


**FIGURE 10.8.** Temperature dependence of the magnetic moment  $\mu$  of a MV  $d^1 - d^2$  dimer with  $J = -0.2$ ,  $w = 2$ , and different vibronic constants: (1)  $F = 0$ , (2)  $F = 1.8$ , and (3)  $F = 3$  (in dimensionless units).

#### Mixed-Valence Trimers: Coexistence of Localized and Delocalized States

Regular three-center triangular clusters with equivalent transition metal centers are rather widespread, the series of carboxylates  $[M_3O(RCOO)_6]L_3$  being a well-known example; Figure 10.9 illustrates the one with  $M = Fe$ ,  $R = CF_3$ , and  $L = H_2O$ .

Consider a trimer MV cluster and assume (as in the cases of simple dimers) that there is only one excess electron over the three metal centers with closed shells and only one nondegenerate state on each center  $\varphi_i$ ,  $i = 1, 2, 3$ , to be occupied by the excess electron. In the triangular symmetry  $C_{3v}$  the three one-electron states  $\varphi_i$  form three MOs of  $A$  and  $E$  symmetry (Section 5.1):

$$\begin{aligned}\Psi_A &= \frac{1}{\sqrt{3}}(\varphi_1 + \varphi_2 + \varphi_3) \\ \Psi_{E\theta} &= \frac{1}{\sqrt{6}}(2\varphi_1 - \varphi_2 - \varphi_3) \\ \Psi_{E\varepsilon} &= \frac{1}{\sqrt{2}}(\varphi_2 - \varphi_3)\end{aligned}\tag{10.39}$$

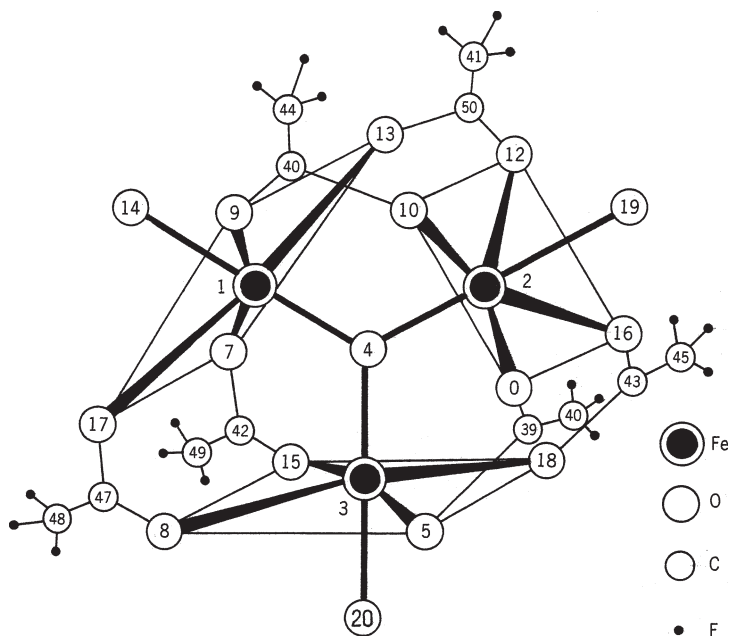


**FIGURE 10.9.** Structure of the MV trimer  $M_3O(RCOO)_6L_3$  with  $M = Fe$ ,  $R = CF_3$ , and three ligands  $L = H_2O$  marked by  $N = 14, 19,$  and  $20$ , respectively.

Denoting, as above, the intercenter resonance integral (the electron transfer parameter) by  $w$  [cf. (10.26)], we find easily that the splitting  $\varepsilon(A) - \varepsilon(E) = 3w$ .

As in the case of dimers, the excess electron, when localized at the center, distorts its environment, thus violating the  $C_{3v}$  (or  $D_{3h}$ ) symmetry of the system, and this distortion is very important for the electron transfer phenomenon. Since the  $\varphi_i$  are nondegenerate, the totally symmetric local breathing (polaron-type) distortions  $Q_i$  ( $i = 1, 2, 3$ ) are affected only by the excess electron. Similar to the wavefunctions (10.39), it is more convenient to take these three local coordinates  $Q_1, Q_2, Q_3$  in symmetrized combinations for the system as a whole (Section 7.1):

$$\begin{aligned} Q_A &= \frac{1}{\sqrt{3}}(Q_1 + Q_2 + Q_3) \\ Q_\theta &= \frac{1}{\sqrt{6}}(2Q_1 - Q_2 - Q_3) \\ Q_\varepsilon &= \frac{1}{\sqrt{2}}(Q_2 - Q_3) \end{aligned} \quad (10.40)$$

While  $Q_A$  is totally symmetric with respect to the  $C_{3v}$  symmetry,  $Q_\theta$  and  $Q_\varepsilon$  form two components of the twofold-degenerate  $E$  displacement. The totally

symmetric coordinate, similar to the dimer, can be separated by an appropriate choice of the energy readoff.

With these denotations, the electronic energy levels  $\varepsilon_0(Q)$  as functions of the coordinates  $Q_\theta$  and  $Q_\varepsilon$  can be found by solving the corresponding secular equation of the type (7.78), which, in polar coordinates (7.37)  $Q_\theta = \rho \cos \phi$ ,  $Q_\varepsilon = \rho \sin \phi$ , is [10.20]:

$$\varepsilon_0^3 - \left( \frac{F^2 \rho}{2} + 3w^2 \right) \varepsilon_0 - 2w^3 - \left( \frac{2}{3} \right)^{1/2} F^3 \rho^3 \cos 3\phi = 0 \quad (10.41)$$

where  $F$  is the constant of vibronic coupling with the  $Q_i$  displacements (10.23). The three roots of Eq. (10.41)  $\varepsilon_0^i$  ( $i = 1, 2, 3$ ), together with the strain (deformation) energy  $\frac{1}{2}K\rho^2$  form three sheets of the APES

$$\varepsilon_i(\rho, \phi) = \frac{1}{2}K\rho^2 + \varepsilon_0^i \quad (10.42)$$

For simplicity, we assume that the  $K$  values (the primary force constants of the  $Q_i$  distortions) are the same for the two oxidation states of the center (with and without the excess electron), and we use dimensionless units for  $Q$ ,  $F$ , and  $w$ .

It can be shown that  $\varepsilon_i$  are periodic functions of  $\phi$  with a period of  $2\pi/3$ . The extremal points of the APES (10.42) are at  $\phi = \pi n/3$ ,  $n = 0, 1, \dots, 5$ . If  $F < 0$ , the even values of  $n$  correspond to maxima along  $\phi$  in the lowest sheet (and saddle points if other coordinates are included; see below), while the odd values give minima, and vice versa for  $F > 0$ .

Consider the radial dependence of the adiabatic potential in the extremal cross section  $\phi = 0$  (or, equivalently,  $Q_\varepsilon = 0$ ). The solutions of Eq. (10.42) in this case are

$$\begin{aligned} \varepsilon_1 &= \frac{-F\rho}{\sqrt{6}} - w \\ \varepsilon_{2,3} &= \frac{1}{2} \left[ w - \frac{F\rho}{\sqrt{6}} \pm 3 \left( \frac{F^2 \rho^2}{6} - \frac{2w\rho}{3\sqrt{6}} + w^2 \right)^{1/2} \right] \end{aligned} \quad (10.43)$$

Investigation of this expression requires knowledge of the sign of the parameter of intercenter electron transfer  $w$ . The sign of  $w$  is not important for dimers but it is essential for trimers. If  $w > 0$ , the electronic doublet is lowest. Its APES is then similar to the Mexican hat in the JT  $E \otimes e$  problem with the quadratic terms of the vibronic interaction included (Section 7.4), but the warping of the trough in the APES (10.43) is produced by simultaneous JT and PJT distortions in the linear approximation without quadratic terms. The three minima of the APES describe the three possibilities of localization of the excess electron at each of the three centers. Since there is no minimum at  $Q_\theta = 0$  (where the three centers are equivalent), it follows that *in trimer MV compounds with  $w > 0$  delocalized electron distributions are not possible.*

The systems with  $w < 0$  seem to be more interesting. Indeed, they have singlet ground electronic terms, and the APES, as in the case of the dimer, is completely determined by the parameter  $|w|/F^2$ . Substituting

$$\rho = \left(\frac{2}{3}\right)^{1/2} \frac{|w|}{F} (2\sqrt{2} \sinh t - 1) \quad (10.44)$$

into Eq. (10.43), we obtain the following transcendent equation for the extremal points of the APES:

$$4\sqrt{2} \sinh 2t + \left[1 - \left(\frac{|w|}{F^2}\right)\right] \cosh t - 3 \sinh t = 0 \quad (10.45)$$

Figure 10.10 illustrates the calculated shapes of the extremal crosssections of the APES at  $\phi = 0$  for different  $|w|/F^2$  values. Its behavior at  $\rho = 0$  can be investigated by means of the expansion of the potential function into a power series of  $\rho$  keeping the terms up to  $\rho^2$ . If  $|w|/F^2 < \frac{2}{9}$  (Fig. 10.10a), the point  $\rho = 0$  is a local maximum, and the APES has three global minima  $M$  at  $\rho \neq 0$ . One more minimum at  $\rho \neq 0$  in Fig. 10.10a (the point  $S$ ) and two other equivalent at  $\phi = 2\pi/3, 4\pi/3$  (not seen in the figure) are in fact three saddle points situated in between the minima along  $\phi$  (similar to the warped Mexican hat). If  $|w|/F^2 > \frac{2}{9}$ , a minimum occurs at  $\rho = 0$ , but this is not necessarily accompanied by disappearance of the minima at  $\rho \neq 0$ . In the interval  $\frac{2}{9} < |w|/F^2 < 0.255$  both types of minima coexist. Finally, when  $|w|/F^2 > 0.255$ , the only minimum exists at  $\rho = 0$ .

The minimum at  $\rho = 0$  describes the state of the excess electron uniformly delocalized over the three centers, whereas the minima at  $\rho \neq 0$  correspond to electron localized at one of the three centers. Thus we conclude that for three-center MV compounds in a certain interval of parameter values, a *coexistence of localized and delocalized electron distributions is possible*. The region of parameter values required for this coexistence of two alternative electron distributions is relatively small; it is expected to increase when the difference in the frequencies of the local one-center totally symmetric vibration (or similarly, the  $K = M\omega^2$  constants) in two valence states is taken into account.

The coexistence of localized and delocalized electron distributions was observed first in a series of compounds of the type  $[\text{Fe(II) Fe}_2\text{(III) (CH}_3\text{COO)}_6\text{L}_3]$  (see Ref. 10.40 and references therein). In these works, it is shown that the Mossbauer spectra (Section 8.5), besides the lines corresponding to the Fe(II) and Fe(III) ions with the intensity ratio 1 : 2, also contain quadrupole doublets that are characteristic of iron ions in the intermediate oxidation state. The MV systems under consideration form, as a rule, molecular crystals in which the interaction between the molecules depends on the intramolecular electron distribution and hence nuclear configuration distortions. It follows that the cooperative properties of MV compounds in the crystal state depend on their electron localization or delocalization state. The APES of the type considered

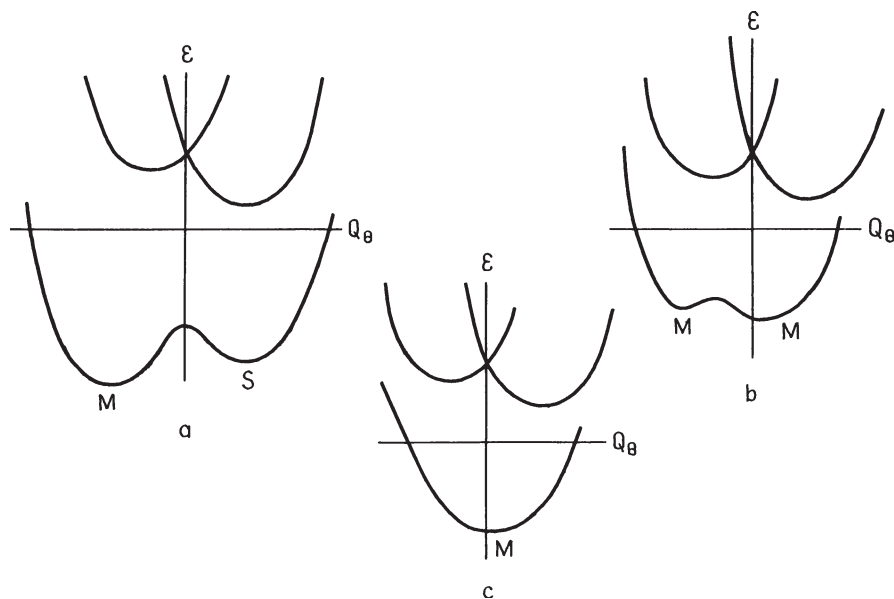


**FIGURE 10.10.** Crosssections  $\varphi = 0$  of the adiabatic potentials of a MV trimer as a function of  $|w|/F^2$ : (a)  $|w|/F^2 < \frac{2}{9}$ , (b)  $\frac{2}{9} < |w|/F^2 < 0.255$ , (c)  $|w|/F^2 > 0.255$  ( $M$  are minima;  $S$  is a saddle point).

above were used to analyze possible types of *phase transitions in crystals of MV trimers* [10.41].

The results presented above are based on the assumption that there is only one excess electron above the three zero-spin cores of the three centers, and the validity of these results for clusters containing Fe(II), Fe(III), ... in the high-spin state (where for each value of the total spin there are several  $A$  and  $E$  energy levels) may be questioned. However, if one includes the exchange anisotropy [i.e., the difference in the exchange parameters in the pairs Fe(II)–Fe(III) and Fe(III)–Fe(III)], then these levels are relatively displaced from each other, and it may be possible to consider each set containing the pair of  $A$  and  $E$  levels separately, as was done above.

For a more detailed evaluation of the trimer properties, the vibronic energy levels and wavefunctions of the MV system with the APES (10.42) should be computed. Such computations were performed for different values of the parameters  $F$  and  $w$ , and the results were used to evaluate the band shapes of the intervalence transfer (IT) spectra.

There are many MV trimers with equivalent centers that are not regular triangles; the linear system *trans*-(NH<sub>3</sub>)<sub>5</sub>Ru(II)pyzRu(II)(NH<sub>3</sub>)<sub>4</sub>pyzRu(III)(NH<sub>3</sub>)<sub>5</sub><sup>7+</sup> (1) [10.46] and the nonlinear system *cis*-(NH<sub>3</sub>)<sub>5</sub>Ru(II)NCRu(II)(bpy)<sub>2</sub>CNRu(III)(NH<sub>3</sub>)<sub>5</sub><sup>5+</sup> (2) [10.47] may serve as examples. Their IT bands have the maxima at 0.59 and 0.95  $\mu\text{m}^{-1}$ , respectively. The IT absorption curve for a derivative of 2

in which one ammonia molecule is substituted by pyridine is given in Fig. 10.2 (Section 10.1).

Another interesting use of the MV trimer vibronic states is in the calculation of their *magnetic characteristics* [10.20].

The delocalization of the excess electron in trimer MV systems is considered above for the case of zero-spin cores, raising the following question: To what extent are these results valid for systems with non-zero-spin cores that have a more complicated electronic energy spectrum? As stated above, in these cases the effect of double exchange should be considered. In Example 10.3 this problem is considered by investigation of a specific trinuclear cluster of biological importance—*tricenter ferredoxin*.

### EXAMPLE 10.3

#### *Tricenter Ferredoxin*

The trinuclear iron–sulfur cluster in the ferredoxin of the sulfate-reducing bacteria *Desulfovibrio gigas* [10.44], for which the presence of double exchange is revealed, seems to be an appropriate system to illustrate the problem of intramolecular electron transfer between centers with open-shell cores.

In the reduced form this ferredoxin cluster has the valence composition Fe(III)–Fe(III)–Fe(II). The ESR and Mossbauer spectra (Sections 8.4 and 8.5) show that the excess electron is delocalized over two out of three centers [10.45]. On the basis of these data, a model was proposed that considers the double exchange between the pair Fe(II)–Fe(III) in addition to the HDVV exchange between all three ions [10.45]. This approach implies that one of the ions is strongly distinguished from the other two, so that its resonance interaction with the latter is negligible. However, X-ray structural data [10.46] show that the structural differences between the three ions, if any, are very small.

Borshch and Chibotaru [10.47] proposed a model based on simultaneous magnetic and vibronic effects, which explains the origin of the peculiar electron distribution in the ferredoxin cluster under consideration. The electronic configuration of the three centers is  $d^5 - d^5 - d^6$  and all the iron ions are in the high-spin states. From experimental data it is known that the ground state of the system is a quintet  $S = 2$ , and the excited states with other  $S \neq 2$  spins lie higher than the ground one by at least  $80 \text{ cm}^{-1}$ . Therefore, approximately, for sufficiently low temperatures, only the quintet states can be considered. With the localized electron, there are five states of this kind.

For simplicity the differences between the exchange integrals  $J_1$  for the Fe(II)–Fe(III) pair and  $J_2$  for Fe(III)–Fe(III) are neglected. In other

words, it is assumed that the system is exchange-isotropic. Then the analytical expressions for the electronic energies [Eq. (10.43)] at  $Q_\theta = Q_\varepsilon = 0$  are:

$$\begin{aligned}\varepsilon[{}^5A^{(1)}] &= \varepsilon[{}^5E^{(1)}] = \varepsilon[{}^5E^{(2)}] = -w \\ \varepsilon[{}^5A^{(2)}] &= \varepsilon[{}^5A^{(3)}] = \varepsilon[{}^5E^{(3)}] = 0 \\ \varepsilon[{}^5A^{(4)}] &= \varepsilon[{}^5A^{(5)}] = \varepsilon[{}^5E^{(5)}] = \frac{5}{6}w\end{aligned}\quad (10.46)$$

where the energies are read off from the position of nonsplit HDVV multiplet with  $S = 2$ . For an arbitrary relation between the exchange parameters  $J_1$  and  $J_2$  and arbitrary values of vibrational coordinates, the electronic energies can be obtained by numerical calculations.

With the known electronic energies at fixed nuclei, one can determine the APES of the system in the space of the active  $Q_\theta$  and  $Q_\varepsilon$  or  $\rho$  and  $\phi$  coordinates [see Eq. (10.41)]. In the case at hand, although the energy-level scheme depends on the sign of  $w$ , the shape of the lowest sheet of the APES undergoes qualitatively the same transformations with the  $|w|/F^2$  parameter for both positive and negative  $w$  values.

For small  $w$  values the minima of the lowest branch of APES are at  $\phi = \pi/3, \pi, 5\pi/3$ , whereas at  $\phi = 0, 2\pi/3, 4\pi/3$  there are saddle points. As a result, the extremal crosssections of the APES have the same shape as in Fig. 10.10a. Similar to the case of a one-electron trimer (considered above), these minima correspond to the localization of the excess electron at one center. For some values of  $|w|/F^2$  a pair of minima occurs instead of each individual minimum. The two minima in the pair occupy a symmetric position with respect to the directions  $\phi = \pi/3, \pi, 5\pi/3$ ; the minima in these directions thus become saddle points. The value  $|w|/F^2$ , for which the number of minima doubles, depends on the relation between the exchange integrals: for the  $|J_1 - J_2|$  values from 0.0 to 0.1,  $0.7 < |w|/F^2 < 0.8$  (for the possible existence of such three pairs of equivalent minima of the APES in the space of  $E$  vibrations, see Refs. 10.36 and 10.48).

On further increase of the ratio  $|w|/F^2$ , the six minima merge in pairs into three minima at  $\phi = 0, 2\pi/3, 4\pi/3$ ; these points thus become minima instead of saddle points, and the surface as a whole again becomes triminimal. However, as opposed to the previous cases, *the excess electron in these minima is delocalized over two centers of the trimer.*

If  $|w|/F^2 \rightarrow \infty$ , the energies of the minima and saddlepoints coincide, and we obtain a continuous set of minima, a trough [10.36, 10.48]. The motion along the trough corresponds to a dynamical delocalization of the excess electron; this is not possible in other MV systems, considered above, neither in dimers nor in one-electron trimers.

The observed charge distribution in the iron-sulfur ferredoxin can thus be attributed to the joint influence of vibronic and interelectron

(double exchange) interactions in a multilevel system with a special relation of parameter values resulting in minima of the adiabatic potential that describe the partial (two-center) delocalization of the excess electron. DFT- $X_\alpha$  calculations [10.49] of the once and twice reduced systems of the type  $[\text{Fe}_3\text{S}_4(\text{SH})_3]^{2-}$  with  $C_{3v}$  symmetry in which the competition between spin–spin coupling and delocalization is considered in detail confirms qualitatively the scheme of double exchange. The calculations show that the exchange constant  $J$  is larger in the reduced form than in the oxidized one, and that  $w$  is negative ( $w/J$  varies from 1.5 to 3.0).

For a model *four-center tetrahedral cluster* (e.g., *four-center ferredoxin* [10.50] with one excess electron over the four closed shells and one electronic state on each center, there are four symmetrized coordinates of the center displacement from regular tetrahedral positions,  $Q_A, Q_{T\xi}, Q_{T\eta}$ , and  $Q_{T\zeta}$  (Table 7.1), which are linear combinations of the local totally symmetric breathing (polaron) displacements on each center  $Q_i, i = 1, 2, 3, 4$ . From these coordinates the totally symmetric combination  $Q = 1/\sqrt{3}(Q_{T\xi} + Q_{T\eta} + Q_{T\zeta})$  in the trigonal space is most informative in the problem under consideration. In the space of this coordinate the four energy levels as functions of  $Q$  (APES in the crosssections along  $Q$ ) are [cf. Eqs. (10.41) and (10.42)]

$$\varepsilon_{1,2} = \frac{1}{2}Q^2 - w - \frac{FQ}{2\sqrt{3}} \quad (10.47)$$

$$\varepsilon_{3,4} = \frac{1}{2}Q^2 + w + \frac{FQ}{2\sqrt{3}} \pm 2 \left( w^2 - \frac{wQ}{2\sqrt{3}} + \frac{F^2Q^2}{12} \right)^{1/2} \quad (10.48)$$

By direct calculation one can easily ensure that if  $w > 0$ , there is always a minimum of the lowest curve at  $Q \neq 0$  corresponding to the excess electron localized at one center. For negative  $w$  values, three possibilities similar to that for the trimers occur: (1) if  $|w|/F^2 < 0.125$ , the lowest curve has two minima from which one is, in fact, a saddle point (in the extended space including other coordinates); (2) if  $0.125 < |w|/F^2 < 0.152$ , there are two minima at  $Q = 0$  and  $Q \neq 0$ , respectively; and (3) if  $|w|/F^2 > 0.152$ , the only minimum point occurs at  $Q = 0$ . As for the electron charge distribution corresponding to these three cases, they are: (1) an electron localized state; (2) coexistence of localized and delocalized states, and (3) electron delocalization.

Thus, for the tetrahedral MV tetramers we again come to the possibility of *coexistence of states with localized and delocalized excess electron distributions*. Apparently this effect has a more general meaning and can also be expected in clusters with larger numbers of MV centers. So far, to our knowledge, there has not been experimental confirmation of the coexistence effect in tetramers.



The lowest pathway between the APES minima of the localized electron goes through the saddle points along the  $Q_{T\xi}$ ,  $Q_{T\eta}$ , and  $Q_{T\zeta}$  directions. Numerical calculation shows that the barrier height for the electron transfer through these saddle points in tetramers is always lower than the corresponding barrier in dimers for the same values of  $w$  and  $F$ . Perhaps this result explains why in the same conditions, that is, for the same structure of the nearest-neighbor environment of the iron ions and the same bridges between them, as well as approximately the same iron–iron distances, in iron–sulfur dimers the excess electron is rather localized, whereas in the similar tetramers it is delocalized.

It is evident that the other problems considered above for dimers and trimers by means of the vibronic theory can be similarly treated for tetramers and other MV systems. However, for MV systems with the number of centers  $n > 3$ , some new problems may occur. In particular, two and more excess electrons migrating among the MV centers may be important in these systems (in trimers two excess electrons are equivalent to one excess hole for which the problem is similar to that of one electron). For two and more excess electrons, the electron distribution and dynamics are determined by the competition of vibronic, intraatomic, and intercenter interactions. Examples of MV systems with two excess electrons are known among cubic [10.50] and quadratic [10.51] tetramers, six-nuclear clusters [10.52], and others.

The coexistence of localized and delocalized electronic distributions in polynuclear clusters considered in this section is somewhat analogous to the coexistence of localized and delocalized excitonic states in crystals [10.53, 10.54].

### 10.3. ELECTRON-CONFORMATIONAL EFFECTS IN BIOLOGICAL SYSTEMS

#### Distortions Produced by Excess Electronic Charge; Special Features of Metalloenzymes

Conformational changes produced by excess electronic charge [*electron-conformational effects* (ECEs)] are of widespread interest, especially in biologic processes. In essence, the ECE problem is a particular case of the TEST paradigm formulated in Section 7.4 realizing electronic control of configuration instability. Similarly, the ECE problem is formulated as follows: Is it possible to predict conformational changes in molecular system induced by the addition or removal of electronic charge?

The solution of this problem is facilitated by the vibronic theory (Sections 7.2 and 7.4). In Section 7.2 the notion of vibronic constants is introduced [see Eq. (7.22)]:  $F_{\Gamma^*}^{(\Gamma, \Gamma')} = \langle \Gamma | \partial V / \partial Q_{\Gamma^*} | \Gamma' \rangle$ , where  $\Gamma$  and  $\Gamma'$  are two electronic states [for the diagonal constant  $F_{\Gamma^*}^{(\Gamma)}$   $\Gamma = \Gamma'$ ],  $V$  is the electron–nucleus interaction in the Hamiltonian of the system, and  $Q_{\Gamma^*}$  is the symmetrized coordinate of nuclear displacements that belongs to the representation  $\Gamma^*$ . The vibronic constant has the dimensionality of a force, and the diagonal constant  $F_{\Gamma^*}^{(\Gamma)}$  also has the physical

meaning of a force (Section 7.2):  $F_{\Gamma^*}^{(\Gamma)}$  means the force with which the electronic cloud in the state  $\Gamma$  acts on the nuclear configuration in the direction of the symmetrized displacements  $Q_{\Gamma^*}$ .

It is clear that in the equilibrium configuration  $F_{\Gamma^*}^{(\Gamma)} = 0$ , but any excess electronic charge (electron addition, proton removal) or positive charge (electron removal, proton addition) violates the equilibrium of forces and results in  $F_{\Gamma^*}^{(\Gamma)} \neq 0$ . The nonzero force distorts the nuclear configuration in the direction  $Q_{\Gamma^*}$ .

How can one determine the direction  $Q_{\Gamma^*}$  of this distortion and its magnitude as a function of the excess charge and electronic state  $\Gamma$ ? If the excess charge is an integer (one or more electrons added or removed), the problem can be solved directly by computing the wavefunction  $|\Gamma'\rangle$  of the new state  $\Gamma'$  with the additional charge (not to be confused with the excited state) and the matrix element for the  $Q_{\Gamma^*}$  coordinates, for which  $F$  is nonzero. But this is a very difficult method, especially for large (biological) molecular systems, and it cannot be carried out, in principle, when the excess charge is fractional (which is often the case).

A more realistic way to solve this problem approximately is provided by the semiempirical method, based on the notion of *orbital vibronic constants*  $f$  introduced in Section 7.2:  $f_{\Gamma^*}^{(i,j)} = \langle i | (\partial V_i / \partial Q_{\Gamma^*})_0 | j \rangle$ , where  $|i\rangle$  are molecular orbitals and  $V_i$  is the one-electron operator of electron–nucleus Coulomb interaction (7.24). The diagonal orbital vibronic constant  $f_{\Gamma^*}^{(i)}$  has the physical meaning of the force with which the electron on the  $i$ th MO acts on the nuclear configuration in the direction  $Q_{\Gamma^*}$ . It is very important that, owing to the additive electron–nucleus interactions, the diagonal integral vibronic constant according to Eq. (7.26) equals the sum of the orbital constants multiplied by their electron occupation numbers (in the state  $\Gamma$ )  $q_i^\Gamma$  [8.36].

In fact, Eq. (7.26) solves the preceding problem approximately. Indeed, for a stable system in the equilibrium configuration

$$F_{\Gamma^*}^{(\Gamma)} = \sum_i q_i^\Gamma f_{\Gamma^*}^{(i)} = 0 \quad (10.49)$$

With the excess charge the population of the MO changes:

$$q_i^{\Gamma'} \rightarrow q_i^\Gamma + \Delta q_i \quad F_{\Gamma^*}^{(\Gamma')} = \sum_i q_i^{(\Gamma')} f_{\Gamma^*}^{(i)} = \sum_i \Delta q_i f_{\Gamma^*}^{(i)} \quad (10.50)$$

This equation is approximate because it implies that the excess charge does not change the orbital vibronic constants. It is valid roughly to the second order of the charge alteration  $(\Delta q/N)^2$ , where  $N$  is the total number of electrons.

Following Eq. (10.50), the distortion force  $F_{\Gamma^*}^{(\Gamma')}$  produced by the excess charge  $\Delta q_i$  can be easily found, provided that the orbital vibronic constants  $f_{\Gamma^*}^{(i)}$  are known. In particular, for one electron added to the system  $F_{\Gamma^*}^{(\Gamma')} = f_{\Gamma^*}^{(i)}$ , where  $i$  is the MO occupied by the excess electron. The numerical value of the constants  $f_{\Gamma^*}^{(i)}$  can be calculated from electronic structure data. In many cases they can

be estimated using empirical data obtained from spectroscopic and diffraction experiments; many examples are given in Sections 7.2 and 11.2. The sign of  $f$  and the symmetry of  $Q_{\Gamma^*}$  (i.e., the direction of distortion) can be established from general considerations without detailed calculations.

As stated in Section 7.2,  $f_{\Gamma^*}^{(i)} > 0$  for bonding MO (in the  $Q_{\Gamma^*}$  direction),  $f_{\Gamma^*}^{(i)} < 0$  for antibonding MO,  $f_{\Gamma^*}^{(i)} \approx 0$  for non-bonding MO, and the absolute value of  $f_{\Gamma^*}^{(i)}$  follows quantitatively the measure of the MO bonding or antibonding. The symmetry of  $Q_{\Gamma^*}$  can be obtained directly from Eq. (7.25) using the selection rules (Section 3.4). Following these rules,  $f_{\Gamma^*}^{(i)}$  [the diagonal matrix element (7.25)] is nonzero if the symmetrical square of the symmetry type  $\Gamma_i$  (to which the  $i$ th MO belongs) contains the symmetry  $\Gamma^*$  of  $Q_{\Gamma^*}$ :  $\Gamma^* \in [\Gamma_i \times \Gamma_i]$ . If  $\Gamma_i$  is nondegenerate, then  $\Gamma_i \times \Gamma_i$  contains only the totally symmetric representation  $A_1$ . Thus addition of electronic charge on nondegenerate MOs produces totally symmetric distortions that do not change the symmetry of the system. But in this case there is a second source of distortion: the PJTE (Section 7.4; see below). If  $\Gamma_i$  is degenerate, then the product  $[\Gamma_i \times \Gamma_i]$  also contains nontotally symmetric representations, and the charges on such MOs produce deformation of the system. These deformations are exactly the same as in the Jahn–Teller effect (Section 7.3); double degenerate  $E$  MOs produce  $E$  deformations with two components  $Q_\theta$  and  $Q_\varepsilon$  (Fig. 7.1) or (for particular cases)  $B_1$  and  $B_2$  deformations (Fig. 9.16), orbital triplets  $T$  produce  $E$  or  $T_2$  deformations, and so on. Each of these deformations is characterized by its own orbital vibronic constant  $f_{\Gamma^*}^{(i)}$ .

If several MOs are populated, the total distortion equals the sum of the distortions produced by each MO. They can be found approximately using Eq. (7.41):

$$Q_{\Gamma^*}^0 = \frac{F_{\Gamma^*}}{K_{\Gamma^*}} \quad (10.51)$$

where  $K_{\Gamma^*}$  is the force constant of the  $Q_{\Gamma^*}$  distortion without the additional charge [a more exact equation for  $Q_{\Gamma^*}^0$  is given in Section 11.2, Eq. (11.24)]. Substituting (7.26) into (10.51), we have

$$Q_{\Gamma^*}^0 = \frac{\sum_i \Delta q_i f_{\Gamma^*}^{(i)}}{K_{\Gamma^*}} \quad (10.52)$$

The symmetrized distortions  $Q_{\Gamma^*}$  determine the Cartesian displacement of the nuclei, as shown in Table 7.1; if several types of  $Q_{\Gamma^*}$  (for several types of  $\Gamma^*$ ) are nonzero, the corresponding Cartesian displacements should be summed as vectors. The PJT distortion [Eq. (7.67)] caused by interaction with an one-electron excited ( $i \rightarrow j$ ) state, denoting  $M = |f^{(ij)}|^2/K_0$ , yields (the  $\Gamma^*$  subscript is omitted here for simplicity)

$$Q^0 = (\Delta q_i - \Delta q_j) \left( \frac{M^2 - \Delta^2}{K_0 M} \right)^{1/2} \quad (10.53)$$

where  $\Delta$  is the energy gap to the excited state (not to be confused with  $\Delta q$ !) and the possible partial occupation of the two orbitals  $\Delta q_i$  and  $\Delta q_j$  is also taken into account (in particular, when  $\Delta q_i = \Delta q_j$ , there is no PJTE).

As seen from Eqs. (10.52) and (10.53), the nuclear configuration distortion is directly proportional to the charge transfers  $\Delta q_i$  and orbital vibronic couplings  $f_{\Gamma^*}^{(i)}$  of the corresponding MOs, and inversely proportional to the rigidity of the system  $K_{\Gamma^*}$  in the  $Q_{\Gamma^*}$  direction. While  $f_{\Gamma^*}^{(i)}$  characterizes quantitatively the participation of the excess charge in the alteration of bonding (and hence the occurrence of the distortion force) along  $Q_{\Gamma^*}$ ,  $K_{\Gamma^*}$  characterizes the resistance of the system to deformations in the  $Q_{\Gamma^*}$  direction.

In general, many biologic systems are very susceptible to vibronic instabilities mainly for two reasons [10.36]:

1. Conformational flexibility, that is, the presence of *soft modes* (small  $K_0$  values)
2. Presence of prosthetic groups with close-in-energy HOMO–LUMO levels (small  $\Delta$  values)

Both sources of vibronic deformation, (10.52) and (10.53), are strongly dependent on  $K_{\Gamma^*}$ , the rigidity of the system with respect to the  $Q_{\Gamma^*}$  distortion. Biologic systems are specific in possessing low rigidity  $K_{\Gamma^*}$  in certain directions  $\Gamma^*$  (soft modes). This circumstance favors large distortions.

Examples of the second special feature in biological systems, the presence of close energy levels, ground and excited (small energy gaps  $\Delta$ ), are provided by metalloenzymes. The latter have a group of such active states due to the metal  $d$  orbitals (organic conjugated prosthetic groups may also be very similar to this type). *The prosthetic group is a site triggering (initiating) electron-conformational transitions due its close-in-energy electronic levels and the soft modes of the biological environment.*

### **Trigger Mechanism of Hemoglobin Oxygenation: Comparison with Peroxidase**

One of the most important properties of hemoglobin is its ability to oxygenate (absorb oxygen) and to deoxygenate (release oxygen) with a special S-type kinetics. In other words, hemoglobin absorbs oxygen sharply (much more sharply than do most absorbers) in an oxygen environment, and releases oxygen sharply in a medium where there is no oxygen. Perutz was the first to show that this kinetics of oxygenation is due to a special mechanism based on the so-called  $T \rightarrow R$  (tense  $\rightarrow$  relaxed) conformational transitions and consequent cooperative effects induced by out-of-plane and in-plane displacements of the iron atom in the metal–porphyrin active center by oxygenation (trigger mechanism) [10.55] (see also Refs. 10.56 and 10.57).

Hemoglobin has four similar active iron centers, each containing an iron porphyrin group. The four centers are linked by protein chains. Figure 10.11 shows

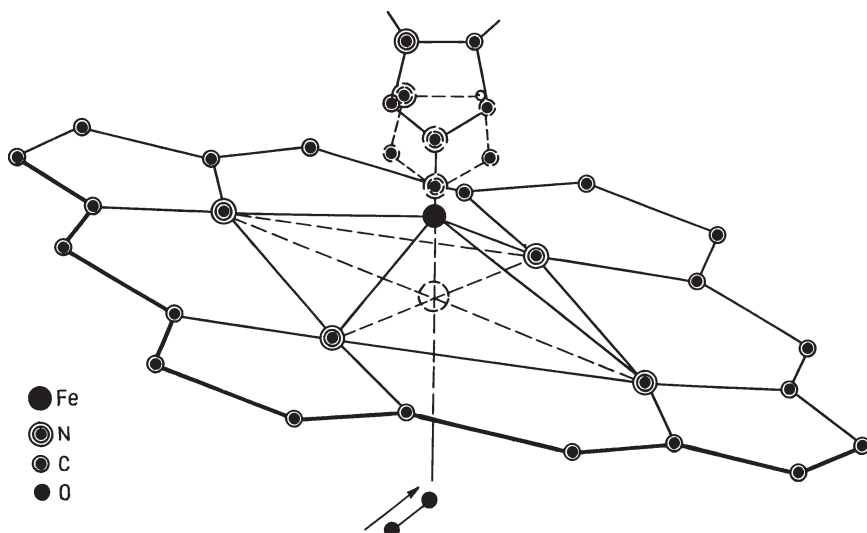


**FIGURE 10.11.** Structure of the active center of hemoglobin (myoglobin)—the iron porphyrin center with the imidazole moiety of the proximal histidine. The in-plane position of the iron atom is shown by dashed lines. The approaching oxygen molecule is also shown.

schematically the structure of the iron porphyrin center with the imidazole moiety as the fifth ligand (cf. Fig. 9.6). The iron centers are linked via this ligand, which is a part of the protein chain. In the Perutz mechanism [10.55] (see also Ref. 10.57) the position of the iron atom in the deoxy form of the hemoglobin centers is out of plane of the porphyrin ring, and in this position only two of the four centers are open to oxygen coordination. When the oxygen molecule occupies the sixth coordination position (Fig. 10.11), the iron metal returns to the porphyrin plane. This displacement pulls the imidazole moiety of the proximal histidine, which, being linked to the protein chain, produces the conformational transition  $T \rightarrow R$ ; this, in turn, opens the other two iron centers for oxygen coordination, thus sharply increasing the oxygenation curve.

In the absence of oxygen the release of one oxygen molecule initiates an inverse process of the iron out-of-plane displacement and  $R \rightarrow T$  transition with corresponding consequences for the desorption curve. Thus the local changes in the iron atom position with respect to the porphyrin ring as a result of oxygen coordination initiate conformational transitions in the protein (trigger mechanism) important to its biologic function.

In Section 9.2 it is shown that the in-plane position of the iron atom in the porphyrin ring is very soft or even unstable with respect to its out-of-plane displacement. In the planar metalloporphyrin symmetry  $D_{4h}$  this displacement has  $A_{2u}$  symmetry, and the instability is due to the sufficiently strong PJTE (Section 7.4), the mixing of the MO  $a_{2u}$  of mainly the porphyrin ring with the metal  $d_{z^2}$  orbital of  $a_{1g}$  symmetry under  $A_{2u}$  displacements ( $A_{1g} \times A_{2u} = A_{2u}$ ).

As seen from Fig. 10.12, the energy-level separation  $2\Delta = \varepsilon(a_{1g}) - \varepsilon(a_{2u})$  is relatively small, making the inequality (7.67) quite real. Under the influence of the imidazole moiety of the proximal histidine residue, these MO energy levels of iron porphyrin, as shown in Fig. 10.12, do not change very much; at least the  $\Delta$  value remains sufficiently small to soften the iron atom out-of-plane displacement.

The picture changes when the oxygen molecule is coordinated to the sixth position. The repulsion of the iron antibonding  $d_{z^2}$  orbital by the oxygen negative charge raises this iron energy level significantly and makes the energy gap  $2\Delta \approx 3$  eV (see Fig. 10.12; for CO as the sixth ligand  $2\Delta \approx 4$  eV). With this  $\Delta$  value the inequality (7.67) does not hold, and there is no more softness or instability of the in-plane position of the iron atom; it returns to the plane of the porphyrin ring.

An important feature of iron out-of-plane and back in-plane displacements is that they change the spin of the ground state of the system (cf. spin crossover, Section 8.4). In Fig. 10.12 the real ground-state spins are indicated. In the out-of-plane position of the iron atom in deoxyhemoglobin the spin is higher than in the oxygenated in-plane position. In accordance with the results of Sections 4.3 and 6.2, the electron distribution over the AOs or MOs depends on the pairing energy  $\Pi$  and its ratio to the energy gap  $\Delta$  between the MO levels occupied by the electrons in the unpaired (high-spin) configuration. Therefore, it is not surprising that in the configuration with larger  $\Delta$  values the ground state is a low-spin one.

Note that both the iron–porphyrin stereochemistry and the spin states are controlled by the same MO energy-level arrangements. It is worth emphasizing this fact because the earlier explanations of the origin of the iron out-of-plane and in-plane displacements by Hoard [10.58] and Perutz [10.55] (see also Refs. 10.56 and 10.59) are based on the fact that the atomic radii in the high-spin configuration are larger (the antibonding  $d$  orbitals of the high-spin configuration are more extended) than in the low-spin case. Hence the iron atom (ion) cannot fit the hole in the porphyrin ring when it is in the high-spin state, while it fits this hole in the low-spin state. Section 9.2 presents some criticism of this rough ball-hole fitting.

In these explanations, cause and effect are inverted. There are many examples with different metals [10.56] when the atom (ion) is in the in-plane position for smaller holes and is out-of-plane for larger holes. A detailed analysis of out-of-plane displacements of the metal atom in metalloporphyrins and the spin state–geometry relationship is given in the review article [10.56], and it is shown that the vibronic approach discussed above qualitatively explains the observed features of the phenomenon.

In real metalloenzymes the metal porphyrin active center is subject to influence of the protein environment that controls a variety of their functions [10.60, 10.61]. For instance, the same iron porphyrin active center with different proximal ligands (and other differences in the next coordination spheres) has quite different activities with respect to the interaction with oxygen; in hemoglobin the coordination of the  $O_2$  molecule initiates  $T \rightarrow R$  conformational transitions

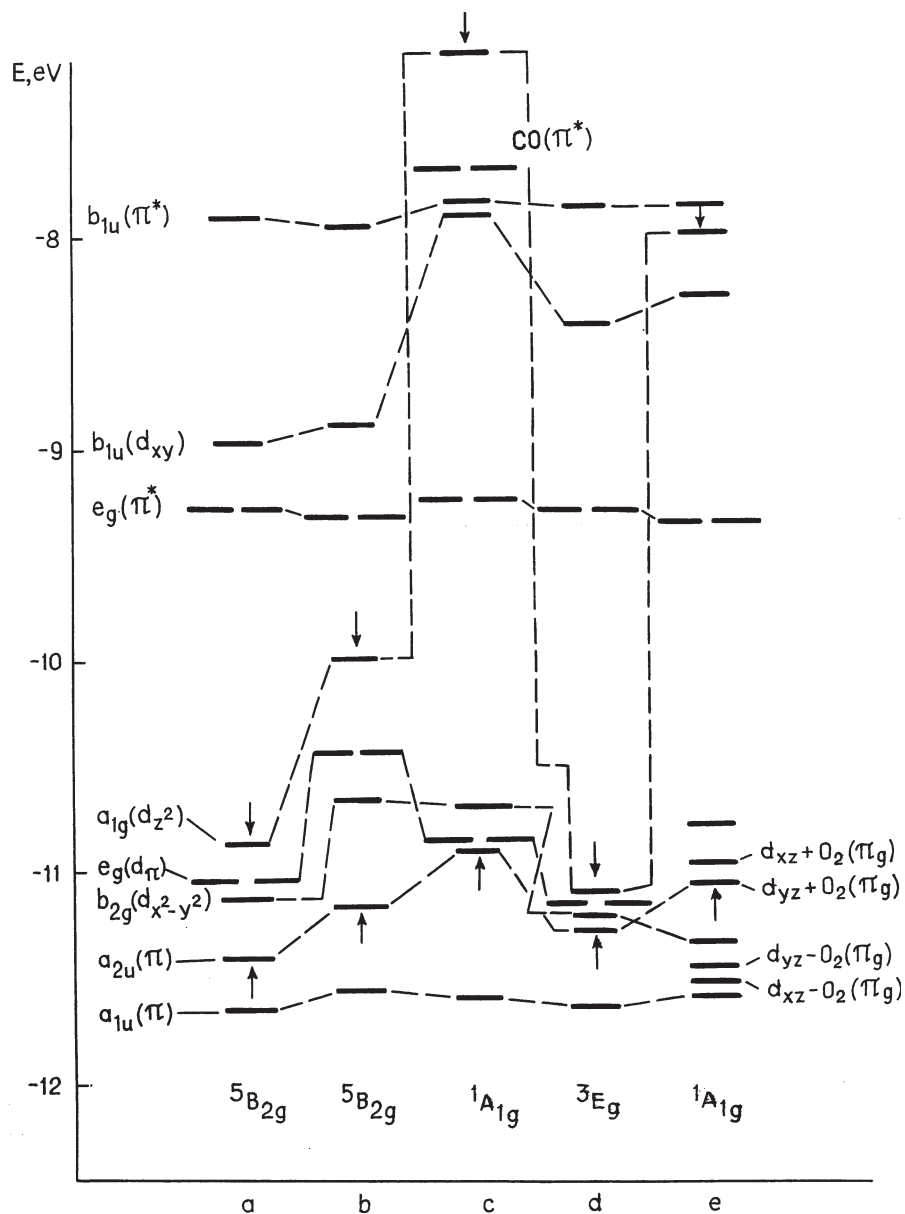


**FIGURE 10.12.** The MO energy levels for several HOMOs and LUMOs of iron porphyrin with indication of the ground term: (a) out-of-plane displacement of the iron atom is  $\Delta R = 0.49 \text{ \AA}$ ; (b) deoxy form of hemoglobin (Hb),  $\Delta R = 0.62 \text{ \AA}$ ; (c) Hb—CO; (d) planar iron porphyrin  $\Delta R = 0$ ; (e) Hb—O<sub>2</sub>. The energy gap  $2\Delta$  between the two states that mix under the iron out-of-plane displacement is shown by arrows.



and is released without being strongly activated, whereas in cytochrome P-450 coordinated oxygen is strongly activated and performs hydroxylation of saturated hydrocarbons (catalase and peroxidase act in a similar way). While chemical activation by coordination (also to cytochrome P-450) is considered in Section 11.2, we present here, by way of example, a comparison of hemoglobin and peroxidase that illustrates the role of the protein environment.

Figure 10.13 is a schematic representation of the configuration of the iron porphyrin active center in the two metalloenzymes, hemoglobin and peroxidase, without (Fig. 10.13, I) and with (Fig. 10.13, II) coordinated oxygen (in peroxidase the coordinated molecule is  $\text{H}_2\text{O}_2$  that is modeled by  $\text{O}_2$ ). The essential difference in these two cases is in the structure of the protein, not shown in the figure. In both cases the iron atom is out-of-plane without oxygen and returns to the in-plane position through oxygenation.

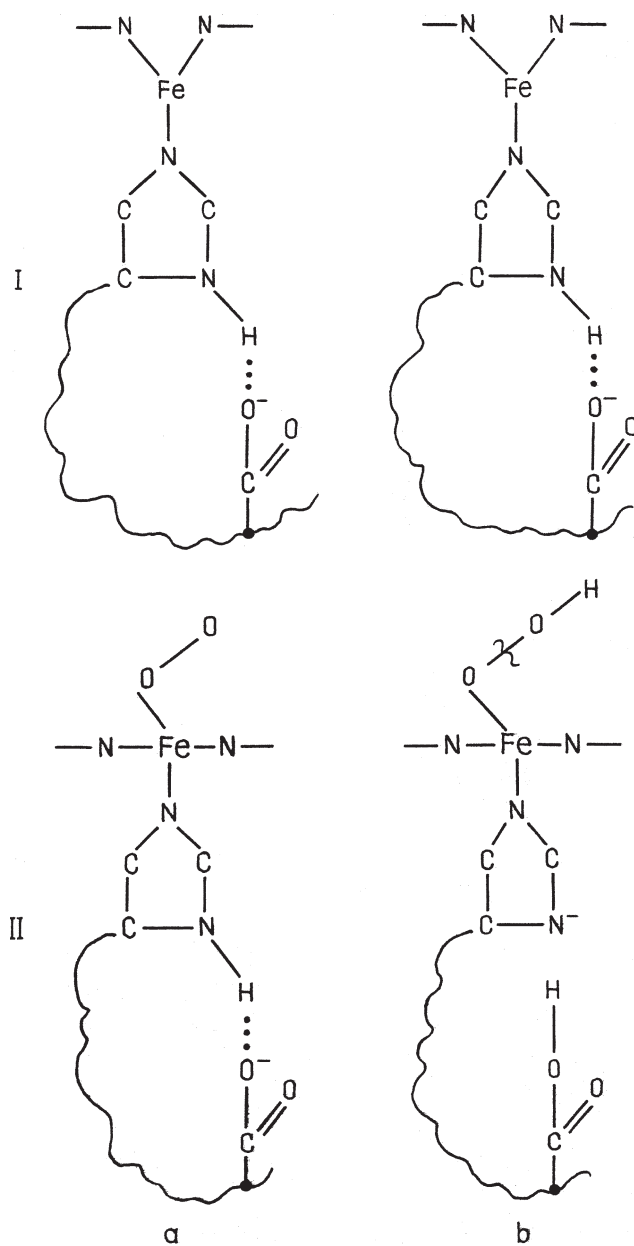
In hemoglobin the iron displacement toward the porphyrin plane triggers the conformational  $T \rightarrow R$  transition, discussed above, without strong activation of the O—O bond, whereas in peroxidase, where the protein environment is different from that of hemoglobin, movement of the iron atom toward the in-plane position deprotonates the imidazole residue with the result that the distal nitrogen acquires an excess electron. This process, initiated by oxygen coordination, has an important backward influence on the coordinated molecule  $\text{O}_2$ .

Figure 10.14 shows the MO energy levels of the oxygenated active center FeP (P = porphyrin) of peroxidase with neutral imidazole,  $\text{Fe}(\text{ImH})\text{O}_2$ , and deprotonated imidazole,  $\text{Fe}(\text{Im}^-)\text{O}_2$ , computed [10.62] in the semiempirical MO LCAO IEH (SCCC) approximation (Section 5.5). It is seen that, due to the excess electron, the energy level of the (mainly) lone-pair hybridized  $sp^3$  orbital of the distal nitrogen rose up to the LUMO, which is (mainly) a strongly antibonding  $\pi^*$  MO of the oxygen molecule; the energy gap between the HOMO and LUMO  $\Delta$  becomes smaller than the pairing energy  $\Pi$  (Sections 4.3 and 6.2). This separates the lone pair of electrons, with one of them occupying the antibonding  $\pi^*$  MO of the  $\text{O}_2$  molecule, which results in its activation (Section 11.2).

Interestingly, the enzyme as a whole acts in the regime of feedback; the oxygen molecule coordinates to the active center of the enzyme and the latter, dependent on its function, activates the O—O bond (peroxidase, cytochrome P-450, catalase), or not (hemoglobin). In the case of cytochrome P-450 the mechanism of population of the antibonding  $\pi^*$  MO of the coordinated oxygen is similar to that of peroxidase. Calculations of the MO energy levels of the oxygenated active center of cytochrome P-450 [10.63] in the same approximation as above show that in the deprotonated form the energy of the lone pair of the sulfur atom goes up, comes near to, and populates the antibonding  $\pi^*$  MO of  $\text{O}_2$ , thus significantly activating the coordinated oxygen molecule. An additional electron acts in the same direction, reducing the O—O bonding up to its cleavage [10.64] (Section 11.2).

In fact, the problem of electron transfer in biologic systems is of general importance. For an instant view of some topics related to this problem see, for example, Refs. 10.60, 10.61, and 10.65–10.67.





**FIGURE 10.13.** Comparison of conformational changes in hemoglobin (a) and peroxidase (b) by oxygenation. The iron atom from the out-of-plane position (I) returns back into the plane (II) with the effect of a  $T \rightarrow R$  conformational transition in hemoglobin (not shown in the figure) and deprotonation of peroxidase that leaves an excess electron on the distal nitrogen atom.

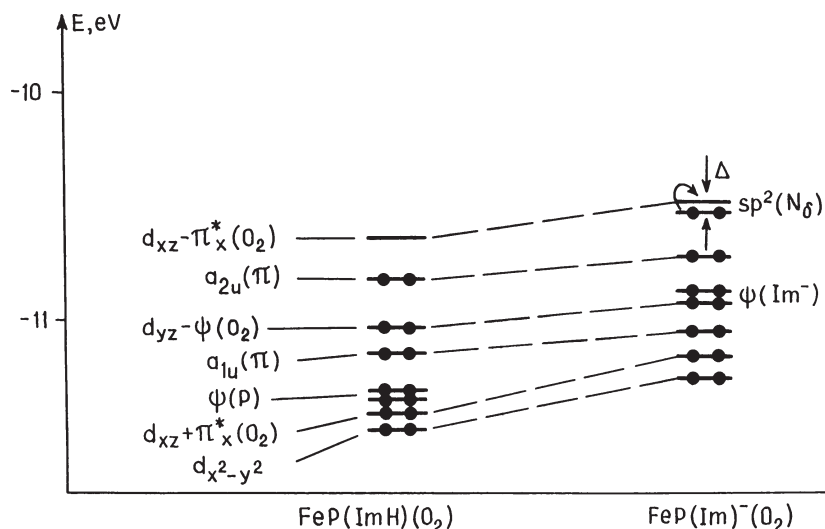


**FIGURE 10.14.** MO energy levels of the active center of oxygenated peroxidase with imidazol, neutral  $\text{FeP}(\text{ImH})\text{O}_2$ , and deprotonated  $\text{FeP}(\text{Im}^-)\text{O}_2$ . In the last case one electron from the distal nitrogen lone pair populates the strongly antibonding  $\pi^*$  MO of the coordinated oxygen molecule [ $\psi(\text{O}_2)$  and  $\psi(\text{Im})$  are the corresponding MOs].

### SUMMARY NOTES

1. *Charge transfer* or charge redistribution takes place at the beginning of any chemical transformation, thus determining the initial conditions of its evolution. Charge transfer by coordination is one of the most important features of any TMS. Integer electron transfer takes place between weakly interacting systems, as well as between the centers in multicenter TMSs, essentially determining their properties.
2. The *direction of charge transfer* between two interacting systems can be determined by comparing their HOMO and LUMO energy levels or chemical potentials. The amount of charge transfer can be estimated by their redox capacitance or their chemical hardness. The notion of *soft and hard acids and bases* is directly related to these magnitudes.
3. In *mixed-valence compounds* the localized–delocalized electron alternative determines their main properties. The probability of electron transfer depends on exchange interaction between the centers and the vibronic coupling to the nuclear displacements on each center, as well as on the exchange interaction with other electrons in case of open-shell cores. Additional complications emerge from possible JT and/or PJT interaction on each center.
4. Charge transfer to any system produces changes in its nuclear configuration via the vibronic coupling, resulting in either small distortions or

more fundamental changes of its conformation, thus serving as a trigger mechanism of *electron-conformational transitions*. Many biological TMSs are very sensitive to such effects because of their soft modes (softness to structural changes in certain directions) and the presence of close-in-energy levels in the transition metal site.

5. Hemoglobin, peroxidase, cytochrome P-450, and catalase are typical examples of TMSs in which the *electron-conformational effects* triggered by charge transfer determine their biological function.

### EXERCISES AND PROBLEMS

- P10.1.** What is the difference between intramolecular charge transfer and intermolecular electron transfer? Give examples.
- P10.2.** *Redox capacitance* is defined as a measure of the ability to accept or donate charge with smaller changes in HOMO energy. What kind of system is expected to have larger capacitance? Is there a quantitative difference between the capacitances for accepting and donating charge? Is there essential difference between redox capacitance and chemical softness (hardness)?
- P10.3.** The charge dependence of the HOMO energy of a molecular system  $\varepsilon(q) = 14.1q^2 + 80.2q + 38.6$  ( $q$  in electrons,  $\varepsilon$  in  $10^3 \text{ cm}^{-1}$ ) was obtained semiempirically from ionization potentials as indicated in Section 5.5. Estimate the redox capacitance of this system and the charge transfer by its coordination to iron porphyrin assuming that the energy gap between them is  $45 \times 10^3 \text{ cm}^{-1}$  (use the data of Example 10.1 for iron porphyrin capacitance).
- P10.4.** One of the main problems of mixed-valence compounds is the localization–delocalization alternative for the excess electron. What parameters of the system characterize this alternative? How can this problem be addressed experimentally; that is, what experimental observations can be related to this phenomenon?
- P10.5.** In three-center and four-center mixed-valence compounds there is a possibility of coexistence of localized and delocalized states of the excess electron. Explain what this means from the physical perspective and how this phenomenon can be confirmed experimentally.
- P10.6.** In Section 10.3 it is stated that some biological systems are susceptible to electron-conformational changes. What are the general conditions for such susceptibility, and why do biological systems feature these conditions? Give examples of such biological systems and identify which of their properties confirm this electron-conformational susceptibility.
- P10.7.** The trigger mechanism of hemoglobin oxygenation is shown to be due to the PJTE, which makes the iron atom position in the porphyrin plane unstable in the absence of oxygen and drives it back in plane

by oxygenation. An earlier explanation of this effect was that the out-of-plane position of the iron atom is caused by its large atomic radius in the high-spin configuration that does not fit the porphyrin cavity, and that it transfers to the low-spin (small-radius) one by oxygenation. Why is this ball-hole-fitting explanation unacceptable? (*Hint*: Utilize the discussion of this issue from Section 9.2.)

- P10.8.** Several metallobiochemical systems, such as hemoglobin, catalase, peroxidase, and cytochrome P-450, have quite similar (almost the same) iron porphyrin active sites, and their function begins by coordination of the oxygen molecule (in peroxidase the coordinated molecule is  $\text{H}_2\text{O}_2$ , which can be modeled by  $\text{O}_2$ ). Meanwhile, their biological function is quite different. How is this explained in terms of electronic structure and vibronic coupling in the active site?

## REFERENCES

- 10.1. L. Pauling, *The Nature of the Chemical Bond*, 3rd ed., Cornell Univ. Press, Ithaca, NY, 1960.
- 10.2. R. Pearson, *Coord. Chem. Rev.* **100**, 403 (1990); *Inorg. Chim. Acta* **198**, 781 (1992).
- 10.3. M. Chanon, M. D. Hawley, and M. A. Fox, in M. A. Fox and M. Chanon, eds., *Photoinduced Electron Transfer*, Part A, Elsevier, Amsterdam, 1988, p. 1.
- 10.4. J. C. Curtis and T. J. Meyer, *Inorg. Chem.* **21**, 1562 (1982).
- 10.5. M. D. Newton, in *The Challenge of d and f Electrons. Theory and Computation*, ACS Series 394, Washington, DC, 1989, p. 378.
- 10.6. V. Balzani and F. Scandola, in M. A. Fox and M. Chanon, eds., *Photoinduced Electron Transfer*, Part D, Elsevier, Amsterdam, 1988, p. 148.
- 10.7. J. Jortner and M. Bixon, *J. Chem. Phys.* **88**, 167 (1988); I. Rips and J. Jortner, *J. Chem. Phys.* **87**, 2090 (1987); J. T. Hynes, *J. Phys. Chem.* **90**, 3701 (1986); A. M. Kjaer and J. Ulstrup, *Inorg. Chem.* **25**, 644 (1986); A. Haim, *Comments Inorg. Chem.* **4**, 113 (1985).
- 10.8. J. Jortner and B. Pullman, eds., *Tunnelling*, Reidel, Dordrecht, 1986; V. I. Gol'danskii, L. I. Trakhtenberg, and V. N. Fleurov, *Tunnelling Phenomena in Chemical Physics*, Gordon & Breach, New York, 1989.
- 10.9. I. B. Bersuker, *Biofizika* **12**, 732 (1967); *Structure and Properties of Coordination Compounds* (Russ.), Khimia, Leningrad, 1971.
- 10.10. I. B. Bersuker and S. S. Budnikov, *Teor. Eksp. Khim.* **3**, 799 (1967); I. B. Bersuker and S. S. Budnikov, *Proc. IV Int. Congress on Catalysis*, Vol. **1**, Nauka, Moscow, 1970, p. 82.
- 10.11. J. E. Huheey, *J. Phys. Chem.* **69**, 3284 (1965).
- 10.12. W. Kauzmann, *Quantum Chemistry. An Introduction*, Academic Press, New York, 1957.
- 10.13. R. Taube, *Chem. Zvesti* **19**, 215 (1965).
- 10.14. Trinh-Toan, B. K. Teo, and J. A. Ferguson, *J. Am. Chem. Soc.* **99**, 408 (1977).

- 10.15. A. F. Shestakov, in G. I. Likhtenshtein, ed., *Redox Metalloenzymes and Their Models: Theoretical and Methodological Aspects* (Russ.), Part 2, AN SSSR, Chernogolovka, 1982, p. 19.
- 10.16. R. G. Parr and R. G. Pearson, *J. Am. Chem. Soc.* **105**, 7512 (1983).
- 10.17. R. F. Nalewajski, *Acta Phys. Polon.* **A77**, 817 (1990).
- 10.18. D. B. Brown, ed., *Mixed-Valence Compounds*, Reidel, Dordrecht, 1980.
- 10.19. K. Prassides, ed., *Mixed-Valency Systems: Applications in Chemistry, Physics and Biology*, NATO ASI Series C, Vol. 343, Kluwer, Dordrecht, 1991.
- 10.20. I. B. Bersuker and S. A. Borshch, *Adv. Chem. Phys.* **81**, 703 (1992).
- 10.21. S. J. Lippard, in D. B. Brown, ed., *Mixed-Valence Compounds*, Reidel, Dordrecht, 1980, p. 427.
- 10.22. N. S. Hush, *Coord. Chem. Rev.* **64**, 135 (1985).
- 10.23. A. R. Bishop, R. L. Martin, K. A. Muller, and Z. Tesanovic, *Z. Phys. B* **76**, 17 (1989).
- 10.24. L. J. de Jongh, in K. Prassides, ed., *Mixed-Valency Systems: Applications in Chemistry, Physics and Biology*, NATO ASI Series C, Vol. 343, Kluwer, Dordrecht, 1991, p. 223.
- 10.25. D. Gatteschi, R. Sessoli, and J. Villain, *Molecular Nanomagnets*, Oxford Univ. Press, 2006.
- 10.26. J. P. Lannay, in F. L. Carter, ed., *Molecular Electronic Devices II*, Marcel Dekker, New York, 1987, p. 39; C. Jioachim and J. P. Lannay, *J. Mol. Electron.* **6**, 37 (1990); I. B. Bersuker, S. A. Borshch, and L. F. Chibotaru, *Chem. Phys.* **136**, 379 (1989).
- 10.27. M. B. Robin and P. Day, *Adv. Inorg. Chem. Radiochem.* **10**, 247 (1967).
- 10.28. C. N. R. Rao, in *Theoretical and Experimental Aspects of Valence Fluctuation in Heavy Fermions*, Plenum, New York, 1987, p. 235.
- 10.29. P. N. Schatz, in K. Prassides, ed., *Mixed-Valency Systems: Applications in Chemistry, Physics and Biology*, NATO ASI Series C, Vol. 343, Kluwer, Dordrecht, 1991, p. 115.
- 10.30. K. Y. Wong and P. N. Schatz, *Progr. Inorg. Chem.* **28**, 369 (1981).
- 10.31. L. T. Zhang, J. Ko, and M. J. Ondrechen, *J. Am. Chem. Soc.* **109**, 1666 (1987).
- 10.32. S. A. Borshch and I. N. Kotov, *Zh. Strukt. Khim.* **32**, 44 (1991).
- 10.33. K. Neuenschwander, S. Piepho, and P. N. Schatz, *J. Am. Chem. Soc.* **107**, 7862 (1985).
- 10.34. M. E. Grees, C. Creutz, and C. O. Quicksoll, *Inorg. Chem.* **20**, 1522 (1981).
- 10.35. U. Furholz, H. B. Burgi, P. E. Wagner, A. Stebler, J. H. Ammeter, E. Krausz, R. J. H. Clark, M. Stead, and A. J. Ludi, *J. Am. Chem. Soc.* **106**, 121 (1984).
- 10.36. I. B. Bersuker, *The Jahn-Teller Effect*, Cambridge Univ. Press, Cambridge, UK, 2006.
- 10.37. G. Blondin, S. Borshch, and J.-J. Jirerd, *Comments Inorg. Chem.* **12**, 315 (1992).
- 10.38. P. V. Anderson and H. Hasegawa, *Phys. Rev.*, **100**, 675 (1955).
- 10.39. S. I. Klokishner, and B. S. Tsukerblat, *Chem. Phys.* **125**, 11 (1988); S. I. Klokishner, B. S. Tsukerblat, and B. L. Kushkulei, *New J. Chem.* **17**, 43 (1993).

- 10.40. H. G. Jang, S. J. Geib, Y. Kaneko, M. Nakano, M. Sorai, A. L. Pheingold, B. Monter, and D. V. Hendrickson, *J. Am. Chem. Soc.* **111**, 173 (1989).
- 10.41. T. Cambara, D. N. Hendrickson, M. Sorai, and S. Oh, *J. Chem. Phys.* **85**, 2895 (1986); R. M. Stratt and S. H. Adachi, *J. Chem. Phys.* **86**, 7156 (1987).
- 10.42. A. von Kameke, G. M. Tom, and H. Taube, *Inorg. Chem.* **17**, 1790 (1978).
- 10.43. C. A. Bignozzi, S. Roffia, and F. Scandola, *J. Am. Chem. Soc.* **107**, 1644 (1985).
- 10.44. B. H. Huynh, J. J. C. Moura, I. Moura, T. A. Kent, J. Le Gall, A. X. Xavier, and E. Munck, *J. Biol. Chem.* **255**, 3242 (1980).
- 10.45. V. Papaefthymiou, J. J. Girerd, I. Moura, J. J. Moura, and E. Munck, *J. Am. Chem. Soc.* **109**, 4703 (1987).
- 10.46. C. P. Kissinger, *J. Am. Chem. Soc.* **110**, 8721 (1988).
- 10.47. S. A. Borshch and L. F. Chibotaru, *Chem. Phys.* **135**, 375 (1989)
- 10.48. I. B. Bersuker and V. Z. Polinger, *Vibronic Interactions in Molecules and Crystals*, Springer, Berlin, 1989.
- 10.49. S. F. Sontum, L. Noodelman, and D. A. Case, in D. S. Salahub and M. C. Zerner, eds., *The Challenge of d and f Electrons. Theory and Computation*, ACS Symposium Series 394, Washington, DC, 1989, p. 366.
- 10.50. T. G. Spiro, ed., *Iron-Sulphur Proteins*, Wiley-Interscience, New York, 1982.
- 10.51. J. J. Girerd and J. P. Launay, *Chem. Phys.* **74**, 217 (1983).
- 10.52. D. Coucovanis, M. G. Kanatzidis, A. Salifogloa, W. R. Dunham, A. Simopoulos, J. R. Sams, V. Papaegthymion, A. Kostikas, and C. F. Strouse, *J. Am. Chem. Soc.* **109**, 6863 (1987).
- 10.53. V. V. Hizhnyakov and A. V. Sherman, *Phys. Stat. Solidi (b)* **92**, 77 (1979).
- 10.54. K. Prassides and P. N. Schatz, *J. Phys. Chem.* **93**, 83 (1989).
- 10.55. M. F. Perutz, *Br. Med. Bull.* **32**, 195 (1976); *Nature* **228**, 726 (1970).
- 10.56. I. B. Bersuker and S. S. Stavrov, *Coord. Chem. Rev.* **88**, 1 (1988).
- 10.57. M. Weissbluth, *Haemoglobin. Cooperativity and Electronic Properties*, Chapman & Hall, 1974.
- 10.58. J. L. Hoard, in K. M. Smith, ed., *Porphyrins and Metalloporphyrins*, Elsevier, Amsterdam, 1975, p. 317.
- 10.59. W. R. Sheidt and C. Reed, *Chem. Rev.* **81**, 543 (1981).
- 10.60. S. J. Lippard and J. M. Berg, *Principles of Bioinorganic Chemistry*, University Science Books, Mill Valley, CA, 1994.
- 10.61. W. Kaim and B. Schwederski, *Bioinorganic Chemistry: Inorganic Elements in the Chemistry of Life. An Introduction Guide*, Wiley, New York, 1994.
- 10.62. S. S. Stavrov, I. P. Decusar, and I. B. Bersuker, *Mol. Biol.* **22**, 837 (1988).
- 10.63. S. S. Stavrov, I. P. Decusar, and I. B. Bersuker, *Mol. Biol.* **21**, 338 (1987).
- 10.64. S. S. Stavrov, I. P. Decusar, and I. B. Bersuker, *New J. Chem.* **17**, 71 (1993).
- 10.65. M. K. Johnson, R. B. King, D. M. Kurtz, Jr., C. Kutal, M. L. Norton, and R. A. Scott, eds., *Electron Transfer in Biology and Solid State: Inorganic Compounds with Unusual Properties*, ACS Advances in Chemistry Series, Vol. 226, 1990.
- 10.66. R. A. Sheldon, ed., *Metalloporphyrins in Catalytic Oxydation*, Sheldon, Marcel Dekker, New York, 1994.
- 10.67. G. Berton, ed., *Handbook of Metal-Ligand Interactions in Biological Fluids. Bioinorganic Chemistry*, Vols. I, II, Marcel Dekker, New York, 1995.

---

# 11

---

## REACTIVITY AND CATALYTIC ACTION

*Chemical transformations form the heart of all of chemistry; the problem is to establish how chemical reactions, including their rates and mechanisms, depend on the structure and properties of the reactants, and to be able to control this phenomenon.*

### 11.1. ELECTRONIC FACTORS IN REACTIVITY

*Chemical reactivity* characterizes the relative ability of a molecular system to interact with other molecules (or atoms) during their collision, determining the reaction rate. It obviously also depends on the properties of the other molecule, the reagent. Therefore, reactivity is reaction-specific, and it depends on the mechanism of the *elementary act* of the reaction. In reactions with the same reagent different reactants may have different reactivities, which, however, may not necessarily be the same for different reagents.

#### **Chemical Reactivity and Activated Complexes**

The main quantitative characteristic of a chemical reaction is the *reaction rate*, which also depends on *kinetic factors*, including temperature and reactant concentrations. While kinetic factors have similar features in many reactions and can be relatively easily controlled, the elementary act is the most important stage

---

*Electronic Structure and Properties of Transition Metal Compounds: Introduction to the Theory, Second Edition* By Isaac B. Bersuker  
Copyright © 2010 John Wiley & Sons, Inc.

determining the specificity and huge diversity of chemical reactions. General presentation of the energetics of elementary chemical reactions is usually given by means of the notion of the *energy barrier of the reaction*, the activation energy  $D$ , and the exponential dependence of the reaction rate constant  $k$  on  $D$  (the *Arrhenius law*):

$$k = A \exp \frac{-D}{k_B T} \quad (11.1)$$

where  $A$  is the frequency factor,  $k_B$  is the Boltzmann constant, and  $T$  is the temperature.

Consider an elementary reaction starting with stable reactants and ending with stable products. To transform the reactant molecules to the products, some of the chemical bonds should break down, while others are formed. Usually a breakdown or activation of some bonds is required first, and then the activated bonds undergo transformations. This means that in the process of the chemical reaction the energy of the system should increase first (activation), and then decrease following the formation of new bonds.

The energy of this process is lower when the displacements of atoms realizing the breakdown of some bonds and formation of others are correlated (concerted). The generalized coordinate  $Q$  of these atomic displacements is called *the reaction coordinate* or *reaction pathway* (more, concisely, the *reaction path*). The latter is thus the generalized coordinate of correlated motions of the atoms of the reactants toward the products along which the activation energy  $D$  is minimal. The reaction pathway follows in detail (in intermediate points) the bond breakdowns and new-bond formation determining the mechanism of the elementary act of the reaction, the *reaction dynamics*.

With respect to the reaction coordinate  $Q$ , the cross section of the APES of the system (Section 7.1) appears as shown in Fig. 11.1 The configuration  $Q_D$  of the point  $M$  for which the energy of the interacting system is maximal is called *the activated state of the reaction* or *activated complex*. Sometimes the activated state is relatively stable (this possibility is shown in Fig. 11.1 by the dashed line). There are reactions with zero activation energy,  $D = 0$  (non-Arrhenius reactions); their rate is determined by kinetic factors only. By definition, the activation energy along  $Q$  is minimal; hence any other way gives a higher value of  $D$ . This means that in the extended space point  $M$  is a saddle point: a maximum along  $Q$  and a minimum along other coordinates orthogonal to  $Q$ .

According to Eq. (11.1), the rate of the elementary reaction increases exponentially with temperature. At low temperatures  $k$  is very small, but the reaction barrier can still be penetrated by quantum-mechanical tunneling. The rate of tunneling reactions is independent of temperature [11.2]. The energy barrier of the reaction is directly dependent on the structure of the reactants and the mechanism of the elementary act. For a specific mechanism, the elementary reaction rate depends on the structure of the reactants.

*The inverse of activation energy  $D^{-1}$  may be taken as a quantitative measure of the reactivity of the molecule in the reaction under consideration.* The activated



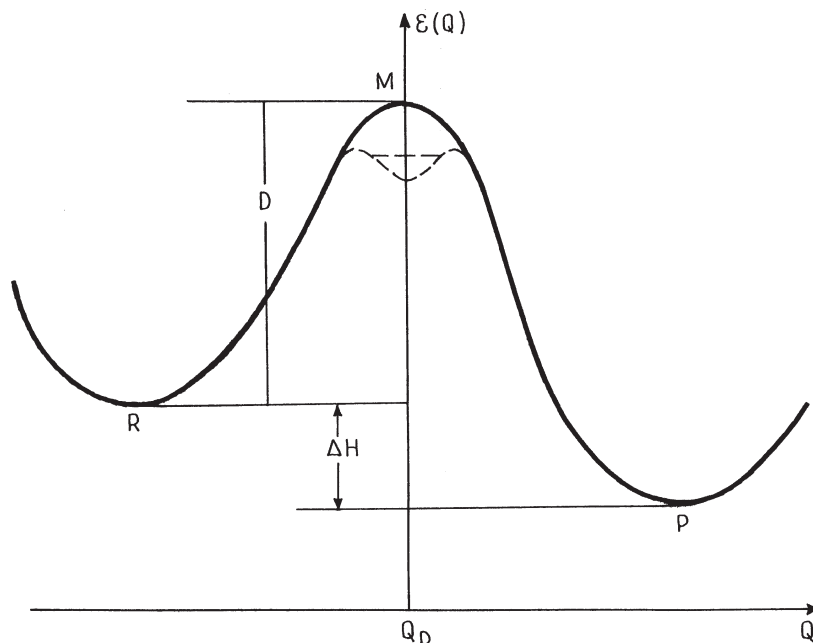


**FIGURE 11.1.** Schematic presentation of the potential energy curve of a chemical reaction along the reaction pathway (generalized coordinate)  $Q$  from the reagents (R) to the products (P) via the activated state (M).  $D$  and  $\Delta H$  denote the activation energy and heat of the reaction, respectively. The dashed line shows the possible relative stability of the activated state.

state (or the activated complex) is most important in the chemical reaction because it determines both the activation energy (the rate of the reaction) and the elementary reaction mechanism. According to quantum mechanics, the Schrödinger equation (1.5) for the saddle-point-type potential at point  $M$  of Fig. 11.1 has no stationary (localized) solutions, meaning that direct spectroscopic observation of an activated state that corresponds to this point is impossible. However, if an additional minimum at the top of the reaction curve exists (dashed line in Fig. 11.1), the state in this well may be observed by high-resolution femtosecond spectroscopy [11.3], provided its depth is greater than the kinetic energy of the corresponding nuclear motions; the state  $M$  can be regarded as an isomeric state of the system.

An interesting relation between the activation energy  $D$  and the reaction energy  $\Delta H$  (the heat of the reaction on Fig. 11.1) is given by the Marcus equation [11.4]. Derived first for electron transfer reactions, it proved to be of more general importance for many other chemical reactions. Assume that the reactants and products can be approximately characterized by two parabolas as shown in Fig. 11.2 with the reaction coordinate  $Q$  changing from  $Q = 0$  at the reactants to  $Q = Q_0$  for the products (the main conclusions do not depend crucially on this

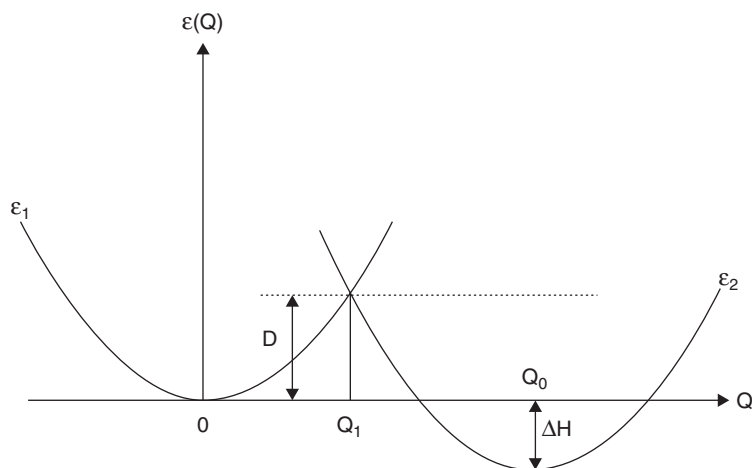


**FIGURE 11.2.** Adiabatic curves of the reactants and products as a function of the reaction path illustrating the Marcus equation.  $Q_1$  and  $Q_0$  are the coordinates of the activated complex and products, respectively;  $D$  is the activation energy, and  $\Delta H$  is the heat of the reaction.

simplified presentation). Then the two parabolas can be presented as  $\varepsilon_1 = \frac{1}{2}KQ^2$  and  $\varepsilon_2 = \left(\frac{1}{2}\right)K(Q - Q_0)^2$  (the force constants  $K$  are taken the same in both parabolas for simplicity). Their intersection at  $Q = Q_1$  may be assumed to characterize the transition state, and hence  $D$  is the activation energy. It can easily be shown that under these conditions

$$Q_1 = \frac{1}{2}Q_0 + \frac{\Delta H}{2KQ_0} \quad (11.2)$$

If the reaction is thermally neutral, that is,  $\Delta H = 0$ , then  $Q_1 = Q_0/2$ , and for such reactions the activation energy (sometimes called *intrinsic activation energy*)  $D_0 = \frac{1}{2}KQ_1^2 = \frac{1}{8}KQ_0^2$ . Obviously,  $Q_1$  decreases with the increase in the negative reaction energy  $\Delta H$  in exothermic reactions. For the activation energy  $D = \frac{1}{2}KQ_1^2$  of such reactions, we obtain

$$D = D_0 + \frac{\Delta H}{2} + \frac{(\Delta H)^2}{16D_0} \quad (11.3)$$

In essence this is the Marcus equation [11.4]. The last term in this equation is usually much smaller than the second one, so the direct conclusion from the Marcus equation is that for similar reactions (reaction with approximately the same  $D_0$ ) the difference in activation energy  $D$  is roughly half the reaction energy  $\Delta H$ , and  $D$  decreases as the reaction becomes more exothermic ( $\Delta H < 0$ ). At approximately  $\Delta H = -4D_0$  a turnover should occur as  $D$  becomes negative, but experimentally such large exothermic reactions are difficult to realize. Also,

of course, the meaning of the intrinsic activation energy  $D_0$  is not rigorously defined and it is not clear when different reactions may be considered to have approximately the same  $D_0$  value.

Some qualitative assumptions similar to the conclusions from the Marcus equation were known earlier as the *Bell–Evans–Polanyi principle* and *Hammond postulate* [11.5].

In Section 7.4 the theorem of uniqueness of the vibronic origin of molecular instability is discussed, and it is shown that in accordance with the TEST paradigm instability of the ground state is due to the vibronic mixing with stable excited states. In application to activated complexes of chemical reactions the theory predicts the existence of stable excited states in the configuration  $Q_D$  of the activated complex, provided that the two-level or a similar several-level approximation is valid.

In the two-level approximation, the curvatures of the adiabatic potential energy curves for the two states, ground 1 and excited 2, that are mixed by the vibronic coupling, are given by Eq. (7.94), from which it follows that if, at point  $Q_D$ , the ground state is unstable in the  $Q$  direction,  $K_1 < 0$ ,  $K_0^{(1)} < F^2/\Delta$ , then the excited state is stable in this direction,  $K_2 > 0$  [11.6]. The energy level of the stable excited state can, in principle, be estimated from the resonances in the *molecular beam experiments* (scattering of the reactants as a function of their kinetic energy). Some further details and useful formulas for this issue are derived and discussed in Ref. 11.7.

### Frontier Orbitals and Perturbation Theory

An important problem is to relate the reactivity and reaction mechanism to the electronic structure of the interacting systems. As mentioned in the introduction to Chapter 7, any molecular transformation begins with changes in the much less inertial electron distribution, which then impels the nuclei (via vibronic coupling) to rearrange. Therefore, the beginning of the chemical reaction should be sought for in the electronic structure of the reactants. In previous sections the interaction between two atomic groups is considered in terms of their possible bonding; here a similar interaction is studied with respect to the chemical reaction.

The outer electrons enter the interaction first. The electronic charge distribution in the separated reactants (as in any other atomic system) decreases exponentially with the distance from their nuclei, with the exponential power proportional to the electron energy (Section 2.1). Hence the outer electrons have the highest energy, and they form the HOMO. However, the interaction of the HOMO of one system with the HOMO of the other one, both occupied (Fig. 11.3a), does not change significantly the electron distribution and bonding because it results in equal population of the bonding and antibonding orbitals (Section 5.2). The inclusion of the LUMO in the bonding makes some of the bonding states uncompensated (Fig. 11.3b). The HOMO–LUMO states form *frontier orbitals*. The theory of molecular interactions in the approximation of frontier orbitals has been developed by Fukui [11.8].

In many cases, particularly with transition metal participation, not one but several HOMOs and LUMOs, as well as single-electron occupied MOs (SOMOs), are active in the intermolecular interaction. In a more rigorous treatment all the orbitals of corresponding symmetry may be involved in the interaction, but in a qualitative treatment some of those MOs that are energetically close to the frontier orbitals may be distinguished as giving the major contribution. This group of active MOs is sometimes called *generalized frontier orbitals*.

With respect to frontier orbitals, chemical reactions can be divided into three types, illustrated schematically in Fig. 11.4. In the first type (Fig. 11.4a) the reactant participates in the interaction with its HOMO, while the reagent provides its LUMO (*electrophilic reagent*). This interaction has a donor–acceptor nature (Sections 6.1 and 10.1). In Fig. 11.4b the second type of reaction, with a *nucleophilic reagent*, is shown. Finally, the reagent shown in Fig. 11.4c has an unpaired electron on the HOMO (*radical reagent*) that participates in the interaction as both a HOMO and a LUMO; the reactant in this condition also takes part with both HOMO and LUMO (*exchange reactions*).

In Section 10.1, it is shown how the interaction between two molecular groups results in electron charge transfer from one of them to another, but the energetics of this interaction, which determines the activation energy and reaction path, is not considered there. At a relatively large distance the interaction energy can be estimated using perturbation theory [11.8, 11.9]. The idea is to consider the frontier orbitals of the reactant perturbed by the formation of MOs with the reagent. The situation is similar to that of weak covalence considered in Section 5.2. Using formulas similar to Eqs. (5.30) and (5.31), and omitting the intermediate transformations, we come to the following expression for the energy of two interacting atoms  $s$  and  $t$  of the molecular groups [11.8, 11.9]:

$$\Delta E = \frac{-q_s q_t}{R_{st} \varepsilon} + 2 \sum_m \sum_n \frac{(c_s^m c_t^n \beta_{st}^{mn})^2}{E_m^s - E_n^t} \quad (11.4)$$

In this equation  $q_s$  and  $q_t$  are the atomic charges of the  $s$  and  $t$  atoms;  $R_{st}$  is the distance between them;  $\varepsilon$  is the effective dielectric constant of the medium (solvent);  $c_s^m$  and  $c_t^n$  are the LCAO coefficients of the MOs  $m$  and  $n$ , respectively, in which the atoms  $s$  of the reactant and  $t$  of the reagent take part;  $\beta_{st}^{mn}$  is the corresponding resonance integral between the two interacting states; and  $E_m$  and  $E_n$  are the MO energies. The summation in (11.4) is carried out over the HOMOs  $m$  in the reactant and LUMOs  $n$  in the reagent in donor–acceptor (electrophilic) reactions (Fig. 11.4a), and vice versa in nucleophilic reactions (Fig. 11.4b). In exchange reactions with radicals both  $m$  and  $n$  contain HOMOs and LUMOs, but in each term one of the indices belongs to HOMOs and the other to LUMOs (otherwise the corresponding contribution to the bonding, as shown in Fig. 11.3, is near zero). If there are more than one pair of interacting atoms, Eq. (11.4) should be summed over all of them.

The first term in Eq. (11.4) denotes the electrostatic interaction between the atoms  $s$  and  $t$ , while the second term represents the covalence contribution

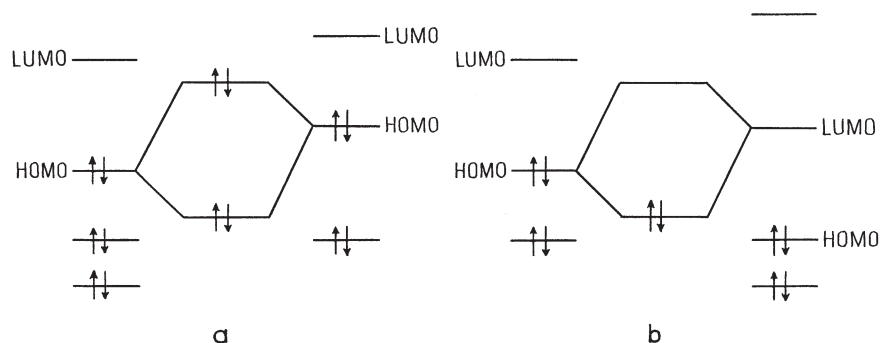


**FIGURE 11.3.** Frontier orbital interactions: HOMO–HOMO interaction in (a) does not result in MO bonding (the bonding and antibonding MO compensate each other), whereas HOMO–LUMO in (b) does.

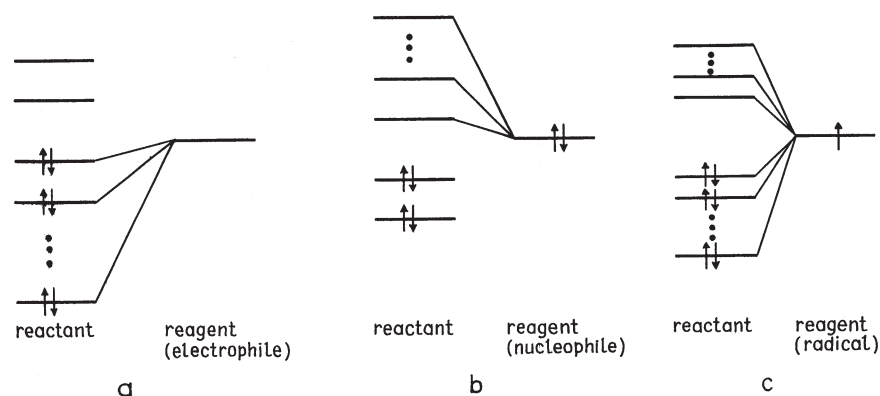


**FIGURE 11.4.** HOMO and LUMO in the interaction of a reactant with an electrophile (a), nucleophile (b) and radical (c) reagent. (From Fukui [11.8].)

of orbital overlap and formation of MOs. The latter demands nonzero overlap between the HOMOs of the reactant with the LUMOs of the reagent, or vice versa, and small energy separation between them. Depending on the electronic structure of the interacting groups, the two terms in Eq. (11.4), *electrostatic* and *covalent*, can be of different orders of magnitude. Therefore, it is convenient to consider two cases: (1) the electrostatic term is predominant and the covalent contribution can be neglected—*charge-controlled reactions*; and (2) the electrostatic term can be neglected as compared with the covalent contribution—*orbital-controlled reactions*. Certainly, there are reactions that may be classified as both charge- and orbital-controlled.

The difference between charge-controlled and orbital-controlled reactions may be very significant. Indeed, electrostatic interactions are scalar and do not require specific orientations of the interacting species, whereas MO formation is possible

only between appropriately oriented orbitals that give nonzero overlap. Hence, unlike charge-controlled reactions, *orbital-controlled reactions are stereoselective* (see discussion of orbital symmetry rules below).

Provided that the mutual orientation of the interacting groups is not restricted, there are always such positions when the overlap of the corresponding orbitals is nonzero. But this does not mean that the reaction is necessarily orbital-controlled, even when the charges are small, because the energy difference  $E_m - E_n$  between the overlapping orbitals may be large, making the corresponding terms in (11.4) small; orbital-controlled reactions require small energy gaps between the overlapping HOMOs of the reactant and the LUMOs of the reagent (Fig. 11.4). In particular, when the HOMOs and LUMOs in question are almost degenerate,  $E_n \approx E_m$ , the perturbation problem should be solved for a degenerate state; then the covalent contribution to the interaction energy  $\Delta E$  is due mainly to this degenerate interaction:

$$\Delta E \approx 2c_s^m c_t^n \beta_{st}^{mn} \quad (11.5)$$

The role of orbital overlap in the reactant–reagent interaction allowed Fukui [11.8] to formulate a *general orientation principle*:

A majority of chemical reactions are liable to take place at the position and in the direction where the overlapping of HOMO and LUMO of the respective reactants is maximum; in the electron-donating species, HOMO predominates in the overlapping interaction, whereas LUMO does so in an electron-accepting reactant; in the reacting species which have SOMO's these play the part of HOMO or LUMO, or both.

The theory of frontier orbitals in reactivity was created mainly for organic compounds [11.8, 11.9], but its basic features, especially the perturbation theory formulas (11.4), (11.5), can also be applied to coordination compounds with the metal atom participation. In these cases, the number of interacting HOMOs and LUMOs is usually larger than for organic compounds. For this reason, and due to the specificity of *d* orbitals, the exploitation of reactivity indices (frontier electron density, delocalizability, superdelocalizability, etc. [11.8]) is less important for transition metal coordination compounds.

The electrostatic term in (11.4) may be more important for transition metal compounds than for organic compounds. Even when the interacting atomic groups are initially neutral, they may become charged as a result of the interaction due to charge transfer. These charges may be small, and hence the covalent term in the interaction can be predominant, but the electrostatic term cannot be a priori neglected.

### Orbital Symmetry Rules in Reaction Mechanisms

Orbital symmetry rules in the mechanisms of chemical reactions follow directly from the above mentioned treatment of intermolecular interactions that precede

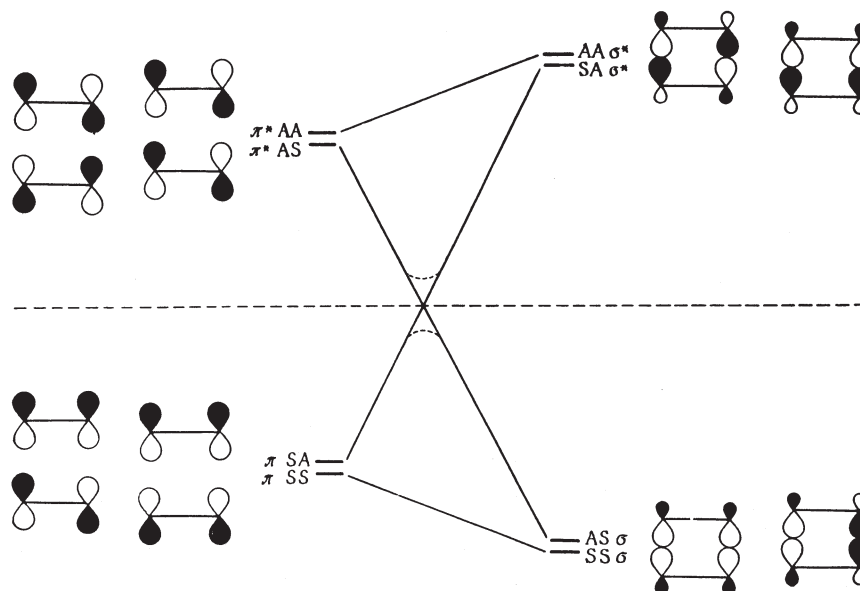


**FIGURE 11.5.** MO energy-level correlation diagram illustrating the Woodward–Hoffmann orbital symmetry rule in formation of cyclobutane from two ethylene molecules. *S* and *A* indicate the symmetry properties, symmetric and antisymmetric, respectively, with respect to reflections in the two symmetry planes of the rectangular transition state. (From Woodward and Hoffmann [11.10].)

the reaction. The covalent contribution to this interaction, discussed above, is determined by the overlap of the orbitals of the interacting atoms, which depends strongly on their mutual orientation. Therefore, for orbital-controlled reactions, the energy of the activated complex (the energy barrier of the reaction) depends strongly on the mutual orientation of the interacting species. The overlap between atomic orbitals is nonzero if they possess the same symmetry properties (Section 2.1) in the molecular configuration of the activated complex. Hence the latter should be chosen to satisfy the condition of the same symmetry of the close-in-energy interacting HOMOs and LUMOs of the reactants and reagents. In other words, in order to ensure a low-energy barrier of the chemical reaction, the orbital overlaps that promote the formation of new bonds should be sufficiently large to compensate for the breakdown of the old bonds in the process of the reaction.

Orbital symmetry rules were suggested and developed for widespread use by Woodward and Hoffmann [11.10]. In Fig. 11.5 the visual treatment of these rules is reproduced for the formation of cyclobutane from two ethylene molecules through the rectangular activated complex. It is seen that the formation of  $\sigma$  bonds between the carbon atoms of the two molecules (before the break of the  $\pi$  bonds in each molecule) can take place only by involving excited MOs that have the same symmetry as the ground state. If the corresponding excited state, as in

ethylene, is too high in energy, the formation of  $\sigma$  bonds does not compensate for the breakdown of the  $\pi$  bonds.

This is seen from the one-electron MO correlation diagram (Fig. 11.5), in which the energy levels of the newly formed MOs and the old MOs that are broken in the process of the reaction are connected by straight lines. Because of the high position of the appropriate excited MO, the corresponding lines in Fig. 11.5 rise steeply, and in the intermediate area corresponding to the activated complex the energy is rather high—the reaction barrier assumes high values. The latter can be estimated approximately by accounting for the fact that the excited state under consideration corresponds to a transition of the bonding electrons to the antibonding MO (in both molecules), resulting in an excitation energy of  $\sim 5$  eV (115 kcal/mol).

A more detailed energy-level diagram for this system [11.10] shows that, along with the abovementioned excited states, there are others much lower in energy but of different symmetry. In particular, if starting from an appropriate excited state, the two ethylene molecules can form the cyclobutane molecule (also in its excited state) without any activation barrier. Consequently, this reaction is allowed as a photochemical reaction.

Further developments and other formulations of the orbital symmetry rules were suggested by Pearson, based on the work of Bader [11.11] and others (see Pearson's book [11.12] and references cited therein). We demonstrate here a treatment that employs the pseudo Jahn–Teller effect (PJTE) [11.6], which seems to be more appropriate to transition metal coordination compounds under consideration. From the results obtained in Section 7.4, we know that if there is only one active excited state  $\Gamma'$  that is sufficiently close in energy to the ground state of the activated complex, the nuclear configuration of the latter softens in a particular direction  $Q_{\Gamma^*}$ , and this coordinate is determined by the condition that the vibronic constant  $F^{(\Gamma\Gamma')} = \langle \Gamma | (\partial V / \partial Q_{\Gamma^*})_0 | \Gamma' \rangle$  is nonzero. The symmetry  $\Gamma^*$  of this  $Q_{\Gamma^*}$  displacement is determined by the symmetries of the wavefunctions of the states  $\Gamma$  and  $\Gamma'$ :  $\Gamma^* = \Gamma \times \Gamma'$ . Therefore, if the symmetries of the ground and corresponding excited states of the activated complex are known, the direction of its labilization (and hence a specific mechanism of the reaction) can be predicted.

Consider two approaching molecular closed-shell systems  $A$  and  $B$ , each of which is stable separately. The interaction forms a united system leading to the activated complex  $AB$  with its own symmetry and own energy spacing  $\Delta$ . What are the directions of the lowest (or even negative) curvature of the adiabatic curve of the  $AB$  system? To answer this question using the vibronic coupling approach, the symmetries of the wavefunctions of the ground and low-lying excited states are needed. If the two molecules  $A$  and  $B$  are approaching each other with an unchanged mutual orientation, meaning that the symmetry group of the complex  $AB$  remains the same (and only intermolecular interatomic distances change), the coordinate of the reaction  $Q_{\Gamma^*}$  is totally symmetric with respect to the activated complex  $AB$ . Therefore, the reaction mechanism under consideration is allowed if and only if the wavefunctions of the HOMO of  $A$   $\psi_1^A$  and LUMO of  $B$   $\psi_2^B$  (or  $\psi_1^B$  and  $\psi_2^A$ ) have the same symmetry (a nonzero overlap integral) in the  $AB$



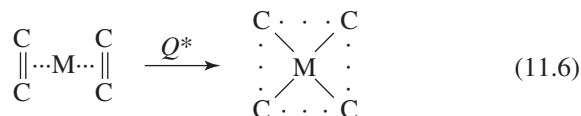
configuration. Otherwise, the reaction mechanism is forbidden. This explains the origin of the expression *preservation of orbital symmetry in chemical reactions*. This term is also related to the general preservation rules [11.13]. If there are several close-in-energy HOMOs and/or LUMOs, the contribution of each pair of these MOs should be examined and the results summarized (strictly speaking, the multilevel problem must be solved). It was shown that the vibronic approach contains all the features of the phenomenon and adds some quantitative criteria for favorable mechanisms of the reaction (the criteria of HOMO–LUMO pseudo JTE).

The orbital symmetry rules in their qualitative version are widely used in the study and prediction of elementary reaction mechanisms. Examples of these applications can be found in monographs, reviews, and original papers [11.10], [11.12]. Following the orbital symmetry rules, a forbidden reaction between two molecular systems may become allowed by interaction with a third molecular system (the catalyst). Example 11.1 elucidates this important issue.

### EXAMPLE 11.1

#### *Orbital Symmetry Rules and Vibronic Coupling in Formation of Cyclobutane from Ethylene with Catalyst Participation*

Without the catalyst, the reaction of formation of cyclobutane from two ethylene molecules via a rectangular activated complex is forbidden. Its MO energy-level correlation diagram is given in Fig. 11.5. Following Mango and Schachtschneider [11.14] (who were the first to consider this case), we assume that both molecules are *cis*-coordinated to the transition metal atom M with the two C=C bonds perpendicular to the plane of the metal–ligand bonds. The two coordinated parallel ethylene molecules, by moving along the  $Q^*$  coordinate, which preserves their rectangular arrangement, produce the coordinated cyclobutane molecule (the atom M is beyond the plane):



One can see that with the participation of the metal atom, the symmetry of the system and the symmetry of the reaction coordinate  $Q^*$  are the same as for the reaction without catalyst participation. In particular, the two planes of symmetry are preserved with respect to reflections, and hence the classification of the MO states remains as shown in Fig. 11.5. However, *the positions of the MO energy levels under the influence of the*

metal atom vary significantly, and this is the main effect of the catalyst in the scheme under consideration.

In Fig. 11.6 the MO correlation diagram for this case with a transition metal M that has the electronic configuration  $d^8$  is given; only the  $\pi$  bonds of the ethylene molecules (transforming to  $\sigma$  bonds in cyclobutane) and the  $d$  states of metal atom are shown; the  $s$  and  $p$  states of the metal are omitted. These energy levels must be populated by six electrons (two electrons from the  $d^8$  metal and two electrons from each of the two ethylene molecules). As compared with the MO correlation diagram without the metal participation (Fig. 11.5), the energy levels of the cyclobutane molecule vary substantially; for the antibonding  $\sigma$  MO ( $\sigma_1^* + \sigma_2^*$ ) with SA symmetry the energy lowers, while the AS ( $\sigma_1 - \sigma_2$ ) MO energy increases. As a result, the energy gap  $\Delta$  between the ground and excited states decreases and the vibronic reduction of the APES curvature in the  $Q^*$  direction increases; the reaction barrier (its top shown in Fig. 11.6 as the  $d^8$  crossing) becomes essentially smaller. For  $d^{10}$  metals these (or somewhat changed) energy levels should be occupied by eight electrons resulting in the population of the  $b_2^*(d_{x^2-y^2})$  and  $b_2(\sigma_1^* + \sigma_2^*)$  levels (Fig. 11.6). It does not significantly increase the reaction barrier (shown in Fig. 11.6 as  $d^{10}$  crossing). These results agree

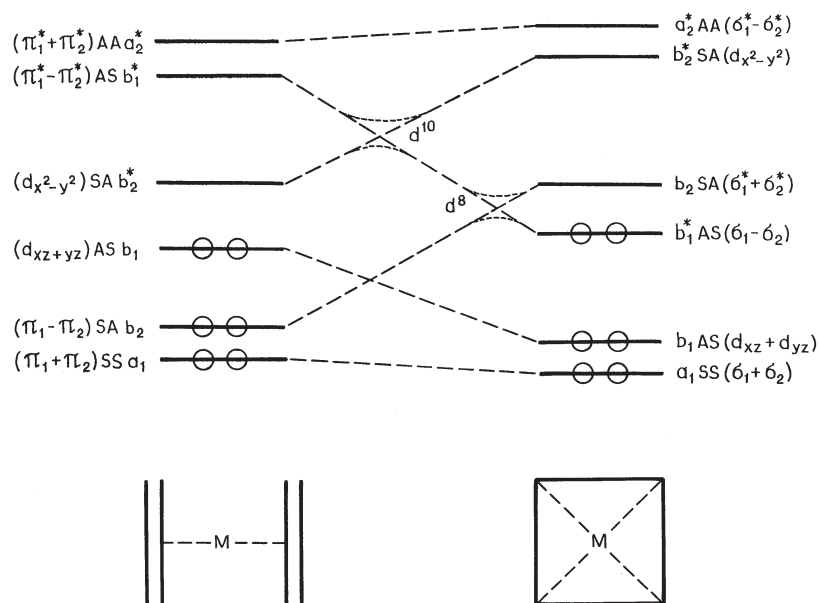


**FIGURE 11.6.** Correlation diagram for cyclobutane formation from two ethylene molecules with catalyst (transition metal M) participation. The crossings  $d^8$  and  $d^{10}$  illustrate the reaction barrier formation for the corresponding metal  $d^n$  configurations.

well with the empirical data on the  $d^8$  and  $d^{10}$  metal activity as catalyst in the reactions in question [11.14]. Quantitatively, the catalyst influence depends critically on the magnitude of the energy level shifts produced by coordination to the metal and the corresponding vibronic constant  $F$  in Eq. (7.71).

## 11.2. ELECTRONIC CONTROL OF CHEMICAL ACTIVATION VIA VIBRONIC COUPLING

### Chemical Activation by Electron Rearrangement

As stated in the previous section, the dependence of the rate of the elementary act of the chemical reaction on the activation energy  $D$  is exponential [Eq. (11.1)], and hence even a small change of  $D$  results in a considerable change of the reaction rate;  $D^{-1}$  can be taken as a measure of reactivity of one of the reactants in the reaction with the other one. To lower the  $D$  value from  $D_0$  to  $D$  means to activate the molecule; therefore, the change  $-\Delta D = D - D_0$  can be called *chemical activation*. How can chemical activation be controlled? To answer this question, consider the rising portion of APES of the chemical reaction from the minimum  $R$  to the maximum  $M$  (Fig. 11.1). For simplicity, let us present this curve by a cubic polynomial (presentation by Morse potentials may also be useful [11.17a]):

$$\varepsilon(Q) = a + bQ + cQ^2 + dQ^3 \quad (11.7)$$

The constants in this polynomial have a clear physical meaning. By choosing the energy reference  $\varepsilon(0) = 0$ , we get  $a = 0$ ;  $(\partial\varepsilon/\partial Q)_0 = F$  is the force acting on the nuclear framework in the  $Q$  direction at  $Q = 0$ , that is, it coincides with the definition of the linear vibronic constant  $F$  (Section 7.2), hence  $b = F$ ;  $\frac{1}{2}(\partial^2\varepsilon/\partial Q^2)_0 = K$  is the curvature at the minimum (or the force constant), hence  $c = \frac{1}{2}K$ ; and  $d$  is the cubic anharmonicity that is convenient to denote by  $d = -\gamma$ . If the point  $Q = 0$  is taken at the minimum, then the system is in equilibrium at this point,  $F = 0$ , and the reaction curve appears as follows (the subscript zero at  $\varepsilon$ ,  $K$ , and  $\gamma$  denotes initial values):

$$\varepsilon_0(Q) = \frac{1}{2}K_0Q^2 - \gamma_0Q^3 \quad (11.8)$$

By differentiating, one can easily ensure that in these notations (where  $Q_{0D}$  is the coordinate of the maximum of the energy barrier)

$$D_0 = \frac{K_0^3}{54\gamma_0^2} \quad (11.9)$$

$$Q_{0D} = \frac{K_0}{3\gamma_0} = \left(\frac{6D_0}{K_0}\right)^{1/2} \quad (11.10)$$

It is seen that if  $F = 0$ ,  $D_0$  is determined by only two parameters,  $K_0$  and  $\gamma_0$ , and by all three parameters  $F$ ,  $K_0$ , and  $\gamma_0$ , if  $F \neq 0$ . Hence, to change the  $D$  value, one must change some or all of these parameters *without changing the reactants*. The only way to do this is to change their electronic state, *to rearrange the electronic structure*. There are several ways to rearrange the electronic structure of the reactants, including excitation, oxidation, reduction, ionization, and chemical perturbation by involving another molecular system. The latter thus acts as a *catalyst*.

To study the influence of electron rearrangements on chemical activation, the results of the vibronic coupling theory (Sections 7.2 and 7.4) and especially the use of orbital vibronic constants (Section 7.2) may be most efficient [11.15–11.17]. The orbital vibronic constants  $f_{\Gamma^*}^{(ij)}$  and orbital contribution to the force constant  $k_{\Gamma^*}^i$  as defined by (7.25) and (7.29), respectively, are employed below. For simplicity, the indication of the representation  $\Gamma^*$  of the reaction coordinate  $Q$  is sometimes omitted.

As formulated in Section 7.2, the diagonal linear orbital vibronic constant (OVC)  $f_{\Gamma^*}^i$  equals the force with which the electron of the  $i$ th MO distorts the nuclear framework in the direction of the symmetrized displacements  $Q_{\Gamma^*}$  minus the proportion of the nuclear repulsion force in this direction per electron. Consequently, the total force distorting the molecule in this direction (the integral vibronic constant  $F_{\Gamma^*}^\Gamma$ ) is given by Eq. (7.26):  $F_{\Gamma^*}^\Gamma = \sum_i q_i^\Gamma f_{\Gamma^*}^i$  (the “addition rule”);  $q_i^\Gamma$  is the electron occupation number for the  $i$ th MO in the electronic state  $\Gamma$  under consideration. If the system is (statically) stable with respect to the  $Q_{\Gamma^*}$  displacement, then  $F_{\Gamma^*}^\Gamma = \sum_i q_i^\Gamma f_{\Gamma^*}^i = 0$ . The OVC are different for different orbitals; the nuclear repulsion per electron is independent of the MO, whereas the electron distribution changes considerably from one MO to another. In particular, in diatomics the bonding influence of the electron of the bonding MO is stronger than the nuclear repulsion per electron,  $f_R^i > 0$  (where  $R$  is the interatomic distance), whereas the opposite is true for the antibonding orbitals:  $f_R^i < 0$ . The OVC are thus a measure of the MO bonding. At the point of stability these different values of OVC are exactly compensating each other and  $F_{\Gamma^*}^\Gamma = 0$  holds. Similar relationships can be obtained for the off-diagonal OVC and orbital force constants given by Eqs. (7.28) and (7.29).

By coordination of a ligand to the activation center their electronic distributions change. If sufficiently small, the variation in electronic structure in the first approximation can be described by the changes in MO electronic occupation numbers—orbital charge transfers  $\Delta q_i$  (Sections 5.2, 10.1, and 6.3). If these  $\Delta q_i$  values are not very large (usually of the order of one electron), one can use them as characteristics of the perturbational intermolecular influence by coordination (the ratio  $\Delta q_i/q$ , where  $q$  is the total electronic charge, may be used as a measure of perturbation of the system by orbital charge transfers).

The electronic redistribution is thus presented by the new orbital occupation numbers  $q_i^\Gamma + \Delta q_i$ . If the initial system is stable,  $F_{\Gamma^*}^\Gamma = 0$  and  $K_{\Gamma^*} > 0$  (the superscript  $\Gamma$  of the electronic state of the system as a whole is omitted), the substitution  $q_i \rightarrow q_i + \Delta q_i$  in Eqs. (7.26) and (7.29) lead to the following

relationships:

$$F_{\Gamma^*} = \sum_i \Delta q_i f_{\Gamma^*}^i \quad (11.11)$$

$$\Delta K_{\Gamma^*} = K'_{\Gamma^*} - K_{\Gamma^*} = \sum_i \Delta q_i k_{\Gamma^*}^i + \sum_{i \neq j} \frac{q_i \Delta q_j |f_{\Gamma^*}^{(ij)}|^2}{\Delta_{ji}} \quad (11.12)$$

Hence the electronic rearrangement, included in the changes in orbital occupancies  $\Delta q_i$ , results in a nonzero distorting force  $F_{\Gamma^*} \neq 0$  and a change in the force constant  $\Delta K_{\Gamma^*}$  in the direction  $Q_{\Gamma^*}$ , for which  $f_{\Gamma^*}^i \neq 0$  and/or  $f_{\Gamma^*}^{(ij)} \neq 0$  ( $i$  is the index of the MO for which  $\Delta q_i \neq 0$ ). The direction of the distorting force  $Q_{\Gamma^*}$  depends on the symmetry  $\Gamma_i$  of the  $i$ th MO. As mentioned in Section 7.2,  $f_{\Gamma^*}^i$  is nonzero if the symmetric product  $[\Gamma_i \times \Gamma_i]$  contains  $\Gamma^*$  (Section 3.4 and Table A1.14). If  $\Gamma_i$  is nondegenerate,  $\Gamma = A_1$  is totally symmetric; electrons of nondegenerate MOs distort the molecule in the direction of totally symmetric displacements  $A_1$  which do not change the symmetry of the system. If  $\Gamma_i$  is degenerate,  $\Gamma^*$  can be nontotally symmetric, but it should be Jahn–Teller active.

As for the change in the force constant  $\Delta K_{\Gamma^*}$ ,  $\Gamma^*$  can be of any symmetry allowed in the corresponding point group. This is seen directly from the second term in Eq. (7.29), in which  $f_{\Gamma^*}^{(ij)}$  is nonzero if  $\Gamma^* = \Gamma_i \times \Gamma_j$ , while  $\Gamma_i$  and  $\Gamma_j$  for the ground and excited states, respectively, may belong to any symmetry representations. Similar expressions can be obtained for the change in anharmonicity constants  $\Delta\gamma$ .

*The occurrence of distorting forces and changes in the force constants and anharmonicities due to electronic rearrangements directly explain the change in the reactivity of the molecule—its chemical activation.* With the new constants of the rearranged electronic structure  $F$ ,  $K = K_0 + \Delta K$ , and  $\gamma = \gamma_0 + \Delta\gamma$ , the rising portion of the reaction curve becomes as follows (Fig. 11.7):

$$\varepsilon(Q) = FQ + \frac{1}{2}KQ^2 - \gamma Q^3 \quad (11.13)$$

This equation differs from (11.8) and yields a different activation energy of the reactions  $D$ :

$$D = \frac{(K - 6\gamma Q_0)^3}{54\gamma^2} \quad (11.14)$$

where  $Q_0$  is the new equilibrium position of the reactants (for the unperturbed system  $Q = 0$ ):

$$Q_0 = \frac{K}{6\gamma} \left[ 1 - \left( \frac{1+12\gamma F}{K^2} \right)^{1/2} \right] \quad (11.15)$$

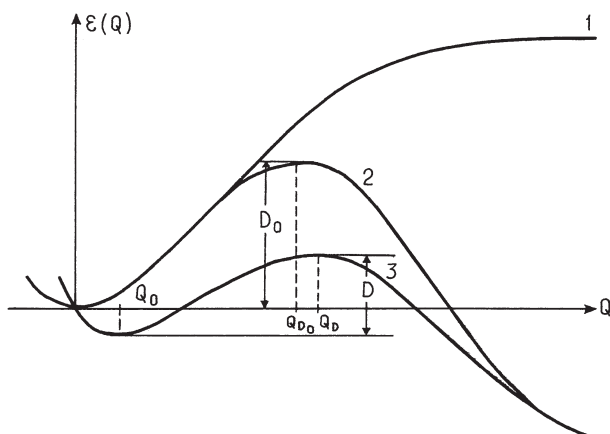


**FIGURE 11.7.** Cross section of the APES of a molecular system in the direction of the reaction path  $Q$ : (1) free molecule (*dissociation curve*); (2) influence of another reactant (*reaction curve*); (3) influence of the catalyst (*activation curve*).

The new position of the maximum of the energy barriers is

$$Q_D = \frac{K}{3\gamma} - Q_0 \quad (11.16)$$

Compared with the nonperturbed values, we have

$$\frac{D}{D_0} = \frac{(K - 6\gamma Q_0)^3 \gamma_0^2}{K_0^3 \gamma^2} \quad (11.17)$$

All the parameters on the right-hand side of (11.17) can be, in principle, estimated from empirical data.  $K$  and  $K_0$  are directly related to IR spectra:  $K_0 = M\omega_0^2$ , and  $K = M\omega^2$ , where  $\omega_0$  and  $\omega$  are the corresponding vibrational frequencies of the reactants in the initial and electronically rearranged states, respectively;  $Q_0$  is the new equilibrium position (distortion) in the rearranged state. The coefficients in the cubic terms  $\gamma_0$  and  $\gamma$  can be expressed by spectroscopic anharmonicity correction  $\omega x$  [11.18]:  $\gamma_0/\gamma = \beta^{1/2}(K_0/K)^{3/2}(\hbar\omega/\hbar\omega_0) = \beta^{1/2}K_0/K$ , where  $\beta = \omega_0 x_0/\omega x$  is the ratio of the anharmonicity corrections in the initial and rearranged system, respectively (usually, for small rearrangements  $\beta$  does not differ very much from a unity).

For chemical activation, as defined at the beginning of this section, we have

$$-\Delta D = D - D_0 = D_0 \left[ 1 - \left( \frac{K}{K_0} \right)^3 \left( \frac{\gamma}{\gamma_0} \right)^2 \right] + \frac{K^2 Q_0}{3\gamma} - 2K Q_0^2 + 4\gamma Q_0^3 \quad (11.18)$$

The last term proportional to  $Q_0^3$  is very small ( $Q_0$  is of the order of  $10^{-1}$  Å) and can be neglected. The remaining expression can be presented by two terms:

$$-\Delta D = D_0 \left( 1 - \beta \frac{K}{K_0} \right) + K Q_0 (Q_D - Q_0) \quad (11.19)$$

where  $Q_D - Q_0 = Q'_D$  is the coordinate distance between the minimum  $R$  and maximum  $M$  in the rearranged system (Fig. 11.10), and in the same notations  $Q_D = (6\beta D_0/K_0)^{1/2} - Q_0$ . The following formula may be convenient:

$$\frac{D}{D_0} = \frac{K}{\beta^{1/2} K_0} \left( \frac{Q'_D}{Q_{0D}} \right)^3 \quad (11.20)$$

The first term on the right-hand side of the equation of chemical activation (11.19) gives the contribution of the softening (hardening) by the electronic rearrangement, while the second term represents a similar contribution of the distortion force (it equals the work of the force  $F = K_0 Q$  along the distance  $Q'_D$ ).

In both terms the anharmonicity is essential since it forms the barrier itself (without anharmonicity there is no maximum of the reaction curve), although the influence of the change in anharmonicity (the ratio of anharmonicities) in the first term presented by the parameter  $\beta$  can be small. With the parameters  $F$  and  $\Delta K$  calculated by Eqs. (11.11) and (11.12), and  $\Delta\gamma$  after a similar equation, one can estimate  $K$  and  $\gamma$  ( $K_0$  and  $\gamma_0$  are assumed to be known) and the chemical activation  $-\Delta D$ . Another, much easier, way to use Eq. (11.17) or (11.18) is to estimate the parameters from empirical data.

For a polyatomic molecule with many degrees of freedom the consideration and conclusions presented above apply to each normal coordinate, in particular, to the reaction path (which may be a linear combination of normal coordinates). In these multidimensional cases the expressions obtained above can also be used for determining the change in molecular geometry by electronic rearrangement (Section 9.2).

Equation (11.19) is approximate and is valid only for small changes in the electronic structure as compared with the initial structure. Such electronic rearrangement occurs in the abovementioned processes of oxidation, reduction, excitation, ionization, and coordination of one molecular system to another molecule (in the process of chemical reaction) or to a coordination center as a ligand, on a solid surface (chemical adsorption), and so on.

The latter cases can be jointed together under a common title of *activation by coordination*. This topic is of special importance. The changes in MO occupancies due to the charge transfers to the coordination center and back are fractional. While the cases of integer charge transfers (oxidation, reduction, ionization, excitation, etc.) can in principle be treated by other methods (e.g., by quantum-chemical calculations of the electronic structure of the initial and final systems), the approximate analysis of the properties of molecular systems with fractional charges can apparently be carried out only by the approach described above involving the OVC, although, of course, there is the possibility of calculating the full electronic structure of the whole system with and without the ligand, and with and without the other reactant, which is impractical in many cases.

The assumption of weak changes in the electronic structure by coordination is valid in many systems. It is confirmed by spectroscopic investigations indicating that the coordinated molecule preserves its main individual structural features moderately changed by coordination. Certainly, this assumption is not always true. For example, the hydrogen molecule may dissociate by coordination, thus changing its structural features. Even in these cases, if the process is evaluated according to the abovementioned approach at an early stage when the coordination is still sufficiently weak, the direction of the reaction, as well as some other features, may be predicted qualitatively.

### Activation of Small Molecules by Coordination: Semiempirical Approach

Chemical activation due to electron rearrangements induced by interaction with (or coordination to) another molecular system are of special interest; they model the activation mechanism in catalysis. To consider this activation in the scheme described above, the orbital charge transfers  $\Delta q_i$ , orbital vibronic constants  $f^i$ , orbital contributions to the force constant  $k^i$ , and anharmonicities for each MO of the activated molecule are needed [see Eqs. (11.11), and (11.12)].

First, we note the importance of the number of MOs involved in the coordination. Mono-, di-, and multiorbital bonds with ligands are considered in Section 6.3. The number of active MOs is important, in particular, because it influences the orbital charge transfers  $\Delta q$ . As mentioned in Section 6.3, the total transfer by coordination  $\Delta q = \sum_i \Delta q_i$  cannot be very large owing to thermodynamic restrictions (cf. the electroneutrality principle proposed by Pauling [11.19]). Therefore, the absolute values of  $\Delta q_i$  may be large, in principle, only if more than one orbital is involved in the bonding and they have different signs. When only two orbitals are involved in the bonding—the HOMO and LUMO (diorbital bonds, Section 6.3)—the two  $\Delta q_i$  values often have opposite signs:  $\Delta q_1 < 0$  and  $\Delta q_2 > 0$ . If the HOMO is bonding [i.e.,  $f^{(1)} > 0$ ] and the LUMO is antibonding [ $f^{(2)} < 0$ ], then the resulting distorting force, according to Eq. (11.11), is

$$F = \Delta q_1 f^{(1)} + \Delta q_2 f^{(2)} = -(|\Delta q_1| |f^{(1)}| + |\Delta q_2| |f^{(2)}|) \quad (11.21)$$

In other words, the contribution of the two orbitals to the distorting force equals the sum of their absolute values, whereas the total charge transfer  $\Delta q = \Delta q_2 + \Delta q_1$  may be very small. Similar conclusions are valid for the contributions to the change of the force constant and anharmonicities. Consequently, the greater the absolute values of the two charge transfers of opposite sign, the greater the mutual vibronic influence of the interacting molecular systems. If there are more than two orbitals active in the bond formation, the possibility of a favorable combination of charge transfers that would increase the vibronic influence (but preserve the required small total charge transfer  $\Delta q$ ) increases.

Hence the conclusion follows concerning *the role of multiorbital bonding in the vibronic influence* of one molecular system on another as, for example, in chemical activation in catalysis. *The special role of transition and rare-earth*



*elements and their compounds in chemical activation and catalysis is due to the ability to form multiorbital bonds with various molecular groups.*

For concrete calculations the values of OVC and orbital charge transfers  $\Delta q_i$  are required. The latter are determined by the electronic structure of both the coordinated molecule and the coordination center, as well as by the geometry of coordination. The mode of coordination determines which orbitals of the coordinated molecule overlapping those of the coordination center have the largest changes  $\Delta q_i$ . Examples in Section 6.3 illustrate how these values can be calculated. Following are some semiempirical schemes and illustrative examples.

Consider the HOMO–LUMO two-orbital approximation. Neglecting the changes in the MO occupation numbers for the inner orbitals, one can essentially simplify Eqs. (11.11) and (11.12), which can be written in the following form (where 1 and 2 refer to HOMO and LUMO, respectively):

$$\begin{aligned} F &= f^{(1)} \Delta q_1 + f^{(2)} \Delta q_2 \\ \Delta K &= k^{(1)} \Delta q_1 + k^{(2)} \Delta q_2 \\ \beta - 1 &= C^{(1)} \Delta q_1 + C^{(2)} \Delta q_2 \end{aligned} \quad (11.22)$$

Here, in addition to  $\Delta K = K - K_0$  as defined above,  $k^{(1)}$  and  $k^{(2)}$  are the force constant coefficients (combinations of the second- and first-order vibronic constants) that show how the force constant changes by adding one electron on the corresponding MO (Section 7.2). The last equation in (11.22) describes the linear dependence of the ratio of anharmonicity constants  $\beta$  on the charge transfers  $\Delta q_i$ , where the coefficients  $C^{(1)}$  and  $C^{(2)}$  are complicated combinations of cubic and lower-order OVC. For the anharmonicity changes, another presentation is also possible:

$$\Delta\gamma = \gamma - \gamma_0 = \gamma^{(1)} \Delta q_1 + \gamma^{(2)} \Delta q_2 \quad (11.23)$$

If there are more than two MOs of the coordinated molecule that are active in the bonding with the metal (see Problem 11.8), the formulas (11.22) and (11.23) should be extended accordingly:

$$\begin{aligned} F &= \sum_i f^{(i)} \Delta q_i \\ \Delta K &= \sum_i k^{(i)} \Delta q_i \\ \Delta\gamma &= \sum_i \gamma^{(i)} \Delta q_i \end{aligned} \quad (11.22')$$

where the sum is taken over the number of active orbitals.

All the coefficients  $f^{(i)}$ ,  $k^{(i)}$ ,  $C^{(i)}$ ,  $\gamma$  or  $\gamma^{(i)}$  instead of  $C^{(i)} \Delta$  in Eqs. (11.22) and (11.22') can be easily determined if the values of  $F$ ,  $\Delta K$ , and  $\beta$  (or  $\Delta\gamma$ ) are known for any two independent processes of electronic rearrangements (for two pairs of values of  $\Delta q_1$  and  $\Delta q_2$  excluding the trivial values  $\Delta q_1 = \Delta q_2 = 0$ ). These processes may be either ionization ( $\Delta q_1 = -1$ ,  $\Delta q_2 = 0$ ), reduction

( $\Delta q_1 = 0, \Delta q_2 = 1$ ), or excitation ( $\Delta q_1 = -1, \Delta q_2 = 1$ ), provided that the above mentioned empirical parameters are available for them.

As mentioned above, the force constants  $K$  and  $K_0$  can be obtained from the corresponding vibrational frequencies, while the magnitude of distortion  $Q_0$  is in general available from X-ray (or other diffraction) measurements, as well as from spectroscopic data. For some systems, especially for simple molecules,  $Q_0$  can be also determined from the known  $K$  value using empirical relations between  $K$  and  $Q_0$ ; then the theory becomes one-parametrical [11.20a]. In many cases calculation of the parameters in Eq. (11.22) are preferable.

With the known values of  $F$ ,  $\Delta K$ , and  $\beta$  (or  $\gamma_0$ ), the change in the activation energy  $-\Delta D$  as a function of the activation energy  $D_0$  of the reaction with the nonactivated molecule can be estimated from Eq. (11.19). The latter can also be used as an empirical relation between  $\Delta D$  and  $D_0$ :

$$-\Delta D = aD_0 + bD_0^{1/2} + c \quad (11.24)$$

where the coefficients  $a, b$ , and  $c$  [not to be confused with  $a, b, c$ , and  $d$  in Eq. (11.7)] are functions of the empirical parameters presented above. The  $D_0$  value is often unknown. In these cases the functions  $-\Delta D = f(D_0)$  can be plotted for different coordination centers for comparison of their ability to lower the activation energy. In Example 11.2 activation of the CO molecule is considered in this approach. Other examples are given below. For activation of CN, see the article by Kushkuley and Stavrov [11.17b] and Problems 11.8 and 11.9.

### EXAMPLE 11.2

#### Activation of Carbon Monoxide

The electronic structure and spectroscopic parameters of the CO molecule and its ions are well studied. This makes it possible to obtain the estimates of its main orbital vibronic constants and force constant coefficients. For CO the HOMO is  $5\sigma$ , while the LUMO is  $2\pi$  (Fig. 6.9). Using the empirical data [11.21–11.23] for the force constant  $K_0$  of the free molecule, and  $K$ ,  $Q_0$ , and  $\beta$  for the  $\text{CO}^+$  ion ( $\Delta q_1 = -1, \Delta q_2 = 0$ ) and the CO excited state  $5\sigma^2 2\pi^0 \rightarrow 5\sigma^1 2\pi^1$  ( $\Delta q_1 = -1, \Delta q_2 = 1$ ), we find the following from Eqs. (11.22) (for the  $5\sigma^1 2\pi^1$  configuration, the values averaged over the two excited states  $A^1\Pi$  and  $a^3\Pi$  were employed):

$$\begin{aligned} f^{(1)} &= -4.54 \cdot 10^{-4} \text{ dyn} & f^{(2)} &= -12.1 \cdot 10^{-4} \text{ dyn} \\ k^{(1)} &= -0.080 \cdot 10^6 \text{ dyn/cm} & k^{(2)} &= -0.83 \cdot 10^6 \text{ dyn/cm} \\ C^{(1)} &= 0.134 & C^{(2)} &= 0.0104 \end{aligned} \quad (11.25)$$

It is evident from both the OVC and force constant coefficients that the two orbitals  $5\sigma$  and  $2\pi$  are both antibonding, with the latter much more antibonding than the former. In addition to the qualitative statement about the nature of the corresponding MO (bonding or antibonding), which can often (but not always) be made without using the vibronic approach, the latter also gives the quantitative degree of MO participation in the chemical bonding, and separately in the distorting force, force constant, anharmonicity correction, and so on.

With knowledge of the constants (11.25), one can analyze the behavior of the CO molecule in various situations, in particular, when it is coordinated to another molecular system or solid surface. If the charge transfers  $\Delta q_1$  and  $\Delta q_2$  are known, then  $F$ ,  $\Delta K$ ,  $\beta$ , and hence  $-\Delta D$  (for given  $D_0$ ) can be evaluated, and vice versa. It is seen from these constants that the greater the positive values of  $\Delta q_1$  and  $\Delta q_2$  (i.e., the greater the increase in the occupancy of the HOMO and LUMO), the larger the negative force  $F$  (which acts as an antibonding factor to lower the activation energy) and the negative  $\Delta K$  (acting in the same way). However, since the HOMO is fully occupied by electrons in the free molecule,  $\Delta q_1$  can be only negative or zero. Consequently, activation of the CO molecule is greater with larger positive values of  $\Delta q_2$  and smaller with negative values of  $\Delta q_1$ ; the former correlation is much more important. Hence in reactions in which the activation energy is determined by the activation of the CO molecule when it is linearly coordinated to a catalyst, the latter is the more efficient, the greater its  $\pi$ -donor properties and the lower its  $\sigma$ -acceptor ability.

Consider the linear end-on coordination of carbon monoxide to the Ni atom on a NiO surface. The value  $K = 1.710 \times 10^6$  dyn/cm is known from empirical data [11.24]. Using the empirical relationship between  $K$  and  $Q_0$  for the CO molecule [11.21]

$$K = [1.7957 - 8.2926Q_0 (\text{\AA})] \times 10^6 \text{ dyn/cm} \quad (11.26)$$

one can obtain  $Q_0 = 0.0126 \text{ \AA}$ ,  $F = -2.119 \times 10^{-4}$  dyn and  $\Delta K = K - K_0 = -0.192 \times 10^6$  dyn/cm, and consequently estimate  $\Delta q_1 = -0.32$ ,  $\Delta q_2 = 0.26$ , and  $\beta = 0.93$  from Eq. (11.22). These data provide in detail the mechanism of activation of the CO molecule when coordinated to the NiO surface; as a result of coordination there is a  $\sim 0.3$  electron charge transfer to the metal from the weak antibonding  $5\sigma$  orbital and about  $\sim 0.3$  electron charge transfer from the metal to the strong antibonding  $2\pi$  orbital of CO.

Using the relationship (11.26) between  $K$  and  $Q_0$ , a general correlation between the CO vibrational frequency and the charge transfers  $\Delta q_1$  and  $\Delta q_2$  from the HOMO  $5\sigma$  ( $-\Delta q_1$ ) and to the LUMO  $2\pi$  ( $\Delta q_2$ ) by

coordination was derived. It is shown in Fig. 11.8 in the form of a correlation diagram. Note, however, that the empirical function  $K = f(Q_0)$  (11.26) is valid in the region where the coordination is sufficiently strong

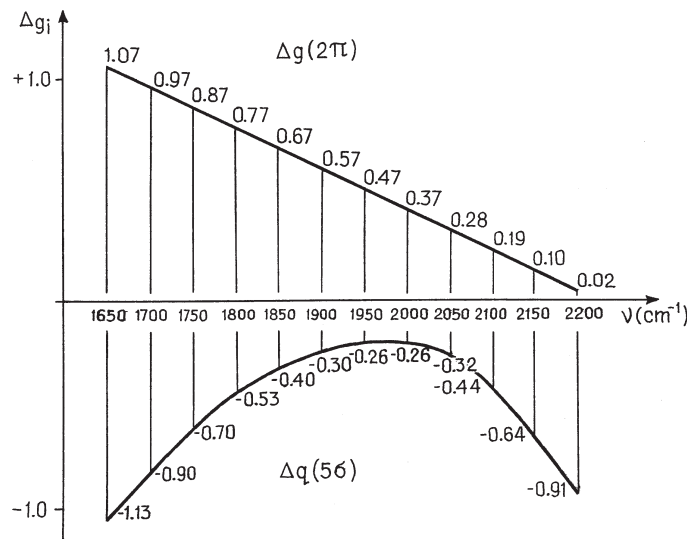


**FIGURE 11.8.** Correlation diagram between CO vibration frequencies  $\nu$  (in  $\text{cm}^{-1}$ ) and orbital charge transfers from the HOMO  $5\sigma$  ( $-\Delta q_1$ ) to the coordination center, and from the latter to the LUMO  $2\pi$  ( $\Delta q_2$ ) in linear end-on coordination.

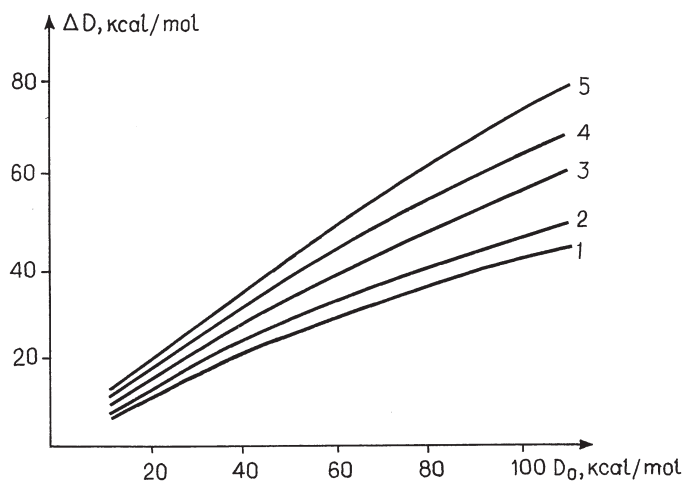


**FIGURE 11.9.** Vibronic activation of carbon monoxide. Curves  $-\Delta D = f(D_0)$  for CO coordination to surfaces PdO (1) and NiO (2), and in carbonyls  $\text{Fe}(\text{CO})_5$  (3),  $\text{V}(\text{CO})_5$  (4),  $\text{Mn}(\text{CO})_5$  (5).

and does not apply to very small charge transfers and CO frequency changes.

The change in CO reactivity when coordinated to the NiO surface can be estimated from Eq. (11.24) ( $D_0$  and  $\Delta D$  in kcal/mol):

$$-\Delta D = 0.17D_0 + 1.40D_0^{1/2} - 0.78 \quad (11.27)$$

This curve  $-\Delta D = f(D_0)$ , together with similar curves for CO activation in a series of coordination systems including metal carbonyls and metal surfaces, is shown in Fig. 11.9.

Some results for activation of CO by coordination to polynuclear clusters, similar to those discussed in Example 11.2, are shown in Table 11.1 [11.20a] (for activation of CO in hemoproteins, see Ref. 11.20b). It is seen that simultaneous (bridged) coordination to two or three centers of the cluster (denoted by  $\mu_2$  and  $\mu_3$ , respectively) results in much stronger activation  $-\Delta D$  than for one-center coordination ( $\mu_1$ ). In  $\text{Rh}_6(\text{CO})_{12}$  and  $\text{Co}_2(\text{CO})_8$  the effect of bridged coordination is seen explicitly (Table 11.1). In the rhodium polynuclear complex triple-bridged coordination to three centers simultaneously results in activation of the CO molecule, which in reactions with  $D_0 = 100$  kcal, is more than 5 times larger than in simple one-center coordination to the same system.

The charge transfers in Table 11.1 explain in more detail the origin of the bridged multicenter coordination effect—the orbital charge transfer from the complex to the strongly antibonding MO  $2\pi$  of CO is much larger ( $\sim 3.5$  times) in triple-bridged coordination than in the monocoordinated case. A numerical estimate of CO activation by coordination to a NiO surface is given in Example 11.3.

**TABLE 11.1. Charge Transfers to the CO Molecule  $\Delta q_1(5\sigma)$  and  $\Delta q_2(2\pi)$  and Chemical Activation  $-\Delta D$  (for  $D_0 = 100$  kcal/mol) in Some Polynuclear Clusters<sup>a</sup>**

Complex (kcal/mol)	$\Delta q_1(5\sigma)$	$\Delta q_2(2\pi)$	$-\Delta D$ for $D_0 = 100$
$\text{Mo}(\text{CO})_6$	-0.31	0.32	30
$\mu_1\text{-Mn}_2(\text{CO})_{10}$	-0.27	0.36	36
$\mu_1\text{-Os}_3(\text{CO})_{12}$	-0.28	0.31	28
$\mu_1\text{-Co}_2(\text{CO})_8$	-0.33	0.27	22
$\mu_2\text{-Co}_2(\text{CO})_8$	-0.42	0.67	74
$\mu_1\text{-Rh}_6(\text{CO})_{16}$	-0.39	0.22	15
$\mu_3\text{-Rh}_6(\text{CO})_{16}$	-0.53	0.77	78

<sup>a</sup>Symbols  $\mu_1$ ,  $\mu_2$ , and  $\mu_3$  denote simultaneous coordination to one, two, and three centers, respectively.

**EXAMPLE 11.3*****Numerical Estimate of CO Activation by Coordination to a NiO Surface***

For numerical estimation of activation  $-\Delta D$ , knowledge of  $D_0$  is needed. For illustration, if we assume that the activation energy of the reaction  $\text{CO} + \text{O}_2 \rightarrow \text{CO}_2 + \text{O}$  in flames is  $D_0 = 48$  kcal/mol [11.25], and this is associated with activation of the CO bond only, then by linear coordination to the NiO surface the activation energy, in accordance with Eq. (11.27) in Example 11.2, is lowered by  $\Delta D = -17$  kcal/mol and becomes equal to  $D = D_0 + \Delta D = 31$  kcal/mol. The experimental value for this reaction on the NiO catalyst (in excess CO) is  $D_{\text{exp}} = 25.4$  kcal/mol [11.26].

In Examples 11.4–11.6 the activation by coordination to transition metal centers is considered and numerical estimations obtained for  $\text{N}_2$ , NO, and  $\text{H}_2$  molecules.

**EXAMPLE 11.4*****Activation of Dinitrogen***

In the nitrogen molecule  $\text{N}_2$  the HOMO is  $5\sigma$  and the LUMO is  $2\pi$  (Fig. 6.7), as in CO. Using the data for  $\text{N}_2^+$  and the excited states  $a^1\Pi_g$  and  $B^3\Pi_g$  emerging from the  $(5\sigma)^2 \rightarrow (5\sigma)^1(2\pi)^1$  excitation ( $\Delta q_1 = -1$ ,  $\Delta q_2 = 1$ ) and Eqs. (11.22), we get

$$\begin{aligned} f^{(1)} &= 3.51 \times 10^{-4} \text{ dyn} & f^{(2)} &= -8.18 \times 10^{-4} \text{ dyn} \\ k^{(1)} &= 0.286 \times 10^6 \text{ dyn/cm} & k^{(2)} &= -0.785 \times 10^6 \text{ dyn/cm} \\ C^{(1)} &= 0.112 & C^{(2)} &= 0.127 \end{aligned} \quad (11.28)$$

It is seen that in contrast to the CO molecule the HOMO  $5\sigma$  is bonding, while the LUMO  $2\pi$  is antibonding as in CO. Therefore an activation center with high  $\pi$ -donor and high  $\sigma$ -acceptor properties is needed for activation of linearly coordinated dinitrogen. If the coordination center is a  $\pi$  acceptor, a charge transfer may take place from either the inner bonding  $\pi_u$  orbital when the coordination is linear end-on (longitudinal), or the antibonding  $\sigma_u$  orbital for transversal (side-on) coordination. It follows that the activation depends on the geometry of coordination.

TABLE 11.2. Semiempirically Calculated Charge Transfers  $\Delta q_1$  and  $\Delta q_2$  and Vibronic Reduction of Activation Energies  $-\Delta D$  by Coordination of the  $N_2$  Molecule to Different Complexes ( $D$  and  $-\Delta D$  in kcal/mol)

Coordination System <sup>a</sup>	$\nu'$ ( $\text{cm}^{-1}$ )	$K'$	$\Delta K = K' - K$ ( $10^6$ dyn/cm)	$Q_0$ ( $\text{\AA}$ )	$F$ ( $10^4$ dyn)	$\Delta q_1$	$\Delta q_2$	$-\Delta D = aD + bD^{1/2} + c$		
								$a$	$b$	$c$
[RuH <sub>2</sub> (N <sub>2</sub> )(PPh <sub>3</sub> ) <sub>3</sub> ]	2147	1.900	-0.394	0.0229	-4.19	-0.16	0.44	0.14	2.72	-2.87
[[Ru(NH <sub>3</sub> ) <sub>5</sub> ] <sub>2</sub> N <sub>2</sub> ] <sup>4+</sup>	2100	1.821	-0.479	0.0303	-5.25	-0.57	0.41	0.21	3.37	-4.81
[Os(NH <sub>3</sub> ) <sub>5</sub> N <sub>2</sub> ][Br <sub>2</sub> ]	2028	1.695	-0.599	0.0428	-6.77	-1.00	0.40	0.31	4.32	-8.94
[(tol)(PPh <sub>3</sub> ) <sub>2</sub> Mo-N <sub>2</sub> -Fe(C <sub>5</sub> H <sub>5</sub> )(dmpe)] <sup>+</sup>	1930	1.536	-0.758	0.0619	-8.54	-1.21	0.52	0.37	5.62	-16.9

<sup>a</sup>tol = toluol; dmpe = Me<sub>2</sub>PCH<sub>2</sub>CH<sub>2</sub>PMe<sub>2</sub>.

The constants (11.28) and empirical data pertaining to the coordinated nitrogen molecule can be employed to estimate the charge transfers  $\Delta q_1$  and  $\Delta q_2$  and the reduction in activation energy  $-\Delta D$  as a function of  $D_0$  using Eqs. (11.22). Table 11.2 presents some examples of such calculations [11.16]. The value  $Q_0$  is estimated from the empirical formula (the  $N_2$  stretching vibrational frequency in the coordinated state  $\nu$  is given in  $10^3 \text{ cm}^{-1}$ ):

$$Q_0 (\text{\AA}) = 0.9482 - 0.7105\nu + 0.1302\nu^2 \quad (11.29)$$

It is seen from Table 11.2 that, as above, the larger contribution to the  $-\Delta D$  value comes from the linear (in  $Q_0$ ) effect, the distorting force ( $b$  term).

### EXAMPLE 11.5

#### Activation of Nitrogen Monoxide

As distinct from the examples presented above, the HOMO and LUMO in the free NO molecules are realized in the same antibonding  $2\pi$  orbital occupied by one electron. Calculations [11.27] show that in addition to this orbital the lower fully occupied  $5\sigma$  orbital takes part in the charge transfers by coordination (the remaining inner orbitals are practically not involved). The coefficients  $a$ ,  $b$ , and  $c$  determining the chemical activation  $-\Delta D$  [Eq. (11.24)] are given in Table 11.3 for several coordination systems. In contrast to the previous examples, the iron complex produces deactivation of the coordinated NO molecule ( $-\Delta D < 0$ ), and is thus an anticatalyst for corresponding reactions with NO.

**TABLE 11.3. The  $a$ ,  $b$ , and  $c$  Coefficients in the Relation  $-\Delta D = aD + bD^{1/2} + c$  for NO Activated by Coordination in Different Complexes**

Coordination System	a	b	c
$\text{Fe}(\text{CN})_5\text{NO}^{2-}$	-0.03	-0.78	-0.19
$\text{Mn}(\text{CN})_5\text{NO}^{2-}$	0.02	0.23	-0.02
$\text{Mn}(\text{CN})_5\text{NO}^{3-}$	0.18	2.6	-2.83
$\text{Cr}(\text{CN})_5\text{NO}^{3-}$	0.27	3.56	-5.77
$\text{Cr}(\text{CN})_5\text{NO}^{4-}$	0.37	4.26	-9.58
$\text{V}(\text{CN})_5\text{NO}^{3-}$	0.35	4.19	-9.07



**EXAMPLE 11.6****Activation of Hydrogen**

Because of the small number of electrons in  $H_2$ , even small charge transfers activate strongly the H—H bond. Therefore, in most cases  $H_2$  decomposes in the coordinated state, although in some cases hydrogen is coordinated as a molecule, with vibrational frequencies observed at about  $\nu = 2600\text{--}3100\text{ cm}^{-1}$  (in the free molecule  $\nu_0 = 4401\text{ cm}^{-1}$ ) with the H—H distance  $R \sim 0.75\text{--}0.86\text{ \AA}$  ( $R_0 = 0.74\text{ \AA}$ ). To employ the one-parameter version of the vibronic theory of chemical activation [11.20], the following relationship between interatomic distance  $R$  and vibrational frequency change  $\Delta\nu = \nu - \nu_0$  can be suggested ( $\Delta\nu$  in  $10^3\text{ cm}^{-1}$ ) [11.25]:

$$R(\text{\AA}) = 0.7412 + 0.5034 \Delta\nu - 0.1541 (\Delta\nu)^2 \quad (11.30)$$

The orbital vibronic constants for the two active MOs, bonding 1 and antibonding 2, are [11.28]

$$\begin{aligned} f^{(1)} &= 1.58 \times 10^{-4} \text{ dyn} & k^{(1)} &= 0.418 \times 10^6 \text{ dyn/cm} \\ f^{(2)} &= -0.41 \times 10^{-4} \text{ dyn} & k^{(2)} &= -0.0348 \times 10^6 \text{ dyn/cm} \end{aligned} \quad (11.31)$$

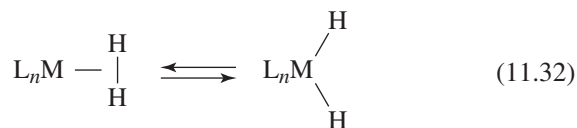
and the anharmonicity ratio  $\beta \approx 0.5$  is much smaller than in the examples above.

With these data one can estimate the charge transfers  $\Delta q_1$  and  $\Delta q_2$  to the bonding and antibonding MOs of  $H_2$ , and the chemical activation  $-\Delta D = D_0 - D$  for different  $\Delta\nu$  values. Some results are given in Table 11.4 ( $-\Delta D$  is given for model reactions with  $D_0 = 103\text{ kcal/mol}$ ).

**TABLE 11.4. Orbital Charge Transfers to Bonding ( $\Delta q_1$ ) and Antibonding ( $\Delta q_2$ ) MOs and Chemical Activation  $-\Delta D$  of Coordinated Molecular Hydrogen as a Function of the Frequency of Stretching Vibration  $\nu(\text{H—H})$  in the Coordinated State for  $D_0 = 103\text{ kcal/mol}$**

$\nu\text{ (cm}^{-1}\text{)}$	$\Delta q_1$	$\Delta q_2$	$-\Delta D\text{ (kcal/mol)}$
4200	-0.06	0.06	30.5
3800	-0.17	0.16	53.7
3400	-0.27	0.25	70.3
3000	-0.35	0.34	81.7
2600	-0.43	0.41	89.4
2200	-0.49	0.38	94.8
2000	-0.52	0.50	96.1

The main conclusion drawn from these data is that the homolytic cleavage of the  $H_2$  molecule



takes place at  $\nu = 2400 - 2100 \text{ cm}^{-1}$  and  $R = 1.0 - 1.2 \text{ \AA}$ , in qualitative agreement with known experimental data.

One version of the vibronic theory of chemical activation is *to calculate the orbital charge transfers*  $\Delta q_i$  to and from the coordinated molecule and, using the equations presented above, to estimate the expected distortion, changes in vibrational frequencies, anharmonicities, and activation by coordination. This version has been employed in the treatment of activation of the oxygen molecule. It provides additional possibilities for verifying the applicability of the vibronic approach by comparison of the estimated frequencies of vibrations with those observed experimentally.

For oxygen coordination the semiempirical scheme used above should be completed because, as shown by calculations, three MOs are active in the orbital charge transfers (oxygen forms a three-orbital bond with the active site of the coordination system). Activation of oxygen by metalloenzymes is of special interest in biology. In Section 10.3 the electronic structure and some electron-conformational effects in these systems are discussed. In Example 11.7 we consider in more detail the mechanism of activation of oxygen by several hemoproteins [11.17a].

### EXAMPLE 11.7

#### *Activation of Oxygen by Hemoproteins*

The active site of several metallobiochemical systems considered below can be presented by a general formula  $Fe(P)(L)$ , where P is porphyrin and L is the amino acid moiety of the protein: hemoglobin ( $L = \text{ImH}$ , where Im denotes imidazol), horseradish peroxidase (HRP,  $L = \text{Im}^-$ ), cytochrome P-420 ( $L = \text{SHCH}_3$ ), and cytochrome P-450 ( $L = \text{SCH}_3^-$ ); the same systems with an additional electron were also tried. Their electronic structures with the coordinated oxygen were calculated using the semiempirical MO LCAO IEH (SCCC) approximation (Section 5.5). The three active MOs participating in the bonding with the active site

TABLE 11.5. Parameters of O<sub>2</sub> Activation by Hemoprotein Models Fe(P)(L) without and with an Additional Electron<sup>a</sup>

Parameter	L												
	ImH			Im <sup>-</sup>			SHCH <sub>3</sub>			SCH <sub>3</sub> <sup>-</sup>			
	Hb	Hb + e	HRP	HRP	HRP + e	P-420	P-420	P-420 + e	P-450	P-450	P-450 + e	P-450 + e	C <sub>6</sub> F <sub>4</sub> HS <sup>-</sup>
$\Delta q(1\pi_u)$	-0.04	-0.04	-0.06	-0.04	-0.04	-0.05	-0.05	-0.06	-0.05	-0.05	-0.05	-0.05	-0.04
$\Delta q(3\sigma_g)$	-0.11	-0.13	-0.13	-0.13	-0.13	-0.11	-0.11	-0.13	-0.11	-0.11	-0.12	-0.12	-0.10
$\Delta q(1\pi_g)$	0.56	0.86	0.60	0.88	0.88	0.55	0.55	0.86	0.74	0.91	0.91	0.91	0.64
$K$ (mdyn/Å)	6.28	5.40	1.30	6.04	5.37	6.27	6.27	5.35	1.21	1.38	5.31	5.31	6.07
$\omega^{(1)}$ (cm <sup>-1</sup> )	1115	1067	1132	1132	1067	1154	1154	1066	1102	1061	1061	1061	1134
$\omega^{(2)}$ (cm <sup>-1</sup> )	1193	1112	979	962	962	1198	1198	1115	1008	989	1111	1111	1174
$\omega_{\text{exp}}$ (cm <sup>-1</sup> )	1160		1111	1110	1110				1150	1111			1140
$R_0$ (Å)	1.30	1.35	1.32	1.35	1.35	1.31	1.31	1.35	1.33	1.36	1.36	1.36	1.32
$R_{\text{exp}}$ (Å)	1.15-1.22		1.41	1.45	1.45				1.42	1.42			
$D$ (eV)	4.62	4.08	4.45	4.05	4.05	4.69	4.69	4.04	4.34	3.97	3.97	3.97	
			4.34	2.63	2.63				3.36	2.98	2.98	2.98	

<sup>a</sup>The data for  $\Delta q$ ,  $K$ , and  $\omega$  obtained from electron lone-pair separation by deprotonation are given in second rows.

of the enzyme are  $3\sigma_g$ ,  $1\pi_u$ , and  $1\pi_g^*$ . The corresponding three orbital vibronic constants  $f^{(i)}$ , force constant  $k^{(i)}$  and anharmonicity  $\gamma^{(i)}$  coefficients were calculated by Eqs. (11.2) using spectroscopic data for oxygen and its ions [11.17a]. The constants were calculated for the coordination of the superoxide ion  $O_2^-$  which is more appropriate to the state of coordinated oxygen in hemoproteins. Unlike the examples above, the Morse potential instead of the cubic polynomials (11.7) was employed in calculation of the vibrational frequencies and interatomic distances in the coordinated state. The  $3\sigma_g$  and  $1\pi_u$  MOs of oxygen are bonding, while  $1\pi_g^*$  is antibonding, but with respect to the superoxide ion their contribution to the force constant has an opposite sign.

Some results for the calculated charge transfers, interatomic distances, vibrational frequencies, and activation of coordinated oxygen are illustrated in Table 11.5. It is seen that the activation is due mainly to the contribution of the charge transfer  $\Delta q(1\pi_g^*)$  to the antibonding  $1\pi_g^*$  MO of oxygen, which in the case of cytochrome P-450 + e- is  $\sim 0.91$ , and in the approximation when the sulfur lone pair is separated (Section 10.3) it is even larger. However, the value of  $\sim 1.4$  electron in Table 11.5 is overestimated because of the use of the "frozen orbital" approximation.

The resulting activation of the O—O bond is significant; in the coordinated state  $D$  is almost half of the dissociation energy  $D_0$ , but it is still larger than the activation energies of the reaction of hydroxylation by cytochrome P-450 ( $\sim 1$  eV). One reason for this discrepancy is that  $D_0$  in Eqs. (11.9) and (11.18) is not the dissociation energy, but the activation energy in the corresponding associative reactions without catalyst participation, which is smaller than the dissociation energy (Fig. 11.7). The calculated frequencies of  $O_2$  stretching vibrations are in good agreement with the experimental data available.

### Jahn–Teller- and Pseudo-Jahn–Teller-Induced Chemical Activation

The influence of the electronic rearrangement on the reactivity of a molecular system, discussed above in this section, is attributed to the occurrence of a distorting force  $F$ , the changes of the force constant  $\Delta K$ , and anharmonicity  $\Delta\gamma$  in this rearrangement [Eq. (11.13)]. The change of the rising portion of the reaction curve as a function of the reaction pathway and the consequent change of the activation energy  $-\Delta D = D_0 - D$  are shown in Fig. 11.7. By comparison, one can see that near the origin  $Q = 0$  these changes are similar to those produced by the JT or PJT effects (Sections 7.3 and 7.4, Fig. 7.5). In the JTE (degenerate electronic states) a nonzero force distorts the high-symmetry nuclear configuration in the direction of JT active coordinates  $Q$ ; if the quadratic terms of vibronic

interactions are taken into account, the force constant (APES curvature)  $K_0$  is also changed. In the PJTE (mixing of the ground and excited electronic states by the nuclear displacements), the force constant  $K_0$  changes as well.

If a JT system enters a chemical reaction, the behavior of its APES both without and with the JTE as a function of the JT active coordinate  $Q$  [ $\varepsilon_0(Q)$  and  $\varepsilon(Q)$ , respectively] follow exactly Eqs. (11.8) and (11.13), respectively, as illustrated in Fig. 11.7. This means that the JTE produces the same kind of chemical activation  $-\Delta D$  as a corresponding electronic rearrangement induced by, say, a catalyst. The chemical activation  $-\Delta D$  is determined here by the same equation [Eq. (11.17)] with  $Q_0$  and  $\Delta K = K - K_0$  taken from the JTE formulas (Section 7.3).

If the quadratic vibronic coupling terms in the JTE are neglected (linear vibronic coupling), then  $K = K_0$ ,  $\gamma = \gamma_0$ , and expression (11.19) is simplified:

$$-\Delta D = (12D_0E_{JT})^{1/2} - 4E_{JT} \quad (11.33)$$

where  $E_{JT}$  is the JT stabilization energy (Section 7.3). For instance, for a system with a double-degenerate electronic  $E$  term  $E_{JT} = F^2/2K_0$  [see Eq. (7.41)] and

$$-\Delta D = |F| \left( \frac{6D_0}{K_0} \right)^{1/2} - \frac{2F^2}{K_0} \quad (11.34)$$

Calculation of the chemical activation  $-\Delta D$  for a PJT system becomes more complicated since an additional important parameter emerges: the energy gap  $2\Delta$  between the ground and excited states whose admixing produces the instability of the ground state of the reactant. Figure 11.10 shows the two reaction curves, without and with the PJTE in the direction of the reaction path  $Q$ . The curve

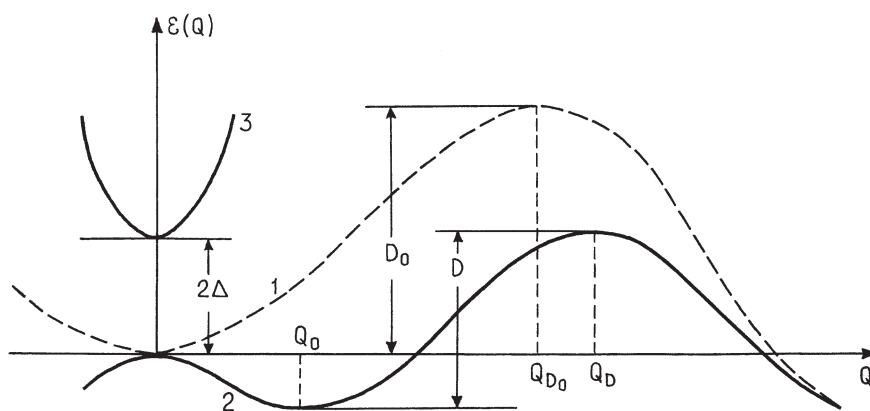


**FIGURE 11.10.** Cross section of APES along the reaction path  $Q$  without (1) and with (2) the strong pseudo-Jahn–Teller effect that mixes the states 1 and 3.

modified by the PJTE differs from the JTE curve (Fig. 11.7) by the behavior near the origin  $Q = 0$ .

If the condition of the strong PJTE (7.71),  $K_0 < F^2/\Delta$ , holds, the ground state is unstable at  $Q = 0$  and the adiabatic potential curve (7.69) has two minima at the points (7.72) with the curvature at the minima points given by Eq. (7.73). Factoring in the anharmonicity produced by the interacting reactants, we can present the reaction curve by adding a negative cubic anharmonicity term to Eq. (7.69), which, unlike (11.8) or (11.13), should be of the sixth order to preserve the symmetry conditions (with regard to inversion of  $Q$ ):

$$\varepsilon(Q) = \frac{1}{2}K_0Q^2 - (\Delta^2 + F^2Q^2)^{1/2} - \gamma Q^6 \quad (11.35)$$

This curve has not been studied in detail as yet. Approximately, by expansion of the square root, we get (cf. (7.66)):

$$\begin{aligned} \varepsilon(Q) &= \frac{1}{2}KQ^2 + \frac{F^4}{8\Delta^3} - \gamma Q^6 \\ K &= K_0 - \frac{F^2}{\Delta} \end{aligned} \quad (11.36)$$

and for the points of the minimum  $Q_0$  (stable reactants), and maximum  $Q_D$  (activated complex), we have

$$Q_{0,D} = \left\{ \frac{F^4}{24\Delta^3\gamma} \left[ 1 \pm \left( 1 + \frac{48\gamma K \Delta^6}{F^8} \right)^{1/2} \right] \right\}^{1/2} \quad (11.37)$$

with the minus sign for  $Q_0$  and plus sign for  $Q_D$ . Note that, due to (7.67),  $K < 0$ , and hence for real roots of Eq. (11.37) the condition  $|48\gamma K| < F^8/\Delta^6$  must be obeyed. If this inequality is sufficiently strong, we have approximately

$$Q_0 \approx \sqrt{2} \frac{\Delta}{F} \left( 1 - \frac{K_0\Delta}{F^2} \right)^{1/2} \quad (11.38)$$

$$Q_D \approx \left( \frac{F^8 + 24K\Delta^6\gamma}{12\gamma\Delta^3F^4} \right)^{1/2} \quad (11.39)$$

By substituting the parameters (11.37) or (11.38) and (11.39) into (11.35), one can estimate the activation energy modified by the PJTE

$$D = \varepsilon(Q_D) - \varepsilon(Q_0) \quad (11.40)$$

and the chemical activation  $-\Delta D = D_0 - D$  [with  $D_0$  after (11.9)].

Thus the JT- and PJT-induced chemical activation (one of the particular cases of the TEST paradigm; Section 7.4) is similar to the effect of electronic rearrangement under the influence of a catalyst as discussed above. However, along with this important similarity there are also essential differences between the two sources of chemical activation. First, they are concerned with the direction  $Q$ , in which the activation energy is lowered, that is, with the allowed mechanism of the reaction. In systems with the JT and PJT effects, this direction is predetermined by the electronic structure of the molecule itself (by the JT and PJT active displacements), whereas in the case of catalyst influence the direction of chemical activation depends on the nature of the catalyst, on the electronic rearrangement it produces in the reagents. Therefore, different catalysts can, in principle, cause different dominating mechanisms. In particular, the catalyst can change the mechanism of the reaction that takes place without the catalyst. On the contrary, for vibronically induced reactions of free molecules the mechanism is known a priori, and this allows us to predict the reaction course and its products. Example 11.8 illustrates this statement for Jahn–Teller-induced reactions.

### EXAMPLE 11.8

#### *Jahn–Teller-Induced Substitution Reactions in Octahedral Complexes with an E Term*

Consider the reaction of substitution in, or monomolecular decomposition of, an octahedral transition metal complex in an orbitally twofold-degenerate electronic  $E$  state [11.6, 11.29], for example, for bivalent copper known to have a strong JTE. The APES of this system has three equivalent minima, in each of which the octahedron is elongated along the tetragonal axis, with two ligands being farther away from the central atom than the other four (Sections 7.3 and 9.2). In  $Q_\theta$  and  $Q_\varepsilon$  coordinates (Fig. 7.1) the distortion takes place along the  $Q_\theta$  direction;  $Q_\theta$  is thus the coordinate along which the activation energy of the reaction is lowered (the system is chemically activated) as compared with other directions, *ceteris paribus*. As a result, the reaction should proceed in the direction of the  $Q_\theta$  displacements, which cause the two axial ligands to move away from (while the other four approach) the CA (Fig. 9.20). For the monomolecular reaction this implies dissociation of the ligands in the *trans* positions, while for the substitution reaction it means the formation of *trans*-substituted complexes. Visually, this conclusion corresponds to the following picture; when elongated octahedrons are formed, in the pulsating motions during a specific lifetime (Section 9.2), the two ligands in *trans* positions are more weakly bonded and reached more easily by the attacking reagents. Thermodynamic considerations (Section 9.3) also support the conclusion about the formation of *trans*-substituted complexes of  $E$ -term metals.

This result is in complete agreement with the well-known empirical data on the behavior of octahedral complexes of Cu(II) in solution or gas phase. It is known that these complexes lose two ligands in the *trans* position, forming square-planar structures, while substitution reactions produce only *trans*-substituted complexes (except for bidentate ligands, which can be *cis*-coordinated only). On the other hand, if the JTE in such a system is quenched (say, by the significant differences between the ligands), the potential barrier essentially increases and the reaction rate decreases. This conclusion also agrees with experimental data [11.30] showing the substitution reaction rate to decrease about 3000 times when passing from  $[\text{Cu}(\text{H}_2\text{O})_6]^{2+}$  to  $[\text{Cu}(\text{tren})\text{H}_2\text{O}]^{2+}$  (where tren = 2, 2', 2''-triaminotriethylamine). According to predictions of the theory, similar effects are expected in octahedral complexes of Cr(II), Mn(III), Ag(II), ... that have *E* ground terms (see also Problem P11.10).

For nonoctahedral molecular configurations with *E* terms and for other terms the expected vibronically induced mechanisms of reactions are different from that considered in Example 11.8 for octahedral Cu(II) complexes. They can be qualitatively determined from known JT and PJT distortions. There are other suggested applications of the vibronic effects in determining the chemical reaction rate and mechanisms ([11.6, 11.31]).

### 11.3. DIRECT COMPUTATION OF ENERGY BARRIERS OF CHEMICAL REACTIONS

Methods of numerical computation of the electronic structure of coordination compounds involving computer and supercomputer calculations (Chapters 5 and 6) allow one, in principle, to obtain the APES for any chemical reaction, including catalytic reactions, and to estimate the numerical value of the energy barrier (activation energy) of the reaction. Practically, the solution of this problem may be very laborious and costly. However, the continuous improvement of methods and algorithms, as well as computer power, makes it possible to solve increasingly complicated problems.

In this section we discuss several examples of numerical calculations of the APES and consequent properties of chemical reactions with coordination compounds, including cases when the latter act as catalysts.

#### Substitution Reactions: The *trans* Effect

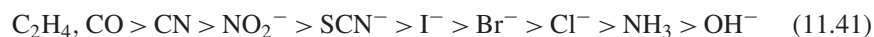
In Section 9.3, which is devoted to the mutual influence of ligands in coordination compounds, the phenomena of *trans* and *cis* influences in stereochemistry



problems are discussed. We emphasized the need to distinguish between the thermodynamic aspect of the problem (*trans influence*), in which the mutual influence is considered from the static (energetic) point of view, and the kinetic aspect (*trans effect*), in which the influence of mutual ligand positions on the reaction rate of substitution or decomposition reactions is discussed. In this section we discuss *mutual ligand effects*—the influence of a given ligand on the energy barrier of the reactions of substitution (or cleavage) of another ligand in the *trans* or *cis* position.

There is an obvious correlation between the mutual influence and mutual effect of ligands as they are defined above. For instance, as shown in Section 9.3, the *trans* influence results in a weakening of the metal–ligand bond in the *trans* position to the influencing ligand. It is clear that the weaker bond is subject to easier cleavage or substitution (see Example 11.8). Hence the *trans* influence also promotes the *trans* effect. On the other hand, for a bimolecular associative  $S_N2$  reaction, the formation of the reaction barrier may be much stronger dependent on (and on more details of) the electronic structure of both reactants (especially the entering, leaving, and *trans*-directing ligands) than the stereochemistry of the initial complex, where mainly one ligand is specified.

Square-planar complexes of Pt(II) were suggested first [11.32] and are best studied (see the reviews in Refs. 11.33–11.36) as demonstrating the *trans* effect in the most explicit way. Usually the series of ligands arranged in decreasing *trans*-effect power (the *trans*-effect series) is given as follows [11.37]:



In Section 9.3, many examples are given (see Tables 9.8–9.11) and the role of some major electronic features of the ligand and the metal in realizing the *trans* influence is discussed. It is shown that the  $\sigma$ -donor properties of the ligand enhanced by its  $\pi$ -acceptor properties are most important in the *trans* influence. Basically, these ideas are also valid in the *trans* effect, with the distinction that in the latter the  $\pi$ -acceptor properties are more important. The qualitative reason for this  $\pi$  effect was discussed first by Chatt et al. [11.38] and by Orgel [11.39] and is illustrated in Fig. 11.11.

If the ligand L in the square-planar complex of Pt(II) has the strongest  $\pi$ -acceptor properties (low-energy empty  $\pi$  orbitals), then there is a backdonation to this ligand from the  $d_{xz}$  orbital of the metal M [which is occupied in the  $d^8$  configuration of Pt(II)]. This backdonation results in a significant rearrangement of the electron distribution in which the electron density along the *trans* bond M—A is decreased. In turn, this lowers the repulsion from the entering group in the *trans* position, thus lowering the energy of the transition state of the reaction and hence the activation energy. Hence the *trans* influence, which weakens and elongates the M—A bond, also contributes to lowering the activation energy by facilitating the approach of the attacking group and removal of the leaving group. Note that if the  $d_{xz}$  orbital is not occupied, this  $\pi$  effect disappears.

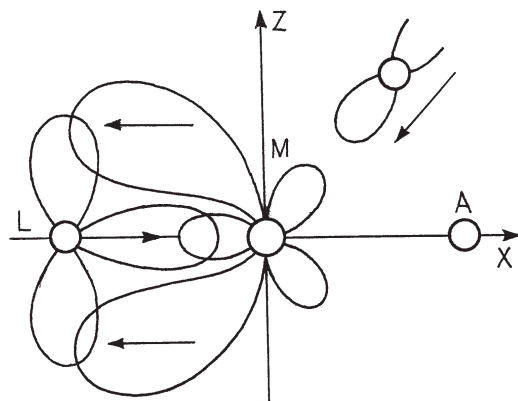
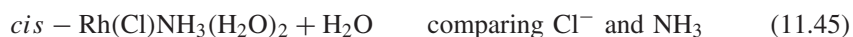
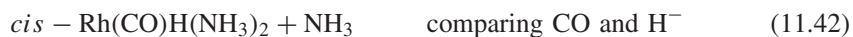


**FIGURE 11.11.** Illustration of the  $\sigma$ - $\pi$  interaction in the *trans* effect: the  $\pi$ -acceptor properties of the *trans*-influencing ligand L enhanced by its  $\sigma$ -donor properties lower the electron density along the *trans* bond M—A, thus favoring the labilization and substitution of the *trans* ligand A.

As discussed elsewhere in this book (Sections 6.3, 9.3, and 11.2), as a result of  $\sigma$ -donor and  $\pi$ -acceptor effects the corresponding orbital charge transfers have opposite signs, and hence their sum is smaller than each of them individually. Therefore, in the presence of strong  $\pi$  donation to the ligand its  $\sigma$ -donor property increases, and vice versa; strong  $\sigma$  donation increases the  $\pi$ -acceptor ability. This mutual enhancing of  $\sigma$ -donor and  $\pi$ -acceptor properties is important in understanding both the *trans* influence (Section 9.3) and *trans* effect. For instance,  $\text{H}^-$  has empty  $\pi$  states ( $2p_z$ ), but in the free ion they are rather high in energy and hence  $\text{H}^-$  is a poor  $\pi$  acceptor. However, in the coordinated states with strong  $\sigma$  donation, its  $2p_z$  orbital energy lowers significantly, and  $\text{H}^-$  becomes a better  $\pi$  acceptor.

It was also shown [11.40] that the competition of the ligands in the  $\sigma$  donation to the metal results in a characteristic *cis* effect—the influence on the reaction rate of ligand substitution in the *cis* position. The *cis* effect is opposite to the *trans* effect; *the larger the trans effect of a given ligand, the smaller its cis effect*. This means that the reaction rate for the substitution of A is determined by (1) the *trans*-effect power of the *trans* ligand L and, (2) the *cis*-effect power (opposite to *trans*-effect power) in the *cis* positions of L and A. The higher the *trans* effect of the *trans* ligand and the lower the *trans* effect of the *cis* ligands, the higher the reaction rate for the given ligand.

These general qualitative considerations were confirmed by direct numerical calculations of transition states and energy barriers of substitution reactions with some square-planar Pt(II) and Rh(I) complexes [11.41]. To reveal the *trans* effect in detail, four reaction systems were computed; for each of them the reactions of substitution of two ligands in *trans* positions to two other ligands were studied to compare their *trans* effects:



In all these reactions the entering and leaving groups are identical [ $\text{NH}_3$  for the first three cases and  $\text{H}_2\text{O}$  for (11.45)]. This simplifies the calculations since it allows one to use additional symmetry considerations. In particular, the identical entering and leaving groups should occupy equivalent positions, provided that there are no additional local minima (intermediates) on the reaction curve. For simplicity, all the groups are chosen neutral.

The computation scheme is as follows. For each substitution reaction the geometry (bond lengths and angles) of the five-coordinated complex (associative  $\text{S}_\text{N}2$  reaction) is optimized, yielding the energy of the transition state. With respect to the energies of the free reactants, this gives the activation energy. In all eight reactions (11.42)–(11.45), the transition state is a trigonal bipyramid with a mirror plane for the two equivalent groups, entering and leaving. Then, allowing one of these groups to move away and calculating the optimized geometry and energy for several fixed positions of this leaving group, one obtains the reaction curve along the reaction coordinate. This curve is illustrated in Fig. 11.12 for the reaction

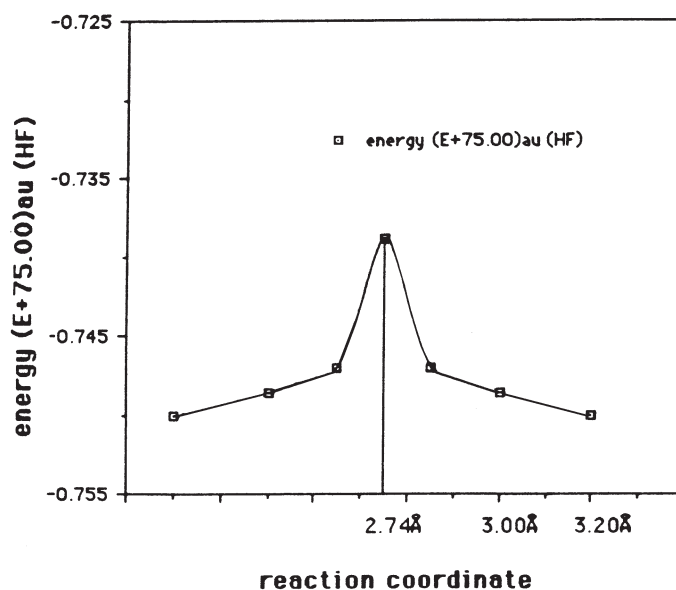


**FIGURE 11.12.** APES along the reaction coordinate for the substitution reaction  $\text{cis}$ - $\text{PtHCl}(\text{NH}_3)_2 + \text{NH}_3$  with  $\text{H}^-$  as a  $\text{trans}$ -directing ligand. (After Lin and Hall [11.41].)

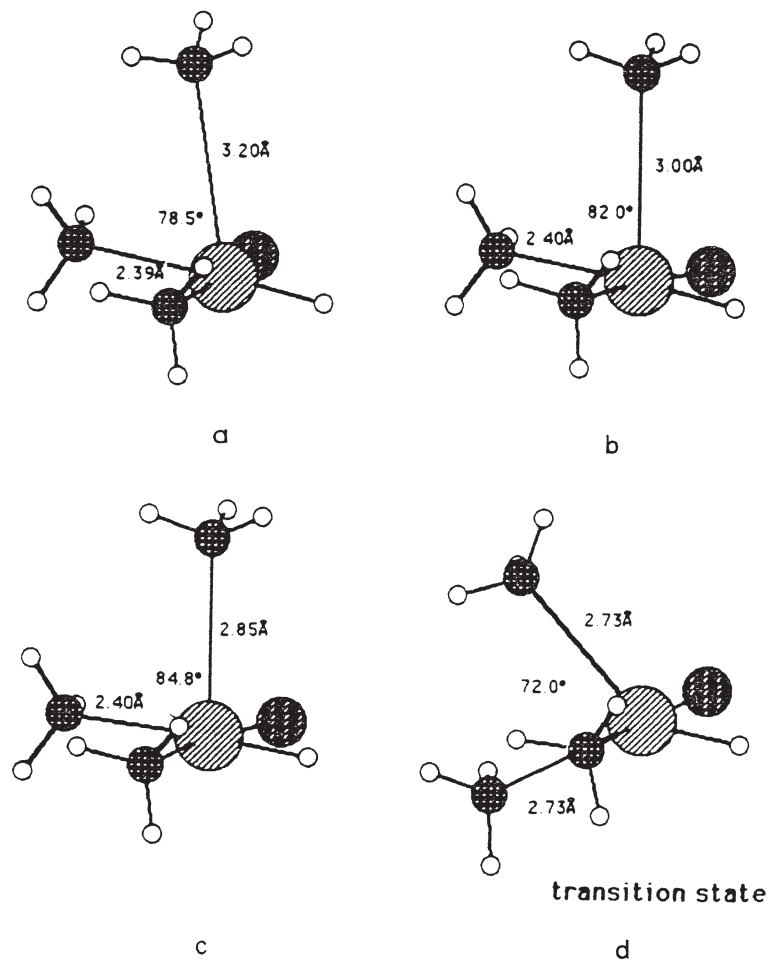


**FIGURE 11.13.** Optimized geometries for several fixed positions of the entering  $\text{NH}_3$  group in reaction (11.43) with  $\text{H}^-$  as the *trans*-directing ligand.

*cis*- $\text{PtHCl}(\text{NH}_3)_2 + \text{NH}_3$  with the substitution *trans* to H. The optimized ligand positions along the reaction path are shown in Fig. 11.13.

All the calculations were carried out by the *ab initio* MO LCAO RHF (restricted Hartree–Fock) method with effective core potentials (Sections 5.3 and 5.4) (calculation details are described well by Lin and Hall [11.41]). The validity of the results, especially the role of electron correlations, was examined by comparison with more sophisticated valence approaches. Total energies and activation energy differences (relative *trans* effects) are given in Table 11.6.

We begin the discussion of these results with Fig. 11.13 showing the optimized geometries for several fixed positions of the entering group  $\text{NH}_3$  in the reaction

**TABLE 11.6. Total Energies of Transition States and Activation Energy Differences for Different *trans*-Directing Ligands (Relative *trans* Effect) in Substitution Reactions (11.42)–(11.45)**

System	<i>Trans</i> -Directing Ligand	Total Energy of Transition State (au)	Activation Energy Difference (kcal/mol)
Rh(CO)H(NH <sub>3</sub> ) <sub>3</sub>	CO	−78.0154	10.92
	H <sup>−</sup>	−78.0239	
PtHCl(NH <sub>3</sub> ) <sub>3</sub>	H <sup>−</sup>	−75.7388	1.57
	Cl <sup>−</sup>	−75.7363	
Pt(CH <sub>3</sub> )Cl(NH <sub>3</sub> ) <sub>3</sub>	CH <sub>3</sub> <sup>−</sup>	−83.3640	0.38
	Cl <sup>−</sup>	−82.3634	
RhCl(NH <sub>3</sub> )(H <sub>2</sub> O) <sub>3</sub>	Cl <sup>−</sup>	−97.8882	7.28
	NH <sub>3</sub>	−97.8766	

Source: Lin and Hall [11.41].

(11.43) with H<sup>−</sup> as the *trans*-directing ligand. To understand the origin of these geometries, let us also employ the qualitative  $\sigma$  MO energy-level scheme for the initial square-planar 16-electron complex M( $d^8$ )L<sub>4</sub> shown in Fig. 11.14. It is seen that the LUMO is the pure  $p_z$  orbital of M, which is perpendicular to the plane of the complex, while the three ( $d_{xy}$ ,  $d_{xz}$ ,  $d_{yz}$ ) orbitals form three occupied lone pairs. When the  $\pi$  bonding is taken into account, these lone pairs form the corresponding MOs that have asymmetric distribution shifted toward the most *trans*-directing ligand (Fig. 11.11).

At large distances  $R = 3.2 \text{ \AA}$  (Fig. 11.13A), when there is no significant orbital overlap and bonding, the entering group NH<sub>3</sub> forms an angle  $\alpha = 78.5^\circ$  with the plane; it is narrower than  $90^\circ$  because of the repulsion from the corresponding  $d_\epsilon$  lone pair, which has the asymmetric distribution, mentioned above (Fig. 11.11). At smaller distances the NH<sub>3</sub> lone pair overlaps with the empty  $p_z$  orbital to form a square-pyramidal structure and the angle  $\alpha$  increases (Fig. 11.13, B and C). At equilibrium distances ( $R = 2.73 \text{ \AA}$ ) the optimized transition state is reached that has a pseudo-trigonal-bipyramidal structure (Fig. 11.13D); here a compromise between the repulsion of the two NH<sub>3</sub> ligands, their repulsion from the  $d_{xz}$  lone pair, and bonding to the rehybridized  $p$ - $d$  metal orbitals (including  $p_z$ ) is reached.

The less the repulsion from the lone pairs (directly dependent on the  $\pi$ -acceptor properties of the *trans*-directing ligand) and the weaker the metal-leaving and metal-entering bonds [dependent on the  $\sigma$ -donor properties of the *trans*-directing ligand, Section 9.3, Eq. (9.30)], the lower the energy of the transition state and hence the activation energy. These features are effective when the metal M has occupied  $d_\epsilon$  orbitals and the latter have a sufficient diffusiveness to overlap strongly with (and to be easily shifted to) the ligands. Second- and third-row  $d^8$  transition metals are good examples. Thus direct numerical calculations confirm the preceding qualitative statements: *The trans*

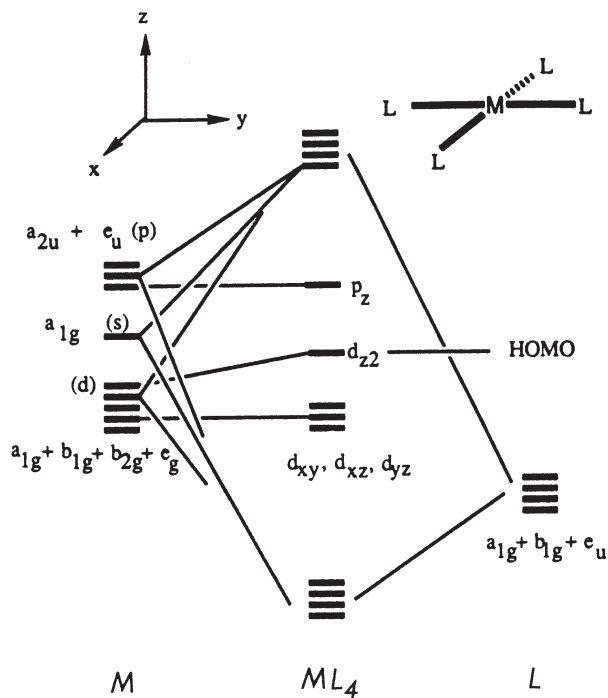


FIGURE 11.14. Schematic presentation of the  $\sigma$  MO energy levels of a 16-electron square-planar  $d^8$  transition metal complex  $ML_4$ .

effect is produced by an appropriate combination of  $\pi$ -acceptor and  $\sigma$ -donor properties of the *trans*-directing ligand and occupied diffuse  $d_\epsilon$  orbitals of the central atom. Numerical data of Table 11.9 show that among the ligands considered, the *trans* effect follows the series  $CO > H^- > CH_3^- > Cl^-$ , in agreement with the experimental order.

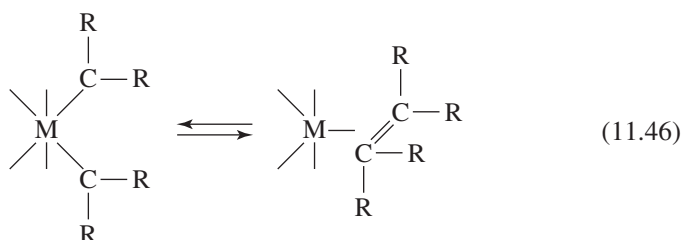
Lin and Hall [11.41] elucidate many other details of the *trans*-effect mechanism. In particular, they show that the monomolecular mechanism of substitution reactions (via dissociation) have an activation energy that is considerably higher than that in the associative mechanism.

### Ligand Coupling and Cleavage Processes

Transition metal systems are often involved in chemical transformations as catalysts. In principle, catalytic reactions are similar to noncatalytic reactions with the distinction that in the former the yield of the reaction leaves one of the reactants unchanged. In Sections 6.3 and 11.2, the specific features of transition metals important to catalytic action are emphasized; because of the active  $d$ -electron configurations, *transition metals and their complexes form multiorbital bonds with ligands, with the effect of strong activation of the latter.*

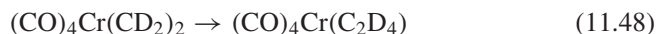
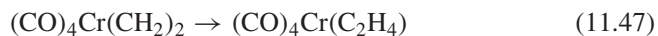
Another important feature is that, owing to high coordination numbers, coordination compounds may serve as a *center of "organization"* of the reactants promoting specific mechanisms of the reaction. This "organizational" aspect of coordination is of special importance in *supramolecular chemistry*, where the coordination system, via *recognition, orientation, and termination*, serves as a center of self-organization, self-assembly, and *templating* [11.42, 11.43].

A relatively simple example of catalytic action of coordination compounds is provided by the bonding of two coordinated carbon ligands  $CR_2$  in *cis* positions forming an olefin  $C_2R_4$ , and the inverse process of cleavage of a coordinated olefin into a bis-carbene complex:



The first attempt to model this reaction was made for the "naked metal"  $M = W$  and  $R = H$  [11.44]. Figure 11.15 illustrates the MO energy-level diagram as a function of the angle between the two carbon ligands obtained by the semiempirical extended Hückel method (Section 5.5). It is seen that for a metal  $M$  with more than two electrons (in  $W$  they are six), the least-motion process of direct bonding of two methylene groups  $CH_2$  to form  $C_2H_4$  is forbidden by symmetry considerations (Section 11.1), since it involves the highly excited state  $2b_2$  of  $C_2H_4$ .

A more complete analysis, using the same approach and the same method of calculation, was carried out for the reactions [11.45]



where  $D$  is a  $\pi$ -donor substituent ( $D = NR_2$ ).

For the reaction (11.47), the MO energy-level diagram [11.45] shows that, as compared with the unligated metal (Fig. 11.15), the ordering of the important MO levels under the influence of the four  $\pi$ -acceptor CO groups changes significantly, and the  $2b_2$  MO is no longer involved in the reaction. Instead, the  $1b_2$  level in the olefin side is pushed up and unoccupied, and hence the reaction of direct least-motion coupling is again formally forbidden. This means that somewhat less symmetric pathways, although formally allowed by symmetry considerations, may still encounter energy barriers.

The qualitative MO energy-level diagrams give no definite information about the relative thermodynamic stability of the two systems and the height of the

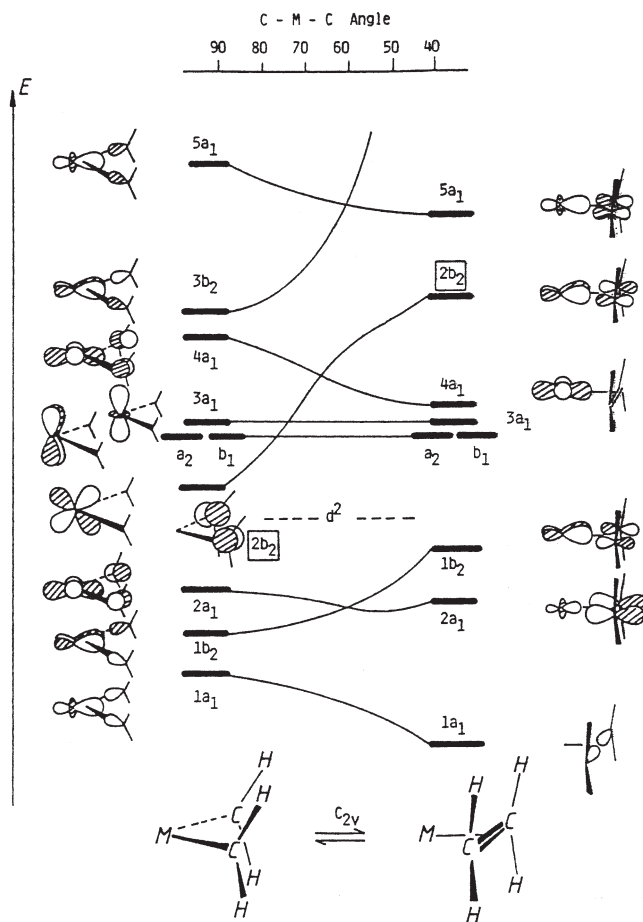


**FIGURE 11.15.** MO energy-level correlation diagram for a  $C_{2v}$  least-motion coupling/decoupling of two methylene groups coordinated to a unligated metal center. Symmetries of the AOs that form the corresponding MOs and the  $d^2$  configuration limit are also shown. (After Hoffmann et al. [11.44, 11.45].)

energy barrier between them. To answer these questions, calculations of the potential energy surface for the least-motion coupling (uncoupling) of the two methyl groups in reaction (11.47) were carried out [11.45]. Two coordinates, the angles  $\theta$  (between the two M—C bonds, Fig. 11.16) and  $\Phi$  (between the  $\text{CH}_2$  plane and the M—C bond) were chosen to describe the reaction pathway. Their variation with the fixed position of the  $\text{Cr}(\text{CO})_4$  group results in the potential energy surface presented schematically in Fig. 11.17. The surface has two minima for the olefin and bis-carbene complexes, respectively. Interestingly, in this model the olefin complex, which is a 16-electron system, is more stable than the 18-electron bis-carbene complex; the allowance for a more relaxed configuration



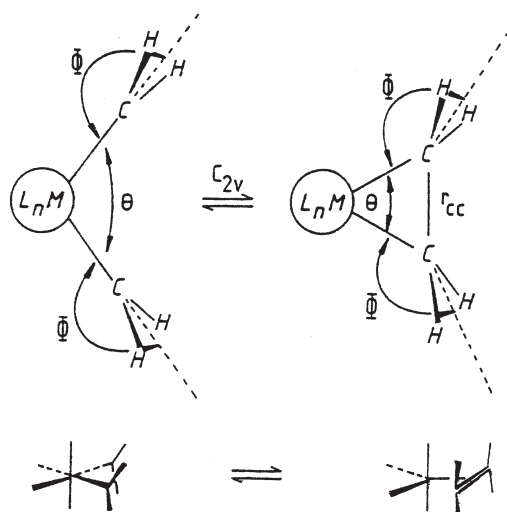


**FIGURE 11.16.** The angles  $\theta$  and  $\Phi$  chosen to describe the least-motion convergence of two  $\text{CH}_2$  groups and their planes bending in the reaction (11.47). Instead of  $\theta$ , the interatomic  $r_{\text{CC}}$  distance can be equally useful. (After Hoffmann [11.45].)

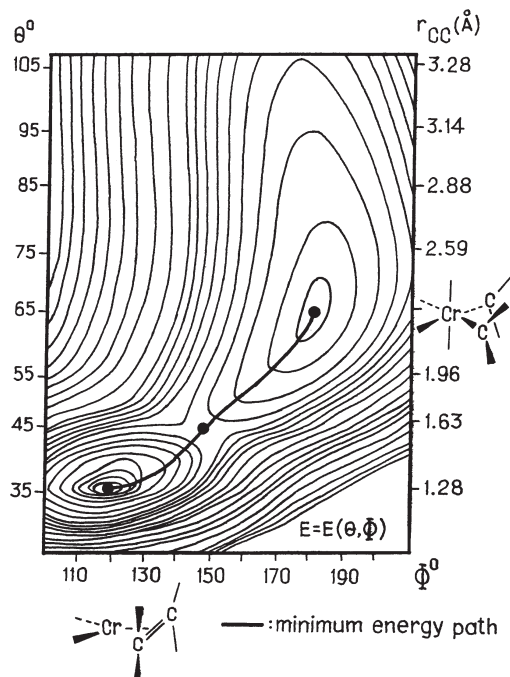
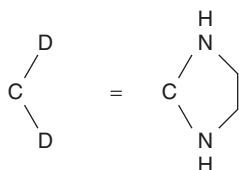


**FIGURE 11.17.** APES of the reaction (11.47) as a function of angles  $\theta$  and  $\Phi$  characterizing the two methyl group least-motion convergence and their planes bending (Fig. 11.16). Contour lines at 0.1 eV separation. (From Hoffmann [11.45].)

with optimization of the CO ligand positions is expected to lower the energy of the olefin complex. The energy barrier between these two minima is rather low, about 10 kcal/mol, and will be probably even lower for a less symmetric reaction pathway.

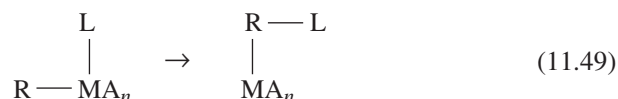
With good  $\pi$ -donor substituents in the methyl groups  $\text{CD}_2$ , the situation changes drastically. The experimental data show that in this instance the *bis*-carbene  $d^6$  complexes  $\text{M}(\text{CO})_4(\text{CD}_2)_2$  are stable compounds and can be obtained from the corresponding olefin. The calculations using the approach described above confirm these results and reveal their origin. The corresponding APES in  $(\theta, \Phi)$  coordinates for



is illustrated in Fig. 11.18. It is seen that here there is only one minimum for the bis-carbene complex, and no minimum for the olefin complex. The MO energy-level diagram [11.45] shows that the reaction under consideration is symmetry-allowed and may proceed without energy barrier, as the olefin complex is thermodynamically less stable (all the MO energy levels are lower in the bis-carbene complex). The reason for this effect can be revealed from the analysis of the MO energy-level reordering produced by the donor D substitution.

### CO Reductive Hydrogenation and Carbonyl Insertion Reactions

Insertion reactions of the type



where R is an unsaturated ligand and  $\text{M}-\text{L}$  is a metal-hydrogen or a metal-carbon bond, are most important in modern organometallic chemistry as the key processes in many catalytic cycles. In this subsection we consider the examples of CO insertion into  $\text{M}-\text{H}$  and  $\text{M}-\text{CH}_3$  bonds and a related reaction of coordinated CO hydrogenation [11.46, 11.47]. The next subsection is devoted to olefin insertion reactions.

Homogeneously catalyzed carbon monoxide hydrogenation underlies many processes, including conversion of the  $\text{CO}/\text{H}_2$  mixture into liquid fuels and production of methanol, ethanol, ethylene glycol, and other compounds. The process can be presented as either a nucleophilic addition of a hydride ion

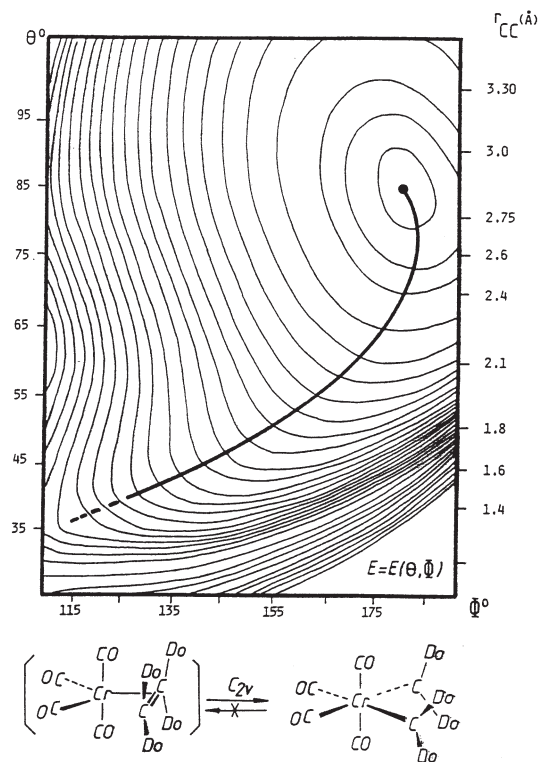
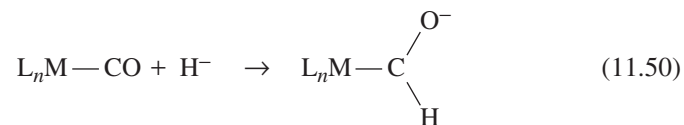
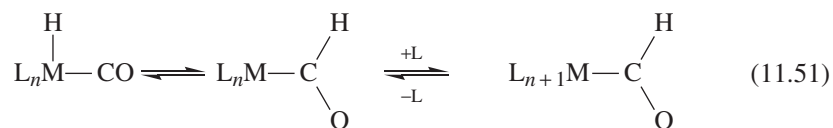


**FIGURE 11.18.** APES for the reaction (11.48). The coordinates  $\theta$  and  $\Phi$  (or  $r_{CC}$ ) are given in Fig. 11.16. (After Hoffmann [11.45].)



or an insertion of a carbonyl ligand into the metal-hydride bond:

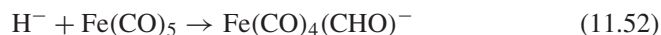


The two reactions (11.50) and (11.51), despite an apparent similarity, are significantly different; many examples of the first reaction are known, whereas examples of the second type, (11.51), are generally lacking, at least when resulting

in a monohaptoformyl ligand. The hydride affinity of coordinated carbonyls is large (ranging from 45 to 55 kcal/mol) as compared with that of bare carbon monoxide (a few kcal/mol only), and this indicates the significant activation of the CO molecule by coordination to transition metals (Section 11.2).

To reveal the reaction mechanism, calculations of the APES in the space of a possible reaction pathway for prototype reactions have been performed [11.46]. The calculations carried out in the ab initio SCF-MO-LCAO approximation (Section 5.3) with extended basis sets and other computational details are discussed by Dedieu and Nakamura [11.46]. The role of electron correlation effects was also elucidated by means of additional CI calculations (Section 5.3).

For the hydrogenation reaction, the reaction of addition of  $\text{H}^-$  to  $\text{Fe}(\text{CO})_5$  has been considered:



The approach of the hydride is restricted by the plane containing two axial ligands and one equatorial ligand. The numerical results are illustrated in Fig. 11.19, and the optimized geometry is shown in Fig. 11.20. In the geometry calculations the axial Fe—C—O angle is allowed to relax, while the Fe—C and C—O distances are kept fixed at 1.81 and 1.22 Å, respectively.

Figure 11.19 shows that the reactions are highly exothermic (~52 kcal/mol) and proceed without any energy barrier. This is in agreement with the corresponding gas-phase studies [11.48]. The calculation details also explain the origin of the high affinity of the activated CO ligand for the  $\text{H}^-$  ion and the role of the metal  $d_{z^2}$  orbital in this process [11.46].

For the CO ligand insertion reaction (11.49), the prototype example is taken as follows:



In principle, there are two main pathways for this reaction to proceed: (1) proper insertion of the CO molecule into the Mn—H bond or (2) migration of the hydrogen atom to the CO ligand to form the CHO ligand. To reveal the true process, a two-dimensional APES as a function of two critical angles,  $\alpha$  and  $\beta$ , has been calculated [11.46]. The two angles are chosen as shown in Fig. 11.21, while the two out-of-plane (perpendicular to the reaction plane) carbonyl ligands are kept frozen; the Mn—C and C—O bond lengths of the nonreacting in-plane CO ligands are also kept fixed at their experimental values. For each point of the surface ( $\alpha$ ,  $\beta$ ), the Mn—H bond length ( $d$ ), the angles  $\gamma$  and  $\delta$ , and the C—O bond length were successively optimized, and then the Mn—C bond length ( $R$ ) was optimized for representative points of the minimum-energy path.

The results are illustrated in Fig. 11.22, and the successive geometries of the system along the resulting reaction path are given in Fig. 11.23. It is seen that

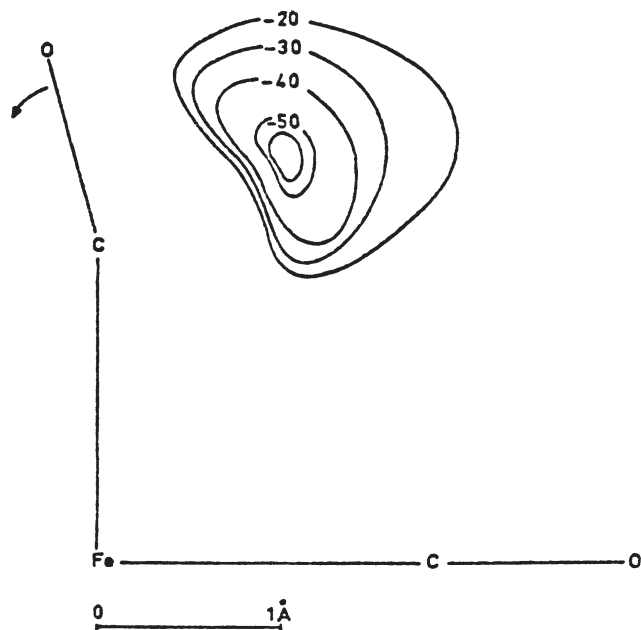


**FIGURE 11.19.** Contour lines of the APES for the approach of the hydride ion (energies in kcal/mol with respect to separated reactants). The inner contour is  $-52$  kcal/mol. (After Hoffmann [11.45].)

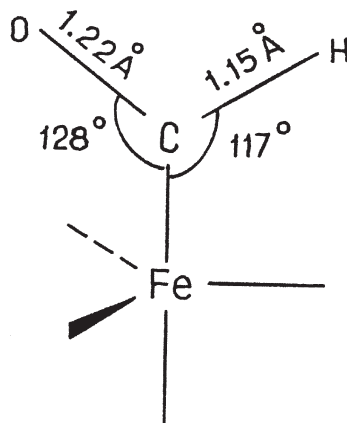


**FIGURE 11.20.** The optimized geometry of the hydrogenated system  $\text{Fe}(\text{CO})_4(\text{CHO})^-$ .

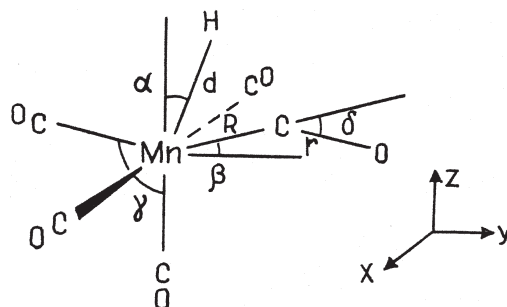


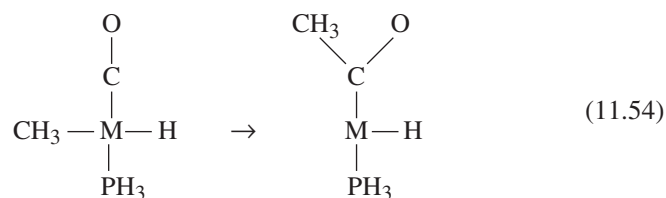
FIGURE 11.21. Variation coordinates for the CO ligand insertion reaction (11.53).

the process is best described as a hydride migration and not CO insertion in agreement with experimental data and other theoretical investigations.

Figure 11.23 shows that the geometry of the CO groups remains virtually unchanged during the reaction. The geometry of the transition state *D* is near that of a five-coordinated formyl intermediate *F*. The energy profile as a function of the H—Mn—C angle  $\eta$  for the configurations from *A* to *F* of Fig. 11.23 is shown in Fig. 11.24. In the SCF approximation the energy barrier of the reactions is about 15 kcal/mol with a small difference between *D* and *F* (about 4 kcal/mol). However, CI calculations with electron correlation effects carried out for the three key structures *A*, *D*, and *F* show a large increase in the reaction barrier of the forward reaction and its decrease (almost to zero) for the inverse reaction (Fig. 11.24). Analysis of computational details [11.46] shows the reason for this result to be the inadequate description of the difference in the  $\pi$  backdonation to CO and CHO without CI. This feature is also inherent in other processes in which similar ligand changes occur. For the whole process  $\text{HMn}(\text{CO})_5 + \text{CO} \rightarrow \text{Mn}(\text{CO})_5\text{CHO}$  in which the number of CO ligands is not changed, the calculated endothermicity 3.7 kcal/mol roughly agrees with the experimental value of 5 kcal/mol.

Thus the failure to observe CO insertion into a metal hydride bond resulting in a monohaptoformyl ligand is well accounted for by the high energy barrier and the close proximity of the transition state with the five-coordinated intermediate.

For a similar reaction of CO ligand insertion into a M—CH<sub>3</sub> bond



with  $\text{M} = \text{Pd}, \text{Pt}$ , calculations were carried out [11.47] for electronic structure, energy, and geometry of the initial complex, activated state, and the product of the

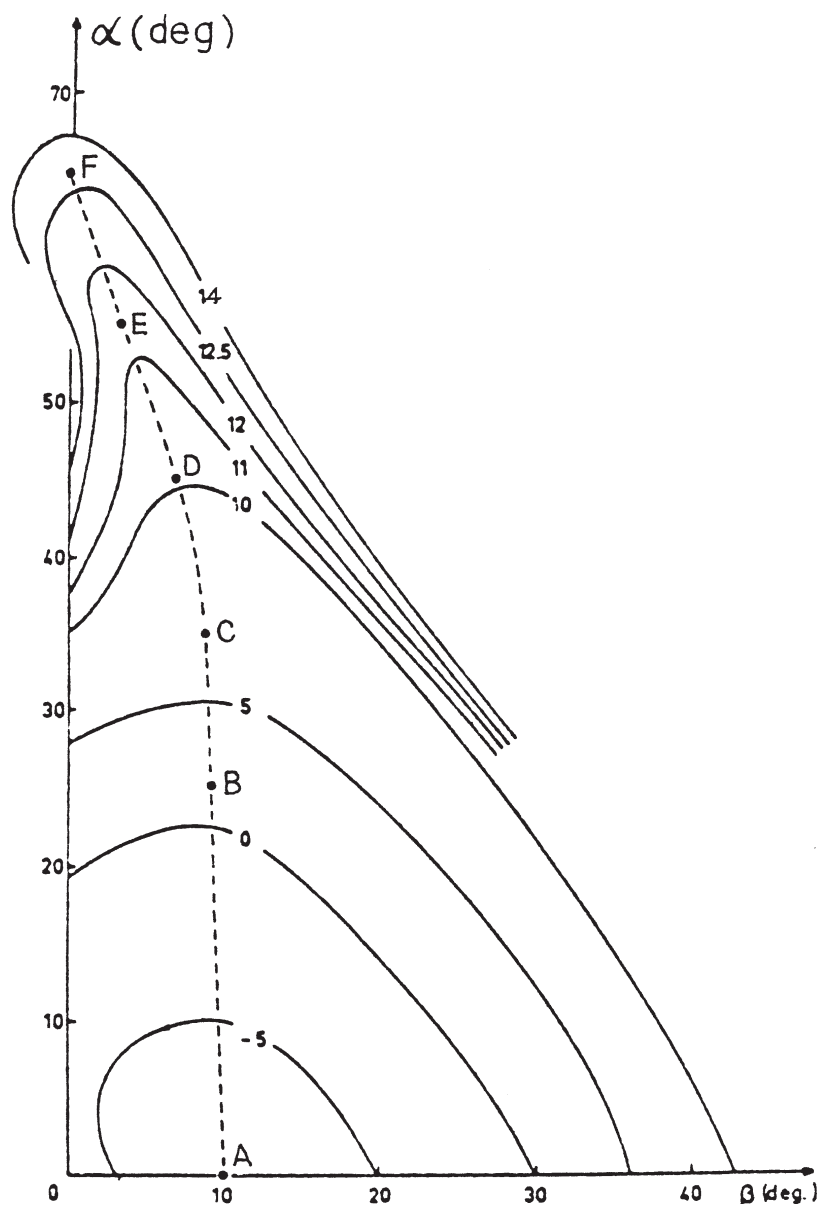


**FIGURE 11.22.** Contour lines of the APES for the reaction (11.53) as a function of the angles  $\alpha$  and  $\beta$  specified in Fig. 11.21. The distance  $R = 1.885 \text{ \AA}$  is kept constant and the energies are read off the point  $\alpha = \beta = 0$ . (From Dedieu and Nakamura [11.46].)

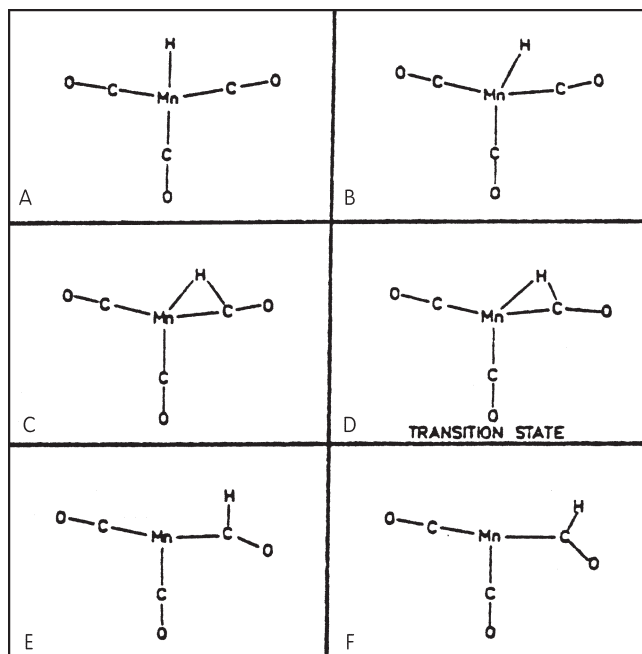


**FIGURE 11.23.** In-plane geometry changes along the reaction path of the hydride migration in the  $\text{HMn}(\text{CO})_5$  system (the two CO ligands perpendicular to the plane are not shown). (After Dedieu and Nakamura [11.46]).

reaction. The authors use the ab initio SCF MO LCAO restricted Hartree–Fock (RHF) approximation with gradient technique for geometry optimization and perturbation theory (MP2) for electron correlation effects (Section 5.3), as well as relativistic effective core potentials for the metal atoms (Section 5.4).

The optimized geometries are illustrated in Fig. 11.25, while relative energies are given in Table 11.7.

It is seen that, similar to the previous case of CO insertion into the  $\text{M—H}$  bond, where, in fact, there is no insertion but H migration, there is no CO insertion into the  $\text{M—CH}_3$  bond, either; the reaction proceeds as a  $\text{CH}_3$  migration toward the CO ligand in accordance with experimental data. The energy of a similar transition state with CO migration instead of  $\text{CH}_3$  [a configuration in which the angles  $(\text{CO})\text{—Pd—(H)}$  and  $(\text{CH}_3)\text{—Pd—(PH}_3)$  of the true transition state in Fig. 11.25 are exchanged] is about 7 kcal/mol higher than the true transition state.

The reason for this reaction pathway is in the strong repulsion of the carbonyl lone pair from the occupied  $d_{xy}$  orbital of the metal in the case of CO migration (Fig. 11.26a). This repulsion is significantly lower when the  $\text{CH}_3$  group migrates (Fig. 11.26b), due to the lower electron density in the hybridized  $sp^3$  orbital pointed toward the lobe of the metal  $d_{xy}$  orbital (approximately one electron instead of two electrons in the CO lone pair) and the longer distance  $\text{M—CH}_3$ .



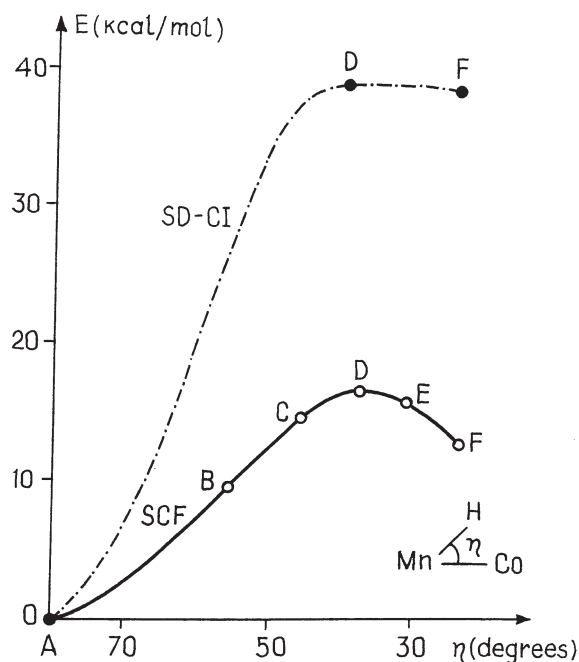


**FIGURE 11.24.** SCF and CI calculated energy profiles for the hydride migration process (Fig. 11.23) as a function of the H—Mn—C angle  $\eta$ .

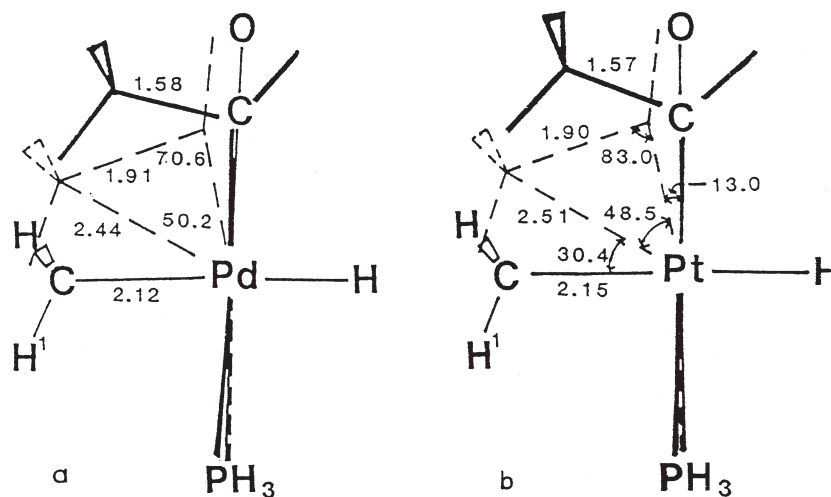


**FIGURE 11.25.** Optimized geometries (in angstroms and degrees) of  $M(\text{CH}_3)\text{H}(\text{CO})\text{PH}_3$  and  $M(\text{COCH}_3)\text{H}(\text{PH}_3)$  (thick solid lines),  $M = \text{Pd}, \text{Pt}$  and the transition states (dashed lines) for the CO insertion ( $\text{CH}_3$  migration) and inverse reaction. (After Koga and Morokuma [11.47].)

**TABLE 11.7. Relative Energies (in kcal/mol) of the Transition States and Products of Reaction  $M(\text{CH}_3)\text{H}(\text{CO})(\text{PH}_3) \rightarrow M(\text{COCH}_3)\text{H}(\text{PH}_3)$ , with  $M = \text{Pd, Pt}$  Calculated without (RHF) and with (MP2) Electron Correlation Effects**

M	Method	Reactant	Transition State	Product
Pd	RHF	0.0	25.8	19.1
	MP2	0.0	13.5	8.8
Pt	RHF	0.0	31.3	23.0
	MP2	0.0	21.8	17.6

Source: Koga and Morokuma [11.47].

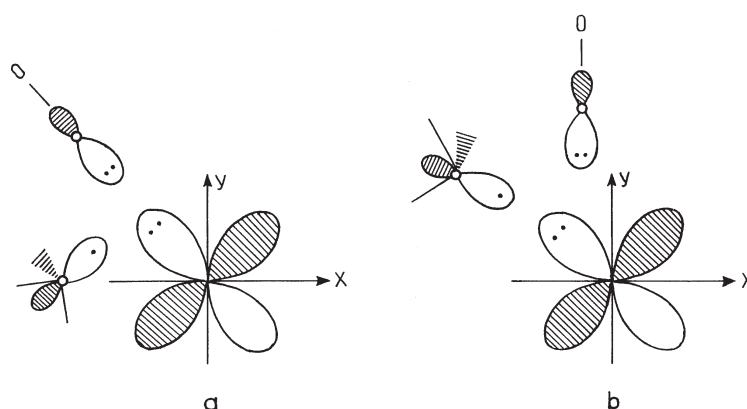


**FIGURE 11.26.** Interaction of two electrons of the CO lone pair and one electron of the  $\text{CH}_3$   $sp^3$  orbital with the metal occupied  $d_{xy}$  orbital in the CO migration (a) and in the true transition state of  $\text{CH}_3$  migration (b).

Although the structural changes in the preceding two reactions with Pd and Pt are almost the same, the energetics is quite different (Table 11.7); the activation energy in the Pt complex is considerably higher than in Pd (at the MP2 levels 21.8 and 13.5 kcal/mol, respectively). This is due to the differences in the  $M-\text{CH}_3$  and  $M-\text{CO}$  bond energies, which are, respectively, higher by 7 and 11 kcal/mol in the Pt complex than in the Pd one, while the  $\text{Pt}-\text{COCH}_3$  bond is stronger by 9 kcal/mol than  $\text{Pd}-\text{COCH}_3$  bond. Therefore, the Pd reaction is more endothermic by  $(7 + 11 - 9) = 9$  kcal/mol, and hence it has a higher energy barrier.

The reaction was also studied for  $\text{CH}_3$ -substituted ligands [11.47]. Some results for the energetics of these reactions obtained for the fixed ligand geometries (Fig. 11.25) are given in Table 11.8.

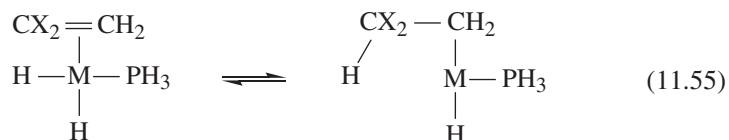
### Olefin Insertion Reactions

Olefin insertion reactions are of great importance in organometallic chemistry and chemical industry as basic models of the corresponding polymerization

**TABLE 11.8. Relative Energies (in kcal/mol) for the CO Insertion (R Migration) Reaction Pd(R)H(CO)(PH<sub>3</sub>) → Pd(COR)H(PH<sub>3</sub>)**

R	Reactant	Transition State	Product
CHF <sub>2</sub>	0.0	40.9	31.2
C <sub>2</sub> H <sub>5</sub>	0.0	23.1	14.6

processes. Formally, olefin insertion is similar to the CO insertion considered above. For ethylene and its derivatives CX<sub>2</sub>=CH<sub>2</sub> insertion into the M—H bond (and inversely, β elimination), the following four reactions were investigated [11.47]:



The method of numerical computation is the same RHF method with the MP2 corrections mentioned above for the CO insertion reactions (for details, see the paper by Koga and Morokuma [11.47]). This method was used to calculate the optimized geometries and energies of the transition states and products of the reaction. The results are illustrated in Table 11.9 and Fig. 11.27. It is seen that the reaction proceeds as a hydrogen migration via a four-center transition state; its optimized geometry is shown for the Pt reaction (11.58).

For other reactions the transition state is similar, with the distinction that for Ni and Pd the transition state is achieved much earlier with smaller distortions of the M—H and C=C bonds (Ni produces smaller distortions than does Pd) and corresponding structural differences in the products (see below). This is also seen from the energy profile of the reaction given by the energies in Table 11.9; the activation barrier is much lower for the Ni reaction (11.56) and increases for similar reactions (11.57) and (11.58) with Pd and Pt. On the other hand, the reaction for the Ni complex is also most exothermic.

These effects are due, first, to the strength of the M—(C<sub>2</sub>H<sub>4</sub>) bond, which is very weak for Ni and increases for Pd and Pt. Therefore, the Pt–ethylene complex is more stable than the ethyl complex. The stability of the ethyl complex increases in the order Pt < Pd < Ni, while the barrier height for the migration reaction decreases in the order Pt > Pd > Ni. In general, the metal–ethylene bonds are relatively weak indicating a strong *trans* influence of the hydride ligand.

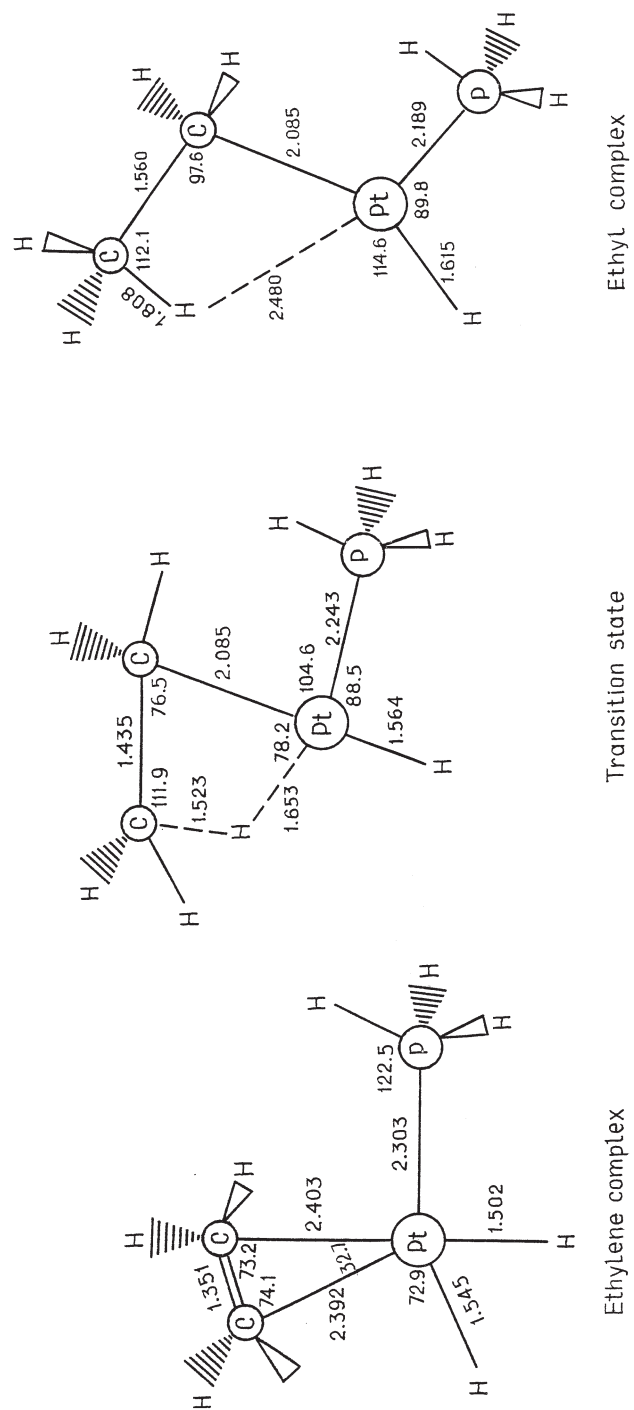


**FIGURE 11.27.** Optimized geometries (distances in angstroms and angles in degrees) of ethylene and ethyl complexes and the transition state of the reaction  $\text{Pt}(\text{CH}_2=\text{CH}_2)(\text{H})_2\text{PH}_3 \rightarrow \text{Pt}(\text{CH}_3-\text{CH}_2)(\text{H})\text{PH}_3$  (for simplicity, some of C—H bond lengths and angles are not indicated; see Koga and Morokuma [11,47]).

**TABLE 11.9. Relative Energies of the Reaction  $M(H)_2(CH_2CX_2)(PH_3) \rightarrow M(CH_2CHX_2)(H)(PH_3)$  (in kcal/mol)**

M	X	Ethylene Complex	Transition State	Ethyl Complex
Pd	H	0.0	8.0	-3.0
		0.0	5.1 <sup>a</sup>	3.0 <sup>a</sup>
Pd	F	0.0	7.3	-11.1
Ni	H	0.0	0.6	-31.5
Pt	H	0.0	12.5	4.2

<sup>a</sup>Calculated including correlation effects in the MP2 approximation with RHF geometries.

**TABLE 11.10. Comparison of Activation Energies of  $\beta$ -Elimination Reactions  $M(CH_2CHX_2)(H)(PH_3) \rightarrow M(H)_2(CH_2CX_2)PH_3$  with a Qualitative Estimate of Inverse and Backdonative Interaction**

M	X	Activation Energy	Inverse Interaction	Backdonation
Pd	H	11.0	Excellent	Good
	F	18.4	Fair	Good
Ni	H	32.1	Good	Poor
Pt	H	8.3	Good	Excellent

Source: Koga and Morokuma [11.47].

As for the inverse reaction of  $\beta$  elimination, its activation energy depends mainly on two effects: (1) the remaining interaction of the migrating hydrogen  $H^\beta$  with the metal atom M via  $\sigma$  donation from the  $CH^\beta$  bonding orbital to the empty  $d + p$  orbital of the free coordination place (the so-called *inverse interaction*), and (2) the backdonation from the occupied metal  $d_{xy}$  orbital to the antibonding  $\sigma^*$  orbital of  $CH^\beta$  that weakens the bonds in the latter. Calculations [11.47] show that the inverse interaction is stronger in the Pd reaction (11.57) and decreases toward Pt and Ni. The backdonation, on the contrary, is stronger in the Pt complex because of its more diffuse  $d_{xy}$  orbital, and is very poor in Ni for similar reasons. The activation energy is thus a result of a combination of these two reasons, illustrated qualitatively in Table 11.10.

As mentioned above, insertion reactions underlie many catalytic processes. As an illustration of this statement, the reaction of catalytic insertion of ethylene in the M—CH<sub>3</sub> bond in the Ziegler–Natta polymerization process is considered in Example 11.9.

### EXAMPLE 11.9

#### *Polymerization with Ziegler–Natta Catalysts*

Ethylene insertion into the M—CH<sub>3</sub> bond is the basic elementary step in the well-known Ziegler–Natta catalytic ethylene polymerization

process:



Cossee [11.49] first considered this process as ethylene coordination to Ti followed by a  $\text{C}_2\text{H}_4$  insertion reaction into the Ti—CH<sub>3</sub> bond in

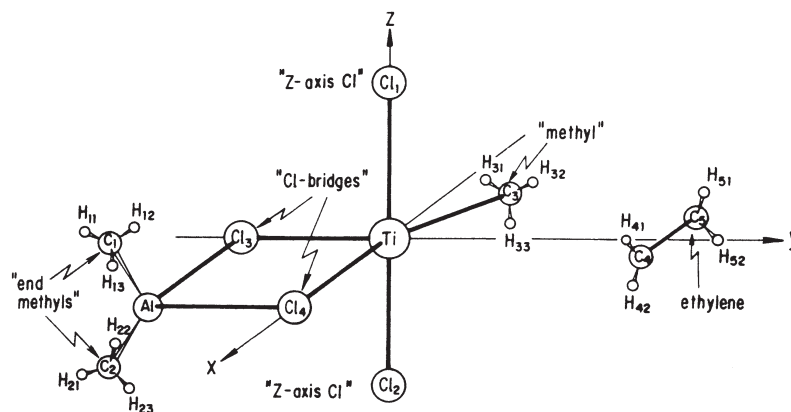


**FIGURE 11.28.** The catalyst-ethylene complex in the Ziegler-Natta catalytic polymerization of ethylene and the denotation of the atoms.

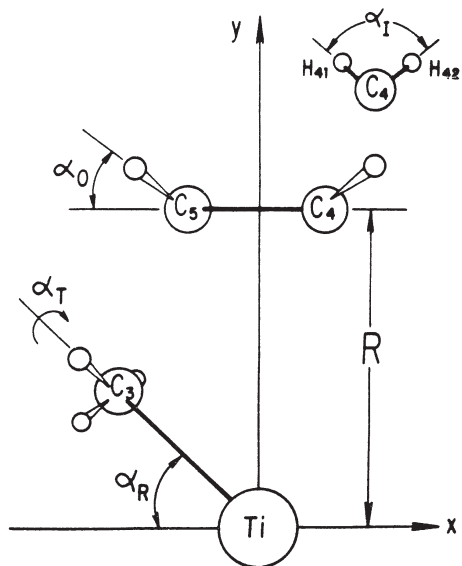


**FIGURE 11.29.** Geometric variation parameters describing the 12 steps in Table 11.11 in the pathway of the reaction (11.60). (After Novaro et al. [11.50].)

the *cis* position, and involved ligand field and semiempirical MO LCAO considerations in support of this reaction mechanism. A more detailed calculation of the energies along the reaction pathway and the activation energy with a detailed analysis of the electronic origin of the phenomenon was carried out by Novaro et al. [11.50].

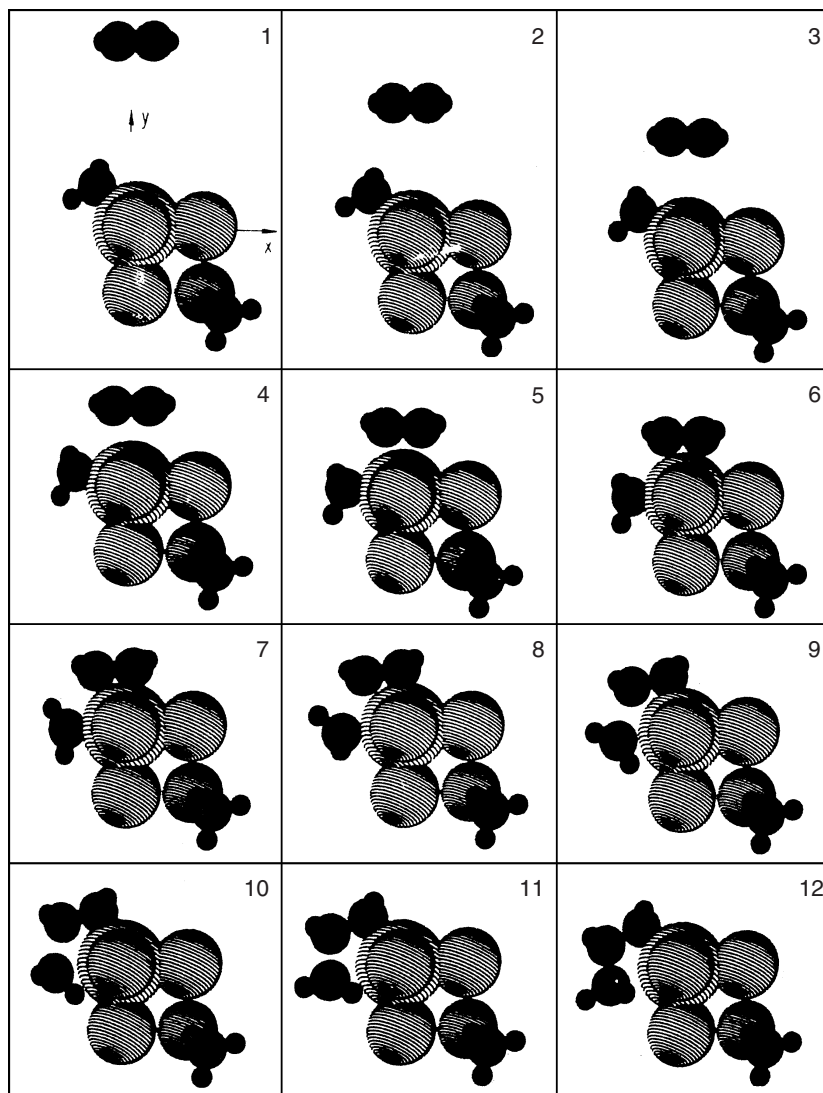


**FIGURE 11.30.** Molecular models for the 12 steps of the reaction (11.60) characterized in Table 11.11. (After Novaro et al. [11.50].)

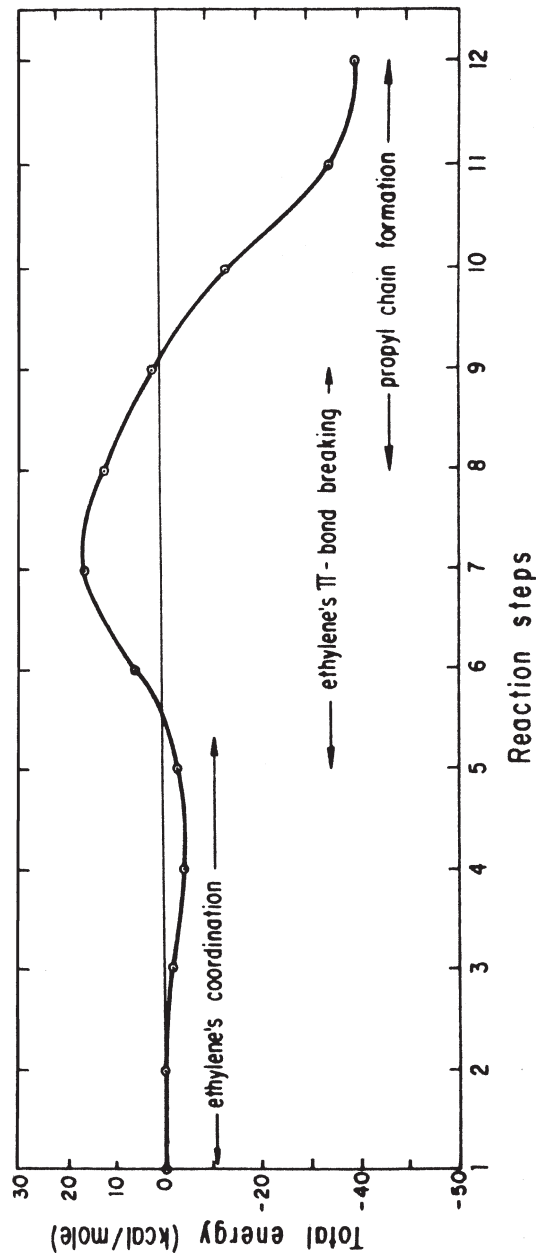


**FIGURE 11.31.** Evolution of the total energy (the reaction curve) in the Ziegler-Natta polymerization process (11.60) along a given pathway specified by the 12 steps in Table 11.11.



**TABLE 11.11. Geometries and Total Energies for a Sequence of Configurations Describing the Pathway of Reaction (11.60)<sup>a</sup>**

Reaction Step	$R(\text{Ti}-\text{C}_4)$ (Å)	$R(\text{Ti}-\text{C}_5)$ (Å)	$R(\text{Ti}-\text{C}_3)$ (Å)	$R(\text{C}_3-\text{C}_5)$ (Å)	$\alpha_R$ (°)	$\alpha_0$ (°)	$\alpha_I$ (°)	$r$ (Å)	$\Delta E = E_i - E_1$ (kcal/mol)
1	7.03	7.03	2.15	5.55	45	0	117	1.337	0
2	5.04	5.04	2.15	3.58	45	0	117	1.337	-0.3
3	4.06	4.06	2.15	3.23	28	0	117	1.337	-1.9
4	3.08	3.08	2.15	2.71	13	8	115	1.383	-4.2
5	2.59	2.59	2.15	2.70	8	16	115	1.383	-3.0
6	2.40	2.43	2.15	2.69	0	19	114	1.406	+5.3
7	2.24	2.39	2.26	2.48	-2.3	23	113.25	1.428	15.0
8	2.18	2.49	2.37	2.31	-4.6	28	112.49	1.451	10.9
9	2.14	2.60	2.48	2.14	-6.9	34	111.74	1.473	1.1
10	2.124	2.73	2.59	1.95	-9.2	40.9	110.98	1.495	-14.2
11	2.126	2.88	2.65	1.75	-11.5	47.8	110.23	1.518	-34.5
12	2.15	3.03	2.81	1.54	-13.8	54.7	109.47	1.54	-40.3

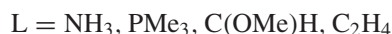
<sup>a</sup>The energy is read off the first step with  $E_1 = -3112.1681$  au. The geometric parameters are defined as shown in Fig. 11.29;  $r = R(\text{C}_4 - \text{C}_5)$ .  
Source: Novaro et al. [11.50].

A schematic representation of the catalyst–ethylene complex and the notation of atoms is shown in Fig. 11.28. The reaction mechanism is assumed, in principle, to be similar to that suggested earlier by Cossee [11.49]; 12 steps, including ethylene bonding and CH<sub>3</sub> migration, are taken as the reaction pathway. Calculations were carried out by means of the ab initio all-electron SCF MO LCAO (RHF) approximation (Section 5.3). The parameters for the 12 steps and the calculated energies are given in Table 11.11, while denotation of the corresponding angles is shown in Fig. 11.29. For each Ti–C<sub>2</sub>H<sub>4</sub> distance, optimization of the other parameters is performed. A visual presentation of the reaction by means of molecular models is given in Fig. 11.30.

Figure 11.31 shows the evolution of the total energy of the system as a function of the reaction path presented by the 12 reaction steps mentioned above. It is seen that at the beginning of the ethylene approach to the complex the energy lowers slightly, due to the metal–ethylene bond formation with a bonding energy of more than 4 kcal/mol. At step 6 with a Ti–C<sub>2</sub>H<sub>4</sub> distance of 2.4 Å, the energy increases, and this increase is attributed mainly to the ethylene's π-bond breaking. The highest activation of the C=C bond is reached at step 7 [ $R(\text{Ti}-\text{C}_4) = 2.24$  Å,  $R(\text{Ti}-\text{C}_5) = 2.39$  Å], after which the bonding to the CH<sub>3</sub> group increases and the energy decreases; at step 8 the π bond finally breaks. These and many other details are seen clearly from the MO populations and charge distribution discussed thoroughly by Novaro et al. [11.50].

### Photochemical Reactions of Organometallics

From the computational perspective, photochemical reactions are more complicated because they involve excited states for which quantum-chemical calculations are in general more difficult. On the other hand, photochemical reactions are rather widespread in chemistry. By way of examples demonstrating theoretical possibilities, the following reactions are considered [11.51]:



The calculations were carried out by the ab initio SCF MO LCAO method with CI (Section 5.3). For all these reactions the APES of the ground and excited electronic states as a function of the corresponding coordinate of the ligand elimination were calculated and analyzed. Strictly speaking, these curves are

cross sections of the multidimensional APES, with some additional symmetry and bond lengths restrictions.

For the first reaction, (11.61), the reaction path of equatorial CO ligand elimination is taken as shown in Fig. 11.32a maintaining  $C_{2v}$  symmetry of the product. For the second reaction, (11.62), both the reactant and the product  $\text{Co}(\text{CO})_4$  belong to  $C_{3v}$  symmetry (in their ground states), and therefore the reaction coordinate is taken as shown in Fig. 11.32b.

The results of the computations for these two reactions are illustrated in Figs. 11.33 and 11.34. It is seen that in both cases there are excited states that lead to the ligand elimination without any energy barrier. However, not all the excited states evolve to the dissociation products in their ground states. A special feature of the two reactions is that their products have a triplet spin ground state,  $^3B_2$  and  $^3A_1$  for reactions (11.61) and (11.62), respectively. This means that, since the ground states are singlets, only singlet–triplet excitation may lead to direct photolysis of the ligands shown above:  $^1A_1 \rightarrow ^3E'$  in CO photoelimination from  $\text{Fe}(\text{CO})_5$ , and  $^1A_1 \rightarrow ^3A_1$  in hydrogen elimination from  $\text{HCo}(\text{CO})_4$ .

These electronic singlet  $\rightarrow$  triplet transitions are spin-forbidden (Section 8.1), and therefore they are difficult to perform experimentally, especially in the presence of close-in-frequency, much more intensive singlet–singlet transitions (e.g.,  $^1A'_1 \rightarrow ^1E'$  in Fig. 11.33). Therefore, another mechanism of photolysis has been suggested [11.51]. It is illustrated in Fig. 11.35; the reactant is photoexcited to a singlet state and then, by way of radiationless transition (via spin–orbital coupling and thermal effects), the corresponding triplet state is populated. From the latter the molecule, according to Figs. 11.33 and 11.34, can dissociate to the products in the ground state without any energy barrier.

In fact, this mechanism of photolysis is valid (qualitatively) in many other photochemical reactions where homolysis of a  $\sigma$  bond takes place with the reactant in a singlet ground state and the products in a triplet state. Daniel and Veillard [11.51] list some examples, including dissociation of hydrogen from

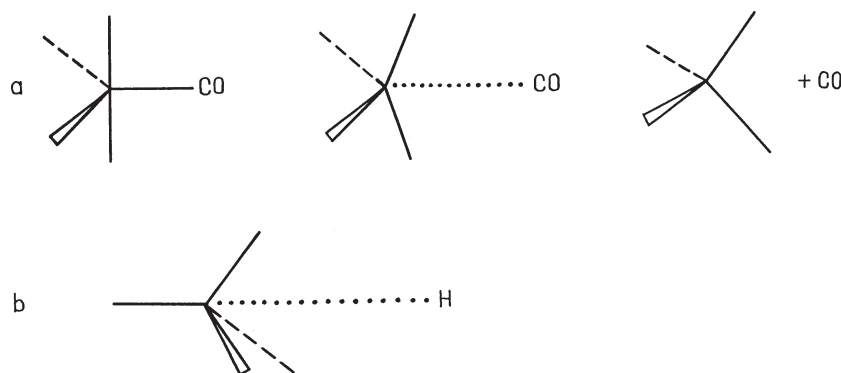


**FIGURE 11.32.** The reaction pathway for CO elimination from  $\text{Fe}(\text{CO})_5$  (a) and hydrogen dissociation from  $\text{HCo}(\text{CO})_4$  (b).

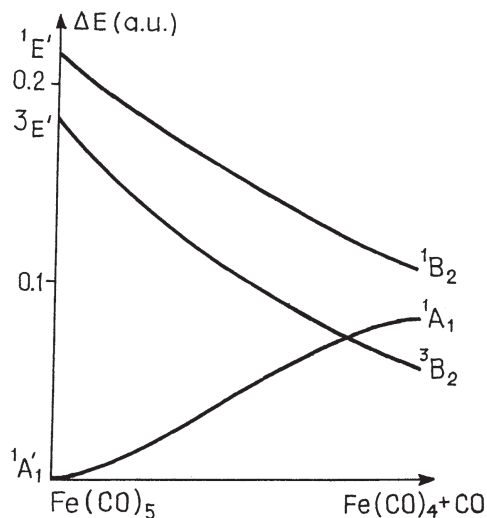


**FIGURE 11.33.** Potential energy curves for the ground state and two excited states in the dissociation process  $\text{Fe}(\text{CO})_4 + \text{CO}$  under the  $C_{2v}$  constraint. (From Daniel and Veillard [11.51].)

metal hydrides  $\text{HMn}(\text{CO})_5$ ,  $\text{HReCp}_2$ ,  $\text{HW}(\text{CO})_3\text{Cp}$ , photochemical cleavage of the metal–carbon bond in  $\text{RMn}(\text{CO})_5$  with  $\text{R} = \text{CH}_3$ ,  $\text{C}_6\text{H}_5$ , metal–silicon bond in  $\text{R}_3\text{SiCo}(\text{CO})_4$ ,  $\text{R} = \text{Et}$ ,  $\text{Ph}$ , and metal–metal bond in  $\text{Mn}_2(\text{CO})_{10}$ .

The photosubstitution reactions (11.63) proceeds via a primary photodissociation of a CO ligand



and subsequent reaction of the unsaturated species  $\text{M}(\text{CO})_4\text{L}$  with  $\text{L}'$ :



One of the most important features of this photoreaction is its stereospecificity: its product,  $\text{M}(\text{CO})_4\text{LL}'$ , is a *cis*-disubstituted derivative. Therefore, one goal of the calculations [11.51] is to explain this characteristic *cis*-stereospecificity.

The photoelimination reaction (11.64) is more complicated than (11.61) or (11.62), and therefore the calculations have been restricted to a number of remarkable points of the potential energy surface. Figure 11.36 illustrates some results of such calculations showing the evolution of two important singlet states of the photoexcitation in the reaction and subsequent transformations [the final product  $\text{M}(\text{CO})_4\text{LL}'$ , as a  $d^6$  hexacoordinated complex, is assumed to have a singlet ground state].

The mechanism of the photoreaction of ligand substitution (11.63) emerging from these computations is as follows. By photoexcitation of the

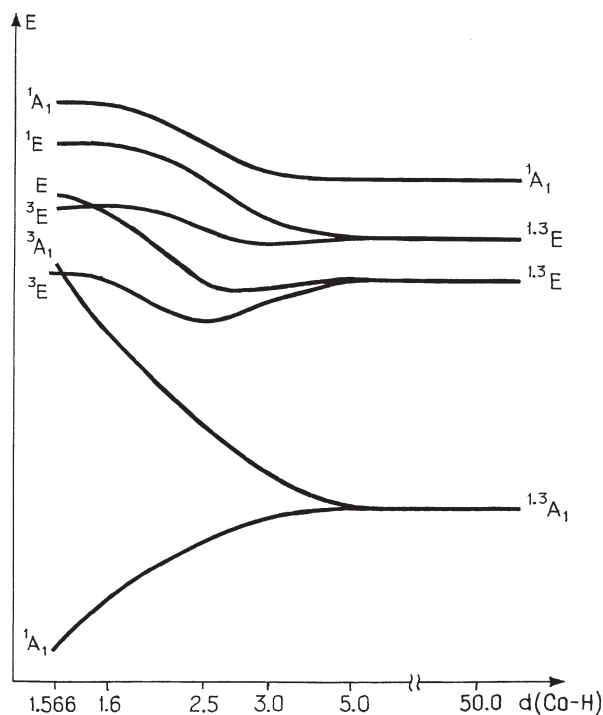


**FIGURE 11.34.** Potential energy curves (ground and excited) for dissociation of the Co—H bond in  $\text{HCo}(\text{CO})_4$  under  $C_{3v}$  constraint. (From Daniel and Veillard [11.51].)

complex  $\text{M}(\text{CO})_5\text{L}$ , the reaction of CO elimination takes place, resulting in a square-pyramidal structure with  $C_{4v}$  symmetry and the axial ligand eliminated (Fig. 11.36a), or a pseudo-square-pyramidal structure if the equatorial ligand is eliminated (Fig. 11.36b).

In the axial elimination, the excited state in the  $C_{4v}$  configuration has no minimum energy (Fig. 36a); by an internal rotation (pseudorotation, or Berry rotation, Section 9.2) via an intermediate trigonal-bipyramidal structure, it transforms itself to the pseudo-square-pyramidal structure shown in the right-hand side of Fig. 11.36a. From this metastable state, a radiationless transition to the ground state takes place. In the case of equatorial ligand elimination the system relaxes to this minimum-energy pseudo-square-pyramidal structure directly, without additional transformations (Fig. 11.36b). It is seen that, beginning with this configuration, the subsequent reaction (11.64) proceeds as an addition of  $\text{L}'$  to the only free coordination place of the photoinduced complex, resulting in a *cis*-bisubstituted system  $\text{M}(\text{CO})_4\text{LL}'$ .

For another example of *ab initio* calculated photochemical reaction, the photochemical cleavage of the metal–hydrogen bond in aluminum porphyrins, see the article by Rohmer and Veillard [11.52].

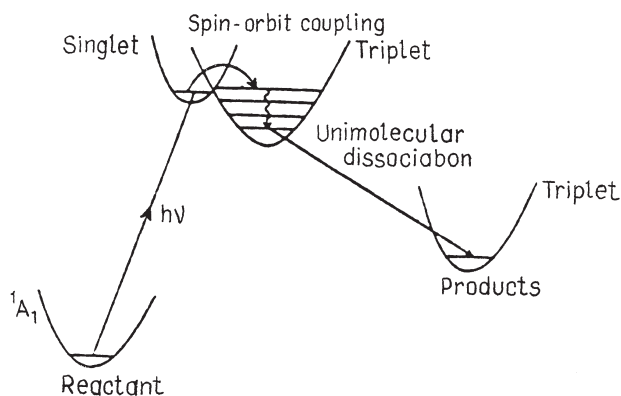


**FIGURE 11.35.** Mechanism of photochemical dissociation starting from a singlet ground state to triplet state products.

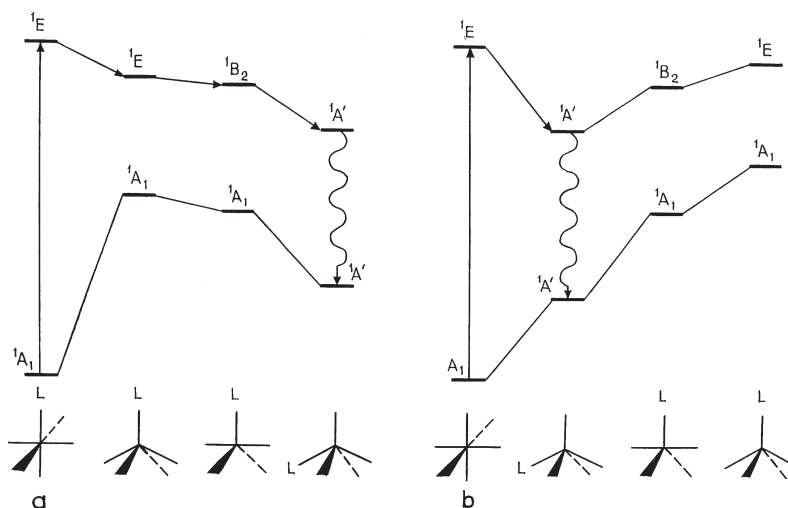


**FIGURE 11.36.** State correlation diagram for the reaction of photoelimination of the axial (a) or equatorial (b) carbonyl ligand from  $\text{Mo}(\text{CO})_5\text{L}$  and consequent internal rotation (the eliminated ligand is not shown in the products). The straight-line arrows show the evolution of the excited state to the configuration of minimum energy, while the wavy-line arrows show the radiationless transitions to the ground state.

### SUMMARY NOTES

1. *Chemical reactivity*—the ability of a system to react with another molecular system—can be measured by the relative rate of chemical transformation in the elementary act of the reaction (the full rate of reaction depends also on kinetic factors).

2. The inverse of *activation energy* of the reaction may serve as a measure of relative reactivity of molecular systems in reactions with the same reagent. There is also an approximate relationship between the activation energy and the heat of the reaction given by the *Marcus equation*; in similar reactions the activation energy decreases with the heat release in exothermic reactions and increases in endothermic reactions.
3. In the first approximation to the problem of *electronic origin of reactivity* the idea of the essential role of frontier orbitals, HOMO and LUMO, is employed. Approximate formulas based on perturbation theory show that in the intermolecular HOMO–LUMO interaction there are charge-based electrostatic and orbital-based covalent contributions that differ significantly in different reactions, with the charge component larger in reactions with TMS participation.
4. The covalent interaction between two molecular groups is directly dependent on the overlap of their wavefunctions when they approach each other. This leads to *orbital symmetry rules* that restricts possible reaction mechanisms with the lowest activation barrier. These rules, although most efficient in reactions with organic compounds, are sometimes also important in reactions with TMS participation, for example, as catalysts (Example 11.1).
5. *Chemical activation by coordination* is a widespread phenomenon with major application in catalysis. By employing orbital vibronic constants, we can estimate the changes in bond lengths, vibrational frequencies, and anharmonicities of coordinated ligands, and hence the activation energies of their reactions with another molecular group. Several specific cases are demonstrated in Examples 11.2–11.6.
6. Instabilities and distortions produced by *the Jahn–Teller and pseudo-Jahn–Teller effects* indicate directly the possible reaction path in reactions with the TMS under consideration. Several formulas show the reduction of activation energy in such reactions as a function of the JTE parameters.
7. *Numerical calculations* of the APES of chemical reactions are presently quite affordable for small and moderate systems. Examples of different kinds of reactions calculated by means of existing methods (Chapter 5) show how this approach works in explaining the origin and mechanism of the reaction and the main factors that control its rate.

## QUESTIONS AND PROBLEMS

- P11.1.** In the Marcus equation (10.3) the activation energy  $D$  decreases with the negative heat release  $\Delta H$  in exothermic reactions. Find the absolute value of  $\Delta H$  at which  $D$  becomes negative for different values of  $D_0$ . What is the physical meaning of negative activation energy? Can we find the  $D_0$  value from experimental data?

- \*P11.2.** According to Eq. (7.87), the instability of the activated complex of the chemical reaction in a two-level problem is accompanied by a stable excited state. Can this latter be observed experimentally? What measurement methods would you suggest?
- P11.3.** According to Eq. (11.4), obtained by perturbation theory for the intermolecular interaction, chemical reactions may be either charge-controlled or orbital-controlled, or by a comparable contribution of both types. How can we distinguish these possibilities in specific reactions? Is there a way to predict these kinds of reaction? Are the orbital symmetry rules applicable to charge-controlled reactions?
- P11.4.** It is well known that transition metal systems, including metal enzymes, are the best catalysts in many reactions. What is special in the electronic structure of the TMS that makes metal enzymes good catalysts? Explain in detail and give examples.
- P11.5.** List the main electronic features of activation by coordination. What electronic parameters do we need to predict the reduction in activation energy of a reactant due to its coordination to a TMS? How can we find these parameters?
- P11.6.** The CO and N<sub>2</sub> molecules are isoelectronic, but their activation by coordination is different. What are the main differences in their electronic structure that makes them different in activation by coordination?
- \*P11.7.** From Fig. 11.9, where the relative values of activation of the CO molecule by coordination to different TMSs are given for different  $D_0$  values (different reactions), we can see that the activation in Mn(CO)<sub>5</sub> is larger than in other similar carbonyls and by coordination on surfaces. Explain the origin of this effect in terms of electronic structure.
- \*\*P11.8.** Using the numerical data of orbital vibronic coupling constants for the CN molecule and orbital charge transfers by its coordination in Fe(III)CN in Ref. 11.17b, derive the equation for the activation energy  $D$  of reactions of the coordinated CN molecule with other systems as a function of the activation energy  $D_0$  of the same reactions of the free molecule, employing the semiempirical equation (11.24') with Eqs. (11.22') for the parameter changes due to coordination. Note that in this case four MOs of CN are active in the bonding with iron. For the anharmonicity constant  $\gamma_0$  use the formula [11.53]:  $\gamma_0 = (K_0/\hbar\omega)(4K_0\hbar\omega x_e/15)^{1/2}$  with the anharmonicity correction  $\hbar\omega x_e$  and vibrational frequency  $\hbar\omega$  from the paper [11.17b].
- P11.9.** Assuming that the reaction  $\text{CN} + \text{X}_2 \rightarrow \text{CX} + \text{NX}$  exists and its activation energy  $D_0 = 100$  kcal/mol, estimate the reduction of the activation energy  $-\Delta D$  for the same reaction when the CN molecule is coordinated to Fe(III) using the results of Problem \*\*P11.8 (cf. Example 11.3).
- P11.10.** The substitution reaction  $\text{CuL}_6^{2+} + \text{M} \rightarrow \text{CuL}_5\text{M}^{2+} + \text{L}$  is assumed to be driven by the strong JTE in octahedral Cu(II) complexes (see



Example 11.8). Estimate the reduction in activation energy of such reactions due to the JTE, assuming that the stabilization energy is known to be  $\Delta E = 0.5$  eV and  $D_0 = 50$  kcal/mol.

## REFERENCES

- 11.1. H. Eyring, J. Walter, and G. E. Kimball, *Quantum Chemistry*, Wiley, New York, 1947.
- 11.2. V. I. Goldanskii, V. A. Benderskii, and L. I. Trakhtenberg, *Adv. Chem. Phys.* **75**, 349 (1989); J. Jortner, B. Pullman, and D. Reidel, eds., *Tunnelling*, Dordrecht, 1986.
- 11.3. A. H. Zewail, *Femtochemistry. Ultrafast Dynamics of the Chemical Bond*, Vols. 1, 2, World Scientific, Singapore, 1994; M. Gruebele and A. H. Zewail, *Phys. Today* **43**, 24 (1990); P. R. Brooks, *Chem. Rev.* **88**, 407 (1988).
- 11.4. R. A. Marcus, *J. Phys. Chem.* **72**, 891 (1968).
- 11.5. R. P. Bell, *Proc. Roy. Soc. Lond. A* **154**, 414 (1936); M. G. Evans and M. Polanyi, *J. Chem. Soc. Faraday Trans.* **32**, 1340 (1936); G. S. Hammond, *J. Am. Chem. Soc.* **77**, 334 (1955).
- 11.6. I. B. Bersuker, *The Jahn-Teller Effect and Vibronic Interactions in Modern Chemistry*, Plenum, New York, 1984.
- 11.7. I. B. Bersuker, *Nouv. J. Chim.* **4**, 139 (1980).
- 11.8. K. Fukui, *Theory of Orientation and Stereoselection*, Springer, Berlin, 1975.
- 11.9. G. Clopman, in G. Clopman, ed., *Chemical Reactivity and Reaction Paths*, Wiley, New York, 1974, Chapter 4.
- 11.10. R. B. Woodward and R. Hoffmann, *The Conservation of Orbital Symmetry*, Verlag Chemie, GmbH., Weinheim/Bergstrasse, 1970.
- 11.11. R. F. W. Bader, *Can. J. Chem.* **40**, 1164 (1962).
- 11.12. R. G. Pearson, *Symmetry Rules for Chemical Reactions*, Wiley-Interscience, New York, 1976.
- 11.13. T. F. George and J. Ross, *J. Chem. Phys.* **55**, 3851 (1971).
- 11.14. F. D. Mango and J. H. Schachtschneider, *J. Am. Chem. Soc.* **89**, 2484 (1967); **93**, 1123 (1971); F. D. Mango, *Adv. Catal.* **20**, 291 (1969).
- 11.15. I. B. Bersuker, *Kinet. Katal.* **18**, 1268 (1977); *Chem. Phys.* **31**, 85 (1978); I. B. Bersuker, in D. Banerjee, ed., (*IUPAC*) *Coordination Chemistry*, Vol. 20, Pergamon Press, Oxford, 1980, p. 201.
- 11.16. I. B. Bersuker and S. S. Budnikov, in A. E. Shilov, ed., *Fundamental Research in Homogeneous Catalysis*, Gordon & Breach, London, 1986, Vol. 2, p. 557.
- 11.17. (a) S. S. Stavrov, I. P. Decusar, and I. B. Bersuker, *New J. Chem.* **17**, 71 (1993); (b) B. Kushkuley and S. S. Stavrov, *Biochim. Biophys. Acta* **1341**, 238 (1997).
- 11.18. E. B. Wilson, Jr., J. G. Decius, and P. C. Cross, *Molecular Vibrations. The Theory of Infrared and Raman Spectra*, McGraw-Hill, New York, 1958; G. Gerzberg, *Infrared and Raman Spectra of Polyatomic Molecules*, Van Nostrand, New York, 1945.
- 11.19. L. Pauling, *J. Chem. Soc.* 1461 (1948); *Proc. Symp. Coord. Chem.*, Copenhagen, 1953, p. 25.

- 11.20. (a) A. P. Svitin, S. S. Budnikov, I. B. Bersuker, and D. V. Korol'kov, *Teor. Exp. Khim.* **18**, 694 (1982); V. I. Bykov and A. P. Svitin, *Methods of Calculation of Parameters of Molecular Activation* (Russ.), Nauka, Novosibirsk, 1988; (b) S. S. Stavrov, in T. S. Németh, ed., *Biopolymer Research Trends*, Nova Publishers, 2008, p 119; A. D. Kaposi, J. M. Vanderkooi, and S. S. Stavrov, *Biophys. J.* **91** (11) (2006).
- 11.21. Yu. Ya. Kharitonov and O. V. Bazileva, *Zh. Neorg. Khim.* **23**, 867 (1978).
- 11.22. K. S. Krasnov, V. S. Timoshinin, T. G. Danilova, and S. V. Mandozhko, *Molecular Constants for Inorganic Compounds* (Russ.), Khimia, Leningrad, 1968.
- 11.23. A. A. Radsig and V. M. Smirnov, *Handbook on Atomic and Molecular Data* (Russ.), Atomizdat, Moscow, 1980.
- 11.24. V. I. Yakerson, L. I. Lafer, and A. M. Rubinshtein, in *Problemi Kinetiki i Kataliza*, Vol. 16, Nauka, Moscow, 1975, p. 49.
- 11.25. V. N. Kondratiev, *Constants for Gas Phase Reactions* (Russ.), Nauka, Moscow, 1970.
- 11.26. A. Belyanskii and G. Dereni, in F. F. Vol'kenstein, ed., *Electronic Effects in Adsorption and Catalysis* (Russ.), Mir, Moscow, 1969, p 227.
- 11.27. R. F. Fenske and K. L. LeCock, *Inorg. Chem.* **11**, 437 (1972).
- 11.28. S. S. Budnikov, *Teor. Exp. Khim.* **28**, 34 (1992).
- 11.29. I. B. Bersuker, *Teor. Exp. Khim.* **1**, 5 (1965).
- 11.30. G. Canley, D. Cross, and P. Knowless, *J. Chem. Soc. Chem. Commun.* **20**, 837 (1976).
- 11.31. I. B. Bersuker, ed., *The Jahn-Teller Effect. A Bibliographic Review*, IFI Plenum, New York, 1984.
- 11.32. I. I. Chernyaev, in *Selected works: Complex Compounds of Platinum* (Russ.), Nauka, Moscow, 1973.
- 11.33. F. R. Hartley, *Rev. Chem. Soc.* **2**, 163 (1973).
- 11.34. E. M. Shustorovich, M. A. Porai-Koshitz, and Iu A. Buslaev, *Coord. Chem. Rev.* **17**, 1 (1975).
- 11.35. V. I. Nefedov and M. M. Hofman, *Mutual Influence of Ligands in Inorganic Compounds* (Russ.), in: *Itogi Nauki i Tekhniki, Ser. Inorg. Chem.*, Vol. 6, VINITI, Moscow, 1978.
- 11.36. J. D. Atwood, *Inorganic and Organometallic Reaction Mechanisms*, Brooks/Cole Publishing, Monterey, CA, 1985.
- 11.37. F. A. Cotton and G. Wilkinson, *Advanced Inorganic Chemistry: A Comprehensive Text*, Wiley, New York, 1992.
- 11.38. J. Chatt, L. A. Duncanson, and L. M. Venanzi, *J. Chem. Soc.* 4456 (1955).
- 11.39. L. E. Orgel, *J. Inorg. Nucl. Chem.* **2**, 137 (1956).
- 11.40. I. B. Bersuker, *Zh. Neorg. Khim.* **9**, 36 (1964), *Zh. Strukt. Khim.* **4**, 461 (1963).
- 11.41. Z. Lin and M. B. Hall, *Inorg. Chem.* **30**, 646 (1991).
- 11.42. J.-M. Lehn, in A. F. Williams, C. Floriani, and A. E. Merbach, eds., *Perspectives in Coordination Chemistry*, VCH, New York, 1992, p. 447; G. Denti, S. Serroni, S. Campagna, A. Juris, M. Ciano, and V. Balzani, *ibid.*, p 153.
- 11.43. D. H. Bush and N. A. Stephenson, *Coord. Chem. Rev.* **100**, 119 (1990).

- 11.44. R. Hoffmann, C. N. Wilker, and O. Eisenstein, *J. Am. Chem. Soc.* **104**, 632 (1982); C. N. Wilker, R. Hoffman, and O. Eisenstein, *New J. Chem.* **7**, 535 (1983).
- 11.45. R. Hoffmann, in A. Veillard, ed., *Quantum Chemistry: The Challenge of Transition Metals and Coordination Chemistry*, Reidel, Dordrecht, 1986, p. 253.
- 11.46. A. Dedieu and S. Nakamura, in A. Veillard, ed., *Quantum Chemistry: The Challenge of Transition Metals and Coordination Chemistry*, Reidel, Dordrecht, 1986, p. 277.
- 11.47. N. Koga and K. Morokuma, in A. Veillard, ed., *Quantum Chemistry: The Challenge of Transition Metals and Coordination Chemistry*, Reidel, Dordrecht, 1986, p. 351; *New J. Chem.* **15**, 749 (1991).
- 11.48. K. R. Lane, L. Sallons, and R. R. Squires, *J. Am. Chem. Soc.* **107**, 5369 (1985).
- 11.49. P. Cossee, *J. Catal.* **3**, 80 (1964).
- 11.50. O. Novaro, E. Blaisten-Barojas, E. Clementi, G. Giunchi, and M. E. Ruiz-Vizcaya, *J. Chem. Phys.* **68**, 2337 (1978).
- 11.51. C. Daniel and A. Veillard, in A. Veillard, ed., *Quantum Chemistry: The Challenge of Transition Metal and Coordination Chemistry*, Reidel, Dordrecht, 1986., p. 363.
- 11.52. M. M. Rohmer and A. Veillard, *New J. Chem.* **15**, 795 (1991).
- 11.53. L. D. Landau and E. M. Liphshits, *Quantum Mechanics: Nonrelativistic Theory*, Nauka, Moseow, 1974, p. 369.

# APPENDIXES

## APPENDIX 1. TABLES OF CHARACTERS OF IRREDUCIBLE REPRESENTATIONS OF MOST USABLE SYMMETRY POINT GROUPS AND DIRECT PRODUCTS OF SOME REPRESENTATIONS

The Cartesian coordinates  $x$ ,  $y$ , and  $z$  and some of their combinations, as well as rotations around the axes  $R_x$ ,  $R_y$ , and  $R_z$  that belong to the corresponding representation are also indicated; for degenerate representations the corresponding degenerate combinations are shown in parentheses.

**TABLE A1.1. Point Groups  $C_s$ ,  $C_2$ , and  $C_i$**

$C_i$		$C_2$		$C_s$	$E$	$I$	
					$E$	$C_{2z}$	
					$E$	$\sigma_z$	
$A_g$	$R_x, R_y, R_z,$ $x^2, y^2, z^2, xy, xz, yz$	$A$	$z, R_z, x^2, y^2, z^2$ $xy$	$A'$	$x, y, R_z,$ $z^2, xy$	1	1
$A_u$	$x, y, z$	$B$	$x, y, R_x, R_y, xz, yz$	$A''$	$z, R_x, R_y,$	1	-1

*Electronic Structure and Properties of Transition Metal Compounds: Introduction to the Theory,*  
 Second Edition By Isaac B. Bersuker  
 Copyright © 2010 John Wiley & Sons, Inc.

TABLE A1.2. Point Groups  $C_{2h}$  and  $C_{2v}$ 

$C_{2h}$		$C_{2v}$		$E$	$C_2$	$\sigma_h$	$I$
				$E$	$C_2$	$\sigma_v$	$\sigma'_v$
$A_g$	$R_z, x^2, y^2, z^2, xy$	$A_1$	$z, x^2, y^2, z^2$	1	1	1	1
$B_g$	$R_x, R_y, xz, yz$	$B_2$	$y, R_x, yz$	1	-1	-1	1
$A_u$	$z$	$A_2$	$R_z, xy$	1	1	-1	-1
$B_u$	$x, y$	$B_1$	$x, R_y, xz$	1	-1	1	-1

TABLE A1.3. Point Groups  $C_{3v}$  and  $D_3$ 

$C_{3v}$		$D_3$		$E$	$2C_3$	$3\sigma_u$
				$E$	$2C_3$	$3C_2$
$A_1$	$z, x^2 + y^2, z^2$	$A_1$	$x^2 + y^2, z^2$	1	1	1
$A_2$	$R_z$	$A_2$	$z, R_z$	1	1	-1
$E$	$(x, y), (R_x, R_y), (x^2 - y^2, xy)(xz, yz)$	$E$	$(x, y), (R_x, R_y)$	2	-1	0

TABLE A1.4. Point Group  $D_{3d}$ 

$D_{3d}$	$E$	$2C_3$	$3C_2$	$I$	$2S_6$	$3\sigma_d$
$A_{1g}$	$x^2 + y^2, z^2$	1	1	1	1	1
$A_{1u}$		1	1	1	-1	-1
$A_{2g}$	$R_z$	1	1	-1	1	-1
$A_{2u}$	$z$	1	1	-1	-1	1
$E_g$	$(R_x, R_y)$	2	-1	0	2	-1
$E_u$	$(x, y)$	2	-1	0	-2	1

TABLE A1.5. Point Groups  $C_{6v}$  and  $D_{3h}$ 

$C_{3v}$		$D_{3h}$		$E$	$C_2$	$2C_3$	$2C_6$	$3\sigma_v$	$3\sigma'_v$
				$E$	$\sigma_h$	$2C_3$	$2S_3$	$3C_2$	$3\sigma_v$
$A_1$	$z, x^2 + y^2, z^2$	$A'_1$	$x^2 + y^2, z^2$	1	1	1	1	1	1
$A_2$	$R_z$	$A'_2$	$R_z$	1	1	1	1	-1	-1
$B_2$		$A''_1$		1	-1	1	-1	1	-1
$B_1$		$A''_2$	$z$	1	-1	1	-1	-1	1
$E_2$	$(x^2 - y^2, xy)$	$E'$	$(x, y), (x^2 - y^2, xy)$	2	2	-1	-1	0	0
$E_1$	$(x, y), (R_x, R_y), (xz, yz)$	$E''$	$(R_x, R_y), (xz, yz)$	2	-2	-1	1	0	0

TABLE A1.6. Point Group  $D_{2h}$ 

$D_{2h}$		$E$	$C_{2z}$	$C_{2y}$	$C_{2x}$	$I$	$\sigma_z$	$\sigma_y$	$\sigma_x$
$A_g$	$x^2, y^2, z^2$	1	1	1	1	1	1	1	1
$A_u$	$xyz$	1	1	1	1	-1	-1	-1	-1
$B_{1g}$	$R_z, xy$	1	1	-1	-1	1	1	-1	-1
$B_{1u}$	$z$	1	1	-1	-1	-1	-1	1	1
$B_{2g}$	$R_y, xz$	1	-1	1	-1	1	-1	1	-1
$B_{2u}$	$y$	1	-1	1	-1	-1	1	-1	1
$B_{3g}$	$R_x, yz$	1	-1	-1	1	1	-1	-1	1
$B_{3u}$	$x$	1	-1	-1	1	-1	1	1	-1

TABLE A1.7. Point Groups  $C_{4v}$  and  $D_{2d}$ 

$C_{4v}$		$D_{2d}$		$E$	$C_2$	$2C_4$	$2\sigma_v$	$2\sigma'_v$
				$E$	$C_2$	$2S_4$	$2C'_2$	$2\sigma_d$
$A_1$	$z, x^2 + y^2, z^2$	$A_1$	$x^2 + y^2, z^2$	1	1	1	1	1
$A_2$	$R_z$	$A_2$	$R_z$	1	1	1	-1	-1
$B_1$	$x^2 - y^2$	$B_1$	$x^2 - y^2$	1	1	-1	1	-1
$B_2$	$xy$	$B_2$	$z, xy$	1	1	-1	-1	1
$E$	$(x, y), (R_x, R_y), (xz, yz)$	$E$	$(x, y), (R_x, R_y), (xz, yz)$	2	-2	0	0	0

TABLE A1.8. Point Group  $D_{4h}$ 

$D_{4h}$		$E$	$2C_4$	$C_2$	$2C'_2$	$2C''_2$	$I$	$2S_4$	$\sigma_z$	$2\sigma_v$	$2\sigma_d$
$A_{1g}$	$x^2 + y^2, z^2$	1	1	1	1	1	1	1	1	1	1
$A_{1u}$		1	1	1	1	1	-1	-1	-1	-1	-1
$A_{2g}$	$R_z$	1	1	1	-1	-1	1	1	1	-1	-1
$A_{2u}$	$z$	1	1	1	-1	-1	-1	-1	-1	1	1
$B_{1g}$	$x^2 - y^2$	1	-1	1	1	-1	1	-1	1	1	-1
$B_{1u}$		1	-1	1	1	-1	-1	1	-1	-1	1
$B_{2g}$	$xy$	1	-1	1	-1	1	1	-1	1	-1	1
$B_{2u}$		1	-1	1	-1	1	-1	1	-1	1	-1
$E_g$	$(R_x, R_y), (xz, yz)$	2	0	-2	0	0	2	0	-2	0	0
$E_u$	$(x, y)$	2	0	-2	0	0	-2	0	2	0	0

**TABLE A1.9. Point Group  $C_{\infty v}$** 

$C_{\infty v}$		$E$	$2C_{\infty}(\varphi)^a$	...	$\infty\sigma_v$
$A_1 \equiv \Sigma^+$	$z, x^2 + y^2, z^2$	1	1	...	1
$A_2 \equiv \Sigma^-$	$R_z$	1	1	...	-1
$E_1 = \Pi$	$(x, y), (R_x, R_y), (xz, yz)$	2	$2 \cos \varphi$	...	0
$E_2 = \Delta$	$(x^2 - y^2, xy)$	2	$2 \cos 2\varphi$	...	0
$E_3 = \Phi$		2	$2 \cos 3\varphi$	...	0
...		...	...	...	...

<sup>a</sup> $\varphi$  is the angle of rotation around the axis of symmetry of infinite order.

**TABLE A1.10. Tetrahedral Point Group  $T_d$** 

$T_d$		$E$	$8C_3$	$3C_2$	$6S_4$	$6\sigma_d$
$A_1$	$x^2 + y^2 + z^2$	1	1	1	1	1
$A_2$		1	1	1	-1	-1
$E$	$(2z^2 - x^2 - y^2, x^2 - y^2)$	2	-1	2	0	0
$T_1$	$(R_x, R_y, R_z)$	3	0	-1	1	-1
$T_2$	$(x, y, z), (xy, xz, yz)$	3	0	-1	-1	1

**TABLE A1.11. Octahedral Point Group  $O_h$** 

$O_h$		$E$	$8C_3$	$3C_2 (= C_4^2)$	$6C_4$	$6C_2$	$I$	$8S_6$	$3\sigma_h$	$6S_4$	$6\sigma_d$
$A_{1g}$	$x^2 + y^2 + z^2$	1	1	1	1	1	1	1	1	1	1
$A_{1u}$		1	1	1	1	1	-1	-1	-1	-1	-1
$A_{2g}$		1	1	1	-1	-1	1	1	1	-1	-1
$A_{2u}$		1	1	1	-1	-1	-1	-1	-1	1	1
$E_g$	$(2z^2 - x^2 - y^2, x^2 - y^2)$	2	-1	2	0	0	2	-1	2	0	0
$E_u$		2	-1	2	0	0	-2	1	-2	0	0
$T_{1g}$	$(R_x, R_y, R_z)$	3	0	-1	1	-1	3	0	-1	1	-1
$T_{1u}$	$(x, y, z)$	3	0	-1	1	-1	-3	0	1	-1	1
$T_{2g}$	$(xy, xz, yz)$	3	0	-1	-1	1	3	0	-1	-1	1
$T_{2u}$		3	0	-1	-1	1	-3	0	1	1	-1

TABLE A1.12. Icosahedral Group  $I_h$ 

$I_h$	$E$	$12C_5$	$12C_5^2$	$20C_3$	$15C_2$	$I$	$12S_{10}$	$12S_{10}^3$	$20S_6$	$15\sigma$
$A_g$	1	1	1	1	1	1	1	1	1	1
$A_u$	1	1	1	1	1	-1	-1	-1	-1	-1
$T_{1g}$	3	$(1 + \sqrt{5})/2$	$(1 - \sqrt{5})/2$	0	-1	3	$(1 - \sqrt{5})/2$	$(1 + \sqrt{5})/2$	0	-1
$T_{1u}$	3	$(1 + \sqrt{5})/2$	$(1 - \sqrt{5})/2$	0	-1	-3	$-(1 - \sqrt{5})/2$	$-(1 + \sqrt{5})/2$	0	1
$T_{2g}$	3	$(1 - \sqrt{5})/2$	$(1 + \sqrt{5})/2$	0	-1	3	$(1 + \sqrt{5})/2$	$(1 - \sqrt{5})/2$	0	-1
$T_{2u}$	3	$(1 - \sqrt{5})/2$	$(1 + \sqrt{5})/2$	0	-1	-3	$-(1 + \sqrt{5})/2$	$-(1 - \sqrt{5})/2$	0	1
$G_g$	4	-1	-1	1	0	4	-1	-1	1	0
$G_u$	4	-1	-1	1	0	-4	1	1	-1	0
$H_g$	5	0	0	-1	1	5	0	0	-1	1
$H_u$	5	0	0	-1	1	-5	0	0	1	-1

$$\begin{aligned}
 & (2z^2 - x^2 - y^2, \\
 & x^2 - y^2, xy, \\
 & xz, yz)
 \end{aligned}$$



**TABLE A1.13. Point Group  $O'$  (Octahedral Double Group)**

Mulliken Notations	Bethe Notations	$E$	$Q$	$4C_3$ $4C_3^2 Q$	$4C_3^2$ $4C_3 Q$	$3C_4^2$ $3C_4^3 Q$	$3C_4$ $3C_4 Q$	$3C_4^3$ $3C_4 Q$	$6C_2$ $6C_2 Q$
$A'_1$	$\Gamma_1$	1	1	1	1	1	1	1	1
$A'_2$	$\Gamma_2$	1	1	1	1	1	-1	-1	-1
$E'$	$\Gamma_3$	2	2	-1	-1	2	0	0	0
$T'_1$	$\Gamma_4$	3	3	0	0	-1	1	1	-1
$T'_2$	$\Gamma_5$	3	3	0	0	-1	-1	-1	-1
$E'_2$	$\Gamma_6$	2	-2	1	-1	0	$\sqrt{2}$	$-\sqrt{2}$	0
$E'_3$	$\Gamma_7$	2	-2	1	-1	0	$-\sqrt{2}$	$\sqrt{2}$	0
$G'$	$\Gamma_8$	4	-4	-1	1	0	0	0	0

**TABLE A1.14. Direct Products of Irreducible Representations of Simple Groups  $\Gamma_i \times \Gamma_j$  (I), Simple with Double Groups  $\Gamma_i \times \Gamma_\alpha$  (II), and Double with Double Groups  $\Gamma_\alpha \times \Gamma_\beta$  (III) Presented as a Sum of  $\Gamma_i$** 

I. $\Gamma_i \times \Gamma_j$	
$\Gamma_1 \times \Gamma_i = \Gamma_i,$	$\Gamma_2 \times \Gamma_2 = \Gamma_1$
$\Gamma_2 \times \Gamma_3 = \Gamma_3,$	$\Gamma_2 \times \Gamma_4 = \Gamma_5$
$\Gamma_2 \times \Gamma_5 = \Gamma_4,$	$\Gamma_3 \times \Gamma_3 = \Gamma_1 + \Gamma_2 + \Gamma_3$
$\Gamma_3 \times \Gamma_4 = \Gamma_4 + \Gamma_5,$	$\Gamma_3 \times \Gamma_5 = \Gamma_4 + \Gamma_5$
$\Gamma_4 \times \Gamma_4 = \Gamma_1 + \Gamma_3 + \Gamma_4 + \Gamma_5$	
$\Gamma_4 \times \Gamma_5 = \Gamma_2 + \Gamma_3 + \Gamma_4 + \Gamma_5$	
$\Gamma_5 \times \Gamma_5 = \Gamma_1 + \Gamma_3 + \Gamma_4 + \Gamma_5$	
II. $\Gamma_i \times \Gamma_\alpha$	
$\Gamma_1 \times \Gamma_6 = \Gamma_2 \times \Gamma_7 = \Gamma_6,$	$\Gamma_2 \times \Gamma_6 = \Gamma_1 \times \Gamma_7 = \Gamma_7$
$\Gamma_3 \times \Gamma_6 = \Gamma_3 \times \Gamma_7 = \Gamma_8,$	$\Gamma_3 \times \Gamma_8 = \Gamma_6 + \Gamma_7 + \Gamma_8$
$\Gamma_4 \times \Gamma_6 = \Gamma_5 \times \Gamma_7 = \Gamma_6 + \Gamma_8$	
$\Gamma_5 \times \Gamma_6 = \Gamma_4 \times \Gamma_7 = \Gamma_7 + \Gamma_8$	
$\Gamma_4 \times \Gamma_8 = \Gamma_5 \times \Gamma_8 = \Gamma_6 + \Gamma_7 + 2\Gamma_8$	
III. $\Gamma_\alpha \times \Gamma_\beta$	
$\Gamma_6 \times \Gamma_6 = \Gamma_7 \times \Gamma_7 = \Gamma_1 + \Gamma_4$	
$\Gamma_6 \times \Gamma_7 = \Gamma_2 + \Gamma_5$	
$\Gamma_6 \times \Gamma_8 = \Gamma_7 \times \Gamma_8 = \Gamma_3 + \Gamma_4 + \Gamma_5$	
$\Gamma_8 \times \Gamma_8 = \Gamma_1 + \Gamma_2 + \Gamma_3 + 2\Gamma_4 + 2\Gamma_5$	

**APPENDIX 2. GENERAL EXPRESSIONS FOR THE MATRIX ELEMENT  $V_{mm'}$  OF PERTURBATION OF THE STATES OF ONE  $d$  ELECTRON IN CRYSTAL FIELDS OF ARBITRARY SYMMETRY**

For the calculation of the matrix element  $V_{mm'}$  after (4.8) we use the following expansion (2.37):

$$\frac{1}{|\mathbf{r} - \mathbf{R}_i|} = \sum_{k=0}^{\infty} K_k(r, R_i) P_k(\cos \gamma_i)$$

where  $K_k(r, R_i)$  is given by Eq. (2.38), and  $\cos \gamma_i = \cos \theta \cos \theta_i + \sin \theta \sin \theta_i \cos(\varphi - \varphi_i)$ . Then

$$V_{mm'} = \int \Psi_m * V \Psi_{m'} d\tau = \sum_{i=0}^N eq_i \sum_{k=0}^{\infty} F_k(R_i) \Theta_k^{mm'}(\theta_i, \varphi_i) \quad (\text{A2.1})$$

where

$$F_k(R) = R^{-(k+1)} \int_0^R r^k R_{n2}^2(r) r^2 dr + R^k \int_R^{\infty} r^{-(k+1)} R_{n2}^2(r) r^2 dr \quad (\text{A2.2})$$

$$\Theta_k^{mm'} = \int_0^{\pi} \int_0^{2\pi} Y_2^m(\theta, \varphi) Y_2^{m'}(\theta, \varphi) P_k(\cos \gamma_i) \sin \theta d\theta d\varphi \quad (\text{A2.3})$$

To simplify the last equation, the expansion of the product of spherical functions  $Y_2^m Y_2^{m'}$  in spherical functions  $Y_l^m$  can be employed [A2.1, p.60]:

$$\begin{aligned} Y_2^m(\theta, \varphi) Y_2^{m'*}(\theta, \varphi) &= \frac{(-1)^{m'}}{(4\pi)^{1/2}} \left[ \frac{5}{3} C_{-m'm}^{224} C_{00}^{220} Y_4^{m-m'}(\theta, \varphi) \right. \\ &\quad \left. + \sqrt{5} C_{-m'm}^{222} C_{00}^{222} Y_2^{m-m'}(\theta, \varphi) + 5 C_{-m'm}^{220} C_{00}^{220} Y_0^{m-m'}(\theta, \varphi) \right] \end{aligned} \quad (\text{A2.4})$$

where  $C_{\alpha\beta}^{abc}$  denotes the Clebsh–Gordan coefficients, which are tabulated [A2.2]. By substituting Eq. (A2.4) into (A2.3), one obtains integrals that are calculable directly by means of the following formula of addition of spherical functions:

$$\int Y_l(\theta, \varphi) P_n(\cos \gamma_i) \sin \theta d\theta = \frac{4\pi}{2n+1} Y_l(\theta_i, \varphi_i) \delta_{ln} \quad (\text{A2.5})$$

In so doing, we obtain

$$\begin{aligned} \Theta_n^{mm'}(\theta_i, \varphi_i) &= A_{mm'} Y_4^{m-m'}(\theta_i, \varphi_i) \delta_{n4} + B_{mm'} Y_2^{m-m'}(\theta_i, \varphi_i) \delta_{n2} \\ &\quad + D_{mm'} Y_0^{m-m'}(\theta_i, \varphi_i) \delta_{n0} \end{aligned} \quad (\text{A2.6})$$

where

$$\begin{aligned} A_{mm'} &= (-1)^{m'} \frac{10\sqrt{\pi}}{27} C_{-m'm}^{224} C_{00}^{224} \\ B_{mm'} &= (-1)^{m'} (2\sqrt{\pi}/5) C_{-m'm}^{222} C_{00}^{222} \\ D_{mm'} &= (-1)^{m'} (10\sqrt{\pi}) C_{-m'm}^{220} C_{00}^{220} \end{aligned} \quad (\text{A2.7})$$

Owing to the  $\delta$  symbols, only three terms in the infinite sum (A2.1) are nonzero, and the summation over the  $N$  nuclei only remains:

$$V_{mm'} = \sum_{i=1}^N e q_i [A_{mm'} F_4(R_i) Y_4^{m-m'}(\theta_i, \varphi_i) + B_{mm'} F_2(R_i) Y_2^{m-m'}(\theta_i, \varphi_i) + D_{mm'} F_0(R_i) Y_0^{m-m'}(\theta_i, \varphi_i)] \quad (\text{A2.8})$$

This is the general formula for the matrix element of the perturbation of  $d$  states (2.1) by crystal fields.

The functions  $F_k(R)$  after (A2.2) depend on the radial part of the  $d$  functions. For instance, taking the  $3d$  function as a hydrogenlike one with an effective screening parameter  $\alpha$  (Section 2.1)

$$R_{32}(r) = \frac{4\sqrt{10}}{3} \alpha^{7/2} r^2 e^{-\alpha r} \quad (\text{A2.9})$$

we obtain

$$F_k^{3d}(R) = \frac{\alpha}{360} \left\{ \left[ \frac{(k+6)!}{(2x)^{k+1}} \right] - (2x)^6 [A_{k+6}(2x) - A_{5-k}(2x)] \right\} \quad (\text{A2.10})$$

where  $x = \alpha R$  and

$$A_n(y) = \int_1^\infty \exp(-yr) r^n dr \quad (\text{A2.11})$$

are auxiliary functions often used in quantum-chemical calculations [see  $A_n(y)$  tables in Ref. A2.3]. If  $n$  is an integer, the integrals (A2.11) can be calculated directly yielding analytical expressions for the functions  $F_k(R)$ . In particular, for  $F_0$ ,  $F_2$ , and  $F_4$  in (A2.8), we have

$$F_0 = \alpha \left[ x^{-1} - e^{-2x} \left( x^{-1} + \frac{5}{3} + \frac{4x}{3} + \frac{2x^2}{3} + \frac{2x^3}{9} + \frac{2x^4}{45} \right) \right] \quad (\text{A2.12})$$

$$F_2 = \alpha \left[ \frac{14}{x^3} - e^{-2x} \left( \frac{14}{x^3} + \frac{28}{x^2} + \frac{28}{x} + \frac{56}{3} + \frac{28x}{3} \frac{11x^2}{3} + \frac{10x^3}{9} + \frac{2x^4}{9} \right) \right] \quad (\text{A2.13})$$

$$F_4 = \alpha \left[ \frac{315}{x^5} - e^{-2x} \left( \frac{315}{x^5} + \frac{630}{x^4} + \frac{630}{x^3} + \frac{420}{x^2} + \frac{210}{x} + 84 + 28x + 8x^2 + 2x^3 + \frac{2x^4}{5} \right) \right] \quad (\text{A2.14})$$

The values  $F_k(R)$  are tabulated [A2.4].

## REFERENCES

- A2.1. G. Ya. Liubarskii, *The Theory of Groups and Its Application in Physics*, Gostekhteorizdat, Moscow, 1957.
- A2.2. A. Simon, in *Deformation of Atomic Nuclei*, Oak Ridge National Laboratory, 1957, pp. 353–379.
- A2.3. M. Kotani, A. Amemiya, E. Ishiguro, et al., *Tables of Molecular Integrals*, Tokyo, Maruzen, 1955; H. Preuss, *Integraltafeln zur Quantumchemie*, Vol. 1, Springer, Berlin, 1956; Vol. 2, 1957; Vol. 3, 1961; Vol. 4, 1960.
- A2.4. C. J. Ballhausen and E. M. Ancmon, *Mat. Fys. Medd. Dan. Vid. Selsk.* **31**, 1–38 (1958).

**APPENDIX 3. CALCULATION OF THE DESTABILIZATION AND SPLITTING OF THE STATES OF ONE  $d$  ELECTRON IN CRYSTAL FIELDS OF DIFFERENT SYMMETRIES**

Calculations of  $d$ -electron energy-level splitting in the field of ligand–point charges performed in Section 4.2 can be extended to the case of ligand–dipoles. Present the dipole system as two charges  $-q$  and  $+q$  situated at a distance  $\Delta R$  from each other and assume that the dipoles of the ligands are oriented along the metal–ligand bonds with the negative pole toward the CA. Performing the calculation of the perturbation of the  $d$  states twice, first in the field of six negative charges  $-q$  at the distances  $R$  from the CA and then in the field of similar positive charges at a larger distance  $R + \Delta R$ , and summing up the results, we have [cf. (4.14)]

$$\begin{aligned}\varepsilon_1 = \varepsilon_2 = e q \{ [6F_0(R) + F_4(R)] - [6F_0(R + \Delta R) + F_4(R + \Delta R)] \} \\ \varepsilon_3 = \varepsilon_4 = \varepsilon_5 = e q \{ [6F_0(R) - \frac{2}{3}F_4(R)] - [6F_0(R + \Delta R) - \frac{2}{3}F_4(R + \Delta R)] \} \end{aligned} \quad (\text{A3.1})$$

For  $\Delta = \varepsilon_1 - \varepsilon_3$  we get

$$\Delta = e q \frac{5}{3} [F_4(R) - F_4(R + \Delta R)] \quad (\text{A3.2})$$

These equation can be simplified if we assume that the ligand dipoles can be considered as point dipoles; that is, the dimensions of the dipoles  $\Delta R$  are much smaller, than the metal–ligand distance  $R$ ,  $\Delta R \ll R$ . Under this assumption

$$\frac{1}{\Delta R} [F_k(R + \Delta R) - F_k(R)] \approx \frac{dF_k(R)}{dR} = F'_k(R)$$

Since  $q \Delta R = \mu$ , we easily obtain Eq. (4.30):

$$\Delta = -\frac{5}{3} e \mu F'_4(R) \quad (\text{A3.3})$$

**Tetragonally Distorted Octahedron and Planar Square (see Problem 4.1)**

If the six ligand–point charges  $q$  form tetragonal symmetry  $D_{4h}$ , then

$$\begin{aligned} R_1 &= R_4 & R_2 &= R_3 = R_5 = R_6 & (R_1 \neq R_2) \\ \theta_1 &= 0 & \theta_2 &= \theta_3 = \theta_5 = \theta_6 = \frac{\pi}{2} & \theta_4 = \pi \\ \varphi_2 &= 0 & \varphi_3 &= \frac{\pi}{2} & \varphi_5 = \pi & \varphi_6 = \frac{3\pi}{2} \end{aligned} \quad (\text{A3.4})$$

With these relations the nonzero matrix elements  $V_{mm'}$  are the same as for the octahedron, and the roots  $\varepsilon$  are the same as in Eqs. (4.13). However, the expressions for  $V_{mm'}$  do not coincide with (4.12):

$$\begin{aligned} V_{22} &= eq\{2F_0(R_1) + 4F_0(R_2) - \frac{4}{7}[F_2(R_1) - F_2(R_2)] + \frac{2}{21}F_4(R_1) + \frac{1}{14}F_4(R_2)\} \\ V_{11} &= eq\{2F_0(R_1) + 4F_0(R_2) + \frac{2}{7}[F_2(R_1) - F_2(R_2)] - \frac{8}{21}F_4(R_1) - \frac{2}{7}F_4(R_2)\} \\ V_{00} &= eq\{2F_0(R_1) + 4F_0(R_2) + \frac{4}{7}[F_2(R_1) - F_2(R_2)] + \frac{4}{7}F_4(R_1) + \frac{3}{7}F_4(R_2)\} \\ V_{2-2} &= \frac{5}{6}eqF_4(R_2) \end{aligned} \quad (\text{A3.5})$$

For this reason all four roots (4.13) are different, and for the description of the splitting one should introduce, alongside the cubic splitting parameter (4.15)

$$\Delta = 10Dq = \frac{5}{3}eqF_4(R) \quad (\text{A3.6})$$

two more parameters of the tetragonal splitting:

$$D_s = \frac{2}{7}eq[F_2(R_2) - F_2(R_1)] \quad D_t = \frac{2}{21}eq[F_4(R_2) - F_4(R_1)] \quad (\text{A3.7})$$

With these parameters the  $d$ -electron energy levels are (the type of symmetry and  $d$  function are indicated in parenthesis)

$$\begin{aligned} \varepsilon_1(A_{1g}; d_{z^2}) &= E'_0 + \frac{3}{5}\Delta - 2D_s - 6D_t \\ \varepsilon_2(B_{1g}; d_{x^2-y^2}) &= E'_0 + \frac{3}{5}\Delta + 2D_s - D_t \\ \varepsilon_3(B_{2g}; d_{xy}) &= E'_0 - \frac{2}{5}\Delta + 2D_s - D_t \\ \varepsilon_{4,5}(E_g; d_{xz}, d_{yz}) &= E'_0 - \frac{2}{5}\Delta - D_s + 4D_t \end{aligned} \quad (\text{A3.8})$$

where  $E'_0 = 2F_0(R_1) + 4F_0(R_2)$ .

In the limit of strong tetragonal distortion with two axial ligands at infinity, the octahedron transforms into a *planar-square configuration* with the CA in the center. The corresponding energy levels can be found by tending  $R_1 \rightarrow \infty$ . This results

in  $F_k(R_1) \rightarrow 0$  [see Eqs. (A2.12)–(A2.14)], and hence  $D_s = \frac{2}{7}eqF_2(R_2)$ ,  $D_t = \frac{2}{21}eqF_4(R_2)$ . Note that in this case the three parameters,  $\Delta$ ,  $D_s$ , and  $D_t$ , are no longer independent:  $D_t = \frac{2}{35}\Delta$ , and the energy levels depend on only two parameters,  $D_s$  and  $\Delta$ .

For  $F_k(R_1) \rightarrow 0$  the nonzero matrix elements (A3.5) become

$$\begin{aligned} V_{22} &= eq[4F_0(R) - \frac{4}{7}F_2(R) + \frac{1}{14}F_4(R)] \\ V_{11} &= eq[4F_0(R) - \frac{2}{7}F_2(R) - \frac{2}{7}F_4(R)] \\ V_{00} &= eq[4F_0(R) - \frac{4}{7}F_2(R) + \frac{3}{7}F_4(R)] \\ V_{2-2} &= eq\frac{5}{6}F_4(R) \end{aligned} \quad (\text{A3.9})$$

This allows one to obtain the energy levels of  $d$  electrons in the square-planar crystal field of the ligands:

$$\begin{aligned} \varepsilon_1(A_{1g}; d_{z^2}) &= E_0^S + \frac{9}{35}\Delta - 2D_s \\ \varepsilon_2(B_{1g}; d_{x^2-y^2}) &= E_0^S + \frac{19}{35}\Delta + 2D_s \\ \varepsilon_3(B_{2g}; d_{xy}) &= E_0^S - \frac{16}{35}\Delta + 2D_s \\ \varepsilon_{4,5}(E_g; d_{xz}, d_{yz}) &= E_0^S - \frac{6}{35}\Delta - D_s \end{aligned} \quad (\text{A3.10})$$

where  $E_0^S = 4F_0(R)$ .

### The Tetrahedron and the Cube

For four ligand–point charges forming a regular tetrahedron with the CA in the center, we have

$$\begin{aligned} q_i &= q \quad R_i = R \quad i = 1, 2, 3, 4 \\ \cos \theta_1 &= \cos \theta_2 = -\cos \theta_3 = -\cos \theta_4 = \frac{1}{\sqrt{3}} \\ \varphi_1 &= \frac{\pi}{4} \quad \varphi_2 = \frac{3\pi}{4} \quad \varphi_3 = \frac{5\pi}{4} \quad \varphi_4 = \frac{7\pi}{4} \end{aligned} \quad (\text{A3.11})$$

For these coordinates the roots of the secular equation (4.7) are given by the same formulas (4.13) as for the octahedron, but with different expressions for the matrix elements  $V_{mm'}$ :

$$\begin{aligned} V_{22} &= eq[4F_0(R) - \frac{2}{27}F_4(R)] \\ V_{11} &= eq[4F_0(R) + \frac{8}{27}F_4(R)] \\ V_{00} &= eq[4F_0(R) - \frac{4}{9}F_4(R)] \\ V_{2-2} &= eq\frac{10}{27}F_4(R) \end{aligned} \quad (\text{A3.12})$$

Here, as in the octahedron (and any other cubic system), we obtain

$$\begin{aligned} V_{22} + V_{2-2} &= V_{11} \\ V_{22} - V_{2-2} &= V_{00} \end{aligned} \quad (\text{A3.13})$$

Therefore, among the five roots (4.13) there are only two different groups with two and three equal roots, respectively:

$$\begin{aligned} \varepsilon_1 = \varepsilon_2 = \varepsilon_3 = \varepsilon(T_2) &= eq[4F_0(R) + \frac{8}{27}F_4(R)] \\ \varepsilon_4 = \varepsilon_5 = \varepsilon(E) &= eq[4F_0(R) - \frac{4}{9}F_4(R)] \end{aligned} \quad (\text{A3.14})$$

Thus the splitting in the tetrahedral field is similar to that of the octahedral field (4.14) with the significant distinction that in the tetrahedron the  $E$  term is lower than  $T_2$ . Besides, the absolute value of the splitting in the tetrahedron  $\Delta_T = \varepsilon(E) - \varepsilon(T_2)$

$$\Delta_T = -eq\frac{20}{27}F_4(R) = -\frac{4}{9}\Delta \quad (\text{A3.15})$$

is  $\frac{4}{9}$  of the splitting in the octahedron, provided the interatomic distances  $R$  and ligand–point charges  $q$  are the same in both types of complexes.

Quite similar to the tetrahedral field, the cubic field created by eight ligand–point charges at the eight corners of a regular cube can be considered simply by doubling the field strength. The resulting d electron energy terms and crystal field splitting  $\Delta_k$  are

$$\begin{aligned} \varepsilon(T_2) &= eq[8F_0(R) + \frac{16}{17}F_4(R)] = E_0^k + \frac{2}{5}\Delta_k \\ \varepsilon(E) &= eq[8F_0(R) - \frac{8}{9}F_4(R)] = E_0^k - \frac{3}{5}\Delta_k \end{aligned} \quad (\text{A3.16})$$

$$\Delta_k = \frac{40}{27}eqF_4(R) = 2\Delta_T = \frac{8}{9}\Delta \quad (\text{A3.17})$$

$$E_0^k = 8eqF_0(R) = 2E_0^T = \frac{4}{3}E_0 \quad (\text{A3.18})$$

**APPENDIX 4. MATRIX ELEMENTS OF CRYSTAL FIELD PERTURBATION OF A TWO-ELECTRON TERM  $F(nd)^2$ ,  $V'_{ij}$ ,  $i, j = 1, 2, \dots, 7$  (AFTER [4.34]) EXPRESSED BY ONE-ELECTRON MATRIX ELEMENTS  $V_{mm'}$  GIVEN IN APPENDIX 2**

$$V'_{11} = V_{11} + V_{22}$$

$$V'_{12} = V_{10}$$

$$\begin{aligned}
V'_{13} &= \left(\frac{3}{5}\right)^{1/2} V_{1-1} - \left(\frac{2}{5}\right)^{1/2} V_{20} \\
V'_{14} &= \left(\frac{1}{5}\right)^{1/2} V_{1-2} - \left(\frac{4}{5}\right)^{1/2} V_{2-1} \\
V'_{15} &= -\left(\frac{3}{5}\right)^{1/2} V_{2-2} \\
V'_{16} &= 0 \\
V'_{17} &= 0 \\
V'_{22} &= V_{00} + V_{22} \\
V'_{23} &= \left(\frac{3}{5}\right)^{1/2} V_{0-1} + \left(\frac{2}{5}\right)^{1/2} V_{21} \\
V'_{24} &= \left(\frac{1}{5}\right)^{1/2} V_{0-2} \\
V'_{25} &= -\left(\frac{2}{5}\right)^{1/2} V_{2-1} \\
V'_{26} &= -V_{2-2} = \left(\frac{5}{3}\right)^{1/2} V'_{15} \\
V'_{27} &= 0 \\
V'_{33} &= \frac{3}{5} (V_{22} + V_{-1-1}) + \frac{2}{5} (V_{00} + V_{11}) \\
V'_{34} &= (\sqrt{3}/5) V_{-1-2} + (2\sqrt{3}/5) V_{21} + (2\sqrt{2}/5) V_{0-1} \\
V'_{35} &= (\sqrt{6}/5) V_{20} + (\sqrt{6}/5) V_{0-2} - \frac{2}{5} V_{1-1} \\
V'_{36} &= -\left(\frac{2}{5}\right)^{1/2} V_{1-2} \\
V'_{37} &= -\left(\frac{3}{5}\right)^{1/2} V_{2-2} \\
V'_{44} &= \frac{1}{5} (V_{22} + V_{-2-2}) + \frac{4}{5} (V_{11} + V_{-1-1}) \\
V'_{45} &= (\sqrt{3}/5) V_{21} + (2\sqrt{3}/5) V_{-1-2} + (2\sqrt{2}/5) V_{10} \\
V'_{46} &= \left(\frac{1}{5}\right)^{1/2} V_{20} \\
V'_{47} &= \left(\frac{3}{5}\right)^{1/2} V_{2-1} - \left(\frac{4}{5}\right)^{1/2} V_{1-2} \\
V'_{55} &= \frac{3}{5} (V_{11} - V_{-2-2}) + \frac{2}{5} (V_{00} + V_{-1-1}) \\
V'_{56} &= \left(\frac{3}{5}\right)^{1/2} V_{10} + \left(\frac{2}{5}\right)^{1/2} V_{-1-2} \\
V'_{57} &= \left(\frac{3}{5}\right)^{1/2} V_{1-1} - \left(\frac{2}{5}\right)^{1/2} V_{0-2} \\
V'_{66} &= V_{00} + V_{-2-2} \\
V'_{67} &= V_{0-1} \\
V'_{77} &= V_{1-1} + V_{-2-2}
\end{aligned}$$



**APPENDIX 5. MATRIX ELEMENTS OF CRYSTAL FIELD PERTURBATION OF  $f$  ELECTRON STATES (AFTER [4.22])**

The wavefunction of the  $f$  electron can be taken in the form.

$$\Psi_{n3m} = R_{n3}(r)Y_{3m}(\theta, \varphi) \quad m = 0, \pm 1, \pm 2, \pm 3 \quad (\text{A5.1})$$

Considering the ligand–point charge perturbation after Eq. (4.2), denoting the ligand coordinates by  $\mathbf{R}(R_j, \theta_j, \varphi_j)$  and the functions  $F_n \equiv F_n(R_j)$  after (A2.2) with  $R_{n3}(r)$  instead of  $R_{n2}(r)$

$$R_{43}(r) = \left(\frac{140}{9}\right)^{1/2} \alpha^{9/2} r^3 e^{-\alpha r} \quad (\text{A5.2})$$

and following the computation procedure of Appendix 2, we get the following matrix elements of the ligand–point charge perturbation of the  $f$  states (the sum is taken over all the ligands  $j$ ):

$$\begin{aligned} V_{00} = e^2 \sum_j & \left[ F_0 + \frac{2}{15} (3 \cos^2 \theta_j - 1) F_2 + \frac{1}{44} (35 \cos^4 \theta_j \right. \\ & - 30 \cos^2 \theta_j + 3) F_4 + \frac{25}{1716} (231 \cos^6 \theta_j - 315 \cos^4 \theta_j \\ & \left. + 105 \cos^2 \theta_j - 5) F_6 \right] \end{aligned} \quad (\text{A5.3})$$

$$\begin{aligned} V_{\pm 1 \pm 1} = e^2 \sum_j & \left[ F_0 + \frac{1}{10} (3 \cos^2 \theta_j - 1) F_2 \right. \\ & + \frac{1}{264} (35 \cos^4 \theta_j - 30 \cos^2 \theta_j + 3) F_4 \\ & \left. - \frac{25}{2288} (231 \cos^6 \theta_j - 315 \cos^4 \theta_j + 105 \cos^2 \theta_j - 5) F_6 \right] \end{aligned} \quad (\text{A5.4})$$

$$\begin{aligned} V_{\pm 2 \pm 2} = e^2 \sum_j & \left[ F_0 - \frac{7}{264} (35 \cos^4 \theta_j - 30 \cos^2 \theta_j + 3) F_4 \right. \\ & \left. + \frac{5}{1144} (231 \cos^6 \theta_j - 315 \cos^4 \theta_j + 105 \cos^2 \theta_j - 5) F_6 \right] \end{aligned} \quad (\text{A5.5})$$

$$\begin{aligned} V_{\pm 3 \pm 3} = e^2 \sum_j & \left[ F_0 - \frac{1}{6} (3 \cos^2 \theta_j - 1) F_2 + \frac{1}{88} (35 \cos^4 \theta_j \right. \\ & - 30 \cos^2 \theta_j + 3) F_4 - \frac{5}{6864} (231 \cos^6 \theta_j - 315 \cos^4 \theta_j \\ & \left. + 105 \cos^2 \theta_j - 5) F_6 \right] \end{aligned} \quad (\text{A5.6})$$

$$\begin{aligned} V_{32} = e^2 \sum_j & \left( \sqrt{6/6} \right) \exp(-i\varphi_j) \sin \theta_j \cos \theta_j [-F_2 \\ & + \frac{5}{22} (7 \cos^2 \theta_j - 3) F_4 - \frac{35}{1144} (33 \cos^4 \theta_j \\ & - 30 \cos^2 \theta_j - 30 \cos^2 \theta_j + 5) F_6] \end{aligned} \quad (\text{A5.7})$$

$$\begin{aligned}
V_{31} = e^2 \sum_j & (\sqrt{15/2}) \exp(-2i\varphi_j) \sin^2 \theta_j \left[ -\frac{1}{15} F_2 \right. \\
& + \frac{1}{22} (7 \cos^2 \theta_j - 1) F_4 - \frac{35}{3432} (33 \cos^4 \theta_j \\
& \left. - 18 \cos^2 \theta_j + 1) F_6 \right] \tag{A5.8}
\end{aligned}$$

$$\begin{aligned}
V_{30} = e^2 \sum_j & \sqrt{5\frac{7}{44}} \exp(-3i\varphi_j) \sin^3 \theta_j \cos \theta_j [F_4 \\
& - \frac{5}{26} (11 \cos^2 \theta_j - 3) F_6] \tag{A5.9}
\end{aligned}$$

$$\begin{aligned}
V_{3-1} = e^2 \sum_j & \sqrt{15\frac{7}{88}} \exp(-4i\varphi_j) \sin^4 \theta_j \\
& \left[ \frac{1}{3} F_4 - \frac{5}{26} (11 \cos^2 \theta_j - 1) F_6 \right] \tag{A5.10}
\end{aligned}$$

$$V_{3-2} = -e^2 \sum_j \sqrt{6\frac{385}{2288}} \exp(-5i\varphi_j) \sin^5 \theta_j \cos \theta_j F_6 \tag{A5.11}$$

$$V_{3-3} = -e^2 \sum_j \frac{385}{2288} \exp(-6i\varphi_j) \sin^6 \theta_j F_6 \tag{A5.12}$$

$$V_{2-2} = e^2 \sum_j \frac{35}{88} \exp(-4i\varphi_j) \sin^4 \theta_j \left[ \frac{1}{3} F_4 + \frac{3}{13} (11 \cos^2 \theta_j - 1) F_6 \right] \tag{A5.13}$$

$$\begin{aligned}
V_{1-1} = -e^2 \sum_j & \exp(-2i\varphi_j) \sin^2 \theta_j \frac{1}{5} F_2 + \frac{5}{66} (7 \cos^2 \theta_j - 1) F_4 \\
& + \frac{175}{2288} (33 \cos^4 \theta_j - 18 \cos^2 \theta_j + 1) F_6 \tag{A5.14}
\end{aligned}$$

$$\begin{aligned}
V_{10} = -e^2 \sum_j & \sqrt{3} \exp(-i\varphi_j) \sin \theta_j \cos \theta_j \left[ \frac{1}{15} F_2 + \frac{5}{132} (7 \cos^2 \theta_j - 3) F_4 \right. \\
& \left. + \frac{175}{3432} (33 \cos^4 \theta_j - 30 \cos^2 \theta_j + 5) F_6 \right] \tag{A5.15}
\end{aligned}$$

$$\begin{aligned}
V_{21} = e^2 \sum_j & \sqrt{10} \exp(-i\varphi_j) \sin \theta_j \cos \theta_j \left[ -\frac{1}{10} F_2 - \frac{1}{33} (7 \cos^2 \theta_j - 3) F_4 \right. \\
& \left. + \frac{35}{2288} (33 \cos^4 \theta_j - 30 \cos^2 \theta_j + 5) F_6 \right] \tag{A5.16}
\end{aligned}$$

$$\begin{aligned}
V_{20} = e^2 \sum_j & (\sqrt{30/6}) \exp(-i\varphi_j) \sin^2 \theta_j \left[ -\frac{1}{5} F_2 - \frac{1}{44} (7 \cos^2 \theta_j - 1) F_4 \right. \\
& \left. + \frac{35}{572} (33 \cos^4 \theta_j - 18 \cos^2 \theta_j + 1) F_6 \right] \tag{A5.17}
\end{aligned}$$

$$\begin{aligned}
V_{2-1} = e^2 \sum_j & \sqrt{10\frac{7}{44}} \exp(-3i\varphi_j) \sin^3 \theta_j \cos \theta_j \left[ \frac{1}{3} F_4 \right. \\
& \left. + \frac{15}{52} (11 \cos^2 \theta_j - 3) F_6 \right] \tag{A5.18}
\end{aligned}$$

# ANSWERS AND SOLUTIONS

Following are answers to questions and solutions to problems at the end of Chapters 2–11. Problems are distinguished from questions by the letter P before its number.

## *Chapter 2*

### *True or False?*

- 2.1. *False.* The atomic  $d$  states are fivefold-degenerate, so for the free atom any linear combination of the  $d$  functions in Table 2.1 and Fig. 2.3 is also a  $d$  function; they become space-oriented only under external perturbations that violate the spherical symmetry of the atom.
- 2.2. *False.* Hybridization of atomic functions takes place during (and is caused by) appropriate chemical bonding.
- 2.3. *True.* The orbital moment of  $s$  electrons is zero, so there is no spin–orbital interaction.
- 2.4. *False.* Separation between orbital and spin functions is possible approximately for light atoms where the spin–orbital interaction is weak and can be considered as a perturbation (Russell–Saunders coupling), but is not possible for heavy-atom compounds where the spin–orbital interaction cannot be considered as a small correction ( $jj$  coupling).
- 2.5. *True.* Since the atomic functions are normalized, the maximum of the overlap integral is achieved only when they fully coincide, and then the integral equals unity.

**2.6. False.** In general, the spin-orbital interaction in transition metal systems (TMSs) is neither small nor insignificant and cannot be neglected. In coordination compounds it may be partially reduced by covalence bonding to organic ligands (Example 6.14). For first-row transition elements it can usually be considered as a perturbation.

**2.7. True.** (See Section 2.2.)

**P2.5.** For the  $\text{Ti}^{2+}$  ion in Table 4.7  $B = 695 \text{ cm}^{-1}$  and  $C = 2910 \text{ cm}^{-1}$ , and following Table 2.6 for the electronic configuration  $d^2$  with  $A = 0$  we find (in  $\text{cm}^{-1}$ ):  $E(^3F) = -8B = -5560$ ,  $E(^3P) = 7B = 4865$ , and so on. This results in the following energy level diagram:

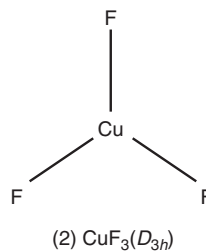
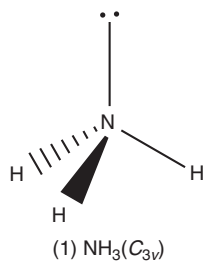
$^1S$ (30100)	
$^1G$ (8600)	
$^3P$ (4865)	
$^1D$ (3735)	
$^3F$ (-5560)	

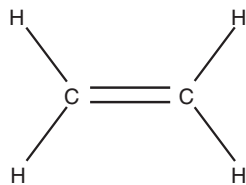
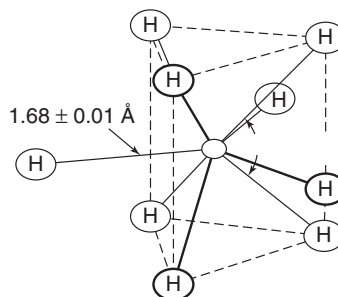
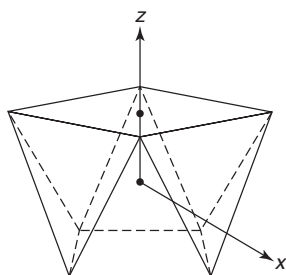
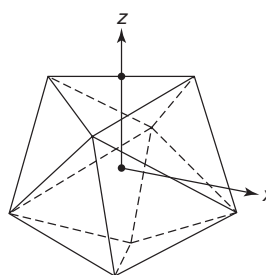
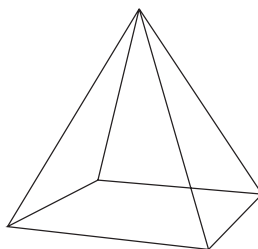
Note that the numbers are relative values of the energy term as we assumed  $A = 0$ . The energy diagrams of the other ions can be obtained in quite a similar way.

### Chapter 3

**P3.1.** A hexagonal prism has an identity element  $E$ , two 2-sided rotational axes  $C_6$  and  $C_3$ , a central  $C_2$  axis, three axes  $C'_2$  in the plane perpendicular to the  $C_6$  axis, cutting the prism in half and connecting two opposite vertices, and three similar axes  $C''_2$  in the same plane connecting the midpoints of two opposite lateral planes; an inversion element  $I$  and an additional five elements that emerge from multiplying the five types of rotational axes  $C_n$  by the inversion element  $I$ , namely,  $C_6I = S_6$  (a six-order rotational-reflection axis),  $C_3I = S_3$ ,  $C_2I = \sigma_h$ ,  $C'_2I = \sigma_v$ ,  $C''_2I = \sigma_d$ . The symmetry group formed by these transformations is  $D_{6h}$ .

**P3.2.** The symmetry group of trigonal pyramidal  $\text{NH}_3$  is  $C_{3v}$ ; planar  $\text{CuF}_3$ ,  $D_{3h}$ ; planar  $\text{C}_2\text{H}_4$ ,  $D_{2h}$ ; tricapped trigonal prism of  $[\text{ReH}_9]^{2-}$ ,  $D_{3h}$  (Section 9.1);



(3)  $\text{CH}_2\text{-CH}_2(D_{2h})$ (4)  $[\text{ReH}_9]^{2-}(D_{3h})$ (5)  $[\text{W}(\text{CN})_8]^{4-}$  in  $\text{H}_4[\text{W}(\text{CN})_8]$  ( $D_{4d}$ )(6)  $[\text{W}(\text{CN})_8]^{4-}$  in  $\text{K}_4[\text{W}(\text{CN})_8]$  ( $D_{2d}$ )(7)  $[\text{Ni}(\text{CN})_5]^{3-}(C_{4v})$ 

square antiprism  $[\text{W}(\text{CN})_8]^{4-}$  in  $\text{H}_4[\text{W}(\text{CN})_8]$ ,  $D_{4d}$ , dodecahedron  $[\text{W}(\text{CN})_8]^{4-}$  in  $\text{K}_4[\text{W}(\text{CN})_8]$ ,  $D_{2d}$ ; and square pyramid  $[\text{Ni}(\text{CN})_5]^{3-}$ ,  $C_{4v}$ . Their structures are shown above.

**P3.3.** Allowed electric-dipolar and magnetic-dipolar transitions from the ground  $A$  state and their polarizations in systems with different symmetries are tabulated as follows:

Symmetry	Electric–Dipolar		Magnetic–Dipolar	
	Transition	Polarization	Transition	Polarization
$O_h$	$A_{1g} \rightarrow T_{1u}$	$x, y, z$	$A_{1g} \rightarrow T_{1g}$	$x, y, z$
$T_d$	$A_1 \rightarrow T_2$	$x, y, z$	$A_1 \rightarrow T_1$	$x, y, z$
$D_{3d}$	$A_{1g} \rightarrow A_{2u}$	$z$	$A_{1g} \rightarrow A_{2g}$	$z$
	$A_{1g} \rightarrow E_u$	$x, y$	$A_{1g} \rightarrow E_g$	$x, y$
$D_{2h}$	$A_g \rightarrow A_u$	$x, y, z$		
	$A_g \rightarrow B_{1u}$	$z$	$A_g \rightarrow B_{1g}$	$z$
	$A_g \rightarrow B_{2u}$	$y$	$A_g \rightarrow B_{2g}$	$y$
	$A_g \rightarrow B_{3u}$	$x$	$A_g \rightarrow B_{3g}$	$x$
$D_{4h}$	$A_{1g} \rightarrow A_{2u}$	$z$	$A_g \rightarrow A_{2g}$	$z$
	$A_{1g} \rightarrow E_u$	$x, y$	$A_{1g} \rightarrow E_g$	$x, y$
$I_h$	$A_{1g} \rightarrow T_{1u}$	$x, y, z$	$A_{1g} \rightarrow T_{1g}$	$x, y, z$

**P3.4.** For the characters of the reducible representation of symmetric products of representations, using formula (3.34),  $[X]^2(G) = \frac{1}{2}\{[X(G)]^2 + X(G^2)\}$  for each class of transformations  $G$ , for both types of  $E$  terms in the  $O_h$  group,  $E_g$  and  $E_u$ , the  $E \times E$  product yields:

$G$	$E$	$C_3$	$C_2$	$C_4$	$C'_2$	$I$	$S_6$	$\sigma_h$	$S_4$	$\sigma_d$
$[X]^2(G) =$	3	0	3	1	1	3	0	3	1	1

Using Eq.(3.33) or by direct inspection, we easily find that this reducible representation is a sum of two irreducible representations (IrReps):  $A_{1g} + E_g$ . Similarly, using Eq. (3.35) we easily solve for the antisymmetric product  $\{E \times E\} = A_{2g}$ . In the same way we find that  $[T \times T] = A + E + T_2$ , and  $\{T \times T\} = T_1$  for any  $T$  term in the cubic groups, while for the  $C_{4v}$  group  $[E \times E] = A_1 + B_1 + B_2$  and  $\{E \times E\} = A_2$  (see also Problem 3.9).

**P3.5.** See Table 5.1.

**P3.6.** See Table 5.1.

**P3.7.** According to the table of characters of the symmetry group  $O_h$ , Table A1.11, the tensor of polarizability belongs to the  $T_{2g}$  IrRep (its components, products of coordinates, transform as  $T_{2g}$  symmetry type). Therefore the matrix elements of this tensor, and hence transition under tensor perturbations (e.g., in Raman spectra; see Section 8.2) are nonzero if the product of the IrReps of the initial and final states contains the  $T_{2g}$  IrRep. Using Eq. (3.33) (or by direct inspection) we can easily find that in the  $O_h$  group

the  $T_{2g}$  IrRep is contained in the products  $A_{1g} \times T_{2g}$ ,  $A_{1u} \times T_{2u}$ ,  $E_g \times T_{2g}$ ,  $E_u \times T_{2u}$ ,  $T_{1g} \times T_{2g}$ , and  $T_{1u} \times T_{2u}$ . Thus transitions between these pairs of states are allowed under tensor perturbations.

- P3.8.** For the seven-atom system  $\text{UF}_6$ , using Eqs. (3.54)–(3.56) and Table A1.11, we find the following reducible vibrational representation  $X(G)$  of the atomic displacements in the octahedral  $O_h$  symmetry:

$G$	$E$	$C_3$	$C_2$	$C_4$	$C_2'$	$I$	$S_6$	$\sigma_h$	$S_4$	$\sigma_d$
$X(G)$	15	0	-1	1	1	-3	0	5	-1	3

Its decomposition into IrReps by means of Eq. (3.33) yields  $X(G) = A_{1g} + E_g + T_{2g} + T_{2u} + 2T_{1u}$ . Thus the possible symmetrized vibrations include one  $A_{1g}$ , one  $E_g$ , two  $T_{1u}$ , one  $T_{2g}$ , and one  $T_{2u}$  vibrations, with a total of  $3 \times 7 - 6 = 15$ .

- P3.9.** In the  $T_d$  group there are two types of  $t^2$  configurations,  $t_1^2$  and  $t_2^2$ . In both cases  $T \times T = A_1 + E + T_1 + T_2$  with the symmetric part  $[T \times T] = A_1 + E + T_2$  (for which the spin state should be antisymmetric, meaning  $S = 0$ ) and antisymmetric product  $\{T \times T\} = T_1$  (for which  $S = 1$ ). Therefore the  $t^2$  configuration in tetrahedral systems produces one triplet term  ${}^3T_1$  and three singlet terms  ${}^1A_1$ ,  ${}^1E$ , and  ${}^1T_2$ . In the  $O_h$  groups there are four types of  $t^2$  configurations:  $t_{1g}^2$ ,  $t_{1u}^2$ ,  $t_{2g}^2$ , and  $t_{2u}^2$ . For all of them  $T \times T = A_{1g} + E_g + T_{1g} + T_{2g}$  with the symmetric part  $[T \times T] = A_{1g} + E_g + T_{2g}$  and antisymmetric product  $\{T \times T\} = T_{1g}$ . Thus the terms of any  $t^2$  configuration in  $O_h$  symmetry are  ${}^3T_{1g}$ ,  ${}^1A_{1g}$ ,  ${}^1E_g$ , and  ${}^1T_{2g}$ .

#### Chapter 4

- 4.1.** See answers in Sections 4.1 and 4.6.
- 4.2.** The equivalence of the five  $d$ -electron distribution (fivefold degeneracy) is due to the spherical symmetry of the atomic field; any additional field of cubic and lower symmetry makes them nonequivalent and removes the degeneracy. In icosahedral fields the five  $d$  electrons remain equivalent (the icosahedral group has five-dimensional IrReps); their levels do not split. The three  $p$  electrons form a threefold-degenerate state in the free atom, and they remain equivalent in the ligand fields of cubic symmetry; their levels do not split (cubic symmetry groups have threefold-degenerate IrReps), but they split in fields of lower symmetry.
- 4.3.** The stability of the complex in the crystal field theory (CFT) model is provided by Coulomb interaction of the central atom (CA) core and ligand ions or dipoles [the term  $W$  in Eq. (4.1)]. The CFT does not consider in detail the CA—ligand bonding energy (Section 4.1).
- 4.4.** See answers in Section 4.3.

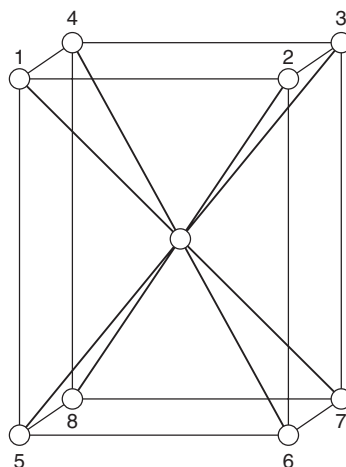
- 4.5. In weak crystal fields the splitting magnitude of  $d$ -electron levels  $\Delta$  is small, so additional electrons prefer to occupy the higher levels forming a configuration with parallel spins (high total spin), which has lower energy in accordance with Hund's rule. When  $\Delta$  is large (in strong fields), the high-spin arrangement becomes inconvenient, while at lower levels the electron spins are paired, resulting in low-spin electron configurations. The number of  $d$  electrons for which two alternative configurations are possible is limited to  $d^4$ – $d^7$  in octahedral systems and  $d^3$ – $d^6$  in tetrahedral complexes. For details, see Section 4.3 and Example 4.2.
- 4.6. The criterion of applicability of perturbation theory to the splitting of separate terms under the influence of the crystal field requires that the splitting magnitude  $\Delta$  be small in comparison to the energy gap to other terms of the same symmetry and multiplicity (see Question 4.7). As we can see from Fig. 4.7 for the case of weak fields, for relatively large  $\Delta$  values some of such terms [e.g.,  ${}^1T_{2g}({}^1D)$  and  ${}^1T_{2g}({}^1G)$ ,  ${}^1E_g({}^1D)$  and  ${}^1E_g({}^1G)$ ] are significantly close in energy, and hence they do not obey the criterion based on which they were evaluated. In more accurate calculation the interaction between such terms should be taken into account (Section 4.3).
- 4.7. The noninteraction, intersection rule for two terms with different symmetries or multiplicities follows from Eqs. (4.55)–(4.58). If two terms have different symmetries or different multiplicities, the integral (4.56) is zero according to group-theoretical selection rules (Section 3.4; the spin functions for different multiplicities are orthogonal), and they do not interact they intersect. Terms with the same symmetry and multiplicity interact and repulse each other; they do not intersect.
- 4.8. The crystal field destabilization is due to the averaged repulsion between the electrons of the CA and the negative charges (or negative ends of dipoles) of the ligands, whereas the electron interaction destabilization is produced by the repulsion and exchange interaction between the  $d$  electrons belonging to the CA. In the strong-field approximation we assume that the ligand field splitting of the  $d$ -electron levels is stronger than the splitting produced by interelectron interaction. When all the ligands are identical (in high-symmetry complexes), both the local and averaged ligand fields depend on the magnitude of the ligand charge, so we can assume that the larger the splitting, the stronger the averaged ligand field, and hence in the strong-field limit the ligand field destabilization is stronger than the electron interaction destabilization. However, in low-symmetry complexes the differences in the local ligand fields that produce the splitting may be large when the averaged field is small.
- 4.9. In tetrahedral complexes the main ligand field splitting magnitude  $\Delta_T$  is approximately four-ninths (44%) of that in octahedral complexes  $\Delta_O$  (Section 4.2), whereas the pairing energy  $\Pi$  is approximately the same in





both cases. Therefore the condition of low-spin systems  $\Delta > \Pi$  is realized much more easily in octahedral complexes than in tetrahedral ones. Low-spin tetrahedral complexes are very rare.

- 4.10.** The differences in ligand field splitting of  $d$  and  $f$  electrons are due to their different symmetries and, most important, to the fact that the ligand field for  $f$  electrons is usually screened by the outer  $d$  electrons of the CA, and the  $f$  electrons have a much larger spin-orbital splitting. See Section 4.4 for details.
- P4.1.** The square prism is shown in the following diagram. Similar to the octahedral and cubic case (Section 4.2), the charges of the eight ligands and their distances to the CA are the same, while the angular coordinates are different:



The ligand coordinates  $R_i$  and charges  $q_i$  are ( $i = 1, \dots, 8$ )

$$\begin{aligned}
 q_i &= q & R_i &= R \\
 \varphi_1 = \varphi_5 &= \frac{\pi}{4} & \varphi_2 = \varphi_6 &= \frac{3\pi}{4} \\
 \varphi_3 = \varphi_7 &= \frac{5\pi}{4} & \varphi_4 = \varphi_8 &= \frac{7\pi}{4} \\
 \cos \theta_1 = \cos \theta_2 = \cos \theta_3 = \cos \theta_4 &= c \\
 \cos \theta_5 = \cos \theta_6 = \cos \theta_7 = \cos \theta_8 &= -c \\
 \sin \theta_i = s & & s^2 + c^2 &= 1
 \end{aligned}$$

To calculate the matrix elements  $V_{mm'}$ , substitute these values into Eq. (4.9) and take into account the data of Table 4.1. The expressions of  $Y_4^{m-m'}$ ,  $Y_2^{m-m'}$ , and  $Y_0^{m-m'}$  can be found, for example, from [http://en.wikipedia.org/wiki/Table of spherical harmonics](http://en.wikipedia.org/wiki/Table_of_spherical_harmonics).

We then obtain

$$\begin{aligned}
 V_{22} = V_{-2-2} &= eq \left[ \frac{35c^4 - 30c^2 + 3}{21} F_4(R) - \frac{24c^2 - 8}{7} F_2(R) + 8F_0(R) \right] \\
 V_{11} = V_{-1-1} &= eq \left[ -\frac{140c^4 - 120c^2 + 12}{21} F_4(R) \right. \\
 &\quad \left. + \frac{12c^2 - 4}{7} F_2(R) + 8F_0(R) \right] \\
 V_{00} &= eq \left[ \frac{70c^4 - 60c^2 + 6}{7} F_4(R) + \frac{24c^2 - 8}{7} F_2(R) + 8F_0(R) \right] \\
 V_{2-2} &= eq \left[ -\frac{5s^4}{3} F_4(R) \right]
 \end{aligned}$$

and zero for the other  $V_{mm'}$  matrix elements. With these matrix elements the roots of Eq. (4.7) are  $\varepsilon_1 = V_{00}$ ,  $\varepsilon_2 = \varepsilon_3 = V_{11}$ ,  $\varepsilon_4 = V_{22} - V_{2-2}$ , and  $\varepsilon_5 = V_{22} + V_{2-2}$ , meaning that the fivefold-degenerate  $D$  term splits into four terms, from which one remains twofold-degenerate, similar to the splitting in a tetragonal distorted octahedron in Appendix 3. In the particular case of a cube,  $c = 1/\sqrt{3}$  and  $s = \sqrt{2/3}$ , and the solution,

$$\begin{aligned}
 \varepsilon_1 = \varepsilon_2 = \varepsilon_5 &= eq \left[ -\frac{8}{9} F_4(R) + 8F_0(R) \right] \\
 \varepsilon_3 = \varepsilon_4 &= eq \left[ \frac{16}{27} F_4(R) + 8F_0(R) \right]
 \end{aligned}$$

with the splitting  $\Delta_c = \frac{40}{27} eq F_4(R)$  coincides with that given in Section 4.2, Eq. (4.22).

**P4.2.** For one  $d$  electron ( $L = 2$ , term  $D$ ) in an icosahedral field we first calculate the reducible representation of the spherical group of the free atom in the octahedral symmetry. Using Eq. (4.31) with  $L = 2$ ,  $X(\phi) = (\sin 5\phi/2)/(\sin \phi/2)$ , we obtain the following characters of the reducible representation for all  $I_h$  symmetry operations  $X(G)$ :

$G$	$E$	$12C_5$	$12C_5^2$	$20C_3$	$15C_2$	$I$	$12S_{10}$	$10S_{10}^3$	$20S_6$	$15\sigma$
$X(G)$	5	0	0	-1	1	5	0	0	-1	1

Looking at the characters of the  $I_h$  group (Table A1.12), we see that this representation is irreducible,  $X(G) = H_g$ . Thus the  $D$  term of one  $d$  electron in icosahedral fields of  $I_h$  symmetry is  $H_g$ ; it does not split. For one  $f$  electron ( $L = 3$ , energy term  $F$ ), using the same procedure, and the formula  $X(\phi) = (\sin 7\phi/2)/(\sin \phi/2)$ , we obtain:

$G$	$E$	$12C_5$	$12C_5^2$	$20C_3$	$15C_2$	$I$	$12S_{10}$	$10S_{10}^3$	$20S_6$	$15\sigma$
$X(G)$	7	$-a$	$-b$	1	-1	-7	$a$	$b$	-1	1

where  $a = (1 + \sqrt{5})/2$  and  $b = (1 - \sqrt{5})/2$ . Decomposing this reducible representation in IrReps using Eq. (3.33) (or by inspection) we easily find that  $X(G) = G_u + T_{2u}$ , meaning that the  $F$  term in icosahedral fields splits into two terms:  $F \rightarrow G_u + T_{2u}$ .

- P4.3.** The splitting is calculated starting from the point where the average influence of the ligand field is taken into account, which means that the averaged splitting should be zero.
- P4.4.** Results of the calculations of pairing energy  $\Pi$  by means of Eq. (4.50) as a function of electronic configuration  $d^n$  and Racah parameters  $B$  and  $C$  with  $B$  from Table 8.3 and  $C = \gamma B$  with  $\gamma$  from Table 4.7 (for  $\text{Rh}^{3+}$  complexes  $\gamma \approx 4.50$ ), and its comparison with the octahedral crystal field splitting  $\Delta$  taken from Table 8.2 for the given coordination systems are presented in the following table [values in wavenumbers ( $\text{cm}^{-1}$ )]:

$d^n$	Complex	$\Delta$	$B$	$\gamma$	$\Pi$	HS versus LS
$d^5$	$\text{Mn}(\text{H}_2\text{O})_6^{2+}$	7,800	790	4.78	24,806	HS
$d^5$	$\text{Fe}(\text{H}_2\text{O})_6^{3+}$	13,700	770	4.73	23,986	HS
$d^6$	$\text{Co}(\text{NH}_3)_6^{3+}$	23,000	660	4.81	14,348	LS
$d^6$	$\text{Co}(\text{CN})_6^{3-}$	34,000	440	4.81	9,566	LS
$d^6$	$\text{RhCl}_6^{3-}$	20,300	400	4.50	8,200	LS
$d^6$	$\text{Rh}(\text{H}_2\text{O})_6^{3+}$	27,000	500	4.50	10,250	LS
$d^7$	$\text{Co}(\text{H}_2\text{O})_6^{3+}$	9,300	970	4.63	21,844	HS

- P4.5.** Tanabe–Sugano diagrams show, in particular, the  $\Delta$  values where the energy levels of low-spin and high-spin states of corresponding octahedral coordination systems with electronic configurations  $d^4$ – $d^7$  intersect, realizing a spin crossover, and hence the approximate  $\Delta$  values for which they coexist. These  $\Delta$  values are calculated for specific magnitudes of Racah parameters  $B$  and  $C$ , which are approximately near the expected average values for corresponding complexes. On the other hand, the  $\Delta_{\text{exp}}$  magnitudes for specific complexes can be determined experimentally; in the series (8.24) they are given for different six-coordinated ligands as a fraction of the  $\Delta$  value for the same CA with water ligands. The latter can be taken from Table 8.2. For instance, for  $\text{Mn}(\text{H}_2\text{O})_6^{2+}$   $\Delta_{\text{exp}} = 7800 \text{ cm}^{-1}$ , and hence even cyanide ligands of  $\text{Mn}^{2+}$  for which  $\Delta_{\text{exp}} = 7800 \times 1.7 = 13,260 \text{ cm}^{-1}$  are far from the spin crossover possibility: according to Fig. 4.11c (Tanabe–Sugano diagram for  $d^4$  systems),  $\Delta \approx 21,000 \text{ cm}^{-1}$ . For similar complexes of  $\text{Fe}^{2+}$  or  $\text{Co}^{3+}$  with  $d^6$  configuration for which in water complexes  $\Delta_{\text{exp}} = 10,400 \text{ cm}^{-1}$  and  $\Delta_{\text{exp}} \approx 18,600 \text{ cm}^{-1}$ , respectively, spin crossover is quite possible in complexes with relatively strong-field ligands for iron and moderate-strength ligands for cobalt. Of course, the series (8.24) is very limited (it serves only as an illustration). In fact, spin

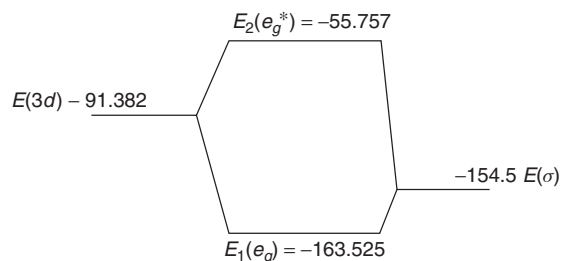
crossover takes place in a huge variety of complexes of transition metals, especially iron and cobalt (see Section 8.4).

### Chapter 5

**P5.1.** The  $E_g$  state is double-degenerate, so its two MOs have the same energy; to find the latter, one should solve the secular equation of the type (5.111) in Example 5.5 with the matrix elements relevant to the atomic orbital  $\psi_0 = d_{x^2-y^2}$  and ligand  $\Phi_\sigma = \frac{1}{2}(\sigma_2 + \sigma_5 - \sigma_3 - \sigma_6)$  (Table 5.1):

$$\begin{vmatrix} H_{3d3d} - E & H_{3d\sigma}^G - EG(3d, \sigma) \\ H_{3d\sigma}^G - EG(3d, \sigma) & H_{\sigma\sigma} - E \end{vmatrix} = 0$$

Using Eqs. (5.11) and (5.11') for, respectively, group overlap and resonance integrals, we easily find that  $G(3d, \sigma) = \sqrt{3}S(3d, \sigma)$  and  $H_{3d\sigma}^G = \sqrt{3}H_{3d\sigma}$ . Then, from the Wolfsberg–Helmholtz formula with  $k = 2$ , we have  $H_{3d\sigma} = (H_{3d3d} + H_{\sigma\sigma})S(3d, \sigma)$ , and with the initial data of the problem, we get (in  $\text{kK} = 1000 \text{ cm}^{-1}$ )  $H_{3d\sigma} = -44.259$ ,  $H_{3d\sigma}^G = -76.659$ ,  $G(3d, \sigma) = 0.312$ , so the secular equation above is  $0.903E^2 + 198.012E + 8233.314 = 0$ . Its two roots are  $E_1 = -163.525$  and  $E_2 = -55.757$ . The MO scheme for these  $E_g$  orbitals is



For the LCAO coefficients of the  $E_g$  MOs, Eqs. (5.7) yield ( $E_1 = -163.525$ )  $c_{3d} = 0.306$  and  $c_\sigma = 0.861$  for the bonding MO. Note that because of the uniformity of two Eqs. (5.7) with respect of the two coefficients  $c_{3d}$  and  $c_\sigma$ , only the ratio  $c_{3d}/c_\sigma = 0.355$  can be obtained from these equations. The second equation determining the two coefficients is the normalization condition:  $(c_{3d})^2 + (c_\sigma)^2 + 2c_{3d}c_\sigma G = 1$ . Thus this MO is

$$\varphi_1(e_g) = 0.306d_{x^2-y^2} + 0.861 \cdot \frac{1}{2}(\sigma_2 + \sigma_5 - \sigma_3 - \sigma_6)$$

while for the antibonding MO ( $E_2 = -40.866$ ), we obtain

$$\varphi_1(e_g^*) = 0.986d_{x^2-y^2} - 0.657 \cdot \frac{1}{2}(\sigma_2 + \sigma_5 - \sigma_3 - \sigma_6)$$

In the same way we estimate the coefficients for the second  $E_g$ -type MO that has the same energies and the same group overlap and resonance

integrals. The bonding MO is

$$\varphi_2(e_g) = 0.370d_{z^2} + 0.821 \cdot \frac{1}{\sqrt{6}}(2\sigma_1 + 2\sigma_4 - \sigma_2 - \sigma_5 - \sigma_3 - \sigma_6)$$

and the antibonding one is

$$\varphi_2(e_g^*) = 0.939d_{z^2} - 0.564 \cdot \frac{1}{\sqrt{6}}(2\sigma_1 + 2\sigma_4 - \sigma_2 - \sigma_5 - \sigma_3 - \sigma_6)$$

For the three  $T_{2g}$ -type  $\pi$  MOs with the data given in the problem we find the following secular equation with respect to the energies  $E$ :  $0.959E^2 + 200.744E + 9674.234 = 0$ , which yields two roots,  $E_1 = -134.096$  and  $E_2 = -75.230$ . The MO energy-level scheme (the very-high-energy  $4p$  electrons of Ti,  $H_{pp} = -46.060$ , are not considered here) is thus as follows (in  $\text{kK} = 10^3 \text{ cm}^{-1}$  with arbitrary scaling):

AO, Ti	MO	AO, F
	_____ $E(a_{1g}^*) = -16.10$	
	_____ $E(e_g^*) = -55.757$	
	_____ $E(t_{2g}^*) = -75.230$	
$E(4s) = -78.898$ _____		
$E(3d) = -91.382$ _____		
		_____ $E(\sigma) = -154.5$
		_____ $E(\pi) = -172.2$
	_____ $E(t_{2g}) = -134.096$	
	_____ $E(e_g) = -163.525$	
	_____ $E(a_{1g}) = -164.64$	

Note that this scheme qualitatively coincides with the most common MO energy-level diagram for octahedral  $O_h$  systems given in Fig. 6.1.

**P5.2.** In the weak covalence approximation, using Eqs. (5.38) and (5.39) and the data in ( $\text{kK} = 10^3 \text{ cm}^{-1}$ )  $H_{00} = H_{4s4s} = -78.90$  and  $H_{11} = H_{\sigma\sigma} = -154.50$  with  $G_{01} = G(4s, \sigma) = \sqrt{6} \cdot S(4s, \sigma) = 0.429$  (Table 5.4), we find  $E_1 = -169.57$  and  $E_2 = -20.88$ . To estimate the coefficients of the wavefunctions (5.32) and (5.33), we use Eq. (5.36'), which yields  $\gamma = 0.448$ , and Eq. (5.34) to obtain the normalization constant  $N_1 = 0.794$ . This gives us the bonding wavefunction:

$$\varphi_1 = 0.794 \times \frac{1}{\sqrt{6}}(\sigma_1 + \sigma_2 + \sigma_3 + \sigma_4 + \sigma_5 + \sigma_6) + 0.356|4s \rangle$$

For the antibonding MO we estimate first  $\lambda = \gamma + G_{01} = 0.877$  and  $N_2 = 0.992$  [Eq. (5.35)], so following Eq. (5.33) we obtain:

$$\varphi_2 = 0.870 \times \frac{1}{\sqrt{6}}(\sigma_1 + \sigma_2 + \sigma_3 + \sigma_4 + \sigma_5 + \sigma_6) - 0.992|4s \rangle$$

Comparing these results with those obtained for the same system by the IEH method in Example 5.1, we can see that they are very close; the discrepancies are within the approximations of both methods, but the calculations are simpler in the method of weak covalence. However, while the latter is limited to mostly ionic compounds (which include the case of  $\text{TiF}_6^{3-}$  under consideration), the IEH method has no such limitations and can be applied to any system.

**P5.3.** The density functional theory (DFT) methods handle the problem via electron densities instead of wavefunctions, and this essentially simplifies the calculations because the former is a function of the three coordinates of space, whereas the latter depends on a much higher number of coordinates and spin of all electrons. This simplification (as do any other simplifications) comes with a cost—electronic density does not depend directly on spin, it cannot handle electronic degeneracy and pseudodegeneracy [and hence Jahn–Teller effect (JTE) and pseudo–JTE (PJTE)] and properties that depend on off-diagonal matrix elements in wavefunction presentation; there are also difficulties in directly treating excited states. However, because of its essential advantages in calculations of ground-state energies for larger systems, the DFT methods achieved widespread use. Different versions combine the main DFT concept with MO LCAO presentations to overcome the difficulties outlined above (Section 5.4); the most commonly used method is the Kohn–Sham (KS) approach. By choosing appropriate KS orbitals, one can impose a definite value of total spin on the system to be calculated by DFT methods. Some (limited) excited states can be determined by employing the time-dependent version of DFT (TD-DFT). But the degeneracy problem remains unresolved in DFT. See also Example 5.3 and Problem P5.6.

**P5.4.** In the program package MOLPRO, the input is similar to that of the Hartree–Fock (HF) method with the lanl2dz basis set in Example 5.4. We give the input here for the square-planar configuration; the reader can produce it for the other two configurations in a quite similar way from those in the Example 5.4:

```
***,MnO_4^-, HF/6-31g* square-planar
! For full explanation see exercise 5.4 input
ro=1.52 Angstrom;
rdummy=1;
ang=90.0;
died=90.;
```

```

geometry={Q1;
  Mn,Q1,rdummy;
  O1,Mn,ro,Q1,ang;
  O2,Mn,ro,Q1,ang,O1,died;
  O3,Mn,ro,Q1,ang,O1,-died;
  O4,Mn,ro,Q1,ang,O2,died}
basis={! The basis is taken from the emsl exchange web page
  (https://bse.pnl.gov/bse/portal)
!
! OXYGEN      (10s,4p,1d) -> [3s,2p,1d]
! OXYGEN      (1d)
s, 0, 5484.6717000, 825.2349500, 188.0469600, 52.9645000,
16.8975700, 5.7996353, 15.5396160, 3.5999336, 1.0137618,
0.2700058
c, 1.6, 0.0018311, 0.0139501, 0.0684451, 0.2327143,
0.4701930, 0.3585209
c, 7.9, -0.1107775, -0.1480263, 1.1307670
c, 10.10, 1.0000000
p, 0, 15.5396160, 3.5999336, 1.0137618, 0.2700058
c, 1.3, 0.0708743, 0.3397528, 0.7271586
c, 4.4, 1.0000000
d, 0, 0.800000
c, 1.1, 1
! MANGANESE   (22s,16p,4d,1f) -> [5s,4p,2d,1f]
! MANGANESE   (1f)
s, MN, 56347.1400000, 8460.9430000, 1927.3250000,
543.2343000, 173.9905000, 59.3600500, 1165.4120000,
277.3276000, 89.4727800, 33.4825600, 13.5403700, 5.5579720,
45.8353200, 15.1877700, 6.5007100, 2.7515830, 1.1454040,
0.4536870, 1.7579990, 0.6670220, 0.1051290, 0.0384180
c, 1.6, 1.771580E-03, 1.357081E-02, 6.690605E-02,
2.318541E-01, 4.799046E-01, 3.495737E-01
c, 7.12, 2.388751E-03, 3.181708E-02, 1.254670E-01,
-2.955431E-02, -6.175160E-01, -4.544458E-01
c, 13.18, -3.665856E-03, 7.231971E-02, 2.544486E-01,
-2.910380E-01, -7.359860E-01, -1.997617E-01
c, 19.21, 0.05628572, 0.2897491, -1.1406530
c, 22.22, 1.000000E+00
p, MN, 1165.4120000, 277.3276000, 89.4727800, 33.4825600,
13.5403700, 5.5579720, 45.8353200, 15.1877700, 6.5007100,
2.7515830, 1.1454040, 0.4536870, 1.7579990, 0.6670220,
0.1051290, 0.0384180
c, 1.6, 3.977318E-03, 3.103112E-02, 1.351894E-01,
3.457387E-01, 4.629205E-01, 2.090592E-01
c, 7.12, -6.887578E-03, -2.846816E-02, 6.031832E-02,
3.938961E-01, 5.013769E-01, 1.792264E-01
c, 13.15, -0.5035024, 0.2345011, 0.9141257
c, 16.16, 1.00000000
d, MN, 20.9435500, 5.5104860, 1.6650380, 0.4617330
c, 1.3, 8.672702E-02, 3.841883E-01, 7.069071E-01
c, 4.4, 1
f, MN, 0.800000
c, 1.1, 1

```



```

}
{rhf;
wf,56,1,0}
{optg;
active,ro}

```

With these inputs the calculations yield

Configuration	Method	Basis	$R_{ml}$ (Å)	Angle Dummy—Mn—O (degree)	Energy (au)
Square	HF	6-31G*	1.852	—	-1447.45309082
Tetrahedral	HF	6-31G*	16.919	—	-1438.01485078
Pyramidal	HF	6-31G*	1.806	138.7	-1448.03592380

We see that here again the pyramidal configuration is the lowest in energy with the square-planar one higher, and the tetrahedral geometry very high; together with the interatomic distance of  $\sim 17$  Å this means that the tetrahedral configuration is dissociated. The results for this system are compared in fuller detail at the end of the solution to the Problem 5.6.

**P5.5.** MP2 calculations are more complicated as they take into account the correlation effects. The method requires the wavefunctions of Hartree–Fock calculations as an input. We give here the input for the tetrahedral geometry; the others are similar.

```

***,MnO_4^-, MP2/6-31g* tetrahedral
! For full explanation see exercise 5.4 and 5.5 input
ro=1.82 Angstrom;
tang=109.471;
died=120.;
geometry={Mn;
  01,Mn,ro;
  02,Mn,ro,01,tang;
  03,Mn,ro,01,tang,02,died;
  04,Mn,ro,01,tang,02,-died}
basis={
!
! OXYGEN      (10s,4p,1d) -> [3s,2p,1d]
! OXYGEN      (1d)
s, 0, 5484.6717000, 825.2349500, 188.0469600, 52.9645000,
16.8975700, 5.7996353, 15.5396160, 3.5999336, 1.0137618,
0.2700058
c, 1.6, 0.0018311, 0.0139501, 0.0684451, 0.2327143,
0.4701930, 0.3585209
c, 7.9, -0.1107775, -0.1480263, 1.1307670
c, 10.10, 1.0000000
p, 0, 15.5396160, 3.5999336, 1.0137618, 0.2700058
c, 1.3, 0.0708743, 0.3397528, 0.7271586

```

```

c, 4.4, 1.0000000
d, 0, 0.800000
c, 1.1, 1
! MANGANESE      (2s,16p,4d,1f) -> [5s,4p,2d,1f]
! MANGANESE      (1f)
s, MN, 56347.1400000, 8460.9430000, 1927.3250000,
543.2343000, 173.9905000, 59.3600500, 1165.4120000,
277.3276000, 89.4727800, 33.4825600, 13.5403700, 5.5579720,
45.8353200, 15.1877700, 6.5007100, 2.7515830, 1.1454040,
0.4536870, 1.7579990, 0.6670220, 0.1051290, 0.0384180
c, 1.6, 1.771580E-03, 1.357081E-02, 6.690605E-02,
2.318541E-01, 4.799046E-01, 3.495737E-01
c, 7.12, 2.388751E-03, 3.181708E-02, 1.254670E-01,
-2.955431E-02, -6.175160E-01, -4.544458E-01
c, 13.18, -3.665856E-03, 7.231971E-02, 2.544486E-01,
-2.910380E-01, -7.359860E-01, -1.997617E-01
c, 19.21, 0.05628572, 0.2897491, -1.1406530
c, 22.22, 1.000000E+00
p, MN, 1165.4120000, 277.3276000, 89.4727800, 33.4825600,
13.5403700, 5.5579720, 45.8353200, 15.1877700, 6.5007100,
2.7515830, 1.1454040, 0.4536870, 1.7579990, 0.6670220,
0.1051290, 0.0384180
c, 1.6, 3.977318E-03, 3.103112E-02, 1.351894E-01,
3.457387E-01, 4.629205E-01, 2.090592E-01
c, 7.12, -6.887578E-03, -2.846816E-02, 6.031832E-02,
3.938961E-01, 5.013769E-01, 1.792264E-01
c, 13.15, -0.5035024, 0.2345011, 0.9141257
c, 16.16, 1.00000000
d, MN, 20.9435500, 5.5104860, 1.6650380, 0.4617330
c, 1.3, 8.672702E-02, 3.841883E-01, 7.069071E-01
c, 4.4, 1
f, MN, 0.800000
c, 1.1, 1
}

{rhf;          ! In order to perform a MP2 calculation
wf,46,1,0}    ! it is necessary to calculate the HF
mp2           ! wavefunction
{optg;
active,ro}

```

The calculations (taking more time than in the previous approximations) yield the following tabulation (where NC means nonconvergent):

Configuration	Method	Basis	$R_{ml}$ (Å)	Angle	Energy (au)
				Dummy—Mn—O (degree)	
Square	MP2	6-31G*	1.832	—	-1449.27703002
Tetrahedral	MP2	6-31G*	17.536	—	-1438.32002622
Pyramidal	MP2	6-31G*	NC	NC	NC

We see that in these calculations the square-planar configuration is the lowest in energy, while the square-pyramidal one does not converge, meaning that it has no stable configurations (minimum of the APES). Again, further discussion is given at the end of the solution to Problem 5.6.

**P5.6.** The DFT methods are different from those described and explained in Section 5.4 and Problem 5.3. We give here the input for the square-pyramidal geometry; for other configurations the input is similar:

```

***,MnO_4^-, B3LYP/6-31g* pyramidal
! For full explanation see exercise 5.4 and 5.5 input
ro=1.52 Angstrom;
rdummy=1;
ang=130.0;
died=90.;
geometry={Q1;
  Mn,Q1,rdummy;
  O1,Mn,ro,Q1,ang;
  O2,Mn,ro,Q1,ang,O1,died;
  O3,Mn,ro,Q1,ang,O1,-died;
  O4,Mn,ro,Q1,ang,O2,died}
basis={
!
! OXYGEN (10s,4p,1d) -> [3s,2p,1d]
! OXYGEN (1d)
s, 0, 5484.6717000, 825.2349500, 188.0469600, 52.9645000, 16.8975700,
5.7996353, 15.5396160, 3.5999336, 1.0137618, 0.2700058
c, 1.6, 0.0018311, 0.0139501, 0.0684451, 0.2327143, 0.4701930,
0.3585209
c, 7.9, -0.1107775, -0.1480263, 1.1307670
c, 10.10, 1.0000000
p, 0, 15.5396160, 3.5999336, 1.0137618, 0.2700058
c, 1.3, 0.0708743, 0.3397528, 0.7271586
c, 4.4, 1.0000000
d, 0, 0.8000000
c, 1.1, 1
! MANGANESE (22s,16p,4d,1f) -> [5s,4p,2d,1f]
! MANGANESE (1f)
s, MN, 56347.1400000, 8460.9430000, 1927.3250000, 543.2343000,
173.9905000, 59.3600500, 1165.4120000, 277.3276000, 89.4727800,
33.4825600, 13.5403700, 5.5579720, 45.8353200, 15.1877700,
6.5007100, 2.7515830, 1.1454040, 0.4536870, 1.7579990,
0.6670220, 0.1051290, 0.0384180
c, 1.6, 1.771580E-03, 1.357081E-02, 6.690605E-02, 2.318541E-01,
4.799046E-01, 3.495737E-01
c, 7.12, 2.388751E-03, 3.181708E-02, 1.254670E-01, -2.955431E-02,
-6.175160E-01, -4.544458E-01
c, 13.18, -3.665856E-03, 7.231971E-02, 2.544486E-01, -2.910380E-01,
-7.359860E-01, -1.997617E-01
c, 19.21, 0.05628572, 0.2897491, -1.1406530
c, 22.22, 1.000000E+00
p, MN, 1165.4120000, 277.3276000, 89.4727800, 33.4825600, 13.5403700,
5.5579720, 45.8353200, 15.1877700, 6.5007100, 2.7515830, 1.1454040,

```

```

0.4536870, 1.7579990, 0.6670220, 0.1051290, 0.0384180
c, 1.6, 3.977318E-03, 3.103112E-02, 1.351894E-01, 3.457387E-01,
4.629205E-01, 2.090592E-01
c, 7.12, -6.887578E-03, -2.846816E-02, 6.031832E-02, 3.938961E-01,
5.013769E-01, 1.792264E-01
c, 13.15, -0.5035024, 0.2345011, 0.9141257
c, 16.16, 1.00000000
d, MN, 20.9435500, 5.5104860, 1.6650380, 0.4617330
c, 1.3, 8.672702E-02, 3.841883E-01, 7.069071E-01
c, 4.4, 1
f, MN, 0.800000
c, 1.1, 1
}
{rks,b3lyp;
wf,56,1,0}
{optg;
active,ang,ro}

```

The results of these DFT calculations of  $\text{MnO}_4^-$  are given in the table below in comparison with those obtained by other methods described in Example 5.4 and Problems 5.4 and 5.5:

Configuration	Method	Basis	$R_{\text{ml}}$ (Å)	Angle Dummy—Mn—O (degree)	Energy (au)
Square	HF	lanl2dz	1.839	—	-401.27643354
Tetrahedral	HF	lanl2dz	1.741	—	-401.42029498
Pyramidal	HF	lanl2dz	1.862	127.6	-401.48928806
Square	HF	6-31G*	1.852	—	-1447.45309082
Tetrahedral	HF	6-31G*	16.919	—	-1438.01485078
Pyramidal	HF	6-31G*	1.806	138.7	-1448.03592380
Square	MP2	6-31G*	1.832	—	-1449.27703002
Tetrahedral	MP2	6-31G*	17.536	—	-1438.32002622
Pyramidal	MP2	6-31G*	NC	NC	NC
Square	LDA	6-31G*	1.654	—	-1446.62509992
Tetrahedral	LDA	6-31G*	NC	—	NC
Pyramidal	LDA	6-31G*	1.686	127.3	-1446.64045661
Square	B3LYP	6-31G*	1.659	—	-1450.72080760
Tetrahedral	B3LYP	6-31G*	17.219	—	-1439.73304091
Pyramidal	B3LYP	6-31G*	1.848	139.43	-1450.75558577

In both DFT methods the pyramidal geometry is lower in energy, in the B3LYP approximation it is lower than in LDA, while in the latter the tetrahedral configuration is nonconvergent. The reason for this nonconvergence is that DFT-LDA usually underestimates the HOMO-LUMO gap, and in

the case under consideration the separation is too small, making the DFT convergence impossible because of pseudodegeneracy (see Problem 5.3).

Comparing the results for all the methods applied to the  $\text{MnO}_4^-$  system in the table above, we see that the total energies obtained with different methods may be incomparable. The first six calculations in this table use the same Hartree–Fock method, but employ two different basis sets. One of them includes all electrons (6-31G\*); the other uses pseudopotentials (lanl2dz) that substitute the core electrons. The huge energy difference between these calculations comes from the interaction of the core electrons with the nuclei that are included in the energy in the HF/6-31G\* method and not included in the HF/lanl2dz one.

The total energy is an indicator of the accuracy of the results in all variational methods (Hartree–Fock, configuration interaction, CASSCF, coupled cluster), where a better solution yields lower energy. Since MP2 is a perturbation method, the energy obtained with it may be either higher or lower than in Hartree–Fock methods. Also, each DFT method uses its own effective Hamiltonian, which is different from the real one used in the Hartree–Fock methods (Section 5.4), so the energy comparisons between them or with other wavefunction methods is not adequate. We also note that the HF/lanl2dz calculations predict that all three conformations of  $\text{MnO}_4^-$  are stable and that the pyramidal one has the lower energy. Comparison with other methods and basis sets shows that HF/lanl2dz is the only one that predicts the tetrahedral configuration to be stable (but it has not the lowest energy). With most of the other methods we find that in this system the metal–ligand distance exceeds 12.0 Å, meaning that the oxygens dissociate. The energy in this dissociated configuration is always higher than in the pyramidal configuration, so the  $\text{MnO}_4^-$  complex exists as a stable species in these approximations.

Finally, all the methods except MP2 predict that the most stable configuration for the in-vacuum  $\text{MnO}_4^-$  complex is pyramidal with a metal–ligand distance around 1.85 Å and a O—Mn—O angle of 130.0°. It is also important to note that LDA underestimates the metal–ligand distance as compared to other methods. This is relatively common in LDA calculations since this method overestimates the binding.

- P5.7.** Similar to Example 5.4 and Problems 5.4–5.6, we first build the geometry of the molecule. We begin with a square-planar  $\text{FeF}_4$  complex, as described above for  $\text{MnO}_4$ , and then place the fifth and sixth fluorine ions above and below the  $\text{FeF}_4$  complex using a dihedral angle F(5,6)—Fe—F1—F2 equal to +90° and –90°. We then define the metal–ligand distance. In GAMESS it will be necessary to produce a different input for each metal–ligand distance, while in MOLPRO a do-loop can be implemented to vary it. We then input the lanl2dz basis and determine that the method of calculation will be CASSCF. In the latter we need to define the active

space, that is, the number of electrons and orbitals. We may also use symmetry restrictions to more clearly specify the active space.

Both GAMESS and MOLPRO use  $D_{2h}$  symmetry internally to represent an octahedral complex such as  $\text{FeF}_6^{4-}$  (this does not restrict the final configuration). In this space group the  $\text{Fe}(4s)$  orbital belongs to the  $A_g$  IrRep, while the  $\text{Fe}(3d)$  orbitals belong to  $a_g$ , and  $e_g$  ( $3z^2-r^2$  and  $x^2-y^2$ ), which in  $D_{2h}$  are  $a_g + a_g$ , and to  $b_{1g}$ ,  $b_{2g}$ , and  $b_{3g}$ , which form the  $t_{2g}$  degenerate orbital in  $O_h$  symmetry. Thus, the active space consists of six orbitals,  $3a_g + b_{1g} + b_{2g} + b_{3g}$ , and contains six electrons coming from the  $\text{Fe}^{2+}$  ion  $d$  shell. In some cases we will also need to know the symmetry of the doubly occupied orbitals containing the  $2s$  and  $2p$  orbitals of the fluorine ions. These are  $10a_g + 6b_{3u} + 6b_{2u} + 2b_{1g} + 6b_{1u} + 2b_{2g} + 2b_{3g}$  occupied by electrons donated by the ligands. In the low-spin configuration of the  $\text{FeF}_6$  complex the  $t_{2g}$  orbital with main  $\text{Fe}(3d)$  character is fully occupied (closed-shell), so that the state is  $^1A_g$  (in the  $D_{2h}$  notation). Thus, we indicate the spin  $S = 0$  and symmetry  $A_g$  (if requested) in the input. The high-spin configuration contains four electrons in the  $t_{2g}$  orbital and two in the  $e_g$  orbital with main  $\text{Fe}(3d)$  character, resulting in a  $^5T_{2g}$  state. In  $D_{2h}$  symmetry the octahedral  $^5T_{2g}$  state spans  $^5B_{1g}$ ,  $^5B_{2g}$ , and  $^5B_{3g}$ , so a calculation of the lowest state with spin  $S = 2$  in any of these IrReps will yield the same energy (we can check this). It is usually helpful to perform a Mulliken population analysis after the CASSCF calculation to verify that the final state corresponds to the one we were trying to obtain. The input in MOLPRO is as follows:

```

***, CASSCF/lanl2dz for 1Ag and 5T2g in FeF6^4-
! This input contains the final result for the calculation
! several test runs can be previously made to obtain
! the number of orbitals necessary to define the CAS spaces
gprint,orbital,civector ! Print the orbitals and ci coefficients
                        ! to check solutions and find which orbitals
                        ! are mainly Fe(3d) ones
rml=2.45 Angstrom;      ! Necessary to create the input, not
                        used later

ang=90.degree;
died=180.;
zero=0.;
geometry={angstrom;
  fe;          ! Geometry definition (see above and Example 5.4)
  f1,fe,rml;
  f2,fe,rml,f1,ang;
  f3,fe,rml,f1,ang,f2,died;
  f4,fe,rml,f2,ang,f1,died;
  f5,fe,rml,f1,ang,f2,ang;
  f6,fe,rml,f1,ang,f2,-ang}
basis=lanl2dz          ! Basis definition
                        ! Be aware that lanl2dz contains a pseudopotential
                        ! to describe the core electrons so that
                        the atoms

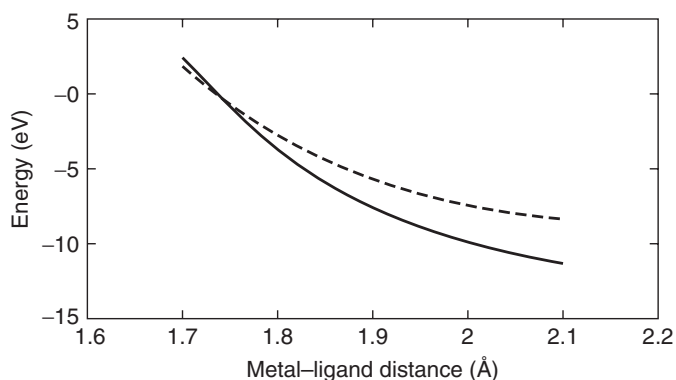
```

```

! do NOT have their nominal number of
! electrons!
do rml=2.1,1.7,-0.05 ! Loop over several metal ligand distances
! starting from 2.1 and finishing at 1.7 Angstrom
! with steps of -0.05 Angstrom
! The negative step allows to avoid
! problems with
! Fe(4s) orbital and memory from previous
! calculations
{rhf; ! A Hartree-Fock calculation required to obtain
wf,74,1,0} ! the initial orbitals. A closed-shell
! configuration
! is usually optimum for this step
pop ! Mulliken population calculation to self-check
{multi; ! CASSCF calculation
occ,13,6,6,3,6,3,3,0; ! All the occupied orbitals including
! closed and
! active space
closed,10,6,6,2,6,2,2,0; ! All the doubly-occupied orbitals
! coming from
! F(2s)+F(2p) orbitals
wf,74,1,0} ! Low spin 1Ag state
pop ! Mulliken population calculation to self-check
{multi; ! CASSCF calculation
occ,13,6,6,3,6,3,3,0; ! All the occupied orbitals including
! closed an
! active space
closed,10,6,6,2,6,2,2,0; ! All the doubly-occupied orbitals coming from
! F(2s)+F(2p) orbitals
wf,74,4,4} ! One state in the triply
! degenerate 5T2g state
pop ! Mulliken population calculation to
! self-check
! The following part of input allows to calculate the other two states
! in the 5T2g degenerate state. Since they have the same energy as the
! other component it is not necessary to perform this calculation
! (although it allows the very important self-check).
!{multi;
!occ,13,6,6,3,6,3,3,0;
!closed,10,6,6,2,6,2,2,0;
!wf,74,6,4}
!rs2
!pop
!{multi;
!occ,13,6,6,3,6,3,3,0;
!closed,10,6,6,2,6,2,2,0;
!wf,74,7,4}
!pop
enddo ! The loop is closed

```

In the following diagram shows the results of CASSCF/lanl2dz energy calculations for the lowest  $^1A_{1g}$  (dashed line) and  $^5T_{2g}$  (solid line) states of the  $\text{FeF}_6^{4-}$  complex as a function of the metal–ligand distance.



We see that the  ${}^5T_{2g}$  state is lower in energy for Fe—F distances exceeding  $\sim 1.75$  Å. The figure thus reproduces the Tanabe–Sugano diagram for  $d^6$  complexes shown in Fig. 4.11e, where for large  $\Delta$  values (with low metal–ligand distances) the low-spin state  ${}^1A_1$  is more stable while at smaller  $\Delta$  values (with larger metal–ligand distances) the high-spin  ${}^5T_{2g}$  term is the ground state. This means that if the  $\text{FeF}_6^{4-}$  complex is compressed to reach the metal–ligand distance around the crossing point ( $R_{\text{ml}} \sim 1.75$  Å), it could, in principle, possess temperature-dependent spin crossover properties (Section 8.4).

Note that the calculation above is not without shortcomings: (1) the solution does not converge to a stable minimum, and this can be attributed to the high charge of the complex, which renders the system unstable in vacuum (such situations should be addressed by correcting the influence of the environment, e.g., the Madelung potential in crystals; this is beyond the scope of this exercise); and (2) depending on how you perform your calculation (the ones shown above are performed correctly), you may observe a nasty energy jump when the metal–ligand distance is  $\sim 1.85$  Å; if you check the Mulliken populations at this point, you will find that there is a large transfer of charge from Fe( $3d$ ) to Fe( $4s$ ) levels. To correctly describe the position of the  $(n+1)s$  levels in transition metals it is necessary to factor in the relativistic  $s$  orbital contraction (Section 6.5).

### Chapter 6

**P6.1.** See Sections 1.2 and 6.1.

**P6.2.** See Section 6.1 and Table 6.2.

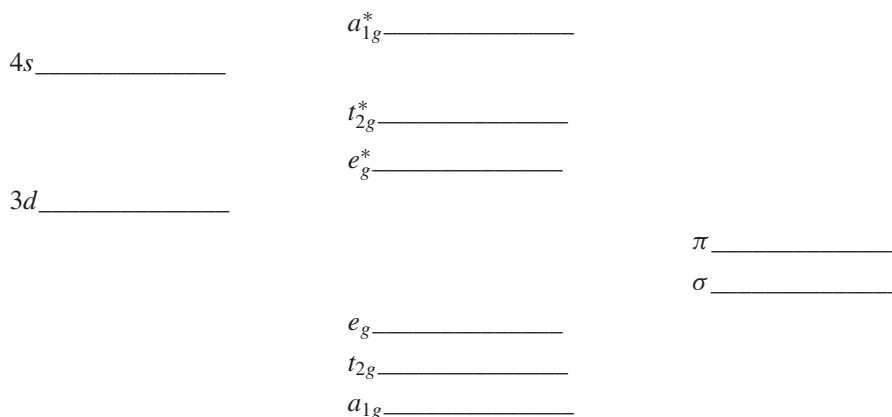
**P6.3.** Answer in Section 6.1.

**P6.4.** From the numerical data in Example 5.1 we find that for this system,  $\text{TiF}_6^{3-}$ ,  $G(4s, \sigma) = \sqrt{6}S(4s, \sigma) = 0.429$ ,  $G(3d, \sigma) = \sqrt{3}S(3d, \sigma) =$



0.312, and  $G(3d, \pi) = 2S(3d, \pi) = 0.202$ , which, indeed, follows the order of magnitude that leads to the most probable MO energy-level scheme in Fig. 6.1 (without the contribution of  $p$  electrons). The calculations in Problem 5.1 of additional MO energy-levels and the total MO energy-level scheme for this complex obtained there follow (qualitatively) the MO scheme in Fig. 6.1. However, in principle, violations of this energy-level scheme are quite possible, especially in coordination systems with different ligands (see also Problem 6.5).

- P6.5.** Lower group overlap integrals  $G$  (and hence reduced group resonance integrals  $H_{ij}^G$ ) result in smaller energy gaps between the corresponding bonding and antibonding MOs. Therefore, the expected MO energy diagram for the inequalities  $G(3d, \sigma) < G(3d, \pi) < G(4s, \sigma)$  is expected to look (qualitatively) as follows:



In this diagram the order of  $e_g$  and  $t_{2g}$  (both bonding and antibonding) is inverted as compared with the usual scheme in Fig. 6.1. This means that, for instance, in octahedral complexes with two electrons donated from each of the six ligands the  $3d^n$  electrons of the CA occupy first the  $e_g^*$  MO, and the remaining  $n-4$  electrons populate the  $t_{2g}^*$  MO, instead of the inverse order in the usual scheme. This leads to essential (some times dramatic) differences in the optical ( $d-d$  spectra), magnetic (low-spin high-spin alternative), and thermodynamic (crystal field extrastabilization) properties of these two types of complexes, described in Chapters 4 and 6.

- P6.6.** Multiorbital bonding occurs when there are more than one bonding MOs that are not compensated by antibonding MOs. The number of such bonding MOs does not necessarily coincide with the multiplicity of the bond (the bond order) in organic compounds because some of the MOs are often degenerate. This difference is significant in the TMS, where the

electronic structure of the metal–ligand bonding is strongly asymmetric, and the charge transfers on different MOs in diorbital or multiorbital bonding may take place in opposite directions involving antibonding states and causing ligand excitation. This effect does not occur in multiple bonds of mostly homogeneous organic and main-group compounds (in the sense of only *sp* electrons involved). Coordination of the CO molecule to transition metals is a simple example. For details, see Section 6.3 and Examples 6.1—6.10.

- P6.7.** The covalence produced by the unpaired electrons as revealed by ESR spectra does not, in general, reflect the covalence of the bonding; the latter is produced by other electrons, namely, by those that occupy the uncompensated bonding MOs (Fig. 6.3), which are different from the MOs of unpaired electrons.
- P6.8.** See Section 6.3, Fig. 6.6, and Problem P8.20.
- P6.9.** In the side-on coordination the H<sub>2</sub> molecule forms diorbital bonding with the metal involving its bonding MO as a  $\sigma$  donor and the antibonding MO as a  $\pi$  acceptor (these two MOs are quite similar to the lowest two  $\sigma$  MOs of N<sub>2</sub> in Fig. 6.8). Since these are the only orbitals participating in the H—H bonding, even small charge transfers  $\Delta q_\sigma$  from its bonding MO to the metal and  $\Delta q_\pi$  from the latter to the antibonding MO strongly activate the H<sub>2</sub> molecule (see Table 11.4), resulting in its homolytic cleavage (11.32) described in Example 11.6.
- P6.10.** According to the N<sub>2</sub> MOs shown in Fig. 6.8, the symmetry of some of these MOs with respect to the line of metal–ligand bonding in the two modes of coordination, linear end-on and side-on, is different. The three most important MOs of N<sub>2</sub> in the bonding to the metal,  $1\pi$ ,  $5\sigma$ , and  $2\pi$ , form, respectively,  $\pi$ ,  $\sigma$ , and  $\pi$  MOs with the metal in the linear end-on coordination, whereas in the side-on coordination the corresponding MOs is  $\sigma$ ,  $\sigma$ , and  $\pi$ . This increases the  $\sigma$ -donor properties of the N<sub>2</sub> molecule, resulting in larger orbital charge transfer to the metal  $\Delta q_\sigma$  and, consequently, larger  $\Delta q_\pi$  values of orbital charge backdonation to the antibonding  $2\pi$  orbital of N<sub>2</sub>, resulting in much stronger activation of the latter. The consequences of this effect are discussed in Section 11.2 and Example 11.4.
- P6.11.** Substitution of the chlorine ligands with more electronegative fluorine ligands makes the Pt atom more electropositive and hence stronger accepting electronic charge  $\Delta q_\sigma$  from the ethylene bonding  $\sigma$  orbital, thus weakening the C—C bond. Larger  $\Delta q_\sigma$  values also increase the  $\Delta q_\pi$  magnitude, which acts in the same direction of weakening this bond. On the contrary, the substitution with less electronegative bromine atoms produces an opposite effect of strengthening the C—C bond. See also Section 11.3.

- P6.12.** Separation in  $\sigma, \pi, \delta, \dots$  orbitals is rigorous with regard to their symmetry properties (quantized projection of the orbital angular momentum, Section 2.1) *with respect to one axis of symmetry* that coincides with the line of bonding. If the molecule has more than one line of bonding, as in coordination systems, the separation of the MOs on symmetry should follow the IrReps of the symmetry group, but the separation in  $\sigma, \pi, \delta, \dots$  MOs still remains valid with respect to the specific lines of bonding taken separately. An MO in coordination systems may have  $\sigma$  symmetry with regard to one of the several lines of metal–ligand bonding and  $\pi$  symmetry with respect to another one; this is termed  $\sigma + \pi$  bonding.
- P6.13.** In the presence of strong relativistic effects (strong spin–orbital interaction) separation of the total momentum into independent orbital and spin moments is invalid, as they are mixed (Section 2.2). Accordingly, the separate quantization of the orbital momentum that leads to  $\sigma, \pi, \delta, \dots$  symmetries is invalid as well, and the orbitals cannot be classified on the basis of these symmetries. Visually, the atomic orbitals lose their purely orbital distribution shown in Section 2.1. As explained in Section 6.5, if two  $p_{1/2}(\frac{1}{2})$  functions from two bonding atoms overlap, they form one-third of  $\sigma$  bonding and two-thirds of  $\pi$  antibonding MOs (Fig. 6.32b), or vice versa for opposite signs: one-third  $\pi$  antibonding and two-thirds  $\sigma$  bonding.
- P6.14.** The essential differences in properties of the three metals Au, Ag, and Cu that have isoelectronic valence shells is due to their different relativistic effects. The main effect is the contraction of the valence  $s$  orbitals (Section 6.5), which renders them less chemically reactive. This effect is very strong in Au, weaker in Ag, and very weak in Cu. The same relativistic effect contributes to their color. For solid Au the refractivity responsible for the color is due to the transition from the  $5d$  band to approximately the Fermi level  $6s$ . Without relativistic contraction this transition falls outside the visible range, thus making the gold expected to be white. Because of the relativistic contraction, this transition becomes  $h\nu = 2.4$  eV, making gold yellow as it is. In Ag the relativistic contraction of the  $5s$  electron is much smaller, and it remains white. The color of Cu has a different origin, the  $d-d$  transition.

### Chapter 7

- P7.1.** The criterion of validity of the adiabatic approximation requires that the electronic state under consideration be nondegenerate and well separated (noninteracting) from other electronic states under nuclear displacements. If this criterion is not fulfilled, the mixing electronic states produce a variety of observable effects, primarily the JTE and RTE in case of degeneracy, and PJTE in case of interacting nondegenerate terms, with all the consequences for observables as described in Chapters 8–11. The non-adiabaticity is seen in many other chemical and spectroscopic effects when

the system jumps from one electronic state (term) to another following their interaction.

- P7.2.** For nondegenerate vibrations the symmetrized (normal) coordinates in Figs. 7.1–7.3 and Table 7.1 are real displacements of the atoms during the vibrations. For degenerate vibration, any linear combination of the components is also a normal vibration with the same frequency, so within such linear combination the real atomic displacements remain uncertain, and only external perturbations or the JTE that split the degenerate vibration (frequency) “fix” the nuclear displacements in the split components.
- P7.3.** See the answer in Section 7.2.
- P7.4.** See examples in Chapter 11: CO, N<sub>2</sub>, NO, C<sub>2</sub>H<sub>4</sub>, and O<sub>2</sub>.
- P7.5.** The one-state distorted configuration is energetically advantageous as it is lower by the amount of JT stabilization energy. In some cases all states of the degenerate term contribute simultaneously to the distortion and JT stabilization (as in the case of the “Mexican hat” of the twofold-degenerate  $E$  term interacting with twofold-degenerate  $e$  nuclear displacements), but this not simply an average of electronic states, as it involves dynamic nuclear distortions, causing the electronic and nuclear motions to become mixed, nonseparable.
- P7.6.** The relatively slow nuclear displacements (as compared with vibrations) along the bottom of the trough of the Mexican hat in the case of strong vibronic coupling (as well as in other similar JT situations where the energy gap to the excited state is relatively large) can be considered in the semiclassical approximation; it will be seen indirectly in a variety of spectroscopic measurements, including ESR (Section 8.4), electron spectroscopy (tunneling splitting of the zero-phonon line, Section 8.1), Mossbauer (Section 8.5), and NMR (Section 9.2) spectroscopy, as well as in direct observation by means of laser femtosecond spectroscopy (Section 9.2).
- P7.7.** The electronic wavefunction for the lowest branch of the APES of the JT  $E \otimes e$  problem (the Mexican hat) is not single-valued, but quantum mechanics requires that the *total* wavefunction as a product of nuclear and electronic wavefunctions be single-valued, not only the electronic wavefunction. To satisfy this condition, a special phase factor (called *topological*, or *Berry phase*) is attached to the nuclear wavefunction in such a way as to compensate for the deficiency of the purely electronic function; the total wavefunction is then single-valued. In the usual case when only one conical intersection is encircled, the additional phase in the phase factor equals  $\pi$ , and the nuclear wavefunction acquires special properties, including a degenerate ground state and half-integer quantum numbers of the vibronic states. When more than one ( $n$ ) conical intersections are encircled, the phase factor equals  $n\pi$ ; the special properties

described above occur only when  $n$  is an odd number. Having initially emerged in the JT problem, the Berry phase theory was later extended to a variety of other physical effects.

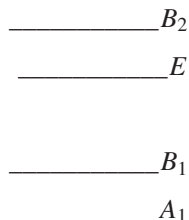
- P7.8.** The term *high-symmetry configuration* in the formulation of the PJTE is employed in the sense that at this point of configuration the first derivative of the APES of the system in the direction of nuclear displacements under consideration is zero, meaning this point is a maximum or minimum (the Coulomb forces are equilibrated). Any configuration of pure ions is not force-equilibrated, and hence its distortion is unrelated to the PJTE. Any system with a PJTE may be used to illustrate this statement.
- P7.9.** Chemical transformations via transition states (a maximum or a saddle point of the APES) may serve as an example of the minimum-two-level paradigm involved [two electronic states in transformation (TEST) paradigm, Section 7.4]. The scheme of such transformation can be seen in Figs. 11.7 and 11.10 of Section 11.2. The difficulty in finding specific illustrative examples is due to the lack of calculations of excited states at the point of instability of the ground (transition) state that produce the instability of the latter. But in all the cases when excited states are revealed, the TEST paradigm is confirmed.
- P7.10.** The two states with different spin are orthogonal in the Russell–Saunders scheme of term separation (Section 2.2), but they become nonorthogonal when the spin–orbital interaction is taken into account. Therefore, there are spontaneous thermal transitions between these two states, and this thermal relaxation of the higher energy state to the lower one at room temperatures is often the main obstacle to the direct use of such systems in electronics. The relaxation rate for  $\text{CuF}_3$  has not been calculated as yet.

### Chapter 8

- P8.1.** From Eqs. (8.12), (8.14), (8.16), and (8.17) we find the following values for  $\text{K}_2\text{NaCrF}_6$ :  $\omega = (\delta\Omega)^2/[4 \ln 2)(\Omega_1 - \Omega_2)] \cong 832 \text{ cm}^{-1}$ ,  $a = (\Omega_1 - \Omega_2)/\omega \cong 4.1$ , and  $\Omega_0 = (\Omega_1 + \Omega_2)/2 = 21,600 \text{ cm}^{-1}$ .
- P8.2.** See Section 8.1.
- P8.3.** The answer to this question is given in Section 8.2.
- P8.4.** See Section 8.1.
- P8.5.** See Section 8.1.
- P8.6.** The approximate correlation between the two series, spectrochemical and nephelauxetic, is not accidental. The  $d$ -level splitting magnitude  $\Delta$ , attributed in CFT to the interaction with ligand charges or dipoles, is in fact directly dependent on the covalence of the metal–ligand bonding

(Section 6.2). This explains the origin of the experimentally observed approximate synchronism in the changes of the parameters in both series.

**P8.7.** According to Section 4.2, Fig. 4.5, the  $d$ -level splitting in a tetragonally compressed tetrahedral field is as follows (the scheme in Fig. 8.21 illustrates a tetragonally elongated tetrahedral field):



From the ground state  $A_1$ , the following  $d-d$  transition can be expected:  $A_1 \rightarrow B_1$ ,  $A_1 \rightarrow E$ , and  $A_1 \rightarrow B_2$ . Using the group-theoretical selection rules (Section 3.4) and Table A1.7 for the characters of the  $D_{2d}$  group we find that the  $z$  component of the electric dipole moment (as of any vector) belongs to the  $B_2$  IrRep of this group, while the  $x$  and  $y$  components belong to the IrRep  $E$ . Then, by evaluating direct products of IrReps (Table A1.14), we find

$$\begin{aligned}
 A_1 \times B_1 \times B_2 &= A_2 \\
 A_1 \times B_1 \times E &= E \\
 A_1 \times E \times B_2 &= E \\
 A_1 \times E \times E &= A_1 + A_2 + B_1 + B_2 \\
 A_1 \times B_2 \times B_2 &= A_1 \\
 A_1 \times B_2 \times E &= E
 \end{aligned}$$

Only two of these products contain the totally symmetric IrRep  $A_1$ , and hence their corresponding transitions are allowed: the  $A_1 \rightarrow B_2$  transition with the highest frequency ( $\sim 12,000 \text{ cm}^{-1}$ ) allowed in the  $z$  polarization of incident light, and the  $A_1 \rightarrow E$  ( $\sim 9000$ ) transition for light polarized in the  $xy$  plane. The  $A_1 \rightarrow B_1$  transition is forbidden in the electric-dipolar approximation.

**P8.8.** For the system  $\text{CuF}_3$  with  $D_{3h}$  symmetry, the vibrational representation, according to Eqs. (3.54)–(3.56), is (cf. Example 3.5)

$G$	$E$	$\sigma_h$	$C_3$	$S_3$	$C_2$	$\sigma_v$
$X(G)$	6	4	0	-2	0	2

Decomposing this reducible representation into IrReps of the  $D_{3h}$  group (Table A1.5) by means of Eq. (3.33) or by direct examination, we find that its components are  $2E' + A_1' + A_2''$ . Thus the  $\text{CuF}_3$  molecule has two double-degenerate  $e'$ , one  $a_1'$ , and one  $a_2''$  vibrations, a total of  $3 \times 4 - 6 = 6$  symmetrized (concerted) vibrations. Table A1.5 also shows that the  $a_1'$  vibration can be seen only in the Raman spectra in different polarizations, the  $a_2''$  vibrations will be manifest in the infrared in  $z$  polarization, while the  $e'$  vibrations can be seen in both infrared and Raman spectra in  $xy$  polarization.

For tetrahedral  $\text{CoCl}_4^{2-}$  a similar analysis employing the table of characters A1.10 for  $T_d$  symmetry yields the following vibrational representation:

$G$	$E$	$C_3$	$C_2$	$S_4$	$\sigma_d$
$X(G)$	9	0	1	-1	3

By decomposing this reducible representation in IrReps of the  $T_d$  group, we find that it contains  $2T_2 + E + A_1$ . This means that in  $\text{CoCl}_4^{2-}$  the nine vibrations are two  $t_2$ , one  $e$ , and one  $a_1$ . Table A1.10 also shows that the  $t_2$  vibrations will be seen in both infrared and Raman spectra in any polarization, while the  $a_1$  vibrations will be manifest in Raman spectra only.

The possible vibrations of the  $\text{UF}_6$  molecule with  $O_h$  symmetry are given in Problem 3.8. According to Table A1.11, only  $t_{1u}$  vibrations can be seen in infrared spectra in any polarization, while  $a_{1g}$  and  $t_{2g}$  vibrations will be seen in Raman spectra.

For the vibrational representation  $X(G)$  of the 21 vibrations of  $\text{OsF}_8$  in  $O_h$  symmetry with the Os atom in the center of a regular cube and fluorine atoms at its apices, we have

$G$	$E$	$C_3$	$C_2$	$C_4$	$C_2'$	$I$	$S_6$	$\sigma_h$	$S_4$	$\sigma_d$
$X(G)$	21	6	1	-1	1	-3	0	1	-1	5

Its decomposition in IrReps yields  $X(G) = A_{1g} + A_{2u} + E_g + E_u + 2T_{1u} + 2T_{2g} + T_{2u}$ . With these values, according to Table A1.11, only the  $T_{1u}$  vibrations are active in the IR spectra in any polarization, while the  $A_{1g}$  and  $T_{2g}$  frequencies will be seen only in the shifts of Raman spectra.

- P8.9.** Raman spectra can be obtained, in principle, with any frequency of incident light larger than the frequency of the vibrations, whereas resonance Raman scattering takes place only when the frequency of the incident light is in resonance with one of the electronic transitions in the system. Since the selection rules for Raman shifts are those of a tensor, while dipolar IR spectra are induced by a vector perturbation, vibrations can be

seen in both types of spectra only if they belong to an IrRep of the symmetry group to which both vector and tensor transformations belong. In particular, this does not take place in the presence of an inversion center, so for such systems the same vibrational mode cannot be seen in both types of spectra. For Stokes and anti-Stokes intensities, see Eq. (8.30).

- P8.10.** With the data given for the system  $\text{VF}_3$ , we calculate (Section 8.2)  $X_A = F_A^2 \coth(\omega_A/2kT) = 0.290$  and  $X_E = F_E^2 \coth(\omega_E/2kT) = 0.637$ ; hence  $X_A < X_E$ , and the  $A \rightarrow E$  optical absorption band is expected to be two-humped (split by the JTE). With increasing temperature,  $\coth(\omega/2kT) \rightarrow 0$  as  $(\omega/2kT) \rightarrow 0$ , and since  $\omega_E > \omega_A$  and  $F_E > F_A$ ,  $X_E > X_A$  at any given temperature.
- P8.11.** The peaks of photoelectron spectra do not necessarily coincide with the calculated energy levels of the system because of electron relaxation, shakeup and shakeoff satellites, and configuration interaction; see Section 8.3 for details.
- P8.12.** In TMS the chemical shift in photoelectron spectra depends not so much on the change of the effective (total) atomic charges on the atom as on the changes in orbital populations by bonding. Indeed, the influence of  $d$  electrons on the shift of inner energy levels may be opposite to that of  $sp$  electrons. Therefore, the change in the total charge by bonding may be small when the absolute values of orbital charge transfers in opposite directions are large (Section 6.3, Fig. 6.6). Hence the shift of the inner levels may be very large when total charge transfers are small.
- P8.13.** In the definition  $\boldsymbol{\mu} = \beta(\mathbf{L} + 2\mathbf{S})$ , all three magnitudes  $\boldsymbol{\mu}$ ,  $\mathbf{L}$ , and  $\mathbf{S}$  are vectors and operators for which observables are their quantum-mechanical averages, and  $\mathbf{L} + \mathbf{S} = \mathbf{J}$ . For the projection of  $\boldsymbol{\mu}$  on  $\mathbf{J}$ , we have  $\mu_J = \beta \times [J + S \cos(\mathbf{J}, \mathbf{S})]$ . On the other hand, following the cosine rule of a triangle with the sides  $\mathbf{L}$ ,  $\mathbf{S}$ , and  $\mathbf{J}$ , we find that  $\cos(\mathbf{J}, \mathbf{S}) = (J^2 + S^2 - L^2)/2JS$ . Hence we can write  $\mu_J = \beta J[1 + (J^2 + S^2 - L^2)/2J^2]$ . In this equation the quantities  $J$ ,  $S$ , and  $L$  are operators. To find observable  $\mu$  values, we should average the latter using quantum-mechanical averages  $\langle M^2 \rangle = M(M+1)$ . Finally we get  $\mu_J = g\beta[J(J+1)]^{1/2}$ , where  $g = 1 + [J(J+1) + S(S+1) - L(L+1)]/2J(J+1)$ .
- P8.14.** The orbital magnetic moment of the CA in coordination systems may be partially or fully quenched by the ligand field, which, by splitting the energy term, fixes the orbital orientation thus restricting its ability to follow external magnetic perturbations (see more details in Section 8.4). The orbital moment in cubic groups belongs to  $T_1$  IrRep, and it is shown that the magnetic moment is quenched in all TMSs where there are no  $T_1$  representations of their symmetry groups. The orbital contribution to the magnetic properties become temperature-dependent when the ligand field splitting of the orbital levels is not very large and the excited



states become significantly thermally populated, thus partially restoring the orbital freedom to follow external fields.

- P8.15.** In the formulas in Table 8.9 the molar susceptibility in two directions,  $n, l$ , is presented as a product  $\chi_{\text{mol},n,l} = C_{n,l}\chi_{n,l}$ , where  $C_{n,l} = N_A\mu_0(g_{n,l})^2\beta^2/kT$  and  $\chi_{n,l}$  is the spin (and temperature)-dependent factor. For high-spin  $[\text{Fe}(\text{urea})_6]\text{Cl}_3$  the spin of the iron atom is  $S = \frac{5}{2}$ , and for the given values of axial splitting  $D = 0.130 \text{ cm}^{-1}$  and  $g_n = g_l = 2.002$  we can calculate its susceptibilities for the two temperatures as follows:

$C_{n,l}(298 \text{ K}) = [6.022 \times 10^{23} \times 4\pi \times 10^{-7} \times (2.002)^2 (9.274 \times 10^{-24})^2 / (1.381 \times 10^{-23} \times 298.15) \text{ m}^3 \text{ mol}^{-1}] = 6.341 \times 10^{-8} \text{ m}^3 \text{ mol}^{-1}$ ; similarly,  $C_{n,l}(20 \text{ K}) = 94.53 \times 10^{-8} \text{ m}^3 \text{ mol}^{-1}$ . The quantity of  $x = D/kT$  should be dimensionless. The corresponding units are:  $D/kT = D(\text{cm}^{-1}) \times hc(\text{J cm})/[k(\text{JK}^{-1})T(\text{K})]$ . This yields for  $T = 298 \text{ K}$ ,  $x(298) = 0.130 \text{ cm}^{-1}/207.23 \text{ cm}^{-1} = 5.79 \times 10^{-4}$  and for  $T = 20 \text{ K}$ ,  $x(20 \text{ K}) = 8.63 \times 10^{-3}$

With these  $x$  values and the expressions  $\chi_n$  and  $\chi_l$  in Table 8.9 for the spin  $S = \frac{5}{2}$ , we obtain (for small  $x$ ,  $e^{-2x} \cong 1 - 2x$ ):  $\chi_l(298 \text{ K}) = 1.249$ ,  $\chi_l(20 \text{ K}) = 2.863$ ,  $\chi_n(298 \text{ K}) = 3.589$ , and  $\chi_n(20 \text{ K}) = 3.668$ . Finally, we obtain

$$X_{\text{mol},l}(298 \text{ K}) = 6.341 \times 10^{-8} \text{ m}^3/\text{mol} \times 1.249 = 7.920 \times 10^{-8} \text{ m}^3/\text{mol}$$

$$X_{\text{mol},l}(20 \text{ K}) = 94.53 \times 10^{-8} \text{ m}^3/\text{mol} \times 2.863 = 270.64 \times 10^{-8} \text{ m}^3/\text{mol}$$

$$X_{\text{mol},n}(298 \text{ K}) = 6.341 \times 10^{-8} \text{ m}^3/\text{mol} \times 3.589 = 22.76 \times 10^{-8} \text{ m}^3/\text{mol}$$

$$X_{\text{mol},l}(20 \text{ K}) = 94.53 \times 10^{-8} \text{ m}^3/\text{mol} \times 3.668 = 346.53 \times 10^{-8} \text{ m}^3/\text{mol}$$

We see that both the temperature dependence and anisotropy of the magnetic susceptibility in this TMS are very strong despite of the small axial splitting  $D$  of the energy levels.

- P8.16.** See Section 8.4; in the absence of purely orbital contribution, spin-orbital interaction and covalence contribute to the values of the  $g$  factors by admixing excited states. The covalence factor retrieved from the ESR spectra characterizes the MOs occupied by the unpaired electrons that contribute to the  $g$  factor, whereas the covalence of the bonding is realized by the inner occupied MOs that are not compensated by their corresponding antibonding MOs (Section 6.2).
- P8.17.** In the MO LCAO approach the coupling is clearly contained in the electronic structure, the MO distributions, and their occupancy. In the semiempirical calculations of the binuclear copper(II) acetate hydrate  $[\text{Cu}(\text{OAc})_2\text{H}_2\text{O}]_2$  the direct Cu—Cu  $d-d$  overlap is weak, yielding small splitting between the corresponding bonding and antibonding MO levels with the result that they are both occupied by electron, and hence do

not contribute considerably to the bonding. The latter is produced by the uncompensated bonding MOs that are formed via the overlaps of the Cu atoms with the commonly shared ligands.

- P8.18.** While ferromagnetic (direct and indirect) interaction between atomic centers depends on the Coulomb integrals (Coulomb interaction between their electronic clouds) and hence takes place in any geometric arrangement of their orbitals, the antiferromagnetic interaction is strongly dependent on the square of the overlap between the latter  $S_{AB}^2$ . Therefore the possibility of antiferromagnetic interaction is limited to special orientation of the “magnetic orbitals,” thus depending on the geometry of the indirect interacting centers, and it is sensitive to their small structural changes.
- P8.19.** See Section 8.5. The main effect of electronic structure in GRS is seen in its chemical shift, quadrupole splitting, and magnetic hyperfine splitting. The chemical shift is due to the electronic charge on the nuclei produced by the  $s$  electrons (and  $p_{1/2}$  electrons in the case of strong relativistic effects), while the quadrupole splitting is created by the population of MOs containing  $d$  and  $f$  electrons. Significant temperature dependence is seen mostly in the magnetic hyperfine structure, and this is due to thermal relaxations between the components of the nuclear energy levels split by interaction with the electronic cloud (Example 8.13 serves as an illustration).
- P8.20.** See full answer in Section 8.4. The measured or calculated total electronic density distribution in TMS does not reflect well the redistribution of charge by bonding because of possible opposite directions of orbital charge transfers in case of multiorbital bonds (Section 6.3; see also Problem 8.12). These mutually compensating charges are accompanied by ligand excitation (Fig. 6.6); neither the former nor the latter are seen in  $DD$ . Another important point is the way the  $DD$  are calculated. The assumption of spherical symmetric charge distribution in free atoms with open shells is valid only when the atom is free, indeed, but introduced in the crystal it becomes immediately nonspherical symmetric (*before* the bonding redistribution) because it acquires zero-order field-oriented distribution (zero-order wavefunction of perturbation theory). This essentially influences the determination of the  $DD$  as a difference between the measured total density and the assumed atomic density before bonding.

## Chapter 9

**P9.1.** See Section 9.1.

**P9.2.** The concept of directed valences is based on the assumption that *localized* bonds between the atoms are formed by hybridization of close-in-energy atomic orbitals, whereas the main feature of electronic structure of TMS is the formation of three-dimensionally delocalized bonds formed due to

the participation of  $d$  electrons. The differences in properties produced by this difference in electronic structure are indicated in Table 6.1.

- P9.3.** The VSEPR model assumes that the lone pair of electrons of the CA is repulsive and distorts the otherwise symmetric arrangements of the ligands, but it cannot explain rigorously why not all lone pairs produce distortions. A qualitative explanation is given in the model where it is assumed that in the symmetric configuration the lone pair occupies an antibonding MO, whereas in the distorted configuration it is nonbonding. Therefore only strong antibonding lone pairs produce distortions. A rigorous treatment of the problem is given based on the vibronic coupling theory, the pseudo-JTE (Section 9.2).
- P9.4.** The “inert-gas rule” in stereochemistry is based on the assumption that the ligands form a spherical-symmetric charge distribution which can be described by means of spherical functions and follow the same rules of stable atomic closed shells; this leads to the magic numbers of most stable systems with 8, 18, 32, . . . , valence electrons. With 8 electrons the model predicts four 2-electron bonds, 18 electrons form nine bonds, and so on. For instance, if in the 18-electron case there are less than nine ligands, the complementary spherical electron density model assumes that the two electrons of the missing bond can be provided by an appropriate occupied nonbonding atomic orbital with required symmetry; this is the “generalized inert-gas rule.” These inert-gas rules are very approximate; they can serve only for orientation and some preliminary qualitative estimates.
- P9.5.** The MO population analysis in Example 9.3 shows electronic configurations that have relatively close energy states, which interact under nuclear displacements of given symmetry and may, in principle, make the system unstable with regard to these displacements, but it does not indicate when the distortions actually take place. To do this, one has to involve the PJTE, which states that for the distortions to take place, the inequality (7.67) should be valid; to check this, one needs to evaluate the energy gap  $\Delta$  between the interacting states, the vibronic coupling constant  $F$ , and the primary force constant  $K_0$ .
- P9.6.** The vibronic theory of lone-pair influence on stereochemistry reveals the condition of instability of the TMS, which, in addition to the general criterion of the PJTE ( $f > 1$ ), differentiates the possible distortions on their symmetries. The parameters that are needed to estimate the possible instabilities are indicated in the inequalities (9.11)–(9.14), with the denotations in Eq. (9.9). They can be obtained mostly by calculations; the energy gap  $\Delta$  can be obtained from spectroscopic data.
- P9.7.** In TMS with a degenerate electronic state the pseudorotation always goes around (sidesteps) the point of highest symmetry (the point of degeneracy), whereas in the Berry case the pseudorotation proceeds via the

high-symmetry transition state, which is a maximum of the APES in the direction of the nuclear displacements; Berry pseudorotations are thus a consequence of the PJTE. In the JT case such pseudorotations are forbidden by symmetry. On the other hand, some pseudorotations sidestepping the point of highest symmetry are also possible in the case of PJTE. The differences between the two types of pseudorotation are seen in NMR spectra of systems with ligands marked by isotope substitutions (Section 9.2).

- P9.8.** The theory of mutual influence of ligands including *cis* and *trans* influences, is presented in Section 9.3 with many examples in Tables 9.8–9.10, and are discussed further together with the *trans* effect in Section 11.3 with Fig. 11.11.
- P9.9.** The plasticity effect in TMS is based on the model of a “soft coordination sphere” around the transition metal formed as a result of the JTE or PJTE, due to which the APES has a continuum of minima, a trough, or several minima with very low barriers between them, so the ligand configuration easily changes under the influence of the environment. Transition metals in double-degenerate *E* states in octahedral and tetrahedral environments are most appropriate for manifesting this effect, but there may be many other metals that obey the conditions of plasticity. Ample examples are provided in Tables 9.14–9.17, and in the literature, data can be obtained from the *Science Citation Index* by searching for papers that cite the original publications on the plasticity effect [9.25].
- P9.10.** The driving force of structural displacive phase transitions in crystals with JT centers is the local JTE, while in dielectric crystals with fully occupied conduction bands the phase transition is triggered by the local distortions produced by the PJTE. Ferroelectric phase transitions take place when the local PJT distortions produce a dipole moment (as, e.g., in BaTiO<sub>3</sub>). For a full answer to this question, see the discussion in Section 7.4 and/or Section 8.3 of Ref. 9.23.

### Chapter 10

- P10.1.** See Section 10.1
- P10.2.** The ability of the system to accept additional electronic charge from a donor depends on the position of its LUMO (which can accept electrons) with respect to the HOMO of the donor, and on how rapidly the LUMO energy increases with its population, the redox capacitance *C*. The latter, roughly speaking, decreases with the increase of the HOMO-LUMO energy gap of the system. The best charge-accepting systems are those with several (many) close energy levels that include both the HOMO and LUMO, such as conjugated systems (see Example 10.1). They may be also good donors of charge. In the same approximation as above, the

redox capacitance of the system as a donor decreases with the HOMO-SOMO energy gap (SOMO denotes the second lower in energy MO), so it may differ from that as an acceptor.

**P10.3.** The redox capacitance of the system, following Eq. (10.4), is  $C_1 = (dq/d\varepsilon)_0 = 1e/(80.2\text{ kK})$  ( $1\text{ kK} = 10^3\text{ cm}^{-1}$ )  $= 0.012e\text{ (kK)}^{-1}$ , the redox capacitance of iron porphyrin in Example 10.1 is  $C_2 = 0.6e\text{ (kK)}^{-1}$ . Hence  $C_2 \gg C_1$ , and using Eq. (10.11) and the value of the energy gap  $\varepsilon_1^u - \varepsilon_2^0 = 45\text{ kK}$  we find for the charge transfer:  $\Delta q = C_1(\varepsilon_1^u - \varepsilon_2^0) = 0.56e$ .

**P10.4.** See Section 10.2.

**P10.5.** Coexistence of two molecular configurations occurs when the APES of the system has two minima of same or close energies, but with an energy barrier between them that distinguishes them physically. This means that the system may be found in either one of the minima or averaged over both of them, dependent on the barrier height and the means of observation (see Section 9.1). In principle, the two configurations can be observed with many spectroscopic methods, but the most impressive so far was GRS ( $\gamma$ -resonance spectroscopy, Section 8.5), which shows a superposition of two spectra, one with the localized electron and the other with the delocalized electron (Section 10.2).

**P10.6.** Adding or removing charge from a system may trigger a change in its nuclear configuration, its conformation, if there are two or more electronic states involved and the electron–vibrational (vibronic) coupling is sufficiently strong to satisfy the condition of instability (see the TEST paradigm in Section 7.4), and if this condition was not in place without the added charge. Equation (7.67) shows that in addition to strong vibronic coupling  $F$ , the condition of instability requires small energy gaps to excited states  $\Delta$  and small primary force constants  $K_0$ . The latter two conditions are satisfied in many biological systems. Because of their organic large size, biological systems are “soft” (have small  $K_0$  values) with regard to conformational changes, and in the presence of transition metal active centers (as, e.g., in metalloenzymes) or organic conjugated systems as prosthetic groups, they have also open shells with small  $\Delta$  values. Examples are given in Section 10.3.

**P10.7.** See answer in Sections 10.3 and 9.2.

**P10.8.** See answer in Section 10.3.

## Chapter 11

**P11.1.** See Section 11.1.

- P11.2.** The stable excited states that produce the instability of the ground transition state of chemical reactions can (in principle) be observed spectroscopically similar to any other excited state, although there may be experimental difficulties in recording the spectra because of the instability of the ground state in this configuration. There should be no insurmountable difficulties in allocating these states by means of femtosecond spectroscopy (attempts to do this are unknown to us). However, the presence of such stable excited states (known as *resonances*) is well recorded in collision experiments.
- P11.3.** Orbital symmetry rules emerge from the overlap of the orbitals of the two interacting molecular systems, and hence these rules are not effective in charge-controlled reactions. For the same reason charge-controlled reactions are not stereoselective, and this is one of the features that distinguish them from orbital controlled reactions. The two limit reactions and their intermediates can be predicted by calculation of the electronic structure of the reactants (Section 11.3) and/or qualitatively by inspection of their HOMO-LUMO and estimating their overlap.
- P11.4.** The electronic features of TMS that facilitate their catalytic properties are due mainly to their ability to form multiorbital bonds with the ligands, which, because of the compensating orbital charge transfers, may produce strong ligand activation without “thermodynamic cost” (i.e., without thermodynamically unfavorable total charge redistribution). Generally, there is no such effect in absence of the strong heterogeneity introduced by *d* electrons. Another important feature of TMS that makes them good catalysts is that by coordinating several molecular groups as ligands, the CA “brings them together,” facilitating their interaction at short distances. Examples are given in Section 11.3.
- P11.5.** Following Eq. (11.19) or (11.20), to estimate the reduction of the activation energy  $-\Delta D$  of reactions with a coordinated molecule, we need to know how the force constant  $K_0$ , interatomic distances, and anharmonicity coefficient of the latter changes by coordination. These changes are expressed approximately by empirical parameters; in Eqs. (11.22) and (11.23) they are presented as functions of HOMO and LUMO orbital charge transfers and orbital vibronic constants (Section 7.2). The latter can be determined from empirical, mostly spectroscopic, data. Conversely, by revealing the changes in vibrational frequencies and interatomic distances of the molecule due to its coordination, one can estimate the charge transfers.
- P11.6.** While the two molecules,  $N_2$  and CO, have the same number of electrons, their electronic structure is different. According to their MO diagrams in Figs. 6.8 and 6.10 and estimation of their orbital vibronic constants in Section 7.2, Fig. 7.4, the HOMO  $5\sigma$  of  $N_2$  is bonding and its LUMO  $2\pi$  is antibonding, whereas in CO the HOMO  $5\sigma$  is weakly

antibonding and the LUMO  $2\pi$  is strongly antibonding. Therefore the orbital charge transfers from and to these two molecules by coordination produce different effects described in detail in Examples 11.2–11.4.

- P11.7.** The activation of the CO molecule in these carbonyls is due to the combined effect of the electron donation from its HOMO  $5\sigma$  and back-donation from the metal to its LUMO  $2\pi$ , both strongly dependent on the metal donor and acceptor properties in this coordination. Therefore a full answer to the question of why the activation of CO is the largest in  $\text{Mn}(\text{CO})_5$  in Fig. 11.9 can be given only after calculation of orbital charge transfers. However, since the only difference in the three carbonyls,  $\text{Fe}(\text{CO})_5$ ,  $\text{V}(\text{CO})_5$ , and  $\text{Mn}(\text{CO})_5$ , is in their  $d$ -electron population ( $3d^64s^2$ ,  $3d^34s^2$ , and  $3d^54s^2$ , respectively), we can assume that the electron-rich Mn complex has better  $\pi$ -donor properties, thus more strongly activating the CO molecule by populating its strongly antibonding LUMO  $2\pi$  (in  $\text{Fe}(\text{CO})_5$  the low-spin configuration  $3d^6$  forms a more stable closed shell).
- P11.8.** From the paper in Ref. 11.17b, we obtain the following parameters for CN coordinated to Fe(III):

MOs	$f_i$	$k_i$	$\gamma_i$	$\Delta q_i$
$4\sigma^*$	-0.397	-3.255	5.758	-0.13
$5\sigma$	0.018	0.649	0.969	-0.49
$1\pi$	0.671	8.136	-2.314	-0.06
$2\pi^*$	0.896	-1.861	5.152	0.14

With these parameters Eq. (11.22') yields

$$F = 0.128 \times 10^{-3} \text{ dyn}$$

$$\Delta K = -0.644 \times 10^{-3} \text{ dyn/\AA}$$

$$\Delta\gamma = -0.36 \times 10^{-3} \text{ dyn/\AA}^2$$

With the value  $K = 16.21 \times 10^{-3} \text{ dyn/\AA}$  from Ref. 11.17b, we have  $K_0 = K - \Delta K = 16.854 \times 10^{-3} \text{ dyn/\AA}$ , and with the formula  $\gamma_0 = (K_0/\hbar\omega)(4K_0\hbar\omega x_e/15)^{1/2}$  and anharmonicity correction  $\hbar\omega x_e = 13.087 \text{ cm}^{-1}$  (adjusting for units), we obtain  $\gamma_0 = 14.020 \times 10^{-3} \text{ dyn/\AA}^2$ . Substituting all these numbers into Eq. (11.24'), we obtain the final formula,  $D = 0.834D_0 - 0.917D_0^{1/2}$ , where  $D_0$  is given in kcal/mol (for other units of energy the coefficient at  $D_0^{1/2}$  changes).

- P11.9.** For a reaction of the free CN molecule, such as  $\text{CN} + \text{X}_2 \rightarrow \text{CX} + \text{NX}$ , for which the activation energy is  $D_0 = 100$  kcal/mol, its coordination to Fe(III), according to the semiempirical relation obtained in Problem 11.8, lowers the activation energy to  $D = 83.4 - 9.17 = 74.2$  kcal/mol. Hence  $-\Delta D = D_0 - D = 25.8$  kcal/mol.
- P11.10.** Using the approximate Eq. (11.33) for the JT-induced chemical activation (which includes linear vibronic coupling only), we find that for reactions that proceed in the direction of JT instability with the activation energy  $D_0 = 50$  kcal/mol, and with the JT stabilization energy  $E_{\text{JT}} = 0.5$  eV = 11.53 kcal/mol, the reduction of the activation energy due to the JTE,  $-\Delta D = D_0 - D = 37.06$  kcal/mol<sup>-1</sup>. A more accurate estimation of  $-\Delta D$  can be obtained by including the quadratic coupling terms.



# SUBJECT INDEX

- Activated complex, 624  
Activated state, 624  
Activation by coordination, 639, 741, 742  
Activation energy, 624, 656  
Adiabatic approximation, 15, 175, 325, 730  
    criterion, 327  
    full, 328  
    simple (Born–Oppenheimer), 327  
Adiabatic potential energy surface (APES), 7, 327  
    in Jahn–Teller problems, *see* JT problems  
Amplification rule, *see* Jahn–Teller distortions  
Angular overlap model, 151  
Anharmonicity  
    corrections, 638, 742  
    vibronic, 335  
Antiferrodistortive interactions (ordering), 567  
Antiferromagnetic interaction (ordering), 444, 457  
Arrhenius reaction rate, 624  
Atomic  
    charge effective, 23, 146, 437  
    functions, 19  
    relativistic, 32  
    Slater type, 22  
    orbital (AO), 19  
    hybridized, 24  
    state, 18  
    one-electron, 19  
    multielectron, 36  
    term, 36  
Auger electron spectroscopy, 422  
Basis set, 24, 157  
    contracted, 159  
    correlation consistent, 160  
    double-zeta, 158  
    extended, 158  
    Gaussian, 158  
    Huzinaga, 159  
    minimal, 158  
    Pople, 159  
    superposition error, 161  
    valence, 158  
Berry pseudorotation, *see* Pseudorotation  
Bispinor, 31, 168, 185  
Bohr magneton, 29, 380  
Bond order, 145  
Bonding  
    coordination, 11, 241  
    diorbital, 257, 261  
    metal–metal, 279

- monoorbital, 257, 259, 728
- multicenter, 273
- multiorbital, 257, 741
- valence, 10
- $\sigma$ ,  $\pi$ ,  $\delta$ , ..., 25
- $\sigma + \pi$ , 27, 269
- Bridging ligand, 279
- Broken symmetry effect, 568
- Charge
  - capacitance, *see* Redox capacitance
  - distribution, 133
  - effective, 22, 144, 434
  - transfer, 144
    - intramolecular, 579
    - mutual compensation, 213
    - orbital, 144, 258, 640
    - spectra, 416
- Charge-controlled reactions, 571
- Chemical activation of
  - carbon monoxide, 642, 646
  - cyan, 742, 743
  - dinitrogen, 646, 729
  - dioxygen, 650
  - double bond, 663
  - hydrogen, 649, 729
  - JT induced, 652
  - nitrogen monoxide, 648
- Chemical bond. *See also* Bonding
  - classification, 11, 238
    - genealogical, 239
  - conjugated (orbital), 11, 240
  - coordination, 11, 241
  - definition, 7, 15
  - donor-acceptor, 11, 241
  - in nontransition elements, 245
  - valence, 10, 239
- Chemical hardness (softness), 588
- Chemical potential, 588
- Chemical reaction
  - carbonyl insertion, 666
  - charge-controlled, 629
  - CO reductive hydrogenation, 666
  - energy barrier, 656
  - ligand coupling and cleavage, 662
  - olefin insertion, 674
  - orbital-controlled, 630
  - photochemical, 682
  - rate, 624
  - stereoselective, 630
  - substitution, 656
  - symmetry rules, 630
  - trans*-effect, 657
  - Ziegler–Natta polymerization, 677
- Chemical reactivity, 623
- Chemical shift, *see* Photoelectron spectra
- cis*-effect, 544
- Clebsh–Gordan coefficients, 73, 93, 187
- Computer
  - experiment, 6
  - programs, 165
- Configuration interaction (CI), 44, 108, 162
  - CI satellites, 434
  - multireference (MRCI), 163
  - s*-configuration interaction, 455
- Coordinates
  - normal, 328
  - symmetrized, 335, 731
- Coordination bond. *See also* Chemical bond
  - definition, 9, 241
  - features, 243
- Coordination compound (system)
  - definition, 10, 241
  - of posttransition elements, 245
  - of pretransition elements, 245
  - mixed-valence, 591
- Coordination theory, 10
- Correlation effects, *see* Electron correlation effects
- Coulomb integral, 45, 134
- Coupled-cluster approximation, 163
- Covalence
  - electrons, 251
  - in ESR, 452
  - in JT distortions, 452
  - weak, 149, 717
- Creutz–Taube ion, *see* Mixed-valence compounds
- Crossover phenomenon, *see* Spin-crossover
- Crystal field
  - extrastabilization, 124, 712
  - icosahedral, 696, 714
  - parameter, 121
  - theory, 84
- Curie law, 448
- d* electron heterogeneity, 149, 175, 211
- Deformation density (DD), 143, 484, 737
  - DD modelling, 490
  - fragment DD, 488
- Density functional theory (DFT), 171, 718, 722
  - time-domain DFT (TD DFT), 177
- Density matrix, 145
- Diamagnetism, 445
- Dichroism (polychroism), 468
  - circular, 468
  - magnetic circular, 468
- Dipolar instability, 376
- Dirac equation, 28, 168

- Doppler effect, 474  
Double exchange, 597  
Dushinsky effect, *see* Optical spectra  
 $\delta$ -function,  $\delta$ -symbol, 47, 58
- Effective charge, 22, 144, 434  
Electron affinity, 580  
Electron-conformational effects, 609  
Electron correlation effects, 115, 157, 161  
Electron potentials, *see* Standard electron potentials  
Electron transfer  
  intermolecular, 579  
  outer-sphere, 583  
  probability (in MV compounds), 600  
  reactions, 580  
Electron spin resonance (ESR) spectra, 449  
  angular dependence, 453  
  covalence reduction, 452  
  fine structure, 455  
  *g*-factor, 446, 450  
  hyperfine structure, 455  
  in the Jahn–Teller effect, 452  
  super-hyperfine structure, 456  
Electronegativity, 580  
Electroneutrality principle, 213, 640  
Electronic configuration, 36, 71, 247  
  complementary, 42, 46, 92  
  high-spin, 100, 105, 251, 715  
  low-spin, 107, 251, 715  
Electronic density, 143  
  reference, 488  
  spherical model, 514  
Electronic equation, 326  
Electronic transitions. *See also* Optical spectra  
  absorption coefficient, 397  
  band shapes, 396  
  charge transfer, 416  
  *d-d*, 406  
    between degenerate states, 422, 735  
  forbidden, 402  
  Franck–Condon principle, 393  
    factor, 393, 401  
  intervalence, 544  
    radiationless, 401  
    vertical, 393  
  vibrational induced, 409  
  zero-phonon line, 401  
ENDOR, 457  
Epikernel principle, 522  
Exchange-correlation potential, 173  
Exchange interaction, 8, 45, 457  
  anisotropic, 465  
  antiferromagnetic, 457  
  antisymmetric, 464  
  biquadratic, 464  
  double exchange, 536  
  ferromagnetic, 457  
  indirect, 457  
  isotropic, 459  
Excitation by coordination, 258  
Extinction coefficient, *see* Optical spectra  
Extrastabilization energy, 124  
EXAFS, *see* X-ray absorption spectroscopy
- Fenske–Hall method, 169  
Fermi  
  contact interaction, 455, 475  
  hole, 161  
Ferrimagnetic ordering, 444  
Ferrodistorive  
  interactions, 567  
  ordering, 567  
Ferroelastic interactions, *see* Structural phase transitions, ferroelastic  
Ferroelectric interactions, *see* Structural phase transitions, ferroelectric  
Ferroelectricity, 568  
Ferromagnetic interaction (ordering), 444, 457  
Ferrimagnetism, 445  
Ferromagnetism, 445  
Fine-structure constant, 32  
Fockian (Fock effective Hamiltonian), 50, 134, 155  
Force constant, primary, 339  
Form-function, *see* Optical spectra  
Fourier transform, 440  
Fragmentary calculations, 202  
Fragment deformation density, 488  
Franck–Condon principle, *see* Electronic transitions  
Frontier orbitals, 627  
  generalized, 628
- $\gamma$ -Resonance spectroscopy (GRS), 472, 737  
  isomer shift, 475  
  quadrupole splitting, 476  
  hyperfine structure, 478  
GAMESS (computer programs), 165  
GAUSSIAN (computer programs), 165  
Gaussian functions, 158  
Geometry optimization, 165  
Group orbital, 137  
Group representation, 64, 692  
  character, 65, 692  
  irreducible (IrRep), 66  
  two-valued (double group), 81, 187

- Hamiltonian, 12  
   Dzyaloshinsky–Moriya, 464  
   HDVV, 459  
   Ising, 465  
   relativistic, *see* Dirac equation  
   spin-Hamiltonian, 448  
 Hard and soft acids and base, 587  
 Harmonic  
   approximation, 329  
   oscillator, 329  
 Hartree approximation, 47, 173  
 Hartree–Fock, 47, 134  
   equation, 49  
   limit solution, 158  
   method, 47  
   restricted, 156  
   unrestricted, 156  
   wavefunction, 23  
 Hartree–Fock–Roothane method, 154  
 Heitler–London approximation, 8  
 Helicoidal structure, 571  
 High-spin complexes, 100, 105, 715  
 Hindered rotations, *see* Pseudorotations  
 HOMO (highest occupied MO), 149  
 Huckel method  
   extended, 192  
   iterative (SCCC), 193, 716  
 Hund rule, 38  
 Hypsochromic series, 413  
 Hybridization, 24, 51, 707  
 Hysteresis, 467  
  
 Icosahedral field, 130, 696, 714  
 Incommensurate phases, 571  
 Inert gas rule, 516, 738  
   generalized, 517  
 INDO, 175  
 Infrared absorption, 417  
 Intersection (nonintersection) rule, 113  
 Intervalence transition, 596  
 Intuition, 2  
 Ionization energy (potential), 22  
 Irreducible representation (IrRep), *see* Group  
   representation  
 Isomer  
   distortion isomers, 559  
   shift, 475  
  
*j-j* coupling, 40, 52, 193, 311, 707  
 Jahn–Teller  
   active modes, 347  
   dynamics, 363  
   distortions  
     amplification rule, 521  
     isomer, 559  
     off-center, 528  
     pulsating, 313  
     static, 309  
   effect, 348  
     cooperative, 567  
     dynamic, 363  
     hidden, 387  
     static, 360  
   problems  
     multimode, 352  
      $E \otimes b_1$ , 543  
      $E \otimes (b_1 + b_2)$ , 353  
      $E \otimes e$ , 353  
      $(E + A) \otimes e$ , 375  
      $T \otimes (e + t_2)$ , 364  
      $T \otimes e$ , 365  
      $T \otimes t_2$ , 366  
      $(A_{1g} + T_{1u}) \otimes t_{1u}$ , 372  
      $(A_{1g} + T_{1u}) \otimes (t_{1u} + e_g + t_{2g})$ , 536  
      $\Gamma_8 \times (e + t_2)$ , 369  
     pseudo-effect, 349, 369, 738. *See also*  
       Pseudo JT effect  
   stabilization energy, 354  
   theorem, 344  
  
 Kohn–Sham equations, 172  
 Koopmans theorem, 50, 254  
 Kramers doublet, 294, 346, 449  
 Kronecker index, *see*  $\delta$ -function,  $\delta$ -symbol  
  
 Landé  
   *g* factor, 446, 450  
   intervals, 39, 446  
 Langeven theory, 443  
 LCAO, 133  
 Ligand  
   activation, *see* Chemical activation  
   coordination  
     bridging, 279  
     geometry, 530  
     mutual influence, 544  
     semibridging, 288  
 Ligand field  
   arbitrary, 112  
   intermediate, 116  
   parameter, 121  
   strong, 106, 117, 251  
   theory, 123  
   weak, 100, 103, 116, 251  
 Local density approximation (LDA), 175  
 Localization–delocalization  
   alternative, 592  
   coexistence, 604, 740

- Lone pairs, 509, 535, 738  
inert, 535
- Low-spin complexes, *see* Electronic configurations
- LUMO (lowest unoccupied MO), 149
- Madelung potential, 193
- Magnetic  
anisotropy, 443  
circular dichroism, 468  
exchange coupling, 457  
hyperfine structure, 479  
moment, 444, 735  
reduction (quenching), 446  
orbitals, 460, 737  
susceptibility, 443, 447, 736
- Magnetization, 443
- Marcus equation, 625
- Metal–metal bond, 236
- Mixed-valence  
compounds, 591  
dimers, 592  
Creutz–Taube ion, 594  
intervalence transition, 596  
parameter, 593  
phase transitions, 605  
trimers, 601
- Molecular  
dynamics, 206  
engineering, 1, 15  
magnets, 465  
mechanics, 206  
modeling, 206  
orbitals, 132  
antibonding, 147  
bonding, 147  
nonbonding, 147  
symmetrized, 74, 137  
vibronic, 343  
shapes, 506  
symmetry, 54  
vibrations, 325
- Mossbauer effect, 472
- Moeller–Plesset (MP) approximation, 163
- Multielectron  
states, 36  
terms, 37  
wavefunctions, 40
- Multimode problem, *see* JT problem, multimode
- Multiorbital bonding, *see* Bonding
- Mutual influence of ligands, 544, 739  
*cis*-influence, 544  
*trans*-effect, 657  
*trans*-influence, 544  
vibronic theory, 549
- Nephelauxetic  
effect, 414  
series, 414, 733
- Neutron diffraction, 493
- Nonintersection rule, 113, 712
- Normal coordinates, 80
- Nuclear hyperfine splitting, *see*  $\gamma$ -Resonance spectroscopy
- Nuclear magnetic resonance (NMR), 540
- Operator, 12, 56
- Optical activity, 468
- Optical spectra. *See also* Electronic transitions  
absorption coefficient, 397  
band  
form function, 398  
maximum, 399, 400  
shape, 396  
width, 400  
*d-d*, 405, 422  
dichroism (polychroism), 403  
dipolar, 396  
Dushinski effect, 398  
extinction coefficient, 404  
oscillator strength, 404, 406  
parity forbidden, 405  
resonance fluorescence, 401  
selection rules, 402, 733  
spectral density, 397  
spin-forbidden (intersystem combinations), 405  
Stocks shift, 401  
vibrational broadening, 393  
vibrational induced, 409  
zero-phonon line, 401
- Orbital. *See also* Molecular orbital (MO)  
chemical shift, 437  
contraction, 303  
frontier, *see* HOMO, LUMO  
Gaussian, *see* Basis set  
hybridization, 24, 27, 52, 508  
overlap, 24  
Slater type, *see* Basis set  
symmetry rules, 741  
vibronic constants, 340, 610, 636
- Orbital-controlled reactions, 571
- Oscillator strength, *see* Optical spectra
- Overlap  
density, 144  
differential, 25  
integral, 24, 140

- Overlap (*Continued*)  
 model, *see* Angular overlap model  
 negative, 151  
 orbitals, 24  
 population, 144  
 zero differential, 188
- Pairing energy, 109, 251, 465, 712
- Paradigm TEST (two electronic states in transformations), 381, 732, 740
- Paramagnetic  
 relaxation, 457  
 susceptibility, 443, 447, 736
- Paramagnetism, 443  
 temperature independent (Van Fleck), 448
- Pauli  
 matrices, 31  
 principle, 8, 36, 40, 72
- Phase transitions, *see* Structural phase transitions
- Photoelectron spectra, 427  
 angular dependence, 436  
 Auger (APS), 422  
 chemical shift, 436, 735  
 moments of distribution, 433  
 multiplet structure, 435  
 projection formula, 76  
 shake-up satellites, 431  
 ultraviolet (UPS), 422  
 X-ray (XPS), 422
- Pseudo-degeneracy, *see* Pseudo JTE
- Pseudo Jahn–Teller effect, 349, 369, 738  
 illustration, 374  
 multilevel, 378  
 strong, 370  
 weak, 370
- Pseudopotentials, 170
- Pseudorotation, 362, 539, 738  
 Berry, 509, 540  
 Jahn–Teller, 541
- Pulse motions (pulsating deformations), 362
- Plasticity effect, 554, 739
- Quasirelativistic  
 approach, 167, 185  
 parameterization, 198
- Quadrupole splitting, 476
- Quantum-mechanical/molecular mechanics (QM/MM) method, 211
- Racah parameters, 36, 42, 46, 107
- Radiationless transition, 401
- Rayleigh scattering, 419
- Raman effect, 418  
 resonance spectra, 421  
 spectra, 420, 734
- Reactivity, *see* Chemical reactivity
- Reagents  
 electrophilic, 628  
 nucleophilic, 628  
 radical, 628
- Redox capacitance, 584
- Redox nobility, 304
- Relativistic. *See also* Quasirelativistic  
 approaches, 167, 184  
 atomic states, 30, 32  
 functions, 34, 51  
 contraction, 303  
 effects, 13, 185, 303, 314
- Renner–Teller effect, 347
- Resonance integral, 134, 140
- Roothaan method, 143
- Russell–Saunders coupling, 36, 52, 707
- Schrodinger equation, 12, 325, etc.
- Secular equation, 11, 135, 141
- Selection rules, 70, 402, 709
- Self-consistent field (SCF) method, 48, 154
- Semiclassical approximation, 358, 398
- Semiempirical methods, 187
- Slater–Condon parameters, 36, 42, 46
- Slater orbitals, 22, 158
- Spectrochemical series, 412, 733
- Spin-crossover, 130, 465, 482, 715, 727
- Spin density, 493
- Spin-Hamiltonian, 448
- Spin-orbital  
 coupling constant, 30, 39  
 interaction, 28, 186  
 splitting, 311  
 reduction, 314
- Spin multiplicity, 36
- Spin-resonance, *see* Electron spin resonance (ESR)  
 ferroelastic, 570  
 ferroelectric, 568  
 helicoidal, 509  
 incommensurate, 571  
 in MV trimers, 605  
 order-disorder, 566  
 structural-magnetic, 572
- Super-exchange (indirect exchange) interaction, 459
- Super-hyperfine interaction, *see* ESR
- Supramolecular chemistry, 663
- Symmetry  
 breaking, 568  
 classification on, 65, 124

- double group, 81
- group, 60
  - representations, 64
  - tables of, 692
- molecular, 54
- transformation (operation), 54, 60
- transformation matrix, 56
  - character, 65, 692
- Symmetrized
  - orbitals, 74, 76, 78
  - vibrations, 74
  
- Tanabe–Sugano diagrams, 112, 130
- TEST, *see* Paradigm TEST
- Topological (Berry) phase, 363, 731
- trans* effect, 657
- trans* influence, 474
- Transition dipole moment, 341
- Tunnelling, 362
  
- Unitary transformation, 49, 58
- Undistinguishability principle, 8, 40
  
- Valence
  - activity, 304
  - basis set, 146
  - bond, 10, 241
  - directed, 27, 508, 737
  - state, energy of ionization (EIVS), 192
- Variational principle, 47, 134
- Vibrational
  - induced transitions, *see* Optical spectra
  - representation, 79
  
- Vibrations, 325
  - classification, 70
  - fundamental frequency, 418
  - harmonic, 328
  - mechanical, 330
  - normal, 70
  - overtone (anharmonic), 418
  - symmetrized, 74, 80, 734
- Vibronic
  - amplification, 521
  - anharmonicity, 335
  - constants, 338
    - dimensionless, 360
    - linear, 338
    - orbital, 340
    - quadratic, 339
  - effect, cooperative, 566
  - interaction (coupling), 326, 337
  - molecular orbital, 343
  - reduction, 363
    - factor, 364
    - in ESR spectra, 452
  - stereochemistry, 519
  
- Wave-particle duality, 3
- Wigner–Eckart theorem, 73
  
- XANES, 440
- $X_\alpha$  method, 375
- X-ray absorption spectroscopy (EXAFS), 440
  
- Zeeman effect, 450, 478
- Zeise salt, 233
- Zero-phonon line, 401, 473

# FORMULA INDEX

For coordination compounds mentioned in this book.

Chemical formulas are listed by the coordination centers as they appear in the periodic table (separate ligands, as a rule, are not listed). Within each element entry the list begins with simple ligands followed by polydentate coordination, crystal structures, and polynuclear compounds, respectively (this separation is not rigorous, though). General formulas of the type  $ML_n$  are listed at the end of this index.

	<b>B</b>		<b>P</b>
BF <sub>3</sub> , 436		PH <sub>4</sub> <sup>+</sup> , 379	
BH <sub>4</sub> , 379		P(C <sub>2</sub> H <sub>5</sub> ) <sub>5</sub> , 310	
BF <sub>3</sub> ·NH <sub>3</sub> , 11		PF <sub>5</sub> , 540, 544	
		H <sub>3</sub> PO <sub>4</sub> , 546	
	<b>C</b>	MPO <sub>4</sub> , M = Tm, Dy, Tb, 568	
CH <sub>4</sub> , 11, 239, 379			<b>S</b>
	<b>N</b>	SH <sub>4</sub> , SH <sub>4</sub> <sup>2+</sup> , 379	
NH <sub>3</sub> , 384		SF <sub>4</sub> , 540, 544	
NH <sub>4</sub> <sup>+</sup> , 239, 379		SF <sub>6</sub> , 524	
	<b>O</b>		<b>K</b>
OH <sub>4</sub> <sup>2+</sup> , 379		KF, 434	
	<b>Na</b>		<b>Sc</b>
NaF, 402		Sc-CO, 268	
	<b>Al</b>	ScF <sub>3</sub> , 299	
AlH <sub>4</sub> <sup>-</sup> , 379		Sc <sub>2</sub> , 289	
	<b>Si</b>		<b>Ti</b>
SiH <sub>4</sub> , 379		Ti(H <sub>2</sub> O) <sub>6</sub> <sup>3+</sup> , 87, 412	
SiF <sub>4</sub> , 10		TiA <sub>6</sub> <sup>3+</sup> , 396	
SiF <sub>6</sub> <sup>2-</sup> , 8, 10		Ti(Enta) <sup>-</sup> , 412	
		TiF <sub>6</sub> <sup>3-</sup> , 196, 230, 728	

*Electronic Structure and Properties of Transition Metal Compounds: Introduction to the Theory, Second Edition* By Isaac B. Bersuker  
Copyright © 2010 John Wiley & Sons, Inc.



TiO<sub>6</sub><sup>8-</sup>, 371, 384, 528, 535, 569  
 TiO<sub>2</sub>, 430  
 TiCl<sub>4</sub>, 299, 303  
 TiCl<sub>6</sub><sup>3-</sup>, 249,  
 TiCl<sub>4</sub>·Al(CH<sub>3</sub>)<sub>3</sub>, 678  
 TiCl<sub>4</sub>·Al(CH<sub>3</sub>)<sub>2</sub>C<sub>3</sub>H<sub>7</sub>, 678  
 Li<sub>2</sub>TiO<sub>4</sub>, 529  
 FeTiO<sub>4</sub>, 502  
 BaTiO<sub>3</sub>, 371, 382, 384, 442, 569, 570  
 PbTiO<sub>3</sub>, 442, 570  
 Ti<sub>2</sub>, 289  
 LiTi<sub>2</sub>O<sub>4</sub>, 592  
*See also* ML<sub>n</sub>

## V

V(H<sub>2</sub>O)<sub>6</sub><sup>3+</sup>, 412  
 V(H<sub>2</sub>O)<sub>6</sub><sup>2+</sup>, 412  
 V(CN)<sub>5</sub>NO<sup>3-</sup>, 648  
 V(CO)<sub>5</sub>, 644, 742  
 VO<sub>4</sub><sup>3-</sup>, 297  
 VF<sub>5</sub>, 299  
 VOCl<sub>3</sub>, 299  
 V(Ox)<sub>3</sub><sup>3-</sup>, 412  
 Oxo(bis-acetylacetonato)V(IV), 456  
 AVO<sub>4</sub>, A = Tb, Dy, and Tm, 568  
 FeV<sub>2</sub>O<sub>4</sub>, 568  
 V<sub>2</sub>, 289  
 [SiV<sub>3</sub><sup>IV</sup>W<sub>9</sub>O<sub>40</sub>]<sup>10-</sup>, 463  
 V<sub>2</sub>, 289  
*See also* ML<sub>n</sub>

## Cr

CrH<sub>6</sub>, 307  
 Cr(H<sub>2</sub>O)<sub>6</sub><sup>3+</sup>, 396, 412, 497  
 Cr(H<sub>2</sub>O)<sub>6</sub><sup>2+</sup>, 130, 296, 412, 442  
 Cr(C<sub>6</sub>H<sub>6</sub>)<sub>2</sub>, 296  
 Cr<sub>2</sub>(C<sub>3</sub>H<sub>4</sub>)<sub>4</sub>, 288  
 Cr(CN)<sub>6</sub><sup>3-</sup>, 412, 414  
 Cr(NH<sub>3</sub>)<sub>6</sub><sup>3+</sup>, 412, 414  
 Cr(En)<sub>3</sub><sup>3+</sup>, 412, 414  
 Cr(Enta)<sup>-</sup>, 412, 414  
 Cr(NO)<sub>4</sub>, 294, 299  
 Cr(CN)<sub>5</sub>NO<sup>3-</sup>, 648  
 Cr(CN)<sub>5</sub>NO<sup>4-</sup>, 648  
 (CO)<sub>4</sub>Cr(CH<sub>2</sub>)<sub>2</sub>, 664  
 (CO)<sub>4</sub>Cr(C<sub>2</sub>H<sub>4</sub>), 664  
 (CO)<sub>4</sub>Cr(C(NR<sub>2</sub>)<sub>2</sub>)<sub>2</sub>, 664  
 (CO)<sub>4</sub>Cr(C<sub>2</sub>(NR<sub>2</sub>)<sub>4</sub>), 664  
 Cr(CO)<sub>6</sub>, 269, 271, 296, 297, 299, 303  
 Cr(Ox)<sub>3</sub><sup>3-</sup>, 412, 414  
 Cr(C<sub>6</sub>H<sub>6</sub>)CO<sub>3</sub>, 298  
 Cr<sub>2</sub>(O<sub>2</sub>CH<sub>3</sub>)<sub>4</sub>(H<sub>2</sub>O)<sub>2</sub>, 238, 287  
 CrO<sub>4</sub><sup>2-</sup>, 297

CrO<sub>8</sub><sup>3-</sup>, 297  
 CrF<sub>2</sub>, 558  
 CrF<sub>6</sub><sup>3-</sup>, 336, 414, 415  
 CrCl<sub>2</sub>, 558  
 CrCl<sub>6</sub><sup>3-</sup>, 412, 414  
 KCrF<sub>3</sub>, 558  
 K<sub>2</sub>NaCrF<sub>6</sub>, 410, 494, 732  
 Cr : Be<sub>3</sub>Al<sub>2</sub>(SiO<sub>3</sub>)<sub>6</sub>, 410  
 FeCr<sub>2</sub>, 568  
 FeCr<sub>2</sub>O<sub>4</sub>, 568  
 NiCr<sub>2</sub>O<sub>4</sub>, 568  
 CuCr<sub>2</sub>O<sub>4</sub>, 568  
 MoCr(O<sub>2</sub>CH<sub>3</sub>)<sub>4</sub>, 290  
*See also* ML<sub>n</sub>

## Mn

Mn(H<sub>2</sub>O)<sub>6</sub><sup>3+</sup>, 130, 296, 412  
 Mn(H<sub>2</sub>O)<sub>6</sub><sup>2+</sup>, 130, 296, 407, 412, 414, 715  
 Mn(C<sub>5</sub>H<sub>5</sub>)<sub>2</sub>, 297  
 Mn(Enta)<sup>2-</sup>, 412, 414  
 Mn(En)<sub>3</sub><sup>2+</sup>, 130, 412, 414  
 Mn(CO)<sub>5</sub>H, 296, 297, 299, 668  
 Mn(CO)<sub>4</sub>(CHO), 668  
 RMn(CO)<sub>5</sub>, R = CH<sub>3</sub>, C<sub>6</sub>H<sub>5</sub>, 685  
 CH<sub>3</sub>Mn(CO)<sub>5</sub>, 297  
 Mn(C<sub>5</sub>H<sub>5</sub>)CO<sub>3</sub>, 296  
 Mn(CO)<sub>5</sub>, 644, 742  
 Mn(CO)<sub>5</sub>CN, 300  
 Mn(CN)<sub>5</sub>NO<sup>2-</sup>, 648  
 Mn(CN)<sub>5</sub>NO<sup>3-</sup>, 648  
 Mn(NO)<sub>3</sub>CO, 299  
 MnO<sub>4</sub><sup>-</sup>, 180, 230, 297, 302, 336, 718, 724  
 KMnO<sub>4</sub>, 445  
 MnF<sub>3</sub>, 558  
 MnF<sub>6</sub><sup>2-</sup>, 415  
 MnF<sub>6</sub><sup>4-</sup>, 415  
 KMnF<sub>3</sub>, 568  
 (NH<sub>4</sub>)<sub>2</sub>MnF<sub>5</sub>, 558  
 K<sub>2</sub>NaMnF<sub>6</sub>, 558  
 KMnF<sub>3</sub>H<sub>2</sub>O, 558  
 Cs<sub>2</sub>KMnF<sub>6</sub>, 558  
 MnCl<sub>4</sub><sup>2-</sup>, 303  
 Mn(acac)<sub>3</sub>, 558  
 Mn(Ox)<sub>3</sub><sup>3-</sup>, 412  
 Mn(picO)<sub>2</sub>2H<sub>2</sub>O, 417  
 Mn-porphyrin, 528. *See also* in ML<sub>n</sub>  
 Mn-phtalocyanine, 528  
 Mn(trop)<sub>3</sub>, 558  
 Mn(Et<sub>2</sub>dtc)<sub>3</sub>, 558  
 La<sub>1-x</sub>Sr<sub>x</sub>MnO<sub>3</sub>, 592  
 Mn<sub>2</sub>(CO)<sub>10</sub>, 488, 645, 684  
 Mn<sub>2</sub>, 289  
 Mn<sub>3</sub>O<sub>4</sub>, 568  
*See also* ML<sub>n</sub>

**Fe**

$\text{Fe}(\text{H}_2\text{O})_6^{3+}$ , 412, 414, 715  
 $\text{Fe}(\text{H}_2\text{O})_6^{2+}$ , 130, 412  
 $\text{Fe}(\text{Cp})_2$ , 292  
 $\text{Fe}(\text{C}_5\text{H}_5)_2$ , 296, 297  
 Ferrocene, 429  
 $\text{Fe}(\text{C}_5\text{H}_5)_2^+$ , 297  
 $\text{Fe}(\text{III})\text{-CN}$ , 742  
 $\text{Fe}(\text{CN})_6^{4-}$ , 130, 293, 412  
 $\text{FeN}_2$ , 263, 317  
 $\text{FeN}_4$ , 376  
 $\text{Fe}(\text{CN})_5\text{NO}^{2-}$ , 485  
 $[\text{Fe}(\text{CN})_5\text{NO}]^{2-}$ , 648  
 $\text{Na}_2[\text{Fe}(\text{CN})_5\text{NO}]$ , 486  
 $\text{K}_3\text{Fe}(\text{CN})_6$ , 445  
 $\text{Fe}(\text{CO})_4(\text{CHO})^-$ , 668  
 $\text{Fe}(\text{CO})_4$ , 542, 682  
 $\text{Fe}(\text{CO})_5$ , 296, 301, 303, 518, 644, 668, 682, 742  
 $\text{Fe}(\text{CO})_2(\text{NO})_2$ , 294, 298, 299  
 $\text{Fe}(\text{NO}_2)_6^{3-}$ , 10  
 $\text{FeF}_6^{3-}$ , 415  
 $\text{FeF}_6^{4-}$ , 231, 725  
 $\text{Fe}(\text{Br})_6^{3-}$ , 110  
 $\text{Fe}(\text{bipyz})_3^{2+}$ , 417  
 $\text{Fe}(\text{Enta})^{2-}$ , 412  
 $\text{Fe}(\text{phen})_2(\text{NCS})_2$ , 442, 482  
 $[\text{Fe}(\text{urea})_6]\text{Cl}_3$ , 736  
 $\text{Fe}(\text{picO})_2\text{2H}_2\text{O}$ , 417  
 $[(\text{tol})(\text{PPh}_3)_2\text{Mo}(\text{N}_2)\text{Fe}(\text{C}_5\text{H}_5)(\text{dmpe})]^+$ , 647  
 Fe-ferredoxines, 608  
 Fe-porphyrin, 587, 612  
 Fe-picket-fence porphyrin, 221  
 $\text{FeP}(\text{ImH})\text{O}_2$ , Im = imidazol, 618  
 Fe-peroxidase, 616, 619  
 Fe-cytochrom P450, P420, 616, 650  
 $\text{Fe}(\text{P})(\text{L})$ , P = porphyrin, L =  $\text{SCH}_3^-$ ,  $\text{SHCH}_3^-$ , 650  
 Fe(II)-phtalocyanine, 491  
 Fe-ditiocarbomate, 479  
 $\text{FeTiO}_4$ , 568  
 $\text{FeV}_2\text{O}_4$ , 568  
 $\text{FeCr}_2\text{O}_4$ , 568  
 $\text{FeCr}_2\text{S}_4$ , 568  
 $\text{CuFe}_2\text{O}_4$ , 568  
 $\text{PbFeF}_3$ , 568  
 $\text{Fe}_2$ , 289  
 $\text{Fe}_3(\text{CO})_{12}$ , 290  
 $[\text{Fe}(\text{II})\text{Fe}_2(\text{III})(\text{CH}_3\text{COO})_6\text{L}_3]$ , 604  
 $[\text{Fe}_3(\text{CF}_3\text{COO})_6(\text{H}_2\text{O})_3]$ , 602  
 $\text{Fe}_3\text{O}_4$ , 445  
 $[\text{Fe}_3\text{S}_4(\text{SH})_3]^{2-}$ , 608  
 $\text{Fe}_4(\eta^3\text{-C}_5\text{H}_5)_4(\mu_3\text{-S})^n$ , 587  
 $\text{Fe}_4[\text{Fe}(\text{CN})_6]_3 \cdot 4\text{H}_2\text{O}$ , 592

$\text{Fe}_4\text{S}_4$ , 592  
*See also*  $\text{ML}_n$

**Co**

$\text{Co}(\text{H}_2\text{O})_6^{3+}$ , 412, 414, 715  
 $\text{Co}(\text{H}_2\text{O})_6^{2+}$ , 412, 414  
 $\text{Co}(\text{C}_5\text{H}_5)_2$ , 297, 514  
 $\text{Co}(\text{NH}_3)_6^{2+}$ , 412, 582  
 $\text{Co}(\text{NH}_3)_6^{3+}$ , 130, 133, 297, 396, 412, 414, 582, 715  
 $\text{Co}(\text{CN})_6^{3-}$ , 130, 293, 412, 414, 715  
 $\text{Co}(\text{CO})_3\text{NO}$ , 299  
 $\text{Co}(\text{CO})_4$ , 683  
 $\text{HCo}(\text{CO})_4$ , 683  
 $\text{R}_3\text{SiCo}(\text{CO})_4$ , R = Et, Ph, 684  
 $\text{Co}(\text{Ox})_3^{3-}$ , 412, 414  
 $[\text{Co}(\text{NH}_3)_5\text{CN}](\text{NO}_2)_2$ , 439  
 $[\text{Co}(\text{NH}_3)_5\text{X}]^{2+}$ , X = F, Cl, Br, I, 416  
 $\text{Copy}_2\text{Cl}_2$ , 568  
 $(\text{NH}_4)_2\text{CoCl}_2$ , 568  
 $\text{CoCl}_4^{2-}$ , 303, 499, 734  
 $\text{Co}(\text{En})_3^{3+}$ , 412, 414  
 $\text{Co}(\text{En})_3^{2+}$ , 412  
 $\text{Co}(\text{Enta})^-$ , 412, 414  
 $\text{Co}(\text{Enta})^{2-}$ , 412, 414  
 $\text{Co}(\text{bipyz})_3^{2+}$ , 417  
 $\text{Co}(\text{sep})_3^{3+}$ , 582  
 $\text{Co}(\text{sep})_3^{3+}$ , 582  
 $\text{Co}(\text{picO})_2\text{2H}_2\text{O}$ , 417  
 $\text{Co}(\text{H}_2\text{fs}_2\text{en})\text{L}_2$ , L =  $\text{H}_2\text{O}$ , pyridine, 442  
 $\text{Co}(\text{H}_2\text{fsa}_2\text{en})(4\text{-}t\text{-Bipy})_2$ , 467  
 Co-tetraphenylporphyrin, 491  
 Co(II)-phtalocyanine, 494  
 $\text{Co}_2$ , 289  
 $\text{Co}_2(\text{CO})_8$ , 289, 645  
 $\text{CpCo}(\mu\text{-CO})_2\text{ZrCp}_2$ , 291  
 $[\text{Co}(\text{NH}_3)_6][\text{ZnCl}_5]$ , 525  
 $[\text{Co}(\text{NH}_3)_6][\text{CuCl}_5]$ , 525  
*See also*  $\text{ML}_n$

**Ni**

$\text{Ni}(\text{H}_2\text{O})_n$ ,  $n = 1, 2$ , 261  
 $\text{Ni}(\text{H}_2\text{O})_6^{2+}$ , 412, 414  
 $\text{Ni}(\text{C}_3\text{H}_5)_2$ , 293, 297, 299  
 $\text{Ni}(\text{C}_4\text{H}_4)_2$ , 296  
 $\text{Ni}(\eta\text{-C}_5\text{H}_5)_2$ , 514  
 $\text{Ni}(\text{NH}_3)_6^{2+}$ , 412, 414  
 $\text{Ni}(\text{CN})_4^{2-}$ , 293, 295, 297  
 $\text{Ni}(\text{CN})_5^{3-}$ , 82, 518  
 $\text{Ni}(\text{C}_2\text{H}_5)\text{NO}$ , 299  
 $\text{NiNO}$ , 275  
 $\text{Ni}(\text{PH}_3)_n$ ,  $n = 1, 2$ , 261  
 $\text{NiO}_6^{10-}$ , 303

$\text{NiF}_6^{4-}$ , 297, 303, 415  
 $\text{NiF}_6^{2-}$ , 415  
 $\text{KNiF}_3$ , 445  
 $\text{NiCl}_2$ , 445  
 $\text{NiCl}_4^{2-}$ , 296, 297  
 $\text{NiCl}_6^{4-}$ , 412, 414  
 $\text{NiBr}_6^{4-}$ , 412, 414  
 $\text{Ni(En)}_3^{2+}$ , 412, 414  
 $\text{Ni(Enta)}^{2-}$ , 412, 414  
 $\text{Ni(picO)}_2\text{2H}_2\text{O}$ , 417  
 $\text{Ni(bipyz)}_3^{2+}$ , 417  
 $\text{K}_2[\text{Ni(dto)}_2]$ , 421  
 $\text{Li}_x\text{Ni}_{1-x}\text{O}$ , 592  
 $\text{NiCr}_2\text{O}_4$ , 568  
 $\text{NiO}\cdot\text{CO}$ , 644, 646  
 $\text{Ni}_2$ , 289

**Cu**

Cu-H, 309  
 $\text{Cu(H}_2\text{O)}_6^{2+}$ , 296, 412, 442, 652  
 $\text{Cu(H}_2\text{O)}_6^+$ , 296  
 $\text{Cu(H}_2\text{O)}_5^{2+}$ , 296  
 $\text{Cu(NH}_3)_6^{2+}$ , 412  
 $\text{Cu(NH}_3)_2(\text{NO})_2$ , 557  
 $\text{Cu(NH}_3)_2\text{X}_2$ , X = Cl, Br, 559  
 $\text{CuF}_2$ , 166  
 $\text{CuBr}_2$ , 557  
 $\text{CuCl}_2$ , 557  
 $\text{CuF}_3$ , 82, 387, 499, 733  
 $\text{CuCl}_4^{2-}$ , 11, 239, 242, 297, 303, 498  
 $(\text{Naem})\text{CuCl}_4$ , 498  
 $\text{CuCl}_5^{3-}$ , 296, 384, 525, 540  
 $\text{CuF}_4^{2-}$ , 297  
 $\text{CuF}_6^{3-}$ , 415  
 $\text{CuL}_6$ , L = F, Cl, Br, 557  
 Bis(acetylacetonato)Cu(II), 456  
 Bis(dimethyldithiocarbomato)Cu(II), 456  
 Bis(salicylaldimino)Cu(II), 456  
 Bis(salicylaldoxymato)Cu(II), 456  
 Bis(8 chinolinato)Cu(II), 456  
 Dichlorophenanthroline-Cu(II), 456  
 bis(terpyridin)Cu, 558  
 $\text{Cu(picO)}_2\text{2H}_2\text{O}$ , 417  
 $\text{Cu(PCP)}_3(\text{ClO}_4)_3$ , 556, 558  
 $\text{Cu(Enta)}^{2-}$ , 412  
 $\text{Cu(En)}_3^{2+}$ , 412  
 $\text{Cu(en)}_3(\text{SO}_4)$ , 556, 558  
 $\text{Cu(en)}_3\text{Cl}_2$ , 556, 558  
 $\text{Cu(dien)}_2(\text{NO}_3)_2$ , 556, 558  
 $[\text{Cu(bpy)}_2(\text{ONO})]\text{NO}_3$ , 563  
 $\text{Cu(NO}_3)_2\text{py}_2(\text{N}_3)$ , 416  
 $[\text{Cu(bpy)}_3]^{2+}$ , 563  
 $\text{Cu(ONC}_5\text{H}_6)_6\text{X}_2$ , 568  
 $[\text{Cu(tren)H}_2\text{O}]^{2+}$ , 652

$\text{KCuF}_3$ , 557  
 $\text{K}_2\text{CuF}_4$ , 557, 558  
 $\text{Ba}_2\text{CuF}_6$ , 557  
 $\text{CuCr}_2\text{O}_4$ , 568  
 $\text{CuFe}_2\text{O}_4$ , 568  
 $\text{CsCuCl}_3$ , 557, 568, 570  
 $\text{K}_2\text{PbCu(NO}_2)_6$ , 557, 558, 569, 572  
 $\text{A}_2\text{BCu(NO}_2)_6$ , 557, 568  
 $(\text{NH}_4)_2\text{Cu(SO}_4)_2\cdot\text{6H}_2\text{O}$ , 556, 558  
 $\text{CuSiF}_6\cdot\text{6H}_2\text{O}$ , 556, 557  
 $\text{Cu}_2$ , 309  
 $[\text{Cu(OAc)}_2\text{H}_2\text{O}]_2$ , 461, 462, 500, 736  
 $\text{Ba}_2\text{Zn}_{1-x}\text{Cu}_x\text{F}_6$ , 558  
 $\text{CuCo(CO)}_4(\text{NH}_3)_2$ , 291  
 $[\text{Co(NH}_3)_6][\text{CuCl}_5]$ , 525  
 $\text{Cu}_4\text{OL}_4\text{X}_6$ , X = Cl, Br, L = Cl, Br, pyridine,  
 OPR<sub>3</sub>, ONR<sub>3</sub>, 464  
*See also*  $\text{MX}_n$

**Zn**

Zn-H, 309  
 $\text{Zn-H}^+$ , 309  
 $\text{ZnCl}_2$ , 178  
 $\text{ZnCl}_5^{3-}$ , 525  
 $\text{Ba}_2\text{ZnF}_6$ , 558  
 $\text{Ba}_2\text{Zn}_{1-x}\text{Cu}_x\text{F}_6$ , 558  
 $[\text{Zn(bpy)}_2(\text{ONO})]\text{NO}_3$ , 563

**As**

$\text{As(C}_6\text{H}_5)_5$ , 310

**Se**

$\text{MX}_6$ , M = Se, Te, X = Cl, Br, I, 514

**Zr**

$\text{CpCo}(\mu\text{-CO})_2\text{ZrCp}_2$ , 291  
 $\text{MX}_4$ , M = Zr, Hf; X = Cl, Br, I, 310

**Nb**

$\text{K}_2[\text{NbOF}_5]$ , 546  
 $\text{KNbO}_3$ , 570  
 $\text{KNb}_x\text{Ta}_{1-x}\text{O}_3$ , 570  
 $\text{Nb}_6\text{I}_{11}$ , 467  
 $\text{Nb}_2$ , 289

**Mo**

$\text{MoH}_6$ , 307  
 $\text{MoCl}_6^{2-}$ , 412  
 $\text{Mo(CO)}_6$ , 272, 518, 645  
 $[\text{Mo(CNbut)}_7]^{2+}$ , 518  
 $\text{MoOF}_5$ , 546  
 $\text{K}_2[\text{MoOF}_5]\text{H}_2\text{O}$ , 546

$K_2[MoOCl_5]$ , 546  
 $(NH_4)_2[MoOBr_5]$ , 546  
 $Mo(CO)_5L$ ,  $Mo(CO)_4LL'$ ;  $L, L' = NH_3, PMe_3,$   
 $C(OMe)H$ , 682  
 $MoCl_5$ , 541  
 $[Mo_2(SO_4)_4]^{3-}$ , 287  
 $Mo_2Cl_8^{4-}$ , 285  
 $Mo_2$ , 309  
 $MoCr(O_2CH)_4$ , 290  
 $M_xMo_6S_8$ , 592  
 $[(tol)(PPh_3)_2Mo(N_2)Fe(C_5H_5)(dmpe)]^+$ , 647

**Tc**

$TcF_6^{2-}$ , 415  
 $Tc_2$ , 289  
 $Tc_2Cl_8^{3-}$ , 287

**Ru**

$RuF_6$ , 415  
 $RuF_6^-$ , 415  
 $RuCl_6^{2-}$ , 416  
 $Ru(CN)_6^{3-}$ , 582  
 $Ru(CN)_6^{4-}$ , 582  
 $Ru(NH_3)_5L^{3+}$ ,  $L = \text{pyridine}$ , 582  
 $[RuH_2(N_2)(PPh_3)_3]$ , 647  
 $[{Ru(NH_3)_5}_2N_2]^{4+}$ , 647  
 $Ru(\eta^6-C_6Me_6)(\eta^4-C_6Me_6)$ , 514  
 $Ru_2$ , 289  
 $[(NH_3)_5Ru(pyraz)Ru(NH_3)_5]^{5+}$ , 583, 594  
 $(NH_3)_5Rupyru(NH_3)_4pyzRu(NH_3)_5^{7+}$ , 605  
 $(NH_3)_5RuNCRu(bpy)_2CNRu(NH_3)_5^{7+}$ , 605

**Rh**

$Rh(H_2O)_6^{3+}$ , 412, 414, 715  
 $Rh(NH_3)_6^{3+}$ , 412, 414  
 $Rh(En)_3^{3+}$ , 412, 414  
 $RhF_6^{3-}$ , 415  
 $RhCl_6^{3-}$ , 412, 414, 715  
 $RhBr_6^{3-}$ , 412, 414  
 $Rh(CO)H(NH_3)_2$ , 659, 661  
 $Rh(Cl)NH_3(H_2O)_2$ , 659, 661  
 $Rh(PPh_3)_2(CCN)_2BrCO$ , 507  
 $Rh(Ox)_3^{3-}$ , 412  
 $Rh(dmgl)_4(PPh)_2$ , 288  
 $Rh_2(OCCH_3)_4(H_2O)_2$ , 288  
 $Rh_6(CO)_{16}$ , 645  
 $Rh_4(CO)_{12}$ , 645

**Pd**

$PdF_6^{2-}$ , 415  
 $Pd(C_2H_4)$ , 279  
 $Pd(C_2H_4)_3$ , 279  
 $Pd(C_2H_4)_4$ , 279

$PdCl_3(C_2H_4)^-$ , 280  
 $M(CH_3)_2(PR_3)$ ,  $M = Pd, Pt$ , 670  
 $PdO-CO$ , 644  
 $M(CH_3)H(CO)PH_3$ ,  $M = Pd, Pt$ , 673  
 $Pd(R)H(CO)(PH_3)$ ,  $R = CHF_2, C_2H_5$ , 674  
 $M(CX_2CH_2)(H)_2PH_3$ ,  $M = Ni, Pd, Pt$ ;  $X = H, F$ ,  
 677

*See also*  $MX_6$  and  $MX_4$

**Ag**

$Ag-H$ , 309  
 $Ag(C_2H_4)^+$ , 277, 297  
 $AgF_6^{3-}$ , 415  
 $Ag_2$ , 309

**Cd**

$Cd-H^+$ , 309

**In**

$InCl_6^{5-}$ , 535

**Tb**

$RXO_4$ ,  $R = Tm, Dy, Tb$ ;  $X = V, As, P$ , 568

**Dy**

$RXO_4$ ,  $R = Tm, Dy, Tb$ ;  $X = V, As, P$ , 568

**Tm**

$RXO_4$ ,  $R = Tm, Dy, Tb$ ;  $X = V, As, P$ , 568

**Hf**

$HfCl_4, HfBr_4, HfI_4$ , 310

**W**

$W_2(CH_3)_8^{4-}$ , 287  
 $H_4[W(CN)_8]$ , 82, 518  
 $K_4[W(CN)_8]$ , 82, 518  
 $W(CO)_6$ , 272  
 $[W(CO)_4Br_3]$ , 518  
 $HW(CO)_3Cp$ , 684  
 $WS_4^{2-}$ , 311  
 $Na_xWO_3$ , 592  
 $W_2$ , 309  
 $[SiV_3^{IV}W_9O_{40}]^{10-}$ , 463

**Re**

$[ReH_9]^{2-}$ , 82, 518  
 $HReCp_2$ , 684  
 $ReF_6^{2-}$ , 415  
 $K_2[ReOCl_5]$ , 546

Re<sub>2</sub>Cl<sub>8</sub><sup>2-</sup>, 284  
 K<sub>2</sub>ReCl<sub>8</sub>·2H<sub>2</sub>O, 284  
 Re<sub>2</sub>Cl<sub>4</sub>(PR<sub>4</sub>), 288  
 Re<sub>2</sub>Cl<sub>5</sub>(dth)<sub>2</sub>, 288

**Os**

[Os(NH<sub>3</sub>)<sub>5</sub>N<sub>2</sub>]Br<sub>2</sub>, 647  
 OsOF<sub>5</sub>, 546  
 OsF<sub>8</sub>, 499, 734  
 OsF<sub>6</sub>, 415  
 OsF<sub>6</sub><sup>-</sup>, 415  
 [OsH<sub>4</sub>(PMe<sub>2</sub>Ph)<sub>3</sub>], 518  
 OsCl<sub>6</sub><sup>2-</sup>, 416  
 OsBr<sub>6</sub><sup>2-</sup>, 416  
 OsI<sub>6</sub><sup>2-</sup>, 416  
 Os<sub>3</sub>O(CO)<sub>12</sub>, 645

**Ir**

IrF<sub>6</sub>, 415  
 IrCl<sub>6</sub><sup>3-</sup>, 412, 414  
 IrBr<sub>6</sub><sup>3-</sup>, 412, 414  
 [Iren<sub>3</sub>](NCS)<sub>2</sub>, 439  
 [Iren<sub>3</sub>](NO<sub>2</sub>)<sub>3</sub>, 439  
 [Iren<sub>2</sub>(NO<sub>2</sub>)<sub>2</sub>]NO<sub>3</sub>, 439  
 [Iren<sub>2</sub>ClNO<sub>2</sub>]NO<sub>3</sub>, 439

**Pt**

H<sub>2</sub>Pt(PH<sub>3</sub>)<sub>2</sub>, 306, 317  
 Pt(C<sub>2</sub>H<sub>4</sub>)(H<sub>2</sub>)PH<sub>3</sub>, 676  
 Pt(P(t-Bu)<sub>3</sub>)<sub>2</sub>, 215  
 Pt-CO, 265  
 M(CH<sub>3</sub>)H(CO)PH<sub>3</sub>, M = Pd, Pt, 673  
 [(PPH<sub>2</sub>Et)<sub>2</sub>PtHCl], 545  
 [(PMe<sub>2</sub>Ph)<sub>2</sub>Pt(SiMePh<sub>2</sub>)Cl], 545  
 PtH(Cl)(NH<sub>3</sub>)<sub>2</sub>, 659, 661, 661  
 Pt(CH<sub>3</sub>)Cl(NH<sub>3</sub>)<sub>2</sub>, 659  
 [PEt<sub>3</sub>]<sub>2</sub>Pt(CO)Cl, 545, 549  
 [PEt<sub>2</sub>Ph]Pt(CNEt)Cl<sub>2</sub>, 545  
 [PMe<sub>2</sub>Ph]Pt(CH<sub>2</sub>SiMe<sub>3</sub>)Cl], 545  
 PtCl<sub>2</sub>(PR<sub>3</sub>)<sub>2</sub>, 546  
 [Pt(PEt<sub>3</sub>)<sub>2</sub>Cl<sub>2</sub>], 545  
 [Pt(NH<sub>3</sub>)<sub>2</sub>Cl<sub>2</sub>], 545, 549  
 PtCl<sub>3</sub>(C<sub>2</sub>H<sub>4</sub>)<sup>-</sup>, 280, 545  
 K[Pt(acac)<sub>2</sub>Cl], 545  
 [PEt<sub>3</sub>]<sub>2</sub>PtCl<sub>2</sub>], 545, 549  
 [p-C<sub>6</sub>H<sub>4</sub>S]<sub>2</sub>PtCl<sub>2</sub>], 545  
 [(PEt<sub>2</sub>PH)Pt(CNEt)Cl<sub>2</sub>], 545  
 [Pt(H<sub>3</sub>NCH<sub>2</sub>CH=CHCH<sub>2</sub>NH<sub>3</sub>)Cl<sub>3</sub>], 545  
 [(PMe<sub>3</sub>)<sub>2</sub>PtCl<sub>2</sub>], 545  
 [PEt<sub>2</sub>Ph]Pt(CNEt)Cl<sub>2</sub>, 545  
 [PMe<sub>2</sub>Ph]Pt(CH<sub>2</sub>SiMe<sub>3</sub>)Cl], 545  
 [Pt(*cis*-MeCH=CHCH<sub>2</sub>NH<sub>3</sub>)Cl<sub>3</sub>], 545  
 K[Pt(C<sub>2</sub>H<sub>4</sub>)Cl<sub>3</sub>]H<sub>2</sub>O, 545

K[PtNH<sub>3</sub>Cl<sub>3</sub>]H<sub>2</sub>O, 545  
 K<sub>2</sub>[Pt(NO<sub>2</sub>)<sub>3</sub>Cl<sub>3</sub>], 549  
 X<sub>3</sub>PtC<sub>2</sub>H<sub>4</sub><sup>-</sup>, X = F, Cl, Br, 317  
 PtF<sub>6</sub>, 310, 415  
 PtF<sub>6</sub><sup>2-</sup>, 415  
 PtCl<sub>4</sub><sup>2-</sup>, 303, 403  
 K<sub>2</sub>[PtCl<sub>4</sub>], 545  
 PtCl<sub>6</sub><sup>2-</sup>, 201, 313, 412, 416  
 PtCl<sub>6</sub><sup>3-</sup>, 416  
 K<sub>2</sub>PtCl<sub>6</sub>, 429, 437  
 PtBr<sub>6</sub><sup>2-</sup>, 412, 416  
 PtBr<sub>6</sub><sup>3-</sup>, 416  
 PtI<sub>6</sub><sup>2-</sup>, 416  
 [Pt(L-methionine H)Cl<sub>2</sub>], 545  
 K<sub>2</sub>Pt(CN)<sub>4</sub>Br<sub>0.30</sub>•3H<sub>2</sub>O, 592

**Au**

Au-H, 309  
 AuF<sub>6</sub>, 415  
 Au<sub>2</sub>, 309  
 Au<sub>9</sub>(PPh<sub>3</sub>)<sub>8</sub><sup>3+</sup>, 469

**Hg**

Hg-H<sup>+</sup>, 309

**Tl**

Tl<sub>2</sub>, 314

**Pb**

Pb-H, 314  
 PbO, 314  
 Pb<sub>3</sub>O<sub>4</sub>, 592  
 PbCl<sub>6</sub><sup>2-</sup>, 310  
 Pb<sub>2</sub>, 314  
 BaBi<sub>1-x</sub>Pb<sub>x</sub>O<sub>3</sub>, 592

**Bi**

BiH<sup>+</sup>, 314  
 BiPh<sub>5</sub>, 310  
 Bi(C<sub>6</sub>H<sub>5</sub>)<sub>5</sub>, 310  
 Sb<sub>3</sub>Bi, 312  
 Sb<sub>2</sub>Bi<sub>2</sub>, 312  
 SbBi<sub>3</sub>, 312  
 Bi<sub>4</sub>, 312  
 BaBi<sub>1-x</sub>Pb<sub>x</sub>O<sub>3</sub>, 592

**Th**

ThHCl<sub>3</sub>, 311  
 ThCH<sub>3</sub>Cl<sub>3</sub><sup>-</sup>, 311  
 RMCl<sub>3</sub>, M = Th, U; R = H, CH<sub>3</sub>, 310

- Pa**  
(NEt)[PaOCl], 553
- Ac**  
MX<sub>6</sub>, M = actinide, 553
- U**  
UHCl<sub>3</sub>, 311  
UCH<sub>3</sub>Cl<sub>3</sub>, 311  
UO<sub>2</sub>, 568  
UF<sub>6</sub>, 499, 710, 734  
UCl<sub>6</sub>, 553  
UBr<sub>6</sub>, 7  
(PPh<sub>4</sub>)[UOCl<sub>5</sub>], 553  
(NEt<sub>4</sub>)<sub>2</sub>[UOCl<sub>4</sub>], 553  
RMCl<sub>3</sub>, M = Th, U; R = H, CH<sub>3</sub>, 310
- ML<sub>m</sub>**  
M-H<sub>2</sub>, 650  
MH<sub>4</sub>, 515  
M-N<sub>2</sub>, 262, 646  
M-O<sub>2</sub>, 650  
M-CO, M = Cr, Fe, Co, Ni, 267  
M = Ti, Cr, Fe, Co, Ni, 273  
M-NO, 275, 648  
M-C<sub>2</sub>H<sub>4</sub>, 276, 534  
M(CH<sub>3</sub>)<sub>2</sub>(PR<sub>3</sub>)<sub>2</sub>, M = Pd, Pt, 310
- M(PR<sub>3</sub>)<sub>2</sub>, M = Pd, Pt, 310  
M(P(CH<sub>3</sub>)<sub>3</sub>)<sub>2</sub>, 215  
M(CH<sub>3</sub>)H(CO)PH<sub>3</sub>, M = Pd, Pt, 673  
M(CX<sub>2</sub>CH<sub>2</sub>)(H)<sub>2</sub>PH<sub>3</sub>, M = Ni, Pd, Pt; X = H, F, 675, 677  
M(PH<sub>3</sub>)<sub>2</sub>, M = Pd, Pt, 310  
M(CN)<sub>6</sub><sup>4-</sup>, M = Fe, Ru, Os, 582  
ML<sub>2</sub>, M = Ca, Sr, Ba; L = H, F, Cl, Br, 385  
MX<sub>n</sub>, 524  
MX<sub>6</sub>, 261, 536, 558  
M = V, Mn, Cr; X = O, S, F, Cl, I, 558  
M = actinide, 553  
M = Se, Te, 514  
MF<sub>6</sub>, M = Ru, Os, Rh, Ir, Pd, Pt, 310  
[MX<sub>5</sub>]<sup>n-</sup>, 511  
MX<sub>4</sub>  
M = Ni(II), Pd(II), Pt(II), 524  
M = Zr, Hf; X = Cl, Br, I, 310  
MXO<sub>4</sub>, M = Tm, Dy, Tb, X = V, As, P, 568  
MPc, Pc = phtalocyanine, 528  
MP, P = porphyrin; M = Mn, Fe, Co, Ni, Cu, Zn, 530  
M(P(CH<sub>3</sub>)<sub>3</sub>)<sub>2</sub>, 215  
MP(CO), MP(NO), MP(O<sub>2</sub>), 531  
[M(12-ane N<sub>4</sub>)]<sup>n+</sup>, 209  
M<sub>2</sub>X<sub>6</sub>, 309  
M<sub>2</sub>Cl<sub>4</sub>(PR<sub>3</sub>)<sub>4</sub>, 309  
[M<sub>3</sub>O(RCOO)<sub>6</sub>]L<sub>3</sub>, 601